THE JOURNAL
OF
CHEMICAL PHYSICS

VOLUME 34, NUMBER 1 JANUARY, 1961

Nuclear Hyperfine Interactions in Orbitally Degenerate States of Aromatic Ions*

H. M. MCCONNELL† AND A. D. MCLACHLAN‡

Gates and Crellin Laboratories of Chemistry,§ California Institute of Technology, Pasadena, California

(Received August 11, 1960)

The dynamical Jahn-Teller effect in the benzene negative ion is investigated by estimating the vibronic eigenfunctions and energies for the lowest energy degenerate and lowest energy nondegenerate vibronic states using Hückel molecular orbital theory and the normal coordinates for the 606 cm^{-1} and 1595 cm^{-1} E_{2g} vibrations of benzene given by Whiffen. It is concluded that the lowest energy vibronic state is doubly degenerate, and that this degeneracy is removed by interactions with a polar solvent when this ion is in solution. The solvent interaction produces a time-dependent oscillation or switching of the electronic spin distribution relative to the nuclear framework, which in turn leads to an enhanced broadening of the hyperfine structure through a corresponding fluctuation in the isotropic hyperfine interaction. The calculated linewidths are the same as those reported by Townsend and Weissman if the switching spin distribution is described by a correlation time of the order of 10^{-9} sec. A similar effect is probably responsible for the anomalously broad proton hyperfine structure reported by Weissman and Townsend in the negative ions of coronene and triphenylene. This effect must also contribute to the linewidth of the hyperfine structure of the negative ion of cyclooctatetraene observed by Katz and Strauss. It is suggested that the enhanced spin-lattice relaxation rate reported by Weissman and Townsend for the negative ion of coronene is due to enhanced spin-orbit interaction, also associated with a degeneracy of the ground vibronic state.

1. INTRODUCTION

HÜCKEL molecular orbital theory predicts that the ground electronic states of the negative ions of benzene (B^-), triphenylene (Tp^-), coronene (C^-) and cyclooctatetraene (O^-) would be orbitally degenerate if the nuclei of these molecules could be constrained to have D_{xh} symmetry, where $x=6$, 3, 6, and 8, respectively.[1] It is naturally of considerable interest to know whether or not this prediction is correct. Unfortunately, however, any experiment that might be devised to investigate this degeneracy must take into account the Jahn-Teller theorem.[2] For example, an attempt to observe a finite electronic angular momentum of the odd electron around the ring in the benzene negative ion must take into account the prediction of the Jahn-Teller theorem that this molecule will *tend* to distort so as to remove the orbital degeneracy and quench the electronic orbital motion. Thus, observable effects due to the theoretical orbital degeneracy *might* be partially or perhaps even completely masked by the effects of nuclear motions and molecular deformations predicted by the Jahn-Teller theorem. On the other hand, experimental evidence that a molecule is not symmetrical is hardly convincing proof that the electronic state of the molecule *would* be orbitally degenerate if the molecule were symmetrical. Although these depressing possibilities apparently apply to many inorganic complexes of metal ions, there are already a number of publications that suggest the consequences of the Jahn-Teller theorem to be a less serious obstacle to the study of orbital degeneracy in symmetrical aromatic and olefinic radicals and ions. Thus Liehr[3] and Snyder,[4] and Hobey and McLachlan[5] have calculated static Jahn-Teller distortions in B^-, C^-, and Tp^-. This calculation determines equilibrium nuclear configurations and distortion

* Sponsored by the National Science Foundation, by the U. S. Public Health Service and by the Office of Ordnance Research, U. S. Army.

† Alfred P. Sloan Fellow.

‡ Harkness Fellow of the Commonwealth Fund.

§ Contribution No. 2609.

[1] See, for example, C. A. Coulson and R. Daudel, *Dictionary of Values of Molecular Constants* (Mathematical Institute, Oxford, 1955), Vol. II, pp. 5, 39, 63.

[2] H. A. Jahn and E. Teller, Proc. Roy. Soc. (London) **A161**, 220 (1937); H. A. Jahn, *ibid.* **A161**, 117 (1937).

[3] A. D. Liehr, Z. physik. Chem. **9**, 338 (1956).

[4] L. C. Snyder, J. Chem. Phys. **33**, 619 (1960).

[5] W. D. Hobey and A. D. McLachlan, J. Chem. Phys. **33**, 1694 (1960).

Copyright © 1961 by the American Institute of Physics

energies ΔU that would apply to these ions if the nuclei were of infinite mass. For example, in the case of the benzene negative ion, Hobey and McLachlan found the distortion energy ΔU to be equal to 345 cm^{-1} and the distortion amplitude ($\sim$bond extension) to be 0.025 A. Even smaller distortion effects were found for Tp^- and C^-. Now the zero-point amplitudes and energies of the normal vibrational modes of these molecules that produce similar molecular distortions are larger than these calculated static Jahn-Teller distortions. This suggests the qualitative semiclassical argument that for at least some part of the time the nuclei pass through the completely symmetrical configuration, thereby permitting electronic orbital degeneracy and, say, electronic orbital angular momentum around the ring. A number of publications by Moffitt and Liehr,[6] Longuet-Higgins *et al.*,[7] Moffitt and Thorson,[8,9] and Hobey and McLachlan[5] discuss quantum-mechanical calculations to handle this so-called dynamical Jahn-Teller situation that arises when the distortion energies and amplitudes are comparable to zero-point energies and amplitudes, and the Born-Oppenheimer approximation is not valid. These papers do, in fact, suggest that the above classical picture that leads to a finite electronic angular momentum around the ring is indeed correct in that the lowest vibronic state of these molecules may remain degenerate even with nuclear distortions. However, none of this previous work has really gone far enough to provide adequate detailed information for the investigator interested in designing an experiment to study this supposed electronic orbital degeneracy. That is, one must know where the molecules in question are to be placed relative to the following three limiting cases:

A. The ground vibronic state is doubly degenerate, and the nearest totally symmetric state is of the order of a vibrational quantum higher in energy.

B. The lowest vibronic state is nondegenerate, and the first degenerate state is of the order of a vibrational quantum higher in energy.

C. The ground vibronic state is very nearly threefold degenerate, and certain (strictly speaking nonstationary state) combinations of the corresponding vibronic functions yield the conventional picture of, say, a benzene-like molecule that is distorted in one of the three directions.

Although the previous theoretical work on the static as well as dynamical Jahn-Teller effects suggested to us that case *A* obtains for the symmetrical radicals under consideration, we felt that it would be highly desirable to demonstrate this result by a detailed calculation for a particular case (B^-), especially in view of the fact in a real molecule there is, in general, more than a single vibrational mode that is coupled strongly to the electronic motion, whereas in most previous theoretical studies of the dynamical effects only idealized models and a single vibrational mode were considered. On the other hand, this previous work on the dynamical effect has served as an extremely helpful guide to us.

Our interest in these problems was originally stimulated by the observations of Townsend and Weissman[10] that the proton hyperfine structure in the paramagnetic resonance of B^-, Tp^-, and C^- is unusually broad when compared to the sharp hyperfine structure seen in less symmetrical but otherwise similar ion radicals. Also, enhanced spin-lattice relaxation in C^- relative to biphenyl negative ion was observed. Katz and Strauss[11] have also reported rather broad proton hyperfine structures in the paramagnetic resonance of O^-. In discussing their experimental results, Townsend and Weissman[10] have suggested that this broadening may be associated with Jahn-Teller distortions and the accompanying fluctuations of spin distribution and hyperfine interactions. In the present work we conclude, on the contrary, that Jahn-Teller distortions have nothing to do with the enhanced linewidths. However, our work, together with the experimental results of Townsend and Weissman, may be taken as good evidence for the orbital degeneracy predicted by the Hückel theory.

The reader will note that the discussion given in the next four sections of this paper is restricted to the case of the benzene negative ion. This is because our calculations of the dynamical Jahn-Teller effect in the negative ions require a detailed knowledge of the normal vibrational modes for the neutral molecules, and this information is only available for benzene. However, the experimental hyperfine linewidths for B^-, Tp^-, C^-, and O^- are all similar, and it is quite likely that a treatment of the dynamical Jahn-Teller effect in these other ions would also lead to a case *A* doubly degenerate vibronic ground state, especially in view of the small static Jahn-Teller distortion energies that have been calculated for these ions.[5]

2. THE DYNAMICAL JAHN-TELLER EFFECT IN $C_6H_6^-$

The nuclear vibrational amplitudes and Jahn-Teller distortions that we shall encounter in this work are indeed small ($\sim$0.05 A), and therefore it will be a good approximation to separate the molecular rotational motion from the internal vibrational-electronic (vibronic) motions. The vibronic eigenfunctions are designated $F_r^{(p)}(\mathbf{x}, \mathbf{X})$, where $\mathbf{x}=\mathbf{x}_1, \mathbf{x}_2, \mathbf{x}_3, \cdots$, and $\mathbf{X}=\mathbf{X}_1, \mathbf{X}_2, \mathbf{X}_3, \cdots$, refer to the electronic and carbon nuclear coordinates, respectively (no explicit reference to proton coordinates is necessary). The carbon nuclei

[6] W. Moffitt and A. D. Liehr, Phys. Rev. **106**, 1195 (1957).

[7] H. C. Longuet-Higgins, U. Öpik, M. H. L. Pryce, and R. A. Sack, Proc. Roy. Soc. (London) **A244**, 1 (1958).

[8] W. Moffitt and W. R. Thorson, "Calcul des fonctions d'onde Moleculaire," Receuil de Memoires, Centre Nationale de la Recherche Scientifique (November 1958).

[9] W. Moffitt and W. R. Thorson, Phys. Rev. **108**, 1251 (1957).

[10] M. G. Townsend and S. I. Weissman, J. Chem. Phys. **32**, 309 (1960).

[11] T. J. Katz and H. L. Strauss, J. Chem. Phys. **32**, 1873 (1960).

are labeled consecutively 1, 2, ···, 6 around the ring. The operator $\mathbf{P}_6$ is used frequently in the following calculations. $\mathbf{P}_6$ is defined as a permutation operator that acts on the nuclear coordinates so that $\mathbf{X}_1$ is replaced by $\mathbf{X}_2$, $\mathbf{X}_2$ is replaced by $\mathbf{X}_3$, etc. when this operator acts on any function of these variables. The operator $\mathbf{P}_6$ commutes with the Hamiltonian for the problem, and the vibronic functions $F_r^{(p)}$ are chosen to be eigenfunctions of $\mathbf{P}_6$

$$\mathbf{P}_6 F_r^{(p)} = \gamma^p F_r^{(p)},$$
$$\gamma = \exp(2\pi i/6). \tag{2.1}$$

Since $\mathbf{P}_6^6 = 1$, the possible eigenvalues γ^p of $\mathbf{P}_6$ are the six roots of unity, which means that $p = 0, \pm 1, \pm 2, 3$. Distinct energy eigenvalues of a given symmetry species p are labeled $E_r^{(p)}$, so that $E_0^{(p)} < E_1^{(p)} < E_2^{(p)}$, ···. In order to estimate the functions $F_r^{(p)}$ and energies $E_r^{(p)}$ for the lowest vibronic states of B^-, we seek to represent the vibronic functions as a series of products of certain electronic and nuclear vibrational functions. The expansion is represented in a severely condensed notation by the following equation.

$$F_r^{(p)} = \sum_{m, v_k, l_k; n_q} a_{m v_k l_k n_q}{}^r \mid m: v_k, l_k: n_q \rangle. \tag{2.2}$$

The quantity $\mid m: v_k, l_k: n_q \rangle$ represents the product of two electronic wave functions, and thirty nuclear vibrational wave functions. That is,

$$\mid m: v_k, l_k: n_q \rangle = \mathfrak{A} \omega^{(m)}(\mathbf{x}, \mathbf{X}) \psi(\mathbf{x}, \mathbf{X}) \Omega \chi(v_k, l_k: n_q). \tag{2.3}$$

Here $\omega^{(m)}(\mathbf{x}, \mathbf{X})$, $m = \pm 2$, is a molecular π orbital that holds the odd electron, $\psi(\mathbf{x}, \mathbf{X})$ is the space part of a single configurational function for the six bonding π electrons, Ω is a suitable seven-electron spin function, and $\chi(v_k, l_k: n_q)$ are the nuclear vibrational functions for the neutral benzene molecule. $\mathfrak{A}$ is the electron antisymmetrization operator. Now consider each of the three space functions in Eq. (2.3), especially with regard to how these functions are affected by $\mathbf{P}_6$.

The indices q and k refer to the qth and kth normal vibrational modes of benzene that are nondegenerate, and twofold degenerate, respectively. The quantity n_q is the usual quantum number of a nondegenerate harmonic oscillator with energy $(n_q + \frac{1}{2})h\nu_q$, where $n_q = 0, 1, 2, \cdots$. The corresponding normal coordinate and nuclear vibrational eigenfunctions are $Q_q = Q_q(\mathbf{X}_1, \mathbf{X}_2, \cdots)$ and $\Phi_{n_q} = \Phi_{n_q}(Q_q)$. The possible eigenvalues of $\mathbf{P}_6$ for this case are easily determined from the symmetry properties of Q_q.

$$\mathbf{P}_6 Q_q = \pm Q_q \tag{2.4}$$

$$\mathbf{P}_6 \Phi_{n_q} = (\pm 1)^{n_q} \Phi_{n_q}. \tag{2.5}$$

The quantities v_k and l_k are quantum numbers of a two-dimensional isotropic harmonic oscillator[7] corresponding to the two-fold degenerate normal vibrational mode k. The energy is $v_k h\nu_k$, and v_k takes on the values $v_k = 1, 2, 3, \cdots$. The "angular momentum" quantum number l_k takes on positive and negative values such that

$$\mid l_k \mid = v_k - 1, \quad v_k - 3, \quad v_k - 5, \cdots 1, \text{ or } 0. \tag{2.6}$$

Let Q_{ka} and Q_{kb} be two *real* normal coordinates for degenerate mode k such that $Q_{ka} + iQ_{kb}$ is an eigenfunction of $\mathbf{P}_6$ with eigenvalue γ^μ.

$$\mathbf{P}_6(Q_{ka} + iQ_{kb}) = \gamma^\mu (Q_{ka} + iQ_{kb}). \tag{2.7}$$

Now write

$$Q_{ka} + iQ_{kb} = Q_k \exp i\phi_k, \tag{2.8}$$

where Q_k is real. The operation $\mathbf{P}_6$ increases ϕ_k by $2\pi\mu/6$:

$$\mathbf{P}_6 \exp(i\phi_k) = \gamma^\mu \exp i\phi_k. \tag{2.9}$$

In terms of the variables Q_k and ϕ_k, nuclear vibrational eigenfunctions of $\mathbf{P}_6$ are[12]

$$\Phi_{v_k}{}^{l_k} \exp(il_k\phi_k) \equiv \Phi_{v_k}{}^{l_k}(Q_k) \exp il_k\phi_k, \tag{2.10}$$

$$\mathbf{P}_6 \Phi_{v_k}{}^{l_k} \exp(il_k\phi_k) = \gamma^{\mu l_k} \Phi_{v_k}{}^{l_k} \exp il_k\phi_k. \tag{2.11}$$

Of course, for a twofold degenerate coordinate, the only possible eigenvalues of $\mathbf{P}_6$ are ± 1, ± 2 (mod 6). For the sake of definiteness, let us say that the Q_{ka} and Q_{kb} in Eq. (2.7) are chosen so that μ in Eqs. (2.9)–(2.11) is a positive number, which is equal to $+1$ for an E_1 vibration, and equal to $+2$ for an E_2 vibration.

The total nuclear vibrational function $\chi(v_k, l_k: n_q)$ is then a product of all the nondegenerate vibrational eigenfunctions Φ_{n_q} and all the degenerate vibrational eigenfunctions $\Phi_{v_k}{}^{l_k}$. Thus χ is an eigenfunction of $\mathbf{P}_6$ with the eigenvalue

$$\prod_k \gamma^{l_k \mu_k} \prod_q (\pm 1)^{n_q}.$$

Here we have replaced μ by μ_k to indicate that μ takes on different values for different normal modes.

Next we must consider the electronic wave functions $\omega^{(m)}(\mathbf{x}, \mathbf{X})$, $m = \pm 2$, and $\psi(\mathbf{x}, \mathbf{X})$ that appear in Eq. (2.3). In the present work, no explicit reference to the σ electrons is necessary; $\omega^{(m)}$, $m = \pm 2$, is the molecular π orbital that holds the odd antibonding π electron, and $\psi(\mathbf{x}, \mathbf{X})$ is the π electron wave function that describes the six bonding π electrons. We use the molecular π orbitals defined below.

$$\omega^{(\lambda)} = \gamma \sum_{j=0}^{j=5} \gamma^{-j\lambda} \pi_{j+1}, \tag{2.12}$$

$$\mathbf{P}_6 \omega^{(\lambda)} = \gamma^\lambda \omega^{(\lambda)},$$
$$\lambda = 0, \pm 1, \pm 2, 3. \tag{2.13}$$

Note that

$$\pi_j(\mathbf{x}) = \pi(\mathbf{x} - \mathbf{X}_j), \tag{2.14}$$

and that

$$\mathbf{P}_6 \pi_j = \pi_{j+1}. \tag{2.15}$$

[12] G. Herzberg, *Infrared and Raman Spectra* (D. Van Nostrand Company, Inc., Princeton, New Jersey, 1949), p. 81.

The coefficients $\gamma^{-j\lambda}$ of the atomic π orbitals π_{j+1} that appear in Eq. (2.18) are the same as those that solve the Hückel molecular π-orbital problem for benzene when the nuclei have D_{6h} symmetry. These π orbitals π_j are centered on the nuclei, and more with the nuclei. However, the atomic orbital coefficients $\gamma^{-j\lambda}$ do not change with nuclear displacements, according to this definition of $\omega^{(\lambda)}$. The space configurational function $\psi(\mathbf{x}, \mathbf{X})$ for the six bonding π electrons is

$$\psi(\mathbf{x}, \mathbf{X}) = \omega^{(0)}(1)\omega^{(0)}(2)\omega^{(1)}(3)\omega^{(1)}(4)\omega^{(-1)}(5)\omega^{(-1)}(6). \tag{2.16}$$

Clearly

$$\mathbf{P}_6\psi(\mathbf{x}, \mathbf{X}) = \psi(\mathbf{x}, \mathbf{X}). \tag{2.17}$$

It is to be understood that electron No. 7 is placed in orbital $\omega^{(m)}$, $m = \pm 2$.

$$\omega^{(m)} \equiv \omega^{(m)}(7).$$

The electronic spin function Ω is simply

$$\Omega = \alpha(1)\beta(2)\alpha(3)\beta(4)\alpha(5)\beta(6)\alpha(7). \tag{2.18}$$

It must be remarked that as the carbon nuclei move from their equilibrium configurations, there is a tendency for each molecular orbital function to change, and in the present work this is not taken into account except for the mixing of the $\omega^{(+2)}$ and $\omega^{(-2)}$ orbitals. We could recognize this variation of all the molecular orbitals with nuclear displacements by including excited π-electron configurations in the summation in Eq. (2.2). Such effects are easily estimated by perturbation theory and can be shown to be of no importance in the present work.

Now consider all low-lying energy states $|\, m{:}v_k, l_k{:}n_q\rangle$ that can contribute significantly to the lowest energy ground vibronic states $F_r^{(p)}$. In the expansion of Eq. (2.2), we only include the two orbital states $\omega^{(+2)}$ and $\omega^{(-2)}$ for the odd electron, only the ground state closed shell configuration $\psi(\mathbf{x}, \mathbf{X})$ for the six bonding electrons and the zero-point vibrational function $\chi(1, 0{:}0)$ as well as all excited vibrational functions $\chi(v_k, l_k{:}n_q)$ that contribute significantly to the ground vibronic states. Since $|\, m{:}v_k, l_k{:}n_q\rangle$ is an eigenfunction of $\mathbf{P}_6$ with eigenvalue

$$\gamma^m \prod_k \gamma^{l_k\mu_k} \prod_q (\pm 1)^{n_q}, \tag{2.19}$$

we see that the terms that can appear in Eq. (2.2) are limited by the following selection rule.

$$p = m + \sum_k l_k\mu_k + \sum_q{}' 3n_q (\text{mod. } 6), \tag{2.20}$$

where the prime on the summation indicates that only vibrations antisymmetric to $\mathbf{P}_6$ are included.

The next problem is to evaluate the matrix elements

$$\langle m'{:}v_k', l_k'{:}n_q' \,|\, \mathfrak{h} \,|\, m{:}v_k, l_k{:}n_q\rangle, \tag{2.21}$$

and to solve the secular equation that leads to the approximate vibronic functions $F_r^{(p)}$ and energies $E_r^{(p)}$. In this maxtrix element $\mathfrak{h}$ is the effective one-electron Hamiltonian of the Hückel theory. The physically interesting effects arise from matrix elements of the form

$$\langle -2{:}v_k', l_k'{:}n_q' \,|\, \mathfrak{h} \,|\, 2{:}v_k, l_k{:}n_q\rangle, \tag{2.22}$$

since these couple the electronic orbital motion around the ring with nuclear vibrational angular momentum, and give rise to the Jahn-Teller effect. To evaluate these matrix elements, consider first the integration over the coordinates of the odd electron.

$$(-2 \,|\, \mathfrak{h} \,|\, 2) = \int \omega^{(-2)*}\mathfrak{h}\omega^{(2)} dv. \tag{2.23}$$

Note that since $\omega^{(-2)}$ and $\omega^{(2)}$ are orthogonal at all nuclear configurations, and since $\mathfrak{h}$ is assumed to be a sum of one-electron operators, there are no contributions from the matrix elements (2.23) or (2.22) that involve the six bonding electrons. It is convenient to develop several eigenfunctions of $\mathbf{P}_6$ using a projection operator $\mathbf{O}^{(\lambda)}$.

$$\mathbf{O}^{(\lambda)} = 6^{-1}\sum_{j=0}^{j=5} \gamma^{-j\lambda}\mathbf{P}_6{}^j. \tag{2.24}$$

Thus,

$$\omega^{(\lambda)} = \gamma\mathbf{O}^{(\lambda)}\pi_1. \tag{2.25}$$

The extra factor of γ that appears here, and in Eq. (2.18), is introduced so as to simplify the following equations, and to yield coefficients $a_{mvkl_kn_q}{}^r$ in Eq. (2.2) that are real. When we make the plausible assumption that the one center "Coulomb integral" of molecular orbital theory, α, does not change appreciably with nuclear displacements, then the electronic matrix element of Eq. (2.23) becomes

$$(-2 \,|\, \mathfrak{h} \,|\, 2) = (\tfrac{2}{3})^{\frac{1}{2}}\mathbf{O}^{(-2)}\beta_{1,2}, \tag{2.26}$$

where $\beta_{1,2}$ is the usual resonance integral of molecular orbital theory.

$$(\pi_1 \,|\, \mathfrak{h} \,|\, \pi_2) = \beta_{1,2}. \tag{2.27}$$

Now we further assume that $\beta_{i,i+1}$ depends only on the distance $d_{i,i+1} = |\, \mathbf{X}_i - \mathbf{X}_{i+1} \,|$ between atoms i and $i+1$. Then expand $\beta_{i,i+1}$ in a Taylor's series about the equilibrium carbon-carbon internuclear distance d^0.

$$\beta_{i,i+1} = \beta^0 + \beta'\delta_{i,i+1} + \tfrac{1}{2}\beta''\delta_{i,i+1}{}^2 + \cdots. \tag{2.28}$$

Here $\delta_{i,i+1}$ is the extension of the bond between atoms i and $i+1$,

$$\delta_{i,i+1} = d_{i,i+1} - d^0. \tag{2.29}$$

Variations of β with bond angles are neglected. Formulas for β' and β'' as a function of internuclear distance may be obtained from the work of Longuet-Higgins and Salem.[13] The values adopted in the present calculations are $\beta^1 = 27\,600$ cm^{-1}/A, and $\beta'' = 88\,900$ cm^{-1}/(A)^2,

[13] H. C. Longuet-Higgins and L. Salem, Proc. Roy. Soc. (London) **A251**, 172 (1959).

which correspond to an internuclear distance 1.413 A. According to the calculations of Hobey and McLachlan,[3] this is the carbon-carbon internuclear distance that the benzene negative ion would have if the nuclei were of infinite mass and if, in the Hückel approximation, the odd electron were constrained to be always in the $\omega^{(+2)}$ orbital, and never in the $\omega^{(-2)}$ orbital (or vice versa). Our reasons for adopting these values of β' and β'' rather than those appropriate to the neutral benzene molecule are probably obvious from a physical point of view. The mathematical basis is indicated by the discussion at the end of this section.

Equations (2.26) and (2.28) can be combined to express the matrix element (2.23) in terms of symmetry coordinates.

$$(-2 \mid \mathfrak{h} \mid 2)=(\tfrac{2}{3})^{\frac{1}{2}}\Big[\beta'\mathfrak{S}^{(-2)}+\frac{1}{2\sqrt{6}}\beta''\sum_{\lambda+\nu=-2,4}\mathfrak{S}^{(\lambda)}\mathfrak{S}^{(\nu)}+\cdots\Big]. \quad (2.30)$$

Here the six symmetry coordinates $\mathfrak{S}^{(\lambda)}$ for $\lambda=0$, ±1, ±2, 3 are

$$\mathfrak{S}^{(\lambda)}=\mathbf{O}^{(\lambda)}\delta_{1,2}. \quad (2.31)$$

The coefficient of β'' in Eq. (2.30) is most readily obtained from Eqs. (2.26) and (2.28) by noting that

$$\delta_{1,2}=6^{-\frac{1}{2}}\sum_{\lambda}\mathfrak{S}^{(\lambda)}. \quad (2.32)$$

The possible values of the pairs of numbers (λ, ν) that appear in Eq. (2.30) are (λ, ν), $(\nu, \lambda)=(0, -2)$; $(1, 3)$; $(-1, -1)$; $(2, 2)$. As a further convenience for the following calculations, we express the symmetry coordinates $\mathfrak{S}^{(\lambda)}$ in terms of the normal coordinates $Q_k^{(\lambda)}$ that are themselves eigenfunctions of $\mathbf{P}_6$

$$\mathbf{P}_6Q_k^{(\lambda)}=\gamma^{\lambda}Q_k^{(\lambda)} \quad (2.33)$$

$$\mathfrak{S}^{(\lambda)}=\sum_k\mathfrak{S}_k'^{(\lambda)}Q_k^{(\lambda)}. \quad (2.34)$$

The nondegenerate normal coordinates $Q_k^{(\lambda)}$ for $\lambda=0, 3$ are identical to those defined in Eq. (2.4). The doubly degenerate normal coordinates $Q_k^{(\lambda)}$ are defined by the equation,

$$Q_k^{(\lambda)}=\sqrt{2}^{-1}Q_k\exp\pm i\phi_k, \quad (2.35)$$

where the plus or minus sign depends on whether λ is a positive or negative number. With this definition the values of $\mathfrak{S}_k'^{(\lambda)}$ that appear in Eq. (2.34) are numerically equal to those tabulated by Whiffen.[14] In terms of these normal coordinates Eq. (2.30) becomes

$$(-2 \mid \mathfrak{h} \mid 2)=(\tfrac{2}{3})^{\frac{1}{2}}\Big[\beta'\sum_k\mathfrak{S}_k'^{(-2)}Q_k^{(-2)}+\tfrac{1}{2}6^{-\frac{1}{2}}\beta''\sum_{\lambda,\nu,m,n}\mathfrak{S}'_m{}^{(\lambda)}\mathfrak{S}_n'^{(\nu)}Q_m^{(\lambda)}Q_n^{(\nu)}+\cdots\Big]. \quad (2.36)$$

[14] D. H. Whiffen, Phil. Trans. Roy. Soc. London **A248**, 131 (1955).

All the possible terms that can arise from the matrix element (2.22) are listed below.

$$(\tfrac{2}{3})^{\frac{1}{2}}\beta'\sum_t\mathfrak{S}_t'^{(-2)}(v_t', l'_t \mid Q_t^{(-2)} \mid v_t, l_t) \quad (2.37a)$$

$$1/6\beta''\sum_m(\mathfrak{S}_m'^{(2)})^2(v_m', l_m' \mid (Q_m^{(2)})^2 \mid v_m, l_m) \quad (2.37b)$$

$$1/6\beta''\sum_{m\neq m'}\mathfrak{S}_m'^{(2)}\mathfrak{S}_{m'}'^{(2)}(v_{m'}', l_{m'}' \mid Q_{m'}^{(2)} \mid v_{m'}, l_{m'})\times(v_m', l_m' \mid Q_m^{(2)} \mid v_m, l_m) \quad (2.37c)$$

$$1/6\beta''\sum_n(\mathfrak{S}_n'^{(-1)})^2(v_n', l'_n \mid (Q_n^{(-1)})^2 \mid v_n, l_n) \quad (2.37d)$$

$$1/6\beta''\sum_{n\neq n'}\mathfrak{S}_n'^{(-1)}\mathfrak{S}_{n'}'^{(-1)}(v_{n'}', l_{n'}' \mid Q_{n'}^{(-1)} \mid v_{n'}, l_{n'})\times(v_n', l_n' \mid Q_n^{(-1)} \mid v_n, l_n) \quad (2.37e)$$

$$1/6\beta''\sum_{n,q}\mathfrak{S}_n'^{(1)}\mathfrak{S}_q'^{(3)}(v_n', l_n' \mid Q_p^{(1)} \mid v_n, l_n)\times(n_q' \mid Q_q^{(3)} \mid n_q) \quad (2.37f)$$

$$1/6\beta''\sum_{x,y}\mathfrak{S}_x'^{(0)}\mathfrak{S}_y'^{(-2)}(n_x' \mid Q_x^{(0)} \mid n_x)\times(v_y', l_y' \mid Q_y^{(-2)} \mid v_y, l_y). \quad (2.37g)$$

The nuclear vibrational matrix elements appearing in the above equation are well known for nondegenerate modes, and are available in the work of Longuet-Higgins *et al.*[7] for the degenerate modes.

For a nondegenerate normal mode, the only nonzero nondiagonal matrix elements of $Q_k^{(\lambda)}$ are

$$(n_k+1 \mid Q_k^{(\mu)} \mid n_k)=[(n_k+1)/2]^{\frac{1}{2}}\xi_k. \quad (2.38)$$

For the degenerate modes, the only nonzero nondiagonal matrix elements of interest are

$$(v_k+1, l_k+1 \mid Q_k^{|\lambda|} \mid v_k, l_k)=\tfrac{1}{2}(v_k+l_k+1)^{\frac{1}{2}}\xi_k \quad (2.39)$$

$$(v_k-1, l_k+1 \mid Q_k^{|\lambda|} \mid v_k, l_k)=\tfrac{1}{2}(v_k-l_k-1)^{\frac{1}{2}}\xi_k \quad (2.40)$$

$$(v_k-1, l_k-1 \mid Q_k^{-|\lambda|} \mid v_k, l_k)=\tfrac{1}{2}(v_k+l_k-1)^{\frac{1}{2}}\xi_k \quad (2.41)$$

$$(v_k+1, l_k-1 \mid Q_k^{-|\lambda|} \mid v_k, l_k)=\tfrac{1}{2}(v_k-l_k+1)^{\frac{1}{2}}\xi_k \quad (2.42)$$

$$(v_m-2, l_m-2 \mid (Q_m^{-|\lambda|})^2 \mid v_m, l_m)=\tfrac{1}{4}[(v_m+l_m-3)(v_m+l_m-1)]^{\frac{1}{2}}\xi_k \quad (2.43)$$

$$(v_m, l_m-2 \mid (Q_m^{-|\lambda|})^2 \mid v_m, l_m)=\tfrac{1}{2}[(v_m+l_m-1)(v_m-l_m+1)]^{\frac{1}{2}}\xi_k \quad (2.44)$$

$$(v_m+2, l_m-2 \mid (Q_m^{-|\lambda|})^2 \mid v_m, l_m)=\tfrac{1}{4}[(v_m-l_m+3)(v_m-l_m+1)]^{\frac{1}{2}}\xi_k \quad (2.45)$$

$$(v_m+2, l_m+2 \mid (Q_m^{|\lambda|})^2 \mid v_m, l_m)=\tfrac{1}{4}[(v_m+l_m+3)(v_m+l_m+1)]^{\frac{1}{2}}\xi_k \quad (2.46)$$

$$(v_m, l_m+2 \mid (Q_m^{|\lambda|})^2 \mid v_m, l_m)=\tfrac{1}{2}[(v_m+l_m+1)(v_m-l_m-1)]^{\frac{1}{2}}\xi_k \quad (2.47)$$

$$(v_m-2, l_m+2 \mid (Q_m^{|\lambda|})^2 \mid v_m, l_m)=\tfrac{1}{4}[(v_m-l_m-3)(v_m-l_m-1)]^{\frac{1}{2}}\xi_k. \quad (2.48)$$

When the matrix elements (2.38)–(2.48) are substituted in formulas (2.37a)–(2.37g), one always ob-

tains factors of the type $\mathfrak{S}_k'^{(\lambda)}\xi_k$. These are equal to the numerical quantities tabulated by Whiffen.[14] The quantity $\mathfrak{S}_k'^{(\lambda)}\xi_k$ represents the amplitude of a real normalized symmetry coordinate in cm for a classical vibration in which the (or a) normal coordinate for mode k has energy $\frac{1}{2}h\nu_k$. This value of the normal coordinate is ξ_k, i.e.,

$$[h/4\pi^2\nu_k]^{\frac{1}{2}}. \tag{2.49}$$

The vibronic state with the lowest zero-order energy is the zero-point state $|\pm 2:1_k, 0_k:0_p\rangle$ which is doubly degenerate in the electronic coordinates alone. In order to obtain a *rough idea* of the strength of the electronic-vibrational coupling, let us suppose *for a moment* that the effects of this coupling may be treated by first-order perturbation theory. We then have the following first-order formulas for the lowest energy vibronic state with symmetry $p=2$

$$F_0^{(2)} \simeq |2:1_k, 0_k:0_p\rangle - \sum_{v_k, l_k, n_p} \Delta E_k^{-1} \langle -2:v_k, l_k:n_p | \mathfrak{H} | 2:1_k, 0_k:0_p\rangle | -2:v_k, l_k:n_p\rangle. \tag{2.50}$$

$$\begin{aligned} F_0^{(2)} \simeq {} & |2:1_k, 0_k:0_p\rangle - \beta'/\sqrt{3}\sum_t (h\nu_t)^{-1}\mathfrak{S}_t'^{(-2)} | -2:2_t, -1_t:0_p\rangle - \beta''/6\sqrt{2}\sum_m (2h\nu_m)^{-1}(\mathfrak{S}_m'^{(2)})^2 | -2:3_m, 2_m:0_p\rangle \\ & - \beta''/12 \sum_{m\neq m'} (h\nu_m + h\nu_{m'})^{-1}\mathfrak{S}_m'^{(2)}\mathfrak{S}_{m'}'^{(2)} | -2:2_m, 1_m; 2_{m'}, 1_{m'}:0_p\rangle \\ & - \beta''/6\sqrt{2}\sum_n (2h\nu_n)^{-1}(\mathfrak{S}_n'^{(-1)})^2 | -2:3_n, -2_n:0_p\rangle \\ & - \beta''/12\sum_{n\neq n'} (h\nu_n + h\nu_{n'})^{-1}\mathfrak{S}_n'^{(-1)}\mathfrak{S}_{n'}'^{(-1)} | -2:2_n, -1_n; 2_{n'}, -1_{n'}:0_p\rangle \\ & - \beta''/12\sum_{n,q} (h\nu_n + h\nu_q)^{-1}\mathfrak{S}_n'^{(1)}\mathfrak{S}_q'^{(3)} | -2:2_n, 1_n:1_q\rangle \\ & - \beta''/12\sum_{p,t} (h\nu_p + h\nu_t)^{-1}\mathfrak{S}_p'^{(0)}\mathfrak{S}_t'^{(-2)} | -2:2_t, -1_t:1_p\rangle. \end{aligned} \tag{2.51}$$

Table I gives the coefficients of all of the first-order singly excited vibronic states, and also illustrative coefficients for some of the more important doubly excited vibronic states. It is clear that the linear terms in the displacements couple the 1595.3 and 605.6 cm^{-1} E_{2g} vibrations vary strongly with the electronic motion—so strongly in fact that the first-order theory can only be at best a crude approximation. The 1178.0 E_{2g} vibration is somewhat less strongly coupled, and the two quantum mixing is indeed quite weak. Now one of the essential points of our study of the dynamical Jahn-Teller effect is to show that the lowest energy vibronic state is doubly degenerate; this plays a crucial role in the subsequent discussion of hyperfine interactions. To show that the ground vibronic state is doubly degenerate, we first carry out a calculation of the energy of the state $F_0^{(\pm 2)}$, and then of the state $F_0^{(0)}$. Since *two* vibrations are strongly coupled to the electronic motion, both of these vibrations are included in the calculations, which are described below. The inclusion of the third moderately strongly interacting vibration (1178.0 cm^{-1}, E_{2g}) is not expected to affect our conclusions regarding the *relative* energies of $F_0^{(\pm 2)}$ and $F_0^{(0)}$.

TABLE I. First-order theory.

Vibronic class	Vibrational excitation	Matrix element	First-order coefficient
$\|-2:2, -1:0\rangle$	1×1595.3 (E_{2g})	2.37*a*	−0.62
	1×605.6 (E_{2g})	2.37*a*	−0.67
	1×3046.8 (E_{2g})	2.37*a*	+0.032
	1×1178.0 (E_{2g})	2.37*a*	+0.24
$\|-2:3, -2:0\rangle$	2×1033 (E_{1u})	2.37*d*	−0.0092
$\|-2:3, 2:0\rangle$	2×1599.3 (E_{2g})	2.37*b*	−0.013
$\|-2:2, -1:1\rangle$	991.6 (A_{1g})+1595 (E_{2g})	2.37*g*	−0.018
$\|-2:2, 1:1\rangle$	1033 (E_{1u})+1648 (B_{2u})	2.37*f*	−0.015

Let v_1, l_1 be the quantum numbers of the 1595.3 cm^{-1} E_{2g} vibration, and v_2, l_2 be the quantum numbers of the 605.6 cm^{-1} E_{2g} vibration. To obtain an estimate of the vibronic function $F_0^{(2)}$ and its energy, one first considers all possible vibronic states that can contribute to $F_0^{(2)}$. These are restricted as follows.

$$\mathbf{P}_6 |\pm 2:v_1, l_1; v_2, l_2:0\rangle = \gamma^C |\pm 2:v_1, l_1; v_2, l_2; 0\rangle \tag{2.52}$$

$$\begin{aligned} C &= \pm 2 + 2l_1 + 2l_2 \\ &= 2, -4 \pmod 6. \end{aligned} \tag{2.53}$$

Secular equations that included *all* zero-order vibronic functions corresponding to $v_1+v_2=2-7$ were set up and solved. The nondiagonal matrix elements contained linear terms only. This secular determinant was 34×34 and was more than sufficiently large for adequate convergence for the lowest state. The corresponding vibronic energy $E_0^{(\pm 2)}$ is 1497 cm^{-1} (compared to the zero-order energy, $v_1+v_2=2201$ cm^{-1}). The *larger terms* of the vibronic function for this state are given in Table II.

A similar calculation—again including only terms linear in the displacements—was made for the lowest

TABLE II. Lowest energy doubly degenerate vibronic eigenfunction, $F_0^{(2)}$.

Quantum numbers $\mid m{:}v_1, l_1, ; v_2, l_2\rangle$					Coefficients[a]
m	v_1	l_1	v_2	l_2	
2	1	0	1	0	0.786
−2	2	−1	1	0	−0.401
−2	1	0	2	−1	−0.394
2	3	0	1	0	0.118
2	2	−1	2	1	0.074
2	2	1	2	−1	0.157
2	1	0	3	0	0.116
−2	4	−1	1	0	−0.032
−2	3	−2	2	1	−0.024
−2	2	−1	3	0	−0.046
−2	3	0	2	−1	−0.050
−2	2	1	3	−2	−0.030
−2	1	0	4	−1	−0.032

[a] All coefficients of higher vibronic states are less than ±0.015.

energy totally symmetric vibronic state. In this case, all zero-order vibronic states were included in the calculation for which

$$C=\pm 2+2l_1+2l_2$$
$$=0 \qquad (\text{mod. } 6). \tag{2.54}$$

The lowest vibronic energy was found to be 1967 cm^{-1}, which is 470 cm^{-1} above the lowest doubly degenerate state. The larger terms of this non-degenerate vibronic eigenfunction are given in Table III. It is convenient to use a special symbol $f_0^{(0)}$ to represent this particular approximate totally symmetric vibronic function that is given in Table III.

It would appear to be clear from these calculations that the ground vibronic state of B^- is doubly degenerate. There is one possible flaw in this conclusion, however. Although the quadratic terms are shown in Table I to have very little effect on the lowest doubly degenerate vibronic state, this may not be so obvious for the nondegenerate vibronic state. The reader will note that the vibronic function $f_0^{(0)}$ given in Table III is *accidentally degenerate* with another vibronic function $f_0'^{(0)}$ that is obtained from $f_0^{(0)}$ by changing the signs of

TABLE III. The vibronic eigenfunction $f_0^{(0)}$.

Quantum number $\mid m{:}v_1, l_1; v_2, l_2{:}0\rangle$					Coefficient[a]
m	v_1	l_1	v_2	l_2	
−2	2	1	1	0	0.128
−2	1	0	2	1	0.750
2	3	2	1	0	−0.058
2	2	1	2	1	−0.382
2	1	0	3	2	−0.446
−2	4	1	1	0	0.015
−2	3	2	2	−1	0.009
−2	3	0	2	1	0.112
−2	2	1	3	0	0.070
−2	2	−1	3	2	0.171
−2	1	0	4	1	0.124

[a] All coefficients of higher vibronic states are less than ±0.05.

the quantum numbers m, l_1, l_2. This accidental degeneracy is removed by the quadratic terms in Eq. (2.36). *The lowest energy totally symmetric state* $F_0^{(0)}$ *is depressed in energy* relative to that of $f_0^{(0)}$ and $f_0'^{(0)}$ by the matrix element

$$\Delta E=|\,(f_0'^{(0)} \mid \mathfrak{h} \mid f_0^{(0)})\,|. \tag{2.55}$$

Now let us represent the expansion coefficients in Table III as follows

$$f_0^{(0)}=\sum_{mv_1l_1v_2l_2} a_{mv_1l_1v_2l_2} \mid m{:}v_1, l_1, v_2, l_2\rangle. \tag{2.56}$$

Thus,

$$\Delta E=\sum_{\substack{mv_1l_1v_2l_2\\ m'v_1'l_1'v_2'l_2'}} a^*_{m'v_1'l_1'v_2'l_2'}a_{mv_1l_1v_2l_2}$$
$$\times\langle m'{:}v_1', l_1'; v_2', l_2' \mid \mathfrak{h} \mid m{:}v_1, l_1, v_2, l_2\rangle. \tag{2.57}$$

One can show that only terms for which $m=-m'$ contribute to this summation, and that the summation can be simplified as follows.

$$\Delta E=2\sum a^*_{-2,v_1'l_1'v_2'l_2'}a_{2v_1l_1v_2l_2}$$
$$\times\langle -2{:}v_1', l_1'; v_2', l_2' \mid \mathfrak{h} \mid 2{:}v_1, l_1; v_2, l_2\rangle. \tag{2.58}$$

As only two doubly degenerate vibrations are involved, with normal coordinates $Q_1^{(\pm 2)}$ and $Q_2^{(\pm 2)}$, this is, from (2.37b) and (2.37c)

$$\Delta E=\tfrac{1}{3}\beta''(\mathfrak{S}_1'^{(2)})^2\sum a^*_{-2v_1'l_1'v_2l_2}a_{2v_1l_1v_2l_2}(v_1'l_1' \mid (Q_1^{(2)})^2 \mid v_1l_1)$$
$$+\tfrac{2}{3}\beta''\mathfrak{S}_1'^{(2)}\mathfrak{S}_2'^{(2)}\sum a^*_{-2v_1'l_1'v_2'l_2'}a_{2v_1l_1v_2l_2}(v_1'l_1' \mid Q_1^{(2)} \mid v_1l_1)(v_2'l_2' \mid Q_2^{(2)} \mid v_2l_2)$$
$$+\tfrac{1}{3}\beta''(\mathfrak{S}_2'^{(2)})^2\sum a^*_{-2v_1l_1v_2'l_2'}a_{2v_1l_1v_2l_2}(v_2'l_2' \mid (Q_2^{(2)})^2 \mid v_2l_2). \tag{2.59}$$

The matrix elements that appear in these expansions are readily obtained from Eqs. (2.39)–(2.48). These matrix elements plus the expansion coefficients of Table III yield $\Delta E=15$–20 cm^{-1}, the upper limit being an estimate of the maximum possible contribution of a large number of small terms. It is quite possible that higher totally symmetric vibronic states will be split by even larger amounts, perhaps as much as 100 cm^{-1}.

Even so, we can be sure that the ground vibronic state is doubly degenerate—and not nondegenerate or triply degenerate—within the framework of the present theory, and with the assumed values of β' and β''.

It is sometimes convenient to write the wave function given in Table II as follows.

$$F_0^{(2)} = \{\omega^{(2)} J + \omega^{(-2)} K\}\psi(\mathbf{x}, \mathbf{X}), \tag{2.60}$$

when J and K are nuclear vibrational functions that are orthogonal,

$$(J \mid K) = 0, \tag{2.61}$$

and normalized in the sense that

$$(J \mid J) + (K \mid K) = 1. \tag{2.62}$$

If we let $\mathfrak{L}_0$ be the expectation value for the π-electron orbital angular momentum around the ring when the nuclei are constrained to have D_{6h} symmetry

$$\mathfrak{L}_0 = (\omega^{(2)} \mid \mathbf{L}_z \mid \omega^{(2)}), \tag{2.63}$$

then the vibronic coupling reduces the expectation value for this orbital angular momentum by the factor $(J \mid J) - (K \mid K)$, that is,

$$\mathfrak{L} = \mathfrak{L}_0[(J \mid J) - (K \mid K)], \tag{2.64}$$

and the reduction factor is 0.30 from the results given in Table II.

The reader will doubtless have noted by this time that nowhere in the above work have we considered matrix elements that are diagonal in the electronic components of the zero-order functions.

$$\langle 2{:}v_k', l_k'{:}n_q' \mid \mathfrak{h} \mid 2{:}v_k, l_k{:}n_q \rangle. \tag{2.65}$$

The rationale behind this omission is given below.

The nuclear diagonal matrix elements of (2.65) corresponding to $v_k' = v_k$, $l_k' = l_k$, $n_q' = n_q$ lead to first-order changes in vibrational frequencies of the benzene ring, and the nuclear nondiagonal matrix elements ($v_k' \neq v_k$, etc.) lead to changes in the vibrational frequencies as well as average internuclear distances. Now these matrix elements are not small relative to those considered above in (2.22). However, we may reasonably expect that the *change* in the normal vibrational frequencies from those of neutral benzene that arise from the matrix elements (2.65) are small compared to the frequencies themselves. Moreover, we may also reasonably expect that the *nuclear vibrational* functions $\chi^0(v_k, l_k{:}n_q)$ that do diagonalize the matrix (2.65) will yield nondiagonal matrix elements of the type (2.22) that are very similar to those employed in the present work, i.e., those derived from neutral benzene vibrational functions. The only really troublesome effect of these neglected diagonal matrix elements as far as our Jahn-Teller calculation is concerned, is their influence on β' and β'' through their effect on the average internuclear distance. As indicated in the discussion following Eq. (2.29), an attempt has been made to take this indirect effect of the diagonal elements into account even though we are using the vibrational functions of the neutral benzene molecule in our calculation.

3. REMOVAL OF THE VIBRONIC DEGENERACY

The ground state vibronic degeneracy of the benzene negative ion discussed in the preceding section can be removed by a magnetic field, by spin-orbit interaction, possibly by coupling between vibration and rotation, and by interaction with a solvent when present. For the paramagnetic resonance experiments under consideration, the charged benzene negative ion is contained in a strongly polar solvent, and it is *almost* self-evident that the strongest interaction tending to remove the degeneracy is the solvent interaction. This is because the vibronic degeneracy is associated with a degeneracy in the charge distribution. A semiquantitative discussion follows.

Let $V = V(t)$ be the time-dependent potential field that acts on B^- due to the surrounding polar solvent molecules. This field is not expected to have perfect C_3 or C_6 symmetry, and thus the ground state vibronic degeneracy is removed. The magnitude of this splitting is probably 100–1000 cm^{-1} and is almost certainly large compared to the reciprocal of the correlation time that describes the oscillations of $V(t)$.

We therefore use the adiabatic approximation. Neglect, for a moment, the vibronic coupling, and suppose that at time $t = 0$, $V(0)$ has a twofold symmetry axis that coincides with one of the in-plane twofold symmetry axes of the benzene molecule. Then the degenerate perturbation theory leads to the two functions

$$\omega^{(a)} = \sqrt{2}^{-1}(\omega^{(2)} - \omega^{(-2)}), \tag{3.1}$$

$$\omega^{(b)} = \sqrt{2}^{-1}(\omega^{(2)} + \omega^{(-2)}), \tag{3.2}$$

for which the corresponding probability distributions of the odd electron are

$$p^{(a)} = \tfrac{1}{2}(\omega^{(-2)}\omega^{(2)} + \omega^{(2)}\omega^{(-2)}) - \tfrac{1}{2}(\omega^{(-2)}\omega^{(-2)} + \omega^{(2)}\omega^{(2)}), \tag{3.3}$$

$$p^{(b)} = \tfrac{1}{2}(\omega^{(-2)}\omega^{(2)} + \omega^{(2)}\omega^{(-2)}) + \tfrac{1}{2}(\omega^{(-2)}\omega^{(-2)} + \omega^{(2)}\omega^{(2)}). \tag{3.4}$$

The second terms in parentheses in Eqs. (3.3) and (3.4) produce oscillating charge distributions around the ring that modulate the uniform charge distribution described by the first terms. In the two cases, the charges centered on atoms j are

$$p_j^{(a)} = \tfrac{1}{6}[1 - \cos(2\pi j/3)], \tag{3.5}$$

$$p_j^{(b)} = \tfrac{1}{6}[1 + \cos(2\pi j/3)]. \tag{3.6}$$

These charge distributions are sketched below.

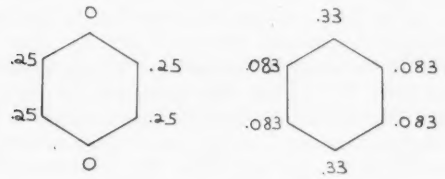

Ia Ib

We assume charge distribution Ia to represent the lower energy state, corresponding to the attack of a positive ion (or the positive end of a dipole) *between* two adjacent carbon atoms.

If we now use as zero-order functions for the degenerate perturbation theory those functions derived in the preceding section for the degenerate ground vibronic state of B^-, then the linear combinations corresponding to Eqs. (3.1) and (3.2) are

$$F_0^{(a)}=\sqrt{2}^{-1}(F_0^{(2)}-F_0^{(-2)}), \tag{3.7}$$

$$F_0^{(b)}=\sqrt{2}^{-1}(F_0^{(2)}+F_0^{(-2)}). \tag{3.8}$$

The corresponding odd-electron probability distributions are

$$p^{(a)}=\tfrac{1}{2}(\omega^{(2)}\omega^{(-2)}+\omega^{(-2)}\omega^{(2)}) -\tfrac{1}{2}[\omega^{(2)}\omega^{(2)}(J^*\mid J)+\omega^{(-2)}\omega^{(-2)}(J\mid J^*)], \tag{3.9}$$

$$p^{(b)}=\tfrac{1}{2}(\omega^{(2)}\omega^{(-2)}+\omega^{(-2)}\omega^{(2)}) +\tfrac{1}{2}[\omega^{(2)}\omega^{(2)}(J^*\mid J)+\omega^{(-2)}\omega^{(-2)}(J\mid J^*)]. \tag{3.10}$$

The effect of the vibronic coupling is to smooth out the probability density for the odd electron; a sketch of this distribution based on the function in Table II and Eqs. (3.9) and (3.10) is given below.

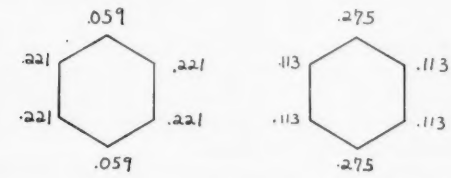

IIa IIb

The vibronic coupling evidently has a larger relative effect on the orbital angular momentum around the ring than it does on the charge distribution. Charge distributions Ia and Ib are appropriate to solute-solvent interactions that are large compared to the vibronic coupling ($\sim$700 cm^{-1}), whereas the charge distribution IIa and IIb are appropriate to solute-solvent interactions that are weak relative to the vibronic coupling. However, these charge distributions [and the associated spin distribution $\boldsymbol{\rho}(\mathbf{r})$] are so nearly equal to one another that it will be of little importance to distinguish between them in the subsequent discussions of hyperfine interactions. Conversely, the solute-solvent interaction is relatively inefficient in breaking down the vibronic coupling. That is, the solute-solvent binding would have to be improbably large, that is of the order of $\sim$7000 cm^{-1} or $\sim$1 ev, if the *gain* in electrostatic binding energy in going from charge distribution IIa to Ia were to be *comparable* to the loss of the vibronic coupling energy ($\sim$700 cm^{-1}).

4. THE SPIN-DENSITY FLUCTUATIONS

Let $\rho(\mathbf{r};\ t)$ be the time-dependent normalized π-electron spin distribution function[15] for B^-. That is, $\hbar\mathbf{s}\rho(\mathbf{r};\ t)$ is the density of electron spin angular momentum (erg-sec/cm^3) at the position $\mathbf{r}$ and at the time t. This time dependence can be expressed by an atomic orbital spin-density matrix $\rho_{\lambda\mu}(t)$,[15]

$$\rho(\mathbf{r};t)=\sum_{\lambda\mu}\rho_{\lambda\mu}(t)\pi_\mu\pi_\lambda. \tag{4.1}$$

Here $\pi_\mu(\mathbf{r})$ and $\pi_\lambda(\mathbf{r})$ are atomic π orbitals centered on carbon atoms μ and λ. In the one-electron approximation employed here, the spin-density distribution function $\rho(\mathbf{r};\ t)$ is numerically equal to the probability distribution $p(\mathbf{r};\ t)$ for the odd electron.

This time dependence can originate in various ways, and it is helpful to enumerate these possibilities by a formal albeit qualitative development.

Let B^- be acted on by $V(t)$, and let the time-dependent wave function $\Phi(t)$ of B^- be expanded in the complete set of vibronic functions $F_r^{(m)}$ that are eigenfunctions of $\mathbf{P}_6$.

$$\Phi(t)=\sum_{r,m}C_r^{(m)}(t)\,F_r^{(m)}\exp(-i\omega_r t). \tag{4.2}$$

This expansion is normalized:

$$\sum_{r,m}|\,C_r^{(m)}\,|^2=1. \tag{4.3}$$

Within the framework of the one-electron approximation that we are using for the odd electron, the time-dependent spin distribution is simply

$$\rho(\mathbf{r};t)=\sum_{r',m';r,m}C_{r'}^{(m')*}(t)\,C_r^{(m)}(t)\,\langle F_{r'}^{(m')}\,||\,F_r^{(m)}\rangle \times\exp[-i(\omega_{r'}-\omega_r)t], \tag{4.4}$$

where the symbol $\langle\ ||\ \rangle$ designates an integration over all space and spin coordinates for all the electrons and nuclei, except for the space coordinates of the odd electron. It is convenient to break up the spin distribution $\rho(\mathbf{r};\ t)$ as follows.

$$\rho(\mathbf{r};t)=\rho_0(\mathbf{r})+\Gamma_a(\mathbf{r};t)+\Gamma_b(\mathbf{r};t). \tag{4.5}$$

Here $\rho_0(\mathbf{r})$ is a uniform spin distribution on the carbon atoms, and this term arises from the diagonal elements

[15] H. M. McConnell, J. Chem. Phys. **28**, 1188 (1958).

in Eq. (4.4); this follows from Eq. (4.3) and the fact that

$$\langle F_r^{(m)} \,||\, F_r^{(m)} \rangle = \rho_0(\mathbf{r}). \tag{4.6}$$

The quantity $\Gamma_a(\mathbf{r};t)$ is defined as a spin density distribution such that $\rho_0(\mathbf{r};t)+\Gamma_a(\mathbf{r};t)$ identical to that sketched in IIa, except that the in-plane twofold symmetry axis of this spin distribution has a direction so that the corresponding charge distribution interacts most favorably with the polar solvent. That is, the spin and charge orientation is such that, at any time t,

$$\int V(t)\,\Gamma_a(\mathbf{r};t)\,dv = \text{a minimum}.$$

The quantity $\Gamma_b(\mathbf{r};t)$ is taken to be the difference between $\rho(\mathbf{r};t)$ and the sum of $\rho_0(\mathbf{r})$ and $\Gamma_a(\mathbf{r};t)$. In the present work, we assume the electrostatic interaction between the polar solvent and B^- to be sufficiently strong that the average *magnitude* of $\Gamma_b(\mathbf{r};t)$ is small relative to $\Gamma_a(\mathbf{r};t)$. Quantitatively, this conclusion is only valid to the extent that (a) the (solvent)—(B^-) interaction is large compared to kT, in the sense that charge distribution IIa is significantly favored relative to IIb, and (b) the excitation energy to the lowest excited totally symmetric vibronic state is significantly higher than kT. When $\Gamma_b(\mathbf{r};t)$ is neglected, we may write the following formula for the time-dependent diagonal elements of the spin-density matrix.

$$\rho_{\lambda\lambda}(t) = \tfrac{1}{6}[1-(J^* \mid J)\cos(2\pi/3)(\lambda - s)]. \tag{4.7}$$

Here s is a function of the time, $s=s(t)$, and takes on the values 0, 1, 2 in a more or less random fashion depending on the details of the mechanism involved in the switching of the spin distribution. There are a number of conceivable mechanisms for this switching process, and we illustrate one below.

Suppose that B^- undergoes f "collisions" per sec, and that, of these, a fraction $\exp(-\Delta E^{\ddagger}/kT)$ puts B^- in the lowest energy totally symmetric vibronic state $F_0^{(0)}$, which has uniform spin distribution $\rho_0(\mathbf{r})$. From this state the molecule will quickly fall back to the ground vibronic state, but with a random spin distribution, i.e., $s=0$, 1 or 2. The activation energy for this process is 470 cm^{-1}, the molecular vibronic excitation energy plus possibly an equal contribution due to the change in the solvent interaction energy. Thus we expect the correlation time for the spin switching to be of the order of magnitude

$$\tau^{-1} \sim f \exp(-\Delta E^{\ddagger}/kT). \tag{4.8}$$

If, say, $f \sim 10^{11}$ sec^{-1} and $\Delta E^{\ddagger} \sim 940$ cm^{-1}, then one obtains a correlation time τ of the order of 10^{-9} sec, equal to that deduced later in this paper on the basis of the hyperfine linewidths. Collisional excitations to other charge and spin distributions, such as IIb, are of course possible.

5. PROTON HYPERFINE INTERACTIONS

The unusually broad proton hyperfine structure reported by Townsend and Weissman[10] in the high-field paramagnetic resonance spectra of B^-, Tp^-, and C^- clearly do not arise from anisotropic proton hyperfine interactions. That is, any time dependence of the spin density distribution is merely superimposed on a tumbling motion that is already fast enough to average effectively the dipolar linewidths. The unusually large linewidths may arise through the time-dependent variations of the isotropic hyperfine interactions that are discussed below, or through spin-orbit induced paramagnetic relaxation that will be discussed in some detail elsewhere.[16]

The time-dependent isotropic hyperfine interaction in B^- is given by the spin Hamiltonian

$$\mathcal{H} = \sum_{\lambda=1}^{\lambda=6} a_\lambda \mathbf{S}\cdot\mathbf{I}_\lambda, \tag{5.1}$$

where the time-dependent isotropic coupling constant $a_\lambda = a_\lambda(t)$ is given, to a good approximation, by the equation,[15]

$$a_\lambda(t) = Q\rho_{\lambda\lambda}(t). \tag{5.2}$$

Here Q is a previously discussed quantity and is equal to -63 Mc.[15] Consider the paramagnetic resonance spectrum that is expected when we take into account the terms in Eq. (5.1) arising from the components of $\mathbf{S}$ and $\mathbf{I}_\lambda$ in the direction of the applied field, S_z, $I_{\lambda z}$.

$$\mathcal{H}_z = \tfrac{1}{6}QS_z\sum_{\lambda=1}^{\lambda=6}[1-\cos(2\pi/3)(\lambda - s(t))]I_{\lambda z}. \tag{5.3}$$

For simplicity, the effect of the vibronic coupling is omitted here; this amounts to replacing $(J^* \mid J) = 0.65$ by one as a factor of the cosine term in Eq. (5.3). The possible values of the individual $I_{\lambda z}$ in Eq. (5.3) are $+\frac{1}{2}$, and there are 2^6 possible combinations of these spin eigenvalues. Now single products of six nuclear spin functions (e.g., $\alpha\alpha\beta\alpha\beta\alpha$) are eigenfunctions of $\mathcal{H}_z$. Therefore, the totality of eigenvalues of $\mathcal{H}_z$ to be considered are those that arise from these 2^6 spin functions and the various possible values of s. The problem can be formulated simply as follows.

Let $s(t)$ have a fixed value, say, $s=0$. In this case the spin distribution is fixed, as in Ia, and the hyperfine structure of the paramagnetic resonance spectrum is a quintet with the normal binomial distribution 1:4:6:4:1. A spectrum of this type is illustrated in the upper portion of Fig. 1. The numbers beside each vertical hyperfine multiplet indicate the *number* of nuclear spin states that contribute to each multiplet, including the two noninteracting protons. In the lower half of Fig. 1, this quintet has been decomposed into contributions that arise from the various nuclear spin arrangements with different F_z values, where F_z is the

[16] H. M. McConnell (following paper).

component of the total proton nuclear spin in the field direction.

$$F_z=\sum_\lambda I_{\lambda z}. \tag{5.4}$$

It should be noted that, in general, *each member* of the hyperfine quintet at the top of Fig. 1 receives a contribution from arrangements of proton spins with different F_z values.

Now consider what happens to the hyperfine spectrum when s is not held fixed but is allowed to vary in a random manner so that the time-dependent cosine term in Eq. (5.3) fluctuates with a correlation time τ. As a very reasonable first approximation we may say that the switching of the electron spin distribution produces no nuclear spin relaxation, so that F_z is unaffected. Thus, the switching spin distribution has no effect on the single resonance line that arises from the $F_z=3$ state. When $F_z=2$, the switching spin distribution causes the spectrum to change back and forth between the *two* multiplets sketched in the lower portion of Fig. 1, as indicated schematically by the arrows. When the correlation time τ is large, $\tau\gg 1/2\pi\Delta\nu$, where $\Delta\nu$ is the hyperfine splitting (15.7 Mc), then these hyperfine multiplets are resolved; when $\tau\ll/12\pi\Delta\nu$ the two multiplets merge into the single vertical dotted line indicated in Fig. 1. Spectra in intermediate cases are readily estimated by introducing the electron spin switching directly into the Bloch equations for the electron spin magnetization, in a manner similar to that used to calculate the effects of chemical exchange on nuclear magnetic resonance spectra.[17] Similarly, rapid switching averages the three lines for $F_z=1$ in the lower part of Fig. 1 to a single line. The net averaged hyperfine spectrum in the rapid switching case is of course a seven-line spectrum with splittings of $1/6\,|\,Q\,|$ and a binomial distribution of

$$1:6:15:20:15:6:1.$$

The spectra reported by Townsend and Weissman clearly belong to the rapid switching case. The linewidths $\Delta\nu_h$ for the individual components of the hyperfine septet are of the order of 1–3 Mc. *If this residual linewidth* is due to the spin switching effect, then we expect the switching frequency to be *of the order of magnitude*

$$\Delta\nu_s\sim(1/6Q)^2/\Delta\nu_h$$
$$\sim 100\text{ Mc}. \tag{5.5}$$

The corresponding correlation time τ is $\sim 10^{-9}$ sec. This frequency, if it does refer to solute-solvent interaction, is of course very low. This suggests that the (B^-+ion), or (B^-+dipole) pair may tumble together in the liquid state, as a semi-stable unit.

Since Townsend and Weissman have reported enhanced spin-lattice relaxation in the C^- ion, it is of

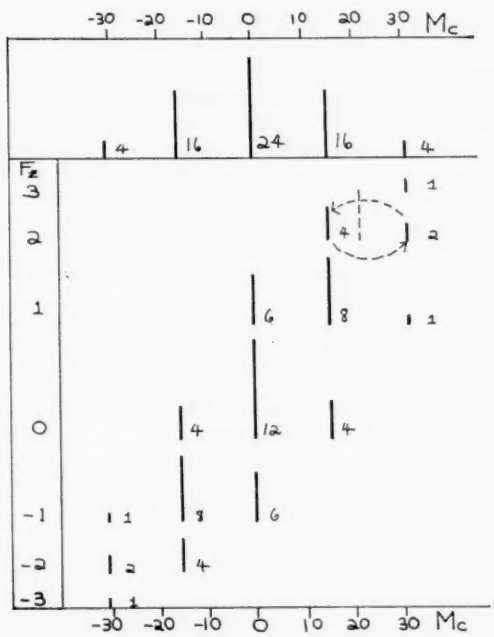

FIG. 1. Hyperfine structure of the benzene negative ion when the spin density on each of four carbon atoms is 0.25. The effect of solvent induced spin switching is indicated schematically by the dotted arrows for the total nuclear spin $F_z=2$ state.

interest to inquire as to possible contributions of the fluctuating isotropic interaction to the spin-lattice relaxation. The pertinent terms in Eq. (5.1) are those that involve

$$\tfrac{1}{2}a_\lambda(S_+I_{\lambda-}+S_-I_{\lambda+}), \tag{5.6}$$

since these give rise to a simultaneous flip of the electron spin and a proton spin. In the limit of fast switching, we assume that the net spin-lattice relaxation rate is simply six times the relaxation rate arising from a fluctuating hyperfine between the electron spin and a single proton. A well-known calculation[18] then leads to the following contribution to the spin-lattice relaxation rate.

$$1/T_1'=(\pi^2/3)Q^2[\tau/(1+\omega^2\tau^2)]. \tag{5.7}$$

Here ω is the difference between the electron and proton resonance frequency (radians/sec). From the present calculation, we see that if the previously discussed low-frequency switching ($1/2\pi\tau=\Delta\nu_s=100$ Mc) is indeed responsible for the observed linewidths, then this switching *cannot* account for an enhanced spin-lattice relaxation since for this value of τ, Eq. (5.7) leads to a $T_1'\sim 10^{-3}$ sec. Since typical paramagnetic

[17] A convenient method for calculating these spectra is described by H. M. McConnell, J. Chem. Phys. **28**, 430 (1958).

[18] See J. A. Pople, W. G. Schneider, and H. J. Bernstein, *High Resolution Nuclear Magnetic Resonance* (McGraw-Hill Book Company, Inc., New York, 1959), p. 486.

relaxation times in most radicals[19] are $\sim 10^{-6}$ sec, this mechanism makes no significant contribution. This conclusion can be stated in a more general fashion. If the fluctuating part of the isotropic hyperfine interaction is described by a single correlation time τ, then the corresponding white spectrum has insufficient power to produce significant spin-lattice relaxation at the frequency ω, and also a simultaneous T_2 broadening due to the Fourier components of $a_\lambda(t)$ near zero frequency. The vibronic coupling, omitted in this section, only further reduces the integrated power in this white spectrum. The term $\Gamma_b(\mathbf{r}; t)$ that we have dropped, could easily have a Fourier spectrum quite different from $\Gamma_a(\mathbf{r}, t)$, but a detailed examination of Eq. (4.4) certainly suggests that this spectrum should not be particularly strong near the frequency ω.

6. REMARKS

The calculations given in Secs. 2–5 of the present paper have dealt almost exclusively with the benzene negative ion. It is very likely that the conclusions of Sec. 2 hold for all cyclic polyene anions (*unless* out-of-plane deformations become important, which may be the case for $C_8H_8^-$), and very probably also the anions of triphenylene and coronene.[20] That is, the vibronic ground states of these ions are doubly degenerate, and, as shown in Sec. 3 for B^-, this degeneracy is removed most effectively by interactions with a polar solvent. This will always lead to a broadening of the paramagnetic resonance if the solvent induced switching of the spin distribution has a correlation time that is of the order of magnitude or more than the reciprocal of the proton hyperfine splittings. The correlation time τ estimated on the basis of the discussion of Sec. 5 is 10^{-9} sec. While we do believe that this is a reasonable correlation time for the switching process under consideration, we hasten to point out that it is conceivable that the correlation time for the spin distribution is really much shorter (it could not be longer in view of the observed spectra). In this case we would be forced to look elsewhere for a relaxation mechanism. The only alternative candidate is the spin-orbit interaction, which is expected to be especially large in vibronically degenerate states. The only suspicion we have that the spin-orbit interactions might be important is that, as pointed out in Sec. 5, the fluctuating isotropic hyperfine interaction with a correlation time of 10^{-9} sec cannot account for the enhanced spin-lattice relaxation reported by Townsend and Weissman for C^-. Unfortunately, it is quite difficult to calculate the spin-orbit interaction theoretically, and it is not known experimentally. This problem will be discussed elsewhere.[16] It is quite possible—in fact we think most probable—that the enhanced spin-lattice relaxation is indeed due to the especially large spin-orbit interaction characteristic of a degenerate or near-degenerate state, but that the enhanced linewidths are due to the fluctuating isotropic hyperfine interaction. Clearly, most of these remaining points of uncertainty can be resolved by experiment. Experiments on perdeutero anions, as well as quantitative T_1 measurements, might convincingly demonstrate the foregoing suggestions.

ACKNOWLEDGMENTS

We are greatly indebted to L. F. Shampine and S. H. Caine for coding and carrying out the machine computations used for the dynamical Jahn-Teller problem in the benzene negative ion. Dr. A. D. Liehr made a number of helpful comments on the manuscript.

[19] M. J. Stephen and G. K. Fraenkel, J. Chem. Phys. **32**, 1435 (1960), J. W. H. Schreurs, G. E. Blomgren, and G. K. Fraenkel, *ibid.* **32**, 1861 (1960).

[20] Townsend and Weissman[16] have pointed out that the enhanced linewidths in B^- *may* be due to electron exchange with neutral B molecules.

THE JOURNAL OF CHEMICAL PHYSICS VOLUME 34, NUMBER 1 JANUARY, 1961

Spin-Orbit Coupling in Orbitally Degenerate States of Aromatic Ions*

HARDEN M. MCCONNELL†

Gates and Crellin Laboratories of Chemistry,‡ California Institute of Technology, Pasadena, California

(Received August 11, 1960)

It is shown that in the orbitally degenerate ground state of the benzene negative ion there is a first-order electron spin-orbit interaction associated with the electronic orbital motion around the ring. This first-order interaction may be as large as a few cm^{-1} and can give rise to enhanced electron spin-lattice relaxation in solution even though most of the time the electronic orbital motion is strongly quenched by electrostatic interaction with the solvent.

INTRODUCTION

RECENTLY Townsend and Weissman[1] have noted that the proton hyperfine structure that is observed in the paramagnetic resonance spectra of the negative ions of benzene (B^-), triphenylene (T_p^-), and coronene (C^-), is unusually broad when compared with the hyperfine structure observed in less symmetrical but otherwise similar negative ion radicals. Also, the linewidths in the hyperfine structure of the negative ion of cyclooctatetraene are rather large.[2] Townsend and Weissman[1] suggested that the enhanced linewidths in these symmetrical ion radicals are due to Jahn-Teller distortions that modulate the spin distribution, and thereby modulate the proton hyperfine interactions. In another paper[3] this problem has been examined in considerable detail for the particular case of B^-. This work shows that the ground vibronic state of B^- (and very probably C^-, T_p^- and O^-) remains twofold degenerate even when allowance is made for the coupling of electronic and nuclear motions (dynamical Jahn-Teller effect). Time-dependent solute-solvent interactions remove this degeneracy and create a fluctuating spin distribution and hyperfine interaction.[3] A fluctuating spin distribution with a correlation time of 10^{-9} sec can account for the observed enhanced linewidths for B^-. However, Townsend and Weissman[1] have made the very important observation that the rate of spin-lattice relaxation in T_p^- is significantly higher than in an otherwise similar but less symmetrical ion radical. Detailed calculations[3] show that the hyperfine interactions very probably cannot account for this enhanced spin-lattice relaxation. It was therefore suggested[3] that spin-orbit effects might be responsible for the relaxation.

The only apparent reason that a symmetrical ion radical of the type under consideration might have a larger spin-orbit interaction than a less symmetrical ion, is the possibility of the interaction between the spin and the π-electronic angular momentum around the ring. At first glance even this does not appear as a very attractive possibility, for a combination of three reasons. In the first place, the orbital angular momentum is quenched by interaction with a polar solvent.[3] Secondly, even if the orbital angular momentum were not quenched, a number of theoretical calculations have argued that the spin-orbit interactions of electrons confined to π-molecular orbitals is indeed very small.[4,5] By small is meant small relative to the first-order spin-orbit coupling in atomic carbon, which is of the order of 28 cm^{-1}.[4] Finally, large spin-orbit effects in the symmetrical ion radicals might reasonably be expected to lead to g factors significantly different from 2.0023, and no such anomalous g factors have been reported for these ion radicals.[6] In private correspondence Weissman has indicated that the g factors for B^- and C^- are not outside the range 2.000–2.006. We know of no independent experimental evidence (phosphorescent lifetimes, intercombination selection rules, observed g factors) that would imply any of the foregoing arguments to be incorrect. In the present paper, however, we examine the seemingly remote possibility that there is a degree of error in each of the above three arguments, and under these circumstances the spin-orbit contribution to the spin-lattice relaxation does become readily understandable.

THE BENZENE NEGATIVE ION

Neglect for a moment the coupling of the electronic and nuclear angular momentum (dynamical Jahn-Teller effect). A correction for this effect is easily introduced as a last step in the present calculation. The simplest approximate Hamiltonian that one can

* Supported in part by the U. S. Public Health Service, by the Office of Ordnance Research, U. S. Army, and by the National Science Foundation.

† Alfred P. Sloan Fellow.

‡ Contribution No. 2617.

[1] M. G. Townsend and S. I. Weissman, J. Chem. Phys. **32**, 309 (1960).

[2] T. J. Katz and H. L. Strauss, J. Chem. Phys. **32**, 1873 (1960).

[3] H. M. McConnell and A. D. McLachlan, J. Chem. Phys. **34**, 1 (1961), preceding paper.

[4] D. S. McClure, J. Chem. Phys. **20**, 682 (1952).

[5] M. Mizushima and S. Koide, J. Chem. Phys. **20**, 765 (1952).

[6] An unusual g factor of 1.95 has however been reported for pentaphenylcyclopentadienyl. B. M. Kozyrev and S. G. Salikhov, Doklady Akad. Nauk S.S.S.R. **58**, 1023 (1947). This radical is expected to have an orbitally degenerate ground state under D_{5h} or C_5 symmetry. J. E. Wertz, C. F. Koelsch, and J. L. Vivo, J. Chem. Phys. **23**, 2194 (1955) report a g factor of 2.0025 for this radical.

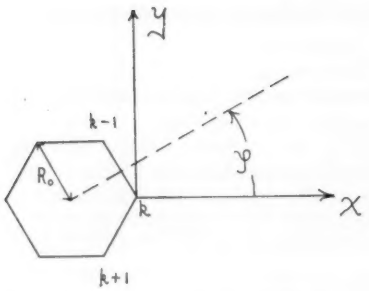

FIG. 1. Coordinate system used in calculating the electron spin-orbit interaction near nucleus k.

use to describe the spin-orbit interaction is[4]

$$H_s = 2\beta^2 \sum_i \sum_{k=1}^{k=6} Z_k r_{ik}^{-3} (\mathbf{r}_{ik} \times \mathbf{p}_i) \cdot \mathbf{S}_i. \qquad (1)$$

Here k labels the six carbon nuclei, Z_k is the effective nuclear charge, r_{ik} is the distance between electron i and nucleus k, $\hbar\mathbf{p}_i$ is the linear momentum of electron i, and $\hbar\mathbf{S}_i$ is the spin angular momentum of electron i. For simplicity we consider only the odd electron in the independent π-electron approximation (Hückel molecular orbital theory or otherwise), and only nucleus k, and only the components in Eq. (1) that are perpendicular to the molecular plane, since we are only concerned with the orbital motion around the ring. Equation (1) is then simplified as follows,

$$H_s = 12\beta^2 Z_k r_{ik}^{-3} l_{kz} S_z. \qquad (2)$$

Here $\hbar l_{kz}$ is the z component of the electronic orbital angular momentum of the odd electron about nucleus k, and $\hbar S_z$ is the z component of the spin of the odd electron. A factor of six has been introduced to account for the fact that there are six nuclei, each of which contributes additively to the spin-orbit interaction. The Hamiltonian in Eqs. (1) and (2) pictures the odd electron as seeing six simple Coulomb potentials $Z_k \mid e \mid r_{ik}^{-1}$ arranged in a hexagon, as far as the magnetic spin-orbit effects are concerned. In this approximation the results obtained with this Hamiltonian are the same as those that are obtained with the Dirac relativistic Hamiltonian employed by Mizushima and Koide.[5]

Conventional Hückel orbital theory for the π electrons of B^- puts these electrons into the molecular orbitals $\omega^{(m)}$,

$$\omega^{(m)} = 6^{-\frac{1}{2}} \sum_{j=0}^{j=5} \exp(im\phi_j)\pi_j. \qquad (3)$$

Here $m = 0, \pm 1, \pm 2, 3$; ϕ_j is the angular coordinate of carbon nucleus j in Fig. 1, and π_j is a $2p_z$ atomic orbital centered on nucleus j. In the ground-state electronic configuration six spin-paired electrons are placed in the three bonding orbitals for which $m = 0, \pm 1$, and the odd electron goes into one of the degenerate antibonding orbitals with $m = \pm 2$.

The reader will note that if (a) the atomic orbitals are real, all first-order one-center contributions to the π-electron spin-orbit interaction vanish since l_{kz} is a pure imaginary operator, and if (b) the π-atomic orbitals are cylindrically symmetric, then all two-center contributions to the spin-orbit interaction vanish. These are essentially the arguments put forth by McClure[4] to the effect that spin-orbit interactions of electrons confined to purely π orbitals are small, since only three center integrals remain, and these must indeed by very small. However, we note two points: the spin-orbit operator is *very* large near a *single* center k, and the assumptions contained in points (a) and (b) above are to some extent artificial. That is, it is important to consider plausible modifications of the molecular orbitals $\omega^{(m)}$ that can lead to one-center contributions to the spin-orbit interaction. An example is the Bloch-type orbital $\psi^{(m)}$,

$$\psi^{(m)} = 6^{-\frac{1}{2}} \sum_{j=0}^{j=5} \exp(im\phi)\pi_j. \qquad (4)$$

Here ϕ is an electronic coordinate, whereas ϕ_j in Eq. (3) is *not* an electronic coordinate. When the atomic orbitals π_j are allowed to be slightly deformed from cylindrical symmetry then, as we shall see below, the odd-electron molecular orbital $\psi^{(2)}$ does give rise to a one-center contribution to the spin-orbit interaction. Our motivation in using $\psi^{(2)}$ for this calculation is apparent: Eq. (4) is not a perfect approximation to the independent π-electron Hartree-Fock function, but neither is Eq. (3), and Eq. (4) must to some extent represent a one-center property of the exact Hartree-Fock function that Eq. (3) fails to completely to do.

The Cartesian axis system x, y, z has its origin at nucleus k and the orientation sketched in Fig. 1. Let $\hbar L_z$ be the operator for the z component of the odd π-electron angular momentum about the center of the benzene ring,

$$L_z = (x + R_0)p_y - yp_x, \qquad (5)$$

where R_0 is the distance from the center of the ring to atom k,

$$L_z = R_0 p_y + l_{kz}. \qquad (6)$$

Thus,

$$H_s = 12\beta^2 Z_k S_z r_k^{-3} [L_z + iR_0(\partial/\partial y)]. \qquad (7)$$

The expectation value of the spin-orbit interaction is

$$(\psi^{(m)} \mid H_s \mid \psi^{(m)}) = 12\beta^2 Z_k S_z \{m(\psi^{(0)} \mid r_k^{-3} \mid \psi^{(0)}) + iR_0[\psi^{(m)} \mid r_k^{-3}(\partial/\partial y) \mid \psi^{(m)}]\}. \qquad (8)$$

The second matrix element on the right-hand side of Eq. (8) is best handled by first expressing the factor $\exp(im\phi)$ in terms of x, y, and R_0, then carrying out the differentiation with respect to y, and then finally expressing the result in a power series of (x/R_0)

and (y/R_0). This leads to the result

$$(\psi^{(m)} \mid H_s \mid \psi^{(m)})$$

$$=12\beta^2 mZ_k S_z \int \mid \psi^{(0)} \mid^2 r_k^{-3} \left\{ \frac{x}{R_0} + \frac{y^2-x^2}{R_0^2} + \cdots \right\} dv. \quad (9)$$

When only the one-center integral and the linear contribution are retained, we have simply

$$(\psi^{(m)} \mid H_s \mid \psi^{(m)}) = 2\beta^2 mZ_k R_0^{-1} S_z (\pi_k \mid x r_k^{-3} \mid \pi_k). \quad (10)$$

Here the required asymmetry in the atomic π-orbital distribution is apparent. Now this asymmetry is probably realized by a slight bending of the $p\pi$ atomic orbital lobes either towards or away from the center of the benzene ring. This is achieved if the π_k orbital has a small amount of $3d$ character of the proper symmetry. A suitable orbital is a $3d_{xz}$ orbital. That is, let us write the π_k orbital as

$$\pi_k = p_k + \lambda d_k, \quad (11)$$

where d_k is this $3d_{xz}$ orbital. We shall later assume that this π orbital has $\sim 1\%$ $3d$ character; that is, $\lambda \sim \pm 0.1$. Thus,

$$(\psi^{(m)} \mid H_s \mid \psi^{(m)}) = 4\beta^2 m\lambda R_0^{-1} Z_k S_z (p_k \mid x r_k^{-3} \mid d_k)$$

$$= (4)(5^{-\frac{1}{2}}) \langle r^{-2} \rangle_{pd} \beta^2 \lambda R_0^{-1} Z_k m S_z. \quad (12)$$

Here

$$\langle r^{-2} \rangle_{pd} = (R_p(r) \mid r_k^{-2} \mid R_d(r)) \quad (13)$$

and $R_p(r)$ and $R_d(r)$ are the normalized radial functions of the p and d orbitals. If we write a spin Hamiltonian $\mathfrak{H}$ for the spin-orbit interaction,

$$\mathfrak{H} = h\Lambda L_z S_z, \quad (14)$$

then the coupling parameter Λ is

$$\Lambda = (4)(5^{-\frac{1}{2}}) \langle r_k^{-2} \rangle_{pd} \lambda R_0^{-1} Z_k \beta^2 h^{-1}. \quad (15)$$

In using Eq. (14) it is necessary to take into account the vibrational-electronic coupling (dynamical Jahn-Teller effect) that reduces the electronic angular momentum around the ring by a factor of η. That is, in our work[3] on the Jahn-Teller effect in B^- it was shown that the doubly degenerate vibronic ground state with symmetry $m=2$ is of the form

$$F^{(2)} = (J\omega^{(2)} + K\omega^{(-2)})\Psi, \quad (16)$$

where J and K are nuclear vibrational functions and Ψ is the remainder of the electronic wave function. In this case the expectation value of the electronic angular momentum around the ring is reduced from that of the simple function $\omega^{(2)}$ by a factor of

$$\eta = (J \mid J) - (K \mid K) \quad (17)$$

and $\eta = 0.3$.

When we assume $\langle r_k^{-2} \rangle_{pd}^{-\frac{1}{2}} = 0.1$ A, $\lambda = 0.1$, $R_0 = 1.5$ A, $Z_k = 1$, then Λ in Eq. (15) has the value, 150 000 Mc, or 5 cm^{-1}. This estimate of Λ is of course extremely uncertain; the values used for $\langle r_k^{-2} \rangle_{pd}^{-\frac{1}{2}}$ and λ are almost sheer guesses. There is one possible shread of experimental evidence that this result may be of the correct order of magnitude. The diagonal elements of the spin-orbit interaction estimated in the present paper for an orbitally degenerate state may be compared with nondiagonal elements of the spin-orbit interaction for nonsymmetrical aromatic molecules such as naphthalene. McClure[4] has inferred from experimental evidence on phosphorescent lifetimes that these nondiagonal elements are of the order of magnitude of a cm^{-1}. Unfortunately, one cannot be sure that this is a pure π-electron spin-orbit interaction rather than a σ-π spin-orbit interaction.

THE SPECTROSCOPIC SPLITTING FACTOR

When the vibronic degeneracy of the ground state of B^- is removed by spin-orbit interaction, and the net spin-orbit interaction energy is large relative to electronic Zeeman energies (e.g., 9500 Mc), then the electronic orbital angular momentum around the ring, $\pm m\eta\hbar$, may be coupled parallel or antiparallel to the spin, and the possible spectroscopic splitting factors parallel, $g_{\parallel}$ and perpendicular $g_{\perp}$ to the sixfold symmetry axis are

$$g_{\parallel} = 2(1 \pm m\eta)$$

$$g_{\perp} = 0. \quad (18)$$

At present there appears to be relatively little immediate prospect of being able to prepare an aromatic system where the orbital degeneracy is removed by the spin-orbit interaction so that this prediction may be tested experimentally. Instead we must probably be content to examine these symmetrical radicals under conditions where the orbital degeneracy is removed by electrostatic interactions with an unsymmetrical environment. In this case the first-order spin-orbit interaction is zero, and a perfectly straightforward calculation of the second-order spin-orbit interaction leads to the following formula for the spectroscopic splitting factors,

$$g_{\parallel} = 2[1 - (h \mid m \mid \eta\Lambda/\Delta E)]$$

$$g_{\perp} = 2.00. \quad (19)$$

Here ΔE is the splitting of the vibronically degenerate states by interaction with the unsymmetrical environment[3]. The sign of Λ is not known, since the sign of λ in Eq. (15) is not known. If ΔE is ~ 500 cm^{-1},[3] $\Lambda = 5$ cm^{-1}, then the increase in the average value of the g factor is only ± 0.004. In view of the uncertainty in the value of Λ, and the fact that the orbital function $\psi^{(m)}$ in Eq. (4) probably overestimates the expectation value of the orbital angular momentum around the ring, it is not surprising that unusual g factors have not been found for B^- (or C^-).

THE SPIN-LATTICE RELAXATION

Even though the average g factors for the symmetrical ion radicals are close to the free-spin g factor, there still exists a mechanism for an unusually effective spin-orbit induced spin-lattice relaxation in the symmetrical ion radicals. Due to the thermal motions of the polar solvent ΔE must surely be a function of the time, and for very short periods Δt it may be assumed that ΔE is very small; that is, in the range

$$|\Delta E| \lesssim |hm\eta\Lambda|. \quad (20)$$

During this period of time Δt the electron spin-orbit interaction is first-order, and the electron spin experiences a "magnetic pulse"[7] that will flip the spin if the pulse is long enough and strong enough. The pulse is long enough if

$$2\pi\Delta t \gtrsim |m\eta\Lambda|^{-1}, \quad (21)$$

and is strong enough if[7]

$$|m\eta\Lambda| \gtrsim \nu_e. \quad (22)$$

Here ν_e is the electron magnetic resonance frequency, equal to 9500 Mc in the experiments of Townsend and Weissman.[1] Even if our estimate of $|m\eta\Lambda| \simeq 100\,000$ Mc were ten times too large, condition (22) would still be met adequately. Condition (21) merely requires that condition (20) hold for approx. 10^{-12} sec, which is not unreasonable. The spin-lattice relaxation rate due to these effects alone is $\sim t$, where t is the average (long) period between magnetic pulses when condition (20) does not hold. Let T_1 be a normal unenhanced spin lattice relaxation rate of the order of 10^{-6} sec, which is characteristic of the unsymmetrical ion radicals in solution.[8] Then, of course, if the enhanced spin-lattice relaxation is to be observed in the symmetrical radicals it is necessary that

$$T_1 > t. \quad (23)$$

This then requires that condition (20) be met more than, say, once in 10^{-6} sec. Condition (23) is hardly any obstacle at all since in the liquid state we are concerned with collision frequencies of $\sim 10^{10}$–10^{13} sec^{-1} and a thermal activation barrier of $\Delta E \simeq 500$ cm^{-1} is of relatively little importance in reducing the frequency of realizing condition (20) at room temperature.

All of the above conditions (20)–(23) are entirely plausible for B^-. It can easily be shown[7] that the principal effect of the magnetic spin-orbit "pulse" considered here is to broaden the paramagnetic resonance lines, but not to shift them, at least in first-order. Therefore the spin-orbit interaction may indeed contribute to an enhanced spin-lattice relaxation rate without manifesting itself through an unusual g factor. Although the present work has not *proven* that spin-orbit interaction *is* the origin of the enhanced spin-lattice relaxation observed by Townsend and Weissman,[1] we have certainly demonstrated the plausibility of this explanation. This is in itself of some importance since no other mechanism is at all evident.

ACKNOWLEDGMENT

I wish to thank Professor S. I. Weissman for a number of helpful conversations concerning the paramagnetic resonance spectra of the negative ions of benzene, coronene, and triphenylene.

Note added in proof. Recent unpublished precision g value determinations by Blois, Brown, and Maling show that the g values of $\bar{C}$ and possibly $\bar{B}$ are significantly higher than those of a half-dozen other less symmetrical negative, aromatic, ion radicals. These observations support the conclusions of this paper.

[7] H. M. McConnell and S. B. Berger, J. Chem. Phys. **27**, 230 (1957); H. M. McConnell, *ibid.* **28**, 430 (1958).

[8] M. J. Stephan and G. K. Fraenkel, J. Chem. Phys. **32**, 1435 (1960); J. W. H. Schreurs, G. E. Blomgren, and G. K. Fraenkel, *ibid.* **32**, 1861 (1960).

Diffusion Coefficients of Helium in Fused Quartz

D. E. SWETS, R. W. LEE, AND R. C. FRANK

General Motors Research Laboratories, Warren, Michigan

(Received April 27, 1960)

The diffusion of helium through the walls of high-purity fused quartz hollow cylinders was studied using a mass spectrometer as a detecting device. By surrounding the outside of the hollow cylinder with helium and observing it diffuse through into the mass spectrometer, permeation rates and diffusion coefficients were measured in the temperature range of 24° to 1034°C. The diffusion process appeared to be relatively simple with only small deviations from Fick's laws occurring. The activation energy was found to be different in the temperature range of 24° to 300°C than in the range of 300° to 1034°C. In the low-temperature range the diffusion coefficients are expressed by

$$D=3.04\times10^{-4}\exp\left(-\frac{5580\pm56\text{ cal/g atom}}{RT}\right)\text{cm}^2/\text{sec},$$

and in the high-temperature range they are expressed by

$$D=7.40\times10^{-4}\exp\left(-\frac{6613\pm40\text{ cal/g atom}}{RT}\right)\text{cm}^2/\text{sec}.$$

The solubility was also determined by dividing the permeability by the diffusion coefficients. This was expressed by

$$S=1.99\times10^{17}\exp\left(-\frac{-680\pm60\text{ cal/g atom}}{RT}\right)\text{atoms/cm}^3$$

in the temperature range of 24° to 300°C and by

$$S=1.28\times10^{17}\exp\left(-\frac{-1174\pm120\text{ cal/g atom}}{RT}\right)\text{atoms/cm}^3$$

in the range 300° to 1034°C.

INTRODUCTION

THE relatively good agreement between the many investigators who have measured the permeability of helium in fused quartz is very encouraging.[1–5] Although there have been a number of good measurements of the permeabilities there have apparently been only a few attempts to determine the diffusion coefficients. Barrer[6] calculated diffusion coefficients by dividing his permeabilities by the solubility values obtained by Williams and Ferguson.[7] Jones[5] measured both the permeabilities and solubilities and divided the first by the second to get the diffusion coefficients. In the present work the diffusion coefficients have been obtained directly by measuring the rate of change of helium permeation through hollow fused quartz cylinders with a mass spectrometer when helium was suddenly introduced or removed from the outside surface of the cylinder. The permeabilities were obtained from the steady state permeation and the solubilities were calculated by dividing the permeabilities by the diffusion coefficients.

[1] L. S. Tsai and T. Hogness, J. Phys. Chem. **36**, 2595 (1932).
[2] E. O. Braaten and G. F. Clark, J. Am. Chem. Soc. **57**, 2714 (1935).
[3] R. M. Barrer, J. Chem. Soc. **1934**, 378.
[4] Francis J. Norton, J. Am. Ceram. Soc. **36**, 90 (1953).
[5] W. M. Jones, J. Am. Chem. Soc. **75**, 3093 (1953).
[6] R. M. Barrer, *Diffusion in and through Solids* (Cambridge University Press, New York, 1951), p. 141.
[7] G. A. Williams and J. B. Ferguson, J. Am. Chem. Soc. **46**, 635 (1924).

EXPERIMENTAL PROCEDURE

The fused quartz diffusion specimens used in these tests were constructed as shown in Fig. 1. Two such samples were used, one having a wall thickness of 1.48± 0.06 mm, the other a wall thickness of 0.905±0.055 mm. The quartz used in these samples were analyzed spectrographically and found to have the following impurities: Al 0.0040%, Mg 0.0015%. Visual and microscopic inspection showed no gross defects although some striations were present.

The diffusion specimen and associated equipment are shown in Fig. 1. The inner volume was connected directly to the ion source of a mass spectrometer. The outer volume was attached to a vacuum and gas inlet system. The entire sample system was enclosed in a resistance oven which was large enough so that the temperature along the length of the sample was uniform. A chromel-alumel thermocouple was mounted as is

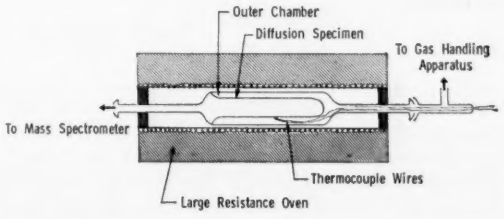

FIG. 1. Diagram of the diffusion specimen mounting and oven.

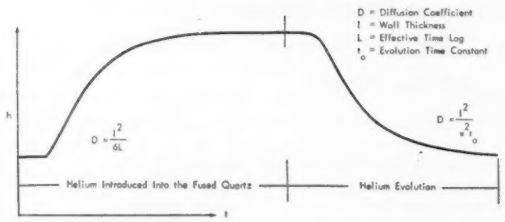

FIG. 2. Typical mass spectrometer record for helium diffusion through fused quartz.

shown in Fig. 1 and used to read the sample temperature. The mass spectrometer was a modified General Electric 60 deg sector field instrument.

The procedure carried out for each test was as follows. The outer volume was evacuated to a pressure of about 1×10^{-5} mm of Hg by an oil diffusion pump, after which the valve to the pump was closed. Helium gas from a lecture bottle was then quickly allowed into the system through a liquid nitrogen cold-trap to remove impurities. The pressure was read with a mercury manometer and held constant. As gas permeated the wall of the inner quartz tube it was continually recorded by the mass spectrometer. After a constant rate had been reached, establishing a value for the steady-state permeation rate, the gas in the outer chamber was evacuated. The mass spectrometer then recorded the evolution of gas from the sample. Both the input and the evolution data were used to obtain values for the diffusion coefficient. See Fig. 2. Tests were made at a number of temperatures chosen at random until the range of 24°C to 1034°C had been covered. Fewer tests were made at the lower temperatures because of the long periods of time required to carry out the tests.

Several tests were made in an attempt to establish the relationship between the permeation rate and the gas pressure on the outside of the specimen. Most of these were carried out at temperatures above 300°C because at temperatures below this the time required to reach steady state each time was rather long. In each test the temperature was held constant and the permeation rate was measured at various pressures. The permeation rate was plotted against pressure on logarithmic graph paper. It was found that the relationship between the permeation rate and pressure could be expressed by

$$h=Kp^x,$$

where h is the mass spectrometer reading, p is the pressure outside the specimen, and K is a constant of proportionality, x was found to be slightly less than 1, varying from about 0.93 to 0.97. The error of the method was such that this value could not be established more accurately without performing a large number of tests.

MATHEMATICS OF THE METHOD

The mathematics of the method used for calculating the diffusion coefficients has been discussed in earlier papers,[8–10] so only a brief discussion is needed here. When gas is suddenly introduced into the outside of the hollow cylindrical specimen, the mass spectrometer reading on the gas can be shown to vary as[10]

$$h=(sADC_0/F_1l)[(k-1)/\ln k]$$

$$\times\{1+2\sum_{n=1}^{\infty}(-1)^n\exp(-\pi^2n^2/l^2)Dt\}\},\ n=1, 2, \cdots, \quad (1)$$

where A = the internal surface area of the specimen; s = the mass spectrometer sensitivity for the gas being used; F_1 = the conductance of the leak used to obtain s; C_0 = the concentration of the gas dissolved in the outside surface of the specimen; l = the wall thickness of the specimen; k = the ratio of the outside to the inside diameter of the specimen. D = the diffusion coefficient; and, t = time.

This equation is applicable only if the following conditions exist: (a) The diffusion coefficient D is a constant. (b) The thickness of the wall must be small compared to the radius of the cylinder ($1<k<1.5$). (c) The time constant for the pump-out rate of the ion source of the mass spectrometer must be much smaller than the time constant for the transient effect of the diffusion process.

When steady state is reached the exponentials drop out and the equation becomes

$$h_0=(sADC_0/F_1l)[(k-1)/\ln k]. \quad (2)$$

If, after steady state has been reached, the gas is suddenly removed from the outside surface of the specimen, the mass spectrometer reading will drop off as

$$h=h_0\{2\sum_{n=0}^{\infty}(-1)^n\exp[-(\pi^2n^2/l^2)Dt]\}. \quad (3)$$

After a short time the mass spectrometer recorder trace becomes a simple exponential decay with a time constant equal to

$$t_0=l^2/\pi^2D. \quad (4)$$

The thickness of the specimen l, can be measured before fabrication using a micrometer, t_0 is measured on the recorder trace and, therefore, D can be easily calculated from Eq. (4).

The "time lag" method used by Barrer[6] is also

[8] A. Van Wieringen and N. Warmoltz, Physica **22**, 849 (1956).
[9] R. C. Frank, D. E. Swets, and D. L. Fry, J. Appl. Phys. **29**, 892 (1958).
[10] R. C. Frank and J. E. Thomas, Jr., J. Phys. Chem. Solids (to be published).

applicable. This can be shown by integrating Eq. (1);

$$\int h dt = h_0 t + (2l^2 h_0/\pi^2 D)\sum_{n=1}^{\infty}[(-1)^n/n^2] \times\{1-\exp[-(\pi^2 n^2/l^2)Dt]\}. \quad (5)$$

A plot of the integral against time becomes a straight line after a short time due to the fact that the exponentials approach zero. The intercept of the straight line with the time axis is found from the equation

$$h_0 t-(2h_0 l^2/12D)=0 \quad (6)$$

since

$$\sum_{n=1}^{\infty}[(-1)^n/n^2]=-\pi^2/12.$$

Rearranging Eq. (6) it is easily shown that

$$t=l^2/6D=L=\text{effective time lag}. \quad (7)$$

Therefore, the first part of the mass spectrometer curve can be integrated with a planimeter and the integral plotted against time. The linear portion of this curve can then be extrapolated to the time axis and the effective time lag L determined. The diffusion coefficient can be calculated from this.

The diffusion coefficients can also be calculated using curve fitting techniques[8,9] or the inflection point technique used by McAfee[11] but it is believed that these rely a little more on the judgment of the experimenter.

The permeability is obtained from the steady state mass spectrometer reading h_0 which is multiplied by $F_1 l/s\{A[(k-1)/\ln k]\}$ to give the permeation constant P in the commonly used units. The factor

$$A[(k-1)/\ln k]$$

is the effective area. As can be seen from Eq. (2)

$$P=DC_0=\text{Permeability}, \quad (8)$$

when the gas pressure outside of the specimen is one atmosphere the concentration C_0 inside the surface is considered to be the solubility S. Therefore,

$$P=DS. \quad (9)$$

Finally, after the diffusion coefficient and permeability have been measured, the solubility can be calculated from Eq. (9).

RESULTS

Values of the diffusion coefficients in the temperature range from 24° to 1034°C were calculated by both the time lag and the decay methods. The values of D found by the two methods agree quite well. However, for reasons which will be described below, the decay values are considered slightly more accurate and were the values used to obtain the plot in Fig. 3. After a preliminary plot of the diffusion coefficients against $1/T\times 1000$ had been made it was found that the curve appeared to have two straight-line portions with a connecting transition region. The actual data points for each of the straight-line portions of the curve were then fed into an IBM 704 computer and the least-mean-square lines were calculated. The computer also calculated the 95% confidence limits on these lines, as well as the correlation coefficients. The least-mean-square curves and the 95% confidence limits have been plotted in Fig. 3. The line in the upper temperature range was calculated from 26 data points while that in the lower range was calculated from 5 points.[12] The straight lines can be expressed mathematically by

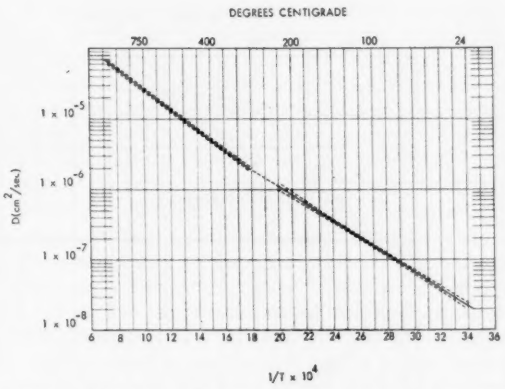

FIG. 3. Diffusion coefficients, D, as a function of temperature.

$$D=D_0 e^{-E/RT},$$

where D_0 is the frequency factor, (a measure of the frequency of vibration of the impurity in the interstitial site); E is the activation energy; R is the gas constant; and, T is the absolute temperature.

In the high-temperature range (300°–1034°C) the least-mean-square line through the points is represented by

$$D=7.40\times 10^{-4}\exp\left(-\frac{6613\pm 40\ \text{cal/g atom}}{RT}\right)\text{cm}^2/\text{sec}.$$

In the lower temperature range the least-mean-square line through the points is represented by

$$D=3.04\times 10^{-4}\exp\left(-\frac{5580\pm 56\ \text{cal/g atom}}{RT}\right)\text{cm}^2/\text{sec}.$$

The errors quoted are 0.67 times the standard deviation of the slope of the lines multiplied by R.

As mentioned above, there was a slight but consistent difference between the values for D found by the time lag and decay methods. In all but two cases the diffu-

[11] K. B. McAfee, Jr., J. Chem. Phys. **28**, 218 (1958).

[12] Actual values are listed in the Appendix.

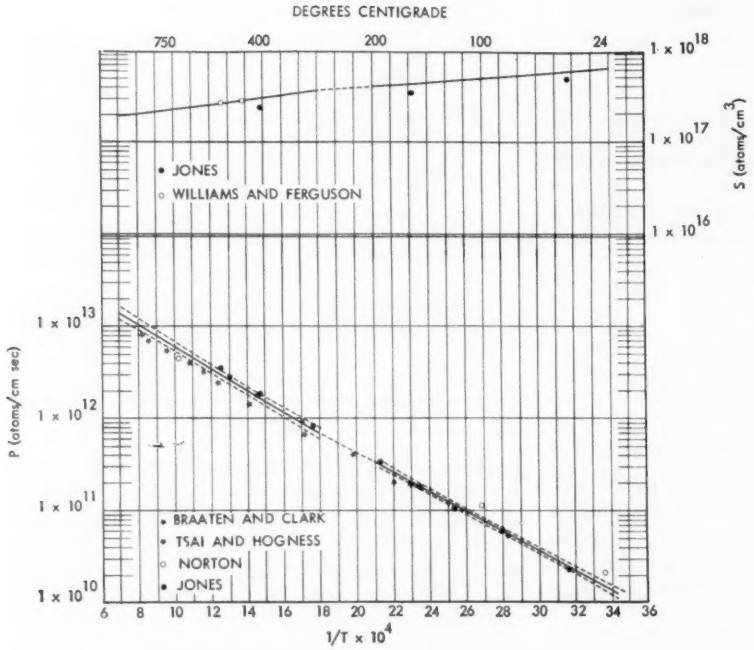

FIG. 4. Permeability, P, and solubility, S, as a function of temperature.

sion coefficients found by the time lag method were a few percent higher than those found by the decay curve method. After the possibility of calculation errors or temperature effects was eliminated it was found that there was a slight dependence of the time lag values upon the pressure of the gas outside of the specimen. The first half of the transient curve is obtained when the specimen is subjected to a gas pressure whereas all of the gas is removed from the chamber during the decay portion of the curve. It was therefore assumed that the gas pressure somehow changed the character of the fused quartz lattice to affect the helium diffusion, and for this reason the decay values were used. Unfortunately there was too much scatter in the time lag results and their deviation from the decay values was too small to establish a mathematical relation between diffusion coefficient values and pressure.

The permeability P, was also measured and is plotted against $(1/T)\times 1000$ in Fig. 4. The units of P are atoms/sec cm for a sample 1 cm thick and a pressure difference across the membrane of 76 cm of Hg. The solid lines in Fig. 4 are the least-mean-square lines obtained from the points of the present work. The dotted lines are the 95% confidence limits on the least-mean-square lines. The results of a number of other investigations, converted to the same units, are also plotted in Fig. 4 and show good agreement with the present work. Barrer's[3] permeability values are about a factor of 5 or 6 below all the other values and have not been included on the curve.

The solubility of helium in fused quartz can be found by dividing the permeability by the diffusion coefficient value at a given temperature. The units for the solubility are then atoms/cm^3 for a pressure of 76 cm of Hg outside of the sample. A plot of solubility vs $(1/T)\times 1000$ is also shown on Fig. 4.

In the upper temperature range the equation for the line is

$$S=1.28\times 10^{17} \times \exp\left(-\frac{-1174\pm 120 \text{ cal/g atom}}{RT}\right) \text{atoms/cm}^3.$$

In the lower temperature range the straight line portion of the curve is represented by

$$S=1.99\times 10^{17} \times \exp\left(-\frac{-680\pm 60 \text{ cal/g atom}}{RT}\right) \text{atoms/cm}^3.$$

The values of solubility found by Jones[5] and also by Williams and Ferguson[7] are plotted on the curve and show very good agreement with the present work.

It is particularly noteworthy that in both temperature ranges the heat of solution is negative. The solubility therefore decreases with increasing temperature. The heat of solution is greater in the upper temperature range than in the lower.

DISCUSSION

Since the permeabilities and solubilities found by Jones agree fairly well with the present work the diffusion coefficients calculated from P/S might also be expected to agree fairly well. The diffusion coefficients calculated by Barrer,[6] which have long been considered the only values, are approximately two orders of magnitude lower than those reported here.

There was extremely good agreement between the diffusion coefficient values obtained in this work from the two specimens of different thicknesses. This indicates two things: (a) The fused quartz is of reproducible quality (b) The diffusion coefficients are not a function of the thickness of the specimens.

The fact that there is some correlation between the time lag diffusion coefficient values and the pressure of the helium outside of the specimen indicates the possibility of the diffusion coefficient being increased when the specimen is under compressive stress. McAfee studied the effect of stress on the diffusion coefficients of helium in Pyrex glass[11] at room temperature but found that the effect of compressive stresses was small or nonexistent. In plastic materials such as iron the increase in diffusion rate produced by subjecting the specimen to stress is believed to be associated with the movement of dislocations.[13] However, little is known about dislocation-like defects in fused quartz and therefore not much can be said about their effects on the diffusion properties of interstitials.

Equation (4), from which values of D were found, is obtained under the assumption that the laws of simple diffusion are applicable. The results indicate that this was a fair assumption for the following reasons: (a) The decay curves exhibited a simple exponential decay over most of the evolution process. In general the tail end of the decay curve deviated slightly from the exponential law but the quantity of gas involved in this deviation was less than 1% of the total gas evolved. (b) There was only a small difference between the time-lag and the decay diffusion coefficient values, particularly at low-gas pressures. Under these circumstances it seems justifiable to define a constant diffusion coefficient at a given temperature.

A commonly accepted model for the lattice structure of fused silica is that proposed by Zachariasen[14] which considers the structure to be a random array of the basic tetrahedra. Thus the lattice is believed to consist of a rather wide assortment of sizes of the interstices. The activation energy for the diffusion of impurities in a crystalline lattice is considered to be the energy required for the impurity atom to jump from one interstitial site to another.[15] Therefore a variation in "jumping" energy corresponding to the assorted sizes of the interstices would be expected, and the activation energy for diffusion would be an average of all possible jumping energies.

The curve of the diffusion coefficients as a function of temperature appears to have a straight line relationship from 24°C to 300°C and from 300°C to 1034°C but the slopes are slightly different for the two ranges and therefore the activation energy for diffusion is slightly different in each range. The change in activation energy implies a change in the average jumping energy. It is perhaps important to note that there is not only a change in activation energy for diffusion but also a change in the heat of solution. In looking for possible explanations for this it is necessary to look for changes in other physical properties which occur in the temperature range near 300°C. Although vitreous or fused silica does not exhibit the presence of inversion points in the volume vs temperature curve, the crystalline forms of silica do. Cristobolite and tridymite, in fact, show very pronounced inversions in the temperature range of 160°C to 280°C. There are also inversions in the birefringency[16] vs temperature curves in this range. The existence of a change in activation energy for helium diffusion in the temperature range in which an inversion occurs in the crystalline forms of silica suggests the possibility that there are characteristics of the crystalline forms of silica which are carried over into the vitreous form of the material. Several experiments, including those by Westman and Crowther[17] and also Prebus and Michene[18] indicate that the Zachariasen picture of the fused silica lattice may not be entirely adequate. They suggest that instead of a completely random arrangement, the glass lattice might actually contain regions in which there is a repeating and somewhat uniform structure. The notion of the existence of extremely small crystallites in glass was apparently proposed many years ago by Lebedev[19] and much experimental work supporting the view has been done in the Soviet Union. It is possible that fused quartz in some subtle way retains some of the properties of cristobolite and that this is what produces the change in activation energy for the diffusion of helium in fused quartz in the region near 300°C.

Investigations of the permeation rate as a function of the gas pressure indicate that at least in the high-temperature range the permeation rate is not a linear function of the pressure. The exponent of the pressure is slightly less than one. The permeation rate-pressure relationship for helium in glass has been investigated by a number of people[1–3,20] but apparently Urey[20]

[13] P. Bastien and P. Azou, Proc. 1st World Met. Cong., 1951. Am. Soc. Metals, p. 535.
[14] W. H. Zachariasen, J. Am. Chem. Soc. **54**, 3841 (1932).
[15] C. Wert and C. Zener, Phys. Rev. **76**, 1169 (1949).
[16] R. B. Sosman, *The Properties of Silica* (Chemical Catalog Company, New York, 1927).
[17] A. E. Westman and J. Crowther, J. Am. Ceram. Soc. **37**, 420 (1954).
[18] A. F. Prebus and J. W. Michener, Ind. Eng. Chem. **46**, 147 (1954).
[19] K. S. Evstropyev, *The Structure of Glass*, translated from Russian (Consultants Bureau, Inc., New York, 1958), p. 9.
[20] W. D. Urey, J. Am. Chem. Soc. **54**, 3887 (1932).

TABLE I. Diffusion coefficients.

Temperature (°C)	Diffusion coefficients (10^{-7} (cm²/sec)
814	355.
857	387.
854	380.
605	158.
608	159.
1038	613.
1034	610.
1028	584.
1032	580.
860	401.
861	416.
861	408.
712	244.
712	237.
717	250.
717	248.
490	90.2
489	89.4
284	19.5
492	94.5
380	48.1
378	43.9
378	47.7
700	241.
705	245.
704	238.
191	7.28
78	1.06
24	.239
112	2.15
148	3.73

is the only one who found anything other than a linear pressure relationship. He found that the permeation rate was an exponential function of the pressure and the exponent was slightly less than unity but varied with the composition of the glass. Since helium cannot dissociate and does not react with the silica, an exponnent less than one is difficult to explain. It might indicate that when the helium enters the quartz it passes through an adsorption phase in which the amount adsorbed is not a linear function of the pressure.

Although the diffusion of helium in fused quartz appears to be relatively simple compared to other diffusion systems it is probably not as simple as the earlier investigators believed and a few minor discrepancies remain to be investigated in the future as better methods become available.

TABLE II. Permeabilities.

Temperature (°C)	Permeabilities (10^{11} Atoms/cm sec)
1034	118.
861	86.1
717	62.8
490	22.2
284	6.92
492	27.3
380	15.3
705	55.8
191	3.00
78	.532
24	.151
112	.995
148	1.76

ACKNOWLEDGMENTS

The authors wish to express their appreciation to Arthur Dolenga for constructing the diffusion specimens and to Robert L. Williams for assistance with the operation of the mass spectrometer and with the data reduction. James E. Dallemand supplied some helpful advice about the statistical treatment of the data.

APPENDIX

The actual diffusion coefficient values used in plotting the curve in Fig. 3 are given in Table I. These values were obtained by substituting the time constants of the evolution curves into Eq. (4). The values above the black line were measured using the specimen which was 1.48 mm thick and those below the line were obtained using the specimen which was 0.905 mm thick.

TABLE III. Additional diffusion coefficient data.

Temperature (°C)	Diffusion coefficients (10^{-7} cm²/sec)
227	11.6
261	17.0
281	20.6
334	32.9
334	33.1
708	240.
430	64.0
430	68.0
607	177.
606	170.

The permeabilities used to obtain the curve in Fig. 4 are listed in Table II. There are more diffusion coefficient values than permeability values since some of the tests were performed at reduced pressures to study the effect of pressure on the permeation rate. The diffusion coefficients calculated from the evolution curves did not vary with the pressure and therefore they are as valid as the values obtained using higher pressures and are included. In the table of permeabilities the black line again separates the data of the 1.48-mm thick specimen from that of the 0.905-mm thick specimen.

Note. Since the initial writing of this paper additional data has been taken which confirms that the $\ln D$ vs $1/T$ plot in Fig. 3 is best represented by two straight lines rather than by one line with continuously varying slope. The additional diffusion coefficient values are given in Table III. As shown, many of these are taken in the temperature range where the change in slope occurs. All of these new points fall almost exactly on the least-mean-square lines shown in Fig. 3.

Dependence of Calculated and Experimental Propane Mass Spectra upon Electron Voltage*

EDWARD M. EYRING† AND AUSTIN L. WAHRHAFTIG

Department of Chemistry, University of Utah, Salt Lake City, Utah

(Received June 13, 1960)

Experimental propane mass spectra have been obtained with bombarding electrons ranging in energy from 14 to 500 v. The quasi-equilibrium theory has been used in calculating the same spectra. The grossly simplified version of the statistical theory that satisfactorily predicts the 70-v mass spectrum is inadequate at low voltages, but if half the theoretical number of oscillators are assumed to be effective in the parent-ion and activation energies that bear no simple relation to experimental appearance potentials are employed, a semiquantitative fit of the experimental data is obtained. The description of the decomposition reaction of a molecule-ion in terms of a collection of harmonic oscillators is clearly unsatisfactory. However, the more general form of the quasi-equilibrium theory, in which it is assumed only that the reaction coordinate is separable, does appear to be applicable.

INTRODUCTION

ACCORDING to the quasi-equilibrium theory of mass spectra,[1] the rate constant for the unimolecular dissociation of a polyatomic molecule is given by

$$k(E)=h^{-1}\int_0^{E-\epsilon_0}\frac{\rho^{\ddagger}(E,\ \epsilon_0,\ \epsilon_t)}{\rho(E)}d\epsilon_t, \qquad (1)$$

where $\rho(E)\delta E$ is the number of states of the ion with energies between E and $E+\delta E$ and $\rho^{\ddagger}(E,\ \epsilon_0,\ \epsilon_t)\delta E$ is the number of states of the ion in the activated complex configuration with potential energy ϵ_0 and translational energy ϵ_t in the reaction coordinate. If this equation is grossly simplified by neglect of all electronic state contributions to the state density functions ρ, and in addition the oscillators in the normal and activated complex configurations of the molecule-ion are assumed to be harmonic, the specific rate constant for a unimolecular decomposition of the polyatomic molecule-ion with internal energy E is[1]

$$k_i=z_i(1-\epsilon_i/E)^p(E-\epsilon_i)^q. \qquad (2)$$

In this expression z_i is a frequency factor calculable from the vibration frequencies and moments of inertia of the parent ion and the ith activated complex and ϵ_i is the activation energy for decomposition along the ith reaction path which presumably may be determined from appearance potentials or thermochemical calculations, $p=(3N'-6)-L/2-1$ where N' is the number of atoms in the parent ion, L is the number of internal rotational degrees of freedom, $q=(L-L^{\ddagger})/2$, and the symbol ‡ indicates quantities relating to the activated complex.

Kropf *et al.*[2] recently described in detail the application of Eq. (2) to the 70-v mass spectrum of propane. The calculations described in the present work are similar, but some modifications have been required. The low-energy reaction paths for unimolecular decomposition of propane ion (see Fig. 1) were predicted from thermochemical considerations.[3] If we assume that only the jth reaction yields the particular product ion A^+, that secondary decomposition of A^+ can be neglected, and that $\sum_i k_i(E)>10^6$ sec^{-1} so that essentially all the parent ion decomposes in the ionization chamber, the relative abundance (R.A.) of A^+ in the mass spectrum of propane at a particular value of E is

$$I_j=k_j(E)/\sum_i k_i(E). \qquad (3)$$

Since not all values of E are equally probable, we denote the relative number of parent ions of internal energy E produced by electrons of energy E_e by the symbol $P(E)$. The numerical integration

$$S_j=\sum_E P(E)I_j(E) \qquad (4)$$

performed with a small increment in E over the range $E=0$ to a maximum value E_m gives the abundance S_j of the ion A^+. The R.A. of this decomposition product in the total mass spectrum is, therefore,

$$(\text{R.A.})_{A^+}=S_j/\sum_i S_i, \qquad (5)$$

where j is, of course, numbered among the i major unimolecular decomposition paths.

With these equations investigators have calculated the mass spectra of compounds as diverse as propane,[1,2] simple esters,[4] lower aliphatic alcohols,[5] and ethyl

* The construction of the mass spectrometer used in this research was initiated under a grant from the University of Utah Research Fund. This research was assisted by the U. S. Atomic Energy Commission.

† Part of a thesis presented in partial fulfillment of the requirements for the degree of Doctor of Philosophy. National Science Foundation Cooperative Fellow.

[1] H. M. Rosenstock, M. B. Wallenstein, A. L. Wahrhaftig, and H. Eyring, Proc. Natl. Acad. Sci. (U. S.) **38**, 667 (1952).

[2] A. Kropf, E. M. Eyring, A. L. Wahrhaftig, and H. Eyring, J. Chem. Phys. **32**, 149 (1960).

[3] M. B. Wallenstein, Ph.D. thesis, University of Utah, 1951.

[4] A. B. King and F. A. Long, J. Chem. Phys. **29**, 374 (1958).

[5] L. Friedman, F. A. Long, and M. Wolfsberg, J. Chem. Phys. **27**, 613 (1957).

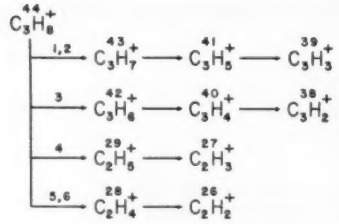

FIG. 1. Unimolecular decomposition scheme for propane under electron bombardment.

mercaptan.[6] In general, the calculated mass spectra have at best agreed only semi-quantitatively with experimental data. At low-electron voltages, serious discrepancies have been noted.[4]

Using a high-speed digital computer program that makes a long series of recalculations of the propane mass spectrum practicable, we have compared calculated and experimental spectra over the range of electron energies $E_e=14$ to 70 v in an attempt to establish values of p and E_m for propane that apply for all values of E_e. A semi-quantitative fit of the experimental data is obtained with some difficulty. Somewhat different calculations for other alkanes[7,8] have also encountered problems. Our results indicate that the general form of the statistical theory is a useful working hypothesis for describing the decomposition of the excited propane molecule-ion, but that application of the simple form given in Eq. (2) is not generally appropriate.

EXPERIMENTAL

Propane mass spectra for bombarding electrons ranging in energy from 14 to 500 v were obtained with a single focusing mass spectrometer of the sector field type described by Nier,[9] but with a magnetic deflection of 90° at an 8-in. radius. The operating conditions were: trap current = 15 μa, repeller plate voltage = 6 v, ion accelerating voltage = 3000 v, ionization chamber temperature ~175°C, minimum detectable ion current $\approx 10^{-15}$ amp. Thirty minutes were required to scan magnetically the region $m/e=12$ to 45. The electron voltage scale was calibrated with neon. Below an ion gauge reading of 4.5×10^{-5} mm Hg peak intensities varied linearly with pressure. With the propane-neon mixture admitted to the ionization chamber the pressure readings ranged from 3 to 6×10^{-6} mm Hg; hence, collision processes were definitely precluded. Although the background pressure was about 5×10^{-7} mm Hg, the $m/e=28$ background accounted for as much as 12% of the sample $m/e=28$ peak at higher electron voltages. Consequently, background mass spectra were subtracted from the propane spectra in all cases. Agreement at 50 and 70 v with published propane spectra[10] was acceptable, particularly considering the lower than customary temperature of the ion source. The points plotted in Fig. 2 indicate the experimental R.A.'s of the principal ions of the propane mass spectrum in the range 14 to 70 v. The total intensity of ions of $m/e=26$ to 29 and 38 to 44 was normalized to unity. Smaller fragments constituting about 8% of the total ionization at 70 v and far less at lower electron voltages were omitted for consistency with our simplified calculated mass spectra. We have not extended the plot beyond 70 v because no important changes occur in the mass spectrum of propane in the 70- to 500-v range. In this range a slight tendency for the primary product ions to regain importance at the expense of the secondary ions is observed as is also a decrease in total ionization.

RESULTS AND DISCUSSION

The relative number $P(E)$ of parent propane molecule-ions with internal energy E may be taken as the product of two independent factors: the distribution $G(E)$ of excited levels along the energy axis and the average transition probability $A(E)$ to the levels of energy E to $E+\delta E$ where all internal energy (electronic, vibrational, and internal rotational) is included. The most frequently used expression for $P(E)$,[4,5,11]

$$P(E)=P_0 \quad \text{for} \quad 0\leq E\leq E_m,$$
$$P(E)=0 \quad \text{for} \quad E>E_m, \qquad (6)$$

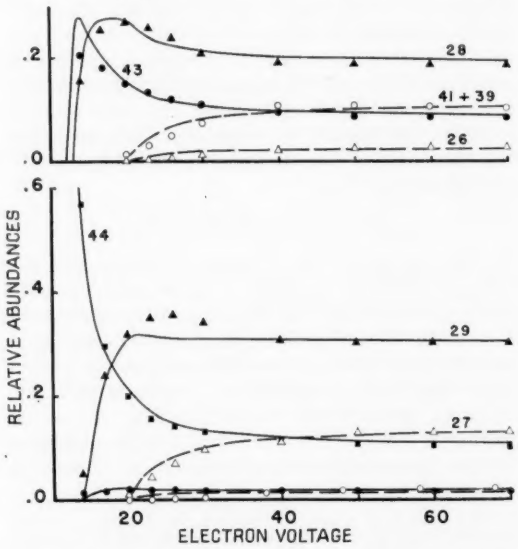

FIG. 2. Experimental (points) and calculated (curves) relative abundances in propane mass spectra. Numbers adjacent to a curve denote the corresponding m/e value. The unmarked continuous and dashed curves at the bottom are for $m/e=42$ and 40+38, respectively.

[6] J. Collin, Bull. soc. roy. sci. Liège **25**, 520 (1956).
[7] F. W. Lampe and F. H. Field, J. Am. Chem. Soc. **81**, 3238 (1959).
[8] L. Friedman, F. A. Long, and M. Wolfsberg, J. Chem. Phys. **30**, 1605 (1959).
[9] A. O. Nier, Rev. Sci. Instr. **11**, 212 (1940); **18**, 398 (1947).
[10] American Petroleum Institute, *Mass Spectral Data*, Research Project 44 (Carnegie Institute of Technology, Pittsburgh, 1954).
[11] D. P. Stevenson, Radiation Research **10**, 610 (1959).

is obtained from the assumption that $G(E)$ is a constant for $0 \leq E \leq E_m$ and zero elsewhere and that $A(E)$ is constant for all E of interest. There is both experimental[12–14] and theoretical[15,16] evidence that the threshold law for the simple process $R+e^- \rightarrow R^+ + 2e^-$ has the linear form $i_{R^+} = a(E_e - I_z)$, and further there is experimental evidence that this form holds for at least 8 v above threshold for He^+.[14,17] It may be inferred from the additivity of molecular ionization cross sections[18] that the value of the coefficient in the last expression is independent not only of the rotational and vibrational excitation of the molecule but also of the particular molecular orbital from which the electron is removed in the ionization process. Thus, we obtain

$$A(E) = A_0[E_e - (I_z + E)]. \quad (7)$$

Since there are ten molecular orbitals in propane, the eigenfunction of the molecule in the ground state can be written as $\psi_m = a^2b^2c^2\cdots j^2$. Let us assume that the energies of these molecular orbitals bear the following relationship to one another: $\epsilon_a < \epsilon_b < \epsilon_c \cdots < \epsilon_j$. The wave function of the ground state of the molecule-ion will then be given by $\psi_i = ab^2c^2\cdots j^2$ while that of the first excited state of the ion will be $\psi_i = a^2bc^2\cdots j^2$. Since removal of an electron from any one of the molecular orbitals of the molecule is presumed to be equally likely, a 70 v electron beam should produce ions in all ten such states. Many other electronic states of the ion have energies in the region 0 to 100 v, but in the molecular orbital approximation these are described by use of orbitals that are not doubly occupied in the ground state of the molecule. To obtain such a state at least a two-electron transition must take place in which one electron is removed from the molecule while a second electron is excited. The probability of such a transition is very small compared to the probability of simple removal of one electron.[19] Then, only the distribution of the electronic states obtained by simple ionization need be considered in the function $G(E)$. These states will be scattered over a several-volt range above the lowest level[20] except for the states, about 200 v higher in energy and so neglected here, obtained by removal of a carbon 1*s* electron. The effect of internal rotation and vibration is to smear out the lower levels; the simplest approximation is a $G(E)$ that is constant for $0 \leq E \leq E_m$ and zero elsewhere. We then obtain $P(E)$ curves of the type shown in Fig. 3(a). The curves numbered 1, 2, and 3 apply for 70-, 30-, and 14-v bombarding electrons, respectively. Since the $P(E)$ vs E curve for $E_e \geq 70$ v closely approximates the rectangle of Eq. (6), the rate of change with increasing E_e of the calculated R.A.'s will rapidly decrease to near zero once E_e exceeds twice $E_m + I_z$. However, at low-electron voltages where $E_e < E_m + I_z$ the use of Eq. (7) and the $G(E)$ function does yield a $P(E)$ curve that is quite different from the simple rectangular distribution. Chupka and Kaminsky[21] have adduced experimental evidence for somewhat similar but more exact conclusions regarding the distribution of accessible states of the propane molecule-ion.

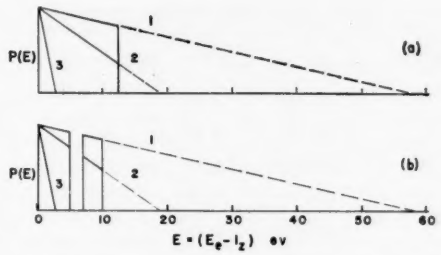

FIG. 3. Relative number $P(E)$ of $C_3H_8^+$ ions formed with internal energy E by electrons of energy E_e.

In our initial calculation we used the parameters which had given a good fit of the experimental 70-v propane mass spectrum[2] and a probability function of the type shown in Fig. 3(a) with $E_m = 12.5$ v. The calculated curves disagreed markedly with the experimental data for low values of E_e. Specifically, for bombarding electron energies a few volts above the first ionization potential, the R.A.'s of those primary product ions resulting from high activation energy decompositions as calculated were much smaller than the corresponding experimental R.A.'s. This same result was noted in calculated low-voltage mass spectra of some simple esters with the explanation "that for the first several volts above the ground state [of the molecule-ion] the distribution of electronic states would consist of a number of highly degenerate, narrow bands with little overlap."[4] Discussions of energy randomization by radiationless transitions among the lower states of simple alcohols and amines have been given by Chupka,[22] and by Chupka and Berkowitz.[23] They conclude that in such molecule-ions where the first excited electronic state is perhaps 2 ev above the ground state, the assumption of energy randomization is frequently

[12] R. E. Fox, W. M. Hickam, T. Kjeldaas, Jr., and D. J. Grove, Phys. Rev. **84**, 859 (1951).
[13] R. E. Fox, W. M. Hickam, and T. Kjeldaas, Jr., Phys. Rev. **89**, 555 (1953).
[14] W. M. Hickam, R. E. Fox, and T. Kjeldaas, Jr., Phys. Rev. **96**, 63 (1954).
[15] G. H. Wannier, Phys. Rev. **90**, 817 (1953); **100**, 1180 (1955).
[16] S. Geltman, Phys. Rev. **102**, 171 (1956).
[17] F. H. Dorman, J. D. Morrison, and A. J. C. Nicholson, J. Chem. Phys. **32**, 378 (1960).
[18] J. W. Otvos and D. P. Stevenson, J. Am. Chem. Soc. **78**, 546 (1956).
[19] G. Herzberg, *Atomic Spectra and Atomic Structure* (Dover Publications, New York, 1944), p. 153.
[20] J. Lennard-Jones and G. G. Hall, Trans. Faraday Soc. **48**, 581 (1952).
[21] W. A. Chupka and M. Kaminsky; presented at the American Physical Society Meeting, Washington, D. C., May, 1959.
[22] W. A. Chupka, J. Chem. Phys. **30**, 191 (1959).
[23] W. A. Chupka and J. Berkowitz, J. Chem. Phys. **32**, 1546 (1960).

TABLE I. Specific rate constant parameters.

Reaction[a]	z_i,[b]	ϵ_i,[b] ev	$q_i=(L-L^{\ddagger})/2$[b]	E_a,[c] ev
1	1.2×10^{16}	3.78	0	4.4
2	5.0×10^{9}	0.52	0	4.4
3	3.2×10^{12}	1.25	$\frac{1}{2}$	4.6
4	1.8×10^{14}	1.38	0	7.8
5	2.9×10^{11}	0.87	1	7.8
6	1.8×10^{12}	0.97	1	7.8

[a] The reaction numbers refer to Fig. 1.
[b] Defined in connection with Eq. (2) of the text. Units for Z_i are sec^{-1} ev^{-9}.
[c] Internal energy of parent ion for which primary product ion undergoes further decomposition to give a secondary product.

invalid. In the absence of electronic states spaced sufficiently closely to give rapid redistribution of electronic energy among the vibrational degrees of freedom, low-energy activation processes on an excited potential surface (hence high-activation energy relative to the ion ground state) could precede the establishment of quasi-equilibrium. We believe a qualitative examination alone of the wide variation of mass spectra of isomers having essentially the same total ionization[24] requires that rapid radiationless transition be possible, in general, between the electronic states of the ion initially obtained with electrons of 50 v and more. Since most ions are formed with excitation energies well under 12 v and since the ionization potential of propane is 11.2 v, radiationless transition should still be important in ions formed by 20-v electrons. While amines and other molecules with nonbonding electrons may well have an isolated ground state for the ion, the evidence favors the assumption that in the alkanes, where all the electrons are in similar C—C and C—H bonds, the ground state—first excited state spacing is not significantly larger than that between the higher levels obtainable by simple ionization. Hence, the concept of energy randomization was retained in these calculations.

There is an alternative explanation for incomplete randomization of energy which may apply in some cases. The statistical theory must fail and true metastable ions be observed if radiationless transitions between excited states of the molecule-ion are impeded by a difference in multiplicity for the crossing potential surfaces.[25,26] While it was assumed in formulating the quasi-equilibrium theory that all potential surfaces can intercombine, it would be more reasonable to expect all doublet excited states of the molecule-ion to drain down into the lowest doublet state and all quartets to drain down into the lowest quartet state, etc. There could then be a considerable delay before such a lowest state made the excitation energy coming from change in multiplicity available to the vibrational modes important in decomposition. However, such considerations probably do not apply in reactions such as $C_3H_8^+\rightarrow C_3H_7^++H$; even though the paramagnetic bombarding electron is presumably capable of exciting all possible states of $C_3H_8^+$, spin angular momentum is conserved if, as seems likely, the ground state of $C_3H_8^+$ is a doublet, that of $C_3H_7^+$ a singlet, and that of H a doublet.

While it was assumed that a redistribution of electronic energy does take place in the propane molecule-ion, the failure of our first calculation suggested that the number of vibrational modes involved is smaller than that required by the simple theory. Since there was some evidence that our previous choices of p and E_m were too large by a factor of 3 or 4,[22] values of E_m ranging from 5 to 12.5 v and values of the exponent p ranging from 8 to 25 were tried in conjunction with arbitrary values of z and ϵ. The best fit (see Fig. 2) of the experimental data was obtained with the values of z and ϵ given in Table I, $p=12$, and the modified probability function of Fig. 3(b). We will consider the characteristics of the experimental R.A. curves that led to this choice of parameters.

In calculating the 70-v propane mass spectrum[2] it was assumed that $C_3H_3^+$ is formed from $C_3H_8^+$ by three consecutive unimolecular dissociations the first of which involves the loss of an H atom while each of the remaining two processes involves the loss of an H_2 molecule. This assumption requires that a plot of the sum of the R.A.'s for $m/e=43$, 41, and 39 vs increasing E_e give a curve with no minima at intermediate values of E_e. However, a minimum does exist in the experimental curve at about 22 v (see Fig. 2). This result is not accounted for by the presumed existence of both a primary hydrogen atom and a competing secondary hydrogen atom abstraction process, $C_3H_8^+\rightarrow C_3H_7^++H$, since the activation energies of the two processes are almost certainly not separated by more than a volt.[27] The observed rapid changes in the R.A. curves at values of E_e well above all the experimental primary product ion appearance potentials can only be obtained from our calculations by a radical change in the postulated activation energies of the major primary dissociations or by use of a very large E_m. The latter gambit results in very large specific rate constants which contradict the fundamental assumption that energy randomization has time to occur before unimolecular decomposition. We have therefore revised our previous interpretation[2] of the probable propane decompositions, Fig. 1, and of the corresponding activation energies.

We have assumed that hydrogen abstraction occurs by two competing processes (reactions 1 and 2 of Fig. 1): one with low activation energy and low fre-

[24] M. B. Wallenstein. A. L. Wahrhaftig, H. M. Rosenstock, and H. Eyring, in Natl. Research Council, *Symposium on Radiobiology* (John Wiley & Sons, Inc., New York, 1952).
[25] A. E. Stearn and H. Eyring, J. Chem. Phys. **3**, 778 (1935).
[26] E. K. Gill and K. J. Laidler, Can. J. Chem. **36**, 1570 (1958).
[27] M. Szwarc, Discussions Faraday Soc. **10**, 336 (1951).

quency factor, the other with much higher values for both these parameters. This can be visualized in either one of two ways neither of which is consistent with the simplifications that led from Eq. (1) to Eq. (2). In the first picture we concede the possibility of dissociation paths on several potential surfaces so that the z's and ϵ's of Table I are in fact some sort of composites of z's and ϵ's for the individual surfaces each with reactions described by Eq. (2). In the other picture we assume that it is meaningless to talk of potential surfaces and resulting vibrations when the estimated residence time on a surface is less than the time for one molecular vibration.[1,4,28] That is, the Born-Oppenheimer approximation involved in the separation of electronic and vibrational eigenfunctions is invalid. Then, the system, described by its electronic and nuclear coordinates with only a reaction coordinate assumed separable, will have activated complex configurations, in general more than one, leading to each product. The values of z_i, p, and q_i in Eq. (2) can then be considered as descriptive of some kind of average set of nuclear motions. These same arguments apply to the use of two rate constants in describing methane loss (reactions 5 and 6 of Fig. 1). The fact that rather reasonable agreement with the observed mass spectra is obtained with two of the reaction paths of Fig. 1 described by two k_i, and the remaining two by only one k_i each, is more easily reconciled with our second picture.

Thus to some extent the values of z_i, ϵ_i, p_i, and q_i must be considered as arbitrary parameters. We have attempted in so far as possible to retain the values used in a previous calculation[2] in which these parameters had the simple meanings noted below Eq. (2). The q_i values were retained unchanged; all p_i were assumed equal as before, but the common value was varied in the several successive calculations. We selected the difference of appearance potentials for $C_3H_8^+$ and s-$C_3H_7^+$ as the value of ϵ_2, the activation energy of reaction 2. The reliability of the value $\Delta A.P.=0.52$ v[29] has been confirmed by a recent investigation[30] of the effect of repeller plate voltage on appearance potentials. A value of ϵ_2 not very different from 0.52 v is necessary to obtain agreement in the initial onset of the experimental and calculated R.A. curves for $C_3H_7^+$, but the selection of this particular value also permits comparison of our final set of activation energies with the assumption that all values of ϵ_i in Eq. (2) are differences of appearance potentials.

To obtain the rapid change in specific rate constants implied by the steep slopes of the experimental R.A. curves of Fig. 2 the exponent p of Eq. (2) must be reduced to about half the theoretical value of 25. However, a p much smaller than 12 is also unsatisfactory; the calculated R.A. curves rise too steeply at low energies, and the ϵ_i's must be spread over a much broader energy range than that predicted by appearance potential differences in order to get satisfactory differentiation of the reaction rates for the several dissociation processes. Hence, as we might expect, the choice for n-propylamine[22] of a p only 0.21 times as large as the theoretical value has little significance for the case of propane in which presumably no atom is preferentially ionized. While small values of p permit the use of z_i's that do not exceed the arbitrary maximum of 10^{14} to 10^{15} sec^{-1} suggested by several investigators,[1,4,5] this is not a valid argument against values of p as large as 12 for propane. Specific rate constants in excess of 10^{14} sec^{-1} contradict the assumption leading to Eq. (2) that several molecular vibrations occur between ionization and dissociation. However, in our calculations the larger z_i's are consistently paired with large values of ϵ_i so that the specific rate constants do not exceed 10^{14} sec^{-1} at the E_m used.

The R.A. of $C_3H_8^+$ ion is a few percent too large unless $G(E)$ for $E=0$ to 0.2 v is taken to be zero. This choice is compatible with the theoretical prediction that "the probability of obtaining ions with no internal excitation is essentially zero because the minima on the potential surfaces of the molecule and the molecule-ion will in general have different equilibrium internuclear distances."[1]

The last step in the calculation is the division of each of the S_j's of Eq. (4) into two sums representing the abundances of the primary and secondary product ions of the jth reaction. An expression devised previously[2] for calculating the internal energy E_a of the parent molecule-ion for which primary product ion undergoes further decomposition to give a secondary product cannot be used here without an elaborate reinterpretation of the effective number of internal degrees of freedom in the parent and primary product ions. As such arguments are necessarily quite arbitrary, we chose to use empirical values of E_a. The selected values of E_a (see Table I) were arrived at after making a further refinement in the probability curve suggested by the prolonged gentle rise with increasing E_e of the experimental secondary ion R.A. curves. If we are to match this effect with the continuous probability function of Fig. 3(a), we must use an implausibly large value of E_m. An alternative that gives a much better fit of the experimental R.A. curves is the assumption that there are two maxima in the $G(E)$ curve in the range $0<E<E_m$. This assumption implies that the bonding electron orbitals in the $C_3H_8^+$ ion form a high- and a low-energy band with relatively few intermediate vibronic states. An alternative possibility is that radiative transitions subsequent to ionization selectively depopulate the intermediate range of the parent-ion energy spectrum. For the purposes of this calculation we used the approxi-

[28] M. Krauss, A. L. Wahrhaftig, and M. Eyring, Ann. Rev. Nuclear Sci. **5**, 252 (1955).

[29] F. H. Field and J. L. Franklin, *Electron Impact Phenomena and the Properties of Gaseous Ions* (Academic Press, Inc., New York, 1957).

[30] L. Friedman, F. A. Long, and M. Wolfsberg, J. Chem. Phys. **31**, 755 (1959).

TABLE II. Parameters for calculating activation energies from appearance potentials.

Ion	A.P.[a]	ϵ_i'[c]	z_i[d]	ϵ_i[e]	ϵ_i[f]
$C_3H_8^+$	11.2_1[b]				
$C_3H_7^+$	11.7_3	0.52	5.0×10^9	0.31	0.52
$C_3H_6^+$	12.2_7	1.06	3.2×10^{12}	0.79	1.25
$C_2H_5^+$	12.2_3	1.02	1.8×10^{14}	0.85	1.38
$C_2H_4^+$	11.7_5	0.54	2.9×10^{11}	0.36	0.87

[a] Appearance potentials of these ions in the propane mass spectrum, ev, taken from Field and Franklin, footnote reference 29, pp. 254–260.
[b] First ionization potential of propane, I_s.
[c] ϵ_i'=A.P.$-I_s$, ev.
[d] Empirical frequency factors (Table I).
[e] Activation energies calculated from $z_i(1-\epsilon_i/\epsilon_i')^{12}(\epsilon_i'-\epsilon_i)^9 i=10^5$.
[f] Empirical activation energies (Table I).

mation that $G(E)$ is unity from 0.2 to 5 v, zero from 5 to 7 v, unity from 7 to 10 v, and zero for all higher energies. The shape of the $P(E)$ curves of Fig. 3(b) is a consequence of this assumption. The effect of these curves is to increase the range in E over which the secondary ion R.A.'s rise in importance. In a recent calculation of $\bar{E}$ for a large number of hydrocarbon parent ions Stevenson[11] concluded that the simple probability function $D(E)=1/E_m=\frac{1}{2}\bar{E}$ is quite satisfactory for use with the simplified quasi-equilibrium theory of mass spectra. This conclusion is based on comparatively good agreement between values of $\bar{E}$ calculated by two independent methods: the one based on an interpretation of appearance potentials yields $\bar{E}=3.1$ v for propane whereas the other method based on a simplified version of the statistical theory yields $\bar{E}=2.1$ v. The split probability function of Fig. 3(b) predicts that for $E_s=70$ v the average internal energy of $C_3H_8^+$ ions is 4.5 v. This disagreement with Stevenson's work is not conclusive evidence for or against the validity of the discontinuous probability function of Fig. 3(b). The value $\bar{E}=2.1$ v is obtained from a calculation based upon the experimentally determined R.A. of $C_3H_8^+$ in the propane mass spectrum. This information, however, can only predict the form of the energy level distribution $G(E)$ over the range for which E satisfies the relation $0<\sum_i k(E)<10^6$. The reliability of the value $\bar{E}=3.1$ v hinges on the correctness of the association of linear extrapolation appearance potentials with the average energy required for the formation of the ion in question plus neutral fragments (if any). This relationship, inferred from the work of Mariner and Bleakney,[31] is not proved.

Stevenson has suggested[11] that the apparent inconsistency of equating appearance potential differences to the activation energies of Eq. (2) can be circumvented by assuming that for the ith reaction $\epsilon_i'=\Delta$A.P. and $k_i(E)=10^5$ when $E=\epsilon_i'$. Using our empirical frequency factors and a set of experimental appearance potentials selected by Field and Franklin[29] (see Table II), we obtain from Stevenson's relation values of ϵ_i for the reaction of Fig. 1 that are about 0.6 times as large as our empirical activation energies. Just as we noted previously for small values of the exponent p, the calculated R. A. curves obtained with these smaller activation energies rise too steeply with increasing E to give a good fit of the experimental data. The inclusion in our calculation of a distribution in bombarding electron energies of the type $Ee^{-E/kT}$ may help to clarify the relationship between experimental appearance potentials and the activation energies of Eq. (2). However, the critical appraisal of such a calculation must be deferred until low voltage propane mass spectra have been obtained with a true monoenergetic electron beam.

ACKNOWLEDGMENT

We wish to thank Professor H. Eyring for several helpful suggestions made in the course of this work.

[31] T. Mariner and W. Bleakney, Phys. Rev. **72**, 807 (1947).

Low-Temperature Chemisorption. I. Flash Desorption of Nitrogen

GERT EHRLICH

General Electric Research Laboratory, Schenectady, New York

(Received May 23, 1960)

Flash desorption (desorption by continuous temperature displacement) is applied to a study of the low-temperature interactions of N_2 with an initially clean tungsten surface. Molecular nitrogen is found to dissociate into atoms on adsorption even at 115°K, at a rate which diminishes with increasing temperature, but is initially independent of surface concentration. Formation of this atomically bound β nitrogen is hindered at low temperatures ($T\sim115$°K) by competitive growth of an additional state γ, in which nitrogen, at $\sim2\frac{1}{2}$ times the concentration in the β state, is bound as molecules with an energy of 9 kcal mole^{-1}, resulting in a total surface concentration of 600×10^{12} molecules cm^{-2}. The population in this γ state depends sensitively upon the arrangement of atoms in the β state. Preadsorption at $T\sim300$°K equalizes the populations in β and γ; annealing at $T\sim1000$°K at impingement rates of 7×10^{15} molecules cm^{-2} min^{-1}, further lowers n_γ/n_β and brings about rearrangement of the tungsten surface as well, without appreciable change in the adatom concentration. A third state α is formed at temperatures up to 400°K, with a binding energy of $\sim$20 kcal mole^{-1}. Initially its rate of formation, just as that of γ at low temperatures, is dictated by the concentration of the atomically held β state. At 300°K and above the α concentration passes through a maximum, then diminishes; at low temperatures, it remains constant, achieving a maximum value 1/30 that of the γ state.

WITHIN the past five years the almost complete lack of information on the kinetics of molecular interactions with metals, which limited understanding of chemisorption phenomena in the past, has been eliminated and we now have at our disposal quantitative rate data on the behavior of simple gases, such as nitrogen, carbon monoxide, and hydrogen, brought into contact with initially clean surfaces at room temperature. These measurements have revealed an unexpected complexity even for such very simple systems, particularly the presence of adsorbed entities in a multitude of binding states with energies in excess of those expected for van der Waals forces. Rate studies under conditions favoring the stabilization of molecules in these states, that is at low temperatures, have so far not been carried out in any detail, and it is the purpose of this work to fill this gap, both for the intrinsic interest in the kinetics of formation of these states, as well as to characterize the nature of the interactions and the binding sites involved.

In this and the following paper we shall report on a detailed study of the interplay of both nitrogen and carbon monoxide with tungsten surfaces. The former is of interest because it dissociates on the surface and can exist there as strongly bound atoms. Nitrogen atoms, however, do not fill all available binding sites on the surface; the remaining sites can still interact with nitrogen molecules and we therefore have a mixed adsorption. Carbon monoxide, in contrast, does *not* lose its molecular identity on interacting with tungsten and therefore serves as a model for entirely molecular adsorption.

The formation and properties of both primary and secondary chemisorbed states have been examined in two ways: Quantitative measurements of adsorption and desorption kinetics have been carried out by the flash filament technique; more qualitative observations have been made in the field emission microscope by electron and ion emission. The first two papers will be devoted solely to the presentation of the experimental results obtained by the first method and rely upon the detailed kinetic analysis presented elsewhere.[1] The work with the field emission microscope, as well as discussion of the results of both types of measurements, will be reported separately.

EXPERIMENTAL TECHNIQUES

Achievement of pressures of the order of 10^{-10} mm is now routine, and we therefore only indicate modifications of our original methods, as well as deviations from the vacuum techniques suggested in Alpert's basic work.[2] The general procedures and equipment which we have adopted for adsorption studies under ultra-high vacuum conditions and for desorption measurements at variable temperatures have already been outlined, and we refer to previous papers for the more detailed experimental background.[3,4]

A. Ultra-High Vacuum Equipment and Procedures

A diagram of the ultra-high vacuum line used in most of these studies is shown in Fig. 1. The flash filament cell C is separated from the rest of the standard vacuum line by magnetically operated ground glass ports, D and E, which can be regulated to adjust the rate of loss of gas out of the cell during the actual measurements. The cell itself is designed for maximum conductance between the sample compartment and the gauge, the diameter of the constriction between the two being 4.1 cm. To establish good thermal contact with

[1] G. Ehrlich (to be published).
[2] D. Alpert, J. Appl. Phys. **24**, 869 (1953).
[3] G. Ehrlich, J. Phys. Chem. **60**, 1388 (1956).
[4] T. W. Hickmott and G. Ehrlich, J. Phys. Chem. Solids **5**, 47 (1958).

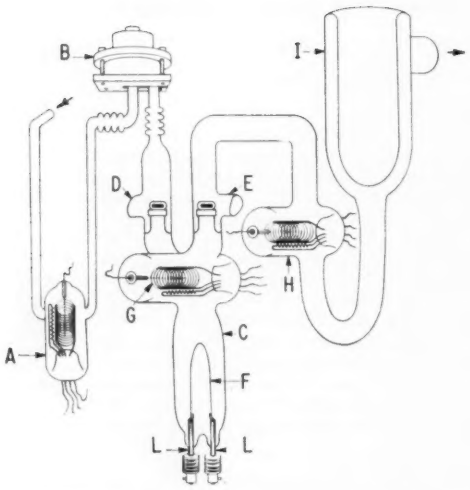

FIG. 1. Ultra-high vacuum equipment for ad- and desorption studies. *A*, *G*, and *H*, Bayard-Alpert inverted ionization gauges; *B*, Granville-Phillips vacuum valve, type C; *C*, flash filament cell, volume = 640 cc up to: *D*, *E*, magnetically operated ground-glass shutters; *F*, sample *W* filament; *I*, liquid nitrogen trap; *L*, glass-covered leads, Mo or W, 0.38 cm diam. Gas introduced into *A*, from 1-liter flask equipped with breakoff, pumped out through *I*.

the outside environment, the sample is arced onto heavy tungsten or molybdenum leads, *L*; these are covered with glass to within 1 cm of the sample ends, in order to minimize gas adsorption. During measurements at temperatures of 243°K and above, the cell up to the ports *D* and *E* is immersed in a thermostat bath, filled either with mineral oil or refined kerosene.

To achieve the vacua necessary for significant measurements ($p \sim 2 \times 10^{-10}$ mm) the system, with all ports and valves at their maximum opening, is subjected to several cycles of baking at 450°C for a minimum of six hours, followed by outgassing of the electrodes by induction or resistance heating. The system is continuously pumped by two mercury diffusion pumps in series, which are separated both from the ultra-high vacuum parts and from the mechanical fore pump by liquid-nitrogen-cooled traps. Cooling of the latter, which collects appreciable amounts of decomposed oil from the fore pump, is never interrupted as long as the trap is in the line, even when the system is at atmospheric pressure for adjustments. Pressures of the order of 10^{-10} mm are maintained in these lines solely through the action of the diffusion pumps, and *not* by the ionization gauges.

Once satisfactory vacua have been obtained we have in working with nitrogen flushed the system with gas from the sample bottle for 1 hr at a pressure of $\sim 10^{-1}$ mm in order to prevent evolution of other residuals when operating our gauges. We have not followed this procedure in studying carbon monoxide because of possible decomposition reactions with hot electrodes at high pressures; in any event this gas is the main impurity present in ultra-high systems of this type. With carbon monoxide it is also inadvisable to bake out the connecting tubing right up to the breakoff seal, since at ~200°C black decomposition products form at the top of the gas bulb. However, to avoid the possible accumulation of mercury our carbon monoxide sample flasks have been equipped with two breakoffs in series. The space between these is evacuated to $\sim 10^{-7}$ mm on an auxiliary line and our regular high temperature baking can then be accomplished right up to the second breakoff seal without difficulties.

B. Adsorption and Gas Samples

All measurements reported here have been on tungsten wires of nominal 2.54×10^{-2} cm diam, from the same spool of prewar 218 tungsten, which were aged at $T > 2600$°K.[3] Prior to this, some were cleaned by electrolytic etching in sodium hydroxide. The wire as received had already been freed of the graphite coating, which it acquires in the drawing process, by caustic cleaning and by annealing in wet hydrogen. Typical impurity concentrations in such a tungsten sample after flashing in vacuum are given as[5]: Mo, 0.002–0.005%; Na, K, Al, Si, Ca, Cr, Fe, Ni, and Cu, less than 0.001%. The carbon content of wire from our spool was determined as 0.006–0.002% by weight. Tungsten emitters fabricated from similar material have been studied in the field emission microscope and have given patterns typical of a clean surface after heating at only 2300°K.

Effective areas for the samples discussed in these reports are: Filament 1, 0.92 cm²; 2, 1.54 cm²; 3, 1.21 cm²; and 7, 1.18 cm². The last of these had been reduced in diameter to 0.239 cm by electrolytic etching.

In routine desorption measurements samples were flashed by connecting to the secondaries of a transformer, set at a voltage which under steady-state conditions maintains the filament at 2200°K. For temperature measurements during desorption we have generally used a bridge circuit in which the filament is heated by a constant current, and the temperature T rises with time t as $1/T = a_0 + b_0 t$.[4] To achieve higher heating rates, we have connected the sample filament directly to storage batteries, and have determined the temperature during heating from the instantaneous potentials across the filament and a standard resistor in the series with it. This technique will be described in detail later. Maximum temperature rise of the 0.380-cm leads when the sample is at 2200°K is estimated at 47°K; this temperature is achieved slowly, rising less than 11° during the first 1½ sec after the start of heating.

The assayed reagent-grade nitrogen and carbon monoxide used in these studies was obtained in 1-liter Pyrex bottles from Airco. Impurities present varied

[5] I am greatly indebted to Dr. C. H. Toensing, G.E. Lamp Division, Cleveland, Ohio, for supplying both the tungsten samples as well as their specifications.

during the four-year period over which measurements are recorded. The best nitrogen was listed as having no impurities above the mass-spectroscopic resolution of 0.005 mole %. For carbon monoxide gas purity was lower, the best samples containing 0.04 mole % carbon dioxide and 0.03 mole % hydrogen. Differences in impurity content did not result in any observable changes in adsorption or desorption experiments.

C. Pressure Measurements

Both in the flash filament cell and outside it (at G and H in Fig. 1) the gas density is monitored by Bayard-Alpert gauges, WL-5966. In the cell the electrodes from a standard gauge were mounted in a cylindrical 7740 Pyrex envelope, slightly larger than that in the commercial design (o.d. 5.72 cm compared with 5.08 cm) to reduce heating of the walls. Gauge H, between the cell and liquid nitrogen trap I, was altered only by substitution of 3-cm glass tubulation for the original 1.2-cm tubulation.

For adsorption measurements gauge G, in the cell, was operated at an emission current $i_e = 5\times10^{-4}$ amp, with cathode at $V_c = +25$ v, grid at $V_g = +170$ v, and the ion collector at no more than +0.5 v above ground. The cathodes are heated with dc from storage batteries to eliminate the 120-cycle ripple in electron emission which arises from the heating and cooling of the cathode when operated on alternating current. Gauge H, used only as an auxiliary pressure monitor, operated at a regulated emission of 5×10^{-3} amp.

Calibration of the gauges was established at pressures of 5.6×10^{-4} mm or less against a sensitive McCleod (designed by T. W. Hickmott). Gauge constants were determined at $g = 11$ and 12 mm^{-1} for nitrogen and carbon monoxide at $T = 298°K$. Our previous calibration,[3] which suggested $g = 15$ mm^{-1}, was performed on a McCleod only $\frac{1}{12}$ as sensitive, and at best these early measurements were reliable to only ±25%. It must be noted that errors in the gauge constant influence only the absolute values of the surface concentrations and have no effect upon the sticking coefficients or estimates of activation energy.

During the adsorption stage ion currents have been measured with a Keithley dc indicating amplifier, the output of which is displayed on a Speedomax G recorder. The details of the ion current rise when gas is desorbed during rapid heating of the filament have been recorded photographically using a Tektronix 532 oscilloscope, equipped with a high-gain dc preamplifier, type 53/54D, as a detector. A detailed description of the techniques for interpreting and evaluating these desorption traces is contained in a separate report.[1]

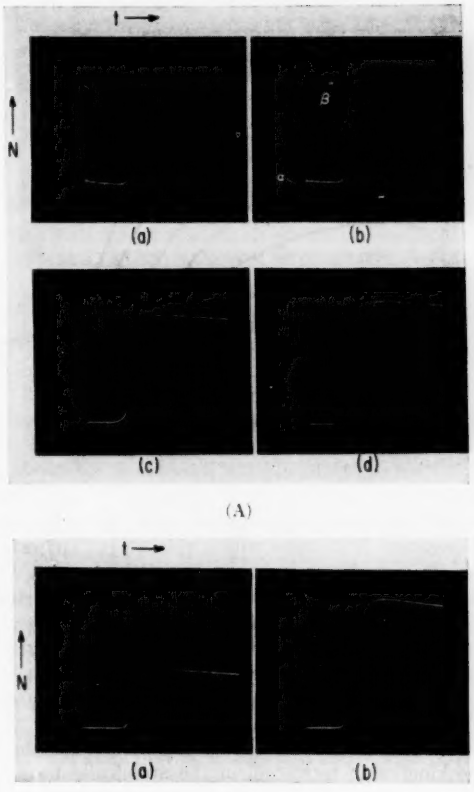

FIG. 2(A). Growth of α and β states during adsorption of N_2 at $T = 243°K$. Filament 3. Time scale: 1 cm = 100 msec. (a) $\Delta t = 4$ min, $n_\alpha = 6.5\times10^{12}$ molecules cm^{-2}, $n_\beta = 39\times10^{12}$; (b) $\Delta t = 12$, $n_\alpha = 16\times10^{12}$, $n_\beta = 114\times10^{12}$; (c) $\Delta t = 21$, $n_\alpha = 14\times10^{12}$, $n_\beta = 204\times10^{12}$; (d) $\Delta t = 26$, $n_\alpha = 13\times10^{12}$, $n_\beta = 233\times10^{12}$. (B). α and β states during adsorption of N_2 at $T = 373°K$. Filament 3. Time scale: 1 cm = 100 msec. (a) $\Delta t = 11$ min, $n_\alpha = 0.7\times10^{12}$ molecules cm^{-2}, $n_\beta = 58\times10^{12}$; (b) $\Delta t = 27$, $n_\alpha = 1.3\times10^{12}$, $n_\beta = 125\times10^{12}$.

KINETICS OF NITROGEN AD- AND DESORPTION

A. Chemisorption at Room Temperature

The phenomena observed when molecular nitrogen is allowed to interact with a bare surface kept at room temperature or above have already been outlined.[3,4,6] Here we shall emphasize those interactions that involve the more weakly bound adsorbed entities, and occur in the range of temperatures around $T = 100°K$.[7] In order to establish the behavior of the primary chemisorbed state on our samples and to check our previous experimental findings we have carried out extensive rate measurements at higher temperatures as well (using more rapid, more sensitive ion-current detectors than heretofore); we shall summarize these briefly.

At $T \sim 300°K$, nitrogen adsorbs on tungsten in two states: the weakly bound α and the primary chemi-

[6] J. A. Becker and C. D. Hartman, J. Phys. Chem. **57**, 157 (1953).

[7] A preliminary presentation of parts of the following has been given at the Gordon Research Conference on Catalysis, 1956, and at the International Conference on Structure and Properties of Thin Films, Bolton Landing, September, 1959.

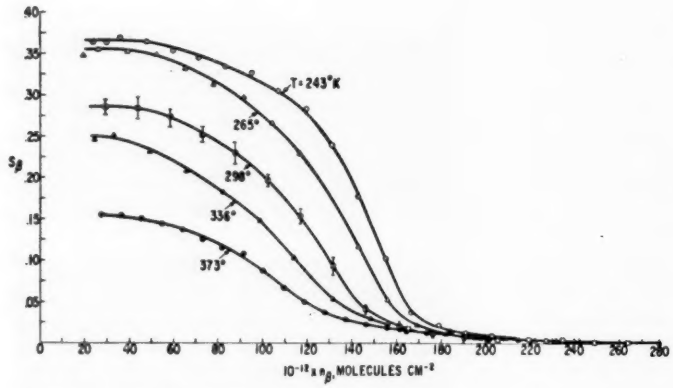

FIG. 3. Sticking probability for formation of β nitrogen on filament 3, as a function of surface concentration n_β and of temperature.

sorbed entity, designated as β. These are clearly resolved in the desorption traces shown in Fig. 2, obtained after adsorption at 243°K and 373°K, respectively. No other breaks in the evolution curve appear as the concentration of adsorbed gas increases, or as the adsorption temperature is changed within this range. The evolution curve itself has a characteristic S shape and with increasing coverage the evolution of the β state starts at lower times after the initiation of heating. These are the criteria for a second-order desorption[1] (and therefore for dissociation into atoms) of nitrogen held in this state, which has been established by more detailed measurements.[3,4]

We shall consider the more weakly held α state later. The kinetics of formation of the atomically bound β state are given (for sample No. 3) as a function of temperature and surface concentration in Fig. 3. Here the sticking coefficient s has been obtained as the ratio of the net rate of increase of the surface concentration, dn/dt, to the instantaneous rate of supply of gas to the surface by Knudsen flow, $p(2\pi mkT)^{-\frac{1}{2}} = pZ$. Evaporation has been neglected, as the desorption traces in Fig. 2 indicate that this is insignificant in the range of room temperature.

The validity of assuming an adsorption process of the first order with respect to the concentration of molecules in the gas phase (which is implicit in our estimates of s) is demonstrated by rate measurements at different pressures, summarized in Fig. 4. The rate of adsorption is linear in the impingement rate for a 3.5-fold increase in pressures; in contrast, a plot of the rate as a function of $p^{\frac{1}{2}}$ not only shows considerably more scatter, but also fails to pass through the origin as is required in the absence of evaporation. The limiting process in the adsorption step thus must involve the undissociated molecule.

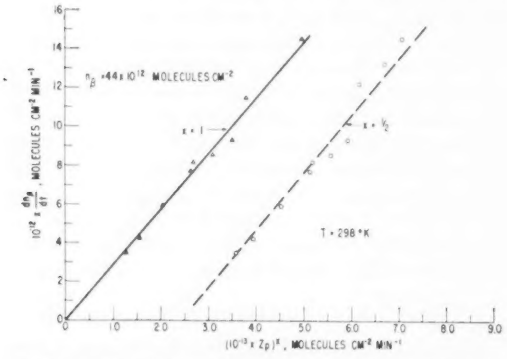

FIG. 4. Rate of formation of β nitrogen on filament 3 as a function of impingement rate Zp at constant surface concentration and temperature.

The rate of formation of β nitrogen on this surface qualitatively follows the course established for other specimens. With the gas and adsorption sample at 300°K or below, the sticking probability is initially high ($0.1 < s < 0.4$) and independent of the concentration of adsorbed gas. The rate then diminishes gradually with increasing concentration, but maintains itself at a small but finite value ($\sim 10^{-3}$) even close to saturation at these pressures ($p \sim 2 \times 10^{-7}$ mm). The absolute value of the sticking coefficient diminishes as the temperature is increased, from 0.36 at $n_\beta \sim 30 \times 10^{12}$ molecules cm^{-2} for $T = 243$°K, to 0.15 at 373°K and the same concentration. With increasing temperature, the onset of the initial concentration dependence of the rate is also shifted towards lower surface concentrations and above 300°K a clearly defined initial region of constant sticking probability is not apparent. Similarly the first inflection point, which marks the change in the rate of diminution of the sticking coefficient at larger values of n_β, also makes its appearance at lower concentrations the higher the temperature. Only at the highest concentrations of nitrogen in the β state ($n_\beta \geq 190 \times 10^{12}$ molecules cm^{-2}), at which the sticking probability has diminished to $\sim 1/20$ of its initial value, do the rates of adsorption become much the same independent of temperature.

The diminution of the rate with increasing temperature is outside the range of error of our measurements.[8]

[8] Absence of any significant variation with temperature has recently been claimed by P. Kisliuk [J. Chem. Phys. **30**, 174 (1959)].

For the rate determinations at 298°K we have in Fig. 3 indicated the average deviation from the mean of 9 runs at different pressures, carried out over a period of more than six months. At low coverages ($n<120\times10^{12}$ molecules cm^{-2}), this deviation amounts to $\sim5\%$ of the mean. Also, despite qualitative similarities it appears from Fig. 5, that the rates of formation of the atomically bound β nitrogen on this filament differ considerably from those found on previous samples. The sticking coefficient, although initially almost three times as great as on filament No. 1 and No. 2, maintains its constancy over a much smaller concentration range, suggesting significant differences in the surface structure of the samples.

B. Chemisorption at Low Temperatures ($T\sim100$°K)

Measurements so far reported have been taken under essentially isothermal conditions.[9] For the adsorption studies at $T<243$°K, which we now outline, only the sample filament has been cooled by immersing the leads in an appropriate refrigerant, and the cell has been kept at room temperature ($T_G\sim300$°K). In these measurements the gas interacting with the sample is thus at the temperature of the cell walls.

With the tungsten filament cooled to $T=115$°K an additional state, of binding energy even lower than that of α, makes its appearance. Desorption traces showing the growth of this state, which we have designated γ, as well as of α and β, when the adsorption interval is increased are displayed in Fig. 6. The size of this additional γ peak exceeds that of β once rapid adsorption of nitrogen has ceased, and the total gas concentration in all states at saturation (at $2<p<6\times10^{-7}$ mm) is double that at 300°K. These traces also show very clearly the displacement of the evolution curve of the β peak toward lower times as the initial concentration is increased, already noted as typical of second-order reactions. Rates of adsorption under these conditions have been plotted in Fig. 7 as the ratio of the net increase in surface concentration per unit time to the rate of supply of gas to the surface.

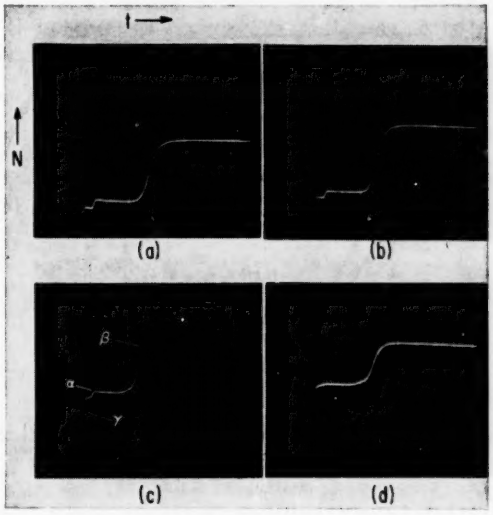

FIG. 6. Formation of α, β, and γ nitrogen during adsorption at $T=115$°K. Filament 3. Time scale: 1 cm = 100 msec. (a) $\Delta t=3$ min, $n_\gamma=4.8\times10^{12}$ molecules cm^{-2}, $n_\alpha=7.5\times10^{12}$, $n_\beta=55\times10^{12}$; (b) $\Delta t=8$, $n_\gamma=32\times10^{12}$, $n_\alpha=12\times10^{12}$, $n_\beta=120\times10^{12}$; (c) $\Delta t=14$, $n_\gamma=100\times10^{12}$, $n_\alpha=12\times10^{12}$, $n_\beta=163\times10^{12}$; (d) $\Delta t=45$, $n_\gamma=342\times10^{12}$, $n_\beta=218\times10^{12}$.

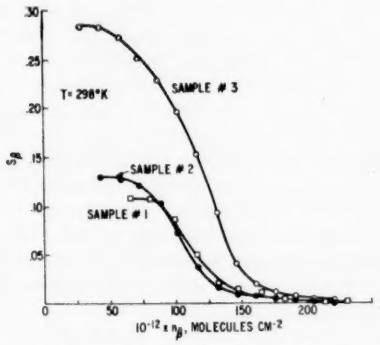

FIG. 5. Sticking probability for β nitrogen on filaments 1, 2, and 3 as a function of surface concentration n_β.

Most striking is the initial high value of the sticking coefficient (for all forms of adsorbed nitrogen $s=0.51$) and the extended concentration range, up to 350×10^{12} molecules cm^{-2} in all states, over which the rate remains constant. This is to be compared with an initial sticking probability, for all states populated at room temperature, of 0.33 which diminishes sharply for $n>75\times10^{12}$ molecules cm^{-2}. Inspection of the data in Fig. 7 also reveals that the rate of formation of the β state itself is somewhat higher at $T=115$°K than at 300°K. The initial sticking coefficients for this state at the two temperatures are $s=0.38$ and 0.29, respectively. At $T=115$°K the rate is comparable to that (found in Fig. 3) for adsorption in an isothermal system at 243°K, both in the absolute value of the sticking probability and its concentration dependence up to $n_\beta\sim200\times10^{12}$ molecules cm^{-2}.

The high rate of adsorption at the low temperatures is thus due to the binding of nitrogen in an additional state γ, which in the range of room temperatures is not significantly populated. Adsorption of nitrogen on tungsten at $T=115$°K also differs from that at higher temperatures in the total amount of the β material that can be formed. At $T=265$°K, for example, up to 280×10^{12} molecules cm^{-2} of β can be adsorbed at a

[9] Only the cathode filament of the ionization gauge in the cell deviates from the temperature of the surrounding thermostat bath. Inasmuch as the gauge is not in a direct line with the adsorption sample, energetic molecules emanating from the cathode are deactivated by the cell walls and therefore should have little effect on the over-all kinetics.

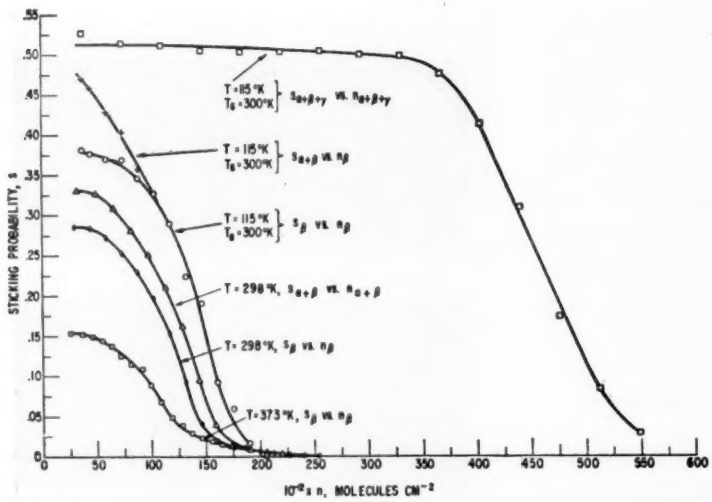
STICKING PROBABILITY, s
10^{-12} n, MOLECULES CM^{-2}
T = 85°K, T_0 = 300°K } $s_{\alpha+\beta+\gamma}$ vs. $n_{\alpha+\beta+\gamma}$
T = 115°K, T_0 = 300°K } $s_{\alpha+\beta}$ vs. n_β
T = 115°K, T_0 = 300°K } s_β vs. n_β
T = 298°K, $s_{\alpha+\beta}$ vs. $n_{\alpha+\beta}$
T = 298°K, s_β vs. n_β
T = 373°K, s_β vs. n_β

FIG. 7. Sticking probability for adsorption of nitrogen on filament 3, as a function of surface concentration n and temperature. T = surface temperature, T_G = gas temperature.

finite rate (as evident in Fig. 3); at $T = 115°K$, however, the maximum concentration of β on the sample was reduced to $\sim 225 \times 10^{12}$ molecules cm^{-2} (Fig. 7). The initial adsorption of β at $T = 115°K$ shows *no* sign of being an activated process. However, at high-surface concentrations ($n_\beta > 200 \times 10^{12}$ molecules cm^{-2}), the sticking probability for β does fall below the values at higher temperatures, indicating for the low-temperature experiments an activation barrier, and therefore also a different mechanism of formation, which must be connected with the presence of the additional γ state.

C. Low-Temperature γ State

1. Kinetics of Formation and Evaporation

The sequence in Fig. 6 demonstrates that during the initial stages of adsorption molecules in the γ peak contribute little to the over-all surface population, and that only towards the conclusion of adsorption does the γ state assume overwhelming proportions. The details of the filling up of this state are given in Fig. 8(a), which shows the γ population as a function of the number adsorbed in the β state at different nitrogen pressures. At a given surface concentration of β, the number of molecules in the γ state is fixed and independent of the pressure, which in these experiments was varied by a factor of 2.75 (for $n_\beta = 117 \times 10^{12}$ molecules cm^{-2}). At a slightly higher filament temperature ($T \sim 125°K$) the data in Fig. 8(b) are suggestive of a possible lowering of the concentration of γ at lower pressures, for $n_\beta > 150 \times 10^{12}$ molecules cm^{-2}.

The total amounts of nitrogen in the γ state at saturation are roughly comparable at these two temperatures. In adsorption runs at higher pressures (for which saturation can be accomplished in less than 1 hr) the γ population goes through a maximum and then diminishes as the sample is maintained at this temperature. This effect (which has also been observed in measurements of the γ peak at high pressures on filament 2, Fig. 9), suggests a competition between the rates of formation of the two states even at the highest coverages. The qualitative dependence of n_γ upon the β population on sample 2 resembles that described for No. 3. The measurements on the former, shown in Fig. 9 were made in a higher pressure range (and at a less well-defined temperature) and at higher concentrations of β a definite increase in γ with increasing impingement rate emerges. The saturation ratio (n_γ/n_β) on this filament is also higher than on filament 3.

The evolution kinetics of material in the γ state are quite different from those in the high-temperature β peak. In Fig. 10 are shown desorption traces for γ at concentrations differing by a factor of 2. At the higher concentration the onset of gas evolution has shifted towards a lower time, but completion of the evolution occurs at the same instant for both.[10] The former characteristic eliminates the possibility of a simple first-order reaction, while the latter cannot occur for a second-order evolution. Such kinetics resemble those for a first-order reaction, with the heat diminishing at higher surface concentration.[1] We therefore conclude from these measurements that nitrogen in the γ state is held in the form of molecules.[11] The temperature range of the desorption (and the absence of a significant pressure dependence for the rate of formation at 115°K) indicate a binding energy of the order of 9 kcal mole^{-1} for this molecularly bound state.

2. Nature of Binding Sites

A dependence of the rate of γ formation upon the number of nitrogen atoms in the β state is suggested by

[10] The significance of the sharp change in slope beyond the midway mark still remains to be established.

[11] Or as pairs isolated from one another.

the curves in Fig. 8. In order to test how the arrangement of the β nitrogen may affect the weaker γ, the sample filament was first allowed to adsorb nitrogen at 300°K for a predetermined interval, and only then was brought to saturation at 115°K and an impingement rate of 18×10^{15} molecules cm^{-2} min^{-1}. The desorption traces in Fig. 11, obtained after this cycle, show that the larger the quantity of nitrogen preadsorbed at room temperature the smaller the amount that can subsequently be taken up in the γ state. The quantitative

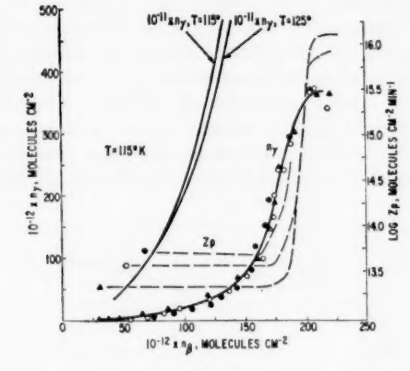

(a)

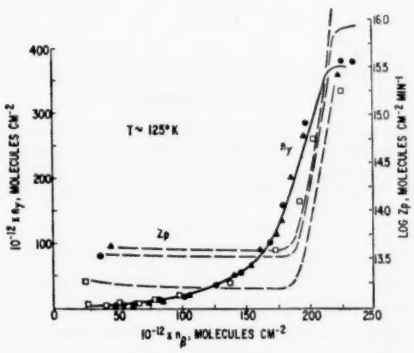

(b)

FIG. 8. Instantaneous concentration of nitrogen in γ and β states during adsorption runs at different pressures on filament 3. (a) $T=115$°K; (b) $T\sim125$°K.

display of these experiments for filaments 2 and 3 in Fig. 12, giving the total number of molecules in the γ state as a function of the total number of β molecules at saturation, suggests an essentially linear diminution of n_γ with increasing n_β: each additional β molecule introduced at room temperature eliminates 2.5γ at the lower temperatures.

Even more significant changes in the concentration of the low-temperature γ state can be brought about by heating the sample above room temperature while exposed to nitrogen, prior to allowing adsorption at 115°K. On filament 7, we have $n_\beta/n_\gamma=0.41$ after saturation entirely at 115°K, which is comparable to the saturation ratio on filament 2. When the sample is saturated with nitrogen at 300°K before adsorption at 115°K (all at an impingement rate of $\sim7\times10^{15}$ molecules cm^{-2} min^{-1}), n_β/n_γ increases to unity. As shown in Fig. 13 this ratio rises still further if the sample is first maintained at 970°K, then is saturated at room temperature and, before testing the formation of γ, at 115°K. The longer the time interval at the high temperature, the higher n_β/n_γ, reaching a value of more than two when high-temperature annealing is carried out for five hours. The effects of this annealing procedure are not completely reversible, moreover. After a 2-hr high-temperature anneal, $n_\beta/n_\gamma=1.7$. In the very next determination, after only room-temperature saturation, this ratio is still 1.14, compared with the initial value of unity.

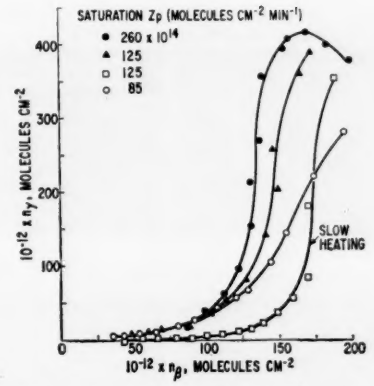

FIG. 9. Instantaneous concentration of nitrogen in γ a and β states during adsorption runs at different pressures on filment 2. $T\sim115$°K. Desorption times: Normal~30 msec; slow heating~800 msec.

The nature of this irreversibility has been more firmly established by the following procedure. Subsequent to a 2-hr anneal at 970°K and saturation at 300°K, the filament was flashed twice for a 1-sec interval, sufficient to remove the adsorbed gas. The filament was then saturated once more at room temperature and tested at

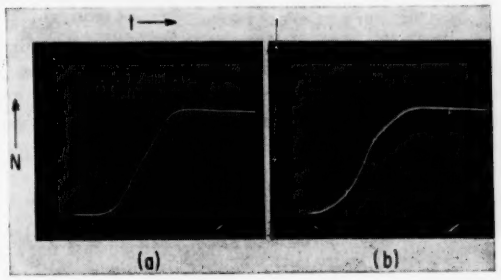

FIG. 10. Desorption of nitrogen in γ state. Adsorption temperature $T=115$°K. Filament 3. Time scale: 1 cm=200 msec. (a) $\Delta t=25$ min, $n_\gamma=184\times10^{12}$ molecules cm^{-2}; (b) $\Delta t=51$, $n_\gamma=266\times10^{12}$. Concentrations not corrected for pumping.

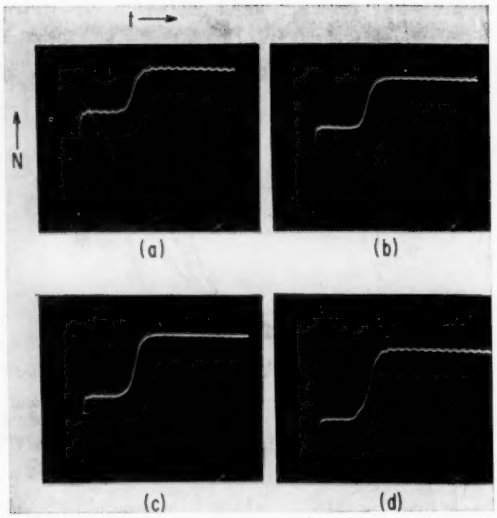

FIG. 11. Effect of preadsorption of N_2 at $T=298°K$ upon saturation concentration in γ and β states at $T\sim115°K$. Filament 2. Time scale: 1 cm = 100 msec. (a) $\Delta t_{298}=0$ min, $n_\beta=167\times10^{12}$ molecules cm^{-2}, $n_\gamma=403\times10^{12}$; (b) $\Delta t_{298}=6\frac{3}{4}$, $n_\beta=196\times10^{12}$, $n_\gamma=338\times10^{12}$; (c) $\Delta t_{298}=11$, $n_\beta=236\times10^{12}$, $n_\gamma=253\times10^{12}$; (d) $\Delta t_{298}=23$, $n_\beta=268\times10^{12}$, $n_\gamma=174\times10^{12}$. Saturation $Zp\sim18\times10^{15}$ molecules cm^{-2} min^{-1}.

115°K. After this cycle the ratio n_β/n_γ still exceeded 1.3, as indicated in Fig. 13. It follows that these changes in the relative population of γ and β are *not* brought about solely by a redistribution of the β material over the surface during the high-temperature anneal—all the adsorbed molecules are removed in the flash, yet there remains an after effect; this must arise from a change in the surface structure of the sample itself.

Diffusion of W atoms away from steps on their own lattice requires an activation energy of 73 kcal mole^{-1},[12,13] and at 970°K the tungsten surface should therefore be able to arrange itself into a configuration minimizing the total surface free energy,

$$\int \sigma dA;$$

σ is now the surface energy in the presence of adsorbed nitrogen, and not that of the clean interface, which dictates the structure during the initial preparation of the sample. During the ~100 msec required for nitrogen desorption, the rearrangement of the surface is negligible, and the desorption kinetics are characteristic of the surface on which adsorption measurements have been made. However, in calorimetric or isotherm measurements at temperatures which insure the mobility of nitrogen atoms over the W surface ($T>650°K$)[14] such rearrangement should occur. Comparison of these [15] with determinations at lower temperatures thus must involve both differences in the distribution of adatoms dictated by equilibrium and by rate considerations, and differences in the surface structure, which are difficult to disentangle.

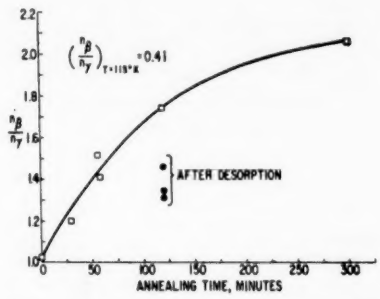

FIG. 13. Ratio of nitrogen concentration in β state to that in γ state, after saturation at $T=115°K$, $Zp\sim7\times10^{15}$ molecules cm^{-2} min^{-1}, on filament 7. □ Heated at $T=970°K$, $Zp\sim7\times10^{15}$, then saturated at $T=300°K$. ● Flashed after anneal at 970°K, then saturated at $T=300°K$.

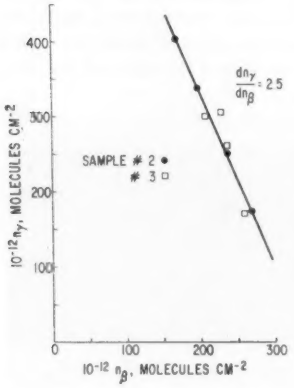

FIG. 12. Concentration of nitrogen in γ state after saturation at $T\sim115°K$, for β concentrations achieved by preadsorption at $T=300°K$. Saturation impingement rate: ● 18×10^{15} molecules cm^{-2} min^{-1} □ 7×10^{15}.

The results of Fig. 12 indicate that the rearrangement of only the nitrogen atoms on the surface does affect the subsequent formation of γ; all our experiments therefore point to a competitive adsorption of nitrogen, either as atoms (β) or molecules (γ) with the latter held at highly specific sites, created on the lattice by the presence of the adatoms, and interfering with the further adsorption of nitrogen in the β state. Measurements of the *absolute* amounts of nitrogen adsorbed after annealing at 970°K have not been carried out with the accuracy of our other determinations; they do show, however, that although high-temperature annealing very drastically lowers the number of nitrogen molecules that can be accommodated in the γ state, the atomic population in the β state is *not* significantly altered, nor is the evolution curve for β.

[12] E. W. Müller, Z. Physik **126**, 642 (1949).
[13] W. P. Dyke and W. W. Dolan, Advances in Electronics and Electron Phys. **8**, 89 (1956).
[14] G. Ehrlich and F. G. Hudda, J. Chem. Phys. **32**, 942 (1960).
[15] P. Kisliuk, J. Chem. Phys. **31**, 1605 (1959).

3. *Conversion to Ad atoms*

Both in this, and in the previous discussion of β formation, we have tacitly assumed that the desorption trace mirrors the distribution of molecules on the surface during adsorption at low temperatures; that is, we have assumed that during the heating of the filament no interconversion between states occurs. That conversion *can* take place during desorption is suggested by a comparison of the plots of n_γ vs n_β in Fig. 9; these have been obtained on sample 2 under normal heating conditions (by imposing a constant voltage on the filament), for which the evolution of γ is complete in $\sim$30 msec, and under slower heating (obtained by passing a constant current through the sample) giving an evolution time of $\sim$800 msec for the γ state. The shape of the two curves is qualitatively the same, but for a fixed surface concentration of the atomically held β material the slow heating gives significantly less of the γ. That such conversion does not affect our measurements as usually performed was established by increasing the heating rate still further till evolution was complete in less than 15 msec. After correction for differences in pumping these measurements were identical to those for normal heating (at $\sim\frac{1}{2}$ the rate).

It may be argued that some of the γ material converts so rapidly that the change to β cannot be prevented, even at our highest heating rate. This would, however, imply such fast conversion that it should already go to completion during the long adsorption interval at 115°K, and certainly at 125°K. More precisely, the fact that an increase in the heating rate does not affect the amount of material in the γ state indicates[1] that on the time scale of the evolution reaction the conversion has become negligible. Conversion prior to the onset of evolution is still possible. However, for the β population to have arisen entirely by conversion prior to the evolution of γ we estimate a rate constant for conversion $k_c \sim 4\times10^{-2}$ sec^{-1} at 125°K. For a simple first-order conversion reaction in competition with adsorption (at a constant pressure) into the γ state directly, the concentration of γ would be just

$$n_\gamma = (Zps/k_c)[1-\exp(-k_c t)].$$

Our estimate of k_c indicates a maximum concentration of γ less than one-hundredth of that actually found. Moreover, the changes in n_γ brought about by the slow heating appear to occur primarily by readsorption of the desorbed gas into the β state—the decay constant for pumping out just after the evolution of the γ has the unusually high value of $S_E/V \sim 5$ sec^{-1}. The absence of conversion of γ to β during the desorption is also strongly suggested by the fact that the rates of formation of β at 115°K and 243°K are comparable. At the lower temperature the *total* rate of adsorption is considerably higher, however, and we would therefore expect a significantly higher concentration of β if conversion had been an important effect. We can therefore conclude that conversion of γ during the temperature rise does not determine the β peak as found by desorption—this is dictated by the kinetics of the *adsorption* process.

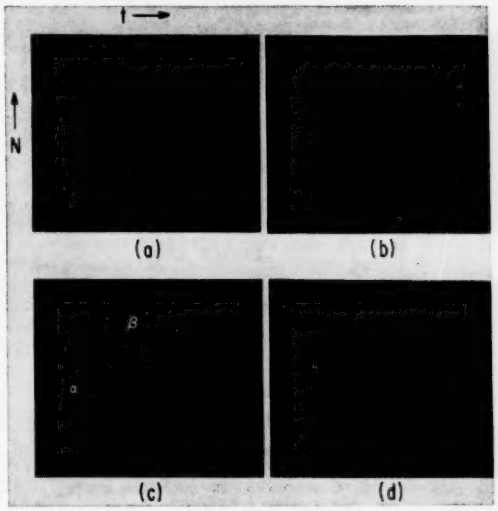

FIG. 14. Growth of α state during adsorption of nitrogen at $T=243°$K. Filament 3. Time scale: 1 cm = 50 msec. Concentration in α state: (a) $\Delta t=4$ min, $n_\alpha=6.5\times10^{12}$ molecules cm^{-2}; (b) $\Delta t=12$, $n_\alpha=16\times10^{12}$; (c) $\Delta t=21$, $n_\alpha=14\times10^{12}$; (d) $\Delta t=26$, $n_\alpha=13\times10^{12}$. β concentrations as in Fig. 2 (A).

D. Formation of the α State

The growth of the α state on increasing the adsorption interval is apparent in the desorption traces of Fig. 14 which were obtained on an enlarged scale for the same over-all concentrations depicted in Fig. 2. At higher concentrations of β the total amount of material in the α peak actually falls and the onset of evolution moves toward lower times. Our data are not sufficient, however, to distinguish between the various possible desorption mechanisms.

It has been shown previously that at higher temperatures the maximum concentration of α that can be achieved diminishes.[3] The α peak is still present when adsorption is carried out at 115°K, as is evident from the desorption traces of the previous section (Fig. 6). The amount of material in this peak does not increase monotonically; just as at the higher temperatures the concentration of α is initially a function *only* of the concentration of nitrogen in the β state, but as shown in Fig. 15 the maximum concentration of the α is comparable at 115° and 300°K. There is no indication that at 115°K the concentration of α actually diminishes as the surface approaches saturation. However, in the desorption traces at saturation the contribution of the α peak has become negligible on the scale of the *total* surface concentration, making up only $\sim$2% of the total peak height, and is thus just barely perceptible

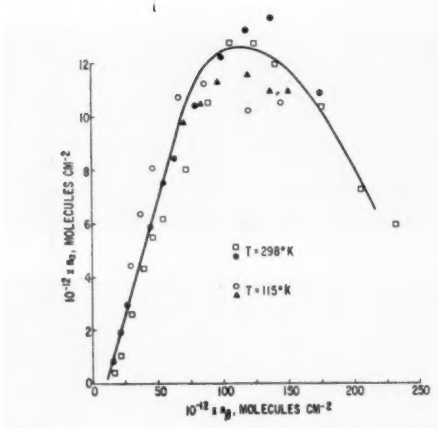

FIG. 15. Instantaneous concentration of nitrogen in α and β states during adsorption on filament 3. Impingement rates (Zp, molecules cm^{-2} min^{-1}) at $n_\beta = 73\times10^{12}$ molecules cm^{-2}: □ 3.6×10^{12}; ● 2.4×10^{12}; ○ 2.2×10^{12}; ▲ 3.7×10^{13}.

in Figs. 6 and 11. From the maximum concentration at 298°K we estimate a binding energy of the order of 20 kcal $mole^{-1}$ for nitrogen held on α sites.

Just as for the γ state we must examine the possibility that the amount of α nitrogen formed in the adsorption step is significantly altered in observing desorption. At 300°K, the distribution of gas over the two peaks does depend upon the rate at which the sample is heated. Under the ordinary schedule, the evolution of α formed at room temperature is complete in ~35 msec. Lowering the rate of temperature rise, until the evolution occurs over a period of 500 msec, lowers the amount of α evolved by only 30%. Just as in the discussion of the possible conversion of γ, the conversion of the α to the β cannot occur so rapidly that the change in heating rate has no effect, inasmuch as it would then have to go to completion during the adsorption step itself.

It is significant that for the desorption pictures obtained after exposing the sample to nitrogen at 115°K, the amount of material found in the α state is in good accord with the observations at 243°K and above. This shows that conversion of γ to the α state has not played an important part. Under standard operating conditions evolution of α is complete ~100 msec after heating the filament, originally at 115°K. An increase of the time interval necessary for desorption to 1.5 sec reduces the size of the peak (uncorrected for any pumping effects) by only 40%. A decrease of the desorption time by a factor of 0.5 increases the amount of α evolved by less than 10%. We conclude that for conversion to be important during the temperature rise of the desorption, it would also have to be rapid at the adsorption temperature. That is, our measurements indicate that the α peak found after low temperature adsorption is again the result of the particular *adsorption* kinetics of the system nitrogen on tungsten. This result is buttressed by the agreement with the concentration of α formed at higher temperatures, where the immediate formation of β has already been demonstrated.

SUMMARY

The formation of the two low-temperature states of nitrogen on tungsten is similar, in that initially the concentration of both α and γ is fixed by the quantity of the atomically held β nitrogen. However, whereas the α population increases fairly linearly with β, nitrogen in the γ state rises almost exponentially as the β concentration increases. The implications of these kinetics will be detailed in a subsequent report.

It should be noted that these weak states are bound to the surface by other than van der Waals forces—the binding energy even of the γ state on tungsten is comparable to that of Xe,[16] with a polarizability twice the mean value for nitrogen. Formation of both α and γ states occurs on well-defined sites. The total number of these for γ is ~30 times that of α, although the binding energy for α is approximately twice as large. For γ we have established that the gas is held to the surface as molecules, and that it preempts sites on the surface that can be occupied by nitrogen atoms.

Our low-temperature measurements demonstrate directly (for the first time) that molecular nitrogen gas adsorbs on tungsten as atoms in the β state, both at 300° and 115°K, and that the initial dissociation on the surface does *not* slow down even at these low temperatures.

[16] G. Ehrlich and F. G. Hudda, J. Chem. Phys. **30**, 493 (1959).

Low-Temperature Chemisorption. II. Flash Desorption of Carbon Monoxide

GERT EHRLICH

General Electric Research Laboratory, Schenectady, New York

(Received July 25, 1960)

Flash desorption studies of the interaction of carbon monoxide with a tungsten surface indicate that this gas forms at an initial rate considerably higher than that for nitrogen (CO sticking coefficient: $s\sim0.5$; N_2 sticking coefficient: $s\sim0.25$). This rate also remains independent of the amount adsorbed for higher coverages, up to $n\sim300\times10^{12}$ molecules cm^{-2}. Unlike nitrogen, CO does not dissociate on the surface. It retains its molecular identity in both the primary chemisorbed state β, and the weaker state of 20 kcal $mole^{-1}$ binding energy α, which forms as the rate of β growth diminishes. At $T=298°K$, the α state reaches a concentration of $\sim200\times10^{12}$ molecules cm^{-2}. No additional weak binding is found even at low temperatures, $T\sim115°K$. The β state is itself made up of three subpeaks, arising from different surface structures, and designated β_1, β_2, and β_3 in order of increasing binding energy. Only β_2 and β_3 form initially, with desorption energies of 75 and 100 kcal $mole^{-1}$, respectively; β_1 appears at higher coverages, at which the desorption energy of β_2 has also diminished.

ALTHOUGH carbon monoxide is isoelectronic with nitrogen, it does not dissociate on tungsten and its behavior is remarkably different from that of nitrogen, presented in the previous paper.[1] A preliminary indication of these differences was reported some time ago,[2,3] and several investigations of this system have appeared since[4] without, however, unraveling the complicated details of the adsorption process. These are apparent in the desorption sequence of Fig. 1, obtained (by the techniques of I) after adsorption of carbon monoxide at $T=298°K$. We can distinguish four separate regions of desorption. One, designated α, occurs just above room temperature and becomes important only toward the later stages of the adsorption. The primary and most heavily populated peak evolves at much higher temperatures ($T>1000°K$); it appears to be constituted of three separate sections, which we denote by β_1, β_2, and β_3, respectively.

Our aim in this report will be the elucidation of the adsorption processes in this strictly molecular system, following the general approach and relying upon the experimental techniques presented in I. We therefore immediately outline our experiments dealing with the qualitative nature of the β peak and its subdivisions; in subsequent paragraphs we will then describe attempts at more quantitative studies of the rate of formation and evolution of carbon monoxide in this state. A discussion of the kinetics of growth of the state of lowest binding energy isolated, α, is reserved for the last section.

A. QUALITATIVE EXAMINATION OF THE β PEAK

The unusual complexity of the β peak of carbon monoxide suggests the possible participation of artifacts. It has been established, for instance, that carbon monoxide is very strongly held to the cell interior[5] and evolution of this gas from the walls may conceivably affect the nature of the observed desorption peak. That this is *not* the origin of the multiple structures of Fig. 1, is, however, demonstrated by the agreement between desorption traces taken in systems maintained at 273° and 373°K, respectively. Evolution of gas from the filament supports also does not appear to have any measurable effect; with the cell walls at 300°K traces differing only in quantitative details are obtained when the filament and leads are cooled from 300° to ~125°K.

The structure of the peak is altered only slightly by changing the rate at which the sample filament is heated. This effect is apparent from Fig. 2, in which the period required for β evolution (after adsorption at 298°K for identical time intervals) has been changed from 240 to 360 msec. Only the β_2 and β_3 peak can be recognized in these traces, since the total concentration is still low ($n_\beta=89\times10^{12}$ molecules cm^{-2}). The total height of the peak is diminished by 17% on desorbing at the slower rate, yet the amount in the β_3 peak actually rises by 22%. The qualitative features remain the same, however, and on increasing the desorption intervals still further (to 800 msec) the total height only diminishes by another 10% with negligible changes in β_3. Since the lifetime of carbon monoxide on glass[5] is of the order of 20 msec, we consider this a good indication that possible delay of gas, desorbed from the filament, in reaching the gauge after adsorption on the cell walls is *not* responsible for these breaks.

Extensive observations of the β subpeaks have been carried out on one filament (No. 3) only. Earlier studies (on filament No. 1) were made with slower ion current detectors, incapable of resolving any fine structure in β. Qualitative measurements have been made on two additional samples. On one of these all of the features of the desorption trace for sample 3 were duplicated. On

[1] G. Ehrlich, J. Chem. Phys. **34**, 29 (1961), preceding paper. Henceforth referred to as I.
[2] G. Ehrlich, J. Phys. Chem. **60**, 1388 (1956).
[3] T. W. Hickmott and G. Ehrlich, J. Chem. Phys. **24**, 1263 (1956).
[4] R. Klein, J. Chem. Phys. **31**, 1306 (1959).
[5] G. Ehrlich, J. Appl. Phys. (to be published).

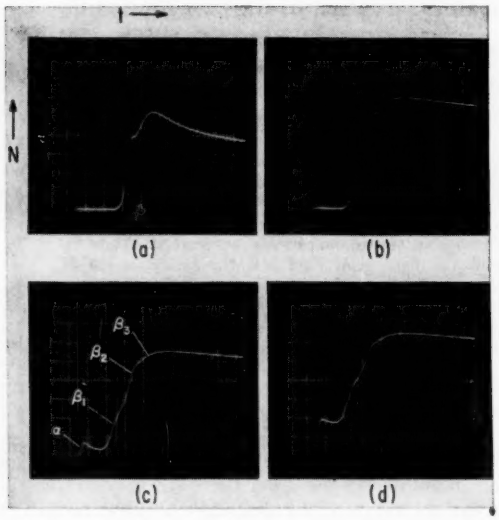

FIG. 1. Formation of multiple peaks during adsorption of CO at $T=298°K$. Filament 3. Time scale: 1 cm = 100 msec. (a) $\Delta t=3$ min, $n_\beta=35\times10^{12}$ molecules cm^{-2}; (b) $\Delta t=20$, $n_\alpha=2.2\times10^{12}$, $n_\beta=188\times10^{12}$; (c) $\Delta t=35$, $n_\alpha=35\times10^{12}$, $n_\beta=338\times10^{12}$; (d) $\Delta t=90$, $n_\alpha=160\times10^{12}$, $n_\beta=433\times10^{12}$.

the other, only low concentrations were examined and for these a definite break marking the onset of evolution of β_3 was not detectable, although the slope of the evolution curve diminished rapidly in that vicinity.

All of these experiments suggest that subpeaks β_1, β_2, and β_3 are *not* artifacts and do represent different states of binding on a tungsten surface. There still remains the possibility of impurities in the cell which could conceivably account for the desorption peaks, both α and β. All of the peaks are of comparable size, however, and therefore would have to be caused by gases present in comparable concentrations. Measurements have been made with gas bottles differing in the concentration of the main impurity, carbon dioxide, by a factor of more than 7 (0.04 to 0.3 mole %) without change in the desorption traces. Similarly, trapping with liquid nitrogen has no observable effect. Examination (by T. W. Hickmott) of the carbon dioxide level within a separate but similar ultra-high vacuum system, using an omegatron, revealed an impurity concentration comparable to that in the original gas supply. Impurities can therefore be rejected, and we conclude that the various desorption peaks are those of carbon monoxide *held in different forms on the surface.*

The diminution in peak height with lower heating rate, which was observed in Fig. 2, appears to stem from losses by pumping. The rapid diminution in gas density after the maximum has been achieved is quite apparent in Fig. 1(a). At higher coverages, that is, for longer adsorption intervals, the rate of this decay diminishes, presumably as the gas cover on the cell walls is restored after the high-temperature equilibration of the sample filament. Correction for this pumping using the decay constant S_E/V derived from the descending portion of the pressure trace *cannot* be properly accomplished. For the two traces in Fig. 2, the pumping correction so derived amounts to 4.4 and 1.2%, respectively, increasing the discrepancy between the high and low heating rate measurements to 20%. Although the reason for this failure is not clearly established, it very likely has two causes: (1) a compensating evolution of gas from the glass walls once the sample filament radiates intensely, which masks the pumping effects during the earlier stages of desorption, and (2) a competition at the slower heating rates between evolution from the filament and pumping by the cell walls, which at the higher temperatures gives an essentially constant gas density and therefore helps to simulate slow pumping. It has been shown,[5] for example, that the pumping speed S_E/V, estimated from the rate of diminution of the density, may be too low by more than 20% compared with the actual value when this lies in the range of 10 sec^{-1}. This difficulty of correcting for pumping, whatever its origin, prevents a quantitative assessment of the error involved in measurements of the adsorbed quantities, or for that matter of the rates of adsorption.

B. KINETICS OF FORMATION FOR THE β STATE

1. Distribution over Substates

As the total concentration of the tightly bound β carbon monoxide on the surface increases on increasing the adsorption interval, the fraction made up of the lower subpeaks β_1 and β_2 rises in proportion to $n_\beta{}^x$, where $x>1$. As indicated in Fig. 3 this fraction is independent of the pressure of the system, and over the range from 273° to 373°K, is fixed by the total concentration of β. A change in the temperature has no clearly resolvable effect upon this distribution which must therefore be dictated by rate processes.

The precise separation of the lower two peaks is difficult, but subject to larger errors than are usual even for this system, the distribution of carbon mon-

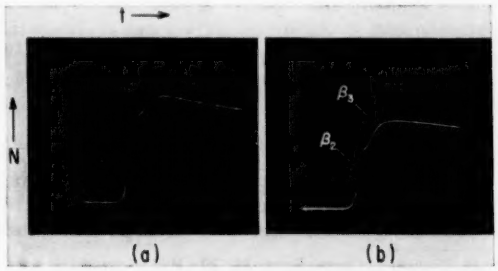

FIG. 2. Desorption of CO as a function of heating rate. Filament 3, $T=298°K$. $\Delta t=10$ min. (a) Normal heating. Time scale: 1 cm = 100 msec. $n_{\beta_2}=71\times10^{12}$ molecules cm^{-2}, $n_{\beta_3}=18\times10^{12}$. (b) Slow heating. Time scale: 1 cm = 200 msec. $n_{\beta_2}=48\times10^{12}$, $n_{\beta_3}=22\times10^{12}$.

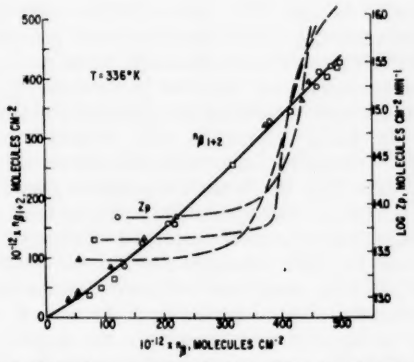

FIG. 3. Instantaneous concentration of CO in subpeaks β_1 and β_2 as a function of total β concentration, during adsorption runs on filament 3 at different impingement rates, Zp.

oxide over the β_1, β_2, and β_3 states is given in Fig. 4 as a function of the total β concentration. Both of the more strongly bound of the β's, β_2 and β_3, form initially but continue to grow to very different dimensions. The concentration of the latter never attains 80×10^{12} molecules cm^{-2}, whereas β_2 reaches $2\frac{1}{2}$ times this concentration. The third peak in β, β_1, becomes discernible only when the over-all β concentration has reached 315×10^{12} molecules cm^{-2}; it then grows linearly, encompassing essentially all additional molecules that are accommodated in this state, and at saturation equals in size the β_2 state.

As already indicated in Fig. 2, the distribution over these states does depend upon the heating schedule for desorption. This conversion of the lower to the higher β peaks at elevated temperatures can also be demonstrated differently. In Fig. 5 are displayed two traces, one (a) obtained after a normal 10-min adsorption interval, giving $n_\beta=82\times10^{12}$ molecules cm^{-2}. The other desorption trace, (c), was again taken after a 10-min interval under the same flow conditions, but was preceded at $t=6$ min by a flash cutoff so that only the low-temperature portion of β was evolved, as shown in (b). It is apparent that only small changes amounting to less than 4% in the total concentration of β were brought about by this intermediate heating. The concentration in the β_3 peak has, however, been increased by approximately 40%. The β_3 state is the most stable, but apparently is not formed rapidly at the lower temperatures, at which interconversion of the β states occurs slowly, if at all. Adsorption therefore results in a nonequilibrium distribution. Only at higher temperatures is this metastable distribution transformed to one dictated by the thermodynamics of the interaction between carbon monoxide and the surface.[6]

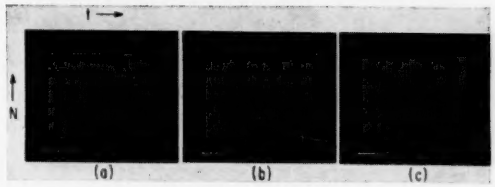

FIG. 5. Interconversion of β_2 and β_3 by preheating. Filament 3, $T=298$°K. Time scale: 1 cm=60 msec. (a) $\Delta t=10$ min, $n_{\beta_2}=63\times10^{12}$ molecules cm^{-2}, $n_{\beta_3}=19\times10^{12}$. (b) $\Delta t=6$ min, low-temperature flash, $n\sim38\times10^{12}$, followed by (c) desorption at $\Delta t=10$ min, $n_{\beta_2}=53\times10^{12}$, $n_{\beta_3}=27\times10^{12}$.

2. Absolute Adsorption Rates

Quantitative measurements of the absolute kinetics of formation of the β peak are difficult, because of the rapid pumping by the interior of the cell. This introduces two sources of error. (1) The surface concentration as estimated from the desorption curve may be less than the actual value. (2) The gas density, determined at the gauge during the adsorption interval, may be higher than that around the filament due to losses on the walls.[5] We have attempted to minimize both effects by operating at relatively high pressures ($Zp>1.5\times10^{13}$ molecules cm^{-2} min^{-1}) and by keeping the cleaning cycles for the filament as short as possible.[7]

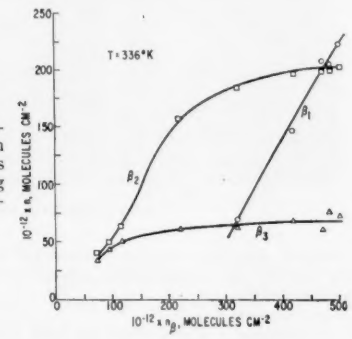

FIG. 4. Instantaneous concentration of CO in subpeaks β_1, β_2, and β_3 during adsorption on filament 3.

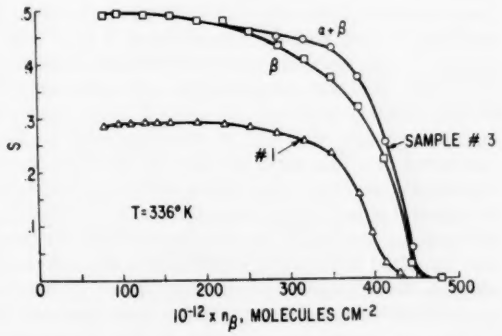

FIG. 6. Sticking probability for CO on filaments 1 and 3, as a function of surface concentration, n_β.

[6] It also follows from these observations that the relative concentrations of the three β states, shown in Fig. 4, have been perturbed by the act of measurement and may differ from the concentrations as formed in the adsorption step by ~20%.

[7] R. E. Schlier [J. Appl. Phys. **29**, 1162 (1958)] resorted to saturation with oxygen.

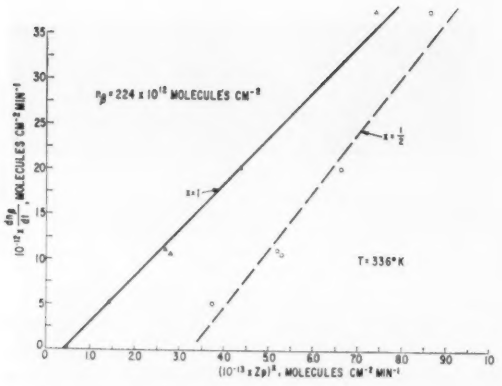

FIG. 7. Rate of formation of β CO on filament 3 as a function of impingement rate, Zp, at constant surface concentration and temperature.

The sticking coefficient for adsorption in β, determined in the same fashion as for nitrogen, is shown for two different filaments (1 and 3) in Fig. 6, and the dependence of the rate of adsorption upon the rate of impingement from the gas is plotted in Fig. 7. Although the rate of formation rises linearly with pressure, the curve does not pass through the origin. Inasmuch as evaporation of the β state at this temperature is negligible on the time scale of the adsorption experiments, this is an indication that the gas density at the filament compartment differs from that determined at the gauge.[5] However, it appears from Fig. 7 that the random deviations from a $p^{\frac{1}{2}}$ dependence for the rate of formation are even more serious, as is the failure of this curve to pass even close to the origin, and we therefore conclude that the rate of adsorption in this state is of the first order in the gas density.

The measurements in Fig. 6 on different filaments show the same trend found with nitrogen[1]: the sticking coefficient at low coverages on filament 3 is 1.7 times that on 1. On both the rate of formation is initially insensitive to the concentration of gas present on the surface, although filament 3 again shows a somewhat earlier diminution with increasing surface concentration. The concentration range over which the sticking coefficient for carbon monoxide maintains its high value is, however, appreciably higher than for nitrogen; for the former the rate has diminished to one-half its initial value at $n_\beta \sim 400\times10^{12}$ molecules cm^{-2}, whereas for nitrogen this halfway point occurs at $n_\beta \sim 110\times10^{12}$ molecules cm^{-2}. We have not been able to obtain any reasonable estimate of the temperature dependence of the adsorption process—our more limited measurements at temperatures other than 336°K have not been sufficiently reproducible. However, on lowering the temperature of adsorption to 298°K there does appear a trend toward higher sticking coefficients.

The difficulties encountered in quantitative rate determinations with carbon monoxide are well illustrated by the adsorption data at 298°K in Fig. 8. The apparent sticking coefficient (that is $Z^{-1}p^{-1}\,dn_\beta/dt$), particularly at the lower pressures, seems to increase as the concentration of adsorbed gas increases; this has been considered as evidence for cooperative chemisorption,[8] in which interaction with several adsorbed entities is required for a successful encounter with the surface. That this is *not* a cooperative effect, however, is evident: the adsorption seems to have a dependence upon a power of the pressure greater than the first, and at higher pressures this increase of the apparent sticking coefficient with cover becomes less pronounced. These deviations from the type of curve found at higher temperatures (Fig. 6) appear to be another manifestation of the rapid pumping by the cell interior, particularly at low pressures and short adsorption intervals for which the walls are not saturated. Because of all the difficulties which obstruct quantitative measurements, the system carbon monoxide on tungsten rather appears as an excellent example of uncooperative chemisorption.

C. KINETICS OF EVOLUTION FOR THE β STATE

1. Qualitative Observations

A qualitative insight into the mechanism of desorption for carbon monoxide in the β peak can be gained from the traces in Fig. 1, and from the more detailed sequence in Fig. 9. It is apparent from these that the location of the *peak* of β_3 and β_2 does not change as the total amount adsorbed increases (by a factor of three for β_2). The β_1 state becomes discernible at higher coverages, but even before the formation of an inflection point in the evolution curve, the foot of the β peak as a whole is shifted towards lower times, and this trend continues once β_1 can be resolved. This peak blends into β_2 so gradually, however, that a clear decision about its termination cannot be made. The

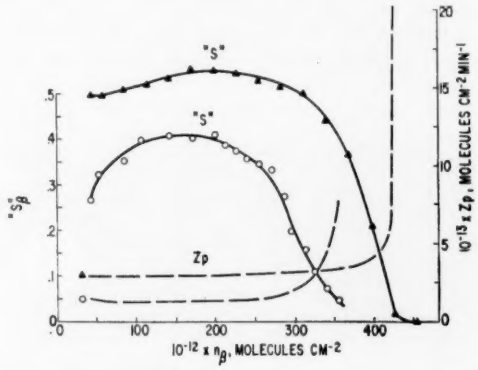

FIG. 8. Apparent "sticking probability" of CO on filament 3, for different impingement rates, Zp, and surface concentrations, n_β. $T = 298$°K.

[8] J. Eisinger, J. Chem. Phys. **27**, 1206 (1957).

fact that the finish of the evolution remains unchanged for different concentrations is an indication that the evolution reaction is first order in the concentration of the particular states[5] and for β_2 such a first-order dependence is therefore established by our observations.

A similar situation holds for β_3, although here the concentration range covered by the measurements is much smaller. This criterion is difficult to apply to the evolution of the β_1 state because its boundaries are indistinct, but for this state as well we assumed a first-order desorption. A second-order evolution would imply the surface dissociation of the carbon monoxide into oxygen and carbon, and some of the carbon (which is very firmly held) should therefore have remained on the sample after desorption. We have not been able to find any evidence of such a residue, however: (1) The resistivity of the sample was unchanged after more than 200 desorption experiments. (2) Measurements of the adsorption of nitrogen, reported in I, were made both before and after studying carbon monoxide, and were in excellent agreement. This could not be expected for a carbon contaminated sample. (3) In the field emission microscope, typical carbon patterns are not found when a tungsten emitter is heated at a low pressure (5×10^{-8} mm) of carbon monoxide. These observations therefore suggest a first-order desorption but not necessarily a *simple* first-order reaction. The onset of evolution of β_1 and β_2 does shift to lower times as the surface concentration is raised, and it therefore appears that the heat of desorption diminishes with increasing coverage. However, all our measurements indicate the presence of molecularly bound carbon monoxide only.

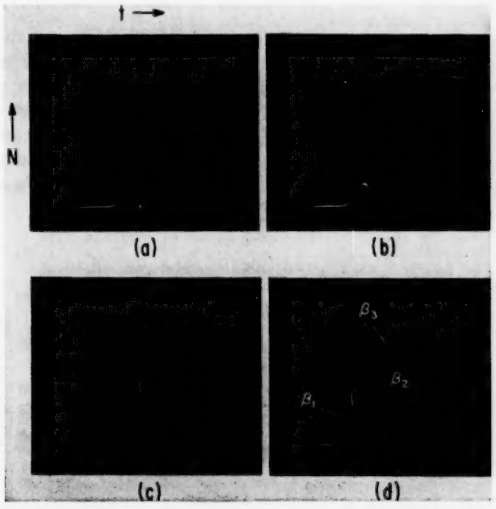

FIG. 9. Population of β states during adsorption of CO at $T=373$°K. Filament 3. Time scale: 1 cm = 100 msec. (a) $\Delta t=5$ min, $n_{\beta_2}=70\times10^{12}$ molecules cm^{-2}, $n_{\beta_3}=48\times10^{12}$; (b) $\Delta t=10$, $n_{\beta_2}=162\times10^{12}$, $n_{\beta_3}=59\times10^{12}$; (c) $\Delta t=20$, $n_{\beta_1}=143\times10^{12}$, $n_{\beta_2}=205\times10^{12}$, $n_{\beta_3}=66\times10^{12}$; (d) $\Delta t=50$, $n_{\beta_1}=228\times10^{12}$, $n_{\beta_2}=215\times10^{12}$, $n_{\beta_3}=68\times10^{12}$.

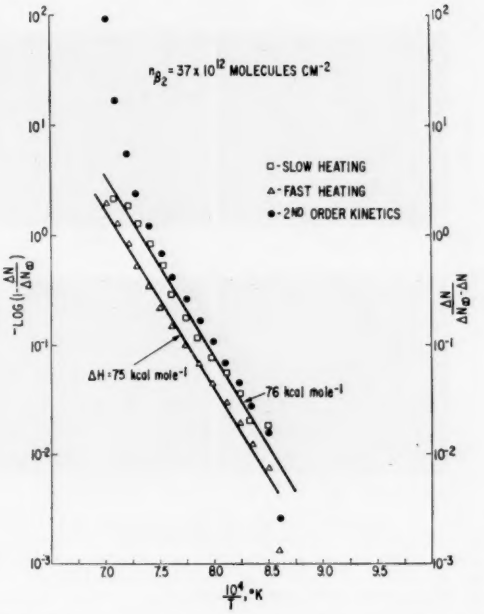

FIG. 10. Desorption of CO in β_2 state from filament 3. Left ordinate: first-order desorption; right ordinate; second-order desorption. Time-temperature curve Δ: $1/T=a_0+b_0t$, $a_0=16.67\times10^{-4}$ (°K)$^{-1}$, $-b_0=5.76\times10^{-4}$ (°K sec)$^{-1}$. □: $-b_0=3.4\times10^{-4}$.

2. Quantitative Measurements

Determination of the desorption kinetics of carbon monoxide is beset by the same difficulties encountered in adsorption experiments and we have not been able to carry out a detailed analysis of the β_3 peak. Semi-quantitative studies suggest that the desorption energy of this state is of the order of 100 kcal mole^{-1}.[9] We have, however, measured the evolution of β_2 under a heating schedule such that the reciprocal temperature varies linearly with time. The desorption at different heating rates is displayed in Fig. 10 for $n_{\beta_2}=37\times10^{12}$ molecules cm^{-2}, following the analysis outlined previously.[5]

The slopes of the two first-order plots yield heats of 75 and 76 kcal mole^{-1}, respectively, of which the former, at the higher heating rate, is the more reliable. The data for this particular desorption have also been plotted as a second-order reaction; the deviation from a straight line is significant and together with the qualitative observations already noted establishes this as a first-order process. Measurements at different initial concentrations again suggest a diminution of the heat of desorption at higher coverages, but have not been detailed enough to establish this trend quantitatively.

[9] In agreement with independent measurements by **R. Gomer** and D. O. Hayward [J. Chem. Phys. **30**, 1617 (1959)].

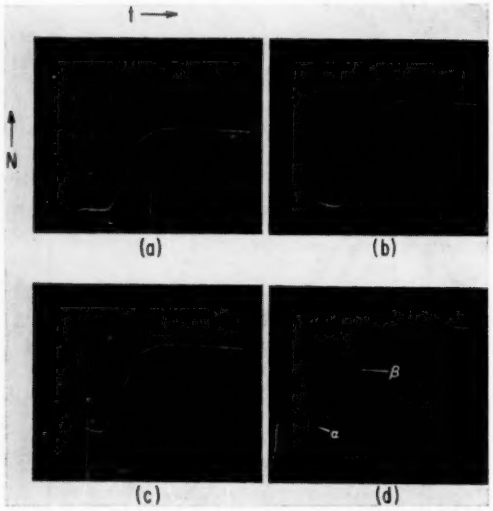

FIG. 11. Growth of α state during adsorption of CO at $T=298°K$. Filament 3. Time scale: 1 cm = 100 msec. (a) $\Delta t = 7\frac{1}{2}$ min, $n_\alpha = 3.1\times10^{12}$ cm^{-2}, $n_\beta = 275\times10^{12}$; (b) $\Delta t = 10$, $n_\alpha = 27\times10^{12}$, $n_\beta = 363\times10^{12}$; (c) $\Delta t = 15$, $n_\alpha = 138\times10^{12}$, $n_\beta = 438\times10^{12}$; (d) $\Delta t = 30$, $n_\alpha = 210\times10^{12}$, $n_\beta = 460\times10^{12}$.

This dependence is not sufficiently pronounced, moreover, to introduce any curvature into the desorption plots for the low concentrations of Fig. 10. At the concentration of β_2, previously given, our measurements yield a first-order rate constant for desorption, k_1, given by

$$k_1 \sim 3\times10^{13} \exp[-(75\times10^3)/RT] \text{ sec}^{-1}.$$

The desorption kinetics of the β_1 peak have not been evaluated, but judging from its evolution curve, evaporation occurs with a heat of desorption considerably below that of β_2.

D. THE α STATE

1. Kinetics of Formation

The weakest of the states in which carbon monoxide adsorbs on a tungsten surface α, is populated to a significant extent only when the β peak has achieved at least two-thirds of its final height. This effect is illustrated qualitatively by the desorption sequence in Fig. 11, obtained after adsorption at 298°K. It is of interest that although the α peak grows from 3.1 to 210×10^{12} molecules cm^{-2}, evolution terminates at the same time after initiating the heating. Desorption out of the α state must therefore occur as a reaction of the first order in the concentration of carbon monoxide in this state, indicating molecular binding.

The formation of the α state is given in greater detail in Fig. 12 as a function of amount in the β state. At saturation (for an impingement rate of 1.4×10^{16} molecules cm^{-2} min^{-1}) the concentration in α at 298°K is approximately $\frac{1}{2}$ that in β. During the early stages of adsorption, for $n_\beta < 280\times10^{12}$ molecules cm^{-2}, the α concentration is less than 3×10^{12} molecules cm^{-2} but then grows rapidly. Over the range $n_\beta = 280$ to 370×10^{12} molecules cm^{-2} n_α increases more than eightfold. The pressure during this growth, however, only increases by 12%. The rise in the concentration of α therefore stems from changes occurring on the surface and not from an increase in the external driving force.

The early stages of formation of α are qualitatively the same at temperatures above 298°K; however, as is shown in Fig. 12, the total amount formed at saturation diminishes the higher the adsorption temperature. At 373°K and an impingement rate of 1.1×10^{16} molecules cm^{-2} min^{-1}, the maximum α concentration is only 36×10^{12} molecules cm^{-2} compared to 200×10^{12} molecules cm^{-2} at 298°K. The amount of carbon monoxide found in this weakly held state also depends upon the pressure, and is *not* just dictated by the concentration of material present in the stronger β state. This dependence is small and during the initial stages of formation of α is within the limit of error of the measurements.

The variation of n_α with pressure is quite definite at saturation at higher temperatures, and is shown in Fig. 13 for adsorption at 373°K. The data have been plotted in the form appropriate to a Langmuir isotherm, the slope of which yields 55×10^{12} for n_s, the apparent number of adsorption sites per unit area. Even here the pressure dependence is small—an increase of the impingement rate by a factor of 3.5 raises the concentration of α by only 65%. It should be noted that at these temperatures and at higher pressures the concentration of α actually passes through a maximum at high concentrations of β, indicating that the slow formation of β in the final stages does interfere with the formation of the α, and that we are not at true equilibrium at the maximum. The number of adsorption sites deduced from the Langmuir isotherm is itself a function of the temperature, increasing with diminishing adsorption temperature. From the con-

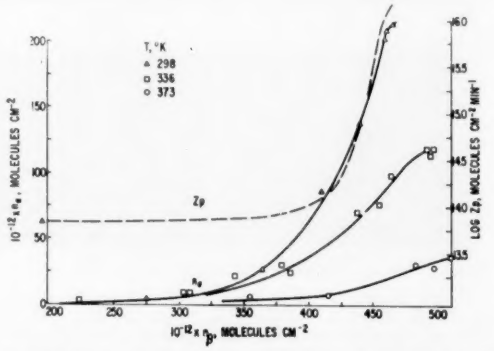

FIG. 12. Instantaneous concentration of CO in α and β states during adsorption runs on filament 3 at different temperatures.

centration of carbon monoxide in the α state at 373°K, we estimate that the binding energy has a minimum value of the order of 20 kcal mole^{-1}.

The rate of formation of the α peak becomes appreciable once the rate of adsorption into the β peak begins to diminish. This is indicated by the difference between the total adsorption rate and that into the β state, plotted for a surface at 336°K in Fig. 6; the effect is therefore to maintain the total adsorption probability at a high value up to higher concentrations. The threshold for resolution of the α peak can be shifted by cooling the adsorption sample to ~130°K (maintaining the remainder of the cell at a constant temperature). At these low temperatures we do not find any additional state of binding as for nitrogen, but rather a displacement of the onset of α formation to considerably lower concentrations of β. Only limited data have been obtained under these conditions, but at the same impingement rate as for the 298°K data in Fig. 12 (6.2×10^{13} molecules cm^{-2} min^{-1}) the concentration of α has a value of 41×10^{12} molecules cm^{-2} at $n_\beta=235\times10^{12}$ molecules cm^{-2}, which is roughly 30 times the concentration of α formed at the higher temperatures. This increase in the α concentration may arise in two ways. (1) There may be sites present on the surface of very low binding energy which can only be populated at low temperatures. The absence of any distinct new peak would then merely indicate a continuous distribution of binding energies. (2) At the lower adsorption temperatures ($T\sim130$°K), sites may be filled which at 300°K and above would be depleted very rapidly by conversion to the β state. We will distinguish between these possible mechanisms later.

2. Kinetics of Interconversion

The appearance of α at smaller β concentrations when the adsorption temperature is lowered has additional significance: it helps to verify our implicit assumption that the concentration of carbon monoxide in the α peak, estimated from the desorption traces, corresponds to the concentration formed during the adsorption process.

There are two possible effects that could invalidate the measurements of the concentration of α. The fact that significant quantities formed only after long adsorption intervals, once much β is on the surface, might be an artifact caused by the rapid pumping of the material evolved initially. This possibility is eliminated, however, since cooling the filament (and leads) could only increase pumping by the cell walls; despite this α is observed after shorter adsorption intervals than, for example, at 298°K. The other possibility to consider is the conversion of weakly bound material, in the α state, to the β state during the desorption flash. The desorption trace, after adsorption of 170×10^{12} molecules cm^{-2} of β at 130°K, suggests complete evolution of α just below 300°K, with a total evolution time of ~1.8 sec. Conversion would have to occur during this short interval, which shows that for adsorption at 298°K conversion, if it occurs at all, would be essentially complete. We conclude that the β peak is formed during the adsorption and is not a product of our technique of observation, and that the same holds for the formation of the α state.[10]

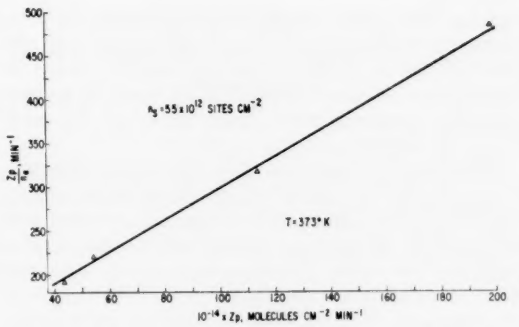

FIG. 13. Langmuir isotherm for α CO on filament 3. n_α = maximum concentration in α state, Zp = impingement rate.

SUMMARY

A detailed analysis of the adsorption and desorption kinetics we have presented will be given later. We wish to emphasize here that our experiments have demonstrated the formation of intermediate states of binding in significant concentrations during adsorption for both nitrogen and carbon monoxide. These states differ greatly for the two gases, however. For nitrogen the primary chemisorbed state β forms as atoms even at 115°K. The secondary states α and γ both adsorb irreversibly, at 300° and 115°K, respectively (the latter definitely as molecules), with the efficiency of formation dictated by the amount of the atomically bound β state present. In contrast carbon monoxide in the primary β state is held as molecules, which fill the surface more efficiently than does nitrogen. At 300°K a total of 480×10^{12} carbon monoxide molecules have been adsorbed per cm^2 in the β state, by comparison with only 280×10^{12} molecules for nitrogen on the identical surface.

The total number of molecules adsorbed in all states at $T=115$°K is, however, similar for the two gases: $N_2\sim600\times10^{12}$ molecules cm^{-2}, $CO\sim680\times10^{12}$ molecules cm^{-2}, and the deficiency in the primary nitrogen adsorption is compensated by the larger number of molecules that can be accommodated in the

[10] Some losses out of the β state may still occur during the desorption. We have not examined the effect of heating rate in detail. However, measurements on filament 1 in which the heating rate was reduced by a factor of 0.25 and evolution occurred over an interval of 160 msec, instead of the 40 msec standard for room temperature desorptions from sample 3, duplicated all the features of the kinetics of formation of α already outlined, and agreed to better than 25% in the absolute amount of α formed under comparable conditions.

γ state. With carbon monoxide, the intermediate state stable at 300°K (α) is not at all comparable with the state of similar stability found for nitrogen, either in numbers or kinetics of formation. In these the α state of carbon monoxide more closely resembles the weak γ state of nitrogen.

The kinetics of formation of the primary chemisorbed state β are alike for both nitrogen and carbon monoxide, the sticking coefficient initially remaining constant and independent of coverage. For nitrogen our results indicated the profound effect of the atomic arrangement of the surface upon adsorption, and also the effect of adsorption in rearranging the surface layer itself. We shall show subsequently that structural differences are also responsible for the presence of strongly chemisorbed carbon monoxide in different β states, and for the appearance of distinct peaks in the desorption spectrum.

ACKNOWLEDGMENTS

In the initial measurements on both nitrogen and carbon monoxide the author was assisted by Philip Gibeau; much of the later work was performed by F. G. Hudda. The author is greatly indebted to his colleagues in the Metallurgy and Ceramics Research Department, particularly to E. W. Hart, for many stimulating suggestions, and to the Glass Development Shop for skillful help in the construction of the experimental equipment.

THE JOURNAL OF CHEMICAL PHYSICS VOLUME 34, NUMBER 1 JANUARY, 1961

Criticality Criteria for Various Configurations of a Self-Heating Chemical as Functions of Activation Energy and Temperature of Assembly

JOHN R. PARKS

Applied Mathematics Section of the Research and Engineering Division of the Monsanto Chemical Company, St. Louis 66, Missouri

(Received May 18, 1960)

In 1939 D. A. Frank-Kamenetsky proposed a criticality criterion that is a dimensionless constant that varies only with configuration of the self-heating chemical. In his studies of the equation equating power production as a function of temperature by the formula of Arrhenius and the power loss by conduction alone, he made a simplifying assumption. A Pace analog computer and an IBM 704 have been used to study the exact equation and it was found that the value of the F-K criticality criterion is a slowly varying function of E/RT_0 in the range from infinity to 30 but becomes a sensitive function for values of E/RT_0 less than 30.

INTRODUCTION

A STEADY-state temperature distribution is possible in a body containing distributed heat power production only if the heat power leakage through the surface of the body to the environs is equal to the volume average of the heat power production within the surface of the body. In those cases in which the power production is greater than the power leakage, the temperature cannot become stable and the bodies will heat to self-destruction. It is for this reason that studies of bodies containing power sources and sinks are of scientific and practical interest.

The problems involving the production of heat by electrical means and by radioactive decay of atoms have been solved and the solutions put to scientific and practical use. In these problems heat was considered to leak from the bodies by thermal conduction only; such situations are quite generally realizable in practice.

Cases involving the presence of self-heating chemicals, the power production of which is a function of temperature, have been studied. The equations describing such cases, however, are nonlinear and are such that present theories of the solution of differential equations are not applicable. Certain approximations have been made to make the equations more tractable with a consequent loss of accuracy and information concerning the solutions.

The work of D. A. Frank-Kamenetzky (1939) on self-heating chemicals contains the latest significant development of the problem to which later investigators have referred.[1] Out of this work came an F-K criticality criterion δ_{cri} for a substance assembled as a sphere, or as an infinitely long cylinder or as an infinite slab of finite thickness. The constant δ_{cri}, is a dimensionless number and is a function of the physical and chemical properties of the material, the temperature at the time of assembly, the concentration of the self-heating chemical and the dimensions of the assembly. For a given material and temperature of assembly there is a continuous set of values of δ for a continuous set of values of the characteristic dimension. However, there is a value of δ which is the lower limit of that subset

[1] D. A. Frank-Kamenetzky, Zhur. Fiz. Khim. **13**, No. 6, 738 (1939). Note: A translation is available at Associated Technical Service Inc., East Orange, New Jersey.

of values of δ for which there is no possible steady-state temperature distribution within the assembly. This value of δ is the critical value and is denoted by δ_{cri}. Frank-Kamenetzky computed the δ_{cri} for several configurations as shown in Table I.

The criterion as a function of the physical and chemical properties and dimensions of the material is shown in Eq. (1)

$$\delta_{cri}=\frac{EQnZ\exp[-E/RT_0]r_0^2}{RT_0^2\lambda}, \tag{1}$$

where δ_{cri}=criticality criterion; E=activation energy of the chemical reaction; Q=heat per mole of reaction; n=molar density; Z=frequency factor for the unimolecular velocity constant; R=the gas constant; T_0=absolute temperature of assembly; λ=thermal conductivity of the material; and, r_0=characteristic dimension of the assembly. If, when a mass of self-heating chemical is assembled,

$$\delta>\delta_{cri}, \tag{2}$$

the mass of material will heat to self-destruction in time; if

$$\delta<\delta_{cri}, \tag{3}$$

then the mass will warm a few degrees and reach a steady temperature distribution. The equality, $\delta=\delta_{cri}$, describes a metastable state; the temperature of the body may reach equilibrium, however, perturbation can cause it to heat without limit. Frank-Kamenetzky has given excellent discussions of conclusions to be drawn from inequalities (2) and (3).[2]

The F-K criteria have been used in studies on thermal instability of gaseous and solid material. O. K. Rice used the criteria extensively in his discussion of the part played by conduction in thermal gaseous explosions.[3] He raised an important question as to whether the δ_{cri} given by F-K are the largest possible theoretical values, since his experimentally determined δ_{cri} are 2 to 4 times larger than theoretical. Robertson used the thermal theory in this study of the decomposition of condensed high explosives.[4] R. M. Hainer also used the F-K criterion in a study of ammonium nitrate and high percentage ammonium nitrate fertilizers.[5]

The importance of the thermal theory of explosion warrants a closer look at the mathematics of the theory than has been taken heretofore. This paper is a discussion of a study of the exact equations of heat flow in a self-heating chemical using numerical and analogic methods on an IBM 704 data processing machine and a Pace analog computer, respectively.

TABLE I. Values of the F-K criticality criteria for several configurations of a self-heating chemical.

δ_{cri}	Configuration
3.32	Sphere
2.00	Infinitely long cylinder
0.88	Infinite slab of finite thickness

PROBLEM

The following differential equation with initial and boundary conditions (i.c. and b.c.) represents the heat power balance in a body of self-heating chemical, the rate of reaction of which follows the equation of Arrhenius,

$$\lambda\nabla^2T=\rho c(\partial T/\partial t)-QnZ\exp[-E/RT], \tag{4}$$

i.c. at $t=0$, $T=T_0$ throughout the body; b.c. $T=T_0$ at the surface of the body; $\nabla T=0$ at the center of symmetry of the body.

These equations represent the power balance within the body of a self-heating chemical in a well-stirred bath or its equivalent. The left-hand term of Eq. (4) is the power leakage per unit volume, which is balanced by the difference between the power storage per unit volume and the power generation per unit volume, the first and second terms, respectively, on the right-hand side. The symbols ρ and c are the density and specific heat, respectively, of the material, the other symbols are as defined in Eq. (1). This equation is best handled on the digital and analog computers if it is put into dimensionless form and referred to regular geometric shapes. In effecting the transformation of Eq. (4), the approximation made by Frank-Kamenetzky will not be used. The origin of coordinates will be taken at the center of symmetry of the geometric bodies. The characteristic dimension of the bodies will be the distance from the center of symmetry to at least one characteristic point on the surface of the body, and will be denoted by r_0. In a sphere the characteristic point is any point on the surface and the characteristic dimension is the radius. In a cube there are six characteristic points which are the centers of the six faces and the characteristic dimension, r_0, is half the length of an edge of the cube, etc.

Equation (4) can be put into the completely dimensionless form shown in Eq. (5)

$$\nabla^2\theta=(\partial\theta/\partial\tau)-(\alpha\beta)\exp[\theta/(1+\theta/\alpha)], \tag{5}$$

i.c. at $\tau=0$, $\theta=0$ throughout the body; b.c. $\theta=0$ at the surface; $\nabla\theta=0$ at the center of symmetry; $\tau>0$. The factor $(\alpha\beta)$ is equivalent to δ as given in Eq. (1), and α is E/RT_0. The steady-state equivalent of Eq. (5) is the main subject of this paper; however, Eq. (5) has been studied as applied to supercritical masses of a

[2] D. A. Frank-Kamenetzky, *Diffusion and Heat Exchange in Chemical Kinetics*, translated by N. Thon (Princeton University Press, Princeton, New Jersey, 1955).

[3] O. K. Rice, Jr., J. Chem. Phys. **8**, 727 (1940).

[4] A. J. B. Robertson, "Sensitiveness of high explosives," Ph.D. thesis, University of Cambridge, 1947 (unpublished).

[5] Arthur D. Little, Inc., "Report on an investigation of the properties and hazards of ammonium nitrate and high percentage ammonium nitrate fertilizers," a report made to the Commandant U. S. Coast Guard Headquarters (1952).

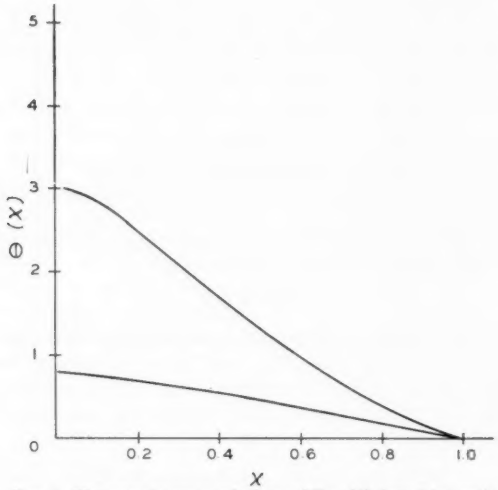

FIG. 1. Two steady-state solutions of Eq. (6) found by analog computer, $\alpha=50$, $\delta=3.0$ (see Fig. 2).

mixture of ammonium nitrate and oil and information was obtained which supports some of the conclusions drawn from the studies of the steady-state equation.

The steady-state equivalent of Eq. (5) is obtained by setting $\partial\theta/\partial\tau=0$ and ignoring the initial condition. The equation studied by Frank-Kamenetzky is obtainable from the steady-state equivalent in two ways: First, by assuming θ to be near zero and hence θ/α is negligible for nonzero α, or second, by assuming α to be so large that θ/α is negligible for any finite θ. The second method implies that β in the quantity $(\alpha\beta)$ must decrease, as α increases, in such a way that $(\alpha\beta)$ remains finite and nonzero. This second method also makes the F-K equation a member of the set of nonlinear equations corresponding to values of α in the range $0<\alpha<\infty$.

In the study of Eq. (5), in either the transient or steady-state form, the Laplacian ∇^2 and the boundary conditions must be put into the form appropriate to the geometrical shape of the body. The boundary conditions show that the gradient of the temperature at the center of symmetry of regular body is zero. This is imposed on the solution by the regular shape. It is here that Harris made his error. Harris used the thermal theory of explosion in his study of diethyl peroxide and refers to the Frank-Kamenetzky work. Harris solved the differential equation for thermal conduction in a body with chemical heat power generation and obtained critical values of δ significantly different from those of F-K.[6] This was so because he used an incorrect boundary condition at the center of the sphere and an infinitely long cylinder in order to effect integration of the equations.

The work reported here was stimulated by the possibility that the product $(\alpha\beta)$ may be a function of α, as implied in the foregoing discussion. The problem then, was to find the largest values of $(\alpha\beta)$ for various values of α and for which Eq. (5) would yield steady-state solutions which meet the boundary conditions. The digital computer is best suited for accurately computing $(\alpha\beta)$ as a function of α and also finding transient solutions of Eq. (5), whereas, the analog computer is best suited to determine the nature of the solutions of the steady-state equivalent.

SOLUTION OF THE PROBLEM

A. Analog Computer

The analog computer was used to explore the solutions of the steady-state equivalent of Eq. (5) expressed in spherical geometry as shown in Eq. (6),

$$(d^2\theta/dx^2)+(2/x)(d\theta/dx)=-\delta\exp[\theta/(1+\theta/\alpha)] \quad (6)$$

$$\text{b.c.} \quad \text{at } x=1, \quad \theta=0$$

$$\text{at } x=0, \quad d\theta/dx=0.$$

The analog program used the usual methods and hardware except for the component used to produce voltages proportional to the exponential function on the right of Eq. (6). This component is special and is referred to as a "log card circuit." Potentiometers were used to enter values of α, δ, and $\theta(0)$ (temperature at the center of the sphere) into the circuit and an X, y plotter was used to draw the function $\theta(x)$ as output data.

The procedure was to enter constant values of α and δ and then try various values of $\theta(0)$ in an effort to find that value (or values) of $\theta(0)$ for which $\theta(x)$ would pass through zero when $x=1$ (the equivalent of 100 v). After finding the value (or values) of $\theta(0)$ that gave a solution (or solutions) within the precision of the machine ($<1\%$), a new value of δ was entered and the procedure repeated. Figure 1 shows two solutions that were found for $\alpha=50$ and $\delta=3.24$. These were

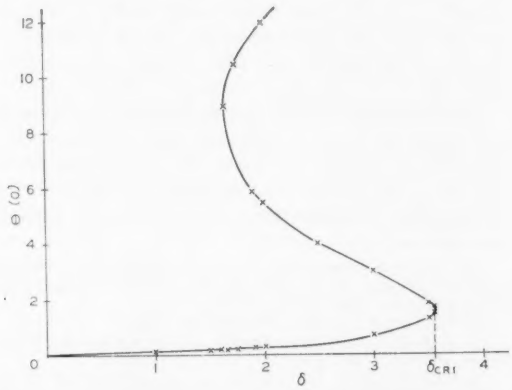

FIG. 2. Center temperatures yielding solutions of Eq. (6) as a function of δ.

[6] E. J. Harris, Proc. Roy. Soc. (London) **A175**, 254 (1940).

the only solutions found within the range of the machine.

Solutions were found for various values of δ from about 1 to 3.5 with $\alpha=50$. Figure 2 shows the results of this search. Here, the data, that are plotted, are the values of $\theta(0)$ yielding solutions that meet the boundary conditions, versus δ. In the range $1<\delta<1.85$ only one solution was found; in the range $1.85<\delta<2.0$ three solutions existed, and in the range $2.0<\delta<3.55$ two solutions were found. No solutions could be found for $\delta>3.55$. The region in the neighborhood of $\delta=3.55$ was carefully explored. It was found that the two solutions approached and became coincident as δ approached and became 3.55. This value of δ was then called the critical δ (or δ_{cri}) for $\alpha=50$.

It is interesting to note that Rice anticipated these results.[3] He solved the F-K steady-state differential equation for a sphere to obtain δ as an alternating and even power series of a dimensionless variable x which could vary from 0 to ∞. The variable x is a function of the temperature at the center of the sphere for which there is a solution that fits the b.c. Figure 1 in his paper shows that δ goes through a maximum at x approximately equal to 4.0, at which point δ has a value in agreement with that calculated by Frank-Kamenetzky. The presence of the maximum indicates that there are at least two values of x for a given δ near its maximum value, and therefore indicating that there are at least two solutions of the equation that fit the boundary conditions. Rice's solution suffers from the limitation that x must be small; otherwise, he would have been able to extend his graph beyond 4.5 in search of an answer to his question regarding the existence of values of δ greater that δ_{cri} and also to more clearly show the existence of multiple solutions.

The behavior of the curve shown in Fig. 2 was studied for a range of α from 30 to 100. For values of α in the high range, the curve maintained the shape shown and δ_{cri} decreased slowly toward 3.32. In the low range the general shape of the curve was maintained but δ_{cri} was increasing more rapidly as α was decreased, furthermore, the value of $\theta(0)$ was also rapidly increasing.

At this point in the work it was decided to use the digital computer for a more accurate determination of δ_{cri} as a function of α.

B. Digital Computer

The digital computer was used to study the steady-state equivalents of Eq. (5) with the ∇^2 and b.c. appropriate to the following geometries; sphere, infinitely long circular cylinder, infinite slab of finite thickness, cube, and right circular cylinder, the diameter of which equaled its height. The differential equations and b.c. for each geometry were reduced to the usual set of difference equations with the increment in x (or x's) set equal to 0.1. For a given value of α a double iterative procedure was devised. The program selected automatically, values of β on a range from a β minimum to a β maximum in small steps indexed by k. For each value of β the computer would numerically develop a solution that met the b.c., if the solution existed. In this way for each value of α a β_k was found such that a solution existed and a β_{k+1} such that the machine could find no solution which met the b.c. The value of δ_{cri} satisfied the following inequality (7) and was computed by Eq. (8),

$$(\alpha\beta_k)<\delta_{cri}<(\alpha\beta_{k+1}) \tag{7}$$

$$\delta_{cri}=\alpha\tfrac{1}{2}(\beta_k+\beta_{k+1}). \tag{8}$$

TABLE II. Criticality criterion δ_{cri} as a function of α.

	$\delta_{cri}=F(\alpha)$				
α	Sphere	Inf. long cir. cylinder	Inf. slab of finite thickness	Cube	Regular right cir. cylinder
20	3.51	2.11	0.927	2.68	2.93
25	3.47	2.08	0.915		
30	3.44	2.07	0.911	2.63	2.88
35	3.42	2.06	0.905		
40	3.41	2.05	0.904	2.58	2.83
45	3.40	2.04	0.894		
50	3.38	2.04	0.892	2.58	2.83
55	3.38	2.03	0.892		
60	3.38	2.03	0.891	2.58	2.83
65	3.37	2.03	0.886		
70	3.36	2.02	0.884	2.58	2.83
75	3.36	2.02	0.882		
80	3.35	2.01	0.881	2.58	2.83
85	3.35	2.01	0.880		
90	3.35	2.01	0.880	2.53	2.78
95	3.34	2.01	0.880		
100	3.34	2.01	0.880	2.53	2.78

Table II shows the results for the various geometric shapes studied. The data shown for the cases of the cube and the regular right circular cylinder are in steps of 10 for α because of the time required to iterate the solution of the partial difference equations involving three and two independent variables, respectively. These values of δ_{cri} are accurate to better than 1%. This table also shows that the analog computer was 6% in error on the high side in the determination of δ_{cri} for $\alpha=50$.

DISCUSSION

Table II shows that in all the cases considered δ_{cri} is a rapidly decreasing function of α for increasing values of α near 20 and slowly decreasing around $\alpha=100$. At $\alpha=20$, δ_{cri} changes by 0.04 for a change of 5 in α; at $\alpha=70$, δ_{cri} changes by 0.02 for a change of 30 in α and in none of these cases has δ_{cri} become that value specified by Frank-Kamenetzky for the cases he studied.

Frank-Kamenetzky solves the equation

$$\nabla^2\theta=-\delta\exp[\theta] \tag{9}$$

for his values of δ_{cri}. Equation (9) is the steady-state equivalent of (5) when $\alpha=\infty$. This value of α corresponds to a chemical which has an infinitely large

activation energy E assembled at a nonzero temperature T_0. It also corresponds to a chemical with a finite activation energy assembled at absolute zero.

In the opposite limit, $\alpha=0$, the steady-state equivalent of Eq. (5) is Eq. (10),

$$\nabla^2\theta=-\delta. \tag{10}$$

As α approaches zero the value of β approaches infinity in such a way that the product $(\alpha\beta)$ is in the limit a finite number δ. Equation (10) is the steady-state equation for constant power generation as in the case of electrical power generation problems or of radioactive power generation by isotopes that have extremely long half-lives. This problem has been solved and it turns out that there are steady-state solutions for all finite values of δ thus indicating that $\delta_{cri}=\infty$.[7,8] The value of zero for α corresponds to a chemical with a finite nonzero activation energy assembled at an infinitely high temperature, and it also corresponds to a chemical of zero activation energy assembled at a finite nonzero temperature.

Table II shows the importance of knowing as accurately as possible the activation energy and temperature of assembly in the experimental studies of thermal explosion of self-heating chemicals. This is especially ture for chemicals that have low activation energies.

Equation (5) was studied on the digital computer to determine the time from assembly of a mixture of ammonium nitrate and oil as a sphere at 165°C to the explosion state as a function of supercriticality. These studies were made for several cases ranging from 10% supercritical to 200%. The percent supercriticality was calculated as the percent increase of the square of the radius over the square of the critical radius. The explosion state was defined as being existent when the center of the sphere had reached 573°K. The computer determined the temperature distribution in the sphere as a function of time. The time was taken in incremental steps. Occasionally the computer would print out the temperature distribution for the time one increment past the time the sphere had reached the defined explosion state. Invariably the temperatures reported were of the order of 10^{10}°K. This work is mentioned to indicate that for values of $\delta>\delta_{cri}$ there appears to be no limiting temperature rise that could be imposed by the differential equation.[9]

The writer realizes that the work reported here is not rigorous proof of the general thermal behavior of a mass of self-heating chemicals, however, it lends strength to the conjecture that there are no values of δ_{cri} greater than the F-K values for the chemicals with moderate or high activation energies assembled at usual experimental temperatures. This work is a partial negative answer to Rice's question. A rigorous answer may have to wait for the development of general existence theorems in the mathematics of nonlinear differential equations.

CONCLUSIONS

1. An analog computer has been used to show the multiplicity of the solutions of the nonlinear steady-state differential equation describing thermal conduction of heat in a mass of self-heating chemical. It is also shown that within the limit of the machine there is but one value of δ_{cri} for a given value of E/RT_0.

2. The digital computer has been used to show, for several geometric shapes and for values of E/RT_0 between 20 and 100, that δ_{cri} is a function of E/RT_0. It is shown that a slowly decreasing function appears to approach the F-K values in the high range; a rapidly increasing function as E/RT_0 decreases in the low range. This throws new light on thermal explosion experiments involving chemicals with low activation energies.

3. O. K. Rice's question regarding the possibility of the existence of values of δ_{cri} greater than those given by Frank-Kamenetzky has been partially answered in the negative within the limits of the Pace analog and IBM 704 digital computers.

ACKNOWLEDGMENTS

The author wishes to acknowledge the assistance of Paul Chen on the digital computer and Paul Parisot on the analog computer Their excellent help made this paper possible.

[7] H. S. Carslaw and J. C. Jaeger, *Conduction of Heat in Solids* (Clarendon Press, Oxford, 1947), p. 207.

[8] Max Jakob, *Heat Transfer* (John Wiley & Sons, Inc., New York, 1949), p. 189.

[9] John R. Parks, Inorganic Chemicals Division of Monsanto Chemical Company, Rept. 4679, March 17, 1960 (unpublished).

Reactions of Active Nitrogen with Hydrogen Bromide, Bromine, and Ethylene

EARL R. V. MILTON AND H. B. DUNFORD

Department of Chemistry, University of Alberta, Edmonton, Canada

(Received June 2, 1960)

Measurement of the specific rate constant for the reaction

$$N+HBr\rightarrow NH+Br$$

indicates that k is 3.8×10^{-14} sec^{-1} (molecules/cc)$^{-1}$ at 40°C. Attempts to obtain complete turbulence of reactants at a pressure of 0.85 mm were unsuccessful so that diffusion techniques were employed. The homogeneous flame reaction accompanying the above reaction was too weak to define the reaction zone, so calculations were based on the reaction tube diameter and the critical flow rates of reactants at which the orange flame initiated by a wall reaction involving active nitrogen and bromine was prevented. Spectra of flames obtained from the N+Br_2 and N+HBr reactions in a stirred-flow reactor indicate that NBr is the source of the orange flame in the latter reaction. The flow rates of atomic nitrogen were calibrated by chemical titration with ethylene. A conventional diffusion flame technique was used to obtain $k=1.6\times10^{-13}$ sec^{-1} (molecules/cc)$^{-1}$ at 40°C for the reaction

$$N+C_2H_4\rightarrow HCN+CH_3.$$

INTRODUCTION

IN a previous study of the kinetics of the reaction of active nitrogen with hydrogen bromide[1] (HBr reaction), it was shown that a plausible reaction scheme to account for the major products is[2]

$$N+HBr\rightarrow NH+Br+0 \text{ kcal}, \quad (1)$$

$$NH+HBr\rightarrow NH_2+Br+3 \text{ kcal}, \quad (2)$$

$$NH_2+HBr\rightarrow NH_3+Br+14 \text{ kcal}, \quad (3)$$

$$NH_3+HBr\rightarrow NH_4Br, \quad (4)$$

$$Br+Br+M\rightarrow Br_2+M. \quad (5)$$

From the stoichiometry of the reaction, it was apparent that about 90% of the atomic nitrogen at 80°C was being destroyed by some mechanism(s) other than step (1). Reactions of the type

$$N+NH\rightarrow N_2+H \quad (6)$$

$$N+NH_2\rightarrow N_2+2H \quad (7)$$

were not felt to be of major importance since it appeared from the NH_4Br/Br_2 ratio observed for reactions at 80° that 60% of the NH formed in reaction (1) was converted into NH_4Br. If, however, the reaction

$$H+Br_2\rightarrow HBr+Br$$

occurred appreciably, it would invalidate the latter statement. From experiments in which various amounts of Br_2 were premixed with HBr and added to an active nitrogen stream, it was concluded that hydrogen atoms do not play a predominant role in the over-all reaction. Furthermore, as will be discussed below, there is an alternative explanation for the extent of inhibition of HBr decomposition which was caused by added Br_2. The simplest explanation for the consumption of a large amount of atomic nitrogen with no product formation is the reaction

$$N+N+HBr\rightarrow N_2+HBr, \quad (8)$$

where HBr is a very efficient third body, perhaps because an intermediate complex is readily formed with atomic nitrogen.[1,3] Steps (1–5) and (8) account for all main features of the reaction. It was felt worthwhile to attempt quantitative measurements of the rate-controlling step (1) in a system in which the flow patterns of reactants are known and in which the flow rate of atomic nitrogen is curtailed to reduce its catalytic recombination. Results of these rate studies, as well as results of further work on the closely related reaction of active nitrogen with Br_2 and incidental work on the reaction of active nitrogen with ethylene (C_2H_4 reaction), used to monitor the atomic nitrogen flow rate, are reported herein. Further work on the mechanism of flame emission when Br_2 on HBr is fed into active nitrogen is also discussed.

EXPERIMENTAL

The general type of flow system employed, the method of producing active nitrogen and of handling reactants and products are discussed in the previous paper.[1] In the present studies, two types of reaction vessels were employed: (A) a modified "stirred-flow"

[1] H. B. Dunford and B. E. Melanson, Can. J. Chem. **37**, 641 (1959).

[2] Heats of reaction are based on $D_{H-Br}=87$ kcal; D_{N-H}, D_{NH-H}, and D_{NH_2-H}: 87, 90, and 101 kcal, respectively [R. J. Reed and W. Snedden, J. Chem. Soc. **1959**, 4132; G. Pannetier and A. G. Gaydon, J. chim. phys. **48**, 221 (1951); A. P. Altschuller, J. Chem. Phys. **37**, 641 (1954); M. Scwarz, Proc. Roy. Soc. (London) **A198**, 267, 285 (1949)]. The rather remarkable efficiency of NH_4Br formation would tend to confirm that reaction (1) is rate-controlling.

[3] H. G. V. Evans, G. R. Freeman, and C. A. Winkler, Can. J. Chem. **34**, 1271 (1956); W. Forst, H. G. V. Evans, and C. A. Winkler, J. Phys. Chem. **61**, 320 (1957).

low-pressure reactor of 200-ml volume of the type used by Kistiakowsky and Volpi[4]; (B) a "diffusion flame" vessel similar to that used by Greenblatt and Winkler[5] (GW), in which, however, the active nitrogen, instead of flowing through the larger tube, was admitted through a coaxial tube 15 mm i.d. which tapered to 4 mm i.d. at its tip. The other reactant was pumped through the 60 mm i.d. outer Pyrex tube. In all reaction systems used, the total pressure was 0.85 mm and the flow rate of molecular nitrogen was 3.6×10^{-5} mole/sec. The flow rate of atomic nitrogen was controlled by means of a Variac on the primary side of the transformer, or by changing the length of tubing between the discharge tube and reaction vessel.

Photographs of the flame spectra were obtained using a Bausch & Lomb 250-mm monochromator in which a 1 in.×3 in. plate holder was placed over the exit slit. Shutters were so arranged that all or any one-third of a plate could be exposed. Mercury and argon emission spectra were used as references. Dispersion was 66 A/mm.

RESULTS AND DISCUSSION

A. Stirred-Flow Reactor

An atomic nitrogen flow rate of 5×10^{-6} mole/sec was indicated by HCN production from the C_2H_4 reaction.

Results which were essentially identical with those obtained in the earlier study of the HBr reaction were obtained. It was apparent that the reaction is too fast to obtain complete turbulence. It is likely that only about 1×10^{-6} mole/sec of the atomic nitrogen is consumed in reaction (1), and using this figure, an estimate of 5×10^{-15} sec^{-1} $(molecules/cc)^{-1}$ is obtained as a lower limit for the specific rate constant of reaction (1) at 70°C. Since it was not possible to obtain complete turbulence of reactants, it was felt worthwhile to switch to conditions where the reactions were diffusion controlled.

B. Diffusion Flame Apparatus

When the active nitrogen was admitted through a jet into a stream of HBr, it was observed that the Lewis-Rayleigh afterglow was quenched in the immediate vicinity of the tip of the jet and was replaced by a very pale orange flame. If the flow rate of HBr were reduced sufficiently, then the more intense orange flame near the walls was obtained. It was felt that at flow rates of HBr sufficiently large to prevent the wall flame, active nitrogen was being consumed by reactions (1)–(5) and (8) only. Since the boundary of the weak homogeneous flame was very ill defined, rate calculations were based on the minimum flow rate of HBr at which the wall flame was not observed and the reaction zone was assumed to have the diameter of the cylindrical tube. When active nitrogen and bromine were mixed, it was found impossible to obtain an intense homogeneous flame; rather, the most intense flame was always in the region of a wall.

To calibrate the atomic nitrogen flow rate, the rate of HCN formation from the C_2H_4 reaction was measured.[6] With C_2H_4 in excess it was found possible to obtain homogeneous, essentially spherical CN diffusion flames, which could be observed against a dark background. Flame sizes were measured with a centimeter scale after allowance of a constant time for dark adaptation of the eye.

C. Spectroscopic Results

The work of Elliott[7] on the emission spectrum obtained from the flame of the reaction of active nitrogen with Br_2 established the radiating species as the diatomic molecule or radical NBr. We have been able to photograph for both the Br_2 and HBr reactions the same band spectra which Elliott observed. It would seem, therefore, that the N+HBr flame is neither a modified nitrogen afterglow[8] nor a bromine emission spectrum,[1] but is due to NBr. Furthermore, since the intensity distributions of the bands obtained from the two systems appear identical, it would appear that the mechanism of formation of the electronically excited NBr is the same whether Br_2 or HBr is introduced into active nitrogen. The upper and lower states involved in the NBr emission remain to be established.

D. General Discussion

Since Br_2 is an efficient quencher of the nitrogen afterglow, although only molecular bromine is recovered as a reaction product, it would appear plausible that homogeneous reactions of the type

$$N+Br_2\rightarrow NBr+Br \qquad (9)$$

$$N+NBr\rightarrow N_2+Br \qquad (10)$$

occur when bromine and active nitrogen are mixed. There is definitely not enough energy available to form electronically excited NBr in reaction (9), however.[9,10]

The Wigner-Witmer correlation rules show that for the combination of a ^4S nitrogen atom and $^2P_{\frac{3}{2}}$ bromine atom, the resultant molecule can be either in the Σ

[4] G. B. Kistiakowsky and G. G. Volpi, J. Chem. Phys. **27**, 1141 (1957).

[5] J. H. Greenblatt and C. A. Winkler, Can. J. Research **B27**, 732 (1949).

[6] R. Kelly and C. A. Winkler, Can. J. Chem. **37**, 62 (1959); J. T. Herron, J. L. Franklin, P. Bradt, and V. H. Dibeler, J. Chem. Phys. **30**, 879 (1959).

[7] A. Elliott, Proc. Roy. Soc. (London) **A169**, 469 (1939).

[8] R. H. Ewart and W. R. Rodebush, J. Am. Chem. Soc. **56**, 97 (1934).

[9] A bond dissociation energy of 69 kcal is indicated for the lower state of NBr involved in the flame reaction, using a very long Birge-Sponer extrapolation of Elliott's data. However, it remains to be proven that this is the ground state of NBr.

[10] When Br_2 and HBr were admitted simultaneously into active nitrogen, in experiments reported in footnote 1, reaction (9) would become competitive with step (1), which would account for the observed inhibition of HBr decomposition.

or II state. Spin conservation rules show that either a triplet or quintet multiplicity is possible.[11] The latter multiplicity corresponds to a repulsive state since no electrons are bound. The possibility of an induced preassociation reaction cannot be overlooked. Such a mechanism has become widely accepted for the recombination of N atoms[12] and has been proposed for the combination of N+O atoms.[13] At any rate, the formation of some excited state of NBr in the reaction

$$N+Br \rightarrow NBr^* \qquad (11)$$

appears feasible, and if the wall acts as a third body, then the observed flame behavior is accounted for. This is admittedly rather speculative, but to the best of our knowledge, the NBr flame reaction is unique; we have been unable to find another flame reaction which occurs preferentially on or near a glass wall.[14] Bromine adsorbed on the wall may influence the reaction.

Rate calculations, summarized in Table I, are based on the diffusion flame equation[15]

$$k = (\ln P_{jet}/P_0 - \ln R/r)^2 D/(R-r)^2\,[\text{substrate}], \qquad (12)$$

where P_{jet} and P_0 are the partial pressures of atomic nitrogen at the jet and edge of the reaction zone, respectively; [substrate] is the concentration of either C_2H_4 or HBr, R is the reaction zone radius, r is the radius of the jet, and D is the diffusion coefficient of atomic nitrogen.

A value of P_0 for the C_2H_4 reaction at 40°C was obtained by reducing the flow rate of atomic nitrogen to the point where the flame was of minimum size and yet no back diffusion occurred into the nitrogen jet. The value obtained, which corresponded to an atomic nitrogen flow rate of 2×10^{-8} mole/sec when the C_2H_4 flow rate was 6.2×10^{-6} mole/sec, was used in all calculations of k. The same value of P_0 was used for the HBr reaction, since no direct method of obtaining P_0 was possible for this reaction. This is an unavoidable error, but because the HBr and C_2H_4 reactions have comparable rates, it should not be a large one. When more rate data become available for other very fast atomic nitrogen reactions, it may be possible to choose a slightly more suitable reference reaction.

TABLE I. Summary of calculations of rates of the reactions

$N+C_2H_4 \rightarrow HCN+CH_3$

$N+HBr \rightarrow NH+Br.$

Flow rates of reactants, mole/sec×10⁶		Reaction zone diameter, cm	k sec⁻¹ (molecules/cc)⁻¹
C_2H_4	N		
7.0	3.5	3.8	1.5×10^{-13}
7.6	3.5	3.5	1.9×10^{-13}
8.3	3.5	3.2	2.2×10^{-13}
6.2	1.75	3.8	1.0×10^{-13}
			1.6×10^{-13}
HBr			
3.0	1.75	6.0	3.8×10^{-14}

The diffusion coefficient of atomic nitrogen in cm²/sec was calculated from the kinetic equations, $D=1/3\lambda\bar{c}$, $\lambda=1/\sqrt{2}\pi n\sigma^2$. A value of 2.8×10^{-8} cm for σ was used, estimated as a mean of the diameters of atomic and molecular nitrogen, since the latter was present in large excess.[16]

The rate constant for the C_2H_4 reaction is higher by a factor of about three than that obtained by GW, which, considering the errors involved in the two determinations, appears to be in reasonable agreement. True measurement of temperature is perhaps one of the greatest limitations of the diffusion "flame" technique. To minimize thermal gradients, very low atomic flow rates should be used; however, larger errors are then introduced into the measurements of R and the ratio P_{jet}/P_0. All factors considered, it seems reasonable to assign a factor of two as the error in the rate constant for the reaction[17]

$$N+C_2H_4 \rightarrow HCN+CH_3,$$

and a factor of three as the error in the rate constant for reaction (1).

ACKNOWLEDGMENTS

This project was supported financially by the National Research Council of Canada. One of us (ERVM) is also indebted to Canadian Industries Limited for two fellowships.

[11] G. Herzberg, *Spectra of Diatomic Molecules* (D. Van Nostrand Company, Inc., Princeton, New Jersey, 1951), 2nd Ed., Chap. VI.
[12] J. Berkowitz, W. A. Chupka, and G. B. Kistiakowsky, J. Chem. Phys. **25**, 457 (1956).
[13] C. A. Barth, W. J. Shade, and J. Kaplan, J. Chem. Phys. **30**, 347 (1959).
[14] An interesting recombination phenomenon on metal surfaces, which may be related, has recently been reported by R. R. Reeves, G. Mannella, and P. Harteck, J. Chem. Phys. **32**, 946 (1960).
[15] A. F. Trotman-Dickenson, *Gas Kinetics* (Butterworths Scientific Publications, London, 1955), p. 215.
[16] R. A. Back and C. A. Winkler, in work submitted for publication, estimated this value of σ from the results of J. T. Vanderslice, E. A. Mason, and E. R. Lippincott, J. Chem. Phys. **30**, 129 (1959).
[17] K. R. Jennings and J. W. Linnett, Quart. Revs. **12**, 116 (1958); H. G. V. Evans and C. A. Winkler, Can. J. Chem. **34**, 1217 (1956); J. W. S. Jamieson and C. A. Winkler, J. Phys. Chem. **60**, 1542 (1956).

Quantum-Mechanical Cell Model of the Liquid State. II. Application to the Zero-Point Properties of Close-Packed Crystals*

R. P. HURST† AND J. M. H. LEVELT‡

Theoretical Chemistry Laboratory, University of Wisconsin, Madison 5, Wisconsin

(Received May 5, 1960)

The quantum-mechanical cell model previously developed for liquids [J. M. H. Levelt and R. P. Hurst, J. Chem. Phys. **32,** 96 (1960)] is adapted and used to evaluate zero-point properties of the noble gases, H_2 and D_2. Specifically, this theory is applied to determine the heats of sublimation, the zero-point energies and the equation of state for these gases at 0°K. By using the Lennard-Jones (6–12) intermolecular potential constants from second virial coefficients measurements as the only experimental parameters included in the theory, good agreement with the experimentally determined zero-point properties is generally obtained.

I. INTRODUCTION

SEVERAL methods have been developed to calculate the zero-point energy and related properties (energy, volume, and compressibility at 0°K) for close-packed van der Waals crystals with central forces, in an *a priori* way, that is, from a knowledge of the forces between pairs of molecules and from a knowledge of the crystal structure. Whereas the earlier computations were restricted to lattice vibrations of an essentially harmonic character, recent efforts are devoted to lattices in which large anharmonicities occur.

Calculations using the harmonic approximation were performed with the Einstein model by Corner,[1] with the Debye model of Herzfeld and Goeppert Mayer,[2] Kane,[3] and de Boer and Blaisse.[4] The work of Blackman[5] has initiated the search for a better representation of the true frequency spectrum of the lattice waves. If the number of vibrations with a frequency between ν and $\nu+d\nu$ is given by $f(\nu)d\nu$, then the zero-point energy follows from

$$\lambda_0=\int_0^{\nu_m} f(\nu)\,(h\nu/2)\,d\nu, \tag{1}$$

where ν_m is the maximum frequency of the lattice. Therefore, for the computation of zero-point energies, it is sufficient to know the first moment of the frequency distribution. The expressions Montroll[6] derived for even moments of the frequency spectrum have been used by Domb and Salter[7] to obtain this first moment. For example, they show that for a fcc lattice with nearest-neighbor interaction only, the zero-point energy is given by the formula

$$\lambda_0=1.0225h\nu_m=1.0225\frac{h(2\alpha/m)^{\frac{1}{2}}}{\pi}. \tag{2}$$

Here α is the force constant of nearest-neighbor interaction. This force constant can be expressed in terms of intermolecular forces. Thus, in this way, the zero-point energy can be derived from the knowledge of the crystal structure and the intermolecular forces. Salter[8] has applied this method to the crystals of noble gases, and obtained satisfactory results as long as the harmonic approximation is valid, i.e., for the heavy noble gases.

In the Einstein theory, the crystal is considered as consisting of independently oscillating particles, the frequency being given by

$$\nu_E=\frac{(\alpha/m)^{\frac{1}{2}}}{2\pi}. \tag{3}$$

It follows that the zero-point energy for the Einstein treatment is equal to

$$(\lambda_0)_E=(\tfrac{3}{2})h\nu_E=1.0607\frac{h(2\alpha/m)^{\frac{1}{2}}}{\pi}. \tag{4}$$

Thus for a fcc lattice with nearest-neighbor interaction it is shown[7] that the Einstein model gives a close approximation to the true zero-point energy, Eq. (2).

This is not the case for the calculations based upon the Debye theory.[2–4] Here the frequency distribution is a quadratic one with a cutoff at a frequency ν_D given by

$$\nu_D=\bar{c}(3N/4\pi V)^{\frac{1}{3}}. \tag{5}$$

The zero-point energy follows from

$$(\lambda_0)_D=\frac{9h\nu_D}{8}=\frac{9}{8}k\theta. \tag{6}$$

Under simplifying assumptions, the average speed of sound, $\bar{c}$ in Eq. (5), may be related to the elastic constants of the crystal. Finally, the zero-point energy

* This research was supported by the U. S. Atomic Energy Commission.

† Present address: Department of Physics, The University of Oklahoma, Norman, Oklahoma.

‡ Present address: Van der Waals Laboratorium, Gemeente Universiteit, Amsterdam, Netherlands.

[1] J. Corner, Trans. Faraday Soc. **35,** 711 (1939).

[2] K. P. Herzfeld and M. Goeppert Mayer, Phys. Rev. **46,** 995 (1934).

[3] G. Kane, J. Chem. Phys. **7,** 603 (1939).

[4] J. deBoer and B. Blaisse, Physica **14,** 149 (1948).

[5] M. Blackman, Proc. Roy. Soc. (London) **A148,** 365, 384 (1935); **A149,** 126 (1935); **A159,** 416 (1937).

[6] E. W. Montroll, J. Chem. Phys. **10,** 218 (1942); **11,** 481 (1943); **12,** 98 (1944).

[7] C. Domb and L. Salter, Phil. Mag. **43,** 1083 (1952).

[8] L. Salter, Phil. Mag. **45,** 360 (1954).

$(\lambda_0)_D$ is obtained from the relation between the intermolecular field and the elastic constants.

Since the Debye spectrum does not well represent the high-frequency part of the lattice vibrations, which contribute most to the zero-point energy, and because of several approximations made in the calculation of ν_D, an *a priori* calculation of the zero-point energy in terms of molecular forces does not yield very good results if the molecular parameters are not adapted to fit other experimental zero-point properties.[4,9]

Although an *a priori* calculation of the Debye θ, and therefore of the zero-point energy, does not yield good results, the experimental θ as derived from specific heat measurements is still a useful means of estimating experimental zero-point energies. Thus, Domb and Salter[7] have demonstrated that, for various crystal structures, formula (6) represents the true zero-point energy [Eq. (1)] closely, if for θ the value of the experimental Debye temperature in the limit of high temperatures is taken. Therefore, in this paper we consider

$$(\lambda_0)_{\text{exptl}}=\frac{9k(\theta_\infty)_{\text{exptl}}}{8} \tag{7}$$

to be the experimental zero-point energy.

It is well known that the harmonic theories, such as those we have been considering, are not adequate for the light noble gases or for hydrogen or deuterium. These substances have such large zero-point motion in the crystal phase that large anharmonicities occur. The usual methods[1–4,7,8] fail because the force constant α becomes negative. To account for specific heat and elastic properties it is necessary to study the anharmonicity of the lattice vibrations. Hooton,[10] for instance, has applied Born's adapted harmonic approximation to describe the anharmonicity of the lattice waves in solid helium, whereas Yoshimori and Matsubara[11] have developed a variational method useful for small anharmonicity and have applied it to neon.

For the computation of the zero-point energy, it may be that the Einstein model is as satisfactory an approximation for anharmonic problems as it is for problems requiring only a harmonic type potential. The Einstein model has the advantage of requiring relatively few further approximations to facilitate computations. Thinking along these lines, Nagamiya[12] developed a crude single-particle model for solid He. This was followed by the calculations of Toda[13] who used the WKB method to compute the zero-point energy of H_2 and D_2 molecules in a sphericalized potential well in the crystal. Unfortunately, due to the lack of information about the intermolecular forces at that time, his numerical results are not as accurate as the method would warrant. A perturbation treatment introduced by Henkel[14] gives good results for the thermal and elastic properties of the argon crystal, but cannot be used for the light gases H_2, D_2, and He.

In this paper we present a calculation of the zero-point energy, volume, lattice energy, and compressibility at 0°K of close-packed van der Waals crystals by means of an anharmonic Einstein theory. We assume central additive forces of the Lennard-Jones (6–12) type. The potential field around a lattice point is sphericalized, i.e., the actual potential is averaged over all directions, holding the other molecules fixed in their lattice positions.

In the present work, the zero-point energy is obtained from an accurate solution of the Schrödinger equation, appropriate to the problem under consideration. The method used in solving the Schrödinger equation is analogous to the method of paper I of this series.[15] It is found that only in cases where the quantum parameter is sufficiently small such that the zero-point energy is a small fraction of the total crystal energy is a perturbation treatment of the harmonic problem sufficient.

This theory has been applied to the series of noble gases and to hydrogen and deuterium. All calculations presented here are based on the Lennard-Jones (6–12) intermolecular potential, and they are performed in reduced units. From the volume dependence of the zero-point energy, the crystal volume, energy, and compressibility at 0°K have been computed. On comparing the present results with experiment, one should recognize that the parameters of the intermolecular field have been derived entirely from second virial coefficient data; no adjustable parameters have been included so as to fit the computed results to the experimental zero-point properties.

II. METHOD AND CALCULATIONS

A. Eigenvalue Problem for the Crystal Field

The total energy U_0 of a crystal at absolute zero is given by the sum of the static potential energy of the lattice $\frac{1}{2}N\phi(0)$ and the zero-point vibrational energy $N\lambda_0$, so that

$$U_0=N[\tfrac{1}{2}\phi(0)+\lambda_0]. \tag{8}$$

Thus, the predicted volume V for the crystal at 0°K and at pressure P is that value of V for which

$$(\partial U_0/\partial V)_{T=0}=-P. \tag{9}$$

Since, as will be shown presently, it is a relatively simple matter to compute $\frac{1}{2}N\phi(0)$, the basic problem reduced to devising a means of obtaining λ_0 as a function of V.

[9] R. J. Lunbeck, thesis, Amsterdam (1951).
[10] D. J. Hooton, Phil. Mag. **46**, 422, 433, 485, 701 (1955).
[11] A. Yoshimori and T. Matsubara, J. Phys. Soc. Japan **9**, 465 (1954).
[12] T. Nagamiya, Proc. Phys. Math. Soc. Japan **22**, 492 (1940).
[13] M. Toda, Proc. Phys. Math. Soc. Japan **22**, 503 (1940).
[14] J. H. Henkel, J. Chem. Phys. **23**, 681 (1955).
[15] J. M. H. Levelt and R. P. Hurst, J. Chem. Phys. **32**, 96 (1960).

In the present treatment, as with the cell theory of liquids,[15–19] it is assumed that each molecule is restricted in its motion to a cell formed by its neighbors. Further, it is assumed that the forces between molecules are additive and that two molecules at a separation r interact according to the well-known Lennard-Jones (6–12) potential

$$\phi_{L-J}(r)=\phi_{L-J}'(\rho)=4\epsilon[(\sigma/r)^{12}-(\sigma/r)^{6}]$$
$$=4\epsilon[(1/\rho)^{12}-(1/\rho)^{6}]. \quad (10)$$

Here ϵ and σ are parameters characteristic of the molecule, representing the depth of the potential well and the distance at which the potential is zero, respectively.

Finally, when computing the potential $\phi(\rho)$ at a distance ρ, measured from the center of the cell considered, we assume that the contribution due to each shell of neighbors can be replaced by a "sphericalized" potential $\phi_i(\rho)$. That is, the contribution $\phi_i(\rho)$, due to the ith spherical shell of radius δ_i and containing N_i molecules is simplified by averaging over all angles so that[15,16]

$$\phi_i(\rho)=\tfrac{1}{2}N_i\int_0^{\pi}\phi_{L-J}'\{(\rho^2+\delta_i^2-2\delta_i\rho\cos\theta)^{\frac{1}{2}}\}\sin\theta d\theta \quad (11a)$$

or

$$\phi_i(\rho)=\frac{\epsilon N_i}{\delta_i\rho}\left\{\frac{1}{2}\left[\frac{1}{(\rho+\delta_i)^4}-\frac{1}{(\rho-\delta_i)^4}\right]\right.$$
$$\left.+\frac{1}{5}\left[\frac{1}{(\rho-\delta_i)^{10}}-\frac{1}{(\rho+\delta_i)^{10}}\right]\right\}. \quad (11b)$$

In Eqs. (11) and in the formulas which follow the lengths, δ_i and ρ are given in the usual reduced units.[15,9,19] Next, to facilitate the solution of the resulting eigenvalue problem, Eq. (11b) is expressed in terms of a Taylor's series expansion in ρ, so that one obtains

$$\phi_i(\rho)=4N_i\epsilon\sum_{n=0}^{\infty}C_{2n}{}^{i}\rho^{2n}, \quad (12a)$$

where

$$C_{2n}{}^{i}=\frac{1}{\delta_i{}^{2n+12}}\frac{(2n+10)!}{10!(2n+1)!}-\frac{1}{\delta_i{}^{2n+6}}\frac{(2n+4)!}{4!(2n+1)!}, \quad (12b)$$

Then, the total potential $\phi(\rho)$ within the cell in question, the sum of the contributions of all neighbors is given by

$$\phi(\rho)=\sum_{i=1}^{\infty}\phi_i(\rho)=4\epsilon\sum_{i=1}^{\infty}\sum_{n=0}^{\infty}N_iC_{2n}{}^{i}\rho^{2n}. \quad (13)$$

Equation (13) is then written

$$\phi(\rho)=4\epsilon\sum_{n=0}^{\infty}B_{2n}\rho^{2n}, \quad (14)$$

where

$$B_{2n}=\frac{(2n+10)!}{10!(2n+1)!}\left[\sum_{i=1}^{\infty}\frac{N_i}{\delta_i{}^{2n+12}}\right]-\frac{(2n+4)!}{4!(2n+1)!}\left[\sum_{i=1}^{\infty}\frac{N_i}{\delta_i{}^{2n+6}}\right], \quad (15)$$

or

$$B_{2n}=\frac{(2n+10)!}{10!(2n+1)!}\frac{1}{\alpha^{2n+12}}\left[\sum_{i=1}^{\infty}\frac{N_i}{(\delta_i/\alpha)^{2n+12}}\right]$$
$$-\frac{(2n+4)!}{4!(2n+1)!}\frac{1}{\alpha^{2n+6}}\left[\sum_{i=1}^{\infty}\frac{N_i}{(\delta_i/\alpha)^{2n+6}}\right]. \quad (16)$$

In Eq. (16) the nearest-neighbor distance δ_1 has been denoted by α.

In this paper calculations are presented for the two close-packed crystal systems, face-centered cubic and hexagonal close-packed. For these calculations the number of neighbors N_i and the ratios δ_i/α were taken from the tables of Kihara and Koba.[20]

Thus, for the static potential energy $\frac{1}{2}N\phi(0)$, one obtains

$$\tfrac{1}{2}N\phi(0)=2N\epsilon B_0$$
$$=2N\epsilon[(12.13188/\alpha^{12})-(14.45392/\alpha^{6})] \quad (17)$$

for the face-centered cubic crystals, and

$$\tfrac{1}{2}N\phi(0)=2N\epsilon[(12.13229/\alpha^{12})-(14.45489/\alpha^{6})] \quad (18)$$

for the hexagonal close-packed crystals.

The zero-point vibrational energy per molecule λ_0 is obtained by solving the Schrödinger equation [See footnote reference 15, Eq. (16)]

$$-(\hbar^2/2m\sigma^2)\nabla^2\psi+[\tilde{V}(\rho)-\lambda_n]\psi=0 \quad (19)$$

for the lowest eigenvalue λ_0. In this case $\tilde{V}(\rho)$ is the potential energy within the cell less the potential at the center of the cell, i.e.,

$$V(\rho)=\phi(\rho)-\phi(0)=4\epsilon\sum_{n=1}^{\infty}B_{2n}\rho^{2n}, \quad (20)$$

where again B_{2n} is obtained from Eq. (16). Further, as with the cell theory for liquids, Eq. (19) is solved subject to the condition

$$\psi=0 \quad \text{at} \quad \rho=\rho_m=r_m/\sigma=(1/\sigma)(3V/4\pi N)^{\frac{1}{3}},$$
the cell boundary. (21)

This Schrödinger equation, Eq. (19), has been shown[15,21] to have solutions of the form

$$\psi_{l,m,n}=Y_{l,m}(\theta,\phi)R_{l,n}(t). \quad (22)$$

[16] J. E. Lennard-Jones and A. F. Devonshire, Proc. Roy. Soc. (London) **A163,** 53, (1937).
[17] J. G. Kirkwood, J. Chem. Phys. **18,** 380 (1950).
[18] R. H. Wentorff, R. J. Buehler, J. O. Hirschfelder, and C. F. Curtiss, J. Chem. Phys. **18,** 1484 (1950).
[19] J. deBoer, Proc. Roy. Soc. (London) **A215,** 4 (1952).
[20] T. Kihara and S. Koba, J. Phys. Math. Soc. Japan **7,** 348 (1952).
[21] K. S. Pitzer, *Quantum Chemistry* (Prentice-Hall, Inc., New York, 1954), pp. 39, 46.

The $Y_{l,m}(\theta, \phi)$ are spherical harmonics and $R(t)_{l,n}$ is a solution of the differential equation

$$(1/t^2)(d/dt)\left[t^2\frac{dR_{l,n}(t)}{dt}\right]$$

$$+\left\{\frac{-l(l+1)}{t^2}+\frac{8\pi^2\rho_m{}^2}{\Lambda^2\epsilon}[\lambda-\tilde{V}(t)]\right\}R(t)_{l,n}=0, \qquad (23)$$

where

$$\tilde{V}(t)=4\epsilon\sum_{i=1}^{\infty}(B_{2n}\rho_m{}^{2n})t^{2n} \quad \text{and} \quad \Lambda^2=h^2/\sigma^2 m\epsilon. \qquad (24)$$

Since $t=\rho/\rho_m$, the boundary condition Eq. (21) becomes

$$R_{l,n}(t)=0 \quad \text{at} \quad t=1. \qquad (25)$$

Using the power series method previously outlined,[15] Eq. (23) is solved for the lowest eigenvalue λ_0. It is well to emphasize that the method used to solve this eigenvalue problem introduces no approximations which are not inherent in the cell model itself or in the shape of the potential.

During the course of making the calculations two effects are noted. First of all, as one proceeds to systems corresponding to progressively smaller quantum parameters, Λ, the number of terms required in the power series to give adequate convergence of the radial eigenfunction increases rapidly. Secondly, it is found that as Λ is decreased fewer terms in the expansion of the potential, Eq. (20), are required to give the same accuracy in the eigenvalues.

These facts suggest a modification in the technique for computing λ_0 for the difficult cases of the systems with small Λ. This modification is quite useful. For example, with argon for which $\Lambda=0.185$, over 1000 terms are required for a satisfactory convergence of the radial wave function. The situation is even worse for the cases with smaller Λ.

First, neglecting all but the first term in Eq. (20), i.e., B_2t^2, the Schrödinger equation is of the harmonic oscillator form. For cases for which

$$(2\pi/\Lambda)(8\rho_m{}^4B_2)^{\frac{1}{4}}>10^2 \qquad (26)$$

the boundary condition $R_{l,n}(t)=0$ at $t=1$ is for practical purposes numerically equivalent to the condition $R_{l,n}(t)\to 0$ as $t\to\infty$.

Then, the radial eigenfunction for the lowest state of the harmonic oscillator is given by[21]

$$R_{0,1}(t)=A\exp(-\tfrac{1}{2}\beta t^2), \qquad (27)$$

where

$$\beta=(2\pi/\Lambda)(8\rho_m{}^4B_2)^{\frac{1}{4}} \qquad (28)$$

and A is a normalization factor given by

$$A=\left[\int_0^{\infty}\exp(-\beta t^2)t^2dt\right]^{-\frac{1}{2}}. \qquad (29)$$

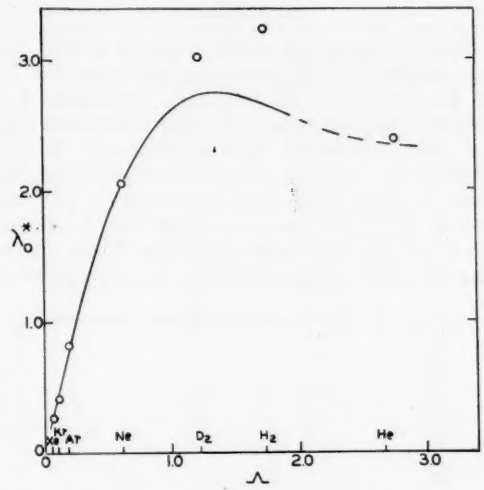

FIG. 1. Reduced zero-point energy $\lambda_0{}^*$ as a function on the quantum parameter Λ. Curve: calculated values at $P=0$ (helium; $P=25$ atm); circles: "average" experimental values.

From first-order perturbation theory we have[22]

$$(2\rho_m{}^2/\epsilon)\lambda_0=(3\beta\Lambda^2/4\pi^2)$$

$$+8\Lambda^2\rho_m{}^2\int_0^{\infty}\exp(-\beta t^2)[B_4(\rho_m t)^4+B_6(\rho_m t)^6+\cdots]t^2dt, \qquad (30)$$

or

$$\lambda_0/\epsilon=(\Lambda^2/8\pi^2\rho_m{}^2)[3\beta+\tfrac{15}{4}(B_4/B_2)\rho_m{}^2$$

$$+(105/8\beta)(B_6/B_2)\rho_m{}^4+\cdots]. \qquad (31)$$

It is to be emphasized that for crystals such as He, H_2, D_2, and Ne, the approximation formula for λ_0 given by Eq. (31) is poor. For example, B_2 for the helium crystal is actually negative so that Eq. (31) could not be applied for this crystal even in the roughest of approximations. Thus Eq. (31) is useful only in those cases where Λ is sufficiently small, and the volume such, that this approximate formula gives results in agreement with the exact method.

In summary, the static potential energy $\frac{1}{2}N\phi(0)$, and the zero-point vibrational energies $N\lambda_0$ are computed as functions of the volume V. The static potential energies are computed from Eq. (17) or (18), and the zero-point vibrational energies are obtained from the exact power series method previously outlined,[15] or from Eq. (31). Finally, from Eq. (8), subject to Eq. (9), the total lattice energies, the volumes, the zero-point energies and the compressibilities are derived. The next section, containing the results, will give some more details of the computation.

[22] H. Margenau and G. M. Murphy, *The Mathematics of Physics and Chemistry* (D. Van Nostrand Co., Inc., Princeton, New Jersey, 1943), p. 373.

III. RESULTS

Computations of the crystal properties at 0°K have been performed for the monatomic substances ^{4}He, Ne, Ar, Kr, and Xe. In addition, these calculations have been made for the crystals of hydrogen and deuterium. The errors introduced by the asymmetry of these molecules are probably small.[23] No attempt has been made to calculate zero-point properties for solid ^{3}He, since its zero-point volume is so large that the application of the cell model seems unjustified. These calculations were made using the form for the potential which

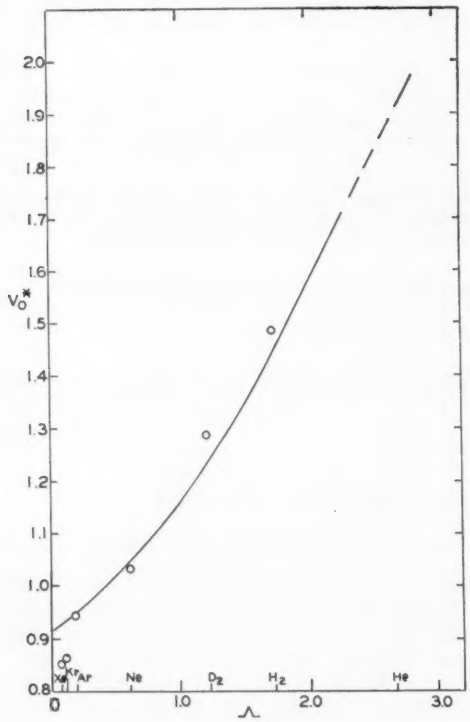

FIG. 2. Reduced molar volume V_0^* at 0°K as a function of the quantum parameter Λ. Curve: calculated values at $P=0$ (helium: $P=25$ atm); circles: "average" experimental values.

coincides with the experimentally observed crystal structure. That is, the calculations for Ne, Ar, Kr, and Xe were made assuming that these substances crystallize in a face-centered cubic lattice. Solid He, H_2, and D_2 are assumed to have hexagonal close-packed structures.

The zero-point energy has been obtained for each of the substances over a range of values of the reduced volume. Here the "exact" procedure[15] has been followed for the crystals of He, H_2, D_2, Ne, and Ar, whereas the approximation method, Eq. (31), has been applied to solid Ne, Ar, Kr, and Xe. The approximation method

[23] J. deBoer, Physica **10**, 357 (1943).

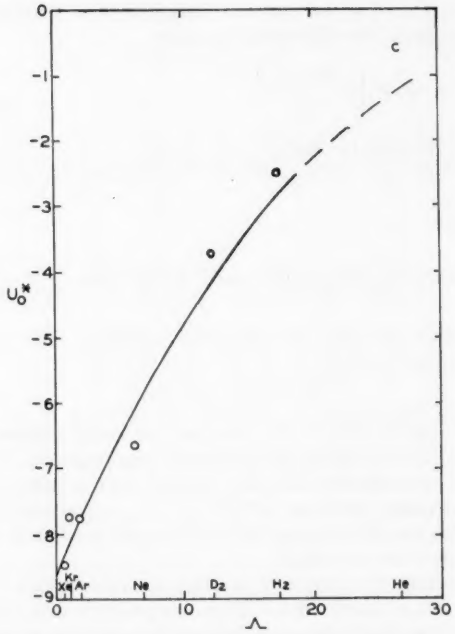

FIG. 3. Reduced crystal energy V_0^* at 0°K as a function of the quantum parameter Λ. Curve: calculated values at $P=0$ (helium: $P=25$ atm); circles: "average" experimental values.

results in a volume dependent deviation from the "exact" answer. This disparity becomes less with decreasing Λ. Thus, the deviation is of the order of 1% in λ_0 for neon, and about 0.1% for argon, when three terms are used in Eq. (31); use of more terms results in slightly increasing deviations.

After the reduced zero-point energy for a substance had been obtained for a number of values of the reduced volume, a polynomial in the volume was fitted to the computed λ_0/ϵ values. The pressure then followed from Eq. (9) with (8). The volume for which the pressure is zero was determined graphically. At this volume, the static potential was obtained from (17)

TABLE I. Parameters of the Lennard-Jones (6-12) potential field.

Gas	ϵ/k in °K	$N\sigma^3$ in cc/mole	$\Lambda=h/\sigma(m\epsilon)^{\frac{1}{2}}$	Reference
^{4}He	10.22	10.06	2.674	a, b
H_2	37.00	15.12	1.729	a, b
D_2	37.00	15.12	1.223	
Ne	33.74	12.61	0.6084	c
Ar	119.5	23.89	0.185	d, e
Kr	166.67	30.05	0.1007	d
Xe	225.3	40.62	0.0625	d

[a] J. de Boer and A. Michels, Physica **5**, 945 (1938).
[b] See footnote reference 9.
[c] G. A. Nicholson and W. G. Schneider. Can. J. Chem. **33**, 589 (1955).
[d] E. Whalley and W. G. Schneider, J. Chem. Phys. **23**, 1644 (1955).
[e] A. Michels, J. M. H. Levelt, and W. de Graaff, Physica **24**, 659 (1958); J. M. H. Levelt, thesis, Amsterdam, 1958.

TABLE II. Calculated zero-point properties.

Substance	V^*	λ_0^*	Properties at 0°K, $P=0$	P in atm	Compressibility V in cc/mole	$\Delta V/V_0 \cdot 10^2$
Helium	1.7	3.232573		20	19.35	
$\Lambda=2.674$	1.8	2.763482		30	18.84	
	1.9	2.376010		40	18.41	
	2.0	2.053062		50	18.04	
	2.2	1.552240		60	17.73	
	2.4	1.189966		70	17.44	
				80	17.17	
Hydrogen	1.3	3.647649	$V^*=1.4422$	0	21.81	
$\Lambda=1.729$	1.4	2.926454	$\lambda_0^*=2.6714$	100	20.90	4.2
	1.45	2.626993	$\frac{1}{2}N\phi^*(0)=-5.5475$	200	20.23	7.2
	1.5	2.360651	$U_0^*=-2.8761$	300	19.70	9.7
	1.6	1.909963				
Deuterium	1.1	3.859419	$V_0^*=1.2323$	0	18.63	
$\Lambda=1.223$	1.2	2.984933	$\lambda_0^*=2.7516$	200	17.84	4.2
	1.3	2.323664	$\frac{1}{2}N\phi^*(0)=-6.8882$	400	17.27	7.3
	1.4	1.812631	$U_0^*=-4.1366$	600	16.82	9.7
	1.5	1.410275				
Neon	1.0	2.337396	$V_0^*=1.0480$	0	13.22	
$\Lambda=0.6084$	1.045	2.048097	$\lambda_0^*=2.0303$	100	13.07	1.1
	1.05	2.018447	$\frac{1}{2}N\phi^*(0)=-8.1315$	200	12.94	2.1
	1.10	1.745798	$U_0^*=-6.10126$	300	12.83	3.0
				400	12.71	3.9
				500	12.59	4.8
Argon	0.916	0.87605	$V_0^*=0.95205$	0	22.74	
$\Lambda=0.185$	0.93	0.83759	$\lambda_0^*=0.7808$	200	22.53	0.9
	0.95	0.78584	$\frac{1}{2}N\phi^*(0)=-8.5630$	400	22.33	1.8
	0.96	0.76126	$U_0^*=-7.7823$	600	22.15	2.6
	0.97	0.73751		800	21.98	3.3
				1000	21.82	4.0
Krypton	0.91	0.48187	$V_0^*=0.93536$	0	28.11	
$\Lambda=0.1007$	0.92	0.46648	$\lambda_0^*=0.4439$	200	27.93	0.6
	0.93	0.45162	$\frac{1}{2}N\phi^*(0)=-8.5959$	400	27.76	1.2
	0.936	0.44300	$U_0^*=-8.1521$	600	27.61	1.8
	0.94	0.43728		800	27.46	2.3
				1000	27.31	2.8
Xenon	0.91	0.29777	$V_0^*=0.92792$	0	37.69	
$\Lambda=0.0625$	0.915	0.29294	$\lambda_0^*=0.2809$	200	37.46	0.6
	0.92	0.28821	$\frac{1}{2}N\phi^*(0)=-8.6047$	400	37.25	1.2
	0.925	0.28355	$U_0^*=-8.3238$	600	37.04	1.7
	0.93	0.27897				

or (18), whereas the appropriate value of λ_0/ϵ followed from the fitted polynomial expression. The sum of these two energies then gave the heat of sublimation U_0/ϵ at 0°K and zero pressure.

In the equations, the only parameter characteristic of the molecule under consideration is the quantum parameter $\Lambda=h/\sigma(m\epsilon)^{\frac{1}{2}}$. It follows that the results, shown in Figs. 1–3, remain valid even if more accurate force constants may be established. In that case, the proper reduced zero-point properties may be obtained by interpolation from Figs. 1–3 for the new value of Λ.

In order to compare these results with experiment, the values of ϵ/k and σ must be known separately. The values of ϵ/k and σ given in Table I have been obtained solely from experimental data for the second virial coefficient. It has been assumed that the potential fields of H_2 and D_2 are identical. This is not entirely justified, but the error is probably small.[9,23]

The results of the calculations of the zero-point properties are summarized in Table II.

IV. COMPARISON WITH EXPERIMENT

The question as to whether theory and experiment agree has two aspects. The first is the reliability of the experimental crystal data available. Some indication of this reliability is obtained when data from different sources are compared. An equally important consideration is the accuracy of the data of Table I, the parameters of the Lennard-Jones (6–12) potential field, since these parameters enter in a straightforward manner into the comparison. In considering this latter factor, one should recognize that the potential parameters of the heavy noble gases are usually not more reliable than 1%. This accuracy can certainly not be claimed for the parameters of ^4He, H_2, and D_2.

The experimental crystal data are summarized in

TABLE III. Experimental data for crystal properties.

Substance	Volume V cc/mole	at T°K	P atm	Energy U_0 cal/mole	Debye θ θ°K	at T°K,	V cc/mole	Reference
Helium	17.4	4.0	130		32.5	2.7–3.7	17.4	a
	18.2	3.6	109					a
	17.4	4.0	130		37–32	1–3	18.4	b
	17.8	3.6	109		32–27	1–2.5	19.3	b
	19.8	2.2	48		30–25	1–2.2	19.9	b
	19.5	1.45	37					c
	21.2	0	25	−11.9				d, from a–d
	17.3	4.0	130		75	5–12	13.0	e
					60	4–7	14.4	e
	18.7	1.15	66		22.7	0	20.6	e, from f
								g
Hydrogen	22.91	2						h
	25.0	11						i
				−183.4				j
	22.9	0						k
					105	11–18	23.5	l
	22.65	4.2						m
Deuterium	20.3	0						k
					94–98	11–21	20.0	l
	20.5	18.7		−274.0				n
	19.56	4.2						m
Neon				−447.6	57–63	11–21		o
	13.9	4.2						p
	14.0	24.57			64–62	12–18		q
	14.0	24.57						r
	13.0	4.2						s
Argon	24.0	40						t
	23.7	20						u
	25.0	84		−1600	79–84	10–17		q
	24.6	84						r
				−1818				v, from w–y
	22.6	0						z
	22.6	0		−1850	81			a′, from a′, q, z
	21.9	4						s
Krypton	26.3	20						b′
	29.1	77						c′
	27.7	82						d′
	27.8	89						d′
	27.8	92						d′
					63	10–15		q
				−2589				v, from q, e′
	28.4	75						f′
	29.1	105						f′
Xenon	35.5	82						g′
	36.5	88						d′
					55	10–20		q
	37.1	161						r
	34.6	0		−3828				v, from r, h′

[a] R. Kaishew and F. E. Simon, Nature **133**, 460 (1934).
[b] W. H. Keesom and A. P. Keesom, Physica **3**, 105 (1936).
[c] W. H. Keesom and K. W. Taconis, Physica **5**, 161 (1938).

Table III and in part of Table V. We will consider energy, volume, Debye temperatures, and compressibilities separately.

Generally, for the crystal energy, only one source of information is available per substance, so the reliability is hard to judge. For the heavy noble gases, large extrapolations have been made to arrive at the experimental sublimation energy at 0°K.

For the crystal volumes (or lattice parameters) more data are available; however, even recent data show discouraging discrepancies, if obtained by different methods (see Ne and Ar). An error of $\frac{1}{2}$-1 cc in the zero-point volume/mole must be expected in most instances.

Debye temperatures from different sources have a tendency to show better agreement. It should be borne in mind, however, that for H_2 and D_2, the measurements of c_v are scarce, and usually not performed at the volume at 0°K. In addition, the experimental ratios $\Delta V/V$ of Table V, as given in footnote references d and e, were not obtained from direct experimental measurements. Only ΔV was measured as a function of the pressure, whereas V was obtained from a semiempirical equation of state.

Comparison of theory and experiment is shown in Table IV and V. The entries labeled "experimental" have been obtained by "averaging" the information of Table III; for the volumes, preference has been given to the newer data; in the case of Debye temperatures, to those at higher temperatures.[7]

The comparison presented in Table IV shows a fair to good agreement for the zero-point volumes, the theoretical values being too high at low Λ and too low at high Λ. The calculated crystal energy is close to the experimental value for the heavy noble gases, but too low for ^4He, H_2, and D_2. One should remember that the calculated value is obtained as a difference of two terms which are almost equal in the case of ^4He. The computed zero-point energy is close to that derived from the experimental Debye θ.

On comparing the experimental and calculated compressibilities as presented in Table V, it is found that the behavior of solid H_2 and Ne is well represented by the theory, whereas the predicted values for the compressibility of D_2 are definitely too low. The volume change of solid ^4He between 50 and 88 atm is rather well predicted. It may be of interest to mention that the results of our computations for ^4He agree in the range where they overlap with the cell-model calculations for liquid ^4He performed by Pekeris.[24]

Finally, it may be of interest to point out that the recent determinations of second virial coefficients of H_2 and D_2[25,26] will lead to new values of the force constants in the Lennard-Jones potential. In fact, there is evidence[27] that the value of ϵ/k for D_2 quoted in Table I should be decreased by 5%. As a consequence, the calculated value of λ_0 and U_0 in Table IV, and of the compressibility in Table V, will increase by about 5%, which gives an appreciable improvement in the agreement of theory and experiment.

---

[d] C. A. Swenson, Phys. Rev. **79,** 626 (1950).
[e] J. S. Dugdale and F. E. Simon, Proc. Roy. Soc. (London) **218,** 291 (1953).
[f] F. J. Webb, K. R. Wilkinson, and J. Wilks, Phys. Rev. **214,** 546 (1952).
[g] D. G. Henshaw, Phys. Rev. **109,** 328 (1958).
[h] W. H. Keesom, J. de Smedt, and H. H. Mooy, Communs. Phys. Lab. Univ. Leiden **209d,** (1930).
[i] H. Kamerlingh Onnes and C. A. Crommelin, Communs Phys. Lab. Univ. Leiden **137a,** (1913).
[j] F. Simon, Z. Physik **15,** 307 (1923).
[k] E. Bartholomé, Z. physik Chem. (Leipzig) **B33,** 387 (1935).
[l] E. Bartholomé and A. Eucken, Z. Electrochem. **42,** 547 (1936).
[m] H. D. Megaw, Phil. Mag. **28,** 129 (1939).
[n] K. Clusius and E. Bartholomé, Z. physik Chem. (Leipzig) **B30,** 237 (1935).
[o] K. Clusius, Z. physik Chem. (Leipzig) **B4,** 1 (1929).
[p] J. de Smedt, W. H. Keesom, and H. H. Mooy, Communs. Phys. Lab. Univ. Leiden **203e,** (1930).
[q] K. Clusius, Z. physik Chem. (Leipzig) **B31,** 459 (1936).
[r] K. Clusius and K. Weigand, Z. physik Chem. (Leipzig), **B46,** 1, (1940).
[s] D. G. Henshaw, Phys. Rev. **111,** 1470 (1958).
[t] F. E. Simon and C. v. Simson, Z. physik **25,** 160 (1924).
[u] J. de Smedt and W. H. Keesom, Physica **5,** 344, (1925).
[v] E. Whalley and W. G. Schneider, J. Chem. Phys. **23,** 1644 (1955).
[w] C. A. Crommelin, Communs. Phys. Lab. Univ Leiden **138a, 140a,** (1914).
[x] F. Born, Ann. Physik **69,** 473 (1922).
[y] A. Eucken and F. Hanck, Z. physik Chem. (Leipzig) **134,** 161 (1928).
[z] E. R. Dobbs, B. F. Figgins, G. O. Jones, D. C. Piercey, and D. P. Riley, Nature **178,** 483 (1956).
[a'] E. R. Dobbs and G. O. Jones, Repts. Progr. Phys. **20,** 516 (1957).
[b'] W. H. Keesom and H. H. Mooy, Nature **125,** 889 (1930).
[c'] G. Natta and A. G. Nassini, Nature **125,** 889 (1930).
[d'] B. Ruhemann and F. Simon, Z. physik Chem. (Leipzig) **B15,** 389 (1932).
[e'] K. Clusius, A. Kruis, and F. Konnertz, Ann. Physik **33,** 642 (1938).
[f'] E. R. Dobbs, Brit. J. Appl. Phys. **7,** 433 (1956).
[g'] G. Natta and A. G. Nassini, Nature **125,** 457 (1930).
[h'] K. Clusius and L. Riccoboni, Z. physik Chem. (Leipzig) **B38,** 81 (1937).

[24] C. L. Pekeris, Phys. Rev. **79,** 884 (1950).
[25] J. J. M. Beenakker, F. H. Varekamp, and A. v. Itterbeek, Physica **25,** 9 (1959).
[26] A. Michels, W. de Graaff, T. Wassenaar, J. M. H. Levelt, and P. Louwerse, Physica **25,** 25 (1959).
[27] W. de Graaff (private communication).

TABLE IV. Experimental and calculated crystal properties at 0° K.

Substance	V in cc/mole		$-U_0$ in cal/mole		Debye θ	$\lambda_0=9/8R\theta_\infty$ λ^0 in cal/mole	
	exptl	calc	exptl	calc	exptl	exptl	calc
Helium (25 atm)	21.2	19.09	11.9	23.6	22	49.2	48.5
Hydrogen	22.5	21.81	183.4	211.4	108	241	196.4
Deuterium	19.5	18.63	274.0	304.1	100	224	202.3
Neon	13	13.22	448	409.0	62	139	136.1
Argon	22.5	22.74	1840	1848	81	181	185.4
Krypton	26	28.11	2590	2700	63	141	147
Xenon	34.6	37.69	3830	3726	55	123	125.7

V. DISCUSSION

In judging the merits and weaknesses of the present theory, the following aspects are to be considered. First, is this theory capable of representing the experimental data, and how does this representation compare with other theories which use the same amount of *a priori* information? Finally, the theory may be judged on its intrinsic qualities. In particular, can such deviations from experiment, as are found, be explained on the basis of the assumptions inherent in the theory?

As to the first point, the conclusion of the preceding section is that this anharmonic Einstein theory, based on Lennard-Jones (6–12) interaction, represents the experimental zero-point properties of van der Waals crystals in a satisfactory way. It is hard to determine whether it is superior to other theories in this respect. Only for the harmonic theories of de Boer and Blaisse[4] and of Salter[8] are the results presented in reduced form, and it is well known that these theories do not apply for values of Λ larger than 1. In most of the other work the potential parameters have been adjusted for better agreement.

The assumptions inherent in the present theory fall into three classes: the use of an Einstein model for calculating zero-point properties, which has been discussed in the Introduction, the use of the (6–12) potential, and the approximations involved in the model proper.

The use of the (6–12) potential may be responsible for the trend found in the comparison of experimental and calculated zero-point volumes. For this potential, the classical reduced crystal volume, which one obtains

TABLE V. Experimental and calculated compressibilities.

Substance	T° K	Experimental P	V in cc/mole	$\Delta V/V_0$	Ref.	Calc at P_{exp}, 0° K V in cc/mole	$\Delta V/V_0$
Helium	0	25 atm	21.18		a	19.08	
	0	50 atm	19.0		b	18.05	
	0	88 atm	18.0		b	16.97	
Hydrogen	4.2	0 kg/cm²	22.65		c	21.81	
	4.2	25 kg/cm²	22.30	0.015	c	21.56	0.011
	4.2	50 kg/cm²	22.01	0.028	c	21.32	0.022
	4.2	75 kg/cm²	21.79	0.038	c	21.11	0.032
	4.2	100 kg/cm²	21.63	0.045	c	20.92	0.041
	4.2	200 atm		0.076	d	20.23	0.072
Deuterium	4.2	0 kg/cm²	19.70		c	18.63	
	4.2	25 kg/cm²	19.45	0.013	c	18.52	0.006
	4.2	50 kg/cm²	19.28	0.021	c	18.41	0.012
	4.2	75 kg/cm²	19.14	0.028	c	18.31	0.017
	4.2	100 kg/cm²	19.06	0.032	c	18.22	0.022
	4.2	200 atm		0.056	d	17.84	0.042
	4.2	400 atm		0.093	d	17.27	0.073
	4.2	600 atm		0.121	d	16.82	0.097
Neon	4.2	200 kg/cm²		0.016	e	12.95	0.020
	4.2	400 kg/cm²		0.031	e	12.73	0.037

[a] C. A. Swenson, Phys. Rev. **79**, 626 (1950).
[b] J. S. Dugdale and F. E. Simon, Proc. Roy. Soc. (London) **A218**, 291 (1953).
[c] H. D. Megaw, Phil. Mag. **28**, 129 (1939).
[d] J. W. Stewart and C. A. Swenson, Phys. Rev. **94**, 1069 (1954).
[e] J. W. Stewart, Phys. Rev. **97**, 578 (1955).

by minimizing the static potential energy $\frac{1}{2}N\phi(0)$ is equal to 0.916. The experimental reduced volumes of Xe and Kr should be slightly larger; however, they are equal to 0.85 and 0.86, respectively. If this discrepancy is not due to experimental errors in measuring the crystal volume, then the assumption about the shape or the additivity of the potential must be in error.

The most serious approximation of the model is made in averaging the potential. The assumption about the fixed position of the neighbors is unjustified when the wave function is spread out over an appreciable part of the cell, as in the case of solid He. The theory could be improved by using the wave functions obtained in first approximation to obtain a new average potential and a more realistic lattice energy. For crystals other than He, the wave function is concentrated in a rather small volume, and the assumptions made in the averaging process should not be too serious. The error introduced by the finite cutoff of the potential, Eq. (21), is probably small in all cases. Even for ^{4}He, it occurs at a value of the potential about 80 times larger than the zero-point energy.

ACKNOWLEDGMENTS

The authors take great pleasure in thanking Professor J. O. Hirschfelder for his encouragement and for helpful discussions and suggestions. In addition, many thanks go to Professor I. Shavitt for his advice on efficient use of the computer.

THE JOURNAL OF CHEMICAL PHYSICS VOLUME 34, NUMBER 1 JANUARY, 1961

Photoconduction Activation Energies in *cis-trans* Isomers of β-Carotene

BARNETT ROSENBERG

Department of Physics, New York University, Washington Square, New York

(Received May 27, 1960)

The activation energies for photoconduction have been measured in all *trans* and 15-15′ *cis* β-carotene powders and in β-carotene glass consisting of a mixture of isomers. The average values of a number of measurements of each are all *trans*, 0.37 ev; 15-15′ *cis*, 0.20 ev; isomerized glass, 0.19 ev. The values predicted by the triplet state theory of photoconduction are 0.35 (or 0.53), 0.18, and 0.18 ev, respectively. The larger activation energy (two or three vibrational quanta) of the all *trans* is attributed to the thermal energy necessary to allow an intersystem crossing from the first singlet excited state (about 2.6 ev) to the triplet state (about 3.0 ev). The activation energy of the *cis-trans* forms of the molecule (1 vibrational quanta) correspond to intersystem crossing from the "*cis* peak" state (about 3.5 ev) to the triplet state. The excitation spectrum of photoconduction in 15-15′ *cis* β-carotene and isomerized glass, peaks in the "*cis* peak" region, in agreement with this assignment. These results, that intersystem crossing occurs more readily from the *cis* peak state than the first singlet excited state, provide an explanation for the shape of the photocurrent excitation spectra in β-carotene and for the lack of phosphorescence in all *trans* lycopene as reported by Lewis and Kasha.

I. INTRODUCTION

IN a previous paper[1] it was pointed out that β-carotene was an anomolous case with regard to the excitation spectrum for photoconduction. Normally, on the basis of previous work, one expects to find a fairly good agreement between the optical absorption spectra and the photoconduction excitation spectra. In the case of all *trans* β-carotene, the main absorption band corresponding to a π-electron transition from the ground singlet state to the lowest excited singlet state occurs in the region from about 4000 to 5000 A and consists of a series of vibrational peaks with an energy spacing of 0.177 ev.[2] In *cis-trans* isomers an additional peak occurs at 3500 A (in benzene), the "*cis* peak." It was shown that the photoconduction excitation spectrum for isomerized β-carotene consists of a single broad band with its peak at 3500 A. If there is any contribution to the current by excitation in the main absorption band it is not evident from the curve. The writer then suggested a tentative explanation of this on the basis of the application of the triplet state theory of photoconduction.[3] The basic assumption is that the intersystem crossing to a triplet state of the molecule after singlet-singlet excitation is an essential step leading to the creation of mobile charges. The available evidence indicates that the photoactive triplet state lies about 3 ev above the ground state. This places it on an energy scale between the lowest singlet excited state (about 2.6 ev) and the *cis* peak

[1] B. Rosenberg, J. Chem. Phys. **31,** 238 (1959).

[2] See, for example, G. Wald, J. N. Loeb, and P. K. Brown, Nature **184,** 614 (1959).

[3] B. Rosenberg, J. Chem. Phys. **29,** 1108 (1958).

state (3.54 ev). It is obvious that thermal activation energy is necessary to accomplish intersystem crossing from the lowest singlet excited state and it will have a magnitude of at least two or three vibrational quanta. It is not so obvious that thermal activation is necessary for intersystem crossing from the *cis* peak state since it lies above the triplet, but previous evidence[3] particularly for the case of aromatic hydrocarbons, indicates that even in the normal case where the triplet state energy level is below the singlet excited state energy level some thermal activation is necessary, and that the density of triplet states N_T, will be given by

$$N_T = \alpha I \tau_T (P/a) \exp(-E/KT), \qquad (1)$$

where αI is the intensity of absorbed radiation; τ_T is the lifetime of the triplet state; (P/a) represents the competition between the intersystem crossing rate P and the rate of fluorescence or direct quenching to the ground state a; and E is equal to a small number times the energy of the predominant vibrational quanta and represents the position of the vibrational level nearest the crossing point of the potential curves. The energy of the vibrational quanta in the *cis* peak state of β-carotene is not known but it seems likely to be roughly the same magnitude as the singlet state and therefore about 0.18 ev. The exact value is not essential to the argument.

The theory therefore suggests that the photocurrent excitation spectrum of isomerized β-carotene can be accounted for if the photoconduction activation energy is larger for the lowest excited singlet state than the *cis* peak state; and that the activation energy should be either 0.35 or 0.53 ev for the all *trans* molecules (where there is no absorption in the *cis* peak region), and about 0.18 ev or less for the *cis-trans* molecules.

We have already pointed out that the same suggestion can explain the results of Lewis and Kasha[4] in determining the phosphorescence of lycopene, a similar C_{40} carotenoid. Here they found that at liquid nitrogen temperature, all *trans* lycopene exhibited little or no phosphorescence, whereas a short heat treatment to produce some *cis* isomers did result in phosphorescence emission.

The experiments discussed in the following describe the attempt to determine the photoconduction activation energies for all *trans* and *cis-trans* forms of β-carotene.

II. PHOTOCONDUCTION ACTIVATION ENERGY MEASUREMENTS

To measure the photocurrent as a function of the temperature, the β-carotene sample was placed in a controlled temperature apparatus, continually flushed with dry nitrogen, and irradiated with light from a 300-w projector through various filters. A dc voltage from batteries was applied and the current was measured with a Keithley 200 B electrometer. The temperature was determined by a copper-constantan thermocouple in contact with the metal of the rear electrode. The temperature range of the equipment was from −30 to 130°C. The front electrode was in all cases electrically conducting glass. All measurements were made in sandwich-type cells with thin sheets of Teflon (1–3 mils thick) as spacer elements. The sample was cycled through the temperature range a few times before measurements were taken.

To prepare glass samples of β-carotene, pure, all *trans* powder was placed between the conductive glass and the metal electrode, with the Teflon spacer between. The sandwich was held together by strong spring clips and heated slowly through the glass electrode until the powder melted. The sample was slowly cooled. The β-carotene glass which formed adhered strongly to both electrodes. The electrical characteristics of these cells were the same whether prepared in a vacuum, in dry nitrogen or in air as long as the temperature did not rise appreciably above the melting point. If this occurred in air, the β-carotene deep red color rapidly bleached to a light orange color and finally to a yellow color as a result of extensive oxidation.

The powder samples were prepared as before, but were not heated to the melting point. The effect of pressure on the powder cells was determined using c clamps to hold the sandwich cell together. There was no measurable change in the magnitude of the currents or the value of the activation energies over a wide range of pressure. Therefore no further attempt was made to control this variable. The following materials were tested as rear electrodes—conductive glass, brass, aluminum, stainless steel, monel metal, and mercury. There was no apparent difference with any of these materials. We are fairly convinced at this state that the phenomena we are measuring are characteristic of the molecular properties of the bulk of the β-carotene and not of the sample-electrode interface so long as no chemical interaction occurs at the interface.

The measurements were made on three types of isomers of β-carotene, pure all *trans*, pure 15−15′ *cis*, and the mixture (predominantly all *trans*) of various isomers resulting from melting to the glass form. The isomers were all purified by chromatography on a calcium hydroxide column and recrystallized four times from benzene-methanol (spectroscopic grade). The 15−15′ *cis* molecule has the largest dipole moment in the perpendicular direction to the *trans* axis and therefore the largest absorption in the *cis* peak region of all β-carotene isomers. The molecular structure of the two pure isomers are shown in Fig. 1.

The excitation spectrum for photoconduction in a film of 15−15′ *cis* is shown in Fig. 2 along with the optical absorption spectrum, and agrees with that of the isomerized glass in exhibiting a single peak in the region of 3500–3600 A. Thus the 15−15′ *cis* isomer can be taken as representative of the isomerized glass.

[4] G. N. Lewis and M. Kasha, J. Am. Chem. Soc. **66**, 2100 (1944).

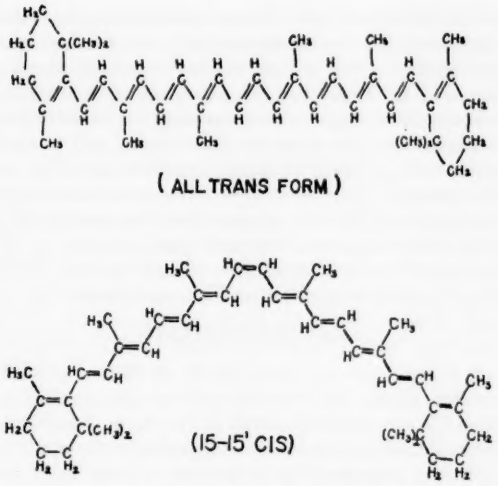

FIG. 1. Molecular structure of all *trans* and 15–15′ *cis* β-carotene.

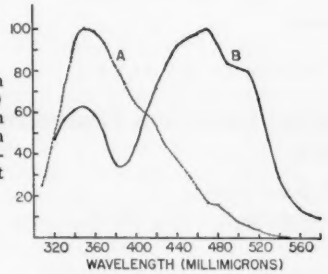

FIG. 2. Photoconduction excitation spectrum (A) and optical absorption spectrum (B) of a thin film of 15–15′ *cis* β-carotene, plotted as percent of maximum.

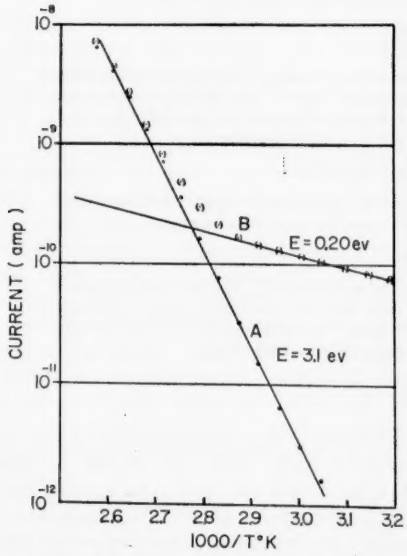

FIG. 3. Activation energy curves in β-carotene isomerized glass. (A) Semiconduction. (B) Photoconduction.

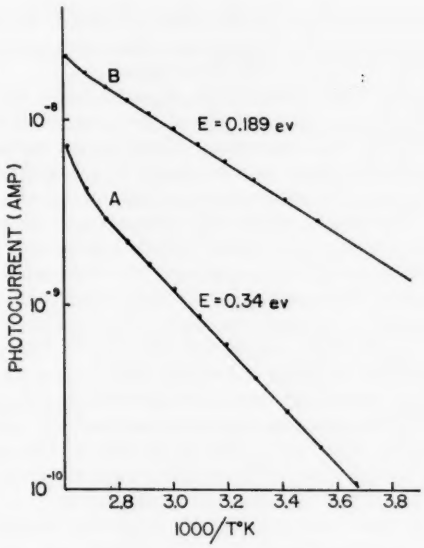

FIG. 4. Photoconduction activation energy curves in all *trans* (A) and 15–15′ *cis* (B) β-carotene.

The curve for all *trans* films has not yet been successfully determined.

The temperature dependence of the photocurrent of the isomerized glass is shown in Fig. 3 with the separate curve of the dark current (semiconduction). It can be seen that at low temperatures the photocurrent is much larger than the dark current, but as the temperature increases the dark current curve begins to dominate and finally at the high-temperature end, the slope is purely that of the dark current. The crossover point is a function of the light intensity only. The intensity was adjusted in this measurement to best illustrate the superposition effect. The photocurrent activation energy [E in Eq. (1)] is 0.20 ev in this case. The results on powdered all *trans* and powdered 15−15′ *cis* are shown in Fig. 4. Here the activation energy of the *cis* isomer is 0.189 ev and agrees fairly well with that of the isomerized glass, while the activation energy of the all *trans* isomer is 0.34 ev. In both of these cases the light intensity was the same, and higher

TABLE I. Photoconduction activation energies of *cis-trans* isomers of β-carotene.

Form	No. of measurements averaged	Activation energy	Value suggested by triplet state theory
All *trans* powder	20	0.37±0.04 ev	0.35 ev or 0.53 ev
15-15′ *cis* powder	5	0.20±0.02 ev	0.18 ev
Isomerized glass	7	0.19±0.02 ev	0.18 ev

than the value used on the isomerized glass. The light was incident from the projection lamp through a 1-56 Corning glass filter in all three cases.

In any single sample, the reproducibility was excellent, but in various samples of the same isomer there were fairly wide variations. Therefore the results of many measurements were averaged. The data clustered well about the mean values except in the all *trans* case. The mean values with the average deviation measures are given in Table I. There was no overlap of any values of the two *cis* groups with those of the all *trans* sets. In the case of the all *trans* isomer, out of the 20 sets of measurements, eight were within 5% of 0.35 ev and three were within 5% of 0.53. Thus it is not possible to decide unambiguously between the two or three vibrational quanta requirement at this time. In the other cases, the dispersion was much less and the agreement with each other is excellent. The mean experimental values of the activation energies are about 10% higher than the theoretical expectation.

It is clear, however, that the activation energy for photoconduction in the all *trans* molecules is about twice the value in the *cis-trans* molecules. At room temperature this implies a rate of intersystem crossing of about a factor of 10^3 larger from the *cis* peak than from the lowest excited singlet state [assuming the other factors in Eq. (1) are the same for both states] and a much larger ratio at lower temperatures. This therefore can adequately account for the excitation spectrum being a maximum at 3500 A in samples where the number of *cis* to all *trans* molecules is greater than one part in 10^3; and for the lack of detectable phosphorescence in all *trans* lycopene at liquid-nitrogen temperatures.

ACKNOWLEDGMENTS

It is a pleasure to thank Dr. R. H. Bunnel of Hoffman-La Roche Inc. for the gift of the synthesized 15—15′ *cis* β-carotene, as well as Mr. P. A. Orlando for his invaluable assistance in the experimental work. This work was supported by a Research Grant from the National Institute of Neurological Diseases and Blindness, Public Health Service.

THE JOURNAL OF CHEMICAL PHYSICS VOLUME 34, NUMBER 1 JANUARY, 1961

Proton Magnetic Resonance Study of Crystalline Potassium Trisoxalatorhodium(III) Hydrate

A. L. PORTE* AND H. S. GUTOWSKY

Noyes Chemical Laboratory, University of Illinois, Urbana, Illinois

AND

G. M. HARRIS

Department of Chemistry, Acheson Hall, University of Buffalo, Buffalo, New York

(Received May 20, 1960)

The broad-line proton magnetic resonance spectrum of crystalline potassium trisoxalatorhodium(III) hydrate, $K_3Rh(C_2O_4)_3 4\frac{1}{2}H_2O$, has been investigated in the temperature range 77°K–330°K. The spectrum at 77°K indicates that some of the protons in the crystal are not present in water of crystallization and an analysis of this same spectrum indicates that the compound should be formulated as

$$K_6[Rh(C_2O_4)_3][Rh(C_2O_4)_2(HC_2O_4)(OH)]8H_2O.$$

This formula is not inconsistent with the chemical reactions that the compound undergoes, and it explains some properties which are not satisfactorily accounted for by the previously accepted formula

$$K_3[Rh(C_2O_4)_3]4\frac{1}{2}H_2O.$$

The absorption spectrum at 318°K substantiates the analysis of the spectrum at 77°K and it also indicates that the water of crystallization can be grouped into at least three sets, the water molecules in different sets having different degrees of mobility. The proton magnetic resonance data also indicate that the "monohydrate," $K_3Rh(C_2O_4)_3H_2O$, is probably $K_6[Rh(C_2O_4)_3][Rh(C_2O_4)_2(HC_2O_4)(OH)]H_2O$.

I. INTRODUCTION

MANY crystalline hydrates lose their water of crystallization in stages when heated and, in most cases, this gradual loss of water can be accounted for by assuming that the water molecules are situated at different sites in the crystal lattice. Water molecules on equivalent lattice sites are subject to identical crystalline forces and will tend to be expelled from the crystal at a temperature which differs from that which characterizes the expulsion of another set at different equivalent sites.

In some instances, however, the stepwise loss of

* Now at the Department of Chemistry, The University of Glasgow, Glasgow W.2, Scotland.

water of crystallization could be accounted for by assuming that the "water molecules" are chemically different. This assumption implies that the empirical formula for the hydrate is correct but that the formula which describes the ionic species present in the crystal is wrong. For example, a hydrate formulated empirically as $A[PQ]xH_2O$ might be $A[P(OH)QH](x-1)H_2O$. This substance, on heating, could lose its water of crystallization over a particular temperature range and then might also have the (OH) and H present in the complex ion $[P(OH) \cdot QH]$ eliminated, as water, at another temperature. The net result, as far as experiment is concerned, would be that the hydrate $A[PQ]xH_2O$ lost "water of crystallization" over two different temperature ranges.

The potassium trisoxalatorhodium (III) hydrate formulated empirically as $K_3Rh(C_2O_4)_3 4\frac{1}{2}H_2O$ loses "water of crystallization" in at least two stages. According to Deléphine,[1] it loses 3.5 moles of water at 150°C, and all water at 190°. Throughout the literature it has always been assumed that the anion in this compound is the complex trisoxalatorhodium (III),

$$[Rh(C_2O_4)_3]^{3-},$$

but while the chemical reactions which the compound undergoes are not inconsistent with this anion, no one has ever proved that the structure of the crystal is represented correctly by the above empirical formula.

This paper describes studies we have made on this substance with the object of finding out if the differences in the "water of crystallization" are due to water molecules situated at different lattice sites or if in fact there are chemical differences in these "water molecules."

A problem of this type is an ideal one for solid state nuclear magnetic resonance studies,[2,3] since studies of this type give information about the distribution and mobility of hydrogen nuclei in a crystal. Such investigations can be carried out either on a large single crystal of the material or on a polycrystalline specimen. However, because of the large number of interproton vectors which must be present in the unit cell of $K_3Rh(C_2O_4)_3 4\frac{1}{2}H_2O$, a single crystal study would be difficult unless something was already known about the crystal structure of the compound. Except for the classical crystallographic work of Dufet[4] involving a determination of the crystal class, the unit cell angles and axial ratios, no crystal structure studies of this compound appear to have been made. For these reasons, the nuclear magnetic resonance studies were all carried out on the polycrystalline material.

II. EXPERIMENTAL PROCEDURE AND RESULTS

Potassium trisoxalatorhodium(III) hydrate was prepared in a manner similar to that described by Werner,[5] starting with water soluble $RhCl_3 3H_2O$.[6] The trisoxalato salt was freed of excess potassium acid oxalate by repeated precipitation with alcohol and several recrystallizations from cold water. The red crystals obtained in this way lose water spontaneously when exposed to the atmosphere at room temperature, crumbling in the process to a yellow powder. A total weight loss of 11.8% occurs when the crystals are stored over calcium chloride, and the resultant powder remains constant in weight indefinitely under these conditions. This yellow material was analyzed for rhodium by hydrogen reduction,[5] for oxalate either by decomposition of the complex with 0.1*N* NaOH and titration with standard $KMnO_4$ (method *A*) or by direct titration of a solution of the complex in dilute sulfuric acid with $KMnO_4$ (method *B*) and for total carbon by conventional semimicro technique.

Found: Rh, 20.58%; C_2O_4, 52.0% (method *A*) and 52.6% (method *B*); total C, 14.0%.
Calculated for $K_3Rh(C_2O_4)_3H_2O$: Rh, 20.4%; C_2O_4, 52.6%; total C, 14.3%.

The initial 11.8% weight loss over calcium chloride corresponds to about 3.5 additional moles of water so that the red crystals appear to have the formula $K_3Rh(C_2O_4)_3 4\frac{1}{2}H_2O$ as reported by Delépine.[1] It is to be noted from the present work, however, that the first 3.5 moles of water can be lost without heating and must, therefore, be rather loosely bound water of crystallization. The resultant monohydrate, on the other hand, is very stable at room temperature.

The broad-line magnetic resonance spectrometer and cryostat used in this study have been described previously.[7] The magnetic field was modulated at 30 cps with an amplitude which depended on the linewidth. This amplitude varied from 0.5 gauss to less than 0.1 gauss. The field was swept linearly in time while the oscillator frequency was kept constant at 29.925 Mc/sec. A permanent magnet with a field strength of 6324 gauss was used.

We have investigated the proton magnetic resonance absorption spectrum of $K_3Rh(C_2O_4)_3 4\frac{1}{2}H_2O$, over the temperature range 77°–343°K. The sample was enclosed in a sealed tube to prevent loss of water; moreover, the spectra were first recorded at the lower temperatures so that these results would not be affected by any change in the extent of hydration upon heating above room temperature.

The variation of the apparent second moment of the

[1] M. Delépine, Anales ffs. y qufm. (Madrid) **27,** 490 (1929).
[2] R. E. Richards, and J. A. S. Smith, Trans. Faraday Soc. **47,** 1261 (1951).
[3] E. O. Bishop, J. L. Down, P. R. Emtage, R. E. Richards, and G. Wilkinson. J. Chem. Soc. **1959,** 2484.
[4] H. Dufet, Bull. Soc. Min. **12,** 466 (1889).
[5] A. Werner and J. Poupardin, Ber. deut. chem. Ges. **47,** 1955 (1914).
[6] Material obtained from Chemical Commerce, Newark, New Jersey, and used without further purification.
[7] H. S. Gutowsky, L. H. Meyer, and R. E. McClure, Rev. Sci. Instr. **24,** 644 (1953).

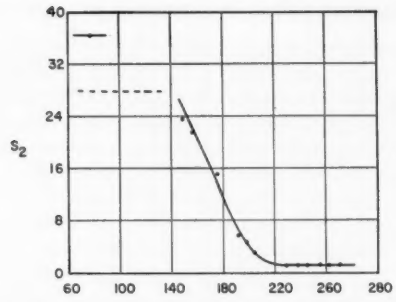

FIG. 1. Second moment (S_2 gauss^2) of the proton magnetic resonance absorption curve observed as a function of temperature (T°K) in polycrystalline $K_3Rh(C_2O_4)_3 4\frac{1}{2}H_2O$. The dashed straight line and the gap in the solid curve, at temperatures below 140°K, are discussed in the text.

proton absorption curve in the temperature range 77°K to 270°K is shown in Fig. 1. These second moments were calculated directly from the experimental derivative curves, and corrected for modulation broadening, by means of the expression given by Andrew.[8] We have not given any experimental points on this curve for temperatures between 80–140°K because of experimental difficulties resulting from serious saturation effects coupled with thermal instabilities in the apparatus in that temperature range. The dashed straight line at temperatures lower than 140°K represents the second moment value to be expected from theory for a rigid hydrate. The value of the second moment observed at liquid nitrogen temperature, 77°K, and its deviation from the expected value at that temperature will be accounted for later.

Figure 2 shows the observed first derivative, and the absorption curve obtained from it by direct integration, at 77°K. The three well-resolved peaks A, B, and C remain prominent features until a temperature of 170°K is reached. Then peaks A and C start to collapse in towards the center of the spectrum, a process which continues until the temperature is 205°K. In the temperature range 205–255°K, the absorption curve consists of a single peak 2.1 gauss wide, the linewidth being defined as the distance between the points of maximum slope. This, in its turn, splits up into two broad peaks between 255°K and 270°K. The separation between the peaks in this "doublet" is 1.2 gauss. As the temperature is raised further, this "doublet" then splits up and at 318°K the proton magnetic resonance spectrum is just resolved into seven peaks, as shown in Fig. 3. Above 325°K the spectrum narrows abruptly to a single narrow peak, less than 0.3 gauss wide, a spectrum expected for highly mobile protons in a crystal.

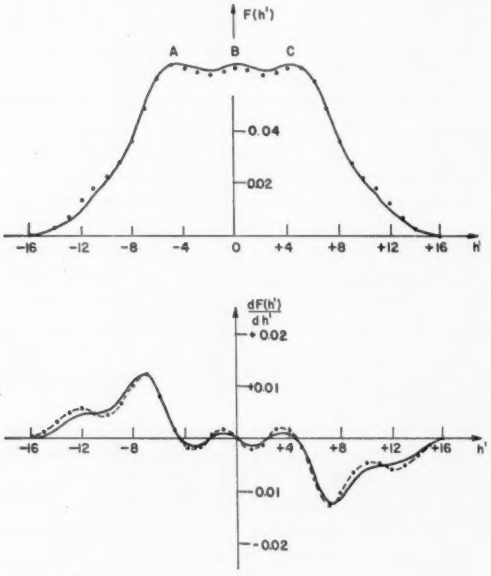

FIG. 2. Proton magnetic resonance spectrum of

$K_3Rh(C_2O_4)_3 4\frac{1}{2}H_2O$

at 77°K. Observed (...) and calculated (—) absorption, $F(h')$, and derivative, $dF(h')/d(h')$, curves. h' is the displacement, in gauss, of the applied magnetic field from the value, 6324 gauss, at the center of the absorption. The calculated absorption and derivative curves are defined by Eq. (3).

[8] E. R. Andrew, Phys. Rev. **91**, 425 (1953).

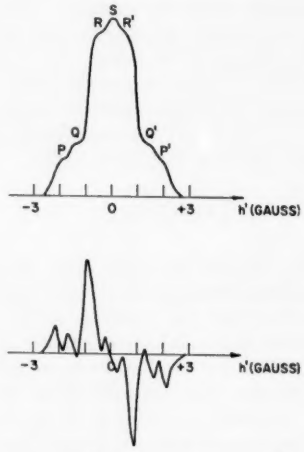

FIG. 3. Proton magnetic resonance spectrum of

$K_3Rh(C_2O_4)_3 4\frac{1}{2}H_2O$

at 318°K. Observed absorption and derivative curves. Modulation amplitude 0.1 gauss. h' is the displacement, in gauss, of the applied magnetic field from the value, 6324 gauss, at the center of the absorption.

III. INTERPRETATION OF RESULTS AND DISCUSSION

The curve of second moment vs temperature shows that there is unlikely to be any motion which could

affect the shape of the absorption curve below about 115°K. Consequently, the derivative of the absorption curve recorded at 77°K represents the proton magnetic resonance absorption of the "rigid lattice." This rigid lattice curve is of immediate importance.

If the hydrogen nuclei in the specimen were only present in water of crystallization then an absorption curve typical of simple hydrates would be obtained. Many nuclear magnetic resonance studies of such systems have been made and both experiment and theory shows that the absorption spectrum of simple hydrates consists of two overlapping, but nevertheless well-resolved, peaks separated by about 10.8 gauss.[9]

The absorption curve obtained from

$$K_3Rh(C_2O_4)_3 4\tfrac{1}{2}H_2O$$

at 77°K consists of three resolved peaks. The outer two of these are at the positions expected for the characteristic peaks of water molecules in a hydrate. The maximum of the third peak is at the center of the absorption curve. This means that some hydrogen nuclei are in an environment which differs from that of the protons in water. If the empirical formula is correct, then these hydrogen nuclei must be associated with the complex ion. They can not be present in coordinated water molecules in this ion since, if they were, they would give rise to a solid state proton magnetic resonance absorption spectrum which could not be distinguished from that of a hydrate. Some of the hydrogen atoms must, therefore, be attached to the oxalate residues of the complex ion, i.e., some of the oxalic acid residues are functioning as monobasic acids. If this is true, then an OH^- radical must be incorporated into the complex ion to maintain the charge on the ion. This implies that at least some of the complex ion is in the form I or its geometrical isomer II. However, the anhydrous salt

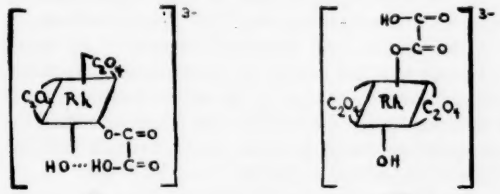

I II

$K_3Rh(C_2O_4)_3$ can be obtained by strongly heating the hydrate and the compound is, furthermore, readily resolvable into "*d*" and "*l*" isomers by suitable manipulation in aqueous solution. The *trans* isomer II must, therefore, be excluded. It should be noted that $K_3[Rh(C_2O_4)_2(HC_2O_4)(OH)]3\frac{1}{2}H_2O$ is consistent with the empirical formula $K_3Rh(C_2O_4)_3 4\frac{1}{2}H_2O$.

The assumption that some of the complex ion is in the form I is further substantiated by a quantitative investigation of the absorption line shape. If I is present then the absorption curve and its derivatives should both consist of a superposition of two curves, one of which is characteristic of water molecules in a hydrate and the other characteristic of the structural unit [HO···HOOC]. Each of the superimposed absorption curves can be described[10] by normalized line shape functions of the form

$$f(h') = (2\pi)^{-\frac{1}{2}}\beta^{-1}\int_{h=-3\mu/r^3}^{+3\mu/r^3} g(h) \times \exp[-(h'-h)^2(2\beta^2)^{-1}]dh. \quad (1)$$

In this, $g(h)dh$ represents the probability that a fine structure component line characteristic of an isolated pair of nuclear dipoles, each of magnetic moment μ, and r cm apart, lies between h and $(h+dh)$ gauss from the center of the absorption curve. When interpair effects are considered, the probability function $g(h)dh$ is broadened out so that a line, originally at h, contributes to the magnitude of the absorption at another point h'. It is not possible to predict the exact form of the broadening parameter, β, unless the structure of the compound is known. In other cases, however,[10,11] it has been found to be a good approximation to regard the broadening function as Gaussian. The line shape function described by Eq. (1) is then obtained by summing the contributions from each of these broadened fine structure components and normalizing the result to give unit intensity for the complete absorption curve.

Various values of r and β were tried in attempts to account for the observed absorption spectrum and an approximate fit was eventually obtained from

$$f(h') = (8.78)^{-1}\sum_{h=-3\mu/r^3}^{+3\mu/r^3} g(h)\exp[-(h'-h)^2(6.04)^{-1}] + (8)^{-1}(7.69)^{-1}\sum_{h=-3\mu/r_1^3}^{+3\mu/r_1^3} g_1(h)\exp[-(h'-h)^2(4.71)^{-1}], \quad (2)$$

where $r=1.53\pm0.03$ A, $r_1=2.43\pm0.03$ A, and $h=0$, ±0.5, ±1.0, $\pm\cdots$, $\pm3\mu/r^3$ or $\pm3\mu/r_1^3$. The limits of error given for r and r_1 represent the sensitivity of the curve fitting. The first summation term is due to a system made up of pairs of protons distributed in a random manner. The components of each pair are separated by 1.53 A and each pair is separated from its nearest neighbors by 2.3 A. This is that part of the spectrum which is due to water of crystallization. The value of 1.53 ± 0.03 A which we adopt for the proton-proton distance in the water molecules is somewhat shorter than the expected value of 1.59 A.

[9] G. E. Pake, J. Chem. Phys. **16,** 327 (1948).

[10] G. E. Pake, J. Chem. Phys. **16,** 327 (1948), Eq. (12).

[11] H. S. Gutowsky, G. B. Kistiakowsky, G. E. Pake, and E. M. Purcell, J. Chem. Phys. **17,** 972 (1949).

However, it is within the range 1.53 to 1.65 A quoted in the literature[12] for water molecules in hydrates.

The second summation term arises from a system, essentially isolated from the first, which is made up of proton pairs in which the components are separated by 2.43 A and each pair is surrounded in a random manner by other proton pairs, the nearest of which is 2.4 A away. This is due to a system [H—O···H—O—] which does not involve water molecules and which can only arise from the complex ion I. These two systems are present in the relative weights of 8:1.

A better description of the observed absorption curve is given by

$$F(h')=1.622[1+10.94f(h')]^{-1}f(h'). \qquad (3)$$

and the calculated absorption curve, and its derivative, obtained by using this expression are compared with the observed curves on Fig. 2. The theoretical reasoning leading to the use of $F(h')$ rather than $f(h')$ in comparing observed and calculated curves is as follows, $f(h')$ only takes account of the geometrical factors involved in the study of solids by the NMR technique. It does not take account of the interaction of the system with the applied radiation, and the application of the radio frequency is well known to alter the excess number of protons in the ground state from the value n_0, in the absence of the radiation, to

$$n=n_0[1+\tfrac{1}{2}\gamma^2H_1^2T_1f(h')]^{-1} \qquad (4)$$

in the presence of the radio field H_1. The observed absorption signal is proportional to this excess number, n, and so the observed absorption signal is proportional to

$$[1+\tfrac{1}{2}\gamma^2H_1^2T_1f(h')]^{-1}f(h'), \qquad (5)$$

which is of the same form as the correction factor derived from experiment. We do not know the value of the spin-lattice relaxation time, T_1, for potassium trisoxalatorhodium(III) hydrate, nor do we know the exact value of H_1 at the cutoff point in our spectrometer. However, we consider the value of 10.94 for $\frac{1}{2}\gamma^2H_1^2T_1$ to be a reasonable one for studies of this type with our instrument. We have not been able to reduce H_1 to a value low enough to ignore this correction factor and still observe the absorption signal.

This tendency to saturate the system appears to reduce the magnitude of the line shape function in the center of the absorption curve and to increase its *relative* value at the wings. This gives rise to an apparent second moment which is larger than the true second moment.[13] In the present case, the second moment calculated on the basis of $f(h')$, i.e., without taking account of the saturation, is found to be 27.8 gauss,[2] while the corresponding value calculated from $F(h')$ is 34.7 gauss.[2] The experimental second moment at 77°K is 36.3 gauss.[2]

These results show that the compound should be formulated as

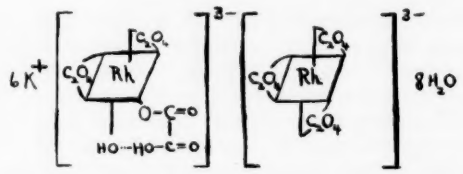

which is exactly twice the empirical formula. There is some uncertainty about the nature of the hydrogen bonding in the neighborhood of the complex ion $[Rh(C_2O_4)_2(HC_2O_4)(OH)]^{3-}$. We have assumed the presence of an internal hydrogen bond but other arrangements of hydrogen atoms in the neighborhood of this complex ion may be visualized. For example, the acidic hydrogen atom may be incorporated into an H_3O^+ ion in the crystal and this may then form hydrogen bonds with water molecules. The observed spectrum would then consist of a superposition of three absorption curves, one due to water of crystallization, one due to H_3O^+ ion and one due to the —OH proton, and it would be somewhat similar to our calculated curve except at the tails. There are serious objections to such an arrangement. First of all, the proton magnetic resonance absorption spectrum characteristic of three protons situated at the corners of an equilateral triangle has been shown, both by theoretical calculation[14] and by experiment,[2] to consist of a peak at the origin which is flanked by shoulders on either side of it. The derivative of this absorption curve has two secondary maxima about 9–10 gauss from the origin. We have not observed any secondary maxima in the derivative curve for $K_3Rh(C_2O_4)_3 4\frac{1}{2}H_2O$ in that region. Another objection to a model involving H_3O^+ ions arises from the fact that oxalic acid dihydrate consists[2,15] of oxalic acid molecules and water of crystallization. It seems unlikely that the charge on the acidic hydrogen atom of the complex ion I would be so much greater than the corresponding charge in oxalic acid dihydrate that the ion would dissociate to give rise to an H_3O^+ ion.

No information can be deduced from the proton magnetic resonance data about the positions of the water molecules in the unit cell. However, a study of the changes in the derivative curves, particularly in the temperature range 300°K to 318°K indicates that at least four sets of proton pairs are present in the crystal. Thus, in the absorption curve shown in Fig. 3, which is characteristic of this temperature range, the peaks Q and Q' which occur at ± 1.4 gauss from the center of the spectrum are in the positions expected

[12] "Tables of Interatomic Distances and Configuration in Molecules and Ions," Spec. Publ. No. 11, (1958) Chem. Soc. (London) p. M68.

[13] The question of saturation broadening is discussed in detail by D. W. McCall, J. Appl. Phys. **29,** 739 (1958).

[14] E. R. Andrew and R. Bersohn, J. Chem. Phys. **18,** 159 (1950).

[15] J. Itoh, R. Kusaka, R. Kiriyama, and S. Yabumoto, J. Chem. Phys. **21,** 1895 (1953).

for rigid pairs of protons 2.43 A apart, and we assign these to the proton pair in the complex ion I. The peaks P, P', R, R', and S, arise from the water of crystallization and they indicate that this water of crystallization can be divided into at least three sets. The water molecules in different sets are subject to different barriers to rotation. Within each set, rotation of the water molecules causes the characteristic rigid hydrate spectrum to collapse, and both the separations between the peaks, and the peak heights, in the resultant spectrum now become functions of the correlation time and of the angle between the re-orientation axis and the interpair vectors within the set.[16] Moreover, the small splittings of the doublets indicate that the re-orientation occurs about more than one axis.

The single narrow peak obtained at temperatures above 325°K shows that the water molecules at these elevated temperatures are highly mobile in the crystal; the dipolar interactions are averaged out by diffusional motions of the protons as well as by reorientations of the H_2O molecules. This, coupled with the fact that water of crystallization can be removed by allowing the compound to stand in a dessicator containing calcium chloride, implies that at these higher temperatures the compound is no longer the stochiometric $K_6[Rh(C_2O_4)_3][Rh(C_2O_4)_2(HC_2O_4)(OH)]8H_2O$.

The structure proposed for $K_3Rh(C_2O_4)_3 4\frac{1}{2}H_2O$ on the basis of this magnetic resonance study is supported by some of the known chemistry of the compound. Recent studies[17] in aqueous solution of the reaction

$$Rh(C_2O_4)_3^{3-} + C_2{}^*O_4^{=} \rightarrow Rh(C_2{}^*O_4)_3^{3-} + C_2O_4^{=}$$

are best interpreted in terms of an intermediate "monoaquated" ion $[Rh(C_2O_4)_2(OC_2O_3)(OH_2)]^{3-}$ the structure of which, we suggest, is identical with the intrahydrogen-bonded ion proposed above. Dehydration data on the crystalline hydrate $K_3Rh(C_2O_4)_3 4\frac{1}{2}H_2O$, while incomplete as yet, confirm unequivocally the existence of at least two different kinds of "bound water." The "monohydrate" formulated empirically as $K_3Rh(C_2O_4)_3H_2O$ should, on the basis of our arguments, be reformulated as

$$K_6[Rh(C_2O_4)_3][Rh(C_2O_4)_2(HC_2O_4)(OH)]H_2O,$$

and it is interesting to note that peaks P and P' in Fig. 3 indicate the presence of some water molecules which are subjected to higher barriers to rotation than those to which the remaining waters of crystallization are subjected. Of the water of crystallization in $K_3Rh(C_2O_4)_3 4\frac{1}{2}H_2O$, that represented by P and P' will be last to be expelled when the substance is heated and, furthermore, the weights of peaks PP' and QQ' in the spectrum are the same, a point which is consistent with the formula proposed for the "monohydrate." More thorough dehydration studies[18] of the very similar ruthenium compound $K_3Ru(C_2O_4)_3 4\frac{1}{2}H_2O$ indicate that there are both a stable "monohydrate" and a "hemihydrate." This latter we believe to be exactly analogous to the double oxalatorhodium(III) ion suggested above, less the eight moles of "loose" crystal water.

ACKNOWLEDGMENTS

The authors wish to express their gratitude to Dr. D. Barton and Dr. W. Plumb for preparing and analyzing the samples of potassium trisoxalatorhodium(III) hydrate used in this investigation. They also thank the donors of the Petroleum Research Fund, administered by the American Chemical Society, and the Office of Naval Research for partial support of this research.

[16] H. S. Gutowsky and G. E. Pake, J. Chem. Phys. **18**, 162 (1950).

[17] D. Barton and G. M. Harris, manuscript in preparation.

[18] R. Charonnat, Ann. chim. et phys. **16**, 124, 156 (1931).

Method of Alternant Orbitals for Allyl*

HENRY H. DEARMAN† AND ROLAND LEFEBVRE‡

Gates and Crellin Laboratories of Chemistry,§ California Institute of Technology, Pasadena, California

(Received June 6, 1960)

The π-electron correlation energy and ground-state wave function for allyl are calculated by the method of alternant orbitals. This method accounts for 98.8% of the correlation energy given by the configuration interaction treatment. The atomic orbital spin density matrix obtained with this approximation is also included.

THE configuration interaction (CI) problem for the π electrons of the allyl radical has been treated by several authors.[1–4] In this note we report the results of the calculation of the ground-state wave function for the π electrons, the energy of electron correlation and the spin density matrix by the method of alternant orbitals (MAO)[5,6] for this molecule. MAO has been applied to the benzene molecule by Itoh and Yoshizumi,[7] and the results of this calculation account for 85% of the correlation energy predicted by the CI treatment of Parr, Craig, and Ross.[8] It is of interest to determine the accuracy of MAO for the estimation of the ground state of an open-shell molecule.

MAO yields for the π electrons of allyl a wave function of the form

$$\psi = |\ (a\phi_1 + b\phi_3)\phi_2(a\bar{\phi}_1 - b\bar{\phi}_3)\ | \qquad (1)$$

with the usual notation for Slater determinants and where

$$a = \cos\theta$$

$$b = \sin\theta.$$

A bar denotes β spin and the absence of a bar denotes α spin. The molecular orbitals ϕ are linear combinations of the atomic $2p_z$ orbitals χ centered on the carbon atoms.

We choose for allyl the model for which the C—C bond distance is 1.40 A, the C—H bond is 1.09 A, and the C_1—C_2—C_3 bond angle is 120°. With the inclusion of overlap the MO's are

$$\phi_1 = 0.424544(\chi_1 + \chi_3) + 0.600395\chi_2$$

$$\phi_2 = 0.721262(\chi_1 - \chi_3)$$

$$\phi_3 = 0.610762(\chi_1 + \chi_3) - 0.888297\chi_2. \qquad (2)$$

Equation (1) is not an eigenfunction of the operator S^2 but can be made to satisfy this condition by the application of the doublet projection operator O^2.[5,6] Writing the proper doublet function now as a function of the mixing parameter θ we find

$$O^2\psi = \frac{\Phi_1 - \sqrt{\frac{2}{3}}\tan\theta\Phi_2 - \tan^2\theta\Phi_3}{(1 + \frac{2}{3}\tan^2\theta + \tan^4\theta)^{\frac{1}{2}}}. \qquad (3)$$

Here the configuration functions Φ are

$$\Phi_1 = |\ \phi_1\bar{\phi}_1\phi_2\ |$$

$$\Phi_2 = (1/\sqrt{6})\,(2\,|\ \phi_1\bar{\phi}_2\phi_3\ | - |\ \phi_1\bar{\phi}_3\phi_2\ | + |\ \phi_2\bar{\phi}_1\phi_3\ |\ )$$

$$\Phi_3 = |\ \phi_2\phi_3\bar{\phi}_3\ |. \qquad (4)$$

The energy is given by the equation

$$E(\theta) = \frac{\mathcal{H}_{11} - 2\sqrt{\frac{2}{3}}\tan\theta\mathcal{H}_{12} + \tan^2\theta(\frac{2}{3}\mathcal{H}_{22} - 2\mathcal{H}_{13}) + 2\sqrt{\frac{2}{3}}\tan^3\theta\mathcal{H}_{23} + \tan^4\theta\mathcal{H}_{33}}{1 + \frac{2}{3}\tan^2\theta + \tan^4\theta} \qquad (5)$$

in which $\mathcal{H}_{ij} = \int\Phi_i\mathcal{H}\Phi_j d\tau$. We have taken the values of the necessary atomic integrals from the CI calculation for benzene[8] and from the tables of Roothaan.[9] Figure 1 shows the variation of the energy with the parameter θ and that the value $\tan\theta = 0.4500$ produces the minimum. With this value of the mixing parameter the ground state is

$$\Psi_{MAO} = 0.9221\ \Phi_1 - 0.3388\ \Phi_2 - 0.1867\ \Phi_3 \qquad (6)$$

and the energy of electron correlation is 1.7767 ev. Equation (6) is to be compared to the CI function for allyl given by Chalvet and Daudel[1]

$$\Psi_{CI} = 0.9249\,\Phi_1 - 0.3133\,\Phi_2 - 0.2049\ \Phi_3 + 0.0660\ \Phi_4 \qquad (7)$$

in which the configuration Φ_4 neglected by MAO is

$$\Phi_4 = (1/\sqrt{2})\,(\,|\ \phi_2\bar{\phi}_1\phi_3\ | - |\ \phi_1\bar{\phi}_3\phi_2\ |\,). \qquad (8)$$

* Sponsored by the National Science Foundation, the Office of Ordnance Research, U. S. Army, and by the U. S. Public Health Service.

† Dow Chemicals Company Fellow 1959–1960.

‡ On leave from Centre de Mécanique Ondulatoire Appliquée, Paris.

§ Contribution No. 2531.

[1] O. Chalvet and R. Daudel, J. chim. phys. **49**, 629 (1952).

[2] H. C. Lefkovits, J. Fain, and F. A. Matsen, J. Chem. Phys. **23**, 1690 (1955).

[3] W. Moffitt, Proc. Roy. Soc. (London) **A218**, 486 (1953).

[4] H. O. Hunt, D. L. Peterson, and W. T. Simpson, J. Chem. Phys. **27**, 20 (1957).

[5] P.-O. Lowdin, Phys. Rev. **97**, 1509 (1955).

[6] P.-O. Lowdin, *Advances in Physics* (Taylor and Francis, Ltd., London, 1956), Vol. 5, p. 161.

[7] T. Itoh and H. Yoshizumi, J. Phys. Soc. Japan **10**, 201 (1955).

[8] R. G. Parr, D. P. Craig, and I. G. Ross, J. Chem. Phys. **18**, 1561 (1950).

[9] C. C. J. Roothaan, Office of Naval Research Report, University of Chicago (1955); J. Chem. Phys. **19**, 1445 (1951).

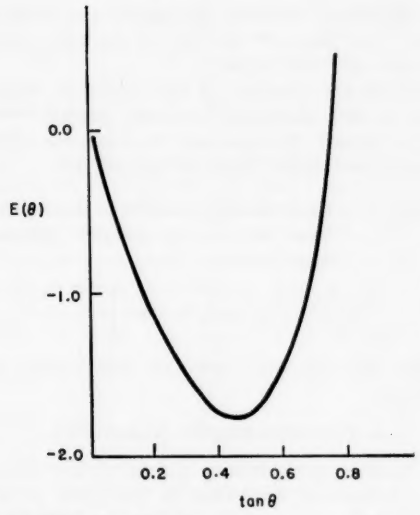

FIG. 1. Variation of electron correlation energy (in ev) with mixing parameter θ.

The correlation energy given by this CI treatment is 1.7975 ev.

McConnell[10,11] has evaluated the spin density matrix for allyl employing (7). Using the MAO function (6) the spin density matrix is

$$\rho=\begin{bmatrix} 0.6388 & -0.1028 & -0.2424 \\ -0.1028 & -0.2645 & -0.1028 \\ -0.2424 & -0.1028 & 0.6388 \end{bmatrix}. \quad (9)$$

MAO then accounts for 98.8% of the correlation energy given by a complete CI treatment. Another important feature of function (6) is that it gives the correct magnitude and sign to the coefficient of Φ_2, which is chiefly responsible for the negative diagonal element of the atomic spin density matrix on the central carbon atom. In previous work[12] we have derived relations between the spin densities in odd alternant hydrocarbon radicals and the mixing parameter θ of MAO. We believe that the excellence of agreement of the wave functions of MAO and CI for allyl gives support to these general calculations.

ACKNOWLEDGMENTS

We wish to thank Professor H. M. McConnell for many stimulating discussions.

[10] H. M. McConnell, J. Chem. Phys. **28**, 1188 (1958).
[11] H. M. McConnell, J. Chem. Phys. **30**, 328 (1959).
[12] R. Lefebvre, H. H. Dearman, and H. M. McConnell, J. Chem. Phys. **32**, 176 (1960).

THE JOURNAL OF CHEMICAL PHYSICS VOLUME 34, NUMBER 1 JANUARY, 1961

Density Expansions of Correlation Functions for Equilibrium Systems

HAROLD L. FRIEDMAN

IBM Research Center, Yorktown Heights, New York

(Received May 9, 1960)

A method of deriving density expansions of correlation functions from density expansions of the excess free energy is based on certain thermodynamic relations between derivatives of the grand partition function and derivatives of the excess free energy. The method also depends on using the most general expansion of the interaction energy into components; it is *not* assumed that this energy is limited to pairwise components. Expansions are obtained for the correlation functions in multicomponent gases and for the correlation functions for solute species in solutions. The method is also applicable to ionic solutions. A mathematical difficulty limits the systems for which these equations are proved to those in which there is a certain flexibility in treating the model.

I. INTRODUCTION

EITHER correlation functions or distribution functions[1] provide a more detailed description of the properties of systems at equilibrium than do the thermodynamic functions. The correlation functions have mostly been used in equilibrium theories as tools for deriving expressions for thermodynamic functions from molecular models or their equivalent, but they are also useful in interpreting certain experimental observations, particularly those relating to association equilibria.[2] There is a strong and obvious connection between the tendency of some molecules to associate and the behavior of the correlation functions which describe the equilibrium spatial distribution of these

[1] T. L. Hill, *Statistical Mechanics* (McGraw-Hill Book Company, Inc., New York, 1956).

[2] See, for example, J. van Kranendonk, Physica **23**, 825 (1957); **25**, 337 (1959).

TABLE I. Notation.

V	extensive volume
$\mathfrak{F}$	extensive Helmholz free energy
$\mathbf{N}$	$=N_1, \cdots, N_s, \cdots N_\sigma$, where N_s is the number of molecules of species s in the system. This is a composition set.
c_s	$=N_s/V$
$\mathbf{c}$	$=c_1, \cdots, c_s, \cdots c_\sigma$, the concentration set.
$\boldsymbol{\mu}$	the chemical potential set
$\mathbf{z}$	the fugacity set
$\{\mathbf{N}\}$	a set of center-of-mass coordinates of the molecules corresponding to $\mathbf{N}$. This is called a coordinate set.
$\{\mathbf{n}\}$	$\subseteq\{\mathbf{N}\}$ means that $\{\mathbf{n}\}$, a set of center-of-mass coordinates of the molecules corresponding to composition set $\mathbf{n}$, is a subset of $\{\mathbf{N}\}$. This implies that $\mathbf{n}\leq\mathbf{N}$, or $n_s\leq N_s$ for every s.
n	$=n_1+\cdots+n_s+\cdots+n_\sigma$
c	$=c_1+\cdots+c_s+\cdots+c_\sigma=N/V$
$\sum''f(\mathbf{n})$	=sum of all $f(\mathbf{n})$ for which $n\geq 2$.
$\prod''f(\mathbf{n})$	=product of all $f(\mathbf{n})$ for which $n\geq 2$.

molecules in a system. On this basis it seems that correlation functions are of interest even when exact and useful expressions for the thermodynamic functions in terms of a model are already available.

The calculation of thermodynamic functions from expressions for correlation functions is a familiar procedure.[1,3] However it is the purpose of this paper to demonstrate the possibility of the reverse procedure, namely the calculation of density expansions for the correlation functions from such expansions for thermodynamic functions. This is of interest in itself as an extension of the known relations among these functions and it also seems to be useful as a practical method for calculating density expansions of correlation functions in certain cases. As an example it is proposed that the method may be used to obtain the correlation functions of ionic solutions from the Mayer[4] expansion for the free energy of these solutions.

In this paper density expansions are obtained only for nonionic systems and the results are of proven validity only for systems that are subject to a certain further restriction described in Sec. 5. Subject to this restriction the present results are a generalization of those previously obtained by Mayer and Montroll,[5] deBoer,[6] and Meeron[3,7] by various methods different from those described below.

The principal features of the notation, which is similar to that employed in earlier papers[3–5,7–9] are given in Table I. We also note the equations defining the spatial correlation function[10] $g_n(\{\mathbf{n}\}, \mathbf{z})$:

$\mathbf{c}^n g_n(\{\mathbf{n}\}, \mathbf{z})$ = the probability density of the configuration $\{\mathbf{n}\}$ in an infinite system of fugacity set $\mathbf{z}$.

$$\lim\left[V^{-n}\int_V g_n(\{\mathbf{n}\}, \mathbf{z})d\{\mathbf{n}\}\right]=1.$$

For the rest we shall use the abbreviation $g_n\equiv g_n(\{\mathbf{n}\}, \mathbf{z})$.

2. THERMODYNAMIC RLEATIONS

The basis of our procedure is a parallelism between certain differential operations on the grand partition function and on a certain free energy function, $\mathfrak{S}$. The definition of the grand partition function is

$$\Xi=\exp(PV/kT). \tag{2.1}$$

The function $\mathfrak{S}$ is defined in terms of the excess free energy,

$$-\mathfrak{S}VkT\equiv\mathfrak{F}^{ex}(\mathbf{c}, V, T)\equiv-N\int_{c=0}^{c}[P-ckT]d(1/c), \tag{2.2}$$

where the integral pertains to a compression of the system at constant T and constant c_1/c, c_2/c, $\cdots$, c_σ/c and where $\mathfrak{F}^{ex}$ is the extensive Helmholtz free energy minus that of the equivalent hypothetical ideal gas at the same T and $\mathbf{c}$.

The relations of interest are the following:

$$\{\partial\ln\Xi/[\partial(1/kT)]\}_{z,V}=\{\partial(V\mathfrak{S})/[\partial(1/kT)]\}_{c,V}$$
$$=-\mathcal{E}^{ex}, \tag{2.3}$$

$$(\partial\ln\Xi/\partial V)_{z,T}-c=[\partial(V\mathfrak{S})/\partial V]_{c,T}=P/kT-c, \tag{2.4}$$

$$(\partial\ln\Xi/\partial x)_{z,V,T}=[\partial(V\mathfrak{S})/\partial x]_{c,V,T}\equiv X. \tag{2.5}$$

The function $\mathcal{E}^{ex}$ is the excess internal energy. It corresponds to $\mathfrak{F}^{ex}$ and in fact is given by the equation

$$\mathcal{E}^{ex}=[\partial(\mathfrak{F}^{ex}/T)/\partial(1/T)]_{c,V}. \tag{2.6}$$

The variable x represents an experimental variable that is independent of $\mathbf{z}$, V, T for an open system and independent of $\mathbf{c}$, V, T for a closed system. An example

[3] E. Meeron, J. Chem. Phys. **27,** 1238 (1957).
[4] J. E. Mayer, J. Chem. Phys. **18,** 1426 (1950).
[5] J. E. Mayer and E. Montroll, J. Chem. Phys. **9,** 2 (1941).
[6] J. de Boer, Repts Progr. in Phys. **12,** 305 (1949).
[7] E. Meeron, J. Chem. Phys. **28,** 630 (1958).
[8] W. G. McMillan and J. E. Mayer, J. Chem. Phys. **13,** 276 (1945).
[9] H. L. Friedman, Mol. Phys. **2,** 23 (1959).
[10] McMillan and Mayer, footnote 8, use $F_{\mathbf{n}}(\mathbf{z}, \{\mathbf{n}\})$ where we use $g_n(\{\mathbf{n}\}, \mathbf{z})$. In this notation as in others where boldface superscripts or subscripts are called for it has been necessary to substitute lightface Roman type to avoid typographical difficulties.

is a uniform electric field, externally controlled. An example of a different kind is a number of molecules of a different species than those counted in the sets $\mathbf{z}$ and $\mathbf{c}$. This possibility, which allows us to have a large number of equations like (2.5), is discussed in a later section.

The existence of such a variable gives us some flexibility in defining the reference states implied in the definitions of $\mathfrak{F}^{ex}$ and $\mathbf{z}$. For instance, the equivalent hypothetical ideal gas in the definition of $\mathfrak{F}^{ex}(\mathbf{c}, V, T, x')$ can be either at $x=0$ or at the particular value x'. The latter choice gives simpler relations between the thermodynamics and the statistical-mechanical procedures in which one expresses the energy of the system relative to the widely separated molecules as zero. In general, then, we treat x like T in defining reference states. Thus in (2.2) the integration is carried out at constant x and in (2.3), (2.4), and (2.6) the differentiations are at constant x, although the subscript to indicate this has been omitted.

Equation (2.4) follows at once from the definitions of Ξ and $\mathfrak{S}$. To derive (2.5) we begin with the expression

$$d(PV)=\mathfrak{S}dT+PdV+\sum N_s d\mu_s + [\partial(PV)/\partial x]_{\mu,V,T}dx, \quad (2.7)$$

where $\boldsymbol{\mu}$ is the chemical potential set. Using the definition of the fugacity,

$$\mu_s(\mathbf{c}, T, x)=\mu_s^{\dagger}(T, x)+kT\ln z_s(\mathbf{c}, T, x), \quad (2.8)$$

where $\mu_s^{\dagger}$ is the chemical potential in a hypothetical reference state of pure species s, we change (2.7) from chemical potentials to fugacities as independent variables to get

$$d(PV)=(\mathcal{E}^{ex}+PV)(dT/T)+kT\sum(N_s/z_s)dz_s+PdV + [\partial(PV)/\partial x]_{z,V,T}dx. \quad (2.9)$$

From this we derive

$$(\partial P/\partial x)_{c,T}=(\partial P/\partial x)_{z,T} + (kT/V)\sum(N_s/z_s)(\partial z_s/\partial x)_{c,T}. \quad (2.10)$$

Substitution of (2.8) (solved for z_s) in $\partial z_s/\partial x$ gives the following expression for the sum in (2.10)

$$kT\sum(N_s/z_s)(\partial z_s/\partial x)_{c,T}=\sum N_s\{(\partial/\partial x)[\mu_s-\mu_s^{\dagger}]\}_{c,T} =\{(\partial/\partial x)[\mathcal{G}-\mathcal{G}^{\dagger}]\}_{c,V,T}, \quad (2.11)$$

where $\mathcal{G}$ is the Gibbs free energy and $\mathcal{G}^{\dagger}$ applies to the same reference state as $\mu_s^{\dagger}$. Now we introduce $\mathcal{G}=\mathfrak{F}+PV$ and note that

$$\{(\partial/\partial x)[\mathfrak{F}-\mathfrak{F}^{\dagger}]\}_{c,V,T}=(\partial\mathfrak{F}^{ex}/\partial x)_{c,V,T} \quad (2.12)$$

because the ideal part of $\mathfrak{F}-\mathfrak{F}^{\dagger}$ is completely determined by $\mathbf{c}$, V, T. Therefore (2.10) becomes

$$0=(\partial P/\partial x)_{z,T}+V^{-1}(\partial\mathfrak{F}^{ex}/\partial x)_{c,V,T}. \quad (2.13)$$

Now we have in general

$$d\ln\Xi=[1/kT]d(PV)+PVd(1/kT) \quad (2.14)$$

and therefore

$$(\partial\ln\Xi/\partial x)_{z,V,T}=[V/kT](\partial P/\partial x)_{z,T}. \quad (2.15)$$

Equation (2.5) is obtained by combining (2.13) and (2.15) with the definition of $\mathfrak{S}$. Equation (2.3) follows from the dT term of (2.9) together with (2.14) and (2.6).

3. DIFFERENTIATION OF Ξ

We use the expansion[1,8]

$$\Xi(\mathbf{z}, V, T)=\sum[\mathbf{z}^{\mathbf{N}}/\mathbf{N}!]Z(\mathbf{N}, V, T), \quad (3.1)$$

where Z is the configuration integral.

$$Z\equiv\int_V \exp(-U(\{\mathbf{N}\})/kT)d\{\mathbf{N}\}. \quad (3.2)$$

We shall assume that $\{\mathbf{N}\}$ is a set of *spatial* coordinates (Cartesian center-of-mass coordinates). This implies a prior integration[8] (or summation!) over internal coordinates and hence $U(\{\mathbf{N}\})$ has the character of a potential of average force.[1] We also assume that we may expand U in component potentials[8,11,12]

$$U(\{\mathbf{N}\})=\sum''_{\{\mathbf{n}\}\subseteq\{\mathbf{N}\}} u_{\mathbf{n}}(\{\mathbf{n}\}), \quad (3.3)$$

where the sum is over all subsets of $\{\mathbf{N}\}$ for which $n=n_1+\cdots+n_\sigma$ is at least two. The $u_{\mathbf{n}}$ are components of the potentials of average force.

Now we apply the operation of (2.5) to (3.1). On the right of (3.1) only Z is a function of x and indeed we have

$$\partial Z/\partial x=\int[\sum''_{\{\mathbf{n}\}\subseteq\{\mathbf{N}\}} x_{\mathbf{n}}] \times\exp[-U(\{\mathbf{N}\})/kT]d\{\mathbf{N}\}/kT, \quad (3.4)$$

where

$$x_{\mathbf{n}}\equiv x_{\mathbf{n}}(\{\mathbf{n}\})\equiv\partial u_{\mathbf{n}}/\partial x. \quad (3.5)$$

If x is the square of the strength of an externally applied electric field, then the significance of (3.5) is clear at once. If x is the number of molecules of species ω, not counted in the sets $\mathbf{N}$, then (3.5) measures the effect on $u_{\mathbf{n}}$ of the fact that $U(\{\mathbf{N}\})$ now includes an average over the coordinates of x molecules of species ω in addition to the average over internal coordinates of the molecules of the set $\mathbf{N}$ at $\{\mathbf{N}\}$.

Among the terms in the sum of (3.4) there will be many of different $\{\mathbf{n}\}$ but the same $\mathbf{n}$, that is, different coordinate sets but the same composition set. All such terms of the integrand give the same integral. Their

[11] B. Kahn and G. E. Uhlenbeck, Physica **5**, 399 (1938).
[12] J. E. Mayer, J. Chem. Phys. **10**, 629 (1942).

number is

$$\binom{\mathbf{N}}{\mathbf{n}} \equiv \mathbf{N}!/\mathbf{n}![\mathbf{N}-\mathbf{n}]!. \tag{3.6}$$

Hence we have

$$kT(\partial Z/\partial x) = \sum_{\mathbf{n}\leq\mathbf{N}}'' \binom{\mathbf{N}}{\mathbf{n}} \int x_{\mathbf{n}} \exp[-U(\{\mathbf{N}\})/kT] d\{\mathbf{N}\}, \tag{3.7}$$

which may be substituted in $\partial \ln \Xi/\partial x$. After rearranging the summation and integration operations with the substitution $\mathbf{N}=\mathbf{n}+\mathbf{m}$ we get

$$kTX = \Xi^{-1} \sum'' [\mathbf{z}^{\mathbf{n}}/\mathbf{n}!] \int x_{\mathbf{n}} d\{\mathbf{n}\} \sum [\mathbf{z}^{\mathbf{m}}/\mathbf{m}!] \times \int \exp[-U(\{\mathbf{n}+\mathbf{m}\})/kT] d\{\mathbf{m}\}. \tag{3.8}$$

Now we introduce the generalization[8] of the grand partition function,

$$\Xi[\mathbf{c}^{\mathbf{n}}/\mathbf{z}^{\mathbf{n}}] g_{\mathbf{n}} = \sum [\mathbf{z}^{\mathbf{m}}/\mathbf{m}!] \times \int \exp[-U(\{\mathbf{n}+\mathbf{m}\})/kT] d\{\mathbf{m}\}, \tag{3.9}$$

where $g_{\mathbf{n}}$ is the spatial generic correlation function[13] in the system of fugacity set $\mathbf{z}$ and is a function of the coordinate set $\{\mathbf{n}\}$. Then (3.8) becomes

$$kTX = \sum'' [\mathbf{c}^{\mathbf{n}}/\mathbf{n}!] \int x_{\mathbf{n}} g_{\mathbf{n}} d\{\mathbf{n}\}. \tag{3.10}$$

This equation has a simple physical meaning. When the perturbation x is applied to the system its effect X is obtained by summing over the changes $x_{\mathbf{n}}$ that it produces in the component potentials for a given configuration and then integrating over configurations using the appropriate weighting factors, the correlation functions.

The same procedure based on (2.3) yields the equation

$$\mathcal{E}^{\mathrm{ex}} = \sum'' [\mathbf{c}^{\mathbf{n}}/\mathbf{n}!] \int e_{\mathbf{n}} g_{\mathbf{n}} d\{\mathbf{n}\}, \tag{3.11}$$

where

$$e_{\mathbf{n}} \equiv e_{\mathbf{n}}(\{\mathbf{n}\}) \equiv \partial(u_{\mathbf{n}}/kT)/\partial(1/kT) \tag{3.12}$$

is the component *energy* corresponding to $u_{\mathbf{n}}$ as a component free energy.[14]

With the same procedure again but based on (2.4) and employing the method used by H. S. Green[6,15] for differentiating the configuration integral with respect to volume, we obtain

$$-3V[P-ckT] = \sum'' [\mathbf{c}^{\mathbf{n}}/\mathbf{n}!] \int v_{\mathbf{n}} g_{\mathbf{n}} d\{\mathbf{n}\}, \tag{3.13}$$

where

$$v_{\mathbf{n}} \equiv v_{\mathbf{n}}(\{\mathbf{n}\}) \equiv \sum_{\{p\} \in \{\mathbf{n}\}} R_{\{p\}} \nabla_{\{p\}} u_{\mathbf{n}} \tag{3.14}$$

is a generalization of the virial.[16] The radius vector from the origin to the particle at $\{p\}$ is $R_{\{p\}}$ and $\nabla_{\{p\}}$ is the gradient operator for a change in $\{p\}$. In Cartesian form

$$v_{\mathbf{n}} = \sum [x_p[\partial/\partial x_p] + y_p[\partial/\partial y_p] + z_p[\partial/\partial z_p]] u_{\mathbf{n}},$$

where the sum has the same range as in (3.14), namely over each particle in $\mathbf{n}$ at its coordinates in $\{\mathbf{n}\}$.

Equations (3.11) and (3.13) are generalizations of those commonly derived[1] for the special case in which $U(\{\mathbf{N}\})$ is a sum of only pairwise components. Our method of deriving the expansions of correlation functions depends on using the more general form, Eq. (3.3).

4. DIFFERENTIATION OF $\mathcal{Z}$

Equations similar in form to the expansions of X, $\mathcal{E}^{\mathrm{ex}}$, and $P-ckT$ just obtained can be derived by differentiating the cluster expansion of $\mathcal{Z}$ and collecting terms in a certain way. We begin with the McMillan-Mayer[8] expansion for an imperfect gas,

$$\mathcal{Z} = \sum'' \mathbf{c}^{\mathbf{n}} B_{\mathbf{n}}, \tag{4.1}$$

where $B_{\mathbf{n}}$ is the irreducible cluster integral,

$$\mathbf{n}! B_{\mathbf{n}} \equiv \int_V S_{\mathbf{n}}(\{\mathbf{n}\}) d\{\mathbf{n}\}. \tag{4.2}$$

The integrand $S_{\mathbf{n}}$ is the sum of all products of cluster functions that correspond to at-least-doubly-connected (ALDC) graphs on the skeleton of $\mathbf{n}$.[9] The general cluster function is[9]

$$\gamma_{\mathbf{n}} \equiv \gamma_{\mathbf{n}}(\{\mathbf{n}\}) = \exp(-u_{\mathbf{n}}/kT) - 1. \tag{4.3}$$

A concise way to write $S_{\mathbf{n}}$ that will be helpful is

$$S_{\mathbf{n}} = [\prod'' [1+\gamma_{\mathbf{m}}]]_{\mathrm{ALDC}}, \tag{4.4}$$

where the subscript ALDC indicates that only those terms are to be retained that correspond to ALDC graphs on the skeleton of $\mathbf{n}$ and the product is over all $\{\mathbf{m}\} \subseteq \{\mathbf{n}\}$ for $m \geq 2$.

The derivative according to (2.5) is

$$X = \partial(V\mathcal{Z})/\partial x = \sum'' [\mathbf{c}^{\mathbf{n}}/\mathbf{n}!] \int [\partial S_{\mathbf{n}}/\partial x] d\{\mathbf{n}\}, \tag{4.5}$$

$$\partial S_{\mathbf{n}}/\partial x = \sum_{\{\mathbf{m}\} \subseteq \{\mathbf{n}\}} [\partial \gamma_{\mathbf{m}}/\partial x] \Big[\prod_{\{\mathbf{k}\} \subseteq \{\mathbf{n}\}}'' [1+\gamma_{\mathbf{k}}] \Big]_{\mathrm{ALDC:m}}. \tag{4.6}$$

[13] This terminology is from Hill, footnote 1.

[14] The potential of average force resembles the free energy in being the reversible work for an isothermal process. For example, see footnote 9.

[15] H. S. Green, Proc. Roy. Soc. (London) **A184,** 103 (1947).

[16] For a discussion of the virial see R. B. Lindsay, *Physical Mechanics* (D. Van Nostrand Company, Inc., Princeton, New Jersey, 1933).

In the last equation we are to retain only those terms of the product which correspond to ALDC graphs on $\mathbf{n}$ when the (differentiated) γ_m bond is included.

We note the derivative

$$\partial\gamma_m/\partial x = x_m[1+\gamma_m]/kT, \tag{4.7}$$

where x_m is the function defined in (3.5). We also note that in (4.6) for every $\{\mathbf{k}\}\subseteq\{\mathbf{m}\}$ the ALDC condition does not depend on whether or not a γ_k bond is present in a graph. In this case for every term from γ_k of $[1+\gamma_k]$ there is also a term from the 1, and hence we may factor every such $[1+\gamma_k]$ from the part of the product to which the ALDC condition applies. In view of

$$\prod_{\{\mathbf{k}\}\subseteq\{\mathbf{m}\}}'' [1+\gamma_k] = \exp[-U(\{\mathbf{m}\})/kT], \tag{4.8}$$

we may write (4.6) as

$$\partial S_n/\partial x = \sum_{\{\mathbf{m}\}\subseteq\{\mathbf{n}\}}'' [x_m/kT] \times \exp[-U(\{\mathbf{m}\})/kT] P(\mathbf{m}:\mathbf{n}-\mathbf{m}), \tag{4.9}$$

where $P(\mathbf{m}:\mathbf{n}-\mathbf{m})$, a function of $\{\mathbf{n}\}$, is the sum of all products of cluster functions that satisfy both of the following conditions.[17,18]

(a) If γ_k appears as a factor in the product then $\{\mathbf{k}\}\subseteq\{\mathbf{n}\}$ but $\{\mathbf{k}\}$ is not a subset of $\{\mathbf{m}\}$.

(b) The product $\gamma_m P(\mathbf{m}:\mathbf{n}-\mathbf{m})$ corresponds to an ALDC graph on the skeleton of $\mathbf{n}$.

An alternative and entirely equivalent way to describe $P(\mathbf{m}:\mathbf{n}-\mathbf{m})\equiv P(\mathbf{m}:\mathbf{u})$ is the following.

$P(\mathbf{m}:\mathbf{u})$ is the sum of all products of cluster functions corresponding to graphs that satisfy the following conditions.

(a) There are no bonds that intersect only the skeleton of $\mathbf{m}$.

(b) Every vertex of $\mathbf{u}$ is connected to at least two vertices of $\mathbf{m}$ by independent paths.

We now integrate (4.9) to obtain

$$\int (\partial S_n/\partial x)\, d\{\mathbf{n}\} \tag{4.10}$$

for substitution in (4.5). The result is

$$kTX = \sum[\mathbf{c}^n/\mathbf{n}!]\sum_{\mathbf{m}\subseteq\mathbf{n}}\binom{\mathbf{n}}{\mathbf{m}}\int x_m \times \exp[-U(\{\mathbf{m}\})/kT] P(\mathbf{m}:\mathbf{n}-\mathbf{m})\, d\{\mathbf{n}\}. \tag{4.11}$$

We substitute $\mathbf{u}\equiv\mathbf{n}-\mathbf{m}$ and again interchange the order of summation and integration to arrive at the result

$$kTX = \sum_{\mathbf{m}}''[\mathbf{c}^m/\mathbf{m}!]\int x_m g_m^*\, d\{\mathbf{m}\}, \tag{4.12}$$

where

$$g_m^*\equiv g_m^*(\{\mathbf{m}\},\mathbf{z}) = \exp[-U(\{\mathbf{m}\})/kT]\sum_{\mathbf{u}}[\mathbf{c}^u/\mathbf{u}!]\int P(\mathbf{m}:\mathbf{u})\, d\{\mathbf{u}\}. \tag{4.13}$$

Equation (4.13) has the form expected for the density expansion of the correlation function g_m but it remains to be proven that g_m^* *defined* by this equation is indeed the correlation function. This problem is considered in the following section.

Just as Eq. (2.5) leads to (4.12), so (2.3) leads to

$$\mathcal{E}^{ex} = \sum''[\mathbf{c}^m/\mathbf{m}!]\int e_m g_m^*\, d\{\mathbf{m}\} \tag{4.14}$$

and (2.4) leads to

$$-3V[P-ckT] = \sum''[\mathbf{c}^m/\mathbf{m}!]\int v_m g_m^*\, d\{\mathbf{m}\}, \tag{4.15}$$

where the definitions of e_m, v_m, and g_m^* are those previously given.

One feature of (4.13) is of particular interest. The low density limit of g_m^* is given by the exponential function times the $u=0$ term of the sum. For the case $m=2$ this is unaffected by the existence of higher component potentials [Eq. (3.3)]. However even for $m=2$, the very next terms in g_m^*, those for $u=1$, contain contributions from the higher component potentials. In fact we have

$$P(1_a, 1_b:1_c) = \gamma_{ac}\gamma_{bc} + \gamma_{abc}[1+\gamma_{ac}][1+\gamma_{bc}]. \tag{4.16}$$

5. COMPARISON OF RESULTS

We rewrite here two of the equations and their difference.

$$kTX = \sum[\mathbf{c}^m/\mathbf{m}!]\int x_m g_m\, d\{\mathbf{m}\}, \tag{3.10}$$

$$kTX = \sum[\mathbf{c}^m/\mathbf{m}!]\int x_m g_m^*\, d\{\mathbf{m}\}, \tag{4.12}$$

$$0 = \sum[\mathbf{c}^m/\mathbf{m}!]\int x_m \delta_m\, d\{\mathbf{m}\}, \tag{5.1}$$

where

$$\delta_m\equiv\delta_m(\{\mathbf{m}\},\mathbf{z})\equiv g_m(\{\mathbf{m}\},\mathbf{z}) - g_m^*(\{\mathbf{m}\},\mathbf{z}). \tag{5.2}$$

There is an equation like (5.1) for every conceivable variable x and in addition one for T and one for V.

Now we wish to consider whether these results allow a proof that $\delta_m=0$ for every $\{\mathbf{m}\}$. No simple proof based on the properties of power series is possible because if δ_m is not zero, it must be a function of $\mathbf{c}$.

[17] If $u=0$, then $P(\mathbf{n};\mathbf{u})\equiv 1$.

[18] This is a generalization of the function for which Meeron, footnote 2, uses the notation $P(\mathbf{n};\mathbf{v})$. However, in his definition Meeron neglects to specify the condition, "The particles of $\mathbf{n}$ are not connected directly." This would be the equivalent, for γ_2 bonds alone, of our condition 1.

Thus by taking the appropriate limit on (4.13) and comparing with (3.8) we see that as $\mathbf{c}\to\mathbf{0}$, $\delta_{\mathbf{m}}\to 0$ and therefore $\delta_{\mathbf{m}}$ is only independent of $\mathbf{c}$ if it is uniformly zero.

There are examples of series of the form of (5.1) in which the integrals are not zero; these are found in the theory of Schlömilch series.[19] This theory is itself difficult and, considering how little is known about the integrals in (5.1) compared to Bessel functions, the investigation of whether (5.1) is true only if every $\delta_{\mathbf{m}}=0$, has the appearance of an obstacle rather than a challenge. One might expect assistance from the fact that we have a large number, perhaps infinite, of equations of the form of (5.1), each with a different set of variables $x_{\mathbf{m}}$. But we have not found an analytical procedure that allows us to use this fact.

There is a restricted class of systems for which it is easy to prove that $\delta_{\mathbf{m}}=0$. Since this class includes most if not all of those for which one can make numerical calculations it is of some interest. We suppose that the system can be represented by a model which may be described by two independent sets of parameters, the set of $u_{\mathbf{n}}$ and a set of $x_{\mathbf{n}}$. In this case the only solution of (5.1) is $\delta_{\mathbf{m}}=0$ for every $\{\mathbf{m}\}$ and $\mathbf{z}$. To prove this, suppose that the contrary is true and that in a certain range of $\{\mathbf{m}\}$, say $\{\mathbf{m}\}^*$, $\delta_{\mathbf{m}}$ has a positive value. Because $g_{\mathbf{m}}$ and $g_{\mathbf{m}}{}^*$ are completely determined by the parameters $u_{\mathbf{n}}$ and the parameters of state, $\mathbf{c}$ and T, the same is true of $\delta_{\mathbf{m}}$ and therefore we may vary one of the $x_{\mathbf{n}}$ without changing any of the $\delta_{\mathbf{m}}$. But if we increase $x_{\mathbf{m}}$ in the range $\{\mathbf{m}\}^*$ we make a positive contribution to the right side of (5.1) without any other effect. But this is impossible because the sum is zero.

A familiar example of a system to which this analysis applies is an electrolyte solution in the usual case that the solvent dielectric constant and its derivatives with respect to temperature, pressure, etc. are introduced as independent parameters in the description of the model. In general we may say that we may treat a set of $x_{\mathbf{m}}$ as independent of the set of $u_{\mathbf{m}}$ only because of our ignorance of the correct relation. In principle for a real quantum-mechanical system both the $x_{\mathbf{m}}$ and the $u_{\mathbf{m}}$ can be calculated from the same Slater sums. In this respect our solution to the comparison problem is not completely satisfactory.

6. DISCUSSION

Our conclusion, subject to the restrictions discussed in the preceding section, is that the density expansion of the correlation function is given by (4.13). According to the most general results of McMillan and Mayer[3] we may at once apply this to solutions provided that we now change from the potentials of average force in a vacuum[1,3]

$$U(\{\mathbf{N}\})=W(\{\mathbf{n}\},\mathbf{0})$$

to the potentials of average force at infinite dilution in the solvent, $W(\{\mathbf{n}\},\mathbf{y},\mathbf{a}=0)$ as the basis for the expansion in component potentials. Here $\mathbf{y}$ is a set of solvent fugacities in the reference state of the pure solvent, and $\mathbf{a}$, the set of solute activities, is zero in this state. Then $g_{\mathbf{n}}$ is the correlation function for a set of solute molecules and $\mathbf{c}$ is a set of solute concentrations, both in the solution that is in osmotic equilibrium with the solvent in its reference state.

In the case of ionic solutions a somewhat more complicated procedure is necessary. In this case we must repeat Sec. 4, but beginning with the Mayer expansion[4,9]

$$\mathfrak{S}=[\kappa^3/12\pi]+\sum{}''[\mathbf{c}^{\mathbf{n}}/\mathbf{n}!]I^{(\mathbf{n})}, \qquad (5.3)$$

which is applicable to ionic solutions. In this case the cluster integral $I^{(\mathbf{n})}$ is a function of the Debye parameter κ as well as of the potentials of average force at infinite dilution. The procedure developed above for an imperfect gas then leads to a density expansion for the correlation function in ionic solutions which is a generalization of that obtained by Meeron[6] for the pairwise correlation function for the case in which $W(\{\mathbf{N}\},\mathbf{y},\mathbf{a}=\mathbf{0})$ is made up of the sum of pairwise contributions. The details of this development will be given in another place.

Finally we note that the density expansion of the potential of average force is readily obtained from (4.13). It is

$$W(\{\mathbf{n}\},\mathbf{c})=-kT\ln(\{\mathbf{n}\},\mathbf{c})=U(\{\mathbf{n}\})$$
$$-kT\sum{}''[\mathbf{c}^{\mathbf{u}}/\mathbf{u}!]\int Q(\mathbf{n}:\mathbf{u})d\{\mathbf{u}\}, \qquad (5.4)$$

where the definition of $Q(\mathbf{n}:\mathbf{u})$ is the same as that of $P(\mathbf{n}:\mathbf{u})$ except for the following additional restriction of the graphs[20,21]:

(c) Every pair of vertices of the skeleton of $\mathbf{u}$ is connected by at least one path that does not pass through any vertices of $\mathbf{n}$.

The corresponding result was first obtained for a one-component system by Mayer and Montroll.[5] Meeron's elegant method[3] of deducing the form of Q from that of P by using the cumulant-moment relation is at once applicable to our more general equations.

ACKNOWLEDGMENTS

I should like to thank Dr. W. R. Heller for many interesting conversations on almost all topics covered in this paper. I also wish to thank Professor J. E. Mayer for valuable criticism.

[19] G. N. Watson, *A Treatise on the Theory of Bessel Functions* (Cambridge University Press, New York, 1944), Chap. 19. The author is grateful to Professor L. H. Thomas for this example.

[20] The additional restriction only applies for $u>1$.

[21] Meeron's definition of $Q(\mathbf{n},\mathbf{m})$ neglects to specify that the vertices of $\mathbf{n}$ are not directly connected. See footnote 17.

THE JOURNAL OF CHEMICAL PHYSICS VOLUME 34, NUMBER 1 JANUARY, 1961

Molecular Statistics of Vinyl Polymers

YASUTAKA SUZUKI

College of Arts and Sciences, Chiba University, Chiba, Japan

(Received March 14, 1960)

A formula is proposed to describe the end-to-end distance and the total dipole moment of the vinyl polymer $(CH_2CHX)_n$. The interaction of neighboring X's is taken into account. The formula treats the general atactic polymer and includes the isotactic polymer and the syndiotactic polymer as special cases.

1. INTRODUCTION

MANY theoretical works have been published about the effect of neighbor interaction upon the end-to-end distance and the total dipole moment of the polymer molecule.[1-6] Some of them are concerned with vinyl polymers, but their descriptions are chiefly on stereospecific polymers and are not sufficient on atactic polymers. The author treated them in a special case (the diamond-lattice model),[7] and now gives a generalized treatment.

2. GENERAL FORMULATION

Various methods have been proposed in the aforementioned works, that of Oka[8] will be adopted here with some modifications.

Generally in a molecular chain, $M_1-M_2-M_3-\cdots-M_i-\cdots-M_n$, n sets of rectangular axes, $(\mathbf{x}_1, \mathbf{y}_1, \mathbf{z}_1)$, $(\mathbf{x}_2, \mathbf{y}_2, \mathbf{z}_2)$, $\cdots(\mathbf{x}_i, \mathbf{y}_i, \mathbf{z}_i)$, $\cdots$ and $(\mathbf{x}_n, \mathbf{y}_n, \mathbf{z}_n)$, are defined as to express the spatial directions of the chain units, M_1, M_2, $\cdots$, and M_n, respectively. Let these vectors be unit vectors, so that the direction cosines of the jth axes to the ith axes are given by the scalar products $\mathbf{x}_i\mathbf{x}_j$, $\mathbf{y}_i\mathbf{y}_j$, etc.

Now we define a matrix to represent the relative direction of M_i to M_j,

$$\mathbf{P}_{i\to j}=\begin{pmatrix} \mathbf{x}_i\mathbf{x}_j & \mathbf{x}_i\mathbf{y}_j & \mathbf{x}_i\mathbf{z}_j \\ \mathbf{y}_i\mathbf{x}_j & \mathbf{y}_i\mathbf{y}_j & \mathbf{y}_i\mathbf{z}_j \\ \mathbf{z}_i\mathbf{x}_j & \mathbf{z}_i\mathbf{y}_j & \mathbf{z}_i\mathbf{z}_j \end{pmatrix}, \tag{1}$$

and set

$$\mathbf{P}_{i\to i+1}=\mathbf{P}_i \tag{2}$$

for abbreviation. Then we have

$$\mathbf{P}_{i\to j}=\mathbf{P}_i\mathbf{P}_{i+1}\cdots\mathbf{P}_{j-1}. \tag{3}$$

If the $\mathbf{P}_i$ are independent of each other, we have the mean value relation[9]

$$\langle\mathbf{P}_{i\to j}\rangle=\langle\mathbf{P}_i\rangle\langle\mathbf{P}_{i+1}\rangle\cdots\langle\mathbf{P}_{j-1}\rangle. \tag{4}$$

And if the $\langle\mathbf{P}_i\rangle$ are constant, independent of i, they are denoted by $\mathbf{P}$, and then Eq. (4) becomes

$$\langle\mathbf{P}_{i\to j}\rangle=\mathbf{P}^{j-i} \quad \text{for} \quad j>i. \tag{5}$$

If we want to obtain the average of a quantity $(\sum a\mathbf{x}_i)^2$, in the calculation of the end-to-end distance or to the total dipole moment of the molecule, it will be expressed by $\mathbf{P}$ as follows:

$$\begin{aligned}\langle(\sum_i a\mathbf{x}_i)^2\rangle &= a^2(\sum_{i=1}^{n}\langle\mathbf{x}_i\mathbf{x}_i\rangle+2\sum_{i<j}\sum\langle\mathbf{x}_i\mathbf{x}_j\rangle)\\ &= a^2\{n+xx \text{ component of } 2\sum_{h=1}^{n-1}(n-h)\,\mathbf{P}^h\}\\ &\simeq a^2(xx \text{ component of } 2n\sum_{h=0}^{\infty}\mathbf{P}^h-n\mathbf{P}^0),\end{aligned} \tag{6}$$

[9] The independence of $\mathbf{P}_i$'s means that the total energy U of a chain is given by

$$U=\Sigma_i u_i, \tag{4a}$$

where u_i is a function of $\mathbf{P}_i$ and independent of other $\mathbf{P}_i$'s. (See Appendix 1.) In this case Eq. (4) is derived as follows:

$$\begin{aligned}\langle\mathbf{P}_{i\to j}\rangle &= \frac{\int\cdots\int\mathbf{P}_{i\to j}\exp(-U/kT)d\mathbf{P}_1d\mathbf{P}_2\cdots d\mathbf{P}_h\cdots d\mathbf{P}_{n-1}}{\int\cdots\int\exp(-U/kT)d\mathbf{P}_1d\mathbf{P}_2\cdots d\mathbf{P}_h\cdots d\mathbf{P}_{n-1}}\\ &= \frac{\prod_{i\le h<j}\int\mathbf{P}_h\exp(-u_h/kT)d\mathbf{P}_h\prod_{h\ge j,\,h<i}\int\exp(-u_h/kT)d\mathbf{P}_h}{\prod_h\int\exp(-u_h/kT)d\mathbf{P}_h}\\ &= \prod_{i\le h<j}\frac{\int\mathbf{P}_h\exp(-u/kT)d\mathbf{P}_h}{\int\exp(-u_h/kT)d\mathbf{P}_h}\\ &= \prod_{i\le h<j}\langle\mathbf{P}_h\rangle.\end{aligned} \tag{4b}$$

[1] M. V. Volkenstein, J. Polymer Sci. **29,** 441 (1958).
[2] S. Lifson, J. Chem. Phys. **30,** 964 (1959).
[3] K. Nagai, J. Chem. Phys. **31,** 1169 (1959).
[4] W. J. Taylor, J. Chem. Phys. **32,** 146 (1960).
[5] C. A. J. Hoeve, J. Chem. Phys. **32,** 888 (1960).
[6] Preceding works are listed in these papers.[1-5]
[7] K. Suzuki and Y. Suzuki, Busseiron Kenkyu **9,** 39 (1947).
[8] S. Oka, Proc. Phys.-Math. Soc. Japan **24,** 657 (1942).

where $\mathbf{P}^0=\mathbf{E}=$unit matrix. Then

$$\langle(\sum a\mathbf{x}_i)^2\rangle/a^2n=\mathbf{xx}\text{ component of }2(\mathbf{E}-\mathbf{P})^{-1}-\mathbf{E}$$

$$=\frac{2\begin{vmatrix}1-\langle\mathbf{yy}\rangle & -\langle\mathbf{yz}\rangle\\ -\langle\mathbf{zy}\rangle & 1-\langle\mathbf{zz}\rangle\end{vmatrix}}{\begin{vmatrix}1-\langle\mathbf{xx}\rangle & -\langle\mathbf{xy}\rangle & -\langle\mathbf{xz}\rangle\\ -\langle\mathbf{yx}\rangle & 1-\langle\mathbf{yy}\rangle & -\langle\mathbf{yz}\rangle\\ -\langle\mathbf{zx}\rangle & -\langle\mathbf{zy}\rangle & 1-\langle\mathbf{zz}\rangle\end{vmatrix}}-1, \quad (7)$$

in which $\mathbf{yz}$, etc. are the scalar products $\mathbf{y}_i\mathbf{x}_{i+1}$ etc.

Generally we have

$$\langle(\sum_i a\mathbf{x}_i+b\mathbf{y}_i+c\mathbf{z}_i)^2\rangle=aaQ_{zz}+abQ_{zy}+acQ_{zz}$$
$$+baQ_{yz}+bbQ_{yy}+bcQ_{yz}+caQ_{zz}+cbQ_{zy}+ccQ_{zz}, \quad (8)$$

where Q_{yz}, etc. are the yz component, etc. of the matrix $\mathbf{Q}$ defined by

$$\mathbf{Q}/n=2(\mathbf{E}-\mathbf{P})^{-1}-\mathbf{E}=(\mathbf{E}+\mathbf{P})/(\mathbf{E}-\mathbf{P}). \quad (9)$$

3. APPLICATION TO VINYL POLYMERS $(CH_2CHX)_n$

Definition of axes[10]

$\mathbf{x}_i$: direction from C_{2i-1} to C_{2i+1}.

$\mathbf{y}_i$: direction from the line $C_{2i-1}C_{2i+1}$ to C_{2i}.

$\mathbf{z}_i$: direction from the plane $C_{2i-1}C_{2i}C_{2i+1}$ to X_i,

where C_{2i}, X_i, etc. means $2i$th carbon atom, ith X radical, etc., and X_i is fixed to C_{2i}.

Then in an isotactic chain all the sets of axes make right-hand systems D or all make left-hand systems L. In a syndiotactic chain D system and L system appear alternately, and in atactic polymers the same system succeeds in a definite probability p_+, which is determined by the condition of polymerization. Here $p_+=0$ means that the polymer is syndiotactic, and $p_+=1$ means isotactic.

Definition of P

The forms DD and LL are the mirror images of each other, so that the mean matrices defined by (2) and (4b) should be the same. The relation of DL to LD is similar. Thus we have only one matrix, $\mathbf{P}_+$, for the isotactic chain, and another for the syndiotactic chain, $\mathbf{P}_-$.

In a single atactic chain $\langle\mathbf{P}_h\rangle$ is not independent of h, and it is $\mathbf{P}_+$ or $\mathbf{P}_-$ according to the relative configuration of the hth and $(h+1)$th units. But we always treat a mixture of stereoisomers, and we want the average over the mixture;

$$\langle\mathbf{P}_{i\to j}\rangle_{\text{mixture}}=\sum_{\text{all the isomers}}^{2^n}\langle\mathbf{P}_{i\to j}\rangle_{\text{an isomer}}$$
$$\times\text{fraction of the isomer}$$
$$=\sum^{2^n}\prod_{h=1}^{j-1}\langle\mathbf{P}_h\rangle_{\text{an isomer}}\times\tfrac{1}{2}\prod_{h=1}^{n-1}p_h, \quad (10)[13]$$

where $\langle\mathbf{P}_h\rangle=\mathbf{P}_+$ and $p_h=p_+$ when the hth unit and $(h+1)$th unit have the same configuration, and $\langle\mathbf{P}_h\rangle=\mathbf{P}_-$ and $p_h=p_-=1-p_+$ when they have different configurations. Therefore, executing the summation in (10), we obtain

$$\langle\mathbf{P}_{i\to j}\rangle_{\text{mixture}}=(\mathbf{P}_+p_++\mathbf{P}_-p_-)^{j-1}. \quad (11)$$

Thus we may use

$$\mathbf{P}=\mathbf{P}_+p_++\mathbf{P}_-p_- \quad (12)$$

in (9) for the atactic polymer. Equation (12) includes isotactic polymer ($p_+=1$) and syndiotactic polymer ($p_-=0$).

Because of the symmetric structure of M_i to M_{i+1}, the elements of $\mathbf{P}_+$ and $\mathbf{P}_-$, and therefore $\mathbf{P}$ and $\mathbf{Q}$, have the relations

$$\langle\mathbf{xy}\rangle=-\langle\mathbf{yx}\rangle,\quad \langle\mathbf{yz}\rangle=\langle\mathbf{zy}\rangle \text{ and } \langle\mathbf{zx}\rangle=-\langle\mathbf{xz}\rangle,$$
$$Q_{zy}=-Q_{yz},\quad Q_{yz}=Q_{zy},\text{ and } Q_{zz}=-Q_{zz}, \quad (13)$$

and Eq. (8) is simplified to

$$\langle(\sum_i a\mathbf{x}_i+b\mathbf{y}_i+c\mathbf{z}_i)^2\rangle=a^2Q_{xx}+b^2Q_{yy}+c^2Q_{zz}+2bcQ_{yz}. \quad (14)$$

4. NUMERICAL EXAMPLES

The most interesting is the effect of interactions of neighboring X's. It can readily be taken into account in Eq. (14). It will be shown in a simplified model. The bond angles are assumed to be the tetrahedral angles. Three successive C—C bonds have three conformations: one is the *trans* form where the third bond is parallel to the first, and the other two are the *gauche* forms where the third bond is rotated about the second bond from the *trans* position as much as $\pm120°$. Then $\mathbf{P}_+$ is the average over nine conformations, and $\mathbf{P}_-$ is the average over other nine. (See Appendix 1.) If we put

$$b=c=0,\quad a=\text{distance of } C_{2i-1}C_{2i+1}=(8/3)^{\frac{1}{2}}d, \quad (15)$$

[10] This choice of the coordinate system is different from the usual one, which assigns a system to each C—C bond; however, they lead to the same result. In fact, with respect to the isotactic and syndiotactic chains, the author's results are essentially equivalent to those of Pstitsyn and Sharonov[11] and of Lifson,[12] whose choices were usual. But, so far as the vinyl polymers are concerned, this choice simplifies the mathematical formulation and gives an easy access to atactic chains.

[11] O. B. Ptitsyn and I. A. Sharonov, Zhur. Tekn. Fiz. **27,** 2744 (1957).

[12] S. Lifson, J. Chem. Phys. **29,** 80 (1958).

[13] The independence of the p_h from each other is assumed; the assumption is reasonable according to the mechanism of polymerization. For an isomer of tetramers, $DDLD$, the $\langle\mathbf{P}_h\rangle$ are $\mathbf{P}_+$, $\mathbf{P}_-$, $\mathbf{P}_-$ and the fraction is $\frac{1}{2}p_+p_-p_-$. The mirror image isomer $LLDL$ has the same $\langle\mathbf{P}_h\rangle$ and fraction.

where d is the length of C—C bond, then Eq. (14) gives the mean square end-to-end distance $\langle r^2 \rangle$. And if we put

$$a=0, \qquad b=(\tfrac{1}{3})^{\frac{1}{2}}m, \qquad c=(\tfrac{2}{3})^{\frac{1}{2}}m, \tag{16}$$

where m is the dipole moment of a C—X, Eq. (14) gives the total square dipole moment of the polymer molecule $\langle \mu^2 \rangle$.

Case 1. Nine Conformations Have the Same Energy

On taking the average of equal weight, we construct $\mathbf{P}_+$ and $\mathbf{P}_-$. We obtain equal values for them, so that $\mathbf{P}$ is independent of p_+:

$$9\mathbf{P}_+=9\mathbf{P}_-=9\mathbf{P}=\begin{vmatrix} 2 & \sqrt{2} & 0 \\ -\sqrt{2} & -1 & 0 \\ 0 & 0 & 0 \end{vmatrix}.$$

By the use of this $\mathbf{P}$ in (8), $\mathbf{Q}$ is determined, and Eq. (15) with (16) and (17) leads to

$$\langle r^2 \rangle / d^2 n = 4, \tag{17}$$

$$\langle \mu^2 \rangle / m^2 n = 11/12 = 0.917. \tag{18}$$

Case 2. X's Are Repulsive

If we exclude the two positions where C$\rightarrow X_i$ and C$\rightarrow X_{i+1}$ becomes parallel, we have

$$7\mathbf{P}_+=\begin{vmatrix} 3/2 & \sqrt{2}/2 & 1/2 \\ -\sqrt{2}/2 & -2 & -\sqrt{2}/2 \\ -1/2 & -\sqrt{2}/2 & -3/2 \end{vmatrix},$$

$$7\mathbf{P}_-=\begin{vmatrix} 1 & \sqrt{2} & 0 \\ -\sqrt{2} & -1 & -\sqrt{2} \\ 0 & -\sqrt{2} & -1 \end{vmatrix},$$

$$7\mathbf{P}=\begin{vmatrix} 1+\frac{1}{2}p_+ & \sqrt{2}(1-\frac{1}{2}p_+) & \frac{1}{2}p_+ \\ -\sqrt{2}(1-\frac{1}{2}p_+) & -1-p_+ & -\sqrt{2}(1-\frac{1}{2}p_+) \\ -\frac{1}{2}p_+ & -\sqrt{2}(1-\frac{1}{2}p_+) & -1-\frac{1}{2}p_+ \end{vmatrix};$$

and similarly to Case 1, Eq. (15) gives

$$\begin{aligned} \langle r^2 \rangle / d^2 n &= 320(3+p_+)/3(97+9p_+) \\ &= 3.30 \quad \text{for} \quad p_+=0, \\ &= 4.03 \quad \text{for} \quad p_+=1, \end{aligned} \tag{19}$$

$$\begin{aligned} \langle \mu^2 \rangle / m^2 n &= (286+23p_+)/6(97+9p_+) \\ &= 0.491 \quad \text{for} \quad p_+=0 \\ &= 0.486 \quad \text{for} \quad p_+=1. \end{aligned} \tag{20}$$

Case 3. X's Are Attractive

The two positions shown before have lower energy. The weights for the two are assumed to be twice as large as the other seven:

$$11\mathbf{P}_+=\begin{vmatrix} 5/2 & 3/\sqrt{2} & -1/2 \\ -3/\sqrt{2} & 0 & 1/\sqrt{2} \\ 1/2 & 1/\sqrt{2} & 3/2 \end{vmatrix},$$

$$11\mathbf{P}_-=\begin{vmatrix} 3 & \sqrt{2} & 0 \\ -\sqrt{2} & -1 & \sqrt{2} \\ 0 & \sqrt{2} & 1 \end{vmatrix},$$

$$11\mathbf{P}=\begin{vmatrix} 3-\frac{1}{2}p_+ & \sqrt{2}(1-\frac{1}{2}p_+) & \frac{1}{2}p_+ \\ -\sqrt{2}(1+\frac{1}{2}p_+) & -1+p_+ & \sqrt{2}(1-\frac{1}{2}p_+) \\ \frac{1}{2}p_+ & \sqrt{2}(1-\frac{1}{2}p_+) & 1+\frac{1}{2}p_+ \end{vmatrix};$$

$$\begin{aligned} \langle r^2 \rangle / d^2 n &= 544(6-p_+)/3(241-9p_+) \\ &= 4.53 \quad \text{for} \quad p_+=0 \\ &= 3.90 \quad \text{for} \quad p_+=1, \end{aligned} \tag{21}$$

$$\begin{aligned} \langle \mu^2 \rangle / m^2 n &= (1994-67p_+)/6(241-9p_+) \\ &= 1.346 \quad \text{for} \quad p_+=0 \\ &= 1.382 \quad \text{for} \quad p_+=1. \end{aligned} \tag{22}$$

5. DISCUSSIONS

Comparing the results (21), (22) with (19), (20), and (17), (18), we can see the effect of the interactions between X's and the dependence of the effect upon the isotactic degree p_+. The repulsion of X's extends the chain if p_+ is large, but it contracts the chain if p_+ is small, and the attraction has the inverse effects. The dipole moment becomes larger by the attraction, and smaller by the repulsion; and the change is always larger in the case of larger p_+.

If the energy distribution among the conformations is varied, we can find closer approximations to various real molecules. We can calculate on the continuous distribution of conformations, if necessary.[14] Although the absolute values of $\langle r^2 \rangle$ and $\langle \mu^2 \rangle$ of real molecules are affected by the excluded volume effect,[15] the relative values will be well shown by such a neighbor-interaction model; it offers at least the basis for the estimation of the volume effect.

So far as the configuration D or L is determined by the state of the end of the growing chain, the method of averaging over the isomeric configurations is available in the statistics of neighbor-interaction model. For a similar reason the method can be applied to copolymers.[7]

[14] Equation (15) leads to the results of other authors[11,12] at $p_+=0$ or 1. See Appendix 1.

[15] J. Marchal and H. Benoit, J. Polymer Sci. **23**, 223 (1957), explained that the effect is small in $\langle \mu^2 \rangle$.

APPENDIX 1. RELATION OF $\mathbf{P}_i$ TO ROTATIONS ABOUT C—C BONDS

The elements of $\mathbf{P}_i$ are expressed by bond angles and angles of rotations around C—C bonds as follows:

$$\mathbf{x}_i\mathbf{x}_{i+1}=c_1c_2c_3+s_1s_2c_3c_4+s_1c_2s_3c_5-c_1s_2s_3c_4c_5-s_2s_3s_4s_5$$

$$\mathbf{x}_i\mathbf{y}_{i+1}=c_1c_2s_3+s_1s_2s_3c_4-s_1c_2c_3c_5+c_1s_2c_3c_4c_5+s_2c_3s_4s_5$$

$$\mathbf{y}_i\mathbf{y}_{i+1}=-c_1s_2s_3+s_1c_2s_3c_4+s_1s_2c_3c_5+c_1c_2c_3c_4c_5+c_2c_3s_4s_5$$

$$\mathbf{y}_i\mathbf{x}_{i+1}=-c_1s_2c_3+s_1c_2c_3c_4-s_1s_2s_3c_5-c_1c_2s_3c_4c_5-c_2s_3s_4s_5$$

$$\mathbf{z}_i\mathbf{x}_{i+1}=-s_1c_3s_4+c_1s_3s_4c_5-s_3c_4s_5$$

$$\mathbf{z}_i\mathbf{y}_{i+1}=-s_1s_3s_4-c_1c_3s_4c_5+c_3c_4s_5$$

$$\mathbf{x}_i\mathbf{z}_{i+1}=s_1c_2s_5-c_1s_2c_4s_5+s_2s_4c_5$$

$$\mathbf{y}_i\mathbf{z}_{i+1}=-s_1s_2s_5-c_1c_2c_4s_5+c_2s_4c_5$$

$$\mathbf{z}_i\mathbf{z}_{i+1}=c_1s_4s_5+c_4c_5.$$

Abbreviations: $c=\cos$, $s=\sin$.

Suffix 1 = angle of vectors $C_{2i}\rightarrow C_{2i+1}$ and $C_{2i+1}\rightarrow C_{2i+2}$,

2 = half of the angle of $C_{2i-1}\rightarrow C_{2i}$ and $C_{2i}\rightarrow C_{2i+1}$,

3 = half of the angle of $C_{2i+1}\rightarrow C_{2i+2}$ and $C_{2i+3}\rightarrow C_{2i+4}$,

4 = rotation angle around $C_{2i}-C_{2i+1}$,

5 = rotation angle around $C_{2i+1}-C_{2i+2}$.

Rotation angles are 0 at *trans* position of the skeletal chain, and are positive and less than π at *trans* position of X. Signs of the last terms are for DD or LL; they are inverse for DL or LD.

When the bond length and the bond angle are constant, the total energy of a chain is a function of rotation angles about C—C axes,

$$U=U(\phi_1, \phi_2, \cdots, \phi_{2n-2}).$$

If the energy can be separated into the functions of single angles,

$$U=u(\phi_1)+u(\phi_2)+u(\phi_3)+\cdots,$$

the mean value of $\mathbf{x}_i\mathbf{x}_{i+1}$, for example, is

$$c_1c_2c_3+s_1s_2c_3\langle c_4\rangle+s_1c_2s_3\langle c_5\rangle-c_1s_2s_3\langle c_4\rangle\langle c_5\rangle\mp s_2s_3\langle s_4\rangle\langle s_5\rangle.$$

And if $\langle c_4\rangle=\langle c_5\rangle$, $\langle s_4\rangle=\langle s_5\rangle=0$, angle 2 = angle 3 = $\frac{1}{2}$ (angle 1) in addition, $\langle \mathbf{x}_i\mathbf{x}_{i+1}\rangle$ becomes

$$\tfrac{1}{2}c_1(1+c_1)+s_1^2\langle c_4\rangle-\tfrac{1}{2}c_1(1-c_1)\langle c_4\rangle^2.$$

Under these conditions Eq. (7) leads to the well-known equation

$$\langle r^2\rangle/d^2n=2(1+c_1)(1+\langle c_4\rangle)/(1-c_1)(1-\langle c_4\rangle).$$

Of course, we can treat the case where $\langle s_4\rangle$ or $\langle s_5\rangle$ is not zero.

Moreover, we can treat the case where U has unseparable terms

$$u(\phi_1, \phi_2)+u(\phi_3, \phi_4)+\cdots,$$

u_i in (4a) means $u(\phi_{2i-1})+u(\phi_{2i})+u(\phi_{2i-1}, \phi_{2i})$. The last term describes the interaction of X_i with X_{i+1}. We have to use $\langle c_4c_5\rangle$ instead of $\langle c_4\rangle\langle c_5\rangle$ and $\langle s_4s_5\rangle$ instead of $\langle s_4\rangle\langle s_5\rangle$, etc.

Furthermore, if U has unseparable terms in addition

$$u(\phi_2, \phi_3)+u(\phi_4, \phi_5)+\cdots,$$

Eq. (14) becomes invalid, because the matrices become dependent on each other. This is the case treated by Suzuki,[16] Lifson,[2] Nagai,[3] and Hoeve.[5]

Generally the rotation $\mathbf{P}_i$ should have three freedoms, two of which are satisfied by the rotations around the C—C bonds. The third freedom is the change of the bond angle $C_{2i}C_{2i+1}C_{2i+2}$ (expressed by suffix 1 in the previous abbreviation), and it can be taken into account. But the change of another series of angles $C_{2i-1}C_{2i}C_{2i+1}$ (2 or 3) needs some corrections of the theoretical formulation[4] as well as the change of the bond length does.

The principle of the use of the average matrix for atactic polymers could be applied with necessary cares to these cases where the formulation in Sec. 1 is too simple to be used.

APPENDIX 2. VALUES OF $\mathbf{P}_i$ OF THE MODEL IN SEC. 4

For DD or LL:

angle 4 \ angle 5 =	0°	+120°	−120°
0°	$\begin{pmatrix} 1 & 0 & 0 \\ 0 & 1 & 0 \\ 0 & 0 & 1 \end{pmatrix}$	$\begin{pmatrix} \frac{1}{2} & a & \frac{1}{2} \\ a & 0 & -a \\ -\frac{1}{2} & a & -\frac{1}{2} \end{pmatrix}$	$\begin{pmatrix} \frac{1}{2} & a & -\frac{1}{2} \\ a & 0 & a \\ -\frac{1}{2} & -a & -\frac{1}{2} \end{pmatrix}$
+120°	$\begin{pmatrix} \frac{1}{2} & -a & \frac{1}{2} \\ -a & 0 & a \\ -\frac{1}{2} & -a & -\frac{1}{2} \end{pmatrix}$	$\begin{pmatrix} -\frac{1}{2} & a & \frac{1}{2} \\ -a & 0 & -a \\ -\frac{1}{2} & -a & \frac{1}{2} \end{pmatrix}$	$\begin{pmatrix} 0 & 0 & -1 \\ 0 & -1 & 0 \\ -1 & 0 & 0 \end{pmatrix}$
−120°	$\begin{pmatrix} \frac{1}{2} & -a & -\frac{1}{2} \\ -a & 0 & -a \\ \frac{1}{2} & a & -\frac{1}{2} \end{pmatrix}$	$\begin{pmatrix} 0 & 0 & 1 \\ 0 & -1 & 0 \\ 1 & 0 & 0 \end{pmatrix}$	$\begin{pmatrix} -\frac{1}{2} & a & -\frac{1}{2} \\ -a & 0 & a \\ \frac{1}{2} & a & \frac{1}{2} \end{pmatrix}$.

[16] K. Suzuki, Busseiron Kenkyu, **16**, 39 (1949).

For *LD* or *DL*:

$$0^\circ \begin{pmatrix} 1 & 0 & 0 \\ 0 & 1 & 0 \\ 0 & 0 & -1 \end{pmatrix} \begin{pmatrix} \frac{1}{2} & a & \frac{1}{2} \\ a & 0 & -a \\ \frac{1}{2} & -a & \frac{1}{2} \end{pmatrix} \begin{pmatrix} \frac{1}{2} & a & -\frac{1}{2} \\ -a & 0 & a \\ \frac{1}{2} & a & \frac{1}{2} \end{pmatrix}$$

$$+120^\circ \begin{pmatrix} \frac{1}{2} & -a & -\frac{1}{2} \\ a & 0 & -a \\ \frac{1}{2} & -a & \frac{1}{2} \end{pmatrix} \begin{pmatrix} 0 & 0 & 1 \\ 0 & -1 & 0 \\ -1 & 0 & 0 \end{pmatrix} \begin{pmatrix} -\frac{1}{2} & a & -\frac{1}{2} \\ -a & 0 & a \\ \frac{1}{2} & a & -\frac{1}{2} \end{pmatrix}$$

$$-120^\circ \begin{pmatrix} \frac{1}{2} & -a & \frac{1}{2} \\ a & 0 & a \\ -\frac{1}{2} & a & \frac{1}{2} \end{pmatrix} \begin{pmatrix} -\frac{1}{2} & a & \frac{1}{2} \\ -a & 0 & -a \\ -\frac{1}{2} & -a & -\frac{1}{2} \end{pmatrix} \begin{pmatrix} 0 & 0 & -1 \\ 0 & -1 & 0 \\ 1 & 0 & 0 \end{pmatrix}.$$

$a=1/\sqrt{2}$. The weighted mean of the upper nine gives $\mathbf{P}_+$, and that of the other nine gives $\mathbf{P}_-$.

THE JOURNAL OF CHEMICAL PHYSICS VOLUME 34, NUMBER 1 JANUARY, 1961

On the Luminescence Minimum in Certain Scintillator Solutions*

J. M. Nosworthy,† John L. Magee, and M. Burton

Department of Chemistry, University of Notre Dame, Notre Dame, Indiana

(Received March 7, 1960)

Several scintillator solutions have been examined for the luminescence minimum previously reported for the case of Co^{60} gamma irradiated cyclohexane+benzene+*p*-terphenyl with oxygen present. The minimum is shown to be dependent on the nature of the solvents and of the quencher. A satisfactory interpretation of the data involves the notion of energy transfer from molecules of the less-efficient ("common") solvent to the molecules of the more efficient ("better") solvent and thence to the scintillator. The latter transfer appears to involve more than one molecule of the solvent. A suggested model of the quenching process explains the existence of two classes of quenchers, one of which does not give a minimum.

1. INTRODUCTION

STUDIES of excitation transfer processes in radiation chemistry[1,2] led to the examination of Co^{60} gamma irradiated scintillator solutions containing two solvents plus scintillator. In the course of that work[3,4] quencher was also introduced, with effects on luminescence intensity that appeared of special significance not only for luminescence processes but also for radiation chemistry. In particular, attention was drawn to the occasional existence of a small, but nevertheless real, luminescence minimum. It was this minimum which appeared to offer a direct clue to the mechanism of the energy transfer processes involved and which has been the stimulus both for decay-time studies and for the more extensive studies of luminescence intensity here reported.

It has long been recognized that, in solutions containing a very low concentration of scintillator solute, energy absorbed in the solvent (either from ultraviolet or high-energy radiation) is re-emitted preferentially by the scintillator molecules, so that the resultant luminescence is characteristic of the solute.[5] By analogy with processes involving direct excitation of the solute it was first thought that quenching (by an additional solute) involves the excited scintillator molecules in all

* Contribution from the Radiation Laboratory operated by the University of Notre Dame and supported in part under Atomic Energy Commission contract. We are indebted also to Wright Air Development Center for support of a portion of this work. This paper was originally intended for the K. F. Bonhoeffer Memorial Volume of the *Zeitschrift für Physikalische Chemie* but was delayed too long in preparation for inclusion in that volume. It is dedicated in memory of Professor Bonhoeffer.

† Present address: Department of Natural Philosophy, University of Edinburgh, Scotland.

[1] J. P. Manion and M. Burton, J. Phys. Chem. **56,** 560 (1952).
[2] M. Burton and W. N. Patrick, J. Phys. Chem. **58,** 421 (1954).
[3] M. Burton, P. J. Berry and S. Lipsky, J. chim. phys. **52,** 657 (1955).
[4] P. J. Berry and M. Burton, J. Chem. Phys. **23,** 1969 (1955).

[5] Cf. T. Förster, *Fluoreszenz Organischer Verbindungen* (Vandenhoeck and Ruprecht, Göttingen, 1951).

cases.[6] At the low scintillator concentrations ordinarily employed, absorption of energy is practically entirely by the solvent. It has now been clearly shown that under such conditions, quencher interacts exclusively with the solvent.[7] Only at high concentrations of the scintillator may the quencher act directly on it.[8,9]

When, instead of one solvent, two are used, it is possible to obtain a scintillator solution with luminescence efficiency greater than might be expected on the basis of an average behavior of the two solvents.[3] Such a result can be interpreted on the basis of energy transfer from the less efficient ("common") solvent *C* to the more efficient ("better") solvent *B*,[3,10] but such an interpretation is not the only one permitted.[3] On the other hand, the effect of quencher seems to introduce a restriction on the number of possible explanations. In the case of cyclohexane+benzene+*p*-terphenyl (scintillator)+oxygen, a luminescence minimum is observed at about 1% benzene.[3,4] A tentative explanation is that isolated excited benzene molecules, produced by energy transfer from cyclohexane, lack an efficient mechanism for transfer of excitation to the scintillator but are relatively efficiently quenched.[3]

2. EXPERIMENTAL

2.1. Measurement of Luminescence

Intensity of luminescence resulting from Co^{60} gamma irradiation was measured by a technique similar to that of Burton, Berry, and Lipsky[3] with the principal difference that 20-ml (rather than 25-ml) samples were used and that the degassing of deaerated solutions was usually by a process of repeated distillation under high vacuum.

2.2. Purification of Materials

The uv spectrum of every solvent was recorded and comparison made with spectra recorded in the literature. Purification was continued until the transmission equalled or exceeded that previously recorded and until no further improvement occurred.

Solvents C

Spectroscopic-grade *cyclohexane* was checked for refractive index and uv absorption spectra; if the latter were found satisfactory, it was usually used without further purification. One batch of cyclohexane was purified by repeated recrystallization, azeotropic distillation with methanol in a 50-theoretical-plate column, and then by washing and passage through an alumina column. Gas chromatographic analysis showed small percentages of two impurities, one of which was identified as 2,4-dimethylpentane and the other of which was almost certainly another heptane isomer. Cyclohexane so purified gave results, in the luminescence experiments, indistinguishable from those obtained with the unpurified material. Moreover, addition of larger quantities of 2,4-dimethylpentane did not eliminate the luminescence minimum in the quaternary solution of cyclohexane, benzene, *p*-terphenyl and oxygen. By contrast, when 2,4-dimethylpentane was substituted entirely for the cyclohexane, no minimum was observed (cf. Table II).

Phillips research grade *n-hexane* was further purified by passage through silica gel and by azeotropic distillation with methanol at 50° on a 50-theoretical-plate column. It was then washed with water and again passed through a silica gel column. $n_D^{25}=1.3753-1.3749$.

Cyclopentane, passed through a silica gel column, was washed three times with sulfuric acid and then with water; it was then distilled through a small column packed with glass helices and the middle fraction (approx. three-quarters) was retained.

Decalin, (mixed isomers) as supplied by Fisher Scientific Company was distilled through a 50-theoretical-plate column.

Phillips "pure grade" 2,4-*dimethylpentane* was passed through silica gel and then purified by distillation through a short column (8 in.$\times\frac{3}{4}$ in. diam.) packed with glass helices.

Dioxane purification involved five steps: refluxing for 9 hrs with 10M by volume of 1 *N* HCl; storage over solid KOH for 48 hrs and subsequent removal of the aqueous layer; drying over sodium for 24 hrs; distillation from sodium on a Todd column, retaining the middle fraction; one crystallization rejecting the last one-fifth of liquid. The *uv* transmission was greatly improved after distillation and further improved by the crystallization process.

Matheson, Coleman and Bell *n-dodecane* was twice thoroughly shaken with conc. H_2SO_4 and then washed with distilled water. Thereafter, it was distilled at approx. 5 mm (bp, 130°C) through a short fractionating column packed with glass helices with retention of the middle fraction. It was then recrystallized three times with rejection each time of the last one-fifth. Finally, the sample was passed twice through silica gel.

Methyl acetate, Eastman-Kodak, was fractionally distilled on a 50-theoretical-plate column with retention of the middle fraction.

Solvents B

Benzene was purified by repeated recrystallization, as previously described.[1,2] The *i-propylbenzene* employed was the middle fraction obtained on distillation through a Todd column.

Naphthalene, Eastman, recrystallized from alcohol was used without further purification.

[6] Cf. B. L. Funt and E. Neparko, J. Phys. Chem. **60**, 267 (1956).
[7] P. J. Berry, S. Lipsky and M. Burton, Trans. Faraday Soc. **52**, 311 (1956).
[8] H. Knau, Z. Naturforsch. **12a**, 881 (1957).
[9] F. H. Brown, M. Furst and H. P. Kallmann, Discussions Faraday Soc. **27**, 43 (1959).
[10] H. P. Kallmann, M. Furst, and F. H. Brown, IRE Trans. on Nuclear Sci. **NS-3**, 51 (1956).

Scintillators

p-Terphenyl, recrystallized once from benzene, had a mp 211–212°C. *m-Terphenyl* was recrystallized twice from Skelly solvent B;[11] mp 84–84.5 as compared with literature values of 83–87°. Pilot Chemical *trans-trans* 1,4-*diphenylbutadiene*-1,3, scintillation grade, mp 148–148.5°, was used without further purification.

Quenchers

Phenylbromide (Eastman) was distilled through a 50-theoretical-plate column with retention of the middle fraction. *Methyl iodide* (Matheson, Coleman and Bell, bp 40–42°), *diphenyl mercury* (Eastman), and *nitromethane* (Commercial Solvents) were used without further purification as were the other quenchers, which were used just as purchased or given to us.

3. RESULTS

Figures 1 and 2 show five illustrative complete luminescence curves. In addition, the systems cyclopentane+benzene+*p*-terphenyl+air, *n*-hexane+benzene+*p*-terphenyl+air, and cyclohexane+benzene+*p*-terphenyl+bromobenzene were also studied over the entire range of solvent concentration but for higher concentrations of scintillator than shown in Figs. 1 and 2. In the case of the bromobenzene solution, air was carefully excluded. Also, a number of other systems have been investigated in the region of low solvent *B* concentration in order to establish the existence or nonexistence of a minimum. All the results bearing on possible minima are summarized in Table I. In all the cases, except one, in which a minimum is indicated, complete quantitative data were established in the neighborhood of the minimum point, which was always found in the region of 0.5–1.2 volume percent of solvent B. In the cases of cyclohexane+*n*-hexane, the existence of a minimum was established qualitatively from the slope of the curve at low *B* concentration.

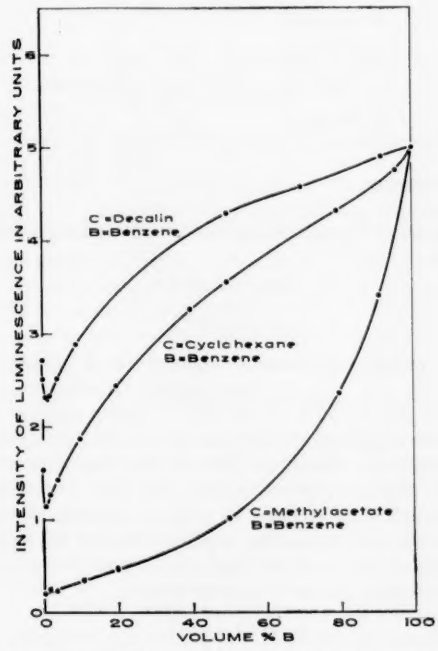

FIG. 1. Some typical Co^{60} gamma-induced luminescence curves of *p*-terphenyl in mixed solvents containing air as quencher.

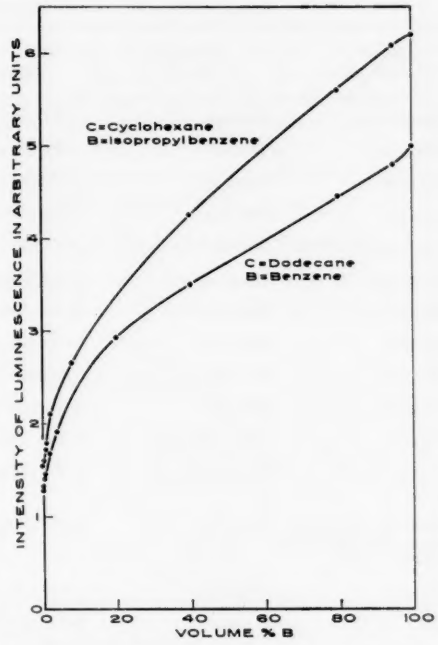

FIG. 2. Some typical Co^{60} gamma-induced luminescence curves of *p*-terphenyl in mixed solvents containing air as quencher. Luminescence intensity in same units as in Fig. 1.

In the case of the air-saturated cyclohexane+benzene systems, four sets of studies at various concentrations of *p*-terphenyl (0.24–0.96 g liter^{-1}) revealed the fact that the position of the minimum is insensitive to concentration of the scintillator.

An effort was made to detect a correlation between the more obvious physical properties of either or both of the solvents and their ability to give a minimum. No such correlation was found. For example, the minimum is not related to the efficiency of the solvent for transfer of energy to the scintillator. Methyl acetate is extremely poor in that respect and dodecane and *n*-hexane have transfer efficiencies comparable to cyclohexane; none of the three give a minimum with benzene but cyclohexane and decalin (transfer efficiency approx. 1.5 times as good as cyclohexane) do.

[11] P. J. Berry, thesis, University of Notre Dame, Indiana (1955), p. 34.

TABLE I. Summary of experiments bearing on existence of luminescence minima.

Solvent C ("common")	Solvent B ("better")	Scintillator	Quencher	Minimum[a]	Investigator[b]
Cyclohexane	Benzene	*p*-Terphenyl	Air-saturated	+	Footnote ref. 3
Cyclohexane	Benzene	*p*-Terphenyl	O_2	+	Footnote ref. 4
Cyclohexane	Benzene	*p*-Terphenyl	C_6H_5Br	+	
Cyclohexane	Benzene	*p*-Terphenyl	$(C_6H_5)_2Hg$	−	
Cyclohexane	Benzene	*p*-Terphenyl	Ferrocene	−	Kropp
Cyclohexane	Benzene	*p*-Terphenyl	CH_3I	+	
Cyclohexane	Benzene	*p*-Terphneyl	Nitromethane	+	
Cyclohexane	Benzene	*m*-Terphenyl	Air-saturated	+	Berry
Cyclohexane	Benzene	Diphenyl butadiene	Air-saturated	+	Berry
Cyclohexane	Toluene	*p*-Terphenyl	Air-saturated	+	Berry
Cyclohexane	*i*-Propylbenzene	*p*-Terphenyl	Air-saturated	−	
Cyclohexane +5% heptane	Benzene	*p*-Terphenyl	Air-saturated	+	
Cyclohexane containing no more than 90% *n*-hexane	Benzene	*p*-Terphenyl	Air-saturated	+	Lipskv
Cyclopentane	Benzene	*p*-Terphenyl	Air-saturated	−	
Decalin	Benzene	*p*-Terphenyl	Air-saturated	+	
2,4-Dimethylpentane	Benzene	*p*-Terphenyl	Air-saturated	−	
Dioxane	Benzene	*p*-Terphenyl	Air-saturated	−	
n-Dodecane	Benzene	*p*-Terphenyl	Air-saturated	−	
n-Hexane	Benzene	*p*-Terphenyl	Air-saturated	−	
Methyl acetate	Benzene	*p*-Terphenyl	Air-saturated	−	Also Kropp
Methyl cyclohexane	Benzene	*p*-Terphenyl	Air-saturated	+	

[a] + indicates a minimum; −, its absence.
[b] Unless otherwise indicated, the observation was made in the course of the work here reported.

According to some notions of the energy-transfer process it is diffusion-controlled; i.e., the viscosity of the solution should be a determining factor. Cyclohexane, like hexane, has low viscosity; decalin and dodecane both have high viscosity. Only cyclohexane gives a minimum. Neither does the existence of the minimum depend on the efficiency of the quencher. Diphenyl mercury and methyl iodide are approximately equal in the latter respect but only the latter gives the minimum.

In summation, neither transfer efficiency nor viscosity of "common" solvent nor quenching efficiency of the quencher have bearing on the existence of a minimum. Section 4 shows that minima are explicable in terms of a conventional kinetic treatment if neighboring molecules of "better" solvent form domains with which, as a unit, the excitation is associated.

4. DISCUSSION

4.1. Energy Transfer

A reasonable view of the related phenomena of radiation chemistry and of luminescence is that a solvent may be energized by high-energy radiation in two ways,

$$M \rightsquigarrow M^+ + e,$$

$$M \rightsquigarrow M^*.$$

The ensuant phenomena depend on a number of factors; e.g., an electron initially produced in an ionization act may escape from a sibling positive hole and be trapped elsewhere; the excited states may be so unstable as to dissociate (without the possibility of any other processes) within approx. 10^{-13} sec; ionization or excitation may transfer to a second solvent or solute molecule; etc. A possible important fate of the initially produced ion is simply neutralization to give a highly excited state (either singlet or triplet),

$$M^+ + e \rightarrow M^\ddagger,$$

which may, in certain circumstances, internally convert within approx. 10^{-13} sec to the lowest excited state permitted by the selection rules.

For an appraisal and interpretation of the essential

TABLE II. Processes included in reaction scheme.

	Processes	Rates[a] (at fixed conc. of scintillator and quencher)
	Energization	
1.	$C\rightsquigarrow C^*$	$\alpha\epsilon_C$
2.	$B\rightsquigarrow B^*$	$\beta\epsilon_B$
	Transfer	
3.	$C^*+S\rightarrow C+S^*$	$k_{C^*S}N_{C^*}$
4.[b]	$B^*+S\rightarrow B+S^*$	$\zeta_{B^*S}N_{B^*}$
5.[c]	$C^*+B\rightarrow C+B^*$	$k_{C^*B}N_{C^*}$
	Quenching	
6.	$C^*+q_i\rightarrow C+q_i$	$\Sigma_i k_{C^*q_i}N_{C^*}$
7.[b]	$B^*+q_i\rightarrow B+q_i$	$\Sigma_i\zeta_{B^*q_i}N_{B^*}$
	Luminescence	
8.[d]	$S^*\rightarrow S+h\nu$	$(r_3+r_4)\phi_e$

[a] Symbol ϵ represents electron fraction; N, mole fraction.
[b] Superficially, the solvent B does not appear to enter into reactions 4 or 7. Nevertheless, the quantities ζ_{B^*S} and $\zeta_{B^*q_i}$ are specifically designated as dependent on N_B; cf Sec. 4.4.
[c] The value of k_{C^*B} is dependent on N_B.
[d] ϕ_e is the luminescence efficiency of the scintillator.

features of the phenomena, we employ a simple model in which the energizing process yields, in each solvent, a single energized species which, in turn, enters into the various energy degradation or transfer processes precedent to luminescence.

The possible variety of processes we specifically consider in a solution containing a common solvent C, a better solvent B, a scintillator solute S, and a quencher system $\sum_i q_i$ is represented in Table II. This table lists a minimal number of processes for a mechanism which has the desired features. In the table, decomposition is included under quenching and the possibility of quenching by the scintillator itself is not ignored.

4.2. Some Correlations

Table I and Figs. 1 and 2 show that (a) both solvents and quencher determine possibility of a luminescence minimum, (b) the only solvents so far found to be effective in that regard are those the individual molecules of which approach some degree of "flatness," (c) the quenchers so far found to be effective in production of a minimum may be classified alternatively as small in size or as electron capturers. Previous work has shown that ionization transfer is not involved in sensitized luminescence of benzene solutions.[7] Thus, if the added quencher does function as an electron capturer, it must be by capturing the electron from an excited state of the solvent B. However, the ionization-transfer process has not been ruled out in the case of cyclohexane solutions. Indeed, the most recent results from our laboratory indicate that this may be the only process by which energy is transferred from energized cyclohexane or similar aliphatic molecule either in processes of true protection in radiation chemistry or in scintillator solutions.[12] However, for the present mathematical analysis of the phenomena it is not necessary to consider such details.

4.3. The Light-Yield Expression

Straightforward kinetic treatment of the reaction scheme of Table II leads to the light-yield expression

$$I=\alpha\epsilon_C\cdot\frac{k_{C^*S}}{k_{C^*S}+k_{C^*B}+\sum_i k_{C^*q_i}}\cdot\left[1+\frac{k_{C^*B}}{k_{C^*S}}\cdot\frac{\zeta_{B^*S}}{\zeta_{B^*S}+\sum_i\zeta_{B^*q_i}}\right]+\beta\epsilon_B\cdot\zeta_{B^*S}/(\zeta_{B^*S}+\sum_i\zeta_{B^*q_i}). \quad (1)$$

This expression can be rearranged to give

$$I=\alpha\rho_C\cdot\frac{1+(k_{C^*B}/k_{C^*S})\rho_B}{1+(k_{C^*B}/k_{C^*S})\rho_C}+\left[\beta\rho_B-\alpha\rho_C\cdot\frac{1+(k_{C^*B}/k_{C^*S})\rho_B}{1+(k_{C^*B}/k_{C^*S})\rho_C}\right]\epsilon_B, \quad (2)$$

where

$$\rho_C=k_{C^*S}/(k_{C^*S}+\sum_i k_{C^*q_i}), \quad (3)$$

$$\rho_B=\zeta_{B^*S}/(\zeta_{B^*S}+\sum_i\zeta_{B^*q_i}), \quad (4)$$

and

$$\epsilon_B+\epsilon_C\approx 1. \quad (5)$$

Since B and S belong to the same general class of compound, we may assume that the relation

$$k_{C^*B}/k_{C^*S}=\gamma N_B=\gamma'\epsilon_B, \quad (6)$$

where γ and γ' are constants, holds throughout the region of small N_B, including the region in which minima occur. Substitution of Eq. (6) into Eq. (2) leads to

$$I=\alpha\rho_C+\{\alpha\rho_C\gamma'(\rho_B-\rho_C)+(\beta\rho_B-\alpha\rho_C)\}\epsilon_B. \quad (7)$$

The parameters ρ_B and ρ_C may be functions of concentration of B and thus Eq. (7) cannot be assumed to be linear in ϵ_B except at very low values of ϵ_B.

4.4. Conditions for a Minimum

In order to give a minimum in the luminescence curve, the value of $dI/d\epsilon_B$ must be negative in the

[12] M. Burton, paper presented at National Academy of Science meeting, Bloomington, Indiana (November, 1959).

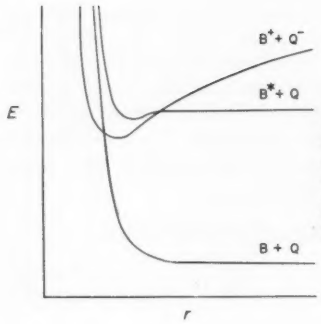

FIG. 3. A proposed system of potential energy relationships for quenching of an excited state of a single molecule of solvent B by a molecule Q, a quencher which is a negative-ion former.

region of very low ϵ_B; i.e., in this region the coefficient of ϵ_B in Eq. (7) must be negative. However, it is also necessary that this coefficient become positive at higher values of ϵ_B. It is interesting to examine the circumstances under which this condition can exist.

The parameters α and β in the rate expressions for reactions 1 and 2 (Table II) are constants of slightly different value which take into account both the different numbers of electrons in reactants C and B and also, in a general sense, the fact that energization of the two different electron systems of C and B is mildly sensitive to the energy states involved. For the present consideration, α and β may be treated as approximately equal.

Thus, the coefficient of ϵ_B in Eq. (7) can be consistent with the occurrence of a minimum when $\rho_B - \rho_C$ is negative for small ϵ_B. The value of ρ_C throughout this region is small[13] and almost certainly constant—or, at most, only slowly varying with concentration. Variation of ρ_B appears the most reasonable way to account for a minimum in the light yield. Thus, we require that ρ_B be initially very small and increase rapidly with concentration of B. This condition may be met (a) if ζ_{B^*S} is a rapidly increasing function of N_B (or ϵ_B), (b) if $\sum_i \zeta_{B^*q_i}$ decreases rapidly with increase of N_B, or (c) if the two quantities together vary in a way to give ρ_B the required properties. Present knowledge of the phenomena of luminescence indicates that (c) is determinant.

Evidence bearing specifically on the minimum in the cyclohexane+benzene+p-terphenyl+oxygen system is now available. In that case it has been shown that τ, the over-all decay time of the luminescence process, varies with benzene concentration reaching a broad maximum at very low values of the latter.[14] This phenomenon is observed both in presence[14] and absence[15] of the quencher. We now know from the work of Burton and Dreeskamp[16] that such a superficially determined value of τ is itself a complex quantity made up of various decay times: of C^*, of B^*, and of S^*. The decay time τ_0 for cyclohexane in this case is now known to be $\ll 0.3\times10^{-9}$ sec[17] and τ_S for p-terphenyl is roughly constant near 2.2×10^{-9} sec; the increase in the over-all τ at low benzene concentration is clearly a property of N_B.

Apparently, isolated B^* molecules, such as exist at low N_B, lack a rapid mechanism for dissipation of energy (as in reaction 4 or as in the summation of processes represented by reaction 7; cf. Table II).[16]

From previous work we now have reason to believe that the high rate of excitation transfer from B^* to S (rate constant k in pure benzene as solvent with p-terphenyl as scintillator estimated to be 9.3×10^{10} liter mole^{-1} sec^{-1}) is to be attributed to the existence of domains of B, every molecule of which is equivalent, so that collision of S with any B molecule in the domain is equivalent to a collision of S with the initially energized B.[18,19] This statement is formally equivalent to a statement that energy transfer may take place by exciton motion within the domain.[19] The reasonableness of the view of the existence of domains in cyclohexane+benzene solutions is evidenced by x-ray studies which Bell and Davey[20] interpret to indicate that benzene has groups —B—B—B—B— floating in a chaotic sea of unorganized molecules, that cyclohexane shows similar groupings and that —B—C—B—C— is also present.

The view of such special organization in cyclohexane and benzene and some survival of organization in their mixtures is supported also by the thermodynamic studies of Scatchard and Wood[21] and of Munster.[22] According to Mulliken,[23] maximum resonance in liquid benzene would be expected if the benzene molecules were stacked as in graphite.

In solutions in which benzene itself is the solvent, quenching and transfer constants are of the same order of magnitude, so that the quenching rate constant would also be high; domains of benzene molecules might again be invoked in explanation of this high rate.[19] However, in solutions of low N_B, with species B^* effectively isolated, we may consider the possible importance of the contribution of a simple diffusion-controlled process between B^* and quencher

$$B^* + q \rightarrow B + q^*.$$

This process can be assumed to occur at a significantly

[13] In all the cases in which a minimum is found C is a compound with high G value for decomposition (cf. cyclohexane, reference 1, also J. Chang and M. Burton, forthcoming publication). In such cases the contribution of reaction 6 (Table II) is high and ρ_C is thus made small.

[14] M. Burton and H. Dreeskamp, Discussions Faraday Soc. **27**, 64 (1959).

[15] Unpublished work in this laboratory.

[16] M. Burton and H. Dreeskamp, Z. Elektrochem. **64**, 165 (1960).

[17] M. Burton, A. Ghosh, and J. Yguerabide, Radiation Research Supplement **2**, 462 (1960).

[18] See especially the *discussion* remarks on footnote reference 16 and also footnote reference 17.

[19] S. Lipsky and M. Burton, J. Chem. Phys. **31**, 1221 (1959).

[20] P. H. Bell and W. P. Davey, J. Chem. Phys. **9**, 441 (1941).

[21] Cf. S. E. Wood, J. Chem. Phys. **15**, 358 (1947).

[22] A. Münster, Trans. Faraday Soc. **46**, 165 (1950); Z. physik. Chem. **196**, 106 (1950).

[23] R. S. Mulliken, J. Am. Chem. Soc. **74**, 811 (1952).

higher rate than a similar process involving direct transfer of energy from the initially energized B^* to scintillator in the specific case where the system B^*, q may become polarized, so that the two species attract each other,

$$B^*+q \rightarrow B^+ \cdot q^- \rightarrow B+q. \qquad (7a)$$

Figure 3 shows a type of potential energy relationship which can account for such a phenomenon.[24] Equation (4) now shows that with such relationship of rates ρ_B is a minimum at low values of N_B, where k_{7a} (the specific rate[25] of reaction 7(a) is the dominant term in $\sum_i \zeta_{B^*q_i}$ and ζ_{B^*S} is relatively small, and increases to a value approximating 0.5 as both ζ_{B^*S} and $\sum_i \zeta_{B^*q_i}$ increase with N_B (because of the contribution of processes involving entire domains of B).

It is interesting to note, on reference to Table I that, in the few examples of different quenchers studied, only those quenchers give a minimum which are electron acceptors in the sense here employed.

[24] H. Linschitz and L. Pekkarinen, J. Am. Chem. Soc. **82**, 2411 (1960).

[25] Note particularly that k_{7a} is substantially independent of N_B.

THE JOURNAL OF CHEMICAL PHYSICS VOLUME 34, NUMBER 1 JANUARY, 1961

On the Solution of the Hartree-Fock Equation in Terms of Localized Orbitals*

WILLIAM H. ADAMS† ‡

Enrico Fermi Institute for Nuclear Studies and Department of Chemistry, University of Chicago, Chicago, Illinois

(Received June 13, 1960)

The Hartree-Fock method is discussed with emphasis placed on the transformation properties of the Hartree-Fock equation. It is emphasized that the Hartree-Fock equation may be solved in terms of nonorthogonal one-electron functions, and that in some cases it may be more convenient to choose such solutions. Equations are developed which define the localized one-electron functions and it is shown how these equations may be solved. For a system of closed shell atoms or ions, it is suggested that the localized orbitals of each atom or ion can be expanded in terms of functions centered on its nucleus. This suggestion is based on the success of the ionic theory of crystals. Due to the symmetry of a crystal, it is suggested that use of the localized orbitals could lead to expressions for the first order, Hartree-Fock density matrix and the Hartree-Fock energy of a crystal, i.e., one could obtain the solution of the Hartree-Fock equation for a crystal.

1. INTRODUCTION

THE Hartree-Fock method gives one the "best possible" one-electron functions from which to construct a single determinant wave function for a system. They are the "best possible" functions in that they minimize the expectation value of the Hamiltonian of the system. Although these functions give the lowest energy obtainable using a single determinant wave function, the error in the energy is quite large in comparison to binding energies. This energy error should not, however, blind us to the importance of the Hartree-Fock method.

The Hartree-Fock method is a mathematically defined approximation to the problems we wish to solve. Furthermore, it is the best approximation to an N-body wave function that we can conveniently evaluate. Added to these two advantages, is the ease with which one may interpret orbital wave functions. These advantages more than compensate for the error we make in the total energy, for in applying the Hartree-Fock method, one should look for an understanding of chemical binding, not accurate, calculated binding energies. By understanding the features of chemical binding in the Hartree-Fock approximation, we may hope to learn what features to look for in a more exact approach to the quantum-mechanical problem of chemical binding.

In spite of the large error in the energy, the so-called correlation energy,[1] one may hope to calculate good binding energies in some cases. In cases in which the atoms or ions of the system are not greatly perturbed by the other members of the system, one may hope that the correlation energy of the system is approximately equal to the sum of the correlation energies of the isolated atoms or ions. Then, if one calculates the binding energy of the system by subtracting the sum of the Hartree-Fock energies of the isolated atoms or ions from the total Hartree-Fock energy of the system,

* Supported by the U. S. Atomic Energy Commission.

† Submitted in partial fulfillment of the requirements for the degree of Doctor of Philosophy at the University of Chicago.

‡ Present address: Quantum Chemistry Group, Uppsala University, Uppsala, Sweden.

[1] The correlation energy is defined to be the difference between the smallest eigenvalue of the Hamiltonian of the system and the Hartree-Fock energy of the system.

the correlation energy of the system will be canceled by the correlation energies of the atoms or ions.[2] This appears to be the case for alkali halide crystals, for Löwdin[3] has calculated cohesive energies for some of the alkali halide crystals which agree closely with the empirical values, in spite of the large correlation energies of the isolated ions.

Löwdin's calculation of the cohesive energies of the alkali halide crystals was done in the Heitler-London approximation, using the ground state Hartree-Fock orbitals of the isolated ions to construct the orbitals of the system. For LiF, Löwdin obtained a cohesive energy of -9.62 ev[3] as compared to the empirical value of -10.638 ev.[4] The correlation energies of Li^+ and F^- are -1.182 ev and -10.69 ev,[5] respectively. Thus the sum of the correlation energies of the isolated ions is greater than the cohesive energy of the crystal. The cohesive energies of the other alkali halide crystals are smaller than that of LiF, while the sum of the correlation energies of the isolated ions is much larger than the sum for Li^+ and F^-.[6]

As we said in the beginning, though, we should not be too much concerned with the accuracy of the calculated energies, but rather with understanding chemical binding. In this respect the result of Löwdin's calculation is suggestive. It suggests that the ions in the crystal do not differ greatly from the isolated ions. It suggests that the viewpoint of the classical theory of ionic crystals[7] is correct, i.e., an ionic crystal can be regarded as being made up of ions which are polarized by the other ions. We shall attempt to apply this interpretation to the Hartree-Fock wave function of a system.

We propose not only to interpret the Hartree-Fock functions of a system in terms of functions localized about the various nuclei, but also to show how one might solve the Hartree-Fock equation directly for these orbitals. In particular, we shall outline a procedure for applying these equations to ionic crystals. It is felt that it will be far easier to solve the Hartree-Fock equation for an ionic crystal in terms of localized orbitals than in terms of the standard Hartree-Fock functions.

2. THE HARTREE-FOCK METHOD

We shall discuss the Hartree-Fock equation for a system of N electrons moving in the electrostatic field due to a number of fixed nuclei. We shall include the spin but we shall not require that the one-electron functions be spin eigenfunctions or that the wave function be an eigenfunction of the total spin.[8] It is better to impose these requirements only when one is discussing special cases. What we shall be interested in are the transformation properties of the Hartree-Fock equation and functions, and the methods used to solve the equation.

The Hamiltonian $\mathcal{H}$ of the system may be written in Hartree's atomic units as

$$\mathcal{H}=\sum_{i=1}^{N}\mathcal{H}_i+\tfrac{1}{2}\sum_{i\neq j}^{N}\sum r_{ij}^{-1}, \tag{1}$$

where

$$\mathcal{H}_i=-\tfrac{1}{2}\nabla_i^2-\sum_a(Z_a/R_{ai}), \tag{1'}$$

when one confines oneself to a nonrelativistic approximation in which the electrons and nuclei interact only through coulombic forces. We have written Z_a for the charge on nucleus a, R_{ai} for the distance from nucleus a to electron i, and $r_{ij}=|\mathbf{r}_i-\mathbf{r}_j|$ for the distance between electrons i and j. The vector $\mathbf{r}_i$ is the position vector of electron i. We use $\mathbf{x}_i$ to represent $\mathbf{r}_i$ and s_i, the spin coordinate of electron i. The Hartree-Fock method defines an approximate solution to the ground-state function for $\mathcal{H}$ in the following manner:

(a) The normalized, approximate wave function, Ψ, is a single determinant of N orthonormal one-electron functions $\psi_1(\mathbf{x})\cdots,\psi_N(\mathbf{x})$.

(b) The integral

$$\langle\mathcal{H}\rangle=\int\Psi^*(\mathbf{x}_1\cdots\mathbf{x}_N)\mathcal{H}\Psi(\mathbf{x}_1\cdots\mathbf{x}_N)d\mathbf{x}_1\cdots d\mathbf{x}_N$$

is a minimum.

The Hartree-Fock equation results from the application of the methods of the calculus of variations to the condition (b). Before we write down the equation, we shall define our notation.[9]

The element $\mathbf{x},\mathbf{x}'$ of the representation in $\mathbf{x}$ space of the first-order density matrix in the Hartree-Fock approximation is

$$\rho(\mathbf{x}\,|\,\mathbf{x}')=\sum_{r=1}^{N}\psi_r(\mathbf{x})\psi_r^*(\mathbf{x}'). \tag{2}$$

We define a matrix $\boldsymbol{\rho}$ which has as its elements $\rho(\mathbf{x}\,|\,\mathbf{x}')$, where $\mathbf{x}$ is the row index of the matrix, and $\mathbf{x}'$ is its column index. We define the matrix $\boldsymbol{\Psi}$ whose elements

[2] P.-O. Löwdin, Advances in Chem. Phys. **2**, 235 (1959).

[3] P.-O. Löwdin, *Advances in Physics* (Taylor and Francis, Ltd., London, 1956), Vol. 5, p. 1. The cohesive energies referred to, are found in Table 10, except for that of LiF, which is in Table 11.

[4] D. Cubicciotti, J. Chem. Phys. **31**, 1646 (1959).

[5] A. Fröman, Phys. Rev. **112**, 870 (1958).

[6] The cohesive energies which Löwdin calculated for the NaCl and KCl crystals were much more accurate than that for LiF, being within 0.15 ev of the empirical values. We have discussed only the LiF crystal because we have accurate correlation energies for Li^+ and F^-, but not for K^+ or Cl^-. The correlation energy of Na^+ is expected to be comparable to that of F^-.

[7] See for example F. Seitz, *The Modern Theory of Solids* (McGraw-Hill Book Company, Inc., New York, 1940), Chap. II.

[8] In order to conform to the usual nomenclature we use the following definitions: Orbital: a function of the position coordinates of one electron. Spin orbital: a function of the position coordinates of one electron which has either spin $+\frac{1}{2}$ or $-\frac{1}{2}$. A spin orbital may be obtained from an orbital by multiplying the orbital by either a spin-up or a spin-down eigenfunction. One-electron function: a function of the position coordinates and the spin coordinates of one electron. It need not be a spin eigenfunction.

[9] The notation is due to G. L. Montet, S. P. Keller, and J. E. Mayer, J. Chem. Phys. **20**, 1057 (1952).

are the $\psi_\nu(\mathbf{x})$'s, the row index being $\mathbf{x}$, and the column index $\nu(1\leq\nu\leq N)$. Multiplication of these matrices is performed according to standard rules, i.e., one sums over discrete indices and integrates over continuous indices. The Hermitian conjugate of $\mathbf{\Psi}$, is $\mathbf{\Psi}^\dagger$. It is formed by application of the standard rules of matrix algebra. We may write

$$\boldsymbol{\varrho}=\mathbf{\Psi}\mathbf{\Psi}^\dagger \tag{3}$$

and

$$\mathbf{\Psi}^\dagger\mathbf{\Psi}=\mathbf{1}, \tag{4}$$

where $\mathbf{1}$ is the N by N unit matrix. The latter relation is a result of the orthonormality of the one-electron functions. The trace is formed in accordance with the standard matrix rules, i.e.,

$$[\boldsymbol{\varrho}]_{tr}=\int d\mathbf{x}\rho(\mathbf{x}\mid\mathbf{x})=N. \tag{5}$$

Similarly, one has

$$[\mathbf{\Psi}^\dagger\mathbf{\Psi}]_{tr}=[\mathbf{1}]_{tr}=N, \tag{6}$$

which, of course, follows from the well-known property of the trace of a product of two matrices,

$$[\mathbf{fg}]_{tr}=[\mathbf{gf}]_{tr}. \tag{7}$$

We shall often have occasion to use this property.

There are three operator matrices which we must define. These quantities will behave like matrices in all cases in which the order of their appearance in a product is not altered, i.e., under matrix transformations, the matrix which they multiply from the left must not change. We define

$$(\mathbf{H})_{\mathbf{x}_i\mathbf{x}_j}=\delta(\mathbf{x}_i-\mathbf{x}_j)\mathcal{H}_j, \tag{8}$$

where $\delta(\mathbf{x}_i-\mathbf{x}_j)$ is the delta function. Similarly, we define

$$(\boldsymbol{\varrho}\mathbf{B})_{\mathbf{x}_i\mathbf{x}_j}=\delta(\mathbf{x}_i-\mathbf{x}_j)\int d\mathbf{x}_k r_{jk}^{-1}\rho(\mathbf{x}_k\mid\mathbf{x}_k), \tag{9}$$

and

$$(\rho\mathbf{A})_{\mathbf{x}_i\mathbf{x}_j}=r_{ij}^{-1}\rho(\mathbf{x}_i\mid\mathbf{x}_j). \tag{10}$$

It must be particularly emphasized that $\boldsymbol{\varrho}\mathbf{B}$ and $\boldsymbol{\varrho}\mathbf{A}$ are the defined matrices, and that $\mathbf{B}$ and $\mathbf{A}$ have no independent meaning in our notation. The matrices $\boldsymbol{\varrho}\mathbf{B}$ and $\boldsymbol{\varrho}\mathbf{A}$ correspond to the Coulomb and exchange operators of the usual formalism.

The total energy of the N-electron system in our notation is

$$E=[\mathbf{H}\boldsymbol{\varrho}+\tfrac{1}{2}\boldsymbol{\varrho}(\mathbf{B}-\mathbf{A})\boldsymbol{\varrho}]_{tr}. \tag{11}$$

Application of the standard variational technique to Eq. (11) and the supplementary condition (4), leads to

$$\mathbf{H}\mathbf{\Psi}+\boldsymbol{\varrho}(\mathbf{B}-\mathbf{A})\mathbf{\Psi}=\mathbf{\Psi}\mathbf{E}. \tag{12}$$

This is the Hartree-Fock equation. No generality is lost by requiring that $\mathbf{E}$ be diagonal since the matrix $\mathbf{E}$ is Hermitian and thus can be diagonalized by a similarity transformation with a unitary matrix. When $\mathbf{E}$ is diagonal and the $\psi_\mu(\mathbf{x})$'s are orthonormal, we shall say that Eq. (12) is the standard form of the Hartree-Fock equation, and that the $\psi_\mu(\mathbf{x})$'s are the standard one-electron functions.

We digress from our discussion of the properties of the Hartree-Fock equation in order to describe how the equation is usually solved. It is an iterative method. One begins by guessing a $\mathbf{\Psi}$, call it $\mathbf{\Psi}^\circ$, and forming $\boldsymbol{\varrho}^\circ=\mathbf{\Psi}^\circ\mathbf{\Psi}^{\circ\dagger}$. Then one replaces $\boldsymbol{\varrho}$ in the Hartree-Fock equation by $\boldsymbol{\varrho}^\circ$ and solves the resulting linear integro-differential equation. There are more than N solutions to this equation. One chooses the N solutions giving the smallest eigenvalues of the equation as the functions to use in a new approximation to $\mathbf{\Psi}$. The outlined procedure corresponds to minimizing $[\mathbf{F}\boldsymbol{\varrho}]_{tr}$ with respect to $\mathbf{\Psi}$ under the assumption that $\mathbf{F}=\mathbf{H}+\boldsymbol{\varrho}(\mathbf{B}-\mathbf{A})$ is independent of $\mathbf{\Psi}$. With the new approximation to $\mathbf{\Psi}$ one goes through the same procedure as with $\mathbf{\Psi}^\circ$, obtaining in the end a third approximation to $\mathbf{\Psi}$. One repeats these operations until the $\mathbf{\Psi}$ used to define the $\boldsymbol{\varrho}$ that is substituted into the Hartree-Fock equation is the same as the $\mathbf{\Psi}$ which is obtained from the equation, to the desired accuracy. The function obtained is called the self-consistent solution of the equation.

With regard to the method of solution outlined, it may be asked if the functions obtained are appropriate to the ground state. If satisfying the Hartree-Fock equation is a sufficient condition for obtaining one-electron functions which minimize E, then there can be no doubt that the solutions of the Hartree-Fock equation obtained in the outlined manner are the correct functions. Although the Hartree-Fock equation must be satisfied by the functions that minimize E, we have been unable to find a proof that a set of N functions satisfying a Hartree-Fock equation necessarily makes E a minimum. Furthermore, the iterative process used corresponds to minimizing not E, but $[\mathbf{F}\boldsymbol{\varrho}]_{tr}$ under the assumption that $\mathbf{F}$ is independent of $\mathbf{\Psi}$.[10]

In outlining the usual derivation of the Hartree-Fock equation, we have required that the $\psi_\mu(\mathbf{x})$'s be orthonormal. It is an unnecessary requirement. Suppose that we had chosen N linearly independent, normalized but nonorthogonal, one-electron functions. From these N linearly independent functions we could have constructed N orthonormal functions. The normalized, single determinant wave function constructed from the nonorthogonal set differs from that constructed from the orthonormalized set by, at most, a phase factor. The conditions of analytic importance are that the

[10] There is one method of solving the Hartree-Fock equation which does not involve making a choice at the end of each iteration. It also seems to be better designed for obtaining rapid convergence of the iteration procedure. The method is that of McWeeny for directly calculating the first-order density matrix. See R. McWeeny, Proc. Roy. Soc. (London) **A235**, 496 (1956).

one-electron functions be normalizable and linearly independent. We could have derived the Hartree-Fock equation by requiring not orthogonality between the different one-electron functions, but by requiring that $\mathbf{\Psi}^\dagger\mathbf{\Psi}=\mathbf{\Delta}$, with $\mathbf{\Delta}$ a matrix of fixed numbers. We could have even omitted all reference to the values of the overlap integrals and still have arrived at an equation of the same form. The linear independence and normalizability of the one-electron functions are the supplementary conditions which can not be omitted. We shall derive the Hartree-Fock equation using only these conditions.

We consider a matrix $\mathbf{\Phi}$ of normalized but nonorthogonal one-electron functions, $\phi_1(\mathbf{x})$, $\phi_2(\mathbf{x})$, $\cdots$, $\phi_N(\mathbf{x})$, where $\mathbf{x}$ is the row index and the subscript ν of $\phi_\nu(\mathbf{x})$, the column index. We require that these N functions be linearly independent. We define the overlap matrix,

$$\mathbf{S}=\mathbf{\Phi}^\dagger\mathbf{\Phi}-\mathbf{1}. \tag{13}$$

The diagonal elements of $\mathbf{S}$ are zero since the $\phi_\mu(\mathbf{x})$'s are normalized. It has been shown[9] that the first-order density matrix of a system described by nonorthogonal one-electron functions is

$$\varrho=\mathbf{\Phi}(\mathbf{\Phi}^\dagger\mathbf{\Phi})^{-1}\mathbf{\Phi}^\dagger \tag{14}$$

$$=\mathbf{\Phi}(\mathbf{1}+\mathbf{S})^{-1}\mathbf{\Phi}^\dagger. \tag{14'}$$

Equation (14) is a valid definition of ϱ even when the $\phi_\mu(\mathbf{x})$'s are not normalized. We replace $\mathbf{\Phi}$ by $\mathbf{\Phi}+\delta\mathbf{\Phi}$. This change in $\mathbf{\Phi}$ causes $\mathbf{S}$ to become $\mathbf{S}+\delta\mathbf{S}$, where $\delta\mathbf{S}=\delta(\mathbf{\Phi}^\dagger\mathbf{\Phi})$. The diagonal elements of $\delta\mathbf{S}$ are not zero for an arbitrary $\delta\mathbf{\Phi}$. To the first order in $\delta\mathbf{S}$, one finds

$$\begin{aligned}(\mathbf{1}+\mathbf{S}+\delta\mathbf{S})^{-1}&=\{(\mathbf{1}+\mathbf{S})[\mathbf{1}+(\mathbf{1}+\mathbf{S})^{-1}\delta\mathbf{S}]\}^{-1}\\&=[\mathbf{1}+(\mathbf{1}+\mathbf{S})^{-1}\delta\mathbf{S}]^{-1}(\mathbf{1}+\mathbf{S})^{-1}\\&=(\mathbf{1}+\mathbf{S})^{-1}-(\mathbf{1}+\mathbf{S})^{-1}\delta\mathbf{S}(\mathbf{1}+\mathbf{S})^{-1}+\cdots.\end{aligned} \tag{15}$$

We write $\delta\varrho$ in terms of $\delta\mathbf{\Phi}$,

$$\begin{aligned}\delta\varrho=&\,\delta\mathbf{\Phi}(\mathbf{1}+\mathbf{S})^{-1}\mathbf{\Phi}^\dagger+\mathbf{\Phi}(\mathbf{1}+\mathbf{S})^{-1}\delta\mathbf{\Phi}^\dagger\\&-\mathbf{\Phi}(\mathbf{1}+\mathbf{S})^{-1}\mathbf{\Phi}^\dagger\delta\mathbf{\Phi}(\mathbf{1}+\mathbf{S})^{-1}\mathbf{\Phi}^\dagger\\&-\mathbf{\Phi}(\mathbf{1}+\mathbf{S})^{-1}\delta\mathbf{\Phi}^\dagger\mathbf{\Phi}(\mathbf{1}+\mathbf{S})^{-1}\mathbf{\Phi}^\dagger+\cdots\end{aligned} \tag{16}$$

$$\begin{aligned}=&\,\delta\mathbf{\Phi}(\mathbf{1}+\mathbf{S})^{-1}\mathbf{\Phi}^\dagger+\mathbf{\Phi}(\mathbf{1}+\mathbf{S})^{-1}\delta\mathbf{\Phi}^\dagger\\&-\varrho\delta\mathbf{\Phi}(\mathbf{1}+\mathbf{S})^{-1}\mathbf{\Phi}^\dagger-\mathbf{\Phi}(\mathbf{1}+\mathbf{S})^{-1}\delta\mathbf{\Phi}^\dagger\varrho+\cdots.\end{aligned} \tag{16'}$$

We vary $\mathbf{\Phi}$ in Eq. (11), requiring that $\mathbf{\Phi}$ minimize E, so that $\delta E=0$,

$$\delta E=[\mathbf{H}\delta\varrho+\varrho(\mathbf{B}-\mathbf{A})\delta\varrho]_{tr}=0. \tag{17}$$

Substitution of Eq. (16') into Eq. (17) will lead to the desired equation. Defining

$$\mathbf{F}=\mathbf{H}+\varrho(\mathbf{B}-\mathbf{A}), \tag{18}$$

we obtain upon substitution of (16') into (17),

$$\begin{aligned}\delta E=\{&\mathbf{F}[\delta\mathbf{\Phi}(\mathbf{1}+\mathbf{S})^{-1}\mathbf{\Phi}^\dagger+\mathbf{\Phi}(\mathbf{1}+\mathbf{S})^{-1}\delta\mathbf{\Phi}^\dagger\\&-\varrho\delta\mathbf{\Phi}(\mathbf{1}+\mathbf{S})^{-1}\mathbf{\Phi}^\dagger-\mathbf{\Phi}(\mathbf{1}+\mathbf{S})^{-1}\delta\mathbf{\Phi}^\dagger\varrho]\}_{tr}.\end{aligned}$$

Using the well-known property of the trace of the product of two matrices, namely, that $[\mathbf{fg}]_{tr}=[\mathbf{gf}]_{tr}$, we obtain

$$\begin{aligned}\delta E=&[\delta\mathbf{\Phi}^\dagger(\mathbf{F}\mathbf{\Phi}-\varrho\mathbf{F}\mathbf{\Phi})(\mathbf{1}+\mathbf{S})^{-1}]_{tr}\\&+[(\mathbf{1}+\mathbf{S})^{-1}(\mathbf{\Phi}^\dagger\mathbf{F}-\mathbf{\Phi}^\dagger\mathbf{F}\varrho)\delta\mathbf{\Phi}]_{tr}=0.\end{aligned}$$

This equation is satisfied if

$$\mathbf{F}\mathbf{\Phi}=\varrho\mathbf{F}\mathbf{\Phi}. \tag{19}$$

If we define

$$\mathbf{E}'=(\mathbf{1}+\mathbf{S})^{-1}\mathbf{\Phi}^\dagger\mathbf{F}\mathbf{\Phi}, \tag{20}$$

then Eq. (19) becomes

$$\mathbf{F}\mathbf{\Phi}=\mathbf{\Phi}\mathbf{E}'. \tag{21}$$

One can show that $(\mathbf{1}+\mathbf{S})\mathbf{E}'$ is a Hermitian matrix, but that $\mathbf{E}'$ is not.

To show that Eq. (21) can be transformed into the standard Hartree-Fock equation, we must use the conditions that the $\phi_\mu(\mathbf{x})$'s be linearly independent and normalized. Since the $\phi_\mu(\mathbf{x})$'s are linearly independent, they may be orthogonalized. It has been shown[9,11] that

$$\chi=\mathbf{\Phi}(\mathbf{1}+\mathbf{S})^{-\frac{1}{2}} \tag{22}$$

is a set of orthonormalized functions;

$$\chi^\dagger\chi=(\mathbf{1}+\mathbf{S})^{-\frac{1}{2}}\mathbf{\Phi}^\dagger\mathbf{\Phi}(\mathbf{1}+\mathbf{S})^{-\frac{1}{2}}=\mathbf{1}. \tag{22'}$$

We multiply Eq. (21) from the right by $(\mathbf{1}+\mathbf{S})^{-\frac{1}{2}}$ to obtain

$$\mathbf{F}\chi=\chi(\mathbf{1}+\mathbf{S})^{\frac{1}{2}}\mathbf{E}'(\mathbf{1}+\mathbf{S})^{-\frac{1}{2}}. \tag{23}$$

The matrix $(\mathbf{1}+\mathbf{S})^{\frac{1}{2}}\mathbf{E}'(\mathbf{1}+\mathbf{S})^{-\frac{1}{2}}$ is Hermitian since $\chi^\dagger\mathbf{F}\chi$ is a Hermitian matrix. Because $(\mathbf{1}+\mathbf{S})^{\frac{1}{2}}\mathbf{E}'(\mathbf{1}+\mathbf{S})^{-\frac{1}{2}}$ is Hermitian, it may be diagonalized by a similarity transformation with a unitary matrix, $\mathbf{U}$. We define

$$\mathbf{E}=\mathbf{U}^\dagger(\mathbf{1}+\mathbf{S})^{\frac{1}{2}}\mathbf{E}'(\mathbf{1}+\mathbf{S})^{-\frac{1}{2}}\mathbf{U} \tag{24}$$

to be the diagonal matrix. We define

$$\mathbf{\Psi}=\chi\mathbf{U}, \tag{25}$$

$$\mathbf{\Psi}^\dagger\mathbf{\Psi}=\mathbf{U}^\dagger\chi^\dagger\chi\mathbf{U}=\mathbf{1}. \tag{25'}$$

Multiplying Eq. (23) from the right by $\mathbf{U}$ and substituting from Eqs. (24) and (25), we obtain the standard form of the Hartree-Fock equation, Eq. (12). We define

$$\mathbf{T}=\mathbf{U}^\dagger(\mathbf{1}+\mathbf{S})^{\frac{1}{2}}. \tag{26}$$

Combining this with Eqs. (22) and (25), we find $\mathbf{\Psi}=\mathbf{\Phi}\mathbf{T}^{-1}$ or

$$\mathbf{\Phi}=\mathbf{\Psi}\mathbf{T}. \tag{27}$$

---

[11] P.-O. Löwdin, J. Chem. Phys. **18**, 365 (1950).

We may also substitute $\mathbf{T}$ into Eq. (24),

$$\mathbf{E}=\mathbf{T}\mathbf{E}'\mathbf{T}^{-1}. \tag{28}$$

From Eq. (26), we see that

$$\mathbf{T}^{\dagger}\mathbf{T}=(\mathbf{1}+\mathbf{S})^{\frac{1}{2}}\mathbf{U}\mathbf{U}^{\dagger}(\mathbf{1}+\mathbf{S})^{\frac{1}{2}}=\mathbf{1}+\mathbf{S}. \tag{29}$$

If $\mathbf{S}=0$, then $\mathbf{T}$ is unitary, the $\phi_\mu(\mathbf{x})$'s are orthonormal and $\mathbf{E}'$ is Hermitian. When $\mathbf{S}\neq 0$, $\mathbf{T}$ is not unitary, the $\phi_\mu(\mathbf{x})$'s are not orthogonal and $\mathbf{E}'$ is not Hermitian.

We have reviewed the transformation properties of the Hartree-Fock equation, putting emphasis on the fact that one need not impose an orthogonality condition. We have pointed out that requiring the N one-electron functions to be linearly independent and normalizable, we obtain the Hartree-Fock equation. We have emphasized it because we wish to make use of that freedom. Briefly, our aim is to obtain "localized" one-electron functions which will be more easily interpreted and more easily evaluated than the usual molecular orbitals.

3. EQUATIONS FOR LOCALIZED ORBITALS

In the introduction, we said that we would attempt to interpret chemical binding in terms of atoms and ions interacting with the other atoms and ions of the system. To do this we must assign a number N_a of the N electrons of the system to each nucleus a of the system. How many electrons we assign to any nucleus is arbitrary, but if we wish to compare our calculations directly with the empirical data and with the classical interpretations, we shall have to assign the same number of electrons to each nucleus as were assigned in the classical interpretations. Having assigned a definite number of electrons to each nucleus, we define an equal number of one-electron functions localized about the respective nuclei.

The one-electron functions are defined by writing them as linear combinations of the standard Hartree-Fock one-electron functions of the system, the $\psi_\mu(\mathbf{x})$'s. The one-electron functions of each "atom" are localized by requiring that they minimize the "self-energy" of that "atom" [Eq. (46)]. These are the "best" localized functions. We form $\mathbf{\Phi}$ from these localized one-electron functions. The standard Hartree-Fock functions of $\mathbf{\Psi}$ will be related to $\mathbf{\Phi}$ by Eq. (27). The localized functions will satisfy the Hartree-Fock equation for nonorthogonal functions, Eq. (21). We shall show that Eq. (21) may be analyzed into equations which may be interpreted as equations for atoms or ions interacting with the other atoms and ions of the system. In accordance with this interpretation, we shall sometimes speak of the "best" localized one-electron functions as "perturbed atomic functions." From the equations for the perturbed atomic functions, we shall develop a "practical" approach for solving the Hartree-Fock equation directly in terms of localized one-electron functions.

In the preceding section we introduced a matrix $\mathbf{\Phi}$ related to the $\mathbf{\Psi}$ of the standard Hartree-Fock equation by the equation $\mathbf{\Phi}=\mathbf{\Psi}\mathbf{T}$. We also defined a matrix $\mathbf{E}'$, which was neither diagonal nor Hermitian. From Eqs. (21) and (27) we shall derive the Hartree-Fock equation appropriate for localized orbitals. This derivation is carried through with the help of a set of auxiliary matrices. We define an N by N matrix $\mathbf{1}_a$ whose only nonzero elements are unity, these elements being the first N_a diagonal elements. We define another N by N matrix $\mathbf{1}_b$ whose only nonzero elements are unity, these elements being the N_a+1th to N_a+N_bth diagonal elements. Matrices $\mathbf{1}_c$, $\mathbf{1}_d$, $\cdots$, are defined in order. The subscripts a, b, c, $\cdots$, refer to the nuclei a, b, c, $\cdots$, of the "atoms" a, b, c, $\cdots$. We require that

$$\sum_a N_a=N, \tag{30}$$

so that

$$\sum_a \mathbf{1}_a=\mathbf{1}, \tag{31}$$

where $\sum_a$ indicates summation over all of the nuclei. These matrices have the properties that

$$\mathbf{1}_a\mathbf{1}_a=\mathbf{1}_a, \tag{31'}$$

$$\mathbf{1}_a\mathbf{1}_b=0, \tag{31''}$$

and

$$[\mathbf{1}_a]_{tr}=N_a. \tag{32}$$

We define

$$\mathbf{T}_a=\mathbf{T}\mathbf{1}_a, \tag{33}$$

$$\mathbf{\Phi}_a=\mathbf{\Phi}\mathbf{1}_a=\mathbf{\Psi}\mathbf{T}_a, \tag{33'}$$

and

$$\mathbf{E}_{ba}'=\mathbf{1}_b\mathbf{E}'\mathbf{1}_a. \tag{34}$$

We shall require that

$$\mathbf{\Phi}_a^{\dagger}\mathbf{\Phi}_a=\mathbf{T}_a^{\dagger}\mathbf{T}_a=\mathbf{1}_a, \tag{35}$$

in other words, that the functions, $\phi_{a1}(\mathbf{x})$, $\phi_{a2}(\mathbf{x})$, $\cdots$, $\phi_{aN}(\mathbf{x})$, of "atom" a be mutually orthogonal. This permits us to define the first-order density matrix of the atom to be

$$\mathbf{n}_a=\mathbf{\Phi}_a\mathbf{\Phi}_a^{\dagger}. \tag{36}$$

We define

$$\mathbf{S}_{ab}=\mathbf{\Phi}_a^{\dagger}\mathbf{\Phi}_b=\mathbf{T}_a^{\dagger}\mathbf{T}_b, \tag{37}$$

for $a\neq b$, and

$$\mathbf{\delta}=\mathbf{\rho}-\sum_a \mathbf{n}_a. \tag{38}$$

We multiply Eq. (21) from the right by $\mathbf{1}_a$ and introduce the quantities defined in Eqs. (33'), (34), and (38).

$$\mathbf{H}\mathbf{\Phi}_a+\mathbf{n}_a(\mathbf{B}-\mathbf{A})\mathbf{\Phi}_a+\sum_{b\neq a}\mathbf{n}_b(\mathbf{B}-\mathbf{A})\mathbf{\Phi}_a + \mathbf{\delta}(\mathbf{B}-\mathbf{A})\mathbf{\Phi}_a=\mathbf{\Phi}_a\mathbf{E}_{aa}'+\sum_{b\neq a}\mathbf{\Phi}_b\mathbf{E}_{ba}'. \tag{39}$$

We define

$$(\mathbf{H}_a)_{\mathbf{x}_i\mathbf{x}_j}=\delta(\mathbf{x}_i-\mathbf{x}_j)\left[-\tfrac{1}{2}\nabla_j^2-(Z_a/R_{aj})\right], \tag{40}$$

and

$$(Z_b/\mathbf{R}_b)_{\mathbf{x}_i\mathbf{x}_j}=\delta(\mathbf{x}_i-\mathbf{x}_j)\,(Z_b/R_{bj}). \tag{41}$$

Substituting Eqs. (40) and (41) into Eq. (39), we obtain

$$\mathbf{H}_a\mathbf{\Phi}_a+\mathbf{n}_a(\mathbf{B}-\mathbf{A})\mathbf{\Phi}_a+\mathfrak{d}(\mathbf{B}-\mathbf{A})\mathbf{\Phi}_a+\sum_{b\neq a}\left[-\frac{Z_b}{\mathbf{R}_b}+\mathbf{n}_b(\mathbf{B}-\mathbf{A})\right]\mathbf{\Phi}_a-\sum_{b\neq a}\mathbf{\Phi}_b\mathbf{E}_{ba}{}'=\mathbf{\Phi}_a\mathbf{E}_{aa}{}'. \tag{42}$$

When we define

$$\mathbf{V}_a=\mathfrak{d}(\mathbf{B}-\mathbf{A})+\sum_{b\neq a}[-(Z_b/\mathbf{R}_b)+\mathbf{n}_b(\mathbf{B}-\mathbf{A})-\mathbf{\Phi}_b\mathbf{E}_{ba}{}'\mathbf{\Phi}_a{}^\dagger], \tag{43}$$

we can write Eq. (42) as

$$\mathbf{H}_a\mathbf{\Phi}_a+\mathbf{n}_a(\mathbf{B}-\mathbf{A})\mathbf{\Phi}_a+\mathbf{V}_a\mathbf{\Phi}_a=\mathbf{\Phi}_a\mathbf{E}_{aa}{}', \tag{44}$$

since $\mathbf{\Phi}_a{}^\dagger\mathbf{\Phi}_a=\mathbf{1}_a$. With Eq. (44), we have reached our goal.

Our goal has been to break the Hartree-Fock equation for the system down into Hartree-Fock type equations for each atom in the external fields due to the other atoms. One could apply this interpretation to Eq. (44) by ignoring the dependence of $\mathbf{V}_a$ on $\mathbf{\Phi}_a$. If $\mathbf{V}_a$ were independent of $\mathbf{\Phi}_a$, we could derive Eq. (44) by minimizing

$$E_a{}'=[\mathbf{H}_a\mathbf{n}_a+\tfrac{1}{2}\mathbf{n}_a(\mathbf{B}-\mathbf{A})\mathbf{n}_a+\mathbf{V}_a\mathbf{n}_a]_{tr}, \tag{45}$$

with respect to $\mathbf{\Phi}_a$ under the supplementary condition (34). Furthermore, if we had solutions for $\mathbf{\Phi}_b$, $\mathbf{\Phi}_c$, $\cdots$, the matrix $\mathbf{\Phi}_a$ being the only unknown one, we could obtain $\mathbf{\Phi}_a$ by minimizing $E_a{}'$ with respect to it. The minimization of $E_a{}'$, assuming that $\mathbf{V}_a$ is independent of $\mathbf{\Phi}_a$, makes the minimization of E and the solution of Eq. (44) easier, just as the requirement that $[\mathbf{F}\varrho]_{tr}$ be a minimum, assuming $\mathbf{F}$ to be independent of $\mathbf{\Psi}$, makes the solution of the standard form of the Hartree-Fock equation easier.

There is an unimportant difficulty with Eq. (45). The number $E_a{}'$ is not necessarily real because $\mathbf{\Phi}_a{}^\dagger\mathbf{V}_a\mathbf{\Phi}_a$ is not Hermitian. This difficulty is unimportant since in practice one uses only real functions. The use of real functions is sufficient, of course, to make all of the quantities in our equations real.

We have not yet imposed the conditions on $\mathbf{\Phi}_a$, $\mathbf{\Phi}_b$, $\cdots$, which will make them localized. To insure that $\mathbf{\Phi}_a$ is a matrix of one-electron functions localized about the nucleus of atom a, we require that

$$E_a=[\mathbf{H}_a\mathbf{n}_a+\tfrac{1}{2}\mathbf{n}_a(\mathbf{B}-\mathbf{A})\mathbf{n}_a]_{tr} \tag{46}$$

be a minimum under the conditions (33) and (35). We shall call E_a the self-energy of atom a. Variation of $\mathbf{T}_a$ in (46) under these conditions leads to

$$\mathbf{\Psi}^\dagger\mathbf{H}_a\mathbf{\Psi}'\mathbf{T}_a+\mathbf{\Psi}'{}^\dagger[\mathbf{n}_a(\mathbf{B}-\mathbf{A})]\mathbf{\Psi}'\mathbf{T}_a=\mathbf{T}_a\boldsymbol{\varepsilon}_a. \tag{47}$$

In other words, the elements of $\mathbf{\Phi}_a$ are the "best possible" one-electron functions for atom a that can be obtained by forming linear combinations of the Hartree-Fock functions of the system. Since $\boldsymbol{\varepsilon}_a$ is Hermitian, we may require that it be diagonal.

These equations for localized orbitals may be solved iteratively in a manner similar to the one used to solve the standard Hartree-Fock equation. Solution in terms of localized orbitals will be most advantageous when the system has high symmetry with respect to the subgroups, e.g., the symmetry of an ionic crystal with respect to the component ions. In carrying through the solution of Eq. (44) by the minimization of $E_a{}'$, one does not necessarily obtain the best localized orbitals. One may, however, construct the best localized orbitals obtainable from the solutions one finds at different stages of the iterative procedure. One does this by using an equation analogous to Eq. (47), namely,

$$\mathbf{\Phi}^\dagger[\mathbf{H}_a+\mathbf{n}_a(\mathbf{B}-\mathbf{A})]\mathbf{\Phi}\boldsymbol{\tau}_a=(\mathbf{1}+\mathbf{S})\boldsymbol{\tau}_a\boldsymbol{\varepsilon}_a. \tag{48}$$

The matrix $\mathbf{\Phi}\boldsymbol{\tau}_a$ contains the N_a best one-electron functions for atom a that can be constructed from $\mathbf{\Phi}$.

4. A METHOD OF SOLVING FOR LOCALIZED ONE-ELECTRON FUNCTIONS

We have derived an equation for localized one-electron functions and have introduced a definition of the best localized functions. We have outlined an iterative approach for obtaining solutions to the equations, but we have not said how the equations might be solved. Certainly, one can not hope to solve the integro-differential equation given in (44) even when we regard $\mathbf{n}_a$ and $\mathbf{V}_a$ as being independent of $\mathbf{\Phi}_a$. The equation can not be separated in the manner in which the Hartree-Fock equation for an isolated atom can be separated, because the system of several nuclei does not have the symmetry that an isolated atom has. There is one promising path open to us. It is to apply Roothaan's method[12] to the minimization of $E_a{}'$. Since $\mathbf{V}_a$ is not a Hermitian operator, we must slightly modify Roothaan's Eq. (58′) in order to use his method.

We write

$$\mathbf{\Phi}_a=\mathbf{f}_a\mathbf{C}_a, \tag{49}$$

where $\mathbf{f}_a$ is a matrix of $N_a{}'$ functions, $f_{a\mu}(\mathbf{x})$, and $N_a{}'>N_a$. The column index of $\mathbf{f}_a$ is μ and the row index is $\mathbf{x}$. The matrix $\mathbf{f}_a$ has $N_a{}'$ columns. The matrix $\mathbf{C}_a$ has $N_a{}'$ rows and N columns. Only the first N_a columns of $\mathbf{C}_a$ are nonzero. Similarly, one may define matrices $\mathbf{f}_b$, $\mathbf{f}_c$, $\cdots$, and $\mathbf{C}_b$, $\mathbf{C}_c$, $\cdots$, but allowing $\mathbf{C}_b$ to have nonzero elements only in columns N_a+1 to N_a+N_b, $\mathbf{C}_c$ to have nonzero elements only in columns N_a+N_b+1 to $N_a+N_b+N_c$, etc. These definitions force $\mathbf{\Phi}_b=\mathbf{f}_b\mathbf{C}_b$, $\mathbf{\Phi}_c=\mathbf{f}_c\mathbf{C}_c$, $\cdots$, to have the forms specified in the preceding section.

[12] C. C. J. Roothaan, Revs. Modern Phys. **23**, 69 (1951).

We define

$$\mathbf{f}_a^\dagger \mathbf{f}_a = \mathbf{\Delta}_a, \tag{50}$$

and require that

$$\mathbf{C}_a^\dagger \mathbf{\Delta}_a \mathbf{C}_a = \mathbf{1}_a. \tag{51}$$

We restrict ourselves to real functions in $\mathbf{f}_a$ and real numbers in $\mathbf{C}_a$, so that E_a' must be real. In terms of these quantities, Eq. (45) becomes

$$E_a' = [\mathbf{C}_a^\dagger \mathbf{f}_a^\dagger \mathbf{H}_a \mathbf{f}_a \mathbf{C}_a + \tfrac{1}{2}\mathbf{C}_a^\dagger \mathbf{f}_a^\dagger [\mathbf{n}_a(\mathbf{B}-\mathbf{A})]\mathbf{f}_a \mathbf{C}_a + \mathbf{C}_a^\dagger \mathbf{f}_a^\dagger \mathbf{V}_a \mathbf{f}_a \mathbf{C}_a]_{tr}. \tag{52}$$

The Hermitian adjoints of $\mathbf{C}_a$ and $\mathbf{f}_a$ are the transposes of these matrices, since they are real. Because $\mathbf{C}_a$ is real, we can not vary $\mathbf{C}_a$ and $\mathbf{C}_a^\dagger$ independently. Minimization of an expression $I = [\mathbf{c}^\dagger \mathbf{h} \mathbf{c}]_{tr}$ when $\mathbf{c}$ is real leads to

$$\delta I = [\delta \mathbf{c}^\dagger \mathbf{h} \mathbf{c} + \mathbf{c}^\dagger \mathbf{h} \delta \mathbf{c}]_{tr} = [\delta \mathbf{c}^\dagger (\mathbf{h} + \mathbf{h}^\dagger)\mathbf{c}]_{tr}. \tag{53}$$

We have used the theorem that the trace of the transpose of a matrix is equal to the trace of the matrix. If $\mathbf{h}$ is symmetric, $\mathbf{h}$ and $\mathbf{h}^\dagger$ will be identical. In Eq. (52), the only matrix which is not symmetric is

$$\sum_{b \neq a} \mathbf{f}_a^\dagger \mathbf{\Phi}_b \mathbf{E}_{ba}' \mathbf{\Phi}_a^\dagger \mathbf{f}_a. \tag{54}$$

In view of Eq. (53), minimization of E_a' under the supplementary condition of Eq. (51) leads to

$$\mathbf{f}_a^\dagger \mathbf{H}_a \mathbf{f}_a \mathbf{C}_a + \mathbf{f}_a^\dagger [\mathbf{n}_a(\mathbf{B}-\mathbf{A})]\mathbf{f}_a \mathbf{C}_a + \mathbf{f}_a^\dagger \mathbf{V}_a \mathbf{f}_a \mathbf{C}_a - \tfrac{1}{2}\sum_{b \neq a} (\mathbf{f}_a^\dagger \mathbf{\Phi}_a \mathbf{E}_{ba}'^\dagger \mathbf{\Phi}_b^\dagger \mathbf{f}_a - \mathbf{f}_a^\dagger \mathbf{\Phi}_b \mathbf{E}_{ba}' \mathbf{\Phi}_a^\dagger)\mathbf{C}_a = \mathbf{\Delta}_a \mathbf{C}_a \mathbf{\varepsilon}_a'. \tag{55}$$

Since the matrix multiplying $\mathbf{C}_a$ on the right-hand side of Eq. (55) is real and symmetric, we may require that $\mathbf{\varepsilon}_a'$ be diagonal without losing generality. The elements of $\mathbf{\varepsilon}_a'$ are the roots of the secular equation

$$\det\{\mathbf{f}_a^\dagger \mathbf{H}_a \mathbf{f}_a + \mathbf{f}_a^\dagger [\mathbf{n}_a(\mathbf{B}-\mathbf{A})]\mathbf{f}_a + \mathbf{f}_a^\dagger \mathbf{V}_a \mathbf{f}_a - \tfrac{1}{2}\sum_{b \neq a} (\mathbf{f}_a^\dagger \mathbf{\Phi}_a \mathbf{E}_{ba}'^\dagger \mathbf{\Phi}_b^\dagger \mathbf{f}_a - \mathbf{f}_a^\dagger \mathbf{\Phi}_b \mathbf{E}_{ba}' \mathbf{\Phi}_a^\dagger \mathbf{f}_a) - \epsilon \mathbf{\Delta}_a\} = 0. \tag{56}$$

We use det { } to indicate that the determinant of the enclosed matrix has been formed. One chooses as the solutions $\mathbf{C}_a$ minimizing $\mathbf{E}_a'$, those which correspond to the N_a lowest roots of Eq. (56). This choice having been made, we may obtain $\mathbf{E}_{aa}'$ by comparing Eqs. (44) and (55). One obtains in this manner

$$\mathbf{E}_{aa}' = \mathbf{\varepsilon}_a' + \tfrac{1}{2}\sum_{b \neq a} \mathbf{C}_a^\dagger (\mathbf{f}_a^\dagger \mathbf{\Phi}_a \mathbf{E}_{ba}'^\dagger \mathbf{\Phi}_b^\dagger \mathbf{f}_a - \mathbf{f}_a^\dagger \mathbf{\Phi}_b \mathbf{E}_{ba}' \mathbf{\Phi}_a^\dagger \mathbf{f}_a)\mathbf{C}_a. \tag{57}$$

Although $\mathbf{\varepsilon}_a'$ may be diagonal, $\mathbf{E}_{aa}'$ certainly need not be diagonal. Their diagonal elements are the same, however.

5. EXPRESSIONS FOR THE ENERGY

In this section we shall not confine ourselves to energy expressions involving solutions of Eq. (44). Instead we shall derive from the expression for the energy in Eq. (11) an expression which is valid when the one-electron functions are solutions of the Hartree-Fock equations for atoms perturbed by an arbitrary external potential. We shall derive this expression for the energy in the same way that Montet, Keller, and Mayer[9] derived their expression for the energy. The approximate wave function of the system that we use resembles that of the Heitler-London approximation. The difference is that we use atomic one-electron functions perturbed by external potentials, whereas the Heitler-London method uses the one-electron functions of the isolated atoms. By choosing the external potentials properly, one should obtain an improvement over the Heitler-London approximation.

There is a good reason for constructing an expression for the total energy of a system in the manner described, instead of deriving a formula valid only for the self-consistent solutions of Eq. (44). To solve Eq. (44) and the corresponding equations for the other atoms, one goes through a long iteration procedure until self-consistent solutions of the equations are obtained. This may not always be practical. But if we derive an expression for the energy of a system when the atomic functions are solutions of a Hartree-Fock equation for atoms perturbed by an arbitrary external potential, then we will have a formula which is valid even when we have not carried the solution of Eq. (44) to self-consistency. The solutions obtained at any point during the iteration calculation may be regarded as solutions of Hartree-Fock equations for atoms in external fields. In these cases, the perturbing potentials will be the $\mathbf{V}_a$'s formed from the $\mathbf{\Phi}_a$'s of the preceding approximation.

The Hartree-Fock equation for atom a in an external potential $\mathbf{P}_a$ is

$$\mathbf{H}_a \mathbf{\Phi}_a + \mathbf{n}_a(\mathbf{B}-\mathbf{A})\mathbf{\Phi}_a + \mathbf{P}_a \mathbf{\Phi}_a = \mathbf{\Phi}_a \mathbf{E}_a''. \tag{58}$$

Equations of the same form can be written for the other atoms. The $\mathbf{E}_a''$'s are allowed to have nonzero elements only in the rows and columns in which the $\mathbf{E}_{aa}''$'s could have nonzero elements. The $\mathbf{\Phi}_a$'s of this section are similarly allowed to have nonzero elements only in the same columns in which the $\mathbf{\Phi}_a$'s, which were solutions of Eq. (44), could have nonzero elements. We require that $\mathbf{\Phi}_a^\dagger \mathbf{\Phi}_a = \mathbf{1}_a$. We define

$$E_a'' = [\mathbf{H}_a \mathbf{n}_a + \tfrac{1}{2}\mathbf{n}_a(\mathbf{B}-\mathbf{A})\mathbf{n}_a + \mathbf{P}_a \mathbf{n}_a]_{tr}. \tag{59}$$

We define the self-energy of atom a, E_a, by Eq. (46), but with the $\mathbf{\Phi}_a$ from Eq. (58) replacing the $\mathbf{\Phi}_a$ from Eq. (44). From Eq. (59) and the definition of E_a we find

$$E_a'' = E_a + [\mathbf{P}_a \mathbf{n}_a]_{tr}. \tag{60}$$

We define a new matrix,

$$\mathfrak{d}_a = -\mathbf{\Phi}_a(\mathbf{1}+\mathbf{S})^{-1}\mathbf{S}\mathbf{\Phi}^\dagger. \tag{61}$$

Using Eqs. (14′), (31), (33′), (36), and (38) one finds that $\mathfrak{d}_a$ has the property

$$\begin{aligned}\sum_a \mathfrak{d}_a &= -\sum_a \mathbf{\Phi}_a(\mathbf{1}+\mathbf{S})^{-1}\mathbf{S}\mathbf{\Phi}^\dagger = -\mathbf{\Phi}(\mathbf{1}+\mathbf{S})^{-1}\mathbf{S}\mathbf{\Phi}^\dagger \\ &= \mathfrak{o} - \mathbf{\Phi}\mathbf{\Phi}^\dagger = \mathfrak{o} - \sum_a\sum_b \mathbf{\Phi}\mathbf{1}_a\mathbf{1}_b\mathbf{\Phi}^\dagger \\ &= \mathfrak{o} - \sum_a \mathbf{\Phi}_a\mathbf{\Phi}_a{}^\dagger = \mathfrak{o} - \sum_a \mathfrak{n}_a \\ &= \mathfrak{d}. \end{aligned} \tag{62}$$

We set

$$\sum_a \mathfrak{n}_a = \mathbf{\Phi}\mathbf{\Phi}^\dagger = \mathfrak{n}. \tag{63}$$

In order to express E in terms of the atomic functions, we perform almost the same manipulations that Montet, Keller, and Mayer performed.[9] In terms of $\mathfrak{n}$ and $\mathfrak{d}$,

$$E = [\mathbf{H}\mathfrak{n} + \tfrac{1}{2}\mathfrak{n}(\mathbf{B}-\mathbf{A})\mathfrak{n}]_{tr} + [\mathbf{H}\mathfrak{d} + \mathfrak{n}(\mathbf{B}-\mathbf{A})\mathfrak{d}]_{tr} + \tfrac{1}{2}[\mathfrak{d}(\mathbf{B}-\mathbf{A})\mathfrak{d}]_{tr}.$$

We substitute from Eqs. (1′), (8), (40), and (41),

$$\begin{aligned}E = &\sum_a [\mathbf{H}_a\mathfrak{n}_a + \tfrac{1}{2}\mathfrak{n}_a(\mathbf{B}-\mathbf{A})\mathfrak{n}_a]_{tr} \\ &+ \tfrac{1}{2}\sum_{a\neq b}\sum [-(Z_b/\mathbf{R}_b)\mathfrak{n}_a - (Z_a/\mathbf{R}_a)\mathfrak{n}_b + \mathfrak{n}_a(\mathbf{B}-\mathbf{A})\mathfrak{n}_b]_{tr} \\ &+ [\mathbf{H}\mathfrak{d} + \mathfrak{n}(\mathbf{B}-\mathbf{A})\mathfrak{d}]_{tr} + \tfrac{1}{2}[\mathfrak{d}(\mathbf{B}-\mathbf{A})\mathfrak{d}]_{tr} \end{aligned} \tag{64}$$

which is exactly the Montet, Keller, and Mayer expression, except that the $\mathfrak{n}_a$'s are now the density matrices of the atoms in the perturbing potentials, the $\mathbf{P}_a$'s. The first sum is the sum of the self-energies of the atoms, while the second sum is the Coulombic energy due to the interaction of the electronic charge densities of the others, plus an electronic exchange energy. The total energy of the system is

$$E_t = E + \tfrac{1}{2}\sum_{a\neq b}\sum \frac{Z_aZ_b}{R_{ab}}, \tag{65}$$

where R_{ab} is the distance between the a and b nuclei. If we define

$$\begin{aligned}Q_{ab} = &(Z_aZ_b/R_{ab}) \\ &+ [-(Z_b/\mathbf{R}_b)\mathfrak{n}_a - (Z_a/\mathbf{R}_a)\mathfrak{n}_b + \mathfrak{n}_a(\mathbf{B}-\mathbf{A})\mathfrak{n}_b]_{tr}, \end{aligned} \tag{66}$$

then

$$\begin{aligned}E_t = &\sum_a E_a + \tfrac{1}{2}\sum_{a\neq b}\sum Q_{ab} \\ &+ [\mathbf{H}\mathfrak{d} + \mathfrak{n}(\mathbf{B}-\mathbf{A})\mathfrak{d}]_{tr} + \tfrac{1}{2}[\mathfrak{d}(\mathbf{B}-\mathbf{A})\mathfrak{d}]_{tr}. \end{aligned} \tag{67}$$

We substitute from Eqs. (62) and (63) into

$$I = [\mathbf{H}\mathfrak{d} + \mathfrak{n}(\mathbf{B}-\mathbf{A})\mathfrak{d}]_{tr} \tag{68}$$

to obtain

$$I = \sum_a [\mathbf{H}\mathfrak{d}_a + \mathfrak{n}_a(\mathbf{B}-\mathbf{A})\mathfrak{d}_a]_{tr} + \sum_{a\neq b}\sum [\mathfrak{n}_b(\mathbf{B}-\mathbf{A})\mathfrak{d}_a]_{tr}. \tag{69}$$

We replace $\mathbf{H}$ by $\mathbf{H}_a - \sum_{b\neq a}(Z_b/\mathbf{R}_b)$.

$$\begin{aligned}I = &\sum_a [\mathbf{H}_a\mathfrak{d}_a + \mathfrak{n}_a(\mathbf{B}-\mathbf{A})\mathfrak{d}_a]_{tr} \\ &+ \sum_{a\neq b}\sum [-(Z_b/\mathbf{R}_b)\mathfrak{d}_a + \mathfrak{n}_b(\mathbf{B}-\mathbf{A})\mathfrak{d}_a]_{tr}. \end{aligned} \tag{70}$$

We shall later show that

$$J_a = [\mathbf{H}_a\mathfrak{d}_a + \mathfrak{n}_a(\mathbf{B}-\mathbf{A})\mathfrak{d}_a + \mathbf{P}_a\mathfrak{d}_a]_{tr} \tag{71}$$

is zero. Substituting $J_a = 0$ into I, we obtain

$$\begin{aligned}I = &-\sum_a [\mathbf{P}_a\mathfrak{d}_a]_{tr} \\ &+ \sum_{a\neq b}\sum [-(Z_b/\mathbf{R}_b)\mathfrak{d}_a + \mathfrak{n}_b(\mathbf{B}-\mathbf{A})\mathfrak{d}_a]_{tr}. \end{aligned} \tag{72}$$

We substitute this into the expression for E_t.

$$\begin{aligned}E_t = &\sum_a E_a + \tfrac{1}{2}\sum_{a\neq b}\sum Q_{ab} + \tfrac{1}{2}[\mathfrak{d}(\mathbf{B}-\mathbf{A})\mathfrak{d}]_{tr} \\ &+ \sum_a [-\mathbf{P}_a\mathfrak{d}_a + \sum_{b\neq a}(-(Z_b/\mathbf{R}_b) + \mathfrak{n}_b(\mathbf{B}-\mathbf{A}))\mathfrak{d}_a]_{tr}. \end{aligned} \tag{73}$$

This is the expression we wished to derive.

To show that J_a is zero, we substitute Eq. (61) into Eq. (71).

$$J_a = -[(\mathbf{H}_a + \mathfrak{n}_a(\mathbf{B}-\mathbf{A}) + \mathbf{P}_a)\mathbf{\Phi}_a(\mathbf{1}+\mathbf{S})^{-1}\mathbf{S}\mathbf{\Phi}^\dagger]_{tr}.$$

Due to Eq. (58) we may rewrite this equation as

$$J_a = -[\mathbf{\Phi}_a\mathbf{E}_a''(\mathbf{1}+\mathbf{S})^{-1}\mathbf{S}\mathbf{\Phi}^\dagger]_{tr}.$$

With the definition of Eqs. (13) and (33′), and using the relation (7), we go through the following steps.

$$\begin{aligned}J_a &= -[\mathbf{1}_a\mathbf{E}_a''(\mathbf{1}+\mathbf{S})^{-1}\mathbf{S}\mathbf{\Phi}^\dagger\mathbf{\Phi}]_{tr} \\ &= -[\mathbf{1}_a\mathbf{E}_a''\mathbf{S}]_{tr} \\ &= -[\mathbf{E}_a''\mathbf{1}_a\mathbf{S}\mathbf{1}_a]_{tr} = 0. \end{aligned} \tag{74}$$

The last step is a consequence of

$$\mathbf{1}_a\mathbf{S}\mathbf{1}_a = \mathbf{1}_a(\mathbf{\Phi}^\dagger\mathbf{\Phi} - \mathbf{1})\mathbf{1}_a = \mathbf{\Phi}_a{}^\dagger\mathbf{\Phi}_a - \mathbf{1}_a = 0.$$

Before we discuss the nature of the $\mathbf{P}_a$'s in Eq. (73), we shall discuss the relative magnitudes of some of the quantities appearing in E_t. If $E_a{}^\circ$ is the Hartree-Fock energy of the isolated, unperturbed atom a, then

$$E_a - E_a{}^\circ \geq 0, \tag{75}$$

since the unperturbed Hartree-Fock functions for atom a are obtained by minimizing E_a. From Eqs. (60) and (75) one obtains

$$E_a'' - E_a{}^\circ \geq [\mathbf{P}_a\mathfrak{n}_a]_{tr}. \tag{76}$$

If γ_a is the Hartree-Fock density matrix of atom a when the atom is unperturbed by external potentials,

then

$$E_a''\leq[\mathbf{H}_a\boldsymbol{\gamma}_a+\tfrac{1}{2}\boldsymbol{\gamma}_a(\mathbf{B}-\mathbf{A})\,\boldsymbol{\gamma}_a+\mathbf{P}_a\boldsymbol{\gamma}_a]_{tr}$$

$$E_a''\leq E_a^\circ+[\mathbf{P}_a\boldsymbol{\gamma}_a]_{tr}$$

$$E_a''-E_a^\circ\leq[\mathbf{P}_a\boldsymbol{\gamma}_a]_{tr}. \tag{77}$$

Equations (76) and (77) serve to bracket $E_a''-E_a^\circ$. From these two equations and Eq. (60), one can show that

$$[\mathbf{P}_a(\boldsymbol{\gamma}_a-\boldsymbol{\eta}_a)]_{tr}\geq E_a-E_a^\circ\geq 0. \tag{78}$$

The binding energy of a system, which is the energy E_t minus that of the isolated atoms, is

$$\Delta E=E_t-\sum_a E_a^\circ$$

$$=\sum_a(E_a-E_a^\circ)+\tfrac{1}{2}\sum_{a\neq b}\sum Q_{ab}+\tfrac{1}{2}[\boldsymbol{\sigma}(\mathbf{B}-\mathbf{A})\,\boldsymbol{\sigma}]_{tr}$$

$$+\sum_a[-\mathbf{P}_a\boldsymbol{\sigma}_a+\sum_{b\neq a}(-(Z_b/\mathbf{R}_b)+\boldsymbol{\eta}_b(\mathbf{B}-\mathbf{A}))\boldsymbol{\sigma}_a]_{tr}. \tag{79}$$

In the Heitler-London approximation one uses the one-electron functions of the unperturbed atoms to calculate the binding energy. Montet, Keller, and Mayer did this using a notation nearly identical to the one used here, and obtained an expression equivalent to

$$\Delta E^\circ=\tfrac{1}{2}\sum_{a\neq b}\sum Q_{ab}^\circ+\tfrac{1}{2}[\boldsymbol{\sigma}^\circ(\mathbf{B}-\mathbf{A})\,\boldsymbol{\sigma}^\circ]_{tr}$$

$$+\sum_{a\neq b}\sum[-(Z_b/\mathbf{R}_b)\,\boldsymbol{\sigma}_a^\circ+\boldsymbol{\gamma}_b(\mathbf{B}-\mathbf{A})\,\boldsymbol{\sigma}_a^\circ]_{tr}. \tag{80}$$

This expression may be obtained from Eq. (79) by setting $\mathbf{P}_a=\mathbf{P}_b=\cdots=0$ and using the one-electron functions of the unperturbed atoms. We want to choose the $\mathbf{P}_a$'s so that $\Delta E<\Delta E^\circ$. If the $\mathbf{P}_a$'s are the $\mathbf{V}_a$'s, and if the iterative calculations are carried through until we obtain the self-consistent solutions of Eq. (44) for each atom, then ΔE will be smaller than ΔE°, since the localized Hartree-Fock one-electron functions of the system minimize E. When the self-consistent solutions of Eq. (44) for each atom are substituted into Eq. (79), we obtain

$$\Delta E=\sum_a(E_a-E_a^\circ)+\tfrac{1}{2}\sum_{a\neq b}\sum Q_{ab}-\tfrac{1}{2}[\boldsymbol{\sigma}(\mathbf{B}-\mathbf{A})\,\boldsymbol{\sigma}]_{tr}$$

$$+\sum_{a\neq b}\sum[\boldsymbol{\Phi}_b\mathbf{E}_{ba}'\boldsymbol{\Phi}_a^\dagger\boldsymbol{\sigma}_a]_{tr}. \tag{81}$$

We can simplify the last sum.

$$\sum_{a\neq b}\sum[\boldsymbol{\Phi}_b\mathbf{E}_{ba}'\boldsymbol{\Phi}_a^\dagger\boldsymbol{\sigma}_a]_{tr}$$

$$=-\sum_{a\neq b}\sum[\boldsymbol{\Phi}_b\mathbf{E}_{ba}'(\mathbf{1}+\mathbf{S})^{-1}\mathbf{S}\boldsymbol{\Phi}^\dagger]_{tr}$$

$$=-\sum_{a\neq b}\sum[\mathbf{E}_{ba}'\mathbf{S}_{ab}]_{tr}=-[\mathbf{E}'\mathbf{S}]_{tr}.$$

The binding energy found from Eq. (81) is the lowest value that can be obtained using a single determinant of one-electron functions to approximate the wave function.

We consider the case in which we have not obtained the self-consistent solutions of Eq. (44) for each atom. In this case

$$\mathbf{P}_a=\mathbf{V}_a^{\mathrm{A}}=\boldsymbol{\sigma}^{\mathrm{A}}(\mathbf{B}-\mathbf{A})$$

$$+\sum_{b\neq a}[-(Z_b/\mathbf{R}_b)+\boldsymbol{\eta}_b^{\mathrm{A}}(\mathbf{B}-\mathbf{A})-\boldsymbol{\Phi}_b^{\mathrm{A}}\mathbf{E}_{ba}^{\mathrm{A}'}\boldsymbol{\Phi}_a^{\mathrm{A}\dagger}], \tag{82}$$

where the $\boldsymbol{\Phi}_a^{\mathrm{A}}$'s are approximations to the self-consistent $\boldsymbol{\Phi}_a$'s and $\boldsymbol{\sigma}^{\mathrm{A}}$, $\mathbf{E}^{\mathrm{A}'}$ and the $\boldsymbol{\eta}_a^{\mathrm{A}}$'s are constructed by using the $\boldsymbol{\Phi}_a^{\mathrm{A}}$'s in place of the self-consistent $\boldsymbol{\Phi}_a$'s in the definitions of $\boldsymbol{\sigma}$, $\mathbf{E}'$, and the $\boldsymbol{\eta}_a$'s. When $\mathbf{P}_a$ is given by Eq. (82), the binding energy is given by

$$\Delta E=\sum_a(E_a-E_a^\circ)+\tfrac{1}{2}\sum_{a\neq b}\sum Q_{ab}$$

$$-[(\boldsymbol{\sigma}^{\mathrm{A}}-\tfrac{1}{2}\boldsymbol{\sigma})\,(\mathbf{B}-\mathbf{A})\,\boldsymbol{\sigma}]_{tr}$$

$$+\sum_{a\neq b}\sum[(\boldsymbol{\eta}_b-\boldsymbol{\eta}_b^{\mathrm{A}})\,(\mathbf{B}-\mathbf{A})\,\boldsymbol{\sigma}_a+\boldsymbol{\Phi}_b^{\mathrm{A}}\mathbf{E}_{ba}^{\mathrm{A}'}\boldsymbol{\Phi}_a^{\mathrm{A}\dagger}\boldsymbol{\sigma}_a]_{tr}. \tag{83}$$

For completely arbitrary functions, $\boldsymbol{\Phi}_a^{\mathrm{A}}$, it is not necessarily true that this ΔE is smaller than $\Delta E'$. However, if the approximate functions, $\boldsymbol{\Phi}_a^{\mathrm{A}}$, are reasonably close approximations to the exact solutions, $\boldsymbol{\Phi}_a$, then one would expect the ΔE of Eq. (83) to be smaller than ΔE°.

Although we know that the ΔE of Eq. (81) is less than ΔE°, we cannot show and we do not know that $\Delta E<\Delta E^\circ$ when we choose $\mathbf{P}_a$'s which are not the $\mathbf{V}_a$'s. This is the case in Eq. (83). We can, however, say something concerning the sign of $\Delta E-\Delta E^\circ$ for some choices of the $\mathbf{P}_a$'s, if we restrict ourselves to a very simple system. From Eq. (79) we subtract Eq. (80).

$$\Delta E-\Delta E^\circ=\sum_a(E_a-E_a^\circ)+\tfrac{1}{2}\sum_{a\neq b}\sum(Q_{ab}-Q_{ab}^\circ)$$

$$+\tfrac{1}{2}[\boldsymbol{\sigma}(\mathbf{B}-\mathbf{A})\,\boldsymbol{\sigma}-\boldsymbol{\sigma}^\circ(\mathbf{B}-\mathbf{A})\,\boldsymbol{\sigma}^\circ]_{tr}$$

$$+\sum_a[-\mathbf{P}_a\boldsymbol{\sigma}_a+\sum_{b\neq a}(-(Z_b/\mathbf{R}_b)+\boldsymbol{\eta}_b(\mathbf{B}-\mathbf{A}))\,\boldsymbol{\sigma}_a]_{tr}$$

$$-\sum_{a\neq b}\sum[-(Z_b/\mathbf{R}_b)\,\boldsymbol{\sigma}_a^\circ+\boldsymbol{\gamma}_b(\mathbf{B}-\mathbf{A})\,\boldsymbol{\sigma}_a^\circ]_{tr}.$$

Into this expression we introduce the inequality of (78).

$$\Delta E-\Delta E^\circ\leq\sum_a[\mathbf{P}_a(\boldsymbol{\gamma}_a-\boldsymbol{\eta}_a)]_{tr}+\tfrac{1}{2}\sum_{a\neq b}\sum(Q_{ab}-Q_{ab}^\circ)$$

$$+\tfrac{1}{2}[\boldsymbol{\sigma}(\mathbf{B}-\mathbf{A})\,\boldsymbol{\sigma}-\boldsymbol{\sigma}^\circ(\mathbf{B}-\mathbf{A})\,\boldsymbol{\sigma}^\circ]_{tr}$$

$$+\sum_a\left[-\mathbf{P}_a\boldsymbol{\sigma}_a+\sum_{b\neq a}\left(-\frac{Z_b}{\mathbf{R}_b}+\boldsymbol{\eta}_b(\mathbf{B}-\mathbf{A})\right)\boldsymbol{\sigma}_a\right]_{tr}$$

$$-\sum_{a\neq b}\sum[-(Z_b/\mathbf{R}_b)\,\boldsymbol{\sigma}_a^\circ+\boldsymbol{\gamma}_b(\mathbf{B}-\mathbf{A})\,\boldsymbol{\sigma}_a^\circ]_{tr}. \tag{84}$$

If we can choose the $\mathbf{P}_a$'s so that the expression on the right in Eq. (84) is negative, then $\Delta E-\Delta E^\circ$ must be

negative. We shall consider the two simplest choices, namely

$$\mathbf{P}_a^{(1)}=\sum_{b\neq a}[-(Z_b/\mathbf{R}_b)+\boldsymbol{\gamma}_b(\mathbf{B}-\mathbf{A})]$$

and

$$\mathbf{P}_a^{(2)}=\sum_{b\neq a}[-(Z_b/\mathbf{R}_b)+\mathbf{n}_b(\mathbf{B}-\mathbf{A})].$$

Substitution of $\mathbf{P}_a^{(1)}$ into Eq. (84) gives

$$\begin{aligned}\Delta E^{(1)}-\Delta E^{\circ}\lesssim&\tfrac{1}{2}\sum_{a\neq b}\sum[(\mathbf{n}_a-\boldsymbol{\gamma}_a)(\mathbf{B}-\mathbf{A})(\mathbf{n}_b-\boldsymbol{\gamma}_b)]_{tr}\\&+\tfrac{1}{2}[\boldsymbol{\delta}(\mathbf{B}-\mathbf{A})\boldsymbol{\delta}-\boldsymbol{\delta}^{\circ}(\mathbf{B}-\mathbf{A})\boldsymbol{\delta}^{\circ}]_{tr}\\&+\sum_{a\neq b}\sum[(\mathbf{n}_b-\boldsymbol{\gamma}_b)(\mathbf{B}-\mathbf{A})\boldsymbol{\delta}_a]_{tr}\\&-\sum_{a\neq b}\sum[-(Z_b/\mathbf{R}_b)\boldsymbol{\delta}_a^{\circ}+\boldsymbol{\gamma}_b(\mathbf{B}-\mathbf{A})\boldsymbol{\delta}_a^{\circ}]_{tr},\end{aligned}$$

when we introduce the definitions of Q_{ab} and Q_{ab}°. If the internuclear distances are large so that the overlap integrals are approximately zero, we can omit any term involving $\boldsymbol{\delta}_a$'s, so that

$$\Delta E^{(1)}-\Delta E^{\circ}\lesssim\tfrac{1}{2}\sum_{a\neq b}\sum[(\mathbf{n}_a-\boldsymbol{\gamma}_a)\mathbf{B}(\mathbf{n}_b-\boldsymbol{\gamma}_b)]_{tr}.$$

Since $[\mathbf{n}_a-\boldsymbol{\gamma}_a]_{tr}=0$, at large internuclear distances the leading term in the expansion of $[(\mathbf{n}_a-\boldsymbol{\gamma}_a)\mathbf{B}(\mathbf{n}_b-\boldsymbol{\gamma}_b)]_{tr}$ in terms of $(R_{ab})^{-1}$ must be a dipole-dipole interaction. If we define the dipole moment of the charge distribution to be

$$\mathbf{d}_a=-\int\mathbf{r}[\eta_a(\mathbf{x}\mid\mathbf{x})-\gamma_a(\mathbf{x}\mid\mathbf{x})]d\mathbf{x},$$

then

$$\Delta E^{(1)}-\Delta E^{\circ}\lesssim\tfrac{1}{2}\sum_{a\neq b}\sum\left[\frac{\mathbf{d}_a\cdot\mathbf{d}_b}{R_{ab}^3}-\frac{3(\mathbf{d}_a\cdot\mathbf{R}_{ab})(\mathbf{d}_b\cdot\mathbf{R}_{ab})}{R_{ab}^5}\right].$$

For two oppositely charged, closed shell ions, a and b, $\mathbf{d}_a$ and $\mathbf{d}_b$ are parallel and directed along the internuclear axis, since the dipole of ion a is induced by the electric field of ion b, and the dipole of b, by a. In this case we find

$$\Delta E^{(1)}-\Delta E^{\circ}\lesssim-\frac{2\mid\mathbf{d}_a\mid\mid\mathbf{d}_b\mid}{R_{ab}^3}<0,$$

i.e., $\Delta E^{(1)}$ will be less than ΔE°. On the other hand, if we had substituted $\mathbf{P}_a^{(2)}$ instead of $\mathbf{P}_a^{(1)}$ into Eq. (84), and then considered the case of two oppositely charged, closed shell ions whose nuclei were far apart, we would have found

$$\begin{aligned}\Delta E^{(2)}-\Delta E^{\circ}&\lesssim-[(\mathbf{n}_a-\boldsymbol{\gamma}_a)\mathbf{B}(\mathbf{n}_b-\boldsymbol{\gamma}_b)]_{tr}\\&\lesssim(2\mid\mathbf{d}_a\mid\mid\mathbf{d}_b\mid/R_{ab}^3)>0.\end{aligned}$$

The sign of $\Delta E^{(2)}-\Delta E^{\circ}$ is not determined by this inequality. The same inequality results if we substitute $\mathbf{V}_a$ into Eq. (84) and consider the case of two oppositely charged, and greatly separated, closed shell ions. In other words, in the case in which we know that $\Delta E\leq\Delta E^{\circ}$, we can not show that it is true by using Eq. (78) and considering a very simple system. On the other hand, if we use the $\mathbf{P}_a$ of Eq. (82) with $\boldsymbol{\Phi}^{\mathrm{A}}=\boldsymbol{\Phi}^{\circ}$, we obtain for the simple system we have been considering, the same inequality that we found for $\Delta E^{(1)}-\Delta E^{\circ}$, so that ΔE will be less than ΔE°.

Looking at Eqs. (78), (80), and (83), one sees that ΔE can be divided into two parts. One part is $\sum_a(E_a-E_a^{\circ})$, which is always positive. The other part, the interaction energy, must be negative and larger in absolute magnitude than $\sum_a(E_a-E_a^{\circ})$, if ΔE is to be negative. Thus one may regard binding as arising from the minimization of ΔE by the balancing of two opposite effects: the increase in the self-energies and the decrease in the interaction energy, arising from the changes in the atomic electron densities.

The equations we have written for ΔE are valid for a system of closed shell ions and for any case in which we do not require the wave function of the system to be an eigenfunction of the total spin. In addition to the formulas for E and ΔE which we have derived, one may also write down expressions of the usual form for E, namely,

$$E=[\mathbf{E}']_{tr}-\tfrac{1}{2}[\boldsymbol{\varrho}(\mathbf{B}-\mathbf{A})\boldsymbol{\varrho}]_{tr},\tag{85}$$

and

$$E=\tfrac{1}{2}[\mathbf{H}\boldsymbol{\varrho}]_{tr}+\tfrac{1}{2}[\mathbf{E}']_{tr}.\tag{85'}$$

These expressions are derived by substituting Eq. (21) into Eq. (11).

6. A SYSTEM OF CLOSED SHELL IONS

Up to this point we have not imposed the requirement that the wave function be an eigenfunction of the total spin of the electrons. In this section we treat the simplest possible case, namely, that in which the total spin of the system is zero and the total spin of each subsystem is zero. A physical example is a system of closed shell ions, such as an ionic crystal or an ionic molecule. We shall place emphasis on the former in what follows.

The easiest way to construct a single determinant wave function having total spin zero is to require that each orbital be doubly occupied. In that case we have

$$\Psi=(\psi_1(\mathbf{x})\psi_2(\mathbf{x})\psi_3(\mathbf{x})\cdots\psi_N(\mathbf{x})),\tag{86}$$

where

$$\left.\begin{aligned}\psi_{2n+1}&=\alpha(s)u_{n+1}(\mathbf{r}),\quad n=0,1,2,\cdots,\tfrac{1}{2}N-1;\\\psi_{2n}&=\beta(s)u_n(\mathbf{r}),\quad n=1,2,\cdots,\tfrac{1}{2}N,\end{aligned}\right\}\tag{87}$$

the functions $\alpha(s)$ and $\beta(s)$ being respectively the spin-up and spin-down eigenfunctions. The matrix $\mathbf{E}$ is diagonal, E_μ being the μth diagonal element, and $E_\mu=E_{\mu+1}$ when μ is odd. We require that $\boldsymbol{\Phi}$ be constructed of doubly occupied orbitals, too. This is auto-

matically true if $\mathbf{T}$ has elements $T_{\mu\nu}$, such that

$$\left.\begin{aligned} T_{\mu\nu}&=0, \qquad \text{if } \mu+\nu=\text{odd integer;}\\ T_{\mu\nu}&=T_{\mu+1,\nu+1}, \quad \text{if } \mu \text{ and } \nu \text{ are both odd.}\end{aligned}\right\} \tag{88}$$

Under these circumstances $\mathbf{T}^{-1}$ and $\mathbf{E}'$ will have the same form; i.e., $(\mathbf{T}^{-1})_{\mu\nu}$ and $(\mathbf{E}')_{\mu\nu}$ are zero if $\mu+\nu=$an odd integer, and $(\mathbf{T}^{-1})_{\mu\nu}=(\mathbf{T}^{-1})_{\mu+1,\nu+1}$ and $(\mathbf{E}')_{\mu\nu}=$ $=(\mathbf{E}')_{\mu+1,\nu+1}$ whenever μ and ν are both odd. This is proven in the Appendix.

In Sec. 4 we indicated that one might solve the equations for localized orbitals in the same way that one solves the standard equation. We shall discuss this in some detail for a crystal composed of two different closed shell ions, one positive and one negative. To be more accurate, we should say that we shall interpret the system in terms of closed shell ions. In line with this interpretation, one might choose as the zeroth approximation to the localized orbitals of the positive and negative ions, the Hartree-Fock orbitals of the isolated ions. One defines the zeroth approximation to $\mathbf{V}_a$, to $\mathbf{V}_b$, $\cdots$, by substituting the $\mathbf{\Phi}_a{}^0$'s for the $\mathbf{\Phi}_a$'s into the defining equation, namely, Eq. (43). One needs to solve for new localized orbitals for only one positive ion and one negative ion, since in the crystal all the positive ions are the same and all of the negative ions are the same. With the new set of localized orbitals one may calculate a new approximation to each $\mathbf{V}_a$ and solve for another set of localized orbitals. One continues this iterative procedure until the orbitals used to define the $\mathbf{V}_a$'s are the same as the orbitals one obtains as solutions; i.e., the calculation is carried to self-consistency. The Hartree-Fock energy of the system can then be evaluated.

One might choose as the starting orbitals in a calculation on an ionic crystal, as we have already said, the Hartree-Fock orbitals of the isolated ions. In view of the excellent cohesive energies calculated by Löwdin[3] for ionic crystals using the Heitler-London method and the Hartree-Fock orbitals of the isolated ions, it may reasonably be hoped that the ions will not be greatly perturbed by their neighbors. In this case one may choose as the functions making up each $\mathbf{f}_a$, the ground-state orbitals of the isolated ion a and other functions, centered on the nucleus a, to allow for the perturbations. If the perturbations are "large," then one may have to use functions centered on the nuclei of neighboring ions as well. Expansion of the localized orbitals of an ion in terms of functions centered at that ion's nucleus should force the orbitals to be localized. Expanding in terms of functions on several centers, one may have to localize the orbitals at various times during the calculation. The expansion of the orbitals on the centers of the ions they belong to, leads to an interpretation in terms of polarized ions. This is, as we have said, the interpretation of the classical theory of ionic crystals.

7. DISCUSSION

With respect to the method we have proposed for solving the Hartree-Fock equation for a large system in terms of localized orbitals, one can ask if one obtains the standard Hartree-Fock ground state. If the Hartree-Fock equation were a sufficient condition for obtaining an energy minimum, then there would be no question. Unfortunately, as we pointed out in the second section, the Hartree-Fock equation is apparently only a necessary condition. There are two things one can do. One can choose the localized orbitals in the same manner that one chooses the standard orbitals, i.e., pick those which give the smallest diagonal elements of $\mathbf{E}'$ and satisfy the equations for the localized orbitals. Alternatively, one could apply McWeeny's method[10] to the minimization of E.

Assuming that by solving our equations with the proper precautions, one can get the standard Hartree-Fock ground state, one must then ask how hard it is to apply. For diatomic molecules there is no apparent advantage in solving directly in terms of localized orbitals, with the exception, perhaps, of ionic molecules. There is a great advantage in using the method in calculations on crystals. Due to the high symmetry of a crystal, one needs localized orbitals only for the various kinds of atoms in the crystal. For example, in the NaF crystal one needs ten orbitals, five for Na^+ and five for F^-. This seems to be a great advantage. The question is whether these advantages outweigh the disadvantages inherent in doing repeated evaluations of $\mathbf{E}'$ and similar matrices. If one is doing the computations with the aid of a computer, then the advantages must outweigh the disadvantages. The Roothaan matrix method,[12] for example, has been programed for computers by a number of groups. Thus one step in the computations can be made automatic. Certainly the computational effort would be worth while in a few cases so that we would have available Hartree-Fock energies and density matrices for some crystals.

If we knew the Hartree-Fock energies and density matrices for several ionic crystals, we could answer a number of questions. We would be able to see how well the sum of the correlation energies of the isolated ions cancel the correlation energy of an ionic crystal when one calculates the cohesive energy of that crystal. We would also be able to compare the resulting electron densities with those that are being obtained experimentally. The Hartree-Fock electron density could also be compared with the electron density obtained from the equations of Montet, Keller, and Mayer,[9] but the most important thing we could do is compare the polarization and van der Waals' contributions to the cohesive energy of an ionic crystal in the classical theory of ionic crystals, with the corrections calculated directly from the Hartree-Fock density matrices of the perturbed ions, i.e., the density matrices constructed from the "best" localized orbitals. This would test the validity of the classical picture of ionic crystals.

Up to this point we have emphasized the usefulness of localized orbitals in obtaining solutions to the Hartree-Fock equation for systems of closed shell ions and in interpreting the Hartree-Fock functions for such systems. We have not discussed "covalent" systems because of the difficulties one encounters in satisfying the requirement that the wave function of the system be an eigenfunction of the total spin. The difficulties arise when one seeks the appropriate equations for solving directly in terms of localized orbitals. We do not wish to discuss these difficulties here. Instead, let us suppose that we have already solved the Hartree-Fock equation of the molecule for the standard orbitals. We may define the "best" localized orbitals for each atom by forming linear combinations of the standard orbitals. In this case there is no problem with the spin because the transformation from the standard orbitals to the localized orbitals can alter the normalized, single determinant wave function by at most a phase factor. Analyzing the standard Hartree-Fock orbitals of a molecule in this manner, may be useful.

If one has solved the Hartree-Fock equation for a molecule for the standard orbitals, the molecular orbitals, one may calculate the binding energy of that molecule, its dipole moment, and whatever else one might want to know about the ground state. One can not, however, use the molecular orbitals from a simpler molecule to approximate the molecular orbitals of a more complicated molecule of the same "type." For example, if we have solved for the Hartree-Fock molecular orbitals of $CH_3CH_2CH_3$, we can not use these orbitals directly to learn anything about $CH_3CH_2CH_2CH_3$. However, the chemist has been very successful in interpreting the properties of molecules in terms of the atoms of which they are composed. In view of this, we suggest[13] that the "best" localized orbitals obtained from the molecular orbitals of a simple molecule might make good approximations to the localized orbitals of a more complicated molecule of the same type. As an example, we again consider $CH_3CH_2CH_3$ and $CH_3CH_2CH_2CH_3$. From the molecular orbitals of the former, one can construct the "best" localized orbitals of the H's of the CH_3 and CH_2 groups, and for the C's of the CH_3 and CH_2 groups. These "perturbed atomic orbitals" may be then used to form a single determinant wave function for $CH_3CH_2CH_2CH_3$, the orbitals appropriate to the C's of the CH_3 groups of $CH_3CH_2CH_3$ being used for the C's of the CH_3 groups of $CH_3CH_2CH_2CH_3$, and so on. To ensure that the determinantal wave function is an eigenfunction of the spin, one can multiply it by a suitable spin projection operator. Whether this method of using molecular orbital calculations on simple molecules to obtain first approximations to the energies and orbitals of more complicated molecules will work, is independent of whether it is practical to solve directly in terms of localized orbitals.

The analysis of the standard Hartree-Fock orbitals in terms of localized orbitals involves the arbitrary choice of atoms or ions as the subgroups in terms of which one investigates the orbitals of the system. Instead of localizing the orbitals about nuclei, one could localize them about groups of nuclei. In the example of the previous paragraph, one could have formed localized orbitals about the nuclei of CH_3 and CH_2 in $CH_3CH_2CH_3$. These localized orbitals could also have been used as the perturbed atomic orbitals were, to obtain a first approximation to the density matrix and Hartree-Fock energy of $CH_3CH_2CH_2CH_3$.

In Sec. 3 we said that we wanted to interpret the Hartree-Fock wave function for a system as a chemist does, in terms of atoms and ions. We obtained equations describing atoms perturbed by the other members of the system. This gives us two things: 1. a picture of chemical binding as due to the balancing of two competing effects—the lowering of the total energy due to the lowering of the interaction energy as the atoms become more and more distorted, and the increase in the total energy due to the increase in the self-energies of the atoms caused by the distortion of their orbitals; 2. from the Φ_a's one can calculate the electron density in an atom as it is brought closer and closer to the other atoms. Thus the qualitative picture of 1 is supplemented by a quantitative picture of the changes in the "atomic" orbitals.

ACKNOWLEDGMENTS

The author thanks Professor J. E. Mayer for suggesting this problem, for innumerable discussions concerning it, and for his searching criticism of each new effort.

The author also thanks E. I. DuPont de Nemours and Company, and the Shell Company Foundation for the award of predoctoral fellowships for the academic years 1957–1958 and 1958–59, respectively.

APPENDIX

We use the summation convention in this Appendix, i.e., we sum over repeated indices. The determinant formed from the matrix $\mathbf{D}$ is written as $|\mathbf{D}|$. We define a quantity $\epsilon(i_1 i_2 \cdots i_n)$, where the i_α's take on the values $1, 2, 3, \cdots n$.

$\epsilon(i_1 i_2 \cdots i_n) = 0$ if two or more of the i_α's are equal.

$\epsilon(i_1 i_2 \cdots i_n) = 1$ if $i_1 i_2 \cdots i_n$ is an even permutation of $1, 2, 3, \cdots n$.

$\epsilon(i_1 i_2 \cdots i_n) = -1$ if $i_1 i_2 \cdots i_n$ is an odd permutation of $1, 2, \cdots n$.

The elements of $\mathbf{D}$ are the $d_j^{\,i}$'s, where the superscript indicates the row, and the subscript, the column. In

[13] The suggestion has been made before, but with reference to other kinds of orbitals. See G. G. Hall, Repts. Progr. in Phys. **15**, 22 (1959).

this notation,[14] one has

$$|\mathbf{D}| = \epsilon(i_1 i_2 \cdots i_n) d_{i_1}{}^1 d_{i_2}{}^2 \cdots d_{i_n}{}^n. \tag{A1}$$

The cofactor of $d_{i_\alpha}{}^\alpha$ in $|\mathbf{D}|$, is

$$D_\alpha{}^{i_\alpha} = \epsilon(i_1 i_2 \cdots i_n) d_{i_1}{}^1 d_{i_2}{}^2 \cdots d_{i_{\alpha-1}}{}^{\alpha-1} d_{i_{\alpha+1}}{}^{\alpha+1} \cdots d_{i_n}{}^n. \tag{A2}$$

The inverse of $\mathbf{D}$ exists and has the elements

$$\bar{d}_\alpha{}^i = |\mathbf{D}|^{-1} D_\alpha{}^i, \tag{A3}$$

if $|\mathbf{D}| \neq 0$.

Theorem 1

If

$$d_j{}^i = 0, \quad \text{for } i+j = \text{odd integer}, \tag{A4}$$

then

$$\bar{d}_l{}^k = 0, \quad \text{for } k+l = \text{odd integer}. \tag{A5}$$

Proof

First we shall show that $D_\alpha{}^{i_\alpha} = 0$ when $i_\alpha + \alpha = \text{odd}$ integer. That result combined with (A3) will give us Eq. (A5).

We first assume that n is even. If $i_\alpha + \alpha$ is to be an odd integer, then either i_α or α must be odd. Suppose that i_α is odd. Then in order not to include $d_{i_\beta}{}^\beta$'s which are zero in the product in Eq. (A2), $i_\beta + \beta$ must be an even integer. Since α was even, there must be $\frac{1}{2}n$ odd i_β's and $\frac{1}{2}n - 1$ even i_β's. But if there are $\frac{1}{2}n$ odd i_β's, one must be equal to i_α since there are only $\frac{1}{2}n$ odd integers in the set of integers 1 through n. Thus $\epsilon(i_1 i_2 \cdots i_n)$ will be zero, and $D_\alpha{}^{i_\alpha} = 0$. We may carry through the same reasoning when i_α is even. The proof may also be carried through for n odd.[15]

Theorem 2

If the elements of $\mathbf{D}$ satisfy Eqs. (A4), and if $\mathbf{E}$ is a diagonal matrix having elements $e_j{}^i$, then

$$\mathbf{E}' = \mathbf{D}^{-1}\mathbf{E}\mathbf{D} \tag{A6}$$

has elements $\bar{e}_j{}^i$ such that

$$\bar{e}_j{}^i = 0, \quad \text{if } i+j = \text{odd integer}. \tag{A7}$$

Proof

According to Eq. (A6) we have

$$\bar{e}_j{}^i = \bar{d}_k{}^i e_l{}^k d_j{}^l. \tag{A8}$$

Since $\mathbf{E}$ is diagonal, $e_l{}^k$ is zero for $k \neq l$. Suppose that i is even and j, odd. When i is even, $\bar{d}_k{}^i$ will be non-zero only if k is even. Because $e_l{}^k \neq 0$ only if $k = l$, l is even. For l even, $l+j$ is odd and $d_j{}^l$ will vanish. Thus $\bar{e}_j{}^i = 0$ when i is even and j is odd. When i is odd and j, even, we may carry through the same arguments to show that $\bar{e}_j{}^i = 0$. This proves the theorem.

[14] The notation and definitions follow those of H. Lass, *Vector and Tensor Analysis* (McGraw-Hill Book Company, Inc., New York, 1950), pp. 260–264.

[15] If we replace (A4) by the requirement that $d_j{}^i = 0$ for $i+j =$ even integer, we find that $\bar{d}_l{}^k = 0$ for $k+l =$ odd integer when n is odd, and for $k+l =$ even integer when n is even.

Theorem 3

If $\mathbf{D}$ is a square matrix of rank n, and n is even, and if

$$d_{j+1}{}^{i+1} = d_j{}^i, \tag{A9}$$

when i and j are both odd integers, then

$$\bar{d}_{j+1}{}^{i+1} = \bar{d}_j{}^i, \tag{A10}$$

where i and j are both odd.

Proof

From the definitions, one has

$$|\mathbf{D}| \bar{d}_\alpha{}^{i_\alpha} = D_\alpha{}^{i_\alpha} = \epsilon(i_1 i_2 \cdots i_\alpha \cdots i_n) d_{i_1}{}^1 \cdots d_{i_{\alpha-1}}{}^{\alpha-1} \times d_{i_{\alpha+1}}{}^{\alpha+1} \cdots d_{i_n}{}^n, \tag{A11}$$

and

$$|\mathbf{D}| \bar{d}_{\alpha+1}{}^{i_\alpha+1} = D_{\alpha+1}{}^{i_\alpha+1} = \epsilon(i_1 \cdots i_\beta, i_\alpha + 1, \cdots i_n) d_{i_1}{}^1 \cdots d_{i_\beta}{}^\beta d_{i_{\beta+2}}{}^{\beta+2} \cdots d_{i_n}{}^n. \tag{A12}$$

In Eq. (A12) we have set $\beta = \alpha$ and $i_{\beta+1} = i_\alpha + 1$. We assume that α and i_α are odd. Replacement of $d_{i_\gamma}{}^\gamma$ in Eq. (A12) by $d_{i_\gamma+1}{}^{\gamma+1}$ when γ and i_γ are odd, and by $d_{i_\gamma-1}{}^{\gamma-1}$ when γ and i_γ are even, does not change the value of the product. The replacement of i_γ in $\epsilon(i_1 i_2 \cdots i_n)$ in (A12) by $i_\gamma + 1$ when γ is odd, and by $i_\gamma - 1$ when γ is even, multiplies the product by $(-1)^{n/2}$. The factor $(-1)^{n/2}$ arises because each interchange corresponds to an odd number of permutations, and every odd permutation gives a factor of (-1).

$$|\mathbf{D}| \bar{d}_{\alpha+1}{}^{i_\alpha+1} = (-1)^{n/2} \times \epsilon(i_1+1, i_2-1, \cdots, i_\beta+1, i_\alpha, \cdots i_n-1) \times d_{i_1+1}{}^2 d_{i_2-1}{}^1 \cdots d_{i_\beta+1}{}^{\beta+1} d_{i_{\beta+2}+1}{}^{\beta+3} \cdots d_{i_{n-1}}{}^{n-1}. \tag{A13}$$

The i_γ's that are summed over may be replaced by new symbols without changing the value of the product.

$$|\mathbf{D}| \bar{d}_{\alpha+1}{}^{i_\alpha+1} = (-1)^{n/2} \epsilon(j_2, j_1, \cdots j_{\beta+1}, i_\alpha, \cdots, j_{n-1}) \times d_{j_2}{}^2 d_{j_1}{}^1 \cdots d_{j_{\beta+1}}{}^{\beta+1} d_{j_{\beta+3}}{}^{\beta+3} \cdots d_{j_{n-1}}{}^{n-1}. \tag{A14}$$

Interchange of the j_γ's to obtain the order

$j_1 j_2 \cdots j_{\alpha-1} i_\alpha j_{\alpha+1} \cdots j_n$, leads to another factor of $(-1)^{n/2}$. Since n is even, $(-1)^n = 1$, and

$$|\mathbf{D}| \bar{d}_{\alpha+1}{}^{i_\alpha+1} = \exp(j_1 j_2 \cdots j_\alpha \cdots j_n) \times d_{j_1}{}^1 d_{j_2}{}^2 \cdots d_{j_{\alpha-1}}{}^{\alpha-1} d_{j_{\alpha+1}}{}^{\alpha+1} \cdots d_{j_n}{}^n. \tag{A15}$$

Comparison of (A12) and (A14) gives us the result we wished to obtain, namely, Eq. (A10).

Theorem 4

If $\mathbf{D}$ is a matrix satisfying the conditions of theorem 3, and if $\mathbf{E}$ is a diagonal matrix whose elements satisfy

$$e_j{}^i = e_{j+1}{}^{i+1} \tag{A16}$$

when i and j are odd, then the elements $\bar{e}_j{}^i$ of

$$\mathbf{E}'=\mathbf{D}^{-1}\mathbf{E}\mathbf{D} \tag{A17}$$

satisfy for i and j odd,

$$\bar{e}_j{}^i=\bar{e}_{j+1}{}^{i+1}. \tag{A18}$$

Proof

By definition we have

$$\bar{e}_j{}^i=\bar{d}_k{}^i e_l{}^k d_j{}^l, \tag{A19}$$

and

$$\bar{e}_{j+1}{}^{i+1}=\bar{d}_k{}^{i+1} e_l{}^k d_{j+1}{}^l. \tag{A20}$$

We assume that i and j are odd. In Eq. (A19) we replace $\bar{d}_k{}^i$ by $\bar{d}_{k+1}{}^{i+1}$, and $d_j{}^l$ by $d_{j+1}{}^{l+1}$.

$$\bar{e}_j{}^i=\bar{d}_{k+1}{}^{i+1} e_{l+1}{}^{k+1} d_{j+1}{}^{l+1}. \tag{A21}$$

The value of the product is not changed due to Eqs. (A9), (A10) and (A16). Since we sum over $k+1$ and $l+1$, we can replace them by new symbols, k and l,

$$\bar{e}_j{}^i=\bar{d}_k{}^{i+1} e_l{}^k d_{j+1}{}^l. \tag{A22}$$

Comparison of Eqs. (A20) and (A22) gives us (A18).

THE JOURNAL OF CHEMICAL PHYSICS VOLUME 34, NUMBER 1 JANUARY 1961

Electron Spin Resonance and Optical Absorption of $K_3[Cr(CN)_5NO]\cdot H_2O$

IVAN BERNAL AND S. E. HARRISON

RCA Laboratories, Princeton, New Jersey

(Received July 19, 1960)

Electron spin resonance of a water solution and of the pure powder of $K_3[Cr(CN)_5NO]\cdot H_2O$ reveal a single sharp resonance line at room temperature. The water solution resonance gives a Cr^{53} hyperfine structure which is further split by a "superhyperfine" structure due to the nitrogen in the NO ligand. From the electron spin resonance the Cr^{1+} ion appears to be in a spin quenched (d^5) orbital singlet ground state. The optical absorption data allows the determination of the splittings of the d levels in concordance with the ESR spectrum.

INTRODUCTION

THE preparation of $K_3[Cr(CN)_5NO]\cdot H_2O$ has been reported recently by Griffith, Lewis, and Wilkinson.[1] They measured the paramagnetic susceptibility of the compound and recorded its infrared spectrum. From these data they concluded that the compound contains Cr^{1+} and NO^+.

Our interest in this compound arises because it has two noteworthy features: (a) Chromium has an unusual valence state. (b) It serves as an illustration of an interaction between a transition metal ion and a free radical.

Cr^{2+} and NO gas can be thought of as interacting to produce a species where the free radical electron is released into the d shell of the Cr^{2+} creating the species $CrNO^{2+}$ with an "effective" Cr^{1+} ion.[2]

Although the free radical electron is transferred to the Cr^{2+} ion, the electron still has a measurable interaction with the nitrogen nucleus; this interaction coming about through the agency of π bonding.

Griffith *et al.*[1] measured the susceptibility of the chromium compound as a function of temperature. Their data indicate that the spin state of the chromium is $S=\frac{1}{2}$, as shown by a plot of $1/\chi$ vs T^1. If the valence of the chromium is assumed to be $+1$, then the ion must be spin quenched.

I. ENERGY LEVELS[3]

The $[Cr(CN)_5NO]^{3-}$ complex has the symmetry C_{4v} (see Fig. 1). The five CN^- bonds transform as $2A_1+B_2+E$ and the NO^+ bond as A_1. These bonds contain the six pairs of electrons from the ligands. The five d electrons from the Cr^{1+} go into the Cr nonbonding orbitals (E and B_2) as shown in Fig. 2. The position of the ligand orbitals has been omitted; suffice it to say that they lie below the Cr^{1+} nonbonding orbitals.

One can justify this assignment of the energy levels by some simple considerations on the effect of the ligands on the free-ion orbitals. An octahedrally arranged sextet of CN^- ligands would split the free-ion orbitals into a lower triplet and a doublet. The substitution of an NO^+ for a CN^- not only changes the symmetry around the Cr^{1+} ion from octahedral to tetragonal, but it also reverses the electrostatic interac-

[1] W. P. Griffith, J. Lewis, and G. Wilkinson, J. Chem. Soc. **1959**, 872.

[2] For an interaction of the opposite kind, where the transition metal releases an electron to the free radical, see C. E. H. Bawn and D. Verdin, Trans. Faraday Soc. **56**, 519 (1960). One of us (I.B., unpublished data) has observed the same effect as Bawn and Verdin observed in the system DPPH—vanadyl acetylacetonate.

[3] Throughout the discussion that follows we shall confine ourselves to a one-electron model.

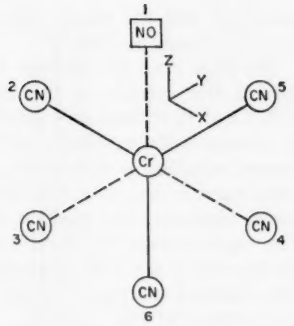

FIG. 1. Configuration of the anion $[Cr(CN)_5NO]^{3-}$.

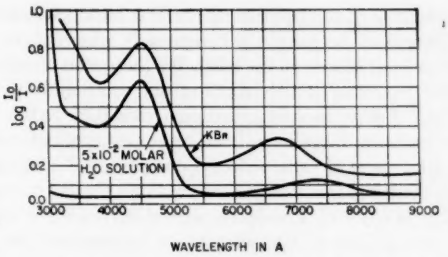

FIG. 3. Optical absorption of $K_3[Cr(CN)_5NO]\cdot H_2O$ in KBr and in H_2O.

tion between the electrons in the d_{xz} and d_{yz} orbitals of the Cr and the ligand. Whereas before the CN^- gave rise to an electrostatic repulsion, we now have an attraction. This gives rise to an enhanced stability of the $E(d_{xz}$ and $d_{yz})$ orbitals over the $B_2(d_{xz})$ orbital. The same argument shows that the $A_1(d_z2)$ orbital should lie below the $B_1(d_{x^2-y^2})$ in this case, hence the just mentioned scheme.

II. OPTICAL SPECTRA

The optical spectrum of $K_3[Cr(CN)_5NO]\cdot H_2O$ was studied in KBr pellets and in water solution using a Cary spectrophotometer that covers the range of 26 000 down to 1900 A. These spectra are shown in Fig. 3. The positions of the maxima and the extinction coefficients are tabulated in Table I.

The optical transitions have been assigned as follows:

$$B_2 \rightarrow A_1 \quad 7300 \text{ A}$$

$$E \rightarrow A_1 \quad 4550 \text{ A}$$

$$B_2 \rightarrow B_1 \quad 3300 \text{ A}.$$

In assigning these transitions we have taken into account (a) the fact that the transitions are d to d transitions (this is shown by the low extinction coefficients), (b) that the splitting of the E state (bonding orbitals) should be larger than that of the T state (nonbonding orbitals).

On examining the optical absorption data given, one notices that the $B_2 \rightarrow A_1$ absorption band (7300 A) is shifted towards the infrared in the water solution sample, which means that the separation between the B_2 and the A_1 state has decreased. Also, the $E \rightarrow A_1$ transition has not been altered. These optical results can be explained by assuming an interaction that affects the axial ligand in such a way as to vary the tetragonality of the crystal field of the complex. This interaction increases the tetragonality of the field in the water solution (i.e., the crystal field of the axial ligands diminishes). Then according to Fig. 2, the E and A_1 levels are lowered while the B_2 and B_1 levels are raised. There are three kinds of interactions that can produce the axial changes necessary to explain our spectral observations:

(a) NO-NO Interactions in the Solid

Interactions between NO groups are well known and the resulting effect on the infrared spectra has often been recorded.[4] Of particular interest to us is the case of $K_2[(SO_3)_2NO]$[5,6] which is a paramagnetic monomer in solution but a diamagnetic dimer in the solid. If intercomplex interactions of this sort were present in our compound we would expect to see a concentration

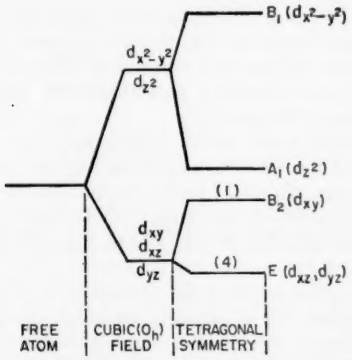

FIG. 2. Energy levels of Cr^{3+} $(3d^3)$ in a crystalline field of C_{4v} symmetry.

TABLE I. Optical absorption spectra of $K_3[Cr(CN)_5NO]$.

KBr pellets		Water solution	
Position of max	Extinction coeff	Position of max	Extinction coeff
6740 A	...	7300 A	15.2
4550 A	...	4510 A	120
		3300 A[a]	80

[a] Shoulder.

[4] See L. J. Bellamy, *Infrared Spectra of Complex Molecules* (John Wiley & Sons, Inc., New York, 1958), 2nd ed.; also W. G. Fately, H. A. Bent, and B. Crawford, Jr., J. Chem. Phys. **31**, 204 (1959).

[5] S. Yamada and R. Tsuchida, Bull. Chem. Soc. Japan **32**, 721 (1959).

[6] R. W. Asmussen, Z. anorg. allgem. Chem. **212**, 316 (1932).

dependence of the position of the first band as observed by Ferguson[7] in some Co compounds where there are similar interactions in the solid. We have seen no change in the positions of the bands of our compound with a tenfold change in concentration (from 0.05 to 0.5 *M*) Furthermore, there have been recent determinations of the structures of some nitrosyl complexes[8–11] and there is no evidence for NO-NO interactions similar to those in $K_2[(SO_3)_2NO]$. Therefore, we feel fairly safe in ruling out interactions in the solid as an explanation for the shifts in the spectra.

(b) Trans Elimination of the Axial CN^- Ligand

As long as there are differences in bonding strengths in the ligands of a complex there is the possibility of *trans* elimination of one of them. Furthermore, some metal complexes are inherently unstable with six ligands, i.e., $Co(CN)_6^{3-}$[12] and some of the nitrosyldithiocarbamates.[10] Others exchange their ligands in water solutions with the medium, i.e., $Cr(NH_3)_6^{3+}$, etc. Therefore, it is possible that our spectral changes may be associated with such effects. In water solution we could have reactions such as

$$[Cr(CN)_5NO]^{3-} \rightleftarrows [Cr(CN)_4NO]^{2-} + CN^-$$

or

$$[Cr(CN)_5NO]^{2-} + H_2O \rightleftarrows [Cr(CN)_4(H_2O)NO]^{2-} + CN^-.$$

The *trans* eliminating power of CN^- and NO^+ are rated as about equal.[13] Fortunately, we can use a more decisive criterion in our case to decide what are the relative strengths of the CN^- and NO^+ bonds with the central ion. Orgel[14] predicted that when there is a change in coordination from octahedral to C_{4v}, the crystal field band should split and the ratio of intensities of the resulting pair should be 2 or $\frac{1}{2}$ according as to whether the new ligand produced a weaker or stronger crystalline field. Furthermore, the size of the splitting is a good measure of the difference in *Dq* between the two kinds of ligands. In our case the intensity ratio is about $\frac{1}{7}$ and the splitting in the solid about 7000 cm^{-1}. Thus, there is a sizable difference in *Dq* between CN^- and NO^+ and the relative intensity predicts that the Cr—NO bonds are stronger.

We have tried to influence the above equilibria by adding free cyanide to the medium up to ratios of CN/Cr of 10 without any spectral changes. This tends to eliminate the possibility of the first equation. The second equation is difficult to eliminate on this basis since water is always in such large excess in these solutions. However, the question that arises to confront this explanation is that if the anion undergoes hydrolysis why did it not form originally as an aquo complex. The chemical analysis of Griffith *et al.*[1] clearly indicates the presence of five cyanides.

(c) Hydrogen Bonding in Solution

Interactions of this type are so well known that they need no further description. We will merely recall that the shift in the $E \rightarrow A_1$ transition we observe is towards the red as in the case of $K_2[(SO_3)_2NO]$.[5] McConnell[15] has proposed an explanation for this phenomenon. His view is that a red shift is due to coupling with solvent molecules which increases slightly the delocalization of electrons. If we assume that the π electron, delocalized between Cr and N, interacts further with the solvent through the agency of H bonds, then we can understand the red shift.

We favor the hydrogen bonding explanation for the shift in spectral absorption. It is possible to account for all the observed data on the basis that in solution there are strong hydrogen bonds. We may note that Cotton *et al.*[16] observed infrared spectral shifts in dehydrating salts similar to ours and that they attributed these shifts to hydrogen bonding.

III. ELECTRON SPIN RESONANCE

Electron spin resonance measurements were carried out in dilute solution and in the pure powdered solid. These measurements were done in a Varian 3-cm spectrometer with a Varian 12 in. magnet. The field was measured with an NMR probe.

The spectrum of a 3×10^{-3} *M* water solution is shown in Fig. 4. The spectrum shows one main triplet flanked by twelve satellites, six on each side. The hyperfine lines are shown in Fig. 5 with increased gain to illustrate the division into two sets of three on either side of the main resonance peak. Figure 6 shows a reconstruction of the spectrum.

The central large triplet in the spectrum is the resonance of the Cr isotope with no nuclear spin split by the nuclear spin of N ($I=1$); the four sets of smaller triplets is caused by the 10% Cr^{53} (isotope ($I=\frac{3}{2}$). The nuclear splitting of Cr is 13.6; that of the N is 5.55 gauss.

The hyperfine constant for chromium is close to a value expected for a strongly covalent complex of Cr^{3+} (see Table II). (Under identical bonding condi-

[7] J. Ferguson, J. Chem. Phys. **32**, 528 (1960).
[8] G. B. Bokii and N. A. Parpiev, Soviet Phys. Crystallography **2**, 681 (1957); also N. A. Parpiev and G. B. Bokii, Russian J. Inorg. Chem. **1959**, 1127.
[9] N. A. Parpiev and M. A. Porai-Koshits, Soviet Phys. Crystallography **4**, 26 (1960).
[10] P. R. H. Alderman and P. C. Owston, Nature **178**, 1071 (1956).
[11] G. Johansson and W. N. Lipscomb, Acta Cryst. **11**, 594 (1958); J. T. Thomas, J. H. Robertson, and E. G. Cox, *ibid.* **11**, 599 (1958).
[12] A. W. Adamson, J. Am. Chem. Soc. **73**, 5710 (1951).
[13] F. Basolo and R. G. Pearson, *Mechanisms of Inorganic Reactions*, (John Wiley & Sons, Inc., New York, 1958), p. 172.
[14] L. E. Orgel, J. Chem. Phys. **23**, 1004 (1953). D. S. McClure (to be published) has recently provided very clear semiquantitative explanation for the spectrochemical series. He arrives at much the same conclusions except he predicts an intensity ratio of 3 or $\frac{1}{3}$.
[15] H. McConnell, J. Chem. Phys. **20**, 700 (1952).
[16] F. A. Cotton *et al.*, J. Inorg. and Nuclear Chem. **10**, 28 (1959).

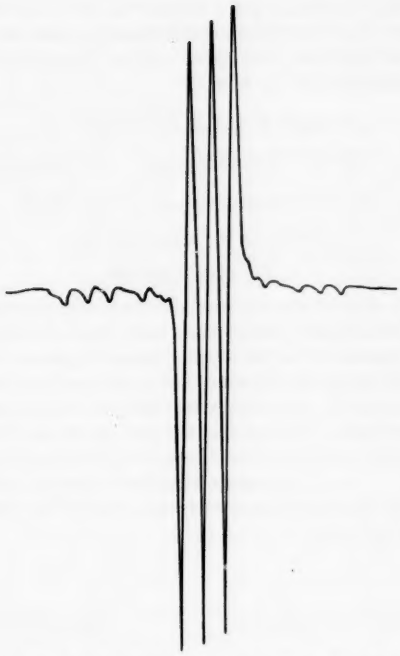

FIG. 4. ESR spectrum of a 3×10^{-3} molar water solution of $K_3[Cr(CN)_5NO]\cdot H_2O$.

FIG. 5. ESR of same solution as in Fig. 4 but at higher gain and sweep field. Note the two sets of three hf lines on each side of the main lines.

tions, one would expect the chromium constant to be larger for the higher charge). The larger the covalent bonding the smaller the Cr hyperfine structure will be. The diminution of hyperfine constant with covalency has been discussed for Mn by Van Wieringer.[17]

TABLE II. Hyperfine splittings in chromium compounds.

Electronic configuration	Host lattice	Chromium splitting (gauss)	Ligand splitting (gauss)
$d\epsilon^3$	$KAl(SeO_4)_2\cdot 12H_2O$[a]	20	...
$d\epsilon^3$	MgO[b]	17.1	...
$d\epsilon^3$	TiO_2[c]	16.7	...
$d\epsilon^3$	$K_3Co(CN)_6$[d]	15.7	...
$d\epsilon^3 d\gamma^2$	NaF[e]	14	13.7
$d\epsilon^5$	$K_3Cr(CN)_5NO$	13.8	5.5
$d\epsilon^3$	ZnF_2[f]	...	3–5

[a] B. Bleaney and K. D. Bowers, Proc. Phys. Soc. (London) **A64,** 1135 (1951).
[b] W. Low, Phys. Rev. **105,** 801 (1957).
[c] H. J. Gerritsen, S. E. Harrison, H. R. Lewis, and J. P. Wittke, Phys. Rev. Letters **2,** 153 (1959).
[d] K. D. Bowers, Proc. Phys. Soc. (London) **A65,** 860 (1952).
[e] W. Hayes, Discussions Faraday Soc., **26,** 58 (1958); W. Hayes and D. H. Jones, Proc. Phys. Soc. (London) **A71,** 503 (1958).
[f] M. Tinkham, Proc. Roy. Soc. (London) **A236,** 535 (1956).

[17] J. S. Van Wieringen, Discussions Faraday Soc. **19,** 118 (1955).

The value of the ligand hyperfine constant in $[Cr(CN)_5NO]^{3-}$ is small compared to value of Cr^{1+} in NaF of 13.7 gauss.[18] In the former compound, as in Cr^{3+} on ZnF_2,[19] the ligand hyperfine splitting is small due to the absence of σ bonding, so that the s electron contact contribution is nil (or very nearly so, due to a small amount of σ-bonding admixture).

Comparisons that can be made for the N "super-hyperfine" splitting are limited because only one such interaction has been measured.[20] The value of 5.5 gauss

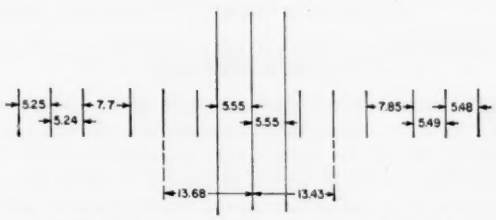

FIG. 6. Reconstruction of the ESR spectrum. Separations are given in gauss.

[18] W. Hayes, Discussions Faraday Soc. **26,** 58 (1958).
[19] M. Tinkham, Proc. Royal Soc. (London) **A236,** 535 (1956).
[20] A. B. Maki and B. R. McGarvey, J. Chem. Phys. **29,** 35 (1958).

for the N ligand hyperfine interaction is less than the value of 11 gauss obtained with a Cu^{2+} chelate,[20] where the σ bonding contribution would be expected to be larger.

We have also looked at the ESR of the undiluted powdered compound and find that the resonance line is only 23 gauss wide. The center of the line is at 3418.81 gauss (DPPH = 3402.01 gauss) whereas for the 3×10^{-3} H_2O solution the center is at 3416.72 gauss. The powder does not show the hyperfine components of the spectrum despite the narrow linewidth. We believe the narrowness of the linewidth in the pure powder is due to exchange narrowing.

The g value is very close to 2 as would be expected from the theoretical values

$$g_{\parallel}=2[1-(4\lambda/\Delta)]$$

$$g_{\perp}=2,$$

where Δ is the separation between the B_2 and B_1 levels (see Fig. 2) and λ is the spin orbit coupling constant. The g value of 2 and the sharp, easily detectable resonance gives support to the assignment of levels (Fig. 2) with an orbital singlet ground state.

The data we have given can be summarized in a Hamiltonian of the kind

$$H=\beta gH\cdot S.+A_1S\cdot I_1+A_2S\cdot I_2$$

$S=\frac{1}{2}$; $A_1=13.8$ gauss; $A_2=5.55$ gauss

$I_1=\frac{3}{2}$(chromium); $I_2=1$ (nitrogen)

$g=1.9950$ for the water solution.

IV. CONCLUSION

The optical spectra and electron spin resonance of $K_3[Cr(CN)_5NO]\cdot H_2O$ have been studied. The Cr^{1+} ion appears to be in a spin quenched state with an orbital singlet state lowest. The results indicate that the NO group in this compound should behave as NO^+ rather than as NO and they support the views of Griffith *et al.*[1] derived from infrared spectra. The relatively small value of the N hyperfine structure constant indicates that the unpaired electron spends most of its time in a $d\epsilon$ orbital of Cr.

THE JOURNAL OF CHEMICAL PHYSICS VOLUME 34, NUMBER 1 JANUARY, 1961

Spin-Spin Interactions in Nuclear Magnetic Resonance. Contact Contribution

S. ALEXANDER

Nuclear Magnetic Resonance Department, The Weizmann Institute of Science, Rehovoh, Israel

(Received December 21, 1959)

A method for calculating the contact contribution to spin-spin interactions between nuclei in nonaromatic molecules is described. The method is based on the valence bond model. The equivalent Hamiltonian of the Dirac vector model is used for a perturbation calculation in a representation where the total spin of the two electrons in each bond in the molecule is a good quantum number. The Ramsey-Purcell contact term in the interaction is calculated by a double perturbation method where only terms linear in the electron-nuclear interactions are considered but the perturbation is carried to higher order in the exchange integrals. In this way the interaction constants can be obtained explicitly in terms of the exchange integrals, and the calculation of the valence bond wave functions is avoided. It is then possible to see how the signs and magnitudes of the interaction constants depend on these integrals and what the dominant interaction mechanisms are. The perturbation series is evaluated explicitly with the electron nuclear contact interaction and the results are compared with the results of a similar calculation based on Ramsey's closure formula. In this way the objections against the closure procedure can be avoided. It is shown that Ramsey's formula can be used when different average energy separations are used for terms of different order in the expansion. The results of Ramsey for H_2 and of Karplus *et al.* for hydrogen atoms separated by two and three bonds and the justification of the method of calculation used by them are discussed in detail. It is found that only perturbation terms of one type are important in each of the cases discussed by these authors and therefore their procedure can be justified. The results previously obtained by the author for spin-spin interactions in the allyl group are also discussed.

I. INTRODUCTION

SPIN-SPIN interactions between nuclei have been measured in a large number of molecules. Recently, the relative signs of such interactions have also been determined in several molecules. In particular, a number of investigations on the relative signs of spin-spin interactions between protons in simple organic molecules have been published.[1–4]

Ramsey and Purcell[5,6] have discussed the various mechanisms responsible for such interactions in detail. Ramsey has also calculated the interaction constant for H_2 in good agreement with experimental results.

Ramsey's formulas have been used by various investigators. Gutowsky, McCall, and Slichter[7] have

[1] S. Alexander, J. Chem. Phys. **28,** 358 (1958).
[2] R. W. Fessenden and J. S. Waugh, J. Chem. Phys. **30,** 944 (1959).
[3] H. S. Gutowsky, M. Karplus, and D. M. Grant, J. Chem. Phys. **31,** 1278 (1959).
[4] S. Alexander, J. Chem. Phys. **32,** 1700 (1960).
[5] E. M. Purcell and N. F. Ramsey, Phys. Rev. **85,** 143 (1952).
[6] N. F. Ramsey, Phys. Rev. **91,** 303 (1953).
[7] H. S. Gutowsky, D. W. McCall, and C. P. Slichter, J. Chem. Phys. **21,** 279 (1953).

used the valence bond model to calculate interactions between nuclei in adjacent atoms. More recently Karplus *et al.*[3,8,9] and McConnell[10] have used this model to calculate the interactions between protons in more complicated cases.

McConnell[11] suggested the use of the Dirac vector model to calculate the contact contributions to spin-spin interactions, within the valence bond approximation. Following this suggestion, the author has developed a method of calculation which brings out clearly the connection between the interaction constant and the various exchange integrals involved.[12,13] The most important feature of this method is that it distinguishes clearly between terms of different order in the exchange integrals. Physically this amounts to a distinction between the different mechanisms responsible for the correlation between the electronic spins at the sites of the interacting nuclei. These calculations, however, have not been published in detail. They will be described in this paper.

McConnell[14] has also used molecular orbital electronic wave functions to calculate spin-spin interactions. There is, however, reason to believe that such functions are not suitable for these calculations.[15]

Numerous other calculations have also been published which will not be enumerated here.

All these calculations are based on Ramsey's results.[6] In particular, they all involve the use of a closure procedure to bring Ramsey's second-order perturbation series to a form which can be evaluated with ground-state wave functions [e.g., the derivation of Eq. (11) of footnote reference 6].

McLachlan[16] has recently pointed out that this procedure is, in general, unjustified. McLachlan points out that the average energy separation (ΔE) defined by Ramsey need not be of the order of the energy separations of the excited states of the molecule. In fact, it can be both positive and negative. This seems to invalidate all calculations of spin-spin interactions hitherto carried out.

For protons, it is usually assumed that spin-spin interactions are mainly due to the scalar contact interaction between the nuclear and electronic spins;

$$\mathcal{H}_e=(16\pi\beta/3)\sum_N\gamma_N\sum_k(\mathbf{S}_k\cdot\mathbf{I}^N)\,\delta(\mathbf{r}_k{}^N), \qquad (1)$$

where β is the Bohr magneton, γ_N the nuclear gyromagnetic ratio, $\mathbf{S}_k$ and $\mathbf{I}^N$ are the spin vectors of the electron (k) and nucleus (N), respectively, and $\mathbf{r}_k{}^N$ is the vector connecting the electron and the nucleus. The summation is over all electrons (k) and magnetic nuclei (N) in the molecule. A second-order perturbation calculation taking $\mathcal{H}_e$ as a perturbation on the electronic Hamiltonian of the molecule, gives the contribution of $\mathcal{H}_e$ to the interaction constant.[6] The interaction energy of the nuclei N and N' is then

$$E_{NN'}{}^2=-(16\pi\beta/3)^2\gamma_N\gamma_{N'}\sum_{kk'n}\times\frac{\langle 0\mid(\mathbf{S}_k\cdot\mathbf{I}^N)\,\delta(\mathbf{r}_k{}^N)\mid n\rangle\cdot\langle n\mid(\mathbf{S}_{k'}\cdot\mathbf{I}^{N'})\,\delta(\mathbf{r}_{k'}{}^{N'})\mid 0\rangle}{E_n-E_0}+\text{c.c.}, \qquad (2)$$

where c.c. stands for the complex conjugates of the terms in the summation. These are obviously the terms one obtains when the order of the operators in the numerator is reversed. The same notation will be used throughout this paper. Summation of the numerators leads to Ramsey's formula,

$$E_{NN'}{}^2=-(2/3\Delta E)\,(16\pi\beta/3)^2\gamma_N\gamma_{N'}\times(\mathbf{I}^N\cdot\mathbf{I}^{N'})\sum_{kk'}\langle 0\mid\mathbf{S}_k\cdot\mathbf{S}_{k'})\,\delta(\mathbf{r}_k{}^N)\,\delta(\mathbf{r}_{k'}{}^{N'})\mid 0\rangle. \qquad (3)$$

As mentioned previously, the use of this equation is, in general, unjustified. In this paper, we will try to evaluate the second-order perturbation series [Eq. (2)] explicitly within the valence bond model. This will require certain assumptions which are not very different from those made (e.g., by Karplus[8,9]) in calculating spin-spin interactions from Eq. (3). It will be shown how the use of an expression equivalent to Eq. (3) can be justified in a double perturbation procedure for evaluating the interactions.[12,13] The calculation is based on the Dirac vector model. In the form presented, it is limited to nonaromatic molecules.

II. VALENCE BOND MOLECULAR WAVE FUNCTIONS WITH THE DIRAC VECTOR MODEL

Valence bond molecular wave functions are linear combinations of functions of the type

$$\phi^r=\sum_j(-1)^jP_j\psi_{eo}(0)\chi_{es}{}^r(0), \qquad (4)$$

where (0) designates a specific permutation of the electrons, P_j is the electron permutation operator, and the summation is over all permutations of the electrons (j) so as to make ϕ^r antisymmetric. The orbital function $\psi_{eo}(0)$ is a single product of linearly independent,

[8] M. Karplus and D. H. Anderson, J. Chem. Phys. **30,** 6 (1959).
[9] M. Karplus, J. Chem. Phys. **30,** 11 (1959).
[10] H. M. McConnell, J. Chem. Phys. **30,** 126 (1959).
[11] H. M. McConnell, J. Chem. Phys. **23,** 2454 (1955).
[12] S. Alexander, Bull. Research Council Israel **7F,** 95 (1958).
[13] S. Alexander, Ph.D. thesis, Hebrew University, 1958 (unpublished).
[14] H. M. McConnell, J. Chem. Phys. **24,** 460 (1956); Ann. Rev. Phys. Chem. **8,** 105 (1957).
[15] In the molecular orbital approximation (without configuration interaction) the spin part of the electronic wave function is determined uniquely by the model (i.e., the function is a single Slater determinant). As it is known that the interactions of the nuclei with the electronic spin are important,[8] such functions are not likely to give good results. It can be shown, for example, that the unique positive sign of proton interactions predicted by McConnell,[14] is solely due to this feature of the model. The same sign would be obtained for any set of real, mutually orthogonal, single electron orbits as long as one puts the electrons in pairs into the orbits.
[16] A. D. McLachlan, J. Chem. Phys. **32,** 1263 (1960). The author is indebted to Professor H. M. McConnell for pointing out McLachlan's objections prior to publication. Some aspects of McLachlan's argument are discussed in the Appendix.

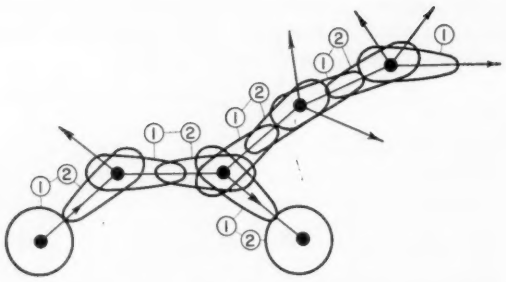

FIG. 1. Schematic description of the notation used in marking the bonds and atomic orbits.

but, in general, nonorthogonal, single electron orbits $(\varphi_i(k_i)]$ each centered on a definite nucleus

$$\psi_{e0}(0)=\prod_{i=1}^{n}\varphi_i(k_i), \tag{5}$$

where i is an index numbering the atomic orbits, k_i is the electron occupying the atomic orbit, and n is the total number of valence electrons (and therefore also of atomic orbits).

The spin function in Eq. (4) is

$$\chi_{es^\nu}(0)=\prod_{i=1}^{n}s_i^\nu(k_i), \tag{6}$$

where the $s_i^\nu(k_i)$ are single electron spin functions. For a definite ψ_{e0} there are obviously 2^n different χ_{es^ν} and therefore also 2^n different ϕ^ν. The valence bond method regards the ϕ^ν as a basis for a variational calculation. The nonorthogonality of the $\varphi_i(k)$ is neglected except for its contribution to the exchange integrals. Ordinarily one also neglects the contribution of polar states and uses just one ψ_{e0}.

To get the best combination of ϕ^ν one can use the Dirac vector model.[17,18] One looks for eigenfunctions of the equivalent Hamiltonian,

$$\mathcal{H}_{eq}=V_1-\tfrac{1}{4}\sum_{i\neq j}V_{ij}[1+4(\mathbf{S}_i\cdot\mathbf{S}_j)], \tag{7}$$

where

$$V_1=\langle\psi_{e0}\mid\mathcal{H}\mid\psi_{e0}\rangle, \tag{8}$$

and

$$V_{ij}=\langle\psi_{e0}\mid\mathcal{H}\mid P_{ij}\psi_{e0}\rangle=\langle\varphi_i(1)\varphi_j(2)\mid\mathcal{H}\mid\varphi_i(2)\varphi_j(1)\rangle. \tag{9}$$

In Eqs. (8) and (9) $\mathcal{H}$ is the true electronic Hamiltonian of the molecule and P_{ij} is the operator exchanging the electrons in the orbits φ_i and φ_j in ψ_{e0}.[19] $\mathcal{H}_{eq}$ operates on linear combinations of functions of the type χ^ν all with the same arrangement of the electrons [e.g., (0)] among the atomic orbitals.

For nonaromatic molecules one can write

$$\mathcal{H}_{eq}=V_1'+\mathcal{H}_0+\mathcal{H}_1, \tag{10}$$

where

$$\mathcal{H}_0=-\tfrac{1}{2}\sum_{\alpha}V^\alpha(1+4\mathbf{S}_1^\alpha\cdot\mathbf{S}_2^\alpha), \tag{11}$$

and

$$\mathcal{H}_1=-\sum_{\alpha\neq\beta}\sum_{i,j=1}^{2}V_{ij}^{\alpha\beta}(\mathbf{S}_i^\alpha\cdot\mathbf{S}_j^\beta). \tag{12}$$

We have included the diagonal terms of $\mathcal{H}_1$ in V_1'. The notation used in Eqs. (11) and (12) to number the electrons (atomic orbitals) is as follows: The upper (greek) indices designate the bonds in the molecule to which the electrons belong in the "ordinary" perfect pairing structure and the summation is over all bonds. The lower (latin) indices number the two electrons participating in each bond. This numbering will always be in a definite direction along the bonds (see Fig. 1). Thus

$$V^\alpha=V_{12}^{\alpha\alpha} \tag{13}$$

is the exchange integral [Eq. (9)] between the two atomic orbits belonging to the bond α. $V_{12}^{\alpha\beta}$ is the corresponding integral for the first orbit in bond α and the second one in β.

The V^α are usually negative and considerably larger than the $V^{\alpha\beta}$. Therefore $\mathcal{H}_1$ can be taken as a perturbation on $\mathcal{H}_0$.

Both $\mathcal{H}_0$ and $\mathcal{H}_1$ commute with the total spin of all electrons. For negative V^α the lowest state of $\mathcal{H}_0$ is obviously a singlet state and therefore only such states have to be considered in the perturbation calculation.

The eigenstates of $\mathcal{H}_0$ have a definite value for the total spin of every pair of electrons belonging to the same bond α. These states can therefore be expressed in terms of the two electron states. For each bond α one has the singlet state

$$\sigma^\alpha=(\mid+-\rangle-\mid-+\rangle)/\sqrt{2}, \tag{14a}$$

(where $+$ and $-$ are the two single electron spin states) and the three triplet states

$$\tau_1^\alpha,\quad\tau_0^\alpha,\quad\tau_{-1}^\alpha, \tag{14b}$$

of the two electrons (the lower index is the magnetic quantum number of the pair). If all V^α are negative, the eigenfunction of $\mathcal{H}_0$ belonging to the lowest eigenvalue is

$$\psi^p=\prod_{\alpha}\sigma^\alpha. \tag{15}$$

This is the perfect pairing state. One then has other singlet states containing triplet functions of the electrons in two, three, or more bonds in addition to states of the type σ for the other bonds. In particular, the

[17] P. A. M. Dirac, Proc. Roy. Soc. (London) **A123,** 714 (1929).
[18] J. H. Van Vleck, Phys. Rev. **45,** 405 (1935); J. H. Van Vleck and A. Sherman, Revs. Modern Phys. **7,** 167 (1935).
[19] The approximations involved are discussed in detail by Van Vleck.[18] They are, however, inherent to the valence bond approximation.

singlet state of the four electrons in bonds α and β is

$$\Sigma^{\alpha\beta}=3^{-\frac{1}{2}}(\tau_0{}^\alpha\tau_0{}^\beta-\tau_1{}^\alpha\tau_{-1}{}^\beta-\tau_{-1}{}^\alpha\tau_1{}^\beta)/\sqrt{3}. \quad (16)$$

This generates a family of eigenstates of $\mathcal{H}_0$ of the type

$$\psi^{\lambda\mu}=\Sigma^{\lambda\mu}\cdot\prod_{\alpha\neq\lambda,\mu}\sigma^\alpha. \quad (17)$$

All $\psi^{\lambda\mu}$ are mutually orthogonal because of the orthogonality of the τ's and σ's. As $\mathcal{H}_1$ contains only two electron operators, it can obviously connect ψ^p only with states of the type $\psi^{\lambda\mu}$. We have

$$\mathcal{H}_0\,|\,\psi^p\rangle=\sum_\alpha V^\alpha\,|\,\psi^p\rangle, \quad (18)$$

$$\mathcal{H}_1\,|\,\psi^p\rangle=(\sqrt{3}/4)\sum_{\alpha\neq\beta}Q^{\alpha\beta}\,|\,\psi^{\alpha\beta}\rangle, \quad (19)$$

$$\mathcal{H}_0\,|\,\psi^{\lambda\mu}\rangle=(\sum_\alpha V^\alpha-2V^\lambda-2V^\mu)\,|\,\psi^{\lambda\mu}\rangle, \quad (20)$$

$$\begin{aligned}\mathcal{H}_1\,|\,\psi^{\lambda\mu}\rangle=&+(\sqrt{3}/2)Q^{\lambda\mu}\,|\,\psi^p\rangle+\tfrac{1}{2}\sum_{\alpha\neq\lambda,\mu}Q^{\lambda\alpha}\,|\,\psi^{\mu\alpha}\rangle\\&+Q^{\mu\alpha}\,|\,\psi^{\lambda\alpha}\rangle+2(P^{\lambda\alpha}-P^{\mu\alpha})\,|\,\psi^{\lambda\mu\alpha}\rangle\\&+(\sqrt{3}/4)\sum_{\alpha\neq\beta;\alpha,\beta\neq\lambda,\mu}Q^{\alpha\beta}\,|\,\psi^{\lambda\mu,\alpha\beta}\rangle, \quad (21)\end{aligned}$$

where we have defined

$$Q^{\alpha\beta}=-V_{11}{}^{\alpha\beta}+V_{12}{}^{\alpha\beta}+V_{21}{}^{\alpha\beta}-V_{22}{}^{\alpha\beta}, \quad (22)$$

$$P^{\alpha\beta}=-V_{11}{}^{\alpha\beta}+V_{12}{}^{\alpha\beta}-V_{21}{}^{\alpha\beta}+V_{22}{}^{\alpha\beta}. \quad (23)$$

$\psi^{\lambda\mu\alpha}$ is a singlet state involving only two-electron triplets (τ's) for the three bonds α, λ, and μ and otherwise σ's and $\psi^{\lambda\mu,\alpha\beta}$ is a singlet state which contains $\Sigma^{\lambda\mu}$,$\Sigma^{\alpha\beta}$, and σ's for all other bonds.[20] The ground-state wave function of $\mathcal{H}_{eq}$ can be expressed as a linear combination of these eigenfunctions of $\mathcal{H}_0$.

The singlet states we use are closely related to the Pauling bond structures, which involve a breaking of the corresponding bonds, but they are orthogonal and therefore easier to use in calculation.[21] In this form the calculation is, however, restricted to nonaromatic molecules. In Eq. (15) it is implicitly assumed that there is a unique "ordinary" bond structure for the molecules and therefore the ground-state wave function of $\mathcal{H}_0$ can be written in the form ψ^p. For aromatic molecules $\mathcal{H}_0$ has to be defined differently.

In the subsequent discussion we will also be interested in the operation of single spin operators on the singlet functions we consider. In this case the resulting functions always describe triplet states. One finds

$$\mathbf{S}_1{}^\alpha\sigma^\alpha=\tfrac{1}{2}(-\tau_-{}^\alpha\mathbf{i}+i\tau_+{}^\alpha\mathbf{j}+\tau_0{}^\alpha\mathbf{k}), \quad (24)$$

$$\mathbf{S}_1{}^\alpha\Sigma^{\alpha\beta}=\sigma_\alpha(-\tau_-{}^\beta\mathbf{i}+i\tau_+{}^\beta\mathbf{j}+\tau_0{}^\beta\mathbf{k})/2\sqrt{3}+\text{h.o.f.}, \quad (25)$$

where $i=\sqrt{-1}$, $\mathbf{i}$, $\mathbf{j}$, $\mathbf{k}$ are the three Cartesian unit vectors. We have defined

$$\text{(a)}\qquad \tau_+{}^\alpha=(\tau_1{}^\alpha+\tau_{-1}{}^\alpha)/\sqrt{2}, \quad (26)$$

$$\text{(b)}\qquad \tau_-{}^\alpha=(\tau_1{}^\alpha-\tau_{-1}{}^\alpha)/\sqrt{2}.$$

It follows that ψ^p [Eq. (15)] is connected by $\mathbf{S}_s{}^\alpha$ only with a special type of triplet function—i.e., one with a τ for one bond (α) and σ's for all other bonds. There are three such states for each "excited" bond α, which are practically degenerate. This gives a certain freedom in choosing the representation.

States of the type $\psi^{\lambda\mu}$ are also connected with these states. In addition, they are connected with more complicated triplet states where both λ and μ are in τ states [h.o.f. in Eq. (25)].

III. METHOD OF CALCULATION

a. Orbital Part

The valence bond ground-state wave function is a linear combination of ϕ_ν [Eq. (4)] all having the same orbital part (ψ_{eo}). Assuming a similar form for the excited states ($|\,n\rangle$) one can separate the orbital and spin parts of the matrix elements in Eq. (2).

The orbital matrix elements will have the form

$$\langle\psi_{eo}{}^0\,|\,\delta(\mathbf{r}_k{}^N)\,|\,\psi_{eo}{}^n\rangle\cdot\langle\psi_{eo}{}^n\,|\,\delta(\mathbf{r}_{k'}{}^{N'})\,|\,\psi_{eo}{}^0\rangle, \quad (27)$$

where $\psi_{eo}{}^0$ and $\psi_{eo}{}^n$ are the products of single electron atomic orbitals appearing in the ground state ($|\,0\rangle$) and the excited state ($|\,n\rangle$), respectively. One can now assume that only atomic orbitals (φ_N) centered on the two nuclei N and N' have significant amplitudes at the sites of the respective nuclei ($\mathbf{r}^N$, $\mathbf{r}^{N'}$).[22] The only important contributions to $E_{NN'}{}^{(2)}$ [Eq. (2)] then come from terms diagonal in the orbital part (i.e., when $|\,n\rangle$ has the same orbital function $\psi_{eo}{}^0$ as $|\,0\rangle$). All other terms involve at least two factors of the order of the overlap of atomic orbitals of different nuclei and are therefore considerably smaller. On neglecting these small terms, the orbital part can be integrated out and, instead of Eq. (2), one is left with

$$E_{NN'}{}^{(2)}=-C\sum_{n_s,k,j}\frac{\langle 0_s\,|\,(\mathbf{S}_k\cdot\mathbf{I}^N)\,|\,n_s\rangle\cdot\langle n_s\,|\,(\mathbf{S}_j\cdot\mathbf{I}^{N'})\,|\,0_s\rangle}{E_n-E_0}+\text{c.c.} \quad (28)$$

where the value of the constant C is clear from Eq. (2).

As the orbital part has been eliminated, one can consider Eq. (28) within the Dirac vector model, i.e.,

[20] The signs of the different V_{ij} in P and Q can easily be verified from the symmetry properties of ψ^p, $\psi^{\lambda\mu}$, and $\psi^{\lambda\mu\alpha}$ as regards an exchange of the two electrons in each bond.

[21] All $\psi^{\lambda\mu}$ and $\psi^{\lambda\mu\alpha}$ are orthogonal to each other and also to the $\psi^{\lambda\mu,\alpha\beta}$. The three independent functions obtainable from the latter by permutation of the indices are, however, not orthogonal. With higher-order functions, the situation obviously becomes even more complicated. As will be seen this is not very important for our purposes. All functions of this type, for a given set of indices, are degenerate in $\mathcal{H}_0$ so that one can always choose the representation in a convenient way.

[22] This assumption is common to all attempts to calculate spin-spin interactions (see, e.g., footnote references 8 and 9).

one can write

$$E_{NN'}{}^{(2)} = -C\sum_n \frac{\langle\psi_{eq} \mid (\mathbf{S}_1{}^N\cdot\mathbf{I}^N) \mid \psi_{eq}{}^n\rangle\cdot\langle\psi_{eq}{}^n \mid (\mathbf{S}_2{}^{N'}\cdot\mathbf{I}^{N'}) \mid \psi_{eq}{}^0\rangle}{E_n - E_0} + \text{c.c.} \quad (29)$$

with the same constant C as in Eq. (28). Here $\psi_{eq}{}^0$ and $\psi_{eq}{}^2$ are eigenfunctions of $\mathfrak{IC}_{eq}$ [Eq. (7)]. The bonds in which N and N' participate are designated by N and N', respectively. The electrons in the bonds (i.e., the lower indices) are numbered in the direction from N to N' along the bonds. Therefore, we have $\mathbf{S}_1{}^N$ in Eq. (29) but $\mathbf{S}_2{}^{N'}$. This notation will be used everywhere subsequently to designate these two electrons.

It was assumed above that the valence bond model can be applied to the excited states of a molecule. Clearly this requires some sort of justification.[23]

Valence bond type wave functions constitute a complete system of functions for the molecular electrons. If Eq. (21) is expanded in terms of these functions, only very special terms in the expansion are important (i.e., those where $\psi_{eo}{}^n = \psi_{eo}{}^0$). The value of $E_{NN'}{}^{(2)}$ is therefore unsensitive to the detailed structure of the excited states. It is sufficient for our purposes if states whose orbital part is mainly $\psi_{eo}{}^0$ do exist. The assumption about the excited states is therefore much weaker than would appear.

By similar arguments it can be shown that the orbital part of the closure expression [Eq. (3)] can be integrated out (see e.g., footnote reference 8). It then follows that the evaluation of Eq. (3) with valence bond wave functions is equivalent to the evaluation of

$$E_{NN'}{}^{(2)} = -(C/\Delta E)(\mathbf{I}^N\cdot\mathbf{I}^{N'})\langle\psi_{eq}{}^0 \mid (\mathbf{S}_1{}^N\cdot\mathbf{S}_2{}^{N'}) \mid \psi_{eq}{}^0\rangle \quad (30)$$

with the Dirac vector model. In Eq. (30) the notation is the same as in Eqs. (3) and (29).

b. Method of Calculation

We will now try to evaluate the perturbation expansion of Eq. (29). In principle this could be done directly by calculating the eigenfunctions of $\mathfrak{IC}_{eq}(\psi_{eq}{}^n)$. This requires a rather tedious calculation. The same result can be obtained more directly if one uses a double perturbation procedure in the representation of $\mathfrak{IC}_0$ [Eq. (11)]. We have two types of perturbations:

(1) The electron nuclear contact interaction[24]:

$$\mathfrak{IC}_{en} = \mathfrak{IC}^N + \mathfrak{IC}^{N'} = D^N(\mathbf{S}_1{}^N\cdot\mathbf{I}^N) + D^{N'}(\mathbf{S}_2{}^{N'}\cdot\mathbf{I}^{N'}). \quad (31)$$

(2) The interbond electron interactions of the equivalent Hamiltonian (i.e., $\mathfrak{IC}_1$) given in Eq. (12).

In Eq. (31) D^N is

$$D^N = (16\pi\beta/3)\gamma_N \mid \psi_N(\mathbf{r}^N) \mid^2, \quad (32)$$

and $D^{N'}$ is defined similarly. Obviously the C of Eq. (28) is $D^N D^{N'}$.

We will now consider perturbation contributions to the ground-state energy which are linear in $\mathfrak{IC}^N$ and $\mathfrak{IC}^{N'}$ but of arbitrarily high order in $\mathfrak{IC}_1$. This is equivalent to evaluating Eq. (29) with wave functions of $\mathfrak{IC}_{eq}$ obtained by perturbing $\mathfrak{IC}_0$ with $\mathfrak{IC}_1$. Our procedure has, however, certain advantages. We only calculate the terms we need. Moreover the dependence of the results on the different exchange integrals comes out clearly.

We will show that the results of this procedure are related to those which would be obtained from the "closure" expression [Eq. (30)] in a similar way. It will then follow that the use of Eq. (30) is justified when one chooses different ΔE's for different types of terms in the double perturbation expansion. It will also be possible to estimate these ΔE's in terms of the V^α's.

We will first consider some simple cases, which are of practical interest, and then discuss in detail the situation for higher order terms.

c. Two-Electron Case

The lowest order terms in the perturbation are of zeroth order in $\mathfrak{IC}_1$. One has

$$E_0{}^{(2)} = D^N D^{N'}\sum_n \frac{\langle 0 \mid \mathbf{S}_1{}^N\cdot\mathbf{I}^N) \mid n\rangle\cdot\langle n \mid \mathbf{S}_2{}^{N'}\cdot\mathbf{I}^{N'} \mid 0\rangle}{E_n - E_0} + \text{c.c.}, \quad (33)$$

where $\langle 0 \mid$ and $\langle n \mid$ are the wave functions and E_0 and E_n the energies of $\mathfrak{IC}_0$ in the corresponding states.

The ground-state wave function ($\mid 0\rangle$) in Eq. (33) is obviously ψ_p [Eq. (15)]. From Eq. (24) it follows that

$$(\mathbf{S}_2{}^{N'}\cdot\mathbf{I}^{N'}) \mid 0\rangle = -\tfrac{1}{2}(-\tau_-{}^{N'}\mathbf{I}_x{}^{N'} + i\tau_+{}^{N'}\mathbf{I}_y{}^{N'} + \tau_0{}^{N'}\mathbf{I}_z{}^{N'})\prod_{\alpha\neq N'}\sigma^\alpha, \quad (34)$$

where the $(-)$ sign is due to the fact that the operator in (34) is $\mathbf{S}_2$ and not $\mathbf{S}_1$. The components of the nuclear spin operator $\mathbf{I}$ can be considered numbers in this context because they do not operate on the wave functions. The right-hand side of Eq. (34) then describes a definite triplet state of the electrons. Moreover one can choose the representation so that it is one of the $\mid n\rangle$'s (except for a normalization factor). The summation in Eq. (33) then reduces to a single term. The numerator is therefore identical with the diagonal element of the matrix product of the two operators,

[23] A similar method is suggested by Karplus (note 15 of footnote reference 8).

[24] $\mathfrak{IC}_{en}$ is obtained from $\mathfrak{IC}_e$ [Eq. (1)] by integrating out the orbital part of the terms involving the respective nuclei and passing to the representation of the Dirac vector model.

i.e.,

$$-\sum_n \frac{\langle 0 \mid (\mathbf{S}_1^N \cdot \mathbf{I}^N) \mid n\rangle \cdot \langle n \mid (\mathbf{S}_2^{N'} \cdot \mathbf{I}^{N'}) \mid 0\rangle}{E_n - E_0} + \text{c.c.}$$

$$= -2\frac{\langle 0 \mid (\mathbf{S}_1^N \cdot \mathbf{I}^N) \cdot (\mathbf{S}_2^{N'} \cdot \mathbf{I}^{N'}) \mid 0\rangle}{E_n - E_0}$$

$$= -\frac{2}{3\Delta E}(\mathbf{I}^N \cdot \mathbf{I}^{N'}) \langle 0 \mid (\mathbf{S}_1^N \cdot \mathbf{S}_2^{N'}) \mid 0\rangle. \quad (35)$$

This is exactly equivalent to Ramsey's result for this case. The factor of two on the right-hand side of Eq. (35) comes from the complex conjugate term in which the order of the two operators is reversed. ΔE is in this case the energy separation of the special triplet state of Eq. (34), i.e.,[25]

$$\Delta E = -2V^N. \quad (36)$$

It follows from Eqs. (18) and (19) that the matrix element in Eq. (35) is different from zero only when N and N' are directly bonded to each other (i.e., when $\mathbf{S}_1^N$ and $\mathbf{S}_2^{N'}$ operate on two electrons in the same bond).

d. Four-Electron Case

There are two types of terms of first order in $\mathcal{H}_1$, namely,

$$\sum_{n,m} \frac{\langle 0 \mid \mathbf{S}_1^N \cdot \mathbf{I}^N \mid n\rangle \cdot \langle n \mid \mathbf{S}_2^{N'} \cdot \mathbf{I}^{N'} \mid m\rangle \cdot \langle m \mid \mathbf{S} \cdot \mathbf{S} \mid 0\rangle}{(E_n - E_0)(E_m - E_0)} \quad (37)$$

and

$$\sum_{n,m} \frac{\langle 0 \mid (\mathbf{S}_1^N \cdot \mathbf{I}^N) \mid n\rangle \cdot \langle n \mid (\mathbf{S} \cdot \mathbf{S}) \mid m\rangle \cdot \langle m \mid (\mathbf{S}_2^{N'} \cdot \mathbf{I}^{N'}) \mid 0\rangle}{(E_n - E_0)(E_m - E_0)}, \quad (38)$$

where $(\mathbf{S} \cdot \mathbf{S})$ stands for any of the operators in $\mathcal{H}_1$. There are four equivalent terms of the first type all equal to Eq. (37). For a definite $(\mathbf{S} \cdot \mathbf{S})$ these correspond to the exchange of N and N' in Eq. (37) and to the complex conjugates of these terms. In the second case there are only two equivalent terms [i.e., (38) and its complex conjugate].

In Eq. (37) there is only one intermediate state $\mid n\rangle$ for the same reasons as in Eq. (33). One can therefore write

$$\sum_m \frac{1}{E_{n'} - E_0} \times \frac{\langle 0 \mid (\mathbf{S}_1^N \cdot \mathbf{I}^N) \cdot (\mathbf{S}_2^{N'} \cdot \mathbf{I}^{N'}) \mid m\rangle \cdot \langle m \mid (\mathbf{S} \cdot \mathbf{S}) \mid 0\rangle}{E_m - E_0}, \quad (39)$$

where n' is the definite triplet state involved. The state $\mid m\rangle$ is necessarily a singlet state [because $(\mathbf{S} \cdot \mathbf{S})$ has no other matrix elements]. It follows that only the scalar part of the $(\mathbf{S} \cdot \mathbf{I})$ operator in (39) contributes. Equation (37) can therefore be written in the form

$$\frac{(\mathbf{I}_N \cdot \mathbf{I}_{N'})}{3(E_{n'} - E_0)} \sum_m \frac{\langle 0 \mid (\mathbf{S}_1^N \cdot \mathbf{S}^{N'}) \mid m\rangle \cdot \langle m \mid \mathbf{S} \cdot \mathbf{S} \mid 0\rangle}{E_m - E_0}. \quad (40)$$

The terms where the order of N and N' is reversed give a similar result, and the complex conjugates of these terms give the complex conjugates of (40).

To show that Eq. (38) can be brought to a similar form, we will assume that the electrons

$$\binom{N}{1} \quad \text{and} \quad \binom{N'}{2}$$

do not belong to the same bond.[26]

There is only one intermediate state $\mid n\rangle$ and one state $\mid m\rangle$ for the reasons discussed previously. Equation (38) can therefore be written, e.g., in the form

$$(E_{m'} - E_0)^{-1} \sum_n \times \frac{\langle 0 \mid (\mathbf{S}_1^N \cdot \mathbf{I}^N) \mid n\rangle \cdot \langle n \mid (\mathbf{S} \cdot \mathbf{S})(\mathbf{S}_2^{N'} \cdot \mathbf{I}^N) \mid 0\rangle}{E_n - E_0}, \quad (41)$$

where we have suppressed the summation over m. There are now two possibilities:

(a) $\mathbf{S}_2^{N'}$ does not appear in $\mathbf{S} \cdot \mathbf{S}$

(b) one of the two electrons in $(\mathbf{S} \cdot \mathbf{S})$ is

$$\binom{N'}{2}.$$

In case (a) the two operators in the right-hand matrix element commute and one can interchange them. It can be seen from Eqs. (18) and (19) that an operator $(\mathbf{S}_i^\alpha \cdot \mathbf{S}_j^\beta)$ connects ψ_p with just one state.[27] The two operators can then be separated again by writing the matrix multiplication explicitly.

$$\sum_{n,l} \frac{\langle 0 \mid (\mathbf{S}_1^N \cdot \mathbf{I}^N) \mid n\rangle \cdot \langle n \mid (\mathbf{S}_2^{N'} \cdot \mathbf{I}^{N'}) \mid l\rangle \cdot \langle l \mid (\mathbf{S} \cdot \mathbf{S}) \mid 0\rangle}{(E_n - E_0) \cdot (E_{m'} - E_0)}. \quad (42)$$

In Eq. (42) l is a new intermediate state while $E_{m'}$ is the energy of the suppressed state $\mid m'\rangle$ in Eq. (41). The equation is of the form of Eq. (37) and differs from it only by a positive numerical factor:

$$(E_{m'} - E_0)/(E_l - E_0). \quad (43)$$

We will now consider case (b). In this case $(\mathbf{S} \cdot \mathbf{S})$ and $(\mathbf{S}_2^{N'} \cdot \mathbf{I}^{N'})$ do not commute. The commutator is

$$[(\mathbf{S}_2^{N'} \cdot \mathbf{S}), (\mathbf{S}_2^{N'} \cdot \mathbf{I}^{N'})] = i\mathbf{S}_2^{N'} \times \mathbf{S} \cdot \mathbf{I}^{N'}. \quad (44)$$

[25] ΔE is, by definition, positive, whereas the V^α are negative.

[26] If this is not true, there is a contribution of the two electron type (Sec. III.c) to the interaction of N and N'. This contribution is of lower order in the perturbation and should therefore be dominant.

[27] Namely, $\psi^{\alpha\beta}$ if $\alpha \neq \beta$ and ψ_p if $\alpha = \beta$. (The latter case is not interesting for our purposes.)

In addition to the matrix elements considered previously [i.e., Eq. (42)], we therefore get a contribution from the commutator:

$$i\sum_n \frac{\langle 0 \mid (\mathbf{S}_1^N \cdot \mathbf{I}^N) \mid n\rangle \cdot \langle n \mid \mathbf{S}_2^{N'} \times \mathbf{S} \cdot \mathbf{I}^{N'} \mid 0\rangle}{(E_n - E_0)(E_{m'} - E_0)}. \quad (45)$$

From the left there are only matrix elements to states $\mid n\rangle$ where solely the bond N is excited (i.e., the two electrons in this bond are in a triplet state). On the other hand, the operator on the right connects $\psi_P(\mid 0\rangle)$ with states where N' is excited (and possibly some other bond is excited too). As N and N' are different bonds (by assumption) the latter states are orthogonal to those "allowed" from the left. It follows that (45) vanishes.

Terms of the type of Eq. (38) are therefore, except for a positive numerical factor, equivalent to those of the type (37). It follows that they can also be brought to the form of Eq. (40).[28]

e. General Case

A general higher-order term in the perturbation expansion will have the form

$$\frac{\langle 0 \mid (\mathbf{S}\cdot\mathbf{S}) \mid i\rangle \cdots \langle j \mid (\mathbf{S}_1^N \cdot \mathbf{I}^N) \mid k\rangle \cdots \langle p \mid 0 \mid l\rangle \cdot \langle l \mid (\mathbf{S}_2^{N'} \cdot \mathbf{I}^{N'}) \mid m\rangle \cdots \langle n \mid (\mathbf{S}\cdot\mathbf{S}) \mid 0\rangle}{(E_0 - E_i)\cdots(E_0 - E_j)(E_0 - E_k)\cdots(E_0 - E_p)(E_0 - E_l)(E_0 - E_m)\cdots(E_0 - E_n)}. \quad (46)$$

We will restrict ourselves to terms of this type where every bond which appears as an index on one of the S's appears twice but only twice. Terms of this type will usually be the most important terms of a given order.

This can be seen easily when one looks on the numerator of Eq. (46) as a series of operators operating on the bonds. In the state $\mid 0\rangle$ all bonds are in σ states (i.e., no bond is excited). When an $\mathbf{S}$ operating on a given bond appears for the first time it will necessarily excite that bond (i.e., it will connect states where the bond is in a σ state only with states of the system where the bond is in a τ state). Obviously some other operator must deexcite the bond before the other end of the perturbation chain is reached. It follows that each bond has to appear at least twice in any nonzero term. Consider now the set of terms of the type (46) characterized by a definite set of bonds which are excited in their intermediate states. The lowest order terms in such a set are, obviously, those in which each bond appears only twice. One would therefore expect these terms to be dominant. In addition, terms where a bond appears more than twice will always correspond to fairly complicated ways of traversing the bonds, and it is hard to imagine molecular structures where such paths would give a larger contribution than a straightforward way along the same bonds. It should be remembered, however, that there are always several terms in $\mathcal{H}_1$ corresponding to any pair of bonds, which may cause a cancellation of terms for the direct paths.[29]

We will now demonstrate that every term of the type (46) can be written in the form

$$\tfrac{1}{3}(\mathbf{I}^N \cdot \mathbf{I}^{N'}) \frac{\langle 0 \mid (\mathbf{S}\cdot\mathbf{S}\cdot) \mid i\rangle \cdots \langle j' \mid \mathbf{S}_1^N \cdot \mathbf{S}_2^{N'}) \mid k'\rangle \cdots \langle n \mid \mathbf{S}\cdot\mathbf{S} \mid 0\rangle}{(E_0 - E_i)\cdots(E_0 - E_j)(E_0 - E_k)\cdots(E_0 - E_l)(E_0 - E_m)\cdots}, \quad (47)$$

where the same $(\mathbf{S}\cdot\mathbf{S})$ terms as in (46) appear in the numerator and the denominators are identical.

The argument is essentially similar to that used in the two previous paragraphs (Secs. IIIc and IIId).

Let us look at the first $(\mathbf{S}\cdot\mathbf{I})$ term from the right in (46). It can be considered as an operator operating on the function to the right ($\mid m\rangle$). As $\mid m\rangle$ is an eigenfunction of $\mathcal{H}_0$ it has a definite spin for the pair of electrons in any bond. Moreover, since all operators to the right are of the $(\mathbf{S}\cdot\mathbf{S})$ type, $\mid m\rangle$ is necessarily a singlet state of the system. In particular it will have a definite spin for the pair of electrons in the bond N' on which $(\mathbf{S}_2^{N'} \cdot \mathbf{I}^{N'})$ operates.

There are two possibilities:

(a) the pair N' is not excited (i.e., it is in a σ state)
(b) it is in a triplet (τ) state.

In case (a) the operator $(\mathbf{S}\cdot\mathbf{I})$ being a single bond operator, couples $\mid m\rangle$ to one definite excited state irrespective of the detailed form of $\mid m\rangle$. This is a state in which the pair N is in a definite triplet state and all other electrons are in the same configuration as in $\mid m\rangle$ [see Eq. (24)]. The situation is essentially similar to that considered in Sec. IIIc.

The next operation to the left [0 in Eq. (46)] can be either an $(\mathbf{S}\cdot\mathbf{S})$ term or the second $(\mathbf{S}\cdot\mathbf{I})$ term. In either case there is only one intermediate state and the summation over the intermediate index can be suppressed. If 0 is the $(\mathbf{S}\cdot\mathbf{I})$ term the $(\mathbf{I}\cdot\mathbf{I})$ part can be separated out and one is left with a term of the required form. As in Sec. IIId there are two possibilities when 0 is of the $(\mathbf{S}\cdot\mathbf{S})$ type. If this term does not contain $\mathbf{S}_2^{N'}$ the two operators can be commuted. To separate the matrix product we have to look at the effect of

[28] Obviously the complex conjugates of (40) can be obtained by permuting the $\mathbf{S}_1^N$ to the right instead of transferring the $\mathbf{S}_2^{N'}$ to the left.

[29] See the discussion in Sec. IV.

$(\mathbf{S}\cdot\mathbf{S})$ on $|m\rangle$. $(\mathbf{S}\cdot\mathbf{S})$ operates on two bonds each of which may be in a τ or σ state in $|m\rangle$. If it is in a τ state an operator acting on this bond has already appeared to the right. Consequently, only matrix elements of $(\mathbf{S}\cdot\mathbf{S})$ connecting $|m\rangle$ with states in which this bond is in a σ state[30] are important. Similarly, for a bond in a σ state, the only significant intermediate states are those where it is in a τ state. Separating the commuted matrix elements one obtains

$$\langle p|\,\mathbf{S}_2^{N'}\cdot\mathbf{I}^{N'})\cdot(\mathbf{S}\cdot\mathbf{S})\,|m\rangle = \sum_q \langle p|\,(\mathbf{S}_2^{N'}\cdot\mathbf{I}^{N'})\,|q\rangle\cdot\langle q|\,\mathbf{S}\cdot\mathbf{S})\,|m\rangle. \quad (48)$$

Our argument shows that only a special sort of intermediate states $|q\rangle$ is possible, namely, states in which a certain well defined group of bonds is excited and all others are in σ states.[31] All other nondiagonal elements of $(\mathbf{S}\cdot\mathbf{S})$ cannot be connected with the rest of the perturbation chain [i.e., $(\mathbf{S}_2^{N'}\cdot\mathbf{I}^{N'})$ will have no elements connecting them to $|p\rangle$]. Now the energy of a state in $\mathcal{H}_0$ depends solely on the excited bonds so that all allowed states $|q\rangle$ are degenerate. It is therefore possible to choose the representation in such a way that there is only one intermediate state $|q\rangle$. It is then possible to separate the matrix product and therefore the $(\mathbf{S}\cdot\mathbf{I})$ operator can be shifted to the right without changing the value of the numerator.

When one of the $\mathbf{S}$ in $(\mathbf{S}\cdot\mathbf{S})$ is $\mathbf{S}_2^{N'}$ the two operators do not commute, however, for the reasons discussed in the previous paragraph [Eq. (45)] the commutator does not contribute to the value of the perturbation term. To separate the permuted matrix elements in this case, one has to consider case (b).[32]

In case (b) the bond N' is in a τ state in $|m\rangle$. In $|l\rangle$ [Eq. (46)] the bond N' is therefore necessarily in a σ state. Using this fact, an argument analogous to the above leads to similar results. It can be shown that the $(\mathbf{S}\cdot\mathbf{I})$ operators can always be permuted to the right without changing the value of the numerator. In addition, whenever the two $(\mathbf{S}\cdot\mathbf{I})$ are adjacent, one can suppress the intermediate index to get a term of the form of Eq. (47).

A straightforward extension of the foregoing arguments shows that the $(\mathbf{S}\cdot\mathbf{I})$ can also be shifted to the right. Similarly it is found that the $(\mathbf{S}\cdot\mathbf{S})$ terms can be shifted and the *order* of all terms is altogether immaterial to the value of the numerator of Eq. (46) The detailed argument is too lengthy to bring here, and does not introduce any new points.

[30] Each bond appears only twice in the perturbation chain. States in which a bond is left in a τ state to the left of these two operators cannot therefore connect to the ground state.

[31] Which bonds these are will obviously depend on $|m\rangle$ and on $(\mathbf{S}\cdot\mathbf{S})$ itself.

[32] In this case the bond N' is obviously excited in the "important" intermediate states $|q\rangle$ of Eq. (48). This also applies when $\mathbf{S}_1^{N'}$ appears in $(\mathbf{S}\cdot\mathbf{S})$ even though the operators commute.

A complete perturbation expansion of the type we have considered is equivalent to the direct evaluation of Ramsey's second-order perturbation series [Eq. (2)] within the valence bond model. We have seen that all terms in such an expansion [i.e., terms of the type (46) are closely related to terms of the type (47)]. In the latter terms the electron nuclear contact interaction does not appear explicitly. It is replaced by an effective interaction of the electrons at the sites of the two nuclei whose interaction we want to calculate [i.e., $(\mathbf{S}_1^{N}\cdot\mathbf{S}_2^{N'})$], which is formally similar to the electron interaction in the closure expression [Eq. (3)]. In the following, we will use Eq. (47) to evaluate the numerators of the terms in our expansion. The similarity with Eq. (3) will enable us to compare our results with those obtained from that expression.

IV. CALCULATION OF SPIN-SPIN INTERACTION

The discussion of Sec. III reduces the evaluation of spin-spin interactions to two separate calculations. These are the evaluation of a typical numerator for each type of perturbation term and the summation of the denominators. We considered only the form of typical terms in the perturbation expansion. There are, however, four different terms in $\mathcal{H}_1$ coupling any two bonds (i.e., the terms coupling each of the two electrons in one bond to each electron in the other bond). All these terms give analogous contributions with the same denominators, which must be added together. This will give the numerators and therefore the signs of the contribution of each type of terms to the interaction constant. It will also give the dependence on the different $V_{ij}^{\alpha\beta}$ involved. The numerators are best evaluated in the reduced form [Eq. (47)] using the results of Sec. II [Eqs. (18)–(21)].

The denominator of an individual term [such as (46)] is easily evaluated. The energy separations in the intermediate states depend only on the excited bonds in these states. The factors in the denominator always have the form

$$E_n - E_0 = -2\sum_\alpha V^\alpha, \quad (49)$$

where the summation is over all the excited bonds in the intermediate state $|n\rangle$. To get the total contribution of a given type of terms, one must sum all the possible denominators for these terms.

To discuss the validity of the closure approximations [i.e., of Eq. (3)] it is convenient to introduce an effective interaction operator

$$J_{NN'}{}^{\mathrm{op}} = -\tfrac{4}{3}\nu_0(\mathbf{S}_1^{N}\cdot\mathbf{S}_2^{N'}). \quad (50)$$

This operator is related to the "closure" interaction [Eq. (30)] in the same way as $\mathcal{H}_{en}$ [Eq. (31)] is related to the electron-nuclear contact interaction [Eq. (1)]. A complete perturbation expansion to all orders in $\mathcal{H}_1$, but linear in ν_0 (i.e., of first order in $J_{NN'}{}^{\mathrm{op}}$) is equivalent to the direct evaluation of the

nuclear spin-spin interaction constant from Eq. (3) [or Eq. (30)] within the valence model. ν_0 is then defined as[33]

$$\nu_0 = D^N \cdot D^{N'}/2\Delta E. \tag{51}$$

On inserting the values for the contact interaction in atomic hydrogen, one finds

$$\nu_0{}^p \approx 4200/\Delta E \text{ cps}, \tag{52}$$

when ΔE is in electron volts.[34]

To compare the expansion based on the $J_{NN'}{}^{op}$ with the expansion based on the $\mathfrak{IC}_{en}$ we will restrict ourselves again to the most important terms. We will only consider terms where each bond which appears in the numerator appears twice. The individual terms in the expansion of $J_{NN'}{}^{op}$ will have a form

$$\frac{\langle 0 \mid (\mathbf{S}\cdot\mathbf{S}) \mid i\rangle \cdots \langle j \mid (\mathbf{S}_1{}^N \cdot \mathbf{S}_2{}^{N'}) \mid k\rangle \cdots \langle l \mid (\mathbf{S}\cdot\mathbf{S}) \mid 0\rangle}{(E_0 - E_i)\cdots(E_0 - E_j)(E_0 - E_k)\cdots(E_0 - E_l)}. \tag{53}$$

For a given coupling scheme of the bonds [i.e., for a certain set of $(\mathbf{S}\cdot\mathbf{S})$] there will always be a number of terms of the type (53) and correspondingly a (larger) set of terms of the type (46) in the expansion based on $\mathfrak{IC}_{en}$. The numerators (53) have the same form as the corresponding numerators (47). It follows that the two sets of terms all have equal numerators. Moreover, the coupling scheme determines the order of the perturbation uniquely so that all denominators will have a definite sign in both sets of terms. It is therefore always possible to choose a positive ΔE of the order of the V^α such that

$$E_{NN'}{}^e(\alpha,\beta) = -(\mathbf{I}^N \cdot \mathbf{I}^{N'})\, A(\alpha,\beta)/\Delta E(\alpha,\beta), \tag{54}$$

where $E_{NN'}{}^e(\alpha,\beta)$ is the contribution to the interaction energy of the two nuclei (N, N') from the coupling scheme (α, β) and $J(\alpha,\beta) = A(\alpha,\beta)/\Delta E(\alpha,\beta)$ is the corresponding contribution in an expansion based on $J_{NN'}{}^{op}$. In general, one will need a different $\Delta E(\alpha\beta)$ for terms of different order (and for different coupling schemes). The resulting expansion is not related to the closure formula in any simple way; however, when the interaction energy of the nuclei is mainly due to one definite coupling scheme (i.e., to one type of perturbation terms), one can use the $\Delta E(\alpha\beta)$ of that scheme as an average energy separation in the closure expression [Eqs. (3), (30), and (51)].

As we have seen, it is possible to evaluate the numerators of our perturbation terms using $J_{NN'}{}^{op}$ instead of $\mathfrak{IC}_{en}$. As $J_{NN'}{}^{op}$ is similar in form to the individual terms in $\mathfrak{IC}_1$ [Eq. (12)] it is convenient to add $J_{NN'}{}^{op}$ to $\mathfrak{IC}_1$ and then look for terms linear in ν_0 in the ground-state energy.[35]

The effect of adding $J_{NN'}{}^{op}$ to $\mathfrak{IC}_1$ is to add $2\nu_0/3$ to $V_{12}{}^{NN'}$ wherever it appears. Henceforth $\mathfrak{IC}_1$ will always denote the extended $\mathfrak{IC}_1$, i.e., $\mathfrak{IC}_1$ plus $J_{NN'}{}^{op}$ [Eq. (50)].

When N and N' are adjacent nuclei, $V_{12}{}^{NN'}$ is of the type V^α and one has by Eqs. (18) and (50) Purcell and Ramsey's result[5] for the hydrogen molecule

$$J_{NN'} = \nu_0 \tag{55}$$

which does not depend on the $V^{\alpha\beta}$.

As we have seen [Eq. (36)] one can take

$$\Delta E = -2V^N \tag{56}$$

in this case. Gutowsky, McCall, and Slichter[7] use a similar model for interactions between adjacent nuclei in more complicated molecules. Evidently, this first-order contribution is dominant in these cases,[36] which justifies the use of Eq. (3). Footnote references 5 and 7 both use a simple Heitler-London wave function (i.e., they assume a perfect pairing ground state). This is equivalent to the complete neglect of $\mathfrak{IC}_1$ and is therefore identical with our treatment. Equation (56) for ΔE is in reasonable agreement with experimental results.

Second-order perturbation gives only one interesting term:

$$E^{(2)} = \langle \psi^p \mid \mathfrak{IC}_1 \mid \psi^{NN'}\rangle \cdot \langle \psi^{NN'} \mid \mathfrak{IC}_1 \mid \psi^p\rangle/(E_0 - E_{NN'})$$
$$= 3(Q^{NN'} + 2\nu_0/3)^2/8(V^N + V^{N'}), \tag{57}$$

and the term linear in ν_0 is

$$J_{NN'}{}^{(2)} = \nu_0 \cdot Q^{NN'}/2(V^N + V^{N'}). \tag{58}$$

A typical numerator [of Eqs. (37) and (38)] is, in this case

$$-\tfrac{1}{8}(\sqrt{3}/2)Q^{NN'} \cdot (\sqrt{3}/4) D^N D^{N'} = -\tfrac{1}{8} D^N D^{N'} Q^{NN'} \tag{59}$$

as can be seen from Eqs. (40), (19), and (21).[37] This is the numerator of all terms (37) and (38). For the denominators we have from the four terms (37) [using Eqs. (18) and (20)]

$$\tfrac{1}{4}[(V^N)^{-1} \cdot (V^N + V^{N'})^{-1} + (V^{N'})^{-1} \cdot (V^N + V^{N'})^{-1}$$
$$+ (V^N + V^{N'})^{-1} \cdot (V^N)^{-1} + (V^N + V^{N'})^{-1} \cdot (V^{N'})^{-1}]$$
$$= \tfrac{1}{2} \cdot [(V^N)^{-1} + (V^{N'})^{-1}] \cdot (V^N + V^{N'})^{-1}. \tag{60}$$

The two terms (38) give

$$2/4V^N V^{N'}. \tag{61}$$

[33] This definition is consistent with Ramsey's definition of ΔE. The factor of $\frac{1}{3}$ is the weight of the scalar part in $(\mathbf{S}\cdot\mathbf{I})\cdot(\mathbf{S}\cdot\mathbf{I})$ and the factor of two is due to the two different orders in which N and N' appear in the original series.

[34] In (52) polar states are altogether neglected. It is, of course, possible to correct partially for the polarity if one uses the actual electron concentration at the site of the proton in the molecule instead of the atomic value.

[35] In this connection ν_0 is not really defined by Eq. (51) but rather serves as a label for the terms we are looking for.

[36] One would expect corrections due to the polar part of the wave function to be more important than the higher-order corrections. Moreover, for H_2 there are no corrections of the type we consider.

[37] All $(\mathbf{S}\cdot\mathbf{S})$ appear with a factor of 2 in $\mathfrak{IC}_1$ whereas $(\mathbf{S}_1{}^N \cdot \mathbf{S}_2{}^{N'})$ appears only once in (47).

On summing (60) and (61), one finds for the interaction constant

$$J_{NN'}{}^{2} = -(D^N D^{N'} Q^{NN'}/8V^N V^{N'}). \quad (62)$$

When the proper ΔE for these terms is inserted in ν_0, the two expressions for $J_{NN'}$ should be equal. Comparison of Eqs. (58) and (62) gives

$$(\Delta E)^{-1} = -[(2V^N)^{-1} + (2V^{N'})^{-1}] \approx V^{-1}. \quad (63)$$

This is about half the value of ΔE in the two electron case [Eq. (36)]. The reduction is due to the terms of Eq. (38), i.e., to the effect of the perturbation $\mathcal{H}_1$ on the excited states.

It can be seen from Eq. (62) that $J_{NN'}{}^{(2)}$ will have the opposite sign from $Q^{NN'}$.

The terms we have considered should be dominant for protons two bonds apart. When the separation is larger, one always has terms of the type (62). However, the $V^{\alpha\beta}$ decrease with the geometric separation between the bonds α and β. Terms which contain only $V^{\alpha\beta}$ between adjacent bonds may therefore be important even when they appear only to higher order in the perturbation.

The third-order perturbation to the ground-state energy contains a term of the type

$$E^{(3)} = \sum_{i,j\neq 0;\, i\neq j} \frac{\langle 0 \mid \mathcal{H}_1 \mid i\rangle \cdot \langle i \mid \mathcal{H}_1 \mid j\rangle \cdot \langle j \mid \mathcal{H}_1 \mid 0\rangle}{(E_0 - E_i)\cdot(E_0 - E_j)}, \quad (64)$$

where all intermediate states are different. This is the only third-order term which interests us.[38]

For the numerator we only need one typical case. On considering the case when all intermediate states are of the type $\psi^{\lambda\mu}$, one finds from Eqs. (18)–(21)

$$-D^N D^{N'} Q^{NI} Q^{IN'}/16, \quad (65)$$

where we have used the fact that the bonds N and N' always appear and therefore there is only one new excited bond (I). Summation of the denominators gives

$$J_{NN'}{}^{(3)} = -(D^N D^{N'} \cdot Q^{NI} Q^{N'I})/(16V^N \cdot V^{N'} \cdot V^I). \quad (66)$$

The corresponding ΔE is then found to be

$$-(\Delta E)^{-1} = \tfrac{1}{2}[(V^N)^{-1} + (V^{N'})^{-1} + (V^I)^{-1} - (V^N + V^I + V^{N'})^{-1}] \approx \tfrac{4}{3}\cdot V^{-1}. \quad (67)$$

Thus the third-order ΔE is even smaller than the second-order one. It is certainly much smaller than the separation of the first triplet state which is of the order of $2V$.

The extension to higher-order terms is quite straightforward. Higher order perturbations will always contain terms similar to Eq. (64) where all intermediate states are different. Only these terms, i.e., terms of the type

$$E^{(m)} = \sum_{i\neq j\neq \ldots \neq k\neq 0} \frac{\langle 0 \mid \mathcal{H}_1 \mid i\rangle \cdot \langle i \mid \mathcal{H}_1 \mid j\rangle \cdots \langle k \mid \mathcal{H}_1 \mid 0\rangle}{(E_0 - E_i)(E_0 - E_j)\cdots(E_0 - E_k)}. \quad (68)$$

need be taken into consideration. All other terms contain fewer intermediate states and the $V^{\alpha\beta}$ which appear will already have made a contribution to terms in lower order perturbations, which should be more important. The corresponding numerators will be products of ν_0 and a number of $Q^{\alpha\beta}$ (the number depending on the order of the perturbation term). Both the numerators and the denominators are easily evaluated by the methods previously discussed.

Each perturbation term (68) can be looked upon as a certain path between N and N' along the bonds. The different terms in $\mathcal{H}_1$ have different ranges depending on the separation between the two bonds on which they act. Long-range terms will naturally tend to appear in lower order perturbations because they bridge a larger part of the separation between the two nuclei. As one expects the $V^{\alpha\beta}$ to decrease with the separation of the bonds, it seems probable that the largest perturbations will be such that the sum of the ranges of the terms in the numerator is just sufficient to bridge the separation of N and N'.[39]

V. RESULTS AND DISCUSSION

As can be seen from Eqs. (55), (62), and (66), the signs of spin-spin interactions depend on the signs of the $Q^{\alpha\beta}$ and on the relative magnitude of different order contributions. If, for example, the dominant perturbations are those involving only terms of range one in $\mathcal{H}_1$, and the corresponding Q's are all positive, the signs of the interactions will alternate with the number of bonds separating the two nuclei. The $V^{\alpha\beta}$ certainly tend to decrease as the separation of the two bonds increases. However the Q's are sums of four terms [Eq. (22)] and their signs and magnitudes depend on a rather delicate balance between these terms. For adjacent bonds, V_{21}, which corresponds to two orthogonal orbits belonging to the same atom, is usually positive and relatively large. If the other terms are small, one will therefore get a positive Q (as McConnell[11] suggests). This effect is, however, counteracted by the overlap contribution to V_{12} and possibly by positive values for V_{11} and V_{22} (see Fig. 1).

It is interesting to compare Karplus' results[8] for methane with our results. Clearly this is a two-bond case so that Eqs. (58) and (62) should apply. Inserting Karplus' values for the exchange integrals one finds

$$Q/4V = (\beta + \gamma - 2\delta)/4\alpha \approx 1/31, \quad (69)$$

where α is the V^{α} of the C—H bond and β, γ, and δ

[38] The other terms in the third-order perturbation contain only one intermediate state and corresponding terms in the second-order perturbation will make a more important contribution.

[39] Incidentally, this also shows why π—σ interactions in a double bond should not be important. These interactions have zero range so that perturbation terms involving them are always of higher order in the perturbation than others which otherwise involve similar Q's.

are respectively V_{12}, V_{21}, and $V_{11}(=V_{22})$ in our notation.

It follows that

$$J_{NN'}=+135/\Delta E \text{ cps}, \tag{70}$$

which means a ΔE of 11 ev in reasonable agreement with Karplus' value of 9 ev.[40] Equation (63) would however give about half this value, i.e.,

$$\Delta E \approx \alpha = 3.8 \text{ ev}. \tag{71}$$

The reduction in the expected value of ΔE is due to the terms of Eq. (38). If only terms of the type (37) were considered, one would get twice the value of ΔE. This would certainly improve the agreement with experiment. Such a procedure does not seem justified. The terms (38) reflect the effect of the electron interactions (i.e., $\mathcal{H}_1$) on the excited (triplet) states. These effects do not appear explicitly in a calculation with the reduced interaction [Eq. (50)], even though they can be represented by it formally. As we have seen, these effects are similar in magnitude to the effects of $\mathcal{H}_1$ on the singlet states, and there is no reason to neglect them.

It follows from Karplus' calculation that Q is negative (and J positive) in methane. The large terms $V_{12}(\beta)$ and $V_{21}(\gamma)$ exactly cancel each other, but V_{11} and $V_{22}(\delta)$ are positive, which makes Q negative

In general, the case of the two protons bonded to the same carbon atom is very similar to that of methane. Such interactions were studied in detail by Gutowsky Karplus, and Grant.[3] The positive value of the interaction in methane is, as we saw, due to the large negative contribution of V_{12} to Q. This is the exchange integral between the two hydrogen atomic orbits and its negative value comes from the overlap of these orbits. V_{12} should decrease in absolute value as the separation between the protons increases, i.e., as the bond angle increases. Other things remaining equal, one therefore expects the (positive) interaction constant to decrease as the bond angle gets larger, till it eventually passes through zero to negative values. As the interaction is determined mainly by the difference of two large quantities (V_{12} and V_{21}), it is rather sensitive to changes in V_{12}.[41]

Experimental results seem to confirm the preceding qualitative conclusions. Interactions among protons bonded to the same carbon atom[42] tend to be rather small and are of the same order as the interactions between protons separated by three bonds. In particular measurements were carried out in many ethylene derivatives[43] where some information on the sign could also be obtained. The interaction between protons bonded to the same carbon is consistently found to be very small in these compounds (of the order of 2 cps). This agrees with the expected decrease in the interaction constant with increasing bond angle. In most cases, the interaction is found to have the same sign as the other (three bond) interactions in the ethylene group, which are probably positive. It is, however, interesting to note that it has a different sign from these interactions in vinyl bromide.[3]

For two adjacent bonds one expects the four electron terms [Eq. (58)] to be dominant. Under this assumption the treatment of GKG[3] is practically equivalent to ours,[44] except for the difficulties mentioned which concern the value of ΔE.

Interactions across three bonds (e.g., J_{13}, J_{23}, J_{3m}, and J_{mm} of Table III, footnote reference 4), have been treated by Karplus.[9] He finds that such interactions should be positive. It is very inviting to assume that this is due to the positive value predicted by Eq. (66) for third-order terms with Q's of equal signs. It seems, however, that this is not the case.

One can express Karplus' ground-state wave functions (Tables I and II of footnote reference 9) in terms of the orthogonal functions we use.[45] It is then found that the contribution of $\psi^{NN'}$ to the ground-state wave function is of the same order as the contributions of ψ^{NI} and $\psi^{IN'}$. This means that $Q^{NN'}$ is of the same order as the Q^{NI} and consequently the direct contribution [Eq. (58)] is dominant. The positive sign found for these interactions is due to the negative sign of $Q^{NN'}$. In fact, one can see that the indirect contribution (which comes from the cross terms of ψ^{NI} and $\psi^{IN'}$) is quite negligible. It is probably for this reason that the total neglect of the π orbitals[9] is not important. Again we see that only one type of term is important so that the use of a closure expression is justified.

---

[40] Karplus uses wave functions of tetrahedral symmetry and diagonalizes the second-order secular equations exactly, whereas our treatment is a perturbation calculation based on a two-bond picture. This may be the reason for the discrepancy in the "empirical" ΔE's. [See, however, footnote 44.]

[41] G K G[3] find that V_{11} (which in these cases is equal to V_{22}) is positive and also decreases as the bond angle increases. This enhances the above effect.

[42] In methane the interaction constant is 12.4 cps [M. Karplus, D. H. Anderson, T. C. Farrar, and H. S. Gutowsky, J. Chem. Phys. **27**, 597 (1957)]. We have found, e.g., the same value for the interaction between the methylene protons in 2-methyl 2-nitro 1,3- propane diol.

[43] See, e.g., footnote references 1, 3, and 4.

[44] The only real difference is that they solve the respective second-order secular equation exactly, whereas Eq. (58) is derived by a perturbation treatment. If one substitutes the values of the V_{ij} and ΔE from Figs. 2 and 3 of footnote reference 3 in Eq. (58), one gets values for the spin-spin interactions which differ from their values by 10–20% at the most. The magnitude of this difference seems surprising since the "error" in the perturbation treatment is certainly smaller.

[45] The connections are as follows:

$$\psi_0=\psi^P$$

$$\psi_1=-\tfrac{1}{2}\psi^P-\tfrac{3}{2}\psi^{NN'}$$

$$\psi_2=\tfrac{3}{4}\psi^{NIN}-\tfrac{3}{4}\psi^{NN'}-\tfrac{3}{4}\psi^{NI}-\tfrac{3}{4}\psi^{IN'}-\tfrac{1}{4}\psi^P$$

$$\psi_3=-\tfrac{1}{2}\psi^P-\tfrac{3}{2}\psi^{NI}$$

$$\psi_4=-\tfrac{1}{2}\psi^P-\tfrac{3}{2}\psi^{IN'},$$

where the ψ_i are defined in footnote reference 9 and we use the notation of Eq. (66) to denote the orbits on the right.

Note added in proof: In a recent paper [J. Chem. Phys. **33,** 941 (1960)] M. Karplus has used arguments somewhat similar to ours to justify the closure approximation.

ACKNOWLEDGMENTS

The author wishes to thank Professor S. Meiboom for guidance and help in the early stages of this work, and Professor W. Low, Professor H. J. Lipkin, and A. Szoke for helpful discussions.

APPENDIX

McLachlan[16] has recently pointed out that the closure procedure used by Ramsey[6] is not justified. In particular, he points out that the average energy separation (ΔE) of Eq. (3) need not be positive or of the order of the energy separations in the molecule. It seems worthwhile to discuss these objections in some detail.

Second-order perturbation theory gives for the ground-state energy

$$E^{(2)}=-\sum_n \frac{\langle 0 \mid \mathcal{H}_1 \mid n\rangle \cdot \langle n \mid \mathcal{H}_1 \mid 0\rangle}{E_n-E_0}, \qquad \text{(A1)}$$

where $\mathcal{H}_1$ is the perturbation and the summation is over all states of some unperturbed Hamiltonian ($\mid n\rangle$). When the excited states are not known, one may try to estimate $E^{(2)}$ from an expression

$$E^{(2)}=-\langle 0 \mid \mathcal{H}_1^2 \mid 0\rangle/\Delta E \qquad \text{(A2)}$$

which involves only ground-state wave functions. Equation (A2) may be regarded as a definition for ΔE.

All the numerators in the summation (A1) are positive because $\mathcal{H}_1$ is Hermitian. The denominators are positive too because E_0 is the ground-state energy. It is therefore clear that the ΔE defined in Eq. (A2) is positive and is some properly weighted average of the energy separations (E_n-E_0).

The case of spin-spin interactions is, however, different. There are two perturbations[46] (say, $\mathcal{H}_N$ and $\mathcal{H}_{N'}$) and the interesting terms are the cross terms between them. The interaction energy

$$E_{NN'}{}^{(2)}=-\sum_n \frac{\langle 0 \mid \mathcal{H}_N \mid n\rangle \cdot \langle n \mid \mathcal{H}_{N'} \mid 0\rangle}{E_n-E_0}+\text{c.c.} \qquad \text{(A3)}$$

is estimated by

$$E_{NN'}{}^{(2)}=-\langle 0 \mid \mathcal{H}_N\mathcal{H}_{N'}+\mathcal{H}_{N'}\mathcal{H}_N \mid 0\rangle/\Delta E_{NN'}. \qquad \text{(A4)}$$

Obviously Eq. (A4) is a legitimate definition of $\Delta E_{NN'}$. The numerators of (A3) can, however, have different signs. As the individual terms are weighted differently in (A3) and in (A4), it is not, in general, possible to say anything about the sign or magnitude of $\Delta E_{NN'}$. It is therefore clear that an equation such as (A4) [e.g., Eq. (3)] are not very useful.

It is interesting to see what the conditions for a "good" $\Delta E_{NN'}$ are. The total contribution of the two perturbation is

$$\begin{aligned} E^{(2)}&=-\sum_n \frac{\langle 0 \mid \mathcal{H}_N+\mathcal{H}_{N'} \mid n\rangle \cdot \langle n \mid \mathcal{H}_N+\mathcal{H}_{N'} \mid 0\rangle}{E_n-E_0} \\ &=-\langle 0 \mid (\mathcal{H}_N+\mathcal{H}_{N'})^2 \mid 0\rangle/\Delta \\ &=-\frac{\langle 0 \mid \mathcal{H}_N{}^2 \mid 0\rangle}{\Delta}+\frac{\langle 0 \mid \mathcal{H}_{N'}{}^2 \mid 0\rangle}{\Delta} \\ &\quad +\frac{\langle 0 \mid \mathcal{H}_N\mathcal{H}_{N'}+\mathcal{H}_{N'}\mathcal{H}_N \mid 0\rangle}{\Delta}, \end{aligned} \qquad \text{(A5)}$$

where Δ is a positive "good" average energy separation. Similarly one has for the separate contributions of $\mathcal{H}_N$ and $\mathcal{H}_{N'}$:

$$E_N{}^{(2)}=-\sum_n \frac{\langle 0 \mid \mathcal{H}_N \mid n\rangle \cdot \langle n \mid \mathcal{H}_N \mid 0\rangle}{E_N-E_0}=-\frac{\langle 0 \mid \mathcal{H}_N{}^2 \mid 0\rangle}{\Delta_N} \qquad \text{(A6a)}$$

and

$$E_{N'}{}^{(2)}=-\frac{\langle 0 \mid \mathcal{H}_{N'}{}^2 \mid 0\rangle}{\Delta_{N'}}. \qquad \text{(A6b)}$$

Δ_N and $\Delta_{N'}$ are, obviously, also positive and "good." Now

$$E^{(2)}=E_N{}^{(2)}+E_{N'}{}^{(2)}+E_{NN'}{}^{(2)} \qquad \text{(A7)}$$

and therefore the $\Delta E_{NN'}$ of Eq. (A4) will be positive and of the same order as the other Δ's if Δ_N and $\Delta_{N'}$ are "sufficiently" close to Δ. The stringency of this condition depends on the relative magnitude of $\mathcal{H}_N{}^2$, $\mathcal{H}_{N'}{}^2$, and $\mathcal{H}_N\mathcal{H}_{N'}$.

To check this $E^{(2)}$, $E_N{}^{(2)}$, and $E_{N'}{}^{(2)}$ must be known with an accuracy which is at least of the order of the magnitude of $E_{NN'}{}^{(2)}$.

[46] That is the interaction of each of the two nuclei with the molecular electrons.

Moment Analysis of Magnetic Resonance Signals*

PETER H. VERDIER, E. B. WHIPPLE, AND VERNER SCHOMAKER

Union Carbide Research Institute, Tuxedo, New York

(Received April 14, 1960)

A relation is given between the moments of a generalized convolution transform of a function, and the moments of the function itself. This relation is applied to the signal obtained with a field-modulated EPR spectrometer, a consequence being that the integrated intensity of an absorption line may be obtained from first moment measurements at any modulation amplitude, regardless of line shape or various instrumental nonidealities. This result has been verified experimentally to within a few percent with a Varian EPR spectrometer. Extension to measurement of higher moments is discussed.

LET two functions, $\Phi(y)$ and $\psi(y)$, be related by (1), where α, β, and the region R of integration are arbitrary,

$$\Phi(y)=\int_R\cdots\int\psi[y-\alpha(x_1,\cdots,x_r)]\times\beta(x_1,\cdots,x_r)dx_1\cdots dx_r. \quad (1)$$

Then the nth moment

$$\Phi_n=\int_{-\infty}^{\infty}y^n\Phi(y)dy$$

can be expressed as a linear combination of the nth and lower moments of ψ; i.e.,

$$\Phi_n=\sum_{j=0}^{n}C_{nj}\psi_j, \quad (2)$$

where the coefficients are given by

$$C_{nj}=\binom{n}{j}\int_R\cdots\int\alpha^{n-j}(x_1,\cdots,x_r)\beta(x_1,\cdots,x_r)dx_1\cdots dx_r \quad (3)$$

and are independent of ψ. Equations (2) and (3) are readily verified by writing Φ_n in terms of (1), inverting the order of integration, and making the change of variable $u=y-\alpha(x_1,\cdots,x_r)$.

The transformation (1) of ψ into Φ may be used to represent the effect of a variety of distortions introduced into the measurement of a function $\psi(y)$ by a linear apparatus. Examples are the effects of constant slit width in optical spectroscopy, arbitrary frequency response of linear electrical or mechanical networks, and certain types of modulation and demodulation.[1]

The application to magnetic resonance spectrometers employing sinusoidal field modulation and synchronous detection is of considerable practical interest, since sensitivity limitations often require modulation amplitudes sufficient to distort the signals from their limiting derivative shapes.[2-5] Analysis in terms of Eq. (2) is particularly appropriate to this problem, since many of the spectral parameters of principal interest can be obtained directly from the lower moments.[6-8]

If $\psi(h)$ represents energy absorption as a function of magnetic field, the signal entering the spectrometer amplifier at fixed h is $\psi(h-H_m\sin\omega t)$, where H_m is the amplitude and ω the angular frequency of the modulating field. The effects of amplifier response and synchronous demodulation can then be represented by a function β in the transformation (1), where $\Phi(h)$ is the observed output of the spectrometer. Since the amplifier does not pass dc, the coefficients C_{nn} vanish, leaving only lower moments of ψ in the expressions for Φ_n. In particular, Φ_0 must vanish and Φ_1, the first moment of the observed curve, is directly proportional to the product of H_m and ψ_0, the integrated intensity, regardless of distortion due to modulation amplitude broadening, amplifier and detector response, detector misphasing, or main-field inhomogeneity. This proportionality is strictly independent of details of line shape and may, for example, be used to obtain the integrated intensity of partially resolved multiplets.

The expressions (2) for the higher moments are simplified by the symmetry of the modulating and demodulating functions, which causes C_{nj} to vanish for $n-j$ even. A proportionality similar to the foregoing

* Advanced Research Projects Agency support is gratefully acknowledged.

[1] The relations (1)–(3) have been given by Flynn and Seymour[6] for the case when $\alpha(x)=x$, and R is $-\infty<x<\infty$, i.e., a convolution transform. It can be shown that every transformation of the form (1) can be written as a convolution, in which case the relations (2), (3) take on a simpler form: If $f*g$ denotes the convolution of f and g, then

$$(f*g)_n=\sum_{j=0}^{n}\binom{n}{j}f_jg_{n-j},$$

where the subscripts denote moments, as before. However, in practical application it may be easier to write the transformation in the more general form (1) than to obtain an equivalent convolution transform.

[2] M. M. Perlman and M. Bloom, Phys. Rev. **88**, 1240 (1952).

[3] E. R. Andrew, Phys. Rev. **91**, 425 (1953).

[4] O. E. Myers and E. J. Putzer, J. Appl. Phys. **30**, 1987 (1959).

[5] A different approach has been formulated by Spry (footnote 9), who has applied the "unfolding" technique of Stokes [A. R. Stokes, Proc. Phys. Soc. (London) **61**, 382 (1948)] to the analysis of magnetic resonance lines.

[6] C. P. Flynn and E. F. W. Seymour, Proc. Phys. Soc. (London) **75**, 337 (1960).

[7] J. H. Van Vleck, Phys. Rev. **74**, 1168 (1958).

[8] W. Anderson and H. M. McConnell, J. Chem. Phys. **26**, 1496 (1957).

then exists between the experimental second moment and true first moment, which defines the centroid of the line. The method is readily extended in principle to a determination of the higher ψ_j. For example, in spectrometers with very narrow band pass the second moment correction inferred by Andrew[3] from a Taylor series expansion is verified for all H_m.

It is possible to obtain values of the coefficients in Eq. (2) experimentally, rather than analytically. Since C_{nj} is proportional to H_m^{n-j}, as may be seen from Eq. (3), the C_{nj} may be determined by measuring each moment at several modulation amplitudes and fitting the resulting Φ_n to polynomials in H_m. Alternatively, the response of the spectrometer to a δ-function input may be determined as suggested by Spry.[9] It can easily be shown that C_{nj} is just the $(n-j)$-th moment of the response of the system to a δ-function input.

As a test of practical applicability, we have studied EPR spectra of a powdered DPPH sample with a Varian Associates Model V-4500 EPR spectrometer using a V-4007 6-in. magnet system at 80 cps field modulation. Since demodulation is accomplished by a synchronous reversing switch, odd harmonics in the input contribute to the output. The spectrometer amplifier, tuned to 80 cps, was found to have relative gains of 1, $\frac{1}{7}$, and $\frac{1}{10}$ at 80, 200, and 400 cps.

The relative gains of the amplifier at different gain settings were determined by measuring dc output with a Leeds and Northrup Type K potentiometer. Ratios of modulation field strengths were obtained by measuring the voltage across the modulation coils with a Ballantine voltmeter.

The DPPH absorption was recorded at modulation ranging from one-quarter to eight times the peak-to-peak linewidth. The wings of the absorption curves were always recorded at higher gain than were the central portions. Zeroth and first moments were obtained for each modulation amplitude. The zeroth moments were always less than 4% of the respective half-curve areas.

TABLE I. Observed first moment G_1 vs relative field modulation amplitude H.

H	1.00	8.33	15.8	31.2
G_1/H	3.26	3.21	3.18	3.12

The observed first moment G_1 is given in Table I for various relative settings of the modulation amplitude H. The ratio G_1/H, which in principle should be proportional to the total absorption intensity and independent of H, is constant to within 5% over the range of H chosen. In particular, the values of G_1/H at relative modulation amplitudes of 8.3 and 1, which are about twice and one-quarter the peak-to-peak linewidth, respectively, differ by less than 2%. Thus to this accuracy, the modulation amplitude for intensity measurements may be chosen anywhere between the small-amplitude derivative limit and the amplitude which yields maximum signal strength.

Attempts to obtain third moments revealed that the calculated integrals were not converging in the wings, although measurements ranged to thirty-six times the peak-to-peak linewidth, or four times the maximum modulation amplitude employed. In contrast, the first-moment integrals were clearly converging; the slight decrease of G_1/H with increasing H is probably a result of small losses in the wings. It is clear that measurement of third and higher moments will require spectra over a considerably wider range than has been employed here, in order to obtain convergence.

[9] W. J. Spry, J. Appl. Phys. **28**, 660 (1957).

THE JOURNAL OF CHEMICAL PHYSICS VOLUME 34, NUMBER 1 JANUARY, 1961

Free-Volume Model of the Amorphous Phase: Glass Transition

DAVID TURNBULL

General Electric Research Laboratory, Schenectady, New York

AND

MORREL H. COHEN

University of Chicago, Chicago, Illinois

(Received August 1, 1960)

Free volume v_f is defined as that part of the thermal expansion, or excess volume $\Delta\bar{v}$ which can be redistributed without energy change. Assuming a Lennard-Jones potential function for a molecule within its cage in the condensed phase, it can be shown that at small $\Delta\bar{v}$ considerable energy is required to redistribute the excess volume; however, at $\Delta\bar{v}$ considerably greater than some value $\Delta\bar{v}_g$ (corresponding to potentials within the linear region), most of the volume added can be redistributed freely. The transition from glass to liquid may be associated with the introduction of appreciable free volume into the system. Free volume will be distributed at random within the amorphous phase and there is a contribution to the entropy from this randomness which is not present in the entropy of the crystalline phase. According to our model all liquids would become glasses at sufficiently low temperature if crystallization did not intervene. Therefore whether or not a glass forms is determined by the crystallization kinetic constants and the cooling rate of the liquid. The experience on the glass formation is consistent with the generalization: at a given level of cohesive energy the glass-forming tendency of a substance in a particular class is greater the less is the ratio of the energy to the entropy of crystallization.

IN earlier publications[1,2] the authors discussed the glass transition and the factors which determine whether an undercooled liquid will solidify to a glass or to a crystalline body. We concluded, on the basis of a simple free-volume theory[3] of molecular transport, that any liquid, when sufficiently undercooled, would solidify to a glass if crystallization did not intervene.[2] From this it follows that whether or not a liquid forms a glass is determined by the magnitude of the crystallization kinetic constants (i.e., the nucleation frequency and the crystal growth rate) and the rate at which the liquid is cooled. We showed that the experience on glass formation is, on the whole, consistent with the generalizations about the magnitudes of the crystallization kinetic constants.

In the earlier papers we did not explicitly define the free volume in microscopic terms nor did we justify the temperature dependence of the free volume which is necessary to account for the molecular transport behavior. Also we did not specifically relate glass-forming tendency to molecular constitution. We have now partly removed this incompleteness in the earlier treatment by developing further the free volume model. This development, though qualitative, illuminates the concept of free volume and leads to a plausible explanation for its temperature dependence through the glass transition. A further outcome of the present development is a more general criterion for glass-forming tendency which permits qualitative interpretation of the effect of molecular constitution. A detailed application of this criterion will appear in a forthcoming review article.[4] A more quantitative development of the free-volume model and its use in interpreting the thermodynamic behavior of amorphous phases will be presented in a later paper.

FREE-VOLUME MODEL OF THE AMORPHOUS PHASE

In molecularly simple substances the "transition" from liquid to glass is manifested by marked changes in viscosity, specific heat, and thermal expansion coefficient within a narrow temperature interval centering about a "glass transition temperature" T_g. Kauzman[5] has pointed out that the extrapolated specific values of the volume, energy, and entropy of molecularly simple liquids become less than the corresponding values for the crystal at temperatures well below T_g. Actually the magnitude of these properties always remains larger in the amorphous than in the crystalline phase because of the intervention of the glass transition as illustrated schematically in Fig. 1 for the specific volume. Such behavior suggests, as Gibbs and DiMarzio[6] have pointed out, that there may exist a uniquely defined amorphous state at low temperatures characterized by minimum specific volume-temperature

[1] D. Turnbull and M. H. Cohen, J. Chem. Phys. **29,** 1049 (1958).

[2] M. H. Cohen and D. Turnbull, J. Chem. Phys. **31,** 1164 (1959).

[3] The first developments of the free volume model of the liquid state are due to Eyring and associates [(a) H. Eyring, J. Chem. Phys. **4,** 283 (1936); J. O. Hirschfelder, D. P. Stevenson, and H. Eyring, J. Chem. Phys. **5,** 896 (1937)] and to Lennard-Jones and Devonshire (b) J. E. Lennard-Jones and A. F. Devonshire, Proc. Roy. Soc. (London) **A163,** 53 (1937); **A169,** 317 (1939)]. The model has been further developed and applied in many subsequent investigations.

[4] D. Turnbull and M. H. Cohen in *Modern Aspects of the Vitreous State*, edited by J. D. Mackenzie (Butterworths Scientific Publications, Ltd., London, 1960).

[5] W. Kauzman, Chem. Rev. **43,** 219 (1948).

[6] J. H. Gibbs and E. A. DiMarzio, J. Chem. Phys. **28,** 373 (1958).

and specific energy-temperature relations which still lie above the corresponding relations for the crystal. This state should be realized, when the liquid is cooled very slowly and constrained so as not to crystallize, at some temperature well above the absolute zero. Gibbs and DiMarzio have presented a statistical mechanical justification of these concepts as applied to polymer systems.

Our previous discussion of the glass transition[1,2] has implicitly identified the glassy state with this uniquely defined amorphous state. Because no structure change appears to accompany the glass transition and because the transition occurs over a range of temperature, we have supposed that the liquid and glass belong to a single thermodynamic phase.[2] If the glass transition is not a thermodynamic phase change, then what is it?

We believe the answer lies in the hypothesis advanced by Fox and Flory[7] that this transition results from the decrease of the free volume of the amorphous phase below some small characteristic value. With this hypothesis Williams, Landel, and Ferry[8] were able to show that the dependence of fluidity ϕ on temperature in the glass transition region is satisfactorily described by the Doolittle[9] equation

$$\phi = A \exp[-(q v_0/v_f)], \tag{1}$$

where q is a constant of order unity, v_0 is the volume of a molecule, $\bar{v}$ is the specific volume, and the free volume v_f is defined as

$$v_f = \bar{v} - v_0. \tag{1a}$$

(We expect v_0 to be pressure dependent, though at large free volume this dependence may be, for most purposes, negligible.)

The authors[2] have derived an expression for the self-diffusion coefficient of a liquid having the same form as the Doolittle equation. Our derivation was based on the assumptions:

(1) Molecular transport may occur only when voids having a volume greater than some critical value v^* form by the redistribution of the free volume.

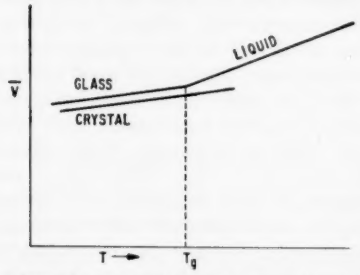

FIG. 1. Schematic specific volume ($\bar{v}$)-temperature relations for amorphous and crystalline phases of a substance.

[7] T. G. Fox and P. J. Flory, J. Appl. Phys. **21,** 581 (1950); J. Phys. Chem. **55,** 221 (1951); J. Polymer Sci. **14,** 315 (1954).
[8] M. F. Williams, R. F. Landel, and J. D. Ferry, J. Am. Chem. Soc. **77,** 3701 (1955).
[9] A. K. Doolittle, J. Appl. Phys. **22,** 1471 (1951).

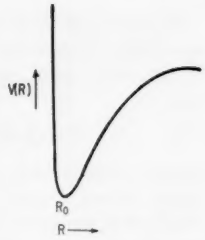

FIG. 2. Schematic diagram showing work $V(R)$ at 0°K required to remove a molecule from the cage formed by its nearest neighbors as a function of the cage radius R.

(2) No energy is required for free volume redistribution.

The resulting expression is as follows:

$$D = g a^* u \exp[-\gamma v^*/v_f], \tag{2}$$

where g is a geometric factor usually taken to be $\frac{1}{6}$, a^* is a molecular diameter, u is the gas kinetic velocity, and γ is an overlap factor which should lie between $\frac{1}{2}$ and unity.

According to the foregoing arguments, the problem of explaining the glass transition is reduced to that of explaining the temperature dependence of the free volume; however, before we can develop such an explanation we must specify the concept of free volume more precisely.

Consider a molecule in a cage formed by its nearest neighbors. If the potential energy of pairwise molecular interaction is described by the Lennard-Jones potential function, the work $V(R)$ at 0°K required to take a molecule from the center of its cage into the vacuum will vary with the cage radius R as shown schematically in Fig. 2. This function $V(R)$ has a minimum at R_0 and rises steeply as R decreases for $R<R_0$. At $R>R_0$ the function rises less steeply and exhibits a linear region, as shown, at R considerably beyond R_0.

The potential of the molecule will vary with its position within the cage. This "inner potential," $V(r)$ where r is the displacement of the central molecule from the mean center of the cage, has been evaluated for various pairwise interaction laws. For example, Fowler and Guggenheim[10] have presented the potential as calculated from the Lennard-Jones interaction law for different volumes corresponding to various cage radii. For R near R_0, $V(r)$ is parabolic at small r with a minimum at $r=0$. At larger R the minimum region of $V(r)$ is shallower and broader. The potential level at the minimum corresponds to $V(R)$ and thus increases with R. A volume ω, which we call the "central volume," is available to the center of the molecule. In the innermost part of this volume the potential difference $\Delta V(r) = V(r) - V(0)$ is small relative to kT and the molecule will move freely with its gas kinetic velocity. However in the peripheral part of the central volume $V(r)$ rises steeply and here the motion of the molecule will be vibrational.

[10] R. Fowler and E. A. Guggenheim, *Statistical Thermodynamics* (Cambridge University Press, New York, 1952), p. 340.

The average $\bar{R}$ of the cage radii will increase with increasing temperature. For $\bar{R}$ not much greater than R_0 the total expansion $\Delta\bar{v}/v_0$ is proportional to $\bar{R}-R_0$, thus

$$(\bar{v}-v_0)/v_0=\Delta\bar{v}/v_0=A(\bar{R}-R_0). \tag{3}$$

Let us consider how this "excess volume" $\Delta\bar{v}$ is distributed among the different cages. From the form of $V(R)$ it is apparent that for $\bar{R}$ near R_0 the potential energy of the system will be least when the excess volume is distributed uniformly among the cages. Let $\Delta\epsilon$ be the increase in potential energy required to redistribute the excess volume nonuniformly. This redistribution energy is very large at $\bar{R}\approx R_0$ and would approach ∞ for a hard sphere repulsive potential. As $\bar{R}$ increases beyond R_0, $\Delta\epsilon$ decreases and, for redistribution within certain limits, approaches zero when $\bar{R}$ reaches values in the linear region of $V(R)$. We shall call that part of the excess volume which may be redistributed with no increase in energy the "free volume" v_f. Thus we may write

$$\Delta\bar{v}=v_f+\Delta v_c. \tag{4}$$

The result that a part of the excess volume can be redistributed with no accompanying energy change was assumed in the authors' earlier treatment of molecular transport in amorphous phases[2] but we then neglected Δv_c and set $\Delta\bar{v}=v_f$.

We may now distinguish two regimes in the thermal expansion of an amorphous phase. In the first regime which occurs at the lowest temperatures all of the thermal expansion arises from the anharmonicity of the vibrational part of the motion of the molecule. The redistribution energy is large and the volume added in expansion will thus tend to be uniformly distributed among the cages. Hence $v_f\approx 0$ and

$$\Delta\bar{v}\approx\Delta v_c. \tag{5}$$

In this regime the increase in entropy due to the volume change alone will be very small. The magnitude of the thermal expansion will be of the order of that for the crystalline solid.

As the temperature of the amorphous phase is increased in the low temperature regime the thermal expansion increases and reaches some value $\Delta\bar{v}_g$ corresponding to $\bar{R}$ near the linear range of $V(R)$. For $\Delta\bar{v}$ greater than $\Delta\bar{v}_g$ a second regime will predominate in the thermal expansion in which most of volume added is "free" for redistribution. The free energy of the amorphous phase should be a minimum when this *free* volume is distributed at random. *Such a random distribution of free volume can occur in the amorphous but not in the crystalline phase.* Hence at $\Delta\bar{v}$ somewhat greater than $\Delta\bar{v}_g$ the amorphous phase should be more stable than a crystalline phase having the same volume. This comes about because of the positive configurational entropy which arises from the randomization of the free volume. This entropy term may constitute a substantial part of the entropy of fusion and an evaluation of it will be described in a forthcoming paper. Even without a quantitative calculation of the randomization entropy certain important inferences of a qualitative nature can be drawn about the transition from glass to liquid. Again we shall take the point of view that the transition results from the appearance of considerable amounts of free volume in the system. Then in the low temperature thermal expansion regime the amorphous phase will be a glass since, according to our arguments, virtually none of the volume added will appear as free volume until $\Delta\bar{v}$ reaches the value $\Delta\bar{v}_g$. In the temperature range in which the total thermal expansion is of the order of $\Delta\bar{v}_g$ free volume will begin to appear and according to the arguments advanced in our earlier paper[2] the fluidity will increase very rapidly to values characteristic of liquidlike behavior. Also the randomization entropy will begin to appear and the increase in entropy with volume, $\delta S(\Delta\bar{v})/\delta\bar{v}$, of the amorphous phase will be much greater than it would otherwise have been. That is, the rapid fall of $\delta S(\Delta\bar{v})/\delta\bar{v}$ from the high value characteristic of a nearly harmonic solid, $3Nk\gamma/\bar{v}$ for a monatomic solid (γ=average logarithmic volume derivative of the vibration frequencies), toward the low value characteristic of a nearly perfect gas $Nk/\bar{v}$ is slowed by the appearance of the entropy of randomization.[10a] The expected form of the entropy derivative and its comparison with the corresponding $V(R)$ derivative are shown in Fig. 3. The intersection of $\delta V(R)/\delta\Delta\bar{v}$ with $T\delta S(\Delta\bar{v})/\delta\Delta\bar{v}$ determines the *equilibrium* excess volume $\Delta\bar{v}_0$ at the

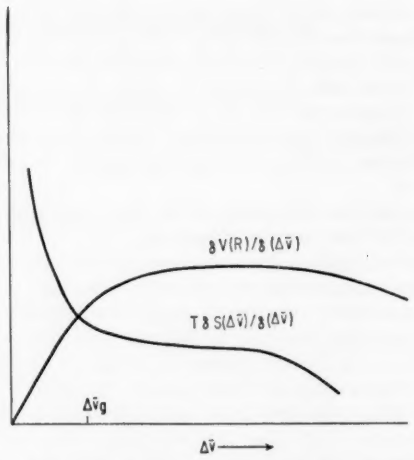

FIG. 3. Schematic diagram showing the derivatives of the potential and entropy functions for an amorphous phase as a function of the excess volume $\Delta\bar{v}$. The volume added starts to become redistributed freely at $\Delta\bar{v}\geq\Delta\bar{v}_g$. This results in a smaller rate of decrease in the entropy derivative.

[10a] The entropy of randomization may be regarded as equivalent to, but perhaps more precisely defined than, the communal entropy discussed by other authors.[3a, 15]

given temperature; $d(\Delta\bar{v}_0)/\bar{v}dT$ is the coefficient of thermal expansion α. If $\delta S(\Delta\bar{v})/\delta(\Delta\bar{v})$ is temperature independent, α must increase rapidly in the transition region, in which the $V(R)$ derivative falls away from its initial linear course, to a value much larger than that characteristic of the low temperature regime. This type of volumetric behavior actually is observed in the glass transition (see Fig. 1). Thus the glass transition temperature T_g may be considered to be approximately the temperature at which the excess volume attains the value $\Delta\bar{v}_g$ and at which free volume begins to appear. From the principle of corresponding states, which will be discussed later, it is expected that $V(R/R_0)/h_v$, where h_v is the heat of vaporization, will be the same for all liquids in a given class. It follows, therefore, that for such liquids T_g should be proportional to h_v as is observed.

According to the simple model just developed the glass transition at $T_g>0°K$ should be a universal characteristic of liquid behavior and would always occur if crystallization did not intervene. Whether or not crystallization intervenes will be determined by the magnitude of the crystallization kinetic constants (the nucleation frequency I, and the crystal growth rate u) and the cooling rate.[10b]

EFFECT OF GLASS TRANSITION ON MOLECULAR TRANSPORT PROPERTIES

The molecular transport properties of interest to us are the fluidity ϕ, the self diffusion constant D, and the kinetic constant for crystal growth D_u. From the limited information available there has emerged some simple semiempirical relations between these properties for amorphous phases. Thus the self-diffusion coefficient and the fluidity are related by

$$D=BT\phi, \tag{6}$$

where the magnitude of the constant B usually is near the Stokes-Einstein value

$$B=k/3\pi a_0, \tag{6a}$$

where a_0 is the molecular diameter. This relation seems to hold well into the glass transition range but the data for this range are very limited.

The velocity of growth of crystals into an undercooled amorphous phase at constant composition may be expressed[11] as

$$u=(fD_u/a_0)[1-\exp(\Delta g/kT)], \tag{7}$$

where Δg is the free energy of crystallization per molecule and f is the fraction of crystal surface sites to which molecules can be attached. If it is assumed that the kinetic constant for growth D_u is equal to the coefficient of diffusion in the amorphous phase, the crystal growth rate and fluidity may be related as follows:

$$u=(fBT\phi/a_0)[1-\exp(\Delta g/kT)]. \tag{8}$$

This relation seems to describe the velocity of crystal growth into very viscous undercooled liquids quite well with reasonable values for f.[11,4] From it we calculate that the velocity of crystal growth at a fluidity of 10^{-13} poise^{-1} is of the order of 1 A per day. Thus a glass once formed should persist for a very long period even though the crystal is the more stable phase.

It is known[12–15] that the equilibrium properties of simple liquids may be correlated by means of a principle of corresponding states. According to this principle the property of the liquid is some universal function of a reduced temperature τ. For our purposes the reduced temperature may be defined somewhat loosely as follows:

$$\tau=kT/h_v, \tag{9}$$

where h_v is the molecular heat of vaporization. There is considerable evidence that the molecular transport properties of liquids also may be correlated by means of the principle of corresponding states. Thus Cino-Castagnoli *et al.*[16] have shown[16a] that the fluidity of some molecularly simple substances are in approximate accord with the principle.

Also the existence of a single fluidity-reduced temperature relation for substances in a given class can be justified crudely on the basis of the free volume model. Thus from the preceding considerations and those of the preceding section we expect that

$$v_f/v_0 \sim (v_f/v_0)(h_v/kT). \tag{10}$$

And since, as shown in our earlier paper,[2] $\phi\beta$ is a function of v_f/v_0 it follows that

$$\phi\beta \sim \phi(kT/h_v) \sim \phi(\tau), \tag{11}$$

where

$$\beta=(mT)^{\frac{1}{2}}/\bar{v}^{\frac{1}{3}}. \tag{11a}$$

Figure 4 shows that this relation is approximately valid in the fluid range for liquids (hereafter called "simple liquids") composed of molecules which are not highly asymmetric in shape and which are bound together only by van der Waals forces. We have found few data on fluidities in the glass transition range. However, the reduced glass transition temperatures reported for substances in this class all fall close to the same value, namely, $\tau_g \sim 0.023$. Therefore we suggest

[10b] In the quantum fluids He_3 and He_4, crystallization does not intervene, the amorphous phase being stable at low temperatures and pressures. What is equivalent in these substances to the entropy of randomization disappears gradually in He_3 and via a phase transformation in He_4; however, the amorphous phase remains fluid down to the lowest temperatures because the structures are blown up by zero point kinetic-energy so that no redistribution of free volume is required for flow.

[11] W. B. Hillig and D. Turnbull, J. Chem. Phys. **24**, 914 (1956).

[12] K. S. Pitzer, J. Chem. Phys. **7**, 583 (1939).

[13] E. A. Guggenheim, J. Chem. Phys. **13**, 253 (1945).

[14] J. DeBoer, Physica **14**, 139 (1948).

[15] I. Prigogine, *The Molecular Theory of Solutions* (North-Holland Publishing Company, Amsterdam, 1957).

[16] G. Cino-Castognoli, G. Pizzella, and F. P. Ricci, Nuovo cimento **11**, 466 (1959).

[16a] See also G. Thomaes and J. Van Itterbeek, Mol. Phys. **2**, 372 (1959).

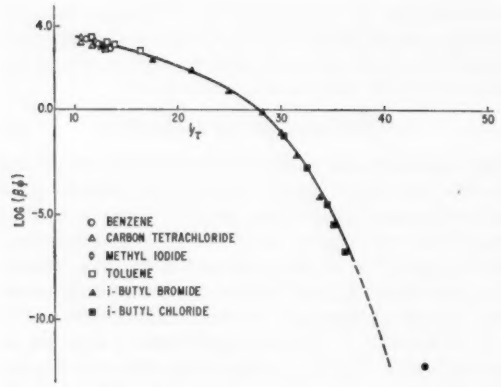

FIG. 4. Relation between fluidity function $\beta\phi$, and reduced temperature τ, for various simple molecular liquids. The solid circle represents the estimated fluidity function at the glass transition for several simple molecular substances.

that Eq. (11) may hold approximately over the entire fluidity range for substances in a given class.

The fluidities of substances composed of short linear molecules fall close to the Fig. 4 curve at relatively high reduced temperatures but are considerably above this curve at lower temperatures. Also the glass transition temperatures of these substances seem to be well below $\tau=0.023$.

The $\phi=\phi(\tau)$ relations for three types of substances are compared in Fig. 5. In making this comparison the factor β was ignored. This factor does not vary markedly from one compound to another though its inclusion significantly improves the accord between the data and the reduced temperature relation. It is seen that the $\phi(\tau)$ relation for the polyalcohols is only a little below that for the simple liquids and gives $\tau_g\sim0.025$; however, it is evident that the form of $\phi(\tau)$ for boron oxide is very different from that for the simpler liquids.

From the correlations stated earlier it follows that for any given class of substances,

$$D_u\sim D_u(\tau) \tag{12}$$

to about the same degree of approximation as the $\phi(\tau)$ relation.

GLASS-FORMING TENDENCY AND ITS RELATION TO MOLECULAR CONSTITUTION

As we have seen, the reduced normal boiling temperature τ_b and the reduced glass transition temperature τ_g seem to be nearly constant for substances in a given class. For example, $\tau_b\sim0.095$ and $\tau_g\sim0.023$ for the simple liquids. According to the considerations advanced in the preceding section the kinetic constant for crystal growth D_u should all off from τ_b to τ_g in the same way as does ϕ (see Fig. 4).

Experience indicates that the other crystallization kinetic constant, the crystal nucleation frequency I, is a very sharply increasing function of undercooling and therefore of τ. Let τ' be the reduced temperature at which the nucleation frequency equals some characteristic measurable value. It is found that,[17] when the reduced thermodynamic melting temperature τ_m is far above τ_g,

$$\tau'=\lambda\tau_m, \tag{13}$$

where λ is approximately constant for substances in a given class. For example, λ is about 0.7 to 0.8 for the simple liquids.[17–19]

The values of τ_m, in marked contrast with those for τ_b and τ_g, may vary widely among different substances within a single class. Hence by Eq. (13) the values of τ' will do the same. It is evident from these considerations that the over-all crystallization velocity $\dot{x}$, which at large undercooling is roughly proportional to ID_u^3, should be smaller the less is τ' or alternatively the less is τ_m. Therefore the glass-forming tendency of a substance within a given class will be greater the less is τ_m where

$$\tau_m=k\Delta U_m/h_v\Delta S_m, \tag{14}$$

and ΔU_m and ΔS_m are, respectively, the energy and entropy of fusion. This generalization about glass-forming tendency can be restated as follows: *The glass forming tendency of a substance in a particular class is greater the less is the energy, at constant cohesive energy, necessary to produce a given amount of disorder.* This statement encompasses the Zacharaisen[20] condition for glass formation as well as the conditions proposed in our 1958 paper.[1]

We can now give a qualitative interpretation of the effect of molecular constitution on glass forming tend-

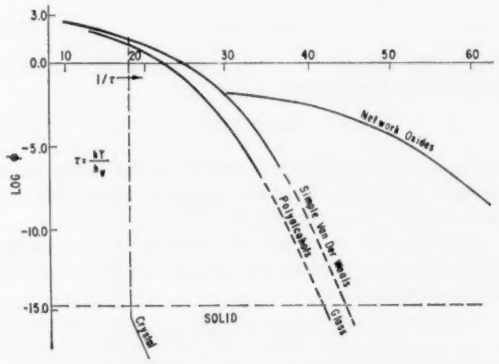

FIG. 5. Relation between fluidity (ϕ) and reduced temperature (τ) for three classes of substances. The curve for network oxides was constructed entirely from data on B_2O_3 [J. D. MacKenzie, Trans. Faraday Soc. **52,** 1564 (1956)].

[17] D. Turnbull, J. Appl. Phys. **21,** 1022 (1950).
[18] D. G. Thomas and L. A. K. Stavely, J. Chem. Soc. **1952,** 4569.
[19] H. J. De Nordwall and L. A. K. Stavely, J. Chem. Soc. **1954,** 224.
[20] W. H. Zachariasen, J. Am. Chem. Soc. **58,** 3841 (1932).

ency. For example, Zachariasen has pointed out that glass formation in ceramics is strongly favored if the coordination polyhedra make point to point contact in an open structure. In this event only a little energy is needed for small changes in the contact angle of the coordination polyhedra. However, as Zachariasen recognized, the long-range order can be destroyed by such small changes and thus the entropy of amorphization is obtained with the expenditure of only a small amount of energy.

In general the glass-forming tendency of simple organic substances is increased by asymmetrization of the molecule. For example, toluene forms glasses much more readily than does benzene. The effect of asymmetrization is to increase the entropy of the amorphous phase so that the amorphization energy at the melting temperature is reduced. Also glass formation would be favored by impurity additions which raise the energy of the crystal relative to the amorphous phase at constant composition.

ACKNOWLEDGMENTS

We are indebted to Bruno H. Zimm for valuable discussions and for encouragement. Also we are pleased to acknowledge several helpful discussions with L. Guttman and M. B. Webb.

THE JOURNAL OF CHEMICAL PHYSICS VOLUME 34, NUMBER 1 JANUARY, 1961

Vacuum Ultraviolet Absorption Spectrum of Phosgene*

S. R. La Paglia and A. B. F. Duncan

Department of Chemistry, University of Rochester, Rochester, New York

(Received July 25, 1960)

The spectrum of phosgene was investigated, for the first time, over the region 2000–600 A with a dispersion of about 4.15 A/mm. A number of resolved transitions were found, some with vibrational structure. The vibrational structure was in each case interpreted as a progression in a totally symmetrical frequency. A tentative interpretation of the electronic transitions is given.

INTRODUCTION

THE electronic transition of phosgene at longest wavelengths[1] consists of many bands between 3050 and 2380 A, followed by a continuum which extends into the vacuum ultraviolet region. The present study revealed several transitions of higher intensity at wavelengths shorter than 2000 A.

Molecules containing the carbonyl group possess a characteristic region of absorption in the near ultraviolet. These molecules also possess transitions in the vacuum ultraviolet which are probably localized in the carbonyl group of the molecule. It is possible to interpret some of the observed transitions of phosgene by analogy with the spectra of other carbonyl compounds. Comparison with the spectra of the chloromethanes is also helpful in the interpretation.

EXPERIMENTAL

The absorption spectrum of phosgene was obtained with a 2-m vacuum spectrograph previously described.[2] In the first order the plate factor of this instrument is about 4.15 A/mm. The background for absorption was provided by the Lyman continuum; Eastman Kodak SWR plates were used.

The emission lines of carbon and silicon which occur in the Lyman continuum were used as wavelength standards.[3] The absorption maxima were read from microphotometer tracings of the plates. The error in measurement was about 10 cm^{-1} for vibrational bands and 2–4 A for the maximum of broad electronic transitions.

The phosgene was obtained from a commercial source and was specified as 99.9% pure. Vapor phase chromatographic and mass spectroscopic analysis showed no detectable impurities. The phosgene was expanded directly into the spectrograph from a calibrated volume to final pressures of 1 to 50 μ Hg. The spectrograph served as a 4-m absorption column.

DESCRIPTION OF THE SPECTRUM

The first electronic transition (I) of phosgene in the vacuum ultraviolet region is a broad absorption region with maximum at 1550 A (64 700 cm^{-1}). At 5-μ pressure in 4 m path length the absorption extends over a spectral region of about 160 A. As the pressure is in-

* Part of a dissertation submitted by S. R. La Paglia to the Graduate School of the University of Rochester in partial fulfillment of the requirements for the degree of Doctor of Philosophy. This research was supported in part by the Office of Naval Research.

[1] V. Henri and O. R. Howell, Proc. Roy. Soc. (London) **A128**, 178, 192 (1930).

[2] C. R. Zobel and A. B. F. Duncan, J. Am. Chem. Soc. **77**, 2611 (1955).

[3] J. C. Boyce and J. T. Moore, "Provisional wavelength identification tables for the vacuum ultraviolet," M.I.T., 1941.

TABLE I. Electronic transitions and vibrational structure below 2000 A in phosgene.

I	II	III	IV	V	VI
64 700 cm^{-1}	66 707 cm^{-1}	72 538 cm^{-1}	74 810 cm^{-1}	80 816 cm^{-1}	88 253 cm^{-1}
(max)	66 976	72 851	75 382	81 185	88 541
	67 253	73 177	75 946	81 514	89 626
	67 514	73 522	76 525		89 918
	67 773	73 867	77 081		90 217
	68 042	74 213	77 620		90 512
	68 301				90 791
	68 573				91 082
	68 848				91 375
	69 116				91 694
	69 388				91 997
	69 668				92 611
	69 936				92 906
	70 209				93 193
	70 458				93 475
	70 716				

creased, the absorption broadens and becomes more intense.

Overlapping the short-wavelength end of this absorption is a second transition (II), which consists of a long vibrational progression. Because of overlapping, the origin of this transition cannot be located with certainty. The first few members appear at 3 μ, and at 20-μ pressure all the bands are revealed. The bands (listed in Table I) have an average separation of 267 cm^{-1}.

The third electronic transition (III) of phosgene begins at 72 538 cm^{-1} and consists of six bands whose average separation is 335 cm^{-1}. This transition is followed by six bands of a very different character. Broader and more diffuse, they have an average separation of 562 cm^{-1}. At a pressure of 8 μ, the bands of this transition (IV) have broadened so that the transition resembles a short continuum while transition III remains well resolved. The intensity maximum in transition IV occurs at about 76 660 cm^{-1}.

The most intense feature of the phosgene spectrum is an electronic transition (V) which occurs at 80 816 cm^{-1}. The transition consists of 2 intense bands followed by a broader band with maximum at 81 514 cm^{-1}. All of these features are revealed at a pressure of 1.5 μ. Increasing pressure causes the transition to spread to the ultraviolet, but it remains quite sharp on the red side. This transition is followed by a region of high transmission. The next transition (VI) has a broad maximum at 89 043 cm^{-1}. The origin of the transition is probably at 88 253 cm^{-1}. The vibrational structure is diffuse and consists of a progression with average separation of 290 cm^{-1}. The maximum is so intense relative to the vibrational structure that the possibility exists that it represents an additional electronic transition.

At very short wavelengths and low pressure (2 μ), absorption is complete from about 1050 A (95 000 cm^{-1}) This long-wavelength limit corresponds to 11.79 ev, and approximately represents the spectroscopic ionization potential. This value agrees with the results of electron impact studies by Morrison and Nicholson,[4] who found 11.77 ev for the ionization potential of phosgene. No Rydberg series of transitions was observed converging to this ionization potential.

VIBRATIONAL STRUCTURE IN THE ELECTRONIC TRANSITIONS OF PHOSGENE

Several electronic transitions of phosgene contain extensive vibrational structure. This structure is well represented by the following equations, derived by least-squares analysis:

$$\nu_{II}=66\,707+270v'-0.15v'^2$$

$$\nu_{III}=72\,537+307v'+5.7v'^2$$

$$\nu_{IV}=74\,810+587v'-5.0v'^2$$

$$\nu_{VI}=88\,253+277v'+0.8v'^2.$$

The electronic transitions are identified by roman numerals. Wherever vibrational structure appears in the vacuum ultraviolet spectrum of phosgene, it is in every case a simple progression in a totally symmetric vibrational mode (a_1). A noteworthy similarity to ground state vibrational frequencies makes their assignment possible. The three totally symmetric

[4] J. D. Morrison and A. J. C. Nicholson, J. Chem. Phys. **20**, 1021 (1952).

vibrational modes of phosgene are ν_1, ν_2, and ν_3 in the notation of Herzberg.[5] These modes have normal state frequencies[6] of 567, 1827, and 285 cm^{-1}, respectively. They correspond to symmetric stretching ν_1, C-O stretching ν_2, and symmetric Cl bending ν_3.

The long progressions in transitions II and VI have frequencies similar to the normal state frequency ν_3 as does the shorter progression found in transition III. The frequency found in transition IV indicates excitation of quanta of ν_1. The anharmonicity constants for these progressions are not large, in keeping with the excitation of totally symmetric vibrations. The lack of excitation of ν_2, the C-O stretching mode, in both the near and vacuum ultraviolet spectrum of phosgene is not unusual for a carbonyl containing compound.

DISCUSSION

In this section a tentative interpretation of the electronic transitions of phosgene is proposed. The proposed assignments in terms of definite orbital transitions is necessarily qualitative since there was insufficient resolution to show the rotational structure of any of the transitions. There are no quantitative conclusions presented here such as could normally follow from analysis of resolved rotational structure. Only conclusions based on analogies to the spectra of related molecules can be made.

Phosgene is planar in its normal state and belongs to symmetry group C_{2v}. The electronic configuration of the normal state of formaldehyde and phosgene have been discussed by Mulliken[7] and the configuration of formaldehyde more recently by Walsh.[8] In order of decreasing negative energy, the highest filled orbitals of formaldehyde are designated as, (y_{CH_2}, b_2), (x_O+x_C, b_1), $(z_O+z_{CH_2}, a_1)$ and $(2p_y, b_2)$ by Mulliken. The orbital $2p_y$ is a nonbonding orbital localized on the oxygen atom; the orbital of symmetry a_1 is bonding in the direction of the twofold axis in the C_{2v} symmetry; the orbital of symmetry b_1 is localized in the CO group perpendicular to the molecular plane (π orbital); and (y_{CH_2}) is CH bonding in the plane of the molecule. In Walsh's description, the a_1 orbital lies lower than b_1 and this idea is supported by recent molecular orbital calculations.[9] In phosgene we substitute CCl for CH bonding and add two nonbonding $(3p\pi)_{Cl}$ orbitals which probably lie between $2py$ and (x_O+x_C). Excitation of electrons from $(3p\pi)$ must also be considered. [Actually, $(3p\pi)$ will be slightly split into b_1 and b_2 components.] Then, in an obvious notation, the normal configuration of phosgene may be written

$$\cdots(Y_1)^2(Z)^2(X)^2(\pi)^4(\pi)^4(Y_2)^2 \qquad {}^1A_1$$

and the low lying excited states of the molecule written,

$$\cdots(Y_1)^2(Z)^2(X)^2(\pi)^4(\pi)^4(Y_2)(\bar{X}) \qquad A_2$$

$$\cdots(Y_1)^2(Z)^2(X)^2(\pi)^4(\pi)^4(Y_2)(\bar{Z}) \qquad B_2$$

$$\cdots(Y_1)^2(Z)^2(X)^2(\pi)^4(\pi)^4(Y_2)(R_o) \qquad A_1, B_2$$

$$\cdots(Y_1)^2(Z)^2(X)^2(\pi)^4(\pi)^3(Y_2)^2(\bar{X}) \qquad A_1$$

$$\cdots(Y_1)^2(Z)^2(X)^2(\pi)^4(\pi)^3(Y_2)^2(\bar{Z}) \qquad B_1, B_2$$

$$\cdots(Y_1)^2(Z)^2(X)^2(\pi)^4(\pi)^3(Y_2)^2(Y_1) \qquad A_1$$

$$\cdots(Y_1)^2(Z)^2(X)^2(\pi)^4(\pi)^3(Y_2)^2(R_{Cl}) \qquad A_1, B_1, B_2$$

$$\cdots(Y_1)^2(Z)^2(X)(\pi)^4(\pi)^4(Y_2)^2(\bar{X}) \qquad A_1,$$

where the orbital symbols with bars are the antibonding forms of the unbarred orbitals and the R_i orbitals are atomic-like (Rydberg) orbitals.

If the lowest energy transition [origin taken at 33 500 cm^{-1} by Henri(1)] is associated with an orbital transition $(Y_2)\rightarrow(\bar{X})$ as is most probably the case, we may consider transition I observed here as, $(Y_2)\rightarrow(\bar{Z})$. The continuous nature of this transition is similar to the next lowest transition observed in formaldehyde[10] at 57 300 cm^{-1}, which is usually taken as $(Y_2)\rightarrow(\bar{Z})$. Furthermore, the term values of these transitions are, respectively, 30 300 and 30 440 cm^{-1} from the experimental ionization potentials of the two molecules.

Transition III is assigned to the transition $(X)\rightarrow(\bar{X})$. The difference in transition energy between III and the near-ultraviolet transition is 38 987 cm^{-1}, which should approximate the difference in ionization potentials, $E(X)-E(Y_2)$. This value for phosgene is to be compared with 35 790 cm^{-1} for the same difference in formaldehyde. Although these differences are in rough agreement for the two molecules, the difference for formaldehyde is not in very good agreement with the experimental difference.[11] It is also larger than the calculated value for the difference in orbital energies.[9]

Transitions I and III (and the near-ultraviolet transition) are apparently the only valence shell transitions which occur from (Y_2) and (X). A possible transition $(X)\rightarrow(\bar{Z})$ would lie higher than the lowest ionization potential of phosgene and could not be observed. However transitions from (Y_2) to Rydberg levels are possible. In order to make a definite assignment of such transition it is, of course, necessary to find a Rydberg series with several members. Such a series cannot be found among the electronic levels of phosgene. However, in the other carbonyl molecules such series have been found to fit a formula,

$$\nu_n=\nu_\infty-R/(n+\alpha)^2, \quad \text{with} \quad \alpha=0.3.$$

If the value of ν_∞ is taken as 95 000 cm^{-1} for phosgene, then $\nu_2=95\,000-R/(2.3)^2=74.256$ cm^{-1}. This is suffi-

[5] G. Herzberg, *Infrared and Raman Spectra of Polyatomic Molecules* (D. Van Nostrand Company, Inc., Princeton, New Jersey, 1945).
[6] E. Catalano and K. Pitzer, J. Am. Chem. Soc. **80,** 1054 (1958).
[7] R. S. Mulliken, J. Chem. Phys. **3,** 564 (1935).
[8] A. D. Walsh, J. Chem. Soc. **1953,** 2306.
[9] F. Birss, P. L. Goodfriend, and A. B. F. Duncan, Revs. Modern Phys. **32,** 307 (1960).
[10] W. C. Price, J. Chem. Phys. **3,** 256 (1935).
[11] T. M. Sugden and W. C. Price, Trans. Faraday Soc. **44,** 116 (1948).

TABLE II.[a]

	Terms of Rydberg transitions			Convergence limit
Cl[b]	19 553	8683	5172	104 991 cm^{-1}
CH_3Cl[c]	19 400	9030	5390	91 180
CCl_2F_2[d]	16 628	8610	...	95 817
CH_2Cl_2[d]	16 308	8631	5048	90 135
$COCl_2$	16 184	8450	...	97 000

[a] The terms for Cl refer to transitions, $3s^23p^5(^2P)\rightarrow 3s^23p^4(^3P)np(^2P)$. Terms are given for all the observed series members in CCl_2F_2 and $COCl_2$ and for 3 members of the series in CH_3Cl and CH_2Cl_2.

[b] Natl. Bur. Standards Circ. 467.

[c] Footnote 12.

[d] Footnote 2.

ciently close to 74 810 cm^{-1}, the origin of transition IV, to allow possible assignment of IV to $(Y_2)\rightarrow(R_0)$. Exact agreement could be obtained with very small adjustment of α. The next higher member of this series, ν_3, would lie at about 85 000 cm^{-1}. Since we are unable to find a transition at this frequency, considerable doubt is cast on this assignment. It is possible that IV represents the orbital transition $(\pi)\rightarrow(\bar{Y}_1)$ which may occur in this spectral region.

Transitions II, V, and VI are believed to originate in transitions from the nonbonded chlorine orbital (π). The ionization potential of (π) is estimated by assignment of II to the orbital transition $(\pi)\rightarrow(\bar{Z})$. From this provisional assignment: $E(\text{II})-E(\text{I})=E(\pi)-E(Y_2)=2000$ cm^{-1}. With the ionization potential of $(Y_2)=95\,000$ cm^{-1} this gives the ionization potential of (π) as $\sim 97\,000$ cm^{-1}. This value is very reasonable in comparison with the spectroscopic ionization potentials of the chloromethanes,[2] and is not very far below the ionization potential of chlorine, 104 991 cm^{-1}. If the value 97 000 cm^{-1} is used, we may try to fit transition V (80 816 cm^{-1}) to the formula

$$\nu_2=97\,000-R/(2+\alpha)^2=80\,816$$

and find $\alpha=0.604$. This value of α is consistent with the value found for Rydberg series in CCl_2F_2, CH_2Cl_2 and CH_3Cl, 0.57, 0.58, and 0.50, respectively.[2,12] When this is done,

$$\nu_3=97\,000-R/(3.604)^2=88\,550.$$

This value is sufficiently close to the experimental value of transition VI. Transitions V and VI are assigned therefore to the orbital excitations: $(\pi)\rightarrow(R_{\text{Cl}})$. The excited states involved in these transitions are probably qualitatively similar to the $4p$ and $5p$ states of Cl(see Table II). Higher electronic transitions in this series would occur so close to the ionization continuum of (Y_2) that observation is not possible.

The vibrational structure in the spectrum of phosgene is of no assistance in explaining the nature of these transitions. Structure, where it is observed, consists exclusively of relatively long vibrational progressions of totally symmetric frequencies. Only the negative conclusion can be drawn that, with the exception of the near-ultraviolet transition, none of the upper states has a symmetry A_2 and most probably all these states are allowed singlet states.

[12] W. C. Price, J. Chem. Phys. **4**, 539 (1936).

THE JOURNAL OF CHEMICAL PHYSICS VOLUME 34, NUMBER 1 JANUARY, 1961

Electronic Conduction in Complexes of Aromatic Hydrocarbons with Iodine

J. KOMMANDEUR AND FRANCES R. HALL

Parma Research Laboratory, Union Carbide Corporation, Parma, Ohio

(Received July 6, 1960)

Molecular complexes of the aromatic hydrocarbons pyrene and perylene with iodine were found to have an electronic conductivity 10 to 12 orders of magnitude higher than that of the constituent compounds. The specific resistivities measured were 75 and 8 ohm-cm, respectively. The materials behaved like semiconductors and plots of $\log \sigma$ vs $1/T$ gave activation energies of 0.14 ev and 0.019 ev. No Hall effect could be found, but an upper limit for the mobility of $\mu \leq .01$ cm^{2}v^{-1} sec^{-1} could be set. Single crystals of the perylene-iodine complex were obtained. The preparation and identification of the complexes are discussed and the results of a phase study on the system of pyrene and iodine are reported.

INTRODUCTION

EXTENSIVE work has by now been carried out on the electronic conduction in molecular solids.[1] The resistivity of these solids is always found to be very high. For the aromatic hydrocarbons, typical specific resistivities are from 10^{12} to 10^{16} ohm-cm. Recently, however, Akamatu and co-workers[2] reported highly decreased resistivities in aromatic hydrocarbons treated with iodine and bromine. Unfortunately, the dependence of the conductivity on time, the lack of well-defined crystal structures, and the nonstoichiometric compositions of the complexes make their work subject to serious criticism. It was, therefore, of interest to see whether similar phenomena could be found in complexes of a more defined nature.

This paper reports on the electronic conductivity of the iodine complexes of pyrene and perylene. Both complexes could be obtained in stoichiometric form, and single crystals of the perylene complex could be grown.

Although these complexes are molecular in character, i.e., no real chemical bonding occurs, their conductivity is from 10 to 12 orders of magnitude higher than that of the constituent compounds. This appears to be the first time that such high conductivities are observed in single crystals of a molecular nature.

After a discussion of the properties of the electronic conduction, the identification and preparation of the complexes are presented.

THE ELECTRONIC CONDUCTION

Both the pyrene-iodine and the perylene-iodine complex were found to be highly conductive with specific resistivities at 300°K of 75 and 8 ohm-cm, respectively. One important question concerning this high conductivity is whether it is electronic or ionic in character. There is some danger in these materials in that the iodine may react with the hydrocarbon and thus produce an iodo-derivative and HI. The protons freed by this process could conceivably be involved in ionic conduction. Although such a reaction is unlikely to take place at the low temperature used in the synthesis of the complex, the following experiment was carried out to test for ionic conduction: A pellet was pressed at 2000 psi and current was run through until the amount of charge passed had exceeded the amount allowed by Faraday's laws by over 10 000 times. No significant change in conductivity took place. This proves that the conduction is electronic in character.

The single crystals of perylene-iodine proved to be very sensitive to thermal shock and generally sheared at the contact points if the temperature was changed at all. Therefore, measurements of conductivity versus temperature were carried out on pressed pellets. Great difficulties were encountered when the conductivity was measured with a two-probe system as used by Akamatu.[2] Apparently contact resistances play an important role. A number of contact materials were tested: platinum, gold, graphite, "Aquadag" (a suspension of graphite in water), and silver paste. All led to a contact resistance, which in its turn gave extra heating at the electrodes. This heat dissipation caused iodine to sublime, which increased the resistance, etc. This may have been the cause of the current-time effects reported by Akamatu. It was found that by enclosing the sample with the electrode no dependence of the current on time existed. However, even then the electrode resistance persists, so it was decided to use the four-probe arrangement as shown in Fig. 1. The current electrodes were graphite rods with the diameter of the pellets (0.160 in.) loaded with a spring, all pressed together by a small bolt. Sample and electrodes were contained inside a closely fitting glass tube with appropriate holes for the platinum voltage probes. The Lavite was covered with a boxlike screen for electrostatic shielding. Thermocouples were attached to the middle of the glass rod and to one of the brass blocks. The whole apparatus could be lowered into a small Dewar flask, which could be charged with nitrogen. The flask was then closed with a cork stopper. In series with the current probes was a 6-v battery and a Sensitive Research microammeter. The voltage probes were

[1] C. B. G. Garrett, *Semiconductors* edited by N. B. Hannay (Reinhold Publishing Corporation, New York, 1959), Chap. 15.

[2] H. Akamatu, H. Inokuchi, and Y. Matsunaga, Bull. Chem. Soc. Japan **29**, 213 (1956).

connected to a high-impedance input Keithley dc voltmeter (No. 200B).

For a temperature run a small amount of liquid nitrogen was added to the Dewar and the assembly was not disturbed. The time for the temperature to rise from 77°K to room temperature was in the order of 8 hr. Thermocouple readings were taken of both couples to make sure that equilibrium was reached. Differences in temperature between the glass and the brass of less than 0.1°K were taken as evidence for equilibrium. In this fashion temperature runs could be made from 90°K to room temperature. Below 90°K equilibrium was not established.

A plot of the logarithm of the specific conductivity versus the reciprocal temperature for the pyrene-iodine complex is given in Fig. 2. Note that this plot gives two straight lines with a break around 200°K. The activation energy[3] for conduction calculated on a basis

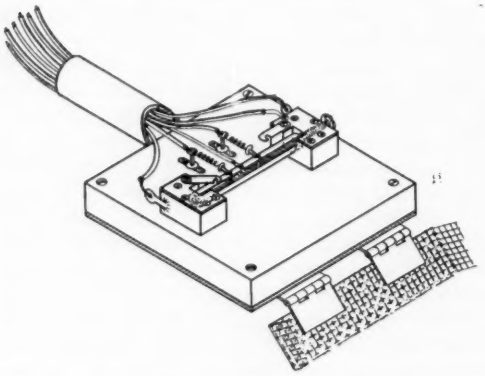

FIG. 1. Apparatus for measuring electronic conductivity as a function of temperature.

of $\sigma=\sigma_0 \exp(-E/kT)$ is 0.14 ev for the upper and 0.07 ev for the lower part of the curve. The position of the break does not seem to depend on the sample. A number of runs were made on samples prepared from different solutions, but the same curve always resulted.

A similar plot for the perylene-iodine complex is given in Fig. 3. The activation energy for conduction is much lower in this case, $E=0.019$ ev. Since this energy becomes in the order of kT at the high temperatures, and the number of carriers is then a significant fraction of the total number of molecules, the line should be slightly curved, which is indeed observed. Although for reasons already stated, a temperature run could not be carried out on a single crystal of perylene-iodine, a number of measurements of specific resistivity were carried out on four single crystals at room temperature. These measurements all agreed

[3] The term "activation energy" as used here means the energy difference between the conducting and the nonconducting state of the system. It has, therefore, no relation to the activation energy, as defined in the theory of rate processes.

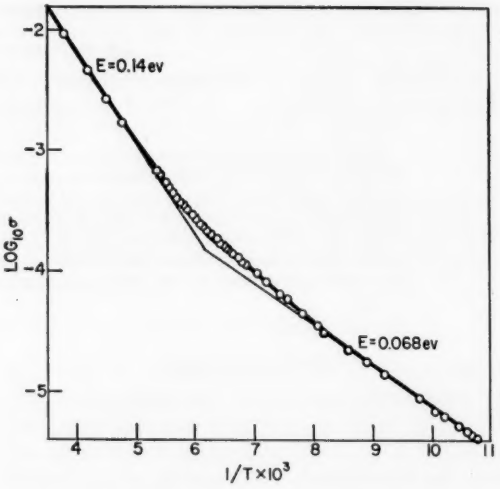

FIG. 2. The variation of the specific conductivity with the reciprocal temperature for pyrene·$2I_2$.

within 5% with each other and with the value found for the pressed pellet.

An attempt was made to measure the Hall effect in these materials. None, however, could be found. Only an upper limit for the mobility of $\mu \leq 0.01$ cm^{2}v^{-1} sec^{-1} could be set for both materials, if the case of an exactly equal number of carriers with exactly equal mobilities can be excluded. With this upper limit for the mobility and the value for the specific conductivity, lower limits for the number of charge carriers can be given. They are for pyrene-iodine and perylene-iodine $N \geq 3\times10^{18}$ carriers/g and $N \geq 3\times10^{19}$ carriers/g, respectively.

Both materials are shiny black in appearance. An effort was made to obtain optical spectra in the near infrared, the visible, and the ultraviolet. The absorption coefficients, however, appeared to be extremely

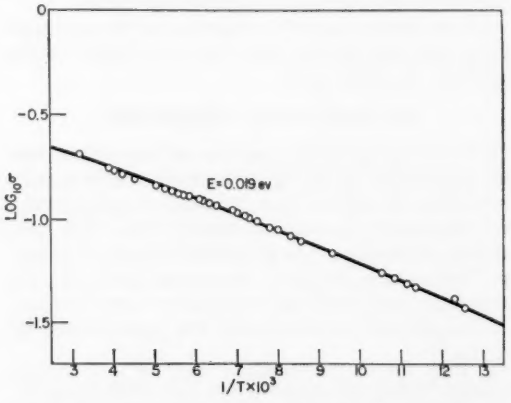

FIG. 3. The variation of the specific conductivity with the reciprocal temperature for 2 perylene·$3I_2$.

high. Even layers of 0.1 μ were not thin enough to obtain an absorption spectrum. The absorption coefficients, therefore, must be at least 5×10^5.

COMPOSITION AND PREPARATION OF THE COMPLEXES

A charge-transfer interaction is known to exist between pyrene and iodine.[4] It was of interest to ascertain whether this interaction is sufficient to allow isolation of the complex. A benzene-bromine complex is known at low temperature,[5] as well as a perylene-iodine complex[6] at room temperature.

To find out whether a pyrene-iodine complex existed, a phase study was carried out in the following way: A small glass container, equipped with stirrer and thermocouple well, was heated in a small oven (Fig. 4). The container was charged with varying amounts of pyrene and iodine in such a way as to allow little iodine in the vapor phase. The stirrer was sealed by means of a high-temperature grease in the glass bearing. Some iodine was lost by sublimation in this arrangement; however, these amounts were insignificant. After all the material was molten, the heaters were turned off, the assembly was left in the oven while stirring, and the temperature was recorded on a Varian G-10 recorder. The resultant cooling curves were examined for breaks at the melting point and at the eutectic. Figure 5 gives the resulting phase diagram. Supercooling of the melt presented a problem, but it could usually be circumvented by making several runs on the same sample. The phase diagram indicated that two complexes exist: one metastable complex $2Py\cdot I_2$ at 33 mole % of iodine and another stable complex $Py\cdot 2I_2$ at 67 mole % of I_2.

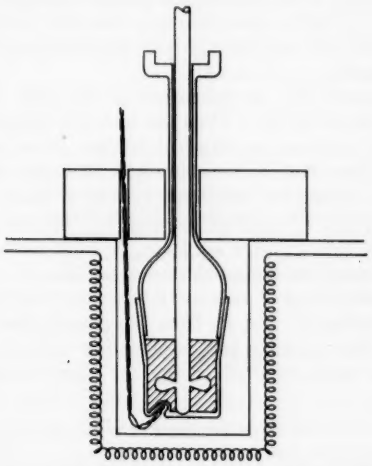

FIG. 4. Apparatus for determining the phase diagram of iodine and pyrene.

[4] R. Bhattacharya and Sadhan Basu, Trans. Faraday Soc. **54,** 1286 (1958).
[5] O. Hassel, Mol. Phys. **1,** 241 (1958).
[6] M. Pestemer and E. Treiber, Chem. Ber. **74,** 964 (1941).

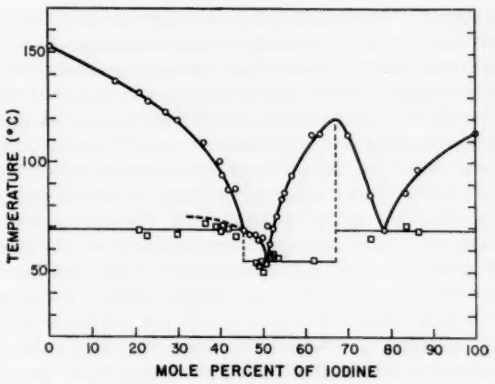

FIG. 5. The phase diagram for the iodine-pyrene system. The squares refer to the eutectic points found.

Since this evidence for the metastable complex depends upon an extrapolation, the density of the pyrene-iodine mixtures was measured in the usual fashion with a pycnometer. The liquid phase to be used in these measurements presented a difficulty. Water had a tendency not to wet the material properly at high pyrene concentrations, while at high iodine concentrations some of the iodine tended to dissolve into the water. This problem was solved by using water with a detergent at one end of the system, and water saturated with iodine on the other. Furthermore, the material was lightly pressed into pellets to decrease the total exposed surface area. These precautions led to good reproducibility of the measurements as can be seen in Fig. 6, which gives the variation of the density with iodine concentration. The discontinuities observed at 33 and 67 mole % of iodine are in excellent agreement with the conclusions drawn from the phase diagram.

Further confirmation was obtained from x-ray patterns obtained with a Norelco powder camera. For the violanthrene-iodine complex, Akamatu[7] found that the x-ray pattern became consistently more diffuse while going to higher iodine concentrations. He therefore concluded that the complex must be an amorphous material. This effect was also found in the present investigation, but by using long exposure times a distinct pattern could always be obtained. The heavy background is probably due to x-ray-excited K-shell fluorescence of the iodine. Table I gives the d values of the lines that were obtained on samples of pure pyrene, a mixture containing 35 mole % I_2, quenched from the melt, a mixture containing 67 mole % I_2 and pure iodine. It will be clear that apart from the pure compounds, two distinctly different phases were observed. It must therefore be concluded that a distinct crystal structure can be assigned to each of the complexes. One relevant observation is that of Hassel and co-

[7] H. Akamatu, Y. Matsunaga, and H. Kuroda, Bull. Chem. Soc. Japan **30,** 618 (1957).

workers,[5] who obtained the x-ray spectrum of an unstable crystalline benzene-bromine complex. From a tentative analysis of his data, Hassel suggested rows of alternating bromine and benzene molecules, with the line joining the bromine atoms very nearly at right angles to the plane of the benzene ring. This may serve as a model for the pyrene-iodine complex, where the pyrene molecule because of its larger size could accommodate two iodine molecules. If the pyrene-iodine complex $Py \cdot 2I_2$ is stable when formed from the melt, it should also be possible to synthesize the complex in solution. By trial and error it was found that a solution of 2 g of iodine and 3 g of pyrene per 100 ml of CCl_4, when cooled from room temperature to $-20°C$, yielded a finely divided crystalline precipitate with the required composition and x-ray pattern. The composition of the precipitate is not critically dependent upon the concentrations, but at high divergencies from the given values either pure iodine or pure pyrene are also precipitated, and it is then impossible to separate the complex. The complex is stable at room temperature if kept under its own vapor pressure. On exposure to the air the iodine sublimes out quickly and the white pyrene powder remains behind. From this and from the synthesis in solution, it seems safe to conclude that the iodine has not reacted with pyrene, but is just loosely bonded to the aromatic system as a whole molecule.

The perylene-iodine complex has been known to exist for quite some time.[6] There has been some argument about its composition, but most authors have concluded that the stable complex is 2 perylene$\cdot 3I_2$. In this investigation it was also found that within wide concentration limits, the precipitate formed on cooling a benzene solution of the parent substances contained 60 mole % iodine. The concentrations most favorable to precipitation of the single complex were 3.5 g of iodine and 1.0 g of perylene per 100 ml benzene. Single crystals of this material were obtained by cooling solutions of these concentrations from 65°C to 35°C over a period of 1 to 2 weeks. Seeding of the solutions was tried but proved to be rather ineffective. Therefore, runs were just repeated until some single crystals were found in the polycrystalline precipitate. The dimensions of these crystals varied: the length from 2 to 5 mm, the width from 1 to 2 mm, and the thickness from 1 to 10 μ.

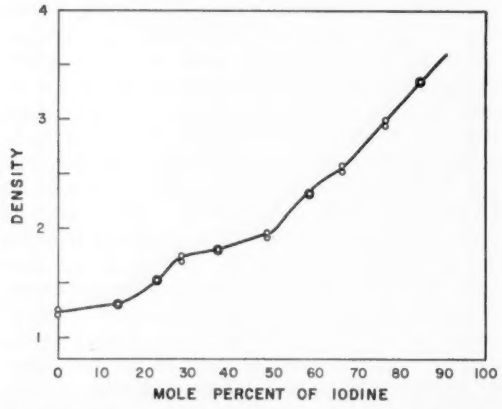

FIG. 6. The variation of the specific density in the iodine-pyrene system.

TABLE I.

d spacings			
Pure pyrene	35% I_2	67% I_2	Pure iodine
8.58	12.69	11.48	3.74
7.75	10.47	9.11	3.64
5.92	8.49	8.42	3.10
5.43	7.62	6.10	2.54
4.91	6.65	5.68	2.45
4.39	5.94	5.16	2.33

The perylene-iodine complex also is only stable when kept under its own vapor pressure. However, when exposed to air the sublimation rate of the iodine is much slower than in the case of pyrene-iodine. Neither the pyrene-iodine nor the perylene-iodine complex showed any change in composition if kept in closed vials for periods up to a year.

DISCUSSION

For a high number of free charge carriers to exist in any material, two conditions must be fulfilled:

1. The energy involved in the separation of charges should not be too high.

2. A charge carrier must have the possibility of transferring from one site to another. The energy required for charge separation in a molecular solid can be approximated qualitatively with the following thought experiment:

Two molecules are taken out of the solid. This requires an energy $2E_s$. Then one molecule is ionized (I) and the electron is attached to the other molecule ($-E$). Then both ions are brought back into the solid without letting the electronic system of either or the lattice relax. The energy required for this last process will, to a high degree of accuracy, be equal and opposite to the energy of taking them out ($-2E_s$). If now the electronic system of ions and lattice is left to relax, the contributions P_- and P_+ from the polarization energy around the negative and positive ion will be gained, i.e., the total required energy for charge separation will be

$$E_{cs}=I-E-P_--P_+.$$

This will be the energy required for charge separation to a distance where no Coulombic interaction of the carriers takes place. It therefore gives an upper limit. If Coulombic interaction still operates, that energy has to be subtracted, too. At the present time, without knowledge of the crystal structure and the anisotropic

polarizabilities of the molecules involved, a more than qualitative approach to E_{cs} is certainly not warranted. However, it is clear that when I is small and E, P_- and P_+ are large, E_{cs} will be small. These conditions seem to be fulfilled in the hydrocarbon-iodine complexes. For the bigger aromatics, like pyrene and perylene, I is relatively small;[8] both iodine and hydrocarbons have high dielectric constants, which will allow a high value for the energies of polarization. Then it is conceivable that E_{cs} can become of the order of 0.1 ev or less, as was found from the conduction measurements.

Since the interaction between molecules in a molecular lattice is very low, transfer of an uncoupled electron from one site to another must be an inherently infrequent process, with a resulting low electronic mobility. This would explain why a Hall effect could not be detected. Alternatively, in his treatment of the electronic spectra of the hydrocarbon-iodine complexes in solution Mulliken[9] explains these anomalous spectra by an almost total transfer of electronic charge from the hydrocarbon to the iodine in the excited state. It is possible that in a solid, where one hydrocarbon molecule can interact at the same time with many iodine molecules, these excited charge transfer states occur at much lower energies. Although this would provide a mechanism for the transfer of charge, processes 1 and 2 as defined before are then closely interrelated and should not be thought of separately. In this context it is interesting to note that the red shift of the fluorescence spectrum of crystalline pyrene and of concentrated pyrene solutions[10] is also explained on a charge transfer basis.[11] The perylene fluorescence spectrum shows essentially the same behavior. Pyrene and perylene, therefore, appear to be particularly sensitive to charge transfer interaction. The extreme opacity of these solids also indicates a number of low-lying excited states.

From the high density of carriers it would appear that at room temperature the conduction in both complexes is intrinsic. The break in the $\log\sigma$ vs $1/T$ curve for pyrene-iodine seems to indicate that at lower temperatures the conductivity becomes extrinsic. The possible role of impurities is presently under investigation in this Laboratory.

ACKNOWLEDGMENT

The authors wish to thank Dr. R. M. Broudy for his cooperation in the determination of the Hall effect.

[8] F. A. Matsen, J. Chem. Phys. **24,** 602 (1956).
[9] R. S. Mulliken, J. Am. Chem. Soc. **74,** 811 (1952).
[10] T. Förster and K. Kasper, J. Electrochem. Soc. **59,** 97 (1955).
[11] J. Ferguson, J. Am. Chem. Soc. **28,** 765 (1958).

THE JOURNAL OF CHEMICAL PHYSICS VOLUME 34, NUMBER 1 JANUARY, 1961

Electron Spin Resonance in Complexes of Aromatic Hydrocarbons with Iodine

L. S. SINGER* AND J. KOMMANDEUR†

Parma Research Center, Union Carbide Corporation, Parma, Ohio

(Received July 6, 1960)

Accurate measurements of electron spin concentration in semiconducting molecular complexes of perylene and pyrene with iodine have indicated an exponential temperature dependence in excellent agreement with the activation energy for electronic conduction. The agreement of the magnitudes of the spin concentrations with the carrier concentration estimates obtained from electrical measurements further confirms the identification of the unpaired spins as charge carriers. At low temperatures, small temperature-independent concentrations of trapped spins or free radicals are observed. Spin resonance line shapes, relaxation times, and g-factor anisotropies also have been determined.

I. INTRODUCTION

THIS paper presents the results of electron spin resonance (ESR) measurements on both powders and single crystals of pyrene-iodine and perylene-iodine molecular complexes at temperatures between 4.2 and 350°K. The purpose of the investigation was to see if the magnetic properties could give additional information concerning the electronic structure and the nature of the conduction process in these and perhaps other organic semiconductors. Since the most important conclusions of this study depend upon the quantitative measurement of spin concentrations at various temperatures, a fairly detailed description of the equipment and experimental procedures is given. The results are presented and discussed mainly from the standpoint of their possible relation to the conduction process.

* Research Laboratory of National Carbon Company, Division of Union Carbide Corporation.
† Parma Research Laboratory of Union Carbide Corporation.

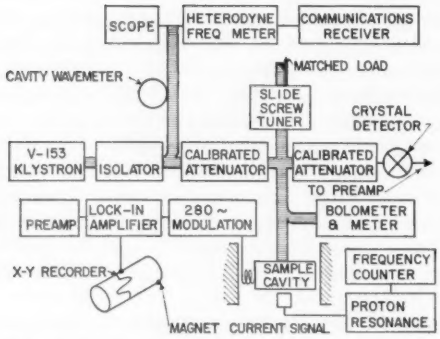

FIG. 1. Block diagram of electron spin resonance apparatus.

II. EXPERIMENTAL METHODS

A. ESR Apparatus

All the ESR experiments were performed at 9500 Mc using a magnetic-field modulation scheme of the conventional type. Figure 1 shows a block diagram of the arrangement. The microwave frequency was locked to that of the sample cavity by an automatic frequency control system. Saturation measurements were made as a function of power by varying the two calibrated attentuators in such a way as to keep the crystal current constant. A bolometer was used to measure the absolute microwave power entering the cavity. The g-factor measurements which were accurate to one part in 20 000 were made by comparing the microwave and proton resonance frequencies with the 10 Mc frequency standard of WWV.

The sample cavity was the Varian V-4500-30 slightly modified to accept either a thin-wall Pyrex Dewar tube for use in a blower arrangement, or the small quartz Dewar shown in Fig. 2. The "paddle wheel" on the left side of the cavity was used conveniently to vary the coupling screw in the Varian adjustable iris. The quartz rod under the cavity was carefully ground and etched with a millimeter scale for accurate positioning of samples in the cavity.

The small quartz Dewar of approximately 200 ml capacity was used for measurements at 77 and 4.2°K, one liquid-helium filling lasting approximately 20 min. The advantages of using such a simple system for certain ESR measurements at 4.2°K are numerous, particularly since there has been no evidence of the Dewar going "soft" after approximately 20 helium fillings. For measurements between 90°K and room temperature, cold N_2 gas was blown through a Pyrex Dewar tube, the desired temperature being attained by controlling the flow rate.

B. Spin Concentration Measurements

Approximate spin concentrations are usually determined by a simple comparison of the integrated ESR absorpiton with that of a standard sample.[1] However, the ESR measurement of spin concentrations over a wide temperature range with an accuracy of better than 10% requires considerable attention to a number of experimental and theoretical details not usually considered. There are two main parts to the problem: first, the relation between certain presumably measurable quantities and the actual number of unpaired spins; and second, the accurate measurement of these quantities. In the following section the basis for the measurements is discussed at some length. The accurate determination of integrated absorptions, line shapes, rf field intensities, and relaxation times are also described.

1. Basis for the Measurement

If an ESR absorption line in the absence of saturation satisfies the Bloch equations modified for a linearly polarized field,[2] the static spin susceptibility χ_0 is given by

$$\chi_0=\frac{2}{\pi\omega}\int_0^\infty \chi''d\omega_0, \tag{1}$$

where ω is the angular frequency of the rf field of amplitude H_1, $\omega_0=\gamma H_0$ is the precession angular frequency, and χ'' is the absorptive part of the total spin susceptibility. χ'' is related to the actual power absorbed by the sample P_a, by $\chi''=2P_a/\omega H_1^2$, so that

$$\chi_0=\frac{4\gamma}{\pi\omega^2 H_1^2}\int_0^\infty P_a dH_0; \tag{2}$$

if P_a is small compared to the total power impinging on the sample, the change in crystal detector signal will be directly proportional to P_a and the necessary data (except for a constant of proportionality) for performing the required integration would be available from a plot of crystal signal versus magnetic field H_0. If a magnetic field modulation scheme is used in which

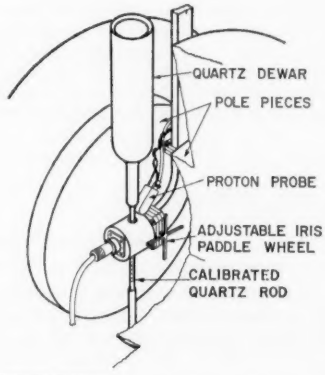

FIG. 2. Close-up view of microwave cavity with small quartz Dewar in place.

[1] D. J. E. Ingram, *Free Radicals* (Academic Press, Inc., New York, 1958), pp. 97–99.
[2] M. A. Garstens, Phys. Rev. **93**, 1228 (1954).

the modulation amplitude is small compared to the linewidth, a quantity proportional to dP_a/dH_0 is measured so that a double integration is necessary. A susceptibility determination thus depends upon the measurement of four quantities: γ (or the g factor), the microwave frequency ω, H_1 inside the sample, and P_a or dP_a/dH_0 as a function of H_0. Assuming almost free spins, the spin concentration is then given by the expression

$$N=\chi_0[3kT/g^2\beta^2S(S+1)]. \quad (3)$$

It should be emphasized that the foregoing simple combination of quantities usually measured in an ESR experiment cannot, in general, be identified with a static susceptibility. The exact form of the Kronig-Kramers relations[3] applies strictly only to the case where the magnetic field is constant and frequency is the variable. Altshuler[4] has attempted to derive similar relations for the case in which frequency is constant and the magnetic field is the variable; however, these relations cannot be obtained in explicit form. Of course, if the ESR line is narrow compared to H_0 at resonance, approximations of the Kronig-Kramers relations lead to the expression (1). The procedures used for justifying the use of (1) and measuring the quantities involved are described in the following.

2. Line Shapes

If an ESR curve can be shown to satisfy the modified Bloch equations, an increase in both simplicity and accuracy can be achieved in determining the spin concentration. For example, if the ESR curve shown in Fig. 3 can be shown to be the first derivative of a Lorentzian curve, the integrated absorption, which is proportional to $S_F{}^2D$, can be compared directly with a Lorentz-shaped curve for a standard sample of known

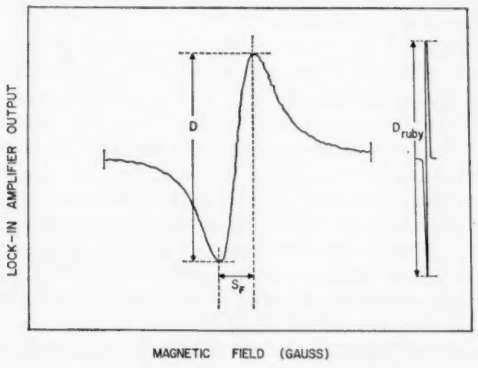

FIG. 3. Recorder chart showing a typical resonance and the ruby calibration signal.

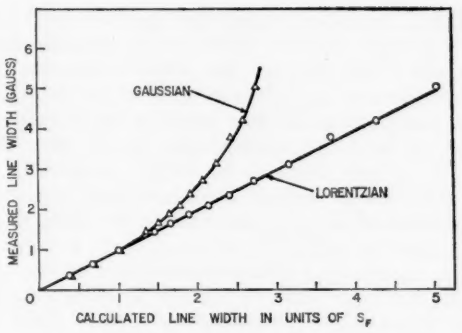

FIG. 4. Line shape analysis of a typical resonance.

susceptibility without resorting to numerical integration procedures.[5]

The method of line shape analysis[6] used was similar to that used by Weidner[7] for an absorption curve. The widths at various fractional heights on the derivative curve in Fig. 3 are plotted against the corresponding widths for a Gaussian and a Lorentzian curve. The straight line in Fig. 4 shows that the experimental curve is Lorentzian, at least out to about five linewidths.[8] The slope of this line also yields a reliable average value for the linewidth S_F. Line shape analyses were performed on all the curves used to obtain spin concentrations.

In the case of the perylene complex, the electrical resistivity of 8 ohm-cm results in a microwave skin depth of the order of 1 mm. As Bloembergen[9] and Feher and Kip[10] have shown, a mixture of χ' and χ'' results when the sample dimensions are $\geqq$ the skin depth. In order to eliminate the complicated shapes observed in the ESR for this material, the powdered sample was dispersed with Al_2O_3 powder.

3. Determination of the rf Field Intensity

It can be seen from (2) that χ_0 and thus the spin concentration is inversely proportional to the square of the rf magnetic field amplitude H_1 inside the sample. Because of the difficulty of accurately determining the absolute magnitude of this quantity, a comparison method was used in which only relative values were required.

[3] G. E. Pake and E. M. Purcell, Phys. Rev. **74,** 1184 (1948).
[4] S. A. Altshuler, Zhur. Eksptl. i Teoret. Fiz. **20,** 1047 (1950).

[5] If one performs an accurate double integration of the derivative curve for a Lorentz-shaped absorption neglecting the wings beyond $\pm 4S_F$, an error of 27% results.
[6] L. S. Singer, W. J. Spry, Jr., and W. H. Smith, *Proceedings of the Third Conference on Carbon* (Pergamon Press, New York, 1959), p. 123.
[7] R. T. Weidner, and C. A. Whitmer, Phys. Rev. **91,** 1279 (1953).
[8] There are, of course, firm theoretical reasons why an ESR curve cannot be exactly Lorentzian. [See, for example, P. W. Anderson and P. R. Weiss, Revs. Modern Phys. **25,** 269 (1953).] However, deviations from the Lorentz shape beyond five linewidths will not significantly change the integrated area calculated in the above manner.
[9] N. Bloembergen, J. Appl. Phys. **23,** 1379 (1952).
[10] G. H. Feher and A. F. Kip, Phys. Rev. **98,** 337 (1955).

It had been found previously[11] that the signal from a small single crystal of synthetic ruby, cemented along one side of the cavity at the correct orientation, is a convenient and accurate monitor of H_1 in the cavity. The signals from the ruby occur at static magnetic fields far from that corresponding to a g value of 2 and have been found to be strictly proportional to H_1 at the sample position. The measurement procedure then consisted of simply determining the height of the ruby signal for each ESR curve as is shown in Fig. 3.

One complication in any determination of spin concentration is the difference between H_1 inside a sample and H_1 immediately outside the sample. Since all materials have a real part of the dielectric constant greater than unity, the density of the E field and H_1 inside will always be somewhat larger than that immediately outside the sample. This means that the effective filling factor of the cavity will be considerably enhanced by samples of sizable dielectric constant. For example, a small solid sample showed an enhancement of signal by a factor of 2 when it was moved from 1 mm above a drop of water in the cavity to inside the water drop. The magnitude of this "sucking in" of the microwave field which, of course, also depends upon the type and thickness of sample tubes, can be estimated by extrapolating the apparent spin concentration to samples of infinitesimal size. Only a slight size effect was observed for the materials reported here. For example, in a pyrene-iodine sample 3 mm in diam, the signal height from a small sample of powdered $MnSO_4 \cdot H_2O$ increased by 20% when it was moved from slightly above the sample to its interior. The absolute spin concentration determinations were performed on samples of 1 mm in diam or less and should, therefore, have an accuracy of about 10%.

4. Saturation

As mentioned previously, an accurate spin concentration measurement requires the determination of both the signal properties and H_1 in the absence of saturation. Saturation curves[12] were, therefore, run on both materials at the lowest temperatures used (see Fig. 9) and the maximum allowable microwave power level was determined. For example, it was necessary to operate at a power less than 100 μw in order not to saturate the signal from the perylene-iodine complex at 4.2°K.

5. Calculation of the Spin Concentration

When the electrical properties of the sample, conditions for measurement, and the ESR line shape were taken into account as already described, the susceptibility was then calculated from the expression

$$\chi_0 = Kg(D/D^*)(G^*/G)(H_m^*/H_m)S_F^2, \qquad (4)$$

where D is the signal height (see Fig. 3), G is the relative amplifier gain measured by a calibrated voltage d vider at the lock-in input, H_m is the modulation amplitude, S_F is the linewidth, and K is a constant determined from a sample of known susceptibility. The starred quantities pertain to the ruby. The spin concentration was obtained from the expression (3).

A convenient material to use for the evaluation of K is $CuSO_4 \cdot 5H_2O$ in single crystal form. It has a very small Weiss constant so that expression (3) is applicable. Single crystals of convenient size (a few hundred micrograms) can be chosen directly from a reagent bottle of the chemical, weighed on a microbalance, and then imbedded in paraffin. No change in the ESR properties has been observed for such standard samples over a period of several years. The ESR linewidth and g factor are both orientation dependent; however, the described method of determining spin concentrations takes both these parameters into account. The line is very closely Lorentzian so that the expression (4) could be used accurately for all the measurements reported in this paper. From a signal-to-noise standpoint, it was found worthwhile to rotate the standard sample in the field until a fairly narrow line with $S_F \approx 30$ gauss was obtained, since the signal height D is inversely proportional to S_F^2.

III. EXPERIMENTAL RESULTS

A. Spin Concentration vs Temperature

The high carrier concentrations of the complexes Py·$2I_2$ and 2 Per·$3I_2$, estimated from the transport properties measured in the preceding paper,[13] suggested that the observed ESR in these materials might be closely related to the conduction process. Detailed measurements of spin concentration for the pyrene and perylene complexes were therefore made over the temperature range from 100 to 300°K. A few measurements of powders and single crystals at 77 and 4.2°K were also carried out.

Figure 5 shows the results for powdered 2 Per·$3I_2$. The solid curve was calculated from the activation energy (as defined in footnote 3 of the preceding paper), $E = 0.019$ ev which was obtained from the electrical conductivity measurements.[13] The maximum deviation of the experimental points (circles) from the calculated solid curve corresponds to 5% of the spin concentration.

The results for the Py·$2I_2$ powder are shown in Fig. 6. It is evident that there are two contributions to the spin concentration, a thermally activated species and a constant number of spins at low temperatures. The solid line was calculated as the sum of this constant (1.4×10^{18} spins/g) and the 0.14-ev activation energy determined from the electrical conductivity measurements. It is again seen that the activation energies for

[11] L. S. Singer, J. Appl. Phys. **30**, 1463 (1959).
[12] N. Bloembergen, E. M. Purcell, and R. V. Pound, Phys. Rev. **73**, 679 (1948).
[13] J. Kommandeur and F. R. Hall, J. Chem. Phys. **34**, 129 (1961), preceding paper.

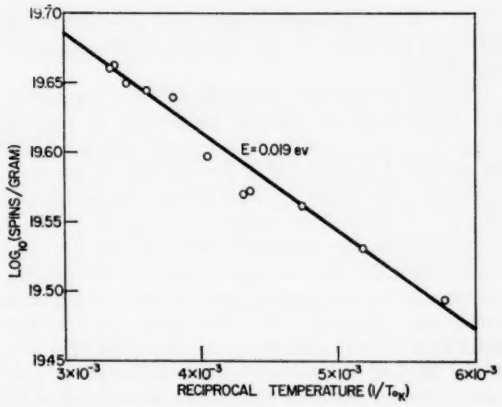

FIG. 5. Temperature dependence of the spin concentration for (2 Per·$3I_2$).

the conduction and the spin resonance are in excellent agreement, at least at temperatures above 200°K.

The room temperature (300°K) spin concentrations, 1.7×10^{19} and 4.6×10^{19} for Py·$2I_2$ and 2 Per·$3I_2$, respectively, are in agreement with the estimates provided by the maximum mobility arguments of the preceding paper. However, our value for 2 Per·$3I_2$ is about 30% lower than that reported recently by Matsunaga.[14] In the case of Py·$2I_2$, the spin concentration results are consistent with a model which depicts every I_2 molecule as a potential paramagnetic site. For 2 Per·$3I_2$, the results indicate a concentration of potential paramagnetic sites about 10 times less than the I_2 molecule concentration.

Measurements of the spin concentration of Py·$2I_2$ powder at 4.2°K indicated no apparent change from the 1.4×10^{18}/g, shown in Fig. 6. On the other hand, a 2 Per·$3I_2$ single crystal showed a decrease in spin

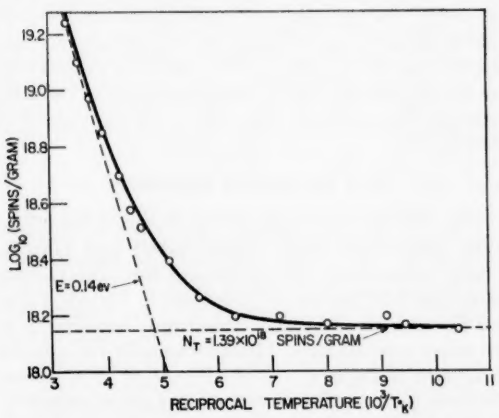

FIG. 6. Temperature dependence of the spin concentration for (Py·$2I_2$).

[14] Y. Matsunaga, J. Chem. Phys. **30**, 855 (1959).

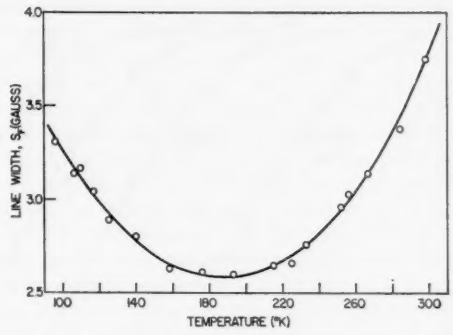

FIG. 7. Linewidth vs temperature for (Py·$2I_2$).

concentration by a factor of 10 in going from 77°K to 4.2°K. This decrease is much less than would be expected for a 0.019-ev activation energy. It is therefore probable that a different paramagnetic species with a temperature-independent spin concentration also occurs in the perylene complex. This would result in a curve similar to Fig. 6, except that the break would occur somewhere between 77 and 4.2°K.

B. Linewidths

Since all the curves measured were found to have essentially identical shapes, a comparison of linewidths is meaningful. In Figs. 7 and 8, the linewidth S_F is plotted as a function of temperature for the powdered pyrene and perylene complexes. S_F is the width between the extreme slope points shown in Fig. 3. The observed ESR lines were all closely Lorentzian so that the full width at half-height can be obtained by multiplying S_F by $\sqrt{3}$. Note that the linewidth miminum for Py·$2I_2$ in Fig. 7 occurs roughly at the same temperature at which the break in spin concentration occurs in Fig. 6.

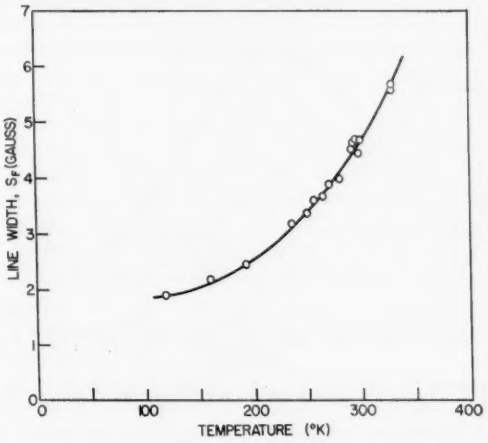

FIG. 8. Linewidth vs temperature for (2 Per·$3I_2$).

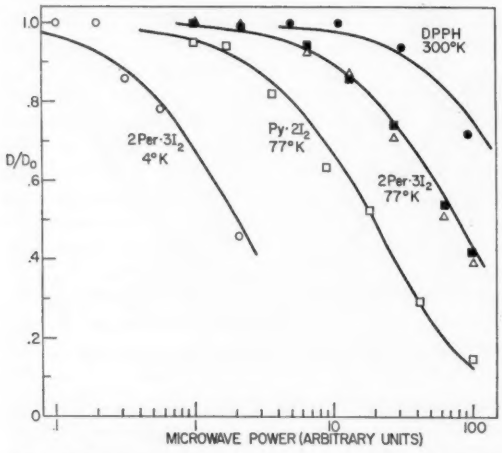

FIG. 9. Saturation curves for the pyrene and perylene complexes at low temperatures.

Much of the linewidth in the perylene complex at low temperatures is due to anisotropy broadening since single crystals exhibited both narrower lines ($S_F=0.5$ gauss at 77°K and 1.1 gauss at 4.2°K) and g-factor anisotropy. However, at room temperature, there was essentially no difference between linewidths for the powder and a single crystal of 2 Per·$3I_2$.

C. Spin-Lattice Relaxation Time, T_1

In order to ensure correct spin concentration measurements, the saturation curves shown in Fig. 9 were measured. The initial part of the saturation curve for a single crystal of diphenyl-picryl hydrazyl (DPPH) is shown for comparison. Since it has been found[15,16] that for DPPH, $T_1=T_2=6\times10^{-9}$ sec, T_1 for the samples could be determined from Fig. 9 at a given extent of saturation from the relation

$$T_1=(P_{(\mathrm{DPPH})}/P)\,T_1^2{}_{(\mathrm{DPPH})}T_2^{-1}, \qquad (5)$$

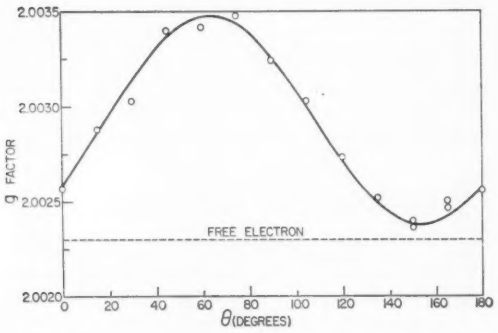

FIG. 10. g-factor anisotropy for a single crystal of (2 Per·$3I_2$) at 77°K.

[15] J. P. Lloyd and G. E. Pake, Phys. Rev. **92**, 1576 (1953).
[16] N. Bloembergen and S. Wang, Phys. Rev. **93**, 72 (1954).

where P is the microwave power and T_2 is the inverse linewidth parameter in the absence of inhomogeneous broadening.

The question of what to use for T_2 is not too obvious. The observation of g-factor anisotropy in perylene single crystals implies that T_2 derived from linewidths for powdered Py·$2I_2$ and 2 Per·$3I_2$ will be incorrect. Unfortunately, single crystals of the pyrene complex were not available. Furthermore, even for the 2 Per·$3I_2$ single crystals, the unknown origin of the linewidth cannot allow one to eliminate completely inhomogeneous broadening mechanisms such as nuclear hyperfine interactions. However, the observation that the linewidth for a 2 Per·$3I_2$ single crystal increased by ~30% at the highest microwave power available is good evidence[17] that the main broadening mechanism is not of the inhomogeneous type. It thus seems highly probable that T_2 is determined by the observed single crystal linewidth. On using a T_2 corresponding to 1-gauss linewidth, the calculated T_1's are 2×10^{-7} and 8×10^{-6} sec for 2 Per·$3I_2$ at 77°K and 4.2°K, respectively; and 9×10^{-7} sec for Py·$2I_2$ at 77°K. Since no evidence for saturation was observed at room temperature for either material, it is probable that $T_1\approx T_2$ in the vicinity of 300°K.

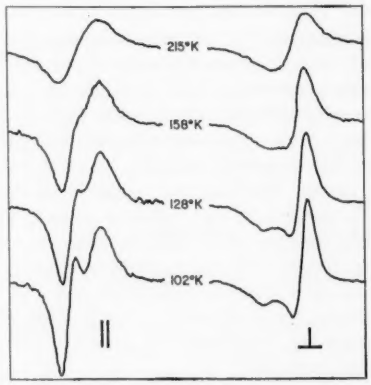

FIG. 11. Temperature dependence of the resonance curves for two different orientations of a "twinned" crystal of (2 Per·$3I_2$).

D. g Factors and Anisotropy

The g factors for powdered Py·$2I_2$ and 2 Per·$3I_2$ at room temperature were 2.0029±0.0001 and 2.0033±0.0001, respectively. The deviations from the Lorentz shape for ESR curves of powdered 2 Per·$3I_2$ below 100°K, strongly suggested anisotropy broadening at the lower temperatures. Measurements of the g-factor anisotropy of single crystals of 2 Per·$3I_2$ at 77°K showed this to be the case. Figure 10 compares the experimental results with those calculated from the expression

$$g=g_\perp+\Delta g\cos^2\theta, \qquad (6)$$

[17] A. M. Portis, Phys. Rev. **91**, 1071 (1953).

where $g_\perp = 2.00238$, $\Delta g = g_{||} - g_\perp = 0.00110$, and θ is the angle between the static magnetic field and the normal to the broad face of the thin crystal prisms. No attempt was made to relate θ, $g_{||}$, or $g_\perp$ to any molecular directions since the crystal structure of this material is at present unknown.

It was found also that this anisotropy was not temperature dependent. Figure 11 shows the ESR curves for a twinned crystal of 2 Per·$3I_2$. Note that as the temperature is increased, only the width of the individual components change. The peak separation remains constant.

IV. DISCUSSION

The close agreement between the activation energies for conduction and spin concentration for the Py·$2I_2$ and 2 Per·$3I_2$ complexes above 200°K is strong evidence that the observed unpaired spins are charge carriers. The agreement of the magnitudes of the spin concentrations with the estimates obtained from the electrical properties[13] further confirms this identification. There are, however, several aspects of the experimental results which require additional explanation.

The source of the constant number of spins which dominate the ESR of the pyrene complex at low temperatures is not understood. One might attempt to associate the spins with shallow traps, but this can be ruled out in the following way. If a constant number of spins, denoted N_T in Fig. 6, exists in shallow traps and thus can take part in the conduction, the 0.07-ev activation energy for the conductivity below 200°K[13] must be due to an activated mobility. However, if this were true, one would not expect the activation energies for conduction and spin concentration to agree at the higher temperatures. A more likely possibility is that the pyrene contains as an impurity about 0.1 mole % of a compound which can form with I_2 a complex having a paramagnetic ground state. The electrical measurements indicate that a 0.07-ev activation energy would be required to promote the carriers from these impurity sites to the conducting state. Since the parent compounds pyrene and I_2 are diamagnetic, this impurity would have to be a molecular complex with an almost completely ionic ground state. These complexes might be similar to those studied by Bijl, Kainer, and Rose-Innes.[18] Impurities probably are involved also in the perylene case. However, due to the small activation energy and the high concentration of the carriers in 2 Per·$3I_2$, the temperature-independent spin concentration becomes evident only at temperatures below 77°K. It is interesting to note that similar phenomena have been observed in mixtures of perylene with sulfuric acid.[19]

Another problem arises when one attempts to relate the total number of complex molecules N, to the number of spins N_1, and the activation energy E. In the case of perylene-iodine, since the activation energy is of the order of kT, one expects to find a spin on every third 2 Per·$3I_2$ molecule at room temperature. However, it is found that only 1 in 10 complex molecules has an unpaired spin. It therefore seems probable that a number of molecules are engaged in stabilizing each charge carrier. If the production of charge carriers is discussed in terms of a localized process,[13] then it is reasonable to assume that the energy of excitation will be increased by the fields of the charge carriers already present. Thus charge carrier formation involves excitation of a small domain, in which a number of molecules is cooperating. Then, instead of using the normal exponential relation $N_1/(N-N_1) = \exp(-E/kT)$, one must use $N_1/(N-N_1-nN_1) = \exp(-E/kT)$, where n is the number of complex molecules engaged in stabilizing the spin. In the case of perylene-iodine this "cooperation factor," n is found to be approximately 3. A similar mechanism should be operative in pyrene-iodine. However, $(n+1)N_1$ is so small compared to N in this case that any such cooperative effect is not observable within the temperature range studied.

Although the other measured spin resonance parameters are not particularly useful in the absence of more structural information, a few qualitative remarks concerning the possible relation of these quantities to other properties may be worthwhile. The observed behavior of T_1 and T_2 for these complexes is consistent with a system of two kinds of spins. At the higher temperatures where the charge carriers are the most numerous magnetic species, $T_1 \approx T_2$, as is to be expected.[20] At low temperatures $T_1 \gg T_2$, as would be the case for localized spins at fairly high dilution. The occurrence of a minimum in the linewidth at about the same temperatures at which the breaks occur in the spin concentration curves is further evidence for the existence of different low- and high-temperature spin species.

The temperature dependence of the ESR linewidth at the higher temperatures is suggestive of a lifetime broadening mechanism, most probably involving a large spin orbit interaction with iodine. From Figs. 7 and 8, it can be seen that both the magnitudes and the temperature dependences of the ESR linewidth at the higher temperatures are approximately the same for the two complexes. Since the carrier concentrations are so different for these two materials, it seems likely that the spin concentration-dependent relaxation mechanisms[20] usually considered for conduction electrons are not applicable. On the other hand, the close similarity of the molecular structures of the two complexes suggests that the variation of lattice motions with temperature is the most important factor in the relaxation process.

The increase in linewidth with decreasing temperature for the localized spins at low temperatures is not

[18] D. Bijl, H. Kainer, and A. C. Rose-Innes, J. Chem. Phys. **30**, 765 (1959).

[19] Y. Yokazawa, J. Phys. Soc. Japan **13**, 727 (1958).

[20] D. Pines and C. P. Slichter, Phys. Rev. **100**, 1014 (1955).

understood. However, it is similar to the linewidth behavior of other free radicals.[21–23] The indication of a homogeneous broadening mechanism for the ESR of the single crystal of the perylene complex at 4.2°K suggests that the linewidth is not due primarily to hyperfine interactions. Since on the basis of pure dipolar broadening,[24] a linewidth of ~0.1 gauss is expected from the observed spin concentration, some unknown line broadening mechanism is involved.

Although the *g*-factor anisotropy, linewidths, and relaxation times furnish in themselves no additional proof, the results are consistent with the conclusions that at higher temperatures the ESR is due to charge carriers while at low temperatures trapped spins are present.

[21] L. S. Singer and E. G. Spencer, J. Chem. Phys. **21**, 939 (1953).
[22] L. S. Singer and C. Kikuchi, J. Chem. Phys. **23**, 1738 (1955).
[23] L. van Gerven, A. van Itterbeek, and E. de Wolf, J. phys. radium **17**, 140 (1956).
[24] J. H. van Vleck, Phys. Rev. **74**, 1168 (1948).

THE JOURNAL OF CHEMICAL PHYSICS VOLUME 34, NUMBER 1 JANUARY, 1961

Effect of Pressure on the Spectra of Crystalline UF_4 and UF_3†

K. B. KEATING AND H. G. DRICKAMER
Department of Chemistry and Chemical Engineering, University of Illinois, Urbana, Illinois

(Received June 28, 1960)

The effect of pressure has been measured on the crystalline spectra of UF_4 and UF_3. The UF_3, which has a structure analogous to PrF_3 and NdF_3, behaved much like those compounds, showing a 15% to 40% increase in intensity for different peaks in 50 000 atm. In UF_4 certain of the peaks increased in intensity while others decreased. The U^{4+} ion is almost at a center of symmetry in this crystal. It is indicated that the intensity behavior is reasonable if a significant fraction of the intensity is obtained due to lattice vibrations. Both red and blue shifts are observed on different peaks.

A STUDY has been made of the effect of pressure on the intensity, half-width, and frequency of maximum absorption, for crystalline UF_3 and UF_4. This work is, in a sense, an extension of our previous work on transitions in rare earth salts.[1] Samples of UF_3 and UF_4 were obtained from R. E. Biggers of Oak Ridge National Laboratory. UF_4 samples were also obtained from Argonne National Laboratory. The chlorides, obtained from the same sources, proved too hygroscopic to handle in our equipment. The UF_4 was studied as a pressure fused polycrystalline pellet, much like the rare earth halides. The UF_3 was diluted about 30% with NaCl to give better optical properties. The experimental methods were identical to those previously described.[1,2] Data were obtained to 180 000 atm on UF_4, but it was not possible to go beyond 53 000 atm with UF_3.

URANIUM TETRAFLUORIDE

Table I shows the absorption bands studied in this work. The position of the peak at 23 500 cm^{-1} is an estimate made necessary by the fact that this band was quite weak relative to the band at 21 140 cm^{-1} and impossible to resolve. The assignments are based on theoretical work by Jorgensen[3] and are tentative.

It has been established that the uranium ion in the UF_4 lattice does not quite occupy a center of symmetry although it is relatively close.[4] The structure is an ionic one in which the uranium atom is surrounded by eight fluorine atoms and each fluorine atom is situated between two uranium atoms. There are two kinds of U—8F coordination, one in which the fluorine atoms are arranged around the uranium atom in such a way that there is a true twofold axis of symmetry, while, in the second, the U—8F group is only slightly distorted from this symmetry. In the first kind of coordination each uranium atom is separated from the fluorine atoms by an average distance of 2.30 A while in the second the average bond distance is 2.28 A. The U—F bond distances and the geometry of the two types of U—8F groups are so similar that the two kinds of atoms are chemically equivalent. On using the uranium atom as a center of coordinates, the average angle between bonds to fluorine atoms in opposing octants is about 147°. The mean deviation in bond distance from the average value for each coordination type is of the order of 0.007 A.

The spectrum of U^{4+} in solids has been studied by Sancier and Freed.[5] They have summarized the experimental facts which are of interest in interpreting the spectrum of the U^{4+} ion.

(1) The spectrum undergoes considerable change in different environments and exhibits evidence of strong

† This work was supported in part by the U. S. Atomic Energy Commission.
[1] K. B. Keating and H. G. Drickamer, J. Chem. Phys. (to be published).
[2] R. A. Fitch, T. E. Slykhouse, and H. G. Drickamer, J. Opt. Soc. Am. **47**, 1015 (1957).
[3] C. K. Jorgensen, Kgl. Danske Videnskab. Selskab, Mat.-fys. Medd. **29**, No. 7 (1955).
[4] R. D. Burbank, U. S. Atomic Energy Commission Rept. K–769 (1951).
[5] K. M. Sancier and L. Freed, J. Chem. Phys. **20**, 349 (1952).

TABLE I. Assignments and observed values of peaks studied in uranium tetrafluoride.

Ion (configuration–ground state)	?	Assignments (3) $^3H_6$	$^3P_0-{}^1G_4$	$^3P_1$	$^1I_6$	$^1D_2$
U^{+4} $5f^2 6s^2 6p^6 - {}^3H_4$)	6825	9490	15 780	18 877	21 140	(23 500)

coupling between the lattice frequencies and the various electronic transitions.

(2) The intensities are greater than those for Pr^{3+} (the analog in the rare earth series) but much less than for an allowed transition.

(3) Magnetic susceptibility data show strong deviations from free ion behavior.

These facts are consistent with the known characteristics of $4f$ and $5f$ orbitals. It is known from theoretical considerations that the $4f$ function is an inner function at atomic numbers corresponding to those of the rare earth elements. Also the energy of a $4f$ orbital is low enough in this region so that the $4f$ levels begin to fill at cerium ($Z=58$). Their spatial extent, however, is very small and they take no part in the chemical binding of the ion. The $5f$ eigenfunctions go through a transformation similar to that of the $4f$ functions. At first they are also outer functions but a critical region of Z is reached where they shrink and become inner functions. At this point the energy levels of the f orbitals begin to fall so that the $5f$ shell starts to fill. In the actinide series, however, the $5f$ orbitals do not appear to shrink as rapidly as in the $4f$ series. They also have a greater spatial extension relative to the $6s$ and $6p$ orbitals than to the $4f$ orbitals relative to the $5s$ and $5p$ orbitals. The result is a lower shielding of the $5f$ electrons and a tendency toward bonding properties.

TABLE II. Intensity ratio, half-width ratio, and peak shift for peaks studied in uranium tetrafluoride at several pressures.

Band location (cm^{-1})	Intensity ratio $p=50\,000$ atm	$p=100\,000$ atm	$p=150\,000$ atm
6825	1.24	1.59	1.87
9490	1.17	1.43	1.63
15 780	0.87	0.69	0.57
18 877	0.89	0.74	0.64
21 140	0.91	0.80	0.72
Band location (cm^{-1})	**Peak shift (cm^{-1}) $p=50\,000$ atm**	**$p=100\,000$ atm**	**$p=150\,000$ atm**
6825	neg.	neg.	neg.
9490	neg.	neg.	neg.
15 780	−30	−75	−100
18 877	+20	+85	+185
21 140	+165	+435	+570
Band location (cm^{-1})	**Half-width ratio $p=50\,000$ atm**	**$p=100\,000$ atm**	**$p=150\,000$ atm**
6825	1.04	1.10	1.12
9490	1.09	1.23	1.33
15 780	1.06	1.13	1.16
18 877	1.07	1.16	1.20
21 140	1.06	1.11	1.14

The band at 23 500 cm^{-1} is not included for the reasons already referred to. This peak, however, clearly decreased in intensity and appeared to be shifting to higher energy.

As Table II indicates, the absorption bands at 15 780, 18 877, 21 140, and 23 500 cm^{-1} decrease in intensity while those at 6825 cm^{-1} and 9490 cm^{-1} increase. Figures 1 and 2 show typical data.

As discussed in our previous paper,[1] a transition allowed by a lack of a center of symmetry should increase in intensity with pressure due to an intensification of the crystalline potential (V_i) causing mixing of the $4f-5d$ ($5f-6d$) wave functions. It is also possible for lattice vibrations to mix f and d orbitals and contribute to the intensity. The mixing due to lattice vibration is proportional to $(r_0/r)^2 V_e$, where V_e is the even part of the crystalline potential, r_0 is the amplitude

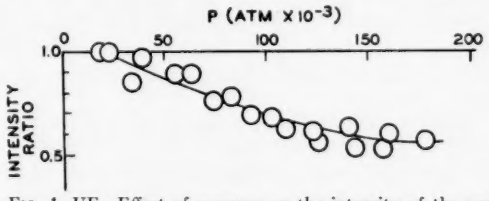

FIG. 1. UF_4. Effect of pressure on the intensity of the peak at 15 780 cm^{-1}.

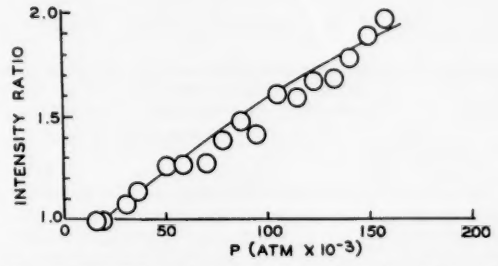

FIG. 2. UF_3. Effect of pressure on the intensity of the peak at 6825 cm^{-1}.

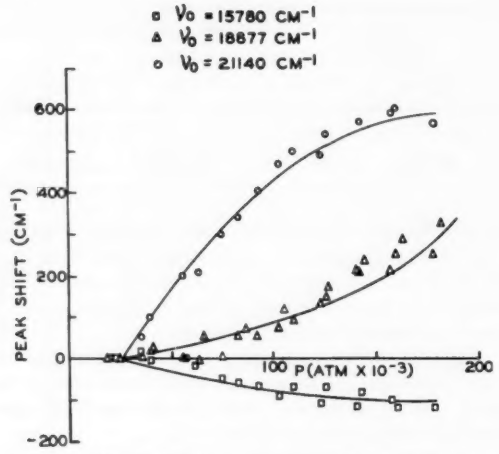

FIG. 3. UF_4. Peak shift versus pressure for three peaks.

of vibration of the metal nucleus, and r is the radius of the f orbital. The change in intensity is proportional to the square of this quantity. V_e will certainly increase with pressure.[1] It is reasonable to assume that r_0 decreases with increasing pressure. Certainly r is essentially independent of pressure.

For a lattice such as UF_4 which is only slightly distorted from having a center of symmetry there are probably significant contributions to the intensity due to mixing induced both by lattice vibrations and by a lack of a center of symmetry. Where the latter are more important the intensity should increase with pressure; where the former dominate there may be an increase or decrease depending on several factors—the extent to which r_0 is reduced and to which V_e is increased with pressure and the nature of the wave functions involved in the transition. It is not surprising, therefore, to find some peaks which increase in intensity with pressure and some which decrease in intensity to different degrees.

Figure 3 shows the shift in energy of the absorption bands at 15 780, 18 877, and 21 140 cm^{-1}. These are 100 cm^{-1} (red), 185 cm^{-1}(blue), and 570 cm^{-1} (blue), respectively (at 150 000 atm). The peaks at 6825 and 9490 cm^{-1} do not show any measurable shift. Table II shows that all of the peaks show significant broadening at 150 000 atm, of the order of 15–30%. The peak at 21 140 cm^{-1} has a very large half-width (about 2200 cm^{-1}) and its shift at 150 000 atm (570 cm^{-1} blue) is the largest found in this study. The shifts are probably due in large part to the intensifications of the crystal field splitting and possibly to some mixing with fluorine atom orbitals induced by pressure. The latter would appear possible in view of the greater spatial extent of the 5f orbital and the extent of covalency in most U^{4+} compounds.

TABLE III. Assignments and observed values of absorption bands studied in uranium trifluoride.

Ion (configuration–ground state)	Assignments (6) $^4I_{11/2}$	$^4I_{15/2}$	$^4F_{7/2}$
U^{3+} ($5f^2 6s^2 6p^6$–$^4I_{9/2}$)	4600	12 180	17 750

URANIUM TRIFLUORIDE

UF_3 diluted with 30% NaCl was used in the 0–50 000 atm cell. The data were normalized at 20 000 atm in order to allow for consistent analysis. Table III shows the absorption bands observed in this thesis along with tentative assignments by Jorgensen.[6]

The crystal structure of UF_3 is isomorphous with PrF_3 and NdF_3. The uranium ion occupies a site of C_{2v} symmetry.

TABLE IV. Half-width ratios, intensity ratios, and peak shifts for UF_3 at 50 000 atm.

Band location (cm^{-1})	Intensity ratio	Half-width ratio	Peak shift (cm^{-1})
4600[a]	1.39	...	+40[b]
12 180	1.15	1.00	neg.
17 750	1.22	1.00	neg.

[a] Crystal field splitting discernible. No half-width measurement made.
[b] Of a crystal field component at 4675 cm^{-1}.

Table IV shows the experimental results. As can be seen a peak at 4860 cm^{-1} shows a shift of approximately 40 cm^{-1} to higher energy. It was possible to observe the behavior of some crystal field components for this group. Unresolved absorption on the blue side of the two peaks at 4600 cm^{-1} made it impossible to make a half-width measurement.

The similarity in behavior to the fluorides of the rare earth elements is noticeable. There is no discernible shift for the peaks at 12 180 and 17 750 cm^{-1} and no measureable increase in the half-width of these two peaks. The shift of the peak at 4680 cm^{-1} is probably due to the intensification of the crystal field.

ACKNOWLEDGMENTS

The authors would like to express their thanks to the Argonne National Laboratory and Oak Ridge National Laboratory (especially R. E. Biggers) for furnishing samples. K. B. Keating would like to acknowledge financial assistance from a Minnesota Mining and Manufacturing Fellowship, and from a Standard Oil Company (Ohio) Fellowship.

[6] C. K. Jorgensen, Kgl. Danske Videnskab. Selskab, Mat.-fys. Medd. **29**, No. 11 (1955).

Effect of Pressure on the Spectra of Rare Earth Ions in Crystals*

K. B. KEATING AND H. G. DRICKAMER

Department of Chemistry and Chemical Engineering, University of Illinois, Urbana, Illinois

(Received May 26, 1960)

The effect of pressure to 180 000 atm has been measured on the absorption spectra of crystalline rare earth ions. The effects observed include:

(1) An increase of intensity due to increased mixing of $5d$ and $4f$ orbitals in the excited state due to an increase of the mixing potential with decreased interionic distance.

(2) Small shifts accompanied by increases in half-width. Except for the shifts of $^3P_0$, $^3P_1$, and $^3P_2$ levels of Pr^{+3}, these can be accounted for by an increase in the splitting of the individual levels due to intensification of the crystal field.

(3) Changes in shape of several of the bands, possibly due to changes in occupation of the various states which make up the bands.

THE effect of pressure to 180 000 atm has been measured on the intensity half-width and energy of maximum absorption for several absorption bands in compounds of praseodymium, neodymium, samarium, holmium, erbium, and thulium. The high-pressure optical techniques have been previously described.[1] The compounds studied, their sources and conditions, are summarized in Table I. The powders were pressure fused; small slices were cut from the single crystals. In all cases the changes observed were reversible with pressure, and considerable care was taken to avoid spurious effects due to fusion or to thickening of the sample with pressure.

The results are discussed in three sections below: (1) intensity changes, (2) shifts and changes in half-width, and (3) changes in peak shape.

1. INTENSITY CHANGES

The absorption bands or line groups (in crystals) of the rare earth ions have oscillator strengths of the order of $10^{-7}-10^{-5}$, about one-millionth that expected for dipole radiation. Broer, Gorter, and Hoogschagen[2] have shown that quadrupole radiation would give oscillator strengths of the order of 10^{-9} and thus can be discounted as a mechanism for transition between states of the rare earth ion in a crystal field. They also show that transitions due to magnetic dipole radiation will be much closer to the proper order ($P\sim 2\times 10^{-8}$) as will transitions due to electric dipole radiation induced by a lack of a center of symmetry ($P\sim 10^{-6}$). Magnetic dipole lines have been observed in the spectra of Dy^{+3} and Eu^{+3}.[3,4]

In salts in which the rare earth ion is not at a center of symmetry, it is possible for the $4f$ orbitals to mix with $5d$ orbitals of opposite parity. Such a perturbed wave function can be written

$$\psi'(4f)=\psi^0(4f)+\sum_{5d}-\int\frac{\psi^0(4f)\mid V_i\mid\psi^0(5d)d\tau}{E_{4f}{}^0-E_{5d}{}^0}, \quad (1)$$

where

$$V_i(r,\theta,\phi)=R_i^{-1}\sum_{n=0}^{\infty}[2/(2n+1)](r/R_i)^n e_i$$

$$\times[\Pi_n{}^0(\theta_i)\Pi_n{}^0(\theta)+2\sum_{m=1}^{n}\Pi_n{}^m(\theta_i)\Pi_m{}^n(\theta)\cos m(\phi-\phi_i)]. \quad (2)$$

Here Π_{nR} is the normalized associated Legendre polynomial of degree n, R_i is the distance between the nucleus and the charge e_i, $\psi'(4f)$ is the new $4f$ wave function, $\psi^0(4f)$ is the unmixed $4f$ wave function, $\psi^0(5d)$ the unmixed $5d$ wave function, $E_{4f}{}^0-E_{5d}{}^0$ the difference in their eigenvalues, and V_i is the crystalline potential. Calculations of this kind have been made in the case of $3d$–$4p$ mixing in transition metal ions by Ballhausen and Liehr.[5]

The integrals of Eq. (1) have nonvanishing values if V_i contains terms in the three coordinate axes which are of odd parity. In this case there will be elements in the integrand of the form (even) (odd) (odd) which will result in a nonzero value. If V_i contains only even terms, then the integrand is of the form (even) (even) (odd) and vanishes leaving the $4f$-eigenfunction unperturbed and retaining its original parity. The prohibition of intercombination by means of electric dipole radiation would then persist. If the integral does not vanish, then $\psi'(4f)$ contains terms of opposite parity to $\psi^0(4f)$ and combination with some other $4f$ state will be possible by means of electric dipole radiation. Due to the high powers, however, the intensity is small.

It can be shown that V_i will contain no terms of odd parity if the charges are arranged so that there is a center of symmetry. Conversely, if there is no center of

* This work was supported in part by the U. S. Atomic Energy Commission.

[1] R. A. Fitch, T. E. Slykhouse, and H. G. Drickamer, J. Opt. Soc. Am. **47**, 1015 (1957).

[2] L. F. J. Broer, C. J. Gorter, and J. Hoogschagen, Physica **11**, 235 (1944–46).

[3] A. M. Rosa, Ann. Physik **43**, 161 (1943).

[4] S. Freed and S. I. Weissman, Phys. Rev. **60**, 440 (1941).

[5] C. J. Ballhausen and A. D. Liehr, J. Mol. Spectroscopy **2**, 342 (1958).

TABLE I. Sources and properties of materials investigated.

Compound	State of aggregation	Source and quality	Method of preparation
$ErCl_3$	Powder	$ErCl_3 \cdot 6H_2O$, Research Chemicals, Inc. Burbank, Calif. 98% Min. purity	Dehydration with gaseous HCl[a]
$HoCl_3$	Powder	Ho_2O_3, Research Chemicals, Inc. 99.8% Min. purity	Treatment with hydrochloric acid and subsequent dehydration with HCl[a]
$NaCl_3$	Powder	$NdCl_3 \cdot 6H_2O$, Research Chemicals, Inc. 99% Min. purity	Dehydration with gaseous HCl[a]
$PrCl_3$	Powder	$PrCl_3 \cdot 6H_2O$, Research Chemicals, Inc. 98% Min. purity	Dehydration with gaseous HCl[a]
$TmCl_3$	Powder	Tm_2O_3, Research Chemicals, Inc. 99% Min. purity	Treatment with hydrochloric acid and subsequent dehydration with gaseous HCl[a]
2% $PrCl_3$-98% $LaCl_3$	Single crystal	C. A. Hutchison, Jr. and E. Wong, Univ. of Chicago	...
NdF_3	Powder	Research Chemicals, Inc. 99% Min. purity	...
PrF_3	Powder	Research Chemicals, Inc. 98% Min. purity	...
$Er(C_2H_5SO_4)_3 \cdot 9H_2O$	Single crystal	Er_2O_3, Research Chemicals, Inc. Min. purity 99.8%	Conversion of oxide to sulfate[b,c] and reaction with previously prepared $Ba(C_2H_5SO_4)_2 \cdot 2H_2O$[d-f]
$Nd(C_2H_5SO_4)_3 \cdot 9H_2O$	Single crystal	Nd_2O_3, Research Chemicals, Inc. Min. purity 99.9%	Conversion of oxide to sulfate[b,c] and reaction with previously prepared $Ba(C_2H_5SO_4)_2 \cdot 2H_2O$[d-f]
$Pr(C_2H_5SO_4)_3 \cdot 9H_2O$	Single crystal	Pr_6O_{11}, Research Chemicals, Inc. Min. purity 99.8%	Same as above.
$Sm(C_2H_5SO_4)_3 \cdot 9H_2O$	Single crystal	Sm_2O_3, Research Chemicals, Inc. Min. purity 99.9%	Same as above.

[a] J. H. Kleinheksel and H. S. Kremers, J. Am. Chem. Soc. **50**, 961 (1928).
[b] P. T. K. Cleve, Sven. Vet. Akad. Handl. Bihang. **2**, No. 8, 5 (1874).
[c] G. Urbain, Compt. rend. **142**, 785 (1906).
[d] M. Berthelot, Bull. Soc. chim. Paris Ser. 2 **19**, 295 (1873).
[e] P. Claesson, J. prakt. Chem. New Ser. **19**, 246 (1879).
[f] J. E. Alen, Kql. Svenska Vetenskapsakad. Handl. **37**, No. 8, 30 (1880).

symmetry, there will be terms of odd parity. The latter is the case in all of the rare earth salts studied.

Here V_i is dependent on R_i^{-n} where R_i is the center-to-center distance between the central ion and the ligand in question. Thus, in the expansion of Eq. (2) for the case where there is not a center of symmetry, terms in R_i^{-4}, R_i^{-5}, R_i^{-6}, etc. appear for the point charge case. If the field is considered to be made of dipoles, then these would be replaced by R_i^{-5}, R_i^{-6}, R_i^{-7}, etc. Obviously, if R_i were to decrease by 15%, which is possible if the crystal were to be subjected to high pressure, the effect on these terms would be large, in the case of R_i^{-4} increasing by a factor of about 1.6. It is clear, therefore, that pressure will cause a pronounced increase in V_i and hence in the degree of mixing of $4f$ and $5d$ orbitals. It is assumed here that the effect of pressure on the coordinates of the electrons is negligible. In the case of a dipole field, a given decrease in the equilibrium distance between the nucleus of the rare earth ion and the center of the ligand would result in more overlap than if the ligand were considered to be a point charge.

Table II lists the intensity ratio at pressures of 50 000 atm, 100 000 atm, and 150 000 atm for all of the rare earth compounds studied. The values have been taken from smoothed plots of the experimental data. Typical plots are shown in Figs. 1–4. Values for the locations of the absorption bands are those observed in this study. In cases where the peaks were near one another in energy it was often not possible to separate them for an intensity measurement without considerable error. In these cases the intensity of the group of peaks was measured. Reversibility checks were made and found to agree within a few percent. There was also no change in the amount of sample in the light path with pressure.

Table II shows that there is no apparent correlation between the effect of pressure on the intensity ratio and the number of electrons in the $4f$ shell or the $L-S-J$ designation of the combining levels. Examination of

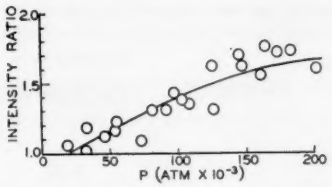

FIG. 1. $PrCl_3$. Plot of intensity of ratio vs pressure for $^3H_4 \rightarrow {}^3P_{0,1,2}$ transitions.

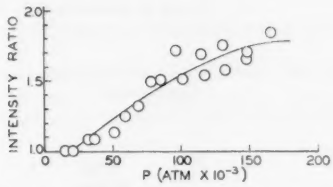

FIG. 3. $Sm(C_2H_5SO_4)_3 \cdot 9H_2O$. Plot of intensity ratio vs pressure for $^6H_{5/2} \rightarrow {}^6H_{13/2}$ transition.

the table also indicates that, at a pressure of 100 000 atm an average value for the intensity ratio for the chlorides and the fluorides is about 1.4. Compressibility data are not available for these substances but, from the data available for other ionic crystals, a reasonable assumption is that there is a 15–20% volume decrease at 100 000 atm. For the chlorides and the fluorides, the crystalline potential V_i in Eq. (2) increases approximately by a factor of $[(R_i)_0/(R_i)_p]^4$ where $(R_i)_0$ and $(R_i)_p$ are the equilibrium ligand-to-ligand distances at atmospheric pressure and at high pressure, respectively. Since the intensity varies directly as V_i^2, if we assume a volume decrease of about 15% at 100 000 atm pressure, we obtain an intensity increase of about 1.45. The term in R_i^{-6} may, of course, raise this estimate slightly, but clearly it is of the right order. The volume decrease estimate is based on the known compressibility (16.5%) of silver chloride at 100 000 kg/cm².[6] The fact that there is a tendency for the fluorides to show a smaller intensity change than the chlorides may be due to a smaller compressibility for the fluoride. The ethylsulfate represents a more complex situation. Here the nearest neighbors to the rare earth ion are six water molecules arranged around the ion such that the oxygen atoms are in D_{3h} positions. The effective charge for these is more nearly approximated by a dipole. Thus V_i varies as R_i^{-5}. Also for a given decrease in the distance between the rare earth nucleus and the center of the water molecule there is a greater potential change seen by the rare earth ion than if the ligand could be represented by a point charge. These two factors indicate that a greater intensity change with pressure might be expected for the ethylsulfates than for the chlorides or fluorides. It is possible, however, that the work of compression is largely dissipated in reducing the distance between the $SO_4^{=}$ radicals and the water molecules instead of the distance between the rare earth ion and the water molecules. This would tend to counterbalance the above two factors and possibly account for the fact that the intensity change with pressure for peaks in the ethylsulfate is only moderately greater than that for the chlorides and fluorides.

Figures 1 through 4 show typical plots of intensity ratio vs pressure for $PrCl_3$, NdF_3, $Sm(C_2H_5SO_4)_3 \cdot 9H_2O$, $HoCl_3$, and $Er(C_2H_5SO_4)_3 \cdot 9H_2O$ for the absorption bands indicated.

2. HALF-WIDTH INCREASES AND SHIFTS IN ABSORPTION MAXIMA

Table III lists half-width ratios and peak shifts at three pressures for the compounds studied. Very small shifts were difficult to detect in the apparatus used for visible and near infrared spectral studies.

At 150 000 atm pressure measurable shifts toward lower energy were observed in low-energy peaks in salts of praseodymium, neodymium, samarium, and thulium. The absorption band at 6580 cm^{-1} ($a^4I_{15/2} \pm {}^4I_{13/2}$ transition) in $Er(C_2H_5SO_4)_3 \cdot 9H_2O$ shifted to higher energy. These were all of the order of 40–90 cm^{-1} and were easily detectable in the infrared apparatus. These energy shifts were entirely reversible and were accompanied by increases in half-width. Figures 5–8 show typical plots of energy shift and a half-width ratio vs pressure for the compounds studied.

Relatively large peaks shifts toward lower energy were observed at 150 000 atm in praseodymium ethylsulfate for the absorption bands at 16 765 cm^{-1}, 20 620 cm^{-1}, 21 270 cm^{-1} and 22 390 cm^{-1} ($^1D_2$, $^3P_0$, $^3P_1$, $^3P_2$) and in anhydrous praseodymium chloride for the bands at 20 675 cm^{-1}, 21 244 cm^{-1}, and 22 452 cm^{-1} ($^3P_0$, $^3P_1$, $^3P_2$). These were of the order of 100 cm^{-1} in the ethylsulfate and from about 100 cm^{-1} to 200 cm^{-1} in the chloride. These effects were all accompanied by increases in the half-width ratio. The corresponding line groups were located at 20 360 cm^{-1}, 21 030 cm^{-1} and 22 120 cm^{-1} (transitions to $^3P_0$, $^3P_1$, $^3P_2$ states) in the single crystal of praseodymium chloride in lanthanum chloride and the peak shifts at 150 000 atm

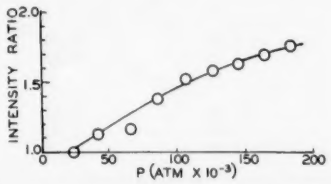

FIG. 2. NdF_3. Plot of intensity ratio vs pressure for $^4I_{9/2} \rightarrow {}^2G_{7/2}$, $^2G_{5/2}$ transition.

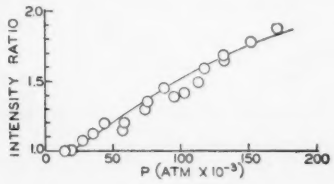

FIG. 4. $HoCl_3$. Plot of intensity ratio vs pressure for peak at 18 550 cm^{-1}.

[6] P. W. Bridgman, Proc. Am. Acad. Arts. Sci. **76**, 1 (1945).

TABLE II. Intensity ratio at three pressures for rare earth compounds studied.

Rare earth ion (ground state) compound-band location (cm^{-1}) (assignment)			Intensity ratio $P=50\,000$ atm	$P=100\,000$ atm	$P=150\,000$ atm
Praseodymium		($^3H_4$)			
PrF_3	6540	($^3F_3$)	1.22	1.50	1.66
	20 830	($^3P_0$)			
	21 410	($^3P_1$)	1.06[a]	1.20[a]	1.30[a]
	22 570	($^3P_2$)			
$PrCl_2$	4990	($^3F_2$)	1.24	1.57	1.79
	6430	($^3F_3$)	1.20	1.45	1.57
	20 675	($^3P_0$)			
	21 244	($^3P_1$)	1.16[a]	1.40[a]	1.59[a]
	22 452	($^3P_2$)			
$Pr(C_2H_5SO_4)_3 \cdot 9H_2O$					
	5100	($^3F_2$)	1.13	1.34	1.48
	6570	($^3F_3$)	1.10	1.26	1.36
	16 765	($^1D_2$)	1.12	1.26	1.38
	20 620	($^3P_0$)			
	21 270	($^3P_1$)	1.20[a]	1.47[a]	1.66[a]
	22 390	($^3P_2$)			
2% Pr^{+3} in $LaCl_3$					
	4960	($^3F_2$)	1.10	1.24	1.32
	6310	($^3F_3$)	1.21	1.54	1.81
	20 630	($^3P_0$)			
	21 030	($^3P_1$)	1.22[a]	1.56[a]	1.77[a]
	22 120	($^3P_2$)			
Neodymium		($^4I_{9/2}$)			
NdF_3	17 230	($^2G_{7/2}$–$^4G_{5/2}$)	1.19	1.47	1.69
	19 160	($^4G_{7/2}$)	1.19[a]	1.45[a]	1.65[a]
	19 570	($^4G_{9/2}$)			
$NdCl_3$	5043	(?)	1.32	1.81	2.08
	17 140	($^2G_{7/2}$ $^4G_{5/2}$)	1.22	1.43	1.54
	19 040	($^4G_{7/2}$)	1.21[a]	1.53[a]	1.75[a]
	19 420	($^4G_{9/2}$)			
$Nd(C_2H_5SO_4)_2 \cdot 9H_2O$					
	5075	(?)	1.19	1.44	1.57
	11 445	($^4F_{3/2}$)			
	12 475	($^4F_{5/2}$) ($^2H_{9/2}$)	1.12[a]	1.32[a]	1.48[a]
	13 465	($^4F_{7/2}$) ($^4S_{3/2}$)			
	17 250	($^2G_{7/2}$ $^4G_{5/2}$)	1.25	1.59	1.78
	19 085	($^4G_{7/2}$)	1.30[a]	1.71[a]	1.99[a]
	19 500	($^4G_{9/2}$)			
$NdCl_3 \cdot 6H_2O$					
	4985	(?)	1.46	2.12	2.54
Samarium		($^6H_{5/2}$)			
$Sm(C_2H_5SO_4)_3 \cdot 9H_2O$					
	5060	($^6H_{13/2}$	1.23	1.55	1.75
	20 770	(?)	1.16	1.39	1.49
	21 370	(?)	1.19	1.45	1.61
Holmium		($^5I_8$)			
$HoCl_3$	18 550	(?)	1.20	1.52	1.76
	22 060	(?)	1.20	1.50	1.72
Erbium		($^4I_{15/2}$)			
$ErCl_3$	18 410	($^4S_{3/2}$)	1.18	1.49	1.73
	19 070	($^2H_{11/2}$)	1.08	1.20	1.29
	20 480	($^4F_{7/2}$)	1.15	1.39	1.57

TABLE II.—*Continued.*

Rare earth ion (ground state) compound-band location (cm^{-1}) (assignment)			Intensity ratio $P=50\,000$ atm	$P=100\,000$ atm	$P=150\,000$ atm
$Er(C_2H_5SO_4)_3 \cdot 9H_2O$					
	6580	$(^4I_{13/2})$	1.13	1.32	1.46
	10 080	$(^4I_{11/2})$	1.14	1.35	1.51
	12 350	$(^4I_{9/2})$	1.21	1.57	1.84
	15 150	$(^4F_{9/2})$	1.13	1.24	1.50
	18 445	$(^4S_{3/2})$	1.29	1.71	1.97
	19 195	$(^2H_{11/2})$	1.20	1.50	1.73
	20 435	$(^4F_{7/2})$	1.21	1.51	1.73
Thulium		$(^3H_6)$			
$TmCl_3$	4970	$(^3H_5)$	1.3	1.74	2.02

[a] Intensity ratio for band group.

were larger than in the anhydrous chloride, being 265 cm^{-1}, 170 cm^{-1}, and 196 cm^{-1}, respectively. Possibly this lattice is more compressible at the praseodymium ion site since the La^{+3} ion (1.15 a.u.) is larger than the Pr^{+3} ion (1.08 a.u.).

In the anhydrous chloride and in the single crystal of Pr^{+3} in lanthanum chloride the shifts are clearly in the order $^3P_0 > {}^3P_1 > {}^3P_2$. This is probably also the case in the ethylsulfate although the difference between the shifts for the states is not large.

Plots of peak shift and half-width ratio vs pressure are shown for the various peaks 2% Pr^{+3} in $LaCl_3$ in Figs. 9–11. The absorption bands ($^3P_0$, $^3P_1$, $^3P_2$) showed a negligible shift and no increase in half-width in praseodymium fluoride.

Examination of Table III indicates that a shift in the energy of a peak is accompanied by an increase in the half-width of the peak. In some cases the peak changes shape radically; these are dealt with in the next section. The order of magnitude of the shifts and the correspondence between the existence of an energy shift and an increase in the half-width suggest that such shifts are results of intensification of the crystal field splitting. The observed shifts also amount to about 15–30% of the crystal field splittings at 1 atm (about 200 cm^{-1}).[2] This is of the same order as the pressure effect observed for transition metal ions[7] at 100 000 atm.

Consider a transition between two states A and B which are essentially of f character and which are split in a given crystal field as in Fig. 12.

When one studies the spectrum of a rare earth ion in a crystal one observes a line group which is the sum of the transitions shown for the crystal field case. The crystal field perturbation energy is increased by pressure and so ΔE increases to an extent depending on the nature of ψ and ψ^*. This increases the splitting and permits transitions over a broader energy range. It is also clear that such a model permits transitions to shift toward a lower or a higher energy, depending on the nature of the wave functions representing the free ion states A and B. This agrees well with the experimental facts. It should also be possible to observe bands which

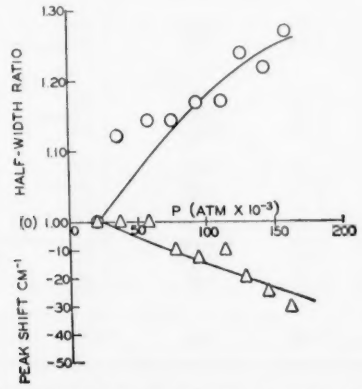

FIG. 5. 2% Pr^{+3} in $LaCl_3$. Plot of half-width ratio and peak shift vs pressure for $^3H_4 \rightarrow {}^3F_2$ transition.

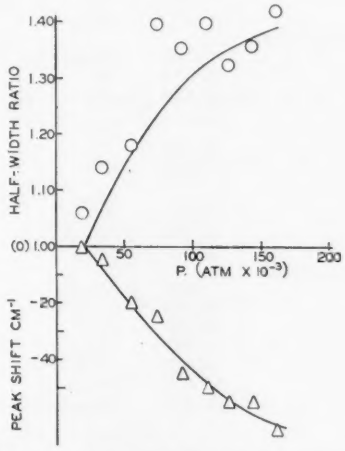

FIG. 6. $Nd(C_2H_5SO_4)_3 \cdot 9H_2O$. Plot of half-width ratio and peak shift vs pressure for peak at 5075 cm^{-1}.

[7] R. W. Parsons and H. G. Drickamer, J. Chem. Phys. **29**, 930 (1958).

TABLE III. Half-width ratio and peak shift at three pressures for rare earth compounds studied.

Rare earth ion (ground state) compound-band location (cm^{-1}) (assignment)			$P=50\,000$ atm		$P=100\,000$ atm		$P=150\,000$ atm	
			Half-width ratio	Peak shift (cm^{-1})	Half-width ratio	Peak shift (cm^{-1})	Half-width ratio	Peak shift (cm^{-1})
Praseodymium		($^3H_4$)						
PrF_3	6540	($^3F_3$)	1.00	Neg.	1.00	Neg.	1.00	Neg.
	20 830	($^3P_0$)	1.00	Neg.	1.00	Neg.	1.00	Neg.
	21 410	($^3P_1$)	1.00	Neg.	1.00	Neg.	1.00	Neg.
	22 570	($^3P_2$)	1.00	Neg.	1.00	Neg.	1.00	Neg.
$PrCl_3$	4990	($^3F_2$)	1.18	−19	1.42	−35	1.58	−42
	6430	($^3F_3$)	1.00	Neg.	1.00	Neg.	1.00	Neg.
	20 675	($^3P_0$)	1.13	−60	1.33	−146	1.50	−194
	21 244	($^3P_1$)	1.14	−38	1.35	−92	1.51	−132
	22 452	($^3P_2$)	1.17	−24	1.40	−62	1.57	−94
$Pr(C_2H_5SO_4)_3 \cdot 9H_2O$								
	5100	($^3F_2$)	1.06	−20	1.18	−39	1.26	−49
	6570	($^3F_3$)	1.00	Neg.	1.00	Neg.	1.00	Neg.
	16 765	($^1D_2$)	1.04	−28	1.10	−64	1.15	−94
	20 620	($^3P_0$)	1.08	−38	1.21	−80	1.29	−108
	21 270	($^3P_1$)	1.06	−32	1.17	−72	1.25	−98
	22 390	($^3P_2$)	1.05	−28	1.14	−64	1.21	−88
2% Pr^{+3} in $LaCl_3$	4960	($^3F_2$)	1.08	−7	1.19	−19	1.26	−27
	6310	($^3F_3$)	1.00	Neg.	1.00	Neg.	1.00	Neg.
	20 360	($^3P_0$)	1.18	−92	1.42	−194	1.55	−256
	21 030	($^3P_1$)	1.17	−52	1.40	−126	1.53	−170
	22 120	($^3P_2$)	1.15	−58	1.35	−138	1.48	−196
Neodymium		($^4I_{9/2}$)						
NdF_3	17 230	($^2G_{7/2}$–$^4G_{5/2}$)	1.00	Neg.	1.00	Neg.	1.00	Neg.
	19 160	($^4G_{7/2}$)	1.00	Neg.	1.00	Neg.	1.00	Neg.
	19 570	($^4G_{9/2}$)	1.00	Neg.	1.00	Neg.	1.00	Neg.
$NdCl_3$	5043	(?)	1.18	−18	1.33	−48	1.61	−72
	17 140	($^2G_{7/2}$–$^4G_{5/2}$)	1.00	Neg.	1.00	Neg.	1.00	Neg.
	19 040[a]	$^4G_{7/2}$	...	...	...	...	...	...
	19 420[a]	$^4G_{9/2}$	...	...	...	...	...	...
$Nd(C_2H_5SO_4)_3 \cdot 9H_2O$								
	5075	(?)	1.17	−18	1.33	−44	1.43	−60
	11 445	$^4F_{3/2}$	1.00	Neg.	1.00	Neg.	1.00	Neg.
	12 475	($^4F_{5/2}$–$^2H_{9/2}$)	1.04	Neg.	1.08	Neg.	1.10	Neg.
	13 465	($^4F_{7/2}$–$^4S_{3/2}$)	1.00	Neg.	1.00	Neg.	1.00	Neg.
	17 250	($^2G_{7/2}$–$^4G_{5/2}$)	1.00	Neg.[b]	1.00	Neg.[b]	1.00	Neg.[b]
	19 085	($^4G_{7/2}$)	1.00	Neg.	1.00	Neg.	1.00	Neg.
	19 500	($^4G_{9/2}$)	1.00	Neg.[b]	1.00	Neg.[b]	1.00	Neg.[b]
$NdCl_3 \cdot 6H_2O$	4985	(?)	1.11	−10	1.26	−44	1.36	−68
Samarium		($^6H_{5/2}$						
$Sm(C_2H_5SO_4)_3 \cdot 9H_2O$								
	5060	($^6H_{13/2}$)	1.12	−15	1.31	−36	1.44	−50
	20 770	(?)	1.00	Neg.	1.00	Neg.	1.00	Neg.
	21 370	(?)	1.05	Neg.	1.10	−30	1.13	−50
Holmium		($^5I_8$)						
$HoCl_3$	18 550	(?)	1.00	Neg.	1.00	Neg.	1.00	Neg.
	22 060	(?)	1.00	Neg.	1.00	Neg.	1.00	Neg.
Erbium		($^4I_{15/2}$)						
$ErCl_3$	18 410	($^4S_{3/2}$)	1.06	Neg.	1.12	Neg.	1.15	Neg.
	19 070	($^2H_{11/2}$)	1.05	Neg.	1.11	Neg.	1.12	Neg.
	20 480	($^4F_{7/2}$)	1.00	Neg.[b]	1.00	Neg.[b]	1.00	Neg.[b]
$Er(C_2H_5SO_4)_4 \cdot 9H_2O$								
	6580	($^4I_{13/2}$)	1.06	+12	1.17	+31	1.27	+45
	10 080	($^4I_{11/2}$)	1.11	Neg.	1.21	+20	1.27	+20
	12 350	($^4I_{9/2}$)	1.07	Neg.	1.15	+20	1.19	+30
	15 150	($^4F_{9/2}$)	1.05	Neg.	1.09	+20	1.11	+20
	18 445[c]	($^4S_{3/2}$)	1.04	Neg.	1.09	+20	1.11	+40
	19 195	($^2H_{11/2}$)	1.04	Neg.[b]	1.09	Neg.[b]	1.11	Neg.[b]
	20 435[c]	($^4F_{7/2}$)	1.09	Neg.	1.22	−40	1.31	−50
Thulium		($^3H_6$)						
$TmCl_3$	4970	($^3H_5$)	1.10	−27	1.25	−62	1.39	−80

[a] Two bands were unresolvable.
[b] Of whole band. Crystal field components were discernible.
[c] Band changing shape.

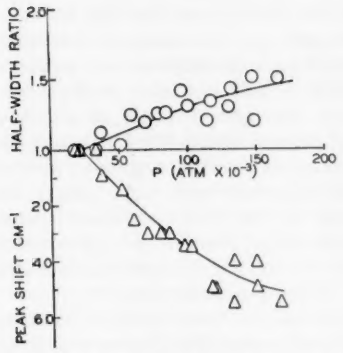

FIG. 7. $Sm(C_2H_5SO_4)_3 \cdot 9H_2O$. Plot of half-width ratio and peak shift vs pressure for ${}^6H_{5/2} \rightarrow {}^6H_{13/2}$ transition.

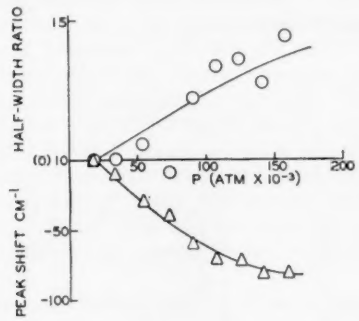

FIG. 8. $TmCl_3$. Plot of half-width ratio and peak shift vs pressure for ${}^3H_6 \rightarrow {}^3H_5$ transition.

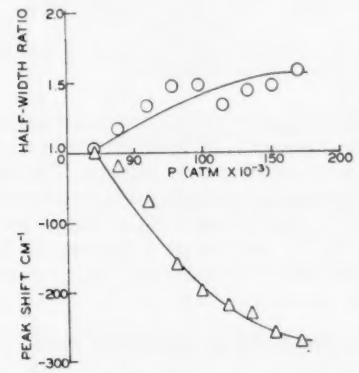

FIG. 9. 2% Pr^{+3} in $LaCl_3$. Plot of half-width ratio and peak shift vs pressure for ${}^3H_4 \rightarrow {}^3P_0$ transition.

broaden but show little or no over-all shift. There are indications that this occurs in the case of the peaks at 10 080 cm^{-1}, 12 350 cm^{-1}, and 15 150 cm^{-1} (transitions to ${}^4I_{11/2}$, ${}^4I_{9/2}$, ${}^4F_{9/2}$, respectively) in erbium ethylsulfate and in the peak at 12 475 cm^{-1} (transition to a mixed ${}^4F_{5/2}-{}^2H_{9/2}$ state) in neodymium ethylsulfate.

It is probably true that all of the bands in the spectra of the rare earth ions broaden to some extent, but they can be detected only when they exceed 10–20 cm^{-1} in the case of the infrared apparatus and 20–30 cm^{-1} in the case of the apparatus used for visible, near infrared and ultraviolet studies.

The rather large red shifts in the ${}^3P_{0,1,2}$ transitions in praseodymium chloride, praseodymium ethylsulfate, and in Pr^{+3} in lanthanum chloride merit further discussion since they are somewhat difficult to reconcile

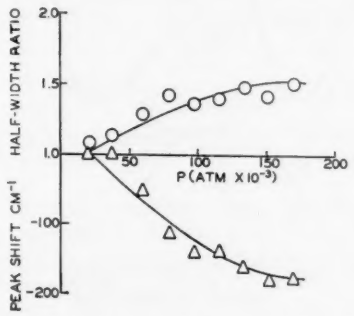

FIG. 10. 2% Pr^{+3} in $LaCl_3$. Plot of half-width ratio and peak shift vs pressure for ${}^3H_4 \rightarrow {}^3P_1$ transition.

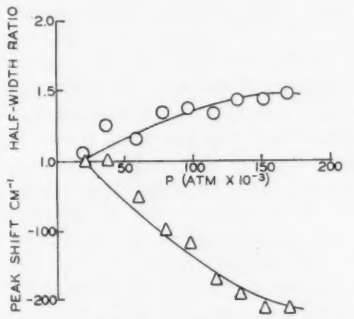

FIG. 11. 2% Pr^{+3} in $LaCl_3$. Plot of half-width ratio and peak shift vs pressure for ${}^3H_4 \rightarrow {}^3P_2$ transition.

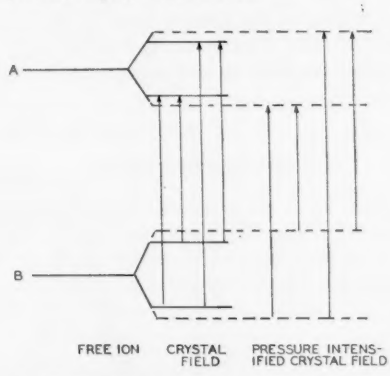

FIG. 12. Schematic representation of splitting of rare earth ion levels in crystal field at atmospheric pressure and at high pressure.

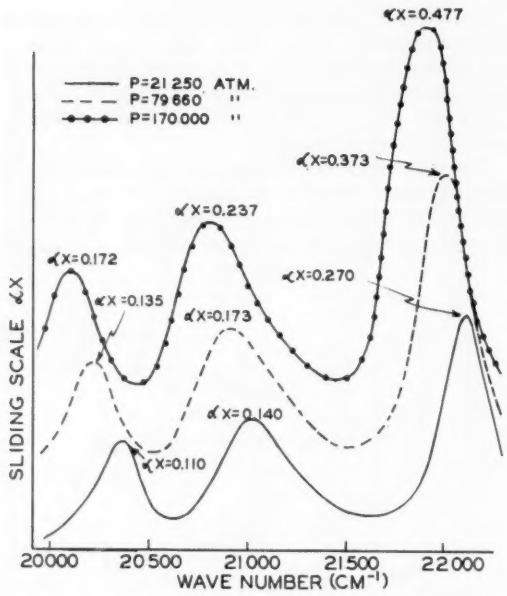

FIG. 13. 2% Pr^{+3} in $LaCl_3$. Plot of αX vs wave number for several pressures $^3H_4 \rightarrow {}^3P_{0,1,2}$ transitions.

with the above theory. Figure 13 shows a plot of αx vs wave number for Pr^{+3} in $LaCl_3$ at 21 250 atm, 79 660 atm and 170 000 atm. The fact that there is a large shift in energy associated with the $^3H_4 \rightarrow {}^3P_0$ transition suggests an intensification of the splitting of the ground level of the order of the shift since a level with $J=0$ is not split in the crystal field. It is also clear that the increase in half-width for these three bands is almost entirely on the low-energy side of the peak. These shifts are also pronounced in the anhydrous chloride and in the ethylsulfate in which the Pr^{+3} ion is also a site of C_{3h} symmetry. They do not occur in the fluoride where the Pr^{+3} ion is at a site of C_{2v} symmetry. All of this evidence points to the influence of the crystal field.

The splitting of the ground level to the extent of 200 cm^{-1} or more with pressure, however, appears to require much too large an intensification of the splitting of this level at atmospheric pressure, which is the same order of magnitude.[8] The weight of evidence suggested by other high-pressure studies on rare earth ion spectra in this work as well as studies on the effect of high pressure on the ground levels of transition metal complexes[7] indicate that a 100–150% intensification of the original crystal field splitting with pressure is highly unlikely. Furthermore such a splitting of the ground levels would require shifts of similar magnitude for other bands (e.g. $^3H_4 \rightarrow {}^3F_2$ at approximately 6500 cm^{-1}) which is not the case; unless, of course, the $^3F_2$ state also shifts by a similar amount.

The effect does not seem attributable to an increase in intensity of a transition between a level derived from the excited state and one derived from the ground state due to an increase in the population of the latter. An effect of this kind would be accompanied by a change of shape of the absorption bands; as can be seen in Fig. 12, this is not discernible.

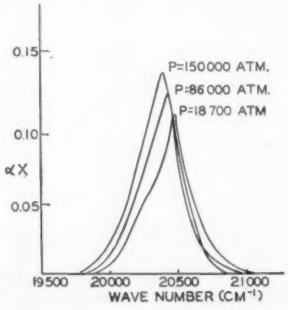

FIG. 14. $ErCl_3$. Plot of αX vs wave number at several pressures. Peak at 20 480 cm^{-1}.

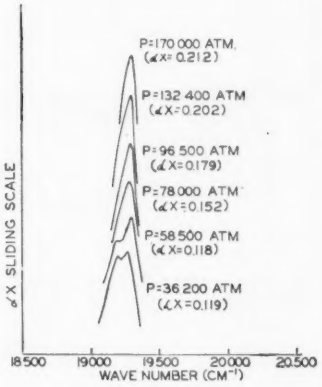

FIG. 15. $Er(C_2H_5SO_4)_3 \cdot 9H_2O$. Plot of αX vs wave number at several pressures. Peak at 19 230 cm^{-1}.

It should be mentioned that it appears unlikely that the observed energy shifts could be due to a change in the spin-orbit coupling with pressure. The spin-orbit coupling constant ζ can be shown to be proportional to $(1/r_i)[\partial V(r_i)/\partial r_i]$ where $V(r_i)$ is the nuclear potential seen by the electron at a distance r_i from the nucleus. The effect of pressure on $V(r_i)$ is undoubtedly negligible.

3. CHANGES OF SHAPE OF PEAKS

In a few runs it was possible to reduce the slit substantially below that normally used and to observe the behavior of some of the crystal field components of the bands in salts of erbium and neodymium. All of the effects observed were reversible.

Figure 14 shows plots of αx vs wave number at several pressures for the band having an apparent

[8] E. V. Sayre, K. M. Sancier, and S. Freed, J. Chem. Phys. **23**, 2060 (1955).

maximum at 20 480 cm^{-1} in erbium chloride. This line group has been assigned as a $^4I_{15/2} \rightarrow {}^4F_{7/2}$ transition.[9] The fine structure is undoubtedly due to transitions between levels arising from the Stark splitting of the $^4I_{15/2}$ and $^4F_{7/2}$ levels. Figure 14 indicates that a high-energy component is shifting toward lower energy and is increasing in intensity at a faster rate than the low-energy component. This causes the apparent peak of the whole band to shift about 80 cm^{-1} to lower energy at 150 000 atm. During this run the bands at 18 410 cm^{-1} ($^4S_{3/2}$) and 19 070 cm^{-1} ($^2H_{11/2}$) were also studied but no effects of this kind could be observed.

The band at 19 230 cm^{-1} ($^2H_{11/2}$) in $Er(C_2H_5SO_4)_3 \cdot 9H_2O$ was studied up to 170 000 atm. This is shown in Fig. 15. This is thought to be a $^4I_{15/2} \rightarrow {}^4H_{11/2}$ transition.[8] Here the high-energy component is apparently shifting to higher energy and also increasing in intensity at a faster rate than the low-energy component. The net result is an apparent shift toward higher energy for the entire band. The bands at 18 445 cm^{-1} and 20 435 cm^{-1} were also studied during this run. These are transitions from $^4I_{15/2}$ to $^4S_{3/2}$ and $^4F_{7/2}$, respectively. The groups at 18 445 cm^{-1} shifted to higher energy (about +40 cm^{-1}) at 170 000 atm and showed a tendency for a high-energy component to increase in intensity. Similarly, the group at 20 435 cm^{-1} showed an apparent red shift of 50 cm^{-1}. The behavior of the latter band in the ethylsulfate thus seemed similar to its behavior in the chloride.

Similar observations were made in the case of neodymium ethylsulfate. Figure 16 shows the band at approximately 17 250 cm^{-1}. This is a transition from the ground state to a mixed $^4G_{7/2} - {}^4G_{5/2}$ level. Here the high energy component shifts red and increases in intensity relative to the low-energy component. This results in an apparent red shift of the peak of approximately 80 cm^{-1} at 157 000 atm. Figure 17 shows a study of the band at approximately 19 500 cm^{-1}. One notes very complex behavior in this case. Both the high-energy component and the low-energy component appear to shift to lower energies. The relative increase in intensity of the high-energy component is of such a degree that the peak appears to be shifting to higher energy at the higher pressures.

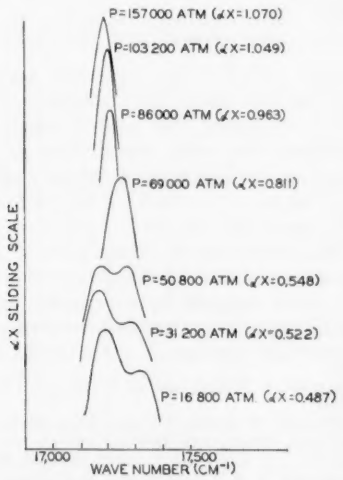

FIG. 16. $Nd(C_2H_5SO_4)_3 \cdot 9H_2O$. Plot of αX vs wave number for several pressures. Peak at 17 250 cm^{-1}.

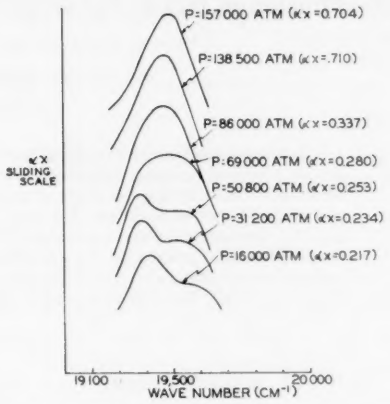

FIG. 17. $Nd(C_2H_5SO_4)_3 \cdot 9H_2O$. Plot of αX vs wave number for several pressures. Peak at 19 500 cm^{-1}.

It is interesting to note that the shift of the center of the four bands in Figs. 14–17 is negligible and that the corresponding broadening of the bands is also negligible. This is consistent with the model suggested in Section 2 if we postulate that the increase with pressure of the splitting of the rare earth levels is very small in this case.

The effects described in this section appear to be due to an increase in intensity of the high-energy component or components of the band. A necessary condition for this would be a substantial increase in the population of the lower-lying Stark levels of the ground state. This is conceivable in the case of the Nd^{+3} ion where, in the ethylsulfate, the maximum splitting of the ground state ($^4I_{9/2}$) is 350 cm^{-1} at atmospheric pressure.[10] This splitting is of the order of 1.7 times kT which would allow some occupation of the upper state at atmospheric pressure.

ACKNOWLEDGMENTS

The authors would like to thank C. A. Hutchison, Jr. for the $LaCl_3$ crystals doped with other rare earth ions. K. B. Keating would like to acknowledge financial assistance from a Minnesota Mining and Manufacturing Company Fellowship and a Standard Oil Company (Ohio) Fellowship.

[9] B. G. Wybourne, J. Chem. Phys. **32,** 639 (1960).

[10] R. J. Elliott and K. W. H. Stevens, Proc. Roy. Soc. (London) **A219,** 387 (1953).

Self-Diffusion of Nearly Spherical Molecules. Neopentane and Tetramethyl Silane

DEAN C. DOUGLASS, DAVID W. MCCALL, AND ERNEST W. ANDERSON

Bell Telephone Laboratories, Inc., Murray Hill, New Jersey

(Received July 14, 1960)

Self-diffusion coefficients have been measured for neopentane and tetramethyl silane by means of the nuclear magnetic resonance spin-echo technique. Both pressure and temperature dependences have been determined, thus allowing evaluation of energies and volumes of activation; neopentane, $E_D=3.5$ kcal/mole and $\Delta V\ddagger=31$ cm³/mole tetramethyl silane, $E_D=1.16$ kcal/mole and $\Delta V\ddagger=22$ cm³/mole. The numbers given for neopentane are average values as the $\ln D$ vs $1/T$ and $\ln D$ vs p plots were not straight lines. Kirkwood's theoretical relation for the self-diffusion coefficient of spherical molecules has been tested for the quasi-spherical neopentane. At 0°C the theoretical value is 6×10^{-5} cm²/sec while the experimental value is 2.6×10^{-5} cm²/sec. The Kirkwood equation for the self-diffusion coefficient is discussed in detail.

I. INTRODUCTION

THE theoretical position regarding transport properties of liquids is, at the moment, unsatisfactory. Various approaches are in use ranging from empirical correlations, through semiempirical modifications of theories more properly applicable to solids or gases, to the modern statistical mechanical method of Kirkwood. As one crosses the range from empiricism to rigor one encounters a range of attitudes; the empiricists are willing to attempt to correlate data for any substance, whereas those interested in rigorous molecular theories wish to consider only spherical molecules. It is with the latter group in mind that we submit the accompanying data. Neopentane and tetramethyl silane are about as spherical as *molecules* can be expected to be and, therefore, if the statistical theories are to be considered useful, they should at least aid us in interpreting the self-diffusion data for these substances. After all, the coefficient of self-diffusion, which involves only averages over the equilibrium ensemble, is the simplest of the transport properties.

II. EXPERIMENTAL

The experiments have been described in detail in earlier publications,[1–4] and no change in procedure has been made. The materials were used as received: neopentane, The Matheson Company, Inc., C.P., tetramethyl silane, K and K. Laboratories, 95–99%. Owing to the fact that neopentane is a gas at room temperature, it was necessary to cool the sample chamber of the pressure apparatus for filling. Where values are quoted above the boiling point, the substance was under its own vapor pressure.

III. RESULTS AND DISCUSSION

Figures 1–4 exhibit the results. It is clear that neopentane does not yield a straight line for either the $\ln D$ vs $1/T$ plot or the $\ln D$ vs p plot. On the other hand, the tetramethyl silane yields rather linear plots. The parameters are given in Table I. Except for the very low activation energy for tetramethyl silane, this is actually the lowest activation energy for self-diffusion known to us, the data are not out of the ordinary. That is to say, the values are close to those found for most other liquids.

Theoretical discussions often treat the phenomenon of self diffusion in terms of the friction constant, $\zeta=kT/D$, and we now examine the result of Kirkwood's theory for this parameter. It can be shown that[5–7]

$$\zeta^2=(4\pi/3)\rho\sigma\epsilon\int_0^\infty[(d^2\gamma/dx^2)+(2/x)(d\gamma/dx)]x^2g_0^{(2)}(x)dx, \quad (1)$$

where ρ is the density (g/cm³) and $\phi(x)=\epsilon\gamma(x)$ is the potential of interaction between two molecules. We shall employ

$$\phi(x)=4\epsilon(x^{-12}-x^{-6}), \quad (2)$$

where $x=R/\sigma$ and R is the separation between the centers of the two interacting molecules; for $x\geq1$. For $0\leq x<1$ we assume that $\phi(x)$ is infinite. Under these conditions the radial distribution $g_0^{(2)}(x)$ has been worked out by Kirkwood, Lewinson, and Alder.[8] The integral of Eq. (1), which we denote I, has been evaluated numerically for $\lambda=27.4$, $\epsilon/kT=0.864$ and $\epsilon/kT=0.792$, and $\lambda=33$, at which point I does not depend upon temperature. The quantity λ is the density parameter which appears in Kirkwood's analysis.[8,9] The potential parameters ϵ and σ have been published by Hamann and Lambert,[10] $\epsilon/k=236$°K and $\sigma=$

[1] D. C. Douglass and D. W. McCall, J. Phys. Chem. **62**, 1102 (1958).
[2] D. W. McCall, D. C. Douglass, and E. W. Anderson, Phys. Fluids **2**, 87 (1959).
[3] D. W. McCall, D. C. Douglass, and E. W. Anderson, J. Chem. Phys. **31**, 1555 (1959).
[4] J. Schwartz, Rev. Sci. Instr. **28**, 780 (1957).
[5] J. G. Kirkwood, F. P. Buff, and M. S. Green, J. Chem. Phys. **17**, 988 (1949).
[6] F. C. Collins and H. Raffel, J. Chem. Phys. **29**, 699 (1958); Advances in Chem. Phys. **I**, 135 (1958).
[7] S. A. Rice and J. G. Kirkwood, J. Chem. Phys. **31**, 901 (1959).
[8] J. G. Kirkwood, V. A. Lewinson, and B. J. Alder, J. Chem. Phys. **20**, 929 (1952).
[9] T. Hill, *Statistical Mechanics* (McGraw-Hill Book Company, Inc., New York, 1956), p. 214.
[10] S. D. Hamann and J. A. Lambert, Australian J. Chem. **7**, 1 (1954).

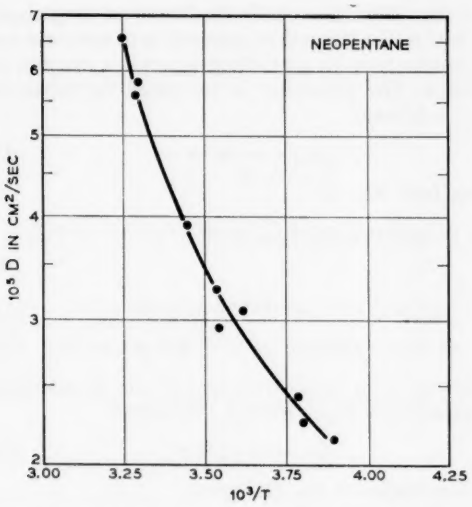

FIG. 1. Logarithm of the self-diffusion coefficient (cm²/sec) for neopentane as a function of reciprocal temperature (°K⁻¹).

7.37×10^{-8} cm, for neopentane. For this choice of ϵ, $\epsilon/kT=0.792$ corresponds to 25°C and $\epsilon/kT=0.864$ corresponds to 0°C. The necessary densities were obtained from the American Petroleum Institute tables.[11] For neopentane $\lambda=30.4$ and $I=59.9$ at 0°C; $\lambda=27.1$ and $I=55.2$ at 25°C.

Theoretical and experimental results for neopentane are compared in Table II, and it is seen that the calculated values are too high but the theoretical temperature coefficient (quoted as the activation energy, $-R[\partial \ln D/\partial(1/T)]$) is too small. Examination of the integrand in Eq. (1) reveals that the major contribution to the integral comes in the range $1.00<x<1.15$, where the repulsive term (x^{-12}) is important. This is unfortunate, as the repulsive part of the Lennard-Jones 6,12 potential is known to be inadequate. Hamann and Lambert[10] have discussed this point at length, and they show that a potential of the form

$$\phi(x)=(\epsilon/3)\,(x^{-23}-4x^{-7}), \tag{3}$$

which increases much more sharply as x decreases below unity, gives a better description of the equilibrium properties.

Collins and Raffel[6] have carried out a similar comparison for argon, ζ(theoretical) $=1.21\times10^{-10}$ g/sec, and ζ(experimental) $=5.93\times10^{-10}$ g/sec[12] (89°K). Their results are similar to ours in that the theoretical diffusion coefficient (kT/ζ) is higher than the measured diffusion coefficient and the integral is almost entirely determined at very small intermolecular separations.

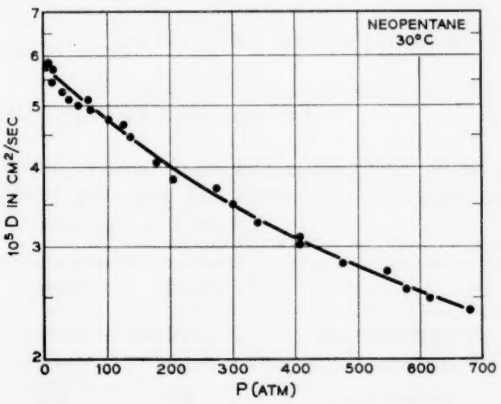

FIG. 2. Logarithm of the self-diffusion coefficient (cm²/sec) for neopentane as a function of the pressure (atm). 30°C.

[11] American Petroleum Institute, Research Project 44, Natl. Bur. Standards, Washington, D. C., 1945.

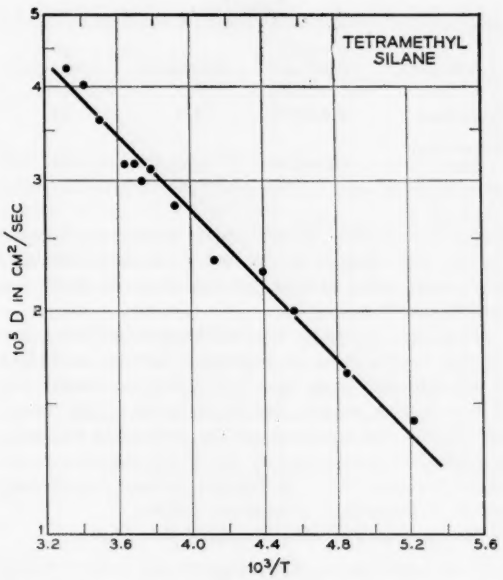

FIG. 3. Logarithm of the self-diffusion coefficient (cm²/sec) for tetramethyl silane as a function of reciprocal temperature (°K⁻¹).

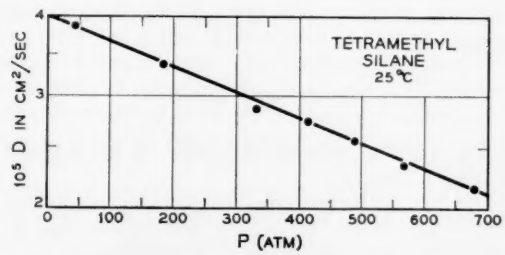

FIG. 4. Logarithm of the self-diffusion coefficient (cm²/sec) for tetramethyl silane as a function of the pressure (atm). 25°C.

[12] J. W. Corbett and J. H. Wang, J. Chem. Phys. **25**, 422 (1956).

TABLE I.

Substance	D(25°C) (cm²/sec)	E_D (kcal/mole)	$\Delta V^{\ddagger}$ (cm³/mole)
Neopentane	4.5×10^{-5}	3.5	31
Tetramethyl silane	3.6×10^{-5}	1.16	22

Collins and Raffel obtained better agreement between theory and experiment by using an experimentally determined radial distribution function; the result was $\zeta=4.84\times10^{-10}$ g/sec.

Since Eq. (1) represents a well-known and impressive attempt to arrive at an expression for the coefficient of self-diffusion from first principles, we should like to take it as representative of the state of the theory and discuss this equation and its derivation in detail. A method of obtaining Eq. (1) which reveals several salient features of the derivation without introducing undue mathematical complexity follows.

The coefficient of self-diffusion is given by

$$D=\langle r^2\rangle/6\tau, \tag{5}$$

where $\langle r^2\rangle$ is the mean square net distance a molecule can be expected to move in time τ. This may be taken as an assumption or definition or may be derived from the Gaussian probability distribution, which, in turn can be assumed or inferred from the fact that the Gaussian form is a solution to the differential equation (Fick's law) of diffusion, which in turn must be assumed. On using the fact that

$$\mathbf{r}=\int_0^t \mathbf{v}(\alpha)\,d\alpha$$

and Eq. (5), Longuet-Higgins and Pople[13] show that Eq. (5) can be written as

$$D=\tfrac{1}{3}\int_0^\infty \langle \mathbf{v}(t+s)\cdot\mathbf{v}(t)\rangle ds, \tag{6}$$

and introducing

$$\rho(s)=\langle \mathbf{v}(t+s)\cdot\mathbf{v}(t)\rangle/\langle v^2\rangle \tag{7}$$

and

$$\langle v^2\rangle=3kT/m, \tag{8}$$

we find

$$D=(kT/m)\int_0^\infty \rho(s)\,ds. \tag{9}$$

$\rho(s)$ is called the normalized velocity (or momentum) correlation function.

Equation (9) is especially interesting because it gives a direct relationship between $\rho(s)$ and D. Some qualitative information regarding $\rho(s)$ is available; e.g., it is an even function of s which decays as s increases. Since it is very difficult to obtain the functional form of $\rho(s)$ in liquids, the theoretical approach is to assume a one-parameter form for $\rho(s)$ which decays in a structureless manner. The parameter is calculated by expanding $\rho(s)$ as follows:

$$\rho(s)=1-a_2s^2+\cdots. \tag{10}$$

Also, from Eq. (7)

$$\langle v^2\rangle\rho(s)=\langle[\mathbf{v}(t)+\dot{\mathbf{v}}(t)s+\ddot{\mathbf{v}}(t)s^2/2+\cdots]\cdot\mathbf{v}(t)\rangle$$

or

$$\langle v^2\rangle\rho(s)=\langle v^2\rangle+s\langle\dot{\mathbf{v}}\cdot\mathbf{v}\rangle+\tfrac{1}{2}s^2\langle\ddot{\mathbf{v}}\cdot\mathbf{v}\rangle+\cdots \tag{11}$$

$$\langle\dot{\mathbf{v}}\cdot\mathbf{v}\rangle=-\langle\nabla\mathrm{H}\cdot\mathbf{p}\rangle/m^2=-\langle\nabla U\cdot\mathbf{p}\rangle/m^2=0, \tag{12}$$

where $\mathbf{p}$ is the momentum and H the Hamiltonian. Comparison of Eqs. (10) and (11) shows

$$a_2=-\langle\ddot{\mathbf{v}}\cdot\mathbf{v}\rangle/2\langle v^2\rangle. \tag{13}$$

Differentiation of Eq. (12) gives

$$\langle\ddot{\mathbf{v}}\cdot\mathbf{v}\rangle+\langle v'^2\rangle=0 \tag{14}$$

or, with Eq. (13),

$$a_2=\langle\dot{v}^2\rangle/2\langle v^2\rangle=m\langle\dot{v}^2\rangle/6kT \tag{15}$$

or

$$a_2=\langle\dot{p}^2\rangle/6mkT. \tag{16}$$

By elementary mechanics,

$$\langle\dot{p}^2\rangle=\langle(\nabla U)^2\rangle, \tag{17}$$

where ∇ denotes differentiation with respect to the particle coordinates and U is the total potential energy of the *system*.[14] On introducing $\beta=1/kT$,

$$a_2=(\beta/6Qm)\int\exp(-\beta U)\,(\nabla U)^2 d\mathbf{q} \tag{18}$$

or

$$a_2=(\beta/6Qm)\left\{\int\nabla[U\exp(-\beta U)]\cdot\nabla U\,d\mathbf{q}+\int\beta U\exp(-\beta U)\,(\nabla U)^2 d\mathbf{q}\right\}. \tag{19}$$

Q is the configurational partition function $\int e^{-\beta U}dq$. On using Green's theorem and neglecting surface

TABLE II. Neopentane.

	Exptl.	Theoret.
D(0°C) (cm²/sec)	2.6×10^{-5}	6×10^{-5}
D(25°C) (cm²/sec)	4.5×10^{-5}	7×10^{-5}
E_D(kcal/mole)	3.5	0.9

[13] H. C. Longuet-Higgins and J. A. Pople, J. Chem. Phys. **25**, 884 (1956).

[14] Dr. H. L. Frisch, of these Laboratories, first pointed out to us this derivation of Eq. (16) from Eq. (9).

integrals,

$$\int \nabla[U\exp(-\beta U)]\cdot\nabla U d\mathbf{q} = -\int U\exp(-\beta U)\nabla^2 U d\mathbf{q}, \tag{20}$$

$$= (d/d\beta)\int \times \exp(-\beta U)\nabla^2 U d\mathbf{q}. \tag{21}$$

Also,

$$\int \beta U\exp(-\beta U)(\nabla U)^2 d\mathbf{q} = -\beta(d/d\beta)\int \exp(-\beta U)(\nabla U)^2 d\mathbf{q}, \tag{22}$$

so that, letting $(6Qma_2/\beta) = J$, we find that

$$J = (d/d\beta)\int \exp(-\beta U)\nabla^2 U d\mathbf{q} - \beta dJ/d\beta$$

or

$$J\beta = \int \exp(-\beta U)\nabla^2 U d\mathbf{q} + C, \tag{23}$$

where C is independent of temperature.

$$6mQa_2 = \int \exp(-\beta U)\nabla^2 U d\mathbf{q} + C. \tag{24}$$

Equation (1) can be derived from Eq. (24) as follows. Setting $C=0$ and specializing to two-body central forces, Eq. (24) becomes[9]

$$a_2 = (2\pi N/3mV)\int_0^\infty \nabla^2 u g_0^{(2)} R^2 dR, \tag{25}$$

where u is the intermolceular pair potential, e.g., $\phi(R)$. On using

$$\nabla^2 u = (\partial^2 u/\partial R^2) + (2/R)(\partial u/\partial R) \tag{26}$$

and

$$x = R/\sigma,$$

$$a_2 = (2\pi\sigma N/3mV)\int_0^\infty [(\partial^2 u/\partial x^2) + (2/x)(\partial u/\partial x)]g_0^{(2)}(x)x^2 dx. \tag{27}$$

In order to relate a_2 of Eq. (27) with ζ^2 of Eq. (1), it is necessary to assume a functional form for $\rho(s)$. For example,

$$\rho(s) = \exp(-\alpha_2 s^2) \tag{28}$$

leads to

$$D = \pi^{\frac{1}{2}}kT/2ma_2^{\frac{1}{2}} = kT/\zeta. \tag{29}$$

Thus, $\zeta^2 = 4m^2 a_2/\pi$, so Eq. (27) yields

$$\zeta^2 = (8\rho\sigma/3)\int_0^\infty [(d^2u/dx^2) + (2/x)(du/dx)]g_0^{(2)}(x)x^2 dx, \tag{30}$$

which differs from Eq. (1) only by the constant $\pi/2$.

In addition to errors in $g_0^{(2)}$ and u, error may be introduced into Eq. (30) by a poor choice of the functional form of $\rho(s)$, and it is important to consider how D is affected by this choice. In gases one expects $\rho(s)$ to decay monotonically, and in solids (neglecting anharmonic motions) one expects $\rho(s)$ to oscillate with no decay. In liquids $\rho(s)$ may oscillate and decay, the oscillation being important near the melting point and the decay being dominant near the boiling point. Thus, the calculation leading to Eq. (30) is pertinent to a high-temperature situation.

A correlation function which has the qualitative properties expected for liquids is

$$\rho(s) = \exp(-\alpha^2 s^2)\cos(\delta\alpha s). \tag{31}$$

On expanding the function and comparing with Eq. (10) we find

$$a_2 = \alpha^2(1+\delta^2/2). \tag{32}$$

Therefore,

$$D = \pi^{\frac{1}{2}}kT[\exp(-\delta^2/4)(1+\delta^2/2)^{\frac{1}{2}}]/2ma_2^{\frac{1}{2}}. \tag{33}$$

The new parameter δ which determines the importance of oscillation in $\rho(s)$, is temperature dependent, decreasing with increasing temperature.

The temperature dependence predicted by Eq. (1) is much too small (see Table II) and, whereas one can rationalize the discrepancies in the absolute values for D, it is difficult to see how a substantially larger temperature coefficient could arise from the variables present. The small temperature dependence of D implied by Eq. (1) arises only through the density ρ and the radial distribution function $g_0^{(2)}$, the density giving the larger effect. These factors alone yield activation energies which are at least four times smaller than those observed for liquids. It is clear that the important temperature dependent terms have been neglected in order to obtain Eqs. (1) and (24). In terms of Eqs. (31) and (33), the major contribution to the temperature variation is to be found in the temperature dependence of the oscillation parameter δ. Physically this corresponds to the onset of vibrations such as one expects in solids. By evaluating higher terms in the expansions for $\rho(s)$ it might be possible, in a limited temperature range, to estimate the importance of the oscillating term. However, independent of any assumed form for $\rho(s)$, it is evident that more information than is contained in Eq. (1) must be obtained if a reasonable temperature coefficient is desired.

In previous publications[2,3] we have employed a semi-empirical modification of a theoretical equation derived

by Longuet-Higgins and Pople,[13]

$$D=(\sigma/2)(\pi RT/M)^{\frac{1}{2}}[(pV/RT)-1]^{-1}. \quad (34)$$

The derivation is based on a hard-sphere model and is good to high densities but does not include intermolecular attractive forces. The modification involves replacing the pressure p by the thermal pressure, $p_t=T/(\partial p/\partial T)_V$. Comparisons of calculated [by Eq. (34) as modified] and experimental diffusion coefficients lead to absolute values in fair agreement, but the calculated activation energies are too small. Thus, Eqs. (1) and (34) yield similar results. Equation (1) is superior in that it involves no empirical adjustments, but Eq. (34) is much more easily handled,[15] and it is based on a simpler model.

On turning to more qualitative aspects of the self-diffusion data, it is of interest to compare our results for tetramethyl silane with viscosity data for the polydimethylsiloxanes.[16,17] Tetramethyl silane can be thought of as the simplest member of this series. The low activation energies for viscosity found for the polydimethylsiloxanes have been interpreted as evidence for weak intermolecular forces which, in turn, were ascribed to the presence of the Si–O–Si group. The unusually low activation energy for self-diffusion found in the present study suggests that the Si–O–Si group is not the only determining factor. That is, the low activation energy is observed even when the Si–O–Si group is not present.

ACKNOWLEDGMENTS

The authors are indebted to H. L. Frisch, E. Helfand, A. D. Liehr, and W. P. Slichter for helpful discussions of this material.

[15] However, in the cases of neopentane and tetramethyl silane we do not have compressibility data and therefore we cannot use Eq. (34).

[16] D. H. Wilcock, J. Am. Chem. Soc. **68**, 691 (1946).

[17] A good summary of this work and related studies is given in E. G. Rochow, *Chemistry of Silicones* (John Wiley & Sons, Inc., New York, 1951), 2nd ed., pp. 108–17.

THE JOURNAL OF CHEMICAL PHYSICS VOLUME 34, NUMBER 1 JANUARY, 1961

Distortion Correction to the Surface Energy of the {110} Face of Alkali Halide Crystals*

G. C. BENSON, E. DEMPSEY,† AND P. BALK‡

Division of Pure Chemistry, National Research Council, Ottawa, Canada

(Received June 9, 1960)

Formulas for the contribution of surface distortion to the surface energy of the {100} and {110} faces of the NaCl-type lattice and of the {110} face of the CsCl-type lattice are obtained by a generalization of a treatment described previously for the {100} face of the NaCl structure. Numerical values of the distortion correction to the surface energy of the {110} faces of all of the alkali halides are presented. These results are discussed in relation to the values calculated previously for the {100} face and to the limited experimental information available.

I. INTRODUCTION

AT present a large discrepancy exists between the experimental values for the surface energies of such of the alkali halides as have been investigated[1,2] and the theoretical values for their {100} faces, the latter being about 50% of the experimental figures. This discrepancy cannot be explained by the uncertainty in the correction of the experimental results for the surface enthalpy to obtain values of the surface energy at 0°K.

Recently it has been suggested[2] that the assumption of thermodynamic equilibrium in the fine NaCl and KCl crystals used experimentally may not be justified. There is some evidence that the small crystals may contain faces of higher index instead of exhibiting exclusively {100} surfaces. In order to make a comparison between theory and experiment it is essential that theoretical values should be available for the energies of those surfaces which are likely to occur.

Theoretical calculations of the surface energy of an ionic crystal are usually carried out in two steps. In the first of these an ideal specific surface energy σ^0 is calculated on the basis that the ions in the surface region of the crystal have no dipole moment and occupy the same relative positions as do the corresponding ions in an infinite crystal. The second stage of the calculation involves the estimation of a distortion correction $\Delta\sigma$, which is the change in energy (per unit area) when the surface is allowed to relax to a configuration of lower energy. In general this spontaneous relaxation involves the displacement and polarization of the ions in the asymmetrical field of the surface region.

Evaluation of σ^0 according to the Born-Mayer classical theory of ionic crystals has been carried out for the {100} and {110} faces of those of the alkali halides possessing the NaCl structure[3,4] and for the {110} faces of those with CsCl-type structures.[4] Consideration of the relaxation term has so far been restricted to the {100} face of NaCl-type crystals. In this case Benson, Balk, and White[5] have shown, on the basis of a Verwey model[6,7] for the distortion, that $\Delta\sigma$ makes a significant correction to σ^0. The present paper describes a unified approach to the calculation of the distortion energy for the three faces of the alkali halides for which σ^0 has already been evaluated; the results of BBW[8] are thus included as a special case.

In the next section the Verwey model used for the consideration of the surface distortion is defined and a general equation for the associated change in energy is given; wherever possible the notation of vZB and BBW is adopted or suitably extended. Some details of the method of handling the repulsive terms are given in Sec. III. Section IV treats the lattice sums which arise in the problem, first from a fairly general point of view, and then for the three particular cases referred to above. The calculation of $\Delta\sigma$ is outlined in Sec. V where numerical results are presented for the {110} face of both NaCl-type and CsCl-type alkali halides. The final section is devoted to a discussion of these results.

II. DISTORTION ENERGY EQUATION

The "generalized NaCl-type" lattice (cf vZB), used in the present work, is defined by three noncoplanar basic vectors ($\mathbf{a}_1$, $\mathbf{a}_2$, $\mathbf{a}_3$) forming a right-handed set. The ions associated with the sites located by the lattice vector

$$\mathbf{R}_l = l_1\mathbf{a}_1 + l_2\mathbf{a}_2 + l_3\mathbf{a}_3 \qquad (l_1, l_2, l_3 \text{ integers}) \qquad (1)$$

alternate in sign as in an ordinary NaCl structure when any one of the l_i takes on successive integral

* Issued as N.R.C. No. 6024.

† National Research Council of Canada Postdoctorate Fellow 1958–1959; on leave from A.W.R.E. Aldermaston, Berkshire, England.

‡ National Research Council of Canada Postdoctorate Fellow 1956–1958; present address: IBM Corporation, Research Laboratory, Poughkeepsie, New York.

[1] G. C. Benson, H. P. Schreiber, and F. van Zeggeren, Can. J. Chem. **34,** 1553 (1956).

[2] P. Balk and G. C. Benson, J. Phys. Chem. **63,** 1009 (1959).

[3] R. Shuttleworth, Proc. Phys. Soc. (London) **A62,** 167 (1949).

[4] F. van Zeggeren and G. C. Benson, J. Chem. Phys. **26,** 1077 (1957).

[5] G. C. Benson, P. Balk, and P. White, J. Chem. Phys. **31,** 109 (1959).

[6] E. J. W. Verwey, Rec. trav. chim. **65,** 521 (1946).

[7] G. C. Benson, H. P. Schreiber, and D. Patterson, Can. J. Phys. **34,** 265 (1956).

[8] For convenience of presentation, footnote references 4 and 5 will be indicated as vZB and BBW, respectively.

values. It is assumed that the surface to be considered is parallel to the plane of $\mathbf{a}_1$ and $\mathbf{a}_2$. A hemicrystal with this type of face is defined by the conditions

$$-\infty \leq l_1 \leq \infty \tag{2}$$

$$-\infty \leq l_2 \leq \infty \tag{3}$$

$$0 \leq l_3 \leq \infty . \tag{4}$$

The area occupied by a surface ion pair, the unit outward normal to the surface, and the perpendicular distance between successive lattice planes parallel to the surface, which is used as a unit of length, are, respectively,

$$\omega = 2 \mid \mathbf{a}_1 \times \mathbf{a}_2 \mid \tag{5}$$

$$\mathbf{v} = -2(\mathbf{a}_1 \times \mathbf{a}_2)\omega^{-1} \tag{6}$$

and

$$\alpha = \mid \mathbf{a}_3 \cdot \mathbf{v} \mid . \tag{7}$$

It may be noted that α is the same as $\mid \alpha \mid$ used by vZB.

In the Verwey model of the distortion, four variables (z_+, z_-, μ_+, μ_-) are used to define relaxed configurations in which the surface positive and negative ions are displaced $z_+\alpha\mathbf{v}$ and $z_-\alpha\mathbf{v}$ from their ideal positions and have dipole moments $\mu_+\mathbf{v}$ and $\mu_-\mathbf{v}$, respectively. The energy of the hemicrystal is obtained by summing u_{ij}, the energy of interaction between a pair of ions, over all possible pairs and adding a correction for the quasi-elastic energy of the ions in the surface layer. The resulting energy is of course infinite but the difference, $\Delta U(z_+, z_-, \mu_+, \mu_-)$, between it and the energy in the ideal configuration, when stated per surface ion pair, is finite and calculable. The potential function u_{ij} used in the present work is the same as that employed previously [see BBW Eq. (2)].

Since the evaluation of ΔU is formally the same as described by BBW for the {100} face it will not be repeated here. After carrying out Taylor series expansions in terms of the displacements of the ions, ΔU can be written as

$$\begin{aligned}\Delta U = &\sum_p {}_1{}^4(A_p z_+{}^p + A_{0p} z_-{}^p) + \sum_p {}_1{}^2 a_{(2p)}(z_- - z_+)^{2p} \\ &+ \sum_p {}_0{}^4 A_{p01}(\mu_+ z_+{}^p - \mu_- z_-{}^p) \\ &+ \sum_p {}_0{}^1 a_{(2p+1)1}(\mu_+ + \mu_-)(z_- - z_+)^{2p+1} \\ &+ \sum_p {}_0{}^2 a_{(2p)11}\mu_+\mu_-(z_- - z_+)^{2p} + a_{02}\mu_+{}^2 + a_{002}\mu_-{}^2,\end{aligned} \tag{8}$$

where terms of order higher than the fourth have been neglected. The coefficients in this polynomial are given by

$$\begin{aligned}A_p = &T_p[1]e^2\alpha^{-1} - (c_+ {}_+G_p[6] + c_+ {}_-U_p[6])\alpha^{-6} \\ &- (d_+ {}_+G_p[8] + d_+ {}_-U_p[8])\alpha^{-8} + R_p\end{aligned} \tag{9}$$

$$\begin{aligned}A_{0p} = &T_p[1]e^2\alpha^{-1} - (c_- {}_-G_p[6] + c_+ {}_-U_p[6])\alpha^{-6} \\ &- (d_- {}_-G_p[8] + d_+ {}_-U_p[8])\alpha^{-8} + R_{0p}\end{aligned} \tag{10}$$

$$\begin{aligned}a_{(2p)} = &-u_{2p}[1]e^2\alpha^{-1} - c_+ {}_-u_{2p}[6]\alpha^{-6} \\ &- d_+ {}_-u_{2p}[8]\alpha^{-8} + r_{(2p)}\end{aligned} \tag{11}$$

$$A_{p01} = (p+1)\,T_{p+1}[1]e\alpha^{-2} \tag{12}$$

$$a_{(2p+1)1} = -u_{2p}[3]e\alpha^{-2} \tag{13}$$

$$a_{(2p)11} = (2p+1)\,u_{2p}[3]\alpha^{-3} \tag{14}$$

$$a_{02} = g_0[3](2\alpha^3)^{-1} + (2\alpha_+)^{-1} \tag{15}$$

$$a_{002} = g_0[3](2\alpha^3)^{-1} + (2\alpha_-)^{-1}. \tag{16}$$

Equations (9)–(16) are the same as those given by BBW [see Eqs. (7)–(14) of that reference] with the unit of length changed to α and the meanings of the symbols for the repulsive coefficients (R_p, R_{0p}, $r_{(2p)}$) and for the lattice sums ($T_p[1]$, $G_p[n]$, $U_p[n]$, $g_p[n]$, $u_p[n]$) extended from their previous usage. These modifications will be explained in the two following sections.

III. REPULSIVE COEFFICIENTS

In evaluating the repulsive contributions to ΔU only the interactions of nearest neighbors at distance a and of next nearest neighbors at distance $k_1 a$ are considered. On this basis the formulas for the repulsive coefficients in Eqs. (9)–(11) can be written as

$$R_p = b_+ {}_-\Psi_p{}' \exp(-\kappa) + b_+ {}_+\Psi_p{}'' \exp(-k_1\kappa) \tag{17}$$

$$R_{0p} = b_+ {}_-\Psi_p{}' \exp(-\kappa) + b_- {}_-\Psi_p{}'' \exp(-k_1\kappa) \tag{18}$$

$$r_{(2p)} = b_+ {}_-\psi_{2p} \exp(-\kappa), \tag{19}$$

where $\Psi_p{}'$, $\Psi_p{}''$, and ψ_{2p} are polynomials of order p in the variable

$$\kappa = a/\rho. \tag{20}$$

The general expressions for these are rather awkward and it is easier to treat directly the three particular cases mentioned in the Introduction. Since the formulas for the {100} face of the NaCl-type structure have been published already, the present considerations are restricted to the remaining two cases.

(i) NaCl Structure {110} Face

The repulsive contribution to ΔU in this case is

$$\begin{aligned}\Delta R = 2b_+ {}_-[&\exp\{-(\kappa/\sqrt{2})[1+(1+z_+)^2]^{\frac{1}{2}}\} \\ &+ \exp\{-(\kappa/\sqrt{2})[1+(1+z_-)^2]^{\frac{1}{2}}\} \\ &+ \exp\{-(\kappa/\sqrt{2})[2+(z_- - z_+)^2]^{\frac{1}{2}}\} - 3\exp\{-\kappa\}] \\ &+ b_+ {}_+[4\exp\{-(\kappa/\sqrt{2})[3+(1+z_+)^2]^{\frac{1}{2}}\} \\ &+ \exp\{-(\kappa/\sqrt{2})(2+z_+)\} - 5\exp\{-\kappa\sqrt{2}\}] \\ &+ b_- {}_-[4\exp\{-(\kappa/\sqrt{2})[3+(1+z_-)^2]^{\frac{1}{2}}\} \\ &+ \exp\{-(\kappa/\sqrt{2})(2+z_-)\} - 5\exp\{-\kappa\sqrt{2}\}].\end{aligned} \tag{21}$$

Expansion of ΔR as a series in the displacements leads to the expressions

$$\Psi_1' = -\kappa \tag{22}$$

$$\Psi_1'' = -3\kappa/\sqrt{2} \tag{23}$$

$$\Psi_2' = (\kappa^2-\kappa)/4 \tag{24}$$

$$\Psi_2'' = \kappa^2/2-3\kappa/4\sqrt{2} \tag{25}$$

$$\Psi_3' = -\kappa^3/24+\kappa^2/8+\kappa/8 \tag{26}$$

$$\Psi_3'' = -\kappa^3/8\sqrt{2}+3\kappa^2/16+3\kappa/16\sqrt{2} \tag{27}$$

$$\Psi_4' = \kappa^4/192-\kappa^3/32-3\kappa^2/64-3\kappa/64 \tag{28}$$

$$\Psi_4'' = 5\kappa^4/384-3\kappa^3/64\sqrt{2}-3\kappa^2/256-3\kappa/256\sqrt{2} \tag{29}$$

$$\psi_2 = -\kappa/2 \tag{30}$$

$$\psi_4 = (\kappa^2+\kappa)/16 \tag{31}$$

for the polynomials in Eqs. (17)–(19).

(ii) CsCl Structure {110} Face

The equations for the {110} face of CsCl corresponding to Eqs. (21)–(31) are

$$\begin{aligned}\Delta R = 2b_+ - [&\exp\{-(\kappa/\sqrt{3})[1+2(1+z_+)^2]^{\frac{1}{2}}\}\\ &+\exp\{-(\kappa/\sqrt{3})[1+2(1+z_-)^2]^{\frac{1}{2}}\}\\ &+2\exp\{-(\kappa/\sqrt{3})[3+2(z_--z_+)^2]^{\frac{1}{2}}\}-4\exp\{-\kappa\}]\\ &+2b_{+\,+}[\exp\{-[\kappa(\tfrac{2}{3})^{\frac{1}{2}}][1+(1+z_+)^2]^{\frac{1}{2}}\}\\ &\qquad-\exp\{-\kappa 2/\sqrt{3}\}]\\ &+2b_{-\,-}[\exp\{-[\kappa(\tfrac{2}{3})^{\frac{1}{2}}][1+(1+z_-)^2]^{\frac{1}{2}}\}\\ &\qquad-\exp\{-\kappa 2/\sqrt{3}\}]\end{aligned} \tag{32}$$

$$\Psi_1' = -4\kappa/3 \tag{33}$$

$$\Psi_1'' = -2\kappa/\sqrt{3} \tag{34}$$

$$\Psi_2' = 4\kappa^2/9-2\kappa/9 \tag{35}$$

$$\Psi_2'' = \kappa^2/3-\kappa/2\sqrt{3} \tag{36}$$

$$\Psi_3' = -8\kappa^3/81+4\kappa^2/27+4\kappa/27 \tag{37}$$

$$\Psi_3'' = -\kappa^3/9\sqrt{3}+\kappa^2/6+\kappa/4\sqrt{3} \tag{38}$$

$$\Psi_4' = 4\kappa^4/243-4\kappa^3/81-7\kappa^2/81-7\kappa/81 \tag{39}$$

$$\Psi_4'' = \kappa^4/108-\kappa^3/12\sqrt{3}-\kappa^2/16-3\kappa/32\sqrt{3} \tag{40}$$

$$\psi_2 = -4\kappa/3 \tag{41}$$

$$\psi_4 = 2(\kappa^2+\kappa)/9. \tag{42}$$

IV. TREATMENT OF THE LATTICE SUMMATIONS

(i) Three-Dimensional Sums

The general form of the three-dimensional lattice sums arising in the present problem can be written as

$$F[n\,|\,z] = \alpha^{\,n}\sum_{l_1 l_2 l_3}{}' \phi\,|\,\mathbf{R}_l - z\alpha\mathbf{v}\,|^{-n}, \tag{43}$$

where z stands for one of the displacements z_+ or z_- and the *GUST* notation of the Appendix of BBW has been adopted with only minor changes. The limits on the summations over l_1 and l_2 are given in Eqs. (2) and (3) and those for l_3 are indicated by

$$1 \le l_3 \le \infty. \tag{44}$$

The particular sums of interest $G[n\,|\,z]$, $U[n\,|\,z]$, $S[n\,|\,z]$, and $T[n\,|\,z]$ are obtained from (43) by assigning to the weight factor ϕ the different values summarized in Table IV of BBW. As in the previous treatment $F[n\,|\,z]$ is approximated by the first five terms of the ascending series in z

$$F[n\,|\,z] = \sum_p{}' \delta^4 F_p[n] z^p, \tag{45}$$

where

$$\begin{aligned}F_p[n] = &\sum_q k^p (-1)^q 2^{2q-p}\\ &\times[(2q-p)(p-q)B(2q-p, p-q)B(n/2, q)]^{-1}\\ &\times F(2q-p, n+2q).\end{aligned} \tag{46}$$

In Eq. (46) k is the smallest integer such that

$$k \ge p/2 \tag{47}$$

and $B(r, s)$ is the Eulerian integral of the first kind. The sums $F(m, n)$ are now defined by

$$F(m, n) = \alpha^{\,n}\sum_{l_1 l_2 l_3}{}' \phi l_3^m R_l^{-n} \tag{48}$$

which is a generalized form of Eq. (A10) in BBW. The evaluation of $T_p[1]$, $G_p[n]$, and $U_p[n]$ in Eqs. (9), (10), and (12) requires the calculation of a number of sums of the form $F(m, n)$. Since the four particular sum types (*GUST*) are not independent of each other but satisfy the relations

$$S = G+U \tag{49}$$

$$T = G-U, \tag{50}$$

it is unnecessary to calculate more than two of them by summation. In the present work $S(m, n)$ and $T(m, n)$ are selected as basic types. On using the methods described by vZB (see also van der Hoff and Benson[9]) these sums can be transformed into the following rapidly convergent forms:

$$\begin{aligned}S(m, n) = (4\alpha^2/\omega)[&\{\pi^{n/2}/\Gamma(n/2)\}\sum_{l_1=-\infty}^{\infty}{}'\sum_{l_2=-\infty}^{\infty}\sum_{l_3=1}^{\infty} l_3^m \exp(-2\pi i\theta l_3)(\tau/l_3)^{(n-2)/2}K_{(n-2)/2}(2\pi\tau l_3)\\ &+\{\pi/(n-2)\}\zeta(n-2-m)]\end{aligned} \tag{51}$$

$$T(m, n) = [\alpha^2\pi^{n/2}/\omega 2^{(n-6)/2}\Gamma(n/2)]\sum_{l_1\ \mathrm{odd}=-\infty}^{\infty}\sum_{l_2\ \mathrm{odd}=-\infty}^{\infty}\sum_{l_3=1}^{\infty}(-1)^{l_3} l_3^m \exp(-\pi i\theta l_3)(\tau/l_3)^{(n-2)/2}K_{(n-2)/2}(\pi\tau l_3). \tag{52}$$

[9] B. M. E. van der Hoff and G. C. Benson, Can. J. Phys. **31**, 1087 (1953).

TABLE I. Basic vectors and expressions for ω, α, θ, and τ for the three special cases.

	NaCl {100} face	NaCl {110} face	CsCl {110} face
$\mathbf{a}_1$	$a\mathbf{i}_1$	$a\mathbf{i}_3$	$a(\mathbf{i}_1-\mathbf{i}_2+\mathbf{i}_3)/\sqrt{3}$
$\mathbf{a}_2$	$a\mathbf{i}_2$	$a(\mathbf{i}_1-\mathbf{i}_2-\mathbf{i}_3)/\sqrt{3}$	$a(\mathbf{i}_1-\mathbf{i}_2-\mathbf{i}_3)/\sqrt{3}$
$\mathbf{a}_3$	$a\mathbf{i}_3$	$a\mathbf{i}_1$	$a(\mathbf{i}_1+\mathbf{i}_2-\mathbf{i}_3)/\sqrt{3}$
ω	$2a^2$	$2\sqrt{2}a^2$	$4\sqrt{2}a^2/3$
α	a	$a/\sqrt{2}$	$\sqrt{2}a/\sqrt{3}$
θ	0	$(l_2-l_1)/2$	$(l_2-l_1)/2$
τ	$(l_1^2+l_2^2)^{\frac{1}{2}}$	$(3l_1^2-2l_1l_2+l_2^2)^{\frac{1}{2}}/2$	$(3l_1^2-2l_1l_2+3l_2^2)^{\frac{1}{2}}/2$

In these equations the usual notation $\Gamma(n)$, $\zeta(n)$, and $K_n(z)$ has been used for the Euler Γ function, the Riemann ζ function, and the modified Bessel function of the second kind, respectively. The quantities θ and τ are given by the equations

$$\theta=\mathbf{n}_l\cdot\mathbf{a}_3 \tag{53}$$

$$\tau=\alpha\eta_l, \tag{54}$$

where $\mathbf{n}_l$ is the lattice vector of the plane lattice reciprocal to that defined by

$$\mathbf{r}_l=l_1\mathbf{a}_1+l_2\mathbf{a}_2. \tag{55}$$

On using the fact that the modified Bessel functions of half-integral order can be expressed in terms of exponentials, the formula for the electrostatic sum $T_p[1]$ can be simply written as

$$T_p[1]=(4\alpha^2/\omega)(-1)^{p+1}\pi^p(p!)^{-1}\sum_{l_1\ \mathrm{odd}}^{\infty}\sum_{l_2\ \mathrm{odd}}^{\infty}\tau^{p-1}\times\exp(-\pi\gamma)[1+\exp(-\pi\gamma)]^{-1}, \tag{56}$$

where

$$\gamma=\tau+i\theta. \tag{57}$$

TABLE II. Values of $T_p[1]$ calculated from Eq. (56).

p	NaCl {110} face	CsCl {110} face
1	0.252730	0.256380
2	−0.147464	−0.322204
3	−0.042056	0.209257
4	0.139053	−0.0093964
5	−0.115801	−0.142958

(ii) Two-Dimensional Sums

The two-dimensional lattice sums $u_p[n]$ and $g_p[n]$ in Eqs. (11) and (13)–(16) can be treated in a manner similar to that described for the three-dimensional forms. Thus the general two-dimensional sum analogous to $F[n\mid z]$ is

$$f[n\mid z]=\alpha^n{\sum_{l_1l_2}}'\phi\mid\mathbf{r}_l-z\alpha\mathbf{v}\mid^{-n}, \tag{58}$$

where z represents the difference z_--z_+ and the sum is taken over all integral values of l_1 and l_2 satisfying conditions (2) and (3), with the omission of the term $l_1=l_2=0$ (indicated by the prime on the summation sign). The two-dimensional forms corresponding to Eqs. (45), (46), and (48) are

$$f[n\mid z]=\sum_p v^4f_p[n]z^p \tag{59}$$

$$\left.\begin{aligned}f_{2p}[n]&=(-1)^p[pB(n/2,p)]^{-1}f(n+2p)\\ f_{2p+1}[n]&=0\end{aligned}\right\} \tag{60}$$

and

$$f(n)=f_0[n]=f[n\mid 0]=\alpha^n{\sum_{l_1l_2}}'\phi r_l^{-n}. \tag{61}$$

The relations (49) and (50) are also valid for the two-dimensional sums.

After transformation the sums $s(n)$ and $t(n)$ can be written as

$$s(n)=2^{(n+5)/2}\pi^{n/2}\alpha^n[\Gamma(n/2)a_1\omega^{(n-1)/2}]^{-1}\sum_{l_1^1}^{\infty}\sum_{l_2^1}^{\infty}\cos[2\pi l_1l_2(\mathbf{a}_1\cdot\mathbf{a}_2)/a_1^2](l_1/l_2)^{(n-1)/2}K_{(n-1)/2}(\pi l_1l_2\omega/a_1^2)$$
$$+2^n\pi^{\frac{1}{2}}\alpha^na_1^{n-2}\Gamma((n-1)/2)[\omega^{n-1}\Gamma(n/2)]^{-1}\zeta(n-1)+2(\alpha/a_1)^n\zeta(n) \tag{62}$$

$$t(n)=16\pi^{n/2}\alpha^n[a_1\omega^{(n-1)/2}]^{-1}\sum_{l_1\ \mathrm{odd}}^{\infty}\sum_{l_2^1}^{\infty}(-1)^{l_2}\cos[\pi l_1l_2(\mathbf{a}_1\cdot\mathbf{a}_2)/a_1^2](l_1/l_2)^{(n-1)/2}K_{(n-1)/2}(2\pi l_1l_2\omega/a_1^2)$$
$$+2^{2-n}(\alpha/a_1)^n(1-2^{n-1})\zeta(n). \tag{63}$$

(iii) Particular Cases

In order to treat the three special cases the vectors of the basis are written in terms of the unit vectors $\mathbf{i}_j(j=1,2,3)$ of an orthogonal Cartesian system. Relations appropriate to each case are summarized in Table I along with expressions for ω, α, θ, and τ. Diagrams illustrating the choice of axes for the two {110} faces may be found in vZB. Substitution of the relations from Table I into Eqs. (51), (52), (56), (62), and (63) yields formulas suitable for the evaluation of the lattice sums for each particular case. Apart from a minor rearrangement of the limits the formulas obtained in this way for the {100} face of the NaCl structure are the same as those used by BBW and will not be considered further here.

TABLE III. Values of $s(n)$ calculated from Eq. (62).

n	NaCl {110} face	CsCl {110} face
3	2.013888	5.316593
5	0.494823	2.038249
7	0.202614	1.183250
8	0.136712	0.931993
10	0.0650514	0.592667
12	0.0318333	0.383151

Values of the lattice sums for the {110} faces under investigation were calculated from the appropriate expressions on a Bendix G15D digital computer and the results are collected in Tables II to VI. It is unnecessary to calculate $t(n)$ directly for the {110} face of NaCl since for this case as for the {100} face of the same structure there is a further relation between the two-dimensional sums, viz.,

$$g(n)=2^{-n/2}s(n). \tag{64}$$

This relation is not true in general and in particular is not valid for the {110} face of CsCl; however, it can be shown that

$$[g(n)]_{\text{CsCl }\{110\}}=[s(n)]_{\text{NaCl }\{110\}}, \tag{65}$$

and accordingly it is only necessary in the case of CsCl to evaluate directly one of the sums given by Eqs. (62) and (63), provided values of $[s(n)]_{\text{NaCl }\{110\}}$ are known. A similar statement holds for the CsCl three-dimensional sums since the relation

$$[G(m,n)]_{\text{CsCl }\{110\}}=[S(m,n)]_{\text{NaCl }\{110\}} \tag{66}$$

is also true.

V. CALCULATION OF Δ_7

The surface configuration corresponding to a minimum of the energy of the hemicrystal is determined by solving the four equations obtained from setting the partial derivatives of ΔU with respect to each of the variables z_+, z_-, μ_+, and μ_- equal to zero. This was done for the {110} faces of all the alkali halides on the Bendix computer using the same iterative Newton-

TABLE IV. Values of $S(m, n)$ for the NaCl {110} face calculated from Eq. (51).

n \ m	0	1	2	3	4
8	0.148700	0.156715			
10	0.0678824	0.0693313	0.0723522		
12	0.0325376	0.0328452	0.0334694	0.0347465	
14			0.0161514	0.0164364	0.0170135
16					0.00814204

TABLE V. Values of $T(m, n)$ for the NaCl {110} face calculated from Eq. (52).

n \ m	0	1	2	3	4
8	−0.107237	−0.104720			
10	−0.0578926	−0.0571524	−0.0556830		
12	−0.0300731	−0.0298689	−0.0294618	−0.0286521	
14			−0.0151641	−0.0149477	−0.0145166
16					−0.00752595

TABLE VI. Values of $S(m, n)$ for the CsCl {110} face calculated from Eq. (51).

n \ m	0	1	2	3	4
8	0.556739	0.571329			
10	0.333421	0.335835	0.340912		
12	0.208499	0.208966	0.209918	0.211883	
14			0.133358	0.133758	0.134573
16					0.0862667

TABLE VII. Summary of results for the equilibrium configuration of the {110} face of alkali halide crystals. The quantity α defined in Eq. (7) is used as a unit for the displacements z_+ and z_- in each crystal.

Crystal	z_+	z_-	μ_+ debye	μ_- debye	$\Delta\sigma_{\{110\}}$ erg cm^{-2}	$\sigma_{\{110\}}$ erg cm^{-2}
LiF	−0.3297	−0.1871	−0.0187	0.7502	−552.1	280
LiCl	−0.2993	−0.0894	−0.0127	1.7687	−340.9	217
LiBr	−0.2938	−0.0707	−0.0114	2.1040	−296.0	190
LiI	−0.2853	−0.0490	−0.0098	2.5629	−241.2	164
NaF	−0.1814	−0.1401	−0.1424	0.4501	−186.7	453
NaCl	−0.1735	−0.0649	−0.0993	1.2210	−137.6	307
NaBr	−0.1723	−0.0488	−0.0903	1.4986	−125.7	270
NaI	−0.1702	−0.0306	−0.0794	1.8909	−109.5	228
KF	−0.1026	−0.1299	−0.5206	0.3111	−111.6	372
KCl	−0.1028	−0.0644	−0.3804	0.9079	−76.1	276
KBr	−0.1034	−0.0501	−0.3502	1.1333	−69.4	247
KI	−0.1033	−0.0337	−0.3140	1.4587	−60.8	213
RbF	−0.0808	−0.1259	−0.6905	0.2751	−95.4	337
RbCl	−0.0833	−0.0642	−0.5163	0.8224	−63.8	259
RbBr	−0.0842	−0.0507	−0.4778	1.0318	−57.9	234
RbI	−0.0847	−0.0355	−0.4320	1.3349	−50.7	203
CsF	−0.0575	−0.1311	−1.0917	0.2595	−98.9	307
CsCl	−0.0315	−0.0375	−0.6159	0.5599	−39.1	205
CsBr	−0.0328	−0.0222	−0.5580	0.7311	−35.8	190
CsI	−0.0416	−0.0102	−0.4947	1.0010	−33.3	168

Raphson program as was employed previously for the {100} case. References to the sources of the numerical data used in the present calculations can be found in vZB and BBW.

Table VII contains a summary of the results for the displacements (in units of α) and for the dipole moments (in debye units). A positive value of z indicates an outward displacement of the ion. The last two columns of the table give values of $\Delta\sigma_{\{110\}}$ and $\sigma_{\{110\}}$ calculated from the equations

$$\Delta\sigma_{\{110\}} = \omega^{-1}[\Delta U]_{\min} \tag{67}$$

and

$$\sigma_{\{110\}} = \sigma_{\{110\}}{}^{0} + \Delta\sigma_{\{110\}} \tag{68}$$

in which the values used for $\sigma_{\{110\}}{}^{0}$ were taken from vZB.

VI. DISCUSSION

It is interesting to compare the results in Table VII with those obtained by BBW for the {100} face. In all cases the relaxation of the ions in the {110} face corresponds to an inward movement. The displacements, expressed in terms of the interplanar distance α, are always larger for the {110} face than for the {100} face. Stable energy minima were found for all of the alkali halides, which contrasts with the {100} case for lithium fluoride. The correction terms for the energy of the {110} faces of the lithium halides are relatively somewhat smaller than those obtained for the {100} faces; in the present instance $\Delta\sigma_{\{110\}}$ amounts to about 60% of $\sigma_{\{110\}}{}^{0}$ for the lithium salts and from 20 to 30% for the other alkali halides. Since the remarks in the discussion of BBW concerning the validity of the numerical results for the {100} calculation are also applicable to the present results, the values given here for the energies of the {110} faces of the lithium halides are probably questionable. Apart from the lithium salts the ratio $\Delta\sigma/\sigma^{0}$ for NaCl-type crystals is very roughly the same for the {100} and {110} faces.

In order to interpret the experimental results[1,2] for the surface energy of NaCl and KCl on the basis of a mixture of {100} and {110} faces as mentioned in the Introduction it would be necessary to have about 75% of the surface in the {110} form. Originally[2] 55% was estimated on the basis of the crude assumption that $\Delta\sigma$ is the same for the {100} and {110} faces.

Finally it should be noted that the values of $\Delta\sigma$ calculated in this paper for the {110} faces and by BBW for the {100} faces are lower limits for the distortion corrections since the relaxation has been restricted to the first layer of ions. It is probable that a successively decreasing contribution will arise from the inner layers; an investigation of this aspect of the problem is currently in progress.

ACKNOWLEDGMENT

We wish to thank the staff, and in particular Dr. D. C. Baxter, of the Analysis and Computation Group of the Division of Mechanical Engineering, N.R.C., for allowing us to use the Bendix computer.

Densities of Solutions of Potassium in Liquid Ammonia and Deutero-Ammonia*

CLYDE A. HUTCHISON, JR., AND DONALD E. O'REILLY† ‡

Enrico Fermi Institute for Nuclear Studies, and Department of Chemistry, University of Chicago, Chicago, Illinois

(Received May 26, 1960)

The densities of solutions of K in liquid NH_3 have been measured at −33.7°, 0.0°, and 20.0°C over a concentration range from 0 to 1.2 mole liter^{-1}. The correlation of these results with paramagnetic resonance measurements is discussed in terms of a cavity trapping model.

IN contrast to the behavior of solutions of inorganic salts in liquid NH_3[1] the densities of solutions of Na in NH_3[2,3] decrease with increasing concentration of solute. With increasing temperature there is a decrease in the ratio of (a) rate of decrease of density with concentration to (b) density of the pure solvent.

In connection with investigations of the paramagnetism of solution of K in liquid NH_3 and ND_3 we have determined the densities of such solutions at −33.7°, 0.0°, and 20.0°C over a concentration range from 0 to about 1.20 mole liter.$^{-1}$ In view of the importance of such information in discussions of the anomalous behavior of these solutions on the basis of various models,[4–12] and because of the lack of data in the literature on solutions of K in NH_3 and of any alkali metal in ND_3, we present the results of our density measurements in this paper.

EXPERIMENTAL

NH_3 used for the measurements was prepared by transferring Armour and Company NH_3 to a steel tank containing Na metal. The H_2 evolved was released from time to time until the reaction was complete. The NH_3 was stored in this tank and just before the density measurements was distilled from the tank to a glass vacuum line and redistilled from Na there before transferring to the pycnometer.

ND_3 was prepared by the reaction of Mg_3N_2 with D_2O. Samples of NH_3 and ND_3 gas were weighed in a Dumas bulb. The ratio of the density of the ND_3 sample to that of NH_3 at the same temperature and pressure was found to be 1.184 whereas the ratio for the pure ideal gases is 1.177.

The pycnometer is shown in Fig. 1. The pycnometer bulb volume (approximately 14 cm^3) to various points above and below the fiducial mark C was measured by weighing the pycnometer filled to various heights with pure water at 0.1° and 5.0°C. The standard taper joint was used for the first evacuation and for filling with NH_3 or ND_3 liquid. Before adding the liquid the K metal was distilled over to point B through arm A. Arm A was then sealed off at the constriction near E. The condensing liquid was used to wash the K down into the bulb. The temperature was then adjusted by placing the pycnometer in a water bath whose temperature was controlled to ±0.05°C at 20.0°C as measured by a Bureau of Standards calibrated thermometer. The height of the meniscus relative to the fiducial mark C was measured with a cathetometer. The pycnometer was weighed. More NH_3 or ND_3 was added

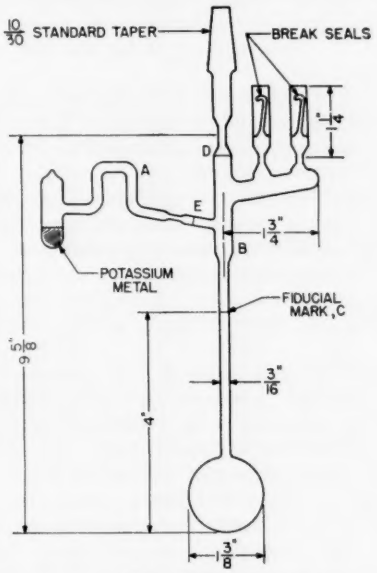

FIG. 1. Pycnometer.

* This research was supported by the U. S. Office of Naval Research.

† Present address: Gulf Research and Development Company Pittsburgh, Pennsylvania.

‡ Argonne National Laboratory, Argonne, Illinois.

[1] S. Kikuti and S. Kudo, J. Soc. Chem. Ind. Japan **47,** 302 (1944); S. Kikuti, J. Soc. Chem. Ind. Japan, Suppl. Binding **42,** 15 (1939).

[2] C. A. Kraus, E. S. Carney, and W. C. Johnson, J. Am. Chem. Soc. **49,** 2206 (1927).

[3] W. C. Johnson and R. Meyer, J. Am. Chem. Soc. **54,** 3621 (1932); **72,** 1842 (1950).

[4] S. Freed and N. Sugarman, J. Chem. Phys. **11,** 354 (1943).

[5] R. A. Ogg, Jr., J. Am. Chem. Soc. **68,** 155 (1946).

[6] T. Hill, J. Chem. Phys. **16,** 394 (1948).

[7] W. N. Lipscomb, J. Chem. Phys. **21,** 52 (1953).

[8] J. Kaplan and C. Kittel, J. Chem. Phys. **21,** 1429 (1953).

[9] W. Bingel, Ann. Physik **12,** 57 (1953).

[10] E. Becker, R. H. Lindquist, and B. J. Alder, J. Chem. Phys. **25,** 971 (1956).

[11] M. F. Deigen and Yu A. Tsvirko, Ukrain. Fiz. Zhur. **1,** **245** (1956).

[12] J. Jortner, J. Chem. Phys. **30,** 839 (1959).

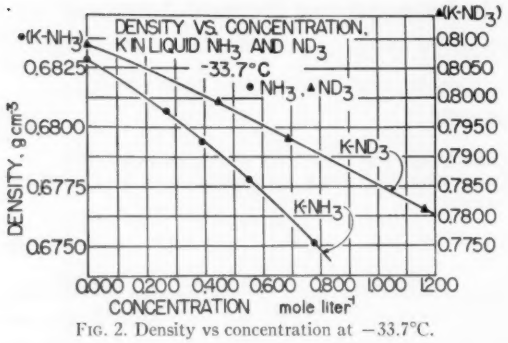

FIG. 2. Density vs concentration at −33.7°C.

through a break seal after adding a weighed taper joint, the meniscus height measured at 0.0°C and the pycnometer and break seal assembly weighed. Still more NH_3 or ND_3 was added and the final measurement of meniscus height was made with the pycnometer immersed in boiling NH_3. The temperature of the NH_3 bath was measured with a copper-constantan thermocouple which had been calibrated at the CO_2 sublimation point, the freezing point of Hg and the boiling point of pure NH_3.

At the end of such a series of measurements the NH_3 or ND_3 was removed and the amount of K determined by conversion to hydroxide with moist air, dissolving in H_2O and titrating with HCl.

Appropriate buoyancy corrections, corrections for weight of vapor in the pycnometer and corrections for the thermal coefficient of expansion of glass were made.

Thirty measurements of the density were made and the results are given in Figs. 2–4. In Table I are given the densities read from the graphs at selected concentrations.

The expected error in the density estimated from assumed reasonable errors in the various individual measurements involved in the procedure leading to a single determination is approximately one part in 7000. Three measurements of the density of pure NH_3 at 0.0°C gave 0.6386 g cm^{-3} with an average deviation of 0.0003 from the mean. Two measurements of the

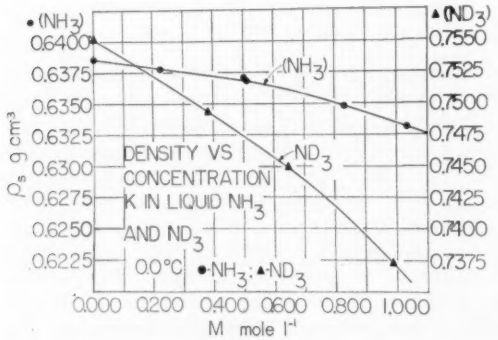

FIG. 3. Density vs concentration at 0.0°C.

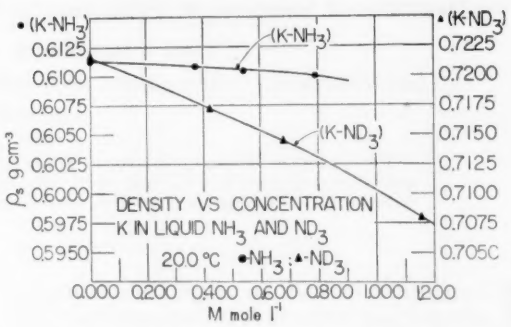

FIG. 4. Density vs concentration at 20.0°C.

density of pure ND_3 at 0.0°C gave 0.7552 g cm^{-3} with an average deviation of 0.0001 from the mean. The error in the determination of the concentration was approximately 0.1%.

The best evidence concerning the extent of the reaction of K with NH_3 in the solutions prepared in the manner described here, came from the measurement of the intensities of paramagnetic resonance absorption.[13] Accurate measurements of absorption intensities of a large number of similarly prepared samples used in the

TABLE I. Density vs. concentration.

M, mole liter^{-1}	ρ, g cm^{-3}	M, mole liter^{-1}	ρ, g cm^{-3}
K—NH_3, 20.0°C		K—ND_3, 20.0°C	
0.000	0.6113	0.000	0.7216
0.150	0.6112	0.150	0.7202
0.300	0.6109	0.300	0.7186
0.600	0.6104	0.600	0.7153
0.900	0.6091	0.900	0.7118
		1.200	0.7074
NH_3, 0.0°C		ND_3, 0.0°C	
M		M	
0.000	0.6386	0.000	0.7552
0.150	0.6381	0.150	0.7530
0.300	0.6375	0.300	0.7506
0.600	0.6363	0.600	0.7457
0.900	0.6343	0.900	0.7395
1.200	0.6316		
NH_3, −33.7°C		ND_3, −33.7°C	
M		M	
0.000	0.6828	0.000	0.8090
0.150	0.6816	0.150	0.8061
0.300	0.6803	0.300	0.8028
0.600	0.6772	0.600	0.7955
0.900	0.6733	0.900	0.7867
		1.200	0.7760

[13] C. A. Hutchison, Jr., and D. E. O'Reilly (unpublished results).

resonance experiments showed no decrease in susceptibility for periods of time several times as large as those employed for the density determinations. In addition no noncondensable gas could be found when the pycnometer was opened at the end of a series of measurements. Consequently the chemical analyses for K could be relied on to give the concentration of unreacted metal.

The only data available heretofore in the literature are the value[14] 0.6816 g cm^{-3} for the density of pure NH_3 at -33.2°C and the value[3] 0.6721 g cm^{-3} for 1.158 molar K in NH_3 at -33.2°C.

DISCUSSION

Many types of evidence[4–12,15–17] indicate that in solutions of metallic K in liquid NH_3 the metal is dissociated into (a) K^+ ions which exist in a form similar to that found in solutions of K salts in NH_3 and (b) electrons trapped or solvated in some manner by the NH_3.

Paramagnetic resonance data[16] enable one to measure the number of unpaired electrons contributing to the spin susceptibility. We will refer to these as singly trapped electrons. The resonance data also permit the calculation of the number of trapped electrons with paired spins assuming that all K exists as K^+ and that all the electrons are trapped in some manner by the solvent. We will refer to these paired electrons as doubly trapped electrons. In the present paper the numbers of unpaired electron spins were computed from measurements[13] of the paramagnetic resonance absorption intensities based on absolute measurements of the detection circuit parameters.

The very marked decrease in density with increasing concentration of solutions of K in liquid NH_3 and ND_3 may be interpreted as the sum of four effects:

(a) the volume increase due to the volume of the K^+ ions;

(b) the volume decrease due to the electrostrictive effects of the K^+ ions;

(c) the volume decrease due to the electrostrictive effects of the singly and doubly trapped electrons;

(d) the volume increases due to the singly and doubly trapped electrons.

We assume that the volume of K^+ is that obtained by using the crystal radius.[18] This volume is $9.9A^3$. The volume decrease due to electrostriction by K^+ is obtained from the available experimental data[1] on

TABLE II. Calculated densities.

M (K) (1)	α (2)	ρ_{wt} (3)	ρ_{exptl} (4)	$\rho_{wt}-\rho_{exptl}$ (5)	$\rho_{wt}-\rho$ (6)
mole liter^{-1}		g cm^{-3}	g cm^{-3}	g mc^{-3}	g cm^{-3}
		NH_3, -33.7°C			
0.000	1.000	0.6828	0.6828	0.0000	0.0000
0.060	0.141	0.6851	0.6823	0.0028	0.0028
0.100	0.100	0.6867	0.6820	0.0047	0.0047
0.200	0.076	0.6906	0.6812	0.0094	0.0095
0.300	0.068	0.6945	0.6803	0.0142	0.0143
0.400	0.052	0.6984	0.6794	0.0190	0.0191
0.500	0.048	0.7023	0.6783	0.0240	0.0240
		ND_3, -33.7°C			
0.000	1.000	0.8090	0.8090	0.0000	0.0000
0.060	0.140	0.8113	0.8078	0.0035	0.0035
0.100	0.111	0.8129	0.8070	0.0059	0.0059
0.200	0.079	0.8168	0.8050	0.0118	0.0119
0.300	0.066	0.8207	0.8028	0.0179	0.0180
0.400	0.060	0.8246	0.8005	0.0241	0.0240
0.500	0.057	0.8285	0.7981	0.0304	0.0301
		NH_3, 0.0°C			
0.000	1.000	0.6386	0.6386	0.0000	0.0000
0.060	0.364	0.6412	0.6384	0.0028	0.0028
0.100	0.258	0.6429	0.6382	0.0047	0.0047
0.200	0.160	0.6473	0.6378	0.0094	0.0094
0.300	0.125	0.6516	0.6375	0.0141	0.0141
0.400	0.109	0.6560	0.6372	0.0188	0.0188
0.500	0.084	0.6603	0.6368	0.0235	0.0236
		ND_3, 0.0°C			
0.000	1.000	0.7552	0.7552	0.0000	0.0000
0.060	0.364	0.7579	0.7543	0.0035	0.0035
0.100	0.262	0.7596	0.7538	0.0058	0.0059
0.200	0.189	0.7641	0.7522	0.0118	0.0118
0.300	0.147	0.7685	0.7506	0.0179	0.0179
0.400	0.124	0.7729	0.7490	0.0239	0.0239
0.500	0.096	0.7773	0.7474	0.0299	0.0299
		NH_3, 20.0°C			
0.000	1.000	0.6113	0.6113	0.0000	0.0000
0.060	0.433	0.6141	0.6112	0.0029	0.0028
0.100	0.338	0.6160	0.6112	0.0048	0.0047
0.200	0.223	0.6207	0.6110	0.0097	0.0096
0.300	0.170	0.6254	0.6109	0.0145	0.0145
0.400	0.144	0.6301	0.6107	0.0194	0.0194
0.500	0.131	0.6348	0.6106	0.0242	0.0243
		ND_3, 20.0°C			
0.000	1.000	0.7216	0.7216	0.0000	0.0000
0.060	0.483	0.7245	0.7210	0.0035	0.0035
0.100	0.361	0.7265	0.7206	0.0058	0.0058
0.200	0.247	0.7313	0.7196	0.0117	0.0118
0.300	0.198	0.7362	0.7185	0.0176	0.0177
0.400	0.168	0.7410	0.7174	0.0236	0.0237
0.500	0.141	0.7459	0.7164	0.0295	0.0296

[14] C. S. Cragoe and D. R. Harper, Natl. Bur. Standards U. S. Sci. Paper 420, 287 (1921).

[15] References to the literature of this subject may be found in C. A. Hutchison, Jr., and R. C. Pastor, Rev. Mod. Phys. **25,** 285 (1953); C. A. Hutchison, Jr., J. Phys. Chem. **57,** 546 (1953).

[16] C. A. Hutchison, Jr., and R. C. Pastor, J. Chem. Phys. **21,** 1959 (1953).

[17] H. C. Clark, A. Horsfield, and M. C. R. Symons, J. Chem. Soc. **1959,** 2478.

[18] L. Pauling, *The Nature of the Chemical Bond* (Cornell University Press, Ithaca, New York, 1948).

TABLE III. Parameters.

		NH_3		ND_3	
T	V A^3	a, A	b, A	a, A	b, A
−33.7°C	0.0	2.85	3.83	2.84	3.91
0.0°C	−11.4	3.05	3.89	3.05	3.99
20.0°C	−21.9	3.05	4.00	3.16	4.03

solutions of KBr in NH_3. It is assumed that the apparent volume per ion pair in such a solution is the sum of the ionic volumes of K^+ and Br^- (taken to be those calculated, from the crystal radii,[18] namely, 1.33 and 1.95 A) and the electrostrictive effects of K^+ and Br^-.[1] The electrostriction volume of K^+ is calculated from the total electrostrictive effect from both ions, assuming that the electrostriction volumes of the two ions are inversely proportional to their radii. The electrostriction volume of the singly trapped electrons is calculated from that for K^+ assuming that for these two species this volume is inversely proportional to the radius of the species. The radius of the singly trapped electronic species is taken to be an adjustable parameter. For the doubly trapped electrons the electrostriction per pair is taken to be twice that for the singly trapped species. This will be seen from the results given in Table III to be essentially the same as assuming that the electrostrictions of the two types of trapped species are inversely proportional to their radii and directly proportional to the square of their charges.

The sum of all these volume changes which have just been described and which are included under (a)–(c) will be referred to as V. It is to be noted that this sum, so calculated, when divided by the number of K atoms in solution is independent of concentration because the electrostrictive effect of the doubly trapped species is taken to be just twice that of the singly trapped species.

We have in this way calculated the densities ρ_{wt} of hypothetical solutions in which the traps do not occupy volume but in which the electrostrictive effects of the traps are taken into account.

In Table II are listed values of (a) ρ_{wt}, (b) the experimental density ρ_{exptl}, and (c) the difference, $\rho_{wt}-\rho_{exptl}$, of these two densities. The value of the radius of the singly trapped species was taken to be the value given in Table III for purpose of calculating the electrostrictive effect described previously.

Paramagnetic resonance data permit the calculation of the numbers of singly and doubly trapped electrons as described previously. The degree of dissociation α of doubly trapped electrons into singly trapped electrons is given by

$$\alpha=[M(\mathrm{K})-2M(e_2^{=})]/M(\mathrm{K})$$
$$=M(e^-)/M(\mathrm{K}),$$

where $M(\mathrm{K})$ is the molarity of K in NH_3 or ND_3, $M(e_2^{=})$ is the molarity of doubly trapped electrons, $M(e^-)$ is the molarity of singly trapped electrons. It is assumed that α is related to the paramagnetic component χ_M of the molar static field susceptibility as determined from the rf susceptibility data by the relation,[16]

$$\alpha=\chi_M(kT/N_{av}\beta^2),$$

where $(N_{av}\beta^2/kT)$ is the paramagnetic static field susceptibility of one mole of free spins. The values of χ_M were obtained from paramagnetic resonance measurements[13] as described previously.

We now assume for simplicity that with each singly trapped electron is associated a spherical cavity of radius a, and with each pair of doubly trapped electrons is associated a spherical cavity of radius b. Assuming such radii to be independent of concentration, we can calculate $\rho_{wt}-\rho$, where ρ is the density of the solution given by the assumed model. The value of this quantity is also listed in Table II.

In Table III we list the values of V calculated as described previously and also the values of a and b used to get the values of $\rho_{wt}-\rho$ which are listed in Table II.

It is clear that the experimental data can be fit very well with this model. It is also to be remarked that the radii a and b are approximately independent of temperature and solvent.

In addition, it should be noted that the radii a and b are very close to the values calculated from the diamagnetic susceptibility of the trapped electrons. This diamagnetic susceptibility is obtained as the difference between the susceptibilities as determined from rf and static measurements. Assuming again that the electrons are trapped in spherical cavities, these cavities must have radii very close to the a and b values given previously in order to account for the observed diamagnetism.

At the boiling point of NH_3 the difference between the molar susceptibilities calculated from rf[13] and dc[4] measurements is 47×10^{-6} cm^3 mole^{-1}. This difference is due mainly to the diamagnetism of the doubly trapped electrons. As seen from Table II, only 5% of the electrons are dissociated into singly trapped species. If the electrons were trapped in a spherical square well 5.0 ev deep and 4.0 A in radius, the observed diamagnetism would be just accounted for.

It is, of course, possible for other models to give good agreement between the very large observed density changes caused by the trapped electrons and the very large diamagnetism of the trapped electrons. The model described gives a good correlation in a particularly simple manner.

ACKNOWLEDGMENT

We thank Edward Bartal for construction of apparatus used in this work.

Potential Energy Curves for OH*

ROBERT J. FALLON, IRWIN TOBIAS, AND JOSEPH T. VANDERSLICE

Institute for Molecular Physics, University of Maryland, College Park, Maryland

(Received June 29, 1960)

Potential energy curves for four of the bound states of OH have been calculated by the Rydberg-Klein-Rees method. Various mechanisms to explain the anomalously high population of the $v'=2$ and 3 levels of the $A\ ^2\Sigma^+$ state are discussed.

INTRODUCTION

THIS is one of a series of papers dealing with the potential energies of interaction of diatomic species existing in flames. A knowledge of the reliable potential energy curves for these species can sometimes lead to the elucidation of the possible kinetics of the reactions that occur.[1–3]

Four of the bound states of OH have been calculated by the Rydberg-Klein-Rees (RKR) method[4–8]: $X\ ^2\Pi$, $A\ ^2\Sigma^+$, $B\ ^2\Sigma^+$, and $C\ ^2\Sigma^+$. Of these, only the $X\ ^2\Pi$ dissociates to ground-state atoms. According to the Wigner-Witmer rules the interaction of an oxygen atom and a hydrogen atom, both in their ground states, gives rise, in addition to a $^2\Pi$, to three other electronic states: $^4\Pi$, $^4\Sigma^-$, and $^2\Sigma^-$. Mulliken[9] has predicted that these three are all repulsive and for a given internuclear distance the order written above is also the order of increasing energy.

TABLE I. Potential energy of the $X\ ^2\Pi_i$ state of OH.[a]

v	$V(\text{cm}^{-1})$	$V(\text{ev})$	$r_{max}(\text{A})$	$r_{min}(\text{A})$
0	1848	0.2291	1.081	0.884
1	5418	0.6717	1.179	0.831
2	8822	1.0937	1.257	0.800
3	12062	1.4954	1.329	0.777
4	15139	1.8769	1.399	0.758
5	18055	2.2384	1.468	0.743
6	20806	2.5795	1.538	0.731
7	23392	2.9000	1.610	0.720
8	25808	3.1996	1.683	0.710
9	28051	3.4777	1.760	0.702

[a] Data from footnotes 14, 15, and 16.

CALCULATION OF CURVES

The results of the RKR procedure for the different bound states of OH are listed in Tables I to IV and are shown as solid lines in Fig. 1. Mulliken's prediction for the three other states dissociating to ground state atoms are indicated by the dotted lines.

The RKR method, a semiclassical procedure for determining potential energy curves from the measured vibrational and rotational energy levels, is both rapid and accurate. It has been sufficiently described in recent articles[4–8,10–12] so that no further details will be given here. In our calculations we have used the spectroscopic data of Barrow,[13] Michel,[14] Herman and Hornbeck,[15] and Dieke and Crosswhite.[16] From the data of Chamberlain and Roesler,[17] which is practically identical to that we used, Jarmain[18] has obtained a potential curve for the $X\ ^2\Pi$ ground state of OH up to $v=6$. His results up to that point agree with ours to ± 0.001 A.

Jarmain[18] has used his own modification of the RKR

TABLE II. Potential energy of the $A\ ^2\Sigma^+$ state of OH.[a]

v	$V(\text{cm}^{-1})$	$V(\text{ev})$	$T_e+V(\text{ev})$[b]	$r_{max}(\text{A})$	$r_{min}(\text{A})$
0	1566	0.1941	4.2462	1.131	0.917
1	4555	0.5647	4.6168	1.244	0.863
2	7348	0.9110	4.9631	1.338	0.832
3	9941	1.2325	5.2846	1.428	0.809
4	12327	1.5283	5.5804	1.518	0.792
5	14491	1.7966	5.8487	1.614	0.777
6	16407	2.0341	6.0862	1.722	0.766
7	18032	2.2356	6.2877	1.856	0.758
8	19306	2.3935	6.4456	2.038	0.752

[a] Data from footnotes 13, and 14.

[b] T_e is the energy difference between the bottom of the potential curve in question and the bottom of the $X\ ^2\Pi_i$ state.

* This work was supported in part by the National Aeronautics and Space Administration.

[1] R. J. Fallon, J. T. Vanderslice, and E. A. Mason, J. Phys. Chem. **63**, 2082 (1959).

[2] R. J. Fallon, J. T. Vanderslice, and E. A. Mason, J. Phys. Chem. **64**, 505 (1960).

[3] R. J. Fallon, I. Tobias, J. T. Vanderslice, and W. G. Maisch, Can. J. Chem. **38**, 743 (1960).

[4] R. Rydberg, Z. Physik **73**, 376 (1931); **80**, 514 (1933).

[5] O. Klein, Z. Physik **76**, 226 (1932).

[6] A. L. G. Rees, Proc. Phys. Soc. (London) **59**, 998 (1947).

[7] J. T. Vanderslice, E. A. Mason, W. G. Maisch, and E. R. Lippincott, J. Mol. Spectroscopy **3**, 17 (1959).

[8] F. Gilmore (Rand Corporation, Santa Monica, California) has corrected the formulas of reference 7. The corrections have appeared as errata [J. Mol. Spectroscopy **5**, 83 (1960) and J. Chem. Phys. **33**, 614 (1960)].

[9] R. S. Mulliken, Revs. Modern Phys. **4**, 1 (1932).

[10] J. T. Vanderslice, E. A. Mason, and E. R. Lippincott, J. Chem. Phys. **30**, 129 (1959).

[11] J. T. Vanderslice, E. A. Mason, and W. G. Maisch, J. Chem. Phys. **31**, 738 (1959).

[12] J. T. Vanderslice, E. A. Mason, and W. G. Maisch, J. Chem. Phys. **32**, 515 (1960).

[13] R. F. Barrow, Arkiv Fysik **11**, 281 (1956).

[14] A. Michel, Z. Naturforsch. **12a**, 887 (1957).

[15] R. C. Herman and G. A. Hornbeck, Astrophys. J. **118**, 214 (1953).

[16] S. H. Dieke and H. M. Crosswhite, "The Ultraviolet Bands of OH Fundamental Data," Bumblebee Report No. 86, The Johns Hopkins University (1948).

[17] J. W. Chamberlain and F. L. Roesler, Astrophys. J. **121**, 541 (1955).

[18] W. R. Jarmain, Can. J. Phys. **38**, 217 (1960).

procedure which involves expressing the classical turning points in a power series in $v+\frac{1}{2}$, where v is the vibrational quantum number. Since the series starts to diverge for large v, Jarmain has arbitrarily limited himself to the calculation of potential curves up to one half of the dissociation limit. In some cases, he finds that the series diverges even at small values of v.[18] Therefore, we have continued to use the original formulation of the RKR procedure[6-8] which does not appear to suffer from this disadvantage except very close to the dissociation limit.[12]

DISCUSSION

The hydroxyl radical is present in a number of flames and there has been much discussion concerning the kinetics of its formation in the $A\,^2\Sigma^+$ state.[19-21] The intensity measurements first made by Kondratiev and Ziskin[22] and later confirmed by other workers[23,24] suggest that the $v'=2$ and 3 levels of the OH $A\,^2\Sigma^+$ state have a greater relative population than that expected under conditions of thermal equilibrium. This has led Gaydon and Wolfhard[23] to propose an inverse predissociation of the $A\,^2\Sigma^+$ state by the $^2\Sigma^-$ state,

$$O(^3P_g)+H(^2S_g)\rightarrow OH(^2\Sigma^-)\xrightarrow[\text{transition}]{\text{radiationless}}OH(^2\Sigma^+). \quad (1)$$

Shuler[21] mentioned that this inverse predissociation reaction should be very weak since it violates selection rules[25] and instead proposes a reaction involving a triatomic complex which should be more efficient than (1),

$$O_2(^3\Sigma_g^-)+H(^2S_g)\rightarrow HO_2(^2A'')\xrightarrow[\text{transition}]{\text{radiationless}}HO_2(^2A'')$$
$$\rightarrow OH(^2\Sigma^+)+O(^3P_g). \quad (2)$$

This reaction, however, is not consistent with the more recent finding that the intensity of emission is approximately proportional to the square of the free-atom concentration, which indicates that an inverse predissociation reaction mechanism contributes a substantial part to the formation of $OH(^2\Sigma^+)$ in the $v'=2$ level.[19,26,27] Also, the anomalously strong excitation of OH bands with $v'=2$ and 3 is accompanied by selective excitation of the f_1 spin levels of the $^2\Sigma^+$ state which again suggests an inverse predissociation.[4]

On the basis of this new information, Charton and Gaydon[19] have again proposed that the $^2\Sigma^-$ state is responsible for this predissociation. Predissociation by the $^2\Sigma^-$ state as well as by either the $^4\Sigma^-$ or the $^4\Pi$ state violates Kronig's selection rules. Therefore, it does not seem possible, on the basis of existing information, to rule out the other two excited states, the $^4\Sigma^-$ and the $^4\Pi$. Indeed, as Fig. 1 shows, Mulliken's predictions of the relative positions of the excited states would favor the $^4\Pi$ state as causing the predissociation. Further investigation of the exact position of these excited states and the details of their interaction with the $^2\Sigma^+$ state is necessary before anything more definite can be said.

TABLE III. Potential energy of the $B\,^2\Sigma^+$ state of OH.[a]

v	$V(\text{cm}^{-1})$	$V(\text{ev})$	$T_e+V(\text{ev})$	$r_{max}(\text{A})$	$r_{min}(\text{A})$
0	441	0.0547	8.7053	2.041	1.627
1	1101	0.1365	8.7871	2.426	1.569

[a] Data from footnote 13.

TABLE IV. Potential energy of the $C\,^2\Sigma^+$ state of OH.[a]

v	$V(\text{cm}^{-1})$	$V(\text{ev})$	$T_e+V(\text{ev})$	$r_{max}(\text{A})$	$r_{min}(\text{A})$
0	1090	0.1351	11.3151	2.193	1.953
1	3364	0.4171	11.5971	2.328	1.893

[a] Data from footnote 14.

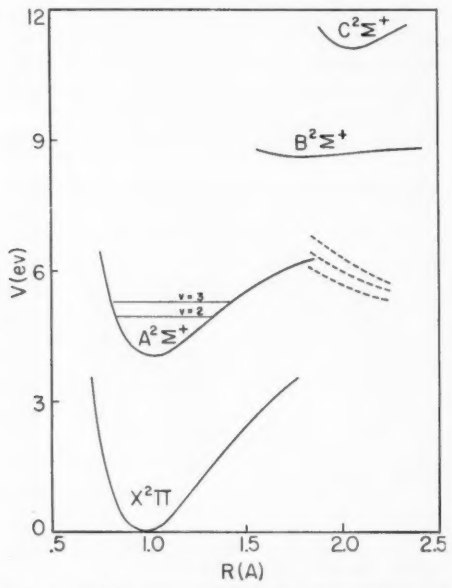

FIG. 1. Potential energy curves for OH. The solid curves were calculated by the RKR method. The dashed curves are those predicted by Mulliken. In order of increasing energy, these are $^4\pi<{}^4\Sigma^-<{}^2\Sigma^-$.

[19] M. Charton and A. G. Gaydon, Proc. Roy. Soc. (London) **A245**, 84 (1958).
[20] K. J. Laidler, *The Chemical Kinetics of Excited States* (Oxford University Press, London, 1955).
[21] K. E. Shuler, J. Chem. Phys. **21**, 624 (1953).
[22] V. Kandratiev and M. Ziskin, Acta. Physiochim. U.S.S.R. 7, 65 (1937).
[23] A. G. Gaydon and H. G. Wolfhard, Proc. Roy. Soc. (London) **A208**, 63 (1951).
[24] H. P. Broida and K. E. Shuler, J. Chem. Phys. **20**, 168 (1952).
[25] G. Herzberg, *Spectra of Diatomic Molecules* (D. Van Nostrand Company, Inc., Princeton, New Jersey, 1950), pp. 416 ff.
[26] E. M. Balewicz, C. G. James, and T. M. Sugden, Proc. Roy. Soc. (London) **A235**, 89 (1956).
[27] W. E. Kaskan, J. Chem. Phys. **31**, 944 (1959).

Linewidths in the Electron Paramagnetic Resonance Spectrum of Gaseous Atomic Hydrogen

R. M. Mazo

Gates and Crellin Laboratories of Chemistry, California Institute of Technology, Pasadena, California*

(Received July 5, 1960)

A theory of the paramagnetic linewidth in gaseous atomic hydrogen, based on the theory of Baranger, and on an expansion of the spin correlation function in powers of the density is presented. To the approximations considered, the line shape is Lorentzian, the linewidth is proportional to the H atom density, and the relevant cross section involves an interference between the scattered amplitudes from the singlet and triplet potential curves. Comparison with experiment yields a velocity averaged cross section of 28.3×10^{-16} cm^2 at 325°K. This value is compared to other estimates found in the literature.

I. INTRODUCTION

THIS paper presents a calculation of the broadening of the hyperfine lines in the electron paramagnetic resonance spectrum of atomic hydrogen. The calculation was prompted by the measurements of Hildebrandt, Booth, and Barth,[1] who determined the linewidth as a function of hydrogen atom density and by the recent theory of linewidths of Baranger.[2] Previous work on this system has been done by Wittke and Dicke,[3] who measured the hyperfine splitting in zero field and gave a theory of the effect of atomic collisions on the linewidth. Relevant calculations have also been made by Purcell and Field,[4] though these authors were not directly concerned with collisional contributions to linewidths, which are negligible under the astrophysical conditions which they considered.

The object of the theory to be presented here is the derivation of an expression for the linewidth in terms of the dynamics of molecular collisions, and thus the construction of the relevant collision cross section. The theory of Wittke and Dicke[3] contains all the physical ideas which bear upon the problem, but does not consider the collision process in detail.

There are several ways of looking at the physical mechanism which gives rise to the broadening. One may say that the exchange forces cause a rapid precession of the electron spins of two colliding hydrogen atoms about each other. Because of this, the atoms may be in different hyperfine states after collision than they were in before collision. This is a lifetime limiting process, and hence broadens the line. Alternatively, one may say that a line is collision broadened when the interaction of emitter and perturber is different in the initial and final states of the emission act. Since, in the EPR spectrum, a spin must flip in the transition, the initial and final states may have different total spin. Because the exchange energy depends on the spin, the line will be broadened. Another related observation, due to Wittke and Dicke,[3] is to consider the hydrogen atoms to be unpolarized before collision. After collision the state of the atom pair will be a mixture of singlet and triplet spin wave functions. This is reflected in the cross section which appears in the theory. Wittke and Dicke have considered other mechanisms besides the exchange interaction, and have found these to be of minor importance.

The formalism of the theory is that of the correlation function method. The spectrum is expressed as the Fourier transform of an electron spin correlation function, which is expanded as a power series in the gas density. The coefficients in this expansion are then investigated using the techniques of Baranger.[2] Indeed, the theory may properly be regarded as an application of that of Baranger, the main difference being that the present case involves "self broadening." The density expansion method, while familiar in the theory of gases, has heretofore been applied to pressure broadening only in the classical path approximation.[5b]

II. THEORY

According to the correlation function theory the shape of the spectrum of an atomic or molecular system is given by

$$P(\omega)=A\hbar\omega\int_{-\infty}^{\infty}dt\,\exp(-i\omega t)\ \mathrm{Tr}\{\rho G^{\dagger}(0)G(t)\},\quad(1)$$

i.e., the line shape is the Fourier transform of a time correlation function.[5] Here A is a combination of constants and the intensity of the incident radiation. This factor only affects the total intensity of the line; we shall ignore it hereafter. Here ρ is the density operator for the entire N body system, and G is the interaction operator between the radiation field and the mtaerial system. $G(t)$ is the Heisenberg operator

$$G(t)=\exp(i/\hbar Ht)\ G(0)\ \exp(-i/\hbar Ht),$$

where H is the Hamiltonian for the entire N body system. The experimentally measured quantity is the

* Contribution No. 2491.

[1] A. F. Hildebrandt, F. B. Booth, and C. A. Barth, J. Chem. Phys. **31,** 273 (1959).

[2] M. Baranger, Phys. Rev. **90,** 791 (1953).

[3] J. P. Wittke and R. H. Dicke, Phys. Rev. **103,** 620 (1956).

[4] E. M. Purcell and G. B. Field, Astrophys. J. **124,** 542 (1956).

[5] (a) P. W. Anderson, Phys. Rev. **76,** 647 (1949); (b) J. van Kranendonk, dissertation, Amsterdam, 1952 (unpublished); (c) S. Bloom and H. Margenau, Phys. Rev. **90,** 791 (1953).

difference between absorption and stimulated emission, $P(\omega)+P(-\omega)$. Spontaneous emission is negligible in the frequency range appropriate to paramagnetic resonance.

In the case of electron spin resonance G is given by

$$G=\sum_{j=1}^{N} s_{jx}\exp(i\mathbf{q}\cdot\mathbf{r}_j)$$

$$q=\omega/c, \tag{2}$$

s_{jx} is the x component of the spin of electron j, and the exponential factor gives the phase of the incident wave at the position of electron j. The exponential factor is usually set equal to unity (dipole approximation), and we shall do so here. However, we should like to point out that retention of this factor brings Doppler broadening into the theory in a natural way. This is shown in the Appendix. The incident radiation has its magnetic vector polarized in the x direction, and for the experiment we consider there is a constant magnetic field $\mathcal{H}$ in the z direction.

The material system interacting with radiation is, in our case, N hydrogen atoms in a volume Ω. We assume that the density, N/Ω, is sufficiently low so that three-body collisions are rare; thus we may neglect recombination to stable molecular hydrogen during the experiment. This assumption is valid in practice; nevertheless, it has a bearing on the derivation of Eq. (1) for our case. The derivation of Eq. (1) from the usual quantum-mechanical radiation formulae involves a summation over all possible final states of the system and the use of the completeness property of the corresponding wave functions. The most stable final states, of course, are those involving $N/2$ molecules of H_2; however, under the hypothesis of binary collisions molecular states can only arise from the initial atomic states by radiative recombination. This is an improbable process and, furthermore, such radiation will not occur in the spectral region of interest to us; i.e., microwaves. Eq. (1) will still apply.

We shall be concerned with the evaluation of the trace in Eq. (1). Because of the identity of the electrons, we may write

$$\mathrm{Tr}\{\rho G^{\dagger}(0)G(t)\}=N\,\mathrm{Tr}\{\rho s_{1x}(0)s_{1x}(t)\}+N(N-1)\,\mathrm{Tr}\{\rho s_{1x}(0)s_{2x}(t)\}. \tag{3}$$

The first term is the time autocorrelation function for a single electron; the second expresses the correlation between different electrons.

It is convenient to introduce the spin raising and lowering operators

$$s_{\pm}=s_x\pm is_y, \tag{4}$$

whose properties are well known. If we are interested in absorption we may write

$$s_x(0)s_x(t)\approx s_-(0)s_+(t). \tag{5}$$

For emission the roles of s_+ and s_- are reversed. The terms which are omitted in Eq. (5) give rise to negligible effects. This corresponds to the fact that we have formulated the problem in terms of linearly polarized incident radiation, and that only one circularly polarized component is effective in absorption, the other in emission.[6]

Although the spectrum has been expressed in terms on one- and two-spin correlation functions, these functions depend on the interactions of all N particles in the system. But, at low densities, the particles will interact predominantly only two at a time, and we should like to incorporate this behavior in the formalism. An analogous situation occurs in the theory of the equation of state of real gases, where the initial departures from the ideal gas laws are ascribed to binary interactions. The effect of molecular interactions is accounted for in the theory by expanding the relevant thermodynamic functions as power series in the density, the well known virial expansion.[7] The coefficient of $(N/\Omega)^n$ involves an integral over the positions of n molecules. At low densities only the terms with $n\ll N$ are needed.

A similar expansion in powers of the density is applicable to the traces in Eq. (3). The theory of density expansions of the thermal average of time-dependent state variables has already been given,[8] and we merely recapitulate here the relevant formulae. As in footnote reference 8, the translational motion of the atoms is assumed to be governed by Boltzmann statistics. At low densities and ordinary temperatures this should be an excellent approximation, even for hydrogen.

Let $\psi_j(n)$ be an eigenfunction of the Hamiltonian H_n for an n particle system in the volume Ω. Define $w_{1,n-1}$ integrals by

$$w_{1,n-1}=[\lambda^{3n}/Q_i{}^n(n-1)!]\int\sum_j\psi_j{}^*(n)\times\exp(-H_n/\kappa T)s_{1-}(0)s_{1+}(t)\psi_j(n)d\mathbf{r}_1\cdots d\mathbf{r}_n, \tag{6}$$

$\lambda=h/(2\pi m\kappa T)^{\frac{1}{2}}$, κ is the Boltzmann constant, Q_i is the internal partition function for a single particle, and the integration sign means integrate over space and spin coordinates. The ordinary w integrals of the theory of gases (integrals of ordinary Slater sums) are given by

$$w_{0,n}=\frac{\lambda^{3n}}{Q_i{}^n n!}\int\sum_j\psi_j{}^*(n)\exp(-H_n/\kappa T)\psi_j(n)d\mathbf{r}_1\cdots d\mathbf{r}_n, \tag{7}$$

[6] N. F. Ramsey, *Molecular Beams* (Clarendon Press, Oxford, 1956), p. 122.

[7] J. E. Mayer and M. G. Mayer, *Statistical Mechanics* (John Wiley & Sons, Inc., New York, 1940).

[8] R. M. Mazo and A. C. Zemach, Phys. Rev. **109**, 1564 (1958).

$u_{1,n}$ integrals are then defined recursively by the relations

$$w_{1,N-1}=\sum_{j=0}^{N-1}u_{1,j}w_{0,N-j-1}, \tag{8}$$

and D coefficients are defined by

$$D_n=u_{1,n}/\Omega. \tag{9}$$

Then the first trace in Eq. (3) can be written

$$\mathrm{Tr}\{\rho s_{1-}(0)s_{1+}(t)\}=D_0+(N/\Omega)(D_1-\beta_1 D_0)$$
$$+(N/\Omega)^2[D_2-2\beta_1 D_1-(\beta_2-\tfrac{1}{2}\beta_1)^2 D_0]+\cdots. \tag{10}$$

Here the β are the usual irreducible cluster integrals of the theory of gases.

The advantage of introducing the u integrals is that the domain of integration is effectively of the order of the range of intermolecular forces, whereas in the w functions, it is effectively the entire space Ω. The two-spin correlation function may be expanded similarly. Define $w_{1,1,n-2}$ functions by

$$w_{1,1,n-2}=\frac{\lambda^{3n}}{Q_i{}^n(n-2)!}\int\sum_j\psi_j{}^*(n)$$
$$\times\exp(-H_n/\kappa T)s_{1-}(0)s_{2+}(t)\psi_j(n)d\mathbf{r}^n, \tag{11}$$

$u_{1,1,n-2}$ functions are then defined recursively by[9]

$$w_{1,1,n-2}=\sum_{j=0}^{n-2}u_{1,1,j}w_{0,n-2-j}, \tag{12}$$

and cluster integrals are defined by

$$I_n=u_{1,1,n}/\Omega. \tag{13}$$

Then

$$(N-1)\ \mathrm{Tr}\{\rho s_{1-}(0)s_{2+}(t)\}=(N/\Omega)I_0$$
$$+(N/\Omega)^2[I_1-2\beta_1 I_0]+\cdots. \tag{14}$$

We have set $(N-1)/N=1$, since N is large.

The definitions of the u and w functions differ slightly from those of footnote reference 8. We have here taken explicit cognizance of the internal structure of the atoms by inserting the factors of Q_i, the internal partition function. Since the magnetic internal energy (Zeeman and hyperfine) is small compared to κT, we may set $Q_i=4$ for the ground electronic state of hydrogen. We have also assumed that the density operator ρ is that appropriate for thermal equilibrium

$$\rho=\exp(-H/\kappa T)/\ \mathrm{Tr}\{\exp(-H/\kappa T)\}. \tag{15}$$

The physical meaning of the expansions (10) and (14) is that the term of order $(N/\Omega)^n$ takes into account the dynamics of $n+1$ particles, but with the effects of collisions accounted for in lower-order terms subtracted out. For example, the coefficient of $(N/\Omega)^2$ has contributions from ternary collisions, and successive collisions of pairs, but *not* from a binary collision and the independent motion of a third particle.

[9] We have omitted here integrals which vanish identically for our case. For the general expansion see footnote 8.

III. EVALUATION OF COEFFICIENTS

D_0 is quite easy to evaluate. We first write down the Hamiltonian for a single hydrogen atom:

$$\mathcal{H}_1=(P^2/2m)+g_e\beta_e\mathcal{H}_z s_z+as_zI_z$$
$$=K+H_i. \tag{16}$$

The first term is the translational kinetic energy, β_e the Bohr magneton, g_e the electron magnetogyric ratio, I_z the z component of nuclear spin, and a, the hyperfine coupling constant, $a=g_e\beta_e g_N\beta_N 8\pi\,|\,\psi(0)\,|^2/3$. We have not written down the electronic energy of ground state, since this is merely an additive constant for our purposes. We have also omitted the Zeeman energy of the nuclear spin, since this is small.

Then

$$D_0=\Omega^{-1}(\lambda^3/Q_i)(\Omega/h^3)\int\exp\frac{(-i/\hbar\mathbf{p}\cdot\mathbf{r})}{\Omega^{\frac{1}{2}}}$$
$$\times\exp(-P^2/2m\kappa T)\frac{\exp(i/\hbar\mathbf{p}\cdot\mathbf{r})}{\Omega^{\frac{1}{2}}}d\mathbf{r}d\mathbf{p}\times\mathrm{Tr}$$
$$\times\{\exp(-H_i/\kappa T)s_{1-}\exp(i/\hbar H_i t)s_{1+}\exp(-i/\hbar H_i t)\}. \tag{17}$$

Defining ω_+ and ω_- by

$$\hbar\omega_\pm=g_e\beta_e\mathcal{H}_z\pm\tfrac{1}{2}a, \tag{18}$$

we easily find

$$D_0=\tfrac{1}{4}\exp(g_e\beta_e\mathcal{H}_z/2\kappa T)\{\exp(i\omega_+ t)+\exp(i\omega_- t)\}. \tag{19}$$

We have set $Q_i=4$ and have neglected the hyperfine energy in the Boltzmann factor, since this is small compared to the Zeeman energy. One is tempted to set the entire Boltzmann factor equal to unity; but this would not be correct since Eq. (19) refers to absorption and we must eventually subtract a similar term for emission with a Boltzmann factor whose exponent has the opposite sign.

If we were content to stop with the calculation of D_0, Fourier transformation would yield delta function lines at ω_+ and ω_-. This should come as no surprise.

The higher coefficients are considerably more difficult to come by. We first consider D_1 and I_0. The Hamiltonian for two hydrogen atoms which we shall use is

$$\mathcal{H}_2=K+V+g_e\beta_e\mathcal{H}_z(s_{1z}+s_{2z})+a(s_{1z}I_{1z}+s_{2z}I_{2z})$$
$$=K+V+H_m$$
$$V=V_1(R)+V_2(R)\mathbf{S}_1\cdot\mathbf{S}_2, \tag{20}$$

K is the translational kinetic energy, and V is the intermolecular potential. For the two-body wave functions we shall use products of translational wave functions and spin wave functions. The electronic spatial wave function is to be thought of as integrated out, giving

use to the effective Hamiltonian (20). V thus contains an exchange contribution and is spin dependent.

It is convenient to consider D_1 and I_0 simultaneously. We have

$$D_1+I_0=(\lambda^6/Q_i^2\Omega)\int\{\tfrac{1}{2}\sum_n\psi_n^*\times\exp(-H_2/\kappa T)s_-(0)s_+(t)\psi_n-\sum_m\phi_m^*\times\exp(-H_2^0/\kappa T)s_{1-}(0)s_{1+}^0(t)\phi_m\}d\mathbf{r}_1d\mathbf{r}_2. \quad (21)$$

Here the ψ_n are two-body wave functions for the Hamiltonian (20), and the ϕ_m are the wave functions for two free particles with Hamiltonian H_2^0, which is obtained from H_2 by setting $V=0$. $s_{1+}^0(t)$ is the Heisenberg spin operator for particle 1, which has evolved according to the Hamiltonian H_2^0. The factor $\frac{1}{2}$ arises because we have symmetrized the part of D_1+I_0 corresponding to interacting particles.

Assume that we know the exact two-body wave functions for the Hamiltonian, Eq. (20); these functions will be rather complicated since the hyperfine energy does not commute with the exchange energy. At large distances the wave functions will describe particles in definite hyperfine states while at small distances the wave functions will have definite values of S^2. Thus, if we consider a scattering problem in which we scatter hydrogen atoms, each of which is a definite, different spin state (neglecting nuclear spin for the moment), the scattered particles will have a certain cross section for scattering with spin exchange. Since this is an exactly resonant process, the amplitude for spin exchange scattering is just half the difference of the singlet and triplet scattering amplitudes.[10] When nuclear spin is not neglected the hyperfine energy makes the process nonresonant; but the energy difference between atomic hyperfine states is so small that the exchange scattering amplitude should have the same form to a very good approximation.

With these remarks in mind we begin the evaluation of D_1+I_0; the integral sign in Eq. (21) carries with it the instruction to take spin matrix elements also. It is convenient to consider separately the contribution from each possible spin combination. We shall take, as the basic functions for evaluating the trace, the exact two-body wave functions for the Hamiltonian H_2, Eq. (20), and shall use the following notational conventions. Electron spin wave functions will be denoted by Greek letters α(spin up) and β(spin down). Nuclear spin wave functions will be denoted by Greek letters with superior bars ($\bar{\alpha}$, $\bar{\beta}$). Positional notation will be used; i.e., $\alpha\beta$ stands for $\alpha(1)\beta(2)$ and $\beta\alpha$ for $\alpha(2)\beta(1)$.

We first note that for states in which the nuclear spins are the same, $\bar{\alpha}\bar{\alpha}$ and $\bar{\beta}\bar{\beta}$, the hyperfine and exchange operators effectively commute. Furthermore, those states whose electron spin function is $\alpha\alpha$ do not contribute (for absorption). Thus the contribution of 10 out of the possible 16 spin states can be evaluated in a completely straightforward manner. The contribution from a single energy is

$$4\exp(-E_3/\kappa T)[\exp(i\omega_+t)+\exp(i\omega_-t)]. \quad (22)$$

The energy E_3 has been given a subscript to indicate that the states yielding this contribution are components of the triplet. In (22) factors of λ^2/Q_i^2, etc., have been omitted, since it is more convenient to put these in all at once at the end of the calculation.

The remaining six states can be treated in the following manner. Consider, for example, a scattering state whose incoming wave is

$$\psi_{1n}=\exp(i\mathbf{k}_1\cdot\mathbf{r})\beta\alpha\bar{\alpha}\bar{\beta}$$
$$\hbar k_1=[2\mu(E+a)]^{\frac{1}{2}}, \quad (23)$$

where E is the energy. The outgoing wave will have two parts, asymptotically, one with wave number k_1 and one with wave number $\hbar k_2=[2\mu(E-a)]^{\frac{1}{2}}$. The elastic part corresponds to no spin flip and has an amplitude approximately given by f_1+f_3, where f_1 and f_3 are the scattering amplitudes for the singlet and triplet potential curves, respectively. The inelastic wave, with wave number k_2, has had a spin flip, and has the amplitude f_3-f_1. These amplitudes are not exactly as stated, since the scattering is not exactly resonant. However, they should be very close to the correct ones.

We now have to evaluate the expectation value of $s_-\exp(iHt/\hbar)s_+\exp(-iHt/\hbar)$ in the state described previously. We use the relations

$$\exp(iHt/\hbar)=\left\{1+(i/\hbar)\int_0^t\exp(i/\hbar Hs)V\times\exp(-i/\hbar(K+H_m)s]ds\right\}\exp[i/\hbar(K+H_m)t] \quad (24)$$

$$\exp(-iHt/\hbar)=\exp[-i/\hbar(K+H_m)t]\times\left\{1-(i/\hbar)\int_0^t\exp[i/\hbar(K+H_m)s]V\exp[-i/\hbar Hs]ds\right\}, \quad (25)$$

and expand the product $s_-(0)s_+(t)$ into four terms. One of these,

$$(s_{1-}+s_{2-})\exp[i/\hbar(K+H_m)t)(s_{1+}+s_{2+})\times\exp[-i/\hbar(K+H_m)t], \quad (26)$$

is quite simple to evaluate, yielding a result of the same form as expression (22). When these terms are added to (22) and are combined with the part of D_1, arising from free particle motion, one gets just β_1D_0, which cancels the β_1D_0 appearing explicitly in the coefficient of (Eq. (10). Thus the free motion is subtracted out, as stated previously.

[10] N. F. Mott and H. W. S. Massey, *The Theory of Atomic Collisions* (Clarendon Press, Oxford, 1949), 2nd ed., p. 148.

The remaining terms are linear or quadratic in the two-body potential, V. They are evaluated using the arguments of Baranger.[2] Consider first the linear terms, one of which is

$$i/\hbar s_-\int_0^t \exp(i/\hbar Hs)\,V\exp[-i/\hbar(K+H_m)s]ds \times \exp(i/\hbar H_m t)s_+\exp(-i/\hbar H_m t), \quad (27)$$

and take the expectation value of this with respect to the state whose incoming part is specified by Eq. (23). Operating to the left with s_- changes all electron spin wave functions to $\alpha\alpha$. Now, operate to the left again with $\exp(iHs/\hbar)$. The incoming wave is propagated outward as a scattered triplet wave, while the original outgoing scattered wave is propagated out of the range of the potential V. We are left with

$$\exp(i\omega_0 s)\,\exp[i/\hbar E_3(k_1)s]\psi_{\mathbf{k}_1}{}^{(3)}\alpha\alpha\bar{\alpha}\bar{\beta}$$

as a result of these operations. Here ω_0 is the Zeeman frequency $g_e\beta_e\mathcal{H}_z/\hbar$, $E_3(k_1)$ is the energy of the triplet scattered wave with wave vector $\mathbf{k}_1$, and $\psi_{\mathbf{k}_1}{}^{(3)}$ is the corresponding wave function.

Now operate to the right with $\exp(-iH_m t/\hbar)$. This multiplies the incoming part of the wave function with spin $\beta\alpha$ by $\exp(i\nu t)$, $\nu=a/2\hbar$, and the part with $\alpha\beta$ (outgoing only) by $\exp(-i\nu t)$. Operating with s_+ to the right changes all spin wave functions to $\alpha\alpha$ and subsequent application of $\exp(iH_m t/\hbar)$ yields a factor $\exp(i\omega_0 t)$. The operator $\exp(-i(K+H_m)s/\hbar)$ then propagates the outgoing part of the wave out of the range of V, and the incoming wave goes on as a plane wave. The net result is that the matrix element is given by

$$\langle\psi_{\mathbf{k}_1}{}^{(3)}\mid V_3\mid\mathbf{k}_1\rangle t\exp(i\omega_+ t) = (-2\pi\hbar^2/\mu)f_{3,\mathbf{k}_1}{}^*(0)t\exp(i\omega_+ t), \quad (28)$$

where V_3 is the triplet potential, and f_3 is the triplet scattering amplitude. These considerations are not valid for very short times, as Baranger points out.[2]

The evaluation of the second term linear in V is quite analogous to the discussion leading to (28). However, in this case, there is a second term proportional to

$$\int_0^t \exp(2i\nu s)ds.$$

Since the times of interest are appreciably greater than ν^{-1} this term is small compared to t and is neglected.

The term quadratic in V appears to be proportional to t^2 at first sight. However, in evaluating the matrix element there is a summation over intermediate states to be performed. This summation reduces the time dependence to a linear one, the calculation being quite analogous to the derivation of time-proportional transition probabilities in time-dependent perturbation theory. The result contains products of the singlet and triplet scattered amplitudes, and is proportional to the time.

Similar calculations must be carried out for each spin state. When all 16 states are taken into account, and the thermal average over energy taken, we obtain for the coefficient of N/Ω,

$$-\frac{\hbar t}{16\pi^2\mu}\frac{\hbar^3}{(2\pi\mu\kappa T)^{\frac{3}{2}}}\int_0^\infty \exp(-\hbar^2k^2/2\mu\kappa T) \times\left[\int\mid f_1-f_3\mid^2 d\Omega\right]k^3dk. \quad (29)$$

The actual calculations are rather lengthy and we have discussed only very sketchily how they are carried out for one particular spin state. We omit further details of our calculation, not because they are particularly easy, but because the technique is just an application of the methods of Baranger, which are very clearly described in footnote reference 2, and the algebraic minutiae are not very enlightening.

We must now consider the higher order terms. These involve the successive solution of 3, 4, etc., body problems, and explicit calculations are hardly possible. However, we have assumed our gas to be very dilute, so that the motion of a molecule can be described by a succession of two-body collisions. It then becomes intuitively reasonable that the higher order terms are just powers of the binary collision term. That is, if we call expression (29) γt, then the nth-order term is expected to be $(\gamma t)^n/n!$. For if the interactions occur as isolated successive binary collisions whose durations are short compared to the time between collisions, one would expect to get, for n collisions in the time t

$$\gamma^n\int_0^t dt_n\int_{t_n}^t dt_{n-1}\cdots\int_{t_2}^t dt_1=\gamma^n t^n/n!.$$

If this be true, then the series for the spin correlation function is just that for an exponential, and the line shape is Lorentzian. A more detailed justification for considering the effects of successive binary collisions to compound in the manner discussed above has been given by Baranger.[11]

IV. DISCUSSION

The expression

$$\sigma_{ex}=\tfrac{1}{4}\int\mid f_1-f_2\mid^2 d\Omega, \quad (30)$$

is just the total cross section for scattering with exchange of electrons.[10] Then (29) can be written

$$-\tfrac{1}{2}(N/\Omega)\bar{V}\bar{\sigma}_{ex}, \quad (31)$$

where $\bar{V}$ is the mean thermal relative velocity $\bar{V}=$

[11] M. Baranger, Phys. Rev. **112**, 855 (1958).

$(8\kappa T/\pi\mu)^{\frac{1}{2}}$ with μ the reduced mass, and $\bar{\sigma}_{ex}$ is given by[4]

$$\bar{\sigma}_{ex}=[2\hbar^4/(2\mu\kappa T)^2]\int_0^\infty \exp(-\hbar^2k^2/2\mu\kappa T)\sigma_{ex}k^3dk; \quad (32)$$

$\bar{\sigma}_{ex}$ is the cross section thermally averaged with a weighting factor proportional to the velocity.

T_2, the experimental line width parameter, is then

$$(N/\Omega)\,T_2=2/\bar{V}\bar{\sigma}_{ex}, \quad (33)$$

and the reported measured value of $(N/\Omega)\,T_e$ is 1.9×10^9 sec cm^3/atom. Assuming 325°K for the temperature,[12] this yields

$$\bar{\sigma}_{ex}=28.5\times10^{-16}\text{ cm}^2\pm15\%, \quad (34)$$

the error being mainly due to uncertainty in the measured H concentration.[12] This number is somewhat larger than the 23×10^{-16} cm^2 estimate given by Wittke and Dicke, which was computed as half the maximum total cross section summed over a suitable range of angular momentum. This difference is not significant since our result is a thermal average, with velocity as a weighting factor, while the estimate of Wittke and Dicke is unweighted.

The cross section at 325°K interpolated from the table given by Purcell and Field is 43.3×10^{-16} cm, about 50% greater than ours. This suggests that these authors' neglect of the triplet interaction was not completely justified.

Since the simple estimate of Wittke and Dicke gives such satisfactory results, laborious and expensive quantum-mechanical calculations of σ_{ex} hardly seem to be called for.

There is another way to get a simple estimate of the cross section.[13] If $\epsilon(r)$ is the difference between the singlet and triplet potential curves, then the spins will precess an amount

$$\int_{-\infty}^{\infty}\epsilon(r)dt/\hbar,$$

due to exchange during a collision. We can say that a spin exchange has taken place when the precession reaches a critical value, say one radian. If b is the distance of closest approach and $\bar{V}$ the relative velocity, we may approximate the integral by $b\epsilon(b)/\bar{V}$, and so b is determined by

$$b\epsilon(b)/\bar{V}\approx\hbar.$$

We have computed $\epsilon(b)$ from the well-known Heitler-London expression for the energy of two hydrogen atoms. This should be quite accurate at the distances that are important: b is easily determined graphically and is found to be about 6.7 a_0. While this is larger than the 5.7 a_0 obtained from Eq. (34), it is clearly of the right order of magnitude and the difference certainly is within the limits of precision of the method of estimation.

Dalgarno[14] has recently computed the momentum-transfer cross section for $H-H$ collisions. We find, by extrapolation of the values he reports, a cross section of 47×10^{-16} cm^2 at an energy of 0.025 ev. This stands in contrast to an old value of about 5×10^{-16} cm^2 [15] based on measurements by Harteck of the viscosity of $H-H_2$ mixtures produced by a Woods discharge in molecular hydrogen. Amdur[16] has recalculated the viscosity (and diffusion coefficients) of atomic hydrogen using Harteck's experimental data and has arrived at results of the same order of magnitude. We suspect that the theoretical data are probably more reliable because of the assumptions made in converting viscosities to cross sections. The momentum-transfer cross section should not be directly compared to our number, which is a spin-exchange cross section; however, it does bear out the contention of Purcell and Field that gas-kinetic cross sections should be abnormally large for $H-H$ collisions. The kinetic theory of atomic hydrogen appears to be due for reconsideration.

V. ACKNOWLEDGMENTS

The author is indebted to Dr. H. M. McConnell for bringing this problem to his attention and to Dr. A. F. Hildebrandt, Dr. C. A. Barth, and F. Booth for discussion of their experiment.

APPENDIX

We have mentioned that the factors $\exp(i\mathbf{q}\cdot\mathbf{r}_i)$, which give the amplitude of the oscillating magnetic field over the sample volume, give rise to the Doppler effect. Though the connection has been stated by Fano,[17] there does not seem to be a derivation of the Doppler effect by the correlation function method in the literature. We would like to just sketch the calculation. We shall consider only the density independent term, i.e., D_0.

We make the dipole approximation as far as the position of the electron relative to the nucleus is concerned, but do not assume the variation of the oscillating magnetic field across the sample is negligible. Equation (17) should then be modified by inserting the operator

$$\exp[-i\mathbf{q}\cdot\mathbf{r}(0)]\exp[i\mathbf{q}\cdot\mathbf{r}(t)]$$

just before the last wave function. Now the solution of the equations of motion for a free particle just give

$$\mathbf{r}(t)=\mathbf{r}(0)+\mathbf{p}(0)t/m. \quad (A1)$$

On making use of the canonical commutation relations to disintangle the noncommuting operators $\mathbf{r}$ and $\mathbf{p}$

[12] A. F. Hildebrandt and C. A. Barth (private communication).
[13] This was pointed out to me by Professor R. P. Feynman.
[14] A. Dalgarno, Proc. Phys. Soc. (London) **75,** 374 (1960).
[15] P. Harteck, Z. physik. Chem. **139,** 98 (1928).
[16] I. Amdur, J. Chem. Phys. **4,** 339 (1936).
[17] U. Fano, Revs. Modern Phys. **29,** 74 (1957).

in the exponent, the integral in (17) can be written

$$\int d\mathbf{p} \exp[-P^2/2m\kappa T + il\mathbf{p}\cdot\mathbf{q}/m - it\hbar q^2/2m]$$
$$\propto \exp[-(q^2l^2\kappa T/2m) - (it\hbar q^2/2m)]. \quad \text{(A2)}$$

(We omit all pre-exponential factors which vary slowly with frequency.) Carrying out the integration over t to get the line shape, we find

$$P(\omega) \propto \exp[-(mc^2/2\kappa T\omega^2)\{(\hbar\omega^2/2mc^2) - (\omega-\omega_0\}^2], \quad \text{(A3)}$$

where ω_0 is the frequency for a stationary emitter. The term $\hbar\omega^2/2mc^2$ is of relativistic origin, and is small in the region where the nonrelativistic treatment of the radiation field is valid. In fact (A3) can be most simply derived just from relativistic energy-momentum conservation. In our derivation the term arises because of the noncommutability of $\mathbf{p}$ and $\mathbf{r}$.

The factor ω^2 multiplying κT can be replaced by ω_0^2 since when ω differs enough from ω_0 for the replacement to be invalid, the exponential is vanishingly small anyway because of the enormous value of $mc^2/\kappa T$. Thus (A3) reduces to the ordinary Doppler shape.

THE JOURNAL OF CHEMICAL PHYSICS VOLUME 34, NUMBER 1 JANUARY, 1961

Reflection Spectra and Absolute Infrared Intensities in Pure Liquids: Benzene, Chloroform, Bromoform, Carbon Disulfide, and Carbon Tetrachloride

P. N. SCHATZ AND SHIRO MAEDA

Department of Chemistry, University of Virginia, Charlottesville, Virginia

AND

J. L. HOLLENBERG AND DAVID A. DOWS

Department of Chemistry, University of Southern California, Los Angeles, California

(Received June 16, 1960)

Reflection spectra of liquid benzene, chloroform, bromoform, carbon disulfide, and carbon tetrachloride have been studied in the infrared region. On using a method developed in this work, absolute intensities of the vibrational transitions involved have been obtained from the experimental data. The results are in reasonable agreement with intensities obtained from dispersion studies except for the case of carbon disulfide. The benzene intensity obtained is in disagreement with the value from absorption measurements on the pure liquid.

IN recent years there has been much interest in the measurement and interpretation of absolute infrared intensities in condensed phases. The appearance of the paper by Polo and Wilson[1] has stimulated particular interest in the comparison of intensities for the same molecule in liquid and gas, one of the ultimate aims being a greater understanding of the liquid state. Although a fair amount of work has been done in solution, very few absolute-intensity measurements have been made on pure liquids. This is largely a result of the exacting requirements for thin samples of accurately known thickness in conventional absorption measurements. In fact, for very intense bands where thicknesses of the order of a micron or less are involved, this problem becomes a very formidable one indeed. Furthermore, the difficult problems of wing[2] and reflection[3] corrections still remain.

As far as we know, there have been only two extensive absorption studies of absolute infrared intensities in a pure liquid, namely, the work of Jayadevappa and Hisatsune on benzene[4] and that of Lisitsa and Tsiashchenko[5] on chloroform. The latter authors also use dispersion and reflection techniques in their work.

It has been pointed out by Schatz[6,7] and Kagarise[8] that liquid infrared dispersion data will also permit a calculation of liquid absolute intensities, and that, in fact, this method becomes increasingly accurate the greater the band intensity. In principle, one should obtain the same absolute intensity from the dispersion and absorption measurements,[6-8] but in the two cases studied so far, the dispersion values have been somewhat higher. Thus for the 14.8-μ band of liquid benzene, the dispersion intensity was about 40% higher than the direct absorption measurement,[7] and for the

[1] S. R. Polo and M. K. Wilson, J. Chem. Phys. **23**, 2376 (1955).
[2] D. A. Ramsay, J. Am. Chem. Soc. **74**, 72 (1952).
[3] D. A. Dows and J. L. Hollenberg, J. Chem. Phys. **32**, 1581 (1960); G. S. Denislov, Optika i Spektroskopiya **6**, 301 (1959).
[4] I. C. Hisatsune and E. S. Jayadevappa, J. Chem. Phys. **30**, 848 (1959); **32**, 565 (1960).
[5] M. P. Lisitsa and Iu. P. Tsiashchenko, Optika i Spektroskopiya **6**, 396 (1959).
[6] P. N. Schatz, J. Chem. Phys. **29**, 959 (1958); see correction, **31**, 1146 (1959).
[7] P. N. Schatz, J. Chem. Phys. **32**, 894 (1960).
[8] R. E. Kagarise, NRL Rept. 5277 (1959); J. Chem. Phys. **31**, 1258 (1959).

9-μ band of liquid CH_2I_2,[8] the difference was about 17%. There is no way of knowing whether these discrepancies will prove typical, but it is interesting to note that the reflection results reported below support the dispersion intensity value in the case of benzene.

The purpose of the present paper is to examine another method of determining absolute infrared intensities of strong bands in pure liquids, namely, through the measurement of the reflection spectrum of the liquid. In principle, it should be possible to make reflection measurements at two different angles of incidence, thereby enabling a unique evaluation of both n and k as a function of frequency.[9] Since the absorption coefficient is given by $\alpha=4\pi nk\nu/c$ (where $I=I_0e^{-\alpha l}$), a straightforward computation of the integrated absorption coefficient (absolute intensity) should be possible. In practice, such a procedure involves considerable experimental and computational difficulties. Robinson and Price[10] have developed another method of extracting n and k from reflection data at normal incidence, and have studied solid polymeric substances. A very similar method has been used by Kislovskii[11] to obtain the optical parameters for solid therilene. These authors have not emphasized the obtaining of absolute intensities from their results. A slightly different approach has been used by Cameo-Bosco[12] to obtain similar data on various liquids; the results are of uncertain accuracy, and the author has not emphasized absolute intensities. In the present work, reflection measurements have been made at a small angle of incidence, and a functional relation between n and k has been assumed. In this way, both the experimental and computational aspects of the problem have been substantially simplified. It will be shown that if one measures the reflection spectrum of a given band, a calculation of the absolute absorption intensity is generally possible, and alternatively, a knowledge of the absolute intensity will permit a calculation of the reflection spectrum.

THEORETICAL

In this work, the following expression has been assumed to be valid[7]:

$$\epsilon'(\nu)-n_v^2(\nu)=(c/\pi^2)\sum_j\frac{A_j\tilde{n}_j}{\nu_j^2-\nu^2+i\gamma_j\nu}; \qquad (1)$$

ϵ' ($\equiv\epsilon_1-i\epsilon_2$) is the complex dielectric constant, n_v^2 is the electronic contribution to n^2 (n being the refractive index), c is the velocity of light, A_j is the integrated absorption coefficient ($\equiv\int\alpha(\nu)d\nu$), ν_j is the resonance frequency, and γ_j is a damping constant characteristic of the transition. The summation extends over all transitions below the visible region of the spectrum. In essence, Eq. (1) results from the assumption that each transition can be represented by a damped harmonic oscillator.[13] The significance of the quantities $\tilde{n}_j$ and A_j as well as the form taken by Eq. (1) at frequencies far from resonance has been discussed in detail previously.[7] It might be noted that one may obtain the Polo-Wilson equation from Eq. (1) by the use of arguments very similar to those recently presented by Ferguson.[14]

In order to obtain the desired relation between n and k for a given band, Eq. (1) is separated into real and imaginary parts. If, for the sake of simplicity, it is assumed that the band under consideration is not appreciably overlapped by other strong bands, the result is

$$\epsilon_1=n_v^2(\nu)+(c/\pi^2)\sum_i\frac{A_i\tilde{n}_i}{\nu_i^2-\nu^2}+(c/\pi^2)\frac{A_p\tilde{n}_p(\nu_p^2-\nu^2)}{(\nu_p^2-\nu^2)^2+\gamma_p^2\nu^2}$$

$$\equiv n'^2(\nu)+(c/\pi^2)\frac{A_p\tilde{n}_p(\nu_p^2-\nu^2)}{(\nu_p^2-\nu^2)^2+\gamma_p^2\nu^2} \qquad (2)$$

$$\epsilon_2=(c/\pi^2)\frac{\gamma_p\nu A_p\tilde{n}_p}{(\nu_p^2-\nu^2)^2+\gamma_p^2\nu^2}, \qquad (3)$$

where the subscript p designates the band under consideration, and the summation is over all other bands. The modifications necessary in Eqs. (2) and (3) when there is appreciable overlap with another band (e.g., in CCl_4) are clear.

If the experimental reflection spectrum has been measured, the absolute intensity (A_p) of the pth band is obtained in the following manner. First, $(n')^2$ must be known in the region of the pth band. Since the major contribution to n' is from n_v, this latter quantity must be known to fair accuracy ($\sim$0.003). Whether additional information is then necessary depends on the individual case. If the pth band represents the only intense absorption beyond the visible, all else can be ignored, and the result is, $n'(\nu_p)=n_v(\nu_p)$. Otherwise, the contributions of other absorptions to $n'(\sim\nu_p)$ must be estimated. This is generally possible if infrared dispersion data are available, and fortunately, a simple method for obtaining such data now exists.[15] Alternatively, n' may be estimated from the observed reflections, and improved by successive approximation. When the pth band is not overlapped appreciably by other strong bands, n' will vary only slightly over the range of the pth band. Accurate values of n' were available for all of the molecules studied in this paper.[6–8,16,17]

[9] I. Simon, J. Opt. Soc. Am. **41**, 336 (1951).
[10] E. T. S. Robinson and W. C. Price, Proc. Phys. Soc. (London) **B66**, 969 (1953); E. T. S. Robinson, *ibid.* **B65**, 910 (1952).
[11] L. D. Kislovskii, Optika i Spektroskopiya **6**, 529 (1959).
[12] M. Cameo-Bosco, Compt. rend. **248**, 1642 (1959).
[13] See, for example, C. J. F. Böttcher, *Theory of Electric Polarisation* (Elsevier Publishing Company, Inc., New York, 1952), Chap. VIII.
[14] E. E. Ferguson, J. Chem. Phys. **30**, 1059 (1959).
[15] R. E. Kagarise and J. W. Mayfield, J. Opt. Soc. Am. **48**, 430 (1958).
[16] M. A. Pittman, J. Opt. Soc. Am. **29**, 358 (1939).
[17] L. P. Lindsay, S. Maeda, and P. N. Schatz, J. Chem. Phys. (to be published).

Assuming that n' is now known, one calculates values for γ_p, ν_p, and $\bar{n}_p A_p$ using Eqs. (2) and (3) to obtain a "best fit" to the experimental reflection curve. The details of this procedure are outlined in an Appendix at the end of this paper. It should be noted that our criteria of a best fit are that the calculated and experimental reflection curves have the same maximum reflectance and the same bandwidth at half-height. These criteria are admittedly somewhat arbitrary, but it seems clear that any other simple criteria will yield values for γ_p, ν_p, and $\bar{n}_p A_p$ which differ but little from our values. The angle of incidence used in our experiments was sufficiently small (11°) that the simple expression $R=[(n_r-1)^2+n_r^2k^2]\times[(n_r+1)^2+n_r^2k^2]^{-1}$ was applicable in calculating the reflection from the surface of the liquid. n_r is the refractive index relative to KBr (the cell window material used in this work). Combination of this expression with the appropriate reflection corrections for the presence of the windows (Experimental section) leads directly to a calculated reflection spectrum. Since the quantity $\bar{n}_p$ can be calculated,[7] the absolute intensity A_p is obtained from the $\bar{n}_p A_p$ which gives a best fit.

In view of the fact that $\alpha=4\pi nk\nu/c$, it is a simple matter to calculate the optical density as a function of frequency, and from such a plot one may obtain the absorption bandwidth (at half-height) and the frequency at maximum absorption. A comparison of these quantities with the experimentally observed values then serves as a partial check of the validity of Eq. (1). Such comparisons are included in Table I.

It is clear from the procedures which have been outlined that one can equally well predict the reflection spectrum if one knows the absolute intensity. Such a predicted curve is shown in Fig. 1 where Hisatsune and Jayadevappa's absorption measurements of the absolute intensity were used to calculate the reflection spectrum. In this procedure, γ_p and ν_p were adjusted so that they reproduced, respectively, the observed maximum reflectance and the frequency of maximum reflectance. Alternately, these parameters could have been chosen to reproduce the observed absorption band width and the frequency of maximum absorption.

EXPERIMENTAL

Reflection spectra were measured in a modified Perkin-Elmer model 13 infrared spectrophotometer, equipped with NaCl and KBr prisms. Liquid samples were contained in a Teflon-bodied cell with a KBr window clamped to its open end. The inside of the cell was machined to an obtuse conical shape, and acted as a light trap to prevent any possible return of light entering the liquid. The cell was mounted on a carriage with fine adjustments to permit accurate and reproducible positioning and focusing. An aluminized plane mirror could be reproducibly placed in the plane of the KBr-liquid surface to serve as a 100% reference.

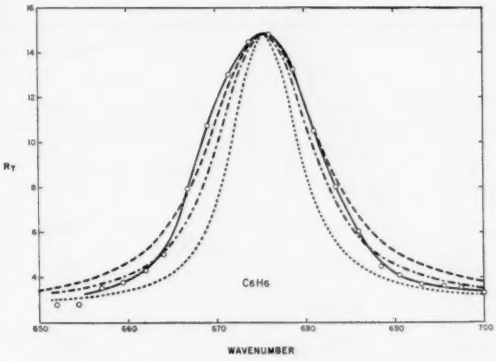

FIG. 1. Benzene; calculated and observed reflection spectrum. The solid line is drawn through the experimental points. The dashed line is the calculated best fit. The dash-dot and dotted lines are, respectively, the reflection spectrum calculated from the dispersion and absorption intensities (see text).

The angle of incidence of the optical beam on the reflecting surface was 11°.

All liquid samples were B and A reagent grade (used without further purification) except for the bromoform, which was Eastman Spectrograde. In each case the reflection spectrum was measured with the appropriate prism, using spectral slit widths as follows: benzene, 2.9; carbon tetrachloride, 2.8; chloroform, 3.0; bromoform, 3.0; and carbon disulfide, 10 cm^{-1}. In the case of carbon disulfide, atmospheric water lines made measurement uncertain, so the whole optical path outside the instrument housings was enclosed in a plastic bag, and the instrument was flushed with dry nitrogen until the accuracy of the reflection measurement was no longer impaired.

When the ratios of observed sample reflection to 100% reflection (aluminized mirror) were plotted, it was observed that the wings of the reflection bands were not as high in reflectivity as would be expected; the front surface of the KBr window alone should reflect 4.2% at 700 cm^{-1}, for example, and the observed benzene wing was about 2.8%. It was discovered that light reflected from the front surface of the cell window was defocused, due to the front surface position being some 6 mm in front of the sample surface. Moving the plane mirror forward by this amount gave almost identical reductions in the "100%" measurement. The data presented in the figures are actual observed reflectivities from the experimental cell. In order to compare with calculated curves, the following procedure was adopted. If R is the calculated reflectivity of the liquid-KBr interface, and, for example, the front of the cell window is expected to reflect 4.2%, the reflection intensity should be

$$R_{\text{obs}}=0.042+(1.00-0.042)\,R(1.00-0.042).$$

The first term is the front-surface reflection, the first parenthesis is the fraction of light passing to the main

TABLE I.

Pure liquid	"Best fit" of experimental reflection spectrum: $\bar{n}_p A_p$[a]	$\bar{n}_p$	A_p[a]	γ_p (cm^{-1})	ν_p (cm^{-1})	ν_{max}^{abs} (calc)[b] (cm^{-1})	Absorption bandwidth (calc) (cm^{-1})
C_6H_6 14.8μ band	24.8± 13%	1.468	16.5± 13%	11.47	670.47	672.5	13.8
CS_2 6.6μ band	170± 12%	1.587	108± 12%	56.2	1497.0	1505	65
$CHCl_3$ 13.2μ band	49.0± 13%	1.432	34.2± 13%	19.7	759.1	763	25.0
$CHBr_3$ 15.2μ band	33.3± 17%	1.576	21.1± 17%	19.5	655.8	659	22.0
CCl_4 12.5μ band	34.8± 5%	1.276	27.3± 5%	11.1	784.3	786	16.0
CCl_4 13.0μ band	34.0± 15%	1.668	20.4± 15%	16.5	760.3	762	17.0

Pure liquid	Dispersion data: $\bar{n}_p A_p$[a]	$\bar{n}_p$	A_p[a]	$n'(\nu_p)$	Absorption data: A_p[a]	ν_{max}^{abs} (obs)[b] (cm^{-1})	Absorption bandwidth (obs) (cm^{-1})
C_6H_6 14.8μ band	20.9[c]± 8.5%	1.488[c]	14.1[c]± 8.5%	1.482[c]	10.0[h]± 8%	673.5[h]	10.8±1.4[h]
CS_2 6.6μ band	118.6[d]± 7.5%	(1.587[g])	74.7[d]± 7.5%	1.585[d]		1510[i]	
$CHCl_3$ 13.2μ band	40.2[e]± 8%	(1.432[g])	28.1[e]± 8%	1.436[e]		757[e]	
$CHBr_3$ 15.2μ band		(1.576[g])		1.567[g]		654[e]	
CCl_4 12.5μ band	66.5[f]± 5%	(1.444[g])	46.0[f]± 5%	1.446[e]		785[j]	
CCl_4 13.0μ band						762[j]	

[a] 10^2 darks; (dark≡cm^{-1}/millimole per cm^2).
[b] ν_{max}^{abs} is frequency at which absorption band is a maximum.
[c] Footnote 7.
[d] Footnote 6.
[e] Footnote 17.
[f] Footnote 8.
[g] Taken from reflection calculation.
[h] Footnote 4 and E. S. Jayadevappa, dissertation, Kansas State University, 1959.
[i] A.P.I. Research Project 44, Serial No. 698.
[j] E. K. Plyler and W. S. Benedict, J. Research Natl. Bur. Standard **47**, 202 (1951).

reflecting surface, the last parenthesis is the fraction of reflected light passing out again through the front surface. It is assumed that all light entering the liquid is lost and that there is no second-pass reflection. Actually, part of the *first* 4.2% reflected is lost by defocusing, so we have simply adjusted that figure to agree with the observed wings of the band, and the calculated curves are the result of this procedure, applied to the values of R calculated as discussed previously.

Some question will arise as to whether the reflection phenomena studied here should be interpreted in terms of bulk properties (index of refraction, etc.) of the liquid, or whether surface phenomena will modify the results. We feel that in these cases it is likely that true bulk properties are being studied. Our belief is based on the fact that the penetration of the light into the reflecting surface is measured roughly by the wavelength of the light, which is in this work about 10μ. This is several orders of magnitude greater than the thickness of molecular films, and in general much larger than the effective distance of intermolecular interactions. Thus most of the reflection process involves liquid a large distance from the surface. In an attempt to check for gross effects of the surface, we measured the reflection of benzene and carbon disulfide with KCl cover windows. Although this window is very similar to KBr, one might expect some changes in the reflection if the surface is of importance. We found only slight differences in the observed bands compared to the KBr window experiments, and the changes were attributable to the change in index of refraction of the window. The question of surface effects is now under further study, and we hope to discuss it in more detail at a later time.[18]

Since the carbon disulfide results were somewhat surprising (integrated intensity 40% too large and width three times as large as any other liquid we studied), and since the CS_2 band lies in the 6-μ water region, we tested the possibility that the CS_2 being wet might change the band shape; two samples were measured, one dried for five days over a molecular sieve, the other saturated with water by shaking with liquid water and allowing to separate. The reflection bands were identical within our limits of error. It has been mentioned that we flushed the whole instrument optical path while studying the CS_2 reflection. Since carbon disulfide is so volatile, we had some trouble with cell leakage. CS_2 vapor absorbs light on the high-frequency shoulder of the reflection band, thus tending to reduce the apparent bandwidth. Experimental adjustment allowed removing most of the CS_2 vapor and permitted estimation of the actual band contour, but some error may still remain.

[18] We have now investigated a simple model which assumes that a 10 A thick surface layer exists which has different optical constants (n, k) than the bulk of the liquid. Detailed calculations show that this layer has no appreciable effect on the reflection properties of the liquid unless one assumes values for n and k which seem completely unreasonable. This would seem to confirm the unimportance of surface effects in infrared reflection spectra.

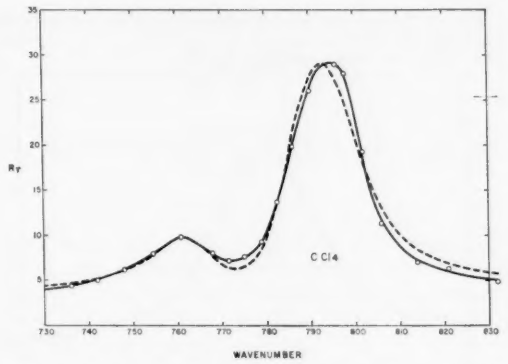

FIG. 2. Carbon tetrachloride; calculated and observed reflection spectrum. The solid line is drawn through the experimental points. The dashed line is the calculated best fit.

RESULTS AND DISCUSSION

The results are shown in Fig. 1–5 and in Table I. Each figure shows the experimental reflection spectrum and the theoretical ("best-fit") reflection spectrum calculated by the method outlined in the Appendix. In addition, Fig. 1 (benzene) shows the reflection curves which are obtained using the dispersion intensity[7] and the absorption intensity[4] with γ_p adjusted in each case to give the experimental peak reflectivity. For benzene, and particularly for CCl_4 and CS_2, it is observed that the assumed form of ϵ' [Eq. (1)] reproduces the experimental shape of the reflection spectrum very well, whereas for $CHCl_3$ and $CHBr_3$ the agreement, while reasonable, is not as good. No other measurable reflection peaks were observed for any of these compounds.

The parameters corresponding to the "best fit" of the experimental reflection spectra are listed in Table I and are compared, when possible, with these same quantities determined by dispersion or absorption measurements. The value of A_p for CCl_4 as determined by dispersion is the total for the 760- and 784-cm^{-1} bands. The percentage errors in Table I for the reflection intensities arise from two sources. First, an uncertainty in R of ± 1 unit has been assumed. This represents the probable error estimated for the experimental reflection measurements. Second, since the shape of the calculated curve is not identical with the experimental one, fitting the bandwidth of the reflection curve at half height is rather arbitrary. Consequently, a certain amount of variation of the intensity is possible before the over-all fit is clearly inferior. This additional uncertainty is also included in the errors listed in Table I. Examination of Table I shows that the intensities obtained from the reflection data ("reflection intensities") are usually higher than those obtained from dispersion measurements. In the cases of benzene

FIG. 3. Carbon disulfide; calculated and observed reflection spectrum. The solid line is drawn through the experimental points. The dashed line is the calculated best fit.

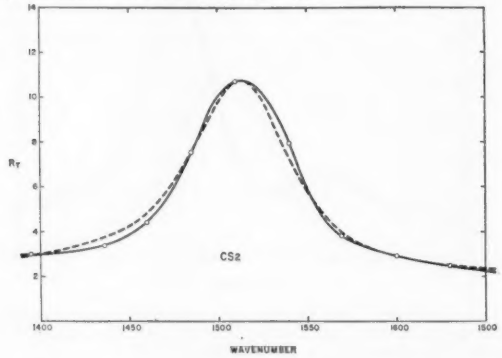

and CCl_4, the two values are in agreement within the combined uncertainties of the two methods, but for $CHCl_3$, and particularly for CS_2, the reflection intensities are substantially higher. A reliable dispersion intensity is not yet available for $CHBr_3$ since there is some evidence of an increasing systematic error at long wavelengths in the existing dispersion data.[17] However, a rough calculation based on these data indicates that the reflection intensity is about 25% higher than the dispersion result. The infrared dispersion data of liquid $CHBr_3$ are now being remeasured,[17] and a more accurate comparison will be possible at a later date. It might be noted that the $CHCl_3$ intensity reported in footnote 5 is only about 60% of our intensity (by dispersion). We can give no explanation for this discrepancy.

Since there are appreciable deviations between the calculated and experimental reflection curves of $CHCl_3$ and $CHBr_3$, it might be hoped that part of the discrepancy between the reflection and dispersion intensities could be attributed to the inadequacy of Eq. (1). However, we note that a small translation of the calculated curves would substantially improve the agreement without the necessity for appreciable changes of the reflection intensities. Much more striking is the case of CS_2 where the fit is truly excellent and yet the discrepancy between the reflection and dispersion intensities is great.

Since the dispersion intensities are based on a very general relation which requires no detailed assumptions about the absorption band,[7] we suggest tentatively that the dispersion intensities are more reliable than the reflection intensities.[19]

In the case of benzene (Fig. 1), it is possible to compare all three methods for determining intensities in pure liquids. The reflection result supports the dispersion intensity over the absorption intensity and agrees fairly well with the limiting intensity in solution (as measured[4] by absorption techniques), but uncertainty will remain until the discrepancy between the dispersion and reflection results is resolved and the pure-liquid absorption results are explained. The reflection curve calculated using the absorption intensity[4] is clearly too narrow and leads to an absorption bandwidth of 8.2 cm^{-1} (experimental $=10.8$ cm^{-1}). If one makes γ larger to increase this width, the calculated peak reflectivity drops rapidly and the discrepancy with the experimental reflection spectrum is even more apparent. The absorption bandwidth corresponding to the dispersion intensity is 11.8 cm^{-1}.

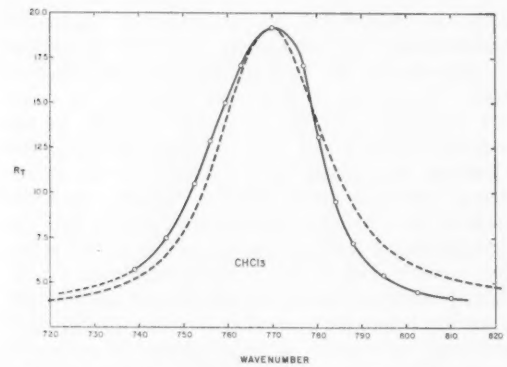

FIG. 4. Chloroform; calculated and observed reflection spectrum. The solid line is drawn through the experimental points. The dashed line is the calculated best fit.

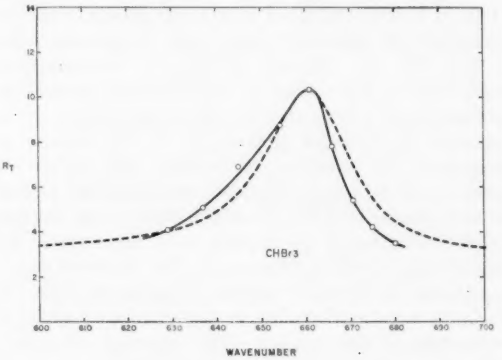

FIG. 5. Bromoform; calculated and observed reflection spectrum. The solid line is drawn through the experimental points. The dashed line is the calculated best fit.

[19] We have investigated the possibility of analyzing our data by the more general method of Robinson and Price (see work cited in footnote 10). However, we find in that case that it is not possible to get accurate absolute intensities. This is so because the refractive indices of our liquids on the wings of the bands approach more or less closely the refractive index of KBr. The resulting very small reflectances in the wings must then be measured very accurately if the method of Robinson and Price is to be successful. The present data are not adequate for this. This difficulty can be overcome by a proper choice of window material, or, of course, by the use of no window at all, if feasible.

In conclusion, it seems clear that absolute intensities of strong infrared bands may be obtained from measurements of the reflection spectra. Of the examples studied in this work, benzene and carbon tetrachloride are in good agreement with the previous dispersion work, and the haloforms are not far from agreeing within the estimated experimental uncertainties. Only carbon disulfide is in serious disagreement. The reason for this is not clear at present. The only case where comparison has been made with absorption intensities, benzene, leaves one in some doubt as to which method provides the correct intensity value. Since the measurements are increasingly difficult in absorption (and increasingly easy in dispersion or reflection) with more intense bands such as the benzene 680-cm^{-1} transition, we favor the results in this work. Our preference is fortified by the agreement between reflection and dispersion values, but it is not at all easy to see where the very careful absorption experiments were in error.

APPENDIX. FITTING THE REFLECTION SPECTRUM

The relevant equations are

$$R=[(n_r-1)^2+n_r^2k^2][(n_r+1)^2+n_r^2k^2]^{-1} \tag{A1}$$

$$\epsilon_1=\theta^2n_r^2(1-k^2)=n'^2+\frac{B_p(\nu_p^2-\nu^2)}{(\nu_p^2-\nu^2)^2+\gamma_p^2\nu^2} \tag{A2}$$

$$\epsilon_2=2\theta^2n_r^2k=\frac{B_p\gamma_p\nu}{(\nu_p^2-\nu^2)^2+\gamma_p^2\nu^2}, \tag{A3}$$

where n_r is the refractive index relative to KBr, θ is the refractive index of KBr (relative to air), and $B_p\equiv c\tilde{n}_pA_p/\pi^2$. All other quantities have been previously defined. It has been assumed that the pth band is not appreciably overlapped by other strong bands so that n' is approximately constant in the vicinity of ν_p. For any reflection band, it follows that

$$(dR/d\nu)_{\nu=\nu_m}=0, \tag{A4}$$

where ν_m is the frequency for which R is a maximum. This differentiation can be performed with the aid of Eqs. (A1)–(A3), and after considerable algebraic manipulation, Eq. (A4) becomes

$$2(n_m^2-3n_m^2k_m^2-1)\nu_m\left[\left(\frac{\nu_p^2-\nu_m^2}{\gamma_p}\right)^2-\nu_p^2\right]$$

$$+k_m(3n_m^2-n_m^2k_m^2-1)\left[\left(\frac{\nu_p^2-\nu_m^2}{\gamma_p}\right)(\nu_p^2+3\nu_m^2)-\gamma_p\nu_m^2\right]=0, \tag{A5}$$

where $n_r(\nu_m)\equiv n_m$, $k(\nu_m)\equiv k_m$. If it is assumed that $\gamma_p\ll\nu_m$, the following approximations may be employed: $x^2-\nu_p^2\approx x^2-\nu_m^2$, $x(\nu_p^2+3\nu_m^2)-\gamma_p\nu_m^2\approx 4\nu_m^2x$, where $x\equiv(\nu_p^2-\nu_m^2)/\gamma_p$, $y\equiv B/\gamma_p$: Eqs. (A2), (A3), and (A5) then become

$$\theta^2n_m^2(1-k_m^2)=n'^2+xy(x^2+\nu_m^2)^{-1} \tag{A6}$$

$$2\theta^2n_m^2k_m=\nu_my(x^2+\nu_m^2)^{-1} \tag{A7}$$

$$(n_m^2-3n_m^2k_m^2-1)(x^2-\nu_m^2)$$
$$+2k_m\nu_mx(3n_m^2-n_m^2k_m^2-1)=0. \tag{A8}$$

The procedure used in fitting the experimental reflection spectrum is the following: Since $R_{\max}$ and ν_m are known, Eqs. (A1) and (A6)–(A8) may be solved simultaneously for n_m, k_m, x and y. [In practice this is conveniently done by first noting from Eq. (A1) that $f^2\geq 1+k_m^2$, where $f\equiv(1+R_{\max})(1-R_{\max})^{-1}$. One first assumes that the equality applies, and this immediately gives a good first approximation to the value of k_m and n_m.] In order to get individual values for ν_p, B, and γ_p, one additional piece of information is necessary. In this work, γ_p was chosen so that the experimentally observed reflection bandwidth (at half-height) was reproduced. This may be done in a straightforward way using Eqs. (A1)–(A3). Once γ_p is known, the values of ν_p and B are obtained immediately. We therefore see that this method insures that the calculated and observed reflection spectra have approximately the same peak height and half-width.

Although the procedure outlined here has involved the use of one approximate equation [Eq. (A8)], in practice no appreciable error was introduced thereby. Comparisons between the experimental and calculated ("best fit") reflection spectra are shown in Figs. 1–5.

THE JOURNAL OF CHEMICAL PHYSICS VOLUME 34, NUMBER 1 JANUARY, 1961

Limit of Stability of Crystalline Helium

LOREN E. RADFORD

University of Virginia, Charlottesville, Virginia

(Received July 5, 1960)

The mobility of a vacancy in a crystal at the absolute zero of temperature is investigated. In this minimum energy configuration movement of the vacancy to an adjacent lattice site occurs by tunneling, the rate being determined by an approximation in which the barrier and adjacent potential wells are formed by nearest neighbor interactions only. There is found a critical volume at which the vacancy begins to move rapidly through the barrier. Identifying this increased mobility with the beginning of the melt, a criterion for stability of the crystalline structure is deduced. On applying this criterion to helium at the absolute zero, general agreement with experimental critical volumes is obtained.

INTRODUCTION

EXTENSIVE local order is known to exist in a liquid which is near its crystallization density. Thus, for example, in a monatomic crystal or dense liquid each atom may, in good approximation, be considered to move in the potential field of its nearest neighbors which are assumed to occupy fixed positions determined by the lattice structure. It is desired here to investigate the mobility of a vacancy in a crystal or liquid using this assumption. The intent is to determine when the crystalline structure becomes unstable, i.e., melting begins. The system, either crystal or liquid, is assumed to be at the absolute zero of temperature, to possess face centered cubic structure as regards nearest neighbor positions, and to consist of atoms with spherically symmetric fields. Being thus in a minimum energy configuration, motion of a vacancy, or, equivalently, movement into the vacancy by an atom occupying an adjacent lattice site, is dependent upon penetration of a potential barrier. The problem is essentially one of motion in two identical potential wells separated by a barrier. It is observed that the probability of penetration of the barrier results in a splitting of the single well ground-state level into two levels. These levels represent states in which the atom moves simultaneously in both wells. The corresponding eigenfunctions are symmetric and antisymmetric in the barrier, the symmetric eigenfunction representing the state of lowest energy. The difference in energy of these levels defines a frequency of transmission through the barrier which is expected, to increase rapidly when the crystal loses its stability.

To determine the energy levels for motion in both wells, and hence the frequency of transmission through the barrier, a trial wave function is chosen. This trial function is a superposition of localized wave functions centered about the two lattice sites in question. The frequency is then found to be extremely sensitive to the amount of overlap of the localized functions. Thus by making the radial extent of the localized wave functions a parameter to be chosen by the variational principle, the rate of transmission through the barrier may be examined and the desired criterion for stability obtained.

PROCEDURE

The variational principle is employed to determine the energy of the symmetric state (E_s). Assuming as a trial wave function $\Psi=\psi_1+\psi_2$ where ψ_1 and ψ_2 are wave functions of the form $\psi_i=p^2-(\mathbf{r}-\mathbf{q}_i)^2$ each centered about its own lattice site $\mathbf{q}_i$, the expression to be minimized is

$$E_s=\int\Psi^*H\Psi d\tau \Big/ \int\Psi^*\Psi d\tau, \qquad (1)$$

where the Hamiltonian has the form

$$H=-(\hbar^2/2m)\nabla^2+\sum_i 4\epsilon[(\sigma/\mathbf{r}-\mathbf{r}_i)^{12}-(\sigma/\mathbf{r}-\mathbf{r}_i)^6].$$

The form of the potential is a Lennard-Jones (6–12). The sum indicated is over nearest neighbors of both lattice sites. After evaluating the integrals E_s may be written

$$E_s=\frac{\hbar^2}{md^2}\left\{\frac{[8\epsilon md^2/\hbar^2][N_1(\sigma/d)^{12}-N_2(\sigma/d)^6]+N_3}{N_4}\right\}, \qquad (2)$$

where the N_i are functions of p/d, the ratio of the radial extent of the wave function at the point where it vanishes (p) to $\frac{1}{2}$ the distance between adjacent lattice sites (d).

To investigate the frequency of penetration through the potential barrier, p must be selected to minimize E_s when a particular set of values of ϵ, m, and d are substituted into (2). This also determines E_a. Then, from the method of beats applied to the two identical potential wells, the frequency for any given interparticle spacing is determined by evaluating $\nu=(E_a-E_s)/\pi\hbar$. It is apparent that were this problem capable of exact solution, the vacancy would have a limited mobility even in the crystalline structure. However, in this approximation, the frequency is zero when p is less than d since the localized wave functions do not overlap. E_a-E_s is observed to increase from zero to values which yield relatively high frequencies as p becomes just greater than d. Thus, using this method, the limit of stability occurs when the localized wave functions overlap. Recalling that the radial extent of the localized

functions is determined by the value of p/d which minimizes E_s, it is clear that the energy surface, $E_s(p/d)$, must have its minimum for some value of $p/d \leqslant 1$. The criterion for stability is then

$$dE_s/d(p/d) \mid_1 \geqslant 0.$$

When evaluated this becomes

$$0.156(\sigma/d)^{10} - 0.436(\sigma/d)^4 \geqslant 3.901\hbar^2/\epsilon m\sigma^2.$$

APPLICATION TO HELIUM

The only element fulfilling the assumptions of this calculation is helium. Using molar volumes of helium at the absolute zero of temperature and zero pressure, as extrapolated from experimental data, the frequency of penetration of the barrier is calculated. For helium 3 with a molar volume of 36 cm^3 a frequency of 3.2×10^{10} secs^{-1} is found; for helium 4 with a molar volume of 27.4 cm^3 a frequency of 1.4×10^{10} secs^{-1} is obtained. Critical volumes for stability are compared in Table I.

It is interesting to apply this criterion to an analysis of nuclear matter. Using potential parameters given by Weisskopf[1] and assuming a close-packed structure, a critical nuclear density of 7×10^{16} g/cm^3 is calculated. The average density of nuclear matter is approximately 2×10^{14} g/cm^3. Nuclear matter is apparently far beyond the limit of crystalline stability as would be expected from the success of its treatment as an independent particle system.

CONCLUSIONS

In this problem, no account can be taken of the difference in symmetry properties of the true wave functions for crystals of helium 3 and helium 4. It is expected that any method which makes a distinction only between the masses of the two would predict that helium 3 occupies a smaller volume than helium 4 at the limit of stability. Hence, it is not surprising to find experimental critical values in opposite relation to those obtained by this method.

Failure to consider correlations between the motion of the atom being observed and nearest neighbors is apparent in the results. Correlated motion of atoms forming the barrier should facilitate its penetration. In turn, the frequency will show the increase associated with instability at a smaller volume, thus bringing calculated data nearer to experimental. In any event, the method, when applied to systems which undergo the solid-liquid transition at absolute zero, predicts limiting volumes of the crystalline phase in general agreement with known data.

TABLE I. Critical molar volumes (cm^3) for stability of Helium.

System	Calculated[a]	Experimental[b]
Helium 3	25.89	22.96
Helium 4	27.01	21.18

[a] Based on values of ϵ and σ from J. DeBoer and A. Michels, Physica **5**, 945 (1938).

[b] Determined or extrapolated from data by H. L. Laquer, S. G. Sydoriak, and T. R. Roberts; F. J. Edeskuty and R. H. Sherman, *Low Temperature Physics and Chemistry* (University of Wisconsin Press, Madison Wisconsin, 1957), pp. 98 and 102.

ACKNOWLEDGMENT

The author is grateful to Dr. J. S. Plaskett for suggesting this problem and for his assistance in this and other endeavors.

[1] V. Weisskopf, *The Many Body Problem* (John Wiley & Sons, Inc., New York, 1959), p. 317.

Condensation Coefficients in the Growth of Cadmium and Zinc from the Vapor

R. A. RAPP,* J. P. HIRTH, AND G. M. POUND†

Metals Research Laboratory, Carnegie Institute of Technology, Pittsburgh, Pennsylvania

(Received June 6, 1960)

Condensation coefficients of essentially unity have been determined for the growth of zinc and cadmium from the vapor phase at high supersaturations in ultra-high vacua. These data indicate that no impingent atoms are reflected, and that all adsorbed atoms are incorporated into the growing crystal by Volmer's disk nucleation and growth mechanism. The adsorption of gaseous impurities at a residual gas pressure of 10^{-4} mm Hg did not affect the condensation coefficient for condensation at high fluxes.

INTRODUCTION

IN this research, the condensation coefficient α is used to describe the growth rates of solid cadmium and zinc from their monatomic vapor phases and is defined by the expression

$$J=\alpha(p-p_e)/(2\pi mkT)^{\frac{1}{2}}, \qquad (1)$$

where J is the net growth rate in atoms/cm²-sec, p the pressure of metal atoms incident on the substrate, p_e the equilibrium vapor pressure, m the mass of the metal atom, k Boltzmann's constant, and T the absolute temperature. At temperatures where the equilibrium vapor pressure of the growing substrate is negligible (as in the present case), the condensation coefficient equals simply the fraction of atoms incident on the substrate that are permanently incorporated into the lattice. There are two ways in which an incident atom may escape back to the vapor phase and thus lead to a value of α less than unity: (a) the atom may retain sufficient kinetic energy on recoil from collision with the surface to escape from the surface, or may remain in a thermally excited state while adsorbed on the surface and reevaporate after a few vibrations on the surface; or (b) even after equilibrating thermally with the surface an adsorbed atom may reevaporate before the atom can diffuse to a site where it will be incorporated into the lattice. These two possibilities will be examined in succession.

Condensation is supposed[1–3] to proceed by a process of adsorption of atoms from the vapor phase onto a low-index crystal plane. These adsorbed atoms then diffuse on the surface until they either reevaporate or reach sites of greater binding energy, such as monatomic ledges or kinks in such ledges, where they are permanently incorporated into the lattice. Thus in considering the possibility of reflection of an atom from the surface one must consider the atom interacting with the low-index surface as depicted in Fig. 1, where ΔG_0 is the free energy of desorption from a low-index surface.[4] Atoms of an atomic beam from an enclosed Knudsen oven[5] are commonly used in condensation experiments, and have an average energy $2kT_B$ per atom, where T_B=temperature of beam source. As such an atom approaches the surface of a metal, it enters the region of strong attractive forces, is accelerated, and finally enters a region of very strong repulsive forces where the atom can be considered to be colliding with the surface atoms. If through either phonon or electron

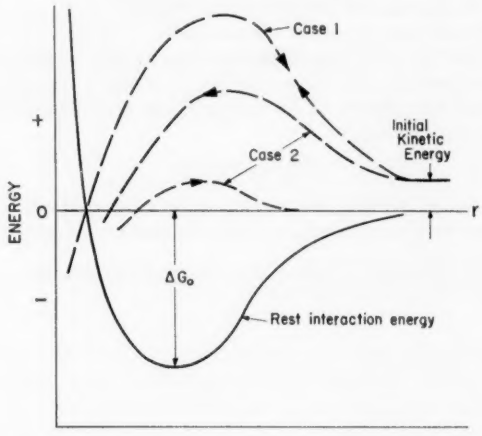

FIG. 1. Interaction energy for an atom as a function of the normal distance r of the atom from a low-index surface. Dashed curves show the kinetic energy of the atom: case 1 for complete reflection; case 2 for adsorption.

interaction the incident atom communicates an amount of energy $2kT_B$ to the surface, the atom will not retain sufficient kinetic energy on rebound to escape, and hence will be adsorbed on the surface.[6] It is noted that if the atom is reflected, the atom will have an energy greater

* Max-Planck-Institut für Physikalische Chemie, Gottingen, Germany.

† Present address: Department of Metallurgy, The University, Sheffield, England.

[1] M. Volmer, *Kinetik der Phasenbildung* (Steinkopff Publishers, Dresden and Leipzig, Germany, 1939).

[2] W. K. Burton, N. Cabrera, and F. C. Frank, Phil. Trans. Roy. Soc. London **A243**, 299 (1951).

[3] J. P. Hirth and G. M. Pound, J. Phys. Chem. **64**, 619 (1960).

[4] The ideas presented here on reflection of an atom from a surface are in essence the same as those developed by J. H. McFee (Ph.D. thesis, Carnegie Institute of Technology, 1960) in considering the thermal accommodation coefficient.

[5] M. Knudsen, Ann. Physik **29**, 179 (1909).

[6] Even without energy exchange, a momentum change leading to motion parallel rather than perpendicular to the surface could reduce the normal component of the kinetic energy to a value less than ΔG_0 leading to adsorption of the atom and a transient excited surface diffusion of the atom.

than that corresponding to the surface temperature so that the thermal accommodation coefficient[7] α_T will be less than unity as will be the condensation coefficient α. Therefore the problems of thermal accommodation and reflection are very closely related.[8]

Massey and Burhop[9], Devienne,[10] and Schäfer[11] review theoretical treatments of the thermal accommodation probability for cases of strong repulsive forces only, or combined with weak attractive forces. However, for metals, ΔG_0 is estimated from the nearest-neighbor bond approximation[1,3] to be approximately one-half the heat of vaporization, or 8 to 88 kcal/mole. These large values of ΔG_0 would indicate that strong attractive forces are active in the adsorption process, so that the above theoretical treatments are not applicable, although they are useful in predicting the onset of rapid energy exchange when the surface temperature T_s exceeds the characteristic vibrational temperature θ for surface atoms. Cabrera,[12] McFee,[13] and Zwanzig[14] have considered a one-dimensional analog of adsorption in the presence of strong attractive forces. Under such strong forces, they consider the collision to consist of multiple phonon excitation. The quantum-mechanical treatment for such a process is quite complex, so they use a classical approximation. The model is a semi-infinite chain of spring-connected particles which interact classically. The result of Cabrera's calculation indicates that the incoming kinetic energy must be $>28\Delta G_0$ for reflection to occur. Even though the model has not been extended to the three-dimensional case, the results suggest that for moderately high T_s (where $T_s>\theta$), complete accommodation will occur for metals on metals where ΔG_0 is large.

Finally, when capture has occurred during the first vibration, escape of an unequilibrated adatom cannot take place if the residence time on the surface τ is much larger than the relaxation time for thermal equilibration τ_r. Langmuir[15] and Lennard-Jones[16,17] estimate $\tau_r=10^{-12}$ to 10^{-15} sec, or about the period of one vibration, while as we shall show $\tau\gg10^{-12}$ sec. Therefore, once adsorbed, an adatom will probably equilibrate thermally with the surface.

Hence, even though a complete treatment of energy exchange between an impingent atom and a surface has yet to be accomplished, available theories predict that α_T, and hence α (reflection), should be unity for metal atoms incident on a clean surface of the same metal as long as $T_s>\theta$. In this work, for Zn, $T_s=340°$K, $\theta=250°$K, $2RT_s\simeq2$ kcal/mole, $\Delta G_0\simeq12$ kcal/mole; and for Cd, $T_s\geq290°$K, $\theta=172°$K, $2RT_s\simeq2$ kcal/mole, $\Delta G_0\simeq14$ kcal/mole, so that we expect no diminution of α because of elastic reflection.

Once an incident atom is adsorbed on a low-index plane and is in thermal equilibrium with the crystal, the atom will have a mean lifetime[18] τ on the plane prior to reevaporation. According to absolute rate theory,[19]

$$\tau=(h/kT)[1-\exp-(h\nu/kT)]^{-1}\exp(\Delta G_0/kT), \quad (2)$$

where ν is the vibration frequency of an adatom. Thus an adatom will have a rms diffusion path on a close-packed plane $\bar{X}=(2D_s\tau)^{\frac{1}{2}}$, where D_s=surface diffusion coefficient. If $\bar{X}>\lambda$, the spacing between monatomic ledges or other sinks for diffusing adatoms, then all adatoms will reach sinks and α will equal unity. If $\bar{X}<\lambda$, some adatoms will reevaporate and α will be less than unity. The modified[20] two-dimensional nucleation treatment of Volmer[1] predicts that nucleation of monatomically thick disks on close-packed surfaces should be extremely rapid for supersaturations

$$(P/P_e)>(P/P_e)_{\text{crit}}=\exp[\pi a^4\gamma^2/B(kT_s)^2], \quad (3)$$

where a=height of monolayer, $\beta\simeq46$ is the exponent of the frequency factor in the nucleation rate equation, and γ=specific interfacial free energy. When the rate of nucleation is very rapid,[21] $\bar{X}>\lambda$ and $\alpha=1$. Taking: for Zn, $a=2.47$ A,[22] $\gamma=750$ ergs/cm^2,[23] $T_s=340°$K, $(P/P_e)_{\text{crit}}\simeq6\times10^2$, while $(P/P_e)=8\times10^6$; for Cd, $a=2.80$ A,[22] $\gamma=650$ ergs/cm^2,[23] $T_s=290°$K, $(P/P_e)_{\text{crit}}\simeq7\times10^2$, while $(P/P_e)=2\times10^7$ (see Table I). Therefore, under the conditions of this experiment we expect $\alpha=1$ for a clean surface of either Cd or Zn.

It was suggested by Langmuir[15] in 1916 that the adsorption of impurities, usually molecules of the residual gas, on a growing substrate may alter the condensation process by shielding the potential well at the surface of the metal and thereby decreasing the energy of desorption.[24] Adsorbed impurities may affect the condensation process in at least four ways, all giving rise to a

[7] M. Knudsen, Ann. Physik **34,** 593 (1911).

[8] α will be less than unity both for specular reflection and for diffuse reflection caused either by scatter from surface asperities or by momentum accommodation.

[9] H. S. W. Massey and E. H. S. Burhop, *Electronic and Ionic Impact Phenomena* (Oxford University Press, New York, 1952), Chap. IX.

[10] F. M. Devienne Compt. rend. **56,** 1 (1953).

[11] K. Schäfer, Fortschr. Chem. Forsch. **1,** 61 (1949).

[12] N. Cabrera, Discussions Faraday Soc. **28,** 16 (1959).

[13] J. H. McFee, Ph.D. thesis, Carnegie Institute of Technology 1960 (to be published in Phys. Rev.).

[14] R. W. Zwanzig, J. Chem. Phys. **32,** 1173 (1960).

[15] I. Langmuir, Phys. Rev. **8,** 149 (1916).

[16] J. E. Lennard-Jones and C. Strachan, Proc. Roy. Soc. (London) **A150,** 442 (1935).

[17] J. E. Lennard-Jones, Proc. Roy. Soc. (London) **A163,** 127 (1937).

[18] The pre-exponent is about equal to the period of one vibration ν_0, so that if $\tau_0\Delta G_0>kT$, $\tau\gg\tau_0$.

[19] C. A. Wert and C. Zener, Phys. Rev. **76,** 1169 (1949).

[20] J. P. Hirth, Acta Met. **7,** 755 (1959).

[21] Burton *et al.*[2] and Hirth and Pound[3] discuss deviations at low supersaturations, $<P/P_e)_{\text{crit}}$, from the behavior postulated by Volmer; however, in this work $(P/P_s)>(P/P_e)_{\text{crit}}$, so these perturbations due to dislocations will not be considered here.

[22] C. S. Barrett, *Structure of Metals* (McGraw-Hill Book Company, Inc., New York, 1943).

[23] T. R. Hogness, J. Am. Chem. Soc. **43,** 1621 (1921).

[24] It is conceivable that, under some conditions, impurity adsorption would increase ΔG_0; however, for the case of metal substrates there is considerable evidence that adsorption lowers ΔG_0. See footnote 30, I. G. Ptushinskii, Zhur. Tekh. Fiz. **28,** 1402 (1958), and S. Wexler, Revs. Modern Phys. **30,** 402 (1958).

TABLE I. Condensation coefficients for zinc and cadmium.

Metal	Time of experiment (min)	Substrate temp. °C	Residual gas pressure[a] (mm Hg)	Zn or Cd flux (atoms/cm²-sec)	Super-saturation[b]	J_M/J_x[c]	Mass of deposit on hot plate[d] ($g\times10^4$)	Mass of deposit on cold plate[d] ($g\times10^4$)	Condensation coefficient α
Zn	30	68	6×10^{-9}	8.3×10^{15}	8×10^6	8.3×10^{15}	137	1.9	0.96 ± 0.01
Cd	30	18	10^{-9}	1.6×10^{16}	2×10^7	1.6×10^{16}	117	1.7	0.97 ± 0.01
Cd	60	19	5×10^{-7}	1.9×10^{16}	2×10^7	1.9×10^{16}	146	0.2	1.00 ± 0.01
Cd	60	23	10^{-4}	1.6×10^{16}	2×10^7	1.6×10^{16}	128	0.1	1.00 ± 0.01

[a] The pressure values listed are those read at the Bayard-Alpert gauge. The pressures in the condensation chamber were thus lower by a factor of about $(T_1/T_2)^{\frac{1}{2}}\simeq(78/323)^{\frac{1}{2}}\simeq0.5$.

[b] The supersaturation is the ratio of the actual Zn or Cd flux to the equilibrium Zn or Cd flux that would obtain at the substrate temperature.

[c] J_M/J_x is the ratio of the flux of Zn or Cd atoms striking the hot plate to the flux of molecules of the residual gas striking that plate.

[d] The chemical analyses of the Zn and Cd on the hot and cold plates were uncertain to about 10% of the weight of condensate on these plates.

condensation coefficient less than the value of unity expected for a clean surface and high supersaturations. First, the contamination may make the initial adsorption of the atom from the vapor more difficult, i.e., increase the difficulty of thermal exchange of the kinetic energy $2kT_B$ with the surface. Secondly, from Eq. (2), a decreased desorption energy reduces the time of stay and therefore the average diffusion distance of the adsorbed atom, so that even after the adsorption step, the atom has a higher reevaporation probability. Thirdly, preferential adsorption of impurities at the ledge may make the attachment of adsorbed atoms at these poisoned ledges more difficult. Finally, the adsorption will affect the surface energy of the critical nucleus and hence change the critical supersaturation for two dimensional nucleation on a contaminated surface. For these reasons, even in condensation at high fluxes and supersaturation, the adsorption of impurities might result in a condensation coefficient less than the expected value of unity. The early experiments of Cockroft[25] showed that the incident flux necessary for the nucleation of a metal on a foreign substrate was much higher for a substrate contaminated by an adsorbed gas than for a "clean" substrate. Estermann[26,27] showed that contamination of a substrate by adsorbed gases decreases the heat of desorption of metal atoms from this substrate. In 1950 Frauenfelder[28] found that contamination of a substrate could decrease the condensation coefficient for such a substrate. He reported condensation coefficients, for Cd at presumably low fluxes and in vacua of 5×10^{-6} mm Hg on mechanically cleaned metal surfaces, of 0.001 to 0.01. On freshly evaporated Ag, Cu, or Au substrates, Cd assumed a condensation coefficient of 0.3 to 0.6. Similarly Devienne[29] in 1953 reported that the condensation coefficient for Cd at 25°C equaled 0.04 to 0.6, dependent on film thickness, for films from 1 to 40 monolayers thick deposited at flux of $\sim10^{10}$ atoms/cm² sec in a vacuum of 10^{-5} mm Hg. Yang *et al.*[30] found a similar dependence of condensation coefficient on film thickness in a study of silver deposition. This was attributed to the initial difficulty of nucleating the condensing metal on a foreign substrate; however, when experimental conditions were fixed to eliminate the effect of a foreign substrate, the condensation coefficient for Ag on Ag[30,31] was shown to equal unity over wide ranges of flux, substrate temperature, and vacua.

The experiments of this research were carried out to determine the condensation coefficient for Cd and Zn, respectively, in deposition on "clean" Cd and Zn substrates (i.e., substrates grown at high fluxes in ultra-high vacua) and the effect of adsorption of gaseous impurities on the condensation coefficient. Zn and Cd were chosen for these experiments because they form thermodynamically stable oxides and therefore are susceptible to contamination from residual gases.

EXPERIMENT

The condensation chamber is shown in Fig. 2 and is very similar to that used previously by the present authors in the determination of the condensation coefficient in the growth of Ag from the vapor.[31] The vacuum system consisted of, in sequence, the condensation chamber, a Bayard-Alpert gauge, a tantalum-filament gettering bulb, a liquid nitrogen trap containing copper-foil rolls, a Philips cold-cathode gauge, a second liquid nitrogen trap, a metal 300 liter/sec octoil diffusion pump, and a Cenco fore pump. There were no greased joints on the high-vacuum side of the octiol pump. The Pyrex tubing in the system was 25 mm in diam. The Philips gauge was used only for pressure measurements during the bake-out procedure. In the experiments, the entire apparatus on the high-vacuum side of the liquid nitrogen trap nearest the oil diffusion pump was baked out at 450°C for three 10-hr periods.

[25] J. D. Cockcroft, Proc. Roy. Soc. (London) **A119,** 293 (1928).
[26] I. Estermann, Z. Physik **33,** 320 (1925).
[27] I. Estermann, Z. Elektrochem. **31,** 441 (1925).
[28] H. Frauenfelder, Helv. Phys. Acta **23,** 347 (1950).
[29] F. M. Devienne, J. phys. radium **14,** 257 (1953).
[30] L. Yang, M. Simnad, and G. M. Pound, Acta Met. **2,** 470 (1954).
[31] R. A. Rapp, J. P. Hirth, and G. M. Pound, Can. J. Phys. **38,** 709 (1960).

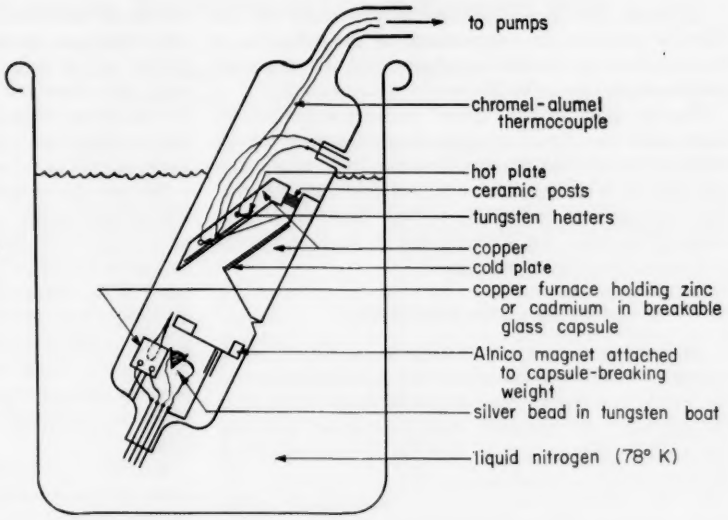

FIG. 2. Cadmium and zinc condensation chamber.

Between the bakeout periods, the ionization gauge was outgassed, and the heaters in the condensation chamber were heated to their maximum operating temperatures for outgassing. During the high-vacuum experimental runs, the cold traps and the condensation chamber were immersed in liquid nitrogen; the gettering bulb was operated intermittently; and except for two 30-sec filament outgassing treatments the Bayard-Alpert gauge was operated continuously, serving both as a vacuum pump and a pressure gauge. In the poor-vacuum runs the procedure was the same, with the exception that the vacuum was lowered by operating the oil diffusion pump at a lower temperature.

In the condensation chamber shown in Fig. 2, the substrate was initially a 25-mm sq glass cover slide which was held snugly in a heated copper block whose temperature was measured with a Chromel-Alumel thermocouple. Facing this "hot plate," but not the incident beam, was another identical, but cold, glass plate which was held in a fixed orientation to the hot plate. This "cold plate" was maintained at 78°K in order to collect all Zn or Cd atoms which might reflect or reevaporate from the growing hot plate deposit to the cold plate. For a fixed geometry, a constant fraction, here 0.33, of the atoms leaving the hot plate will strike the cold plate. Knudsen[32] has shown that Cd and Zn vapors condense completely on a glass substrate at 78°K. All of the walls of the condensation chamber were held at 78°K by immersion of the system in liquid nitrogen to insure that the cold plate did not receive atoms from sources other than the hot plate. For the atomic beam source, either Cd (99.9% purity) or Zn (99.98% purity) was sealed off under 10^{-6} mm Hg vacuum into an evacuated glass capsule which could be separately heated in the vacuum system.[33] Prior to an experiment, after all of the heated elements and the cold walls of the system had reached a constant temperature and the vacuum in the system was constant, 5 to 10 monolayers of silver were evaporated onto the hot plate from an auxiliary source in the vacuum system. The freshly deposited silver on the hot plate provided an initial "clean" surface for the Cd or Zn deposition. The glass capsule containing the Cd or Zn was then broken by a magnetically operated hammer and a Zn or Cd flux, ranging from 10^{15} to 4×10^{16} atoms/cm^2-sec (0.8 to 30 monolayers/sec) was deposited on the hot plate for either 1 hr or 30 min. These high fluxes were used to further ensure that the condensation coefficient was not affected by the nature of the initial substrate and that the condensation coefficients which were measured therefore describe Zn condensation on Zn or Cd on Cd. After the experiment, the glass hot and cold plates were examined metallographically, their areas measured, and the amount of Zn or Cd deposited on the plates was measured by quantitative chemical analysis.[34] From the area of the plate, time of the experiment, and amount of the deposit, the value of the flux incident on the hot plate could be calculated. The condensation coefficient was calculated from the equation

$$\alpha=\frac{Wt_{\text{Cd, hot plate}}}{Wt_{\text{Cd, hot plate}}+Wt_{\text{Cd, cold plate}}/0.33},$$

where 0.33 is a geometric factor, i.e., the calculated fraction of the atoms which strike the cold plate after reevaporating from the hot plate.

[32] M. Knudsen, Ann. Physik **50**, 472 (1916).

[33] It was necessary to seal off the Cd or Zn so that the three 10-hr periods of bakeout of the system at 450°C, requisite for the attainment of ultra-high vacua of 10^{-9} mm Hg, could be accomplished.

[34] E. B. Sandell, *Colorimetric Determination of Traces of Metals* (Interscience Publishers, Inc., New York, 1944), Vol. 3.

Although the Chromel-Alumel thermocouple did not directly measure the temperature of the substrate, a heat transfer calculation has shown that the measured temperatures cannot be in error by more than 5°C.

Finally, even in the "poor" vacuum experiments, there were two liquid nitrogen traps between the oil diffusion pump and the condensation cell, which was also immersed in liquid nitrogen, so that the impurity gas impingent on the substrate may have differed in composition from the impurity gas in the experiments of Frauenfelder[28] and Devienne.[29]

RESULTS AND DISCUSSION

The experimental results are given in Table I. The estimated error includes only errors in measurement of the weights on the hot and cold substrates. Because of the necessity for bakeout, each experiment required one week in preparation, so that the reproducibility of the data was not determined.

For the Zn and Cd experiments conducted in ultra-high vacua, the experimental values of the condensation coefficients were 0.96 and 0.97, respectively, in fair agreement with the theoretical value of unity predicted for clean metal surfaces by the theories reviewed previously. The small deviation from unity could have arisen because of: (a) reevaporation of some of the incident flux during the initial nucleation of Cd or Zn on the Ag substrate; (b) scattering of the beam atoms at the source immediately after breaking the capsule where the Cd or Zn pressure prior to breaking was about 1 mm Hg; or (c) reevaporation from the growing substrate. The authors favor explanations (a) or (b) and hope to test these explanations at a later date.

Condensation coefficients of unity were determined for Cd condensation at residual pressures of 5×10^{-7} mm Hg. This shows that the *dynamic*[35] adsorption of the residual gas molecules on a Cd surface during growth from the vapor at high fluxes does not alter the nature of the substrate or the value of the adsorption energy enough to cause a reflection or a rapid reevaporation of atoms. The low condensation coefficients reported by Frauenfelder[28] and Devienne[29] may be a result of: (a) initial difficulty in nucleation on a foreign substrate, (cf. Yang *et al.*[30]); (b) *static*, or steady-state contamination of the substrate by impurity; (c) dynamic contamination of the substrate by some impurity other than that impingent on the substrate in the present investigation; or (d) reflection of Cd to the Geiger counter or cold plate from parts of the apparatus other than the hot substrate. Considering the low beam fluxes used by Frauenfelder and Devienne, it is likely that cause (a), perhaps influenced by (b) and (c), was predominant.

Microscopic examination of the deposits showed preferred orientation and hexagonal symmetry of the crystallites regardless of the degree of evacuation, between 10^{-9} and 10^{-4} mm Hg, during the growth process.[36] X-ray diffraction revealed a preferred orientation of (0002) parallel to the plane of the substrate. In addition, only lines corresponding to the metal lattice were found. These metallographic results tend to confirm the two-dimensional nucleation model of Volmer[1] which is supported by the quantitative experimental findings.

Further experiments are planned for the measurement of condensation coefficients for the growth of Zn and Cd from the vapor at lower supersaturations and higher substrate temperatures. During growth from the vapor at higher temperatures where the substrate is undergoing gross evaporation (net growth), the possible influence of the adsorption of gaseous impurities on the condensation process can more sensitively be investigated. Also, experiments are planned for the condensation of Cd and Zn from an intermittent beam, in which the influence of *steady-state* adsorption can be studied.

CONCLUSIONS

1. The condensation coefficient for growth of Zn or Cd from the vapor at high supersaturations and in ultra-high vacua is nearly unity in agreement with theoretical expectation.

2. Dynamic adsorption of residual-gas impurity did not affect the condensation coefficient, which was also unity for condensation in vacua as poor as 10^{-4} mm Hg.

ACKNOWLEDGMENTS

This work was carried out in the Metals Research Laboratory at Carnegie Institute of Technology, and was supported by a Thompson-Ramo Wooldridge Fellowship and the Office of Naval Research.

[35] By "dynamic" adsorption we mean adsorption taking place under conditions where the metastable concentration of adsorbate, corresponding to the residual gas pressure in the system, is not attained.

[36] Levinstein [H. Levinstein, J. Appl. Phys. **20**, 307 (1949)] has also found Zn and Cd films deposited in 10^{-5} mm Hg vacua to be oriented with respect to the substrate. However, he reports that Zn and Cd films deposited at room temperature in 10^{-2} mm Hg vacua had a uniform mirrorlike surface, presumably randomly oriented.

Photoionization of Alkanes. Dissociation of Excited Molecular Ions*

BRUCE STEINER, CLAYTON F. GIESE, AND MARK G. INGHRAM
Department of Physics, The University of Chicago, Chicago, Illinois

(Received June 13, 1960)

This report describes studies of photoionization and subsequent dissociation of all saturated paraffins from C_2 to C_6, plus *n*-heptane and *n*-octane, as a function of photon energy. The studies include data on all processes which occur below a photon energy of 11.9 ev. The instrument used was a mass spectrometer, combined with a Seya-Namioka monochromator. The direct experimental data are presented as parent, fragment, and metastable ionization efficiency curves. For each molecule the family of curves obtained by dividing the derivatives of each normalized ionization efficiency curve by the derivative of the total ionization are presented. These derived curves facilitate the test of theories of dissociation kinetics.

From a study of the total ionization curves, it is concluded that the adiabatic ionization transition is not accessible within the Franck-Condon region and that it is therefore not possible to determine the ionization potentials of these molecules by ordinary impact experiments.

The influence of stored thermal energy was studied by determining the ionization efficiency curves (except for metastables) at two temperatures, 300° and 415°K, and comparing the shifts in the curves with the differences in average stored energy. An analysis of transit times in the mass spectrometer was made which (in addition to providing information necessary to the understanding of the curve shapes and metastable intensities) suggests the existence of "missing metastables," i.e., ions which dissociate in the regions of acceleration (fast metastables) or deflection (slow metastables) and hence are spread out in the mass spectrum so that they do not contribute appreciably to a mass peak. The experimental results confirm the existence of these missing metastables, although the intensity attributed to them is statistically rather uncertain. Changing the ion drawing-out potential in the ionization chamber permitted variation of the extraction time by a factor of 3.3 and the effect of this variation upon several fragment ionization efficiency curves was determined.

The experimental results have been compared with the predictions of the statistical theory of dissociation kinetics, a theory which has been widely used in the interpretation of mass spectra. This theory in simplified form involves three parameters, the threshold energy for dissociation E_0, a frequency ν, and the number of oscillators n. The results of the comparison may be summarized as follows.

(1) The effects of temperature cannot be reconciled with the theory unless n is made a free parameter which takes on a variety of values less than or equal to the total number of oscillators.

(2) The statistical theory requires, as an energy randomization mechanism, the presence of many closely spaced electronic states. The experimental evidence is that these states do not exist.

(3) The statistical theory predicts the energy excess needed to give a rate constant such that dissociation will occur within the ionization chamber. Comparison with experimental results shows that this excess energy, calculated with reasonable values for E_0 and ν and with n equal to the total number of oscillators, is much too large. Reducing n removes the difficulty.

(4) The shapes of the fragment and metastable curves, and the metastable intensity, may be calculated from the theory. The tails of the predicted curves are much too large, as is the predicted metastable intensity. Agreement may be obtained by using physically implausible values for E_0 and/or ν, or by using reasonable values for E_0 and ν, and reduced values of n. The reduced values of n do not agree with those obtained in (1).

(5) The shifts in fragment curves resulting from changing the extraction time require either unreasonable values for E_0 and/or ν, or a reduced n. The reduced n which is required does not agree with that determined from (1) or (4).

(6) The intensity of the missing metastables, though statistically rather uncertain, apparently cannot be reconciled with the statistical theory regardless of what values are taken for E_0, ν, and n.

(7) In many cases, the dissociation processes leading to different fragments compete (i.e., maintain approximately a constant intensity ratio) over a range of photon energy. Again, one cannot obtain this behavior from the statistical theory with any choice of E_0, ν, and n which are consistent with the other data. Individually, these comparisons perhaps are not conclusive, but it is believed that collectively they constitute a definite failure of the statistical theory in its simple form.

The lack of a quantitative understanding of the excess energies demanded in the kinetics of dissociation prevents the use of the data for determination of reliable bond dissociation energies. Nevertheless, tentative values have been determined, and these are tabulated and discussed.

INTRODUCTION

THE ionization and dissociation of diatomic molecules is rather well understood. The roles of the Franck-Condon principle and the energetics of the process have been treated by a number of authors.[1] By contrast, the case of polyatomic molecules is not well understood. Two complications which make the polyatomic case more difficult are: (1) The excitation energy of molecular ions is shared among a number of different degrees of freedom. Thus, fragmentation does not occur immediately when the dissociation threshold is reached as it does with diatomic molecules but, rather, is delayed until the molecular vibrations cooperate to produce a particular dissociation. (2) The fragments can carry away energy in the form of vibrational excitations, so that the excess energy need not appear as kinetic energy or as electronic excitation of the fragments.

Some detailed studies of the dissociation of polyatomic ions have been done, using electron impact ionization,[2–5] and there has been one study of two

* Supported jointly by the National Science Foundation and the Geophysics Research Directorate, Air Force Cambridge Research Center.

[1] See, for example, the article by H. D. Hagstrum, Revs. Modern Phys. **23,** 185 (1951).

[2] M. B. Wallenstein, A. L. Wahrhaftig, H. M. Rosenstock, and H. Eyring, *Oberlin Symposium on Radiobiology, June,* 1950 (John Wiley & Sons, Inc., New York, 1952); H. M. Rosenstock, M. B. Wallenstein, A. L. Wahrhaftig, and H. Eyring, Proc. Natl. Acad. Sci., U.S. **38,** 667 (1952); H. M. Rosenstock, A. L. Wahrhaftig, and H. Eyring, J. Chem. Phys. **23,** 2200 (1955).

[3] L. Friedman, F. A. Long, and M. Wolfsberg, J. Chem. Phys. **27,** 714 (1957); **30,** 1605 (1959); **31,** 755 (1959).

[4] A. Kropf, E. M. Eyring, A. L. Wahrhaftig, and H. Eyring, J. Chem. Phys. **32,** 149 (1960).

[5] W. A. Chupka and J. Berkowitz, J. Chem. Phys. **32,** 1546 (1960).

molecules using photoionization.[6] The use of photoionization has an advantage in this type of study because the results are more precise and are more easily interpreted.[7–9] The present paper describes a systematic study of the photoionization and dissociation of all alkanes from ethane through hexane, as well as *n*-heptane and *n*-octane, in the energy range up to 11.9 ev.

EXPERIMENTAL PROCEDURE

The apparatus used was essentially that previously described.[8] A Seya-Namioka monochromator[10] disperses the radiation from a hydrogen-discharge light source. This radiation traverses the ionization chamber of a 60° sector-field mass spectrometer with a 12-in. magnetic radius. An electron multiplier detects the resolved ion beam. After traversing the ionization chamber, the photon beam strikes a metal surface producing secondary electrons. An electrometer-amplifier, which measures this current, serves as a photon intensity monitor. The bandwidth of the ionizing radiation (full width at half-maximum) was about 6.7 A, or, in the energy range covered, about 0.05 ev. The effect of stored internal energy was studied by determining the ionization efficiency curves first at room temperature and then at an elevated temperature. The high-temperature data were obtained by heating the entire source housing of the mass spectrometer. In addition, the sample gas was introduced through a spiral of 3 mm glass tubing, of total length 1 m, located within this ion source housing. This length of tubing was used to ensure that the molecules made many collisions with the heated walls and hence that they were at temperature equilibrium. A chromel-alumel thermocouple attached to the ionization chamber with leads coming directly to a potentiometer and reference junction, through insulated Kovar tubing, enabled direct determination of the temperature to an accuracy of about 1°C. Since the temperature of the ionization chamber is important it was necessary to locate the mass peaks without heating the ion source. This ruled out periodic use of an electron emission filament to produce the usual electron impact spectrum. The necessary mass identification was attained by using a proton resonance gaussmeter and a potentiometer to measure the magnetic field and the accelerating potential.

The high-energy limit of the photons in the present study was fixed by the limit of transmission of the lithium fluoride window used to isolate the discharge from the rest of the instrument.

The sensitivity of the electron multiplier to parent and fragment ions was determined and found to be essentially independent of mass for the parent and fragment ions studied here. This is a surprising result since, using monatomic ions, one expects the gain of a directly integrated multiplier to vary, roughly, inversely as the square root of the mass.[11] For the polyatomic ions used here, it would appear that fragmentation effects[12] counteract this variation and result in a multiplier gain which is approximately independent of mass. Metastable ions are different in that they are accelerated as parent ions and deflected as fragment ions. Thus the energy contained in the neutral fragment is lost and the ion strikes the multiplier with reduced energy as compared with parent ions. For the metastable ions the gain was taken to be the normal gain multiplied by the square root of the ratio of fragment to parent masses.

The calibration of the photon monitor has been discussed in a previous paper,[8] where the calibration curve was obtained from a study of the NO molecule. For the present studies it was necessary to extend this calibration to higher energies. This was done by extrapolation of the calibration curve previously obtained. Using this calibration, the parent ionization efficiency curves were all found to be roughly flat above the first dissociation limit. It could not be determined whether the departures from this characteristic were real or were due to variations in the photoelectric sensitivity curve resulting from changes in the photoemitter surface conditions as different gases were introduced into the mass spectrometer. Therefore, since we could not justify modified curves, the same calibration curve was used for all the data reported. The calibration curve used is subject to some uncertainties. It is, however, smooth and monotonic and has the same general form obtained by others for metal surfaces.[13] We therefore feel that it is doubtful that the calibration curve used differs in any significant way from the true curve.

RESULTS

The direct experimental results of this investigation are in the form of parent, fragment, and metastable ionization efficiency curves given in Figs. 1–89. Parent ionization efficiency curves for propene, butene, pentene, and hexene are given in Figs. 90–93. These curves are included because they are useful in the interpretation of certain of the alkane data. In the case of the parent and fragment ions two ionization efficiency curves are shown, one at room temperature and one at an elevated temperature. For metastable

[6] W. A. Chupka, J. Chem. Phys. **30**, 191 (1959).
[7] J. D. Morrison, Revs. Pure and Appl. Chem. **5**, 22 (1955); J. Appl. Phys. **28**, 1409 (1957).
[8] H. Hurzeler, M. G. Inghram, and J. D. Morrison, J. Chem. Phys. **27**, 313 (1957).
[9] J. D. Morrison, H. Hurzeler, M. G. Inghram, and H. E. Stanton, J. Chem. Phys. **33**, 821 (1960).
[10] M. Seya, Sci. of Light (Tokyo) **2**, 8 (1952); T. Namioka, *ibid.* **3**, 15 (1954).
[11] M. G. Inghram and R. J. Hayden, "Handbook of Mass Spectrometry," National Academy of Sciences, National Research Council Publication No. 311 (1954).
[12] H. E. Stanton and M. G. Inghram, Rev. Sci. Instr. **27**, 109 (1956).
[13] G. L. Weissler, *Handbuch der Physik* (Springer-Verlag, Berlin, 1956), Vol. XXI, p. 354.

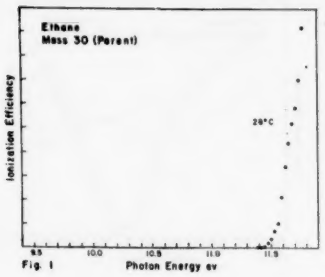

Fig. 1

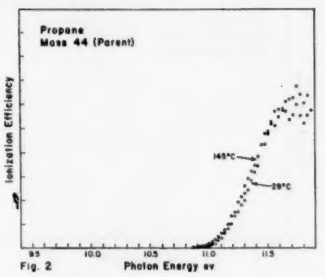

Fig. 2

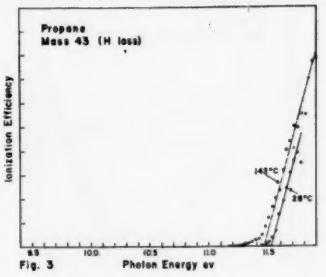

Fig. 3

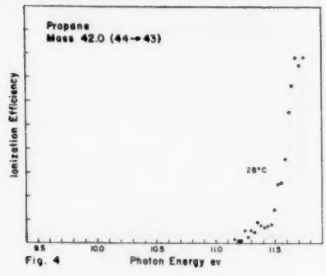

Fig. 4

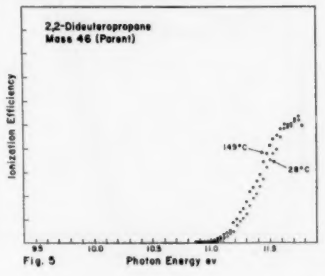

Fig. 5

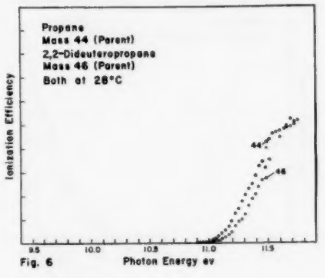

Fig. 6

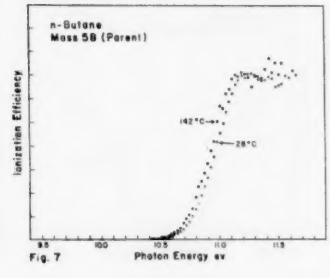

Fig. 7

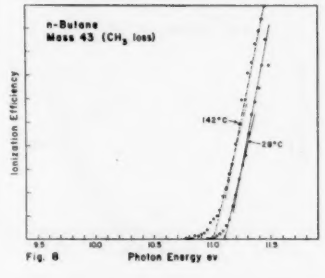

Fig. 8

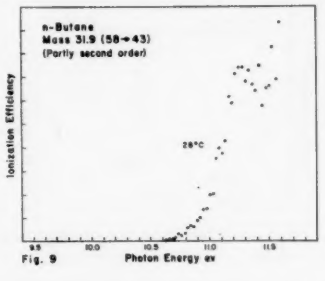

Fig. 9

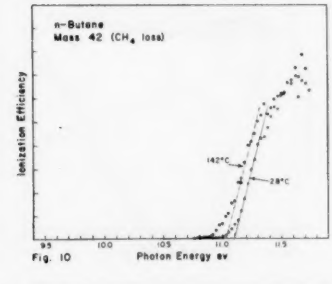

Fig. 10

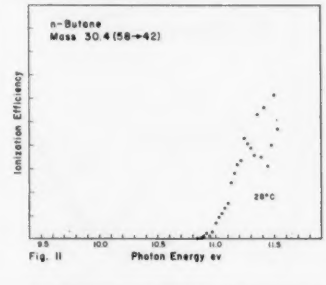

Fig. 11

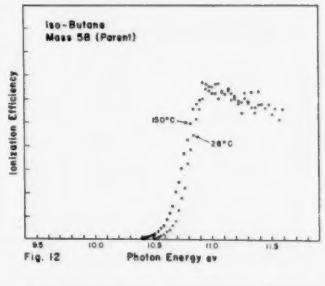

Fig. 12

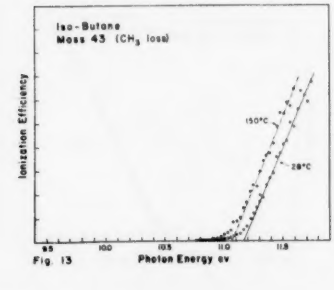

Fig. 13

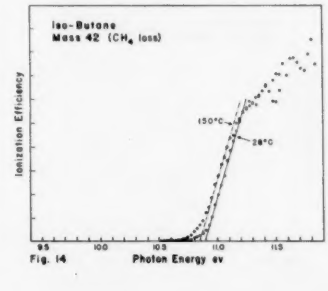

Fig. 14

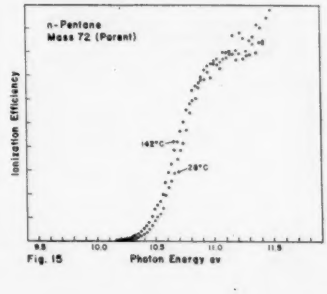

Fig. 15

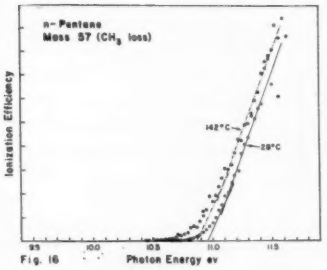

Fig. 16

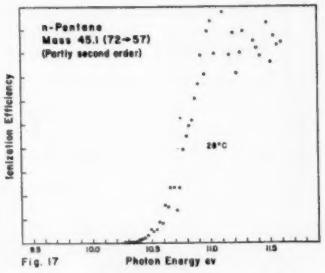

Fig. 17

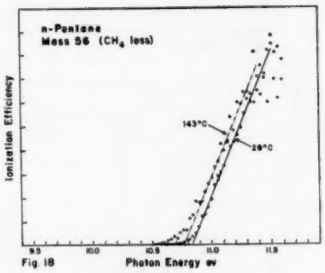

Fig. 18

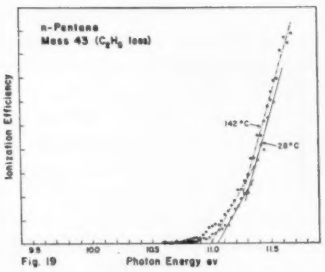

Fig. 19

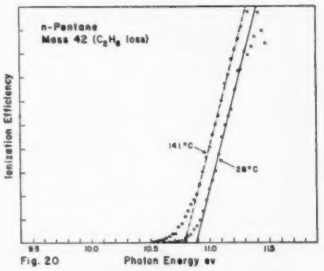

Fig. 20

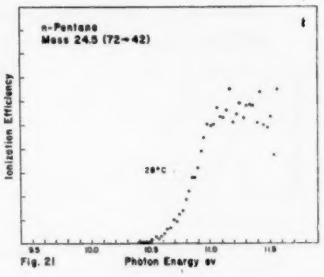

Fig. 21

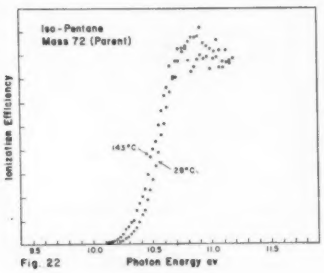

Fig. 22

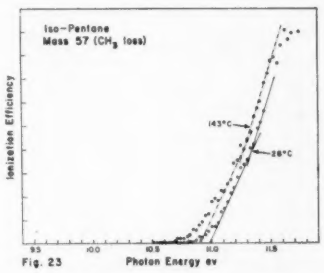

Fig. 23

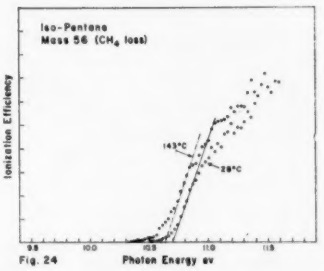

Fig. 24

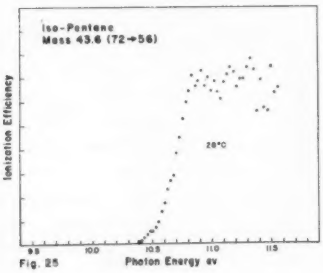

Fig. 25

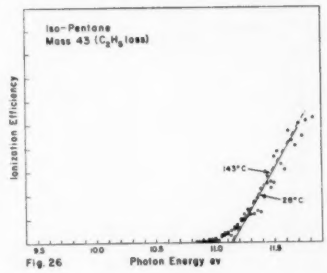

Fig. 26

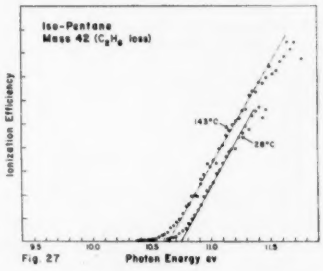

Fig. 27

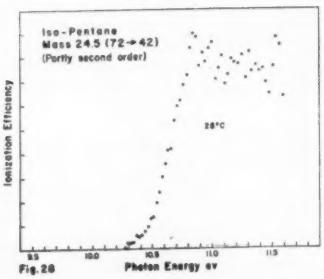

Fig. 28

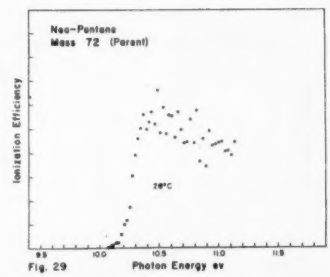

Fig. 29

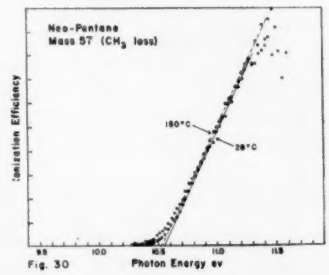

Fig. 30

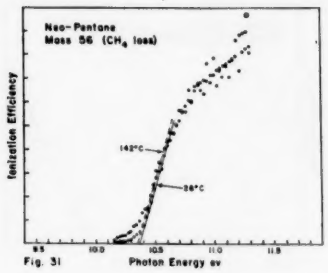

Fig. 31

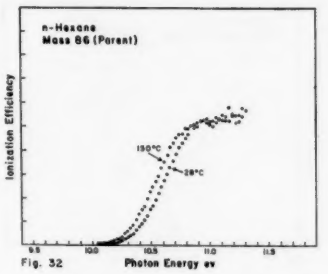

Fig. 32

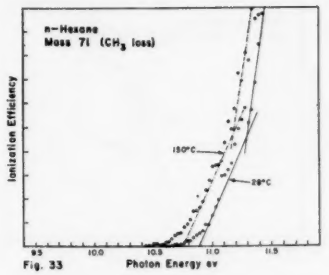

Fig. 33

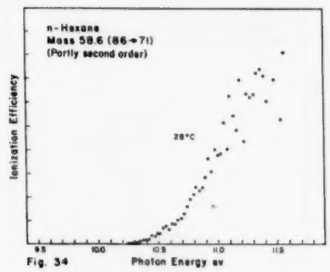

Fig. 34

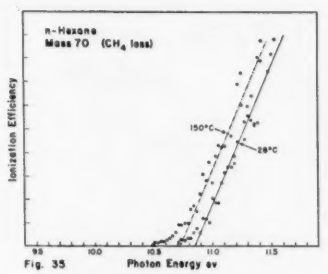

Fig. 35

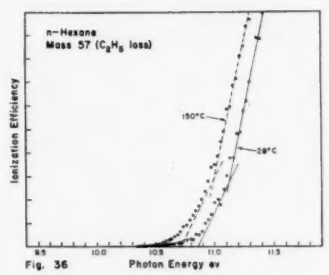

Fig. 36

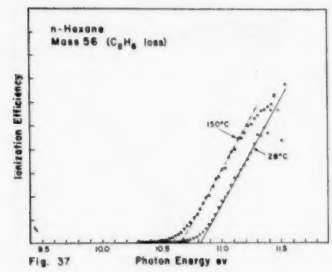

Fig. 37

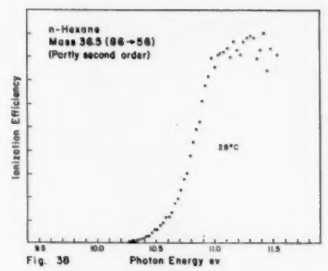

Fig. 38

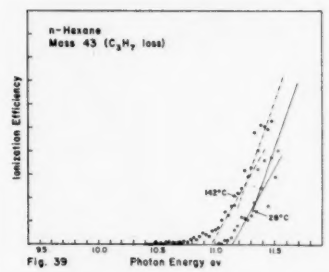

Fig. 39

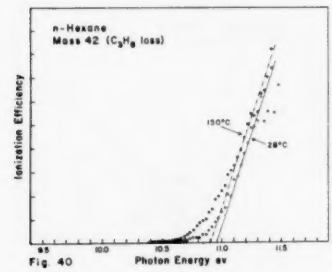

Fig. 40

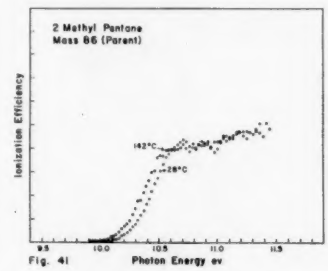

Fig. 41

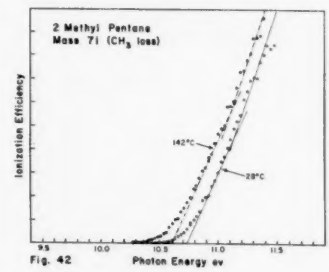

Fig. 42

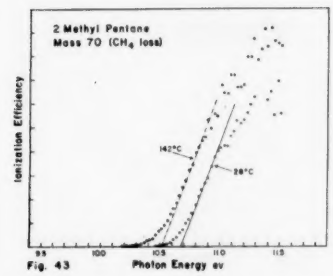

Fig. 43

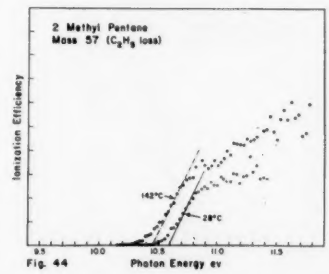

Fig. 44

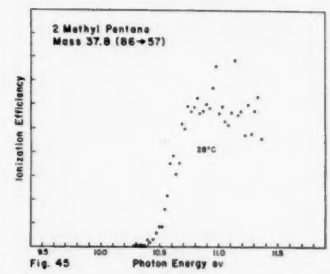

Fig. 45

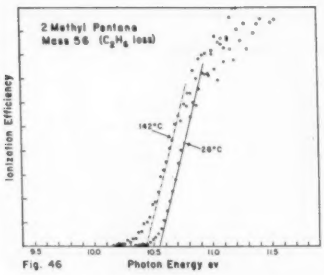

Fig. 46

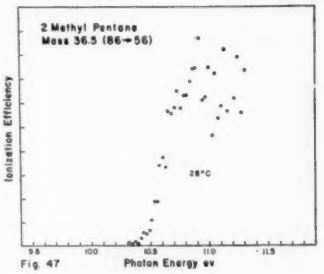

Fig. 47

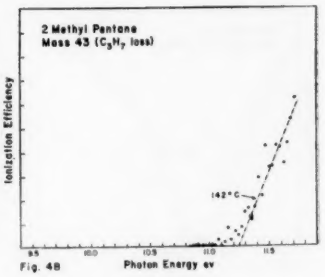

Fig. 48

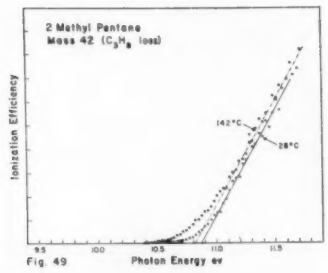

Fig. 49

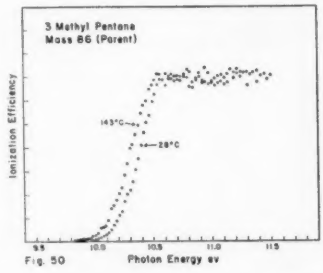

Fig. 50

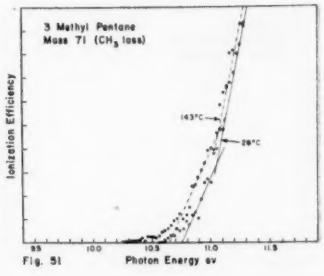

Fig. 51

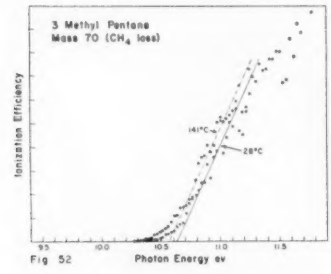

Fig. 52

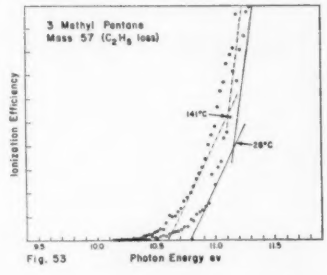

Fig. 53

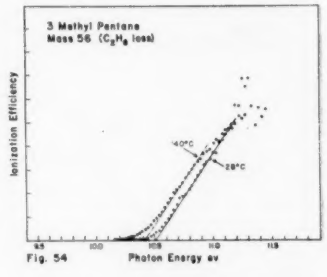

Fig. 54

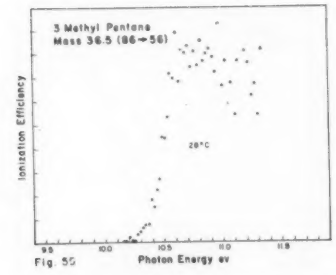

Fig. 55

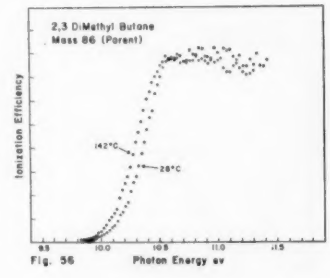

Fig. 56

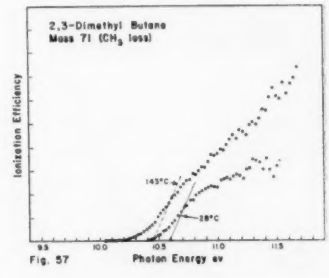

Fig. 57

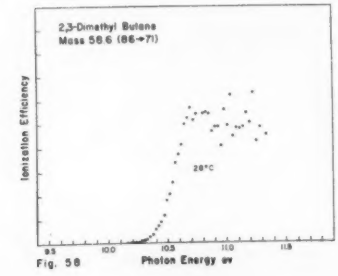

Fig. 58

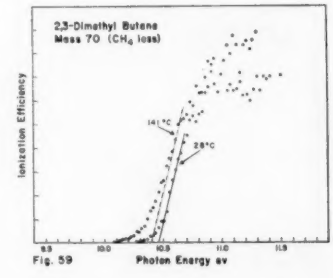

Fig. 59

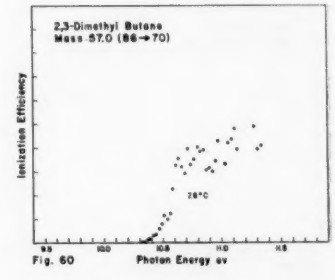

Fig. 60

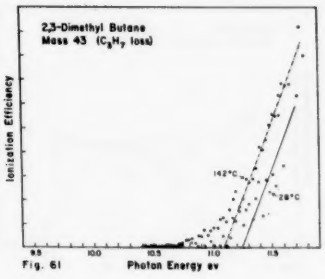

Fig. 61

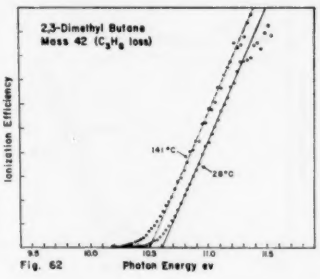

Fig. 62

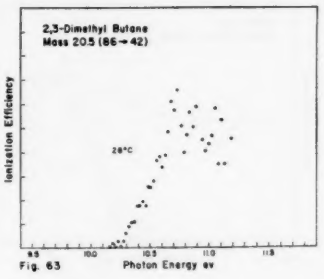

Fig. 63

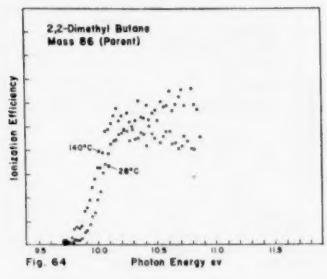

Fig. 64

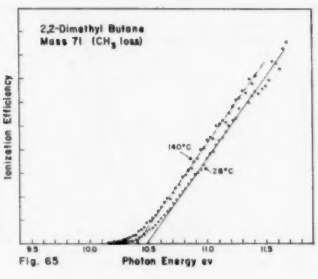

Fig. 65

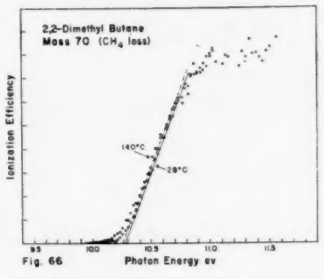

Fig. 66

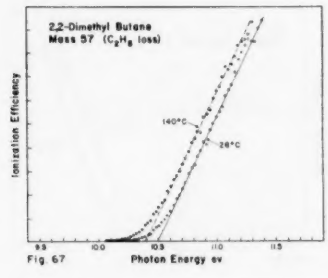

Fig. 67

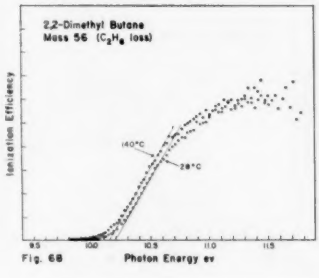

Fig. 68

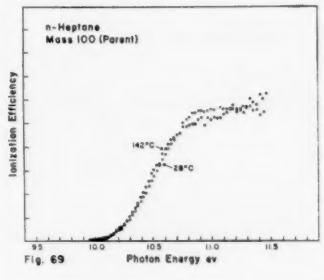

Fig. 69

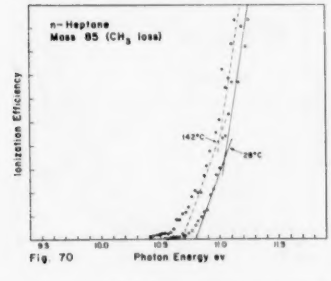

Fig. 70

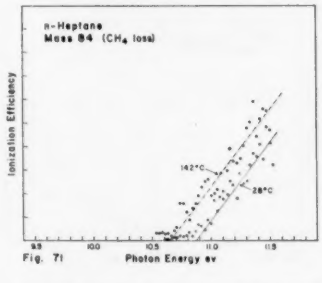

Fig. 71

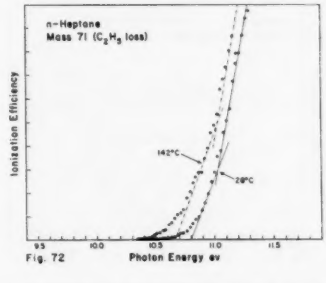

Fig. 72

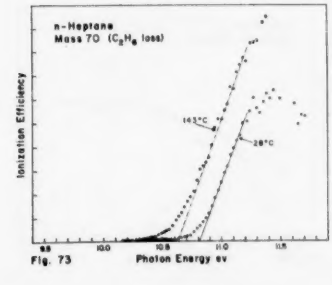

Fig. 73

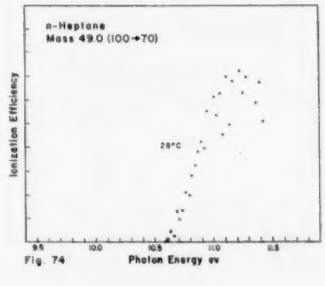

Fig. 74

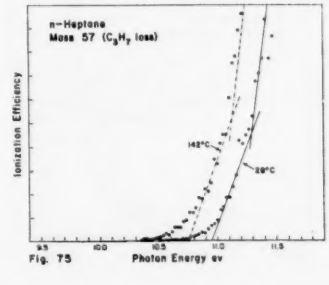

Fig. 75

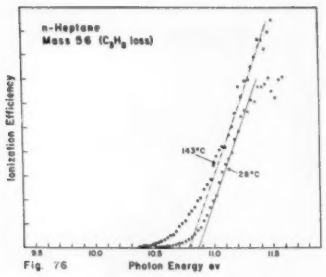

Fig. 76

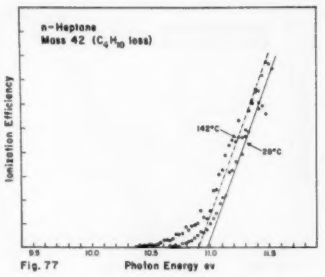

Fig. 77

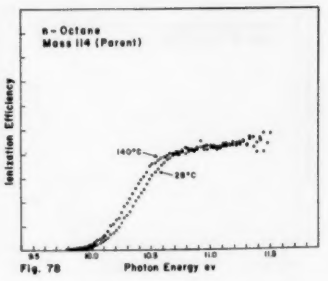

Fig. 78

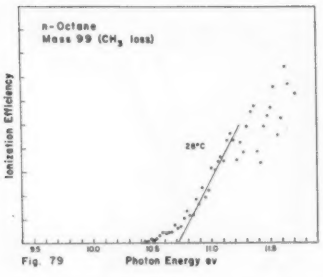

Fig. 79

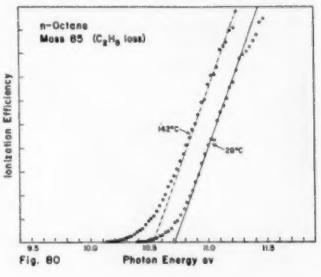

Fig. 80

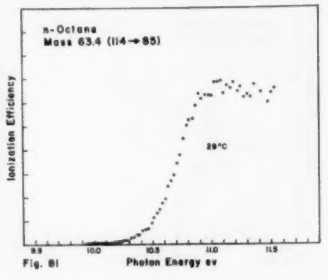

Fig. 81

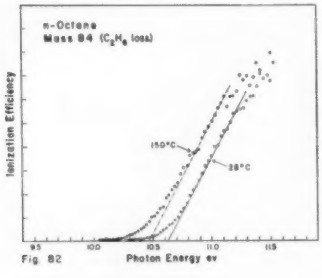

Fig. 82

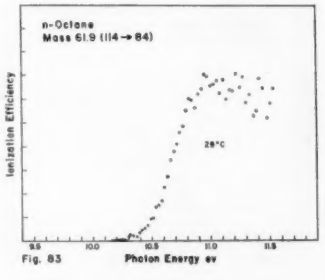

Fig. 83

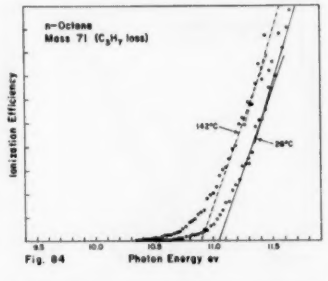

Fig. 84

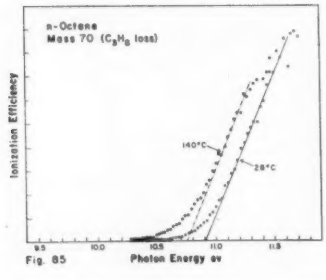

Fig. 85

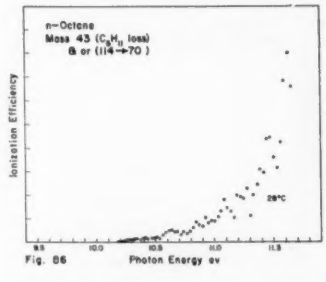

Fig. 86

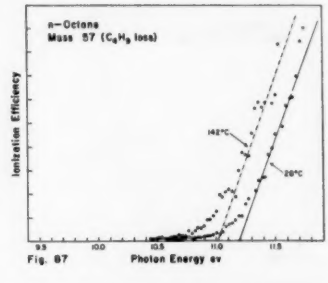

Fig. 87

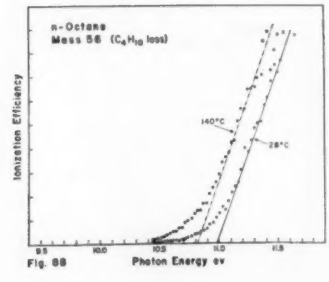

Fig. 88

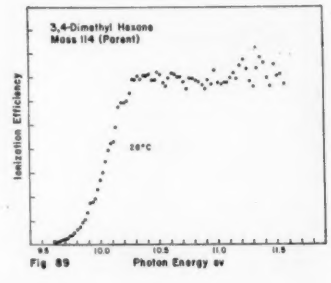

Fig. 89

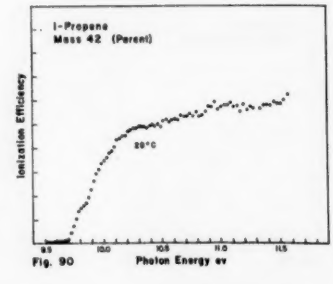

Fig. 90

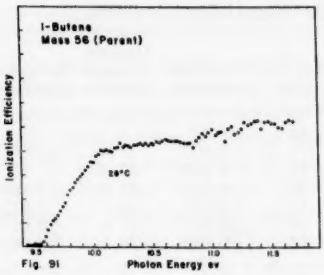

Fig. 91

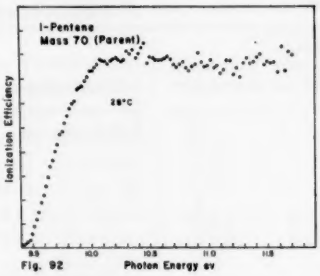

Fig. 92

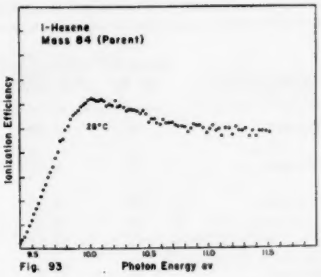

Fig. 93

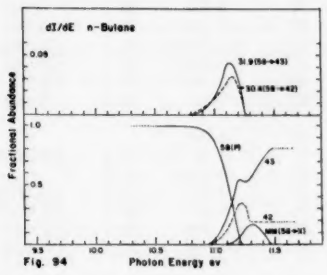

Fig. 94

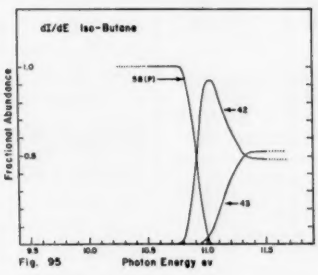

Fig. 95

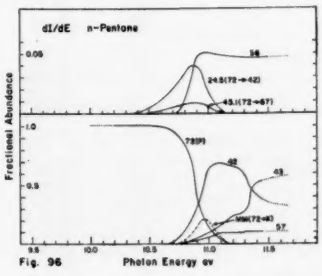

Fig. 96

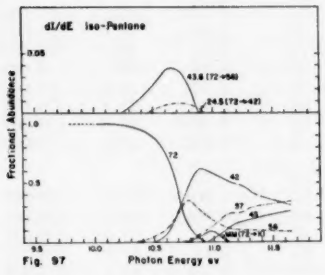

Fig. 97

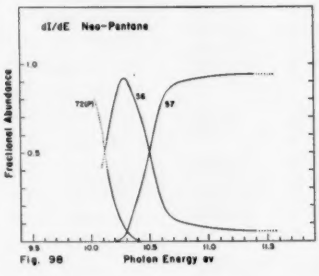

Fig. 98

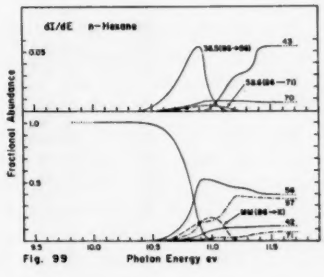

Fig. 99

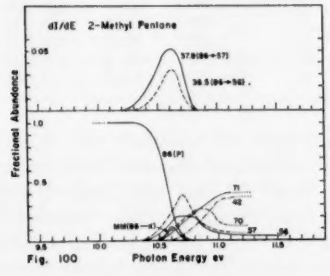

Fig. 100

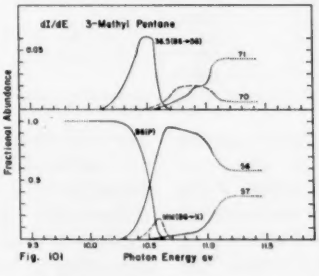

Fig. 101

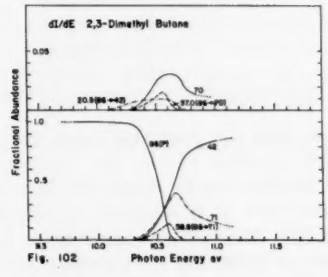

Fig. 102

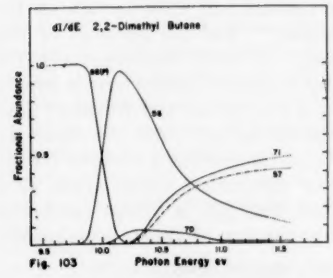

Fig. 103

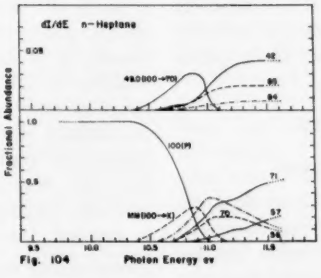

Fig. 104

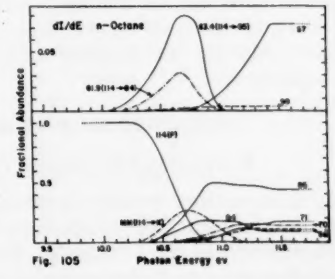

Fig. 105

TABLE I. Normalized abundance of ions produced after photoionization, photon energy 11.25 ev, $T=300°K$.

Parent molecule	Mass no. of ion	Normalized abundance	Mass no. of metastable ion	Normalized abundance
Ethane	30	1.00		
Propane	44	1.00		
n-Butane	58	0.63		
	43	0.20	31.9	0.020
	42	0.13	30.4	0.017
i-Butane	58	0.21		
	43	0.11	31.9	≲0.005
	42	0.68	30.4	≲0.006
n-Pentane	72	0.43		
	57	0.041	45.1	~0.0004
	56	0.031	43.6	≲0.001
	43	0.064	25.7	≲0.0004
	42	0.42	24.5	0.015
i-Pentane	72	0.24		
	57	0.066	45.1	0.0001
	56	0.20	43.6	0.008
	43	0.017	25.7	≲0.0001
	42	0.47	24.5	0.0025
Neo-pentane	72	0.0006		
	57	0.86	45.1	≲0.0001
	56	0.14	43.6	≲0.0001
	43	0.0006	25.7	≲0.002
	42	0.0006	24.5	≲0.002
n-Hexane	86	0.43		
	71	0.015	58.6	0.002
	70	0.005	57.0	
	57	0.14	37.8	~0.003
	56	0.32	36.5	0.017
	43	0.006	21.5	≲0.001
	42	0.057	20.5	≲0.001
2-Methylpentane	86	0.25		
	71	0.20	58.6	≲0.002
	70	0.13	57.0	
	57	0.14	37.8	0.017
	56	0.092	36.5	0.008
	43	≲0.002	21.5	≲0.008
	42	0.16	20.5	≲0.008
3-Methylpentane	86	0.19		
	71	0.013	58.6	≲0.006
	70	0.013	57.0	
	57	0.074	37.8	≲0.006
	56	0.70	36.5	0.012
	43	≲0.013	21.5	≲0.04
	42	≲0.013	20.5	≲0.04
2,3-Dimethylbutane	86	0.25		
	71	0.18	58.6	0.026
	70	0.013	57.0	0.004
	57	≲0.0013	37.8	≲0.004
	56	≲0.0013	36.5	≲0.004
	43	0.003	21.5	≲0.04
	42	0.52	20.5	0.005
2,2-Dimethylbutane	86	0.005		
	71	0.28	58.6	≲0.0005
	70	0.040	57.0	
	57	0.23	37.8	≲0.0005
	56	0.45	36.5	≲0.0005
	43	≲0.009	21.5	≲0.027
	42	≲0.009	20.5	≲0.027
n-Heptane	100	0.50		
	85	0.008	72.3	≲0.0015
	84	0.0026	70.6	≲0.005
	71	0.14	50.4	≲0.0025
	70	0.19	49.0	0.012
	57	0.024	32.5	≲0.0025
	56	0.10	31.4	≲0.005
	43	0.0018	18.5	≲0.007
	42	0.012	17.6	≲0.0025
n-Octane	114	0.37		
	99	0.0018	86.0	≲0.002
	98	≲0.0015	84.2	≲0.004
	85	0.31	63.4	0.032
	84	0.13	61.9	0.012
	71	0.038	44.2	≲0.004
	70	0.065	43.0	≲0.006
	57	0.009	28.5	≲0.004
	56	0.038	27.5	≲0.004
	43	≲0.002	16.2	≲0.004
	42	≲0.0015	15.5	≲0.004

ions, only the curve for room temperature is shown since, because of the low intensity, no significant information can be obtained from a comparison of this curve with that obtained at elevated temperature. Straight lines are drawn on those figures where such lines are helpful in the interpretation of the data. The relative intensities of the mass peaks, all taken at 11.25 ev, are given in Table I. This table also includes upper limits for the intensity of other mass peaks of interest.

INTERPRETATION OF DATA

A. Fractional Derivative Curves

It is convenient, in the interpretation of data, to separate the excitation process (i.e., formation of the excited molecular ion) from the dissociation. In the excitation process, a photon and a neutral molecule interact to produce a molecular ion and a single electron. For processes of this type the threshold law, that is, the variation of the ionization efficiency with energy immediately above threshold, has been treated both theoretically and experimentally. The theoretical treatments predict a sharp onset for the ionization, and, depending on the strength of noninverse-square forces, a relatively slow dependence of cross section on the energy above threshold.[14,15] For the purposes of this report, it is necessary to verify experimentally the validity of this "step function" characteristic over a range of only about 2 ev. Po Lee and Weissler[16] have determined the photoionization cross sections for helium and argon. From threshold to 2 ev above threshold, the cross section for helium varies about 17% and that for argon less than 5%. A similar conclusion is reached from examination of other experimental

[14] S. Geltman, Phys. Rev. **102**, 171 (1956).
[15] E. P. Wigner, Phys. Rev. **73**, 1002 (1948).
[16] Po Lee and G. L. Weissler, Phys. Rev. **99**, 540 (1955).

data except in those cases where the polarizability of the atom is high.[17]

The degree of validity of the step function approximation is also evident in data on photoionization of simple molecules. The data of Watanabe[18] on NO clearly show a series of abrupt increases in ionization cross section corresponding to successive vibrational levels in the NO^+ molecular ion. Between these increases the cross section remains constant within experimental error, i.e., within about 10%. The data can thus be represented as a series of step or Heaviside functions.

Experimental verification of the step function approximation for polyatomic molecules is not so direct as in the above cases. The vibrational levels in these molecules are so closely spaced that one cannot, at present, investigate the behavior of the cross section between the thresholds corresponding to these different levels. We resort, therefore, to the following indirect analysis. Consider the parent ionization curves for 3-methylpentane (Fig. 50) and 2,3-dimethylbutane (Fig. 56) which show the variation of the ionization efficiency with energy over a relatively wide range. The rising portions of these curves are the summation of many threshold functions corresponding to closely spaced transitions to the various vibrational levels. Above a critical energy the curves level off and remain flat. This occurs because, as one concludes from a study of the fragment ion curves, essentially all molecules excited above this critical level dissociate. Thus the summation terminates at this energy. The probability is small that the sum of a large number of threshold functions which vary with energy above their onset would give this constant behavior. Thus, from the observation that the summation of these threshold functions yields a total cross section independent of energy above the dissociation limit, we infer that each of the functions is Heaviside.

In the case of transitions to a single upper energy state where the threshold law is a Heaviside function, the derivative of the ionization efficiency curve with respect to energy is the profile of the photon energy distribution. The amplitude of the derivative is proportional to the transition probability. For polyatomic molecules, the derivative of the total ionization efficiency curve represents the sum of a number of individual transitions. If those transitions are closer together than the photon bandwidth, as they are in the case of the alkanes, they will not be resolved. Nevertheless, the amplitude is proportional to the sum of the transition probabilities and represents the probability of producing an excited molecule of a particular energy. This interpretation is rigorous as long as the threshold laws for the individual transitions are Heaviside functions.

[17] G. L. Weissler, *Handbuch der Physik* (Springer-Verlag, Berlin, 1956), Vol. XXI.

[18] K. Watanabe, J. Chem. Phys. **22**, 1564 (1954).

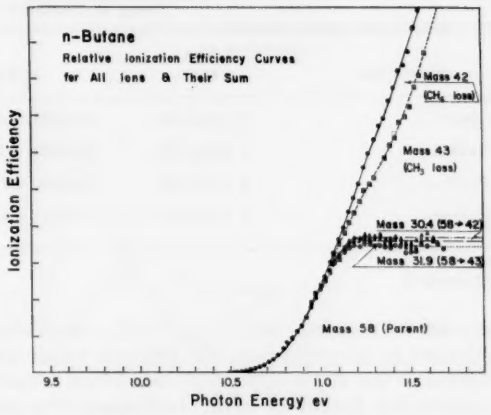

FIG. 106. The successive partial sums of the normalized ionization efficiency curves for *n*-butane derived from Figs. 7–11 and the intensity data of Table I. The differences between the ordinates of the curves give, at a particular photon energy, the relative contribution of each type of ion to the total. The deviation from a smooth sum curve is attributed to the missing metastables, i.e., ions which are not observed as a specific peak in the mass spectrum.

Where dissociation is also involved the relative amplitudes of the fragment derivative curves at a particular energy give the relative probabilities for formation of the fragment after the molecule has been excited to that particular energy. The ratios of the fractional derivatives to their sum, give the relative probability of particular dissociation processes at a particular energy in a form which is completely independent of the probability for formation of the molecular ion at that energy. The normalized fractional derivative curves, Figs. 94–105, thus describe the dissociation processes of molecules excited to particular energies. The curves are derived from the exact data of Figs. 1–89. They are smoothed so as to present what we believe to be the most probable dissociation patterns.

B. Total Ionization Curves and Ionization Potentials

The ionization efficiency curves for *n*-butane given in Figs. 7–11, adjusted in scale according to the relative intensities given in Table I, are summed to give the total ionization curve shown in Fig. 106. This sum curve gives information concerning the relative shapes of the potential surfaces of the molecule and the molecular ion. If the shapes of the potential surfaces are similar, i.e., if the molecule and molecular ion in their ground vibrational states have the same shape, then the adiabatic ionization potential would be measurable. The total ionization curve would, in this case, have a sharp onset. Such an onset is observed in the 1-alkenes, Figs. 90–93. Sharp onsets have also been observed in acetaldehyde, acetone and methylethylketone.[8] The onset for *n*-butane, shown in Fig. 106, is not of this type. A survey of all other alkane parent ionization efficiency curves in this work shows similar

TABLE II. Ionization potentials of 1-alkenes (ev).

Substance	This work	Interpretation	Published photoionization[a]	Published electron impact[b]
Propene	9.73±0.02	Probably adiabatic	9.73±0.01	9.76—10.1
1-Butene	9.61±0.02	Probably adiabatic	9.58±0.01	9.65—10.0
1-Pentene	9.50±0.02	Possibly not adiabatic	9.50±0.02	9.66
1-Hexene	9.45±0.02	Possibly not adiabatic	9.46±0.02	9.59

[a] Footnote 20.
[b] Footnote 19.

behavior. We therefore conclude that, with a sensitivity equivalent to that used here, the adiabatic ionization potential of the alkane molecules studied here cannot be determined directly by impact techniques. One can say only that the adiabatic ionization potential is equal to or less than the threshold for ionization. The only adiabatic ionization potentials which can be given from this study are those for the 1-alkenes. The ionization potentials for these molecules are given in Table II, where they are compared with other recent measurements.[19,20]

In photoionization where only one upper state is involved, and where the adiabatic transition is not accessible, the total ionization curve should be S-shaped.[8] In other words, neglecting fine structure, the slope increases smoothly to a maximum and then decreases to zero. The vertical ionization potential is the energy at which the derivative of the total ionization efficiency curve is a maximum. Over the range of energies covered in Fig. 106, one finds no clear evidence for an inflection beyond which the slope decreases continually, which could correspond to this vertical ionization potential. We therefore believe that the vertical ionization potential of this molecule lies near the upper limit or above the range of energies covered. In the case of the larger molecules, the ionization thresholds are at lower energies and one can study the ionization curves over a wider range of energies. One finds that the total ionization curves do indeed begin to round off within the range of energies covered. However, because the "straight" portion of the curves is relatively long, and because of a complication (to be discussed later) involving what will be called "missing metastable ions," the inflection point cannot be located with useful precision. Hence no vertical ionization potentials will be given.

The interpretation of the data to determine the minimum energy required for dissociation necessitates a detailed knowledge of the kinetics of dissociation, and the contribution of internally stored energy. In the absence of such detailed knowledge an approximate method for locating the thresholds must be used. In the section on bond energies the method used involves a linear extrapolation of the fragment ionization efficiency curves. It will be seen, from Fig. 106, that this method should give the correct thresholds provided the total ionization efficiency curve is linear in the energy range involved and provided also there is no complication caused by competition between different dissociation processes.

C. Influence of Internally Stored Thermal Energy

The discussion so far has ignored the fact that before the molecules absorb the ionizing photon they contain thermal energy. The average energies contained in the molecules involved in this work are given in Table III. They have been calculated by subtracting the contributions of translation and rotation from the heat content functions.[21] It is also necessary to know how the internal energy of the molecule is distributed about the average value. To obtain information on this question, the thermal energy distribution functions for *n*-butane, *n*-hexane, and *n*-octane have been calculated using a method described in Appendix I. These distribution functions are given in Figs. 107–109. From a study of the energy distributions in these figures one can estimate the energy distributions for all of the molecules here studied.

If the molecule is at 0°K, if only a single dissociation process is involved, and if the parent ion having energy greater than the dissociation limit dissociates immediately, then the slope of the parent curve becomes zero abruptly at the dissociation limit, and the fragment ion curve rises abruptly from this limit with a slope equal to that of the parent just below the dissociation limit. For a molecule above 0°K, the internally stored energy will affect the fragment ionization efficiency curve in two ways. The curve will be shifted to lower energies, and the transition from parent to fragment will occur gradually. The observed shifts in the fragment ionization curves are given in Table III, where they are compared with the average stored internal energies of the molecules. A shift which is less than the average stored

[19] F. H. Field and J. L. Franklin, *Electron Impact Phenomena* (Academic Press, Inc., New York, 1957).
[20] K. Watanabe (private communication).
[21] F. D. Rossini, K. S. Pitzer, R. L. Arnett, R. M. Braun, and G. C. Pimentel, *Selected Values of Physical and Thermodynamic Properties of Hydrocarbons and Related Compounds* (Carnegie Press, Pittsburgh, Pennsylvania, 1953).

energy implies that not all of this energy is effective in producing dissociation of the molecule during the time dissociation can be detected. A quantitative discussion of the shift, as well as the shapes of the fragment ionization curves thus involves also the kinetics of the dissociation. This will be discussed in a later section.

Although temperature shifts of parent curves are included, it appears at present to be impossible to make any quantitative analysis of the effect of temperature, because, as already stated, the adiabatic transition is not accessible so that the significance of the observed ionization thresholds is not known.

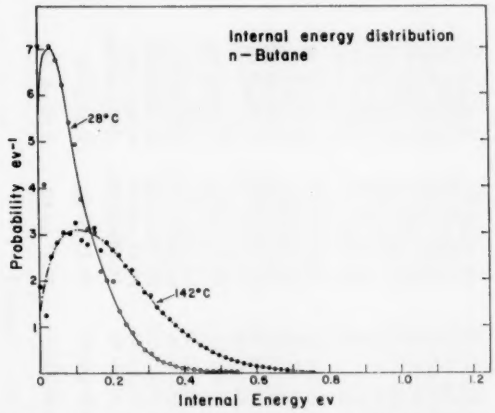

FIG. 107. The distribution function for the internal energy in *n*-butane, calculated by the method described in Appendix I.

D. Kinetic Energies of Fragments

As mentioned earlier, in the case of polyatomic molecules, internal energy, in excess of that necessary to cause dissociation, need not appear as kinetic energy of the fragments but may remain as internal vibrational energy. Stanton,[22] using a cylindrical electrostatic energy selector followed by a mass spectrometer, has studied the kinetic energy distribution of the fragments from a number of alkane molecules. We cite here his study of *n*-butane as an example. Using the parent peak as standard the most probable kinetic energy of the mass 43 fragment was found to be 0.007 ev, that of the 42, 0.004 ev. The most probable kinetic energies of the fragments of mass 41, 39, and 38, resulting from more complicated dissociative processes, are 0.051, 0.065, and 0.041 ev, respectively. The total kinetic energy of fragmentation is the sum of the energies of the ion plus that of the neutral fragment. The total energy of fragmentation of *n*-butane is, therefore, 0.03 ev in the case of CH_3 loss and 0.02 ev for CH_4 loss. The more complicated fragmentation processes leading to masses 41, 39, and 38 have total kinetic energies which are indeterminate, since the details of the fragmentation processes are not known. It can be shown that they have most probable energies equal to or greater than 0.20, 0.22, and 0.13 ev, respectively. Data concerning the detailed energy distribution are that the fraction of mass 43 and mass 42 fragments having 0.20 ev fragmentation energy is about twice that observed for a thermal distribution of energies at room temperature. These results demonstrate experimentally the assumption made by numerous workers that almost all of the excess energy of excitation appears as internal vibrational energy of the fragments and not as translational energy. In the interpretations of data in this report we will make use of this conclusion.

[22] H. E. Stanton (private communication).

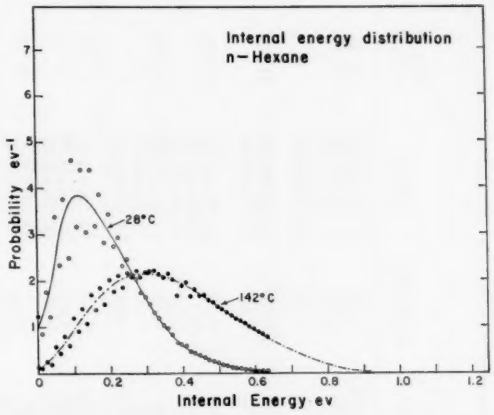

FIG. 108. The distribution function for the internal energy in *n*-hexane, calculated by the method described in the Appendix I.

E. Characteristic Transit Times in the Mass Spectrometer

The question of whether an unstable molecular ion will contribute to the parent peak, "metastable" peak,

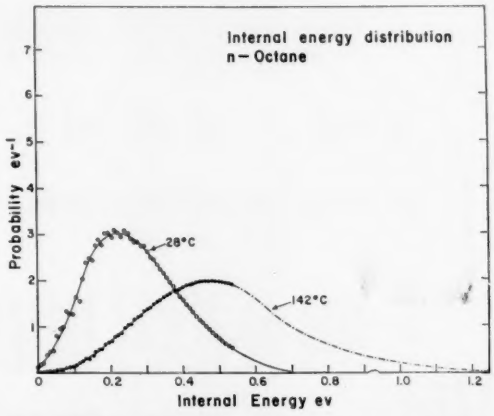

FIG. 109. The distribution function for internal energy in *n*-octane, calculated by the method described in the Appendix I.

TABLE III. Ionization thresholds and stored energy of alkanes (ev).

Reaction identification number[a]	Substance	Ion	Process[b]	$U_{415°K}$[c]	$U_{300°K}$[d]	$\Delta U_{(415°-300°K)}$	$AP_{415°K}$[e]	$AP_{300°K}$[f]	$\Delta AP_{(300°-415°K)}$	$\Delta AP_f/\Delta U$[g]	$AP_{0°K}$[h]	Best fit. $AP_{0°K}$[i]
1	Propane	43	1st	0.117	0.050	0.067	$11.45_5 \pm 0.02$	11.53 ± 0.01	$0.075 \pm 0.02_5$	1.20	$11.58_5 \pm 0.03$	11.58_5
2	*n*-Butane	43	1st	0.197	0.100	0.097	11.01 ± 0.01	11.10 ± 0.01	$0.09 \pm 0.01_5$	0.93	11.19 ± 0.02	11.19
3	*n*-Butane	43	2nd	0.197	0.100	0.097	11.16 ± 0.04	11.23 ± 0.04	0.07 ± 0.06	0.72	11.30 ± 0.07	
4	*n*-Butane	42		0.197	0.100	0.097	$11.03 \pm 0.02_5$	$11.09_5 \pm 0.00_5$	$0.06_5 \pm 0.03$	0.67	11.16 ± 0.03	
5	*i*-Butane	43		0.182	0.084	0.098	$11.07 \pm 0.02_5$	$11.15_5 \pm 0.01_5$	$0.08_5 \pm 0.03$	0.87	11.23 ± 0.03	11.23
6	*i*-Butane	42		0.182	0.084	0.098	10.84 ± 0.02	10.89 ± 0.01	$0.05 \pm 0.02_5$	0.51	10.93 ± 0.03	
7	*n*-Pentane	57	1st	0.276	0.145	0.131	$10.86_5 \pm 0.04$	$10.95_5 \pm 0.04$	$0.09 \pm 0.05_5$	0.69	$11.05_5 \pm 0.07$	11.05_5
8	*n*-Pentane	57	2nd	0.276	0.145	0.131	11.08 ± 0.04	$11.09_5 \pm 0.04$	$0.01_5 \pm 0.05_5$	0.11	11.11 ± 0.07	
9	*n*-Pentane	56		0.276	0.145	0.131	10.77 ± 0.03	$10.84_5 \pm 0.00_5$	$0.07_5 \pm 0.03$	0.57	10.93 ± 0.03	
10	*n*-Pentane	43	1st	0.276	0.145	0.131	10.98 ± 0.03	11.04 ± 0.03	$0.06 \pm 0.04_5$	0.46	$11.10_5 \pm 0.05$	11.10_5
11	*n*-Pentane	43	2nd	0.276	0.145	0.131	11.29 ± 0.04	11.29 ± 0.04	0.00 ± 0.06	0.00	11.29 ± 0.07	
12	*n*-Pentane	42		0.276	0.145	0.131	$10.79 \pm 0.00_5$	10.89 ± 0.01	$0.10 \pm 0.01_5$	0.76	10.99 ± 0.02	
13	*i*-Pentane	57	1st	0.253	0.122	0.131	10.90 ± 0.04	$10.97_5 \pm 0.04$	$0.07_5 \pm 0.05_5$	0.57	$11.14_5 \pm 0.07$	11.12
14	*i*-Pentane	57	2nd	0.253	0.122	0.131	11.28 ± 0.04	$11.32_5 \pm 0.04$	$0.04_5 \pm 0.05_5$	0.34	$11.36_5 \pm 0.02$	
15	*i*-Pentane	56		0.253	0.122	0.131	10.63 ± 0.01	$10.68_5 \pm 0.00_5$	$0.05_5 \pm 0.01_5$	0.42	$10.73_5 \pm 0.02$	
16	*i*-Pentane	43		0.253	0.122	0.131	$11.14_5 \pm 0.04$	$11.14_5 \pm 0.02$	$0.00 \pm 0.04_5$	0.00	$11.14_5 \pm 0.05$	11.14_5
17	*i*-Pentane	42		0.253	0.122	0.131	$10.64_5 \pm 0.01_5$	$10.74_5 \pm 0.01$	0.10 ± 0.02	0.76	$10.84 \pm 0.02_5$	
18	Neo-pentane	57		0.250	0.117	0.133	$10.53_5 \pm 0.02$	$10.55 \pm 0.00_5$	$0.01_5 \pm 0.02$	0.11	$10.56_5 \pm 0.02$	
19	Neo-pentane	56		0.250	0.117	0.133	$10.35 \pm 0.01_5$	10.37 ± 0.01	0.02 ± 0.02	0.16	10.39 ± 0.02	
20	*n*-Hexane	71	1st	0.355	0.190	0.165	$10.75_5 \pm 0.05$	10.89 ± 0.05	$0.13_5 \pm 0.07$	0.82	$11.04_5 \pm 0.08_5$	11.04_5
21	*n*-Hexane	70		0.355	0.190	0.165	$10.72_5 \pm 0.03$	$10.85_5 \pm 0.03$	$0.13 \pm 0.04_5$	0.79	$11.00_5 \pm 0.05_5$	
22	*n*-Hexane	57	1st	0.355	0.190	0.165	$10.71_5 \pm 0.04$	10.86 ± 0.04	$0.14_5 \pm 0.05_5$	0.88	$11.02_5 \pm 0.07$	10.97_5
23	*n*-Hexane	57	2nd	0.355	0.190	0.165	10.99 ± 0.04	$11.11_5 \pm 0.04$	$0.12_5 \pm 9.05_5$	0.76	11.26 ± 0.07	
24	*n*-Hexane	56		0.355	0.190	0.165	$10.66_5 \pm 0.00_5$	$10.82 \pm 0.00_5$	$0.15_5 \pm 0.01$	0.94	$11.00 \pm 0.01_5$	
25	*n*-Hexane	43	1st	0.355	0.190	0.165	$10.96_5 \pm 0.03$	11.14 ± 0.03	$0.17_5 \pm 0.01_5$	1.06	$11.33 \pm 0.05_5$	11.33
26	*n*-Hexane	43	2nd	0.355	0.190	0.165	$11.26_5 \pm 0.04$	$11.34_5 \pm 0.04$	0.08 ± 0.06	0.48	$11.43_5 \pm 0.07$	
27	*n*-Hexane	42		0.355	0.190	0.165	$10.90_5 \pm 0.02_5$	10.95 ± 0.02	$0.04_5 \pm 0.03$	0.27	$11.00 \pm 0.03_5$	
28	2-Methylpentane	71	1st	0.323	0.164	0.159	10.61 ± 0.05	$10.73_5 \pm 0.05$	$0.12_5 \pm 0.07$	0.79	$10.86_5 \pm 0.08_5$	
29	2-Methylpentane	70		0.323	0.164	0.159	10.51 ± 0.01	$10.67 \pm 0.01_5$	0.16 ± 0.02	1.00	$10.83_5 \pm 0.02_5$	
30	2-Methylpentane	57		0.323	0.164	0.159	$10.45_5 \pm 0.02$	$10.59 \pm 0.00_5$	$0.13_5 \pm 0.02$	0.85	10.73 ± 0.02	
31	2-Methylpentane	56		0.323	0.164	0.159	$10.43_5 \pm 0.00_5$	$10.54 \pm 0.00_5$	$0.10_5 \pm 0.01$	0.66	$10.65 \pm 0.01_5$	
32	2-Methylpentane	43		0.323	0.164	0.159	$11.25 \pm 0.02_5$	...	...	...	(11.35±0.10)	
33	2-Methylpentane	42		0.323	0.164	0.159	10.81 ± 0.04	$10.86 \pm 0.01_5$	$0.05 \pm 0.04_5$	0.31	10.91 ± 0.05	
34	3-Methylpentane	71	1st	0.327	0.166	0.161	$10.64_5 \pm 0.05$	10.75 ± 0.05	$0.10_5 \pm 0.07$	0.65	$10.86 \pm 0.08_5$	
35	3-Methylpentane	70		0.327	0.166	0.161	10.56 ± 0.03	10.63 ± 0.03	$0.07 \pm 0.04_5$	0.43	$10.70 \pm 0.05_5$	
36	3-Methylpentane	57	1st	0.327	0.166	0.161	$10.59_5 \pm 0.04$	$10.78_5 \pm 0.04$	$0.19 \pm 0.05_5$	1.18	10.95 ± 0.07	11.01_5
37	3-Methylpentane	57	2nd	0.327	0.166	0.161	$11.12_5 \pm 0.04$	$11.12_5 \pm 0.04$	$0.00 \pm 0.05_5$	0.00	$11.12_5 \pm 0.07$	
38	3-Methylpentane	56		0.327	0.166	0.161	10.41 ± 0.01	$10.49_5 \pm 0.00_5$	$0.08_5 \pm 0.01_5$	0.53	$10.58 \pm 0.01_5$	
39	2,3-Dimethyl-butane	71		0.325	0.163	0.162	10.44 ± 0.05	10.58 ± 0.05	0.14 ± 0.07	0.83	$10.72 \pm 0.08_5$	
40	2,3-Dimethyl-butane	70		0.325	0.163	0.162	10.40 ± 0.01	10.47 ± 0.02	$0.07 \pm 0.02_5$	0.43	10.54 ± 0.03	

TABLE III.—*Continued.*

Reaction identification number[a]	Substance	Ion	Process[b]	$U_{415°K}$[c]	$U_{300°K}$[d]	$\Delta U_{(415°-300°K)}$	$AP_{415°K}$[e]	$AP_{300°K}$[f]	$\Delta AP_{(300°-415°K)}$	$\Delta AP_f/\Delta U$[g]	$AP_{0°K}$[h]	Best fit: $AP_{0°K}$[i]
41	2,3-Dimethyl-	43		0.325	0.163	0.162	$11.08_5 \pm 0.05$	11.24 ± 0.04	$0.15_5 \pm 0.06_5$	0.96	$11.39_5 \pm 0.07$	
42	2,3-Dimethyl-	42		0.325	0.163	0.162	$10.49_5 \pm 0.01_5$	$10.59_5 \pm 0.00_5$	0.10 ± 0.02	0.62	$10.69_5 \pm 0.02$	
43	2,2-Dimethyl-butane	71		0.316	0.157	0.159	$10.39_5 \pm 0.01_5$	$10.47_5 \pm 0.03$	$0.08 \pm 0.03_5$	0.50	$10.55_5 \pm 0.04_5$	
44	2,2-Dimethyl-butane	70		0.316	0.157	0.159	10.25 ± 0.01	$10.26_5 \pm 0.01$	$0.01_5 \pm 0.01_5$	0.09	10.28 ± 0.02	
45	2,2-Dimethyl-butane	57		0.316	0.157	0.159	$10.39 \pm 0.01_5$	$10.49_5 \pm 0.01$	$0.10_5 \pm 0.02$	0.66	$10.60 \pm 0.02_5$	
46	2,2-Dimethyl-butane	56		0.316	0.157	0.159	10.15 ± 0.01	10.19 ± 0.005	$0.04 \pm 0.01_5$	0.25	$10.23 \pm 0.01_5$	
47	*n*-Heptane	85	1st	0.432	0.234	0.198	$10.67_5 \pm 0.06$	10.79 ± 0.06	$0.11_5 \pm 0.08_5$	0.58	$10.92_5 \pm 0.10_5$	10.96_5
48	*n*-Heptane	84		0.432	0.234	0.198	$10.64_5 \pm 0.05$	$10.87_5 \pm 0.02$	0.23 ± 0.03	1.16	$11.14_5 \pm 0.03_5$	
49	*n*-Heptane	71	1st	0.432	0.234	0.198	$10.66_5 \pm 0.05$	10.80 ± 0.05	$0.13_5 \pm 0.07$	0.68	$10.96 \pm 0.08_5$	10.96_5
50	*n*-Heptane	70		0.432	0.234	0.198	$10.62 \pm 0.01_5$	10.81 ± 0.01	0.19 ± 0.02	0.96	$11.03_5 \pm 0.02_5$	
51	*n*-Heptane	57	1st	0.432	0.234	0.198	10.75 ± 0.04	10.95 ± 0.04	$0.08 \pm 0.05_5$	0.40	$11.18_5 \pm 0.07$	11.19_5
52	*n*-Heptane	56		0.432	0.234	0.198	$10.78_5 \pm 0.02_5$	$10.87 \pm 0.00_5$	$0.08_5 \pm 0.02_5$	0.43	10.97 ± 0.03	
53	*n*-Heptane	42		0.432	0.234	0.198	10.95 ± 0.07	$10.96 \pm 0.01_5$	$0.01 \pm 0.07_5$	0.05	10.97 ± 0.08	
54	*n*-Octane	99		0.507	0.279	0.228		$10.70_5 \pm 0.07_5$			(10.90 ± 0.10)	
55	*n*-Octane	85		0.507	0.279	0.228	10.53 ± 0.03	$10.70_5 \pm 0.01$	$0.17_5 \pm 0.03_5$	0.74	$10.91 \pm 0.03_5$	10.88_5
56	*n*-Octane	84		0.507	0.279	0.228	$10.46 \pm 0.02_5$	10.62 ± 0.01	$0.16 \pm 0.02_5$	0.67	10.81 ± 0.03	
57	*n*-Octane	71	1st	0.507	0.279	0.228	$10.89_5 \pm 0.05$	$11.04_5 \pm 0.05$	0.15 ± 0.07	0.67	$11.22 \pm 0.08_5$	11.19
58	*n*-Octane	70		0.507	0.279	0.228	$10.74_5 \pm 0.02$	$10.90 \pm 0.01_5$	$0.15_5 \pm 0.02_5$	0.65	11.08 ± 0.03	
59	*n*-Octane	57		0.507	0.279	0.228	11.01 ± 0.04	11.19 ± 0.04	$0.18 \pm 0.05_5$	0.76	11.40 ± 0.07	11.40
60	*n*-Octane	56		0.507	0.279	0.228	10.81 ± 0.06	$10.98_5 \pm 0.02$	$0.17_5 \pm 0.06_5$	0.73	11.19 ± 0.07	

[a] Reaction number is an identification number, for reference use throughout the text.
[b] Process, 1st or 2nd, refers to whether the break in the ionization efficiency curve is the 1st or 2nd.
[c] $U_{415°K}$ is the internally stored energy of the specified molecule at 415°K, as derived from heat capacity data.[21]
[d] $U_{300°K}$ is the internally stored energy of the specified molecule at 300°K, as derived from heat capacity data.[21]
[e] $AP_{415°K}$ is the experimental threshold energy for the appearance of the ion specified in columns 2 and 3 at 415°K as determined in the present paper.
[f] $AP_{300°K}$ is the experimental threshold energy for the appearance of the ion specified in columns 2 and 3 at 300°K as determined in the present paper.
[g] $\Delta AP/\Delta U$ is the ratio of experimental to theoretical temperature shifts as given in columns 10 and 7.
[h] $AP_{0°K}$ is the extrapolated threshold for the appearance of the ion specified in columns 2 and 3 at 0°K scaled according to the factor $\Delta AP/\Delta U$.
[i] Best fit $AP_{0°K}$ is the value of the threshold which gives the minimum error in the determination of bond dissociation energies. They are valid only insofar as the kinetic shifts are constant.

or a fragment peak depends on how its lifetime compares with various transit times for an ion passing through the mass spectrometer.[23] Those ions dissociating within the ionization chamber (or before acceleration to more than a few volts of energy) contribute to the fragment ion peak. Ions dissociating in the region of strong acceleration are spread over a wide range in energy so that they contribute to the background but do not contribute significantly to a mass peak. In the present paper these will be termed "fast metastables." The familiar "metastables" (which we will call "ordinary metastables"), are those ions which dissociate in the drift space between acceleration and deflection in the magnet. Since they have been accelerated as parent ions and deflected as fragments they appear as a mass peak at m_f^2/m_p, where m_f is the mass of the fragment and m_p is the mass of the unstable ion which decays to form the fragment. The ions which dissociate in the magnetic field will be spread out in a manner similar to the fast metastables and do not contribute significantly to a mass peak. We will term these ions "slow metastables." Finally, those ions which dissociate in the drift space beyond the magnetic field are detected as though dissociation had not taken place. In order to treat the data quantitatively we must calculate the transit time between the boundaries of each of these regions.

To calculate the drawout time, i.e., the time spent in the ionization chamber, it is necessary to calculate the potential distribution in this chamber. The ionization chamber is a rectangular box, 0.42 in. wide, 0.52 in. long, and 0.55 in. deep. Five of the sides are at the same potential; and the sixth, with the aperture through which the ions are extracted, is maintained at an adjustable negative potential relative to the rest. Ions are formed from 0.223–0.357 in. away from this plate. The potential distribution was calculated by solution of LaPlace's equation, neglecting the influence of the drawout aperture and the apertures which provided for the photon beam. The drawout times were taken to be the times required for ions to reach the plane of the exit aperture since beyond this aperture, the ions are accelerated strongly. The results of the calculation are

$$T_d(0.223\text{ in.}) = 3.6\times10^{-7}\ (M/V_d)^{\frac{1}{2}}\text{ sec} \qquad (1)$$

$$T_d(0.357\text{ in}) = 7.8\times10^{-7}\ (M/V_d)^{\frac{1}{2}}\text{ sec}, \qquad (2)$$

where $T_d(0.223$ in.) is the drawing-out time for ions formed 0.223 in. from the drawout slit, $T_d(0.357$ in.) is the drawing-out time for ions formed 0.357 in. from the slit, M is the mass of the ion in atomic mass units, and V_d is the potential applied to the drawout plate in volts. For the data of Figs. 1–93 this potential was held constant at 13 v. The remaining transit times are readily calculated from the dimensions of the mass spectrometer and the ion accelerating potential (3000 v). The time for acceleration is

$$T_a = 7.8\times10^{-8}\ M^{\frac{1}{2}}\text{ sec}. \qquad (3)$$

The time for free flight between acceleration and the magnetic field is

$$T_f = 7.0\times10^{-7}\ M^{\frac{1}{2}}\text{ sec}. \qquad (4)$$

The time for deflection in the magnetic field is

$$T_B = 4.2\times10^{-7}\ M^{\frac{1}{2}}\text{ sec}. \qquad (5)$$

For example, a hexane molecular ion produced approximately in the middle of the ionization chamber has a drawout time of 1.4 μsec, reaches the end of its acceleration after a total of 8.6 μsec, and emerges from the magnet after a total of 12.5 μsec.

F. Effect of Varying the Drawout Time

In order to gain some information on the lifetimes of the molecular ions, one can vary the time spent in the ionization chamber by changing V_d, the drawout potential. Similar studies using electron impact have been carried out by Friedman *et al.*[23] Unfortunately, the variation can be done only over a limited range, because the intensity decreases greatly when V_d is changed from its optimum value. It was possible to decrease V_d to 2.5 v, or increase it to 27 v. Thus, the drawout time could be varied by a factor of 3.3. The results of these experiments are shown in Figs. 110–113. The first two of these curves show the drawout shifts for the fragment ions from *n*-butane. It is apparent that some excited molecular ions do have lifetimes in the range of 1 μsec.[24] The shifts are about equal for the two fragments and they are in the direction expected if a higher excitation produces lower average lifetimes. Since the appearance potentials are about equal, these shifts do not give any information on the correlation of drawout shift with the order of appearance of fragments. Figures 112–113, however, do show this correlation. Figure 112 shows the drawout shift for the lowest energy fragment occurring from *n*-octane. The shift is clear and is again in the expected direction. Figure 113 shows the third lowest energy fragment, mass 70. Clearly the drawout shift on this higher energy process is much less than that for mass 84, the lowest energy fragment. Within the limits of the experiment it is zero. We believe that the upper energy process (Fig. 111) has no drawout shift. The apparent shift is thought to be due to that of the lower process since the breaks in the curves occur apparently at the same energy.

G. Metastable Ions

The ionization efficiency curves corresponding to measurable ordinary metastable transitions are given in the set of Figs. 1–89, following in each case the

[23] L. Friedman, F. A. Long, and M. Wolfsberg, J. Chem. Phys. **31**, 755 (1959).

[24] J. A. Hipple, R. E. Fox, and E. U. Condon, Phys. Rev. **69**, 347 (1946).

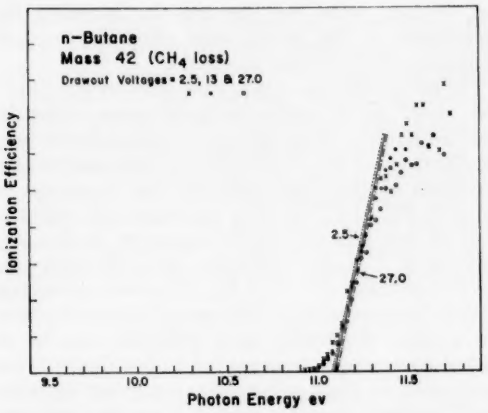

FIG. 110. Drawout effect for the mass 42 fragment from *n*-butane, i.e., ionization efficiency curves for different times spent in the ionization chamber. This time is varied by changing the drawout voltage across the ionization region.

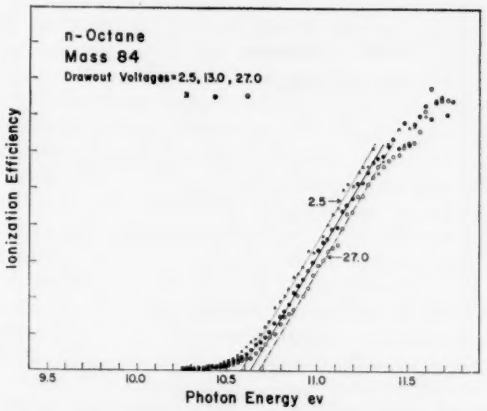

FIG. 112. Drawout effect for the mass 84 fragment from *n*-octane, i.e., ionization efficiency curves for different times spent in the ionization chamber. The time is varied by changing the drawout voltage across the ionization region. The mass 84 fragment is the lowest energy fragmentation process occurring in the *n*-octane ion.

associated fragment curve. The intensities given in Table I, however, include a correction factor. This factor must be used because the metastable mass peaks are broader than the fragment of the parent peaks. Since the profiles of the parent and fragment peaks are the same, within experimental error, the relative intensities are taken to be the ratio of the maximum ion currents. For a given peak height the area under a metastable profile was found to be about 2.7 times the area under a parent or fragment profile. This factor is an average taken after examining the profiles of the fragments of mass 43 and 42 from *n*-butane and their corresponding metastables, and mass 85 and 84 from *n*-octane and their corresponding metastables. This broadening in the direction normal to the slits implies that there is also a loss in intensity caused by a spreading in the direction along the slits. The slits are, however, long in comparison with their width and the correction is negligible. The metastable correction factor is a function of the parameters of the mass spectrometer. The particular factor used, therefore, applies only to the present data.

Two possible causes for the metastable peak broadening are: (1) The drift space between ion acceleration and the deflecting magnet is not really field free, but contains the fringe field of the magnet. Thus the trajectories of the ions depends slightly on the position of the dissociation within this section. (2) If there is

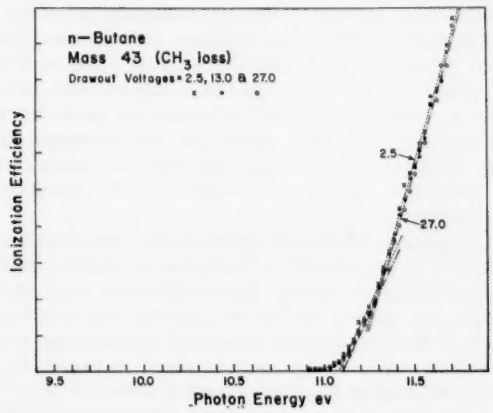

FIG. 111. Drawout effect for the mass 43 fragment from *n*-butane, i.e., ionization efficiency curves for different times spent in the ionization chamber. This time is varied by changing the drawout voltage across the ionization region.

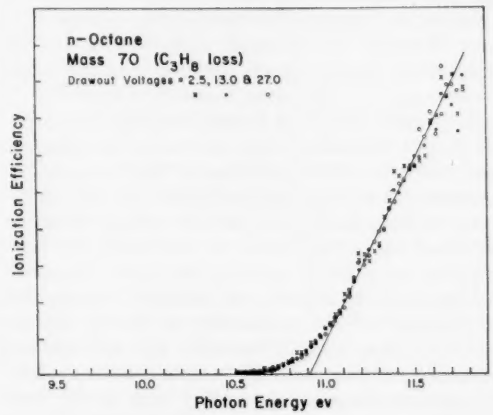

FIG. 113. Drawout effect for the mass 70 fragment from *n*-octane, i.e., ionization efficiency curves for different times spent in the ionization chamber. The time is varied by changing the drawout voltage across the ionization region. The mass 70 fragment is the third from lowest energy fragmentation process occurring in the *n*-octane ion. It is evident that no drawout shift can be detected in the higher energy fragmentation processes.

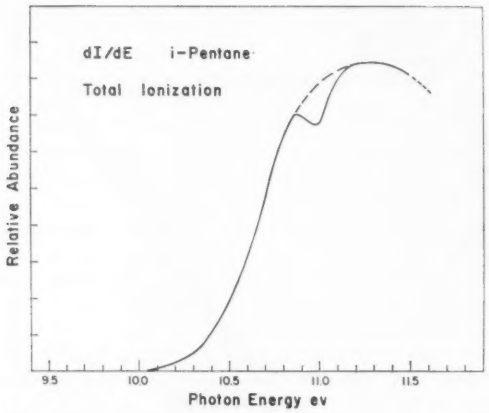

FIG. 114. The smoothed total ionization curve for *i*-pentane derived from Figs. 22–29 along with the intensities from Table I. The departure from the expected monotonic smooth function indicated by a dotted line is attributed to the missing metastable ions. The functional derivative attributed to the missing metastable ions in this case is shown in Fig. 97, indicated by the symbol *MM*.

any kinetic energy of dissociation the components of velocity normal to the trajectory will broaden the peak. In an attempt to determine the relative importance of these two causes, we placed magnetic shielding around the drift space to reduce the fringe field. The reduction in the fringe field was about a factor of four. Within experimental error, the profiles were unchanged. We therefore attribute the broadening mainly to kinetic energy of dissociation. That this is consistent with the data on kinetic energy may be seen from the following rough estimate. A mean kinetic energy of 0.03 ev (see section on kinetic energy) will result in a variation in direction of about 0.003 rad. This would be equivalent to changing the accelerating voltage by a factor of 0.003. The increase in half-width at half-height of the metastable as compared with the parent is, within experimental error, equal to this quantity in the four cases studied. It is surprising that the correction factor is the same for the four cases. The measurement is of course difficult because of the low intensity. However, since the correction factor has been determined for both the lightest and the heaviest molecule and found to be the same, we have used the same correction factor for all ordinary metastable intensities. On Figs. 9, 17, 28, and 38, the comment is made that the intensity of the metastable is partly "second order." In these cases the intensity was very low and it was necessary to use high sample pressures, about 10^{-4} mm resulting in about 10^{-5} mm in the drift space. Thus some collision-induced dissociations occur in this drift space and contribute to the ion peak corresponding to the ordinary metastable transition. This second-order contribution will vary in ionization efficiency in the same way as the parent. The intensity of the effect should vary as the square of the pressure and, in fact, when the pressure was increased the contribution of this second-order effect increased in comparison with all other intensities.

The metastable ions which have been termed "fast" and "slow," in the section on transit times, cannot be detected directly. Their existence can be inferred from the derivative of the total ionization. One example, the derivative of the total ionization for isopentane, is shown in Fig. 114. This curve rises smoothly, begins to level off, and then rises again, suggesting, at first, the presence of a second electronic state. However, the parent ionization curve (see Fig. 22) shows no increase in slope corresponding to the second electronic state. We consider it unlikely that molecular ions in an excited electronic state would fail to contribute to the parent ions. An alternative explanation is that the curve would continue smoothly upward if the fast and slow metastable ions were included. Consequently, we attribute the departure from a smooth curve to the combination of fast and slow metastables, and determine the total intensity of these missing metastables (labeled *MM* in Figs. 94–105) on this basis. This explanation is supported by the following corroborative evidence: (1) The intensity attributed to the missing metastables, though quite uncertain, correlates with the intensity of the ordinary metastables. Specifically, in cases where there are no ordinary metastables, there is also no missing metastable. (2) The shapes and positions, though also quite uncertain, are similar to the ordinary metastables. In particular, we do not believe that the departure from a smooth curve can be attributed to a systematic error in fragment intensities, caused by kinetic energy of the fragments.

THEORY

A. Rate-Determined Dissociation

The dissociative process studied here can be termed unimolecular reactions in the zero-pressure limit. Theories of unimolecular reactions typically consider these processes to be rate-determined. That is, the assumption is made that the probability per unit time that a *given* molecule will dissociate is a constant (independent of time) called the rate constant, k. The theories predict this rate constant k as a function of excitation energy and various other molecular parameters.

Calculation of k requires some assumptions about the behavior of an ensemble of coupled oscillators which contain excitation energy that is shared in some way among the various oscillators. An assumption often made is that, within the lifetime of the molecule (or molecular ion) energy is exchanged between the oscillators a great many times, and in a manner which may be treated as random. Once this assumption is made, a statistical treatment is possible, by which the dissociation process is seen as a statistical fluctuation. That is, dissociation occurs when, by chance, an

amount of energy accumulates at a particular bond (or, in a rearrangement, some combination of reaction coordinates) which is sufficient to cause dissociation.

Unimolecular gas reactions studied by chemical methods generally involve pressures high enough so that the molecule sustains many collisions in its lifetime. These collisions provide a mechanism for the energy randomization mentioned previously. For unimolecular gas reactions, Hinschelwood,[25] Kassel,[26] and Rice and Ramsperger[27] have given, after making various approximations, expressions for k which are all of the form

$$k=\nu[(E-E_0)/E]^{n-1}\ \text{sec}^{-1}, \qquad (6)$$

where ν, the "frequency factor," is related to the vibration frequencies of the molecule. (It may be calculated by different methods or treated as a free parameter.) E is the excitation energy, E_0 is the threshold energy for dissociation, and n is the number of internal degrees of freedom.

Dissociation, in the zero pressure limit, of an excited molecular ion differs from the unimolecular gas reactions, discussed previously, in that there are no collisions to provide a mechanism for energy randomization. Rosenstock, Wallenstein, Wahrhaftig, and Eyring[2] have developed a statistical theory of rate constants for dissociation, in the zero pressure limit, again using the assumption of energy randomization. This randomization, however, must occur among the oscillators within the isolated molecule. The mechanism they have assumed for this intramolecular randomization may be described as follows. The motions of the oscillators in a molecule, for a single electronic state, may be described in terms of a point moving about on a multidimensional surface in phase space. Rosenstock *et al.* assume that there are, in fact, many electronic states accessible and, therefore, many such potential surfaces. These surfaces intersect in complicated ways, and the phase point in its motion, frequently encounters such crossings. At each crossing the phase point may continue on the surface it was on, or may jump to another (a radiationless transition) according to the relative probabilities for these two alternatives. If encounters with crossings occur frequently, i.e., many times in the lifetime of the ion, they provide a mechanism for randomization, as required in the theory.

The statistical theory of Rosenstock *et al.* results in an expression for k which, in the extreme idealization, for molecular ions having no free rotors, may be written in the form of Eq. (6). In addition, the theory makes a prediction of the frequency factor ν. This frequency is the product of the frequencies for all the oscillators in the quiescent molecule divided by the product of the frequencies for the oscillators in the "activated complex," the frequency corresponding to the reaction coordinate being omitted from the latter product. If the molecular ion has free rotors, the equations are more complex (see for example footnote 4).

It is of interest to mention another type of theory, due to N. B. Slater[28] even though it does not apply to the present case of zero pressure. In contrast with the theories outlined previously, which regard energy as the crucial variable, Slater's theory focuses attention upon the reaction coordinates. The dissociation takes place when a reaction coordinate exceeds some critical value. For any particular dissociation, the reaction coordinate is expressed as a linear combination of the normal mode coordinates, the coefficients in the sum being related to the transformation from interatomic distances to normal mode coordinates. The lifetime of the molecule is the time from excitation until the reaction coordinates reaches the critical extension, i.e., until all of the oscillators have the proper phase to produce this critical extension. Slater's original theory also assumes that the oscillators are classical and perfectly harmonic. In later treatments, he attempts to include the effects of anharmonicity and also to treat the problem quantum mechanically. The assumption of perfect harmonicity means that there will be no energy transfer from mode to mode. In this picture a molecule must satisfy two conditions before it can dissociate. In addition to having enough excitation energy, the energy must be distributed (at the start), among the normal modes in such a way that the required critical extension can be attained. Calculation of rate constants in Slater's theory reduces to the problem of calculating the average frequency with which a sum of sinusoidal functions, representing the normal modes, exceeds a critical value. On using the assumption that the distribution of energy among the normal modes is continually randomized by collisions, Slater calculates this frequency and arrives at a rate constant which is of the form of Eq. (6). The frequency factor in his theory is expressed as a weighted average of the normal mode vibration frequencies, the weighting factors being the squares of the coefficients in the expansion of the reaction coordinate in terms of normal mode coordinates.

The two types of theories discussed may be regarded as taking opposite extremes concerning the importance of energy transfer between normal modes in the molecule, Rosenstock *et al.* assuming that energy transfer occurs rapidly and is of the greatest importance, and Slater assuming that it does not occur at all. After comparing the predictions of the statistical theory of Rosenstock *et al.* with experiment, we will return to a discussion of these contrasting theories.

[25] C. N. Hinshelwood, Proc. Roy. Soc. (London) **A113,** 230 (1927).

[26] L. S. Kassel, J. Phys. Chem. **32,** 225 (1928); *Kinetics of Homogeneous Gas Reactions* (Reinhold Publishing Corporation New York, 1932), Chap. 5.

[27] O. K. Rice and H. C. Ramsperger, J. Am. Chem. Soc. **49,** 1617 (1927); **50,** 617 (1928).

[28] N. B. Slater, *Theory of Unimolecular Reactions* (Cornell University Press, Ithaca, New York, 1959).

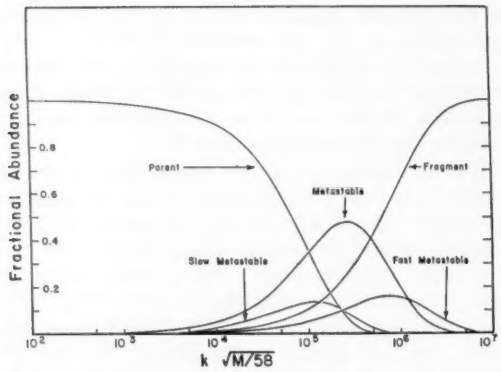

FIG. 115. The relative fractions of ions which will appear as parent, fragment, metastable, slow metastable, or fast metastables—as functions of $k(M/58)^{\frac{1}{2}}$, where k is rate constant for dissociation and M is the mass of the parent ion in amu. The curves are calculated from the information in the section on "Characteristic Transit Times in the Mass Spectrometer."

B. Comparison With Experiment

Before making specific comparisons with experiment, it is necessary to calculate, for a given rate constant for dissociation, the probability that a molecular ion will appear as parent, fragment, ordinary metastable, or will be in the category of "missing metastable" (see section on transit times). This calculation yields the results given in Fig. 115. These results will be used in a number of the following sections.

1. *Temperature Effects*

If energy transfer between modes occurs as rapidly as in the statistical theory of Rosenstock *et al.*, then neglecting the influence of thermal excitation upon the ionization process one may assume that the thermal energy stored in the molecule and the energy added by photons during ionization, are equivalent in regard to the dissociation. Thus one would expect temperature shifts of the fragment ionization efficiency curves equal to the difference in the average stored energy. The results in Table III indicate that this is not the case. The shifts are, in fact, distributed from 0 to 100% of the average stored energy, and they are even different for different fragments from a given molecule.

2. *Evidence Concerning Density of Electronic States*

The mechanism assumed by Rosenstock *et al.*,[2] for energy randomization within the molecular ion has already been discussed. If this theory applies to the present case of low excitation, the existence of many closely spaced electronic states in the range of energy up to a few volts above the ionization threshold is necessary. In none of the ionization efficiency curves of this work do we find evidence for such a plurality of electronic states. For a single electronic state of a polyatomic molecule, one expects the total ionization efficiency to increase approximately linearly with energy above the rounded portion of the curve near threshold. This linear portion may be regarded, as it was with fractional derivative curves, as the superposition of many individual Heaviside functions. More precisely, the cross section for ionization involves a statistical weight factor giving the number of different ways in which excess energy may be divided between vibrational excitation and kinetic energy of the electron. If the density of vibrational levels is constant in the region of interest, this statistical weight factor increases linearly with energy. In any case, when a number of electronic states are accessible, each should give rise to an increase in slope of the total ionization efficiency curve. If many states are involved, individual states could not be distinguished, but the ionization efficiency curve would exhibit a constantly increasing slope. The curves do not show this. Operation of selection rules would permit some electronic states to be present which would not be evidenced in the ionization curves but which could be instrumental in the energy randomization. However, since the departing electron carries away angular momentum and the molecules considered here have only low orders of symmetry, it is doubtful that selection rules can be very important. Thus, the experimental evidence seems to contradict a fundamental assumption in the theory of Rosenstock *et al.*, when it is applied to the present case of low excitation.

3. *Excess Energies Needed to Give Adequate Rate Constants*

According to Fig. 115, a rate constant of about 5×10^6 sec^{-1} insures that virtually all ions dissociate by the time they emerge from the magnetic field. This corresponds, on fractional derivative curves, to the energy at which the parent derivative curve drops to zero. The excess energy required to give this rate constant may be calculated from Eq. (6). In order to make the calculation, it is necessary to estimate E_0. For the simple abstraction of CH_3, C_2H_5, or C_3H_7, E_0 would normally be determined by comparing the adiabatic ionization potential with the sum of the bond dissociation energy and the ionization potential of the remaining radical. However, in the section on total ionization curves and ionization potentials, it was concluded that the adiabatic ionization potentials cannot be determined by ordinary impact techniques. We are left, therefore, with no reliable means for determining E_0. However, it is unlikely that typical dissociation energies for ground-state molecular ions are much less than for neutral molecules, especially in the case of polyatomic molecules. For the present purposes we will assume that E_0 is not appreciably less than 2v.

To obtain $k=5\times10^5$ sec^{-1} for butane, using $\nu=10^{14}$ sec^{-1} and $E_0=2.0$ ev, we find that $E=4.7$ ev. For octane, making similar assumptions, we find that $E=8.4$ ev. On referring to Figs. 94–105, we see that

parent derivative curves for *n*-butane and *n*-octane become zero at 11.2 and 10.9 ev, respectively. This would imply that the adiabatic ionization potentials for the molecules are 6.5 and 2.5 ev. While the former result cannot be ruled out, it is not possible that the adiabatic ionization potential of *n*-octane is 2.5 ev. Other reasonable values for E_0 and the frequency factor may be tried; but, in general, it appears that the theory of Rosenstock *et al.* requires, for the necessary rate constant, too much excess energy in the molecule. This is particularly true in the case of the large molecules.

4. *Shapes of Fragment and Metastable Curves. Metastable Intensities*

Before calculating theoretical curve shapes, it is necessary to make an assumption concerning the probability distribution function for different degrees of excitation. It is assumed that all partitions of energy between kinetic energy of the *single* departing electron and vibrational excitation of the molecular ion are equally probable. This is equivalent to the assumption that the density of vibrational levels is constant in the energy range of interest. The predicted fragment and metastable curves shapes, then, are generated in the following way. A convenient energy increment ΔE is chosen. On using Eq. (6), with appropriate estimated values for E_0 and the frequency factor, one determines from the curves of Fig. 115 the probability that, for a given energy of excitation, a molecular ion appears as fragment or metastable. This is done for energies equal to $E_0+\Delta E$, $E_0+2\Delta E$, $E_0+3\Delta E$, etc. The nth point on the predicted fragment and metastable curves is then the sum of these probabilities for all energies up to $E=E_0+n\Delta E$. The resulting functions shall be called $F_0(E)$ and $M_0(E)$, respectively.

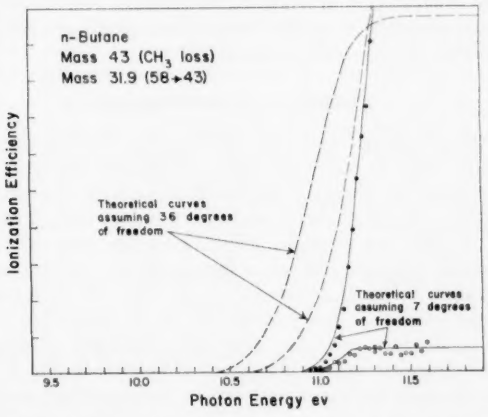

FIG. 116. Comparison between experimental data and theoretical fragment, mass 43, and metastable, mass 31.9 (58→43), ionization efficiency curves for *n*-butane. The theoretical curves are calculated from the statistical theory of dissociation kinetics according to the method given in the section on "Shapes of Fragment and Metastable Curves. Metastable Intensities." Theoretical curves are shown for the full number of degrees of freedom, 36, and for the adjusted number, 7, which results in a predicted metastable intensity which agrees with the experimental value.

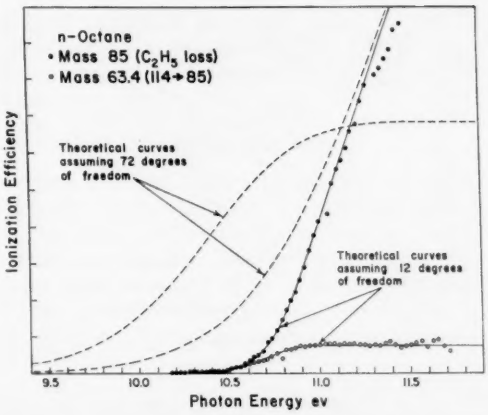

FIG. 117. Comparison between experimental and theoretical fragment, mass 85, and metastable, mass 63.4 (114→85), ionization efficiency curves for *n*-octane. The theoretical curves are calculated from the statistical theory of dissociation kinetics according to the method given in the section on "Shapes of Fragment and Metastable Curves. Metastable Intensities." Theoretical curves are shown for the full number of degrees of freedom, 72, and for the adjusted number, 12. The latter results in a predicted metastable intensity in agreement with the experimental value.

The foregoing has ignored the effect of the stored thermal energy in the molecule. The thermal energy distribution functions, calculated by the method of Appendix I, are given in Figs. 107–109. Assuming that the behavior of the ion is determined by its total excitation energy, i.e., by the sum of its stored thermal energy and the excitation it acquired in the ionization, one expects the fragment or metastable curves to have the form

$$F(E)=\int_0^\infty F_0(E+E')\,P(E')\,dE'$$

and

$$M(E)=\int_0^\infty M_0(E+E')\,P(E')\,dE',$$

where $P(E)$ is the thermal energy distribution function. This integration was performed numerically. The resulting predicted curves for *n*-butane and *n*-octane assuming $E_0=2$ ev and $\nu=10^{14}$ sec^{-1} are given in Figs. 116 and 117, where they are compared with experimental results. The experimental curves were normalized so as to make the slope of the linear portion of the fragment curve equal to the (arbitrary) slope of the predicted curve. The energy scales were placed so as to make these linear portions coincide.

Figures 116 and 117 show that the theory of Rosenstock *et al.* results in a predicted metastable intensity which, for the assumed E_0 and ν, is much too high, and

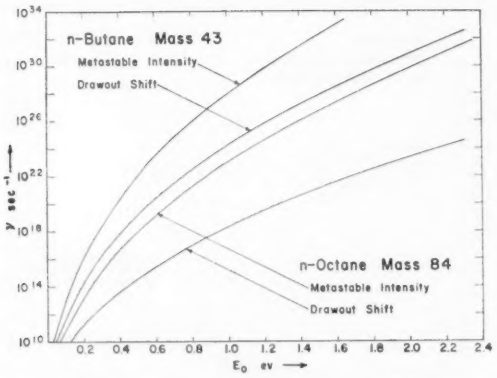

FIG. 118. Relationships between the frequency factor ν and the threshold energy for dissociation E_0, required to give agreement with experimental results on metastable intensity and drawout shifts. Curves are calculated using the assumption that the effective number of degrees of freedom equals the full number.

also in predicted tails on the fragment and metastable curves which are much too large. The agreement can be improved by reducing E_0 or increasing the frequency factor. The relationships between E_0 and ν required to give the observed metastable intensities for *n*-butane (58→43) and *n*-octane (114→84) are given in Fig. 118. Taking, for example, a reasonable well depth of 2 v, one finds that ν must be 10^{26} sec^{-1} for *n*-butane and 10^{30} sec^{-1} for *n*-octane. On the other hand, if one assumes a reasonable frequency factor of 10^{14} sec^{-1}, one finds that the well depth must be 0.13 ev for *n*-butane and 0.25 ev for *n*-octane. Neither these nor any other combination of well depth and frequency factor appear to be physically reasonable.

Another possibility, to improve agreement with theory, is to suggest that all degrees of freedom do not participate in the exchange of energy, and therefore, to reduce the value of n in Eq. (6). This modification will be discussed in a later section.

5. *Drawout Effect*

The curves in Figs. 110–113 show the effect of increasing the drawout time by a factor of 2.3(V_d= 2.5 v) and of decreasing it by a factor of 1.4(V_d=27 v) in comparison with the usual drawout time (V_d=13 v).

With normal drawout voltage, the intercept, on the energy scale, of the linear extrapolation of the theoretical curves corresponds, to good approximation, to the energy required to give a rate constant equal to 5×10^5 sec^{-1}. The shifts in the linear extrapolations can be calculated to sufficient precision by determining, from Eq. (6), the energy change (ΔE_1) required to reduce the rate constant by a factor of 2.3, or the energy change (ΔE_2) required to increase the rate constant by a factor of 1.4. The results of this calculation for *n*-butane (mass 43) and *n*-octane (mass 84) are given in Fig. 118, which also gives the relationships between ν and E_0 required to give the observed shifts ($\Delta E_1+\Delta E_2$). Again, as in the case of the metastable intensities, one cannot find a combination of ν and E_0 which is physically reasonable. Furthermore, the curves for the metastable intensity and drawout shift for a given fragment not only do not cross (which would imply that a specific combination of ν and E_0 could be given which would agree with both experimental results), but also are well separated. This means, that without varying n (a possibility to be discussed later) one cannot find values for ν and E_0 which agree with experimental results.

6. *Missing Metastables*

Examination of Figs. 94–105 shows that when metastables occur, the missing metastables (MM), (see section on metastable ions) as they appear in the fractional derivative curve, are about three times as intense as the ordinary metastables. To obtain the proper theoretical curves to compare with Figs. 94–105, one would have to perform the numerical double integrations described in Sec. 4. These integrations provide for the fact that the total energy of the molecular ion is the sum of thermal energy and excitation energy. One would then differentiate the resulting curves with respect to total energy and divide by the total derivative curve. Without performing these lengthy calculations, however, it is apparent from an inspection of Fig. 115 that, if k varies smoothly with energy as Eq. (6) predicts, the amplitude of the missing metastable (sum of fast and slow metastable) derivative curve should be roughly half that of the ordinary metastable. Thus, regardless of the choice of ν and E_0, the intensities of the missing metastable, even though experimentally uncertain, are in striking disagreement with the theory of Rosenstock *et al.*

7. *Competition between Fragments*

The fractional derivative curves, Figs. 94–105, show many cases in which a number of different fragments compete, i.e., their relative intensities remain constant within a factor of about four over a considerable range of energy. For example, the ratio of the mass 42 to mass 43 fragment intensities from isobutane is constant within a factor of 2 from 11.2 to 11.6 ev, although the onset energies differ by 0.17 ev. It is impossible to reconcile this behavior with the statistical theory. The difficulty may be illustrated as follows. In Fig. 95, the mass 42 fractional derivative curve goes from zero to maximum in about 0.2 ev. This transition is spread out in energy for three reasons: (a) The photon band width is 0.05 ev at half-maximum. Thus, in the absence of all other effects, the transition would require an energy range of about 0.1 ev. (b) The internally stored thermal energy is distributed over a range of values as illustrated, for this particular case, in Fig. 107. Figure 14 and Table III show that the thermal

shift is 0.51 times that to be expected if the thermal energy were fully effective. From this information we estimate that, in the absence of all other effects, thermal energy would broaden the transition by 0.12 ev. (c) There remains broadening due to the kinetics of dissociation. The contributions due to a–c do not combine additively, but approximately as the square root of the sum of the squares. We thus conclude that the rate constant changes from 10^4 sec^{-1} to 10^7 sec^{-1} in about 0.1 ev. At 11.0-v photon energy, i.e., 0.2 ev, above threshold for the first process, the mass 43 appears and competes with the mass 42. This competition occurs in spite of the fact that the process producing the mass 42 will have achieved a very high rate, perhaps 10^{10} sec^{-1}, at this energy. This means that the process producing the mass 43 must: (a) achieve at 11.1 ev a rate comparable to that which the process producing the mass 42 has at that energy; and (b) maintain a rate reasonably close to that of the mass 42 process above 11.1 ev. Requirement (a) can be satisfied by using a sufficiently high frequency factor, but then the rate for the mass 43 process would rise so rapidly that this process would completely dominate at higher energies. Figures 94–105 show many examples of such competition which cannot be reconciled with the statistical theory.

C. Comparison of Experiment with a Modified Statistical Theory

In the foregoing section we have made comparisons of the experimental results with the simple form of the statistical theory. In certain of the sections we made assumptions about E_0 and ν, and in other sections we regarded them as free parameters. Throughout the discussion, however, we regarded the effective number of degrees of freedom as equal to the total number. In each of the comparisons, the agreement of theoretical prediction with the experimental result was not satisfactory. Specifically, temperature effects, missing metastable intensities, and competition between fragments at higher photon energies cannot be brought into agreement with the theory, despite the use of a wide variation in E_0 and ν. We therefore consider the result of allowing n, the effective number of degrees of freedom, to be a free parameter. The use of an effective number of degrees of freedom which is not the total number is not an attractive modification of the theory, because it is difficult to understand how the coupling between some of the oscillators can be strong enough to make use of a statistical theory valid while the coupling with other oscillators is weak enough effectively to exclude them from the dissociation process as treated statistically. Further, if this is so, then the roles of these excluded oscillators in the energetics of the process is not clear, i.e., do they gradually "leak" energy into or away from the active group of oscillators? Nevertheless, such a modification of the theory has been considered by other workers.[3–6] We will, therefore, proceed to re-examine each of the experimental results discussed above, regarding n as a free parameter.

1. *Temperature Effects*

Figures 1–94 and Table III show many instances in which the temperature shift is significantly less than the prediction based on the assumption that all degrees of freedom participate. This may be explained if it is assumed that the number of oscillators participating in a particular dissociation process is less than the total. To calculate an effective number of oscillators from these results is an extremely complicated problem because it would involve a compete understanding of the roles played by each of the oscillators in the dissociation process and in the thermal equilibrium. One crude but simple estimate of the effective number of degrees of freedom may be obtained from the formula

$$n' = n(\Delta AP/\Delta U), \tag{7}$$

where n' is the effective number of degrees of freedom, n is the total number, ΔAP is the temperature shift in the appearance potential, and ΔU is the difference in the average stored thermal energy. As examples for subsequent reference, Eq. (7) gives, for mass 43 from normal n-butane $n'=33$, and for mass 85 from n-octane $n'=53$. As is evident from Table III, n' for different molecules (and even for different dissociation processes in a single molecule) assumes a whole range of values with no obvious systematic behavior. However, allowing n in Eq. (6) to vary does facilitate explanation of the temperature effect. To test the validity of making this variation of the theory we must compare the value of n' obtained from the temperature effect with the values necessary to explain other experimental results.

2. *Evidence Concerning Density of Electronic States*

The previously presented evidence concerning density of electronic states applies equally to a theory in which n is allowed to vary as it does to the original theory. Thus the objection stated there is not removed.

3. *Magnitude of Excess Energy Needed to Give Adequate Rate Constants*

The effect of reducing n in Eq. (6) is that less energy, in excess of the dissociation energy, is required to give a specified rate constant. Referring again to the example of n-octane, we calculate that for $E_0=2$ ev and $\nu=10^{14}$ sec^{-1}, a value for n' of 33 (as computed from the temperature shift) yields $E=4.4$ ev. This corresponds to an adiabatic ionization potential of 6.5 ev. Such a low value is improbable but cannot be ruled out experimentally. Note, however, that any value of n' less than 33 would be equally acceptable. At the present time, therefore, analysis using the odd-

mass fragments cannot be used to determine n' because in addition to the uncertainty in E_0 and ν, the adiabatic ionization potential is also uncertain.

A more definitive argument can be made using the even mass fragments. The best example is the mass 42 fragment from 2,3-dimethylbutane,

$$(CH_3)_2CHCH(CH_3)_2+h\nu\rightarrow C_3H_6^+ + C_3H_8 + \text{kinetic shift} + \text{fragment energy} \quad (8)$$

$$(CH_3)_2CHCH(CH_3)_2+\Delta(\Delta H_f)+I(C_3H_6) \rightarrow C_3H_6^+ + C_3H_8. \quad (9)$$

Subtracting these equations,

$$\text{kinetic shift} \leq h\nu-\Delta(\Delta H_f)-I(C_3H_6). \quad (10)$$

From Table III, reaction 42, $h\nu$ (0°K) = 10.69$_5$ ev; from footnote 21, $\Delta(\Delta H_f)=0.94$ ev and from Table II, $I(C_3H_6)=9.73$ ev. Thus the calculated kinetic shift is equal to or less than 0.02 ev. Considering the errors in the values and the possible systematic error in assuming that the temperature effect can be scaled linearly, we believe that an absolute upper limit for the kinetic shift is 0.06 ev. The process involved here is not a simple dissociation, and for processes of this kind Rosenstock *et al.*[2,4] use an equation for k which is different from Eq. (6). For our present purpose, we will continue to use Eq. (6), but will replace ν with a coefficient which is two orders of magnitude smaller than a normal frequency factor (see footnotes 3 and 6).

On assuming $E_0=2$ ev and the coefficient of the power term $=10^{12}$ sec^{-1}, a maximum of 5 degrees of freedom is required to account for the maximum possible kinetic shift. By contrast, the thermal shift leads to a value of 34 for the number of degrees of freedom.

Subject to this assumption this evaluation is open to question only in so far as the ionic product might be cyclo-propane rather than propene as assumed. Data are not available to evaluate this possibility.

4. *Shapes of Fragment and Metastable Curves. Metastable Intensities*

As discussed earlier, the calculated shapes of fragment and metastable ionization efficiency curves, as well as the metastable intensity assuming $E_0=2$ ev, $\nu=10^{14}$ sec^{-1} and n equal to the total number of oscillators, are in striking disagreement with the experimental results. On using the methods previously described, with n now taken to be a free parameter, we have calculated fragment and metastable curves for the mass 43 fragment from n-butane and the mass 85 from n-octane. In performing this calculation the thermal energy distribution function has been scaled down by the ratio of the temperature shifts to the difference in stored energy (see Table III). The value of n' which gives agreement with experiment, i.e., which predicts the correct metastable intensity, is 7 for n-butane and 12 for n-octane. The resulting curves are shown in Figs. 116 and 117, where they are compared with the experimental points. While the agreement is quite good, it should be noted that for these small values of n the shapes of the curves are determined principally by the thermal energy distribution functions, Figs. 107 and 109. The values of n' determined from the metastable intensities, 7 for n-butane and 12 for n-octane, disagree markedly with the values of 33 and 53 obtained from the temperature shifts.

5. *Drawout Effect*

As discussed before, agreement between predicted and experimental drawout shifts, maintaining n equal to the total number of oscillators, can be obtained only by assuming physically unreasonable values for ν and/or E_0. If reasonable values for ν (10^{14} sec^{-1}), and E_0 (2 ev) are used, n' can be determined by demanding a correct prediction for the drawout shifts (Figs. 110–113). The results are, for the mass 43 fragment from n-butane, $n'=8$, and for mass 85 from n-octane, $n'=19$. These values are in poor agreement with those itemized in the previous section.

6. *Missing Metastables*

Experimentally, the intensities of the missing metastable derivative curves (Figs. 94–105), are about three times those of the ordinary metastable. To obtain a fractional derivative curve for the missing metastable which is larger than that for the ordinary metastable, the rate constants in the range 10^6 to 10^7 sec^{-1} (see Fig. 115) must have a much greater weight than the lower rate constants. Equation (6) gives a relation between log$k$ and energy which does not depart strongly from linearity. The derivative of log$k$ with respect to energy decreases with energy. This tendency becomes more pronounced as n' decreases. This somewhat enhances the importance of the higher values of k. Even with $n'=1$, however, the contribution of rates around $k=5\times10^6$ sec^{-1} cannot be accentuated enough to produce agreement with the experiment.

The large intensity of the missing metastables presents a striking disagreement with the statistical theory, since it appears that no theory which assumes the dissociation to be rate-determined and predicts a smooth dependence of rate upon energy can give this result. The argument is weakened by the fact that the metastable intensities are quite uncertain. Should they be incorrect, even by a factor of two, the argument is still strong.

7. *Competition between Fragments*

Reduction of n in Eq. (6) has the effect of making rate constants change more rapidly with energy. This modification of the theory causes more difficulty in explaining competition between decay processes over a range of energies than does the assumption of

the full number of degrees of freedom. This competition, like the missing metastable intensities, coupled with other experimental facts discussed previously, is an effect which, as long as reasonable values of E_0 and ν are used, cannot be reconciled with any statistical theory.

BOND DISSOCIATION ENERGIES

Since, in the light of the preceeding discussion, we do not know the true thresholds for the production of fragment ions of odd mass, and since we do not have reliable values for the adiabatic ionization potentials of the radicals, we cannot determine, from the present data alone, the absolute value of any bond dissociation energy. To the extent that the kinetic shifts are all equal, the data can be used to determine *differences* in bond dissociation energies.[29] Because we have no direct method of determining whether or not the kinetic shifts for different processes are equal, we will proceed to calculate bond dissociation energies assuming that the shifts are all equal. If the results are inconsistent, the inconsistency can be used as a measure of the differential shifts.

In calculations of differences in bond dissociation energies, two situations arise in which one might expect appreciable differential shifts. The first is the case of a difference taken between the lowest energy dissociation for any molecule and any other fragmentation which is not the lowest energy dissociation of a molecule. The other is a difference taken between a C—C bond break and a C—H bond break. These two situations occur in Table IV only in calculations which involve the threshold for the formation of $C_3H_7^+$ from C_3H_8. This ion is used in all calculations either directly or indirectly as the CH_3—H bond dissociation energy. This threshold is therefore treated in a special way in Table IV as will be discussed later. The same difficulty is involved when treating data on the even mass peaks.

The primary results obtained in the present work are differences in bond dissociation energies. In order to put these energies on an absolute basis, it is necessary to know the absolute value for one dissociation energy. The value employed is the dissociation energy of the H_2 molecule which, when combined with the appropriate heats of formation, yields absolute bond dissociation energies for the hydrocarbons studied in this work.

A review of the fragment ionization efficiency curves indicates that a large share of the curves are linear over a considerable energy range. As observed in an earlier section, this linear portion reflects the linearity of the total ionization efficiency curve when only a single fragmentation process is involved. Examination of Figs. 1–88 shows that, apparently, competition between fragments does not alter the essential linearity of fragment curves except at energy intervals corresponding to the onsets of dissociation processes. Evaluation of the experimental thresholds is therefore performed by linear extrapolation to the axis. This extrapolation is justified provided the total ionization curve is linear in the region above the threshold, and provided competition does not obscure the linear characteristic. An example of a case where this method is questionable is that of the first fragment, mass 56, from neo-pentane, where the first fragmentation process (Fig. 31) begins only 0.1 ev above the onset of the parent. Mass 71 from 2,3-dimethylbutane (Fig. 57) illustrates a case in which competition clearly makes meaningful extrapolation difficult.

For all ions of even mass and some ions of odd mass, the form of the ionization curve from the onset to the linear portion is consistent with the expected threshold behavior due to the thermal energy distribution within the molecule and to the resolution of the instrument. For some ions of odd mass, however, the curves near the onset have a much more extended region before linearity. In several cases, notably mass 43 from *n*-butane and *n*-pentane, the curve can be seen to be the sum of two curves of simple type with different thresholds, i.e., a curve which begins with the usual thermal "tail" rounding to a straight portion followed by a second "break," with its own thermal tail. The corresponding breaks do not occur in the curves for ions of mass 43 from *i*-butane and *i*-pentane. The break in the fragment curves from normal compounds thus indicates that two different ions of mass 43 are formed from normal molecules; while, by comparison, only one is formed from the iso molecules. Presumably, the two forms are the primary and secondary ions, the secondary ion being formed directly in the iso molecules, but only after rearrangement in the normals. A lower heat of formation of the secondary ion would explain its observation in the spectrum of *n*-butane at energies below that at which the primary ion could be formed. At energies where formation of the primary ion is possible, its formation is favored because the mechanism forming it is simpler than that forming the secondary ion.

Extension of the foregoing reasoning explains the large tails in the curves of many ions of odd mass from the heavier molecules. The greater internal energy in such molecules obscures the first linear portion, but its presence may be inferred from the excessive rounding of the curve. If the extent of the thermal tail were known accurately, then the intercept could be determined with precision. In the absence of such information, a good estimate of the thermal tail can be made from the curves for ions from molecules of similar size with temperature shifts of similar extent. The position of the first linear portion of the complex curves (Figs. 1–88) has been determined by superimposing the corresponding tail of the curve for a simple process, selected as noted above, on the suitably normalized curve in question.

The thresholds must be corrected to 0°K before they can be used in calculations of bond energies. Since we lack precise information, this temperature correction

TABLE IV. Bond dissociation energies (ev).

Bond	Reactions and bonds used in calculation[a]	Individual determinations	Weighted average values	Adjusted values based on CH_3—H≡4.38 ev	Published values[b]
CH_3—H	5–1	4.56	4.56	4.38	4.38
C_2H_5—H	16–1	4.35	4.34$_5$	4.17	4.17
	10–2+CH_3—H	4.34$_5$			
	22–7+CH_3—H	4.34$_5$			
	36–13+CH_3—H	4.34			
	45–18+CH_3—H	4.47			
	49–20+CH_3—H	4.34$_5$			
	55–47+CH_3—H	4.34$_5$			
p-C_3H_7—H	32–1	4.54	4.54	4.36	4.34
	25–2+CH_3—H	4.54			
	51–7+CH_3—H	4.54			
	57–20+CH_3—H	4.54			
s-C_3H_7—H	41–1	4.55$_5$	(4.55$_5$)	(4.38)	4.21
p-C_4H_9—H	59–7+CH_3—H	4.76$_5$	(4.76$_5$)	(4.58)	4.39
	59–22+C_2H_5—H	4.76$_5$			
	59–51+p-C_3H_7—H	4.76$_5$			
CH_3—CH_3	Twice CH_3—H	3.97$_5$	3.97$_5$	3.62	3.60
	Twice (2–10)+twice C_2H_5—H	3.98			
	Twice (7–22)+twice C_2H_5—H	3.97$_5$			
	Twice (13–36)+twice C_2H_5—H	3.98			
	Twice (18–45)+twice C_2H_5—H	3.72			
	Twice (20–49)+twice C_2H_5—H	3.97$_5$			
	Twice (20–57)+twice p-C_3H_7—H	3.97			
C_2H_5—C_2H_5	Twice C_2H_5—H	3.81	3.80$_5$	3.45	3.39
	Twice (10–2)+twice CH_3—H	3.80$_5$			
	Twice (45–18)+twice CH_3—H	4.06$_5$			
	Twice (22–7)+twice CH_3—H	3.80$_5$			
	Twice (36–13)+twice CH_3—H	3.80			
	Twice (49–20)+twice CH_3—H	3.81			
	Twice (49–57)+twice p-C_3H_7—H	3.80$_5$			
p-C_3H_7—p-C_3H_7	Twice p-C_3H_7—H	4.25$_5$	4.25	3.89	
	Twice (25–2)+twice CH_3—H	4.25			
	Twice (25–10)+twice C_2H_5—H	4.25$_5$			
	Twice (51–7)+twice CH_3—H	4.24$_5$			
	Twice (51–22)+twice C_2H_5—H	4.24$_5$			
	Twice (57–20)+twice CH_3—H	4.25$_5$			
	Twice (57–49)+twice C_2H_5—H	4.25$_5$			
s-C_3H_7—s-C_3H_7	Twice s-C_3H_7—H	4.36$_5$	4.36$_5$	4.00	
p-C_4H_9—p-C_4H_9	Twice p-C_4H_9—H	4.66	4.66	4.30	
	Twice (59–7)+twice CH_3—H	4.65$_5$			
	Twice (59–22)+twice C_2H_5—H	4.65$_5$			
	Twice (59–51)+twice p-C_3H_7—H	4.66$_5$			
C_2H_5—CH_3	5–16+C_2H_5—C_2H_5	3.86	3.86$_5$	3.50	3.69
	16–5+CH_3—CH_3	3.86$_5$			
	2–10+C_2H_5—C_2H_5	3.86$_5$			
	10–2+CH_3—CH_3	3.86$_5$			
	22–7+CH_3—CH_3	3.86$_5$			
	7–22+C_2H_5—C_2H_5	3.86$_5$			
	36–13+CH_3—CH_3	3.86			
	13–36+C_2H_5—C_2H_5	3.86$_5$			
	45–18+CH_3—CH_3	3.99$_5$			
	18–45+C_2H_5—C_2H_5	3.73$_5$			
	20–49+C_2H_5—C_2H_5	3.86			
	49–20+CH_3—CH_3	3.86$_5$			
	55–47+CH_3—CH_3	3.86$_5$			
	47–55+C_2H_5—C_2H_5	3.86			

TABLE IV.—*Continued.*

Bond	Reactions and bonds used in calculation[a]	Individual determinations	Weighted average values	Adjusted values based on CH_3—H=4.38 ev	Published values[b]
p-C_3H_7—CH_3	25–2+CH_3—CH_3	4.11$_5$	4.11	3.75	
	2–25+pC_3H_7–pC_3H_7	4.11			
	32–5+CH_3–CH_3	4.11			
	5–32+pC_3H_7—pC_3H_7	4.11			
	51–7+CH_3—CH_3	4.11			
	7–51+pC_3H_7—pC_3H_7	4.11$_5$			
	57–20+CH_3—CH_3	4.11$_5$			
	20–57+pC_3H_7—pC_3H_7	4.10$_5$			
s-C_3H_7—CH_3	41–5+CH_3–CH_3	4.20	(4.20)	(3.84)	
	[5–41+sC_3H_7—sC_3H_7	4.20$_5$]			
p-C_4H_9—CH_3	59–7+CH_3—CH_3	4.31	4.31	3.95	
	7–59+pC_4H_9—pC_4H_9	4.31$_5$			
p-C_3H_7—C_2H_5	32–16+C_2H_5—C_2H_5	4.02$_5$	4.02$_5$	3.67	
	16–32+pC_3H_7—pC_3H_7	4.03			
	25–10+C_2H_5—C_2H_5	4.02$_5$			
	10–25+pC_3H_7—pC_3H_7	4.02$_5$			
	51–22+C_2H_5–C_2H_5	4.02			
	22–51+pC_3H_7—pC_3H_7	4.03			
	57–49+C_2H_5—C_2H_5	4.02$_5$			
	49–57+pC_3H_7—pC_3H_7	4.02$_5$			
s-C_3H_7—C_2H_5	41–16+C_2H_5—C_2H_5	4.11	(4.11)	(3.75)	
	[16–41+sC_3H_7—sC_3H_7	4.11$_5$]			
p-C_4H_9—C_2H_5	59–22+C_2H_5—C_2H_5	4.23	(4.23)	(3.87)	
	[22–59+pC_4H_9—pC_4H_9	4.23$_5$]			
s-C_3H_7—pC_3H_7	41–32+pC_3H_7—pC_3H_7	4.32	(4.32)	(3.96)	
	[32–41+sC_3H_7—sC_3H_7	4.32]			
p-C_4H_9—pC_3H_7	59–51+pC_3H_7—pC_3H_7	4.45$_5$	(4.45$_5$)	(4.10)	
	[51–59+pC_4H_9—pC_4H_9	4.45$_5$]			

[a] Reactions refer to the reaction identification number as tabulated in Table III.
[b] Footnote 30.

was made by assuming that the difference between the room temperature threshold and that which would be obtained at zero degrees is given by the stored energy at room temperature, multiplied by the ratio $\Delta AP/\Delta U$ from Table III. On using these thresholds, together with the well-known values for the heats of formation of hydrocarbons and the dissociation energy of H_2,[21] we obtain D(R—H) by the following scheme:

$$R'H+h\nu_1=R'^{+}+H \tag{11}$$

$$-RR'-h\nu_2=-R'^{+}-R \tag{12}$$

$$2H=H_2+D(H—H) \tag{13}$$

$$RH+D(R—H)=R+H \tag{14}$$

$$RR'=nC+(n+1)H_2+\Delta H_f^{\circ}{}_{RR'} \tag{15}$$

$$-RH=-mC-(m+1)H_2-\Delta H_f^{\circ}{}_{RH} \tag{16}$$

$$-R'H=-(n-m)C-(n-m+1)H_2-\Delta H_f^{\circ}{}_{R'H}. \tag{17}$$

Addition of these equations yields

$$D(R—H)=D(H—H)+h\nu_2-h\nu_1+\Delta H_f^{\circ}{}_{RR'}-\Delta H_f^{\circ}{}_{RH}-\Delta H_f^{\circ}{}_{R'H}. \tag{18}$$

By similar methods the symmetrical carbon-carbon bond energy, R—R, may be determined from D(R—H). From the values of D(R—R), those of the more general asymmetrical bonds, R—R′, may be determined. To minimize the number of assumptions involved concerning the ion structure, only ions formed by analogous processes are employed; i.e., the molecules in Eqs. (11) and (12) must both lead by simple dissociation to only primary or secondary or tertiary ions. In compliance with this restriction, an assumption must be made concerning the nature of $C_3H_7^+$ from propane. The assumption that a secondary ion is formed in the range of energies studied is consistent with the observed break in the curve for $C_3H_7^+$ from n-butane, and the absence of a break in the similar curve for i-butane. To confirm this assumption, an experiment was undertaken with labeled 2,2-dideuteropropane. The onset for production of the mass 44 ion was observed at a

photon energy consistent with the loss of D from the secondary position. The peak observed at mass 45 was all due to an impurity, C_3H_7D. We thus conclude that the $C_3H_7^+$ fragment from propane is s-$C_3H_7^+$. This experiment is in agreement with similar electron impact experiments.[29]

While, in general, knowledge of the exact structure of the ions is not necessary, because they cancel in bond dissociation energy calculations, the structure of the remaining radical must be known. No ambiguity exists for radicals with one or two carbons. For radicals with three or four carbons, the assumption has been made that no rearrangement occurs.

The bond dissociation energies determined in the above manner are summarized in Table IV. If the various assumptions involved in their determination are valid, then the bond energies offer a number of checks for consistency of the thresholds themselves. These checks indicate that many of the 0°K thresholds employed are consistent within 0.01 ev. In some cases, however, adjustment of the 0°K thresholds within the error limits improves the consistency. However, we are not completely free to change the thresholds, even by 0.01 ev, because, in general, a given threshold is involved in both a positive and a negative sense in the determination of different bonds, and even in different calculations of a given bond.

For the bond dissociation energies tabulated in Table IV we have used a set of appearance potentials adjusted within their error limits to give a "best fit" set of values. The best fit thresholds are tabulated in the last column of Table III. As an example, the C_2H_5—CH_3 bond dissociation energy may be determined in 14 independent ways with the ions $C_3H_7^+$, $C_4H_9^+$, $C_5H_{11}^+$, and $C_6H_{13}^+$ from a variety of molecules, as listed in Table IV. The various determinations give the value 3.86 ± 0.03 ev, omitting calculations involving $C_4H_9^+$ from neo-pentane and 2,2-dimethylbutane, where an unexplained discrepancy exists. Use of the best fit thresholds makes all determinations for this bond, as well as all other bonds, consistent to within ±0.01 ev, with the exception noted above.

Unfortunately, no consistency checks are available for the bonds s-C_3H_7—R and p-C_4H_9—R. These bonds are therefore more uncertain than the others, and consequently are parenthesized in Table IV.

A survey of the literature for bond energy determinations indicates that the generally accepted values are lower than the direct set determined in this paper (Table IV, compare columns 4 and 6).[30] Since a number of previous bond dissociation energy determinations are subject to considerable question, the difference may indicate inaccuracy in the earlier values. On the other hand, the discrepancy might be ascribed to the uncertainties, noted at the beginning of this section, involving formation of mass 43, $C_3H_7^+$, from propane. Use of this ion in calculations involves the two questionable assumptions: comparison of the lowest energy process from one molecule with higher energy processes from other molecules, and comparison of C—C bond breaks with C—H bond breaks. The discrepancies between columns 4 and 6 (Table IV) could thus be ascribed to differential kinetic shifts between the first, or lowest energy, processes forming $C_3H_7^+$ from propane and those of all other ions involved in bond dissociation energies. If the Kistiakowsky value for the CH_3—H bond is presumed correct,[31] then the difference between his value and the value derived here is a measure of the difference in kinetic shifts between H abstraction from propane and all other processes. Such an assumption will not affect the *differences* measured in this work. All the C—H bond energies will be shifted by an equal amount, and all the C—C bond dissociation energies will be shifted by twice this amount (see column 2, Table IV). The values determined by adjusting the threshold energy for reaction 1 to give agreement with Kistiakowsky's value for CH_3—H are listed in column 5, Table IV. At present, no decision can be made between the two explanations for lack of agreement of the CH_3—H value with earlier values.

Heats of formation of the various radicals may be obtained directly from the bond energies. These are listed in Table V. From these the heats of formation of the various ions may be obtained. Such heats of formation are useful in the interpretation of the structure of the ions. They are listed in Table VI. Note that in the case of $C_3H_7^+$, the ions from the isomolecules have a ΔH_f° only 0.03 ev different from that of the products of lower energy process from the normal molecules. This difference is within the precision of appearance potentials and substantiates the assumption that the structure of the $C_3H_7^+$ ion from the isomolecules and from the lower energy process in the normals is the same. The difference between the appearance potential of the lower and upper states in the normal molecules is 0.10 to 0.19 ev. If the preceeding analysis is correct, this value represents the difference between the heat of formation of primary and secondary $C_3H_7^+$. The heat of formation of s-$C_3H_7^+$ so determined is given in column 3 of Table VI.

The heats of formation of $C_4H_9^+$ from all normal molecules as well as i-pentane and 3-methylpentane suggest that these ions have similar structure. The significance of breaks in the curves of the latter two molecules is unexplained, as is the difference in heat of formation of the (presumably) tertiary ions from neopentane and 2,2-dimethylbutane.

The heats of formation of $C_5H_9^+$, in conjunction with breaks in the ionization efficiency curves, can be interpreted into one consistent picture of the structure

[29] D. P. Stevenson, Trans. Faraday Soc. **49**, 867 (1953); Discussions Faraday Soc. **10**, 35 (1951).

[30] T. L. Cottrell, *The Strengths of Chemical Bonds* (Butterworths Scientific Publications, Ltd., London, 1958).

[31] G. B. Kistiakowsky and E. R. van Artsdalen, J. Chem. Phys. **12**, 469 (1944).

and the heats of formation of the various ions produced. However, until the discrepancy in the heats of formation of $C_4H_9^+$ is resolved, such a presentation is not justified.

The present paper has dealt primarily with fragmentation processes leading to ions of odd mass number, $C_nH_{2n+1}^+$, and free radicals of the same general formula, C_mH_{2m+1}. Energetically, however, another fragmentation process is usually favored; during the carbon-carbon bond rupture a hydrogen atom may be transferred, producing an alkene ion, and an alkane. Since the standard heats of formation of such hydrocarbons are known and the adiabatic ionization potential of the alkenes have been measured (Table II), the energy necessary for the formation of these products in their ground states can be calculated. Such energies are usually below the ionization thresholds for the ions of odd mass.

TABLE V. $\Delta H_f°$, radicals, 0°K (ev).

Formula	Structure without rearrangement	$\Delta H°$ From weighted average dissociation energies[a]	$\Delta H°$ From adjusted dissociation energies[b]
CH_3	...	1.63	1.45
C_2H_5	...	1.39	1.21
C_3H_7	Primary	1.45_5	1.27_5
C_3H_7	Secondary	(1.47)	(1.29)
C_4H_9	Primary	(1.50)	(1.32)

[a] Column 4 of Table IV.
[b] Column 5 of Table IV.

Experimentally the thresholds for production of even mass ions are found to be somewhat higher than those calculated. The difference can be ascribed to two major sources. First, the excess energy necessary to produce fragmentation in a relatively short time may raise the thresholds. Second, the products may be formed in excited vibrational states even at the threshold for the dissociation process. That is, the activation energy for the forward direction is much less than that for the reverse direction. Physically this may be seen from the following qualitative argument. The process which produces the alkene ion and the alkane involves the breaking of a C—C bond and the simultaneous transfer of a hydrogen atom to the alkane radical. Such a transition is essentially unidirectional, i.e., the probability of returning to the original state is negligible, in other words there is a large steric barrier. Since the hydrogen is bound more firmly to the alkane, in making the transition the hydrogen will transfer to the alkyl radical with kinetic energy. It, however, picks up this energy *after* the molecule is committed to the particular decay; i.e., dissociation has taken place simultaneously with the transfer. Thus this energy is not available for lowering the threshold. We therefore expect excess vibrational energy in the fragments for even mass peaks. Table VII gives the total excess energy attributed to the two effects discussed above. The energies are also of importance because they are upper limits to the

TABLE VI. $\Delta H_f°$, ions, 0°K (ev).

Parent molecule	$C_3H_7^+$ First process	$C_3H_7^+$ Second process	$C_4H_9^+$	$C_5H_{11}^+$
Propane	8.50	...	...	...
n-Butane	8.53_5	8.64_5		...
i-Butane	8.50_5			...
n-Pentane	8.53_5	8.62	8.24_5	
i-Pentane	8.50_5		8.24	
Neo-pentane	...		7.58	
n-Hexane	8.53_5	8.64	8.24_5	8.07_5
2-Methylpentane	8.50		7.95	7.84_5
3-Methylpentane	...		8.24	7.84_5
2,3-Dimethylbutane	8.50_5		...	7.67
2,2-Dimethylbutane	...		7.71	7.42_5
n-Heptane			8.24	8.07_5
n-Octane			8.24_5	8.08

TABLE VII. Comparison of experimental thresholds for even mass ions with thresholds calculated for the products in their ground state (ev).

Parent molecule	Ion	0°K Threshold comparison (experimental-calculated)
n-Butane	42	0.72
i-Butane	42	0.42
n-Pentane	42	0.43
	56	0.61
i-Pentane	42	0.21
	56	0.34 (?)[a]
n-Hexane	42	0.40
	56	0.55
	70	0.90
2-Methylpentane	42	0.26
	70	0.68 (?)[a]
3-Methylpentane	56	0.09 (?)[a]
2,3-Dimethylbutane	42	0.02
n-Heptane	42	0.40
	56	0.49
	70	0.81
n-Octane	56	0.73
	70	0.81

[a] Uncertainty concerning the structure of the products makes these values tentative.

TABLE VIII. Upper limits for the adiabatic ionization potentials of alkyl radicals (ev).

s-C_3H_7		p-C_3H_7	
Reaction used (Table III)	Value	Reaction used (Table III)	Value
1	7.20_5	3	7.37
2	(7.26)	11	7.44
5	7.21	26	7.36_5
10	(7.25_5)		
16	7.21_5		
25	(7.26)		
32	7.21		

excess energy necessary for dissociation within the ionization chamber.

IONIZATION POTENTIALS OF RADICALS

Assuming that the adjusted set of dissociation energies is correct, the data may be used to calculate the sum of the kinetic shift and the adiabatic ionization potential of some alkyl radicals. If the kinetic shift is zero, the calculations yield the true adiabatic ionization potential. If the kinetic shift is not zero, the calculation may be regarded as giving an upper limit to the adiabatic ionization potential.

In practice the number of these calculations which can be made without ambiguity is limited by uncertainties in the structures of the various ions produced. This situation is in contrast to that of the bond energy calculations where it was necessary to assume only that ions of the same structure were produced from similar molecules. For the present purpose it is necessary to know the actual structure of those ions.

The only ions whose structures can be assigned with some certainty are the primary and secondary $C_3H_7^+$. A variety of different thresholds may be used to calculate the upper limit for the adiabatic ionization potential of these radicals. The values obtained are summarized in Table VIII. As an example, we consider the production of s-$C_3H_7^+$ from C_3H_8,

$$C_3H_8+h\nu\rightarrow s\text{-}C_3H_7^+ + H + \text{kinetic shift} \quad (19)$$

$$C_3H_8 + D_0(s\text{-}C_3H_7\text{—}H) + I(s\text{-}C_3H_7) \rightarrow s\text{-}C_3H_7^+ + H. \quad (20)$$

Subtracting these two equations,

$$I(s\text{-}C_3H_7) = h\nu - D_0(s\text{-}C_3H_7\text{—}H) - \text{kinetic shift}. \quad (21)$$

For this case, from Tables III and IV,

$$h\nu = 11.58_5 \text{ ev and } D_0(s\text{-}C_3H_7\text{—}H) = 4.38 \text{ ev}, \quad (22)$$

so that

$$I(s\text{-}C_3H_7) \leq 7.20_5 \text{ ev}. \quad (23)$$

Calculation of the C_3H_7 ionization potential using ionization thresholds above the first fragmentation process involves a correction which has been evaluated in the section on bond dissociation energies, i.e., the differential kinetic shift (0.18 ev) between the first and higher fragmentation processes. The remaining kinetic shift is then the kinetic shift in the $C_3H_7^+$ threshold from C_3H_8.

The value obtained by Farmer and Lossing[32] for this s-C_3H_7 ionization potential using electron impact on s-C_3H_7 is 7.90 ev. The disagreement with electron impact is similar to that usually obtained and is due in part to the fact that the electron impact method usually used with large molecules measures something different from the adiabatic ionization potential.

DISCUSSION

The conclusions reached in this paper are seemingly all negative. Rather than determining ionization potentials, we have concluded that for the alkanes the adiabatic transition is not accessible in ordinary impact experiments. Instead of arriving at an experimental verification of the statistical theory of dissociation rates, we have found that the theory cannot be made to agree with the totality of the experimental results. A lack of quantitative understanding of the energy excesses needed to make dissociation occur within the ionization chamber prevents an unequivocal determination of bond energies. It is our hope, however, that the present paper with its extensive experimental data, will prompt the development of an improved theory of unimolecular dissociation kinetics, and improved experiments to give further information on this problem. It is the purpose of this section to present suggestions concerning the form of future theories and experiments.

The general lack of agreement between experimental results and the predictions of the statistical theory, together with the experimental evidence that the high density of electronic states necessary to the theory does not occur, leads us to reject the theory as applied to low excitations of molecular ions. Furthermore, complication between the different dissociation processes and the importance of missing metastables cast doubt upon the validity of any theory of dissociation which treats the process as rate-determined, where the rate is some smooth function of energy.

In the absence of a mechanism for rapid randomization of energy among the oscillators in the molecules, the justification for a statistical theory vanishes. However, some mechanism for transfer of energy is required for an explanation of thermal shifts. The anharmonicity of the oscillators provides a coupling mechanism which makes it possible for energy to flow from oscillator to oscillator. To be more precise, the presence of the anharmonicities makes it impossible to find a normal mode representation in terms of which the energy

[32] J. B. Farmer and F. P. Lossing, Can. J. Chem. **33**, 861 (1955).

matrix is diagonal. Approximately normal modes may be found, but the energy "contained" in each is not constant; it varies with time in a manner determined by the magnitudes of the anharmonic terms. Thus energy may be said to flow from mode to mode. We regard this as a mechanism for energy *transfer* from oscillator to oscillator, but not as a mechanism for energy *randomization* as required in the statistical theory. Dissociation is thought to occur in a manner which is more closely describable in terms of assumptions similar to those of Slater's theory of unimolecular reactions.[28] His detailed calculations do not apply, however, because he did not consider the zero pressure case.

The dissociation process is pictured as taking place as follows. Photoionization produces a molecular ion with excitation energy distributed among its oscillators in a way determined by the initial distribution of thermal energy and by the detailed nature of the ionization transition. The system of oscillators then undergoes a complicated motion, the amplitudes of motion changing with time in a manner determined by the anharmonicities, until a "reaction coordinate" (see footnote 28) reaches a critical extension, at which time the corresponding dissociation takes place. According to this picture, the lifetime of the ion and its mode of dissociation are determined at the time of formation of the ion, i.e., by the amplitudes and phases of the oscillators in the ion at the time of its formation, and possibly by the isomeric form of the ion. The particular dissociation which occurs is determined by whichever reaction coordinate happens to reach a critical extension first. In this picture different dissociation processes do not compete with each other on the basis of relative rate constants. There is no reason why the branching between different modes of dissociation may not be almost constant over a range of energies, as is the experimental situation. There are other reasons for believing that a theory which treats dissociation as rate determined may not be applicable. In rate-determined processes, the probability per unit time that the process occurs is a constant independent of time. In the foregoing there appears to be no reason for supposing that this is so. The most probable elapsed time before decay, i.e., most probable lifetime, in rate-determined dissociation is zero. By contrast, it would seem that the actual probability that a molecule dissociates immediately after ionization is very small. The ionization transition probably results in rather general excitation of the oscillators; and it would seem that some minimum time is required before this energy, together with thermal energy, redistributes in such a way as to permit any dissociation. In this connection, it is of interest to note that, if a few decays occur immediately after ionization, but a large number occur after a time interval of 10^{-6} to 10^{-7} sec, the intensity of the missing metastables would be explained.

A quantitative theory based on these qualitative ideas would perhaps be organized into two parts: (1) the distribution of lifetimes as a function of energy would be calculated, on the basis of assumptions similar to Slater's, in terms of elapsed time occurring before *any* reaction coordinate reaches a critical extension. It would be necessary to average over the different initial states of the molecular ion. (2) The branching ratios into the different modes of dissociation as functions of energy would be calculated, again, averaged over the initial states. It might be possible to treat this problem in terms of dissociation channels in multidimensional phase space, and possibly in terms of *relative* numbers and "cross-sections" of the channels corresponding to different decay modes.

After study of the present results, it is possible to suggest refinements in the experiments here described, as well as additional experiments.

Since the most striking disagreement of theory with experiment occurs in the cases of the missing metastable ions and in the observations of competition between different dissociation processes, it is extremely important to reduce the uncertainties in these measurements. To improve these measurements, it will be necessary to develop light sources of much greater intensity and/or to improve the efficiency of the monochromator. It would also be highly desirable to extend the range of photon energies.

Using a photon beam of greatly increased intensity has the additional advantage that one would be able to follow the tail of the parent ionization curve further down in energy. If such data show that below some energy the ionization drops rather quickly to zero, this energy would correspond to the adiabatic ionization potential.

Data which would be of great value in improving the determination of the bond dissociation energies and the kinetic shifts would be direct determinations of the adiabatic ionization potentials of the alkyl radicals. These could perhaps be determined by photoionization of the alkyl radicals produced by pyrolysis or possibly by photolysis. Experiments of this type using electron impact have been performed by a number of workers.[32,33]

The ideal experiment would involve measurement of the ionization efficiency curves at 0°K, with complete control over the elapsed time between photoionization and mass analysis. A step in this direction would be to build equipment capable of operation at the lowest temperature consistent with the requirement of an adequate vapor pressure, and to provide drift spaces or ion traps which would allow variation over a wide range of the elapsed time from ionization to analysis. An

---

[33] See, for example, J. A. Hipple and D. P. Stevenson, Phys. Rev. **63**, 121 (1943); F. P. Lossing and A. W. Tickner, J. Chem. Phys. **20**, 907 (1952); F. P. Lossing, K. U. Ingold, and A. W. Tickner, Discussions Faraday Soc. **14**, 34 (1953); F. P. Lossing, K. U. Ingold, and I. H. S. Henderson, J. Chem. Phys. **22**, 1489 (1954).

TABLE IX. Adjusted frequencies[(cm⁻¹)] used in calculation of thermal energy distribution.

n-Butane $\omega_0=115$ cm^{-1}	*n*-Hexane $\omega_0=77$ cm^{-1}	*n*-Octane $\omega_0=55$ cm^{-1}
115 (1)	77 (1)	55 (2)
230 (2)	154 (2)	165 (3)
345 (2)	308 (6)	330 (8)
1035 (13)	1001 (15)	1045 (10)
1495 (8)	1309 (16)	1375 (23)
2990 (10)	2926 (14)	2915 (18)

alternative would be a pulsed light source combined with gated counting equipment. One would hope that experiments of this type will be undertaken in the future.

APPENDIX

Calculation of Thermal Energy Distributions

Thermal energy distributions were calculated for *n*-butane, *n*-hexane, and *n*-octane. To make these calculations it was necessary first to assign a complete set of vibration frequencies. To make the calculations tractable, the frequencies were all adjusted to be expressible as integral multiples of a base frequency. These adjusted frequencies are given in Table IX.

For *n*-butane the assignments are identical to those used by Chupka.[6] These are based on a summary by Pitzer.[34] For *n*-hexane and *n*-octane, the spectral assignments of Stepanov[35] provide all of the frequencies except for out-of-plane motions and the CH_3 torsional oscillations.

The out-of-plane frequencies for *n*-hexane were taken from Pitzer[34] and those for *n*-octane were estimated using the methods of Pitzer. The CH_3 torsional oscillation frequencies were taken to be the same for all three molecules and were estimated by assuming, with Pitzer, a reduced moment of inertia of 5×10^{-40} g-cm^2 and a sinusoidal well with a 3600-cal barrier to free rotation.

In thermal equilibrium, the probability that the set of oscillations will contain a total energy $E=nhc\omega_0$, where n is an integer, is given by

$$p=Se^{-E/kT},$$

where S the statistical weight, is given by

$$S=\sum_{a,b,c,d,\cdots}\left(\frac{M!}{a_0!a_1!\cdots}\right)\left(\frac{N!}{b_0!b_1!\cdots}\right)\left(\frac{O!}{c_0!c_1!\cdots}\right)\times\left(\frac{P!}{d_0!d_1!\cdots}\right)\cdots,$$

where M = the number of oscillators of type A, N = the number of oscillators of type B, etc., a_r = the number of oscillators of type A with r quanta, b_s = the number of oscillators of type B with s quanta, etc., and the sum is carried out subject to the conditions

$$\sum_r a_r=M,\ \sum_s b_s=N,\ \cdots$$

$$\sum_r ra_r\alpha+\sum_s sb_s\beta+\cdots=n;$$

α = the frequencies of the oscillators (expressed in units of ω_0) of type A, β = the frequencies of the oscillators (expressed in units of ω_0) of type B, etc. However, from an extension of the treatment of Fowler,[36] S is just equal to the coefficient of Z^n in

$$(1+Z^\alpha+Z^{2\alpha}+\cdots)^M(1+Z^\beta+Z^{2\beta}+\cdots)^N\times(1+Z^\gamma+Z^{2\gamma}+\cdots)^O\cdots.$$

The calculation then reduced to multiplying together six multinomials (seven in the case of *n*-octane) by hand calculation. The coefficients of the resulting products were then the required values for S. The thermal energy distributions obtained gave an average energy approximately 20% lower than the thermodynamic data of Table III. We believe, however, that the shape of the distribution is essentially correct. Figures 107–109 give these distributions with the abscissa modified to give the measured average energy.

ACKNOWLEDGMENTS

We wish to express our appreciation to Fred Elder for his enthusiastic assistance during the latter half of the work reported in this paper. The work was presented at the 137th meeting of the American Chemical Society. We appreciate their releasing that paper and permitting publication in *The Journal of Chemical Physics*.

[34] K. S. Pitzer, J. Chem. Phys. **8**, 711 (1940).
[35] B. Stepanov, Acta Physicochim. **22**, 238 (1947).
[36] R. H. Fowler, *Statistical Mechanics* (The Macmillan Company, New York, 1936), 2nd ed., pp. 31–33.

THE JOURNAL OF CHEMICAL PHYSICS VOLUME 34, NUMBER 1 JANUARY, 1961

On the Fluorine Molecule. Part I.* The Pilot Calculation

KATSUNORI HIJIKATA†

Physics Department, University of Oklahoma, Norman, Oklahoma

(Received July 13, 1959)

The energy levels of the fluorine molecules F_2 are calculated by ASMO method. First and second quantum orbitals and configurations therefrom are all taken into account, resulting in $D_0=1.99$ ev and $R_e=1.41$ A. Vertical excitation energies of $^1\Sigma_g^+-{}^1\Pi_u$ and $^1\Sigma_g^+-{}^3\Pi_g$ are 5.21 ev and 3.93 ev, respectively. The importance of the configurations and of the inner-shell electrons to the ground state is discussed. Finally, the ionicities of the states are evaluated.

INTRODUCTION

WHEN the electronic structure of a molecule is investigated as a quantum-mechanical many-body problem, enormous difficulties in computation prevent us from obtaining exact solutions. The most conventional way out of these difficulties is to rely on the molecular orbital picture, in which the behavior of each electron is assumed to be described by a molecular orbital (MO). Usually and most simply, the molecular orbitals are composed as the linear combinations of the atomic orbitals of the constituent atoms (LCAO). All the electrons are assigned to these LCAO MO's, representing an electronic configuration. The wave function (MWF) of a state of the molecule is expressed by a linear combination of the antisymmetrized products of these LCAO MO's in conformity with the symmetry property of the state. The actual molecular state, however, is not precisely described by a MWF for a single configuration, but by a linear combination of MWF's for infinite number of configurations, the coefficient of which are so determined that the total energy of the state may be stationary. In ordinary treatments a limited number of configurations are taken into account to give a tractable description of the real molecular state.

The method mentioned above, that is, the method of antisymmetrized products of molecular orbitals (ASMO), has been applied to several molecules composed of the second row elements. A few diatomic molecules have been worked out to the extent of approximation that we are taking in this work.[1-3] Although the nature of the approximation does not enable us to expect the precise results in agreement with the spectroscopic data, various features of the molecules have been better understood after these treatments. In this series of papers the author will mainly describe the application of ASMO method to the fluorine molecule F_2, the result of which will be compared with the experimental data. The MO's are restricted up to those based on the second quantum atomic orbitals. Since the 1*s* electrons are located deep enough in the fluorine atom the configurations of the molecule with 1*s* vacancy may be neglected, and thus there are 120 states, some of which are degenerate in the absence of spin-orbit rotational interactions. This does not mean, however, that the effect of 1*s* electrons is entirely neglected, since in a particular state the 1*s*-core contributes to the total energy through the core energy itself and through the interaction with the higher orbitals.

Part I of this series is called the pilot calculation, in which is performed the calculation with two pairs of parameters

$$\alpha=\delta_1 R \qquad 20.0 \qquad 25.0$$

$$\beta=\delta_2 R \qquad 6.0 \qquad 7.5,$$

where δ_1 and δ_2 are the effective nuclear charges of the first and the second quantum orbitals of the atom, and R is the interatomic distance. The value of the effective nuclear charges are $\delta_1=8.665\cdots$ and $\delta_2=2.600\ldots$ which almost minimize the total energy of the ground state of the fluorine atom and give round numbers for α and β with $R=2.308$ and 2.885 a.u. (1.221 and 1.526 A). (Throughout this work we used the atomic units 27.204 ev and 0.529 A.) The total energies of the ground state and the excited states are calculated. In this part the discussion is concentrated mainly on the technical aspect of the calculation.

In Part II the calculation is refined by taking several sets of effective nuclear charges which really minimize the total energies of various atomic constituents. We see how the calculated dissociation energy varies with the choice of effective nuclear charges. The full discussion on the adiabatic potential curves of the variety of states is also developed. Furthermore, the same type of calculations are applied to F_2^+ in its lower states which will reveal some particularities of the fluorine molecule and its ion.

* The greater part of the work incorporated in Part I was performed when the author was at the Mallinckrodt Chemical Laboratory, Harvard University.

† In sojourn from the University of Electro-Communications, Tokyo, Japan.

[1] M. Kotani, Y. Mizuno, K. Kayama, and E. Ishiguro, J. Phys. Soc. Japan **12,** 707 (1957).

[2] E. Ishiguro, K. Kayama, M. Kotani, and Y. Mizuno, J. Phys. Soc. Japan **12,** 355 (1957).

[3] H. Brion, C. Moser, and M. Yamazaki. J. Chem. Phys. **30,** 673 (1959).

TABLE I. Coefficients of the orthogonalized MO's.

	$R=1.221$ A	$R=1.526$ A
A	−0.25122 72	−0.24259 88
A'	−0.22708 38	−0.23571 22
B	−0.19615 91	−0.10496 22
B'	0.29075 77	0.12492 60
C	0.02860 54	0.10954 24
C'	−0.04533 12	−0.02352 53
$N(k_g)$	0.70710 67	0.70710 68
$N(k_u)$	0.70710 69	0.70710 68
$N(s_g)$	0.66673 36	0.69860 45
$N(s_u)$	0.81081 72	0.76200 71
$N(\sigma_g)$	0.64371 69	0.66650 91
$N(\sigma_u)$	0.85433 17	0.76711 28
$N(\pi_g)$	0.74073 64	0.71859 99
$N(\pi_u)$	0.67767 75	0.69582 12

ORBITALS AND STATES

The atomic orbitals on which our calculations are based are hydrogenlike:

$$(1s)=(\delta_1^3/\pi)^{\frac{1}{2}}\exp(-\delta_1\gamma),$$

$$(2s)=(\delta_2^5/3\pi)^{\frac{1}{2}}r\exp(-\delta_2 r),$$

$$(2p\sigma)=(\delta_2^5/\pi)^{\frac{1}{2}}r\exp(-\delta_2 r)\cos\theta,$$

$$(2p\pi^{\pm})=(\delta_2^5/\pi)^{\frac{1}{2}}r\exp(-\delta_2 r)\sin\theta\exp(\pm i\phi).$$

Let two fluorine atoms be called a and b, and denote the atomic orbitals belonging to a particular atom with the suffix a or b. We construct the LCAO MO's which are orthogonal to each other and conform to the symmetry of the molecule:

$$k_g=N(k_g)\{(1s)_a+(1s)_b\}$$

$$k_u=N(k_u)\{(1s)_a-(1s)_b\}$$

$$s_g=N(s_g)\{[(2s)_a+(2s)_b]+A[(1s)_a+(1s)_b]\}$$

$$s_u=N(s_u)\{[(2s)_a-(2s)_b]+A'[(1s)_a-(1s)_b]\}$$

$$\sigma_g=N(\sigma_g)\{[(2p\sigma)_a+(2p\sigma)_b]+B[(2s)_a+(2s)_b]+C[(1s)_a+(1s)_b]\}$$[4]

$$\sigma_u=N(\sigma_u)\{[(2p\sigma)_a-(2p\sigma)_b]+B'[(2s)_a-(2s)_b]+C'[(1s)_a-(1s)_b]\}$$

$$\pi_g^{\pm}=N(\pi_g)\{(2p\pi^{\pm})_a-(2p\pi^{\pm})_b\}$$

$$\pi_u^{\pm}=N(\pi_u)\{(2p\pi^{\pm})_a+(2p\pi^{\pm})_b\}.$$

The normalization constants and the orthogonalization coefficients are listed in Table I. The suffixes g and u represent symmetric and antisymmetric properties, respectively, under the inversion in the center of the molecule. At infinite separation of the atoms all the orthogonalization coefficients tend to zero except A and A' which become $A_0=-0.23915\,55$. Namely, s_g and s_u tend to the linear combinations of $2s$ orbitals orthogonalized to $1s$,

$$N[r\exp(-\delta_2 r)+A_0\exp(-\delta_1 r)].$$

The antisymmetrized products constructed from these MO's are all orthogonal to one another, and this orthogonality gives a great technical advantage to ASMO method.

The orbital energies of the LCAO MO's of the fluorine molecule are believed to be in the order

$$k_g,\ k_u,\ s_g,\ s_u,\ \sigma_g,\ \pi_u^{\pm},\ (\text{or } \pi_u^{\pm},\ \sigma_g),\ \pi_g^{\pm},\ \sigma_u.$$

The 18 electrons are located in these 10 LCAO MO's, each having the capacity of two electrons. The electronic configurations in which k-orbitals are unfilled may be disregarded, since their contributions are practically insignificant and much less important than those arising from the neglected higher quantum orbitals.[5] Thus, the possible electronic configurations are as shown in Table II. These configurations are simply denoted by their electron defects in the first column. In the second column are shown the molecular states belonging to these configurations. There are 8 $^1\Sigma_g^+$, 5 $^1\Sigma_u^+$, and $^3\Sigma_u^+$, 4 $^1\Pi_u$, $^1\Pi_g$, $^3\Pi_u$, and $^3\Pi_g$, 2 $^1\Delta_g$, $^3\Sigma_g^-$, and $^3\Sigma_g^-$, and 1 $^1\Sigma_u^-$, $^1\Delta_u$, $^3\Sigma_u^-$, and $^3\Delta_u$. There is no $^1\Sigma_g^-$. Of these states, the $^1\Sigma_g^+$ state is supposed to be the ground state of the fluorine molecule.

The MWF's for these molecular states are expressed by the antisymmetrized products, for instance,

$$^1\Sigma_g^+,\quad (\sigma_u^2)\sim\mathfrak{A}(k_g\bar{k}_g k_u\bar{k}_u s_g\bar{s}_g s_u\bar{s}_u\sigma_g\bar{\sigma}_g\cdot\pi_u^+\bar{\pi}_u^+\pi_u^-\bar{\pi}_u^-\pi_g^+\bar{\pi}_g^+\pi_g^-\bar{\pi}_g^-),$$

which is denoted by $|\sigma_u\bar{\sigma}_u|$, meaning two σ_u defects, or by their linear combinations conforming to the symmetry and the multiplicity of the state; $\mathfrak{A}$ is the antisymmetrizer and the symbols χ and $\bar{\chi}$ mean the MO's with plus and minus spin, respectively. The MWF's are shown in the second column of Table III.

TABLE II. Configurations and states.

(σ_u^2)	$^1\Sigma_g^+$	$(\pi_g\pi_u)$	$^{1,3}\Sigma_u^{\pm}$, $^{1,3}\Delta_u$
(π_g^2)	$^1\Sigma_g^+$, $^1\Delta_g$	$(\pi_g\sigma_g)$	$^{1,3}\Pi_g$
(π_u^2)	$^1\Sigma_g^+$, $^1\Delta_g$	$(\pi_g s_u)$	$^{1,3}\Pi_u$
(σ_g^2)	$^1\Sigma_g^+$	$(\pi_g s_g)$	$^{1,3}\Pi_g$
(s_u^2)	$^1\Sigma_g^+$	$(\pi_u\sigma_g)$	$^{1,3}\Pi_u$
(s_g^2)	$^1\Sigma_g^+$	$(\pi_u s_u)$	$^{1,3}\Pi_g$
$(\sigma_u\pi_g)$	$^{1,3}\Pi_u$	$(\pi_u s_g)$	$^{1,3}\Pi_u$
$(\sigma_u\pi_u)$	$^{1,3}\Pi_g$	$(\sigma_g s_u)$	$^{1,3}\Sigma_u^+$
$(\sigma_u\sigma_g)$	$^{1,3}\Sigma_u^+$	$(\sigma_g s_g)$	$^{1,3}\Sigma_g^+$
$(\sigma_u s_u)$	$^{1,3}\Sigma_g^+$	$(s_u s_g)$	$^{1,3}\Sigma_u^+$
$(\sigma_u s_g)$	$^{1,3}\Sigma_u^+$		

[4] The z axis of each atom is directed toward the other atom.

[5] In the case of O_2, the inclusion of $1s$-vacancy configurations lowered the total energy by 0.0005 a.u. (Private communication from M. Kotani.)

If the atoms are separated to infinity, these molecular states tend to so-called valence states, each being expressed by a simple linear combination of the wave functions expressing the stationary states of the atomic constituents. Since the LCAO MO's are composed of AO's having the principal quantum numbers 1 and 2, these stationary states must be ^1S of F^-, ^2P and ^2S of F, and ^3P, ^1D, ^1S, $^3P'$, ^1P and $^1S'$ of F^+. Table III shows how the MWF's are related to the atomic wave functions, which are denoted by the notations of atomic terms. The numbers in the parentheses after the atomic term symbols mean the orbital angular momentum components with respect to the bond axis. There are two ^3P and two ^1S state of F_2^+, the latter having the configuration interaction to give the mixing coefficients p and q. If the antisymmetrized atomic wave function of the atom a in the stationary state Q is denoted by $(Q)_a$, that is,

$(Q)_a$ =linear combination of

$$\mathfrak{A}_a[(1s)_a(\bar{1}\bar{s})_a(2s)_a(\bar{2}\bar{s}_a)\cdots]$$

the so-called composite atomic function at infinity separation is in the form

$$QQ=\mathfrak{A}(Q)_a(Q)_b{}^6$$

for equivalent states of atom a and b, and in the form

$$QQ'=(1/\sqrt{2})\mathfrak{A}\{(Q)_a(Q')_b\pm(-1)^i(Q')_a(Q)_b\},$$

for nonequivalent atomic states. The $\pm$ sign corresponds to g and u state of the molecule and i is the parity of the combined state. Table III relates MWF's to these composite atomic functions.

ASMO METHOD

The Hamiltonian of the system is of the form

$$\mathfrak{H}=\sum_i\mathfrak{H}_i{}^0+\tfrac{1}{2}\sum_{ij}r_{ij}{}^{-1}+(Z^2/R),$$

$$\mathfrak{H}_i{}^0=-\tfrac{1}{2}\Delta_i-(Z/r_{ai})-(Z/r_{bi}),$$

where i and j are the numbering of electrons, R is the internuclear distance and $Z=9$. Express a particular symmetry species by Ω and the MWF's belonging to the species by Ω_1, Ω_2, $\cdots$. The elements of the energy matrix of the molecular state Ω are given by

$$H_{mn}=\int\Omega_m{}^*\mathfrak{H}\Omega_n d\tau,$$

where the integration is with respect to all the coordinates and spins. The actual molecular stationary states are represented by linear combinations of Ω_m,

$$\mathbf{\Omega}_l=\sum_m c_{lm}\Omega_m,$$

the coefficients c_{lm} being determined by solving the secular equation

$$|H_{mn}-E|=0,$$

which has roots $E_l(l=1, 2, \cdots)$. The matrix elements H_{mn} are expressed in terms of the integrals of MO, which are further reduced into the integrals of AO, χ_a and χ_b. These integrals are tabulated in Tables IV and V.[7]

The most laborious part of this work is to evaluate these atomic integrals. The integrals in which all the AO's have equal effective nuclear charge are evaluated in the tables by Kotani *et al.*[8,9] However, those including $1s$ and other orbitals were not given when we started this work. The method of evaluation is mainly based on the expansion of $1/r_{ai}$ and $1/r_{ij}$ in terms of Legendre polynomials. This method reduces some of the exchange and the hybrid integrals to infinite series which converge very slowly. The first 7 terms were taken in order to obtain accuracy to the 6th decimal place. In Table V, therefore, the numbers in the 7th digit are not accurate. Although the author started with 14 digit numbers for the basic functions, denoted by A and B in Kotani's table,[10] the recurrence formula used afterward decreased the accuracy enormously.

These atomic integrals were combined into the integrals of the orthogonalized MO's by use of the IBM 650 at the Carnegie Institute of Technology. This calculation was only subject to the usual rounding-off errors. Finally, the matrix elements of the Hamiltonian were constructed from these molecular integrals; this process introduced errors into 5th decimal place. The matrix elements for $^1\Sigma_g{}^+$ are shown in Table VI. The diagonal elements are $H_{mn}-E_\infty$, where E_∞ means the energy of the ground state of the neutral fluorine atoms calculated with the orthogonalized AO's. That is,

$$E_\infty=2\times(-98.93430\,9).$$

The solution of the secular equations for all the states were carried out on the IBM 650 at the Bell Telephone Laboratory, Murray Hill, New Jersey, accurate to the fourth decimal places.

DISCUSSIONS

The roots of the secular equations for $^1\Sigma_g{}^+$ are shown in Table VI, the lowest of which are -1.220 ev at

[6] We must take account of the appropriate spin factor.

[7] The author took the notations of integrals in C. C. J. Roothaan, J. Chem. Phys. **19,** 1445 (1951), and K. Rüdenberg, J. Chem. Phys. **19,** 1459 (1951). Since the complex π-orbitals are used, an additional definition is necessary for

$$(2p\pi^+2p\pi^+\,|\,2p\pi^-2p\pi^-)$$
$$=\int[2p\pi^+(1)]^*[2p\pi^-(2)]^*(1/r_{12})[2p\pi^-(1)][2p\pi^+(2)]d\tau_{12}$$
$$=(+--+).$$

The last notation is that in the tables by Kotani *et al.*[8,9]

[8] M. Kotani, A. Amemiya, E. Ishiguro, and K. Hijikata, J. Phys. Soc. Japan **8,** 463 (1953).

[9] M. Kotani, E. Ishiguro, and K. Hijikata. J. Phys. Soc. Japan **9,** 553 (1954).

[10] M. Kotani, A. Amemiya, and T. Shimose, Proc. Phys.-Math. Soc. Japan **20,** extra No. 1 (1938).

TABLE III. MWF's and their relation to the composite atomic functions at infinity.

		$F+F$				$F^+ + F^-$			
	$^1\Sigma_g^+$	$^2P(0)$ $^2P(0)$	$^2P(1)$ $^2P(-1)$	$^2P(0)^2S$	$^2S^2S$	$^1D\,^1S$	$^1S\,^1S$	$^1P\,^1S$	$^1S'\,^1S$
1	$\lvert \sigma_u\bar{\sigma}_u \rvert$	$1/\sqrt{2}$				$1/\sqrt{3}$	$p/(6)^{\frac{1}{2}}$		$q/(6)^{\frac{1}{2}}$ [a]
2	$(1/\sqrt{2})\{\lvert s_u\bar{\sigma}_u \rvert - \lvert \bar{s}_u\sigma_u \rvert\}$			$-1/\sqrt{2}$				$1/\sqrt{2}$	
3	$(1/\sqrt{2})\{\lvert \pi_g{}^+\bar{\pi}_g{}^- \rvert - \lvert \bar{\pi}_g{}^+\pi_g{}^- \rvert\}$		$-1/\sqrt{2}$			$1/(6)^{\frac{1}{2}}$	$-p/\sqrt{3}$		$-q/\sqrt{3}$
4	$(1/\sqrt{2})\{\lvert \pi_u{}^+\bar{\pi}_u{}^- \rvert - \lvert \bar{\pi}_u{}^+\pi_u{}^- \rvert\}$		$1/\sqrt{2}$			$1/(6)^{\frac{1}{2}}$	$-p/\sqrt{3}$		$-q/\sqrt{3}$
5	$\lvert \sigma_g\bar{\sigma}_g \rvert$	$-1/\sqrt{2}$				$1/\sqrt{3}$	$p/(6)^{\frac{1}{2}}$		$q/(6)^{\frac{1}{2}}$
6	$\lvert s_u\bar{s}_u \rvert$				$1/\sqrt{2}$		$-q/\sqrt{2}$		$p/\sqrt{2}$
7	$(1/\sqrt{2})\{\lvert s_g\bar{\sigma}_g \rvert - \lvert \bar{s}_g\sigma_g \rvert\}$			$1/\sqrt{2}$				$1/\sqrt{2}$	
8	$\lvert s_g\bar{s}_g \rvert$				$-1/\sqrt{2}$		$-q/\sqrt{2}$		$p/\sqrt{2}$

		$F+F$		$F^+ + F^-$	
	$^{1,3}\Pi_g$	$^2P(0)^2P(0)$	$^2P(1)^2S$	$\left.\begin{matrix}^1D\\ ^3P\end{matrix}\right\}{}^1S$	$\left.\begin{matrix}^1P\\ ^3P'\end{matrix}\right\}{}^1S$ [b]
1	$(1/\sqrt{2})\{\lvert \sigma_u\bar{\pi}_u \rvert \mp \lvert \bar{\sigma}_u\pi_u \rvert\}$ [b]	$-1/\sqrt{2}$		$1/\sqrt{2}$	
2	$(1/\sqrt{2})\{\lvert \sigma_g\bar{\pi}_g \rvert \mp \lvert \bar{\sigma}_g\pi_g \rvert\}$	$1/\sqrt{2}$		$1/\sqrt{2}$	
3	$(1/\sqrt{2})\{\lvert s_u\bar{\pi}_u \rvert \mp \lvert \bar{s}_u\pi_u \rvert\}$		$-1/\sqrt{2}$		$1/\sqrt{2}$
4	$(1/\sqrt{2})\{\lvert s_g\bar{\pi}_g \rvert \mp \lvert \bar{s}_g\pi_g \rvert\}$		$1/\sqrt{2}$		$1/\sqrt{2}$
	$^{1,3}\Pi_u$				
1	$(1/\sqrt{2})\{\lvert \sigma_u\bar{\pi}_g \rvert \mp \lvert \bar{\sigma}_u\pi_g \rvert\}$ [b]	$-1/\sqrt{2}$		$1/\sqrt{2}$	
2	$(1/\sqrt{2})\{\lvert \sigma_g\bar{\pi}_u \rvert \mp \lvert \bar{\sigma}_g\pi_u \rvert\}$	$1/\sqrt{2}$		$1/\sqrt{2}$	
3	$(1/\sqrt{2})\{\lvert s_u\bar{\pi}_g \rvert \mp \lvert \bar{s}_u\pi_g \rvert\}$		$-1/\sqrt{2}$		$1/\sqrt{2}$
4	$(1/\sqrt{2})\{\lvert s_g\bar{\pi}_u \rvert \mp \lvert \bar{s}_g\pi_u \rvert\}$		$1/\sqrt{2}$		$1/\sqrt{2}$

		$F+F$	$F^+ + F^-$		
	$^1\Sigma_u^+$	$^2P(0)^2S$	$^1D(0)^1S$	$^1S\,^1S$	$^1P(0)^1(S)$	$^1S'^1S$
1	$\frac{1}{2}\{\lvert \pi_u{}^+\bar{\pi}_g{}^- \rvert - \lvert \bar{\pi}_u{}^+\pi_g{}^- \rvert + \lvert \pi_u{}^-\bar{\pi}_g{}^- \rvert - \lvert \bar{\pi}_u{}^-\pi_g{}^+ \rvert\}$		$1/\sqrt{3}$	$-(\frac{2}{3})^{\frac{1}{2}}p$		$-(\frac{2}{3})^{\frac{1}{2}}q$
2	$(1/\sqrt{2})\{\lvert \sigma_g\bar{\sigma}_u \rvert - \lvert \bar{\sigma}_g\sigma_u \rvert\}$		$(\frac{2}{3})^{\frac{1}{2}}$	$p/\sqrt{3}$		$q/\sqrt{3}$
3	$(1/\sqrt{2})\{\lvert \sigma_g\bar{s}_u \rvert - \lvert \bar{\sigma}_g s_u \rvert\}$	$-1/\sqrt{2}$			$1/\sqrt{2}$	
4	$(1\sqrt{2})\{\lvert s_g\bar{\sigma}_u \rvert - \lvert \bar{s}_g\sigma_u \rvert\}$	$1/\sqrt{2}$			$1/\sqrt{2}$	
5	$(1/\sqrt{2})\{\lvert s_g\bar{s}_u \rvert - \lvert \bar{s}_g s_u \rvert\}$			$-q$		p

		$F+F$				$F^+ + F^-$
	$^3\Sigma_u^+$	$^2P(0)^2P(0)$	$^2P(1)^2P(-1)$	$^2P(0)^2S$	$^2S^2S$	$^3P'(0)^1S$
1	$\frac{1}{2}\{\lvert \pi_u{}^+\bar{\pi}_g{}^- \rvert + \lvert \bar{\pi}_u{}^+\pi_g{}^- \rvert + \lvert \pi_u{}^-\bar{\pi}_g{}^+ \rvert + \lvert \bar{\pi}_u{}^-\pi_g{}^+ \rvert\}$		1			
2	$(1/\sqrt{2})\{\lvert \sigma_g\bar{\sigma}_u \rvert + \lvert \bar{\sigma}_g\sigma_u \rvert\}$	1				
3	$(1/\sqrt{2})\{\lvert \sigma_g\bar{s}_u \rvert + \lvert \bar{\sigma}_g s_u \rvert\}$			$1/\sqrt{2}$		$1/\sqrt{2}$
4	$(1/\sqrt{2})\{\lvert s_g\bar{\sigma}_u \rvert + \lvert \bar{s}_g\sigma_u \rvert\}$			$-1/\sqrt{2}$		$1/\sqrt{2}$
5	$(1/\sqrt{2})\{\lvert s_g\bar{s}_u \rvert + \lvert \bar{s}_g s_u \rvert\}$				1	

TABLE III.—*Continued.*

		$F+F$	$F^+ + F^-$
	$^1\Delta_g$	$^2P(1)^2P(1)$	$^1D(2)^1S$
1	$\lvert \pi_g\bar{\pi}_g \rvert$	$-1/\sqrt{2}$	$1/\sqrt{2}$
2	$\lvert \pi_u\bar{\pi}_u \rvert$	$1/\sqrt{2}$	$1/\sqrt{2}$
		$F+F$	$F^+ + F^-$
	$^3\Sigma_g^+$	$^2P(0)^2S$	$^3P'(0)^1S$
1	$(1/\sqrt{2})\{\lvert s_u\bar{\sigma}_u \rvert + \lvert \bar{s}_u\sigma_u \rvert\}$	$-1/\sqrt{2}$	$1/\sqrt{2}$
2	$(1/\sqrt{2})\{\lvert s_g\bar{\sigma}_g \rvert + \lvert \bar{s}_g\sigma_g \rvert\}$	$1/\sqrt{2}$	$1/\sqrt{2}$
		$F+F$	$F^+ + F^-$
	$^3\Sigma_g^-$	$^2P(1)^2P(-1)$	$^3P(0)^1S$
1	$(1/\sqrt{2})\{\lvert \pi_g^+\bar{\pi}_g^- \rvert + \lvert \bar{\pi}_g^+\pi_g^- \rvert\}$	$-1/\sqrt{2}$	$1/\sqrt{2}$
2	$(1/\sqrt{2})\{\lvert \pi_u^+\bar{\pi}_u^- \rvert + \lvert \bar{\pi}_u^+\pi_u^- \rvert\}$	$1/\sqrt{2}$	$1/\sqrt{2}$
$^1\Delta_u$	$(1/\sqrt{2})\{\lvert \pi_g\bar{\pi}_u \rvert - \lvert \bar{\pi}_g\pi_u \rvert\}$		$F^+ + F^-$ $^1D(2)^1S$
$^1\Sigma_u^-$	$\frac{1}{2}\{\lvert \pi_u^+\bar{\pi}_g^- \rvert - \lvert \bar{\pi}_u^+\pi_g^- \rvert - \lvert \pi_u^-\bar{\pi}_g^+ \rvert + \lvert \bar{\pi}_u^-\pi_g^+ \rvert\}$		$F+F$ $^2P(1)^2P(-1)$
$^3\Sigma_u^-$	$\frac{1}{2}\{\lvert \pi_u^+\bar{\pi}_g^- \rvert + \lvert \bar{\pi}_u^+\pi_g^- \rvert - \lvert \pi_u^-\bar{\pi}_g^+ \rvert + \lvert \bar{\pi}_u^-\pi_g^+ \rvert\}$		$F^+ + F^-$ $^3P(0)^1S$
$^3\Delta_u$	$(1/\sqrt{2})\{\lvert \pi_g\bar{\pi}_u \rvert + \lvert \bar{\pi}_g\pi_u \rvert\}$		$F+F$ $^2P(1)^2P(1)$

[a] $p^2+q^2=1$.
[b] Upper ∞singlet, lower∞triplet.

$R=1.221$ A and -1.904 ev at $R=1.526$ A. Note that no single MWF gives the stable molecule, and it is the result of the configuration interaction that the dissociation energy appears positive. In order to estimate the dissociation energy and the equilibrium internuclear distance from the values of energy at two points, the Morse curve for the adiabatic potential function is supposed

$$E(R)=D_e+D_e\{1-\exp[-\beta(R-R_e)]\}^2,$$

and the experimental value of Raman frequency 892.1 cm^{-1} is used.[11] The zero-point energy is 0.055 ev. In the first row of Table VII is shown the value of D_e and r_e calculated in this manner. Therefore, $D_0=D_e-0.055=1.99$ ev.

In Table VI the lowest state (σ_u^2) interacts strongly with $(s_u\sigma_u)$ and (σ_g^2), but very weakly with (π_u^2) and (π_g^2). It is expected, therefore, that one may obtain almost the same result for the ground state by taking into account only the states having s and σ defects. Disregarding the states (π_u^2) and (π_g^2), the 6-dimensional secular equations are solved, the result of which is shown in the second row of Table VII. Also shown is the result from the $\sigma\pi$ approximation in the third row, in which all the states having s defects are neglected. Although the value of D_e coincides very well with the experimental value, this agreement is fortuitous. In fact, in O_2, Li_2, etc., where the dissociation energies were calculated to be lower than the experimental value, the $s\sigma$ interaction is important for obtaining the better results.[1,2] The importance of the configurations with s-vacancies will be partly removed if LCAO SCF MO is taken as the orthogonalized MO. The larger interatomic distance in this approximation shows that the attractive effect of $2s$-electrons is underestimated.

The same calculation was performed by neglecting the interaction between $1s$ and the other electrons. That is to say, the effect of the $1s$ electrons is assumed only to reduce the nuclear charge by two. $s_{g,u}$ and $\sigma_{g,u}$ are, however, still kept orthogonal to $k_{g,u}$. The total energy of the molecule is compared with the total energy of all the second quantum electrons in the separated atoms calculated by using the orthogonalized $2s$ orbital as before, resulting in higher D_e and in shorter R_e. The fourth row of Table VII shows these results. Amith[12] treated $1s$ in almost the same manner.

[11] D. Andrychuk, J. Chem. Phys. **18**, 233 (1950).

[12] Avraham Amith, Ph.D. thesis submitted to the Department of Chemistry, Harvard University.

TABLE IV. One-center integrals.

χ_1	χ_2	$(\chi_{1a} \mid -\frac{1}{2}\Delta \mid \chi_{2a})$	$(\chi_{1a} \mid 1/r_a \mid \chi_{2a})$
$1s$	$1s$	37.54136 11	8.66502 87
$1s$	$2s$	−1.19709 63	0.89799 19
$2s$	$2s$	1.12624 08	1.29975 43
$2p\sigma$	$2p\sigma$	3.37872 25	1.29975 43
$2p\pi$	$2p\pi$	3.37872 25	1.29975 43

$[\chi_{1a}\chi_{2a} \mid \chi_{3a}\chi_{4a}]$

χ_1	χ_2	χ_3	χ_4	
$1s$	$1s$	$1s$	$1s$	5.41564 29
$1s$	$1s$	$1s$	$2s$	0.79318 57
$1s$	$1s$	$2s$	$2s$	1.29039 72
$1s$	$1s$	$2p\sigma$	$2p\sigma$	1.29039 72
$1s$	$1s$	$2p\pi$	$2p\pi$	1.29039 72
$1s$	$2s$	$1s$	$2s$	0.14764 73
$1s$	$2p\sigma$	$1s$	$2p\sigma$	0.03131 93
$1s$	$2p\pi$	$1s$	$2p\pi$	0.03131 93
$1s$	$2s$	$2s$	$2s$	0.29728 82
$1s$	$2s$	$2p\sigma$	$2p\sigma$	0.29728 82
$1s$	$2s$	$2p\pi$	$2p\pi$	0.29728 82
$1s$	$2p\sigma$	$2s$	$2p\sigma$	0.04716 91
$1s$	$2p\pi$	$2s$	$2p\pi$	0.04716 91
$2s$	$2s$	$2s$	$2s$	0.94435 27
$2s$	$2s$	$2p\sigma$	$2p\sigma$	0.94435 27
$2s$	$2s$	$2p\pi$	$2p\pi$	0.94435 27
$2s$	$2p\sigma$	$2s$	$2p\sigma$	0.20872 79
$2s$	$2p\pi$	$2s$	$2p\pi$	0.20872 79
$2p\sigma$	$2p\sigma$	$2p\sigma$	$2p\sigma$	1.01746 39
$2p\sigma$	$2p\sigma$	$2p\pi$	$2p\pi$	0.90799 71
$2p\sigma$	$2p\pi$	$2p\sigma$	$2p\pi$	0.05483 34
$2p\pi^+$	$2p\pi^+$	$2p\pi^+$	$2p\pi^+$	0.96263 05
$2p\pi^+$	$2p\pi^+$	$2p\pi^-$	$2p\pi^-$	0.10966 68

His $2s$ orbital, however, is orthogonalized to $1s$ in the form: $N(r+a)\exp(-\delta_2 r)$. He obtained $D_e=4.16$ ev and $R_e=1.16$ A. The larger value of the dissociation energy comes from the fact that the $2s$ orbitals orthogonalized in his manner gives higher total energy of the separated atoms.

The calculated value of the dissociation energy $D_0=1.99$ ev is higher than the experimental value 1.62 ev.[13] Eve[14] started with LCAO SCF MO and took five configurations at the experimental internuclear distances, resulting in 1.91 ev, which is in good agreement with our calculations.

The energies of the excited states were calculated in the same scheme as (1) in Table VII. These states can be grouped into "ground complex" which is adiabatically traced to the ground atomic structure $^2P+^2P$ at infinite separation, and "excited complex" which tends to the excited atomic structures. These two groups do not overlap at the larger distances than R_e of $^1\Sigma_g^+$. Table VIII shows the energies of the ground complex. In the first three columns the zero-point of the energy is the energy of $^2P+^2P$. Apparently no states seem to have minima in this range and the continuous band of the fluorine is mainly $^1\Sigma_g^+-{}^1\Pi_u$. The vertical distance between these two states at $R_e(^1\Sigma_g^+)$ is calculated to be 5.21 ev, which is related to the frequency at the maximum intensity and is to be compared with the experimental value 4.28 ev. There is a $^3\Pi_u$ state below $^1\Pi_u$. Theoretically, by the comparison of the energy matrices of $^3\Pi_u$ and $^1\Pi_u$, we note that each diagonal element of $^3\Pi_u$ is lower than the corresponding diagonal element of $^1\Pi_u$, and that the corresponding off-diagonal elements are of the same order of magnitude. Therefore, we are quite certain for the existence of $^3\Pi_u$ state below $^1\Pi_u$. The same thing is true for $^3\Pi_g$ and $^1\Pi_g$. Rees[15] derived by the analysis of the spectra the vertical distance between $^1\Sigma_g^+$ and $^3\Pi_u$ as 3.16 ev. He stated that $^3\Pi_u$ has a minimum at 1.8∼1.9 A. This calculation, however, is not enough to locate this minimum. The author purposely did not show the energy levels of the excited complex, since in Part II these calculated energy levels for the excited complex will turn out to be almost meaningless from the physical point of view.

The wave functions have also been calculated for each state. Here are shown those for the lowest $^1\Sigma_g^+$, $^1\Pi_u$ and $^3\Pi_u$:

$^1\Sigma_g^+$: $R=1.221$ A

$$0.9718(\sigma_u^2)-0.1620(s_u\sigma_u)-0.0492(\pi_g^2)-0.0219(\pi_u^2)$$
$$-0.1606(\sigma_g^2)-0.0177(s_u^2)+0.0092(s_g\sigma_g)-0.0185(s_g^2)$$

$R=1.526$ A

$$0.9344(\sigma_u^2)-0.0740(s_u\sigma_u)-0.0856(\pi_g^2)-0.0352(\pi_u^2)$$
$$-0.3338(\sigma_g^2)-0.0301(s_u^2)-0.0038(s_g\sigma_g)-0.0197(s_g^2)$$

$^1\Pi_u$: $R=1.221$ A

$$0.9493(\sigma_u\pi_g)-0.2505(\sigma_g\pi_u)-0.1899(s_u\pi_g)$$
$$+0.0037(s_g\pi_u)$$

$R=1.526$ A

$$0.8891(\sigma_u\pi_g)-0.4443(\sigma_g\pi_u)-0.1092(s_u\pi_g)$$
$$+0.0097(s_g\pi_u)$$

$^3\Pi_u$: $R=1.221$ A

$$0.9585(\sigma_u\pi_g)-0.2078(\sigma_g\pi_u)-0.1953(s_u\pi_g)$$
$$+0.0031(s_g\pi_u)$$

$R=1.526$ A

$$0.9097(\sigma_u\pi_g)-0.4002(\sigma_g\pi_u)-0.1101(s_u\pi_g)$$
$$+0.0075(s_g\pi_u).$$

For the ground state $^1\Sigma_g^+$ the mixing of the lowest configuration with the others is small, but this small mixing gives the ground state the binding character.

[13] H. O. Pritchard, Chem. Rev. **52**, 529 (1953). In this article the electron affinity was determined in various methods as 83.7 kcal/mole, resulting in $D_0=37.4$ kcal/mole (1.62 ev).

[14] J. Eve, Proc. Roy. Soc. (London) **A246**, 582 (1958).

[15] A. L. G. Rees, J. Chem. Phys. **26**, 1567 (1957).

TABLE V. Two-center integrals.

One-electron integrals

R (in A)		$(\chi_{1a}) \mid -\frac{1}{2}\Delta \mid \chi_{2b})$		$(\chi_{1a}) \mid (1/r_b) \mid \chi_{2a})$		$(\chi_{1a}) \mid (1/r_a) \mid \chi_{2b})$	
χ_1	χ_2	1.221 A	1.526 A	1.221 A	1.526 A	1.221 A	1.526 A
$1s$	$1s$	0.00000 87	0.00000 01	0.43325 14	0.34660 12	0.00000 04	0.00000 00
$1s$	$2s$	−0.01466 75	−0.00560 13	0.10361 45	0.08289 16	0.05060 84	0.01427 16
$2s$	$1s$	−0.01466 75	−0.00560 13	0.10361 45	0.08289 16	0.00551 61	0.00124 82
$1s$	$2p\sigma$	−0.02076 78	−0.00885 00	0.00920 34	0.00589 02	0.08717 86	0.02463 27
$2p\sigma$	$1s$	−0.02076 78	−0.00885 00	0.00920 34	0.00589 02	0.00944 17	0.00214 59
$2s$	$2s$	−0.02065 82	−0.03850 32	0.43293 73	0.34657 90	0.15142 32	0.05777 95
$2s$	$2p\sigma$	0.06866 17	−0.01888 10	0.10367 17	0.06666 47	0.21205 02	0.08482 43
$2p\sigma$	$2s$	0.06866 17	−0.01888 10	0.10367 17	0.06666 47	0.15996 78	0.06718 48
$2p\sigma$	$2p\sigma$	0.24287 54	0.03141 81	0.46838 39	0.36501 87	0.20941 49	0.09498 11
$2p\pi$	$2p\pi$	0.01842 48	−0.00864 28	0.41521 41	0.33735 91	0.06121 35	0.01958 94

Coulomb integrals $[\chi_{1a}\chi_{2a} \mid \chi_{3b}\chi_{4b}]$

χ_1	χ_2	χ_3	χ_4	1.221 A	1.526 A
$1s$	$1s$	$1s$	$1s$	0.43325 14	0.34660 12
$1s$	$1s$	$1s$	$2s$	0.10361 45	0.08289 16
$1s$	$1s$	$1s$	$2p\sigma$	0.00920 34	0.00589 02
$1s$	$1s$	$2s$	$2s$	0.43290 02	0.34657 60
$1s$	$1s$	$2s$	$2p\sigma$	0.10360 75	0.06665 96
$1s$	$1s$	$2p\sigma$	$2p\sigma$	0.46827 29	0.36501 00
$1s$	$1s$	$2p\pi$	$2p\pi$	0.41521 38	0.33735 91
$1s$	$2s$	$1s$	$2s$	0.02478 00	0.01982 40
$1s$	$2s$	$1s$	$2p\sigma$	0.00220 10	0.00140 87
$1s$	$2p\sigma$	$1s$	$2p\sigma$	0.00039 10	0.00020 02
$1s$	$2p\pi$	$1s$	$2p\pi$	0.00019 55	0.00010 01
$1s$	$2s$	$2s$	$2s$	0.10349 76	0.08288 29
$1s$	$2s$	$2s$	$2p\sigma$	0.02742 19	0.01593 73
$1s$	$2s$	$2p\sigma$	$2p\sigma$	0.11189 33	0.08728 61
$1s$	$2s$	$2p\pi$	$2p\pi$	0.09929 97	0.08068 12
$1s$	$2p\sigma$	$2s$	$2s$	0.00917 78	0.00588 82
$1s$	$2p\sigma$	$2s$	$2p\sigma$	0.00424 92	0.00225 35
$1s$	$2p\sigma$	$2p\sigma$	$2p\sigma$	0.01124 26	0.00681 31
$1s$	$2p\pi$	$2s$	$2p\pi$	0.00218 63	0.00113 15
$1s$	$2p\pi$	$2p\sigma$	$2p\pi$	0.00111 98	0.00046 94
$1s$	$2p\sigma$	$2p\pi$	$2p\pi$	0.00814 54	0.00542 58
$2s$	$2s$	$2s$	$2s$	0.42936 41	0.34609 91
$2s$	$2s$	$2s$	$2p\sigma$	0.09816 88	0.06590 83
$2s$	$2p\sigma$	$2s$	$2p\sigma$	0.04067 69	0.02441 25
$2s$	$2p\sigma$	$2p\sigma$	$2p\sigma$	0.11491 03	0.07532 34
$2s$	$2s$	$2p\pi$	$2p\pi$	0.41425 51	0.33725 05
$2s$	$2p\pi$	$2s$	$2p\pi$	0.02389 58	0.01271 87
$2s$	$2p\pi$	$2p\sigma$	$2p\pi$	0.01128 15	0.00515 80
$2p\sigma$	$2p\pi$	$2p\sigma$	$2p\pi$	0.00643 03	0.00268 97
$2p\sigma$	$2p\sigma$	$2p\pi$	$2p\pi$	0.44017 51	0.35262 62
$2s$	$2s$	$2p\sigma$	$2p\sigma$	0.45958 20	0.36369 65
$2s$	$2p\sigma$	$2p\pi$	$2p\pi$	0.08979 80	0.06120 07
$2p\sigma$	$2p\sigma$	$2p\sigma$	$2p\sigma$	0.49839 60	0.38613 70
$2p\pi^+$	$2p\pi^+$	$2p\pi^+$	$2p\pi^+$	0.40129 52	0.32956 26
$2p\pi^+$	$2p\pi^+$	$2p\pi^-$	$2p\pi^-$	0.00394 08	0.00143 28

Exchange integrals $[\chi_{1a}\chi_{2b} \mid \chi_{3a}\chi_{4b}]$

χ_1	χ_2	χ_3	χ_4	R	1.221 A	1.526 A
$1s$	$1s$	$1s$	$1s$		0.00000 00	0.00000 00
$1s$	$1s$	$1s$	$2s$		0.00000 00	0.00000 00
$1s$	$1s$	$1s$	$2p\sigma$		0.00000 00	0.00000 00
$1s$	$1s$	$2s$	$2s$		0.00000 0[a]	0.00000 00
$1s$	$1s$	$2s$	$2p\sigma$		0.00000 0[a]	0.00000 00
$1s$	$1s$	$2p\sigma$	$2p\sigma$		0.00000 0[a]	0.00000 00
$1s$	$1s$	$2p\pi$	$2p\pi$		0.00000 0[a]	0.00000 00
$1s$	$2s$	$1s$	$2s$		0.00039 10	0.00003 92
$1s$	$2s$	$2s$	$1s$		0.00006 91	0.00000 56
$1s$	$2p\sigma$	$1s$	$2p\sigma$		0.00115 19	0.00011 64
$1s$	$2p\sigma$	$2p\sigma$	$1s$		0.00020 54	0.00001 66
$1s$	$2s$	$1s$	$2p\sigma$		0.00067 02	0.00006 75
$1s$	$2s$	$2p\sigma$	$1s$		0.00012 01	0.00000 96

TABLE V.—*Continued.*

Exchange integrals $[\chi_{1a}\chi_{2b} \mid \chi_{3a}\chi_{4b}]$

χ_1	χ_2	χ_3	χ_4	R	1.221 A	1.526 A
$1s$	$1s$	$2p\sigma$	$2s$		0.00000 00	0.00000 00
$1s$	$2p\pi$	$1s$	$2p\pi$		0.00000 15	0.00000 01
$1s$	$2p\pi$	$2p\pi$	$1s$		0.00000 00	0.00000 00
$1s$	$2s$	$2s$	$2s$		0.00189 73	0.00020 81
$1s$	$2s$	$2s$	$2p\sigma$		0.00265 03	0.00030 54
$1s$	$2s$	$2p\sigma$	$2s$		0.00209 08	0.00024 97
$1s$	$2p\sigma$	$2s$	$2p\sigma$		0.00453 93	0.00052 52
$1s$	$2p\sigma$	$2p\sigma$	$2s$		0.00357 95	0.00042 93
$1s$	$2p\sigma$	$2s$	$2s$		0.00324 92	0.00035 78
$1s$	$2s$	$2p\sigma$	$2p\sigma$		0.00276 02	0.00036 43
$1s$	$2p\sigma$	$2p\sigma$	$2p\sigma$		0.00472 59	0.00061 05
$1s$	$2s$	$2p\pi$	$2p\pi$		0.00076 80	0.00007 03
$1s$	$2p\sigma$	$2p\pi$	$2p\pi$		0.00131 50	0.00012 09
$1s$	$2p\pi$	$2s$	$2p\pi$		0.00001 69	0.00000 11
$1s$	$2p\pi$	$2p\pi$	$2s$		0.00003 16	0.00000 24
$1s$	$2p\pi$	$2p\sigma$	$2p\pi$		0.00001 71	0.00000 12
$1s$	$2p\pi$	$2p\pi$	$2p\sigma$		0.00004 90	0.00000 38
$2s$	$2s$	$2s$	$2s$		0.02918 99	0.00538 20
$2s$	$2s$	$2s$	$2p\sigma$		0.03736 53	0.00740 70
$2s$	$2p\sigma$	$2s$	$2p\sigma$		0.04732 41	0.01013 86
$2s$	$2s$	$2p\sigma$	$2p\sigma$		0.04577 73	0.00998 60
$2s$	$2p\sigma$	$2p\sigma$	$2s$		0.04927 11	0.01037 36
$2p\sigma$	$2p\sigma$	$2p\sigma$	$2s$		0.06006 94	0.01394 25
$2p\sigma$	$2p\sigma$	$2p\sigma$	$2p\sigma$		0.07645 15	0.01916 90
$2s$	$2p\pi$	$2s$	$2p\pi$		0.00259 63	0.00037 93
$2s$	$2s$	$2p\pi$	$2p\pi$		0.01239 11	0.00187 32
$2s$	$2p\pi$	$2p\pi$	$2s$		0.00287 48	0.00042 57
$2p\sigma$	$2p\pi$	$2p\sigma$	$2p\pi$		0.00403 50	0.00067 78
$2p\sigma$	$2p\sigma$	$2p\pi$	$2p\pi$		0.01874 19	0.00337 15
$2p\sigma$	$2p\pi$	$2p\pi$	$2p\sigma$		0.00547 38	0.00089 12
$2s$	$2p\pi$	$2p\sigma$	$2p\pi$		0.00327 72	0.00051 09
$2s$	$2p\sigma$	$2p\pi$	$2p\pi$		0.01562 51	0.00254 38
$2s$	$2p\pi$	$2p\pi$	$2p\sigma$		0.00390 71	0.00061 00
$2p\pi^+$	$2p\pi^+$	$2p\pi^+$	$2p\pi^+$		0.00550 37	0.00068 67
$2p\pi^+$	$2p\pi^+$	$2p\pi^-$	$2p\pi^-$		0.00058 92	0.00007 18

Hybrid integrals $[\chi_{1a}\chi_{2a} \mid \chi_{3a}\chi_{4b}]$

χ_1	χ_2	χ_3	χ_4	R	1.221 A	1.526 A
$1s$	$1s$	$1s$	$1s$		0.00000 04	0.00000 00
$1s$	$1s$	$1s$	$2s$		0.04150 30	0.01172 79
$1s$	$2s$	$1s$	$1s$		0.00000 01	0.00000 00
$1s$	$1s$	$2s$	$1s$		0.00551 61	0.00124 82
$1s$	$1s$	$1s$	$2p\sigma$		0.07142 00	0.02022 91
$1s$	$2p\sigma$	$1s$	$1s$		0.00000 0[a]	0.00000 00
$1s$	$1s$	$2p\sigma$	$1s$		0.00944 17	0.00214 59
$1s$	$1s$	$2s$	$2s$		0.15088 63	0.05762 89
$1s$	$2s$	$1s$	$2s$		0.00746 77	0.00211 58
$1s$	$2s$	$2s$	$1s$		0.00131 92	0.00029 85
$2s$	$2s$	$1s$	$1s$		0.00000 03	0.00000 00
$1s$	$1s$	$2s$	$2p\sigma$		0.21112 29	0.08456 39
$1s$	$1s$	$2p\sigma$	$2s$		0.15984 82	0.06715 00
$1s$	$2s$	$1s$	$2p\sigma$		0.01283 36	0.00364 64
$1s$	$2p\sigma$	$1s$	$2s$		0.00054 50	0.00016 25
$1s$	$2p\sigma$	$2s$	$1s$		0.00013 39	0.00002 02
$1s$	$2s$	$2p\sigma$	$1s$		0.00225 80	0.00051 32
$2s$	$2p\sigma$	$1s$	$1s$		0.00000 0[a]	0.00000 00
$1s$	$1s$	$2p\sigma$	$2p\sigma$		0.20920 89	0.09492 09
$1s$	$2p\sigma$	$1s$	$2p\sigma$		0.00095 57	0.00027 99
$1s$	$2p\sigma$	$2p\sigma$	$1s$		0.00020 82	0.00003 50
$2p\sigma$	$2p\sigma$	$1s$	$1s$		0.00000 03	0.00000 00
$1s$	$1s$	$2p\pi$	$2p\pi$		0.06117 21	0.01958 00
$1s$	$2p\pi$	$1s$	$2p\pi$		0.00019 55	0.00005 54
$1s$	$2p\pi$	$2p\pi$	$1s$		0.00000 29	0.00000 03
$2p\pi$	$2p\pi$	$1s$	$1s$		0.00000 03	0.00000 00
$1s\pi$	$2s$	$2s$	$2s$		0.03554 14	0.01362 80
$2s$	$2s$	$1s$	$2s$		0.01491 71	0.00424 63
$2s$	$2s$	$2s$	$1s$		0.00550 39	0.00124 79
$1s$	$2s$	$2s$	$2p$		0.04955 71	0.01995 81

TABLE V.—*Continued.*

Hybrid integrals $[\chi_{1a}\chi_{2a} \mid \chi_{3a}\chi_{4b}]$						
χ_1	χ_2	χ_3	χ_4	R	1.221	1.526
1s	2s	2pσ	2s		0.03801 38	0.01599 57
1s	2pσ	2s	2s		0.00375 68	0.00140 34
2s	2s	1s	2pσ		0.02557 46	0.00730 71
2s	2s	2pσ	1s		0.00942 11	0.00214 53
2s	2pσ	1s	2s		0.00112 85	0.00033 90
2s	2pσ	2s	1s		0.00138 58	0.00025 13
1s	2s	2pσ	2pσ		0.04966 53	0.02259 14
1s	2pσ	2s	2pσ		0.00548 98	0.00215 38
1s	2pσ	2pσ	2s		0.00610 97	0.00223 16
2pσ	2pσ	1s	2s		0.01506 72	0.00429 47
2pσ	2pσ	2s	1s		0.00600 40	0.00132 14
2s	2pσ	1s	2pσ		0.00192 20	0.00058 14
2s	2pσ	2pσ	1s		0.00237 16	0.00043 19
1s	2pσ	2pσ	2pσ		0.00909 93	0.00345 66
2pσ	2pσ	1s	2pσ		0.02583 69	0.00739 13
2pσ	2pσ	2pσ	1s		0.01027 68	0.00227 16
1s	2s	2pπ	2pπ		0.01455 47	0.00466 56
1s	2pπ	2s	2pπ		0.00140 05	0.00039 82
1s	2pπ	2pπ	2s		0.00299 99	0.00095 18
2s	2pπ	1s	2pπ		0.00039 17	0.00008 96
2s	2pπ	2pπ	1s		0.00002 92	0.00000 36
2pπ	2pπ	1s	2s		0.01484 21	0.00422 21
2pπ	2pπ	2s	1s		0.00525 39	0.00121 12
1s	2pσ	2pπ	2pπ		0.00123 15	0.00037 81
1s	2pπ	2pσ	2pπ		0.00123 15	0.00037 81
1s	2pπ	2pπ	2pσ		0.00471 98	0.00153 48
2pσ	2pπ	1s	2pπ		0.00007 08	0.00001 71
2pσ	2pπ	2pπ	1s		0.00001 60	0.00000 09
2pπ	2pπ	1s	2pσ		0.02544 35	0.00726 50
2pπ	2pπ	2pσ	1s		0.00899 32	0.00208 21
2s	2s	2s	2s		0.13095 02	0.05170 53
2s	2s	2s	2pσ		0.17771 70	0.07451 67
2s	2s	2pσ	2s		0.14647 04	0.06295 54
2s	2pσ	2s	2s		0.02893 05	0.01161 33
2s	2pσ	2pσ	2s		0.04452 88	0.01775 28
2s	2pσ	2s	2pσ		0.03961 50	0.01716 85
2s	2s	2pσ	2pσ		0.18701 10	0.08783 66
2pσ	2pσ	2s	2s		0.13810 28	0.05467 08
2s	2pσ	2pσ	2pσ		0.06172 51	0.02637 67
2pσ	2pσ	2s	2pσ		0.18771 99	0.07901 88
2pσ	2pσ	2pσ	2s		0.15955 45	0.06821 73
2pσ	2pσ	2pσ	2pσ		0.20558 94	0.09588 00
2s	2s	2pπ	2pπ		0.05640 88	0.01844 19
2pπ	2pπ	2s	2s		0.12737 38	0.05022 28
2s	2pπ	2pπ	2s		0.01755 42	0.00594 98
2pπ	2s	2s	2pπ		0.01100 81	0.00334 74
2s	2pσ	2pπ	2pπ		0.01087 45	0.00353 22
2pπ	2pπ	2pσ	2s		0.13992 82	0.06032 45
2pπ	2pπ	2s	2pσ		0.17271 55	0.07226 56
2s	2pπ	2pπ	2pσ		0.02608 14	0.00922 25
2pπ	2s	2pσ	2pπ		0.01087 45	0.00353 22
2pπ	2pσ	2pπ	2s		0.00527 60	0.00191 04
2pσ	2pπ	2s	2pπ		0.00428 17	0.00131 38
2pσ	2pπ	2pπ	2pσ		0.00756 48	0.00292 24
2pπ	2pσ	2pσ	2pπ		0.00580 16	0.00178 48
2pπ	2pπ	2pσ	2pσ		0.17772 19	0.08381 47
2pσ	2pσ	2pπ	2pπ		0.05775 09	0.01893 20
$2p\pi^+$	$2p\pi^+$	$2p\pi^+$	$2p\pi^+$		0.05573 79	0.01819 68
$2p\pi^+$	$2p\pi^+$	$2p\pi^-$	$2p\pi^-$		0.00378 88	0.00104 97

[a] The seventh digit was not calculated.

At the infinite interatomic distance these states will tend to

$$^1\Sigma_g^+ \sim (1/\sqrt{2})\{(\sigma_u^2) - (\sigma_g^2)\}$$

$$^{1,3}\Pi_u \sim (1/\sqrt{2})\{(\sigma_u\pi_g) - (\sigma_g\pi_u)\},$$

which are the atomic stationary state $^2P + ^2P$. Therefore, if we observe the difference between the coefficients of these terms and $1/\sqrt{2}$, it may be seen how "atomic" the state is. The $^{1,3}\Pi_u$ states are more atomic than $^1\Sigma_g^+$.

The ionicity of the states may be investigated as follows. The molecular eigenfunctions are transformed into the expressions based on the normalized composite

TABLE VI. The energy matrix of $^1\Sigma_g^+$.

$R=1.221$ A	(σ_u^2)	$(s_u\sigma_u)$	(π_g^2)	(π_u^2)	(σ_g^2)	(s_u^2)	$(s_g\sigma_g)$	(s_g^2)
	0.05477	0.27028	0.04799	0.03880	0.28625	0.11035	−0.00574	0.08109
		1.42447	0.03197	0.02321	0.12676	0.31543	0.32899	−0.00952
roots			0.85786	0.33618	−0.03604	−0.15618	−0.02984	−0.12168
−0.04485	0.67616			1.32609	−0.04478	−0.13085	−0.00729	−0.15590
1.18960	1.48599				1.53763	0.10096	−0.19586	0.12682
1.64333	2.40457					2.63751	0.11964	0.25399
2.88215	3.53464						2.56099	−0.21486
								3.37184
$R=1.526$ A								
	0.06741	0.14456	0.04323	0.03995	0.32363	0.10970	0.01025	0.08936
		1.26040	0.01665	0.01180	0.08492	0.16660	0.37380	0.00566
roots			0.45956	0.37105	−0.03640	−0.15561	−0.01762	−0.12875
−0.06998	0.16776			0.64245	−0.04039	−0.13599	−0.00137	−0.14608
0.82776	0.90215				0.81455	0.09273	−0.07382	0.11525
1.14758	1.89013					2.28281	0.07980	0.28797
2.23659	2.84313						1.80806	−0.08116
								2.60913

TABLE VII. Dissociation energy and equilibrium internuclear distance.

	No. of Configurations	D_e	R_e
(1) Exact Solution	8	2.04 ev	1.409 A
(2) Configurations with $s-\sigma$ defects	6	1.90	1.403
(3) Configurations with $\sigma-\pi$ defects	4	1.67	1.458
(4) Shrunk 1s-core	8	2.63	1.314
(5) Experiment		1.68[a]	1.435

[a] D_0+zero-point energy.

TABLE VIII. Energies of the ground complex.

	$r=1.221$ A	$r=1.526$ A	$E(r_e)$	$E(r_e)-E(GS)$
$^3\Delta_u$	0.9628 a.u.	0.3948 a.u.	0.5660 a.u.	17.16 ev
$^1\Delta_g$	0.7588	0.3117	0.4382	13.96
$^1\Sigma_u^-$	0.8030	0.2323	0.3738	12.21
$^1\Sigma_g^+$	0.6762	0.1678	0.2685	9.83
$^3\Sigma_u^-$	0.3301	0.1239	0.1804	6.95
$^3\Sigma_u^+$	0.4366	0.1023	0.1786	6.90
$^1\Pi_g$	0.4841	0.0959	0.1793	6.92
$^3\Pi_g$	0.4741	0.0929	0.1744	6.78
$^1\Pi_u$	0.2918	0.0658	0.1166	5.21
$^3\Pi_u$	0.2518	0.0327	0.0694	3.93
$^1\Sigma_g^+$	−0.0449	−0.0700	−0.0751	0.00

TABLE IX. Ionicity of states.

State	R	C	I	$2M$	Ionicity
$^1\Sigma_g^+$	1.221 A	0.5302	0.1423	0.3276	0.3061
	1.526	0.7382	0.1022	0.1596	0.1820
$^1\Pi_u$	1.221	0.6800	0.1554	0.1646	0.2377
	1.526	0.8670	0.0659	0.0671	0.0995
$^3\Pi_u$	1.221	0.6307	0.1729	0.1964	0.2711
	1.526	0.8300	0.0919	0.0781	0.1309

atomic functions. We have:

$^1\Sigma_g^+$: $R=1.221$ A

$$0.6947[^2P(0)\ ^2P(0)]+0.0150[^2P(1)\ ^2P(-1)]$$
$$+0.1146[^2P(0)\ ^2S]-0.0061[^2S\ ^2S]$$
$$+0.2519[^1D(0)\ ^1S]+0.2347[^1S\ ^1S]$$
$$-0.0896[^1P(0)\ ^1S]+0.0219[^1S'\ ^1S]$$

$R=1.526$ A

$$0.8560[^2P(0)\ ^2P(0)]+0.0329[^2P(1)\ ^2P(-1)]$$
$$+0.0487[^2P(0)\ ^2S]-0.0044[^2S\ ^2S]$$
$$+0.1935[^1D(0)\ ^1S]+0.2426[^1S\ ^1S]$$
$$-0.0242[^1P(0)\ ^1S]+0.0515[^1S'\ ^1S]$$

$^1\Pi_u$: $R=1.221$ A

$$-0.8314[^2P(0)\ ^2P(1)]+0.1262[^2P(1)\ ^2S]$$
$$+0.3913[^1D(1)\ ^1S]-0.1198[^1P(1)\ ^1S]$$

$R=1.526$ A

$$-0.9300[^2P(0)\ ^2P(1)]+0.0808[^2P(1)\ ^2S]$$
$$+0.2500[^1D(1)\ ^1S]-0.0662[^1P(1)\ ^1S]$$

$^3\Pi_u$: $R=1.221$ A

$$-0.8004[^2P(0)\ ^2P(1)]+0.1292[^2P(1)\ ^2S]$$
$$+0.4345[^3P(1)\ ^1S]-0.1238[^3P'(1)\ ^1S]$$

$R=1.526$ A

$$-0.9099[^2P(0)\ ^2P(1)]+0.0798[^1P(1)\ ^2S]$$
$$+0.2972[^2P(1)\ ^2S]-0.0684[^3P'(1)\ ^1S].$$

The first four terms of $^1\Sigma_g^+$ and the first two terms of $^1\Pi_u$ and $^3\Pi_u$ are of covalent structures, and all the rest are of ionic structures. Since these composite atomic functions strongly overlap with one another, it is not easy to have a clear-cut definition of ionicity. Tentatively, the wave functions are squared and integrated. The terms are grouped as follows

$$\Omega=\sum_{i}{}_{\text{covalent}}a_i\Psi_i+\sum_{i}{}_{\text{ionic}}a_i\Psi_i=\Psi_C+\Psi_I$$

$$\int|\Omega|^2d\tau=\int|\Psi_C|^2d\tau+\int|\Psi_I|^2d\tau$$

$$+\int(\Psi_C^*\Psi_I+\Psi_I^*\Psi_C)d\tau.$$

We call these terms C, I and $2M$. The quantity $I+M$ is taken as a measure of ionicity. Table IX shows the result of this calculation. Although this definition has such a defect that sometimes values of ionicity are less than zero or greater than one, at least there is a rough qualitative picture. In no case are we using these numbers except to convince ourselves of the predominance of covalency or of ionicity of states.

ACKNOWLEDGMENTS

For the accomplishment of this paper the author is indebted to many people. First of all he owes much to the late Professor W. E. Moffitt who gave support and encouragement. The author is also obligated to Professor R. G. Parr, Carnegie Institute of Technology, Dr. S. O. Morgan, Dr. W. P. Slichter and Dr. A. D. Liehr, Bell Telephone Laboratories, Murray Hill, New Jersey, who gave free time on their IBM 650. The author would also like to express his appreciation to Professor R. S. Mulliken, Professor J. C. Slater, and Dr. G. Herzberg for their valuable suggestions.

THE JOURNAL OF CHEMICAL PHYSICS VOLUME 34, NUMBER 1 JANUARY, 1961

On the Fluorine Molecule. II. Energy Levels of F_2 and F_2^+

KATSUNORI HIJIKATA*

Physics Department, University of Oklahoma, Norman, Oklahoma

(Received July 13, 1959)

The same ASMO treatment as in Part I [K. Hijikata, J. Chem. Phys. **34**, 221 (1961), preceding paper] is applied to the fluorine molecule with several pairs of effective nuclear charges, and the best value of the effective nuclear charge is determined for each state. The ground state $^1\Sigma_g^+$ has $D_e=2.02$ ev, $R_e=1.437$ A and the effective nuclear charge 2.58. It is found that the explanation for the effective nuclear charge of each state from the "atomic point of view" is difficult. The vertical excitation energies $^1\Sigma_g^+-{}^1\Pi_u$, $^1\Sigma_g^+-{}^3\Pi_u$, and $^1\Sigma_g^+-{}^1\Pi_g$ are calculated to be 4.49, 3.73, and 6.50 ev, respectively. The lower energy levels of the molecular ion F_2^+ are also calculated, showing that the ground state is $^2\Pi_g$, that two more states appear to have potential minima, and that the higher energy levels of F_2 calculated by ASMO are almost meaningless except $^1\Sigma_u^+$. The energy level of this ionic state $^1\Sigma_u^+$ at $R=1.625$ A is 10.8 ev above the minimum of $^1\Sigma_g^+$. The energy diagram summarizing the calculations is shown. The discrepancy is indicated between the experimental and the theoretical ionization potentials.

INTRODUCTION

RECENTLY a variety of methods have been used to calculate the electronic energy levels of the molecule. Each of them has its own advantage, but none is good for all the molecules. If our interest is in calculating molecular quantities in good agreement with the experiments, we have to choose one method best fitted to the particular case. In this article the author is not discussing the theoretical background of the method, but trying to explain and to predict the experimental features of the electronic spectra of the fluorine molecule and its ion. In Part I[1] it was seen that the straightforward application of LCAO ASMO method gives good results for the ground state and the lower excited states of this molecule. In this article, therefore, the same treatment is pursued.

In the conventional ASMO calculation, a limited number of atomic orbitals are taken, on which the whole scheme of calculation is based. Namely, only the first and the second quantum orbitals for the molecules of the second-row elements are considered. With the development of digital computors the possibility is gradually brought forth to perform the calculation taking account of the higher orbitals. Since these higher orbitals are supposed to have orbital energies very close to one another, it is difficult to decide where to stop calculating. For the time being, therefore, one is compelled to have the restriction upon the number of orbitals. Consequently, a certain theoretical basis is lost in ASMO method. This theoretical difficulty was

* In sojourn from the University of Electro-Communications, Tokyo, Japan.

[1] K. Hijikata, J. Chem. Phys. **34**, 221 (1961), preceding paper, hereafter referred to as I.

TABLE I. Ratio of atomic radius to interatomic distance.

Li_2	Be_2	B_2	C_2	N_2	O_2	F_2	
61	...	52	49	50	39	29	%

critically pointed out when the methods of atoms in molecules and its modified forms were invented. In an earlier article[2] the author showed that these methods do not work for the ground state of the fluorine molecule in the present scheme of calculation. On the other hand, several molecules have been treated by ASMO,[3,4] showing that the results are not so absurd as was very often indicated by the people who are skeptical about ASMO. These ASMO treatments, however, have never been performed to the limit of accessibility. Before the accuracy of ASMO is discussed, therefore, (1) all the configurations arising from the arrangement of the electrons in the limited number of LCAO must be considered, (2) the calculations at several interatomic distances must be carried out, and (3) the variation of the molecular energies with the effective nuclear charges must be investigated. The calculation with a number of effective nuclear charges gives a standpoint to discuss the validity of methods such as HLSP, MAM, etc., in which the individual entity of the atoms in the molecule are admitted. In the following discussion it will be shown how the individuality of the atom is or is not maintained in the molecule by comparing the effective nuclear charges of corresponding atomic and molecular states.

The author took two interatomic distances and three different sets of effective nuclear charges and performed the same scheme of calculation as in I for these six cases. That is, we formed LCAO MO of $1s$, $2s$, and $2p$ atomic orbitals, built up the antisymmetrized products and calculated the configuration interaction for every state, resulting in the energies of molecular stationary states. These stationary states of the molecule can be traced back to the stationary states of the atomic constituents, and thus the curves of adiabatic potential may be obtained. When one considers the molecular states which are connected to the higher atomic states, however, one encounters difficulty because the calculated atomic term values are much different from the experimental values, and these discrepancies between the calculated and experimental values differ from state to state. In the case of fluorine this discrepancy ranges from 0.6 to 1.4 a.u. Thus nothing can be expected from the calculation of these excited states. E (molecule)$-$ E (atoms) are calculated, therefore, and added to the experimental values of the atomic energies in order to obtain the energies of the excited states of the molecule. The basis of this procedure is that the binding energy is a very small portion of the total molecular energy and that this is just the extension of the procedure used for the ground state. In other words, the author regarded the calculation of each state as an independent problem and followed the way of calculating the ground state.

Before proceeding, we have to pay attention to the following characteristics of fluorine. First of all, in the fluorine molecule the atoms are a large distance apart from each other. If the ratio of the atomic radius to the equilibrium interatomic distance for the homonuclear diatomic molecules of the second-row elements are taken, Table I is obtained. Here the atomic radius is that given by Slater[5] for maximum electron density. This ratio helps very much in guessing the difference in the effective nuclear charge between the molecule and the atom. For instance, in Li_2, two atoms overlap very strongly, making the molecular effective nuclear charges much different from the atomic values. On the other hand, there is little overlap in the fluorine molecule. It may be expected, therefore, that the best values of the atomic and the molecular effective nuclear charges do not differ so much from each other, and that the correlation energy in the molecule is almost the same as in the atom. Secondly, the excited states of the fluorine atom are all very high, and are located between 12.7 ev $[^2P,\ (2s)^2(2p)^e(3s)]$ and the ionization potential 17.42 ev. Therefore, the higher orbitals, which are neglected in our treatment, do not contribute very much to the ground state. On the other hand, if we try to obtain some information about the higher excited state, we have to look at the states of the molecular ion F_2^+.

At the beginning of this article, the states of the fluorine atom and of its ions will be discussed in order to fix the best effective nuclear charges for each state. Next, the ground state of the molecule will be investigated and the dissociation energy, effective nuclear charges, and interatomic distance will be discussed. In the same manner the excited states are treated; by the variation of the effective nuclear charges the energy of each state is calculated. Finally, the ground and lower excited states of F_2^+ are worked out in almost the same scheme of calculation, and these results are combined in order to draw the energy diagrams.

In this paper all the notations are the same as in I. The numerical calculations were performed by the use of IBM 650 in the University of Oklahoma.

ATOMIC STATES OF FLUORINE

The author calculated the energies of the states of the fluorine atom and its ions on the basis of the hydrogenic atomic orbitals. The orthogonalized form of $2s$ was taken;

$$(2s) = N[r\exp(-\delta_2 r) + A\exp(-\delta_1 r)].$$

[2] K. Hijikata, Rev. Mod. Phys. **32**, 445 (1960).
[3] M. Kotani *et al.*, J. Phys. Soc. Japan **12**, 707, 1355 (1957).
[4] H. Brion, C. Moser, and M. Yamazaki, J. Chem. Phys. **30**, 673 (1959).
[5] J. C. Slater, Phys. Rev. **36**, 57 (1930).

TABLE II. Total energy of ^2P.

δ_2 \ δ_1	8.64	8.65	8.66	8.67
2.53	98.939 471	98.939 632	98.939 624	98.939 408
2.54	941 013	941 159	941 117	940 886
2.55	941 799	941 900	941 843	941 597
2.56	941 821	*941 918*	941 816	941 556
2.57	941 119	941 192	941 076	940 761
2.58	939 637	939 701	939 548	939 230
2.59	937 480	937 474	937 308	936 953
2.60	930 669	930 715	930 582	930 261

The minimum energy for the variation of the effective nuclear charges δ_1 and δ_2 was determined for each state. As an example Table II shows the total energy of the ground state of the neutral atom (^2P). The minimum occurs for $\delta_1=8.65$ and $\delta_2=2.56$. If we vary δ_1 by 0.01 in the neighborhood of the minimum, the change in the total energy is only 0.0001 a.u.$\sim$0.0003 ev, while the variation of δ_2 by the same amount gives rise to the change by $0.0004>0.01$ ev. The dependence of the total energy upon δ_2 is more critical than upon δ_1.

Table III shows the minima of various states and the corresponding effective nuclear charges. For all the states of F^-, F, and F^+ the best δ_1 changes only between 8.64 and 8.66, while the range of the best δ_2 is between 2.39 and 2.72.

From these tables we may expect that the slight variation of δ_1 does not give appreciable change in the total energy and that if one assumes the value 8.65 for all the states in the atom and in the molecule, the error from this assumption should be very small. This value of 8.65 for δ_1 will be taken throughout the following calculations and the effect of the variation of δ_2 will be emphasized.

Next, δ_2 is determined to minimize the sum of energies of the atomic constituents in various states as shown in Table IV. In this table it is found that the values of δ_2 differ very little for the states of the same ionicity. By these single values of the effective nuclear charge, a hypothetical case is represented where the electrons are not localized in a particular atom but still no interaction exists between the atoms.

In the last column of Table IV is shown the difference between the energies calculated in this manner and those from Table III. It is interesting that the difference depends mainly on the ionicity and the multiplicity.

TABLE III. Effective nuclear charges.

States	δ_1	δ_2	Total energy
$F^-(^1S)$	8.66	2.39	−98.68470 a.u.
F (^2P)	8.65	2.56	−98.94192
(^2S)	8.65	2.54	−97.96064
$F^+(^3P)$	8.64	2.71	−98.55145
(^1D)	8.64	2.71	−98.43721
(^1S)	8.64	2.70	−98.26623
(^3P)	8.64	2.72	−97.68831
$(^1P')$	8.64	2.70	−97.27661
$(^1S')$	8.64	2.70	−96.50339

TABLE IV. Effective nuclear charges for ionic structure and molecular ion.

F^-	F^+	δ_2	E a.u.	Δ[a]
^1S	^3P	2.53	−197.04914	0.19470
^1S	^1D	2.53	−196.94241	0.17950
^1S	^1S	2.53	−196.78231	0.16862
^1S	$^3P'$	2.53	−196.18949	0.18352
^1S	^1P	2.52	−195.80044	0.16087
^1S	$^1S'$	2.52	−195.02681	0.16128
F	F^+			
^2P	^3P	2.63	−197.45022	0.04335
^2P	^1D	2.62	−197.33927	0.03986
^2P	^1S	2.62	−197.17342	0.03473
^2P	$^3P'$	2.63	−196.58682	0.04341
^2P	^1D	2.62	−196.18537	0.03316
^2P	$^1S'$	2.62	−195.41026	0.03505

[a] Δ is obtained by subtracting the values in Table III from E. The author did not show the structure $F(^2S)+F^+$, but found $\delta_2=2.61$ or 2.62.

In the following calculation, therefore, the three pairs of δ_1 and δ_2 are tentatively taken; that is,

δ_1	8.65	8.65	8.65
δ_2	2.53	2.56	2.62.

Although the physical significance of these values is not very apparent, these may be called the effective nuclear charges of the ionic structure, the covalent structure, and the molecular ion, respectively.

GROUND STATE

With the values of effective nuclear charges just shown, the author repeated the same calculation as in I. He took account of all the first and the second quantum orbitals and the configurations therefrom, built up the energy matrix, and solved the secular equations.

Before showing the results, the convenient method of calculation of the integrals must be mentioned. The total energy of the molecule is about 197 a.u., while the expected dissociation energy is less than 0.1 a.u. The accuracy of at least five digits must, therefore, be secured. This does not mean, however, that all the

TABLE V. Parameters of α, β.

	δ_2	R in A	α
$\beta=6.00$			
	2.53	1.2545...	20.51383 40
	2.56	1.2398...	20.27347 75
	2.62	1.2115...	19.80916 00
$\beta=7.50$			
	2.53	1.5682...	25.64229 27
	2.56	1.5498...	25.34179 69
	2.62	1.5143...	24.76145 02

TABLE VI. Dissociation energy.

			r_e	D_e	
(1)	$\delta_1=8.65$	$\delta_2=2.53$	1.456 A	1.81 ev	1.93 ev
(2)	$\delta_1=8.65$	$\delta_2=2.56$	1.441	1.99	1.99
(3)	$\delta_1=8.65$	$\delta_2=2.62$	1.441	1.84	2.26
(4)	$\delta_1=8.665\ldots$ (I)	$\delta_2=2.599\ldots$	1.409	1.83	2.04
(5)	$\delta_1=8.65$	$\delta_2=2.582$ [interpolated from (1), (2) and (3)]	1.437	2.02	
(6)	Experiment		1.435	1.68	

integrals listed in I should be calculated with five-digit accuracy, because most of the intra-atomic (one-center) integrals and the one-electron integrals, which are easy to calculate, have large values and amount to greater portions of 197 a.u. The difficult two-electron, two-center integrals are very often less than 0.01 au. Hence, if one calculates only three digits of these integrals, it is expected that the results may have some physical meaning.

In I was calculated all the integrals for two pairs of values of $\alpha=\delta_1 R$ and $\beta=\delta_2 R$, as exactly possible. Here the value of β at 6.00 and 7.50 is fixed as in I, and the values of R for each δ_2 are determined as in Table V. The values of α are determined as these R's multiplied by $\delta_1=8.65$, which are shown in the same table. The author performed exact calculation for the one-electron and the one-center integrals; the two-center integrals are calculated as follows. Each integral is reduced to the form

$$\alpha^m\beta^n[\xi+\eta(\alpha,\beta)],$$

where ξ is either a one-electron integral or a function of β, and η is a function of α and β. ξ was calculated exactly and η was obtained by logarithmic interpolation from the values given in I.

In the calculation of the dissociation energy the author again used the Morse curve and the experimental vibrational frequency 892 cm^{-1}. The results are shown in Table VI. In the third column is the value of D_e obtained by subtracting the total energy of the atoms calculated with $\delta_1=8.65$ and $\delta_2=2.56$ from the total energy of the molecule for each set of effective nuclear charges. $\delta_2=2.56$ gives the lowest energy. Therefore, there is no appreciable difference between the values of effective nuclear charge for the atom and for the molecule. In fact, if quadratic interpolation is applied, $D_e=2.02$ ev and $\delta_2=2.58$. This D_e is the "minimum to minimum" dissociation energy. It is found that $\delta_2=2.56$ is close to this minimum δ_2, and that $D_e(2.56)$ differs very little from $D_e(\min)$. In some other molecules the atomic δ is far from the minimum δ of the molecule, which makes the choice of δ very critical to the value of dissociation energy. Quadratic relation between r_e and δ_2 is assumed, and $(r_e)_{\min}=1.437$ A obtained.

In the last column of Table VI is shown the dissociation energy obtained by the subtraction of the total atomic energy from the total molecular energy, both calculated with the same value of effective nuclear charges. The increasing tendency of D_e with δ_2 is mainly attributed to the increase of the atomic energy. It may be easily expected from Table II that the same increasing tendency is observed if δ_2 is decreased below 2.53.

As mentioned in I, it is a peculiarity of F_2 that the calculated value of D_e by ASMO is greater than the experimental value. The experimental value of D_e was determined from the electron affinity, which is about 84 kcal/mole in various experiments.[6] By taking the experimental value of D_e as 1.68 ev, the appearance of the result of ASMO is curious.

The atomic ground state ^2P is the state of a single configuration as far as the first and second quantum orbitals are considered. If the molecule is formed, eight configurations interact to lower the energy of the ground state $^1\Sigma_g^+$. The correlation energy is, therefore, partially covered by the configuration interaction. On the other hand, some of the upper orbitals will come down and mix with the lower orbitals. If the interatomic distance is small, this effect of the upper orbitals is not negligible. The lower values of the dissociation energy which have been calculated for the other molecules may be corrected into higher value if the effect of the third quantum orbitals is considered. However, since the interatomic distance of F_2 is large compared with the atomic radius, this mixing effect of the higher orbitals is expected to be small. Therefore, one does not see the floating-up of the ground state due to the neglect of higher orbitals as conspicuously as in oxygen and in lithium.[3]

Table VII shows the eigenfunctions of the ground state. The coefficients do not vary so much with the effective nuclear charge. In all the cases the contribution of the ground configuration (σ_u^2) is so large that this single configuration seems almost accurate representation for the ground state. This is not true, however, because, as seen in I, the single configuration does not give the stable molecule. The increase in the coefficient of (σ_g^2) with the interatomic distance shows that the state becomes more covalent as R increases. Since

[6] H. O. Pritchard, Chem. Revs. **52**, 529 (1953).

TABLE VII. Coefficients of molecular wave functions for $^1\Sigma_g^+$.

	$\delta_2=2.53$		$\delta_2=2.56$		$\delta_2=2.62$	
β	6.0	7.50	6.0	7.50	6.0	7.50
(σ_u^2)	0.97328	0.92856	0.97270	0.93129	0.97106	0.93602
$(s_u\sigma_u)$	−0.13191	−0.05713	−0.14564	−0.06482	−0.16975	−0.07952
(π_g^2)	−0.05588	−0.09122	−0.05272	−0.08890	−0.04822	−0.08289
(π_u^2)	−0.02358	−0.03495	−0.02286	−0.03503	−0.02126	−0.03545
(σ_g^2)	−0.17522	−0.35160	−0.16881	−0.34355	−0.15731	−0.32885
(s_u^2)	−0.02412	−0.03094	−0.02113	−0.03055	−0.01644	−0.02951
$(s_g\sigma_g)$	0.00610	−0.00529	0.00741	−0.00462	0.01002	−0.00305
(s_g^2)	−0.01823	−0.01916	−0.01835	−0.01943	−0.01814	−0.01974

in this paper, the author is describing mainly the energy levels, the detailed discussion on the eigenfunctions will be left to the other paper, where various properties of the molecule, the magnetic shielding in NMR, the spin-orbit interaction, etc., will be treated.

EXCITED STATES

Table VIII shows the result of calculation for almost all the states. The states which do not have experimental significance are omitted from this table. For each state and for each value of β the best value of δ_2 is fixed, assuming the function $E(\delta_m)$ is quadratic. In the column denoted by δ_m are shown these values of δ_2. The values of the energies for δ_m are also shown in the column E_m.

The states numbered from (1) to (7) tend to the ground atomic structure $^2P+^2P$ at infinite separation, and all of these except (1) appear to have no minima within the range of our calculation. In almost all the cases δ_m decreases with the approach of the atoms and also with the excitation of the molecule. Since the value of β is kept constant, the decrease in δ_m means the increase of R. Therefore, the energy curve is shifted to the larger value of R as the state is higher.

The author evaluated the ionicity of some states as was described in Part I. The eigenfunction obtained in I was used. As seen in Table VII, the coefficients are not much different with the change in the effective nuclear charges. Therefore, the eigenfunctions in I will give the ionicity which is sufficient for this discussion. Table IX shows the result of evaluation. It is clearly seen that the states (1) to (7) are strongly covalent, while the others are ionic. It is interesting to look at this table with Table VIII. In the ground state δ_m is larger than 2.56, and in the higher excited states it is smaller than the ionic value 2.53. From the ground state to (7) the ionicity decreases from state to state. If the "atomic" consideration is pursued, the effective nuclear charge should increase from a value between 2.53 and 2.56 as the state is higher. Any such clear-cut correspondence between the ionicity and the effective nuclear charge cannot be found, however. Therefore, the atomic picture does not help in guessing the effective nuclear charge in the molecular state.

The author calculated the vertical distance between the minimum of $^1\Sigma_g^+$ and the first four excited states by assuming the interpolation formula $A\exp(-ar)$. The results are

$^1\Pi_u$	4.49 ev
$^3\Pi_u$	3.73
$^1\Pi_g$	6.50
$^3\Pi_g$	6.31.

The first two values are to be compared with the experimental values, 4.28 ev and 3.16 ev, respectively. Since the agreement is fairly good, one may expect the same

TABLE VIII. Energies and effective nuclear charges of molecular states (in a.u.).

	$\beta=6.00$					$\beta=7.50$				
	$\delta_2=2.53$	2.56	2.62	δ_m	E_m	$\delta_2=2.53$	2.56	2.62	δ_m	E_m
(1) $^1\Sigma_g^+$	−0.02985	−0.03731	−0.01488	2.563	−0.03737	−0.06328	−0.06856	−0.06467	2.581	−0.07012
(2) $^3\Pi_u$	0.22733	0.23692	0.29815	2.523	0.22654	0.02693	0.02724	0.04755	2.539	0.02527
(3) $^1\Pi_u$	0.26485	0.27554	0.33261	2.520	0.26471	0.04394	0.04413	0.06580	2.543	0.04303
(4) $^3\Pi_g$	0.42922	0.44565	0.52914	2.513	0.42573	0.08370	0.08616	0.11186	2.551	0.08320
(5) $^1\Pi_g$	0.43644	0.45415	0.53148	2.518	0.43518	0.08675	0.08936	0.11563	2.539	0.08376
(6) $^3\Sigma_u^+$	0.39619	0.41108	0.47966	2.509	0.39298	0.08702	0.09050	0.11346	2.526	0.08712
(7) $^1\Sigma_g^+$	0.59969	0.63240	0.73259	2.459	0.56748	0.14501	0.15081	0.18926	2.525	0.14483
(8) $^3\Pi_g$	1.05365	1.09140	1.20452	2.454	1.01358	0.64219	0.65546	0.70492	2.493	0.63636
(9) $^3\Pi_u$	1.23400	1.28090	1.40980	2.426	1.16326	0.68893	0.70476	0.75788	2.511	0.69315
(10) $^1\Pi_g$	1.15125	1.18872	1.30222	2.459	1.11508	0.74461	0.75852	0.80904	2.489	0.73748
(11) $^1\Pi_u$	1.32477	1.37285	1.50525	2.424	1.25021	0.78613	0.80277	0.86734	2.473	0.77329
(12) $^1\Sigma_u^+$	0.88420	0.89591	0.96656	2.525	0.88466	0.68219	0.69522	0.73140	2.442	0.66677
(13) $^3\Sigma_u^+$	1.15949	1.20271	1.32414	2.431	1.09697	0.71700	0.73163	0.78364	2.419	0.68143
(14) $^1\Sigma_g^+$	1.14055	1.15928	1.23535	2.500	1.13397	0.79481	0.80685	0.84756	2.485	0.78868

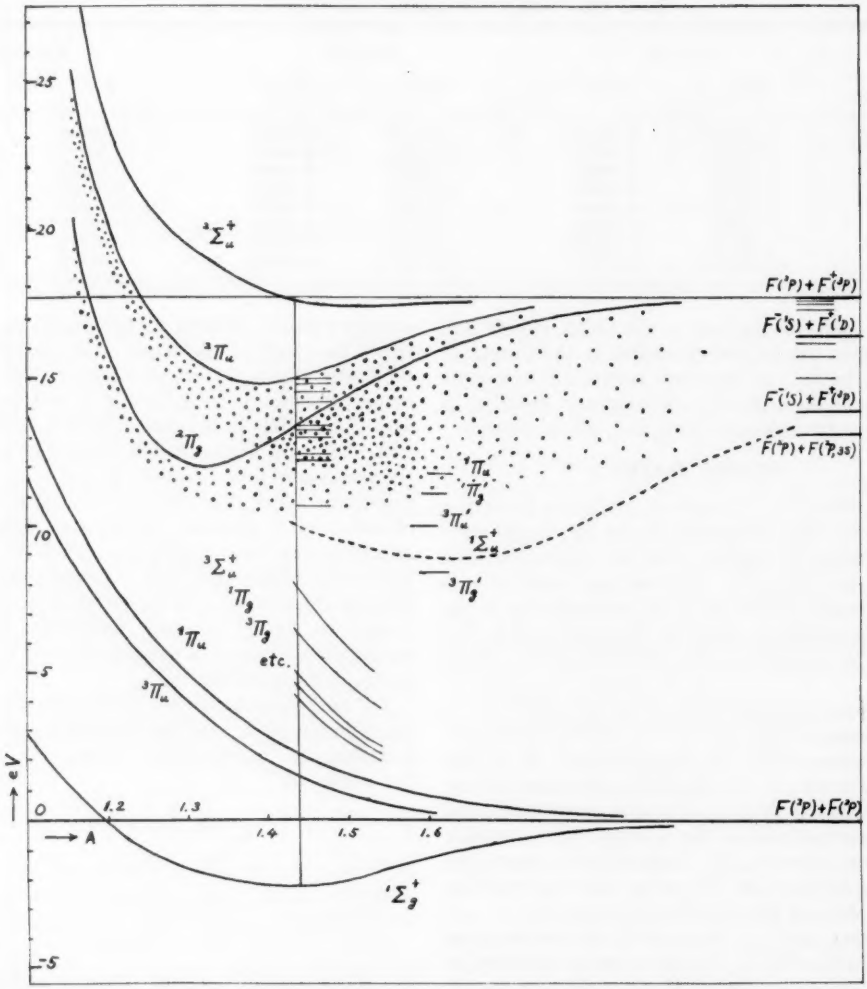

FIG. 1. Energy diagram. The ground states and the lower excited states of F_2 and F_2^+, which converge to the ground states of the atomic constituents, are shown by full lines. The dotted region is the possible Rydberg region below the two lowest states of F_2^+ in accordance with the experimental data. Most of the higher excited states of F_2 are in the Rydberg region except $^1\Sigma_u^+$, which is shown by a dotted line.

degree of accuracy for $^1\Pi_g$, which is important for the calculation of the magnetic shielding in NMR. As mentioned in I, $^3\Pi_{u,g}$ are always lower than $^1\Pi_{u,g}$.

Since the upper states (8) to (14) do not tend to the ground state of the atomic constituents, and since the ionic character of these states are very predominant, the difference of these energies is calculated from the calculated values of the total energy of the ions in $^3P+^1S$ or $^1D+^1S$, resulting in the values shown in Table X. By using the experimental atomic term values

$^3P+^1S$ 0.50122 a.u.

above $^2P+^2P$,

$^1D+^1S$ 0.59632

the energy levels can be located. In Fig. 1, however, are shown the positions of the energy levels of these states for $\beta=7.50$ only.

LOWER STATES OF FLUORINE MOLECULE ION

In order to understand the features of the molecular spectra and to have the physical insight of various properties of the molecule, it is very helpful to consider the molecule and its ion simultaneously. The author took the effective nuclear charge $\delta_1=8.65$ and $\delta_2=2.62$ and calculated the lower energy levels of the fluorine molecule ion. If the fluorine molecule loses one electron in the antibonding orbital π_g, it becomes the molecular ion in its ground configuration. Therefore, it is to be

expected that the interatomic distance of the ion is smaller than that of the neutral molecule. This tendency is seen in the oxygen molecule ion, although very small. On the other hand, however, the atomic ion usually has a considerably smaller radius. Hence, the ratio of the averaged atomic radius to the interatomic distance in the fluorine molecule ion is still as small as the same ratio in the molecule. For this reason, one can also expect a good result from the calculations of the same scheme as was done for F_2.

The main reason for presenting this article on the molecular ion with the description of the energy levels of the molecule is as follows. Do the results given in the preceding paragraph for the excited states of the fluorine have some practical meaning? A criterion for the physical significance of the calculated higher excited levels by the investigation of the energy levels of the molecular ion will be found. Secondly, little is known about the ionization potential and the spectra of F_2^+. We wish to stimulate experimentalists to measure these.

Table XI shows the MWF's of the state $^2\Pi_g$ of F_2^+. Here the notation by the vacant orbital as in I is used. Since there are 20 states which have configuration interaction, a short-cut method was used. Interest is only in the lowest state, because, as is clear from the configuration, all the other states are expected to be very high. In I it was shown that the states having weak configuration interactions with the ground state can be neglected to give a result not appreciably different from that of exact calculation. In the last columns of Table XI are shown the off-diagonal elements between the lowest state and the others. Only seven states marked by * were taken, and the configuration interaction then calculated. Among the neglected configurations J has the largest interaction with the lowest state, but the quantity $H_{ij}^2/H_{ii}-H_{jj}$ is about 0.002 a.u. (0.054 ev). The energy matrix is given in Table XII with the lowest root.

The wave function of $^2\Pi_u$ is easily written down by interchanging π_g and π_u in the wave functions of $^2\Pi_g$. In the same manner seven states were obtained and

TABLE IX. Ionicity of States.

States	No. in Table VIII	$\beta=6.00$	$\beta=7.50$
$^1\Sigma_g^+$	(1)	0.306	0.182
$^3\Pi_u$	(2)	0.271	0.131
$^1\Pi_u$	(3)	0.238	0.100
$^3\Pi_g$	(4)	0.166	0.062
$^1\Pi_g$	(5)	0.114	0.041
$^1\Sigma_g^+$	(7)	0.096	0.015
$^3\Pi_g$	(8)	0.891	0.937
$^3\Pi_u$	(9)	0.734	0.868
$^1\Pi_g$	(10)	0.883	0.958
$^1\Pi_u$	(11)	0.768	0.873
$^1\Sigma_u^+$	(12)	0.912	1.000[a]
$^1\Sigma_g^+$	(14)	0.747	0.620[b]

[a] From the defect of the definition of ionicity, this value turns out to be slightly greater than 1, showing this state is strongly ionic.

[b] The irregularity of these values is attributed to the crossing of two states.

TABLE X.

	r	E	r	E	From
(8) $^3\Pi_g$	1.265 A	0.17988	1.591	−0.19734 A	$^3P+^1S$
(9) $^3\Pi_u$	1.308	0.32956	1.580	−0.14055	$^3P+^1S$
(10) $^1\Pi_g$	1.291	0.17465	1.594	−0.19295	$^1D+^1S$
(11) $^1\Pi_u$	1.309	0.30978	1.604	−0.16714	$^1D+^1S$
(12) $^1\Sigma_u^+$	1.257	−0.05577	1.625	−0.27366	$^1D+^1S$
(13) $^3\Sigma_u^+$	1.306	0.26327	1.640	−0.15227	$^3P+^1S$
(14) $^1\Sigma_g^+$	1.270	0.19354	1.597	−0.15175	$^1D+^1S$

the configuration interaction calculated. The next lowest states which have allowed transition to these states are $^2\Sigma_u^+$ and $^2\Sigma_u^-$. The wave functions of these are

$^2\Sigma_u^+$:

$$A\ 2^{-\frac{1}{2}}\{\,|\,\pi_g^+\bar{\pi}_g^-\sigma_u\,|-|\,\bar{\pi}_g^+\pi_g^-\sigma_u\,|\,\}$$

$$B\ 2^{-\frac{1}{2}}\{\,|\,\pi_u^+\bar{\pi}_u^-\sigma_u\,|-|\,\bar{\pi}_u^+\pi_u^-\sigma_u\,|\,\}$$

$$C\ \tfrac{1}{2}\{\,|\,\sigma_g\bar{\pi}_g^+\pi_u^-\,|+|\,\sigma_g\bar{\pi}_g^-\pi_u^+\,|-|\,\sigma_g\pi_g^+\bar{\pi}_u^-\,|-|\,\sigma_g\pi_g^-\bar{\pi}_u^+\,|\,\}$$

$$D\ 12^{-\frac{1}{2}}\{\,|\,\sigma_g\bar{\pi}_g^+\pi_u^-\,|+|\,\sigma_g\bar{\pi}_g^-\pi_u^+\,|+|\,\sigma_g\pi_g^+\bar{\pi}_u^-\,|+|\,\sigma_g\pi_g^-\bar{\pi}_u^+\,|-2\,|\,\bar{\sigma}_g\pi_g^+\pi_u^-\,|-2\,|\,\bar{\sigma}_g\pi_g^+\pi_u^-\,|\,\}$$

$^2\Sigma_u^-$:

$$A\ 6^{-\frac{1}{2}}\{\,|\,\pi_g^+\bar{\pi}_g^-\sigma_u\,|+|\,\bar{\pi}_g^+\pi_g^-\sigma_u\,|-2\,|\,\pi_g^+\pi_g^-\bar{\sigma}_u\,|\,\}$$

$$B\ 6^{-\frac{1}{2}}\{\,|\,\pi_u^+\bar{\pi}_u^-\sigma_u\,|+|\,\bar{\pi}_u^+\pi_u^-\sigma_u\,|-2\,|\,\pi_u^+\pi_u^-\bar{\sigma}_u\,|\,\}$$

$$C\ \tfrac{1}{2}\{\,|\,\sigma_g\bar{\pi}_g^+\pi_u^-\,|-|\,\sigma_g\bar{\pi}_g^-\pi_u^+\,|-|\,\sigma_g\pi_g^+\bar{\pi}_u^-\,|+|\,\sigma_g\pi_g^-\bar{\pi}_u^+\,|\,\}$$

$$D\ 12^{-\frac{1}{2}}\{\,|\,\sigma_g\bar{\pi}_g^+\pi_u^-\,|-|\,\sigma_g\bar{\pi}_g^-\pi_u^+\,|+|\,\sigma_g\pi_g^+\bar{\pi}_u^-\,|-|\,\sigma_g\pi_g^-\bar{\pi}_u^+\,|-2\,|\,\bar{\sigma}_g\pi_g^+\pi_u^-\,|+2\,|\,\bar{\sigma}_g\pi_g^-\pi_u^+\,|\,\}.$$

In both cases the state A interacts strongly with B but not with the others. Therefore, simply solved 2×2 secular equations.

The zero point in Table XII is the calculated value of the ground atomic structure $^2P+^3P$. The roots of these secular equations together with the lowest energy levels of $^2\Pi_u$, $^2\Sigma_u^+$ and $^2\Sigma_u^-$ are expressed in ev in Table XIII. Since there are no measurements of the vibrational frequency and the equilibrium distance, Morse curve cannot be applied to these states in order to calculate the dissociation energies. In Fig. 1 are shown the potential curves with reasonable shapes, by adjusting the energy at infinite separation to the experimental value of $^2P+^3P$. Thus the ground state of F_2^+ is seen as really a $^2\Pi_g$ state and that $^2\Pi_g$, $^2\Pi_u$ and $^2\Sigma_u^+$ have potential minima. The author emphasizes that this calculation for F_2^+ is not so accurate as the calculation for F_2. If the calculation for F_2^+ is performed in the same scheme of perfect configuration interaction, of several interatomic distances and of varied effective nuclear charges, these curves will be lower.

TABLE XI. Wave functions of $^2\pi_g$-states of F_2^+.

	Configuration	Antisymmetrized product (MWF)	Off-diagonal elements with the lowest state $\beta=6.00$	$\beta=7.50$
A^*	$(\pi_g\sigma_u^2)$	$\lvert\ \sigma_u\bar{\sigma}_u\pi_g^+\ \rvert$	...	...
B	(π_g^3)	$\lvert\ \pi_g^+\bar{\pi}_g^+\pi_g^-\ \rvert$	0.03421	0.03081
C	$(\pi_u^2\pi_g)$	$\lvert\ \pi_u^+\bar{\pi}_u^+\pi_g^-\ \rvert$	0	0
D	$(\pi_u^2\pi_g)$	$2^{-\frac{1}{2}}\{\lvert\ \pi_u^+\bar{\pi}_u^-\pi_g^+\ \rvert-\lvert\ \bar{\pi}_u^+\pi_u^-\pi_g^+\ \rvert\}$	0.03910	0.04026
E	$(\pi_u^2\pi_g)$	$6^{-\frac{1}{2}}\{\lvert\ \pi_u^+\bar{\pi}_u^-\pi_g^+\ \rvert+\lvert\ \bar{\pi}_u^+\pi_u^-\pi_g^+\ \rvert-2\lvert\ \pi_u^+\pi_u^-\bar{\pi}_g^+\ \rvert\}$	0	0
F^*	$(\sigma_g\pi_u\sigma_u)$	$2^{-\frac{1}{2}}\{\lvert\ \sigma_g\bar{\pi}_u^+\sigma_u\ \rvert-\lvert\ \bar{\sigma}_g\pi_u^+\sigma_u\ \rvert\}$	−0.19348	−0.21881
G^*	$(\sigma_g\pi_u\sigma_u)$	$6^{-\frac{1}{2}}\{\lvert\ \sigma_g\bar{\pi}_u^+\sigma_u\ \rvert+\lvert\ \bar{\sigma}_g\pi_u^+\sigma_u\ \rvert-2\lvert\ \sigma_g\pi_u^+\bar{\sigma}_u\ \rvert\}$	0.27285	0.31455
H^*	$(\pi_g\sigma_g^2)$	$\lvert\ \sigma_g\bar{\sigma}_g\pi_g^+\ \rvert$	0.28847	0.32618
I^*	$(\pi_g s_u^2)$	$\lvert\ s_u\bar{s}_u\pi_g^+\ \rvert$	0.11160	0.11046
J	$(s_g\sigma_g\pi_g)$	$2^{-\frac{1}{2}}\{\lvert\ s_g\bar{\pi}_g^+\sigma_g\ \rvert-\lvert\ \bar{s}_g\pi_g^+\sigma_g\ \rvert\}$	−0.06393	−0.04018
K	$(s_g\sigma_g\pi_g)$	$6^{-\frac{1}{2}}\{\lvert\ s_g\bar{\pi}_g^+\sigma_g\ \rvert+\lvert\ \bar{s}_g\pi_g^+\sigma_g\ \rvert-2\lvert\ s_g\pi_g\bar{\sigma}_g\ \rvert\}$	0.03691	0.02320
L^*	$(s_u\pi_g\sigma_u)$	$2^{-\frac{1}{2}}\{\lvert\ s_u\bar{\pi}_g^+\sigma_u\ \rvert-\lvert\ \bar{s}_u\pi_g^+\sigma_u\ \rvert\}$	0.23576	0.11245
M		$6^{-\frac{1}{2}}\{\lvert\ s_u\bar{\pi}_g^+\sigma_u\ \rvert+\lvert\ \bar{s}_u\pi_g^+\sigma_u\ \rvert-2\lvert\ s_u\pi_g^+\bar{\sigma}_u\ \rvert\}$	−0.01316	−0.00685
N	$(s_g\pi_u\sigma_u)$	$2^{-\frac{1}{2}}\{\lvert\ s_g\bar{\pi}_u^+\sigma_u\ \rvert-\lvert\ \bar{s}_g\pi_u^+\sigma_u\ \rvert\}$	−0.01572	−0.00764
O		$6^{-\frac{1}{2}}\{\lvert\ s_g\bar{\pi}_u^+\sigma_u\ \rvert+\lvert\ \bar{s}_g\pi_u^+\sigma_u\ \rvert-2\lvert\ s_g\pi_u^+\bar{\sigma}_u\ \rvert\}$	0.00908	0.00441
P	$(s_u\pi_u\sigma_g)$	$2^{-\frac{1}{2}}\{\lvert\ s_u\bar{\pi}_u^+\sigma_g\ \rvert-\lvert\ \bar{s}_u\pi_u^+\sigma_g\ \rvert\}$	0	0
Q		$6^{-\frac{1}{2}}\{\lvert\ s_u\bar{\pi}_u^+\sigma_g\ \rvert+\lvert\ \bar{s}_u\pi_u^+\sigma_g\ \rvert-2\lvert\ s_u\pi_u^+\bar{\sigma}_g\ \rvert\}$	0	0
R	$(s_g\pi_u s_u)$	$2^{-\frac{1}{2}}\{\lvert\ s_g\bar{\pi}_u^+s_u\ \rvert-\lvert\ \bar{s}_g\pi_u^+s_u\ \rvert\}$	0	0
S		$6^{-\frac{1}{2}}\{\lvert\ s_g\bar{\pi}_u^+s_u\ \rvert+\lvert\ \bar{s}_g\pi_u^+s_u\ \rvert-2\lvert\ s_g\pi_u^+\bar{s}_u\ \rvert\}$	0	0
T^*	$(s_u^2\pi_g)$	$\lvert\ s_g\bar{s}_g\pi_g^+\ \rvert$	0.09967	0.08995

POTENTIAL CURVES AND COMPARISON WITH EXPERIMENTS

The results obtained are all illustrated in Fig. 1. There has been enough discussion about the ground state and lower excited state of F_2. Here will be discussed the higher excited states of F_2 and the lower states of F_2^+. The ground state of F_2^+ dips down for the shorter interatomic distance, and all the higher excited states calculated before appear above this $^2\Pi_g$ for $\beta=6.00$. Since each state of F_2^+ must be accompanied with the Rydberg series which are related to the higher orbitals, these calculated levels of the excited states do

TABLE XII. Energy matrix of $^2\Pi_g$ (in a.u.).

	A	F	G	H	I	L	T
$R=1.211$ A							
	0.05046	−0.19348	0.27285	0.28847	0.11160	0.23576	0.09967
		1.20250	−0.15058	−0.13388	0.00000	−0.09660	0.00000
			1.45905	0.30397	0.00000	−0.09401	0.00000
				1.51323	0.09967	−0.06393	0.12722
					2.52110	−0.12927	0.25574
						1.47840	−0.00486
Lowest root −0.11620							3.30419
$R=1.514$ A							
	0.09691	−0.21881	0.31455	0.32618	0.11046	0.11245	0.08995
		0.75693	−0.17188	−0.15977	0.00000	−0.64870	0.00000
			1.05432	0.34675	0.00000	−0.06379	0.00000
				0.82774	0.09324	−0.04283	0.11591
					2.23948	−0.06216	0.28995
						1.32299	0.00281
Lowest root −0.14800							2.52581

not have any physical meaning at all. Any information at shorter distances cannot be derived, unless account is taken of the third, fourth, etc. quantum orbitals which are supposed to mix with the lower orbitals appreciably. Therefore, only the levels calculated at the larger value of R are shown.

Recently Iczkowski and Margrave[7] measured the far-ultraviolet spectra of the fluorine molecule and discovered a Rydberg series converging to 15.7 ev above $^1\Sigma_g^+$. They found also many higher states of F_2, among which the most interesting is the ionic state $^1\Sigma_u^+$. This state is located 11.96 ev above the ground state and has very small fundamental vibrational frequency 430 cm^{-1}. From their data the author roughly marked with dots two possible Rydberg regions in the figure. Since the values of energy of $^2\Pi_g$ are 16.28 ev at 1.221 A and 15.41 A above the minimum of $^1\Sigma_g^+$, the vertical distance from the ground state must be lower than these. If the calculations for the molecular ion were performed as accurately as for the neutral molecule, these values must be still lower. Eve's calculation by LCAO SCF method[8] shows that the orbital energy of π_g is -12.325 ev. In various diatomic molecules the energy of the highest occupied LCAO SCF orbital coincides very well with the observed ionization potential as shown in Table XIV. Since Eve's value can be reasonably understood in the diagram, the problem remains in discrepancy between the calculated and experimental ionization potentials of F_2. The author hopes that the measurement will be done for the transition $^2\Pi_g - ^2\Sigma_u^+$ in order to determine the lower limit of the dissociation energy of F_2^+.

TABLE XIII. Lowest states of F_2 (in ev).

	$R=1.211$ A	$R=1.514$ A
$^2\Pi_g$	-3.161	-4.026
$^2\Pi_u$	2.446	-2.518
$^2\Sigma_u^+$	7.158	-0.023
$^2\Sigma_u^-$	10.347	3.515

[7] R. P. Iczkowski and J. L. Margrave, J. Chem. Phys. **30,** 403 (1959).
[8] J. Eve, Proc. Roy. Soc. (London) **A246,** 582 (1958).

TABLE XIV. Ionization potential calculated by LCAO SCF.

Molecule	N_2	NO	O_2	F_2
Highest occupied orbital	σ_g	2π	π_g	π_g
$-$(Orbital energy) (in ev)	14.82[a]	9.14[c]	10.73[e]	12.33[f]
Observed ionization potential	15.58[b]	9.25[d]	12.08[d]	(15.7)

[a] C. W. Sherr, J. Chem. Phys. **23,** 569 (1955).
[b] R. E. Worley and F. A. Jenkins, Phys. Rev. **54,** 305 (1938).
[c] Footnote reference 4.
[d] K. Watanabe, J. Chem. Phys. **26,** 542 (1957).
[e] Footnote reference 3.
[f] Footnote reference 8.

$^1\Sigma_u^+$ is only one singlet state which is located clearly outside the Rydberg region. As seen before, this state is strongly ionic and does not rise up so rapidly at the smaller distance. The position of $^1\Sigma_u^+$ in Fig. 1 is 10.8 ev above the minimum of $^1\Sigma_g^+$.

The spectra measured by Gale and Monk[9] are still beyond the scope of this calculation. They reported the emission spectra $^1\Sigma - ^1\Pi$, the peculiarity of which is the short interatomic distance 1.28 A of the $^1\Pi$ state. The only possibility of finding a state with such a short interatomic distance is in the Rydberg region below $^2\Pi_g$. Many factors of approximation, such as the exclusion of higher orbitals and the rather artificial use of experimental atomic term values, however, prevent further discussion on the higher excited states. As is clear in Fig. 1, almost all the high states are in the Rydberg region. The same tendency may be expected in other molecules having smaller interatomic distances as compared with atomic radii. Therefore, the study of Rydberg will throw a new light on the theoretical investigation of molecular spectra.

ACKNOWLEDGMENT

We express our thanks to Professor Kotani, University of Tokyo, for his constant encouragement. We owe much to the University of Oklahoma for the free use of IBM 650.

[9] H. G. Gale and G. S. Monk, Astrophys. J. **69,** 77 (1929).

High-Energy Radiation Damage to Fluorescent Organic Solids

CHARLES F. SHARN*

U. S Naval Research Laboratory, Washington, D. C.

(Received March 2, 1960)

Radiation damage to organic solids exposed to Co^{60} gamma rays has been studied through the analysis of the induced fluorescent changes. From the fluorescence degradation for two series of aromatic hydrocarbons, correlations between chemical structure and radiation damage have been established. In addition, modifications in a conventional model used to describe the fluorescent degradation mechanism in organic materials are suggested by the data. Some of the organic materials studies have potential application in a dosimetry system based on fluorescence degradation.

INTRODUCTION

THE relationship between radiation damage and fluorescence changes in organic solids has been studied by Birks and Black,[1] Hardwick and McMillian,[2] and Schulman, Etzel, and Allard.[3] From the irradiation of aromatic hydrocarbons with either alpha rays, gamma rays, or electrons, all these investigators observed that the degradation behavior of the materials could be described by the expression: $(I/I_0)=(1+AD^n)^{-1}$ where I/I_0 is the ratio of luminescence efficiency of the irradiated solid to that of the unirradiated solid, A is a constant characteristic of the material, D is the absorbed dose, and the exponent n is generally found to be equal to 1.0. It can be simply shown that the constant A is equal to $(D_{\frac{1}{2}})^{-n}$ where $D_{\frac{1}{2}}$ is the absorbed dose required to reduce the optically excited fluorescence to $\frac{1}{2}$ its initial value. In all cases, it was stated or assumed that the constants in this expression were the same for all the emission peaks of a material, i.e., the spectrum degraded uniformly, and that the degradation process was completely irreversible. The amenability of the degradation data to analytical treatment was demonstrated by Rosenstock and Schulman[4] in their derivation of the so-called "smeared-out" model. In this model they assumed, as had Birks,[5] that the large degree of fluorescent degradation resulted from the production of a "poison" which absorbs excitons and "quenches" a large number of normal molecules. It is implied in the "smeared-out" model that there is a constant probability that excitation of a molecule throughout the material, results in quenching independent of the distance from the poison molecule. This model agrees with the conclusion of Hardwick[2] that the excitons have a very long range.

The extent of fluorescent degradation in organic solids was suggested as the basis for dose determination,[3] and such a dosimetry system using anthracene and *p*-quaterphenyl has been developed.[6]

In the present study the preceding work was extended with the goal of furthering the understanding of the fluorescence degradation process and relating the fluorescence changes to damage detectable by other means. From a comparison of damage detectable by chemical changes ("chemical damage") with that observable through changes in fluorescence ("fluorescence damage"), a link between these phenomena is suggested. The mechanisms used to describe chemical and fluorescent damage have many similarities. According to deHalas,[7] at low doses ,i.e., the minimum doses necessary to produce detectable chemical effects ($\sim 10^8$r), a first-order (exponential) rate reaction can be used to describe chemical damage to aromatic hydrocarbons. At the much lower doses ($\sim 10^3$ lower) for minimal fluorescence damage in the materials it has been shown that the data fits several models including that for an exponential-type mechanism. However, at the higher relative doses it develops that both damage mechanisms are no longer exponential in nature. Colichman and Gercke[8] attributed the high-dose behavior in chemical damage to the "protective nature" of the higher polymers formed in the irradiation. Rosenstock and Schulman[4] showed that the D^{-1} dependence of the luminescence degradation at high doses follows from the smeared-out model.

Fluorescence changes in compounds of two homologous organic series were studied as a function of total dose, dose-rate, temperature of irradiation, and time after irradiation, (recovery of fluorescence). In addition, experiments were performed to determine the effect of optical self-absorption and annealing on luminescence degradation. Reference was made to the reported data of chemical damage to polyphenyls in order to compare

* This work used in partial fulfillment of the requirements for the degree of Ph.D. in Chemical Engineering at the University of Maryland.

[1] J. B. Birks and F. A. Black, Proc. Phys. Soc. (London) **64A**, 511 (1951).

[2] E. R. Hardwick and W. G. McMillian, J. Chem. Phys. **26**, 1463 (1957).

[3] J. H. Schulman, H. Etzel, and J. Allard, J. Appl. Phys. **28**, 792 (1957).

[4] H. B. Rosenstock and J. H. Schulman, J. Chem. Phys. **30**, 1, 116–125 (1959).

[5] J. B. Birks, Proc. Phys. Soc. (London) **63A**, 1044 (1950).

[6] F. H. Attix, Nucleonics **17**, No. 4, 142 (1959).

[7] D. R. de Halas, "Radiolytic and pyrolytic decomposition of organic coolants," *Proceedings of the Second International Conference on the Peaceful Uses of Atomic Energy Geneva, 1958* (United Nations, Geneva, 1959).

[8] E. L. Colichman and R. H. Gercke, Nucleonics **14**, No. 7, 50 (1956).

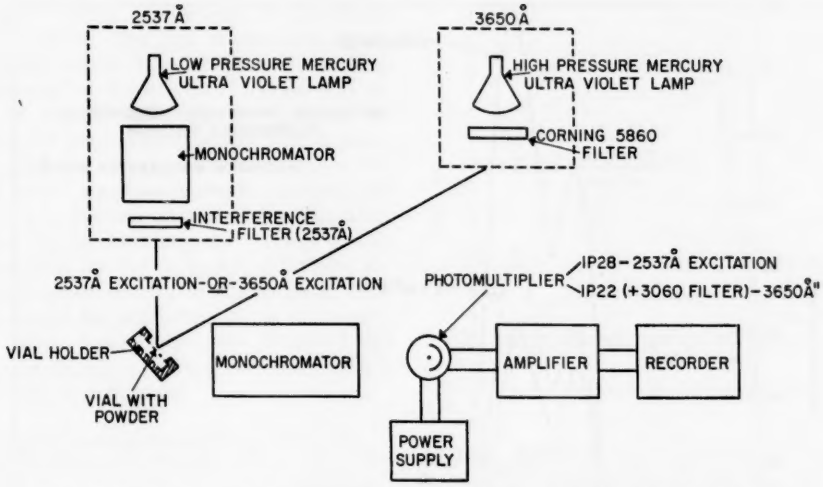

FIG. 1. Schematic diagram of radiometer system with facilities for 2537 and 3650 A excitation.

the chemical-structural and fluorescence changes. The systematic study of several members of the different series provides additional insight into the relation between ring numbers, chemical linkage, and fluorescence and chemical change. The results of this study suggest the potential use of fluorescence degradation, in the form of a luminescent *G*-value for example, as a tool to determine the extent of radiation damage.

EXPERIMENTAL

The radiation used in this study was Co^{60} gamma rays. Seven phosphors (biphenyl, *p*-terphenyl, *p*-quaterphenyl, naphthalene, anthracene, tetracene, and fluorene) were studied. Because minute traces of impurities influence the fluorescence phenomena, only materials of suitable purity were used. In the absence of commercially-available materials of desired purity (purity determined by comparison of the fluorescence spectra to those of Sangster[9] and Pringsheim[10]) the phosphors were specially purified by a combination extraction-filtration chromatographic adsorption-recrystallization apparatus described by Herington *et al.*[11]

The materials, in powdered form, were irradiated in glass vials enclosed in a graphite vial holder. This arrangement ensured that the flux of secondary electrons penetrating the powder was always the same, and that this flux was characteristic of low atomic number materials only. That is, the condition of "electronic equilibrium" was approximated. In order to study the temperature dependence during the irradiation, special facilities were designed to permit temperature control ($\pm 2°C$) over a range of $-90°$ to $+300°C$. The low temperatures were obtained by intermittently circulating precooled gas through the irradiation can. High temperatures were achieved by a heating coil wound around the sample cup. For each material the maximum irradiation temperature investigated was less than the temperature at which pyrolytic effects on luminescence were determined to be significant. Dose-rate dependence was studied by irradiating the materials at 2.2×10^4 and 1.6×10^5 r/hr to the same dose. Calibrations were made by ferrous sulfate and silver-activated phosphate glass was used to determine the flux distribution in the irradiation facilities.[12]

The emission spectra of both the pre- and post-dosed samples were measured at room temperature with the radiometer shown schematically in Fig. 1. The material, packed in small glass or quartz vials, was excited with low intensities (to minimize ultraviolet degradation) of 2537 A or 3650 A light. Radiometer readings were taken within two hours after irradiation in order to minimize any error due to the recovery of fluorescence. For the purposes of this paper, true emission spectra are not presented, a record of photomultiplier current vs wavelength being sufficient. For materials of low brightness—due either to low initial luminescence efficiency or to low radiation stability—the precision of the fluorescent reading was reduced. However, it is believed that the combined error in measuring relative peak heights, from this and other sources, was less than 10%.

The maximum-dosed samples were re-read from time to time over a period of from three to eleven months. The effect of temperature on the recovery process was investigated by heat treating samples for 1 hr at 100°C immediately following irradiation. The contri-

[9] R. C. Sangster and J. W. Irvine, Jr., J. Chem. Phys. **24**, 670 (1956).
[10] P. Pringsheim, *Fluorescence and Phosphorescence* (Interscience Publishers, Inc., New York, 1949), p. 1.
[11] E. F. Herington, R. Handley, and A. J. Cook, Chem. & Ind. (London) 292 (1956).
[12] W. E. Price and H. Rabin, Nucleonics **13**, No. 33 (1955).

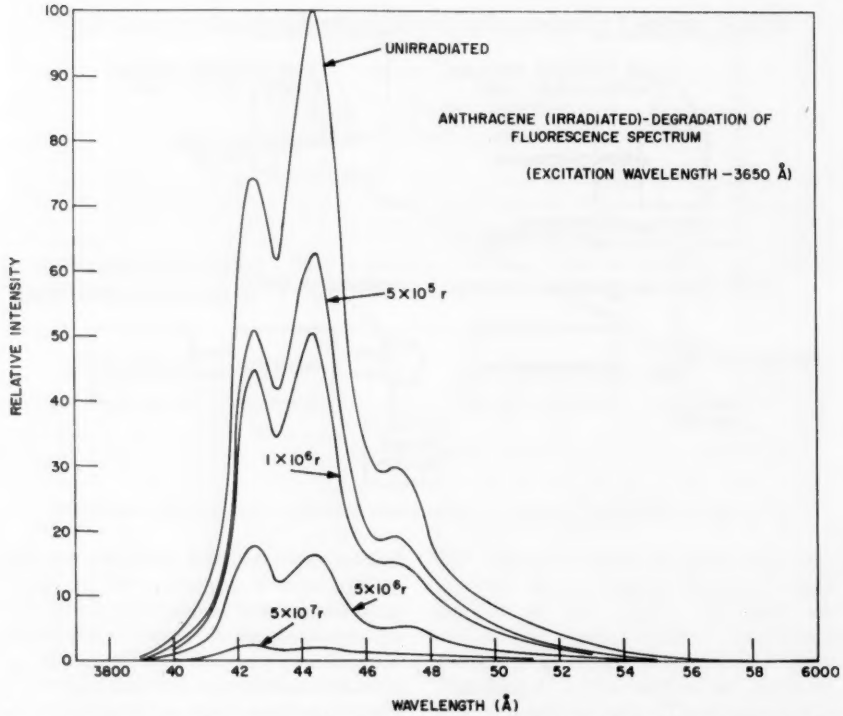

FIG. 2. Pre- and post-dosed fluorescence spectra (uncorrected for wavelength dependence of the radiometer) of anthracene.

bution of optical self-absorption to observed degradation was studied by determining the change in the optical density of a pre- and post-dosed anthracene flake.

RESULTS

Dose-rate independence of the degradation for all materials was found over the range of dose rates studied.

Study of the total-dose parameter resulted in data that conflicted with that of other workers. As illustrated in Fig. 2, in which is plotted the progressive degradation of the anthracene spectrum, the peaks degrade nonuniformly. It is noted that after irradiation to $\sim 10^7$ r, the relative heights of the 4260 A and 4440 A peaks are completely reversed, with the 4260 A peak becoming the higher of the two peaks. In Table I a comparison of the peak ratios of pre- and post-dosed ($\sim 5\times 10^5$ r) materials indicates that nonuniform degradation is general for all the phosphors studied. In order to determine if the degradation rate was a result of an overlapping of emission peaks, the anthracene curves for unirradiated and irradiated ($\sim 10^7$ r) material were resolved by estimating the individual peak shapes. A comparison of the resolved spectra indicates that even the presence of maximum-possible overlapping was not sufficient to explain the observed differences in degradation between the various emission peaks of the same phosphor.

Also investigated was the possibility of an "absorption edge" moving toward longer wavelengths overlapping the emission spectrum at higher doses, and therefore distorting the true emission spectrum. This possibility was investigated by determining the self-absorption in a thin anthracene crystal (thickness -4.5×10^{-4} cm) from the change of optical density with dose. The absorption spectra for the unirradiated and dosed material are presented in Fig. 3. It can be calculated from the absorption at 3650 A that most of the ultraviolet light is absorbed in the material within a depth of 1.4×10^{-4} cm. With this data it was determined that self-absorption of fluorescence from 4000 A to 6000 A in the dosed material is approximately 5%. Therefore, at least for anthracene, absorption effects are negligible.

It is interesting to note from Fig. 3 that the optical density at 3650 A shows an increase of approximately twofold after irradiation with 10^8 r rather than an expected decrease. This result suggests that some of the damaged molecules themselves, absorb ultraviolet light directly. Part of the luminescence degradation could therefore be due to the creation of absorbing nonluminescent molecules which compete for the exciting light. Although the increase in optical density is not of sufficient magnitude to explain all the observed luminescence degradation, it might be partially responsible for it and, in addition, could also be involved in the recovery with time. The dashed curve in Fig. 3—obtained by

subtracting curve 1 from 2—represents the growth of new absorption centers. The lack of structure in the curve suggests that several different types of absorbing species are produced in the irradiation. These may be new species of organic molecules or alternatively, trapped-electron or trapped-hole centers, such as those formed on irradiation of inorganic solids. Since the latter type of center are often thermally unstable, the small recovery of fluorescence on storage or on annealing may be understood by assuming that centers of this type are responsible for the increased ultraviolet absorption. It may be postulated that absorption in these centers is ineffective for production of the anthracene fluorescence. When these centers are destroyed the "useless" absorption ceases and the ultraviolet light is absorbed only by the anthracene.

TABLE I. Comparison of peak ratios (pre- and post-dose).

Material	I_{max}/I ratio	Unirradiated	Irradiated ($\sim 5\times 10^7$r)
Biphenyl	3200/3310	1.12	0.77
	3200/3380	1.11	0.79
	3200/3530	1.30	0.93
	3200/4020	5.78	2.02
p-Terphenyl	3710/3580	1.48	1.39
	3710/3890	1.07	1.24
p-Quaterphenyl	4360/4150	1.54	1.30
	4360/4640	1.90	1.82
Fluorene	4100/3940	7.63	4.81
	4100/4330	1.70	1.48
	4100/4600	6.54	3.25
Naphthalene	3390/3600	3.03	0.28
	3390/3680	5.00	0.28
	3390/3780	11.1	0.25
Anthracene	4440/4260	1.35	0.83
	4440/4700	3.34	1.82
Tetracene	5700/6400	5.0	5.6

A convenient method of presenting degradation data is to plot I/I_0 vs dose for the peak emission of an irradiated phosphor. In this study, the degradation of each emission peak was followed and plotted individually. This is illustrated in Fig. 4 for the degradation of *p*-quaterphenyl (Eastman). The general empirical form of these and all other such curves obtained from this study is consistent with the relation $(I/I_0)=(1+AD^n)^{-1}$. The degradation data was also analyzed by plotting $(I_0/I)-1$ vs dose. This is illustrated by the degradation of fluorene (Eastman) in Fig. 5. If the peaks degrade according to the mechanism postulated in the smeared-out model and in accordance with other reported data, the plot of the degradation data would give a straight line of slope unity ($n=1.0$). That this is not always the case is seen from an inspection of the n-values in Table II.

The temperature-dependence study indicated that

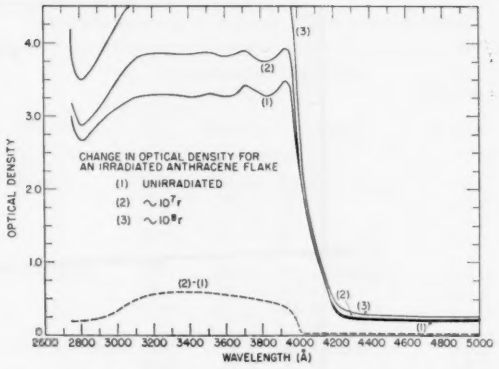

FIG. 3. Optical density in an anthracene flake as a function of dose.

for the materials and temperatures observed, the fluorescence degradation process for most peaks is essentially independent of the temperature during the irradiation. This is pointed out in Table III for anthracene and *p*-quaterphenyl. The presence of pyrolytic effects prevented the use of irradiation temperatures higher than 100°C. It is noted that for the −90°C irradiation that all peak degradations are temperature independent as compared to room temperature. For the high-temperature irradiations, the degradation rate for only one peak—the shortest wavelength emission—is temperature dependent.

Contrary to previous reports,[1,3] the fluorescent degradation process is reversible to a certain extent. The

TABLE II. Degradation constants.

Material	Emission Band (A)	$D_{\frac{1}{2}}$ ($\times 10^6$ r)	n
Biphenyl	3200	4.1	0.97
	3310	5.4	0.98
	3380	4.8	0.90
	3530	3.4	0.77
p-Terphenyl	3580	10.0	0.97
	3710	7.8	0.94
	3890	4.0	0.77
p-Quaterphenyl	4150	39.0	0.66
	4360	24.0	0.67
	4640	24.0	0.65
Fluorene	3940	29.0	0.90
	4100	12.0	0.84
	4330	16.0	0.91
	4600	41.0	0.85
Naphthalene	3390	0.84	1.00
	3600	4.5	0.47
	3680	19.0	0.46
Anthracene	4260	1.4	0.89
	4440	1.0	0.94
	4700	1.1	0.83
Tetracene	5700	60.0	1.00
	6400	45.0	0.68

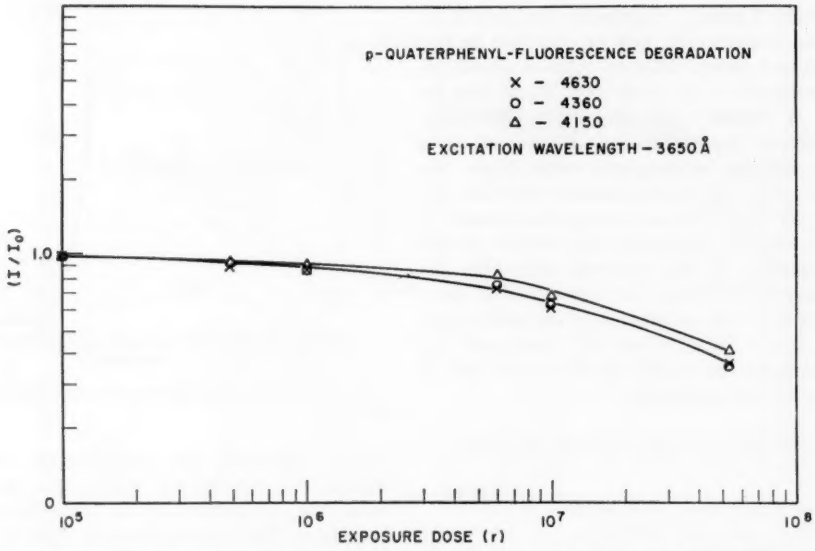

FIG. 4. The fraction of fluorescence degradation with dose for the emission peaks of *p*-quaterphenyl.

recovery of the fluorescence is rapid at first and then decreases to a relatively slow rate after several days. The recovery data is presented in Table IV. The difference between the percent of initial degradation (reading taken within 2 hr t_0 after dosing to $\sim 5\times 10^7$ r) and the percent degradation observed after storage at room temperature to time t represents the percent of recovery relative to I_0. Fluorene appears to exhibit little or no recovery.

It was observed that heat treating the irradiated samples accelerated the recovery process with the result that a constant fluorescent value was obtained. This value is about 7% higher, on the average, than the value observed after several days of room-temperature

TABLE III. Temperature-irradiation data for anthracene and *p*-quaterphenyl.

Material	Emission (A)	−90°C	+25°C	50°C	100°C
Anthracene	4260	0.289*A*[a]	0.294*A* 0.173*B*[b]	0.146*B*	...
	4440	0.206*A*	0.220*A* 0.123*B*	0.124*B*	...
	4700	0.251*A*	0.245*A* 0.139*B*	0.139*B*	...
p-Quaterphenyl	4150	0.889*A*	0.875*A* 0.415*B*	0.423*B*	0.392*C*[c]
	4360	0.827*A*	0.810*A* 0.365*B*	0.377*B*	0.353*C*
	4640	0.844*A*	0.850*A* 0.371*B*	0.392*B*	0.358
Fluorene	3940	0.824*A*	0.862*A* ...	...	...
	4100	0.727*A*	0.710*A* ...	...	...
	4330	0.761*A*	0.747*A* ...	...	...
	4600	0.850*A*	0.863*A* ...	...	...
Tetracene	5700	0.960*A*	0.970*A* 0.550*B*	...	0.346*C*
	6400	0.910*A*	0.925*A* 0.490*B*	...	0.335*C*

[a] *A*—3.8×10^6 r exposure dose.
[b] *B*—8.8×10^6 r exposure dose.
[c] *C*—5.0×10^7 r exposure dose.

recovery. The annealing time and temperature used in the experiment were by no means optimum and further study of these variables is warranted. It was also noted that extensive post-irradiation heat treatment tended to distort the emission spectrum.

DISCUSSION

In Table II it is noted that for the majority of the principal peaks of those materials studied, the n-values are within 10% of unity. This result is in agreement with the experimental data of other workers. However, for the minor peaks of these materials and also for the principal emission of p-quaterphenyl, the deviation from unity is quite pronounced. Several explanations based on a modification of the model of Rosenstock and Schulman[4] are offered to account for these discrepancies. Essentially this model assumed that one type of poison is produced by the irradiation and that the excitons are all of one energy.

The unequal degradation of the various emission peaks in a phosphor can be explained if it is assumed that one poison is produced but that the excitons created by the exciting ultraviolet light are of different energies. The poison might then selectively quench more excitons of one energy than of another. This would cause those emissions excited by the more readily quenched excitons to exhibit the greatest degradation among the spectral peaks. The similar degradation rates ($D_{\frac{1}{2}}$ values) for the p-quaterphenyl peaks are then explainable on the basis that in this material the poison absorbs energy from all excitons with equal probability.

Another assumption is that several poisons are produced during the irradiation and that each poison has a unique selectivity for excitons of different energy.

A third possibility is that one poison is produced and the excitons are all of one energy. However, the excitons excite the molecules to different energy states and the poison then interacts with the excited molecules as well as with the excitons.

Further experimentation is needed to determine which, if any, of these three models best describes all the luminescence-degradation phenomena.

In order to gain a better understanding of radiation damage vs chemical structure, a comparison of damage data was made among the homologous members of the two aromatic series studied. Since it was observed that the emission peaks of a phosphor exhibit different degradation characteristics, for this study it was interesting to determine which peak was most representative of the true chemical degradation. This was done by comparing the $D_{\frac{1}{2}}$ values for all emission peaks of a material to the reported data for the chemical damage in the materials. From the G_{gas} and G_{polymer} values obtained for aromatic hydrocarbons by Colichman *et al.*,[8] Bolt and Carroll,[13] and Burns, Williams, and Wild,[14] it was found that the $D_{\frac{1}{2}}$ values of the maximum emission peaks showed closest agreement to the damage trends indicated by the chemical analysis of the radio-

TABLE IV. Recovery of degraded fluorescence with time.

Material	Emission (A)	% Degradation $(1\text{-}I/I_0)100$ Time-t_0	Time-t	% Recovery $\%(t_0-t)$
Biphenyl	3530	88.4	80.1 (2400 hr)	+8.3
	3380	88.3	83.9	+4.4
	3310	87.9	84.4	+3.5
	3200	91.7	89.6	+2.1
p-Terphenyl	3890	86.4	82.8 (2400 hr)	+3.6
	3710	84.3	81.9	+2.4
	3580	83.2	81.2	+2.0
p-Quaterphenyl	4640	63.2	56.6 (8040 hr)	+6.6
	4360	64.9	57.8	+7.1
	4150	58.6	52.6	+6.0
Fluorene	4600	53.6	54.2 (4536)	−0.8
	4330	73.5	73.5	0.0
	4100	43.3	44.4	−1.1
	3940	27.3	21.8	+5.5
Naphthalene	3780	16.7	$(I/I_0>1.0)$ (2400 hr)	...
	3680	66.0	30.5	+35.0
	3600	79.7	61.2	+18.5
	3390	98.1	96.8	+1.3
Anthracene	4700	96.0	94.7 (8040 hr)	+1.3
	4440	98.0	97.2	+0.8
	4260	96.8	96.3	+0.5
Tetracene	6400	51.0	...	...
	5700	45.1	38.8 (3456 hr)	+6.3

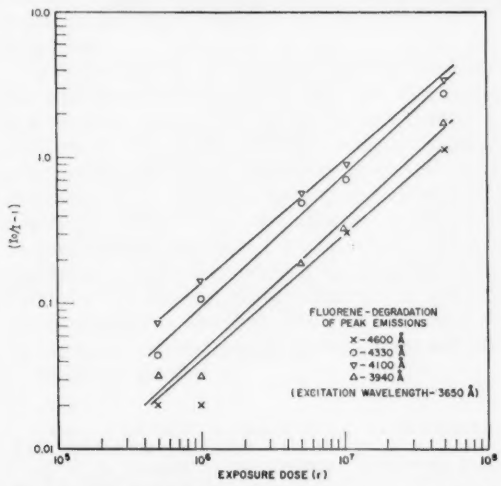

FIG. 5. Plot of $(I_0/I)-1$ vs dose for the emission peaks of fluorene.

[13] R. O. Bolt and J. G. Carrol, "Organics as reactor moderator-coolants," *Proceedings of the First International Conference on the Peaceful Uses of Atomic Energy Geneva, 1955* (United Nations, New York, 1956), p/742.

[14] W. G. Burns, W. Wild, and T. F. Williams, "The effect of fast electrons and fast neutrons on polyphenyls at high temperature," *Proceedings of the Second International Conference on the Peaceful Uses of Atomic Energy, Geneva, 1958* (United Nations, Geneva, 1959), p/51.

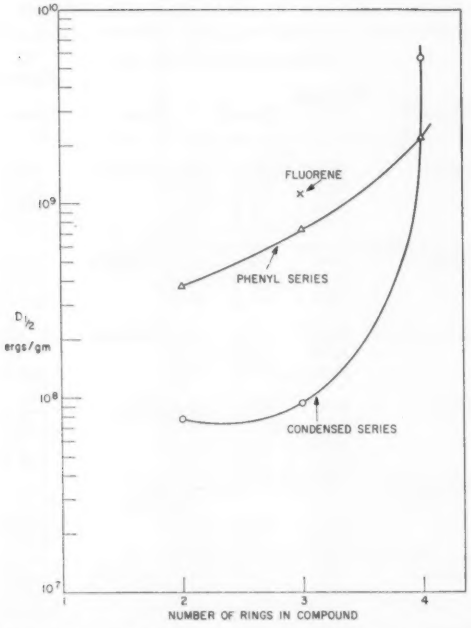

FIG. 6. A comparison of the relative stability between the phenyl-linked and condensed-ring series using the $D_{\frac{1}{2}}$ values for the maximum emission peak as an index of the chemical damage.

lysis products. In Fig. 6, $D_{\frac{1}{2}}$ values of the maximum emission peak are taken as representative of the luminescence damage to illustrate the relationship of luminescence degradation to the chemical and structural properties of the two series of compounds. It is noted that there is no clear-cut advantage in radiation stability of phenyl-linked over condensed-ring chemical linkage. Fluorene, as a sort of "hybrid" of these two linkage types, is more stable than either one. Within each series, stability is seen to increase with increasing number of ring members.

The radiation and thermal properties exhibited by anthracene, *p*-quaterphenyl and fluorene are of interest in the development of a high-level dosimeter based on luminescence degradation. Specifically, the recovery and temperature-irradiation data of this study has application to such a dosimetry system. Fluorene, in particular, shows promise as a dosimetry material because of its negligible recovery effect, its excellent radiation stability and its high luminescence efficiency.

A desirable feature of a luminescence dosimetry system is the high sensitivity of fluorescence changes to radiation. This can be demonstrated by comparing the chemical and fluorescence damage in a polymer resulting from the absorption of an equal amount of radiation. For example, a luminescence G value can be calculated for the major emission of *p*-terphenyl from its $D_{\frac{1}{2}}$ value and the material's density and molecular weight. This value is 580 molecules quenched per 100 ev of radiation absorbed in the material. The G_{polymer} value reported for *p*-terphenyl is 0.065 molecules destroyed per 100 ev absorbed. Taking *p*-terphenyl as typical of radiation damage to the polymers studied, it is evident that the luminescent changes are about 2000 times more sensitive than the detectable chemical changes.

ACKNOWLEDGMENTS

The author wishes to express his appreciation to J. H. Schulman for his invaluable assistance throughout this research, F. H. Attix for his many vital contributions, R. D. Kirk for purifying the materials used, H. W. Etzel, J. G. Allard, and other members of the NRL Dielectrics Branch for their helpful advise. The research was supported in part by the U.S. Air Force, monitored by Materials Laboratory, Directorate of Research, Wright Air Development Center.

Paramagnetic Resonance Study of Irradiated Single Crystals of Calcium Tungstate

HENRY ZELDES AND RALPH LIVINGSTON

Oak Ridge National Laboratory, Oak Ridge, Tennessee*

(Received July 27, 1960)

Gamma irradiation of calcium tungstate at 77°K produces two paramagnetic species in high yield. Measurements of yields and of rates of disappearance upon warming indicate the two species are formed and disappear upon warming in one to one correspondence. The principal axis directions and g tensors have been measured and indicate that one species contains a surplus electron while the other is electron-deficient (hole). Hyperfine effects of W^{183} have been observed. The electron-deficient species contains two tungsten atoms with small isotropic hyperfine interactions. Its unpaired electron must be highly localized in orbitals of atoms other than tungsten. The electron-surplus species contains one tungsten atom with an anisotropic hyperfine interaction. This center could be WO_4^{3-}, but from the lack of symmetry of the measured g values it must be formed near a lattice defect. Experiments with heat-treated crystals indicate lattice defects to be important in the radiation effect.

THE paramagnetic resonance spectrum of single crystals of calcium tungstate at 77°K after irradiation with gamma rays consists of two characteristic groups of four lines. Both groups of lines are anisotropic and well separated. It can easily be shown that the two groups originate from two different paramagnetic species. The work described in this paper was undertaken to elucidate some of the properties of the two species.

There are several favorable features for a study of this system. Both species are formed with high radiation yield, and moderately high quantities can be stably trapped at the low temperature. Single crystals of calcium tungstate have been made available commercially for use in gamma scintillation counters, and the essential details of the crystal structure are known and are relatively simple. Moreover, hyperfine effects from one of the tungsten isotopes (W^{183}) can be observed which makes it possible to learn considerably more about the paramagnetic species. Although much can be deduced from the measurements, a positive, unambiguous identification of the two species has not been made.

Calcium tungstate is tetragonal and has space group C_{4h}^6 with four molecules in the unit cell.[1] The calcium and tungsten parameters are known, but there is uncertainty in the oxygen positions. Unless a paramagnetic species has special symmetry there will be four absorption lines for each species, and these will be related by fourfold axes parallel to the c axis. If the magnetic field is parallel to the c axis the four lines will appear as a single line, while if the magnetic field is parallel to the ab plane the four lines will be merged in pairs to appear as two lines. The groups of lines originating from the two paramagnetic species had these symmetry properties.

EXPERIMENTAL

All observations were made with a simple paramagnetic resonance spectrometer operating at 9000 Mc and employing a TE_{101} mode rectangular transmission cavity. Magnetic fields were measured with a proton magnetic-resonance probe, and g values as well as numbers of unpaired electrons were measured relative to those of a sample of α,α-diphenyl-β-picrylhydrazyl (DPPH) taking $g=2.0037$ for DPPH.[2] Magnetic modulation at 60 cps and oscilloscope display of the spectra gave adequate sensitivity for a large portion of the work. Chart recording was used where higher sensitivity was needed, particularly in studying the weaker hyperfine lines. Most measurements were made at 77°K (liquid nitrogen) and ≈64°K (pumped liquid nitrogen). A few observations were also made at 20°K.

Single crystals of calcium tungstate from two sources were used. Most of the work including essentially all of the measurements of resonance frequencies were made with crystals obtained from the Linde Company. These were made by the Verneuil[3] or flame process. Subsequently single crystals were grown[4] by lowering the temperature of a melt of LiCl and NaCl saturated with $CaWO_4$. In a typical experiment, a mixture of reagent-grade chemicals consisting of 125 g of LiCl, 52 g of Na_2WO_4, and 17.9 g of $CaCl_2$ was heated in a covered platinum crucible to 900°C and held at this temperature for 2 hr to remove nuclei of crystal growth. This temperature was at least 150°C higher than that needed to keep all of the $CaWO_4$ in solution. The melt was allowed to cool rapidly to 750°C and was then slowly (30°C per day) cooled to 550°C. Essentially all of the crystal growth took place during the interval of slow cooling. The temperature was then lowered to room temperature and the crystals recovered by dissolving away extraneous salts in water. Spectroscopic

* Operated for the U. S. Atomic Energy Commission by the Union Carbide Corporation.

[1] R. W. G. Wyckoff, *Crystal Structures* (Interscience Publishers, Inc., New York, 1951), Chap. VIII.

[2] C. A. Hutchison and R. C. Pastor, Phys. Rev. **81**, 282 (1951).

[3] A. Verneuil, Ann. chim. et phys. **3**, 20 (1904).

[4] I. N. Anikin, *Growth of Crystals*, edited by A. V. Shubnikov and N. N. Sheftal (translated from Russian by Consultants Bureau, Inc., New York, 1958), Vol. 1, p. 259.

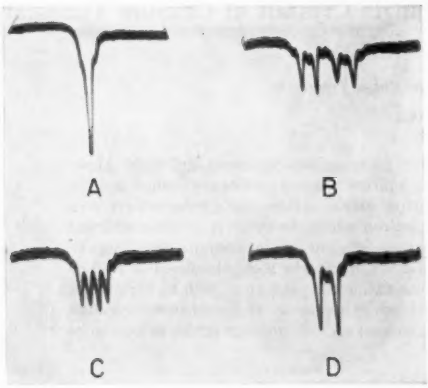

FIG. 1. Low-field lines with the magnetic field parallel to the ac crystallographic plane. The magnetic field is (A) parallel to the c axis, (B) 65° from the c axis, (C) 85° from the c axis, and (D) parallel to the a axis.

analyses were obtained for both the Linde crystals and those grown from a melt. These were identical except with regard to molybdenum which was absent in the crystals from the melt but present in the Linde crystals in the amount of 0.001 to 0.01%. The most abundant impurity was silicon; both kinds of crystals contained 0.01 to 0.1%.

Crystals were oriented by x-ray diffraction and cemented to $\frac{1}{16}$-in. diam rods which were inserted into the microwave cavity at right angles to the steady magnetic field and which served as rotation axes for changing the crystal orientations. Two orientations of crystal relative to rod were used, one with the crystallographic c axis parallel to the rod and the other with the a axis parallel to the rod. All irradiations were carried out at 77°K in a nominal 1000-C Co^{60} source of gamma rays. The doses used in the various experiments ranged from 10^{18} to in excess of 10^{21} ev/g. After irradiation the crystals were transferred to the cooled microwave cavity without warming. Since the magnetic field was perpendicular to the rod attached to the crystal, rotation of the appropriate rod with crystal gave all orientations of the field perpendicular either to the crystallographic a axis or c axis.

SPECTROSCOPIC SPLITTING FACTORS

One group of lines appeared at magnetic field strengths near that corresponding to the free electron g value while the other group was at much higher fields (lower g values). These will be referred to as the *low-* and *high-field* lines or species. The appearance of the low-field lines for a few orientations of the field parallel to the *ac* plane are shown in Fig. 1. A basic four-line pattern appears which merges to a single line when the field is parallel to the c axis and to a pair of lines when the field is along the a axis. All stable tungsten isotopes have zero spin except the 14.3% abundant W^{183} which has a spin of $\frac{1}{2}$. The weak lines that appear in Fig. 1 are hyperfine components involving W^{183} and will be separately described later. The x-ray diffraction orientation of the crystal with respect to its rod was used only to determine the plane of orientations of the magnetic field; for example, the data of Fig. 1 were known from x-ray measurements to be for the field parallel to the *ac* crystallographic plane. The measured angular orientation in the plane was related to the crystallographic axes by symmetry properties; for example, the c- and a-axis directions can easily be identified from Fig. 1. Only a pair of lines appears when the field is parallel to the *ab* plane, but the a axis (or equivalent b axis) can be located from the known locations of lines deduced from measurements in the *ac* plane. In this way a large number of measurements were made at known orientations. The data considerably over-determined the g tensor. The high-field group also consisted of four lines with the same symmetry properties, and measurements were made in a similar manner. The high-field lines were more anisotropic and considerably broader than the low-field lines. They also were accompanied by weak hyperfine components.

The measurements for the four strong lines for each species could be accurately described by the simple Hamiltonian with electron spin of $\frac{1}{2}$ of the form

$$\mathcal{H}=\beta\mathbf{S}\cdot\mathbf{g}\cdot\mathbf{H}, \tag{1}$$

where β is the Bohr magneton, $\mathbf{S}$ the electron spin operator in units of $\hbar$, $\mathbf{H}$ the magnetic field, and $\mathbf{g}$ a symmetric rank two tensor. The value of the spectroscopic splitting factor g for each orientation of the crystal was computed from the data and the definition $h\nu=g\beta H$. It is related to the tensor $\mathbf{g}$ of the Hamiltonian of Eq. (1) by

$$g=(h'\cdot\mathbf{g}\cdot\mathbf{g}\cdot h')^{\frac{1}{2}}, \tag{2}$$

where h' is a unit vector parallel to the applied field. In component form Eq. (2) may be written

$$g^2=G_{aa}h_a^2+G_{bb}h_b^2+G_{cc}h_c^2+2G_{ab}h_ah_b+2G_{ac}h_ah_c+2G_{bc}h_bh_c, \tag{3}$$

where the h's are direction cosines of the applied field with respect to the crystallographic axes and the G's are elements of the symmetric tensor $\mathbf{G}=\mathbf{g}\cdot\mathbf{g}$. If Eq. (3) relates to any one of the four lines from one of the species, the three additional equations relating to the

TABLE I. Principal axis directions and principal values of $\mathbf{g}$ for the low field lines.

	Direction cosines			g
	a	b	c	
g_1	0.101	0.540	−0.836	2.0010
g_2	0.699	−0.636	−0.326	2.0065
g_3	0.708	0.551	0.442	2.0354

remaining lines may be generated from Eq. (3) by fourfold rotations of the tensor about the c axis. On using the spectral data and the four symmetry related equations, the elements of **G** may easily be evaluated. This tensor is then diagonalized and the principal axis directions deduced. These are also the principal axis directions for the tensor **g**. The principal values of **g** are simply the square roots of the corresponding values of **G**. One set of principal axis directions and the corresponding principal values of **g** are given in Tables I and II for the low- and high-field lines. Spectroscopic splitting factors computed from the parameters of Table I are estimated to have a maximum error of 0.001 while those computed from the parameters for the broader lines of the high-field group (Table II) are estimated to have a maximum error of 0.0015.

The various lines showed anisotropy in width. This was particularly noticeable for the relatively sharp low-field lines. It was first ascertained that the concentration of paramagnetic species was low enough that linewidths did not change with variations in the concentration. Moreover, the widths of the low-field lines were essentially unchanged when observations were made at 77°K and then at lower temperatures. Also, the widths were invariant to extensive changes in microwave power level. The anisotropy in width was best seen by intercomparing widths of the four lines at the same orientation of the crystal. For some orientations the sharpest line had a full width at half-height of about 2 gauss while that of the broadest line was as much as three times greater. An example for the spectrum taken at 20°K is illustrated in Fig. 2. The fifth weak line that shows in Fig. 2 is a resolved hyperfine component from W^{183}. The linewidths for different lines were related by the same symmetry properties as for the g values.

Similar observations were made on the high-field group of lines. Here, however, the lines always showed some sharpening in cooling from 77° to 64°K. This probably results because the thermal relaxation time for this species is short enough at the higher temperatures to give pronounced uncertainty broadening. At 64°K widths with typical values of about 11 gauss and varying by 25% were observed.

The anisotropy in linewidths may arise from mosaic spread in the crystal. The sample may be a mosaic of

TABLE II. Principal axis directions and principal values of **g** for the high field lines.

	Direction cosines			g
	a	b	c	
g_1	0.547	−0.837	0.008	1.5716
g_2	0.832	0.543	−0.111	1.6334
g_3	0.089	0.068	0.994	1.8482

FIG. 2. Low-field lines at 20°K showing the width anomaly.

many crystallites slightly misaligned with respect to each other rather than a single perfect crystal. On several occasions samples prepared from seemingly good single crystals were found to have spectra expected from two or more single-crystal pieces with small angular misalignments between the pieces. The usual four-line spectrum appeared for most orientations, but occasionally the lines clearly showed small splittings into components representing the separate crystal pieces. This observation adds to the plausibility that mosaic spread causes the anisotropy in linewidth.

HYPERFINE EFFECTS

The prominent lines of both groups are accompanied by weaker lines that result from hyperfine interactions with 14.3% abundant W^{183}. These weaker lines for the low-field group may be seen in Fig. 1. If the paramagnetic species were to contain a single tungsten nucleus that interacts with the electron, the presence of W^{183} with $I=\frac{1}{2}$ would give rise to a doublet. The two components would be spaced symmetrically to each side of each main line, and from the isotopic abundance of W^{183} the intensity of one hyperfine component relative to the main line would be 0.0835.

It was difficult to make accurate measurements of the high-field group of lines because they were broad and weak. The results of a number of measurements showed the hyperfine components to have the same width as the corresponding main line with an uncertainty of about 20% and to have a relative strength of 0.075. This was regarded as satisfactory evidence that the high-field lines result from a paramagnetic species containing a single tungsten atom that interacts with the electron.

Many observations on the low-field lines indicated that the hyperfine components were too intense to be accounted for by a single W^{183} nucleus. Initially it was thought that the hyperfine lines might result from an impurity atom with isotopes of nuclear spin zero and either $\frac{1}{2}$ or 1. Lead and cadmium were considered possibilities. Crystals were grown containing 0.01 to 0.1% lead and also cadmium, but the presence of these impurities in no way affected the spectra. It was then realized that the high intensity of the hyperfine components could result from a paramagnetic species containing two tungsten nuclei which are equivalent or nearly equivalent. This model requires that there be an additional pair of very weak hyperfine lines with equal spacings from the center and spacings twice those for the first pair of hyperfine lines. Thus each main line would be the center of a group of five equally spaced hyperfine lines where the outermost very weak lines

originate from paramagnetic species having both tungsten atoms as W^{183}, the inner pair originate from species with one of the two tungsten atoms as W^{183}, and the strong central line results primarily from species with no W^{183} but also partly from some of the species with two nuclei of W^{183}. From the abundance of W^{183} the intensities from center to outside should vary as 1:0.164:0.0068. A number of measurements (Fig. 1) were in good agreement with the theoretical relative intensity 0.164 for the first hyperfine lines in support of the two-tungsten model. A search was then made with a more sensitive chart recording spectrometer for the weaker lines. These were found with the expected intensity. This leaves no doubt that the low-field paramagnetic species contains two tungsten nuclei. If the species contained more than two equivalently coupled nuclei, the relative line intensities would have been very different.

The spacings of the hyperfine lines in the low-field group were found to be independent of crystal orientation within the experimental error of about 1 gauss. The widths of the stronger, first hyperfine lines were as much as 1.4 times greater than those of the central line for some orientations. This could result from a slight anisotropy in the hyperfine interactions for the two tungsten positions. Likely, the two positions are crystallographically equivalent, and there is a very slight anisotropic contribution to the hyperfine interaction. The different principal axes for the two tungsten atoms lead to slightly different splittings. The first hyperfine lines originate from species in which one or the other tungsten position is occupied by W^{183} and are thus split in two (broadened). Only a negligible fraction of the central line is similarly broadened. Since the anisotropic coupling which is to be accounted for is only a small part of the total coupling and since the isotropic part is the same for each tungsten it is likely that the two tungsten atoms in the species are equivalent.

The hyperfine interactions may be regarded as a small perturbation to the Hamiltonian given by Eq. (1) of the form $\sum_i \mathbf{S}\cdot\mathbf{A}_i\cdot\mathbf{I}_i$, where $\mathbf{I}_i$ is the nuclear spin operator in units of $\hbar$ for the ith nucleus and where $\mathbf{A}$, in general, is a rank two symmetric tensor. Since the low-field lines showed an isotropic hyperfine interaction $\mathbf{A}$ may be regarded as a scalar, and since the selection rule is $\Delta m_I = 0$, the value of A is simply the separation between hyperfine components (strictly, in energy units) originating from a single W^{183}. This spacing is that between the two strong hyperfine components (or half that between the two weak components) and was found to be 9 ± 1 gauss. The hyperfine interaction for the high-field lines was observed to be anisotropic, but the measurements were not sufficiently detailed to evaluate $\mathbf{A}$. Spacings between the two hyperfine components varying between 35 and 65 gauss were observed.

SUPPLEMENTAL EXPERIMENTS

The two paramagnetic species always appeared to be formed together upon irradiation at 77°K and to disappear together when the crystal was warmed. This suggested that the two species are related in the sense that they result from the unpairing of electrons which were paired in the initially diamagnetic crystal. Their simultaneous disappearance upon warming could be back reaction. To test this idea a Linde crystal was irradiated until the concentration of both species reached saturation. Within an experimental uncertainty of 30% the concentrations of the two species were the same. If the crystal was annealed by warming and then reirradiated at 77°K the yields for the two species were again found to saturate at the same concentrations. The concentrations were compared by measuring areas of the two groups of lines, using the appropriate g values for the lines, and considering the g tensors to be sufficiently close to axial symmetry that the relationship of Bleaney and Stevens[5] could be used. An annealing experiment was carried out at −132°C, and each species was found to disappear with the same rate and with second-order kinetics in the concentration of either species. Initial radiation yields of the two species were not compared because the high-field lines were so broad and weak that a low enough radiation dose to give a valid initial yield value was not high enough to permit an accurate measurement. The initial yield was, however, measured for the low-field species in a Linde crystal and found to be two unpaired electrons for 100 ev of absorbed gamma ray energy. These experiments support the concept that the two species formed by radiation are associated with the fate of two previously paired electrons and that the process for their disappearance is back reaction. The system is, however, more complex than this simple concept as indicated by a few optical experiments described later.

The yield of paramagnetic species from crystals grown from a NaCl-LiCl melt was strikingly lower than from the Linde crystals. The saturation concentrations were also lower, and comparisons were made for the low-field lines. While a Linde crystal gave 5×10^{17} low-field species per gram, crystals from the melt gave only 2×10^{16} centers per gram. On the other hand, if crystals from the melt were heated to a high temperature before cooling to 77°K and irradiating, a much higher concentration could be prepared. Thus heating to 1000°C for three days (in air) resulted in a saturation concentration of 5×10^{16} centers per gram while heating to 1325°C for five days (in argon) gave 1.5×10^{17}. A still higher temperature was obtained by melting most of a crystal held with platinum tongs in a natural gas-oxygen flame and then allowing the melt to recrystallize over a period of about 1 min as the flame was removed. Small crystals remained single after

[5] B. Bleaney and K. W. H. Stevens, Repts. Progr. Phys. **16**, 108 (1953).

this treatment, and those prepared from a NaCl-LiCl melt gave a saturation concentration of low-field species of 1.8×10^{17}/g. This concentration is nearly the same as that obtained from the Linde crystals. In a number of experiments, the saturation concentrations of previously irradiated crystals were found to be unchanged after warming to room temperature, recooling to 77°K and reirradiating. The Linde crystals were grown by a high-temperature flame process while crystals from the melt were prepared by a comparatively low-temperature process. It is clear that a high-saturation concentration is associated with a previous high-temperature treatment with or without an oxygen atmosphere. Some crystals were grown from the melt containing lead and cadmium as impurities as indicated earlier. The presence of these impurities did not affect the saturation concentrations of paramagnetic species either with or without heat treatment.

A few optical experiments were carried out by placing an irradiated crystal in the spectrometer at 77°K and piping light to the sample through a fused silica rod. One end of the rod contacted the sample in the cavity and the other end was exterior to the Dewar containing the cavity. The exposed end of the rod was illuminated with various light sources. Very heavily gamma-irradiated samples were opaque and black. Incandescent light from a 100-w microscope lamp caused the low-field lines to disappear after several minutes. The color of the sample bleached during this time. The high-field lines initially weakened, but they had only partially disappeared by the time the low-field lines had vanished. These results were unchanged when the incandescent light was first passed through a red filter and a 2-cm path of water. The same results were also obtained after annealing the irradiated crystal at room temperature, recooling to 77°K, and reirradiating with gamma rays. Ultraviolet light from a high-pressure mercury source with visible and infrared light filtered out produced a very small concentration of the low field species at 77°K. This experiment was carried out with a Linde crystal that had previously been gamma irradiated but had then been annealed at room temperature before the start of the experiment.

DISCUSSION AND SUMMARY

The observations on the hyperfine lines clearly show that the high-field species contains a single atom of tungsten while the low-field species contains two equivalent or nearly equivalent atoms of tungsten. Finding the same quantity of each species after prolonged irradiation, and, moreover, finding the same rates of disappearance upon warming strongly supports the view that the two species are formed in one to one correspondence. They then disappear upon warming by back reaction. This view is further supported by the measured g values (Tables I and II). The species with one tungsten atom has g values much less than the free electron value like that expected for less than a half-filled shell of electrons while the two-tungsten center has g values close to that of the free electron but with principal values averaging slightly higher which is indicative of a center containing more than a half-filled shell. It would appear that the two centers are formed from the diamagnetic crystal by the loss of an electron at one site giving rise to the low-field two-tungsten center and the trapping of the electron at another site to produce the one-tungsten species.

The isotropic hyperfine interaction for the two-tungsten species indicates that the unpaired electron (hole) has very little probability distribution of being in tungsten orbitals. The isotropic interaction arises from unpaired electrons occupying s orbitals of tungsten The most likely orbitals are the $5s$ or $6s$ for which very large hyperfine interactions would be expected. This is illustrated, for example, by Weissman's observation[6] of the W^{183} hyperfine structure of octacyanotungstate ion in solution where the paramagnetism is attributed to an unpaired electron in a d orbital, yet enough admixture of s orbitals was present to give a 52-gauss isotropic hyperfine splitting. The 9-gauss isotropic splitting in the present case must mean that the unpaired electron is mostly in orbitals of atoms other than tungsten, and these are most likely those of one or more oxygen atoms which are present as a part of the two-tungsten species. The variation in hyperfine separation from 35 to 65 gauss observed for the high-field one-tungsten species clearly arises from contributions from tungsten orbitals other than s orbitals. Since the hyperfine interactions expected from these orbitals are generally much smaller than those expected from s orbitals, it is likely that the observed variation of 30 gauss represents a substantial contribution from tungsten orbitals other than s orbitals.

The finding that the concentration of paramagnetic species after irradiation to saturation depends upon prior heat treatment indicates the radiation effect is associated with defects in the crystal. One view has been that the crystal is initially deficient in oxygen to an extent determined by the heat treatment, and that by the loss of oxygen there are formed diamagnetic two-tungsten complexes. These then become paramagnetic by the loss of an electron upon irradiation. Possible evidence against this model is that heat treatment in the presence and absence of oxygen did not result in different concentrations of radicals, but these experiments were not definitive. Pursuing this model further, another difficulty appears with the high field species. The simplest view is that the electron attaches to a tungstate ion to form WO_4^{3-}. If this process occurred in an otherwise perfect $CaWO_4$ structure the resulting g tensor would have axial symmetry in conflict with the experimental tensor (Table II).

[6] S. I. Weissman and C. S. Garner, J. Am. Chem. Soc. **78**, 1072 (1956).

There would then be a single line rather than four lines. Although proposing specific models is, at best, speculative a preferred interpretation is that the two-tungsten center is analogous to Cl_2^- formed in irradiated alkali chloride crystals.[7] Upon loss of an electron two tungstate ions displace towards each other and share the loss. This center, however, will only persist if the electron can be stably trapped elsewhere in the crystal. The trapping site is presumed to be a tungstate ion associated with a lattice defect (nature unspeculated) and to form WO_4^{3-} stabilized by the neighboring defect. The disappearance of the two-tungsten center with optical illumination indicates that it is converted to still another type of center not observed in the present experiments. On the other hand, warming of the sample leads to simple back reaction.

We wish to acknowledge with thanks the help of R. D. Ellison in aligning crystals by x-ray diffraction.

[7] T. G. Castner and W. Känzig, J. Phys. Chem. Solids **3**, 178 (1957).

THE JOURNAL OF CHEMICAL PHYSICS VOLUME 34, NUMBER 1 JANUARY, 1961

Study of the Wurtzite-Type Compounds. V. Structure of Aluminum Oxycarbide, Al_2CO; A Short-Range Wurtzite-Type Superstructure*

E. L. Amma and G. A. Jeffrey

Crystallography Laboratory, The University of Pittsburgh, Pittsburgh, Pennsylvania

(Received July 18, 1960)

Al_2CO has a long-range disordered structure based on the wurtzite lattice and a short-range $\sqrt{3}a$, $2c$ superstructure. The long-range atomic parameters were determined from the single crystal sharp diffraction data with Mo K radiation. The diffuse spectra, although very apparent on the single-crystal x-ray photographs, were inadequate to completely define the short-range structure; however, the general features of this structure could be inferred and some analogies made to known structures which are wholly or in part wurtzite-lattice superstructures.

INTRODUCTION

THIS work is a continuation of the series of experimental and theoretical investigations of structural and physical properties associated with the wurtzite lattice, which have been published in this Journal.[1]

Aluminum oxycarbide, Al_2CO, has a hexagonal crystal structure based on the wurtzite-type lattice, as originally shown by powder diffraction work by Foster, Long, and Hunter[2] and confirmed by single crystal observations by Jeffrey and Lynton.[3] When written as $Al\cdot\frac{1}{2}(CO)$, it is iso-electronic with AlN, and, from that point of view, might be expected to have a structure systematically related to that of the wurtzite type. With the more metallic elements for which the corresponding III/V compound has the cubic zinc-blende structure, the ordered replacement of atoms to form an isoelectronic II, IV/V_2 compound results in the tetragonal chalcopyrite structure. Examples of this type of extension of the well-known Grimm-Sommerfeld (8-n) rule have been provided recently by the structures of $ZnGeP_2$, $CdSnAs_2$, etc.[4,5] In some other "mixed valence" compounds of this type, a random distribution of the metal atoms over the metal sites occurs and the higher symmetry is maintained, e.g., $ZnSnAs_2$.[6]

A corresponding ordered substitution in the wurtzite-type lattice would lead to a reduction in symmetry from hexagonal to orthorhombic, i.e., from space group $P6_3mc$ to $Pmc2_1$. This hypothetical orthorhombic structure, which bears the same relationship to wurtzite as the chalcopyrite has to zinc blende, is shown in Fig. 1. Aluminum oxycarbide does not have this structure nor are we aware of any compounds which do. $BeSiN_2$ is reported[7] to have the wurtzite structure; however, the true symmetry of these crystals might not be apparent from the powder diffraction data alone, and single crystals of this compound have not yet been studied.[8] Al_2CO is, so far, unique in this general class of "mixed valence" wurtzite and zinc blende type structures in that it is the nometallic atoms which are "mixed."

We have undertaken this single crystal study of Al_2CO in order to investigate the somewhat complex structural situation which appears to exist in this

* The research was supported by the Office of Ordnance Research, U. S. Army.

[1] G. A. Jeffrey, G. S. Parry, and R. L. Mozzi, J. Chem. Phys. **25**, 1024 (1956); F. Keffer and A. Portis, *ibid.* **27**, 675 (1957); W. O'Sullivan, *ibid.* **30**, 379, (1959); F. Keffer, *ibid.* **32**, 62 (1960).

[2] L. M. Foster, G. Long, and M. S. Hunter, J. A. Ceram. Soc. **39**, 1 (1956).

[3] G. A. Jeffrey and H. Lynton, Bull. Am. Phys. Soc. Ser. II, **3**, 231 (1958).

[4] C. H. L. Goodman, Nature **179**, 829 (1957).

[5] H. Pfister, Acta Cryst. **11**, 221 (1958).

[6] Von O. G. Folberth and H. Pfister, Acta Cryst. **13**, 199 (1960).

[7] A. Rabenau and P. Eckerlin, Naturwissenschaften **46**, 106 (1959).

[8] A. Rabenau (private communication).

compound, and which results in the appearance of a comparatively well-defined diffuse x-ray diffraction pattern in addition to the sharp Bragg pattern.

It is believed from the crystal data and methods of preparation, that Al_2CO is the same compound as that described as an aluminum suboxide, Al_2O, by Belecky and Rapoport,[9] except possibly for some differences in nonstoichiometry.

CRYSTAL DATA

Al_2CO is formed, together with Al_4O_4C, by the reaction of Al_2O_3 and Al_4C_3 at temperatures up to 2000°C, as described by Foster, Long, and Hunter.[2] The crystals of Al_2CO are long hexagonal needles about the unique axis, with unit cell dimensions $a=3.17$ A, $c=5.06$ A, $c/a=1.60$, $Z=1$, whence $D_x=3.09$ g cc; $D_m=2.94$ to 3.05. These cell dimensions are 2% greater than those of AlN, while the c/a ratio is the same. The Laue symmetry of the diffraction patterns is 6/mm, as for AlN.

The data reported[9] for Al_2O is $a=3.02$ A, $c=5.00$ A, $c/a=1.61$, $Z=1$; whence $D_x=2.76$, and $D_m=2.74$ g cc, space group $P6_3/mmc$, $P6_3mc$ or $P\bar{6}2c$.

EXPERIMENTAL

The single crystals were provided by Dr. L. M. Foster of the ALCOA Research Laboratories. They ranged in size up to 3 mm long and 0.2 mm in diam. Some of the crystals were dendritic laths elongated about $[2\bar{1}1]$, others were needles about the hexagonal axis with hexagonal cross section. The latter were used in this investigation. Weissenberg and precession photographs were taken of various layers of the crystal reciprocal lattice, using Cu K and Mo K radiation in order to investigate the diffuse scattering superlattice.

The three-dimensional intensity measurements of the sharp diffraction spectrum were made with Cu K and Mo K radiation by the moving-crystal moving-counter method,[10] using a GE single-crystal orienter with a proportional counter on an XRD-3, and with a scintillation counter on an XRD-5. On the XRD-3, the intensity was recorded linearly on a chart and planimetered. On the XRD-5 the intensity was both scanned on the chart and integrated by the cumulative counting facility. The crystals used for the intensity measurements were regularly hexagonal in cross section, 0.2 mm in diam and 1.0 mm long. The usual Lorentz-polarization corrections were made. No corrections were made for absorption or extinction.

The density of the crystals was measured by flotation in hexane and methylene iodide mixtures.

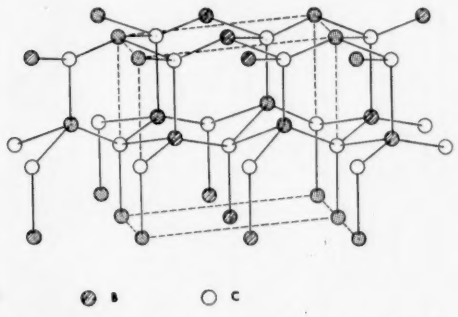

FIG. 1. Hypothetical ABC_2 structure derived by ordered replacement in wurtzite.

TABLE I. Observed structure amplitudes.

h	k	l	AlN single crystal Mo K	Al_2CO single crystal Mo K	Al_2CO single crystal Cu K
1	0	0[a]	16.9	22.6	19.8
2	0	0	17.4	16.0	16.1
3	0	0	23.4	19.0	19.3
1	1	0[a]	24.3	29.4	27.1
1	2	0	16.2	11.9	11.9
0	0	2[a]	16.0	16.1	16.9
0	0	4	13.1	7.3	6.1
0	0	6	15.8	8.4	6.6
1	0	4	9.4	3.1	3.0
2	0	4	7.4	2.6	2.7
1	1	4	15.4	5.9	5.6
2	1	4	6.3	1.9	1.3

[a] Strongly affected by extinction in AlN, as shown by comparison with powder data.[1]

STRUCTURE DETERMINATION

Although the crystal lattice of Al_2CO differs from that of AlN merely by a 2% expansion of the unit cell, the x-ray diffraction spectra differ in two very obvious respects, of which the former was noted on the original powder photographs by Foster *et al.*[2] These are (i) large differences in some of the sharp Bragg reflection intensities, notably the $(00l)$ and $(hk4)$, see Table I, (ii) the appearance of strong diffuse spectra in certain zones of the single crystal x-ray patterns.

The diffuse spectra persisted unchanged when photographs were taken in a cold air stream at about −100°C and were also unaffected when the crystals were heated to about 500°C for several hours. It is concluded therefore that the diffuse spectra do not have their origin in thermal motion but must be associated with some disorder which is a characteristic and permanent feature of the crystal structure. The Laue symmetry of the diffuse spectra is 6/mm, as for the sharp spectra, and the sharp and diffuse spectra together could be indexed on a short-range order hexagonal superlattice of $c'=2c$ and $a'=3a$. The reciprocal lattice layers in the c' direction were then alternately all sharp and all diffuse, with the third (diffuse) layer particularly intense. The superimposed zero and third layer Weissenberg photographs are shown diagrammatically, together with the corresponding layers in the reciprocal lattice, in Fig. 2.

[9] M. S. Beletskii and M. P. Rapoport, Doklady Akad. Nauk. S.S.S.R. **80,** 751 (1951); Structure Repts., **15,** 174 (1951).

[10] T. C. Furnas, *Single Crystal Orienter Instruction Manual* (General Electric Company, Schenectady, New York, 1957).

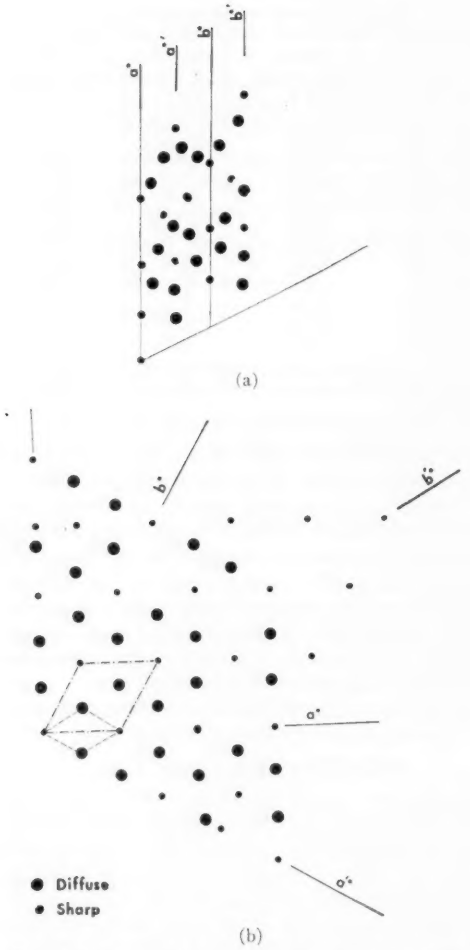

FIG. 2. Diagrammatical representation of Weissenberg photographs and the corresponding reciprocal lattice. Superposition of sharp zero-layer spectra and diffuse third-layer spectra about the c axis.

It was immediately apparent that neither the difference in intensity in the sharp spectra between AlN and Al_2CO nor the intensities of the diffuse spectra could be accounted for solely by the difference in atomic scattering factors for the nonmetallic elements. Some disordering of the aluminum atoms must therefore occur in the structure.

In the (*hk*0) zone, there is a close correspondence between the intensities of the sharp reflections for Al_2CO and AlN. In fact, when scaled against the AlN intensities, these differences were barely significant above the experimental errors, (cf. Tables I and II). There is also a complete absence of diffuse spectra in this zone. These observations indicate that when viewed in projection down the hexagonal axis, the structures of Al_2CO and AlN are nearly indistinguishable. This eliminates any

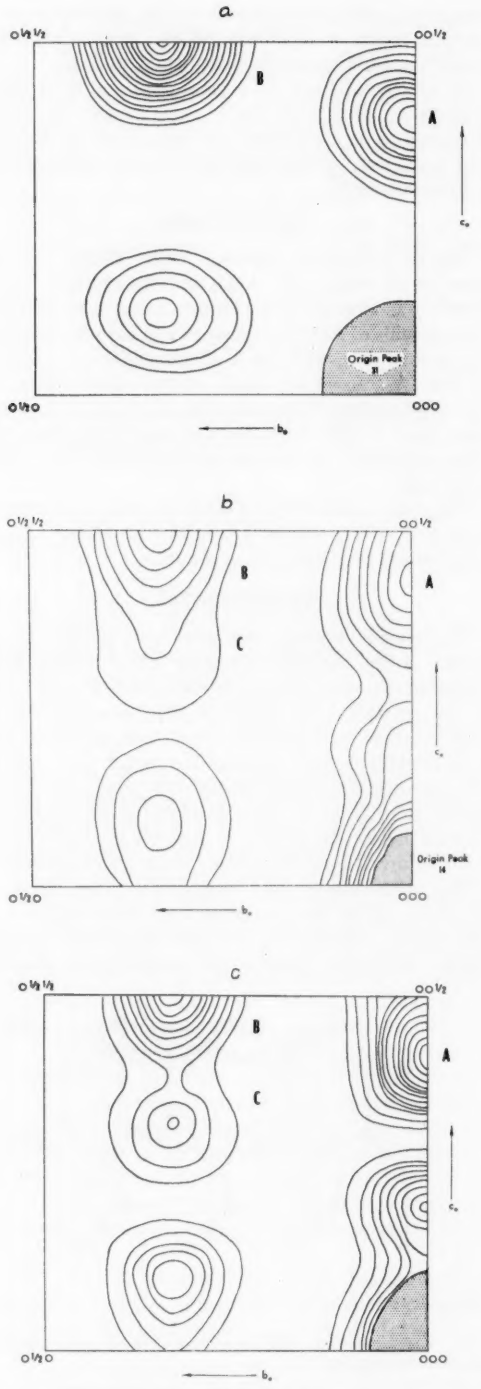

FIG. 3. Three-dimensional Patterson section in plane (120). (a) AlN with Cu K data; (b) Al_2CO with Cu K data; (c) Al_2CO with Mo K data.

consideration of disorder of the stacking-fault type, where the structure alternates between the wurtzite and zinc-blende arrangements. There was also no evidence of the streaking of the diffraction spectra which is commonly associated with strain in the crystal arising from stacking faults.

The disorder must therefore involve only the atomic coordinates in the z direction of the wurtzite lattice. This was studied by means of the comparison of the Patterson F^2 syntheses for AlN and Al_2CO. Since there is a variable parameter, the u parameter, in the wurtzite structure, it was possible to study the disorder by means of the sharp Bragg reflections alone; (this is not possible in the more familiar order-disorder problems of a fixed parameter structure with all the atoms in special positions, such as Cu_3Au).

The interatomic vectors relevant to this problem all appear on the section at $x=0$ of the equivalent C-centered orthorhombic cell, which was used for convenience in computing. Figure 3 shows this section (a) for AlN with CuK data, (b) for Al_2CO with CuK data, (c) for Al_2CO with Mo K data.

With the structure factors scaled on the $hk0$ reflections, the peak at the origin of (b) was lower than that of (a) with the same amount of data. This is also indicative of a disorder in the structure which involves the aluminum atoms.

The peaks A and B correspond in the AlN structure to (Al–N) and (Al–Al)+(N–N), respectively. Their relative peak heights are reversed in Al_2CO. A new vector peak occurs at C in Al_2CO. This peak is unresolved with the Cu data but appears well defined with the increased number of terms of the Mo data synthesis.

TABLE II. Observed and calculated structure amplitudes.

$h\ k\ l$	$\lvert F_{obs}\rvert$	F_{calc}	$h\ k\ l$	$\lvert F_{obs}\rvert$	F_{calc}
1 0 0[a]	22.6	−26.0	3 0 2	10.6	−9.6
2 0 0	16.0	−16.1	4 0 2	3.0	3.0
3 0 0	19.1	18.9	1 1 2	17.8	17.6
4 0 0	5.7	−5.6	1 2 2	6.2	−5.7
5 0 0	4.5	−3.3	1 3 2	4.0	−3.7
6 0 0	3.9	4.0	1 4 2	4.7	4.6
1 1 0[a]	29.4	−36.8	2 2 2	8.5	−7.8
1 2 0	11.9	11.6	2 3 2	2.6	2.6
1 3 0	7.5	6.9	1 0 3	8.9	10.6
1 4 0	6.9	−8.3	2 0 3	6.7	7.2
2 2 0	13.4	14.8	4 0 3	3.3	3.3
2 3 0	4.8	−4.7	1 2 3	5.9	−5.6
2 4 0	2.9	−2.9	1 3 3	5.5	3.8
3 3 0	6.1	−6.0	1 0 4	3.1	3.5
4 4 0	2.3	2.4	2 0 4	2.5	2.5
0 0 2[a]	16.1	−29.9	3 0 4	3.1	−2.8
0 0 4	7.3	−7.6	1 2 4	5.9	5.5
0 0 6	8.4	7.9	1 3 4	1.8	−1.7
1 0 1[a]	9.0	10.9	2 2 4	2.1	−2.0
2 0 1	9.8	−9.8	1 0 5	16.0	−16.3
4 0 1	3.2	2.8	2 0 5	12.8	12.7
1 2 1	7.8	−7.4	4 0 5	5.0	−5.9
1 3 1	4.4	3.8	1 2 5	10.6	10.2
1 0 2	13.0	9.8	1 3 5	8.2	−7.0
2 0 2	8.4	7.7	2 3 5	5.1	−5.0
1 0 6	3.0	−2.7			

[a] Strongly affected by extinction.

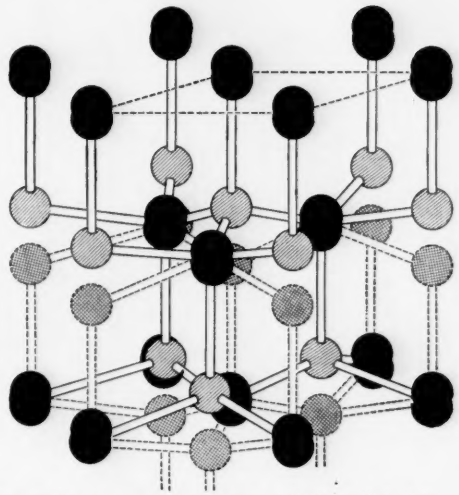

FIG. 4. Long-range order structure of Al_2CO, full circles, 0.45 (C, O); lined circles, $\frac{1}{2}$Al.

With atoms at 0, 0, 0; $\frac{1}{3}$, $\frac{2}{3}$, $\frac{1}{2}$; 0, 0, u; $\frac{1}{3}$, $\frac{2}{3}$, $\frac{1}{2}+u$, as in the wurtzite lattice, this peak corresponds to the occupation of interstitial sites at 0, 0, $-u$; $\frac{1}{3}$, $\frac{2}{3}$, $\frac{1}{2}-u$. The peak heights and vectors on the Al_2CO Patterson section could then be accounted for by placing $\frac{1}{2}$(C+O) at the origin and its related position, $\frac{1}{3}$, $\frac{2}{3}$, $\frac{1}{2}$, and $\frac{1}{2}$Al at the normal sites 0, 0, u; $\frac{1}{3}$, $\frac{2}{3}$, $\frac{1}{2}+u$, and at the interstitial sites 0, 0, $1-u$, and $\frac{1}{3}$, $\frac{2}{3}$, $\frac{1}{2}-u$, with $u=0.410$, i.e., appreciably greater than the theoretical value of 0.375 for an ideal wurtzite lattice.

With this model, successive Fourier synthesis refinement was carried out using the IBM 650 structure factor and differential synthesis programs of Shiono.[11] The scattering power of $\frac{1}{2}$(C+O) is indistinguishable from that of a N atom, and N scattering factors were used throughout the analysis. These atoms are hitherto referred to as (C, O) atoms. The agreement index R, where $R=\sum \lvert\lvert F_{obs}\rvert-\lvert F_{calc}\rvert\rvert/\sum \lvert F_{obs}\rvert$, improved from about 0.3 for Al_2CO with the ideal wurtzite structure to $R=0.18$ for this model. On refinement using a uniform isotropic temperature factor, R was further reduced to 0.15 with $u=0.41$, $B_{Al}=1.0$ A^2. It was then noted that the peak heights and curvatures of the half-aluminums at 0, 0, 0.41 and 0, 0, 0.59 were identical to four decimal places. This suggested that in the long-range average structure there were mirror planes of symmetry perpendicular to the hexagonal axis at the level of the (C, O) atoms, thereby increasing the space group symmetry to the centrosymmetrical $P6_3/mmc$, as compared with the noncentric $P6_3mc$ for the wurtzite lattice.

[11] R. Shiono, University of Pittsburgh, Computation and Data Processing Center, Tech. Rept. No. 2 (1957); IBM 650 Library Program File No. 84001, 84002.

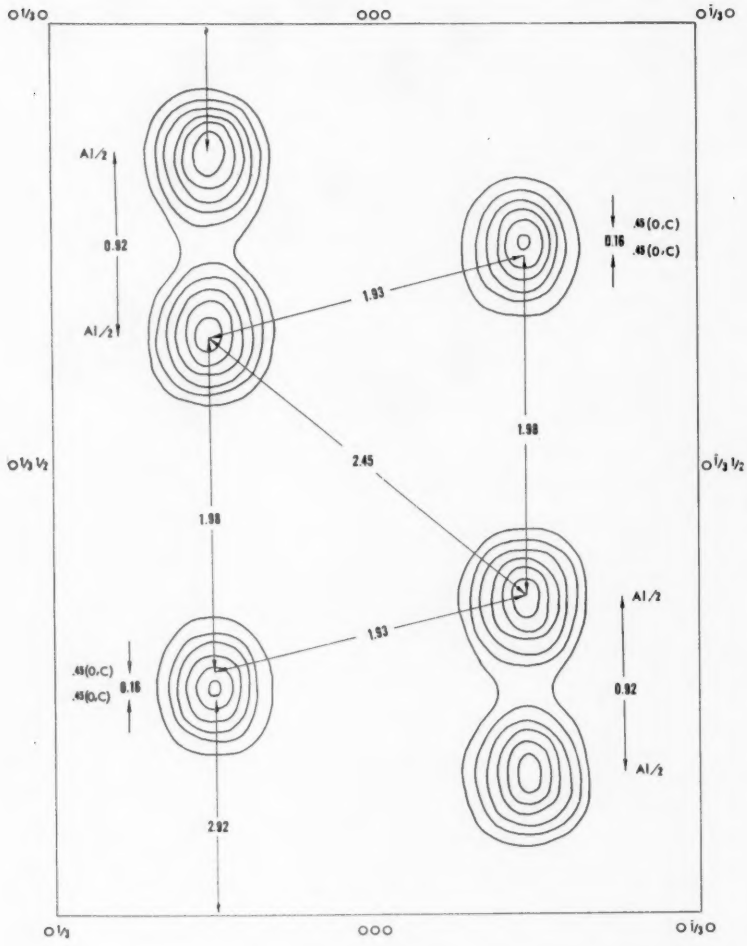

FIG. 5. Three-dimensional Fourier section of Al_2CO in plane (120). Electron density contour intervals $2.5e/A^3$, zero contour omitted.

Although the observed curvature of the aluminum atoms showed that their thermal motion was not appreciably anisotropic, the curvature of the (C, O) atoms was significantly anisotropic, being least in the direction of the c axis. This was interpreted as a small degree of disorder in these sites also, and could be accounted for by displacing these atoms ± 0.015 z above and below the mirror plane and occupying them with half-atoms. This small change further reduced the R factor to 0.13. The average long-range structure is now as shown in Fig. 4. The three-dimensional Fourier section in the plane (120) of the wurtzite cell is shown in Fig. 5. To compare this further with the model, a $(F_O - F_C)$ difference synthesis in this plane was computed and is shown in Fig. 6(a). As compared with the model structure, the observed structure now appears to have a significant deficiency of electron density at the (C, O) sites. This cannot be corrected by transferring electron density to the Al sites, since this would imply greater than half occupancy of these sites and a real interatomic distance between atoms of 0.9 A. in the short-range structure. Since the experimental data had been scaled on the assumption of stoichiometry, the occupancy of the (C, O) sites could be reduced and the structure factors rescaled. This was, in fact, the only chemically feasable interpretation. The best fit with experiment was then obtained by reducing the occupancy of these (C, O) sites from 0.5 to 0.45. This removed the significant features in the difference synthesis, which now appears as in Fig. 6(b). It also brings the calculated x-ray density to 2.99 g/cc, within the range of measured values for a number of single crys-

tals. With a small readjustment of the isotropic temperature factors the R factor dropped to 0.105. With the omission of the intense low-order reflections 100, 110, 101, 002, which by comparison with the single-crystal and powder-diffraction data for AlN[1] are likely to be affected by extinction, the final agreement factor is 0.074. Table II shows the observed and calculated structure factors for the 52 independent observed sharp reflections indexed on the wurtzite hexagonal cell.

LONG-RANGE ORDER STRUCTURE

The data on the atomic sites and their occupancy are summarized in Table III and compared with those of AlN, which is the most nearly comparable normal wurtzite-type structure, and has the same c/a ratio.

Disregarding, for the moment, the small separation between the two (C, O) sites, the nonmetallic atoms form the usual hexagonal closepacked (hcp) arrangement of one component of the wurtzite lattice. In a normal wurtzite structure the metal atoms then lie in *one or other* of the two sets of hcp tetrahedral interstices. The choice of which of the two sets is occupied determined the polar sense of the crystal, since it determines the direction of the bonds along the hexagonal axis. In this structure, on the average, both sets of interstices are occupied by half-aluminum atoms. Since the separation between an immediately adjacent pair of sites of the two sets is less than 1 A, both cannot be occupied simultaneously. The appearance of strong localized diffuse scattering in the reciprocal lattice indicates that this occupation is not random but is ordered with a short periodicity. From the spread of the diffuse spectra it is estimated that this short-range order persists over about 50 A. This is, therefore, compatible with the observed nonstoichiometry, in that it corresponds approximately to a misfit after every 10 unit cells.

TABLE III. Long-range order structure parameters.[a]

Atomic sites	Al_2CO $P6_3/mmc$	AlN $P6_3mc$
0, 0, z; $\frac{1}{3}$, $\frac{2}{3}$, $\frac{1}{2}+z$;	0.45 (C, O)	N
0, 0, $\bar{z}$; $\frac{1}{3}$, $\frac{2}{3}$, $\frac{1}{2}-z$;	0.45 (C, O)	...
0, 0, u; $\frac{1}{3}$, $\frac{2}{3}$, $\frac{1}{2}$+u;	0.5 Al	Al
0, 0, u; $\frac{1}{3}$, $\frac{2}{3}$, $\frac{1}{2}-u$;	0.5 Al	...

[a] $z=0.016$ for Al_2CO and AlN (arbitrary choice of origin along the c axis, since the structure is polar). $u=0.409$ for Al_2CO and 0.401 for AlN. The isotropic temperature factors are $B_{Al}=0.26$ A², $B_N=0.79$ A², AlN (from powder data).[1] $B_{Al}=0.85$ A² $B_{C,O}=0.96$ A², in Al_2CO (from single-crystal data).

The separation of the (C, O) sites is 0.16 A, which is close to the difference between the sums of the tetrahedral covalent radii for Al–C, 2.03 A and Al–O, 1.92 A. The splitting of the nonmetal sites is therefore compatible with the existence of two different bond lengths in the structure.

SHORT-RANGE ORDER STRUCTURE

The appearance of the diffuse reflections with intensities, which are approximately constant over a wide temperature range, indicates the existence of a short-range order structure extending over regions of about 50 A throughout the crystal lattice.

Indexing both the sharp and diffuse spectra on the $a'=\sqrt{3}a$, $c'=2c$ superlattice gives the following observed systematic extinctions: sharp spectra, present only for $h-k=3n$ and $l=2n$, $00l$ present only for $l=4n$, hkl present for $l=2n$; diffuse spectra, present only for $h-k=3n+1$ and for $l=2n+1$.

With the Laue symmetry 6/mm, these extinctions are compatible with special positions of the space groups $P6_3/mmc$, $P6_3mc$ and $P\bar{6}2c$. These special positions in the $\sqrt{3}a$, $2c$ cell are, however, incompatible with the long-range order atomic sites.

The use of the general positions (i.e., ignoring the extinctions), or the reduction of the Laue symmetry to permit space groups $P6_3/m$ or $P6_3$, results in model structures for the short-range order which either have aluminum atoms less than 1 A apart or in a most unlikely layer-type structure of alternate Al and (C, O) atoms 1.8 A. apart. It is concluded, therefore, that the short-range order must be of lower symmetry, and that the apparent hexagonal symmetry of the diffuse diffraction pattern is a consequence of internal hexagonal twinning of lower symmetry domains. This will superimpose diffuse reflections with the same spacings but different hkl indices, and makes it impossible to resolve the intensities and hence solve the short-range order

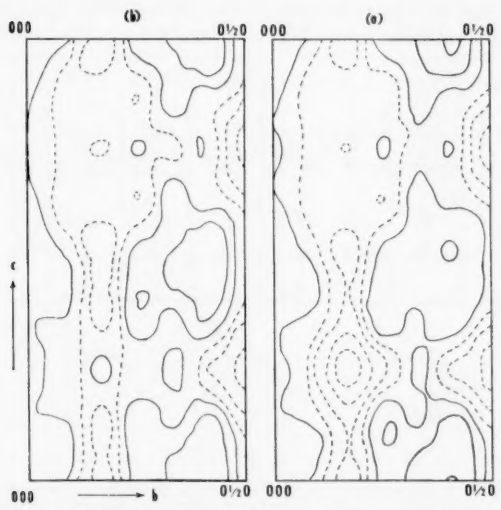

FIG. 6. Three-dimensional Fourier difference synthesis for Al_2CO. Section in plane (120). Electron density contour intervals $0.25e/A^3$ with negative contours dotted. (a) Stoichiometric model, (b) nonstoichiometric model.

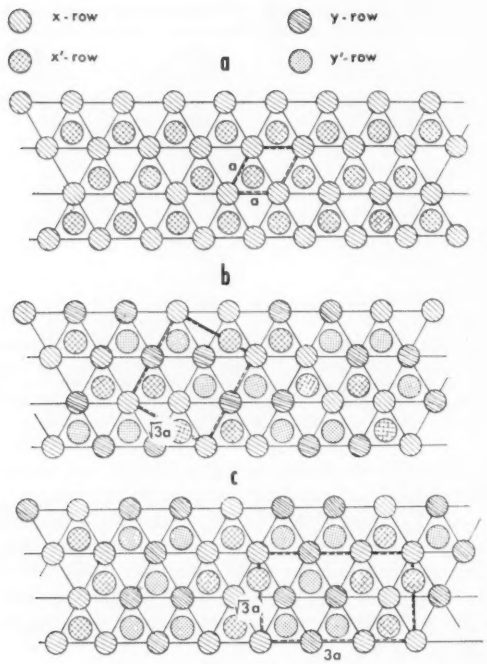

FIG. 7. Basal plane periodicities in wurtzite structure and superstructures obtained by inverting B sites. Row X, A atoms at 0, 0, 0; B atoms at 0, 0, $+u$. Row X′, A atoms at $\frac{1}{3},\frac{2}{3}$, $\frac{1}{2}$; B atoms at $\frac{1}{3},\frac{2}{3}$, $\frac{1}{2}$, $+u$. Row Y, A atoms at 0, 0, 0; B atoms at 0, 0, $-u$. Roy Y′, A atoms at $\frac{1}{3}$, $\frac{2}{3}$, $\frac{1}{2}$; B atoms at $\frac{1}{3}$, $\frac{2}{3}$, $\frac{1}{2}$, $-u$. (a) Normal Wurtzite structure; (b) $\sqrt{3}a$, $2a$, superstructure; (c) $\sqrt{3}a$, $3a$, superstructure (cubanite, $CuFe_2S_3$).

structure directly from intensity measurements of the diffuse spectra, even if sufficient of them could be accurately measured. What is possible, however, is to define the general relationship of this short-range superstructure to the normal wurtzite structure and to point out some analogies with a few known structures.

TABLE IV. Orthogonal cell dimensions for wurtzite and some mineral structures.

	a	b	c	Space group
ZnS wurtzite	6.65 ($\sqrt{3}a_0$)	11.5 ($3a_0$)	6.26 (c_0)	$P6_3mc$
$CuFe_2S_3$ cubanite	6.46	11.12	6.23	$Pcmm$
$AgFe_2S_3$ argentopyrite	6.64	11.47	6.45	$Pmmn$
$AgFe_2S_3$[a] sternbergite	6.62	11.66	12.70	$Cmma$
$Ag_2Fe_3S_5$[b] "freiseit"	6.61	11.61	12.64	$Cmma$

[a] N. W. Buerger, Am. Min. **22**, 847 (1937).
[b] M. A. Peacock, Am. Min. **27**, 229 (1942).

The $\sqrt{3}a$ periodicity in a wurtzite superstructure can be obtained by periodically replacing a sequence of atoms along the c axis by one in which the inverted metal sites are occupied, thus giving structural parameters for the long-range ordered structure consistent with those observed in this case.

This is illustrated in Fig. 7. Both the examples (b) and (c) are compatible with the strong $\sqrt{3}a$ basal periodicity observed in the Al_2CO superstructure, since the twinning of the short-range order domains which produces the observed hexagonal Laue symmetry of the diffuse spectra also obscures the periodicity in the other direction.

The ferromagnetic mineral cubanite $CuFe_2S_3$, which when written as ($Cu_IFe_{III}S_2 \cdot Fe_{II}S$) could be regarded as a mixed valence II/VI compound, has a structure[12]

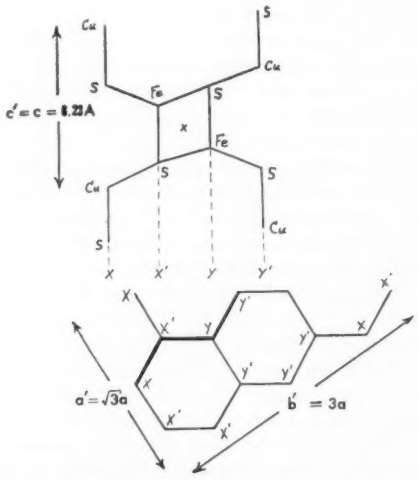

FIG. 8. Structure of $CuFe_2S_3$, cubanite.

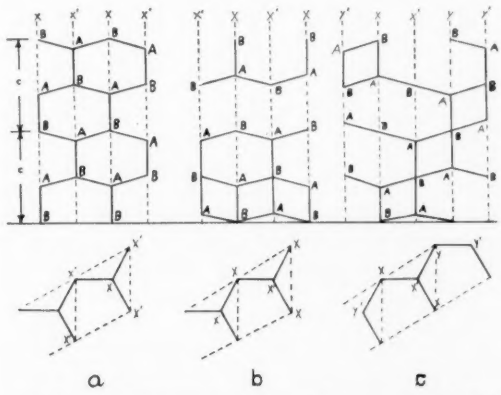

FIG. 9. Superstructures of the wurtzite structure obtained by inverting sites so as to give $2c$ periodicity. (a) normal wurtzite structure; (b) superstructure with $2c$ periodicity; (c) superstructure with $2c$ and $\sqrt{3}a$ periodicities.

[12] L. V. Azaroff and M. J. Buerger, Am. Min. **40**, 213 (1955).

which is a slightly distorted form of the structure shown in Fig. 7(c) in which the B atoms are sulfur and the A atoms are Cu in rows X and Y', Fe in rows X' and Y. A consequence of this inversion of adjacent rows in the wurtzite lattice is the diamond-shaped configuration shown in Fig. 8 with the close Fe–Fe approach of 2.81 A and a valence angle at the sulfur atom of $\sim 70°$.

In sulvanite, Cu_3VS_4, which is based on the zinc blende structure, an analogous occupation of inverted sites also leads to a short metal to metal distance (V–Cu 2.685) and a 70° angle at the sulfur atom.[13]

Argentopyrite, $AgFe_2S_3$, has a similar unit cell to that of cubanite, (see Table IV), but would appear to be a different arrangement since a different space group is reported.[14] This structure is not known.

In order to obtain a $2c$ superlattice periodicity which is also observed in the short-range structure of Al_2CO, it is necessary to occupy alternatively inverted sites along the c axis direction. Figure 9(b) shows the structural features associated with such a $2c$ superstructure and Fig. 9(c) is an arrangement which would combine both the $2c$ and the $\sqrt{3}a$ periodicities. As in cubanite, this structural arrangement would occur at the junction of blocks of normal wurtzite lattice where the polarity of the local structure (and the occupancy of the metal sites) is reversed. The cell dimensions of a second mineral form of $AgFe_2S_3$, sternbergite, suggests that this might provide an example of this type of structure (see Table IV).

The frequency with which this regular occupation of inverted sites occurs in Al_2CO cannot be determined from the experimental diffuse diffraction data. Where it does occur it will embody similar structural features to those found in cubanite and sulvanite, i.e., a short Al–Al separation, 2.45 A in Al_2CO, and an acute valence angle at the nonmetal atom. The coordination around the metal atom is invariably fourfold in a distorted tetrahedron. Somewhat similar structural arrangements

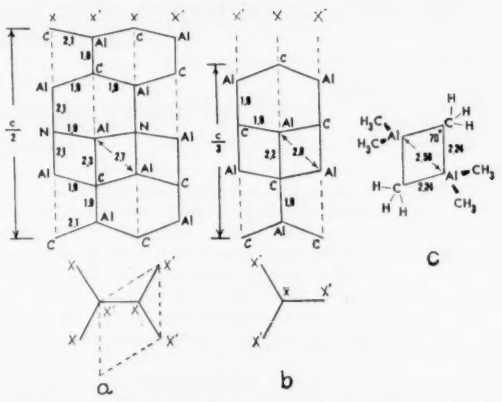

FIG. 10. (a) Structure of Al_4C_3; (b) structure of Al_5C_3N; (c) structure of $Al_2(CH_3)_6$.

have been reported to exist in aluminum carbide,[15] Al_4C_3, and aluminum carbonitride,[16] Al_5C_3N (see Fig. 10). The short Al–Al distance and the 70° angle also invites comparison with the structure of trimethyl aluminum[17] (see Fig. 10).

Further investigation of the structural features associated with the inversion of adjacent rows or blocks of wurtzite-type structure is most necessary. This will have to be carried out on single crystals of compounds in which the structures are completely ordered, or at least the order persists over a longer range than in Al_2CO, if sufficient x-ray diffraction data is to be obtained for a definite determination of the local structural parameters.

Note added in proof. Single crystals of $BeSiN_2$ have been studied by P. Eckerlin and H. Nortmann, Deutsche Philips Industries GmbH, Aachen, who find a wurtzite super-structure, space group $Pna2_1$.

[13] L. Pauling, *The Nature of the Chemical Bond* (Cornell University Press, Ithaca, New York, 1960), 3rd ed.
[14] J. Murdock and L. G. Berry, Am. Min. **39,** 475 (1954).
[15] M. von Stackelberg and E. Schnornenberg, Z. physik. Chem. (Leipzig) **B27,** 37 (1934).
[16] M. von Stackelberg, E. Schnornenberg, R. Paulus, and K. F. Spress, Z. physik Chem. **A175,** 127, 140 (1935).
[17] P. H. Lewis and R. E. Rundle, J. Chem. Phys. **21,** 986 (1953).

Effect of Dissolved Oxygen on the Spin-Lattice Relaxation Time of Free Radicals in Petroleum Oils

A. J. SARACENO AND N. D. COGGESHALL

Gulf Research & Development Company, Pittsburgh, Pennsylvania

(Received June 14, 1960)

Electron paramagnetic resonance studies of free radicals in petroleum oils reveal that the presence of dissolved oxygen significantly affects the free radical spin-lattice relaxation time, T_1. Changes in T_1 can occur upon: (a) dilution with solvents, (b) exposure to light, (c) bubbling with oxygen, and (d) stripping of dissolved oxygen. In this investigation it is shown that these changes all result from the influence of dissolved oxygen. Dilution with ordinary cp solvents results in a decrease of T_1. If the solvent is first stripped of dissolved oxygen, there will be no changes in T_1. The effect is reversible, i.e., the value of T_1 for free radicals in a petroleum oil may be arbitrarily decreased or increased by adding or removing dissolved oxygen, respectively. It was observed that free radicals in oil, or in oil in solution, experienced an increase in spin-lattice relaxation time when allowed to remain sealed in a quartz tube. This change was traced to the effect of light and appears to occur for wavelengths of the order of 5400 A and lower. It is concluded that this phenomenon is due to the photochemical takeup of dissolved oxygen whose presence decreases T_1. This is based on the fact that T_1 may be lowered to its original value merely by adding molecular oxygen to the petroleum oil. Depending upon the degree of saturation being effected, changes in T_1 will be reflected as changes in "apparent" free radical content. The true free radical content was unchanged by the processes studied.

MANY full crudes, petroleum bottoms, and oil distillates have been observed to yield a single paramagnetic resonance peak near a g value of 2.00[1–3] The resonance is in addition to and superimposed upon that arising from the presence of any V^{+4} as vanadyl.[2,3] Nickel porphyrin also occurs in petroleum oils but it exists in a diamagnetic state. Hence, the single resonance can only be explained by the presence of free radicals in petroleum oils. The fact that a large number of free radicals become trapped during the carbonization of organic matter[4–6] is probably related to the mechanism by which free radicals were formed in petroleum.

Previous EPR measurements on petroleum crudes[1,2] reveal no hyperfine structure which may arise from the nuclear moments of surrounding atoms such as hydrogen.

While engaged in the measurement of the free radical content of petroleum oils by EPR, we observed that saturation of the free radical resonance occurred at relatively low rf levels (~1 mw). Subsequently, it was found that the degree of saturation (and hence the value of the spin-lattice relaxation time) depended greatly upon the manner in which a given petroleum oil was treated prior to examination. This investigation is concerned with the variation of the spin-lattice relaxation time T_1 for the free radical resonance which was systematically studied with respect to effects of solvents, dissolved oxygen, and radiation in the visible and ultraviolet region.

[1] H. S. Gutowsky, B. R. Ray, R. L. Rutledge, and R. R. Unterberger, J. Chem. Phys. **28,** 744 (1958).
[2] D. E. O'Reilly, J. Chem. Phys. **29,** 1188 (1958).
[3] A. J. Saraceno, D. T. Fanale, and N. D. Coggeshall, Anal. Chem. (to be published).
[4] J. E. Bennett, D. J. E. Ingram, and J. G. Tapley, *Defects in Crystalline Solids* (Physical Society, London, 1954), p. 65; Phil. Mag. **45,** 545 (1954); Nature **174,** 797 (1954).
[5] J. Uebersfeld, A. Etiene, and J. Combrisson, Nature **174,** 614 (1954).
[6] D. E. G. Austen, D. J. E. Ingram, and J. G. Tapley, Trans. Faraday Soc. **54,** 400 (1958).

APPARATUS AND EQUIPMENT

A Varian Associates X-band spectrometer, model V–4500, employing audiomagnetic field modulation and phase-sensitive detection was used. The standard 6-in. diam pole face magnet (V–4007) with a 2.00-in. air gap and matching power supply (V–2200A) comprised the magnet system. The derivative of the absorption line was traced out in all cases by a pen recorder.

Special, clear fused quartz tubing (General Electric Lamp Glass Department, Cleveland, Ohio) was used in making tubes for holding oil samples in the resonant cavity. The tubes, sealed at one end and about 4.5 in. in length, had the following tolerance specifications: 3 mm±12% i.d.×4.75 mm±0.25 mm o.d.

Ultraviolet and Visible Radiation

Petroleum oils were exposed to relatively narrow frequencies in the visible and ultraviolet region through the use of glass color filters with nominal wavelengths of 600, 540, 500, 420, and 400 mμ. The light source was direct (through window glass) or reflected sunlight.

EXPERIMENTAL RESULTS

Saturation Behavior

Electron resonance experiments were conducted at rf power levels varying from about 1 to 80 mw. The general saturation behavior of free radicals in petroleum can be seen in Fig. 1. This curve is also characteristic of asphaltenes. The latter saturate easily even at 1.0 mw and, for this reason, it is difficult to obtain an accurate measure of spin concentration in this case. In the low microwave power region, there is only a negligible

saturation of the free radicals in oils. A nonsaturating resonance, in the region of rf levels employed, is indicated by the dotted line for V^{+4} as vanadyl ion.

The saturation method is generally used in measuring T_1.[7,8] This consists of measuring the absorption at high (saturating) rf levels and at relatively low power. From the variation of signal with microwave power a saturation parameter, defined as the ratio of the complex susceptibility under saturating conditions to the complex susceptibility under nonsaturating conditions, can be determined and, together with a knowledge of the spin-spin relaxation time (T_2), T_1 can be calculated. T_2 is approximated from the linewidth at very large dilution and at lower power. Since precise and absolute determinations of T_1 are difficult, relative values of the spin-lattice relaxation time are emphasized here.

Depending upon the degree of saturation being effected, changes in T_1 will be reflected as changes in "apparent" free radical content. The true free radical content was unchanged by the processes studied. The larger T_1 becomes, the smaller becomes the observed or "apparent" free radical content. Such changes have been at times interpreted as a real change in free radical content.

Portis[7] treats different types of homogeneous and inhomogeneous broadening and gives four cases for the variation of the saturation parameter with the variable s where $s=\frac{1}{4}\gamma^2H_1^2T_1T_2$. We compared our data with each of the four cases and found about equally good fit for either of Portis' cases 2 or 3. Since case 2 is simple, giving the saturation parameter b_1 as

$$b_1=1/(1+s),$$

it was used to determine the order of magnitude of T_1 which is 10^{-6} sec. Spin-lattice relaxation times of smaller magnitude are difficult to evaluate because of limitations of the klystron power output in obtaining saturation data. The linewidth of the free radical resonance is approximately 6.0 gauss which corresponds to 10^{-9} sec for the value of T_2.

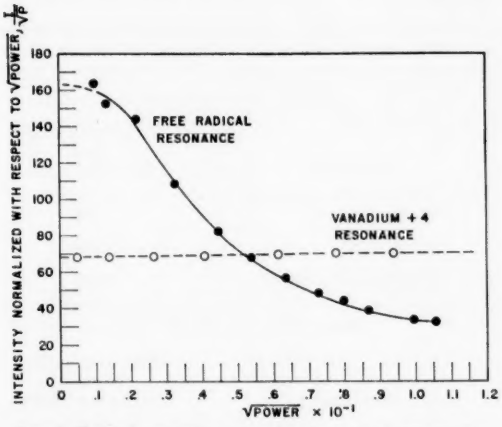

FIG. 1. Typical saturation curve for free radical resonance.

[7] D. J. E. Ingram, *Free Radicals as Studied by Electron Spin Resonance* (Butterworths Scientific Publications, Ltd., London, 1958).

[8] A. M. Portis, Phys. Rev. **91**, 1071 (1953).

TABLE I. Effect of reflected sunlight on the relative value of spin-lattice relaxation time for free radicals in a Kuwait fuel oil containing 10^{16} spins/g.

Time of exposure (hr)	Relative relaxation time (arbitrary units)	Relative relaxation time of oil shielded from light (arbitrary units)
0	0.22	0.22
1	0.59	0.22
2	0.80	0.22
3	0.98	0.23
4	1.00	0.23

In each case the signal divided by $P^{\frac{1}{2}}$, where P is microwave power, was extrapolated to zero power. This provided a base point for determination of saturation parameter b_1 as a function of power. Since none of Portis[7] cases matched the data exactly, we may take $b_1=f(s)$ wherein the exact functionality of f is unknown. In each experiment we interpolate the data to determine the power for $b_1=\frac{1}{2}$. From the foregoing we have $s=kPT_1$ where k is a constant. We may then use this expression to calculate relative values of T_1 as s will necessarily have the same value in all cases where $b_1=\frac{1}{2}$. Parameters such as the volume of the cavity, klystron frequency, etc., which are involved in computing the absolute value of T_1 remain constant and need not be evaluated.

For a given type of treatment (dilution with solvents, exposure to sunlight, etc.) the longest observed T_1 in each case was assigned an arbitrary value of unity. Changes in T_1 are with reference to the oil subjected to the specific treatments listed in Tables I–V.

Effects on Free Radical Concentration

We may briefly state the observations (conducted at nonsaturating rf levels) as follows: exposure of the oils to sunlight or ultraviolet radiation caused no change in the free radical concentration; the addition of either benzene, carbon dislufide, *n*-hexane, or isooctane similarly produced little or no observable effects; and, bubbling molecular oxygen into a petroleum oil had no effect on the radical concentration.

Changes in Spin-Lattice Relaxation Time

Table I contains a tabulation of approximate relative values of T_1 for a fuel oil which was exposed to reflected sunlight for varying periods of time. Corresponding values of T_1 for the oil sample retained in complete darkness are also listed. Values of T_1 for the same oil

TABLE II. Effect of different wavelengths on the relative value of spin-lattice relaxation time for free radicals in a Kuwait fuel oil containing 10^{16} spins/g.

Wavelength (mμ)	Time of exposure (hr)	Relative relaxation time (arbitrary units)
600	1	0.22
540	1	0.28
500	1	0.60
420	1	0.64
400	1	0.80
Direct sunlight	1	1.00
Complete darkness	1	0.22

exposed to specific wavelengths of light for a time of 1 hr are given in Table II. The oil was exposed to radiation while sealed in quartz tubes which could be immediately scanned for the free radical resonance.

The variation of T_1 as a function of the type of solvent added is summarized in Table III for a Kuwait petroleum residue. Analogous data are presented in Table IV for the residue and an asphalt containing ordinary cp benzene at three concentrations.

The effect of oxygen on T_1 is illustrated in Table V for the residue and its benzene solution (50%) by weight). Since little or no change in T_2 was observed throughout this work, its value is not tabulated.

DISCUSSION OF RESULTS

No effects on the free radical concentration were observed as due to light, oxygen, and organic solvents. Consequently, we may conclude that the free radical species in oil are stable and are not created through dissociation of diamagnetic molecules upon dilution with solvents. This is in contrast to the results reported for coal asphaltenes.[9]

Striking changes in the spin-lattice relaxation time were observed for the free radicals in petroleum oils when subjected to the various treatments described. These changes are so pronounced that, at high rf levels

TABLE III. Effect of oxygen-containing solvents on relative spin-lattice relaxation time for a free radical in a Kuwait residue containing 10^{17} spins/g.

Solvent	Wt %	Relative relaxation time (arbitrary units)
Methylene chloride	50	0.26
Benzene	50	0.24
Carbon disulfide	50	0.10
n-Hexane	50	0.97
Original oil sample	...	1.00

[9] R. A. Friedel, J. Chem. Phys. **31,** 280 (1959).

TABLE IV. Influence of oxygen-containing benzene on relative value of T_1 at various concentrations of solvent.

Kuwait residue (10^{17} spins/g)	
Wt % benzene (cp)	Relative relaxation time (arbitrary units)
0	1.00
10	0.32
50	0.23
90	0.22
Asphalt (10^{18} spins/g)	
Wt % benzene (cp)	Relative relaxation time (arbitrary units)
0	1.00
10	0.14
50	≃0.012
90	≃0.010

(∼80 mw), the free radical signal can differ by as much as an order of magnitude.

When a petroleum oil was sealed in a quartz tube and exposed to sunlight, a progressive increase in the spin-lattice relaxation time is easily detected. When the same oil was kept in the dark, however, little or no change in T_1 was observed (Table I). By contrast, the addition of ordinary cp solvents to a petroleum oil had the effect of shortening the relaxation time. Not only was the decrease in T_1 initially proportional to the concentration of solvent (Table IV), but the net change in T_1 differed considerably for each solvent (Table III).

Shortening of T_1 was found for petroleum oils saturated with molecular oxygen, whereas purging the same

TABLE V. Effect of oxygen on spin-lattice relaxation time of free radicals in a Kuwait residue containing 10^{17} spins/g.

Original oil sample	
Environment	Relative relaxation time (arbitrary units)
Under nitrogen	1.00
Air exposed	0.44
Bubbled with oxygen	0.31
Diluted 50% by weight in benzene	
Environment	Relative relaxation time (arbitrary units)
Under nitrogen	1.00
Air exposed	0.11
Bubbled with oxygen	≃0.05

oils with either hydrogen or nitrogen resulted in an increase. Since oxygen was found to play such an important role in reducing T_1, the experiments on oil diluted with solvents were repeated after both had been purged free of dissolved oxygen. Very little change in T_1 was observed upon dilution in this instance. Upon exposure to air, however, T_1 became appreciably shorter (Table V). Again it was found that benzene, carbon disulfide, and methylene chloride solutions of the oil displayed much greater changes than *n*-hexane with respect to T_1. The addition of nitric oxide, another simple paramagnetic molecule, also results in a shortening of T_1 for the free radical species in a petroleum oil.

Qualitative experiments on photochemical effects, mentioned previously, showed that a spin-lattice relaxation time, which had been increased by exposure to light, could be reduced by bubbling molecular oxygen through the oil. Re-exposure of the oil to light of appropriate wavelength was found to result in an increase of T_1.

Only wavelengths of light below 600 mμ are responsible for altering T_1, as observed with the use of filters (Table II). As can be seen from Table II, there is a greater change of T_1 in going from a light-shielded environment to one exposed to progressively shorter wavelengths. These observations can be explained in the following manner. First, the presence of dissolved oxygen shortens the spin-lattice relaxation time as noted in Table V. Second, it is postulated that, during exposure of oils to light of suitable wavelengths, a chemical reaction between atmospheric or dissolved oxygen and certain photochemically sensitive materials in the oil is accelerated. The free radical species, as well as diamagnetic hydrocarbons, are probably involved in the chemical reaction with dissolved oxygen but, because of the large excess of the latter, a radical change is presumably too slow to be detected. The photochemical uptake of dissolved O_2 results in the removal of a magnetic environment within the spin system and this in turn lengthens T_1. The effect of light on T_1 is therefore an indirect influence acting by a mechanism involving oxidation of the oil. Since many hydrocarbons undergo very slow autoxidation even in the absence of light, we may expect that slight changes in T_1 will occur for the free radical species in an oil upon standing in air.

This phenomenon offers an indirect method for detecting, measuring, and following the content of dissolved oxygen, provided that the radical concentration remains constant over a sufficiently long period of time.

The details of the saturation behavior of a spin system depend markedly on the nature of the broadening mechanism. Two types of broadening are recognized[7]: (1) homogeneous broadening in which the line shape is altered by interactions within the spin system or from external interactions which fluctuate rapidly compared with the time taken for a spin transition (e.g., dipolar spin-spin interaction, spin-lattice interaction, and exchange narrowing); (2) inhomogeneous broadening arising from interactions which come from outside the spin system and which vary slowly in time compared with the spin transition. It is possible to distinguish between these two general types by observing any changes accompanying the linewidth upon variation in power. Homogeneous broadening is characterized by an increase in linewidth on saturation, while to a first approximation inhomogeneous broadening does not result in such a change of line shape but only in a reduction of expected power absorption which will be proportional across its whole width. Measurements on linewidth changes at various stages of saturation do not show line broadening between points of maximum slope for the free radical resonance in petroleum oils. This would appear to indicate, therefore, that the shape of the line is remaining constant and inhomogeneous saturation is occuring. This is consistent with the idea that the linewidth of the free radical resonance in petroleum oils is governed by hyperfine interaction with protons.

ACKNOWLEDGMENTS

The authors wish to acknowledge the assistance of J. F. Itzel in obtaining experimental data and the benefit of discussions on this subject with Dr. D. E. O'Reilly and Dr. C. P. Poole, Jr.

Composition Dependence of the Thermal Conductivity of Regular Solutions*

RICHARD J. BEARMAN AND V. S. VAIDHYANATHAN

Department of Chemistry, University of Kansas, Lawrence, Kansas

(Received July 25, 1960)

It is demonstrated from the statistical mechanics of transport processes that the product $\kappa\eta$ of the coefficients of thermal conductivity and viscosity may be expected to be independent of composition in regular solutions. This conclusion is verified for the system benzene-carbon tetrachloride.

IN a previous communication,[1] one of us (*RJB*) established the following general expression for the coefficient of thermal conductivity κ of binary liquid mixtures, basing the calculation upon the principles of the statistical mechanics of transport processes and the method of the pair space linear relations:

$$\kappa=\sum_\alpha\sum_\beta c_\alpha c_\beta \frac{D_\alpha^2}{D_\alpha+D_\beta}\frac{\partial h_{\alpha\beta}}{\partial T}-\tfrac{1}{6}\sum_\alpha\sum_\beta c_\alpha c_\beta\frac{D_\alpha D_\beta}{D_\alpha+D_\beta}$$
$$\times\int\left[V_{\alpha\beta}-r\frac{dV_{\alpha\beta}}{dr}\right]rg_{\alpha\beta}^{(2,0)}\frac{d}{dr}\left[\frac{\partial\ln g_{\alpha\beta}^{(2,0)}}{\partial T}\right]d^3\mathbf{r}$$
$$-\tfrac{1}{2}c_1c_2\frac{(D_1-D_2)^2}{D_1+D_2}\left\{2\frac{\partial h_{12}}{\partial T}-\int\tfrac{2}{3}rg_{12}^{(2,0)}\frac{dV_{12}}{dr}\right.$$
$$\left.\times\left[\frac{d\chi_{12}\dagger}{dr}-\frac{\partial\ln g_{12}^{(2,0)}}{\partial T}\right]d^3\mathbf{r}\right\}$$
$$h_{\alpha\beta}=h_{\beta\alpha}=\tfrac{1}{2}\int\left[V_{\alpha\beta}-\frac{r}{3}\frac{dV_{\alpha\beta}}{dr}\right]g_{\alpha\beta}^{(2,0)}d^3\mathbf{r}, \quad (1)$$

where D_α is the self-diffusion coefficient of species α in the mixture, c_α is the concentration of α, $V_{\alpha\beta}$ is the potential of intermolecular force between two molecules separated by a distance of magnitude r (assumed central, spherically symmetric, and pairwise additive), $g_{\alpha\beta}^{(2,0)}$ is the equilibrium radial distribution function, and $\chi_{12}\dagger$, a nonequilibrium perturbation to the distribution function, obeys the different equation

$$g_{12}^{(2,0)}\frac{d^2\chi_{12}\dagger}{dr^2}+\left(\frac{dg_{12}^{(2,0)}}{dr}+\frac{2}{r}g_{12}^{(2,0)}\right)\frac{d\chi_{12}\dagger}{dr}$$
$$-\frac{2g_{12}^{(2,0)}}{r^2}\chi_{12}\dagger=\frac{d}{dr}\left(\frac{\partial g_{12}^{(2,0)}}{\partial T}\right), \quad (2)$$

where T is absolute temperature.

To facilitate comparison with experiment, an approximate formula was developed, valid for solutions regular in behavior with additive volumes and composition independent radial distribution functions:

$$\kappa=\left[x_1\kappa_1\left(\frac{v_1}{v}\right)^2\left(\frac{D_1}{D_1^0}\right)+x_2\kappa_2\left(\frac{v_2}{v}\right)^2\left(\frac{D_2}{D_2^0}\right)\right]$$
$$+x_1x_2\left[(D_1-D_2)/(D_1+D_2)\right]\left[\kappa_2\left(\frac{D_2}{D_2^0}\right)\left(\frac{v_2}{v}\right)^2\right.$$
$$\left.-\kappa_1\left(\frac{D_1}{D_1^0}\right)\left(\frac{v_1}{v}\right)^2\right]+\tfrac{1}{3}\left(\frac{x_1x_2}{v^2}\right)\left[(D_1-D_2)^2/(D_1+D_2)\right]$$
$$\times\int rg_{12}^{(2,0)}\left(\frac{dV_{12}}{dr}\right)\left[\frac{d\chi_{12}\dagger}{dr}-\left(\frac{\partial\ln g_{12}^{(2,0)}}{\partial T}\right)\right]d^3\mathbf{r}, \quad (3)$$

where κ_1 and κ_2 are the thermal conductivities of the pure components, x_1 and x_2 are the mole fractions of species 1 and 2, respectively, v_1 and v_2 are their molar volumes, D_1^0 and D_2^0 are the self-diffusion coefficients of species 1 and 2, respectively, in the pure state, and v is the molar volume of solution. We now derive for the case of regular solutions an alternative relationship of especially simple form. Into Eq. (1), we introduce the equation

$$(D_1/D_2)=(v_2/v_1) \quad (4)$$

obtained by Bearman[2] for the ratio of the self-diffusion coefficients. Upon rearrangement of terms, with the use of additivity of volumes, we find,

$$\frac{x_1}{x_2}v_1^2\left(\frac{\kappa}{D_1}-\frac{\kappa_1}{D_1^0}\right)+2\frac{\kappa}{D_1}v_1v_2+\frac{x_2}{x_1}v_2^2\left(\frac{\kappa}{D_1}-\frac{\kappa_2}{D_1^\infty}\right)=\kappa_{12}$$

$$\kappa_{12}=\frac{v_2}{(v_1+v_2)}\frac{\partial h_{12}}{\partial T}-\tfrac{1}{6}\frac{v_1}{(v_1+v_2)}\int\left[V_{12}-r\frac{dV_{12}}{dr}\right]rg_{12}^{(2,0)}$$
$$\times\frac{d}{dr}\left(\frac{\partial\ln g_{12}^{(2,0)}}{\partial T}\right)d^3\mathbf{r}-\frac{(v_2-v_1)^2}{(v_2+v_1)}\frac{\partial h_{12}}{\partial T}$$
$$-\frac{(v_2-v_1)^2}{2v_2(v_1+v_2)}\int\tfrac{2}{3}rg_{12}^{(2,0)}\frac{dV_{12}}{dr}\left[\frac{d\chi_{12}\dagger}{dr}-\frac{\partial\ln g_{12}^{(2,0)}}{\partial T}\right]d^3\mathbf{r}, \quad (5)$$

where D_1^∞ is the self-diffusion coefficient of 1 in pure 2. The term κ_{12} is independent of composition. In view of the first of Eqs. (5), this condition can be met only if κ/D_1 is independent of composition, provided that the molar volumes are unequal and κ/D_1 is analytic in the

* This research was supported in part by Grant No. AF-AFOSR-61-7 from the Office of Scientific Research of the U. S. Air Force to the University of Kansas, Lawrence, Kansas.

[1] R. J. Bearman, J. Chem. Phys. **29**, 1278 (1959).

[2] R. J. Bearman, J. Chem. Phys. **32**, 1308 (1960).

mole fraction. Under the same hypotheses and with the use of an identical argument, Bearman and Jones[3] have demonstrated that the product of the self-diffusion coefficient with the viscosity coefficient $D_1\eta$ also may be expected to be independent of composition. We conclude therefore that $\kappa\eta$ will be independent of mole fraction at a specified temperature and pressure. This somewhat surprising result may prove useful in a practical way for the prediction of thermal conductivities of liquid mixtures from the conductivity and viscosity of a single pure component and the viscosity of the solution at a composition of interest.

To test our conclusion, we consider the system benzene-carbon tetrachloride (apparently the only solution of approximate regularity for which thermal conductivity data are available). The thermal conductivities at 30°C may be interpolated from the graph published by Fillipov and Novoselova.[4] The coefficients of viscosity at 30°C may be obtained from an article of Thorpe and Rodgers[5] published some years ago.

TABLE I.

$x_{C_6H_6}$	η centipoises	κ kcal/ mole-hr-deg	$\kappa\eta$ kcal-cpoise/ mole-hr-deg
0.0	0.84	0.0874±3%	0.073
0.2	0.79	0.0896	0.070
0.4	0.73	0.0935	0.068
0.8	0.62	0.1083	0.067
0.9	0.59	0.1161	0.068
1.0	0.56	0.1235	0.069

Their data when plotted versus mole fraction lie nearly on a straight line with intercepts which are in agreement with the more recent values of Grunberg[6] and Grunberg and Nissan[7] for the pure components. The results of these calculations are presented in Table I. The product $\kappa\eta$ is constant with an average value of 0.069 kcal-cpoise/mole-hr-deg and a mean deviation within the 3% maximum experimental error reported by Fillipov and Novoselova.[4]

[3] R. J. Bearman and P. F. Jones, J. Chem. Phys. **33,** 1432 (1960).
[4] L. P. Filippov and N. S. Novoselova, Vestnik Moskov. Univ. **10,** No. 3, Ser. Fiz. Mat. i Estestvan. Nauk. No. 2, 37 (1955).
[5] T. E. Thorpe and J. W. Rodgers, J. Chem. Soc. **71,** 360 (1897).
[6] L. Grunberg, Trans. Faraday Soc. **50,** 1293 (1954).
[7] L. Grunberg and A. H. Nissan, Trans. Faraday Soc. **45,** 125 (1949).

THE JOURNAL OF CHEMICAL PHYSICS VOLUME 34, NUMBER 1 JANUARY, 1961

Infrared Spectrum and Force Field of Crystalline Hydrogen Peroxide*

R. L. MILLER†

Metcalf Chemical Laboratories, Brown University, Providence, Rhode Island

AND

D. F. HORNIG

Frick Chemical Laboratory, Princeton University, Princeton, New Jersey

(Received May 31, 1960)

The infrared spectrum of crystalline and vitreous hydrogen peroxide was studied from 300 cm^{-1} to 4000 cm^{-1}. A normal coordinate analysis of the tetragonal crystal with four molecules/unit cell is given. The hydrogen bonds are only slightly weaker than in H_2O but the O—H linewidths are only 80 cm^{-1}. From the coupled motion of the torsion and the high-frequency libration, the torsional frequency in the gas is estimated to be about 230 cm^{-1}.

INTRODUCTION

HYDROGEN peroxide offers an example of an ordered crystal in which the O—H···O hydrogen bond may be studied. In addition, the molecule itself is interesting because there is still a substantial question as to the magnitude of the forces restricting rotation about the O—O bond. Consequently, we undertook a study of the infrared spectrum of this substance in the region of its fundamental vibrations in the hope of shedding some light on the force field characterizing this hydrogen bond and on the structure of the molecule.

An investigation of the structure of the hydrogen peroxide crystal[1] determined the symmetry of the oxygen lattice to be $D_4^4(P4_12_1)$. The tetragonal unit cell contains four molecules and has dimensions $a=b=4.06$ A and $C=8.00$ A. The O—O bond length is 1.49 A. Each oxygen atom has two nearest-neighbor

* Based on a thesis submitted in partial fulfillment of the requirements for the Ph.D. degree, Brown University, May, 1954. This work was supported in part by ONR.

† E. I. du Pont de Nemours and Co. Graduate Fellow in Chemistry, 1952–1953. Present address: Monsanto Chemical Company, Springfield, Massachusetts.

[1] S. C. Abrahams, R. S. Collins, and W. N. Lipscomb, Acta Cryst. **4,** 15 (1951).

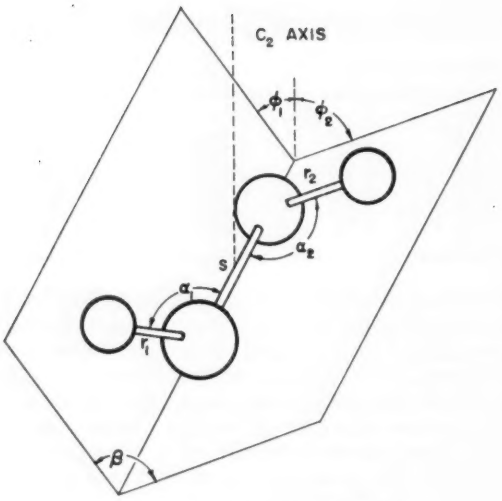

FIG. 1. The hydrogen peroxide molecule.

oxygen atoms (other than the oxygen atom to which it is bonded) at a distance of 2.78 A and two more at 2.90 A. If the hydrogen atoms are placed along the lines of the 2.78 A contacts, the H_2O_2 molecules have the structure proposed by Penney and Sutherland,[2] illustrated in Fig. 1, with $\alpha=97°$ and $\beta=94°$. In these positions the hydrogen atoms do not lower the symmetry and the C_2 axis of the free H_2O_2 molecule is also present in the crystal. The *ab* projection of the unit cell is shown in Fig. 2. It is seen that with hydrogens placed as shown, infinite 'helices with alternating oxygen and hydrogen are formed with the fourfold screw axes at their center.

The infrared spectrum of H_2O_2 vapor has been studied often,[3–6] as has the Raman spectrum of the liquid.[7–12] The infrared and Raman spectra of the crystal had been studied only by Taylor[11–12] when this work was undertaken. Subsequently he has reported the Raman spectrum of a single crystal,[13] and Giguere and Harvey[14] have reported further on the infrared spectrum of the crystal.

NORMAL VIBRATIONS OF THE CRYSTAL

In the structure of Fig. 1 the free hydrogen peroxide molecule has symmetric and antisymmetric O—H stretching (ν_1 and ν_5) and H—O—O bending frequencies (ν_2 and ν_6), an O—O stretching frequency (ν_3), and a torsional frequency about the O—O axis (ν_4). The values for these frequencies which have been arrived at by previous investigators are summarized in Table I. Most of the frequencies are reasonably certain but the magnitude of the torsional frequency is in serious doubt. Whereas Zumwalt and Giguère have found a value of 495 cm^{-1}, recent microwave measurements[15,16] have been interpreted to indicate that the barrier to rotation about the O—O bond is 113 cm^{-1}.

In passing from the vapor to the crystal, intermolecular forces are added. In order to discuss their effect two routes are possible: (a) one can start from the normal modes of the free molecule with symmetry C_2 and consider the coupling between the four molecules in a unit cell, or (b) one can note that for all the modes involving hydrogen motion, the O—H···O spirals, of symmetry C_4, form a basic unit and that two such spirals couple to give the crystal frequencies. Either point of view leads to the same result, and their relation is shown in Fig. 3.

The latter viewpoint is easier to visualize. Inspection of Table I shows that the frequency differences $\nu_1-\nu_5$ and $\nu_2-\nu_6$ are small in the free molecule, indicating a small intramolecular interaction between the O—H groups, so the spiral chain should be nearly an

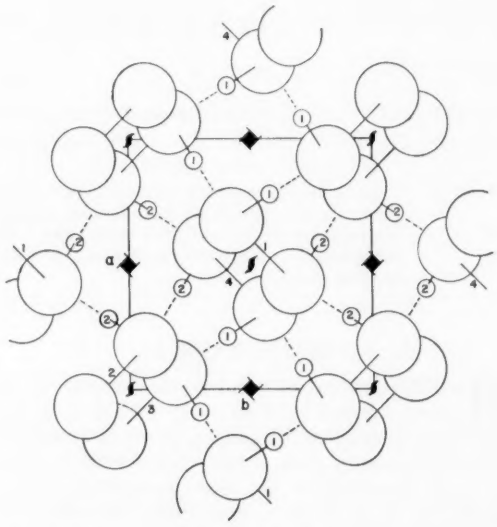

FIG. 2. Projection of unit cell of the hydrogen peroxide crystal perpendicular to the tetragonal axis.

[2] W. G. Penney and G. B. B. M. Sutherland, Trans. Faraday Soc. **30,** 898 (1934); J. Chem. Phys. **2,** 492 (1934).
[3] C. R. Bailey and R. R. Gordon, Trans. Faraday Soc. **34,** 1133 (1938).
[4] F. Feher, Ber. deut. Chem. Ges. **72B,** 1778 (1939).
[5] P. A. Giguere, J. Chem. Phys. **18,** 88 (1950).
[6] P. A. Giguere and O. Bain, J. Phys. Chem. **56,** 340 (1952); O. Bain and P. A. Giguere, Can. J. Chem. **33,** 527 (1955).
[7] S. Venkateswaren, Phil. Mag. vii, **15,** 263 (1933).
[8] A. Simon and F. Feher, Z. Elektrochem. **41,** 290 (1935).
[9] A. Simon, Z. angew. Chem. **51,** 792 (1938).
[10] L. R. Zumwalt and P. A. Giguere, J. Chem. Phys. **9,** 458 (1941).
[11] R. C. Taylor, J. Chem. Phys. **18,** 898 (1950).
[12] R. C. Taylor and P. C. Cross, J. Chem. Phys. **24,** 41 (1956).
[13] R. C. Taylor, Ohio State Symposium, 1957.
[14] P. A. Giguere and K. B. Harvey, J. Mol. Spectroscopy **3,** 36 (1959).
[15] J. T. Massey and D. R. Bianco, J. Chem. Phys. **22,** 442 (1954).
[16] J. T. Massey and R. W. Hart, J. Chem. Phys. **23,** 942 (1955).

TABLE I. Vibrational frequencies of hydrogen peroxide.

Gas, IR[5]	Liquid IR	Liquid Raman	Crystal IR(−190°C)	Crystal (−73°C)	Crystal Assignment
(490?)			650	635	$\nu_7(A_2)$
			690	668	$\nu_4(E)$
			808	800	ν_7+lattice
877	880	880	882	880	$\nu_3(E)$
			1332	1310	$\nu_4+\nu_A$
1266	1350	...	1385	1384	$\nu_6(E)$
1315	...	1400	1407	1404	$\nu_2(E)$
2649	2780	...	2821	2732	$2\nu_2$, $2\nu_6$, $\nu_2+\nu_6$
3610	...	3400	3192	3208	$\nu_5(A_2)$
3614	3400	...	3285	3291	$\nu_1(E)$

independent unit if this situation does not change in the crystal.

In these terms the anticipated spectrum can be analyzed qualitatively. Any given proton displacement (e.g., r, α, or ϕ) in the four molecules can be combined in four linearly independent ways to give four chain coordinates of symmetry A, B, and E. The A and E coordinates are infrared active and are polarized parallel and perpendicular to the C_4 axis, respectively. All three coordinates are Raman active. In this approximation, then, one might expect three frequencies each for the O—H stretching and O—H bending motions, all Raman active but only two of them infrared active. When the two chains are coupled, each of the previous should split in two. If the coupling is weak this results in a pattern of three doublets but if it is strong we expect two triplets. Since under D_4 the species A_2 and E are infrared active, each proton motion may generate three infrared-active-crystal frequencies. Similarly, A_1, B_1, B_2, and E are Raman active, so there might be five Raman frequencies, only two of them coinciding with infrared frequencies.

It should be noted that proton displacement in the ϕ direction (Fig. 1) gives rise to both the torsional motion and rotation about the O—O bond in the free molecule. Similarly, in the crystal it gives rise to torsion and libration so that the pattern of three infrared frequencies expected for this motion corresponds to both torsion and libration.

There is no difficulty in setting up the entire vibrational problem quantitatively. For a free (gas) molecule, six internal-displacement coordinates are necessary and they are indicated in Fig. 1. In the crystal translational and librational coordinates, three each, must be added. The translational frequencies should be low and will be neglected. As for the librations, since one of the principal axes of H_2O_2 nearly coincides with the O—O bond and two are perpendicular, two of the librations involve oxygen motions and should be nearly as low in frequency as the translations, while the third is a hydrogen motion which should have a frequency similar to that of the libration in ice, 850 cm^{-1}. Consequently, we shall include only the high frequency libration.

In discussing the crystal it is convenient to replace the torsional angle β by the angles of twist of the two O—H groups ϕ_1 and ϕ_2 with respect to the C_2 axis of the crystal. The reason is that if the molecule approaches a free rotator, the force constant k_β approaches zero in the free molecule and the torsional and librational frequencies become very similar. In these terms the complete harmonic potential for the molecule may be written

$$f^0 = \begin{array}{ccccccc} s & r_1 & r_2 & \alpha_1 & \alpha_2 & \phi_1 & \phi_2 \\ \hline k_s & k_{sr} & k_{sr} & dk_{s\alpha} & dk_{s\alpha} & dk_{s\phi} & dk_{s\phi} \\ & k_r & k_{rr} & dk_{r\alpha} & dk_{r\alpha}' & dk_{r\phi} & dk_{r\phi}' \\ & & k_r & dk_{r\alpha}' & dk_{r\alpha} & dk_{r\phi}' & dk_{r\phi} \\ & & & d^2k_\alpha & d^2k_{\alpha\alpha} & d^2k_{\alpha\phi} & d^2k_{\alpha\phi}'. \\ & & & & d^2k_\alpha & d^2k_{\alpha\phi}' & d^2k_{\alpha\phi} \\ & & & & & d^2k_\phi & d^2k_{\phi\phi} \\ & & & & & & d^2k_\phi. \end{array} \quad (1)$$

Here d is the equilibrium length of the O—H bonds. For the free molecule $k_\phi = k_{\phi\phi} = k_\beta$ and $k_{i\phi} = k_{i\phi}' = k_{i\beta}$, since $\phi_1+\phi_2=\beta$. The elements of the corresponding kinetic energy matrix, g,[0] may be evaluated from published tables.[17]

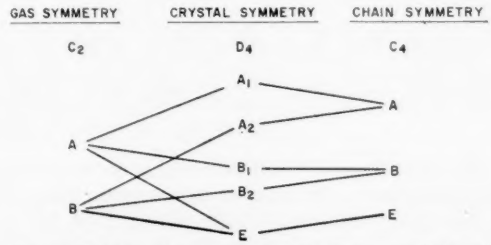

FIG. 3. Relation of symmetry species for gaseous H_2O_2, spiral chains of H—OH and H_2O_2 crystal.

[17] J. C. Decius, J. Chem. Phys. **16**, 1025 (1948).

These matrices satisfy the equation $|f^0g^0-\lambda^0 I|=0$, where I is the identity matrix.

In the crystal it may be anticipated on the one hand that these force constants will change in value and on the other that the motions of the various molecules will be coupled.[18] If it is assumed that the low-frequency lattice modes involving translation of the center of mass and libration about axes perpendicular to the O—O bond can be neglected, and that coupling takes place only between nearest neighbor molecules, the potential energy matrix for the crystal with four molecules in its unit cell is

$$f^c=\begin{array}{c|cccc} & 1 & 2 & 3 & 4 \\ \hline & f^0 & A & A' & 0 \\ & A' & f^0 & 0 & A \\ & A & 0 & f^0 & A' \\ & 0 & A' & A & f^0, \end{array} \qquad (2)$$

where f^0 is given by Eq. (1) and the matrix A contains the interaction constants between the coordinates of a molecule and its neighbor. A' is the transpose of A and 0 is the null matrix. A similar crystalline matrix g^c may be written but in this case the interaction matrices corresponding to A and A' vanish. If the protons are numbered as in Fig. 2, A is symmetrical and $A'=A$. If we assume further that the only important interactions connect protons bonded or hydrogen bonded to the same oxygen atom, the interaction matrix A, Eq. (2), takes the form

$$A=\begin{array}{c|ccccccc} & s' & r_1' & r_2' & \alpha_1' & \alpha_2' & \phi_1' & \phi_2' \\ \hline & 0 & 0 & 0 & 0 & 0 & 0 & 0 \\ r_1 & 0 & k_{rr'} & 0 & dk_{r\alpha'} & 0 & dk_{r\phi'} & 0 \\ r_2 & 0 & 0 & k_{rr'} & 0 & dk_{r\alpha'} & 0 & dk_{r\phi'} \\ \alpha_1 & 0 & dk_{r\alpha'} & 0 & d^2k_{\alpha\alpha'} & 0 & d^2k_{\alpha\phi'} & 0 \\ \alpha_2 & 0 & 0 & dk_{r\alpha'} & 0 & d^2k_{\alpha\alpha'} & 0 & d^2k_{\alpha\phi'} \\ \phi_1 & 0 & dk_{r\phi'} & 0 & d^2k_{\alpha\phi'} & 0 & d^2k_{\phi\phi'} & 0 \\ \phi_2 & 0 & 0 & dk_{r\phi'} & 0 & d^2k_{\alpha\phi'} & 0 & d^2k_{\phi\phi'}. \end{array} \qquad (3)$$

The 28×28 secular equation which occurs in the direct solution can be factored by a suitable transformation to symmetry coordinates. This is most readily accomplished by transforming first to molecular symmetry coordinates, labelled S_i, and thereafter to unit cell symmetry coordinates R_j. Thus

$$\begin{aligned} S_1^i(A)&=(r_1^i+r_2^i)/\sqrt{2} \\ S_2^i(A)&=(\alpha_1^i+\alpha_2^i)/\sqrt{2} \\ S_3^i(A)&=s \\ S_4^i(A)&=(\phi_1^i+\phi_2^i)/\sqrt{2}=\beta/\sqrt{2} \\ S_5^i(B)&=(r_1^i-r_2^i)/\sqrt{2} \\ S_6^i(B)&=(\alpha_1^i-\alpha_2^i)/\sqrt{2} \\ S_7^i(B)&=(\phi_1^i-\phi_2^i)/\sqrt{2}=\theta\sqrt{2}, \end{aligned} \qquad (4)$$

where i represents molecule 1, 2, 3, or 4 and θ is the angle of rotation about the O—O axis. These symmetry coordinates have been numbered to correspond to the normal modes of vibration of a free molecule except for S_7 which corresponds to rotation about the O—O bond. The symmetry coordinates R_j transform as the irreducible representations of D_4. A set of possible R_j is

$$\begin{aligned} R_j(A_1)&=\tfrac{1}{2}(S_j^1+S_j^2+S_j^3+S_j^4), && j=1,\ 2,\ 3,\ 4 \\ R_j(A_2)&=\tfrac{1}{2}(S_j^1+S_j^2+S_j^3+S_j^4), && j=5,\ 6,\ 7 \\ R_j(B_1)&=\tfrac{1}{2}(S_j^1-S_j^2-S_j^3+S_j^4), && j=1,\ 2,\ 3,\ 4 \\ R_j(B_2)&=\tfrac{1}{2}(S_j^1-S_j^2-S_j^3+S_j^4), && j=5,\ 6,\ 7 \\ R_{ja}(E)&=\tfrac{1}{2}(S_j^1+S_j^2-S_j^3-S_j^4) \\ R_{jb}(E)&=\tfrac{1}{2}(S_j^1-S_j^2+S_j^3-S_j^4) \end{aligned} \Bigg\} \quad j=1,\ 2,\ 3,\ 4,\ 5,\ 6,\ 7. \qquad (5)$$

The transformation of f^c and g^c according to Eqs. (4) and (5) yields

$$F^c(D_4)=\begin{array}{|c|c|c|c|c|c|c|c|} \hline F(A_1) & & & & & & & \\ \hline & F(A_2) & & & & & & \\ \hline & & F(B_1) & & & & & \\ \hline & & & F(B_2) & & & & \\ \hline & & & & F(E') & & & \\ \hline & & & & & F(E'') & & \\ \hline & & & & & & F(E') & \\ \hline & & & & & & & F(E'') \\ \hline \end{array} \qquad (6)$$

and a matrix of similar form for $G^c(D_4)$. In Eq. (6)

$$F(i)=\begin{array}{|cccc|c} F_1(i) & dF_{12}(i) & F_{13}(i) & dF_{14} & (i) \\ & d^2F_2(i) & dF_{23}(i) & d^2F_{23} & (i) \\ & & F_3(i) & dF_{34} & (i) \\ & & & d^2F_4 & (i) \end{array} \qquad (7)$$

[18] D. F. Hornig, J. Chem. Phys. **16**, 1063 (1948).

wherein

$$\begin{aligned}
F_1&=(k_r+k_{rr}+2\Delta k_{rr'})\\
F_2&=(k_\alpha+k_{\alpha\alpha}+2\Delta_{\alpha\alpha'})\\
F_3&=k_3\\
F_4&=(k_\phi+k_{\phi\phi}+2\Delta k_{\phi\phi'})\\
F_{12}&=(k_{r\alpha}+k_{r\alpha'}+2\Delta_{r\alpha'})\\
F_{13}&=k_{r3}\sqrt{2}\\
F_{14}&=(k_{r\phi}+k_{r\phi'}+2\Delta k_{r\phi'})\\
F_{23}&=k_{3\alpha}\sqrt{2}\\
F_{24}&=(k_{\alpha\phi}+k_{\alpha\phi'}+2\Delta k_{\alpha\phi'})\\
F_{34}&=k_{3\phi}\sqrt{2}\\
i&=A_1,\ B_1 \text{ or } E'
\end{aligned} \tag{8}$$

and

$$\begin{aligned}
\Delta&=+1 \text{ for } A_1\\
&=-1 \text{ for } B_1\\
&=0 \text{ for } E'.
\end{aligned}$$

Also,

$$F(j)=\begin{vmatrix} F_5(j) & dF_{56}(j) & dF_{57}(j)\\ & d^2F_6(j) & d^2F_{67}(j)\\ & & d^2F_7(j)\end{vmatrix}, \tag{9}$$

where

$$\begin{aligned}
F_5&=(k_r-k_{rr}+2\Delta k_{rr'})\\
F_6&=(k_\alpha-k_{\alpha\alpha}+2\Delta k_{\alpha\alpha'})\\
F_7&=(k_\phi-k_{\phi\phi}+2\Delta k_{\phi\phi'})\\
F_{56}&=(k_{r\alpha}-k_{r\alpha}'+2\Delta k_{r\alpha'})\\
F_{57}&=(k_{r\phi}-k_{r\phi}'+2\Delta k_{r\phi'})\\
F_{67}&=(k_{\alpha\phi}-k_{\alpha\phi}'+2\Delta k_{\alpha\phi'}),
\end{aligned} \tag{10}$$

and

$$\begin{aligned}
j&=A_2,\ B_2 \text{ or } E''\\
\Delta&=1 \quad \text{for } A_2\\
&=-1 \text{ for } B_2\\
&=0 \quad \text{for } E''.
\end{aligned}$$

The G matrices are constructed similarly but all G elements connecting different molecules (i.e., $G_{ij'}$,) vanish.

To a good approximation, particularly for hydrogen stretching vibrations, the off-diagonal elements in the GF matrix may be neglected, not because they are small, but because of the large separation in the stretching, bending and torsional frequencies. In that case a similar pattern of six frequencies is obtained in each of the three regions

FIG. 4. Frequency pattern in crystal for each normal mode; (a) $2k_{zz'}\gg k_{zz}$ (b) $2k_{zz'}\ll k_{zz}$.

$$\begin{aligned}
\lambda(A_1)&=g_{xx}(k_x+k_{xx}+2k_{xx'}) && R\\
\lambda(B_1)&=g_{xx}(k_x+k_{xx}-2k_{xx'}) && R\\
\lambda(E')&=g_{xx}(k_x+k_{xx}) && IR,\ R\\
\lambda(A_2)&=g_{xx}(k_x-k_{xx}+2k_{xx'}) && IR\\
\lambda(B_2)&=g_{xx}(k_x-k_{xx}-2k_{xx'}) && R\\
\lambda(E'')&=g_{xx}(k_x-k_{xx}) && IR,\ R,
\end{aligned} \tag{11}$$

where $x=r$, α, or ϕ. The frequency patterns corresponding to $2k_{xx'}\gg k_{xx}$ and $2k_{xx'}\ll k_{xx}$ are shown in Fig. 4(a) and 4(b), respectively.

In terms of the infrared active modes, then

$$\begin{aligned}
2g_{xx}k_{xx}&=\lambda(E')-\lambda(E'')\\
2g_{xx}k_{xx'}&=\lambda(A_2)-\lambda(E'').
\end{aligned} \tag{12}$$

As a further aid in analyzing the spectrum, it is convenient to have a rough idea of the intensity distribution within each pattern. In the same approximation as Eqs. (11), the normal coordinates, Q, are simple multiples of the symmetry coordinates and the intensities are simply proportional to $(\partial\mu/\partial R)^2$. With two more assumptions, (a) that the dipole moments of the various molecules are simply additive and (b) that the O—H bonds are directed along the O···O lines, the predicted relative intensities are:

$$\begin{aligned}
I\nu_1(E'):I\nu_5(A_2):I\nu_5(E'')&=0.89:1.00:0.04\\
I\nu_2(E'):I\nu_6(A_2):I\nu_6(E'')&=0.09:1.00:12.5\\
I\nu_4(E'):I\nu_7(A_2):I\nu_7(E'')&=1.31:1.00:0.07.
\end{aligned} \tag{13}$$

It should be noted in using these relations that if there are terms in the intermolecular potential not included in Eq. (3) the two species E vibrations may be coupled. In that case the total intensity would be roughly conserved but might be distributed quite differently between the modes, notably in the direction of more equal intensities.

EXPERIMENTAL

The H_2O_2 used was concentrated from 95% peroxide generously donated by Dr. N. S. Davis of the Buffalo Electrochemical Company. It was further purified by bulb to bulb distillation in a closed system at reduced pressure. Before introducing the H_2O_2 to be distilled,

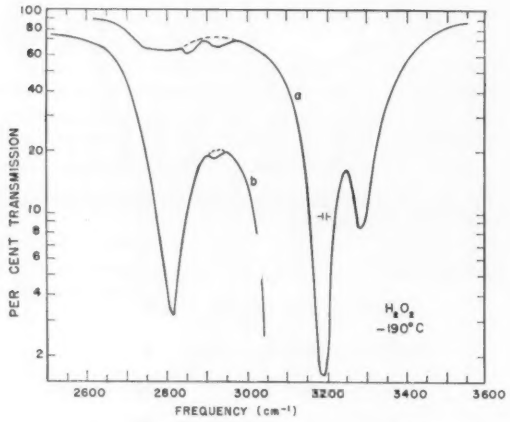

FIG. 5. Infrared spectrum of crystalline H_2O_2 in the region of the stretching vibrations.

the Pyrex apparatus was treated with boiling concentrated HNO_3, rinsed with distilled water, treated with boiling 90% H_2O_2, and finally rinsed with conductivity water. The tubes were then dried in a vacuum dessicator and stored there until used. In the distillation, approximately the last third of the distillate was collected for further use. It generally analyzed better than 99%, the average being about 99.5%. The material was analyzed by titration of an acid solution with $KMnO_4$, following the procedure of Huckaba and Keyes.[19]

Samples were prepared by evaporating H_2O_2, contained in a reservoir as either room-temperature liquid, supercooled liquid, or solid (at $-1°C$, $-78°C$, $-195°C$) to a carrier plate maintained in the infrared cell[20] at a temperature of either $-78°C$ or $-195°C$. No variation in the spectrum due to the state of the material in the reservoir was observed. Since we were concerned that the crystal habit might be affected by the backing material, carrier plates of NaCl, KBr, CaF_2, AgCl, and KRS-5 were used, but there were no noticeable variations in the spectra obtained. When the H_2O_2 was condensed on a plate at $-195°C$ a glass was always obtained but when the plate was at $-78°C$ a crystalline film formed part of the time.

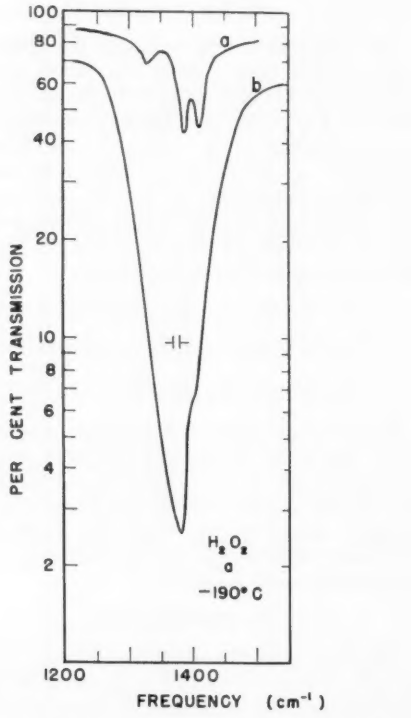

FIG. 6. Infrared spectrum of crystalline H_2O_2 in the region of the bending vibrations.

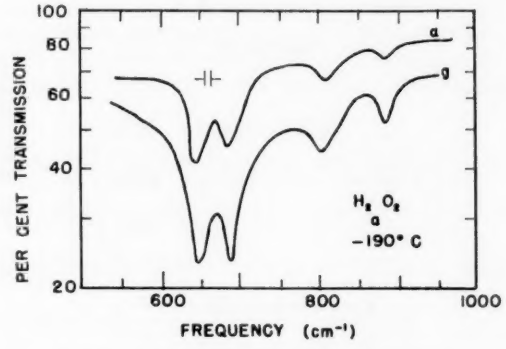

FIG. 7. Infrared spectrum of crystalline H_2O_2 in the region of the torsional, librational and O—O stretching vibrations.

The spectra were studied on a spectrometer similar to that described previously,[21] using LiF, CaF_2, NaCl, KBr, and KRS-5 prisms. The spectra are thought to be free of the effects of stray radiation, which was negligible at frequencies above 800 cm^{-1}, since at lower frequencies the light was reflected from a Reststrahlen plate of LiF or CaF_2 before the entrance slit. The stray radiation amounted to 4% at 500 cm^{-1} and about 10% at 260 cm^{-1}.

Films of varying thicknesses were investigated at both $-73°C$ and $-190°C$ in the spectral range from 300 cm^{-1} to 9000 cm^{-1}. Thirty separate runs were made, each consisting of a series of successively thicker films. Six of these yielded spectra of the type shown in Figs. 5–7, believed to be those of crystals; the remainder of the spectra, which we believe are the

[19] C. E. Huckaba and F. G. Keyes, J. Am. Chem. Soc. **70,** 1640 (1948).

[20] E. L. Wagner and D. F. Hornig, J. Chem. Phys. **18,** 296 (1950).

[21] D. F. Hornig, G. E. Hyde, and W. A. Adcock, J. Opt. Soc. Am. **40,** 497 (1950).

spectra of the glass, were similar to those reported by Giguere.[14] The bands at 2920 cm^{-1} and 2846 cm^{-1} in Fig. 5 are caused by hydrocarbons on the backing plate. The frequencies of maximum absorption are listed in Table I, together with those reported previously. For comparison, the frequencies in the gaseous and liquid state are also included.

DISCUSSION

The general features of the spectra are fairly clear. Absorption occurs in the hydrogen stretching (ν), hydrogen bending (α), and torsion-libration (ϕ) regions. In addition the O—O stretching fundamental is found at 882 cm^{-1} and a bending overtone at about 2800 cm^{-1}. Nevertheless the spectrum proves to be more difficult to interpret in detail, particularly when Taylor's Raman frequencies are also included. We will, therefore, take up each of the absorption regions in succession.

A. O—H Stretching Region

Three infrared active frequencies are expected in this region but from Eq. (13) $\nu_5(E'')$ is expected to be very weak. The observed doublet probably arises from $\nu_1(E')$ and $\nu_5(A_2)$, the more intense low-frequency component presumably arising from the latter. From Eq. (11) the frequency separation is

$$\lambda_1(E')-\lambda_5(A_2)=2g_{rr}{}^2(k_{rr}-k_{rr'}),$$

so that

$$k_{rr}-k_{rr'}=0.169\times10^5 \text{ d/cm}. \qquad (14)$$

This much seems fairly secure but the separation of the two force constants is more difficult. If, as deduced by Giguere,[5] ν_1 and ν_5 are nearly coincident in the gas, k_{rr} must be nearly vanishing. Two difficulties then arise. (a) The combined infrared and Raman spectra show no sign of the pattern of three doublets (Fig. 2) which would then be expected and (b) a value of $k_{rr'}=-0.17\times10^5$ d/cm would be much greater than the corresponding force constant in ice, -0.12×10^5 d/cm[22], although the hydrogen bond distance is slightly longer and the angular geometry less favorable. Therefore, this possibility seems unlikely.

The opposite assumption might also be advanced, that since the two O—H's within a molecule are so much closer together than two O—H's in adjacent molecules, $k_{rr}\gg k_{rr'}$. The only real objection to this assumption is that the expected pattern of two triplets (Fig. 2) cannot be found in the combined infrared and Raman spectra and no matter how hard we have tried, it has been impossible to find a solution of this sort.

The most reasonable possibility may be derived from the following arguments. The intermolecular OH···OH coupling constant, $k_{rr'}$, is -0.099 in H_3BO_3[23] and -0.123 in ice; the effective proton charges which would give rise to these force constants are $0.58e$ and $0.63e$, respectively. If we assume that in H_2O_2 the corresponding effective charge on the protons is about $0.60e$, that the protons lie along the O···O lines, and that $k_{rr'}$ is produced entirely by interaction between these effective charges, we calculate that $k_{rr'}=-0.10\times10^5$ dynes/cm. It follows from Eq. (14) that $k_{rr}=+0.07\times10^5$ dynes/cm, and from Eq. (11) that $k_r=5.79\times10^5$ dynes/cm. The expected pattern of frequencies would then be:

$$\begin{aligned}
&\nu_5(A_2)=3192 \text{ cm}^{-1} && IR\\
&\nu_1(A_1)=3230 \text{ cm}^{-1} && R\\
&\nu_5(E)=3247 \text{ cm}^{-1} && R, IR \text{ (very weak)}\\
&\nu_1(E)=3285 \text{ cm}^{-1} && R, IR\\
&\nu_5(B_2)=3302 \text{ cm}^{-1} && R\\
&\nu_1(B_1)=3340 \text{ cm}^{-1} && R. \qquad (15)
\end{aligned}$$

The mean O—H frequency would be 3266 cm^{-1}. It is interesting to note that this value very nearly coincides with that in the glassy state.

B. O—H Bending Region

In the infrared spectrum of the gas and liquid, only ν_6 has been observed, so that ν_2 is very weak as would be expected from the geometry of the molecule. On the other hand, only ν_2 appears in the Raman spectrum of the liquid. The frequency of ν_6 is not much affected by change of state and ν_2 is about 50 cm^{-1} higher in frequency than ν_6.

In the Raman spectrum of a single crystal Taylor[13] has reported an intense peak at 1410 cm^{-1} and a weaker peak at 1377 cm^{-1}. It seems probable, therefore, that the infrared peak at 1407 cm^{-1} is associated with ν_2 and that at 1386 cm^{-1} with ν_6. It also seems likely that the line at 1310 cm^{-1} is not associated with the bending motion.

A serious problem arises in this interpretation since according to Eq. (13) a single line $\nu_6(E)$ was expected to predominate in the spectrum whereas the two lines observed are of nearly equal intensity. The only reasonable explanation for this anomaly which occurs to us is that the two components of the same symmetry $\nu_2(E)$ and $\nu_6(E)$ are strongly coupled by force constants not included in Eq. (2) so that the intensity is divided between the two. Small intensity changes might also occur from mixing with stretching and torsion-libration modes but these effects seem less likely to produce such a large effect.

If the two species E modes are coupled in the infrared spectrum the same must be true in the Raman spectrum. However, the very strong Raman peak is almost certainly $\nu_2(A_1)$ so that $\nu_2(A_1)$ must be very near in frequency to $\nu_2(E)$ which must lie under it. Since the $\nu_2(A_1)-\nu_2(E)$ splitting depends on $k_{\alpha\alpha'}$, this intermolecular force constant appears to be small. This supports our original conclusion that the observed splitting is largely intramolecular.

[22] C. Haas and D. F. Hornig, J. Chem. Phys. **32**, 1763 (1960).
[23] D. F. Hornig and R. C. Plumb, J. Chem. Phys. **26**, 637 (1957).

A definite solution to these problems can be obtained when the spectra of crystalline HO_2D and D_2O_2 are known but it seems relatively certain that despite the difficulties the assignment proposed here is correct. The weak line at 1310 cm^{-1} is probably the overtone of the torsion-libration region.

C. Torsion-Libration Region

This is one of the most interesting regions of the spectrum because of the light it sheds on hindered rotation in the H_2O_2 molecule. According to Eq. (13) two components $\nu_4(E)$ and $\nu_7(A_2)$ should be observed as almost equally strong peaks, possibly accompanied by a weak satellite $\nu_7(E)$. Two strong peaks do indeed appear at 690 and 650 cm^{-1} but there is a question concerning whether or not the weaker peak at 808 cm^{-1} is also a member of this cluster.

It seems most unlikely that the peak at 808 cm^{-1} is a fundamental vibration for several reasons. If it is, it must be $\nu_7(E'')$. In that case the intermolecular interaction is much greater than the intramolecular and the frequency pattern is that of Fig. 4b. If $\nu_7(E'')$ has a higher frequency than either $\nu_7(A_2)$ or $\nu_4(E')$, Eq. (12) requires that both $k_{\phi\phi}$ and $k_{\phi\phi'}$ be approximately equal and *negative*. If the crystalline perturbation is relatively weak, $k_{\phi\phi}$ is roughly equal to k_β in the free molecule. A negative $k_{\phi\phi}$ would imply a negative k_β so that the molecule would be bound in the crystal in an unstable configuration. This seems most improbable.

In addition, any dipole-dipole or effective charge interaction energy between molecules predicts that $k_{\phi\phi'}$ is about equal to $k_{aa'}$. Since we have already concluded that $k_{aa'}$ is very small this argument leads to the conclusion [from Eq. (12)] that $\nu_7(E)$ cannot be far separated from $\nu_7(A_2)$. Therefore the peak at 808 cm^{-1} almost certainly is not a torsion-libration fundamental.

If we accept the assignment of Table I the torsional frequency in the gas can be estimated. According to Eq. (11), the separation between these peaks is

$$\lambda_4(E)-\lambda_7(A_2)=2g_\phi^2(k_{\phi\phi}-k_{\phi\phi'}).$$

If the intermolecular coupling can be neglected this becomes simply

$$\lambda_4-\lambda_7=2G_\phi k_{\phi\phi}. \tag{16}$$

Now, if the hydrogen bond results only in the superposition of an external force field on the protons, it would change the value of k_ϕ in going from gas to crystal but it would not change the interaction constant $k_{\phi\phi}$ which in the gas is equal to k_β. Hence, since in the gas $\lambda_7=0$, Eq. (16) may be rewritten

$$\lambda_4-\lambda_7=\lambda_4(\text{gas}), \tag{17}$$

from which

$$\nu_4(\text{gas})=231\ cm^{-1}.$$

This result makes it seem likely that the double band at 465–575 cm^{-1} found by Bain and Giguere,[6] which has been attributed to the torsional oscillation about the O—O bond, is actually the first overtone of the torsional frequency.

If the torsional frequency is as high as 230 cm^{-1} the barrier to rotation about the O—O bond is substantial.

CONCLUSIONS

A. Hydrogen Bonding

The most direct measure of the strength of the hydrogen bond is given by the librational frequency, since the restoring force is purely determined by the hydrogen bond. Its frequency, 650 cm^{-1}, in H_2O_2 is decidedly smaller than in ice where it is 850 cm^{-1}. The force constant for the displacement of a proton perpendicular to the hydrogen bond is therefore 0.25×10^5 dynes/cm, a value of $(850/650)^2=1.71$ times smaller than in ice, so the strength of the hydrogen bond in H_2O_2 must be substantially smaller although the O—H···O distance is only 0.02 A greater.

The same conclusion is reached from the frequency shifts from vapor to crystal. The value in H_2O_2 is about 334 cm^{-1} (3600–3266) whereas in ice it is 425 cm^{-1} (3700–3275).

One of the most interesting questions concerns the linewidths of the stretching vibrations. It is often stated that the widths of hydrogen stretching bands for an O···O distance of 2.78 A are several hundred wave numbers.[24] Yet each of the two individual peaks in the H_2O_2 spectrum have a width at half height of only 85 cm^{-1}. This is almost identical with the value, 80 cm^{-1}, in H_3BO_3[23] and of the O—H stretching vibration of HOD in crystalline D_2O.[22] It seems almost safe to generalize that the width of a fundamental O—H transition in crystals with O···O distance of 2.75 A is about 80 cm^{-1}.

The much broader bands observed in liquids and more complicated crystals are undoubtedly an unresolved superposition of a number of such individual transitions. This is readily seen in that the width of the O—H band in vitreous H_2O_2, 250 cm^{-1}, is consistent with the usual correlations of line width and frequency shifts.[24] Such correlations are apparently more nearly related to the splitting by intermolecular coupling than they are to a true linewidth effect.

B. Barrier to Internal Rotation

If the assumption that the crystal field is simply superimposed on the molecular field is valid, the frequency of the torsional vibration in gaeous H_2O_2 is about 230 cm^{-1} and the absorption in the region 465–575 cm^{-1} in the vapor[6] must be an overtone. A similar conclusion has also been reached in a recent analysis of the microwave and infrared data by Hirota,[25] who estimated that the torsional frequency ought to lie in the range 100 to 250 cm^{-1}.

[24] E.g., see G. Pimentel and E. McLellan, *The Hydrogen Bond* (W. H. Freeman and Company, San Francisco, 1960), p. 94.
[25] E. Hirota, J. Chem. Phys. **28**, 839 (1959).

THE JOURNAL OF CHEMICAL PHYSICS VOLUME 34, NUMBER 1 JANUARY, 1961

Sum Rule for Transition Probabilities*

WILLIAM L. CLINTON†

Chemistry Department, Brookhaven Laboratory, Upton, New York

(Received May 20, 1960)

A sum rule is derived for the spontaneous emission transition probability. In particular it is shown that for an atom

$$\sum_m^\infty W_{nm} = Z\rho_n(0),$$

where W_{nm} is the spontaneous emission transition probability, Z is the nuclear charge, and $\rho_n(0)$ is the electron density of the nth electronic state evaluated at the nucleus.

I. INTRODUCTION

THERE are many sum rules that are utilized in spectroscopy. Most, however, are only applicable to special cases (e.g., hydrogen atom sum rules). A much more general and consequently more useful rule is the oscillator strength rule due to Thomas, Reiche, and Kuhn.[1] The purpose of this paper is to present a new sum rule of equivalent generality. The rule is derived in Sec. II. In later sections it is specialized to several different systems.

Of particular interest are the atomic and molecular cases where, for electronic transitions, the sum of the transition probabilities is simply related to the electron density at the nuclei; and for vibrational transitions the sum is related to the force constant.

Among other things, the rule proves useful in discussing lifetimes and natural linebreadths, since the latter are related to partial sums over transition probabilities. This is discussed in Sec. V.

Finally, in Sec. VI a discussion of the importance of the continuous spectrum is given in which the oscillator strength and transition probability sum rules are used to supplement each other.

II. GENERAL SUM RULE

The probability that an atomic system will undergo a spontaneous transition from a state $|\,m\rangle$ to a lower energy state $|\,n\rangle$ with the emission of one photon is[2]

$$W_{nm} = [(E_m - E_n)/2\pi]\,|\,\langle m\,|\,\mathbf{D}\,|\,n\rangle\,|^2, \quad (1)$$

where we have used atomic units and E_m and E_n are the energies of the states $|\,m\,\rangle$ and $|\,n\rangle$. Since we will work throughout on the assumption that the dipole approximation is valid for all W_{nm}, $\mathbf{D}$ can be written in terms of the momenta or position vectors so that

$$\langle m\,|\,\mathbf{D}\,|\,n\rangle = i\langle m\,|\,\mathbf{p}\,|\,n\rangle = (E_n - E_m)\langle m\,|\,\mathbf{r}\,|\,n\rangle, \quad (2)$$

where, for many particles, $\mathbf{p} \equiv \sum_k \mathbf{p}_k$ and $\mathbf{r} \equiv \sum_k \mathbf{r}_k$. More generally $\mathbf{D}$ will contain a retardation term $\exp(i\mathbf{k}\cdot\mathbf{r})$, where $\mathbf{k}$ is the photon propagation vector. Our results then will include only the first term in the expansion of the exponential. Higher terms involve quadrupole, etc., radiation. A discussion of the validity of considering only dipole radiation can be found in footnote reference 1.

On using the relationship

$$\langle m\,|\,\mathbf{p}\,|\,n\rangle = -i\langle \nabla V\rangle_{mn}/E_n - E_m,$$

where V is the total potential energy operator of the system, Eq. (1) becomes

$$W_{nm} = (1/2\pi)\,\langle n\,|\,\nabla\,|\,m\rangle\cdot\langle m\,|\,\nabla V\,|\,n\rangle$$
$$= -(1/2\pi)\,\langle n\,|\,\nabla V\,|\,m\rangle\cdot\langle m\,|\,\nabla\,|\,n\rangle, \quad (3)$$

since ∇ is anti-Hermitian. We now sum (3) over all states and, assuming the eigenstates form a complete set,[3] we have

$$\sum_m W_{nm} = (1/2\pi)\,\langle n\,|\,\nabla\cdot\nabla V\,|\,n\rangle$$
$$= -(1/2\pi)\,\langle n\,|\,\nabla V\cdot\nabla\,|\,n\rangle, \quad (4)$$

or, finally, in terms of the commutator of ∇ and ∇V, (4) becomes

$$\sum_m W_{nm} = (1/4\pi)\,\langle n\,|\,[\nabla, \nabla V]\,|\,n\rangle$$
$$= (1/4\pi)\,\langle n\,|\,(\nabla\cdot\nabla V)\,|\,n\rangle, \quad (5)$$

where $(\nabla\cdot\nabla V)$ is now simply a multiplicative operator. Equation (5) is the most general statement of the sum rule.

Before considering particular potentials a word is necessary concerning the propriety of forming the infinite sum in Eqs. (4) and (5). We recollect that W_{nm} is only defined in the case where $E_m > E_n$, i.e., only downward spontaneous transitions are meaningful. But the derivation of the sum rule requires a

* Research performed under the auspices of the U. S. Atomic Energy Commission.

† Present address: National Bureau of Standards, Washington 25, D. C.

[1] See, for example, H. A. Bethe and E. E. Salpeter, *Quantum Mechanics of One and Two-Electron Systems* (Academic Press, Inc., New York, 1957), p. 256.

[2] Footnote 1, p. 248.

[3] The question of the validity of the dipole approximation arises most seriously at this point. It is well known that for states high in the continuum $\exp(i\mathbf{k}\cdot\mathbf{r}) \neq 1$ and thus higher terms appear. In any event the sum rule gives the contribution due to dipole radiation.

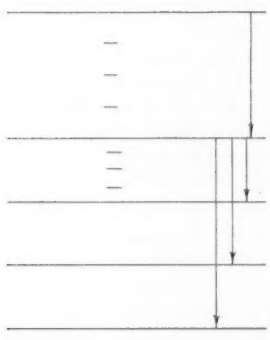

FIG. 1. Diagrammatic representation of the method of summing over all spontaneous emission transition probabilities. The $n \rightarrow m$ transition appears with a minus sign in the sum.

complete set of eigenstates. Thus, when summing over terms for which $E_m < E_n$ the sign must be reversed. A diagramatic representation of the actual sum carried out in (4) and (5) is given in Fig. 1. It is seen from this diagram that we have summed over all transitions downward to n and then subtracted all transitions downward from n. That is,

$$\sum_m W_{nm} \equiv \sum_{m>n} W_{nm} - \sum_{m<n} W_{mn}.$$

III. COULOMB POTENTIAL

In atomic and molecular systems Eq. (5) takes a particularly interesting form. Working in the fixed nucleus approximation for an N electron system, we have

$$\nabla \cdot \nabla \equiv \sum_k^N \nabla_k \cdot \sum_j^N \nabla_j, \tag{6}$$

and

$$V = -\sum_{k,\alpha} Z_\alpha / |\mathbf{r}_k - \mathbf{r}_\alpha| + \tfrac{1}{2}\sum_{k,j} 1/|\mathbf{r}_k - \mathbf{r}_j| + \tfrac{1}{2}\sum_{\alpha,\beta} Z_\alpha Z_\beta / |\mathbf{r}_\alpha - \mathbf{r}_\beta|,$$

where Greek indices refer to nuclei. It is clear, first of all, that the nuclear repulsions will vanish when operated on by the electronic gradients. Secondly, since $\nabla_k(1/|\mathbf{r}_k - \mathbf{r}_j|) = -\nabla_j(1/|\mathbf{r}_k - \mathbf{r}_j|)$, the sum $\sum_k \nabla_k (\sum_{i,j} 1/|\mathbf{r}_i - \mathbf{r}_j|)$ vanishes identically. Finally, since $\nabla_i \cdot \nabla_j (1/|\mathbf{r}_k - \mathbf{r}_\alpha|) = 0$ unless $i = j = k$, we have

$$\sum_m W_{nm} = (1/4\pi) \langle n | \sum_k^N \{\nabla_k^2 (-\sum_\alpha Z_\alpha / |\mathbf{r}_k - \mathbf{r}_\alpha|)\} | n \rangle. \tag{7}$$

Equation (7) is just the average value of a sum of one-electron operators and can therefore immediately be put in terms of the three-dimensional electron density[4] so that

$$\sum_m W_{nm} = (1/4\pi) \left\{ -\sum_\alpha Z_\alpha \int \rho_n(\mathbf{r}) \nabla^2(\mathbf{r}) |\mathbf{r} - \mathbf{r}_\alpha|^{-1} d\mathbf{r} \right\}, \tag{8}$$

where $\int d\mathbf{r}$ implies a volume integration. Now, $|\mathbf{r} - \mathbf{r}_\alpha|^{-1}$ is a solution to Poisson's equation so that $\nabla^2(\mathbf{r}) |\mathbf{r} - \mathbf{r}_\alpha|^{-1} = -4\pi\delta(\mathbf{r}_\alpha)$, whereby Eq. (8) becomes

$$\sum_m W_{nm} = \sum_\alpha Z_\alpha \rho_n(\mathbf{r}_\alpha). \tag{9}$$

In Eq. (9) we recall that $\mathbf{r}_\alpha$ is the position vector of the αth nucleus. Thus, the sum over all transition probabilities is equal to a linear sum of all the densities at the various nuclei with the nuclear charges as coefficients. Obviously, in the atomic case the right-hand side of (9) is just the nuclear charge times the electron density evaluated at the nucleus.

It is an immediate result of Eq. (9) that the ground electronic state of any atom cannot have a nonvanishing electron density at the nucleus. For, if the latter were true, every W_{nm}, all of which must be positive for the ground state, would be zero which is clearly impossible. This result is in agreement with our expectations since, crudely speaking, every atom in its ground state must have $1s$ electrons and thus a nonvanishing density at the nucleus.

Equation (9) is somewhat analogous to the more general theorem which states that for any system the lowest energy eigenstate must be nodeless and nondegenerate. This theorem however is not generally applicable to many fermion systems because of the antisymmetry principle.[5]

Another application of the nonvanishing property of $\rho_n(0)$ is to molecular potential energy curves. Bingel[6] has recently given a power series expansion for the electronic energy of any molecule in terms of the nuclear position vectors $\mathbf{r}_\alpha$. He has shown that the coefficients of the linear terms is zero and the coefficient of the quadratic terms involves $\rho_n(0)$ of the united atom. Our results show that for the lowest energy state the coefficients of the quadratic terms in Bingel's expansion can never vanish.

Finally we note that for an atom in an excited state having no S component in the density (e.g., a hydrogen atom in a P state) the sum of all the transition probabilities to lower states must equal the sum of all transition probabilities from higher states. That is, the total probability that such a state will be populated from above is equal to the total probability that the state will be depopulated (i.e., if all states were equally populated).

IV. HARMONIC OSCILLATOR

We now consider the general quadratic potential most commonly used in molecular vibrations. Suppose that the potential is harmonic in all the coordinates. We assume that the principle axis transformation has been performed so that $\nabla^2 V$ is diagonal. The sum rule is

[4] P. O. Löwdin, Advances in Chem. Phys. **2**, 207 (1959).

[5] L. D. Landau and E. M. Lifshitz, *Quantum Mechanics Non-Relativistic Theory* (Pergamon Press, New York, 1958), p. 56.

[6] W. Bingel, J. Chem. Phys. **30**, 1250 (1959).

then

$$\sum_m W_{nm} = (1/4\pi) \sum_L^{3N-6} K_L, \tag{10}$$

where K_L is the force constant of the Lth vibration and unit masses have been assumed.

In this case the sum rule is easy to verify independently. For example, in the simplest case of a one-dimensional oscillator there is only one nonvanishing matrix element[7] to the ground state so that

$$\sum_m W_{nm} = W_{10} = \pi\nu^2 = K/4\pi m, \tag{11}$$

which agrees with (10) for a unit mass.

V. LIFETIMES AND NATURAL LINEBREADTHS

If we attribute to each energy level E_n a natural level breadth γ_n, which is the inverse of the lifetime of the state, we may write[8]

$$\gamma_n = \sum_{m<n} W_{mn}. \tag{12}$$

Thus the breadth γ_{n0} of any line resulting from a transition $n \rightarrow 0$ where 0 represents the ground state is given by (12) since the ground state is infinitely sharp. Now the sum rule can be used to derive an alternate expression for γ_{n0}. That is, in an atomic system

$$\gamma_{n0} = \sum_{m>n} W_{nm} - Z\rho_n(0). \tag{13}$$

From Eqs. (12) and (13) it is apparent that when $\rho_n(0) = 0$ the linebreadth is given by either of the expressions

$$\gamma_{n0} = \sum_{m<n} W_{mn} = \sum_{m>n} W_{nm}. \tag{14}$$

This is the case for a hydrogen atom in a P state, for example. In general (14) is true for any atomic state having no S component in the electron density.

VI. AVERAGE EXCITATION ENERGY AND THE OSCILLATOR STRENGTH SUM RULE

It sometimes proves useful to estimate the average excitation energy $\langle E_n - E_m \rangle_{Av}$ with the use of sum rules. To do this we combine Eqs. (1), (2), and (5) and write

$$\sum_m (E_n - E_m) \mid \langle n \mid \mathbf{p} \mid m \rangle \mid^2 = \tfrac{1}{2} \langle n \mid (\nabla^2 V) \mid n \rangle. \tag{15}$$

Upon extracting an average value of the excited state energy E_m from the sum in Eq. (15) the result is, for an atomic system,

$$\bar{E}_m = +[2\pi Z\rho_n(0)/\langle n \mid p^2 \mid n \rangle] + E_n, \tag{16}$$

which, by virtue of the virial theorem, becomes

$$\bar{E}_m = -[\pi Z\rho_n(0)/E_n] + E_n. \tag{17}$$

Thus for the ground state of the hydrogen atom where $\rho_n(0) = Z^3/\pi$ and $E_n = -Z^2/2$, we have $\bar{E}_m = \frac{3}{2}Z^2$. On the other hand, the oscillator strength sum rule for the same state leads to $\bar{E}_m = 0$.

The previous results indicate that the main contribution to W_{nm} comes from the continuum. This is in agreement with other estimates[9] of the importance of the continuous spectrum. However, the fact that there are two general sum rules may lead to more accurate estimates of the continuum which would be useful in perturbation theory.

Since the Thomas-Reich-Kuhn rule for the oscillator strength f_{mn} may be written

$$\sum_m f_{mn} = 2\sum (E_m - E_n) \mid \langle n \mid x \mid m \rangle \mid^2 = N, \tag{18}$$

where N is the total number of particles in the system, the preceding results for hydrogen imply that momentum matrix elements weight the continuous spectrum more heavily than coordinate matrix elements.

A final comparison of the two sum rules is also interesting. We may write

$$W_{nm} = [(E_m - E_n)^2/4\pi] f_{mn} \tag{19}$$

so that, in terms of an average of $\langle (E_m - E_n)^2 \rangle_{Av}$,

$$Z\rho_n(0) = [\langle (E_n - E_m)^2 \rangle_{Av}/4\pi] N. \tag{20}$$

One rather trivial result of Eq. (20) is that $\rho_n(0)$ is proportional to the total number of electrons. The average excitation energy of course just serves to weight the density according to the degree of excitation of the electronic state n.

VII. ACKNOWLEDGMENTS

The author is indebted to Dr. Max Wolfsberg of this department for many helpful suggestions, and to the reviewer for clarifying several points.

[7] E. B. Wilson, J. C. Decius, and P. C. Cross, *Molecular Vibrations* (McGraw-Hill Book Company, Inc., New York, 1955), p. 289.

[8] W. Heitler, *Quantum Theory of Radiation* (Oxford University Press, New York, 1944), p. 110.

[9] P. O. Löwdin, M. Wolfsberg, and others (unpublished results).

Emission Spectra of Trivalent Thulium

L. G. VAN UITERT AND R. R. SODEN

Bell Telephone Laboratories, Inc., Murray Hill, New Jersey

(Received June 10, 1960)

Trivalent thulium can be caused to fluoresce selectively from different levels by choice of the wavelength of exciting radiation. This has made it possible to correct the assignments of emission transitions occurring in the visible range. As a consequence, the detailed data of Gobrecht have been found to be in much closer agreement to the theoretical predictions than formerly realized.

INTRODUCTION

THE absorption spectrum of trivalent thulium has been investigated in the optical region by Prandtl and Scheiner[1] (1934) and by Meehan and Nutting[2] (1939). Considering the information gained by these efforts, Bethe and Spedding[3] were able to calculate the approximate positions of absorption lines expected to occur in the infrared and ultraviolet regions. Subsequent measurements by Gobrecht[4,5] employing $Tm_2(SO_4)_3 \cdot 8H_2O$ and borax beads fixed the positions of these absorption lines, with the exception of the $^3H_4$ level calculated to be at 5565 cm^{-1} and the $^1S_0$ level. Gobrecht also reported detailed emission spectra for trivalent thulium[4] in K_2SO_4 and CaO. On failing to find an absorption level in the neighborhood of 5565 cm^{-1}, he correlated his absorption and emission data in a manner differing extensively from that to be expected from the earlier calculations.

Measurements on $CaWO_4$ and $SrWO_4$ containing thulium, described herein, show that there are fluorescent transitions to the above ^3H level. Indeed, infrared absorption measurements made on these materials by R. Pappalardo[6] of these Laboratories have confirmed its presence at about 5815 cm^{-1}. Gruber and Conway[7] have recently presented an up-to-date theoretical treatment of the electronic energy levels of trivalent thulium. In the course of their work they also ascertained the presence of an absorption level at about 5900 cm^{-1} for $TmCl_3$ in D_2O solution. This and other experimental evidence described below have made it possible to correct the assignments of the originating and terminal levels for many of the previously reported emission lines.

MATERIALS

Crystals having the scheelite structure and the compositions $Sr_{1-2x}Na_xTm_xWO_4$, where $x = 10^{-4}$, 3×10^{-4}, 10^{-3}, 3×10^{-3}, 10^{-2}, 0.03, 0.1, 0.3, and 0.5, and $Ca_{0.98}Na_{0.01}Tm_{0.01}WO_4$ were prepared employing a $Na_2W_2O_7$ flux, as previously described.[8]

MEASUREMENTS

Measurements were made employing a Gaertner high-dispersion spectrometer adapted with an AMINCO photomultiplier microphotometer using a 1P22 tube. Ten micron slit widths were employed at the entrance and exit to the spectrometer. The system was calibrated against a tungsten lamp to give relative values of brightness of the emitting surface in units of power per unit wavelength range.

Emission was excited by illuminating a sample 1 in. long by $\frac{1}{2}$ in. wide by $\frac{1}{4}$ in. deep with, alternately, four different light sources: first, a 3660 A rich Hanovia CH4 spotlight through a Corning 5860 filter; second, a 2537 A mineralight through a Corning 9836 filter; third, energy from a 2537 A mineralight passed through a Geartner quartz prism monochromator set at 2537 A (with 100-μ entrance and exit slits) and fourth, a Sylvania Try-Flector tungsten filament projection lamp through a 1-in. layer of saturated copper sulfate solution and a Wratten H filter which passes a band in the blue.

The intensity measurements shown in Figs. 1 and 2 are relative to 100 for the 5450 A peak of a comparable sample of $Na_{0.5}Tb_{0.5}WO_4$ under the same excitation in keeping with previous intensity measurements on other series of scheelite compounds.[9]

DISCUSSION

The emission of $Ca_{0.98}Na_{0.01}Tm_{0.01}WO_4$, excited by the CH4 spotlight, is shown in curve A of Fig. 1. The intensities of the line groups observed are very sensitive to temperature under this excitation. Brightness decreases by a factor of 20 upon going from room temperature to 77°K. This is due to (1) the narrowness of the band of energy (about 27 300 cm^{-1}) supplied by the CH4 lamp, (2) the narrowness of the absorption band (about 27 780 cm^{-1}) responsible for the observed emis-

[1] W. Prandtl and K. Scheiner, Z. anorg. u. allgem. Chem. **220,** 107 (1934); **232,** 267 (1937).
[2] P. J. Meehan and G. C. Nutting, J. Chem. Phys. **1,** 1002 (1939).
[3] H. A. Bethe and F. H. Spedding, Phys. Rev. **52,** 454 (1937).
[4] H. Gobrecht, Ann. Physik [5] **31,** 600 (1938).
[5] H. Gobrecht, Ann. Physik [6] **7,** 88 (1950).
[6] R. Pappalardo (private communication).
[7] J. B. Gruber and J. G. Conway, J. Chem. Phys. **32,** 1178 (1960).
[8] L. G. Van Uitert and R. R. Soden, J. Appl. Phys. **31,** 328 (1960).
[9] L. G. Van Uitert and R. R. Soden, J. Chem. Phys. **32,** 1161 (1960), and others (to be published).

sion, and (3) their energy relationship. The absorption band is wide enough to receive energy from the CH4 lamp at room temperature. At 77°K, it is narrower, receives less energy, and consequently the sample is less bright. These temperature effects are not observed when broad-band long-wave ultraviolet excitation is employed.

These experiments relate the emission lines of curve A of Fig. 1 to the absorption lines at about 27 780 cm^{-1}, either by direct emission from this level or through energy transfer from this to a lower level and emission

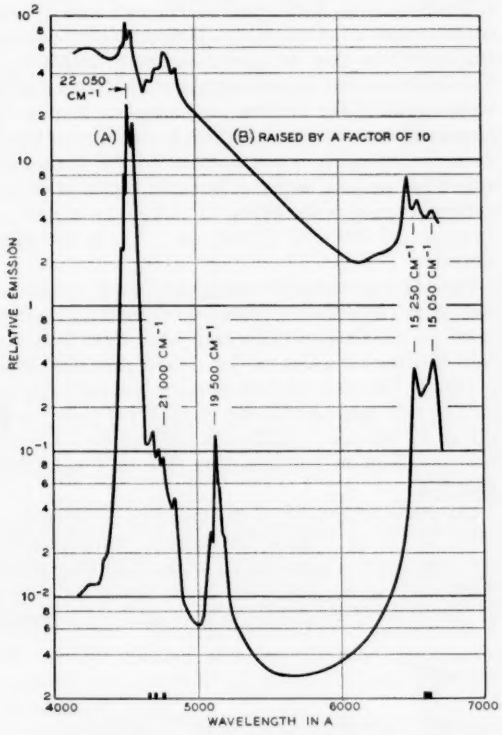

FIG. 1. Emission vs wavelength for $Ca_{0.98}Na_{0.01}Tm_{0.01}WO_4$ excited by (A) the CH4 spotlight and (B) the 2537 A mineralight.

from there. The experiments described below show that the latter case applies to the weak lines about 21 000 cm^{-1}. The others are due to emission from 27 780 cm^{-1} directly. The lines about 22 050 cm^{-1} in particular are due to transitions to the absorption level at about 5815 cm^{-1}.

The emission of the calcium tungstate sample under excitation from a 2537 A mineralight is shown in curve B of Fig. 1. Here the broad-band host lattice emission of $CaWO_4$ obscures much of the detail of the thulium spectrum. However, it appears that the lines about 21 000 cm^{-1} have increased markedly in intensity as compared to those about 22 050 cm^{-1}, and a new peak at 15 400 cm^{-1} is observed.

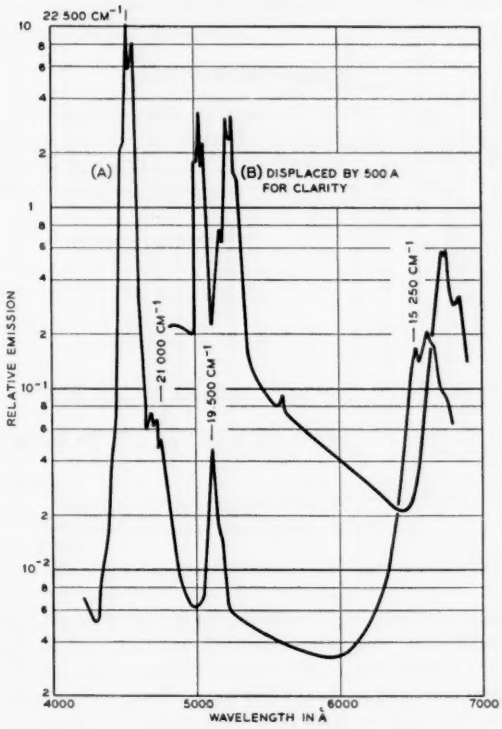

FIG. 2. Emission vs wavelength for $Sr_{0.98}Na_{0.01}Tm_{0.01}WO_4$ excited by (A) the CH4 spotlight and (B) the 2537 A mineralight.

To clarify these observations, data comparable to those shown in Fig. 1 were obtained on

$$Sr_{0.98}Na_{0.01}Tm_{0.01}WO_4,$$

which has a much smaller background emission at room temperature than the calcium composition. Figure 2

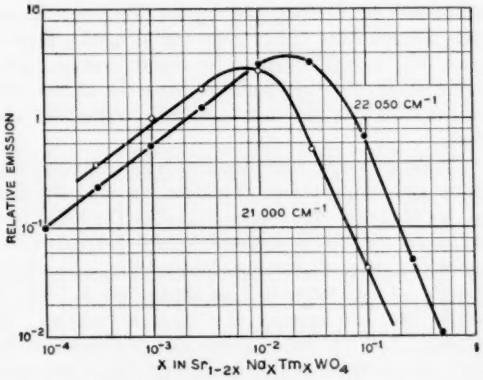

FIG. 3. The dependencies of emission upon thulium content for the peaks at 22 050 cm^{-1} and 21 000 cm^{-1} when the samples are excited by the 2537 A mineralight.

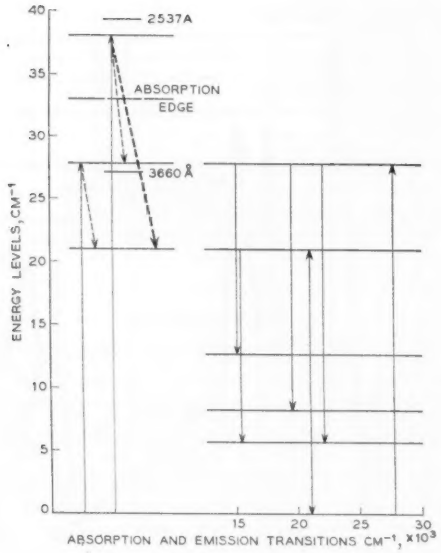

FIG. 4. Absorption and emission transitions found in this work.

confirms that the intensity of the group of lines about 21 000 cm^{-1} is greatly enhanced when excited by the 2537 A mineralight. This source, however, emits in the 3660 A as well as the 2537 A band. Hence, to ascertain the effect of the higher frequency excitation, the output of the mineralight was passed through a monochromator set at 2537 A. Since the exciting energy was greatly attenuated by this procedure, it was only possible to compare the intensities of the 22 050 and 21 000 cm^{-1} peaks. The 21 000 cm^{-1} emission is at least a factor of four brighter under these conditions. This shows that energy gained by thulium through its ^3P absorption levels finds its way preferentially to the 21 000 cm^{-1} level. This is in the absence of the concentration quenching effects discussed below.

The origin of the emission peak at 15 400 cm^{-1} was established by exciting the calcium tungstate sample with filtered blue light from the tungsten filament lamp. The energy accepted by the absorption lines at about 21 000 cm^{-1} produces emission at 15 400 cm^{-1}. This peak is also due to a transition to the 5815 cm^{-1} level.

The dependencies upon thulium concentration shown by the emission peaks at 22 050 cm^{-1} and 21 000 cm^{-1}, for members of the series $Sr_{1-2x}Na_xTm_xWO_4$ when excited by the 2537 A mineralight, are shown in Fig. 3. As for the series studied previously,[9] the quenching of emission at high rare-earth concentrations is probably due to the development of exchange coupling. The emission at 21 000 cm^{-1} (which also originates at that level) shows concentration quenching effects at a lower thulium content than the emission at 22 050 cm^{-1} (which originates at 27 780 cm^{-1}). This behavior appears to be the reverse of that noted previously[9] for terbium and europium where quenching occurs first for the higher emitting states as the rare earth concentration increases. However, as discussed previously, the 21 000 cm^{-1} level of thulium derives its energy from levels that are higher (35 000–38 000 cm^{-1}) than that providing the 22 050 cm^{-1} emission (27 780 cm^{-1}). Hence, the effect noted is consistent with the previous behavior.

Figure 4 graphically presents the electronic transitions of trivalent thulium found to occur in the course of these experiments. Emission lines which Gobrecht found at 16 650 cm^{-1} in K_2SO_4 and 25 000 cm^{-1} in CaO were not observed in the tungstates. Gobrecht attributes the origin of these lines to a level at about 38 000 cm^{-1}. This indicates that the level at about 27 780 cm^{-1} is the highest level of the thulium producing emission in the tungstate structure under 2537 A excitation. Under these conditions, it is not unexpected for energy absorbed by the host lattice (above the region of its absorption edge at ~33 000 cm^{-1}) to find its way to the levels at 27 780 and 21 000 cm^{-1} by radiationless processes.

Figure 5 represents the energy levels and associated absorption and emission transitions of trivalent thulium based on the data of Gobrecht,[4,5] the recent calculations of Gruber and Conway,[7] and the transitions shown in Fig. 4. The data of Gobrecht are satisfactorily related by this diagram with the exception of a very weak line at 17 760 cm^{-1}, which was omitted by Gobrecht from his diagram and could be due to a samarium impurity.

The center of gravity of the group of emission lines about 33 200 cm^{-1} lies a few hundred wave numbers above the position expected for a transition from about 38 000 cm^{-1} to the 5565 cm^{-1} level. The exact reason for this displacement has not been ascertained; however,

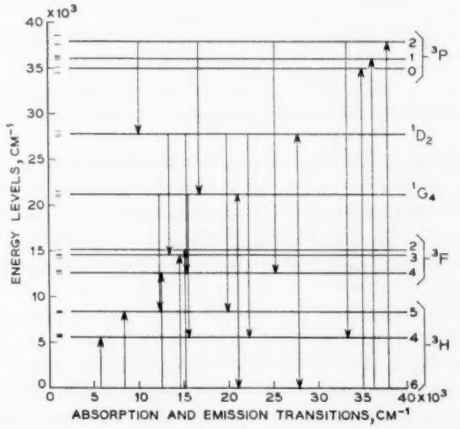

FIG. 5. Absorption and emission transitions of trivalent thulium based on Fig. 4 and the work of Gobrecht.

displacements of this type are not limited to thulium. If one compares the spacings between the members of the emission multiplets for transitions from the two emission levels of terbium in calcium tungstate,[9,10] it is observed that the spacings for the set originating at the higher level are larger, with the greater deviations occurring for the lines terminating in the ground state. In the case of terbium, the difference is about 300 cm^{-1} between the full multiplets.

[10] M. Ch. de Rohden, Ann. Chem. **3**, 338 (1915).

ACKNOWLEDGMENTS

The authors wish to thank C. G. B. Garrett, W. Kaiser, and D. L. Wood for their helpful discussions and, in particular, R. Pappalardo for permission to cite his infrared absorption measurements.

THE JOURNAL OF CHEMICAL PHYSICS VOLUME 34, NUMBER 1 JANUARY, 1961

Composition of the Electronic States of Nd(IV) and Er(IV)

B. G. WYBOURNE*

Physics Department, University of Canterbury, Christchurch, New Zealand

(Received July 5, 1960)

The eigenvectors of the electronic states of the trivalent neodymium and erbium ions are tabulated for use in calculating the crystal field and Zeeman splittings of the ground and excited states.

IN a recent paper[1] on the analysis of the solid-state spectra of neodymium and erbium, the energy matrices for the f^3 and f^{11} configurations, corresponding to the trivalent neodymium and erbium ions, respectively, were diagonalized and theoretical energy level schemes constructed from the eigenvalues of those matrices which were then compared with the experimentally determined energy level schemes. This allowed the assignment of LSJ labels to most of the experimentally known energy levels. The appropriate Racah parameters E^1, E^2, and E^3, together with the spin-orbit coupling constant ζ were derived by a least-squares method and are tabulated in Table I.

Several requests have been made that the eigenvectors of these matrices should be also published. These appear in Tables II and III. The calculated energies of the levels for a given J value are given in the first row of each block, while the normalized eigenvectors pertaining to these energy levels are listed directly below. The eigenvectors are given the labels of the pure LS states. The left superscript of the eigenvector labels refers to the multiplicity, the left subscript to the seniority number v, and the right subscript to the Racah U quantum number. In general the energy levels labeled in the earlier paper[1] were given the LS values of the state possessing the largest eigenvector. These eigenvectors are printed in heavy type. Naturally, the LS labels used can only be regarded as convenient labels having little meaning in themselves as in most cases the effects of intermediate coupling are sufficient, to strongly mix states of different L and S. Due to the small effect of crystal field mixing J remains as a fairly "good" quantum number. An inspection of the eigenvectors for the $J=\frac{9}{2}$ matrix of Er(IV) indicates that the assignments given in the previous paper to the line groups B and D should be reversed.

TABLE I. The parameters in units of cm^{-1} for which the energy matrices were diagonalized.

	E^1	E^2	E^3	ζ
Nd^{3+}	4988	24.51	493.0	906
Er^{3+}	6683	31.19	642.7	2471

These eigenvectors have been found useful in making intermediate coupling calculations of the splittings of the energy levels of the neodymium and erbium ions.

ACKNOWLEDGMENTS

The author wishes to express his thanks to the staff of the Adolph Basser Computing Laboratory at the University of Sydney for performing the calculations on the Silliac computer and to W. A. Runciman for several helpful discussions. Part of this work was done during the tenure of a New Zealand University Research Fund Fellowship.

* Present address: Physics Department, The Johns Hopkins University, Baltimore, Maryland.

[1] B. G. Wybourne, J. Chem. Phys. **32**, 639 (1960).

TABLE II. The eigenvectors and energies of the states of Nd^{3+}.
(All energies, E, are expressed in terms of the spin-orbit coupling constant ζ.)

	Calc. E	25.549	32.313				
$J=1/2$	$^2_3P_{11}$	**0.9760**	0.2426				
	$^4_3D_{20}$	0.2178	**0.9701**				
	Calc. E	14.852	29.085	31.616	23.454	37.279	12.721
	$^4_3S_{00}$	**+0.9697**	−0.1247	+0.0201	+0.2014	−0.0097	−0.0563
	$^2_3P_{11}$	+0.2265	**+0.6955**	−0.1327	−0.6602	+0.0867	−0.0622
$J=3/2$	$^4_3D_{20}$	+0.0151	+0.0981	**+0.8974**	−0.1247	−0.4113	−0.0121
	$^2_3D_{20}$	−0.0409	+0.6727	+0.1013	**+0.6750**	+0.1687	+0.2268
	$^2_3D_{21}$	+0.0020	−0.1490	+0.4080	−0.1159	**+0.8914**	−0.0577
	$^4_3F_{10}$	+0.0808	−0.1278	+0.0044	−0.1972	+0.0135	**+0.9685**
	Calc. E	31.831	26.360	38.602	13.916	43.785	77.133	19.162
	$^4_3D_{20}$	**+0.8912**	−0.0013	−0.4500	−0.0026	−0.0530	+0.0179	−0.0085
	$^2_3D_{20}$	−0.0337	**+0.9855**	−0.0700	+0.1502	−0.0004	+0.0108	−0.0025
	$^2_3D_{21}$	+0.4290	+0.0741	**+0.8013**	−0.0156	+0.4096	−0.0064	−0.0160
$J=5/2$	$^4_3F_{10}$	+0.0089	−0.1496	+0.0067	**+0.9874**	+0.0434	+0.0002	+0.0254
	$^2_3F_{21}$	−0.1012	−0.0133	−0.3097	−0.0320	**+0.7065**	−0.6220	+0.0806
	$^2_1F_{10}$	−0.0964	−0.0233	−0.2276	−0.0282	+0.5646	**+0.7826**	+0.0794
	$^4_3G_{20}$	+0.0302	+0.0104	+0.0520	−0.0203	−0.0975	−0.0120	**+0.9931**
	Calc. E	34.225	15.025	45.385	75.828	21.228	19.157	54.163
	$^4_3D_{20}$	**+0.9937**	+0.0032	+0.1042	+0.0413	+0.0076	+0.0019	−0.0037
	$^4_3F_{10}$	−0.0070	**+0.9615**	+0.0416	+0.0028	+0.1340	+0.2361	+0.0090
	$^2_3F_{21}$	−0.0620	−0.0393	**+0.8200**	−0.5556	+0.0542	−0.0143	+0.1013
$J=7/2$	$^2_1F_{10}$	−0.0918	−0.0300	+0.5521	**+0.8258**	+0.0487	−0.0141	−0.0357
	$^4_3G_{20}$	+0.0145	+0.0355	−0.0658	−0.0116	**+0.8045**	−0.5885	−0.0225
	$^2_3G_{20}$	+0.0107	−0.2094	−0.0717	+0.0524	+0.4500	**+0.5856**	+0.6346
	$^2_3G_{21}$	+0.0004	+0.1673	−0.0253	+0.0685	−0.3562	−0.5046	**+0.7650**
	Calc. E	16.451	21.768	23.463	53.155	36.129	13.922	0
	$^4_3F_{10}$	**+0.8735**	−0.1975	+0.2816	+0.0156	+0.0044	−0.3441	+0.0032
	$^4_3G_{20}$	−0.0314	**+0.8420**	+0.5143	−0.0226	+0.0682	−0.1422	+0.0079
	$^2_3G_{20}$	−0.1422	−0.3005	**+0.6062**	+0.6391	−0.0121	+0.3362	−0.0175
	$^2_3G_{21}$	+0.0972	+0.2827	−0.4876	**+0.7634**	−0.1036	−0.2812	+0.0156
$J=9/2$	$^2_3H_{11}$	−0.1488	−0.1268	−0.0028	+0.0821	**+0.9312**	−0.2909	+0.0580
	$^2_3H_{21}$	+0.4227	+0.2539	−0.2243	+0.0344	+0.3426	**+0.7483**	−0.1672
	$^4_3I_{20}$	+0.0739	+0.0347	−0.0245	+0.0005	+0.0042	+0.1570	**+0.9839**
		Calc. E	24.093	37.663	17.645	2.128	31.675	
		$^4_3G_{20}$	**+0.9630**	+0.1166	−0.2323	+0.0074	−0.0712	
		$^2_3H_{11}$	−0.2154	**+0.8348**	−0.3661	+0.0369	−0.3482	
	$J=11/2$	$^2_3H_{21}$	+0.1609	+0.3933	**+0.8937**	−0.0964	−0.1065	
		$^4_3I_{20}$	+0.0166	+0.0119	+0.1011	**+0.9945**	+0.0175	
		$^2_3I_{20}$	+0.0112	+0.3669	−0.0546	−0.0153	**+0.9285**	
			Calc. E	4.389	33.193	20.949		
			$^4_3I_{20}$	**+0.9975**	+0.0169	−0.0681		
		$J=13/2$	$^2_3I_{20}$	−0.0238	**+0.9946**	−0.1024		
			$^2_3K_{21}$	+0.0660	+0.1028	**+0.9925**		
			Calc. E	6.732	23.211	32.468		
			$^4_3I_{20}$	**+0.9927**	−0.1193	−0.0172		
		$J=15/2$	$^2_3K_{21}$	+0.1201	**+0.9683**	+0.2189		
			$^2_3L_{21}$	−0.0095	−0.2194	**+0.9756**		
				Calc. E	34.141			
			$J=17/2$	$^2_3L_{21}$	**1.0000**			

TABLE III. The eigenvectors and energies of the states of Er^{3+}.
(All energies E are expressed in terms of the spin-orbit coupling constant ζ.)

	Calc. E	13.607	19.380				
$J=1/2$	$^2{}_3P_{11}$	**+0.9756**	+0.2916				
	$^4{}_3D_{20}$	−0.2195	**+0.9565**				
	Calc. E	7.497	17.655	17.334	12.975	22.582	9.187
	$^4{}_3S_{00}$	**+0.8134**	+0.1725	−0.0522	+0.3529	+0.0276	−0.4250
	$^2{}_3P_{11}$	−0.4411	**+0.6220**	−0.1812	+0.5980	+0.1551	−0.0629
	$^4{}_3D_{20}$	+0.0444	+0.3183	**+0.7963**	−0.1816	+0.4793	−0.0032
$J=3/2$	$^2{}_3D_{20}$	−0.2914	−0.4889	+0.4572	**+0.4468**	−0.2418	−0.4571
	$^2{}_3D_{21}$	−0.0214	−0.4734	−0.2610	+0.1855	**+0.8203**	+0.0063
	$^4{}_3F_{10}$	+0.2376	−0.1374	+0.2307	+0.5009	−0.1190	**+0.7788**
	Calc. E	15.844	14.128	20.073	9.033	25.791	37.813	13.749
	$^4{}_3D_{20}$	**+0.6483**	+0.3836	+0.6329	−0.0519	−0.1636	−0.0448	+0.0238
	$^2{}_3D_{20}$	−0.5568	**+0.7257**	+0.0839	−0.3711	−0.0713	−0.0271	−0.1129
	$^2{}_3D_{21}$	−0.4753	−0.4179	**+0.6619**	+0.1469	−0.3591	−0.0200	−0.1017
$J=5/2$	$^4{}_3F_{10}$	−0.1112	+0.3873	−0.0633	**+0.9103**	−0.0580	−0.0102	+0.0377
	$^2{}_3F_{21}$	−0.0856	−0.0297	+0.2930	+0.0764	**+0.8007**	−0.4702	−0.1948
	$^2{}_1F_{10}$	−0.0336	+0.0201	+0.1969	+0.0429	+0.3981	**+0.8794**	−0.1616
	$^4{}_3G_{20}$	−0.1514	+0.0139	+0.1603	−0.0401	+0.1905	+0.0491	**+0.9544**
	Calc. E	16.058	8.384	22.383	39.392	11.476	14.025	26.376
	$^4{}_3D_{20}$	**+0.9736**	+0.0123	−0.2026	−0.0699	−0.0627	+0.0442	−0.0057
	$^4{}_3F_{10}$	−0.0391	**+0.9591**	−0.1033	−0.0006	−0.2013	−0.1653	−0.0054
	$^2{}_3F_{21}$	+0.0976	+0.0568	**+0.7448**	−0.6107	−0.1543	+0.0376	−0.1856
$J=7/2$	$^2{}_1F_{10}$	+0.1650	+0.0477	+0.5847	**+0.7765**	−0.1495	+0.0509	+0.0276
	$^4{}_3G_{20}$	+0.1118	+0.0307	+0.1742	+0.0134	**+0.6401**	−0.7380	+0.0417
	$^2{}_3G_{20}$	+0.3358	+0.2190	+0.1425	−0.0854	+0.5143	**+0.5273**	+0.6171
	$^2{}_3G_{21}$	−0.0085	−0.1598	+0.0329	−0.1088	−0.4849	−0.3796	**+0.7630**
	Calc. E	6.252	11.307	10.074	28.130	19.150	15.102	5.057
	$^4{}_3F_{10}$	**+0.7367**	−0.0127	−0.4971	−0.0265	−0.0003	−0.1900	+0.4162
	$^4{}_3G_{20}$	+0.0918	**+0.8858**	+0.2618	+0.0571	−0.0943	−0.3548	+0.0189
	$^2{}_3G_{20}$	+0.2667	+0.0007	**+0.4366**	+0.6287	+0.0845	+0.4881	+0.3124
$J=9/2$	$^2{}_3G_{21}$	−0.1965	−0.0456	−0.3889	**+0.7544**	+0.1674	−0.3877	−0.2466
	$^2{}_3H_{11}$	−0.0207	−0.0976	+0.2638	−0.1582	**+0.8740**	−0.3013	+0.2018
	$^2{}_3H_{21}$	+0.1308	+0.3850	−0.3783	−0.0816	+0.4368	**+0.5642**	−0.4192
	$^4{}_3I_{20}$	+0.5671	−0.2354	+0.3604	+0.0040	−0.0350	−0.2009	**−0.6720**
	Calc. E	10.882	20.523	7.854	4.215	16.360	
	$^4{}_3G_{20}$	**+0.7735**	−0.1275	+0.5951	+0.1253	−0.1246	
	$^2{}_3H_{11}$	+0.3334	**+0.7394**	−0.1345	−0.1119	+0.5582	
$J=11/2$	$^2{}_3H_{21}$	−0.5121	+0.3161	**+0.6754**	+0.4055	+0.1312	
	$^4{}_3I_{20}$	+0.1669	+0.1149	−0.4102	**+0.8959**	−0.0341	
	$^2{}_3I_{20}$	−0.0208	−0.5805	+0.0577	+0.0685	**+0.8090**	
	Calc. E	2.742	17.540	13.297			
	$^4{}_3I_{20}$	**+0.9951**	−0.0623	+0.0773			
$J=13/2$	$^2{}_3I_{20}$	+0.0332	**+0.9427**	+0.3319			
	$^2{}_3K_{21}$	−0.0935	−0.3277	**+0.9401**			
	Calc. E	0	11.092	19.131			
	$^4{}_3I_{20}$	**+0.9838**	+0.1773	−0.0268			
$J=15/2$	$^2{}_3K_{21}$	−0.1783	**+0.9512**	−0.2518			
	$^2{}_3L_{21}$	−0.0191	+0.2525	**+0.9674**			
	Calc. E	16.486					
$J=17/2$	$^2{}_3L_{21}$	**1.0000**					

Electron Spin Resonance in a Gamma-Irradiated Single Crystal of *L*-Cystine Dihydrochloride*

YUKIO KURITA† AND WALTER GORDY

Department of Physics, Duke University, Durham, North Carolina

(Received August 8, 1960)

The electron spin resonance of a gamma-irradiated single crystal of *L*-cystine dihydrochloride,

$$\mathrm{HOOC-CH(NH_2)-CH_2-S-S-CH_2-CH(NH_2)-COOH\cdot 2HCl},$$

has been measured at 9 kMc/sec and at 24 kMc/sec for various orientations of the crystal in the magnetic field. The resonance pattern was found to be a doublet, the spacing between the components of which is independent of the crystal orientation as well as of the strength of the static magnetic field. The spectroscopic splitting factor was found to be anisotropic with the principal values: $g_u=2.003$, $g_v=2.025$, and $g_w=2.053$. A model of the free radical,

$$\mathrm{HOOC-CH(NH_2)-CH_2-S\cdot},$$

in which the electron spin density is mainly concentrated in a nonbonding 3 p orbital of the sulfur atom, is proposed. The model accounts very well for the principal values of the g tensor as well as their directions relative to the atomic configuration. It also can give rise to the observed proton hyperfine structure.

INTRODUCTION

PREVIOUS studies of the electron spin resonance (ESR) of irradiated amino acids containing sulfur atoms have shown that the odd electron giving the resonance is essentially localized on sulfur atoms.[1,2] In an effort to learn the particular structure of the free radical, we have examined the ESR of gamma-irradiated single crystals of *L*-cystine dihydrochloride:

$$\mathrm{HOOC-CH(NH_2)-CH_2-S-S-CH_2-CH(NH_2)-COOH\cdot 2HCl}.$$

Well-developed single crystals can be grown. The crystal structure is known from x-ray diffraction work.[3] The interpretation of the electron spin resonance of cystine will help explain the nature of radiation damage to proteins since a number of different proteins give the cystinelike resonance when they are subjected to ionizing irradiations.[1,4]

EXPERIMENTAL PROCEDURE

The crystal of *L*-cystine dihydrochloride was grown in a saturated solution of *L*-cystine in 5 *N* hydrochloric acid. Crystals of the type reported by Becke[5] were obtained. They are hexagonal prisms, elongated along the *b* axis, and have the developed forms of {101}, {10$\bar{1}$}, and {100}. The crystal structure has been determined by Steinrauf, Peterson, and Jensen.[3] The crystal is monoclinic and the space group is $C2$ with $\beta=103.6°$, $a_0=18.61$ A, $b_0=5.25$ A, and $c_0=7.23$ A. The unit cell contains two molecules, both of which are equivalent in their orientations. Each molecule has a twofold rotation axis, which is perpendicular to the S—S bond and is parallel to the *b* axis. By comparison of the observed interfacial angles with those calculated from the unit cell dimensions, the crystallographic axes are identified.

A new rectangular coordinate system a', b, and c', was defined for convenience (Fig. 1). The b axis is the same as the crystal b axis. The a' axis was selected in ($\bar{1}$01) plane, perpendicular to the b axis, and the c' axis is perpendicular to the $a'b$ plane. The atomic coordinates ($a'bc'$) with regard to the $a'bc'$ axes were calculated by the following equations:

$$\begin{aligned} a' &= x\cos(a'a)+z\cos(a'c) \\ &= 0.923x+0.156z, \\ b &= y, \\ c' &= x\cos(c'a)+z\cos(c'c) \\ &= 0.384x-0.988z, \end{aligned}$$

where x, y, and z are the atomic coordinates with regard to the *abc* axes shown in Table II of footnote 3. The results are shown in Table I.

The single crystals were irradiated by a kilocurie cobalt-60 gamma-ray source at room temperature. The ESR of irradiated single crystals was measured at 9.03 kMc/sec and 24.3 kMc/sec for various orientations of the crystal in the magnetic field at room temperature. The ESR spectrometer and the method of measurement were the same as those employed in the previous work.[2,6]

* This research was supported by the Office of Ordnance Research, Department of the Army and by the Air Force Office of Scientific Research of the Air Research and Development Command.

† Fellow of the Visiting Research Scientist Program, National Academy of Sciences.

[1] W. Gordy, W. B. Ard, and H. Shields, Proc. Natl. Acad. Sci. U. S. **41**, 983 (1955).

[2] H. Shields and W. Gordy, J. Phys. Chem. **62**, 789 (1958).

[3] L. K. Steinrauf, J. Peterson, and L. H. Jensen, J. Am. Chem. Soc. **80**, 3835 (1958).

[4] W. Gordy and H. Shields, Radiation Research **9**, 611 (1958).

[5] F. Becke, Z. Krist. **19**, 336 (1891).

[6] I. Miyagawa and W. Gordy, J. Chem. Phys. **30**, 1590 (1959).

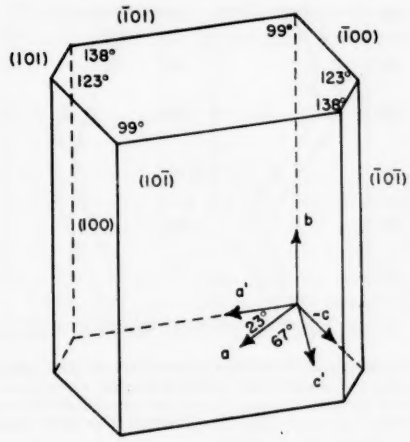

FIG. 1. The crystal form of *L*-cystine dihydrochloride and the coordinate axes employed.

EXPERIMENTAL RESULTS

Some typical spectra of a single crystal are shown in Figs. 2 and 3. The free radical formed is stable, and spectra obtained a year after irradiation are identical with those obtained initially. The resonance pattern was found to have two doublets in general, designated I and II.

Figure 4 compares the ESR of an irradiated powdered sample of *L*-cystine 2HCl with that of a similarly irradiated sample of *L* cystine in the powdered form. The similarity of these patterns indicates that the bound acid has no pronounced influence on the ESR and that the free radicals in the two are similar. Thus, conclusions drawn from the study of single crystals of *L*-cystine 2HCl probably also apply equally well to normal *L* cystine. In cystine dihydrochloride there

TABLE I. Atomic coordinates in the undamaged molecule with regard to the $a'bc'$ axes.

Atom	a'	b	c'
C_1	1.38	4.02	−1.26
C_2	2.86	3.57	−1.13
C_3	3.17	2.45	−2.05
N	3.19	3.20	0.27
O_1	3.79	1.44	−1.69
O_2	2.71	2.52	−3.27
S	0.17	2.63	−1.01
Cl^-	3.63	0.47	−5.22
H_1	1.26	4.78	−0.24
H_2	1.39	4.73	−2.21
H_3	3.66	4.46	−1.35
H_4	2.61	2.42	0.84
H_5	2.99	4.33	0.99
H_6	4.19	2.42	0.47
H_7	3.04	1.89	−3.81
S(*a*)	1.71	5.45	−2.39
(*b*)	1.04	2.59	−0.13
(*c*)	1.71	2.59	−2.39
(*d*)	1.04	5.45	−0.13

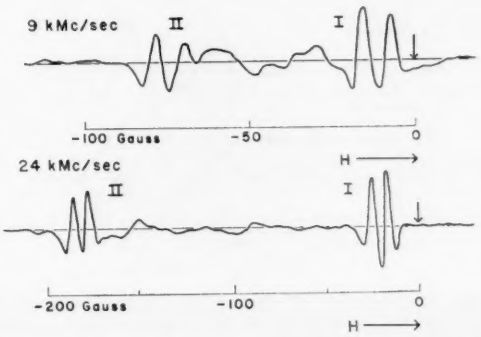

FIG. 2. Electron spin resonance curves of a gamma-irradiated single crystal of *L*-cystine dihydrochloride. The static magnetic field is turned away from the b axis towards the c' axis by 30° in the bc' plane. Arrows show the position for the DPPH reference signal for which $g=2.0036$.

are only two molecules in the unit cell, both of which are equivalent in their orientations. This makes the dichloride simpler for this study than normal cystine, for which the unit cell contains six molecules.

The observed angular dependencies of the spectra in the $a'b$, bc', and $a'c'$ planes (see Fig. 1) are shown in Figs. 5 and 6. The angular dependencies in the bc' and $a'b$ planes are symmetric across the $a'c'$ plane. Two doublets coalesce when the magnetic field is along the b axis and in the $a'c'$ plane.[7] These facts indicate that doublets I and II arise from two chemically equivalent radicals which have different orientations and that they are related to each other by the symmetry operation of the same space group as that of the undamaged crystal. Therefore, if the orientation of a free radical with regard to the $a'bc'$ axes is denoted by (l_1, l_2, l_3), the orientation of others are (l_1, l_2, l_3) or $(-l_1, l_2, -l_3)$. The doublet separation is independent of the strength of the static magnetic field within experimental error,

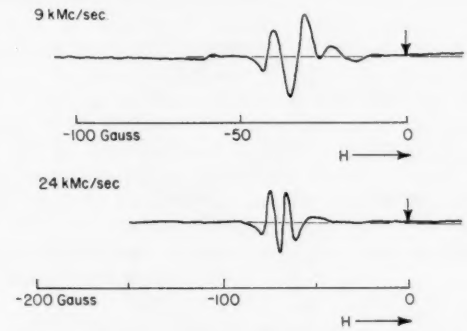

FIG. 3. Electron spin resonance curves of a gamma-irradiated single crystal of *L*-cystine dihydrochloride with the static magnetic field along the a' axis. Arrows show the position of the reference DPPH signal for which $g=2.0036$.

[7] Two doublets coalesce when the magnetic field is in the $a'b$ plane. This is an accidental coincidence arising from $G_{12}=0$.

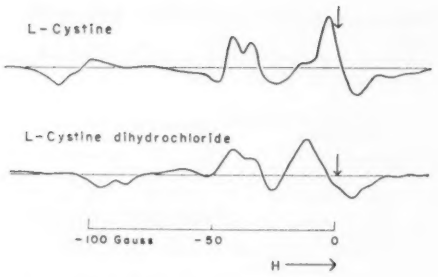

FIG. 4. Comparison of electron spin resonance curves at 9 kMc/sec for powdered samples of gamma-irradiated *L* cystine and *L*-cystine dihydrochloride.

and the two components of the doublet have equal intensity for most orientations. These facts suggest that the doublet must arise from a nuclear coupling of a single proton. The doublet separation is essentially isotropic, indicating that the coupling is mainly the Fermi contact type arising from *s*-orbital spin density. The separation of the components of each of the doublets is the same and is only 9 gauss. The separation between the two doublets is accurately proportional to the frequency of measurements. This dependence on frequency of measurement shows that the separation of doublet I from doublet II is determined by a *g*-value variation, not by nuclear hyperfine structure.

EVALUATION OF THE PRINCIPAL ELEMENTS OF THE SPECTROSCOPIC SPLITTING FACTOR

The resonant field strengths for the two components of the doublet can be expressed as

$$H=(g_0/g)H_0\pm A/2, \tag{1}$$

where A is the isotropic coupling constant of the electron for the hydrogen nucleus, and g_0 and H_0 are the spectroscopic splitting factor and the resonant field strength for DPPH, respectively. The spectroscopic

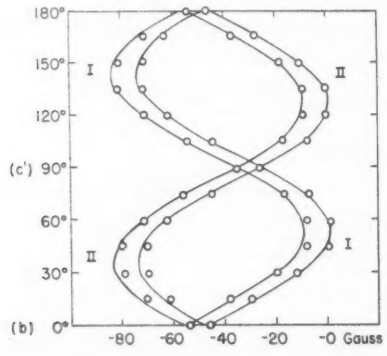

FIG. 5. Calculated (solid lines) and observed (solid dots) positions of the components of the electron spin resonance at 9.03 kMc/sec of gamma-irradiated *L*-cystine dihydrochloride relative to the resonance of DPPH ($g=2.0036$). The static magnetic field is in the bc' plane.

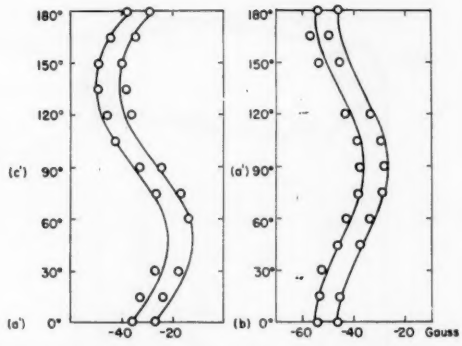

FIG. 6. Calculated (solid lines) and observed (solid dots) positions of the components of the electron spin resonance at 9.03 kMc/sec of gamma-irradiated *L*-cystine dihydrochloride relative to the resonance of DPPH ($g=2.0036$). The static magnetic field is in the $a'c'$ and ba' plane.

splitting factor, g, for various orientations of the single crystal was thus calculated from the observed values of H. The g tensor was determined from the g-value variation as follows.

If the magnetic field has direction cosines, l_1, l_2, and l_3 with respect to $a'bc'$ axes, the square of the corresponding g value is given by the expression[8]

$$g^2=\sum_{i,j=1}^{3}B_{ij}l_il_j(B_{ij}=B_{ji}). \tag{2}$$

As the anisotropy $(g-g_0)/g_0=(H_0-H)/H_0$ is small (smaller than 0.025), the equation is expressed to a good approximation as

$$\Delta g=\sum_{i,j=1}^{3}G_{ij}l_il_j, \tag{3}$$

where $\Delta g=g-g_0$. The principal g values and principal axes are found by diagonalizing the matrix G, the coefficients (G_{ij}) of which are determined from the Δg variation in the $a'b$, bc', and $a'c'$ planes. The three roots λ_u, λ_v, λ_w of the secular equation

$$\det(G-\lambda I)=0, \tag{4}$$

TABLE II. Principal elements of the spectroscopic splitting factor (g) and the matrix elements (G_{ij}).[a]

	Observed	Calculated	Direction cosine with regard to $a'bc'$ system		
g_u	2.003	2.003	±0.35	+0.53	±0.77
g_v	2.029	2.025	±0.92	−0.35	∓0.17
g_w	2.052	2.053	±0.18	+0.77	∓0.61

[a] $G_{11}=0.0197$, $G_{13}=0$, $G_{22}=0.0322$, $G_{13}=-0.0088$, $G_{33}=0.0191$, $G_{12}=\mp 0.0222$. Upper signs for radicals I, lower signs for radicals II.

[8] D. S. Schonland, Proc. Phys. Soc. (London) **A73**, 788 (1959).

where I is the unit matrix, are the principal Δg values. The direction cosines of the principal axes satisfy the relation

$$\sum_{j=1}^{3} G_{ij} l_{kj} = \lambda_k l_{ki}, \quad i=1, 2, 3 \quad \text{and} \quad k=u, v, w, \qquad (5)$$

where the $l_{kj}(j=1, 2, 3)$ are the direction cosines corresponding to the root λ_k of Eq. (4). This procedure was applied to the experimental data at 9 kMc/sec. The results are shown in Table II. In the same table the observed results are given. Angular variations of ΔH at 9 kMc/sec calculated from the results given in Table II are shown graphically in Figs. 5 and 6.

CHEMICAL FORM AND ELECTRONIC STRUCTURE OF THE FREE RADICAL

The anisotropy in the g value of organic free radicals composed of H, C, N, and O atoms is very small. For example, the difference between g(max) and g(min) is 0.0008 for DPPH[9] and 0.0069 for gamma-irradiated dimethylglyoxime,[6] in which the electron spin density is concentrated primarily on nitrogen. The corresponding value for gamma-irradiated *L*-cystine dihydrochloride is an order of magnitude larger, or 0.050. This marked anisotropy in the g value indicates that an unpaired electron is localized mainly on a sulfur atom rather than on a C, N, or O atom of the cystine. Evidence for localization of the spin density on the sulfur atoms has already been obtained by Gordy, Ard, and Shields,[1] who proposed the ionized-molecule free radical. Subsequent work by Shields and Gordy[2] revealed that SH compounds such as cysteine give resonances similar to those of the disulfide compounds like cystine and thus indicated a neutral free radical of the from R–S·. The present work gives confirmation of this neutral radical. The crystal of *L*-cystine dihydrochloride has two S—S bonds in the unit cell, but they have equivalent orientations. Since two different magnetic centers, I and II, were observed, the free radical must be associated with sulfur sites rather than with the S—S bond. Therefore, the probable chemical form of the free radical produced by ionizing radiations on either cysteine or cystine at ordinary temperatures is

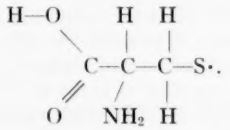

It will be shown below that this model can account for both the anisotropy in the spectroscopic splitting factor and the nuclear hyperfine structure observed for gamma-irradiated single crystals of *L*-cystine dihydrochloride.

Because it seemingly would give the system the lowest energy, we postulate that the unpaired electron of the above free radical is in a π orbital, the principal component of which is a $3p$ orbital of the sulfur. It is reasonable to assume that the bonding orbital of the sulfur has some 20 to 30% s character; and, for simplicity, we postulate it to be an sp_2 hybrid with $\frac{1}{3}$ s character. If small d orbital contributions are neglected, the occupied atomic orbitals of the valence shell are then three sp_2 hybrids directed in a common plane and a pure p orbital perpendicular to this plane. We choose the z axis along the CS bond and the y axis in the plane of the sp_2 hybrid, perpendicular to the CS bond. The x axis is then perpendicular to the CS bond, also to the plane of the sp_2 hybrid. From the symmetry of the electron charge distribution about them, we can expect the x, y, and z axes thus chosen to be principal axes of the magnetic susceptibility and hence of the spectroscopic splitting factor, g. The p_x orbital, perpendicular to the sp_2 plane, should, to a good approximation, contain the unpaired electron.

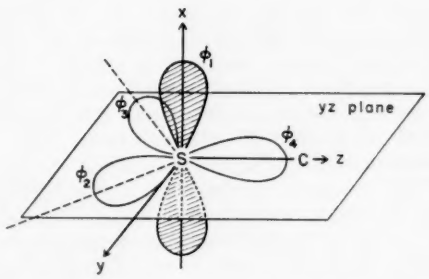

FIG. 7. Diagram indicating the orbitals and reference axes for the free radical shown in Fig. 8. The electron spin density is concentrated in the ϕ_1 orbital, the axis of which is along x and perpendicular to the CS bond. The other three orbitals are directed in the yz plane. Two of these, ϕ_2 and ϕ_3, contain unshared electron pairs. The other, ϕ_4, directed along z forms the CS σ bond.

Figure 7 shows the designation of the orbitals relative to the coordinate system as chosen above. We designate as ϕ_1 the p_x orbital with the odd electron. The p_y and p_z orbitals form with s the three sp_2 hybrids which have their axes directed in the yz plane, 120° apart. Two of these hybrids, which we designate as ϕ_2 and ϕ_3, have unshared electron pairs. The other is directed along the z axis, which is chosen along the CS bond. It forms the σ bonding molecular orbital with the appropriate orbital of the carbon. With these assumptions and designations, the four occupied orbitals can be expressed by

$$\phi_1 = (3p_x)_S, \qquad (6)$$

$$\phi_2 = (\tfrac{1}{3})^{\frac{1}{2}}(3s)_S - (\tfrac{1}{6})^{\frac{1}{2}}(3p_z)_S + (\tfrac{1}{2})^{\frac{1}{2}}(3p_y)_S, \qquad (7)$$

$$\phi_3 = (\tfrac{1}{3})^{\frac{1}{2}}(3s)_S - (\tfrac{1}{6})^{\frac{1}{2}}(3p_z)_S - (\tfrac{1}{2})^{\frac{1}{2}}(3p_y)_S, \qquad (8)$$

$$\phi_4 = (\tfrac{1}{2})^{\frac{1}{2}}\{(\tfrac{1}{3})^{\frac{1}{2}}(3s)_S + (\tfrac{2}{3})^{\frac{1}{2}}(3p_z)_S + \psi_C\}. \qquad (9)$$

Here ψ_C represents the CS bonding orbital of the

[9] A. van Roggen, L. van Roggen, and W. Gordy, Phys. Rev. **105**, 50 (1957).

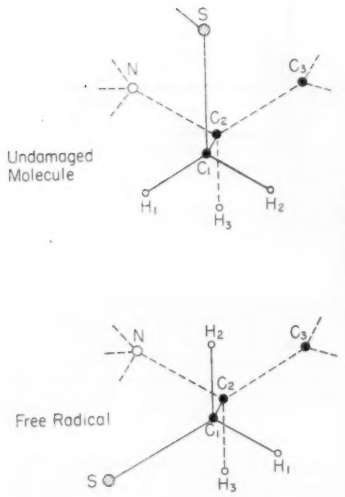

FIG. 8. Diagrams showing the difference in structural arrangement in the free radical from that of the original undamaged molecule.

carbon, which is probably an sp_3 hybrid. Here we do not require the specific form of the ψ_C.

The configuration of lowest energy E_1 will be $\phi_1^1\phi_2^2\phi_3^2\phi_4^2$. If interactions of the electron clouds with nonbonded neighboring atoms are neglected, the configurations $\phi_1^2\phi_2^1\phi_3^2\phi_4^2$ and $\phi_1^2\phi_2^2\phi_3^1\phi_4^2$, in which the odd electron is in one of the nonbonding sp_2 hybrids, will have equal energy. The configuration, $\phi_1^2\phi_2^2\phi_3^2\phi_4^1$, in which the odd electron is in the bonding σ orbital will have highest energy, E_4. The relative energy of these configurations should be $E_1<E_2=E_3<E_4$. Interactions with atoms not bonded to the sulfur should be smaller than the difference between E_1, E_2, and E_4 and are thus not expected to change this relative order. However, such interactions can cause the states 2 and 3 to have different energies and may thus cause a principal axis of the g tensor not to lie exactly along the CS bond as we have assumed. Such interactions, together with the π character of the odd electron orbital, are thought to prevent the orbitals ϕ_1, ϕ_2, and ϕ_3 from rotating about the CS bond and thus causing axial symmetry in the g factor.

The excited states 2, 3, and 4 will be mixed to some extent with the ground state 1 by spin orbital coupling. This mixing will cause an anisotropy in g which can be estimated from second-order perturbation theory. In the formulation given by Pryce[10]

$$g_{ij}=g_f\left\{\delta_{ij}-\lambda\sum_{n=2}^{n=4}\frac{(\phi_1\mid L_i\mid\phi_n)(\phi_n\mid L_j\mid\phi_1)}{E_n-E_1}\right\}, \quad (10)$$

in which λ is the spin orbit coupling, g_f is the free spin value of g, and $\delta_{ij}=1$ when $i=j$ and 0 when $i\neq j$. For sulfur, the spin orbit coupling λ approximately equals[11] -382 cm^{-1}. With the relations $L_x\mid p_x)=0$, $L_y\mid p_x)=-ip_z$, and $L_z\mid p_x)=ip_y$, which are easily proved, and with the wave functions of Eqs. (6)–(9) it follows from Eq. (10) that

$$g_{xx}=g_f, \quad (11)$$

$$g_{yy}=g_f\{1-(\lambda/6)[1/(E_2-E_1)+1/(E_3-E_1)+2/(E_4-E_1)]\}, \quad (12)$$

$$g_{zz}=g_f\{1-(\lambda/2)(1/(E_2-E_1)+1/(E_3-E_1))\}, \quad (13)$$

and

$$g_{xy}=g_{yz}=g_{zx}=0.$$

With $E_3=E_2$ and $\lambda=-382$ cm^{-1}, Eqs. (12) and (13) reduce to

$$g_{yy}=g_f+[255/(E_2-E_1)]+[255/(E_4-E_1)], \quad (14)$$

$$g_{zz}=g_f+[764/(E_2-E_1)], \quad (15)$$

where the energy difference is measured in cm^{-1}.

The smallest principal element observed, $g_u=2.003$, is in reasonable agreement with the free spin value, $g_f=2.0023$. We therefore identify g_u as g_{xx}. It is evident from the equations that $g_{yy}<g_{zz}$. We can thus identify the observed principal element $g_v=2.025$ as g_{yy} and the principal element $g_w=2.053$ as g_{zz}. With these g factors, Eqs. (13) and (14) yield

$$E_2-E_1=15{,}000\ \text{cm}^{-1},$$

$$E_4-E_1\approx 43{,}000\ \text{cm}^{-1}.$$

These values are reasonable, although they must be regarded as only approximate.

In accordance with the above results, the molecular configuration of the free radical

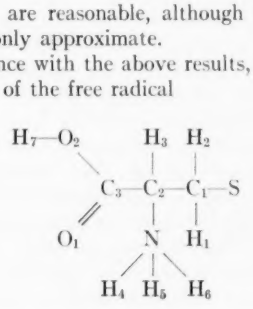

was calculated with the following assumptions: (1) Atomic coordinates of atoms in the radical are the same as those in the undamaged molecule except S, H_1, and H_2. Atomic coordinates in the undamaged molecule with regard to the $a'bc'$ axes are calculated from the crystallographic data by Steinrauf[3] and are shown in Table I. (2) The direction of the C—S bond in the radical is along the observed direction of g_w, the possible direction cosines of which, with regard to the $a'bc'$ axes, are: (a) 0.18, 0.77, −0.61; (b) −0.18, −0.77, 0.61; (c) 0.18, −0.77, −0.61; and (d) −0.18, 0.77, 0.61. (3) The C—S distance is taken as 1.86 A. The atomic coordinates of the sulfur atom in the free radical are shown in Table I.

[10] M. H. L. Pryce, Proc. Phys. Soc. (London) **A63**, 25 (1950).
[11] D. S. McClure, J. Chem. Phys. **17**, 905 (1949).

It was found that the assignment (a), (b), and (c) leads to unstable configurations with shorter interatomic distances than the van der Waals distances and with an unreasonably small angle of $\angle C_2C_1S$. The molecular configurations about the C_1C_2 bond are shown in Fig. 8. The configuration shown in Fig. 8 for the free radical [assignment (d)] is one of the most stable configurations in which $\angle C_2C_1S$ is 110° and the C_1S bond is in trans and gauche position with regard to the C_2C_3 bond and the C_2N bond, respectively. This configuration is more stable than that in the undamaged molecule in which the C_1S bond is in gauche position with regard to both the C_2C_3 bond and the C_2N bond.

Thus, it seems definite that the SS bond is broken by the ionizing radiation. After the bond is broken, thermal motions rotate the $C_1SH_1H_2$ group to the more stable configuration through the potential barrier of *cis* configuration.[12] Electronic interactions between the sulfur atom and nearby atoms determine the orientation of the orbitals ϕ_2, ϕ_3, and ϕ_1 (see Fig. 7) about the C_1—S bond. In this configuration, the sulfur atom is close to the NH_3 group (see Fig. 8). Hydrogen bonding between the electrons in the orbitals ϕ_2 and ϕ_3 and the hydrogen atoms attached to the nitrogen probably help to fix the orientation of the orbitals.

The anisotropy in the g factor is caused by the difference in energy of the orbitals ϕ_1, ϕ_2, ϕ_3, and ϕ_4, as shown above. Since these energy differences result primarily from the CS bond and the mutual interaction of the electron in the orbitals of the S, it is understandable that a comparable spread in the resonance of powdered samples is obtained from many different irradiated disulfide and sulfur hydryl compounds including certain proteins. However, it is apparent that the Coulomb interaction of the orbitals of the S with nearby, nonbonded atoms will cause an additional perturbation which should should lead to small differences in anisotropy in the g tensor of these different substances and to a measurable difference in the spread of the resonances for the different powdered or polycrystalline samples. For the same reason, a temperature change, or a change in solvent medium, for a given one of these substances should lead to a small change in the spread of the resonance. All these features are in accord with the numerous observations carried out in this laboratory on S—H and S—S compounds during the past several years.

HYPERFINE STRUCTURE

The observed doublet indicates coupling of the unpaired electron to one proton, and the isotropic spread of 9 gauss indicates that the unpaired electron density is $9/507=0.02$ in the 1s orbital of the hydrogen atom.

Although the doublet hyperfine splitting is better resolved in the single crystal, it is evident even in the resonance of the irradiated powder. To ascertain whether the doublet splitting arises from a hydrogen bonded to carbon or from one to oxygen or nitrogen, we compared the ESR of irradiated powdered samples with the ESR of samples which had been treated with D_2O before irradiation. The D atoms of the D_2O exchange with the H atoms bonded to oxygen or nitrogen, but not with an H atom bonded to carbon. The resonances of the treated and untreated samples were found to be the same within the experimental error. Therefore, the origin of the doublet observed in *L*-cystine dihydrochloride single crystal is one of the hydrogens bonded to carbon.

If the odd electron mainly localized in the sulfur atom were to interact equally with the two protons of the CH_2 group next to the sulfur atom, it would give a triplet. Since the analysis of the g factor indicates that the ϕ_1 orbiral in which the spin density is concentrated does not rotate about the S—C bond in the crystal, one proton, H_1, might be situated closer to the orbital ϕ_1 of the unpaired electron than is the other proton, H_2. It is, therefore, reasonable that the electron spin density on one proton is too small to give a resolvable splitting, whereas that on the other proton is sufficient to give the observed doublet.

The most probable mechanism for putting the necessary spin density on the CH_2 protons is the π character of the ϕ_1 orbital which arises through hyperconjugation. The isotropic hyperfine splittings of protons H_1 and H_2 caused by hyperconjugation can be expressed as[13]

$$A(H_1)=A_0\cos^2\theta_1,$$

$$A(H_2)=A_0\cos^2\theta_2,$$

where θ_1 and θ_2 are the dihedral angles between the C_1Sx plane and the SC_1H_1 plane and the SC_1H_2 plane, respectively. With the assumption that $\angle C_2C_1H_1$ and $\angle C_2C_1H_2$ are tetrahedral and that the $C_2C_1H_1$ and $C_2C_1H_2$ planes form dihedral angles of 120° with the C_2C_1S plane and with each other, θ_1 and θ_2 are calculated from the molecular configuration for the assignment (d) and the direction cosines of $x=g_u$, -0.35, 0.53, -0.77 as $\theta_1=187°$ and $\theta_2=67°$ (see Fig. 8). Hence,

$$A(H_1)=A_0,$$

$$A(H_2)=0.2A_0.$$

If we assume $A_0=9$ gauss, then $A(H_1)=9$ gauss and $A(H_2)=2$ gauss, which give rise to a doublet, in agreement with the observation. The assumed value of A_0, 9 gauss, seems reasonable as compared with 40 gauss[13] of the A_0 for the isotropic π electron—π proton

[12] See, for example, S. I. Mizushima, *Structure of Molecules and Internal Rotation* (Academic Press, Inc., New York, 1954).

[13] C. Heller and H. M. McConnell, J. Chem. Phys. **42**, 1535 (1960).

interaction in a free radical

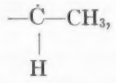

because the S=C π bonding is weaker than the C=C π bonding.

In the early work already mentioned, Shields and Gordy[2] made an incomplete investigation of a single crystal of *L* cystine. Because of the greater number of molecules in a unit cell, its spectrum is generally more complicated that that of cystine dichloride. However, for the magnetic field perpendicular to one face of the crystal, a simple doublet like that found here was observed. For another orientation, a pair of similar doublets was observed. These observations provide additional evidence to support that shown in Fig. 4 that the free radical in irradiated cystine dihydrochloride is like that in irradiated cystine or other sulfur compounds, including the proteins, which in the powdered form give a similar, but not identical, resonance pattern to that of cystine.

THE JOURNAL OF CHEMICAL PHYSICS VOLUME 34, NUMBER 1 JANUARY, 1961

Bonding in Icosahedral Complexes*

JOSEPH H. MACEK AND GEORGE H. DUFFEY

Physics Department, South Dakota State College, Brookings, South Dakota

(Received July 29, 1960)

Results of a group theoretical investigation of icosahedral AB_{12} are presented. These are used in setting up twelve equivalent, orthogonal bond orbitals. Each of the orbitals exhibits a Pauling strength of 3.921. Crystal-field splitting of valence levels of *A* is also discussed.

VAN Vleck,[1] Kimball,[2] Eisenstein,[3] Shirmazan and Dyatkina[4] have used group theory to determine which central atom orbitals can be used in forming bonds to hold two to nine ligands arranged in various ways. The results so obtained are used in both[1] directed covalent[5] and crystal field splitting[6] theories.

Coordination numbers as high as twelve are often observed.[5] As part of an investigation of these bigger structures, we have considered the icosahedral arrangement, which seems to be the most efficient way to place twelve groups around a central atom. Indeed in packing spheres thus, one may make the central sphere about 10% smaller than the surrounding ones before they touch.

The congruent transformations—that is, the symmetry operations—which leave icosahedral AB_{12} unchanged make up group I_h, or if operation *i* is absent, group *I*. Characters for the latter appear in Lomont.[7]

TABLE I. Characters of each class for representations of the *I* group.

Basis orbitals	Representation	E	$12C_5$	$12C_5^2$	$20C_3$	$15C_2$
s	A	1	1	1	1	1
p_x, p_y, p_z	F_1	3	$\frac{1}{2}(1+\sqrt{5})$	$\frac{1}{2}(1-\sqrt{5})$	0	-1
f_{t1}, f_{t2}, f_{t3}	F_2	3	$\frac{1}{2}(1-\sqrt{5})$	$\frac{1}{2}(1+\sqrt{5})$	0	-1
$f_{\eta 1}$, $f_{\eta 2}$, $f_{\eta 3}$, $f_{\eta 4}$	G	4	-1	-1	1	0
$d_{3z^2-r^2}$, $d_{x^2-y^2}$, d_{xy}, d_{yz}, d_{zx}	H	5	0	0	-1	1
Bond orbitals	σ	12	2	2	0	0

* Supported in part by the National Science Foundation.

[1] J. H. Van Vleck, J. Chem. Phys. **3**, 803 (1935).

[2] G. E. Kimball, J. Chem. Phys. **8**, 188 (1940).

[3] J. C. Eisenstein, J. Chem. Phys. **25**, 142 (1956).

[4] M. G. Shirmazan and M. E. Dyatkina, J. Phys. Chem. (U.S.S.R.) **27**, 491 (1953). This paper was translated by M. Kasha, Department of Chemistry, Florida State University, Tallahassee, Florida.

[5] L. Pauling, *The Nature of the Chemical Bond* (Cornell University Press, Ithaca, New York, 1960), 3rd ed.

[6] D. S. McClure in *Solid State Physics*, edited by F. Seitz and D. Turnbull (Academic Press, Inc., New York, 1959), Vol. 9, p. 399; P. George and D. S. McClure, *Progress in Inorganic Chemistry* (Interscience Publishers, Inc., New York, 1959), Vol. 1, p. 381.

[7] J. S. Lomont, *Applications of Finite Groups* (Academic Press, Inc., New York, 1959). The table in Wilson, Decius, and Cross, *Molecular Vibrations* (McGraw-Hill Book Company, Inc., New York, 1955) contains an error.

TABLE II. Coefficients of atomic orbitals in icosahedral bond orbital functions.

	s	p_x	p_y	p_z	$d_{3z^2-r^2}$	d_{xz}	d_{yz}	$d_{x^2-y^2}$	d_{xy}	f_{z1}	f_{z2}	f_{z3}
ψ_1	$\frac{1}{\sqrt{12}}$	0	0	$\frac{1}{2}$	$\frac{\sqrt{5}}{\sqrt{12}}$	0	0	0	0	$\frac{1}{2}$	0	0
ψ_2	$\frac{1}{\sqrt{12}}$	$\frac{1}{\sqrt{5}}$	0	$\frac{1}{\sqrt{20}}$	$\frac{-1}{\sqrt{60}}$	$\frac{1}{\sqrt{5}}$	0	$\frac{1}{\sqrt{5}}$	0	$\frac{-1}{\sqrt{20}}$	$\frac{1}{\sqrt{5}}$	0
ψ_3	$\frac{1}{\sqrt{12}}$	$\frac{1}{\sqrt{5}}\cos 72°$	$\frac{1}{\sqrt{5}}\sin 72°$	$\frac{1}{\sqrt{20}}$	$\frac{-1}{\sqrt{60}}$	$\frac{1}{\sqrt{5}}\cos 72°$	$\frac{1}{\sqrt{5}}\sin 72°$	$\frac{1}{\sqrt{5}}\cos 144°$	$\frac{1}{\sqrt{5}}\sin 144°$	$\frac{-1}{\sqrt{20}}$	$\frac{1}{\sqrt{5}}\cos 144°$	$\frac{1}{\sqrt{5}}\sin 144°$
ψ_4	$\frac{1}{\sqrt{12}}$	$\frac{1}{\sqrt{5}}\cos 144°$	$\frac{1}{\sqrt{5}}\sin 144°$	$\frac{1}{\sqrt{20}}$	$\frac{-1}{\sqrt{60}}$	$\frac{1}{\sqrt{5}}\cos 144°$	$\frac{1}{\sqrt{5}}\sin 144°$	$\frac{1}{\sqrt{5}}\cos 72°$	$\frac{-1}{\sqrt{5}}\sin 72°$	$\frac{-1}{\sqrt{20}}$	$\frac{1}{\sqrt{5}}\cos 72°$	$\frac{-1}{\sqrt{5}}\sin 72°$
ψ_5	$\frac{1}{\sqrt{12}}$	$\frac{1}{\sqrt{5}}\cos 144°$	$\frac{-1}{\sqrt{5}}\sin 144°$	$\frac{1}{\sqrt{20}}$	$\frac{-1}{\sqrt{60}}$	$\frac{1}{\sqrt{5}}\cos 144°$	$\frac{-1}{\sqrt{5}}\sin 144°$	$\frac{1}{\sqrt{5}}\cos 72°$	$\frac{1}{\sqrt{5}}\sin 72°$	$\frac{-1}{\sqrt{20}}$	$\frac{1}{\sqrt{5}}\cos 72°$	$\frac{1}{\sqrt{5}}\sin 72°$
ψ_6	$\frac{1}{\sqrt{12}}$	$\frac{1}{\sqrt{5}}\cos 72°$	$\frac{-1}{\sqrt{5}}\sin 72°$	$\frac{1}{\sqrt{20}}$	$\frac{-1}{\sqrt{60}}$	$\frac{1}{\sqrt{5}}\cos 72°$	$\frac{-1}{\sqrt{5}}\sin 72°$	$\frac{1}{\sqrt{5}}\cos 144°$	$\frac{-1}{\sqrt{5}}\sin 144°$	$\frac{-1}{\sqrt{20}}$	$\frac{1}{\sqrt{5}}\cos 144°$	$\frac{-1}{\sqrt{5}}\sin 144°$
ψ_7	$\frac{1}{\sqrt{12}}$	0	0	$-\frac{1}{2}$	$\frac{5}{\sqrt{12}}$	0	0	0	0	$-\frac{1}{2}$	0	0
ψ_8	$\frac{1}{\sqrt{12}}$	$\frac{-1}{\sqrt{5}}$	0	$\frac{-1}{\sqrt{20}}$	$\frac{-1}{\sqrt{60}}$	$\frac{1}{\sqrt{5}}$	0	$\frac{1}{\sqrt{5}}$	0	$\frac{1}{\sqrt{20}}$	$\frac{-1}{\sqrt{5}}$	0
ψ_9	$\frac{1}{\sqrt{12}}$	$\frac{-1}{\sqrt{5}}\cos 72°$	$\frac{-1}{\sqrt{5}}\sin 72°$	$\frac{-1}{\sqrt{20}}$	$\frac{-1}{\sqrt{60}}$	$\frac{1}{\sqrt{5}}\cos 72°$	$\frac{1}{\sqrt{5}}\sin 72°$	$\frac{1}{\sqrt{5}}\cos 144°$	$\frac{1}{\sqrt{5}}\sin 144°$	$\frac{1}{\sqrt{20}}$	$\frac{-1}{\sqrt{5}}\cos 144°$	$\frac{-1}{\sqrt{5}}\sin 144°$
ψ_{10}	$\frac{1}{\sqrt{12}}$	$\frac{-1}{\sqrt{5}}\cos 144°$	$\frac{-1}{\sqrt{5}}\sin 144°$	$\frac{-1}{\sqrt{20}}$	$\frac{-1}{\sqrt{60}}$	$\frac{1}{\sqrt{5}}\cos 144°$	$\frac{1}{\sqrt{5}}\sin 144°$	$\frac{1}{\sqrt{5}}\cos 72°$	$\frac{-1}{\sqrt{5}}\sin 72°$	$\frac{1}{\sqrt{20}}$	$\frac{-1}{\sqrt{5}}\cos 72°$	$\frac{1}{\sqrt{5}}\sin 72°$
ψ_{11}	$\frac{1}{\sqrt{12}}$	$\frac{-1}{\sqrt{5}}\cos 144°$	$\frac{1}{\sqrt{5}}\sin 144°$	$\frac{-1}{\sqrt{26}}$	$\frac{-1}{\sqrt{60}}$	$\frac{1}{\sqrt{5}}\cos 144°$	$\frac{-1}{\sqrt{5}}\sin 144°$	$\frac{1}{\sqrt{5}}\cos 72°$	$\frac{1}{\sqrt{5}}\sin 72°$	$\frac{1}{\sqrt{20}}$	$\frac{-1}{\sqrt{5}}\cos 72°$	$\frac{-1}{\sqrt{5}}\sin 72°$
ψ_{12}	$\frac{1}{\sqrt{12}}$	$\frac{-1}{\sqrt{5}}\cos 72°$	$\frac{1}{\sqrt{5}}\sin 72°$	$\frac{-1}{\sqrt{20}}$	$\frac{-1}{\sqrt{60}}$	$\frac{1}{\sqrt{5}}\cos 72°$	$\frac{-1}{\sqrt{5}}\sin 72°$	$\frac{1}{\sqrt{5}}\cos 144°$	$\frac{-1}{\sqrt{5}}\sin 144°$	$\frac{1}{\sqrt{20}}$	$\frac{-1}{\sqrt{5}}\cos 144°$	$\frac{1}{\sqrt{5}}\sin 144°$

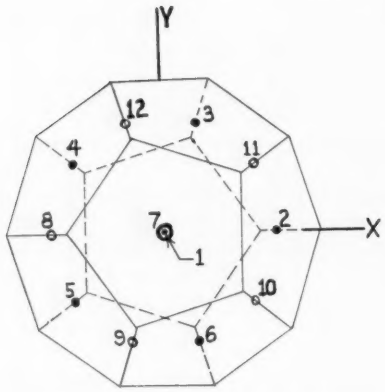

FIG. 1. Location of B atoms at face centers of a regular dodecahedron pierced symmetrically by coordinate axes. The solid circles represent B's on upper faces; the open circles those on lower ones. The corresponding regular icosahedron has a vertex at each B.

These are listed in Table I together with those for the reducible representation based on σ bonds. Also, the s, p, d, and f atomic orbitals that serve as basis functions for the irreducible representations are given.

For each well-known function, the homogeneous-polynomial subscript gives the nonradial variation of the orbital.[3] The f orbitals are defined in terms of such functions as follows:

$$f_{\xi 1}=f_{z(5z^2-3r^2)}, \tag{1}$$

$$f_{\xi 2}=(\sqrt{3}/\sqrt{5})f_{z(x^2-y^2)}+(\sqrt{2}/\sqrt{5})f_{x(x^2-3y^2)}, \tag{2}$$

$$f_{\xi 3}=(\sqrt{3}/\sqrt{5})f_{xyz}-(\sqrt{2}/\sqrt{5})f_{y(3x^2-y^2)}, \tag{3}$$

$$f_{\eta 1}=f_{x(5z^2-r^2)}, \tag{4}$$

$$f_{\eta 2}=f_{y(5z^2-r^2)}, \tag{5}$$

$$f_{\eta 3}=(\sqrt{2}/\sqrt{5})f_{z(x^2-y^2)}-(\sqrt{3}/\sqrt{5})f_{x(x^2-3y^2)}, \tag{6}$$

$$f_{\eta 4}=(\sqrt{2}/\sqrt{5})f_{xyz}+(\sqrt{3}/\sqrt{5})f_{y(3x^2-y^2)}. \tag{7}$$

Using Table I, one finds that the σ representation breaks down into the irreducible representations

$$A+F_1+F_2+H. \tag{8}$$

Likewise with group I_h, one breaks the σ representation down into

$$A_g+F_{1u}+F_{2u}+H_g. \tag{9}$$

Here the s orbital forms the basis for representation A_g; the p orbitals for F_{1u}; the f_ξ orbitals for F_{2u}; and the d orbitals for H_g. Thus including operation i gives one no new results.

We shall use this breakdown in discussing both (a) covalent and (b) electrovalent bonding in icosahedral AB_{12} oriented as in Fig. 1.

Since the configuration is $sp^3d^5f^3$, each bond orbital contains $\frac{1}{12}s$, $\frac{1}{4}p$, $\frac{5}{12}d$, and $\frac{1}{4}f$. To obtain ψ_1 directed upward along and cylindrically symmetric about the z axis, one combines s, p_z, $d_{3z^2-r^2}$ and $f_{\xi 1}$ in the required proportions. Then one obtains ψ_i for bond i from ψ_1 by acting on it with the proper operation of the group. Thus one gets the orbitals described in Table II.

The first bond orbital in Table II is

$$\psi_1=(1/\sqrt{12})s+\tfrac{1}{2}p_z+(\sqrt{5}/\sqrt{12})d_{3z^2-r^2}+\tfrac{1}{2}f_{\xi 1}. \tag{10}$$

The others can likewise be written down from the table and then checked for orthogonality. The Pauling strength[8] S of each is found to be 3.921. Since this is not far below 4.000, the greatest S can be in a single $spdf$ hybrid orbital, the icosahedral bond orbitals overlap quite well those of the attached atoms.

Effects that oppose covalent bond formation in AB_{12} include (a) steric repulsion between the B's and (b) concentration of charge on A. Effect (a) is less in the icosahedral structure than in the corresponding cubic or hexagonal close packed structures.[5] Effect (b) depends on the relative electronegativities of A and B as well as on their valences.[5]

When the bonding is essentially ionic, the electrons in central-atom orbitals which would otherwise be used for σ covalent bonds are repelled more by the electron clouds of the ligands than those valence electrons not in such orbitals—other things being equal. Thus in an icosahedral field, the $f_{\xi 1}$, $f_{\xi 2}$, and $f_{\xi 3}$ are shifted upward with respect to $f_{\eta 1}$, $f_{\eta 2}$, $f_{\eta 3}$, and $f_{\eta 4}$. The p and d orbitals are not split.

Within some crystals, icosahedral coordination is found.[5,9] In none of these, however, is the entire crystal of such symmetry because space cannot be filled with units possessing fivefold rotation axes.[10] In the observed cases, icosahedral symmetry extends outward through only a limited region. The interaction between the central atom and far units is of lower symmetry; thus it causes a small splitting in levels that are not split in an icosahedral field.

[8] G. H. Duffey, J. Chem. Phys. **18**, 510 (1950).
[9] B. R. Judd, Proc. Roy. Soc. (London) **A241**, 122 (1957).
[10] K. Lonsdale, *Crystals and X-Rays* (D. Van Nostrand Company, Inc., Princeton, New Jersey, 1949).

Microwave Spectrum of *cis*-Difluoroethylene. Structures and Dipole Moments of Fluoroethylenes

VICTOR W. LAURIE*

National Bureau of Standards, Washington 25, D. C., and Department of Chemistry, University of California, Berkeley, California

(Received July 29, 1960)

The microwave spectrum of *cis*-difluoroethylene, HFC=CHF, has been investigated in the region 17–36 kMc. Observed rotational constants (Mc) for the ground vibrational state of $C_2^{12}H_2F_2$ are $a_0=21103.31$, $b_0=5930.35$, $c_0=4622.27$; for $C^{12}C^{13}H_2F_2$, $a_0=20752.10$, $b_0=5900.17$, $c_0=4586.92$. From these constants a structure is obtained with $r_{CC}=1.324$ A, $r_{CF}=1.337$ A, $r_{CH}=1.080$ A, $<FCC=122°9'$, and $<HCC=121°16'$. Rotational constants for $v_b=1$ have also been determined. A dipole moment of 2.42 D is calculated from the Stark effect. Comparison with previously existing data for ethylene, vinyl fluoride, and vinylidene fluoride shows that there is a shortening of both the CF and the CC bonds with increasing fluorine substitution.

INTRODUCTION

ALTHOUGH it is a small, reasonably stable molecule there seem to have been no previous investigations of any kind of *cis*-difluoroethylene (HFC=CHF). The molecule is of interest, however, because of its simple relation to the prototype molecule ethylene. Accurate studies of simple derivatives of ethylene are important for helping to settle questions about the extent of the usefulness of theoretical concepts such as conjugation, hybridization, and resonance. The geometry of HFC=CHF is particularly favorable for the determination of a structure from rotational data, and the present study was undertaken to obtain the structure and dipole moment.

EXPERIMENTAL

The sample of HFC=CHF was a small amount obtained from Professor F. G. A. Stone of Harvard University and was used without further purification. Spectra were observed in the region 17–36 kMc with the Stark modulation spectrograph which has been described elsewhere.[1] Frequency measurements are estimated to be accurate to ±0.05 Mc. Lines of HFC^{13}=CHF were observed from the isotopic species present in a natural abundance of ~2%. These transitions were distinguished from vibrational satellites by the temperature dependence of their intensities.

Spectra and Rotational Constants

The spectra were characteristic of an asymmetric rotor with *b*-type selection rules. Measured frequencies of identified transitions are given in Table I, together with frequencies calculated from the rotational constants of Table II. Identifications of the rotational transitions were made from Stark effects.

In addition to the transitions of molecules in the ground vibrational state, rotational transitions of molecules in excited vibrational states were also observed. The strongest of these were measured and have been assigned to the symmetric in-plane bending of the FCCF skeleton (ν_5). No vibrational data are available for HFC=CHF, but analogy with other molecules suggests that this mode has the lowest frequency. Furthermore, as discussed elsewhere,[2] the observed value for the inertial defect, $I_c-I_a-I_b$, supports this assignment.

Some centrifugal distortion is apparent in the ob-

TABLE I. Identified rotational transitions (Mc).

Transition	Obs. freq.	Calc. freq.	Centrif. dist.
	$C_2^{12}H_2F_2$ (ground vib. state)		
$2_{02}\rightarrow2_{11}$	17 870.03	17 870.03	−0.07
$3_{03}\rightarrow3_{12}$	20 101.45	20 101.43	−0.39
$4_{04}\rightarrow4_{13}$	23 336.67	23 336.70	−1.28
$5_{23}\rightarrow4_{32}$	24 090.66	24 089.69	...
$0_{00}\rightarrow1_{11}$	25 725.58	25 725.58	...
$5_{05}\rightarrow5_{14}$	27 750.08	27 750.15	−3.26
$3_{13}\rightarrow4_{04}$	29 158.73	29 161.26	...
$6_{06}\rightarrow6_{15}$	33 478.20	33 478.20	−6.99
$1_{01}\rightarrow2_{12}$	34 970.12	34 970.12	...
	$C_2^{12}H_2F_2$ (excited vib. state)		
$2_{02}\rightarrow2_{11}$	18 006.54	18 006.54	−0.07
$3_{03}\rightarrow3_{12}$	20 243.53	20 243.53	−0.39
$4_{04}\rightarrow4_{13}$	23 485.96	23 485.94	−1.28
$0_{00}\rightarrow1_{11}$	25 848.69	25 848.69	...
$5_{05}\rightarrow5_{14}$	27 908.28	27 908.28	−3.25
$3_{13}\rightarrow4_{04}$	29 020.76	29 022.89	...
$1_{01}\rightarrow2_{12}$	35 083.75	35 083.75	...
	$C^{12}C^{13}H_2F_2$ (ground vib. state)		
$3_{03}\rightarrow3_{12}$	19 808.46	19 808.39	−0.37
$4_{04}\rightarrow4_{13}$	23 070.58	23 070.60	−1.22
$0_{00}\rightarrow1_{11}$	25 339.02	25 339.02	...
$5_{05}\rightarrow5_{14}$	27 524.86	27 524.91	−3.09
$3_{13}\rightarrow4_{04}$	29 198.25	29 200.73	...
$6_{06}\rightarrow6_{15}$	33 305.61	33 305.61	−6.60
$1_{01}\rightarrow2_{12}$	34 512.86	34 512.86	...

* National Research Council, National Bureau of Standards Research Associate 1958–1959; National Science Foundation Postdoctoral Fellow 1959–1960. Present Address: Chemistry Department, Stanford University, Stanford, California.

[1] D. R. Lide, Jr., D. E. Mann, and R. M. Fristrom, J. Chem. Phys. **29**, 444 (1958).

[2] V. W. Laurie and D. R. Herschbach (to be published).

TABLE II. Rotational constants (Mc) and moments[a] of inertia (amu A²).

	$C_2^{12}H_2F_2$ (gnd.)	$C^{12}H_2F_2$ (exc. vib.)	$C^{13}C^{12}H_2F_2$ (gnd.)
a	21103.31	21231.16	20752.10
b	5930.35	5929.68	5900.17
c	4622.27	4617.53	4586.92
D^{b}	0.01082	0.01076	0.01007
I_a	23.9551	23.8108	24.3605
I_b	85.2447	85.2543	85.6807
I_c	109.3686	109.4808	110.2114
$I_c-I_a-I_b$	0.1688	0.4157	0.1702

[a] Conversion factor 5.05531×10^5 Mc amu A².
[b] Distortion constant which is defined in the text.

served transitions. This is particularly true in the Q-branch series where deviations from the rigid rotor frequencies of as much as 7 Mc occur. A one-parameter correction of the form $DJ(J+1)[dE(\kappa)/d\kappa]$ has been applied to the Q-branch energy levels and the fit is within the experimental error of ±0.05 Mc. Calculated centrifugal distortion corrections are given in the last column of Table I. No correction has been applied to the R-branch lines since it is not felt that the small number of observed transitions justifies the introduction of additional parameters. The R-branch transitions used in the calculation of the rotational constants were the $0_{00}\rightarrow1_{11}$ and the $1_{01}\rightarrow2_{12}$. Centrifugal distortion should be small for these transitions and is expected to introduce very minor errors into the rotational constants.

Inertial Defect

For a completely rigid planar body, $I_c=I_a+I_b$. For planar molecules, however, the effective moments of inertia contain contributions from the interaction of vibration and rotation. Thus $I_c^{\text{eff}}=I_a^{\text{eff}}+I_b^{\text{eff}}+\delta$, where δ is the inertial defect.[3] Values of δ found in this study are given in Table II.

There are several points of interest. First, the observed values are within the typical range for planar molecules, supporting the anticipated result that HFC=CHF is planar. We also see that the change in δ resulting from substitution of C^{13} for C^{12} is small and within experimental error. This supports the assumption which is often made that isotopic substitution for a heavy atom causes only a minor shift in the inertial defect. This result is also consistent with recent theoretical calculations.[2] Larger shifts of the order of 0.01 amu A² are characteristic when hydrogen is replaced by deuterium.

In contrast to the relatively small isotope effects, there is an increase of 0.247 amu A² in going to the observed excited vibrational state. From the values for δ, it can be calculated that this vibrational mode contributes 0.123 amu A² to the ground state value for δ as compared with 0.045 amu A² for the sum of the contributions of all other modes. Calculations have shown that this result is expected of a low-frequency in-plane mode. It is interesting to note that $\delta=0.14$ amu A² in[4] $H_2C=CF_2$. Here the lowest frequency modes are in-plane.[5] On the other hand in[6] $H_2C=CHF$ $\delta\approx0$. Here the mode of lowest frequency is out-of-plane. These results are characteristic of the difference in the effect of in-plane and out-of-plane vibrations on the inertial defect.[2] From the observed inertial defect, it is estimated that $\nu_b\approx400$ cm⁻¹ in HFCCHF.

Dipole Moment

Quantitative measurements were made of the Stark effect of the $0_{00}\rightarrow1_{11}$ and the $1_{01}\rightarrow2_{12}$ transitions in the ground vibrational state of HFCCHF. Observed Stark coefficients are listed in Table III. The Stark effect of the OCS transition at 24325.92 Mc was used to calibrate the electric field strengths.[7] The calculated dipole moment is 2.42±0.03 D. This value may be compared with the reported dipole moment[8] of 1.37 D for CH_2CF_2. These two values allow one to estimate that the as yet unmeasured dipole moment of CH_2CHF will be ~1.5 D, directed more or less along the CF bond.

The dipole moment of CH_2CF_2 is rather small compared to the 2.30 D found[9] in CH_3CHF_2. This lesser value may be qualitatively discussed in terms of the 'resonance dipole" concept.[10] In CHFCHF, on the other hand, the geometry is such that the influence of the resonance dipole largely vanishes and the dipole moment is comparable to the aliphatic value.

Determination of Structure of HFC=CHF

For the determination of a structure, there are the six effective ground state moments of inertia given in Table II. The planarity of the molecule reduces the number of independent data to four. The coordinates of the C atom in the principal axis system of the $C_2^{12}H_2F_2$ species can be calculated from the shifts in the moments of

TABLE III. Stark coefficients[a] and dipole moment of CHFCHF.

Transition	m	$\Delta\nu/E^2$	μ
$0_{00}\rightarrow1_{11}$	0	$1.53\pm0.03\times10^{-5}$	2.42±0.02 D
$1_{01}\rightarrow2_{12}$	1	$2.45\pm0.04\times10^{-5}$	2.42±0.02 D

[a] Mc/(V²/cm²).

[3] B. W. Darling and D. M. Dennison, Phys. Rev. **57,** 128 (1940).
[4] W. Edgell, P. A. Kinsey, and J. W. Amy, J. Am. Chem. Soc. **79,** 2691 (1957).
[5] J. R. Scherer and J. Overend, J. Chem. Phys. **32,** 1720 (1960).
[6] H. W. Morgan and J. H. Goldstein, J. Chem. Phys. **30,** 1025 (1959).
[7] S. A. Marshall and J. Weber, Phys. Rev. **105,** 1502 (1957).
[8] A. Roberts and W. F. Edgell, J. Chem. Phys. **17,** 742 (1949).
[9] G. H. Kwei and D. R. Herschbach, J. Chem. Phys. **32,** 1270 (1960).
[10] For example, see L. Pauling, *The Nature of the Chemical Bond* (Cornell University Press, Ithaca, New York, 1948), p. 153.

inertia occurring when C^{13} substitution is made.[11,12] If the axis parallel to the double bond is denoted by "z" and the molecular plane by "xz" then $|x_c| = 0.643$ A and $|z_c| = 0.662$ A. The length of the CC bond is $2|z_c| = 1.324$ A. The ambiguities in the C coordinates that are present because of the inertial defect are small here because of the near equivalence of δ for the two isotopic species. For example, essentially the same result is obtained whether ΔI_b or $\Delta(I_c - I_a)$ is used. We have used I_a and I_b. Use of I_a and I_c gives $r_{CC} = 1.326$ A.

For the determination of the two F and the two H coordinates, there remain three relations, including the center of mass condition. Since there is one more unknown than relations, one parameter must be assumed. The least uncertainty in the structure is introduced by assuming the CH bond length. This bond length has been fairly well characterized by studies of other molecules and a value of 1.08 A seems to be the most likely choice. Any reasonable variation from this value causes only minor changes in the z coordinate of F. The x coordinate of F and all C coordinates are independent of the choice. The x coordinates of F and H were obtained by using the observed coordinates for carbon and the relations $I_a = \sum m_i x_i^2$, $\sum m_i x_i = 0$. The z coordinates were obtained from the observed z coordinate for carbon, the assumed CH bond length, and $I_b = \sum m_i z_i^2$. Table IV shows the results of this analysis. Also in Table IV are the coordinates obtained if $r_{CH} = 1.07$ A and 1.09 A. Corresponding bond distances and angles are given in Table V. It can be seen that F parameters are insensitive to the choice of r_{CH}.

Estimation of the uncertainties in the parameters is not straightforward because of the interaction of vibration and rotation. An estimate of ± 0.005 A for the CC and CF bonds and $\pm 20'$ for the CCF angle seems reasonable, however, and is more than adequate to encompass experimental errors in the measured quantities.

Structures of $H_2C{=}CF_2$ and $H_2C{=}CHF$

Microwave studies of vinylidene fluoride[4] and vinyl fluoride[6,13] have been reported and it is instructive to compare the structural results with those found for HFC=CHF. In order that the comparisons be as meaningful as possible, however, it is desirable that the three structures be calculated by a uniform procedure. Consequently, the data for $H_2C{=}CF_2$ and $H_2C{=}CHF$ have been reanalyzed. The absolute values obtained for the structural parameters do not differ very much from those reported by the original workers, but the relative values should have more significance.

For the determination of the structure of $H_2C{=}CHF$, the microwave data of Morgan and Goldstein[6] and of Bak *et al.*[13] have been combined. These data include an isotopic substitution for every atom except F, as well as several doubly substituted species. Thus it is possible to obtain values for the coordinates in the principal axis system[11,12] of $C_2{}^{12}H_3F$ for every atom but F. The F coordinates could then in principle be obtained from the center of mass condition. However, there are several atoms which are near a principal axis and their position is accordingly poorly determined. For example, if we accept at face value the isotopic shifts in the moments of inertia for C^{13} subsitution, we calculate a C=C bond length of 1.351 A. Such a long bond seems incompatible with the ethylene value of ~1.335 A and the *cis*-difluoroethylene value of 1.324 A. The discrepancy is mostly in the apparent "a" coordinate for the interior C atom. From the data for CH_2CHF and $CH_2C^{13}HF$, one calculates an "a" coordinate of 0.0908 A. However, this apparent value contains zero-point effects which cause it to be ~0.03 A too small, a general effect which is to be expected for any atom which is near to a principal axis.[14] Accordingly, in the location of atoms near axes, the first moment and cross-product equations have been used. It is also necessary to use the moments of inertia of CH_2CHF to locate the F atom. All other coordinates are obtained from isotopic shifts. The results are given in Table VI. The calculated structure is still subject to rather large uncertainties because of the basic insensitivity of the microwave data to some of the parameters, but it is felt that it is the best available from the present data. The probable error is difficult to assess but an estimate of ± 0.01 A in bond lengths is indicative. Previous estimates of errors have been somewhat optimistic.

Edgell *et al.*[4] have reported microwave spectra for

TABLE IV. Coordinates[a] (A) of atoms in principal axis system of HFC=CHF.

	$r_{CH} = 1.07$	$r_{CH} = 1.08$	$r_{CH} = 1.09$
x_C	0.6428	0.6428	0.6428
x_F	−0.4891	−0.4891	−0.4891
x_H	1.5659	1.5659	1.5659
z_C	0.6620	0.6620	0.6620
z_F	1.3745	1.3735	1.3725
z_H	1.2031	1.2225	1.2416

[a] Masses were taken from C. H. Townes and A. L. Schawlow, *Microwave Spectroscopy* (McGraw-Hill Book Company, Inc., New York, 1955), Appendix VII.

TABLE V. Structure[a] of CHFCHF.

	I	II	III
r_{CC}	1.324_0	1.324_0	1.324_0
r_{CF}	1.337_5	1.337_0	1.336_5
r_{CH}	(1.070)	(1.080)	(1.090)
<FCC	122°11′	122°9′	122°7′
<HCC	120°23′	121°16′	122°8′

[a] In each case the CH bond is assumed. Structure II is preferred by the author.

[11] J. Kraitchman, Am. J. Phys. **21,** 17 (1953).
[12] C. C. Costain, J. Chem. Phys. **29,** 864 (1958).
[13] B. Bak, D. Christensen, L. Hansen-Nygaard, and J. Rastrup-Andersen, Spectrochim. Acta **13,** 120 (1958).
[14] D. R. Herschbach and V. W. Laurie (to be published).

TABLE VI. Structure of CH_2CHF.

r_{CC}	1.332	<FCC	121°10′
r_{CF}	1.348	<FCH	117°55′
r_{CH}(CF)	1.071	<HCH	120°31′
r_{CH} (*trans*[a])	1.086	<HCC (*trans*)	120°43′
r_{CH} (*cis*)	1.079		

[a] *cis* and *trans* refer to H.

CH_2CF_2, CD_2CF_2, and $CHDCF_2$. The observed rotational constants give four independent data for the determination of a structure. Since there are five parameters it is necessary to make an assumption. If we assume for the CF bond the electron diffraction value[15] of 1.321 A, the structure shown in Table VII is consistent with the microwave data. The proximity of the middle carbon to the center of mass means the microwave data are very insensitive to the values of the CC and CF bonds taken separately, but the data place restrictions on the two parameters considered together which definitely favors a shortening of the bonds.

DISCUSSION

Some collected structural data for fluorine substituted ethylenes are given in Table VIII. There are several interesting points. First, the CF bonds are all shorter than in the aliphatic compounds. For example, the CF bond in CH_3CH_2F[16] is 1.38 A. This shortening is characteristic of halogenated unsaturated systems and is a familiar phenomenon.[17]

Another definite trend is the progressive shortening of the CF bond with increasing fluorination. The same behavior has been noted in the fluoromethanes,[18] fluorosilanes,[19] and methylfluorosilanes.[20] It would now seem that as a general rule increasing fluorination of a compound leads to a shortening of the bonds involving F. For example, the length of the CF bond in the substituted ethanes is probably in the order $CH_3CH_2F > CH_2FCH_2F > CH_3CHF_2 > CH_2FCHF_2 > CH_3CF_3$, etc.

There also appears to be a shortening of the CC double bond when F is substituted. Unfortunately, the CC bond length is not so accurately determined in any of the fluoroethylenes, except perhaps HFCCHF, that quantitative comparisons can be made. Nevertheless,

TABLE VII. Structure of CH_2CF_2.

r_{CC}	1.320	<FCF	109°26′
r_{CF}	1.321	<HCH	121°
r_{CH}	1.076		

[15] I. L. Karle and J. Karle, J. Chem. Phys. **18,** 963 (1950).
[16] B. Bak, S. Detoni, L. Hansen-Nygaard, J. T. Nielsen, and J. Rastrup-Andersen (to be published).
[17] For example, see L. Pauling, footnote reference 10, p. 214.

TABLE VIII. Comparison of the structures of fluorinated ethylenes.

Molecule	r_{CC}	r_{CF}
CH_2CH_2[a]	1.337	...
CH_2CHF	1.332	1.348
CHFCHF	1.324	1.337
CH_2CF_2	1.320	1.321
CF_2CF_2[b]	1.313	1.313

[a] Infrared study of H. C. Allen and E. K. Plyler, J. Am. Chem. Soc. **80,** 2673 (1958).
[b] Footnote reference 15.

the trend shown in Table VIII is reasonable and probably gives the proper qualitative description. We may note that it also seems that the carbonyl bond lengths in[21] HCOF and[22] CH_3COF are shorter than in H_2CO and CH_3CHO. Additional support for the shortening of multiple bonds by fluorine substitution is the value 1.198 A reported[23] for the CC bond in FC≡CH. This is the shortest C≡C bond reported to date and may be compared with the normal length of 1.205 A.

[18] D. R. Lide, Jr., J. Am. Chem. Soc. **79,** 2691 (1957).
[19] V. W. Laurie, J. Chem. Phys. **26,** 1359 (1957).
[20] L. C. Krisher and L. Pierce, J. Chem. Phys. **32,** 1619 (1960).
[21] O. LeBlanc, V. W. Laurie, and W. D. Gwinn, J. Chem. Phys. **33,** 598 (1960).
[22] L. Pierce and L. C. Krisher, J. Chem. Phys. **31,** 875 (1959).
[23] J. Sheridan, Symposium on Molecular Structure and Spectroscopy, Columbus, Ohio, June, 1960.

Strong Coupling in Nuclear Resonance Spectra. IV. Exact Analysis of Three-Spin Spectra*

S. CASTELLANO† AND J. S. WAUGH‡

Department of Chemistry and Research Laboratory of Electronics,§ Massachusetts Institute of Technology, Cambridge, Massachusetts

(Received July 5, 1960)

A method is developed for calculating the chemical shifts and spin-spin coupling constants for a system of three spin-½ nuclei (*ABC*) directly from the nuclear resonance spectrum. Trial-and-error adjustment of these parameters is avoided entirely, and the values obtained are exactly consistent with the input information. The use of experimental intensities is kept separate from that of experimental frequencies, and the former may be omitted entirely when experimental values of sufficient accuracy are not available. It is shown that previously unknown ambiguities in the assignment of parameters sometimes arise, and that conventional iterative analyses may occasionally lead to the wrong answer. The proton resonance spectra of four compounds containing vinyl groups are discussed as illustrations of the method.

INTRODUCTION

THE analysis of high-resolution nuclear magnetic resonance spectra has become rather popular in recent years.[1] It always involves some sort of attack on the quantum-mechanical problem associated with the Hamiltonian

$$H=\nu_0\sum_i\delta_i I_{zi}+\sum_i\sum_{j>i}A_{ij}\mathbf{I}_i\cdot\mathbf{I}_j. \qquad (1)$$

(The notation used here is the same as that employed in previous papers,[2-4] except that here the external field is taken to be in the negative z direction. The Zeeman energy has been omitted, since in large fields it influences only the location of the spectrum and not its form.) In nearly every case, analyses have been performed by the iterative method well known to spectroscopists in general: one guesses trial values for the chemical shifts δ_i and spin-spin coupling constants A_{ij} and performs a numerical diagonalization of (1), making any possible use of symmetry. The result is compared with the experimental spectrum, new trial values of the parameters are chosen, and the whole process is repeated until one converges on constant values, hopefully the correct ones.

The trouble with this procedure is, in fact, that it offers no assurance that the final result is correct or unique. Sometimes convergence is not obtained at all.[5] In other cases[3,5] it has been accidentally found that two (or more) entirely different sets of parameters are consistent with experiment within ordinary experimental error. Which set is actually obtained is an accidental result of the particular set of trial parameters originally chosen and the criteria used to effect convergence. Whether or not a complex spectrum arising from a spin system of low symmetry is ever in *exact* agreement with more than one set of parameters is not known with certainty. It will be shown here that such ambiguities *always* occur insofar as the transition frequencies alone are concerned. It is clear, in any case, that the problem of uniqueness is serious enough to warrant considerable caution in applying the usual iterative analyses and to justify the investigation of other methods which display clearly any ambiguities that may arise.

It should of course be mentioned that there already exists one method, the moment method of Van Vleck,[6] Anderson, and McConnell,[7] which in principle avoids the previously mentioned difficulties by proceeding forthrightly from the experimental spectrum to the desired chemical shifts and coupling constants. It, however, has the serious drawback that its application depends critically on the availability of accurate intensity measurements, which are difficult to obtain in the present state of the art. Moreover, it does not offer any way of putting heavier weight on the accurately measurable frequencies than on these intensities. In fact, it would seem that the moment method cannot now be applied to the complete analysis of the proton spectra arising from three or more spins in an arrangement of low symmetry. Its considerable usefulness derives mainly from its use as a check on the internal consistency of calculations done by other methods and for approximate or partial analyses.

Our aim here is to develop a compromise between

* Briefly reported in MIT Research Lab. of Electronics Rept. QPR-52 (January 15, 1959), and at the IVth International Meeting on Molecular Spectroscopy, Bologna, September, 1959.

† Present address: Istituto di Chimica Industriale, Politecnico di Milano, Milan.

‡ Sloan Fellow.

§ This work was supported in part by the U. S. Army Signal Corps, the U. S. Air Force Office of Scientific Research, Air Research and Development Command, and the U. S. Navy Office of Naval Research.

[1] J. A. Pople, W. G. Schneider, and H. J. Bernstein, *High Resolution Nuclear Magnetic Resonance* (McGraw-Hill Book Company, Inc., New York, 1958), Chap. 6.

[2] R. W. Fessenden and J. S. Waugh, J. Chem. Phys. **30,** 944 (1959).

[3] R. W. Fessenden and J. S. Waugh, J. Chem. Phys. **31,** 996 (1959).

[4] J. S. Waugh and F. W. Dobbs, J. Chem. Phys. **31,** 1235 (1959).

[5] N. Sheppard (private communication).

[6] J. H. Van Vleck, Phys. Rev. **74,** 1168 (1948).

[7] W. A. Anderson and H. M. McConnell, J. Chem. Phys. **26,** 1496 (1957).

(a) The methods used in this section constitute a somewhat more complete and systematic use of the consequences of trace invariance than a similar procedure very recently described by S. Alexander [J. Chem. Phys. **32,** 1700 (1960)], and are also related to the methods employed by C. A. Reilly and J. D. Swalen [J. Chem. Phys. **32,** 1378 (1960)] in finding the eigenvalues.

TABLE I. Definition of basis functions and matrix elements of the spin Hamiltonian H in the uncoupled (product) representation for three spin-$\frac{1}{2}$ nuclei ABC, ν_0, the origin of frequency measurements, has been so chosen that $\delta_A+\delta_B+\delta_C=0$ (see text), $M=\Sigma m_i$.

n	$\psi_n(ABC)$	M	H_{nn}
1	$\alpha\alpha\alpha$	$+\frac{3}{2}$	$(+A_{AB}+A_{AC}+A_{BC})/4$
2	$\alpha\alpha\beta$	$+\frac{1}{2}$	$(+A_{AB}-A_{AC}-A_{BC})/4-\nu_0\delta_C$
3	$\alpha\beta\alpha$	$+\frac{1}{2}$	$(-A_{AB}+A_{AC}-A_{BC})/4-\nu_0\delta_B$
4	$\beta\alpha\alpha$	$+\frac{1}{2}$	$(-A_{AB}-A_{AC}+A_{BC})/4-\nu_0\delta_A$
5	$\beta\beta\alpha$	$-\frac{1}{2}$	$(+A_{AB}-A_{AC}-A_{BC})/4-\nu_0\delta_C$
6	$\beta\alpha\beta$	$-\frac{1}{2}$	$(-A_{AB}+A_{AC}-A_{BC})/4-\nu_0\delta_B$
7	$\alpha\beta\beta$	$-\frac{1}{2}$	$(-A_{AB}-A_{AC}+A_{BC})/4-\nu_0\delta_A$
8	$\beta\beta\beta$	$-\frac{3}{2}$	$(+A_{AB}+A_{AC}+A_{BC})/4$
			$H_{23}=H_{56}=A_{BC}/2$
			$H_{34}=H_{67}=A_{AB}/2$
			$H_{24}=H_{57}=A_{AC}/2$

the approaches mentioned. We shall separate the intensities completely from the frequencies for computational purposes. Insofar as possible within the limitation of input information this may imply, we shall, however, still calculate the chemical shifts and coupling constants from the spectrum, and not vice versa. It is not surprising that we shall sometimes find more than one satisfactory solution. What is important is that we shall always be able to find *all* of the "satisfactory" ones, including those that might be overlooked in an analysis by the iterative method.

The chief drawback of this (and some other) methods is that to apply them completely one must be able to resolve and measure most of the lines that are theoretically present. For that reason we have limited our attention to the case of three nonequivalent spin-$\frac{1}{2}$ nuclei, where this number is 15. A solution in closed form already exists for two spins[1] (four lines). Four spins give rise to 56 lines, relatively few of which are seen in proton resonance spectra. For such a system and more complicated ones the usual method of successive approximations, applied with forbearance and caution, will undoubtedly remain the most satisfactory.

The analysis is divided into three main parts. First we use the experimental frequencies to derive all the sets of energy eigenvalues that are consistent with them. This procedure depends solely on making use of the trace invariance property of the Hamiltonian. Several of these sets may be eliminated by the use of some simple sum rules for the intensities. Then all the sets of chemical shifts and coupling constants consistent with each remaining set of eigenvalues are found. We shall find that as many as 40 sets of parameters are in principle consistent with the frequencies alone. In practice, nearly all of them can be eliminated at an early stage. The ones that remain are often not even approximately related by reversal of the relative signs of certain coupling constants, as has often been assumed. These procedures and their consequences will finally be discussed in terms of several experimental examples.

DETERMINATION OF EIGENVALUES FROM FREQUENCIES[7a]

It was shown in a previous paper[3] that the 15 allowed transition frequencies for the system ABC obey certain simple regularities, resembling those found when the influence of spin coupling can be treated by first-order perturbation theory. These regularities can be conveniently discussed in the framework of the present paper in terms of the following classification of the transitions:

	A	B	C	
1	E_1-E_4	E_1-E_3	E_1-E_2	
2	E_2-E_6	E_2-E_7	E_3-E_7	
3	E_3-E_5	E_4-E_5	E_4-E_6	
4	E_7-E_8	E_6-E_8	E_5-E_8	(2a)
X	E_4-E_7	E_3-E_6	E_2-E_5.	(2b)

Here E_1 is the energy (in frequency units) of the state with total magnetic quantum number $M=+\frac{3}{2}$; E_2, E_3, and E_4 correspond to $M=+\frac{1}{2}$, etc.

The regularities mentioned are found by comparing H in the product representation appropriate to the usual first-order perturbation theory with the matrix of the eigenvalues, i.e., H in the "experimental" representation. We use the fact that the trace of H and of each of its submatrices for a given M is invariant to the unitary transformation that connects these representations. Thus it was shown[3] that

$$\nu(A_1)+\nu(B_1)+\nu(C_1)+\nu(A_4)+\nu(B_4)+\nu(C_4) = 2\nu_0(\delta_A+\delta_B+\delta_C), \quad (3)$$

where the chemical shifts are referred to whatever origin was used in measuring the frequencies of the lines. We will find it convenient to choose this origin so that both sides of (3) vanish. Then the matrix elements of (1) in the product representation take the particularly simple form given in Table I.

It is now easy, using the trace invariance property, to verify the following statements:

(a) The sum of all the line frequencies is zero. So are the sums over (2a) and (2b) separately. This fact makes it possible to find the proper origin from observed frequencies, before any eigenvalues or chemical shifts are known. (It may be shown[5] that this origin is at the center of *gravity* of the spectrum as well.)

(b) $\nu(A_1)+\nu(A_4)=\nu(A_2)+\nu(A_3)=-\nu(A_X)$, and similarly for columns B and C of (2). This property aids in the construction of a frequency table such as (2)

from the experimental lines when one or more of them is vanishingly weak or unresolved.

$$\begin{aligned}(c)\quad \nu(A_1)-\nu(A_2)&=\nu(A_3)-\nu(A_4)\\ &=\nu(C_1)-\nu(C_3)=\nu(C_2)-\nu(C_4)\\ \nu(A_1)-\nu(A_3)&=\nu(A_2)-\nu(A_4)\\ &=\nu(B_1)-\nu(B_3)=\nu(B_2)-\nu(B_4)\\ \nu(B_1)-\nu(B_2)&=\nu(B_3)-\nu(B_4)\\ &=\nu(C_1)-\nu(C_2)=\nu(C_3)-\nu(C_4).\end{aligned}$$

(This is the property of repeated spacings employed in footnote reference 2 and independently by Bernstein.[8])

(d) $E_1=E_8=(A_{AB}+A_{AC}+A_{BC})/4$. We shall call this quantity $\mathcal{E}$. (Note that this apparent peculiarity arises only because the Zeeman energies have been omitted, and the "eigenvalues" under discussion really are deviations from an "average" behavior.)

(e) Among the 64 sums $\mathfrak{S}_{ijk}\equiv\nu(A_i)+\nu(B_j)+\nu(C_k)$, $i, j, k=1, \cdots, 4$, are exactly eight values which occur only once. These fall into pairs, one member of a pair being the negative of the other. They are the sums of the repeated spacings in (c) with the eight possible permutations of sign.

(f) *One* pair of these nonrepeating values is

$$\mathfrak{S}_{111}=-\mathfrak{S}_{444}=4\mathcal{E}.$$

Of the foregoing, (a), (b), (c), and (e) are experimentally accessible criteria for gathering the observed lines into a table such as (2). Once this has been done a set of eigenvalues can be found, using (f) to determine E_1 and a comparison, line by line, with (2) to find E_2 through E_8.

Unfortunately, though not surprisingly, the construction of this table is not unique. Suppose we begin by choosing the "combination" lines A_X, B_X, and C_X. Condition (b) now dictates the classification of the remaining 12 lines into three columns, A, B, and C, but does not specify the ordering of these lines in detail. We shall call such a classification, obeying (b), a *grouping*. A grouping can always be established by making sure that $\nu(A_X)+\nu(B_X)+\nu(C_X)=0$. It is easily seen from Table I that for each of the 15 lines in the spectrum there are six ways of serially choosing two more lines to satisfy this condition. There are thus $15(6)=90$ groupings possible for a three-spin system. They include groupings that differ only by permutation of whole columns and hence by permutations of the labels A, B, C of the three nuclei. We shall say, then, that only $90/3!=15$ *independent* groupings exist. (See the discussion of acrylonitrile.)

It should be remarked that when the chemical shifts are very much larger than the relevant spin coupling constants (weak coupling), the choice of the proper independent grouping is obvious on the basis that the combination lines are weak or invisible and the others are strong and of roughly equal intensity. In strongly coupled spectra, however, the choice is by no means easy. The term "combination" line in such a case has no precise meaning, and merely reflects a particular way of thinking about the spin system in terms of an arbitrary set of basis functions.

Considering now the further criteria for establishing (2), we see that, because of (e) and (f), there is a fourfold ambiguity in the ordering of lines within columns of a grouping. That is, there are four possible *arrangements* of each grouping. We require only that (c) be satisfied and that the lines in the first and fourth rows be chosen so that the frequency sums over these rows are one pair of the nonrepeating sums of (e). Each arrangement of a grouping can be obtained from the others, without violating (c), by suitable simultaneous permutations of lines within that grouping. [Permutation of $\mathfrak{S}_{111}$ with $\mathfrak{S}_{444}$ inverts the whole table and results in reversal of the signs of all the coupling constants, according to (d) and (e). Such an inversion cannot be detected from the nuclear resonance spectrum alone.] Each of the arrangements is capable of yielding a value of $\mathcal{E}$ and hence a consistent set of eigenvalues. It would thus appear that $90(4)=360$ sets of eigenvalues are obtainable in all.

These are, however, not all independent or physically different. The energies E_2, E_3, and E_4 all correspond to the value $+\frac{1}{2}$ for the observable M, but no significance can be attached to their ordering within this triplet. All permutations of this order are, however, included among the sets of eigenvalues derived from the 360 arrangements. Since there are $(3!)^2$ permutations of this type, counting both the $M=\frac{1}{2}$ and $M=-\frac{1}{2}$ blocks of H, the number of physically distinguishable sets of eigenvalues obtainable is only $360/36=10$. This result can be obtained in another way: From the four arrangements of each of the 15 *independent* groupings one obtains 60 sets of eigenvalues. From each such set one can, however, obtain only six independent groupings, through the 3! permutations of E_2, E_3, E_4 *or* of E_5, E_6, E_7. (Simultaneous permutations of both sets do not lead to new independent groupings.) Therefore only $60/6=10$ sets of eigenvalues are of physical interest.

In principle, all 10 sets must be treated by the methods of the next section to find all the possible chemical shifts and coupling constants. In practice, as we shall see, many of them can often be ignored almost from the beginning.

In applying the foregoing rules to an actual spectral analysis, one begins by examining the spectrum for the repeated spacings required by (c). When some lines are missing or unresolved, reasonable frequencies are assumed which satisfy (c) fully. The origin is then adjusted so as to make the sum of the frequencies which are to go into (2a) vanish. A trial grouping is thus established, (b) being used to fill in the lines in (2b).

[8] H. J. Bernstein (private communication).

The 64 sums $\mathfrak{S}_{ijk}$ are now evaluated and the trial table permuted so as to satisfy (f), in turn, in each of the four ways possible under (e). A set of eigenvalues is calculated for each of these arrangements by using (f) and making a detailed comparison of the table with (2). The indices on E_2, E_3, E_4, and E_5, E_6, E_7 are then permuted and the resulting new groupings are tabulated by using (2) in reverse. Each new grouping is rearranged to obtain new sets of eigenvalues. The process is repeated until all 10 independent sets of eigenvalues have been found. This sounds like a lengthy procedure, but turns out to be relatively easy with the wisdom that comes with practice. One need deal only with the groupings that are independent. When new arrangements of old independent groupings occur they are immediately discarded, since they cannot lead to new sets of eigenvalues.

When the proper independent grouping is evident because of the weakness of spin coupling, only the four sets of eigenvalues appropriate to that grouping need be computed. In the limit of applicability of first-order perturbation theory they lead to identical chemical shifts and to sets of coupling constants that differ only in the distribution of relative signs. It is well known that in this case reversal of sign of one or more coupling constants leads to no observable change in the spectrum. When the coupling is stronger, the numerical values as well as (perhaps) the signs of the coupling constants will differ, and the chemical shifts will no longer be identical.

CALCULATION OF CHEMICAL SHIFTS AND COUPLING CONSTANTS

It is evident from Table I that all the desired parameters can be expressed in terms of the diagonal elements of H in the product representation

$$\begin{aligned}
\delta_A &= (H_7-H_4)/2\nu_0 \\
\delta_B &= (H_6-H_3)/2\nu_0 \\
\delta_C &= (H_5-H_2)/2\nu_0 \\
A_{AB} &= -(H_3+H_4+H_6+H_7) \\
A_{AC} &= -(H_2+H_4+H_5+H_7) \\
A_{BC} &= -(H_2+H_3+H_5+H_6). \qquad (4)
\end{aligned}$$

Here the double subscripts on the diagonal elements have been replaced by single ones for brevity. Evidently our problem is solved if we can find the diagonal elements of Table I from the eigenvalues. Because of the M factorization of H, it is obvious that $H_1=E_1$ and $H_8=E_8$. We need six independent relations between the remaining eigenvalues and diagonal elements in order to complete the solution of the problem.

One pair of such relations follows from trace invariance, and was the basis of our calculation of the eigenvalues,

$$\begin{aligned}
H_2+H_3+H_4 &= E_2+E_3+E_4 = -E_8 \\
H_5+H_6+H_7 &= E_5+E_6+E_7 = -E_1. \qquad (5)
\end{aligned}$$

Since H^2 is also a Hermitian operator, its trace is likewise invariant to the unitary transformation of interest. We define the quantities $W_\pm$ through

$$\begin{aligned}
H_2^2+H_3^2+H_4^2+(A_{AB}^2+A_{AC}^2+A_{BC}^2)/2 \\
= E_2^2+E_3^2+E_4^2 = W_+ \\
H_5^2+H_6^2+H_7^2+(A_{AB}^2+A_{AC}^2+A_{BC}^2)/2 \\
= E_5^2+E_6^2+E_7^2 = W_-. \qquad (6)
\end{aligned}$$

(The same relations follow from the more general invariance of

$$\sum_i \sum_j |H_{ij}|^2.)$$

Further invariants can be generated at will from higher powers of H. Of course they are not all independent. We will find it convenient to obtain the two remaining ones we need from the invariance of $\det(H)$;

$$\begin{aligned}
H_2H_3H_4 \\
+(A_{AB}A_{AC}A_{BC}-H_2A_{AB}^2-H_3A_{AC}^2-H_4A_{BC}^2)/4 \\
= E_2E_3E_4 = R_+ \\
H_5H_6H_7 \\
+(A_{AB}A_{AC}A_{BC}-H_5A_{AB}^2-H_6A_{AC}^2-H_7A_{BC}^2)/4 \\
= E_5E_6E_7 = R_-. \qquad (7)
\end{aligned}$$

The relations (5)–(7), after substitution of (4) to eliminate the coupling constants, suffice to determine the diagonal elements as desired. The algebra necessary to do this is relatively simple but very lengthy, and we shall show most of the steps in Appendix A. Here we simply give the final recipe which one uses in practice to perform the spectral analysis.

We first evaluate the expressions

$$T_\pm = W_\mp(1+\sqrt{3})/2+W_\pm(1-\sqrt{3})/2-3\mathcal{E}^2 \qquad (8)$$

$$k = (T_+/T_-)^{\frac{1}{2}} \qquad (9)$$

$$Q_\pm = \mp 4\sqrt{2}\mathcal{E}(T_\pm^{\frac{1}{2}}/T_\mp) = -k^{\pm 3}Q_\mp. \qquad (10)$$

Then, using the quantities $R_\pm$ defined in (7), we form

$$N_\pm = R_\pm - \mathcal{E}(W_\mp - 2W_\pm + 9\mathcal{E}^2)/6 \qquad (11)$$

$$P_\pm = \pm 6\sqrt{2}[(1+\sqrt{3})N_\mp + (1-\sqrt{3})N_\pm]/T_\pm^{\frac{1}{2}}. \qquad (12)$$

Now (see Appendix A) the solutions to the problem must satisfy the fourth-degree polynomial equation

$$\sum_{n=0}^{4} \beta_n \mathfrak{W}^n = 0, \qquad (13)$$

where

$$\beta_0=4[k^2P_+^2+k^{-2}P_-^2-(k+k^{-1})^2]$$
$$\beta_1=4[k^2P_+Q_-+k^{-2}P_-Q_++P_+P_-+2(k+k^{-1})]$$
$$\beta_2=k^2Q_-^2+k^{-2}Q_+^2+2(P_+Q_++P_-Q_-)+(k+k^{-1})^2-4$$
$$\beta_3=Q_+Q_--2(k+k^{-1})$$
$$\beta_4=1. \tag{14}$$

This equation may be solved exactly, e.g., by Ferrari's method, thus vindicating our description of the present method of analysis as an exact one. As a practical matter it is frequently easier to solve (13) by successive approximations.

On choosing one of the four roots of (13), we then calculate the angle ϕ defined by

$$\mathfrak{S}=-2\cos 2\phi \tag{15}$$

and the angle θ from

$$\sin 3\theta=-\frac{(Q_--Q_+)\mathfrak{S}^2+\lambda\mathfrak{S}+\mu}{4\sin\phi(k+k^{-1}-\mathfrak{S})^2}, \tag{16}$$

where

$$\lambda=2(P_+-P_-)+(k^{-2}+2k^{-1}-1)Q_+-(k^2+2k-1)Q_-$$
$$\mu=2(k^{-2}+2k^{-1}-1)P_--2(k^2+2k-1)P_+. \tag{17}$$

From θ and ϕ (principal values), we define

$$\chi=\theta-\phi; \qquad \eta=\theta+\phi. \tag{18}$$

The desired diagonal elements H_2 through H_7 are then

$$H_2=-\tfrac{1}{3}\{\mathcal{E}-[(2-\sqrt{3})T_+]^{\frac{1}{2}}\cos(\chi-\tfrac{1}{3}\pi)-[(2+\sqrt{3})T_-]^{\frac{1}{2}}\cos(\eta-\tfrac{1}{3}\pi)\}$$
$$H_3=-\tfrac{1}{3}\{\mathcal{E}+[(2-\sqrt{3})T_+]^{\frac{1}{2}}\cos\chi+[(2+\sqrt{3})T_-]^{\frac{1}{2}}\cos\eta\}$$
$$H_4=-\tfrac{1}{3}\{\mathcal{E}-[(2-\sqrt{3})T_+]^{\frac{1}{2}}\cos(\chi+\tfrac{1}{3}\pi)-[(2+\sqrt{3})T_-]^{\frac{1}{2}}\cos(\eta+\tfrac{1}{3}\pi)\}$$
$$H_5=-\tfrac{1}{3}\{\mathcal{E}+[(2+\sqrt{3})T_+]^{\frac{1}{2}}\cos(\chi-\tfrac{1}{3}\pi)+[(2-\sqrt{3})T_-]^{\frac{1}{2}}\cos(\eta-\tfrac{1}{3}\pi)\}$$
$$H_6=-\tfrac{1}{3}\{\mathcal{E}-[(2+\sqrt{3})T_+]^{\frac{1}{2}}\cos\chi-[(2-\sqrt{3})T_-]^{\frac{1}{2}}\cos\eta\}$$
$$H_7=-\tfrac{1}{3}\{\mathcal{E}+[(2+\sqrt{3})T_+]^{\frac{1}{2}}\cos(\chi+\tfrac{1}{3}\pi)+[(2-\sqrt{3})T_-]^{\frac{1}{2}}\cos(\eta+\tfrac{1}{3}\pi)\}. \tag{19}$$

The final chemical shifts then follow by (4). While they can be expressed directly in even more compact form than the diagonal elements (19), it is useful if a complete analysis is desired to calculate the diagonal elements themselves. The reason for so doing is connected with the ordering of these elements with respect to the eigenvalues from which they were derived. While, as remarked earlier, no physical significance can be attached to the ordering of the E_i themselves within 3×3 blocks of the energy matrix, it is important that the diagonal elements corresponding to the same 3×3 blocks be ordered in the same way as the eigenvalues. This is because of a magnetic noncrossing rule[9] which states in this case that the eigenvalues corresponding to a given M cannot cross as we imagine the diagonal elements to be adiabatically increased from zero to their true values. The algebra preceding (19), however, does not guarantee that this ordering will be preserved. For this reason the diagonal elements obtained in (19) must be rearranged if they are not already in the correct order. If this can be done by an identical simultaneous permutation of the indices 2, 3, 4, and 5, 6, 7 there is no effect on (4) except a relabeling of the nuclei. Mathematically, these permutations correspond to the transformations $\theta\rightarrow\theta\pm\frac{1}{3}\pi$ or $\theta\rightarrow\theta\pm\frac{2}{3}\pi$, which are permissible under (16). If such permutations are not sufficient the eigenvalues with which we started must be reassigned within 3×3 blocks; that is, a different independent grouping is chosen. The same quartic equation (13) is obtained [as is evident from the form of (5)–(7)], but the lines which "belong" to a given nucleus in the first-order perturbation limit are scrambled.

In view of the fact that a quartic equation results for each of the 10 independent sets of eigenvalues, it would appear that 40 sets of chemical shifts and coupling constants are in general consistent with a three-spin system. Because of our avoidance of any use of the experimentally measured intensities, however, it turns out that a number of these sets contain some complex parameters and are therefore spurious. It is by no means necessary to carry out the whole analysis before these are rejected. From (19) we see that in order for all the parameters to be real two conditions must be satisfied:

(i) $T_\pm>0$

(ii) χ and η are real.

Point (i) constitutes a criterion by which some groupings (and therefore some sets of eigenvalues) may be discarded early in the calculation. Point (ii) restricts the choice of roots of (13) to real ones lying in the range $-2<\mathfrak{S}<+2$.

The existence of complex solutions to the analysis problem explains the fact that sometimes, in attempting to perform a conventional iterative analysis starting from an arbitrary set of trial parameters, convergence is not obtained at all.[5] The methods employed simply do not permit the introduction of the necessary imaginary components; and the local shape of the multidimensional surface on which the iteration is performed does not lead to any improvement in the result, beyond a certain point, by varying the real parts of the parameters alone.

[9] J. Von Neumann and E. Wigner, Physik. Z. **30**, 467 (1929); see also L. D. Landau and E. M. Lifschitz, *Quantum Mechanics* (Addison-Wesley Publishing Company, Reading, Massachusetts, 1958), pp. 262–266.

Even after narrowing the choice of chemical shifts and coupling constants by the methods outlined, it is common to find more than one "acceptable" set. The choice among them must be made (when it can be made at all) by comparison of theoretical and experimental intensities. One way of doing this is to perform a conventional diagonalization and intensity calculation for each of the sets of parameters involved and to compare the results, line by line, with experiment. We shall show that there is a somewhat easier method for calculating all the intensities by using intermediate results of this analysis. More important, there exist two sets of simple sum rules for the intensities, on the basis of which some of the groupings may be eliminated before the calculations described in the present section are performed at all.

INTENSITIES

Let us denote the intensities of the transitions of Eq. (2) in the following manner:

$$\begin{array}{ccc} I_4 & I_3 & I_2 \\ I_{26} & I_{27} & I_{37} \\ I_{35} & I_{45} & I_{46} \\ I_7 & I_6 & I_5 \end{array}$$

$$I_{47} \quad I_{36} \quad I_{25}.$$

It has been shown previously that when the sum of the intensities is normalized to 12, the following relations exist[3],

$$\sum_i I_i = 3, \qquad i = 2, 3, 4;$$

$$\sum_j I_j = 3, \qquad j = 5, 6, 7;$$

$$\sum_{i,j} I_{ij} = 6. \tag{20}$$

It can now easily be shown (see Appendix B) that the following additional sum rules are obeyed

$$\sum_j I_{ij} = 1 + I_i; \qquad \sum_i I_{ij} = 1 + I_j. \tag{21}$$

Moreover, it is possible to write explicit expressions for intensities individually, in terms of the energies of the states they connect and other parameters defined in this paper:

$$I_i = 3 + \frac{6(\mathcal{E}^2 - E_i^2) + (T_+T_-)^{\frac{1}{2}}(k + k^{-1} - \mathcal{D})/4}{\prod_m (E_i - E_m)};$$

$$m \neq i = 2, 3, 4,$$

$$I_j = 3 + \frac{6(\mathcal{E}^2 - E_j^2) + (T_+T_-)^{\frac{1}{2}}(k + k^{-1} - \mathcal{D})/4}{\prod_n (E_j - E_n)};$$

$$n \neq j = 5, 6, 7,$$

$$I_{ij} = 1 + (I_i - 1)(I_j - 1)/2 + \frac{\alpha_+ E_i + \alpha_- E_j + \beta_+ E_i^2 + \beta_- E_j^2 + \delta_{ij} E_i E_j + K}{\prod_m (E_i - E_m) \prod_n (E_j - E_n)}. \tag{22}$$

The last of these contains the new quantities

$$\alpha_\pm = 4R_\mp + R_\pm + 1/2\mathcal{E}W_\mp - 9/2\mathcal{E}^3$$

$$\beta_\pm = 5\mathcal{E}^2 + (W_\pm - W_\mp)/4 - (T_+T_-)^{\frac{1}{2}}\mathcal{D}/4$$

$$\delta_{ij} = \mathcal{E}^2 + (W_+ + W_-)/2 + 2\mathcal{E}(E_i + E_j) - 3E_iE_j$$

$$K = -5\mathcal{E}^4 + 2\mathcal{E}(N_+ + N_-) + 2\mathcal{E}(R_+ + R_-) + (T_+ + T_-)^2/32 + T_+T_-/12 + [7/6\mathcal{E}^2 + (T_+ + T_-)/16](T_+T_-)^{\frac{1}{2}}\mathcal{D} - 5T_+T_-\mathcal{D}^2/96.$$

These formulas appear very complicated at first sight, but actually shorten the work of calculating the intensities appreciably, as compared with the usual method of obtaining the matrix elements of rotating magnetic moment between states defined as linear combinations of the product spin functions. Once the constants $\alpha_\pm$, $\beta_\pm$, and K are determined, only the value of δ_{ij} need be reevaluated for each line. Moreover, the chemical shifts and coupling constants are not needed; Only the value of $\mathcal{D}$ is required. (Care must be taken, however, that the eigenvalues are ordered in the same way as the diagonal elements of H; *vide supra.*).

Probably the most important application of the intensity relations lies in the use of the simple sum rules (20) and (21) as criteria by which certain of the independent groupings may be eliminated at an early stage of the analysis. In this respect they supplement conditions (i) and (ii) of the preceding section. Further, the same sum rules can be used as the basis of an averaging procedure for the experimental intensities, in much the same way as the interval rules derived earlier permit an averaging of the frequencies. These statements will be made more concrete in the following section, where they are applied to the analysis of the proton resonance spectrum of acrylonitrile.

The first two of Eqs. (22) can be solved in reverse to obtain a value of $\mathcal{D}$ from the eigenvalues and experimental intensities, without solving the fourth-degree equation (13). This matter, likewise, will be illustrated in the discussion of the acrylonitrile spectrum.

ILLUSTRATIVE APPLICATIONS

Experimental Details

The compounds studied were all commercial materials (Eastman Kodak White Label). They were distilled *in vacuo* and run as pure liquids without any reference compounds, either external or internal. No attempt was made to find out whether the spectra were temperature dependent or shifted with concentration. The apparatus and calibration procedured have been described previously.[2,3]

Experimental line positions were measured in arbitrary units. Chemical shifts and coupling constants were expressed in parts per million and cps, respectively, only after the analyses were complete. Frequencies and

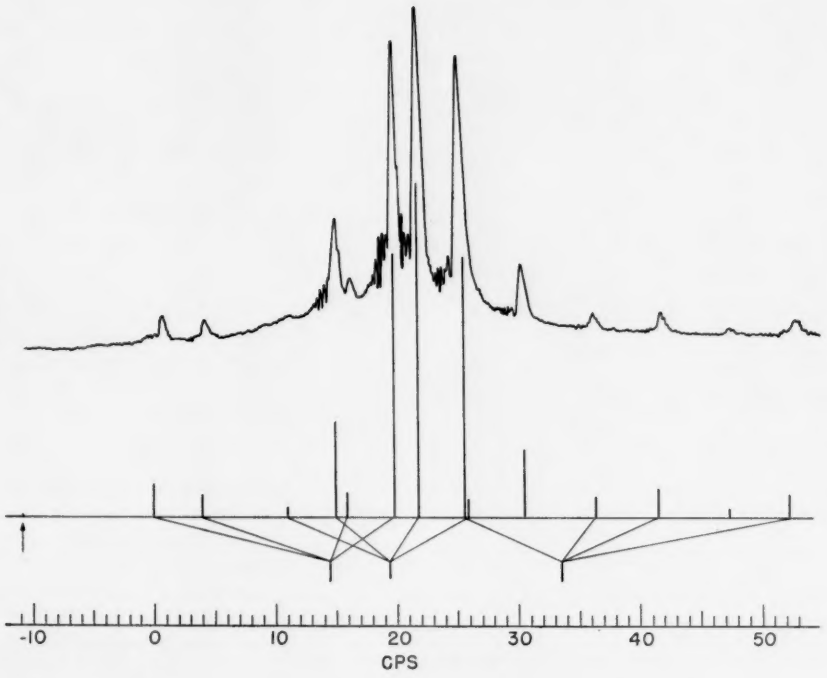

FIG. 1. Proton resonance spectrum of acrylonitrile at 40.00 Mc. The lower part of the figure is the theoretical spectrum calculated from the parameters summarized in Table IV.

intensities were averaged over about 30 spectra in each case: The scatter of individual values amounted to several tenths of a cycle in frequencies and perhaps 10% in intensities. The averaged frequencies needed to be adjusted typically by 0.01–0.02 cps to bring them into exact conformity with the requirements of preceding sections. We think that the final parameters are reliable at worst to 0.1 cps in coupling constants and 0.002 ppm in chemical shifts. We have reported them here to somewhat higher precision than is probably warranted in order that the reader may more easily reproduce our calculations.

Acrylonitrile

The analysis of this spectrum, which is shown in Fig. 1, will be discussed in some detail in order to illustrate the methods developed here.

After drawing up a spectrum which represented the averaged experimental results, a search for repeated spacings was made with a pair of dividers. When these were found, the lines were gathered, using criterion (c) given before, into the following preliminary table:

19.89	(25.74)	52.27
3.96	14.99	41.52
15.93	21.78	36.34
0.00	11.03	25.59.

The arbitrary frequency scale of Fig. 1 has been used, and the lines observed at 47.37 and 30.49 cps have been omitted as "combination" lines. The averaged experimental frequencies have been adjusted by small amounts to make the foregoing table agree exactly with spacing rule (c). The line at 25.74 was not observed, but had to be assigned that frequency in order to make the table just given internally consistent.

The sum of all of the given frequencies is 269.02 cps. In order to satisfy (a), we now choose a new origin by substracting $269.02/12=22.42$ cps from each of them. The combination lines are then filled in by using (b). The resulting arrangement is

−2.53	3.32	29.85
−18.46	−7.43	19.10
−6.49	−0.64	13.92
−22.42	−11.39	3.17
24.95	8.07	−33.02.

The lines A_x and B_x agree in frequency with the two observed lines which were omitted in the preliminary classification. The line at −33.02 cps is not observed and is presumably weak.

The arrangement given already satisfies criterion (e) for a satisfactory arrangement. Had it not done so, the necessary permutations of lines would have been performed *before* filling in the predicted combination lines. The arrangement we have corresponds, according to (f) and (d), with $A_{AB}+A_{AC}+A_{BC}=30.64$ cps, a value which is not inconsistent with previous analyses

TABLE II. Observed and calculated spectra of pure liquid acrylonitrile at 40.00 Mc. Column I of the calculated intensities corresponds to the choice $\delta_A=0.482$, $\delta_B=0.360$, $\delta_C=0.839$, $A_{AB}=1.27$, $A_{AC}=11.28$, $A_{BC}=18.10$. Column II is calculated for $\delta_A=0.441$, $\delta_B=0.420$, $\delta_C=0.820$, $A_{AB}=2.06$, $A_{AC}=21.05$, $A_{BC}=7.54$. The calculated line positions in both cases agree, of necessity, with the (averaged) experimental ones.

Position (cps)	Intensity (obs)	Intensity (calc I)	Intensity (calc II)
−10.60	...	0.016	0.007
0.00	0.281	0.319	0.193
3.96	0.164	0.231	0.165
11.02	0.062	0.092	0.314
14.99	0.940	0.955	0.987
15.93	0.245	0.243	0.246
19.89	2.910	2.618	2.431
21.78	3.351	3.330	3.240
25.59	2.808	2.589	2.493
25.74		0.180	0.409
30.49	0.579	0.655	1.116
36.34	0.168	0.205	0.032
41.52	0.253	0.281	0.047
47.37	0.073	0.083	0.158
52.22	0.168	0.202	0.160
Mean deviation	0.000 (defined)	0.054	0.158

of the proton spectra of vinyl groups. We have $\mathcal{E}=E_1=E_8=7.66$ and

$$E_2=-22.19 \qquad E_5=10.83$$
$$E_3=4.34 \qquad E_6=-3.73$$
$$E_4=10.19 \qquad E_7=-14.76.$$

Proceeding with the analysis, we find four real roots of (13), two of which lie in the specified range

$$\mathfrak{D}_{\mathrm{I}}=-0.90306; \qquad \mathfrak{D}_{\mathrm{II}}=-0.19284.$$

They lead to the following sets of parameters:

	I	II
$\nu_0\delta_A$	−8.02 cps	−4.77 cps
$\nu_0\delta_B$	−3.13	−5.62
$\nu_0\delta_C$	11.15	10.39
A_{AB}	1.27	2.06
A_{AC}	18.10	21.05
A_{BC}	11.28	7.54.

The chemical shifts are to be converted to the scale of Fig. 1 by adding 22.42 cps to each.

These parameters were calculated directly through Eq. (A15). Now, using Table I to find the diagonal elements of the Hamiltonian, we find for the two alternatives

	I	II
H_2	−18.16 cps	−17.02 cps
H_3	4.50	8.48
H_4	6.00	0.89
H_5	4.12	3.77
H_6	−1.74	−2.76
H_7	−10.03	−8.66.

The first set is already ordered in the same way as the eigenvalues listed previously, but the second is not. No simultaneous identical permutation of the indices 2, 3, 4 and 5, 6, 7 is capable of accomplishing such an ordering, and we are therefore forced to permute E_3 with E_4 without making a corresponding permutation of E_6 and E_7. The resulting new set of eigenvalues corresponds to the new independent grouping

3.32	−2.53	29.85
−18.46	−7.43	24.95
−0.64	−6.49	8.07
−22.42	−11.39	3.17
19.10	13.92	−33.02.

Note that this generation of the new grouping is not needed to find the chemical shifts and coupling constants for assignment II, and is required only if it is desired to make a line-by-line comparison (perhaps of intensities) between experiment and theory.

A decision between these two assignments can be make only through the intensities. These may be calculated conventionally or through the relations developed in the previous section and Appendix B. They are given in Table II. Evidently, while I is slightly superior to II, either one would probably have been accepted as satisfactory had it been reached by the usual iterative method in ignorance of the existence of the other. As it is, a final decision between the two should probably be made by running the spectrum in a magnetic field of strength considerably different from the 9400 gauss used here.

It may be noted that both assignments as discussed here give 30.65 cps for the sum of the coupling constants, rather than the predicted 30.64. The calculation was actually done in arbitrary (not frequency) units to a large number of significant figures. The small discrepancy arises from a later conversion of all experimental line positions to cps for purposes of this discussion.

In view of the possible existence of many more independent groupings and sets of eigenvalues, discussed earlier, it should be remarked that all of the others may be rejected in the case of acrylonitrile on the basis of the requirements that T_+ and T_- be positive and that χ and η be real.

An alternative procedure for deciding between $\mathfrak{D}_{\mathrm{I}}$ and $\mathfrak{D}_{\mathrm{II}}$ can be employed which does not require the calculation of all the chemical shifts and coupling constants for both assignments, but is based instead on the intensity relations developed in the preceding section. We begin by constructing a table of experimental intensities which corresponds, line for line, with the arrangement previously written down for the frequencies

2.910	(0.151)	0.168
0.164	0.940	0.253
0.245	3.351	0.168
0.281	0.062	(2.657)
0.073	0.579	(0.063).

The values in parentheses cannot be measured directly. either because of the near coincidence of two lines or because of lack of intensity. They can, however, be filled in by using the appropriate sum rules from the preceding section. In the present case,

$$I_5=3-I_6-I_7=2.657$$

$$I_3=2.808-I_5=0.151$$

$$I_{25}=(2+I_2+I_5-I_{35}-I_{45}-I_{26}-I_{27})/2=0.063.$$

We now use the intensities from the first and fourth rows of the intensity table to solve Eqs. (22) in reverse for $\mathfrak{M}$. In this way we find $\mathfrak{M}=-0.9895$, which agrees better with $\mathfrak{M}_{\mathrm{I}}$ than with $\mathfrak{M}_{\mathrm{II}}$.

It is to be noted that the value of $\mathfrak{M}$ calculated in this way is independent of whether the intensity table is arranged according to grouping I, as we have done, or grouping II, because the eigenvalues enter in a way that leaves the answer unaltered when E_3 and E_4 are permuted.

This procedure can, in principle, be made more accurate by making full use of the intensity rules to adjust the experimental intensities to values that are fully internally consistent, in much the same way as the line frequencies have been adjusted previously. While this procedure is of necessity somewhat involved, requiring the solution of nine quadratic equations, it in principle removes all of the ambiguity which is embodied in multiple values of $\mathfrak{M}$ when only the frequencies are used. It may be mentioned that a much simpler partial adjustment procedure, using only the first two of Eqs. (22), leads to $\mathfrak{M}=-1.02793$ and the rather good approximate parameters

$$\nu_0\delta_A=-7.71 \text{ cps} \qquad A_{AB}=1.65 \text{ cps}$$

$$\nu_0\delta_B=-3.73 \qquad A_{AC}=18.02$$

$$\nu_0\delta_C=11.45 \qquad A_{BC}=10.95.$$

Before leaving this spectrum, it is perhaps desirable to make more concrete the statement in an earlier section that there are 15 independent groupings of any three-spin spectrum which satisfy the requirements of repeated spacings. We shall do so by actually displaying all of them for the acrylonitrile spectrum shown in Fig. 1. Listing all 15 lines shown there from left to right, the grouping of Fig. 1 may be written

$$X\ B\ B\ A\ A\ B\ B\ A\ C\ A\ X\ C\ C\ X\ C,$$

where X indicates a "combination" line and the other letters identify lines supposedly associated with particular nuclei. The result obtained by interchanging all the A's with all the B's, for example, does not represent a new independent grouping. With the same conventions, the other independent groupings are

$$\begin{array}{ccccccccccccccc}
X & A & A & A & A & B & B & B & X & B & C & C & C & C & X \\
X & A & A & B & B & B & B & A & C & A & C & X & X & C & C \\
A & X & A & A & X & B & C & B & A & C & B & B & C & C & X \\
A & X & A & B & C & A & X & B & B & C & A & B & C & X & C \\
A & X & A & B & C & B & C & A & X & B & B & A & X & C & C \\
A & A & X & X & A & B & C & B & A & C & C & C & B & B & X \\
A & A & X & B & C & X & A & B & C & C & A & C & B & X & B \\
A & A & X & B & C & B & C & X & A & C & C & A & X & B & B \\
A & B & C & X & A & A & X & B & B & C & C & X & A & B & C \\
A & B & C & X & A & B & C & A & B & X & X & C & B & A & C \\
A & B & C & A & X & X & A & B & C & C & B & X & A & C & B \\
A & B & C & A & X & B & C & X & C & A & X & B & C & A & B \\
A & B & C & B & C & X & A & A & X & X & B & C & B & C & A \\
A & B & C & B & C & A & X & X & X & A & C & B & C & B & A.
\end{array}$$

No preference can be given to any one of these on the basis of line frequencies alone. The intensity sum rules given earlier can be used to reject some of them (for example, the last) unequivocally.

Acrylic Acid

For this spectrum, shown in Fig. 2, the only grouping which appears to be consistent with validity criteria (i) and (ii) and with the intensity sum rules (20) and (21) is

$$\begin{array}{ccc}
5.96 & -8.63 & -26.33 \\
13.61 & 4.01 & -13.74 \\
14.69 & 0.11 & -18.67 \\
(22.34) & 12.76 & -6.09 \\
\\
-28.30 & -4.02 & (32.41).
\end{array}$$

These frequencies are obtained from those of Fig. 2 by adding 14.69 cps to each. They are averaged experimental frequencies, but have not yet been adjusted to comply exactly with the various spacing rules. Evidently the necessary adjustments amount to an average of only 0.01-0.02 cps per line.

Forming the sums $\mathfrak{S}_{ijk}$ and choosing the arrangement that maximizes the sum of the coupling constants, we obtain the following four real roots of (13):

$$\mathfrak{M}_1=-0.85611$$

$$\mathfrak{M}_2=-1.99916$$

$$\mathfrak{M}_3=2.47229$$

$$\mathfrak{M}_4=9.88891;$$

$\mathfrak{M}_1$ and $\mathfrak{M}_2$ lead to the parameters and intensities listed in Table III. The first set clearly gives the better fit, and is assumed to be the correct one.

It has often been implicitly assumed that, once a three-spin spectrum has been grouped into three quartets, only four possible sets of chemical shifts and coupling constants exist,[9a,10] these being the ones corre-

[10] E. O. Bishop and R. E. Richards, Mol. Phys. **3**, 114 (1960).

[9(a)] H. S. Gutowsky, M. Karplus, and D. M. Grant, J. Chem. Phys. **31**, 1278 (1959), and other papers referred to there.

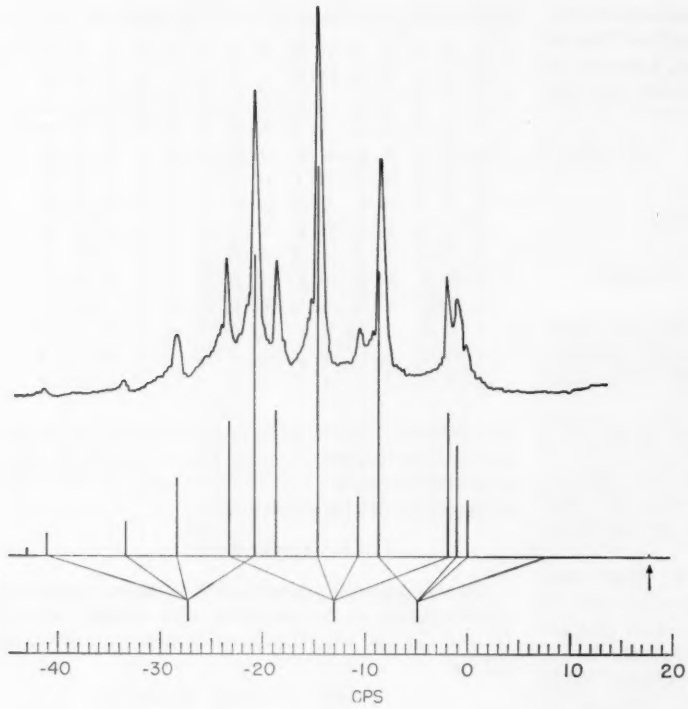

FIG. 2. Proton resonance of the vinyl group of acrylic acid. The acid proton (in the pure liquid at "room temperature") was found at −106.2 cps, a value to which very little attention should be paid.

sponding to the four possible permutations of relative sign of the coupling constants. In acrylic acid we have two quite different sets of parameters, corresponding to the same grouping of the lines, the same sum of the coupling constants, and the same arrangement of relative signs (all positive). The fact that a conventional iterative analysis could produce the correct result in this case must be ascribed to the accidental circumstance that the three repeated experimental spacings, which would be used as first approximations to the coupling constants, lie closer to the correct values than to those resulting from the use of $\mathfrak{D}_2$.

TABLE III. Observed and calculated spectra of pure liquid acrylic acid at 40.00 Mc. The first set of calculated intensities corresponds to $\delta_A=-0.120$ ppm, $\delta_B=-0.656$, $\delta_C=-0.325$, $A_{AB}=1.32$ cps, $A_{AC}=10.44$, $A_{BC}=17.24$. (See Table IV.) The second set (see text) is calculated for $\delta_A=-0.065$, $\delta_B=-0.698$, $\delta_C=-0.339$, $A_{AB}=9.63$, $A_{AC}=7.60$, $A_{BC}=11.80$.

Position (cps)	Intensity (obs)	Intensity (calc I)	Intensity (calc II)
17.70	...	0.001	0.041
8.08	...	0.005	0.337
0.00	0.381	0.382	0.367
−1.08	0.845	0.725	0.964
−1.93	1.053	0.963	0.453
−8.73	1.992	1.946	2.135
−10.68	0.416	0.414	0.291
−14.58	2.709	2.648	2.800
−18.71	0.879	0.992	0.244
−20.78	2.102	2.032	2.208
−23.32	0.946	0.913	0.568
−28.43	0.425	0.538	0.958
−33.36	0.152	0.246	0.248
−41.02	0.073	0.140	0.296
−42.99	0.027	0.052	0.089
Mean deviation	0.000 (defined)	0.056	0.234

It is interesting to note that roots such as $\mathfrak{D}_4$, which lie outside the range $(-2, \mathfrak{D}, +2)$, lead to parameters which are mathematically, if not physically, consistent with the frequencies of all the lines. On writing

$$2\phi=\pi+2i\gamma,$$

we obtain $\gamma=1.14052$. Then, putting

$$3\theta=3\pi/2+3i\delta,$$

we obtain $\delta=-0.20628$. Working out the complex values of χ and η that result, we finally have

$\nu_0\delta_A=-14.39+17.56i$ cps $\quad A_{AB}=-4.87+2.25i$ cps

$\nu_0\delta_B=-15.29 \quad A_{AC}=38.79$

$\nu_0\delta_C=-14.39-17.56i \quad A_{BC}=-4.87-2.25i.$

This is, of course, simply an illustration of the fact that adventitious, physically meaningless solutions are bound to result when the input information is arbitrarily limited to a smaller amount than is contained in the experiment—in this case, to the frequencies alone. In fact, the algebraic transformations used here

TABLE IV. Finally chosen chemical shifts and coupling constants for the compounds studied.[a] Chemical shifts are referred to the arbitrary origins of Figs. 1–4. By analogy with other studies of the vinyl group, the structural assignments are assumed to be as follows:

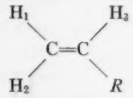

	Chemical shifts (ppm)			Coupling constants (cps)		
R	δ_1	$\delta_2-\delta_1$	$\delta_3-\delta_1$	A_{12}	A_{13}	A_{23}
—CN	0.482	−0.122	0.357	1.27	11.28	18.10
—COOH	−0.120	−0.536	−0.205	1.32	10.44	17.24
—$COOCH_3$	−0.256	−0.533	−0.302	1.76	10.18	17.16
CH_3COO—[b]	−0.100	−0.311	−2.748	1.44	6.37	13.80

[a] We do not claim that these coupling constants are accurate to 0.01 cps. See text.
[b] See footnote reference 11.

are such that the preceding complex parameters lead to the correct frequencies only if the Hamiltonian (1) is treated as symmetric, i.e., not Hermitian!

Methyl Acrylate

While we have not exhausted all the possibilities in this case, it is probable that the correct assignment is that given in Table IV, which leads to the calculated intensities shown in Fig. 3. It is to be noted that this spectrum, like that of acrylic acid, permits two different assignments corresponding to the *same* grouping and having all coupling constants positive. The second assignment involves coupling constants which are considered unreasonable for a vinyl group.

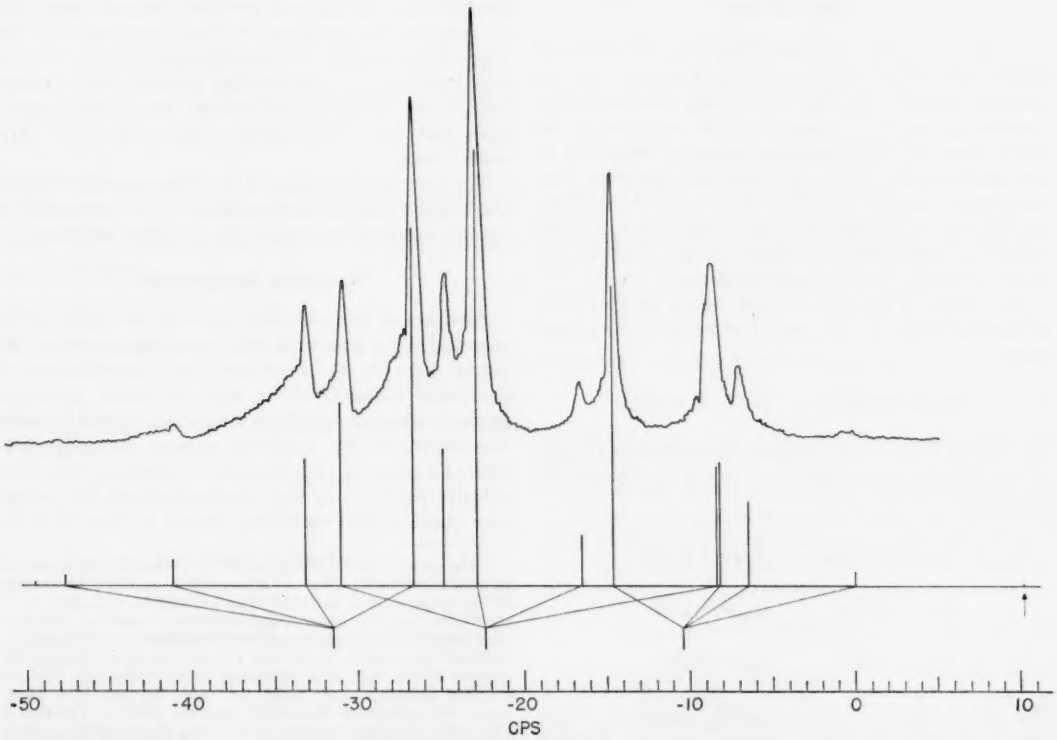

FIG. 3. Proton resonance of the vinyl group of methyl acrylate. The resonance of the methyl group is at +80.4 cps on this scale.

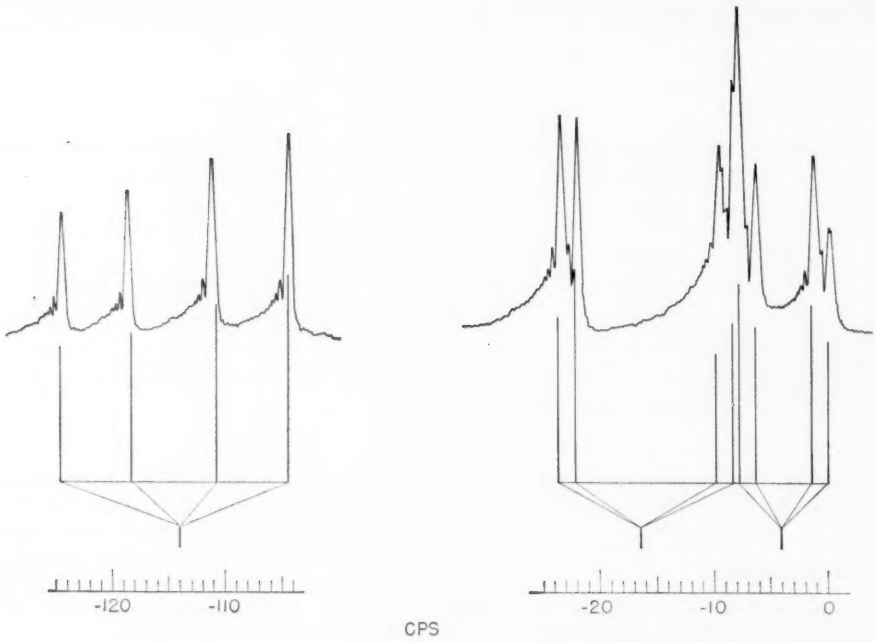

FIG. 4. Proton resonance of the vinyl group of vinyl acetate. The resonance of the methyl group is at +93.4 cps.

Vinyl Acetate

In this case, like the preceding one, we have not carried out an exhaustive analysis. Starting with the grouping indicated in Fig. 4 (the only reasonable one considering the close approach of this spectrum to the ABX type and the consequent expected weakness of the combination lines), we find the following four possibilities for the quantity $\mathfrak{S}_{111}$: ± 21.61, ± 18.65, ± 8.99, and ± 6.03 cps. The combination lines, none of which are experimentally detected, are predicted to lie at -126.59, -102.39, and 94.60 cps.

The choice of the first of these values for $\mathfrak{S}_{111}$ leads to four real roots of (13), two of which lie in the proper range

$$\mathfrak{D}_1 = -0.99576; \qquad \mathfrak{D}_2 = -0.94187.$$

The first of these yields the parameters listed in Table IV and the intensities indicated in Fig. 4. The second root gives

$$\delta_A = 0.276 \text{ ppm} \qquad A_{AB} = 1.52 \text{ cps}$$

$$\delta_B = -0.326 \qquad A_{AC} = -1.96$$

$$\delta_C = -2.832 \qquad A_{BC} = 22.05.$$

This set, besides including coupling constants which appear atypical for vinyl groups, can be rejected without explicit calculation of the intensities on other grounds, i.e., the diagonal elements obtained from (19), in order to be consistent in their ordering with the eigenvalues, require the permutation $E_6 \leftrightarrow E_7$. This in turn leads to a new independent grouping which makes two of the strong lines observed into "combination" lines and two unobservably weak ones into "first order" lines.

We have not investigated the other arrangements of the original independent grouping which correspond to smaller values of the sum of the coupling constants.[11]

Structural Assignments

Analyses of the preceding type tell us which pair of chemical shifts goes with which coupling constant, but cannot provide in themselves any identification of particular chemical shifts with particular hydrogen atoms in the molecule. Such assignments could be made experimentally by studying various partially deuterated analogs of each compound, assuming that such substitution has only very small effects on the nuclear spin states of the remaining proton system. It is far

[11] The paper by E. O. Bishop and R. E. Richards[10] which reached us as this manuscript was being completed, contains an analysis of the vinyl acetate spectrum which disagrees with ours in its conclusion that the *gem*-coupling constant is negative. Probably their result is correct and our failure to obtain it arose because, as remarked previously, we did not exhaust the possibilities of the analysis in this case. It is significant in this connection that our coupling constants agree rather well with the ones they obtain under the assumption that all of them are positive. The sum of their final coupling constants is 19.1 cps, which agrees approximately with the second largest of our possible values of $\mathfrak{S}_{111}$ (18.65 cps).

easier, and probably by now correct, to rely instead on analogies with similar compounds for which this has been done[1,10] or on theoretical predictions of the magnitudes expected for coupling constants.[9,12] By such methods it is known that the coupling constants between protons in vinyl groups tend to be about: *gem*, $\sim$0 cps; *cis*, $\sim$10 cps; *trans*, $\sim$17 cps. It is on this basis alone that the assignments of Table IV have been made.

ACKNOWLEDGMENTS

One of us (S.C.) wishes to thank the Italian Consiglio Nazionale delle Ricerche and the Montecatini Company for fellowship support during the first part of this work. We are both indebted to the National Science Foundation for a grant in support of this research.

APPENDIX A

On using (4) to eliminate the coupling constants, the first of Eqs. (6) becomes

$$W_+=\sum_{n=2}^{6}\sum_{m=2}^{6}H_n\Omega_{nm}{}^{+}H_m, \tag{A1}$$

where the transformation Ω^+ is

$$\Omega^+=(\tfrac{1}{2})\begin{vmatrix} 4 & 1 & 1 & 2 & 1 & 1 \\ 1 & 4 & 1 & 1 & 2 & 1 \\ 1 & 1 & 4 & 1 & 1 & 2 \\ 2 & 1 & 1 & 2 & 1 & 1 \\ 1 & 2 & 1 & 1 & 2 & 1 \\ 1 & 1 & 2 & 1 & 1 & 2 \end{vmatrix}. \tag{A2}$$

Here W_- is obtained in the same way. The corresponding transformation Ω^- is obtained from Ω^+ by transposing about the secondary diagonal.

Transformations Ω^+ and Ω^- are positive definite and symmetric, and can therefore be simultaneously diagonalized by a suitable choice of new variables s_i,

$$H_n=\sum\Xi_{ni}s_i. \tag{A3}$$

The procedure for finding Ξ is straightforward but tedious.[13] We ultimately obtain

$$\Xi=\tfrac{1}{6}\begin{vmatrix} -2 & [3(3-\sqrt{3})]^{\frac{1}{2}} & (3-\sqrt{3})^{\frac{1}{2}} & (3+\sqrt{3})^{\frac{1}{2}} & [3(3+\sqrt{3})]^{\frac{1}{2}} & 2\sqrt{2} \\ -2 & 0 & -2(3-\sqrt{3})^{\frac{1}{2}} & -2(3+\sqrt{3})^{\frac{1}{2}} & 0 & 2\sqrt{2} \\ -2 & -[3(3-\sqrt{3})]^{\frac{1}{2}} & (3-\sqrt{3})^{\frac{1}{2}} & (3+\sqrt{3})^{\frac{1}{2}} & -[3(3+\sqrt{3})]^{\frac{1}{2}} & 2\sqrt{2} \\ 4 & -[3(9+5\sqrt{3})]^{\frac{1}{2}} & -(9+5\sqrt{3})^{\frac{1}{2}} & -(9-5\sqrt{3})^{\frac{1}{2}} & -[3(9-5\sqrt{3})]^{\frac{1}{2}} & -\sqrt{2} \\ 4 & 0 & 2(9+5\sqrt{3})^{\frac{1}{2}} & 2(9-5\sqrt{3})^{\frac{1}{2}} & 0 & -\sqrt{2} \\ 4 & [3(9+5\sqrt{3})]^{\frac{1}{2}} & -(9+5\sqrt{3})^{\frac{1}{2}} & -(9-5\sqrt{3})^{\frac{1}{2}} & [3(9-5\sqrt{3})]^{\frac{1}{2}} & -\sqrt{2} \end{vmatrix}. \tag{A4}$$

With this transformation, Eqs. (6) become the pure quadratic forms

$$\begin{aligned} W_+&=s_2{}^2+s_3{}^2+s_4{}^2+s_5{}^2+s_6{}^2+s_7{}^2 \\ W_-&=2s_2{}^2+(2+\sqrt{3})s_3{}^2+(2+\sqrt{3})s_4{}^2+(2-\sqrt{3})s_5{}^2 \\ &\quad +(2-\sqrt{3})s_6{}^2+\tfrac{1}{2}s_7{}^2. \end{aligned} \tag{A5}$$

On combining these with (5), and using the functions $T_\pm$ defined in (8), we have

$$\begin{aligned} s_2&=-\mathcal{E} \\ s_7&=-\sqrt{2}\mathcal{E} \\ (3+\sqrt{3})(s_3{}^2+s_4{}^2)&=T_+ \\ (3-\sqrt{3})(s_5{}^2+s_6{}^2)&=T_-. \end{aligned} \tag{A6}$$

It is now convenient to make the trigonometric substitution

$$\begin{aligned} \sin^2\chi&=(3+\sqrt{3})s_3{}^2/T_+ & \cos^2\chi&=(3+\sqrt{3})s_4{}^2/T_+ \\ \sin^2\eta&=(3-\sqrt{3})s_6{}^2/T_- & \cos^2\eta&=(3-\sqrt{3})s_5{}^2/T_-. \end{aligned} \tag{A7}$$

In terms of these variables, Eqs. (7) may be written

$$\begin{aligned} \cos3\chi&=P_+-Q_-\cos(\chi-\eta)-k^{-2}\cos(\chi+2\eta) \\ &\quad -2k^{-1}\cos(2\chi+\eta) \\ \cos3\eta&=P_--Q_+\cos(\chi-\eta)-k^{2}\cos(2\chi+\eta) \\ &\quad -2k\cos(\chi+2\eta), \end{aligned} \tag{A8}$$

where $P_\pm$, $Q_\pm$, and k are the quantities defined in (9)–(12).

It is easily seen that Eqs. (A7) are satisfied by any choice of χ and η whatever; their values are determined only by Eqs. (7) in the new form (A8). Moreover, it can be verified by direct substitution that there are always six pairs (χ, η) consistent with (7),

$$\{\pm\chi_0\pm 2n\pi/3;\ \pm\eta_0\pm 2n\pi/3\},\quad n=0, 1, 2. \tag{A9}$$

These six solutions correspond to the 3! possible simultaneous identical permutations of H_2, H_3, H_4, and H_5, H_6, H_7, as discussed in an earlier section. That is, they

[12] Footnote reference 1, Chap. 8.

[13] S. Perlis, *Theory of Matrices* (Addison-Wesley Publishing Company, Reading, Massachusetts, 1956), Chap. 9.

represent the six possible ways of labeling three nuclei with the indices A, B, and C. For our purposes any one of these pairs, as long as we have no trouble with the noncrossing rule, conveys the desired information.

Now, defining the angles θ and ϕ by

$$\chi=\theta-\phi, \qquad \eta=\theta+\phi, \tag{A10}$$

and making simple rearrangements, we have

$$\begin{aligned}
&P_++P_--(Q_++Q_-)\cos2\phi\\
&\quad=[2\cos3\phi+(k^2+k^{-2}+2k+2k^{-1})\cos\phi]\cos3\theta\\
&\qquad+[(k^2-k^{-2}-2k+2k^{-1})\sin\phi]\sin3\theta,\\
&P_--P_+-(Q_+-Q_-)\cos2\phi\\
&\quad=[(k^2-k^{-2}+2k-2k^{-1})\cos3\theta\\
&+[(k^2+k^{-2}-2k-2k^{-1})\sin\phi-2\sin3\phi]\sin3\theta.
\end{aligned}\tag{A11}$$

On treating these as a pair of linear equations in $\sin3\theta$ and $\cos3\theta$, defining $\mathfrak{S}=-2\cos2\phi$, and solving by Cramer's method, we obtain Eq. (16) and

$$\cos3\theta=-\frac{(Q_-+Q_+)\mathfrak{S}^2+\lambda'\mathfrak{S}+\mu'}{4\cos\phi(k+k^{-1}-\mathfrak{S})^2}, \tag{16'}$$

where

$$\lambda'=2(P_++P_-)+(k^{-2}-2k^{-1}-1)Q_++(k^2-2k-1)Q_-$$

$$\mu'=2(k^{-2}-2k^{-1}-1)P_-+2(k^2-2k-1)P_+. \tag{17'}$$

Setting $\sin^3\!3\theta+\cos^2\!3\theta=1$ leads to the sixth-degree polynomial equation

$$\sum_{m=0}^{6}\alpha_m\mathfrak{S}^m=0, \tag{A12}$$

with

$$\begin{aligned}
\alpha_6&=1\\
\alpha_5&=Q_+Q_--4(k+k^{-1})\\
\alpha_4&=Q_+F-Q_-G+6(k+k^{-1})^2-4\\
\alpha_3&=Q_+M+Q_-L-FG-4(k+k^{-1})^3-4(k+k^{-1})-5\alpha_5\\
\alpha_2&=Q_-M+Q_+L+FL-GM+(k+k^{-1})^4-16-4\alpha_4\\
\alpha_1&=FM-GL+Q_-F-Q_+G+LM+4(k+k^{-1})^3\\
&\qquad+8(k+k^{-1})-10\alpha_5-3\alpha_3\\
\alpha_0&=(Q_++F-L)^2+(Q_--G-M)^2-4(k+k^{-1})^4,
\end{aligned}\tag{A13}$$

in which

$$\begin{aligned}
F&=k^{-2}Q_+-2kQ_-+2P_+\\
&=12\sqrt{2}T_+^{-\frac{1}{2}}[(1+\sqrt{3})R_-+(1-\sqrt{3})R_+\\
&\qquad-(W_++W_-)\mathcal{E}/3]\\
L&=Q_++F+2(k^2-1)P_+-4k^{-1}P_-\\
&=12\sqrt{2}T_+^{-1}T_-^{-1}\{(3+\sqrt{3})R_++(3-\sqrt{3})R_-\\
&\qquad-[(1+\sqrt{3})W_-+(1-\sqrt{3})W_++30\mathcal{E}^2]\mathcal{E}/6\}\\
M&=Q_--G+2(k^{-2}-1)P_--4kP_+\\
&=12\sqrt{2}T_+^{-1}T_-^{-1}\{(3-\sqrt{3})R_++(3+\sqrt{3})R_-\\
&\qquad-[(1-\sqrt{3})W_-+(1+\sqrt{3})W_++30\mathcal{E}^2]\mathcal{E}/6\}.
\end{aligned}\tag{A14}$$

It can be verified by direct substitution that $\mathfrak{S}=k+k^{-1}$ is a double root of (A12) and is adventitious since it sends both (16) and (16') to infinity. On dividing (A12) by $[\mathfrak{S}-(k+k^{-1})]^2$, we obtain (13) and (14). Tracing back through the series of substitutions (15), (16), (18), (A7), (8), and (A6), we obtain the values of the variables s_i. Application of (A4) then gives the diagonal elements (19). Explicit use of (4) results in the chemical shifts and coupling constants themselves:

$$\begin{aligned}
\nu_0\delta_A&=6^{-\frac{1}{2}}[-T_+^{\frac{1}{2}}\cos(\chi+\tfrac{1}{3}\pi)-T_-^{\frac{1}{2}}\cos(\eta+\tfrac{1}{3}\pi)]\\
\nu_0\delta_B&=6^{-\frac{1}{2}}[T_+^{\frac{1}{2}}\cos\chi+T_-^{\frac{1}{2}}\cos\eta]\\
\nu_0\delta_C&=6^{-\frac{1}{2}}[-T_+^{\frac{1}{2}}\cos(\chi-\tfrac{1}{3}\pi)-T_-^{\frac{1}{2}}\cos(\eta-\tfrac{1}{3}\pi)]\\
A_{AB}&=\tfrac{1}{3}[4\mathcal{E}-(2T_+)^{\frac{1}{2}}\cos(\chi-\tfrac{1}{3}\pi)+(2T_-)^{\frac{1}{2}}\cos(\eta-\tfrac{1}{3}\pi)].\\
A_{AC}&=\tfrac{1}{3}[4\mathcal{E}+(2T_+)^{\frac{1}{2}}\cos\chi-(2T_-)^{\frac{1}{2}}\cos\eta]\\
A_{BC}&=\tfrac{1}{3}[4\mathcal{E}-(2T_+)^{\frac{1}{2}}\cos(\chi+\tfrac{1}{3}\pi)+(2T_-)^{\frac{1}{2}}\cos(\eta+\tfrac{1}{3}\pi)]
\end{aligned}\tag{A15}$$

APPENDIX B

Let the orthogonal normalized eigenfunctions ϕ_i for the interacting spin system be written in terms of product spin functions u_n as follows,

$$\phi_i=\sum_n a_{in}u_n. \tag{B1}$$

The intensity of the transition between ϕ_1 and ϕ_2 is then proportional to a quantity I_2 which may be written

$$I_2=(a_{22}+a_{23}+a_{24})^2=1+2(a_{22}a_{23}+a_{23}a_{24}+a_{24}a_{22}), \tag{B2}$$

with similar relations for I_3, $\cdots$, I_7. The first two of Eqs. (20) follow immediately by summing over the appropriate indices, and the remaining member of (20) is obtained by difference.

Now consider the transitions connecting eigenstates ϕ_2, ϕ_3, ϕ_4 ($M=\frac{1}{2}$) with ϕ_5, ϕ_6, ϕ_7 ($M=-\frac{1}{2}$). On expanding as before in product functions, we obtain, for

example,

$$I_{25}=[a_{22}(a_{56}+a_{57})+a_{23}(a_{55}+a_{57})+a_{24}(a_{55}+a_{56})]^2$$
$$=a_{22}^2(a_{56}^2+a_{57}^2+2a_{56}a_{57})+a_{23}^2(a_{55}^2+a_{57}^2+2a_{55}a_{57})$$
$$+a_{24}^2(a_{55}^2+a_{56}^2+2a_{55}a_{56})+2(a_{22}a_{23}+a_{23}a_{24}+a_{24}a_{22})$$
$$\times(a_{55}a_{56}+a_{56}a_{57}+a_{57}a_{55})+2a_{22}a_{23}a_{57}^2+2a_{23}a_{24}a_{55}^2$$
$$+2a_{24}a_{22}a_{56}^2$$
$$=1+(I_2-1)(I_5-1)/2-a_{22}^2a_{55}^2-a_{23}^2a_{56}^2-a_{24}^2a_{57}^2$$
$$+2a_{56}a_{57}a_{22}^2+2a_{55}a_{57}a_{23}^2+2a_{55}a_{56}a_{24}^2+2a_{22}a_{23}a_{57}^2$$
$$+2a_{23}a_{24}a_{55}^2+2a_{24}a_{22}a_{56}^2.$$

On proceeding in the same way with I_{26} and I_{27}, and combining the three results, we obtain

$$\sum_j I_{2j}=I_{25}+I_{26}+I_{27}=3+2(a_{22}a_{23}+a_{23}a_{24}+a_{24}a_{22})$$
$$-(a_{22}^2+a_{23}^2+a_{24}^2)$$
$$=1+I_2.$$

This result, and the other similar ones obtained in the same way, is summarized by (21).

To derive the explicit expressions (22) for the intensities, we begin by writing down the simultaneous equations which must be satisfied by the eigenvalues and the coefficients a_{in}. We will find it convenient to abandon the normalization condition for the moment, and will denote the unnormalized coefficients of the product spin functions by c_{in}. The eigenvalue E_2 must satisfy

$$c_{22}(H_2-E_2)+c_{23}(A_{BC}/2)+c_{24}(A_{AC}/2)=0$$
$$c_{22}(A_{BC}/2)+c_{23}(H_3-E_2)+c_{24}(A_{AB}/2)=0$$
$$c_{22}(A_{AC}/2)+c_{23}(A_{AB}/2)+c_{24}(H_4-E_2)=0. \qquad \text{(B3)}$$

By setting c_{22} temporarily equal to unity, we can thus obtain three relations for c_{23} and $c_{3'}$. By performing various manipulations on these, it is possible to obtain

$$c_{22}^2+c_{23}^2+c_{24}^2=\frac{\prod_m(E_2-E_m)}{(H_3-E_2)(H_4-E_2)-A_{AB}^2/4}, \quad m=3, 4.$$

On reinstating the normalization condition, we obtain

$$a_{22}^2=\frac{(H_3-E_2)(H_4-E_2)-A_{AB}^2/4}{\prod_m(E_2-E_m)}$$
$$a_{23}^2=\frac{(H_2-E_2)(H_4-E_2)-A_{AC}^2/4}{\prod_m(E_2-E_m)}$$
$$a_{24}^2=\frac{(H_2-E_2)(H_3-E_2)-A_{BC}^2/4}{\prod_m(E_2-E_m)}. \qquad \text{(B4)}$$

Similar expressions are easily obtained for the components of ϕ_3 through ϕ_7.

Consider now products of the type $a_{22}a_{23}$. From (B4) we have

$$a_{22}a_{23}=\frac{\{[(H_3-E_2)(H_2-E_2)(H_4-E_2)-(H_2-E_2)A_{AB}^2/4-(H_3-E_2)A_{AC}^2/4](H_4-E_2)+A_{AB}^2A_{AC}^2/16\}^{\frac{1}{2}}}{\prod_m(E_2-E_m)}.$$

Now, remembering that

$$(H_3-E_2)(H_2-E_2)(H_4-E_2)-(H_2-E_2)A_{AB}^2/4-(H_3-E_2)A_{AC}^2/4-(H_4-E_2)A_{BC}^2/4+A_{AB}A_{AC}A_{BC}/4=0,$$

we obtain

$$a_{22}a_{23}=\frac{A_{AB}A_{AC}/4-(H_4-E_2)A_{BC}/2}{\prod_m(E_2-E_m)} \qquad \text{(B5)}$$

and similar relations for $a_{22}a_{24}$ and $a_{23}a_{24}$ involving permutations of spin coupling constants and diagonal elements of H. On substituting (B5) and (B4) into (B2) and related formulas, we ultimately obtain Eqs. (22) after a good deal of manipulation.

THE JOURNAL OF CHEMICAL PHYSICS VOLUME 34, NUMBER 1 JANUARY, 1961

Absorption Spectrum and Magnetic Properties of Osmium Hexafluoride

J. C. EISENSTEIN

National Bureau of Standards, Washington, D. C.

(Received April 22, 1960)

This paper is devoted to a discussion of the optical absorption spectrum and the susceptibility of OsF_6. It is assumed that two $5d$ electrons, which move in a ligand field of octahedral symmetry, are responsible for the magnetic and optical properties of the molecule. The calculated positions of the energy levels depend on the strength of the ligand field, the Coulomb integrals and the spin-orbit coupling constant. These quantities are treated as parameters. If they are given appropriate values, excellent agreement with observed energy level positions is obtained. The calculated susceptibility is also in good agreement with experimental values. In order to fit the magnetic data it is necessary to assume that the orbital reduction factor is approximately 0.7.

1. INTRODUCTION

BOTH magnetic and spectroscopic data on OsF_6 are now available. The absorption spectrum between 250 and 1500 cm^{-1} has been observed by Weinstock, Claassen, and Malm[1]; the absorption spectrum between 3800 and 42 000 cm^{-1} has been observed by Moffitt, Goodman, Fred, and Weinstock.[2] The magnetic susceptibility has been measured between 81.5 and 297°K by Hargreaves and Peacock[3] and by Lewis. The first theoretical work on OsF_6 was done by Moffitt *et al.*[2] who calculated the energy levels and showed that satisfactory agreement between theory and experiment could be achieved. The theory given in the present paper takes into account more physical factors than were considered by Moffitt *et al.*; in addition, the susceptibility as well as the spectrum is considered in detail.

The OsF_6 molecule has predominantly octahedral symmetry. It is one of twelve hexafluorides for which the symmetry has been established by analysis of their Raman and infrared vibrational spectra. For some of these hexafluorides electron diffraction data are also available which confirm the octahedral structure. In the ground state of OsF_6 there may be small deviations from perfect octahedral symmetry because of the requirements of the Jahn-Teller theorem. In fact, Weinstock, Claassen, and Malm[1] state that the distinctive behavior of the vibrational frequency σ_2 and its binary combination bands in OsF_6 is probably a consequence of the Jahn-Teller effect.

The model of the OsF_6 molecule which will be used here is that of an Os^{6+} ion at the center of a regular octahedron at whose vertices lie six F^- ions. There is a strong possibility that the bonding is partially covalent instead of strictly ionic. The $5d$, $6s$, and $6p$ orbitals of the osmium ion can be hybridized to form six equivalent bonding orbitals which extend toward the corners of the octahedron, where they can overlap suitably hydridized fluorine orbitals.

The electrons in the bonding orbitals together with the fluorine ions give rise to a ligand field which can be assumed to have octahedral symmetry. Two electrons are left over in d orbitals on the Os^{6+} core. Their motion is perturbed by the ligand field. More generally, one can say that the two remaining electrons occupy antibonding molecular orbitals whose character is predominantly that of osmium $6d$ atomic orbitals. These two electrons are responsible for the magnetic properties and the optical absorption spectrum.

2. INTERACTION MATRICES

The problem of two d electrons in an octahedral field has been discussed frequently in the literature. The wave functions are most conveniently classified in terms of the irreducible representation of the cubic group for which they form a basis. The one-electron wave functions γ_1, γ_2, ϵ_1, ϵ_2, ϵ_3 (Bethe's notation) which span the representations e and t_2 (Mulliken's notation) can be multiplied together and linear combinations of the products can be selected which form bases for the following product representations: $e\times e=A_1+A_2+E$, $e\times t_2=T_1+T_2$, $t_2\times t_2=A_1+E+T_1+T_2$. When the orbital functions are multiplied by the possible spin functions the products can be classified as singlets or triplets. The zero-order wave functions used here will be designated by the multiplicity, the orbital representation, the one-electron orbital functions, and the over-all representation in that order. For example, $|{}^3T_1\epsilon^2T_2\rangle$, denotes a wave function which is a product of two one-electron functions which belong to the representation t_2. It is a triplet function; the orbital and the over-all representations are T_1 and T_2, respectively.

After the zero-point two-electron wave functions with appropriate symmetry and transformation properties have been formed, the matrix elements of the various interactions can be calculated. The Coulomb interaction does not connect singlets with triplets, and does not connect states which belong to different orbital representations. The spin-orbit interaction does

[1] B. Weinstock, H. H. Claassen, and J. G. Malm, J. Chem. Phys. **32**, 181 (1960).
[2] W. Moffitt, G. L. Goodman, M. Fred, and B. Weinstock, Mol. Phys. **2**, 109 (1959).
[3] G. B. Hargreaves and R. D. Peacock, Proc. Chem. Soc. **1959**, 85.

TABLE I. Experimental and calculated energy levels for OsF_6.

Experimental position of peak (cm^{-1})	Tentative identification	Location calculated by Moffitt *et al.* (cm^{-1})	Location calculated here (cm^{-1})
0	$^3T_1\epsilon^2E$	0	0
<250	$^3T_1\epsilon^2T_2$	0	122
3936	?		
4316	$^3T_1\epsilon^2T_1$	~3900	4305
4371	$^3T_1\epsilon^2A_1$	~4270	4327
4587	$(^3T_1\epsilon^2T_1+\sigma_4)$		(4584)
4815	$(^3T_1\epsilon^2T_1+\sigma_4+\sigma_6)$		(4814)
	$(^3T_1\epsilon^2T_1+2\sigma_5)$		(4820)
5013	$(^3T_1\epsilon^2A_1+\sigma_2)$		(5003)
	$(^3T_1\epsilon^2T_1+\sigma_3)$		(5036)
5092	$(^3T_1\epsilon^2A_1+\sigma_3)$		(5091)
	$(^3T_1\epsilon^2A_1+\sigma_1)$		(5104)
5750	$(^3T_1\epsilon^2T_1+2\sigma_3)$		(5756)
8163	?		
8482	$^1T_2\epsilon^2T_2$	~8170	8670
?	$^1E\epsilon^2E$		8826
9090	$(^1T_2\epsilon^2T_2+\sigma_2)$		(9114)
9488	$(^1T_2\epsilon^2T_2+\sigma_1+\sigma_4)$		(9483)
9996	$(^1T_2\epsilon^2T_2+2\sigma_2+\sigma_5)$		(9998)
16892	?		
17301	$^1A_1\epsilon^2A_1$	~16300	17383
17778	$(^1A_1\epsilon^2A_1+\sigma_5+\sigma_6$		(17783)
35700	$^3T_2$ (av)		35737
40800	$^3T_1$ (av)		40744

not connect states which belong to different over-all representations. The ligand field has only diagonal matrix elements.

If the spin-orbit interaction is neglected, the most complicated equation one has to solve in order to find the energy levels is quadratic. Consequently spin-orbit interaction has usually been neglected in papers dealing with two-electron ions in crystal fields. For the iron group compounds the Racah[4] parameters B and C, in terms of which the Coulomb matrix elements can be expressed, are larger than the spin-orbit coupling constant. Therefore, for this group, the neglect of spin-orbit interaction is conceivably justifiable. For the $4d$ and $5d$ compounds a complete calculation is required in which no approximations are made which involve the relative magnitudes of the ligand field, the Coulomb interactions and the spin-orbit interaction.

Liehr and Ballhausen[5] have calculated all the matrix elements and have given the fully reduced interaction matrices for two d electrons in an octahedral field. Their work will be generalized for the purposes of the present paper. Here the effects of covalent bonding on the Racah parameters and on the spin-orbit coupling constant will be taken into account in the interaction matrices. One can argue that the radial functions may not be the same for the e and the t_2 orbitals since they are inequivalent in the ligand field. Therefore the matrix elements should show this lack of equivalence.

We take account of this covalent (or inequivalence) effect by replacing the Racah parameters B, C by

TABLE II. First-order perturbation calculation of changes in energy levels induced by changes in the parameters.

	ΔV	ΔA_0	ΔA_2	ΔA_4	ΔB_0	ΔB_1	ΔB_2	ΔB_4	ΔC_0	ΔC_2	ΔC_4	$\Delta\zeta$	$\Delta\zeta'$
$^3T_1\epsilon^2E$	0	0	0	0	0	0	0	0	0	0	0	0	0
$^3T_1\epsilon^2T_2$	−0.004	0.004	−0.004	0.000	−0.054	0.253	0.014	0.000	−0.012	0.007	0.000	0.013	0.071
$^3T_1\epsilon^2T_1$	−0.011	0.011	−0.011	0.000	−0.571	0.619	0.025	0.000	−0.172	0.002	0.000	1.346	0.321
$^3T_1\epsilon^2A_1$	−0.015	0.016	−0.016	0.001	1.401	1.273	−0.057	0.005	0.493	−0.046	0.002	0.756	0.375
$^1T_2\epsilon^2T_2$	−0.008	0.007	−0.007	0.000	4.906	0.739	0.019	0.000	1.648	0.001	0.000	1.193	0.202
$^1E\epsilon^2E$	−0.013	0.013	−0.014	0.000	4.866	1.303	−0.096	0	1.644	0	0.001	1.209	0.274
$^1A_1\epsilon^2A_1$	0.006	−0.001	−0.004	0.005	12.234	0.656	−0.580	0.043	4.076	−0.331	0.021	1.927	0.232
$^3T_{2\gamma\epsilon}$(mean)	0.980	−0.977	0.973	0.003	4.380	1.345	−6.994	−0.016	−0.168	0.036	0.002	0.529	0.481
$^3T_{1\gamma\epsilon}$(mean)	0.980	−0.979	0.977	0.002	4.409	1.610	2.886	0.001	−0.161	0.392	0.004	0.684	0.412

[4] G. Racah, Phys. Rev. **62**, 438 (1942).
[5] A. D. Liehr and C. J. Ballhausen, Ann. Phys. **6**, 134 (1959).

B_i, C_i. The subscript i refers to the number of e radial wave functions contained in the Coulomb integral. Since the Racah parameter A is also affected by possible inequivalence of the radial wave functions it must be introduced explicitly into the interaction matrices. The spin-orbit coupling constant will be denoted by ζ if two t_2 orbitals are involved in calculating a matrix element and by ζ' if one t_2 and one e orbital are involved. There are no matrix elements of the spin-orbit interaction between two e orbitals. V will denote the amount an e orbital is raised over a t_2 orbital in the ligand field.

Evaluation of the matrix elements leads to the following five interaction matrices. There is one matrix for each of the five representations to which a complete wave function can belong.

$$
\begin{array}{c}
\begin{array}{cccc}
|\,^1A_1\epsilon^2A_1\rangle & |\,^1A_1\gamma^2A_1\rangle & |\,^3T_1\epsilon^2A_1\rangle & |\,^3T_1\gamma\epsilon A_1\rangle
\end{array} \\
\begin{pmatrix}
A_0+10B_0+5C_0 & 6^{\frac{1}{2}}(2B_2+C_2) & -2^{\frac{1}{2}}\zeta & +2^{\frac{1}{2}}\zeta' \\
 & 2V+A_4+8B_4+4C_4 & 0 & 3^{\frac{1}{2}}\zeta' \\
 & & A_0-5B_0+\zeta & -6B_1+\zeta' \\
 & & & V+A_2+4B_2-\tfrac{1}{2}\zeta
\end{pmatrix}
\end{array}
$$

$$
\begin{array}{c}
|\,^3T_2\gamma\epsilon A_2\rangle \\
(V+A_2-8B_2-\tfrac{1}{2}\zeta)
\end{array}
$$

$$
\begin{array}{c}
\begin{array}{ccccc}
|\,^1E\epsilon^2E\rangle & |\,^1E\gamma^2E\rangle & |\,^3T_1\epsilon^2E\rangle & |\,^3T_1\gamma\epsilon E\rangle & |\,^3T_2\gamma\epsilon E\rangle
\end{array} \\
\begin{pmatrix}
A_0+B_0+2C_0 & 2(3^{\frac{1}{2}})B_2 & \tfrac{1}{2}(2^{\frac{1}{2}})\zeta & 2^{\frac{1}{2}}\zeta' & 0 \\
 & 2V+A_4+2C_4 & 0 & -\tfrac{1}{2}(6^{\frac{1}{2}})\zeta' & \tfrac{1}{2}(6^{\frac{1}{2}})\zeta' \\
 & & A_0-5B_0-\tfrac{1}{2}\zeta & -6B_1-\tfrac{1}{2}\zeta' & \tfrac{3}{2}\zeta' \\
 & & & V+A_2+4B_2+\tfrac{1}{4}\zeta & \tfrac{3}{4}\zeta \\
 & & & & V+A_2-8B_2+\tfrac{1}{4}\zeta
\end{pmatrix}
\end{array}
$$

$$
\begin{array}{c}
\begin{array}{cccc}
|\,^1T_1\gamma\epsilon T_1\rangle & |\,^3T_1\epsilon^2T_1\rangle & |\,^3T_1\gamma\epsilon T_1\rangle & |\,^3T_2\gamma\epsilon T_1\rangle
\end{array} \\
\begin{pmatrix}
V+A_2+4B_2+2C_2 & \tfrac{1}{2}(2^{\frac{1}{2}})\zeta' & \tfrac{1}{4}(2^{\frac{1}{2}})\zeta & -\tfrac{1}{4}(6^{\frac{1}{2}})\zeta \\
 & A_0-5B_0+\tfrac{1}{2}\zeta & -6B_1+\tfrac{1}{2}\zeta' & -\tfrac{1}{2}(3^{\frac{1}{2}})\zeta' \\
 & & V+A_2+4B_2-\tfrac{1}{4}\zeta & -\tfrac{1}{4}(3^{\frac{1}{2}})\zeta \\
 & & & V+A_2-8B_2+\tfrac{1}{4}\zeta
\end{pmatrix}
\end{array}
$$

$$
\begin{array}{c}
\begin{array}{cccccc}
|\,^3A_2\gamma^2T_2\rangle & |\,^3T_1\epsilon^2T_2\rangle & |\,^3T_1\gamma\epsilon T_2\rangle & |\,^1T_2\epsilon^2T_2\rangle & |\,^1T_2\gamma\epsilon T_2\rangle & |\,^3T_2\gamma\epsilon T_2\rangle
\end{array} \\
\begin{pmatrix}
2V+A_4-8B_4 & 0 & 0 & 0 & -\zeta' & -\sqrt{2}\zeta' \\
 & A_0-5B_0-\tfrac{1}{2}\zeta & -6B_1-\tfrac{1}{2}\zeta' & \tfrac{1}{2}(2^{\frac{1}{2}})\zeta & -\tfrac{1}{2}(6^{\frac{1}{2}})\zeta' & -\tfrac{1}{2}(3^{\frac{1}{2}})\zeta' \\
 & & V+A_2+4B_2+\tfrac{1}{4}\zeta & -\tfrac{1}{2}(2^{\frac{1}{2}})\zeta' & \tfrac{1}{4}(6^{\frac{1}{2}})\zeta' & -\tfrac{1}{4}(3^{\frac{1}{2}})\zeta \\
 & & & A_0+B_0+2C_0 & 2(3^{\frac{1}{2}})B_1 & \tfrac{1}{2}(6^{\frac{1}{2}})\zeta' \\
 & & & & V+A_2+2C_2 & -\tfrac{1}{4}(2^{\frac{1}{2}})\zeta \\
 & & & & & V+A_2-8B_2-\tfrac{1}{4}\zeta
\end{pmatrix}
\end{array}
$$

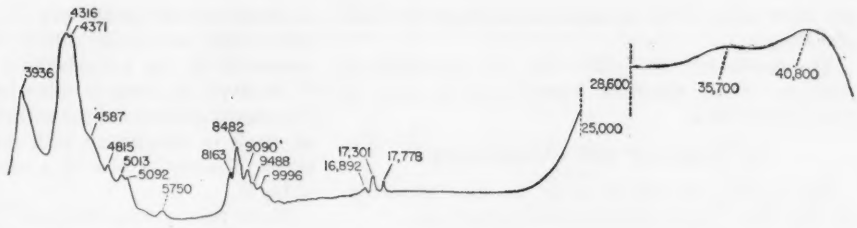

FIG. 1. Optical absorption spectrum of OsF_6.

The matrices agree with those given by Liehr and Ballhausen if one sets $A_i=A$, $B_i=B$, $C_i=C$, $\zeta'=\zeta=2\lambda$, if one introduces the Racah parameters into their matrices in place of the Condon and Shortley F_i integrals, and if the phases of the wave functions are suitably altered.

Eigenvalues and eigenvectors of these matrices were calculated on the IBM 704 machine at the National Bureau of Standards. After each calculation with a particular set of parameters V, ζ, A_i, B_i, C_i the results were compared with the known absorption spectrum. One or more of the parameters was then changed and another calculation made. The results of the final calculation are given in column four of Table I, and are discussed in Sec. 4.

3. OPTICAL ABSORPTION SPECTRUM

The optical absorption spectrum obtained by Moffitt *et al.*[2] is shown in Fig. 1. Six or seven of the peaks probably correspond to electronic transitions; the rest must be ascribed to vibrational fine structure. The vibrational frequencies in the ground state, according to Weinstock, Claassen, and Malm,[1] are as follows: σ_1 733 cm^{-1}, σ_2 632 cm^{-1}, σ_3 720 cm^{-1}, σ_4 268 cm^{-1}, σ_5 252 cm^{-1}, σ_6 230 cm^{-1}. The evidence that the σ_6 frequency is 230 cm^{-1} is not very strong.

Identification of the peaks in the optical absorption spectrum has to be attempted, but is subject to considerable uncertainty. Some highly tentative suggestions regarding the identification are contained in Table I. In columns two and four of this table the peaks ascribed to vibrational fine structure are distinguished by being placed in parentheses. For these peaks the "calculated" locations are the sums of the experimental positions ascribed to the purely electronic transitions and the vibrational energies given above.

The peak at 3936 cm^{-1} is a "hot" peak[6]; that is, it is due to transitions from the vibrationally excited ground state. The first observed peak which may be due to a purely electronic transition is that at 4316 cm^{-1}. It is possible that the small separation between this peak and the next at 4371 cm^{-1} is a manifestation of a Jahn-Teller splitting of the ground state. At present there is no other evidence to support this interpretation. It will be assumed here that the peaks at 4316 cm^{-1} and 4371 cm^{-1} are due to purely electronic transitions to the $^3T_1\epsilon^2T_1$ and $^3T_1\epsilon^2A_1$ states, respectively. However, these two states lie so close to one another that small changes in the parameters suffice to invert their order.

The $^1T_2\epsilon^2T_2$ and $^1E\epsilon^2E$ states also lie close to one another; the latter is slightly higher in energy. The two peaks are probably not resolved in the experimental spectrum; this point is discussed more fully in the following section. We shall assume that the experimental position of the $^1T_2\epsilon^2T_2$ level is 8482 cm^{-1}.

The peak at 17 301 cm^{-1} is probably due to transitions from the ground state to $^1A_1\epsilon^2A_1$.

The three peaks in the spectrum whose identification is most obscure all lie about 400 cm^{-1} below peaks identified here as due to purely electronic transitions. One of these peaks is definitely known to be a hot peak; it seems quite possible that the other two are also hot peaks.

The strongest conclusion one can draw from Table I is that plausible assignments of nearly all the absorption peaks below 20 000 cm^{-1} can be made. The frequencies which have to be assigned to the vibrational modes in the electronically excited states are, in all cases, very near the frequencies for the vibrational modes in the ground electronic state. The frequencies should be nearly the same for all these states because, in all of them, the charge distribution is approximately the same. In all the states below 20 000 cm^{-1} both electrons are predominantly in t_2 orbitals.

The two peaks at 35 700 and 40 800 cm^{-1} are considerably broader and much more intense than the lower energy peaks. Because of their breadth and intensity perhaps they should be ascribed to charge transfer transitions. If they are charge transfer transitions there is no very reliable way to calculate the energy at which they should occur.

Another possibility is that these two peaks are due to transitions to $^3T_2\gamma\epsilon$ and $^3T_1\gamma\epsilon$ states, respectively. There are four of each, belonging to four different over-all representations. The energy spread (if off-diagonal elements of the interaction matrices are neglected) of the $^3T_2\gamma\epsilon$ and the $^3T_1\gamma\epsilon$ states is $3\zeta/4$. Another factor, responsible in part for the width, is the change of the charge distribution which accompanies the transition (from ϵ^2 to $\gamma\epsilon$). One might expect this change to be accompanied by extensive vibrational structure. It is

[6] G. L. Goodman (private communication). Before I received this information from Dr. Goodman I had tentatively classified this peak as a "hot" peak because detailed calculations made it seem unlikely that the splitting of the $^3T_1\epsilon^2T_1$ and $^3T_1\epsilon^2A_1$ states could be as large as 380 cm^{-1}.

not observed for OsF_6 but seems to be present for ReF_6 and PtF_6.

To summarize, we shall take the experimental positions of the electronic levels to be as given in Table I, column 2.

4. VALUES OF THE PARAMETERS

The parameters which occur in the interaction matrices have been assigned the following values:

$$V=34\,540\ \text{cm}^{-1}$$
$$A_0=A_2=A_4 \qquad \text{(arbitrary)}$$
$$B_i=400\ \text{cm}^{-1} \qquad (i=0,\ 1,\ 2,\ 4)$$
$$C_i=1493\ \text{cm}^{-1} \qquad (i=0,\ 2,\ 4)$$
$$\zeta=3200\ \text{cm}^{-1}$$
$$\zeta'=1900\ \text{cm}^{-1}.$$

The calculated positions of the energy levels are then as given in Table I, column 4. The rms deviation of the calculated $^3T_1\epsilon^2T_1$, $^3T_1\epsilon^2A_1$, $^1T_2\epsilon^2T_2$, $^1A_1\epsilon^2A_1$, $^3T_2\gamma\epsilon$ (mean), and $^3T_1\gamma\epsilon$ (mean) energy levels from their experimentally observed positions, as given in the preceding section, is 90 cm^{-1}.

A problem which arises in connection with the interpretation of the spectrum given here is whether, by a different choice of the parameters, one could interpret the spectrum in a substantially different way. If off-diagonal matrix elements are omitted from the calculation, the lowest-lying energy levels are as follows:

$^3T_1\epsilon^2E$ and $^3T_1\epsilon^2T_2$	0
$^3T_1\epsilon^2T_1$	ζ
$^3T_1\epsilon^2A_1$	$3\zeta/2$
$^1T_2\epsilon^2T_2$ and $^1E\epsilon^2E$	$6B_0+2C_0+\frac{1}{2}\zeta$
$^1A_1\epsilon^2A_1$	$15B_0+5C_0+\frac{1}{2}\zeta$
$^3T_2\gamma\epsilon$ (mean)	$V-(A_0-A_2)-8B_2+5B_0+\frac{1}{2}\zeta$
$^3T_1\gamma\epsilon$ (mean)	$V-(A_0-A_2)+4B_2+5B_0+\frac{1}{2}\zeta$.

The identification of $^3T_1\epsilon^2T_1$ and $^3T_1\epsilon^2A_1$ with the peaks near 4000 cm^{-1}, of $^1T_2\epsilon^2T_2$ and $^1E\epsilon^2E$ with the peaks near 8500 cm^{-1}, of $^1A_1\epsilon^2A_1$ with the peaks near 17 000 cm^{-1}, of $^3T_2\gamma\epsilon$ with the peak at 35 700 cm^{-1}, and of $^3T_1\gamma\epsilon$ with the peak at 40 800 cm^{-1} follow almost automatically. No rearrangement of these assignments seems possible. Furthermore, one obtains immediately approximate values for the parameters. We have, for example, $\zeta\sim2800\ \text{cm}^{-1}$, $3B_0+C_0\sim3500\ \text{cm}^{-1}$, $B_2\sim400\ \text{cm}^{-1}$ and $V-(A_0-A_2)\sim35\,000\ \text{cm}^{-1}$.

For the purpose of discussing the finer details of the identification of the absorption peaks and the choice of the parameters it is useful to make a first-order perturbation calculation of the effect on the energy levels of changes in the parameters. If the changes are small a first-order calculation suffices because, of the levels connected by the perturbations, only the $^3T_2\gamma\epsilon$ and $^3T_1\gamma\epsilon$ levels lie closer to other levels than 8000 cm^{-1}. The matrix elements of the perturbations will therefore be small in comparison with the separations of the states. The results of such a calculation are given in Table II.

These results were originally used to exclude the possibility of identifying the levels $^3T_1\epsilon^2T_1$ and $^3T_1\epsilon^2A_1$ with the absorption peaks at 3936 and 4316 cm^{-1}. One can easily see from Table II that unreasonable changes in the parameters are required to make this identification.

One also sees from Table II that the separation of $^1T_2\epsilon^2T_2$ and $^1E\epsilon^2E$ can be substantially increased only by a very large increase in B_1. Therefore it seems quite unlikely that the separation of these two levels is even as large as the 319 cm^{-1} difference between the experimental absorption peaks at 8163 and 8482 cm^{-1}.

Furthermore one sees from Table II that $^3T_1\epsilon^2E$ is without a doubt the ground state, provided the ligand field is predominantly octahedral. No reasonable changes in the parameters will make the $^3T_1\epsilon^2T_2$ state lower. It is possible that a trigonal or tetragonal distortion of the fluorine octahedron would push the $^3T_1\epsilon^2T_2$ state below the $^3T_1\epsilon^2T$ state but the distortion would evidently have to be quite large. There is some evidence for such a distortion in the ReF_6 spectrum[7] but it is difficult to assess its magnitude.

We shall now consider the limits of possible variation of the parameters. We note first that the values of B_4 and C_4 are nearly irrelevant as far as the energy levels below 40 800 cm^{-1} are concerned. Their largest effect is on $^1A_1\epsilon^2A_1$ which is shifted only a few tens of wave numbers by a 100% change in B_4 or C_4. B_4 and C_4 therefore cannot be determined from the absorption spectrum.

Very little is known about the value of the Racah parameter A. Let us assume that A_0 has a value of approximately 20 000 cm^{-1}, although this figure is probably a substantial overestimate. A change in A_0 of 5000 cm^{-1} will shift $^3T_1\epsilon^2A_1$ by 78 cm^{-1} and the other levels below 30 000 cm^{-1} by less. A change of 5000 cm^{-1} in A_2 will have a maximum effect of 81 cm^{-1}, a change in A_4 of 5000 cm^{-1} will have a maximum effect of 26 cm^{-1}. It follows that the values of A_0, A_2, and A_4 cannot be reliably determined from the positions of the levels below 30 000 cm^{-1}. The quantity which can be determined from the experimental positions of the $^3T_2\gamma\epsilon$ and $^3T_1\gamma\epsilon$ levels is $V-(A_0-A_2)$. One sees from the perturbation calculations that changes in A_4 have very little effect on the positions of these levels, and that one cannot distinguish with certainty between the effect of increasing A_0-A_2 and the effect of decreasing V. Consequently we might as well assume that $A_0=$

[7] J. C. Eisenstein, J. Chem. Phys. **33**, 1530 (1960).

TABLE III. Matrix elements of L_z+2S_z between the E and T_2 states.

	$^1E\epsilon^2E$	$^1E\gamma^2E$	$^3T_1\epsilon^2E$	$^3T_1\gamma\epsilon E$	$^3T_2\gamma\epsilon E$
$^3A_2\gamma^2T_2$	0	0	0	0	$i2(6k_\gamma k_\epsilon)^{\frac{1}{2}}/3$
$^3T_1\epsilon^2T_2$	0	0	$i(2-k_\epsilon)$	$-i(k_\gamma k_\epsilon)^{\frac{1}{2}}$	$i(k_\gamma k_\epsilon)^{\frac{1}{2}}$
$^3T_1\gamma\epsilon T_2$	0	0	$-i(k_\gamma k_\epsilon)^{\frac{1}{2}}$	$i(2+\frac{1}{2}k_\epsilon)$	$ik_\epsilon/2$
$^1T_2\epsilon^2T_2$	$-i2k_\epsilon$	0	0	0	0
$^1T_2\gamma\epsilon T_2$	0	$-i2(k_\gamma k_\epsilon)^{\frac{1}{2}}$	0	0	0
$^3T_2\gamma\epsilon T_2$	0	0	$-i(3k_\gamma k_\epsilon)^{\frac{1}{2}}$	$-i\sqrt{3}k_\epsilon/2$	$-i(2-\frac{1}{2}k_\epsilon)/\sqrt{3}$

TABLE IV. Matrix elements of L_z+2S_z between the T_2 and T_2 states.

	$^3A_2\gamma^2T_2$	$^3T_1\epsilon^2T_2$	$^3T_1\gamma\epsilon T_2$	$^1T_2\epsilon^2T_2$	$^1T_2\gamma\epsilon T_2$	$^3T_2\gamma\epsilon T_2$
$^3A_2\gamma^2T_2$	2	0	0	0	0	$-(2k_\gamma k_\epsilon)^{\frac{1}{2}}$
$^3T_1\epsilon^2T_2$	0	$-1+\frac{1}{2}k_\epsilon$	$(k_\gamma k_\epsilon)^{\frac{1}{2}}/2$	0	0	$-(3k_\gamma k_\epsilon)^{\frac{1}{2}}/2$
$^3T_1\gamma\epsilon T_2$	0	$(k_\gamma k_\epsilon)^{\frac{1}{2}}/2$	$-1-\frac{1}{4}k_\epsilon$	0	0	$-\sqrt{3}k_\epsilon/4$
$^1T_2\epsilon^2T_2$	0	0	0	k_ϵ	$(3k_\gamma k_\epsilon)^{\frac{1}{2}}$	0
$^1T_2\gamma\epsilon T_2$	0	0	0	$(3k_\gamma k_\epsilon)^{\frac{1}{2}}$	$\frac{1}{2}k_\epsilon$	0
$^3T_2\gamma\epsilon T_2$	$-(2k_\gamma k_\epsilon)^{\frac{1}{2}}$	$-(3k_\gamma k_\epsilon)^{\frac{1}{2}}/2$	$-\sqrt{3}k_\epsilon/4$	0	0	$1+\frac{1}{4}k_\epsilon$

$A_2=A_4$; in this case the A's drop out of the energy level calculations.

The absorption peaks at 35 700 and 40 800 cm^{-1} are so broad that the positions of the corresponding energy levels cannot be accurately determined. The consequent uncertainty in the value of V is probably 500 to 1000 cm^{-1}. The separation of these peaks depends principally on B_2 and, according to Table I, is 9.88 B_2. An uncertainty of about 80 cm^{-1} in the value of B_2 is another consequence of the breadth of the absorption peaks.

The remaining parameters—B_0, B_1, C_0, C_2, ζ, and ζ'—cannot be very precisely determined because of their mutual dependence. For example, if B_0 is changed by ± 100 and C_0 is simultaneously changed by ∓ 300 the calculated spectrum is not significantly altered. Similarly, simultaneous changes of B_1 by ± 100 cm^{-1} and of ζ by ∓ 100 cm^{-1} are not incompatible with the interpretation of the experimental spectrum. Finally the values of ζ and ζ' could be brought closer together by dropping ζ to 3100 cm^{-1}, say, and raising ζ' to 2400 cm^{-1}.

5. SUSCEPTIBILITY OF OsF_6

The susceptibility of OsF_6 may depend on two factors which cannot be determined from the optical absorption spectrum in the gaseous state. In the first place, the ground state in the octahedral field has twofold orbital degeneracy. According to the Jahn-Teller theorem the molecule should spontaneously distort so as to remove the degeneracy. The first excited state, which has an intrinsic moment, and which is also coupled to the ground state by the magnetic moment operator, is about 120 cm^{-1} above the ground state according to the preceding calculations. If the Jahn-Teller splitting of the ground state is not small in comparison with 120 cm^{-1} this splitting will have an appreciable effect on the susceptibility. Secondly, the molecular solid OsF_6, on which susceptibility measurements have been made, is not magnetically dilute.[8] Exchange interaction effects will therefore probably exist. They are, in fact, known to exist[9] in K_2IrCl_6 and $(NH_4)_2IrCl_6$.

In the following calculation of the susceptibility both these effects will be ignored since existing magnetic data are not sufficiently accurate and do not extend to sufficiently low temperatures to warrant their inclusion. Even with this simplification the calculation of the susceptibility is rather lengthy. Since the ground state is nonmagnetic, but is coupled to low-lying states by the magnetic moment operator, the usual simple formulas for the susceptibility cannot be used. It is necessary to use Eq. (16) on page 191 of Van Vleck's[10] book.

In calculating the matrix elements for the magnetic moment operator, orbital reduction will be allowed for. The orbital reduction factors will be written as $(k_\gamma)^{\frac{1}{2}}$ and $(k_\epsilon)^{\frac{1}{2}}$ for γ and ϵ orbitals, respectively. The matrix

[8] There is a very interesting possibility that at low temperatures OsF_6 really is magnetically dilute. This possibility arises because the ground state is nonmagnetic and the first excited state (which has a permanent moment) has only a small occupation.

[9] J. H. E. Griffiths, J. Owen, J. G. Park, and M. F. Partridge, Proc. Roy. Soc. (London) **A250,** 84 (1959); A. H. Cooke, R. Lazenby, F. R. McKim, J. Owen, and W. P. Wolf, *ibid.* **A250,** 97 (1959); B. R. Judd, *ibid.* **A250,** 110 (1959).

[10] J. H. Van Vleck, *The Theory of Electric and Magnetic Susceptibilities* (Oxford University Press, New York, 1932).

TABLE V. Matrix elements of L_z+2S_z between the T_2 and T_1 states.

	$^3A_2\gamma^2T_2$	$^3T_1\epsilon^2T_2$	$^3T_1\gamma\epsilon T_2$	$^1T_2\epsilon^2T_2$	$^1T_2\gamma\epsilon T_2$	$^3T_2\gamma\epsilon T_2$
$^1T_1\gamma\epsilon T_1$	0	0	0	$-(k_\gamma k_\epsilon)^{\frac{1}{2}}$	$-\sqrt{3}k_\epsilon/2$	0
$^3T_1\epsilon^2T_1$	0	$1+\frac{1}{2}k_\epsilon$	$(k_\gamma k_\epsilon)^{\frac{1}{2}}/2$	0	0	$-(3k_\gamma k_\epsilon)^{\frac{1}{2}}/2$
$^3T_1\gamma\epsilon T_1$	0	$(k_\gamma k_\epsilon)^{\frac{1}{2}}/2$	$1-\frac{1}{4}k_\epsilon$	0	0	$-\sqrt{3}k_\epsilon/4$
$^3T_2\gamma\epsilon T_1$	$-(2k_\gamma k_\epsilon)^{\frac{1}{2}}$	$(3k_\gamma k_\epsilon)^{\frac{1}{2}}/2$	$\sqrt{3}k_\epsilon/4$	0	0	$1-\frac{1}{4}k_\epsilon$

TABLE VI. Matrix elements of L_z+2S_z between the T_2 and A_2 states.

	$^3A_2\gamma^2T_2$	$^3T_1\epsilon^2T_2$	$^3T_1\gamma\epsilon T_2$	$^1T_2\epsilon^2T_2$	$^1T_2\gamma\epsilon T_2$	$^3T_2\gamma\epsilon T_2$
$^3T_2\gamma\epsilon A_2$	$i2(k_\gamma k_\epsilon/3)^{\frac{1}{2}}$	$-i(2k_\gamma k_\epsilon)^{\frac{1}{2}}$	$-ik_\epsilon/\sqrt{2}$	0	0	$i(4-k_\epsilon)/\sqrt{6}$

TABLE VII. Matrix elements of L_z+2S_z between the T_1 and T_1 states.

	$^1T_1\gamma\epsilon T_1$	$^3T_1\epsilon^2T_1$	$^3T_1\gamma\epsilon T_1$	$^3T_2\gamma\epsilon T_1$
$^1T_1\gamma\epsilon T_1$	$\frac{1}{2}k_\epsilon$	0	0	0
$^3T_1\epsilon^2T_1$	0	$1-\frac{1}{2}k_\epsilon$	$-(k_\gamma k_\epsilon)^{\frac{1}{2}}$	$-(3k_\gamma k_\epsilon)^{\frac{1}{2}}/2$
$^3T_1\gamma\epsilon T_1$	0	$-(k_\gamma k_\epsilon)^{\frac{1}{2}}/2$	$1+\frac{1}{4}k_\epsilon$	$-\sqrt{3}k_\epsilon/4$
$^3T_2\gamma\epsilon T_1$	0	$-(3k_\gamma k_\epsilon)^{\frac{1}{2}}/2$	$-\sqrt{3}k_\epsilon/4$	$-1-\frac{1}{4}k_\epsilon$

TABLE VIII. Matrix elements of L_z and $2S_z$ between the T_1 and A_1 states.

	$^1A_1\epsilon^2A_1$	$^1A_1\gamma^2A_1$	$^3T_1\epsilon^2A_1$	$^3T_1\gamma\epsilon A_1$
$^1T_1\gamma\epsilon^2T_1$	$-i2(6k_\gamma k_\epsilon)^{\frac{1}{2}}/3$	$i2(k_\gamma k_\epsilon)^{\frac{1}{2}}$	0	0
$^3T_1\epsilon^2T_1$	0	0	$i(6^{\frac{1}{2}})(2+k_\epsilon)/3$	$i(6k_\gamma k_\epsilon)^{\frac{1}{2}}/3$
$^3T_1\gamma\epsilon T_1$	0	0	$i(6k_\gamma k_\epsilon)^{\frac{1}{2}}/3$	$i(4-k_\epsilon)/\sqrt{6}$
$^3T_2\gamma\epsilon T_1$	0	0	$-i(2k_\gamma k_\epsilon)^{\frac{1}{2}}$	$-ik_\epsilon/\sqrt{2}$

TABLE IX. Matrix elements of L_z+2S_z between the E and T_1 states.

	$^1E\epsilon^2E$	$^1E\gamma^2E$	$^3T_1\epsilon^2E$	$^3T_1\gamma\epsilon E$	$^3T_2\gamma\epsilon E$
$^1T_1\gamma\epsilon T_1$	$-i4(k_\gamma k_\epsilon/3)^{\frac{1}{2}}$	$-i2(k_\gamma k_\epsilon)^{\frac{1}{2}}$	0	0	0
$^3T_1\epsilon^2T_1$	0	0	$-i(2+k_\epsilon)/\sqrt{3}$	$-i(k_\gamma k_\epsilon/3)^{\frac{1}{2}}$	$-i(3k_\gamma k_\epsilon)^{\frac{1}{2}}$
$^3T_1\gamma\epsilon T_1$	0	0	$-i(k_\gamma k_\epsilon/3)^{\frac{1}{2}}$	$-i\sqrt{3}(4-k_\epsilon)/6$	$-i\sqrt{3}k_\epsilon/2$
$^3T_2\gamma\epsilon T_1$	0	0	$i(k_\gamma k_\epsilon)^{\frac{1}{2}}$	$ik_\epsilon/2$	$i(4+k_\epsilon)/2$

TABLE X. Calculated susceptibility of OsF_6 at various temperatures for selected values of the orbital reduction factors. The numbers given in the table are $10^6\,\chi_M$.

k_γ	k_ϵ	300°K	250°K	200°K	150°K	100°K	50°K
1.0	1.0	331.3	361.7	402.6	458.8	530.3	569.3
0.7	0.7	617.4	707.4	834.0	1020.0	1296.4	1595.9
0.5	0.5	923.5	1075.4	1290.8	1612.4	2106.0	2691.5
1.0	0.49	876.5	1017.2	1215.4	1508.8	1951.1	2451.1

elements are given in Tables III through IX. The introduction at this point of the orbital reduction factors does not affect the energy levels as previously calculated. By using Racah parameters and a spin-orbit coupling constant which can differ from their free-ion values we have explicitly taken account in the interaction matrices, of the electron wandering effect which is also responsible for the orbital reduction in the magnetic moment operator.

When the eigenvalues and eigenvectors corresponding to the parameters of the preceding section are inserted into Van Vleck's equation one obtains the following expression for the susceptibility of OsF_6:

$$\chi=(0.75046/T\Sigma)\{0.823+0.197(k_\gamma k_\epsilon)^{\frac{1}{2}}-0.964k_\epsilon$$
$$+0.012k_\gamma k_\epsilon-0.115(k_\gamma k_\epsilon)^{\frac{1}{2}}k_\epsilon+0.283k_\epsilon^2\}$$
$$\times\exp(-175.39/T)+(0.52162/121.91\Sigma)$$
$$\times\{3.329-1.270(k_\gamma k_\epsilon)^{\frac{1}{2}}-3.922k_\epsilon+0.121k_\gamma k_\epsilon$$
$$+0.748(k_\gamma k_\epsilon)^{\frac{1}{2}}k_\epsilon+1.156k_\epsilon^2\}\{1-\exp(-175.39/T)\}$$
$$+(0.52162\times10^{-4}/\Sigma)\{3.183-0.508(k_\gamma k_\epsilon)^{\frac{1}{2}}+3.140k_\epsilon$$
$$+1.422k_\gamma k_\epsilon-0.248(k_\gamma k_\epsilon)^{\frac{1}{2}}k_\epsilon+0.787k_\epsilon^2\}$$
$$+(0.52162\times10^{-4}/\Sigma)\{2.286-0.129(k_\gamma k_\epsilon)^{\frac{1}{2}}+2.252k_\epsilon$$
$$+1.137k_\gamma k_\epsilon+0.043(k_\gamma k_\epsilon)^{\frac{1}{2}}k_\epsilon+0.567k_\epsilon^2\}$$
$$\times\exp(-175.39/T),$$

where

$$\Sigma=2+3\exp(-175.39/T).$$

The first term here is due to diagonal matrix elements of the magnetic moment operator; the second term is due to matrix elements of the magnetic moment operator between the ground state and the first excited state; the third term is the Van Vleck high-frequency term corresponding to virtual transitions from the ground state; and the fourth term is the Van Vleck high-frequency term corresponding to virtual transitions from the first excited state.

This expression for the susceptibility has been evaluated for a few values of the orbital reduction factors. The results of the calculations are given in Table X; some of the results are plotted in Fig. 2. There is very good agreement between calculated and experimental values of the susceptibility provided k_ϵ is sufficiently small (about 0.5). Such a value implies that the magnetic electrons are about equally likely to be found on the Os^{6+} ion, and on the six F^- ions. The calculated susceptibility is not as sensitive to changes in k_γ as to changes in k_ϵ.

This value of k_ϵ may seem unreasonable since it is smaller than values of the orbital reduction factor generally quoted in the literature. For example,

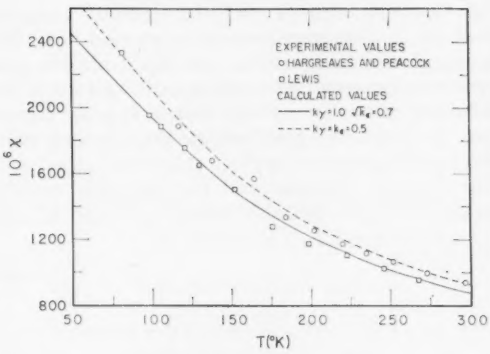

FIG. 2. Susceptibility of OsF_6 as a function of the temperature. The data are taken from footnote reference 3.

Griffiths and Owen[11] give values 0.66 and 0.74 for k_ϵ in ammonium chloroiridate. In this compound the separation[9] of the Ir^{6+} and the Cl^- ions is 2.47 A. The separation[1] of the Os^{6+} and the F^- ions in OsF_6 is only 1.83 A. The overlap of the osmium and the fluorine orbitals is consequently probably greater than the corresponding overlap in the chloroiridates so the smaller value of k_ϵ is not, after all, unreasonable.

6. MICROWAVE RESONANCE

The g value, which in this case is the diagonal matrix element of L_z+2S_z in the lowest magnetic state of the molecule, can readily be deduced from Table IV. If one uses the eigenvector for this state corresponding to the values of the parameters previously introduced, one obtains

$$g=-0.907+0.532k_\epsilon-0.109(k_\gamma k_\epsilon)^{\frac{1}{2}}.$$

It seems unlikely that resonance will be observed in OsF_6. In experiments by Hutchison and Weinstock[12] on the NpF_6 molecule the resonance signal was only two or three times noise at 20°K. Failure to observe resonance at higher temperatures is possibly associated with rotation of the molecule. The problem is discussed in a recent paper by Eisenstein and Pryce.[13] At 20° only about one OsF_6 molecule in 4000 is in the lowest state which has a magnetic moment.

7. CONCLUSION

The optical absorption spectrum and the magnetic properties of OsF_6 have been discussed on the basis of a simple model for the molecule. It has been shown that very satisfactory agreement between calculated and observed energy levels can be achieved provided the parameters of the theory are suitably chosen. These parameters are the strength of the ligand field,

[11] J. H. E. Griffiths and J. Owen, Proc. Roy. Soc. (London) **A226**, 96 (1954).
[12] C. A. Hutchison, Jr. and B. Weinstock, J. Chem. Phys. **32**, 56 (1960).
[13] J. C. Eisenstein and M. H. L. Pryce, Proc. Roy. Soc. (London) **A255**, 181 (1960).

the Coulomb integrals, and the spin-orbit coupling constant. If these same parameters are used in a calculation of the susceptibility, one again obtains good agreement between theory and experiment if the orbital reduction factors are suitably chosen. It is not claimed that the parameters used here are the only ones which will lead to agreement between theory and experiment. The Coulomb integrals and the spin-orbit coupling factors chosen are probably correct to within 25%; the strength of the ligand field is probably not off by more than 10%.

ACKNOWLEDGMENTS

Miss Irene Stegun and Miss Ruth Zucker coded the secular equations for the IBM 704 machine and obtained the eigenvalues and eigenvectors. I am indebted to Dr. G. L. Goodman for valuable comments on a preliminary version of this paper.

THE JOURNAL OF CHEMICAL PHYSICS VOLUME 34, NUMBER 1 JANUARY, 1961

Paramagnetism of Uranyl Ion. Effect of 6*d* Orbitals and Pi Bonding*

R. LINN BELFORD

Noyes Chemical Laboratory, University of Illinois, Urbana, Illinois

(Received June 1, 1960)

Second-order perturbation calculations of the paramagnetism of OUO^{++} ion were done. The contribution from pi bonds may be considerable. Although a bonding scheme utilizing only the 6*d* and 7*s* orbitals of U could account for experimental values, some involvement of 5*f* orbitals is suggested. There is no clear-cut evidence for strong involvement of 5*f* orbitals in bonds.

THE possible electronic structure of the linear OUO^{++} ion has been the subject of some speculation.[1-4] Visible and ultraviolet spectra, chemical behavior, ion entropy, and magnetic susceptibility have been considered as evidence. At least two groups of workers[5,6] measured the molar susceptibility of uranyl salts and found a paramagnetic contribution, after correction for diamagnetism, of about 100×10^{-6} cm^3 $mole^{-1}$. Freed and Kasper report the susceptibility to be nearly temperature independent. This fact suggests that the paramagnetic contribution is due to magnetic interactions which mix excited states into the zero-field ground state of the uranyl ion.[7] Eisenstein and Pryce[1] noted that the order of magnitude of the susceptibility can be accounted for by the assumption of a strongly covalent two-electron oxygen-$5f_\sigma$-oxygen sigma bond, whose electrons are paramagnetic because of mixing with $5f_{\pm1}$ orbitals (which are not supposed to be involved in strong π bonds). They suggested a 50% participtaion of the $5f_\sigma$ orbital in the bond and a $(\sigma)^2(5f_{\pm1})^0\rightarrow(\sigma)^1(5f_{\pm1})^1$ transition frequency of about 40 000 cm^{-1}. They presumed a smaller participation of the $6d_\sigma$ orbital in a sigma bond and a higher $(d\sigma)^2\rightarrow(d\sigma)^1(6d_{\pm1})^1$ transition energy. Thus the *d* bond—principally by presumption—was supposed to be less important than the *f* bond.

In light of the orbital overlap integral calculations by Coulson and Lester[4] and by Belford and Belford,[8] which indicate that the 5*f* uranium orbitals do not overlap much with the oxygen orbitals but that the 6*d* orbitals do, and in view of the fairly small energy of separation of the 6*d* and 5*f* levels,[4,9] we suggest that the uranium 6*d* orbitals might be more strongly involved in both pi and sigma bonds than the 5*f* orbitals are in either.

The aim of this paper is to extend the straightforward perturbation calculation of temperature-independent paramagnetism to the cases in which *d* and *f* pi-type bonds are important in the linear OMO molecule or ion, and to apply the results to the OUO^{++} ion in particular. Eisenstein and Pryce had noted that pi bonding would affect the details of their calculation.

CALCULATION

(1) The formula of Van Vleck[7] was used:

$$\chi_{nq}=2\mu_0N_0\beta^2\mid\langle n\mid\sum_j l_{qj}\mid 0\rangle\mid^2/3\bar{h}^2\Delta_{0n},\qquad(1)$$

where χ_{nq} is the (additive) contribution (for the bulk

* This work was supported by a grant from the National Science Foundation.

[1] J. C. Eisenstein and M. H. L. Pryce, Proc. Roy. Soc. (London) **A229,** 20 (1955).

[2] S. McGlynn, presentation at the Symposium on Molecular Spectra, American Chemical Society, Cleveland, 1960.

[3] R. E. Connick and Z. Z. Hugus, Jr., J. Am. Chem. Soc. **74,** 6012 (1952).

[4] C. A. Coulson and G. R. Lester, J. Chem. Soc., **1956,** 3650.

[5] S. Freed and C. Kasper, J. Am. Chem. Soc. **52,** 4671 (1930).

[6] R. W. Lawrence, J. Am. Chem. Soc. **56,** 776 (1934).

[7] J. H. Van Vleck, *Theory of Electric and Magnetic Susceptibilities* (Oxford University Press, New York, 1932).

[8] R. L. Bedford and G. Belford, (unpublished).

[9] I. Borovskii and R. Barinskii, Izvest. Akad. Nauk S.S.S.R., Ser. Fiz. **15,** 225 (1951).

molar susceptibility of a randomly oriented sample) of the nth excited molecular state for the coordinate q ($q=x, y, z$), μ_0 is the magnetic permeability of empty space, N_0 is Avogadro's number, β is the Bohr magneton, Δ_{0n} is the excitation energy from 0 to n, and l_{qj} is the orbital momentum operator for electron j about q. Only a few excited states expected to be relatively low-lying were considered. It is hoped that our simple representation of the ground and these excited state wave functions are sufficiently good and that the perturbation series converge sufficiently rapidly so that extreme errors were not introduced from these sources. (Our hope may be in vain, but this shall be the subject of a later paper. In any case, we do not now intend to improve this treatment for a system as complicated as OUO^{++} ion.)

(2) We used the sums-of-determinants wave functions for 12 electrons, constructed from one-electron LCAO-MO's, with spin function α or β. The LCAO-MO's were constructed from six oxygen orbitals (three from each O) and 11 central ion orbitals (d_0, $d_{\pm1}$, $d_{\pm2}$, f_0, $f_{\pm1}$, $f_{\pm2}$, s). Certain criteria diminished some of the work:

(a) The ground state is a spin singlet; the only excited states giving nonzero matrix elements with it are also spin singlets.

TABLE I. Molecular orbitals of OUO^{++}.

Index j	Name	ψ_j
1	σsd	$[C_1(sd)+(p_0'-p_0'')/\sqrt{2}]/[1+2C_1S_1+C_1^2]^{0.5}$
2	σf	$[C_2f_0+(1-C_2^2)^{0.5}(p_0'+p_0'')/\sqrt{2}]$
3, 4	πd	$[C_3d_{\pm1}+(p_{\pm1}'+p_{\pm1}'')/\sqrt{2}]/[1+2C_3S_3+C_3^2]^{0.5}$
5, 6	πf	$[C_4f_{\pm1}+(1-C_4^2)^{0.5}(p_{\pm1}'-p_{\pm1}'')/\sqrt{2}]$
11	$\sigma^* sd$	$[(sd)-C_5(p_0'-p_0'')/\sqrt{2}]/[1-2C_5S_1+C_5^2]^{0.5}$
12	$\sigma^* f$	$[(1-C_2^2)^{0.5}f_0-C_2(p_0'+p_0'')/\sqrt{2}]$
13, 14	$\pi^* d$	$[d_{\pm1}-C_6(p_{\pm1}'+p_{\pm1}'')/\sqrt{2}]/[1-2C_6S_3+C_6^2]^{0.5}$
15, 16	$\pi^* f$	$[(1-C_4^2)^{0.5}f_{\pm1}-C_4(p_{\pm1}'-p_{\pm1}'')/\sqrt{2}]$
7, 8	$\delta^n d$	$d_{\pm2}$ (nonbonding)
9, 10	$\delta^n f$	$f_{\pm2}$ (nonbonding)
17	$\delta^n sd$	$[(1-\nu^2)^{0.5}d_0-\nu s]$ (nonbonding)

Relationships:

$S_1 \equiv \langle sd \mid (p_0'-p_0'')/\sqrt{2}\rangle$

$S_3 \equiv \langle d_1 \mid (p_1'+p_1'')/\sqrt{2}\rangle$

$C_5 = (C_1+S_1)/(1+C_1S_1)$

$C_6 = (C_3+S_3)/(1+C_3S_3)$

$\langle f_0 \mid p_0'\rangle$ and $\langle f_1 \mid p_1'\rangle$ are assumed negligible.

Note: The ground state configuration is taken as

$$(\sigma sd)^2(\sigma f)^2(\pi d)^4(\pi f)^4.$$

TABLE II. Coefficients of Eq. (2).

k	j	q	$\lvert C_{kjq}^2\rvert_{Av}$
1	13 or 14	x	$3C_1^2\nu^2(1-C_6S_3)^2/2(1+2C_1S_1+C_1^2)\times(1-2C_6S_3+C_6^2)$
1	15 or 16	x	$C_4^2/2(1+2C_1S_1+C_1^2)$
2	15 or 16	x	$3C_4^2(1-C_4^2)$
2	13 or 14	x	$(S_3-C_6)^2(1-C_4^2)/2(1-2C_6S_3+C_6^2)$
3	11	x	$3\nu^2C_3^2(1-C_5S_1)^2/2(1+2C_5S_3+C_3^2)\times(1-2C_5S_1+C_5^2)$
3	17	x	$3(1-\nu^2)C_3^2/2(1+2C_3S_3+C_3^2)$
3	12	x	$C_3^2/2(1+2C_3S_3+C_3^2)$
3	7	x	$C_3^2/(1+2C_3S_3+C_3^2)$
4	8, 11, 12, 17	x	Same as for $k=3$ with $j=7, 11, 12, 17$
5	9	x	$2.5\ C_4^2$
5	12	x	$3C_4^2(1-C_4^2)$
5	11	x	$(1-C_4^2)(C_5-S_1)^2/2(1-2C_5S_1+C_5^2)$
6	10, 11, 12	x	Same as $k=5$ with $j=9, 11, 12$
All		y	The problem has axial symmetry. Equal contributions come from x and y.
All		z	No contributions

(b) Since the $\sum l_i$ can affect only one electron at a time, only matrix elements for states corresponding to excitation of a single electron can be nonzero.

(c) The one-electron orbitals were set up so as to be normalized and orthogonal.

(d) If

$$(il_q/\hbar)\psi_k = \sum_{j=1}^{17} C_{kjq}\psi_j$$

[where ψ_k is a one-electron function (without spin) occupied in the ground state, and ψ_j is any one-electron orbital], then

$$\chi_q = \sum_n \chi_{nq} = \frac{4N_0\beta^2\mu_0}{3}\sum_{k=1}^{6}\sum_{j=7}^{17} \lvert C_{kjq}^2\rvert/\Delta_{kj},$$

or finally

$$\chi = \sum_{q=x,y,z}\sum_{j=7}^{14}\sum_{k=1}^{6}\left(\lvert C_{kjq}^2\rvert/\Delta_{kj}\right)\cdot\tfrac{4}{3}N_0\beta^2\mu_0. \qquad (2)$$

Here the excited state n corresponds to excitation of an electron from ψ_k to ψ_j. This formula was derived with little trouble from the sums-of-determinants wave functions for the system, inserted into Eq. (1).

(3) The atomic orbitals are as follows (the notation is obvious, except that $'$ and $''$ represent the two oxygens): p_0', p_0'', p_1', p_1'', p_{-1}', p_{-1}'', s, d_0, d_1, d_{-1}, d_2, d_{-2}, f_0, f_1, f_{-1}, f_2, f_{-2}. From these are formed a $7s$,$6d_0$ hybrid, $\nu d_0+(1-\nu^2)^{\frac{1}{2}}s=ds$. The molecular orbitals are listed in Table I. We neglected the small nonorthogonality between the $5f$ orbitals and the oxygen orbitals (cf. Coulson and Lester[4]).

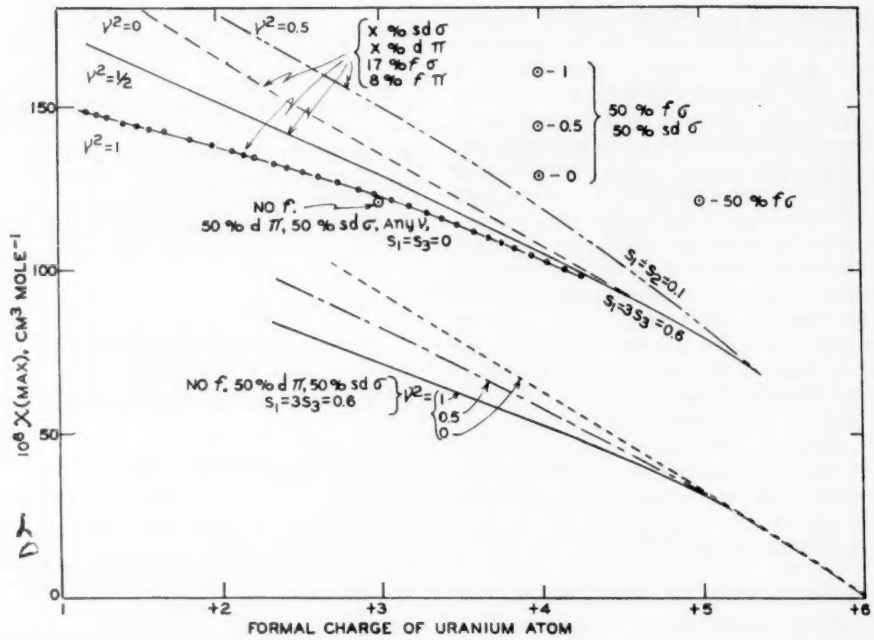

FIG. 1. Dependence of calculated magnetic susceptibility of uranyl ion on formal charge of the central atom. The % figures refer to the amount of a uranium atomic orbital which is used to form a bonding molecular orbital—i.e., if a wavefunction is written $a\phi_U+b\phi_0$ the % figure is $100a^2/(b^2+a^2)$.

(4) Operating upon these functions, we found the C_{kjq} as given in Table II. (All C_{kjq}'s not listed are zero or correspond to $j=1$ to 6, which do not concern us.)

RESULTS

For several cases we show in the figures some results of application of the scheme we have described. In each case, owing purely to our ignorance of the *detailed* energy level structure of OUO^{++} and like ions, we did not attempt to distinguish between the various excitation energies, $\Delta_{k\to j}$, but rather took all Δ's to be a peculiar kind of average, "Δ." Since the lowest optically observed frequencies are 20 000 cm^{-1} for uranyl compounds, we list one calculated value for χ in each instance, i.e., χ(max), which denotes the value obtained by setting "Δ"$=$20 000 cm^{-1}. A "Δ" of 30 000 to 40 000 cm^{-1} is perhaps more realistic; this would produce χ values of two-thirds to one-half of χ(max).

The calculations of Coulson and Lester[4] and of Belford and Belford[8] indicate that the 6*d* and 5*s* uranium orbitals overlap the oxygen 2*p* orbitals rather extensively, but that the 5*f* orbitals do not. We used arbitrary values $S_1=0.6$, $S_3=0.2$; $S_1=S_2=0.1$; or $S_1=S_3=0$ for various trial calculations.

DISCUSSION[10]

Several points may be noted. First, although the use of *f* orbitals in covalent binding is the most effective way to obtain a paramagnetic susceptibility, it does seem just possible to account for the general magnitude of the experimental value by models which involve only covalent σsd and πd bonds. For example, with six bonding electrons in $(\sigma d)^2(\pi d)^4$, with the formal charge distribution $O^{-0.5}U^{+3}O^{-0.5}$, we found $\chi(\max)=122\times10^{-6}$ for the most favorable choice of overlap integrals. Any purely *d*-bonding scheme which places less of the electron charge on the metal atom seems incapable of producing sufficient paramagnetism.

Second, addition of largely ionic σf and πf bonds to a more covalent *d*-bond structure produces a significant increase in the calculated susceptibility. Figure 1 shows how χ(max) varies with polarity of the *d* bonds for the cases corresponding to 17% use of uranium in the σf orbital and 8% in the πf orbitals. For example, with a σd and two πd bonds, having 25% of uranium orbitals, this produces a $\chi(\max)\approx107$ to 130×10^{-6} and a formal structure $O^{-.92}U^{+3.84}O^{-.92}$. (The same σd and πd bonds alone give a χ(max) of only $\sim45\times10^{-6}$.)

Third, admixture of uranium 7*s* into the σd bond causes an *increase* in χ(max), for most cases. We do not, therefore, believe that loss of *d* character in the σsd bond is a good argument for nearly neglecting this source of contribution to paramagnetism. Figure 2 demonstrates the dependence of χ(max) upon *s* character of the *sd* hybrid for several cases. [It is amusing to notice that in some cases, involving strong πd and σd bonding, the ratio of *s* to *d* character in the bonding σsd orbital has no effect upon χ(max).]

[10] All χ's are molar susceptibilities expressed in irrational emu, or cm^3 mole^{-1}.

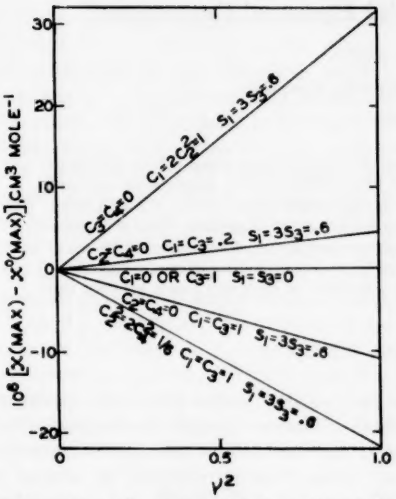

FIG. 2. Dependence of χ on the utilization of the d orbital in the sd hybrid for various cases. Ordinate represents the contribution of the ν-dependent part of χ(max). χ^0(max) denotes the calculated susceptibility for $\nu=0$.

The contributions which we have calculated are somewhat smaller because the excitations which produce them cannot all be the 20 000 cm^{-1} lowest-energy transition. We would expect this to be the πd (or possibly πf)$\rightarrow\delta^n f$. Complete assignments of the excited states would be most helpful. Very few attempts have been made to interpret the pattern of excited states of uranyl compounds.[1,2,11,12] None have been unambiguously successful, though McGlynn's assignments[2] are most complete and give promise that an adequate scheme will be obtained.

[11] R. L. Belford and J. Muirhead (work in progress).
[12] C. K. Jørgensen, Acta Chem. Scand. **11**, 166 (1957).

CONCLUSION

Within the framework of simple LCAO-MO and second-order magnetic perturbation approximations, several bonding schemes can account for the temperature independent paramagnetic part of the susceptibility of uranyl salts. Most of these schemes would assign the metal ion a charge of three to four. Although we mildly object to Eisenstein and Pryce's contention that d bonding alone *cannot* account for the observed susceptibilities, we agree with them that schemes involving some f bonding produce the desired magnitudes with more plausible structures. In particular, since Connick and Hugus[3] were able to explain the observed entropies of aqueous uranyl ion by the model $O^{-1}U^{+4}O^{-1}$, plausible structures might be those in which the formal uranium charge is about three to four.[13] Such a structure, involving moderate d bonding and slight f bonding, does indeed produce satisfactory calculated values. In this scheme, π bonds are necessary. In order to obtain similar values without pi bonding, one would have to postulate highly covalent σf and σd bonds. These seem to us unlikely unless accompanied by moderately covalent π bonds.

[13] An effective charge of +4 on the uranium atom ought to correspond to a somewhat smaller positive formal charge. Since the effective charge is that seen by a nearly equatorial water of hydration, and since the formal charge is a +6 spherical core surrounded by electron clouds bunched (in the d_0, f_0, $d_{\pm1}$, $f_{\pm1}$ orbitals) along the z axis, there will be an angular magnifying factor in the electric field as seen a short distance from the ion in its equatorial plane.

THE JOURNAL OF CHEMICAL PHYSICS VOLUME 34, NUMBER 1 JANUARY, 1961

Structure of the Water Molecule in Solid Hydrated Compounds*

J. W. McGrath and A. A. Silvidi

Department of Physics, Kent State University, Kent, Ohio

(Received July 28, 1960)

The proton-proton separations in hydrated water in 10 compounds have been measured by the Pake method using proton magnetic resonance. The mean value is 1.595±0.003 A with a range in values from 1.56 to 1.61 A. However, consideration of experimental error in individual values of the p-p separation indicates that this range does not prove that this separation varies between compounds. Thus it appears that intermolecular forces on the protons in the water molecule are not appreciable compared to intramolecular forces. The orientations of the water molecules have been determined for eleven compounds. In every instance the orientation appears to be determined by formation of hydrogen bonds between the water oxygen and the nearest pair of electronegative atoms.

INTRODUCTION

THE determination of crystal structure by x-ray diffraction has failed to give the positions of whatever hydrogen atoms may be present because of their small scattering cross section for x rays. Within the past dozen years the nuclear magnetic resonance technique and neutron diffraction have been used for this purpose with the former being more often used, at least for hydrated compounds.

Adjacent protons in proton pairs, such as exist in water molecules, can be expected on a classical basis to augment or lessen at each other whatever external magnetic field is applied to the material. Thus the proton resonance line is split into a doublet whose separation is determined by the interproton distance and the orientation of the proton pair with respect to the external field. Quantum-mechanical analysis[1] indicates that the splitting is greater than the classical splitting by a factor of $\frac{3}{2}$ due to the spin exchange process. In the case of solids with stationary proton pairs there is no motional narrowing of the resonance line. Thus the dipolar magnetic interaction between protons causes a resonance line broadening. Two ways of utilizing this broadening were first used by Pake[1] to determine proton-proton separations in hydrated compounds. When polycrystalline solids are studied the second moment of the broadened proton resonance line is determined and from this the proton-proton separation can be computed. When single crystals are studied actual resonance line doublets appear. As the orientation of the crystal with respect to the external field is changed the doublet separation varies. The proton-proton separation and orientation can be determined from the observed doublet separation as a function of crystal orientation. The latter method has been most often employed since it also can give proton-proton orientations and is inherently more accurate in measuring proton-proton separation.

We began a general study of proton-proton separations in hydrated compounds because previous investigations had yielded values of r (the proton-proton separation) different enough to suggest that this distance is not the same in different compounds. The fact that values were determined by several groups using different sets of apparatus and some differences in procedure may have introduced small systematic discrepancies. In most instances experimental error in r had not been estimated. Further, the orientations of the $p-p$ vector (line segment between the two protons in a pair) often were not computed nor fitted into the crystal structures. Determination of many values of r, on one apparatus, by one procedure with careful estimation of experimental error, presumably could indicate whether any apparent variation in r is real.

Such an experimental study can be helpful at this time since it appears that a theoretical answer to the problem of the structure of the water molecule in solid hydrated compounds is not feasible now. Theoreticians are still working on the simpler problems of the structure of isolated water molecules[2] and hydrogen bonding[3] between two isolated electronegative atoms. The importance of the latter to this discussion will become apparent.

The method used, that of measuring the proton magnetic resonance doublet separation as a function of the orientation of a single crystal in a magnetic field, has been described well by Pake.[1] Details of procedure have been described elsewhere.[4,5] A Pound-Knight-Watkins spectrometer[6,7] was used.

The compounds chosen were primarily those that had already been investigated. However, some were deleted from that list because they had been shown to contain hydronium ions or because they would gain or lose water in single crystal form. Others were sub-

* This research was partially supported by the U. S. Air Force through the Air Force Office of Scientific Research.

[1] G. E. Pake, J. Chem. Phys. **16**, 327 (1948).

[2] For example, R. McWeeny and K. A. Ohno, Proc. Roy. Soc. (London) **A255**, 367 (1960).

[3] For example, E. R. Lippincott and R. Schroeder, J. Chem. Phys. **23**, 1099 (1955).

[4] A. A. Silvidi and J. W. McGrath, J. Chem. Phys. **30**, 1028 (1959).

[5] J. W. McGrath, A. A. Silvidi, and J. C. Carroll, J. Chem. Phys. **31**, 1444 (1959).

[6] R. V. Pound and W. D. Knight, Rev. Sci. Instr. **21**, 219 (1950).

[7] G. D. Watkins, Ph.D. thesis, Harvard, 1952.

stituted. Some hydrated compounds are more amenable to study than others. The ideal crystal would contain only one orientation of water molecule, would contain hydrogen only in hydrated water and would contain no magnetic nuclei other than those in hydrogen. The first two requirements arise so as to have well resolved resonance spectra suitable for measurement. The latter requirement arises since other magnetic nuclei cause line broadening and further fine structure. So far as we know there is no such compound that can be grown as a single crystal of sufficient size (0.5 to 2 cc). The maximum possible number of water molecule orientations is equal to the product of the number of waters of hydration and the number of molecules per unit cell. Hence, we worked with monohydrates and dihydrates. Since growing, or otherwise obtaining, large crystals of hydrates was our most vexing problem; we had to use some crystals that were not nearly the ideal.

RESULTS

Our results for 11 hydrates, including 19 values of r and 21 orientations for the water molecules, are shown in Table I. Wherever possible, values of r are compared to those obtained by others. Not all of the other investigators obtained orientations and none stated orientations in so simple a manner as we have. Hence, the orientations that were obtained by others are not listed in Table I. Wherever comparisons were possible, the orientations were in good agreement.

The standard deviations quoted on individual values of r represent our best judgement on how much error might be present. These quoted deviations vary from ± 0.01 A to ± 0.03 A. Resolution of spectra and signal-to-noise ratio were the primary factors determining error. The smaller errors are quoted for those crystals for which the resonance lines were narrow (full linewidth at half-height, about 1.5 gauss) and which did not contain hydrogen other than that in the hydrated water. The larger errors are quoted for those crystals for which the resonance lines were wide (about 3.5 gauss) and/or whose spectra were not so well resolved due to the multiplicity of water orientation or the presence of other hydrogen. The weighted mean, which is the most probable value of r, and its standard error were computed in the usual fashion.[8]

Errors in the direction angles for the $p-p$ vector are not quoted in order to simplify the table. They range from 1° to 6° with the average error being about 2°.

The complexes listed in Table I show how the hydrogen atoms in the water molecule bind it to neighboring electronegative atoms. The subscripts on the electronegative atoms are those found in the indicated literature on crystal structure. In about half the cases no subscript was originally given nor was it necessary to designate the water oxygen.

Footnotes a, e, and i represent oral papers presented at meetings so that detailed results on the compounds represented have not been given before. In this paper, while the individual values of r are important, a comparison between experimental values of r and a discussion of revealed generalities as to the construction and orientation of hydrated water molecules is of more interest.

DISCUSSION

NMR spectra indicated definitely that the hydrated water molecules in crystals have preferred orientations at room temperatures. Since hydrogen bonds are known to determine molecular orientations in other cases[9,10] we computed possible water orientations by assuming that the hydrogen atoms in the water molecule form hydrogen bonds with the closest electronegative atoms. A less important factor used in determining the orientation was that the water molecule, being polar, orients itself so as to presents its negative pole toward the nearest positive ion in the crystal. We found these two factors to be consistent in every instance.

In general, hydrogen bonds are stronger between pairs of the more electronegative and smaller atoms. Thus, hydrogen bonds between pairs of atoms of fluorine, oxygen, or chlorine are common. While known hydrogen bonds between oxygen and bromine are rare, we nevertheless proceeded with one such computation on water orientation.

Upon computing likely water orientations of the hydrated water molecule on this basis we obtained the atomic complexes shown in Table I. The direction angles computed for the $p-p$ vector on this basis agreed[11] with those obtained from the NMR spectra with an average discrepancy of 1.8°.

For purposes of discussion we assumed that the O—H distances in every water molecule were the same (0.97 A). Then, knowing the values of r, we computed H–O–H angles. These angles ranged from 107° to 112° with an average of 100°. Comparison of these angles to those formed by the water oxygen and the two electronegative atoms in the complexes yielded the amounts by which the H bonds were bent.[12] The average angle of bend was 6.5°.

The uniformity and excellence of agreement between

[8] W. M. Smart, *Combination of Observations* (Cambridge University Press, New York, 1958), pp. 96–99 and 101–102.

[9] L. Pauling, *The Nature of the Chemical Bond* (Cornell University Press, Ithaca, New York, 1960), p. 450.

[10] G. C. Pimentel and A. L. McClellan, *The Hydrogen Bond* (W. H. Freeman and Company, San Francisco, California, 1960), pp. 3, 5, and 255.

[11] Orientation angles determined from NMR and from x-ray structure agreed within 7° in every instance, except for the second values of β_0 and γ_0 listed for potassium pentaborate in Table I. An uncertainty about some atomic positions in potassium pentaborate exists, as mentioned in footnote c. Hence, ignoring these two values for potassium pentaborate, the average discrepancy in orientation angle was 1.8°. In 24 out of 63 comparisons the discrepancy was zero.

[12] The largest angles of bend were 20° and they occurred in lithium sulfate for which there is some uncertainty about atomic positions as determined by x rays. The next largest angle was 12°. *H* bonds that are bent as much as 16° are already known.

TABLE I. Summary of results; r is the proton-proton separation. α_0, β_0, and γ_0 are the direction angles of the p-p vector measured away from the positive a, b, and c crystallographic axes, respectively. The complexes formed by hydrogen bonding to neighboring electronegative atoms are given. Results of others are also listed.

Crystal	Our ref.	Our r	α_0	β_0	γ_0	Complex	Crystal ref.	Others' r	Others' ref.
$CaSO_4 \cdot 2H_2O$	a	1.58±0.02 A	117°	37°	76°	$O_I - - H - O - H - - O_I$	j	1.58 A	Pake[u]
		1.58	64	37	103				
$K(H_4B_2O_{10}) \cdot 2H_2O$	b, c	1.59±0.02	90	37	53	$O_{II} - - H - O_{VI} - H - - O_I$	k	1.55	Smith and Richards[v]
		1.61	90	56	146				
$Li_2SO_4 \cdot H_2O$	a,d,e	...	97	45	48	$O_V - - H - O_V - H - - O_I$	l	See footnote 5	w–a′
			74	38	127				
$Ba(ClO_3)_2 \cdot H_2O$	f	1.61±0.01	31	89	124	$O_{II} - - H - O_{VI} - H - - O_{II}$	m	1.56	Spence[b′]
$Ba(BrO_3)_2 \cdot H_2O$	f	1.61±0.01	30	95	122	$O_{II} - - H - O_{VI} - H - - O_{II}$	n	...	...
$BaCl_2 \cdot 2H_2O$	g	1.58±0.02	90	58	148	$O_I - - H - O_{II} - H - - Cl_I$	o	...	...
		1.58	90	58	32				
		1.59	148	58	90	$Cl_I - - H - O_I - H - - Cl_{II}$			
		1.57	32	58	90				
$BaBr_2 \cdot H_2O$	h	1.56±0.02	89	1	90	$Br_I - - H - O - H - - Br_{II}$	p	...	...
$K_2HgCl_4 \cdot H_2O$	i	1.60±0.01	21	69	90	$Cl_I - - H - O - H - - Cl_I$	q	1.61	Itoh[e′,c′,d′]
		1.59	21	111	90	$Cl_{II} - - H - O - H - - Cl_{II}$			
$K_2SnCl_4 \cdot H_2O$	i	1.59±0.01	38	52	90	$Cl_{III} - - H - O - H - - Cl_{III}$	r, s	1.62	Itoh[e,c′]
		1.59	38	128	90				
$K_2CuCl_4 \cdot 2H_2O$	...	1.61±0.02	45	45	90	$Cl_{II} - - H - O - H - - Cl_{II}$	t	1.62	Itoh[e′,f′]
		1.61	45	135	90				
$(NH_4)_2CuCl_4 \cdot 2H_2O$	...	1.61±0.03	45	45	90	$Cl_{II} - - H - O - H - - Cl_{II}$	t	1.59	Itoh[e′,f′]
		1.61	45	135	90				
Weighted mean		1.595±0.003 A							

[a] J. W. McGrath, A. A. Silvidi, and J. C. Carroll, Bull. Am. Phys. Soc. Ser. II, **3,** 349 (1958).
[b] A. A. Silvidi and J. W. McGrath, J. Chem. Phys. **30,** 1028 (1959).
[c] We studied potassium pentaborate early when we were not so aware of the importance and wide applicability of the H bond concept in determining molecular orientation. Using this concept, we now determine a slightly different orientation of the water molecule from that reported earlier. When we compute the orientations on this basis from x-ray crystallographic positions of atoms, we obtain $\alpha_0=89°$, $\beta_0=30°$, $\gamma_0=59°$; and $\alpha_0=89°$, $\beta_0=38°$, $\gamma_0=129°$. The complex is as given in the table. The discrepancies (18°) for the latter values of β_0 and γ_0 are much larger than those we have obtained for all other crystals. However, the crystal structure parameters reported by Zachariasen are incomplete so we had to estimate some of them and this is probably part of the origin for large discrepancies.
[d] J. W. McGrath, A. A. Silvidi, and J. C. Carroll, J. Chem. Phys. **31,** 1444 (1959).
[e] K. F. Wylie and A. A. Silvidi, Bull. Am. Phys. Soc. Ser. II, **5,** (1960).
[f] A. A. Silvidi and J. W. McGrath, J. Chem. Phys. (to be published).
[g] A. A. Silvidi and J. W. McGrath, J. Chem. Phys. **32,** 924 (1960).
[h] J. W. McGrath and A. A. Silvidi, J. Chem. Phys. **33,** 644 (1960).
[i] A. A. Silvidi and J. W. McGrath, Bull. Am. Phys. Soc. Ser. II, **4,** 471 (1959).
[j] W. A. Wooster, Z. Krist. **94,** 375 (1936).
[k] W. H. Zachariasen, Z. Krist. **98,** 266 (1937).
[l] A. C. Larson and L. Helmholz, J. Chem. Phys. **22,** 2049 (1954).
[m] G. Kartha, Proc. Indian Acad. Sci. **36,** 501 (1952).
[n] G. Kartha, Proc. Indian Acad. Sci. **A38,** 1 (1953).
[o] A. T. Jensen, Kgl. Danske Videnskab. Selskab Mat.-fys. Medd. **22,** No. 3 (1945).
[p] B. K. Vainstein and Z. G. Pinsker, Zhur. Fiz. Khim. **24,** 432 (1950).
[q] C. H. MacGillavry, J. H. de Wilde, and J. M. Bijvoet, Z. Krist. **100,** 212 (1938).
[r] H. Brasseur and A. de Rassenfosse, Z. Krist. **101,** 389 (1938).
[s] J. Itoh, R. Kusaka, Y. Yamagata, R. Kiriyama, and H. Ibamoto, J. Phys. Soc. Japan **8,** 293 (1953).
[t] L. Chrobak, Z. Krist. **A88,** 35 (1934).
[u] G. E. Pake, J. Chem. Phys. **16,** 327 (1948).
[v] J. A. S. Smith and R. E. Richards, Trans. Faraday Soc. **48,** 307 (1952).
[w] G. E. Pake, Ph.D. thesis, Harvard, April 1948.
[x] G. E. Pake, J. chim. phys. **50,** C104 (1953).
[y] M. Soutif, B. Dreyfus, and Y. Ayant, Compt. rend. **233,** 395 (1951).
[z] M. Soutif and Y. Ayant, J. chim. phys. **50,** C107 (1953).
[a′] E. Hirihara and M. Murakami. J. Phys. Soc. Japan **11,** 239 (1956).
[b′] R. D. Spence, J. Chem. Phys. **23,** 1166 (1955).
[c′] J. Itoh, R. Kusaka, Y. Yamagata, R. Kiriyama, H. Ibamoto, T. Kanda, and Y. Masuda, J. Phys. Soc. Japan **8,** 287 (1953).
[d′] J. Itoh, R. Kusaka, Y. Yamagata, R. Kiriyama, and H. Ibamoto, J. Chem. Phys. **20,** 1503 (1952).
[e′] J. Itoh, R. Kusaka, Y. Yamagata, R. Kiriyama, and H. Ibamoto, Physica **19,** 415 (1953).
[f′] J. Itoh, R. Kusaka, R. Kiriyama, and Y. Saito, Mem. Inst. Sci. Ind. Research **14,** 1 (1957).

water orientations obtained directly from NMR spectra and those obtained by computation on the assumption of hydrogen bonding indicate strongly that this is the primary mechanism that determines the orientations of hydrated water molecules.

Values of r, the proton-proton separation, ranged from 1.56 to 1.61 A with an average of 1.595 A. Only one[13] of the values of r is farther from the mean than the sum of their standard deviations and it does not deviate far. In view of the magnitudes of the experimental errors in the individual results we have not shown that the proton-proton distances in hydrated water vary between compounds.

The mean of the seven comparable values of r is 1.594 A and their range is 0.07 A. Unfortunately, none of the quoted investigators estimated his experimental error. We have essentially the same mean value of r and a smaller range, 0.05 A.

We were unable to make quantum-mechanical computations on the structure of the hydrated water molecule. Hence, we attempted simply to compute on an electrostatic basis the effect on r caused by electronegative atoms in various likely positions near the water molecule. The question of how much effective change to allow on the atoms arose. However, after using several arbitrary charge values and atom positions, we concluded that this mechanism produces forces on the hydrogen atoms so small in comparison to the intramolecular force on hydrogen already present (and known from infrared spectra) that it could not appreciably affect r.

The stronger view, that we have experimental evidence that the $p-p$ separations in different hydrated water molecules are all the same, possibly may be accepted. This would mean that the intermolecular forces on the protons in the water molecule are very much less than the intramolecular forces.

There is additional material, not referred to in the text, that involves NMR measurements on hydrated compounds.[14]

CONCLUSION

Values of the proton-proton separations in and orientations of the hydrated water molecules in eleven solid inorganic salts have been obtained. The mean value of the separations is 1.595 ± 0.003 A.

Experimental results support these two statements. (1) The structure and dimensions of the water molecule in hydrated compounds are not affected by atomic environment. (2) The hydrated water molecule is oriented in solids so as to form hydrogen bonds between the water oxygen and the nearest electronegative atoms.

ACKNOWLEDGMENTS

We deeply appreciate the helpful advice and steady encouragement given us by Professor G. E. Pake, Stanford University.

We thank Professor R. D. Spence, Michigan State University, for a barium chlorate crystal and Professors J. Itoh and R. Kiriyama, Osaka University, for a potassium mercuric chloride crystal.

[13] The value obtained for $BaBr_2 \cdot H_2O$ is 1.56 ± 0.02 A. We feel that there may be a systematic error present here tending to make the quoted value of r about 0.01 A too small. We necessarily operated with saturation present. We took derivatives of the resonance lines with a magnetic field sweep. Under these conditions the derivative of the side of the resonance line first encountered is emphasized and this tends to make the line splitting too large and the computed value of r too small.

[14] Y. Kakiuchi, H. Shono, H. Komatsu, and K. Kigoshi, J. Chem. Phys. **19**, 1069 (1951); R. E. Richards and J. A. S. Smith, Trans. Faraday Soc. **47**, 1261 (1951); Y. Kakiuchi, H. Shono, H. Komatsu, and K. Kigoshi, J. Phys. Soc. Japan **7**, 102 (1952); Y. Kakiuchi and H. Komatsu, *ibid.* **7**, 330 (1952); J. Itoh, R. Kusaka, R. Kiriyama, and S. Yabumoto, J. Chem. Phys. **21**, 1895 (1953); S. Maricic and J. A. S. Smith, Report on the 4th International Congress of the International Union of Crystallography, Paper S1.4 (1957); R. D. Spence and John Muller, J. Chem. Phys. **26**, 706 (1957); J. W. McGrath and A. A. Silvidi, *ibid.* **29**, 103 (1958).

Proton Spin Polarization of Water Adsorbed on Sucrose Chars

JAMES J. KREBS*

U. S. Naval Research Laboratory, Washington, D. C.

(Received June 21, 1960)

By saturating forbidden electron-nuclear double transitions in paramagnetic materials, it is possible to considerably enhance the nuclear polarization in a positive or negative sense. This effect has been investigated experimentally using the protons of water adsorbed on paramagnetic charred sucrose. The dependence of the enhancement on the saturating microwave power is derived for the case of overlapping allowed and forbidden transitions, and predicts a linear change in polarization at low power levels. The general features of the enhancement found are in agreement with those predicted by perturbation theory using a simple dipole-dipole electron-nuclear interaction. However, the plot of log (polarization change) vs log (power) has a slope of 0.82 ± 0.04 instead of 1.0. In addition, the field separation between the points of maximum positive and maximum negative enhancement is too small in those chars for which inhomogeneous broadening is suspected.

THE dynamic polarization of nuclear spins in solids by saturating forbidden transitions involving other magnetic species has previously been observed.[1-3] In addition, it has been shown possible to produce a similar polarization in the nuclei of a fluid adsorbed on the surface of a paramagnetic material.[4] We report here a somewhat more detailed investigation of a system of of the latter type, water adsorbed on sucrose chars.

Electron spin resonance (ESR) in charred sugars, in common with other charred organic materials, has been known for some time.[5] The relatively narrow ESR lines and the excellent adsorptive properties of sucrose chars make them suitable materials for a study of the type undertaken here. In addition, by varying the temperature at which such a char is prepared it is possible to have some control over the ESR parameters, in particular, the spin-lattice relaxation time T_1.

THEORY

The energy level diagram of a system of free electrons and magnetic nuclei of spin $\frac{1}{2}$ in a strong magnetic field H_0 is shown in Fig. 1. There $\omega_e=|\gamma_e|H_0$ and $\omega_n=|\gamma_n|H_0$, where γ_e and γ_n are the electronic and nuclear gyromagnetic ratios, respectively. For a nucleus with a positive magnetic moment the states $|a\rangle$, $|b\rangle$, $|a'\rangle$, and $|b'\rangle$ are $|-,+\rangle$, $|-,-\rangle$, $|+,+\rangle$, and $|+,-\rangle$, respectively, where the first sign is that of the electronic magnetic quantum number m_S and the second is that of the nuclear magnetic quantum number m_I.

If there is a weak dipole-dipole interaction between the electrons and the nuclei such that the nuclear Zeeman splitting is large in comparison to this interaction, then the pure states are mixed and the normally forbidden transitions indicated by the dashed arrows can be induced by a microwave field.[6] Saturating these transitions can result in a large enhancement of the nuclear polarization. Transition A (for which $\omega=\omega_e-\omega_n$) leads to an increase in the nuclear polarization, while transition B (for which $\omega=\omega_e+\omega_n$) leads to a change of sign of the polarization as well as an increase in magnitude.

We shall now derive an expression for the steady-state nuclear polarization as a function of the saturating microwave field strength. In this derivation we make use of the methods and notation of Abragam.[6] Since in many actual cases ω_n is less than the ESR linewidth $\Delta\omega_e$, the main transition will be induced at the same time as the forbidden ones. Let V be the probability of an induced electronic transition per unit time at the center of the main ESR line. Then $V=\frac{1}{2}\gamma_e^2H_1^2T_2$, where $2H_1$ is the amplitude of the microwave field and T_2 is the electronic spin-spin relaxation time. Let $g(\omega)$ be the shape function for this line. Then the probability per unit time of inducing a $\Delta m_I=0$ transition at the center of a forbidden line is given by KV, where $K=g(\omega_e\pm\omega_n)/g(\omega_e)$. Thus K is a measure of the overlap of the main and the forbidden transitions.

We assume the ESR line is homogeneously broadened and that the relaxation of the nuclei in the solid is

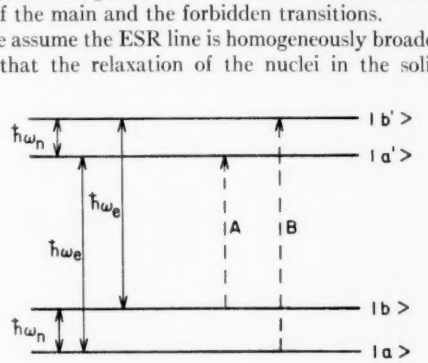

FIG. 1. Energy levels of an electron-nuclear system in a strong magnetic field. The forbidden transitions A and B are used to enhance the nuclear polarization.

* Work performed in part as NAS-NRL postdoctoral research associate.

[1] A. Abragam and W. G. Proctor, Compt. rend. **246**, 2253 (1958).

[2] M. Abraham, M. A. H. McCausland, and F. N. H. Robinson, Phys. Rev. Letters **2**, 449 (1959).

[3] N. Borghini and A. Abragam, Compt. rend. **248**, 1803 (1959).

[4] E. Erb, J. Motchane, and J. Uebersfeld, Compt. rend. **246**, 3050 (1958).

[5] D. J. E. Ingram, *Free Radicals* (Academic Press, Inc., New York, 1958), Chap. 7.

[6] A. Abragam, Phys. Rev. **98**, 1729 (1955).

entirely due to the interaction with the free electrons. We then note that the probability per unit time of inducing a forbidden transition at $\omega_e \pm \omega_n$ may be written as λV. The value of λ is given in footnote 6 and is proportional to $(H_{SI}/H_0)^2$, where H_{SI} is the static field produced by the free electron at the nucleus.

Referring to Fig. 1, let a, b, a', and b' be the populations of the corresponding states. Also let $|\gamma_e|\hbar H_0 = 2\Delta kT$ and $|\gamma_n|\hbar H_0 = 2\delta kT$. Then, if a microwave field is applied at the frequency of transition A, the rate of change of a' in the steady state is

$$da'/dt = 0 = (2T_1)^{-1}[a\exp(-\Delta) - a'\exp(\Delta) + \lambda b\exp(-\Delta+\delta) - \lambda a'\exp(\Delta-\delta)] + KV(a-a') + \lambda V(b-a') \quad (1)$$

with similar equations for a, b, and b'.

The average value of $I_z = m_I$ is given by

$$\langle I_z\rangle = \tfrac{1}{2}\frac{(a+a')-(b+b')}{a+a'+b+b'}. \quad (2)$$

By solving Eq. (1) and its partners simultaneously, and retaining only first-order terms in the expansion of the exponentials, we can show that to a very good approximation

$$(\langle I_z\rangle - \langle I_z\rangle_0)/\langle I_z\rangle_0 = \pm(\Delta/\delta)F(S'), \quad (3)$$

where

$$F(X) = X[(1+X)(1+2KX)]^{-1}. \quad (4)$$

In these expressions $\langle I_z\rangle_0$ is the thermal equilibrium value of $\langle I_z\rangle$ and $S' = VT_1 = \frac{1}{2}\gamma_e^2 H_1^2 T_1 T_2$ is one-half the usual saturation parameter. The function $F(X)$ is shown plotted in Fig. 2 for various values of K.

Equations (3) and (4) show that for $K=0$ the nuclear polarization is enhanced by a factor $\pm(\Delta/\delta) = \pm|\gamma_e/\gamma_n|$ when the forbidden transition is saturated ($S' \gg 1$). Here the upper and lower signs apply to the transitions A and B, respectively. When the forbidden transition lies within the main ESR line, or equivalently, $K>0$, there is a decrease in the maximum polarization attainable, and the position of the maximum polarization shifts to lower values of S' as K increases to its maximum value of 1.0. For $S'<10^{-2}$ we note that $(\langle I_z\rangle - \langle I_z\rangle_0)/\langle I_z\rangle_0$ essentially varies directly as S' for all K.

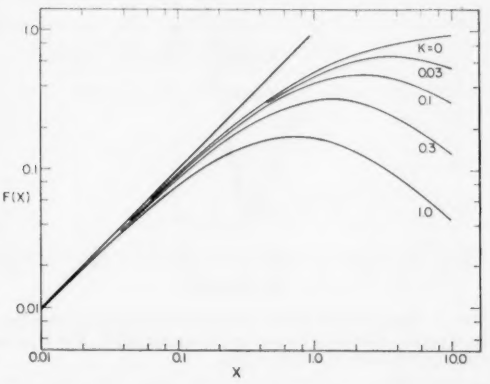

FIG. 2. The enhancement function $F(X)$. The parameter K is a measure of the overlap of the strong and forbidden transitions. The straight line is a common asymptote of unit slope.

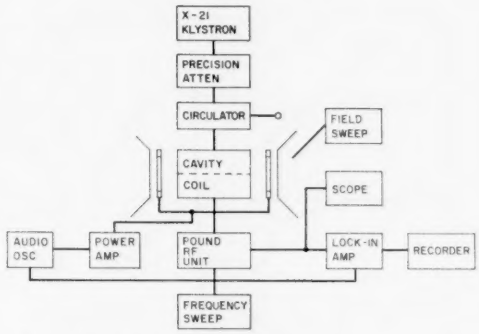

FIG. 3. Block diagram of the double-resonance apparatus.

Note added in proof. It has come to the attention of the author that the result of Eq. (3) has been derived somewhat more generally by J. I. Motchane and J. Uebersfeld [J. phys. radium **21**, 194 1960)].

Previous work[7] has shown that the results which are applicable to nuclei in the solid material are also valid for nuclei of adsorbed fluids, provided that the primary nuclear relaxation is via the same electrons used for polarizing. This is in accord with our previous assumption, and may be safely assumed to be true as long as there is no inhomogeneous broadening of the ESR line.

EXPERIMENTAL

The experiments described here were performed at an ESR frequency of 10.1 kMc which corresponds to a static field H_0 near 3600 gauss and a proton resonance frequency of 15.3 Mc. Figure 3 is a block diagram of the apparatus used. The proton polarization is monitored by observing the nuclear resonance with a modified Pound-Knight spectrometer of conventional design. The X-band power of approximately 2 w is furnished by an X-21 klystron. The microwave power reaching the cavity is controlled by a precision attenuator and can be monitored by a power meter. The cylindrical cavity operates in the TE_{011} mode, and this allows an rf coil that has an elongated rectangular cross section to be inserted along the axis of the cavity without producing excessive losses. The microwave frequencies were measured with a calibrated wavemeter, while the rf frequencies were determined by heterodyning with a crystal-calibrated oscillator.

[7] H. C. Torrey, J. Korringa, D. O. Seevers, and J. Uebersfeld, Phys. Rev. Letters **3**, 418 (1959).

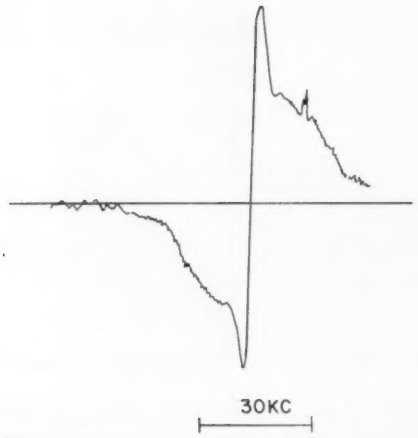

FIG. 4. Derivative trace of the proton resonance signal of an air-activated 400°C sucrose char. The narrow line is that due to the adsorbed water.

In practice the magnetic field H_0 was varied rather than the klystron frequency. The dependence of the polarization on the magnetic field in the neighborhood of the main ESR line was determined point by point by setting H_0, adjusting the rf oscillator frequency for proton resonance, increasing the microwave power to a given level, and observing the change in the proton resonance signal. This process was repeated for each field value. In order to obtain the dependence of the change in polarization on the microwave power (and hence on H_1^2), the magnetic field was adjusted to the previously determined value for maximum positive enhancement, and the change in proton signal was measured at various microwave power levels.

The samples used in these experiments were prepared by charring analytical grade sucrose at 250°C in a nitrogen atmosphere. The samples were then ground and reheated to the desired activation temperature in a cylindrical quartz furnace under a stream of dried air or argon. The samples were outgassed for 20 hrs and cooled under argon. They were then exposed to air and allowed to equilibrate with the water vapor present. Figure 4 shows the derivative trace of the proton signal from a sample activated in dry air at 400°C. The trace shows the presence of two types of protons. The narrow line is due to the adsorbed water and can be removed by heating in air to 170°C, but returns slowly thereafter. The broad line is due to protons bound in the body of the char, and heating the sample does not affect this line. Traces of this type have previously been observed in other hydrogen-containing hygroscopic materials.[8] The signal shown has been increased by a factor of 3.3 from the original signal by pumping on the transition A. Typical signal-to-noise ratios for unenhanced proton signals were 10:1 or better. The ESR of these samples is quite strong and has a g value of 2.0028 for the 400°C samples and 2.0026 for the 600°C samples.[9]

[8] T. M. Shaw and R. H. Elsken, J. Chem. Phys. **21**, 565 (1953).

RESULTS AND DISCUSSION

The dependence of the polarization of the water protons on the magnetic field for a given microwave power level is shown in Fig. 5 for a sample activated in argon at 400°C. In this figure I is the proton signal height with the microwave power on, and I_0 is that with the power off. The ratio (I/I_0) is just the enhancement of the proton polarization. The proton resonance frequency ν_H is plotted on the abscissa of Fig. 5 and is, of course, proportional to the magnetic field. The polarization change should essentially trace out the sum of the line shape of transition A minus that of transition B. The experimental curve shows qualitative agreement with this expectation. It can be seen that the maximum negative change in polarization (15.9) is equal to the maximum positive change (16.2) to within experimental error. This is as predicted by Eq. (3), and follows from the equal probabilities of the two forbidden transitions. This property was found in every sample investigated.

The center frequency, at which there is no change in the proton signal, is given by $\nu_H = |\gamma_H/\gamma_e|\nu_k$, where ν_k is the klystron frequency. Using $\nu_k = 10.096$ kMc and $\nu_H = 15.334$ Mc as found by experiment, we obtain $g = 2.0028$—in complete agreement with the known value. It can be seen that an experiment of this type may allow the determination of the g value of an electron resonance which is too weak or broad to be detected by other means.

A third quantity of interest is the field separation between the maximum positive and negative enhancements. For a fixed klystron frequency ν_k, the forbidden

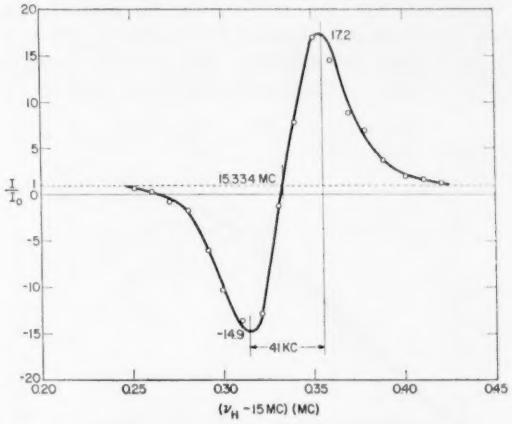

FIG. 5. Enhancement of the proton resonance signal as a function of proton resonance frequency (magnetic field). The klystron frequency was fixed at 10.096 kMc.

[9] L. S. Singer, W. J. Spry, and W. H. Smith, *Proceedings of the Third Conference on Carbon* (Pergamon Press, New York, 1959), p. 121.

transitions occur at the field values H_A and H_B given by

$$2\pi\nu_k=(|\gamma_e|-|\gamma_n|)H_A$$
$$2\pi\nu_k=(|\gamma_e|+|\gamma_n|)H_B. \quad (5)$$

For $\nu_k=10.096$ kMc, Eq. (5) gives $H_A-H_B=(11.0\pm0.2)$ gauss; the probable error being due to the uncertainty of the g value of the char. The value of H_A-H_B found for the 400°C samples was (9.9 ± 0.3) gauss and for the 600° sample (11.3 ± 0.3) gauss. The reason for the discrepancy in the case of the 400°C chars is not known, but it may be associated with nonhomogeneous broadening of sugar chars prepared below 450°C.[10]

Figure 6 shows the dependence of the change in the water-proton polarization on the microwave power for the same sample. In this figure we have set $\Delta I=I-I_0$. The significant fact here is that the change in polarization is not proportional to the microwave power over the range covered. At higher power levels than shown here the results were not reproducible, due to sample heating. The average slope of the $\log(\Delta I/I)$ vs log (power) plots for all samples was found to be 0.82 ± 0.04. It should be noted that in the one case where the power dependence of the broad-line proton signal was also measured, the slope was in agreement with that found for the water protons.

The magnitude of the actual polarization change produced can be compared with that predicted from Eq. (3). For a power input of 2 w and using the measured cavity parameters, $H_1=0.77$ gauss. For a 600°C sample $T_1=T_2$,[9] and $T_2=1.1\times10^{-8}$ sec from the measured maximum-slope linewidth of 5.9 gauss. This gives $S'=1.0\times10^{-2}$ and $K=0.46$, hence $(\Delta I/I_0)=6.4$. The actual value found was 5.9. It is somewhat more difficult to obtain a reliable value of T_1 for the 400°C samples. However, a suitable estimate from the results of Singer, Spry, and Smith[9] yields $T_1\approx10^{-7}$ sec, while $T_2=1.1\times10^{-8}$ sec. The calculated value of $(\Delta I/I_0)$ at half-power is 32, as compared to the value of 30 found. It is surprising and probably fortuitous that the agreement is this good, considering the uncertainties in the value of Q, the cavity coupling, and the electronic T_1. It is evident, however, that the magnitude of the enhancement produced is in agreement with that expected.

[10] R. C. Pastor and R. H. Hoskins, J. Chem. Phys. **32**, 264 (1960).

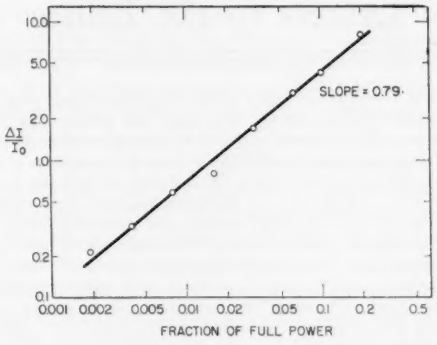

FIG. 6. Change in proton signal with saturating microwave power. Full power corresponds to microwave field $2H_1$ equal to 1.5 gauss.

SUMMARY

The experiments described indicate that the general features of the nuclear polarization of fluids adsorbed on paramagnetic materials are in agreement with the predictions based on a simple dipole-dipole interaction between the nuclei and the paramagnetic electrons. The magnitude and field dependence of the effect are as expected, although it would seem that it may be necessary to take into consideration inhomogeneous broadening to properly treat the separation of the points of maximum positive and negative enhancement. The principal point of disagreement lies in the rather anomalous dependence found for the change in nuclear polarization as a function of saturating microwave power.

ACKNOWLEDGMENTS

The author wishes to thank Dr. J. K. Thompson for preparation of the samples and both him and Dr. L. M. Matarrese for many helpful discussions of the resonance properties of sucrose chars. Appreciation is also extended to Dr. W. A. Barker for his initial stimulation toward investigation of dynamic nuclear polarization.

Letters to the Editor

THE Letters to the Editor section is subdivided into three parts entitled Communications, Comments and Errata, and Notes. These three sections are all subject to the same limitations on length. The textual material of each Letter is limited to a number of words equal to 950 minus the following; (a) 200 words for each average-sized figure: (b) 50 words for each displayed equation: (c) 7 words for each line of table including headings and horizontal rulings. No proof will be sent to the authors of "Communications" and "Comments and Errata." Proof will be sent to the authors of "Notes." The publication charge for Letters is $30 per page, with a minimum of $30 per Letter. If honored, the Institution will be entitled to 100 reprints without covers. See issues of May–September, 1957, for descriptions of categories.

Communications

Collision-Induced Dissociation of HD^+†

A. P. IRSA AND L. FRIEDMAN

Department of Chemistry, Brookhaven National Laboratory, Upton, Long Island, New York

(Received July 29, 1960)

THE collision-induced dissociation of H_2^+ has become the focus of recent interest.[1,2] The reaction of relatively low-velocity ions gives a broad peak in the mass spectrograph at m/e of 0.5, corresponding to protons with half the kinetic energy of the reactant H_2^+ ions.[3] A discrepancy has been noted in the respective cross-section determinations of Federenko *et al.*[1] and Sweetman[2] in the 100-kev range. It is the purpose of this communication to report a mass spectrometric study of HD^+ which may be compared with the Federenko data at their lower limit, 5000 v. General interest in ion-molecule reactions stimulated a study of this reaction at the lowest ion velocities compatible with production of detectable yields of product.

The molecule ion HD^+ was selected rather than H_2^+. This facilitates a determination of the collection efficiency of ions from the scattering chamber, through the magnetic analyzer, and to the Faraday cup behind the collector slit in the mass spectrometer. Both Federenko[1] and Sweetman[2] used magnetic analysis of their ionized products but neglected to discuss possible losses in a single-focusing magnetic analyzer. Such losses may be trivial at very high ion velocities but, as will be shown below, can be serious with reactant ions having energies equal to or less than 5 kev. The basic assumptions in the experiment are, that on excitation HD^+ will produce equal amounts of H^+ and D^+ and that the velocity components of the products in the direction of initial ion acceleration, and transverse or normal to this direction, may be computed classically. One determines the integrated peak intensity of the collision-induced metastable ions at m/e 0.3 and 1.3, and if these are equal, all product ions have been collected. An observed inequality in yields arises from discrimination in collection of H^+ over D^+. Equations set up by Berry[4] suffice, with the above assumptions and a knowledge of the spectrometer geometry, to calculate a ratio of velocity components, u/v, for the transverse and forward velocities of the respective ions. A crude check of the plausibility of the value for u/v can be obtained from an analysis of the peak contour. This is not as sensitive, however, as the discrimination calculation for determination of u/v. The resulting velocity ratio may then be used to relate the observed yields at the collector to the number of ions formed in the field-free region of the magnetic analyzer, i.e., the effective scattering chamber.

A 5-in. radius 60° sector spectrometer with differentially pumped ion source, and an auxiliary inlet system for introduction of scattering gases in the field-free region of the analyzer tube, was used for these experiments. The analyzer tube was fitted with a calibrated VGIA ionization gauge for pressure measurements and with probes which served to measure the intensity and contour of the primary, ion beam.

HD^+ ion currents of the order of 10^{-9} amp were collected. Scattering gases, He, Ne, and Ar, at pressures of roughly 10^{-5} mm were maintained on the analyzer tube. Secondary or product H^+ and D^+ yields of roughly 10^{-12} amp were measured. All ion currents were measured with Applied Physics Corporation model 31 vibrating-reed electrometers. The over-all statistical error in the cross-section determination is estimated at less than 20%.

H^+ and D^+ were detected with HD^+ ions of 800-v energy; yields increased with increasing HD^+ velocity. The sharpness with which product appeared at the calculated m/e values for collision-induced metastable ions, indicated trivial transfer of energy or momentum to the scattering gas. The computed ratio u/v with 4250-v HD^+ ions was 0.0024. This corresponds to a very narrow angular distribution of product ions. If one assumes a random distribution of velocities associated with the kinetic energy liberated in the process of HD^+ going from its ground state vertically to the $2\Sigma_u$ repulsive state and thence to H^+ and D or D^+ and H, the ratio of u/v would be more than an order of magnitude greater. The result may, in part, be explained by the fact that the HD^+ reactant is produced by electron impact in vibrationally excited states and that the cross section for dissociation of excited HD^+ is what is actually being observed. This would imply a larger value for the cross section or average distance of interaction between the scattering gas and the HD^+ ion. An alternative assumption leading to the same general conclusion may be made, namely, that only specific orientation of ions which gives products with all their energy in the forward direction,

are readily excited to dissociation. The hypothesis concerning the role of vibrational excitation in H_2^+ or HD^+ may explain the discrepancy between the results of Sweetman and Federenko.

The discrimination calculation indicates a loss of 30% of ion product in the scattering chamber, magnetic analyzer, etc., up to the collector slit. Cross sections for dissociation of 4250-v HD^+ on collision with He, Ne, and Ar, are, respectively, 1.7, 2.14, and 2.5×10^{-16} cm^2. If the effect on the cross section of isotopic substitution of D for H in H_2^+ is relatively small, then the results above agree with the H_2^+, He cross section of Federenko *et al.* No data are available for comparison with our Ne result, and our Ar data are somewhat higher than results reported graphically by Federenko.

† Research performed under the auspices of the U. S. Atomic Energy Commission.

[1] N. V. Federenko, V. V. Afromisov, R. N. Il'in, and D. M. Kaminken, J. Exptl. Theoret. Phys. (U.S.S.R.) **36,** 385 (1959).
[2] D. R. Sweetman, Proc. Roy. Soc. (London) **A256,** 416 (1960).
[3] F. W. Aston, Proc. Cambridge Phil. Soc. **19,** 317 (1920).
[4] C. E. Berry, Phys. Rev. **78,** 597 (1950).

Elimination of Molecular Hydrogen from Alkyl Free Radicals

ALVIN S. GORDON AND S. RUVEN SMITH*

Chemistry Division, U. S. Naval Ordnance Test Station, China Lake, California

(Received August 29, 1960)

WE wish to report that alkyl radicals (other than methyl or ethyl) eliminate molecular hydrogen as one of their pyrolysis reactions. McNesby and Gordon[1] have previously postulated that cyclopentyl radicals, generated by photolysis (no light in the 2537 A region) of a mixture of cyclopentane and acetone-d_6, eliminated molecular hydrogen as one of their reactions. They noted that hydrogen was produced from 250° to over 500°C, the highest temperature of their work. The H_2/HD ratios were much greater than the CD_3H/CD_4 ratios in the same reaction mixture. We have now generated H atoms and CD_3 radicals (by photolysis and pyrolysis of a mixture of C_2H_6 and acetone-d_6) simultaneously over a temperature range, and shown that an H-atom mechanism could not account for the H_2/HD ratios. Using the same photolysis apparatus as well as a pyrolysis apparatus, our results show that the molecular hydrogen elimination reaction occurs in all cyclo-alkyl radicals from C_4 through C_7, as well as from propyl and butyl radicals. As an example, a comparison of the CD_3H/CD_4 and the H_2/HD ratios in the products of a propane-acetone-d_6 mix are shown in Table I. The ratios show that molecular hydrogen must be eliminated from the propyl radical, at least in part. Consistent with the earlier work,[1] hydrogen yield always increases with temperature. At the temperatures of hydrocargon pyrolysis this molecular elimination must be one of the sources for the production of hydrogen.

TABLE I. Ratios of deuterated methanes, hydrogens, and total hydrogens to total methanes in the products of the photolysis of propane-acetone-d_6 mixes.

T°C	CD_3H/CD_4	H_2/HD	$\frac{\text{Total hydrogens}}{\text{Total methanes}}\times100$
345	6.6	24.8	1.6
367	6.4	21.4	4.7

Our results are in accord with the following general reaction mechanism,

$$R\,\dot{C}HCH_2CH_2R' \rightarrow R\,\dot{C}HC{=}C\,R' + H_2, \qquad (1)$$

where R, R'=H or an alkyl radical; *n*-butyl radicals and *s*-butyl radicals (formed from methyl radical attack on *n*-butane) also eliminate molecular hydrogen. The postulated mechanism predicts that the resonance stabilized butenyl radical would be a product of reactions (2) and (3),

$$\dot{C}H_2CH_2CH_2CH_3 \rightarrow \dot{C}H_2CH{=}CHCH_3 + H_2$$
$$\updownarrow$$
$$CH_2{=}CH\dot{C}HCH_3 \qquad (2)$$

$$CH_3\dot{C}HCH_2CH_3 \rightarrow CH_3\dot{C}HCH{=}CH_2 + H_2$$
$$\updownarrow$$
$$CH_3CH{=}CH\dot{C}H_2. \qquad (3)$$

This radical would add a methyl radical to form pentene-2 and 3 methyl butene-1, and both these compounds have been identified in the products of the reaction. In addition, two hexenes were identified. They are formed by the addition of ethyl radicals (produced from the competitive pyrolysis reaction of *n*-butyl radicals to form an ethyl radical and ethylene) to the resonance forms of the butenyl radical. Since there are so many hexene isomers, positive identification of the hexene isomers was not possible. Likewise, methyl cyclohexene has been identified in the products of the reaction of cyclohexane and methyl radicals. The resonance energy of the allylic type of radical is about 15–20 kcal/mole so that the reaction involving the elimination of molecular hydrogen is endothermic only about 10–15 kcal/mole. We have not succeeded in obtaining a quantitative measure of the kinetic constants of the molecular-hydrogen elimination reaction. It is competitive with the cleavage of the C—C bond of an alkyl radical to form an unsaturated compound, over the 200°C temperature range where we have been able to make our studies, so that the energy of activation for the molecular H_2 elimination reaction

must be about 30 kcal/mole. Our results indicate that the pre-exponential factor for the molecular hydrogen elimination reaction is considerably smaller than for the corresponding cleavage of the C—C bond.

In cycloalkyl radicals the hydrogen atoms cannot fit into the ring and are forced close together. However, the molecular dehydrogenation reaction also occurs as noted above in linear alkyl radicals where the hydrogen atoms on adjacent carbon atoms can be in staggered positions.

Molecular hydrogen is not readily eliminated from a resonance stabilized radical, even at temperatures of 400°C, since we observe no evidence of molecular hydrogen elimination from the cyclohexenyl radical at these temperatures.

We plan to publish results which show that ethyl radicals probably pyrolyze to form only H atoms and no molecular hydrogen in the temperature range 425°–525°C.

* Present address: Department of Chemistry, University of Connecticut, Storrs, Connecticut.

[1] J. R. McNesby and A. S. Gordon, J. Am. Chem. Soc. **79**, 4593 (1957).

Clustering in the Critical Region

GEORGE W. BRADY AND JOHN I. PETZ*

Bell Telephone Laboratories, Inc., Murray Hill, New Jersey

(Received October 24, 1960)

WE would like to report some interesting results obtained by measuring the temperature variation of the small angle x-ray scattering of a two-component liquid system in the region above its consolute curve. The system C_7F_{16}—*i*—C_8H_{18}, which had been previously studied at one temperature only[1] and had been found to exhibit clustering, or large inhomogeneities in structure, was again chosen. The temperature range chosen was one which started within ~0.5°C of the consolute curve and extended to ~16°C above it. The three compositions, 30, 40, and 50 mole % C_7F_{16} were chosen for study because the previous work had shown that in this range the x-ray requirements were best served. The small-angle apparatus used was an improved version of the previous one and along with the temperature control system, will be described in a later communique.

Figure 1 shows the scattering curve for the 40% C_7F_{16} solution at the temperatures indicated. (The scattering curves for the 30% solution are qualitatively similar to these, but those for the 50% solution differ markedly, showing complex interaction effects; they will not be discussed further here.) Radii of gyration $\bar{R}$, calculated by means of Guinier plots are given in Table I. Slit corrections were not applied to the data so these results may be regarded for the present as semi-quantitative only.

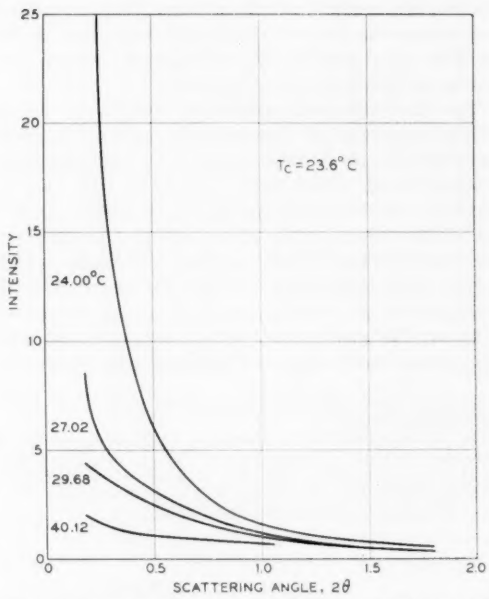

FIG. 1. Scattering curves for 40% C_7F_{16}. T_c is the critical temperature solution.

The most significant fact brought out by these experiments is the surprising length of the "critical" region. Even at 40.1°C there is significant scattering, indicating a surprising degree of clustering. As the temperature is lowered, the size appears to increase rather slowly until near the region of the consolute curve a large increase is apparent. The scattering becomes very intense in the region within 1°C of the consolute curve and is perfectly reproducible. An average experiment takes about 3 hr to complete, and certainly in this period there was no change in intensity inducating that although the clusters are very large, there is still no tendency toward complete phase separation. The shape of the curves indicates that they approximate to a cylindrical scattering function. When the analysis is carried further, we hope to be able to

TABLE I.

30% C_7F_{16}		40% C_7F_{16}	
t°C	$\bar{R}$	t°C	$\bar{R}$
23.40	57	24.00	85
25.38	50	27.02	43
29.07	36	29.68	36
35.26	28	40.12	27

correlate the intensity curves with the size and number of the clusters.

The obvious question arises as to whether these phenomena are unique to the system under study or whether they are general. Because of the difference in electron density between C_7F_{16} and C_8H_{18}, and also because of the good x-ray absorption characteristics of the system, the scattering effects are readily observable here, whereas in other systems this is not likely to be so. In any case, the results are so novel that we felt that we should present them briefly now because it will take some time to work up the data completely. A full report will follow as soon as possible.

* Bell Telephone Laboratories Summer Employee, 1960, from the University of Arkansas, Department of Physics, Fayetteville, Arkansas.

[1] George W. Brady, J. Chem. Phys. **32**, 45 (1960).

Temperature Dependence of the Isotopic Fractionation of Nitrogen in the NO-NO_3^- System*

MARVIN J. STERN, LOIS NASH KAUDER, AND W. SPINDEL

Department of Chemistry, Rutgers, The State University, Newark, New Jersey

(Received November 1, 1960)

ISOTOPIC fractionation of nitrogen isotopes between nitric oxide and nitric acid solutions has been the subject of several recent publications.[1,2] Brown and Begun[2] have measured the effective separation factor α at several temperatures (26°–70°) and acid concentrations, and have reported a rather sharp decrease in the factor with increasing temperature. For $\sim 1M$ HNO_3, they measured a drop in α from 1.064 at 26° to 1.023 at 70°.

The equilibrium constant for the reaction $N^{15}O + N^{14}O_3^- \rightleftarrows N^{14}O + N^{15}O_3^-$, can be calculated from spectroscopic data by the method of Bigeleisen and Mayer.[3] Such calculations predict a much smaller decrease in isotopic fractionation at elevated temperatures, than is indicated by the published data.[2] At high nitric acid concentrations, both phases contain appreciable amounts of several chemical species, so that the over-all exchange constant is a weighted average of the equilibrium constants for a number of reactions. As the authors[2] have pointed out, detailed chemical data is not available for the system at elevated temperature, so comparison of measured separation factors with equilibrium constants for individual exchange reactions is not yet possible for such solutions at temperatures other than 25°. In the case of 1M nitric acid, however, at 25°, greater than 99% of the nitrogen in the gas phase is in the form of NO.[4] At elevated temperatures, even though detailed chemical analyses are not available, the colorless appearance of both phases indicates that nitrogen is present in the gas predominantly as NO, and in the liquid, predominantly as NO_3^-. Thus, in dilute nitric acid solution, over the temperature range 25°–70°, the separation factor should be primarily governed by the equilibrium constant for the indicated reaction, with a small correction for the NO which "dissolves" in the solution. In calculating the equilibrium constant from the measured α, it is assumed that the NO dissolved ($\sim$12% to 6% of total nitrogen in the liquid phase, depending upon the temperature) has the same isotopic composition as the NO in the gas phase. This correction is small and diminishes at elevated temperature as the solubility decreases.

In view of the apparent discrepancy between the reported[2] and expected temperature dependencies of

TABLE I. Single-stage fractionation factors for the NO – NO_3^- system.

Temperature, °C	Initial liquid phase	Mole fraction dissolved NO	a_{N_l}	$(m/M)_{N_l}$	α[a]	K[b] derived	K[c] spect.
25±2	0.98M HNO_3	0.121	1.0523	0.190	1.062±0.001	1.071	1.079
	4.5M $Ca(NO_3)_2$	...	1.0683	0.061	1.073±0.001	1.073	
40±1	0.98M HNO_3	0.103	1.0494	0.164	1.058±0.001	1.065	1.073
	4.5M $Ca(NO_3)_2$	...	1.0613	0.058	1.065±0.002	1.065	
55±1	0.98M HNO_3	0.082	1.0460	0.145	1.053±0.002	1.058	1.067
	4.5M $Ca(NO_3)_2$	...	1.0558	0.051	1.059±0.001	1.059	
70±1	0.98M HNO_3	0.065	1.0401	0.115	1.045±0.002	1.048	1.062
	4.5M $Ca(NO_3)_2$	...	1.0534	0.044	1.056±0.001	1.056	

[a] Error is average deviation of 4-6 equilibrations.

[b] Calculated from α by correcting for "dissolved NO".

[c] Calculated from spectroscopic data. The zero-order frequency [see G. Herzberg, *Molecular Spectra and Molecular Structure* (D. Van Nostrand Company, Inc., Princeton, New Jersey, 1950) 2nd ed., p. 558] of NO was used while for NO_3^-, the latest values of the observed frequencies [see G. M. Begun and W. H. Fletcher, J. Chem. Phys. **33**, 1083 (1960)] were used.

the isotopic separation, we have made measurements of the fractionation factors at several temperatures by equilibrating NO gas with liquid phases consisting either of 0.98M HNO_3 or of 4.5M $Ca(NO_3)_2$. Although exchange in the case of the neutral salt solution is considerably slower than in the case of the acid, the use of a nitrate salt is advantageous because NO is only negligibly soluble in the solution. The observed α is thus a direct measure of the equilibrium constant for the exchange reaction; no correction is required for "dissolved NO" and no assumptions are made as to its isotopic composition.

Exchange was studied by saturating the liquid phase with NO gas at 1 atm pressure in an ~150-ml jacketed flask. The solutions were stirred for several days in the case of the acid and for periods of ~1–2 weeks with the salt solutions. For the 25° equilibrations, unjacketed flasks were shaken at room temperature, 25°±2°. Samples of the gas before and after equilibration were mass-spectrometrically analyzed for nitrogen-15 content after being reduced to N_2 with Cu at 700°–800°. The separation factor was calculated from the isotopic abundances using the relationship $\alpha = a + (m/M)(a-1)$, where a is the quotient of N^{15}/N^{14} ratios in the gas phase before and after equilibration, and m and M are the moles of nitrogen in the gas and liquid phases, respectively. The nitric oxide was prepared by complete reduction of the same nitrate or nitric acid used for the equilibration, so that the initial isotopic abundances in the two phases were the same.

The results of our experiments are shown in Table I. It may be noted that the separation factors for ~1M HNO_3 at 55° and 70° are considerably higher than those previously reported.[2] Further, the equilibrium constants for the reaction, derived from the separation factors for ~1M HNO_3 by correcting for "dissolved NO", agree quite well with the values measured with the salt solution where no correction is used. The difference of 0.008 between the derived equilibrium constant for ~1M HNO_3 at 70° and the value for the salt solution at this temperature may be due to some change in the chemical composition of the acid system. The agreement between the measured equilibrium constants and those calculated from spectroscopic data is reasonable considering that the statistical, mechanical equations used in the calculations are strictly applicable only to ideal gaseous substances. As Urey,[5] has pointed out, equilibrium constants calculated by applying such equations to a condensed phase without considering interactions between molecules may be in error by as much as a factor of 1.01. It is interesting to note that the measured equilibrium constants show the temperature dependence as those calculated from spectroscopic data.

A complete investigation of the separation factor as a function of temperature and liquid phase composition is in progress in this laboratory.

* Supported in part by a grant from the U. S. Atomic Energy Commission.

[1] W. Spindel and T. I. Taylor, J. Chem. Phys. **23,** 981 (1955); **24,** 626 (1956); Trans. N. Y. Acad. Sci. **19,** 3 (1956); T. I. Taylor and W. Spindel, *Proceedings of the International Symposium on Isotope Separation* (North-Holland Publishing Company, Amsterdam, Holland, 1958), p. 158; L. N. Kauder, T. I. Taylor, and W. Spindel, J. Chem. Phys. **31,** 232 (1959).
[2] L. L. Brown and G. M. Begun, J. Chem. Phys. **30,** 1206 (1959).
[3] J. Bigeleisen and M. G. Mayer, J. Chem. Phys. **15,** 261 (1947).
[4] E. Abel, H. Schmid, and M. Stein, Z. Elektrochem. **36,** 692 (1930).
[5] H. C. Urey, J. Chem. Soc. **1947,** 562.

Ionization Potentials of Benzene, Hexadeuterobenzene, and Pyridine from Their Observed Rydberg Series in the Region 600–2000 A*

MOSTAFA F. AMR EL-SAYED† AND M. KASHA‡

Department of Chemistry, Harvard University, Cambridge, Massachusetts, and Florida State University, Tallahassee, Florida

AND

Y. TANAKA

Geophysics Research Directorate, U. S. Air Force Research Division (ARDC), Bedford, Massachusetts

(Received November 15, 1960)

IONIZATION potentials of the nitrogen heterocyclics are of considerable interest for quantum chemistry, expecially in relation to calculations on molecules of biological importance. The only sources of data on the lowest I.P.'s of these molecules have been the electron impact and photoionization methods, neither of which gives sufficient information to distinguish electrons originating from different orbitals, e.g., the π orbitals and the (nearly) nonbonding n orbitals of the molecule. We have undertaken a vacuum spectroscopic investigation in the range 600–2000 A of pyridine, pyrimidine, pyrazine, and some of their methyl derivatives, as well as of benzene and hexadeuterobenzene. Numerous new molecular transitions were found and several previously unobserved Rydberg series were recorded and analyzed. Here we report the higher ionization potentials of benzene, hexadeuterobenzene, and pyridine, because of their central interest.

The Rydberg series of benzene in the 1300–1850 A region was first analyzed by Price and Wood[1] and carefully reinvestigated recently by Wilkinson.[2] The latter author gave as the lowest I.P. a value of 9.247±0.002 ev, which he assigned to the ionization of an (e_{2g}) π electron. The present investigation agrees well with this value (cf. Table I). In addition, intense well-developed groups of Rydberg series were observed in two higher

energy ranges. In the range 1050–1350 A, several rather sharp and well-developed series were found, the strong bands of which fit the two main series converging to the same limit of 11.48_9 ev for benzene and 11.52_0 ev for benzene-d_6. Some vibrationally coupled series are observed, the most prominent one having a spacing of 640 cm^{-1}. The lowest two members of these series were observed by Price and Wood,[1] from which an I.P. of 11.7 ± 0.3 ev was estimated. Because of an observed 250 cm^{-1} isotopic blue shift, and the fact that these series converge to the paraffin I.P. region (observed by electron impact and photoionization methods), it was thought that this I.P. in benzene is due to σ_{C-H}-electron ionization. This interpretation was supported by Mulliken.[3] However, the present authors suggest another assignment for the following reasons: (a) an isotopic blue shift of 200 cm^{-1} is observed in the lowest $\pi \rightarrow \pi^*$ transition of benzene,[4] (b) the sharpness of the observed series makes it hard to correlate with the continuous absorption observed for a σ_{C-H} electron ionization in the paraffins,[5] (c) there is only a small effect on the vibrational structure upon deuteration. These facts suggest that these series arise from excitation of an electron from an (a_{2u}) π-electron MO (the lowest π orbital). A very intense continuous absorption is observed under these series which might be due to a σ_{C-H}-electron photoionization (and/or photodissociation).

In the region 700–850 A, Rydberg series are observed with the 0,0 series converging at 16.84 ev, for benzene. This series is relatively diffuse with a simple, strong vibrational coupling. At least five quanta of an $\sim$960 cm^{-1} excited-state vibration are observed in the first member of this series in benzene. Deuteration blue-shifts these series $\sim$250 cm^{-1} and reduces the vibrational frequency to $\sim$930 cm^{-1}. The isotopic ratio for the vibrational frequency is so close to unity as to suggest that this vibration is a ring mode, and thus might be correlated with the ν_2 mode of the ground state, which has a frequency of 992 cm^{-1}. From these observations, the assignment of these highest series to the ionization of a σ_{C-C}-electron is suggested.

For pyridine, a well-developed Rydberg series is found converging to 9.26 ev, a slightly higher value than that of the lowest I.P. of benzene. This is a somewhat more diffuse series compared with the corresponding one in benzene. Higasi[6] as well as Watanabe[5] and their co-workers, assigned their observed lowest I.P. for pyridine as an n-orbital ionization. We believe, however, that the lowest I.P. of pyridine represents the ionization of a π electron from the highest filled MO (a_2). A second Rydberg series converging to a value close to the second I.P. of benzene is observed for pyridine (Table I). Two series of some five members each are found to converge to a common limit of 11.56 ev. This might be due to ionization of an electron from the lowest MO (b_2) in pyridine. The analogy of the two groups of Rydberg series of pyridine and benzene may serve to confirm the assignment of the values given in Table I for pyridine as π-orbital electron-ionization potentials.

TABLE I. Ionization potentials calculated from observed Rydberg series.

Benzene	Hexadeuterobenzene[a]	Pyridine
9.24_8	9.25_1	9.26_8
11.48_9	11.52_0	11.56
16.84	16.87	

[a] The hexadeuterobenzene used in this research was obtained from the Volk Radiochemical Company, Chicago, Illinois.

A group of a few rather strong lines in the range 1200–1266 A were also observed for pyridine. This group can be arranged in a Rydberg series which converges in the neighborhood of 10.3 ev. This may represent either ionization of an electron from the middle filled π-MO (b_2) of pyridine or ionization from the n orbital (a_1). Unique Rydberg series in the other N-heterocyclics studies, corresponding to the nearly nonbonding (lone pair) n orbitals have not been observed in general. The many strong molecular transitions found in the region studied, may steal sufficient intensity from the Rydberg series to make the latter unobservable.

The spectra were photographed on a 2-m normal-incidence Hilger spectrograph with a 15 000 lines/in. grating which gave a dispersion of 8.7 A/mm. Tanaka's[7] rare-gas-continuum light sources were used for the background. The complete paper on our general spectral results, with full experimental details, is in preparation.

We would like to thank Dr. M. Ogawa for his assistance during the course of this work.

* This work was supported mainly by a contract between the Florida State University, Tallahassee, and the Chemistry Division, Office of Scientific Research, ARDC, U. S. Air Force; and partly by the Chemical Research Fund of Harvard University. Research was carried out in the spectroscopy laboratories of the Geophysics Research Directorate, Hq. Detachment 2 U. S. Air Force Research Division (ARDC), L. G. Hanscom' Field, Bedford, Massachusetts.

† Present address: Gates and Crellin Laboratories, California Institute of Technology, Pasadena, California.

‡ On leave from the Florida State University for the academic year September 1959–1960.

[1] W. C. Price and R. W. Wood, J. Chem. Phys. **3,** 439 (1935).
[2] P. G. Wilkinson, Can. J. Phys. **34,** 596 (1956).
[3] R. S. Mulliken, J. chim. phys. **46,** 703 (1949).
[4] F. Garforth, C. K. Ingold, and H. Poole, J. Chem. Soc. **1948,** 508.
[5] K. Watanabe, T. Nakayama, and J. Mottl, Final Report (Project No.: Department of Army, No. 5B99-01-004, Ordnance R and D, No. TB2-0001, 00R-No. 1624), Department of Physics, University of Hawaii, December, 1959.
[6] K. Higasi, I. Omura, and H. Baba, J. Chem. Phys. **24,** 623 (1956).
[7] Y. Tanaka, A. S. Jursa, and F. LeBlanc, J. Opt. Soc. Am. **48,** 304 (1958).

Comments and Errata

Comments on the EPR Spectrum of Mn^{++} in Calcite

L. M. MATARRESE

U. S. Naval Research Laboratory, Washington, D. C.

(Received November 1, 1960)

THE purposes of this letter are: (a) to provide an explanation for the weak lines in the EPR spectrum of Mn^{++} in calcite reported by Kikuchi and Matarrese[1] (KM); (b) to call attention to a feature that was neglected in their treatment of the doublet splitting of the fine structure; and (c) to mention briefly the results of a low-temperature experiment and an investigation of the $\Delta M=\pm 2$ spectrum that has been found in this system.

The weak lines have been identified as belonging to transitions of the type $\Delta M=-1$, $\Delta m=\pm 1$, where M and m are the electronic and nuclear magnetic quantum numbers, respectively. The positions and intensities of these lines are consistent with the mechanism proposed by Ludwig and Woodbury,[2] in which states of different M are mixed by the DS_z^2 term and states of different m by the $\frac{1}{2}B(S_+I_-+S_-I_+)$ term in the spin Hamiltonian. Transitions of this kind have also been observed in the EPR spectrum of Mn^{++} in $ZnSiF_6\cdot 6H_2O$ by Friedman and Low.[3] The transition probabilities for the transitions $M\rightarrow M-1$, $m\rightarrow m\pm 1$, as calculated from the first-order wave functions for the case $g_{\|}=g_{\perp}$, $A=B$ applicable to Mn^{++} in calcite, and for $H_{rf}\perp H$, are

$$T_{\pm}=T_0[I(I+1)-m(m\pm 1)]\left(\frac{D}{g\beta H}\right)^2\sin^2\theta \times\cos^2\theta\left[\frac{S(S+1)+3M(M-1)}{2M(M-1)}\right]^2, \quad (1)$$

where T_0 is the transition probability for the transition $M\rightarrow M-1$, $m\rightarrow m$, and θ is the angle between the magnetic field H and the c axis of the crystal. All predictions of Eq. (1) have been verified by experiment. The transitions are not observable at $\theta=0°$ and 90° and have maximum intensity at $\theta=45°$, although they are most clearly seen at $\theta\approx 30°$, where there is minimum interference from the lines of the regular ($\Delta m=0$) spectrum. The dependence on $(D/g\beta H)^2$ explains the much greater intensity at X band than at K band. In fact, at X band some of these lines are almost as intense as the weakest lines of the regular spectrum and no longer can be described as "weak." According to Eq. (1), there should be five pairs of lines for each of the five $M\rightarrow M-1$ transitions, adding 50 lines to the 30 lines of the regular spectrum. The five pairs belonging to $M=\frac{1}{2}$, however, are by far the strongest and are the ones appearing in the K band spectrum illustrated in Fig. 8 of KM. The weaker satellites mentioned by KM are assumed to belong to $M\neq\frac{1}{2}$ transitions, and as such their positions vary considerably with angle.

The line positions of the $M=\frac{1}{2}$ pairs have been analyzed. It was found necessary to include the direct nuclear interaction term—$g_N\beta_N\mathbf{H}\cdot\mathbf{I}$ in the Hamiltonian and carry out the perturbation calculation to third order to explain the observed facts about them, especially the magnitudes of the component separation of the pairs at X band and K band, and their variation across the spectrum.

Weak lines assumed to correspond to the transitions $\Delta M=\pm 1$, $\Delta m=\mp 1$, allowed only for $H_{rf}\|H$, have also been observed.

The interpretation by KM of the doublet splitting of the strong and weak satellites of the regular spectrum, was incomplete in that it considered only the *magnitude* of the splitting and its variation with the azimuthal angle ψ, whereas a *shift* in the mean positions of the doublets also occurs. This can be seen clearly in Fig. 5 of KM by comparing the traces for $\psi=-30°$ and $\psi=30°$. Thus, if we set $b_3^{(P)}$ of Eq. (25) of KM equal to $a-ib$ and take the *mean* of the matrix elements rather than the difference, we find the position of the center of the doublet varies as $a_0 a\sin^3\theta\cos\theta\sin 3\psi$. Experimentally, the amplitude of the $\sin 3\psi$ function for the strong doublet is 6.75 gauss at $\theta=60°$.

From the differences in intensities of the lines of the EPR spectrum at 4.2°K, it has been determined that D is negative. From a knowledge of the relative signs of D, A, and a_0, and under the sign convention adopted by KM [Eq. (21)], this means that A is negative and a_0 is positive. An interesting feature of the low-temperature spectrum is that the lines in the middle of the spectrum appear to saturate less readily than the lines at either end. In addition, the g factor becomes anisotropic ($g_{\|}\approx 2.004$, $g_{\perp}\approx 1.997$) and the numerical values of A and D are slightly greater.

Finally, a spectrum of 24 lines corresponding to $\Delta M=\pm 2$ transitions has been found, centered at $\frac{1}{2}H_0$. This "half-field" spectrum has maximum intensity at $\theta=90°$, $H_{rf}\|H$. It has not been found possible to fit satisfactorily the observed line positions, even using third-order perturbation corrections; the discrepancy in some cases amounts to ten times the experimental error.

A more detailed treatment of the foregoing subjects is planned for later publication.

[1] C. Kikuchi and L. M. Matarrese, J. Chem. Phys. **33,** 601 (1960).
[2] G. W. Ludwig and H. H. Woodbury, Bull. Am. Phys. Soc. Ser. II, **5,** 158 (1960).
[3] E. Friedman and W. Low, Phys. Rev. (to be published).

Dipole Moment of Lithium Hydride

F. A. MATSEN

Departments of Chemistry and Physics, The University of Texas, Austin, Texas

(Received November 3, 1960)

THE failures of *ab initio* polyelectronic, molecular quantum mechanics are well known. It may be appropriate, therefore, to call attention to one of its apparent successes, particularly since this success was not indicated in the communication[1] containing the necessary documentation.

The dipole moment of lithium hydride has been calculated by a number of different methods. (See Table I.)

It is seen that several different types of basis functions in the hands of several different research groups, predict the dipole moment of lithium hydride in the range 5.6–6.3 debye in comforting agreement with the experimental 5.9 debye. The calculated energies, however, lie ~2 ev below the experimental energy, so that none of the wave functions can be regarded as extremely good wave functions. In fact, in the two cases[2,3] in which the calculations have been made, $(du/dR)R_e$ is off by more than a factor of two. This is, however, admittedly more difficult to calculate than the moment itself. We have no direct assurance that calculations will not be made in the future, which while yielding a better energy, may nevertheless give a poorer dipole moment. However, we can expect considerable improvement in the energy by choosing wave functions which include more electron correlation, an inclusion which might have only a small effect on the dipole moment.[4]

The fact remains that at least eight different *ab initio* four-electron calculations were made on the dipole moment before it was measured and all agree

TABLE I.

Method	Dipole moment debye units
I. Classical, nonpolarizable ions $\mu=eR$	7.6
II. Classical, polarizable ions $\mu=eR\left[1-\frac{R^3[\alpha(Li^+)+\alpha(H^-)]+4\alpha(Li^+)\alpha(H^-)}{R^6-4\alpha(Li^+)\alpha(H^-)}\right]$	
(a) Klemperer and Margrave[a] (1952) $\alpha(H^-)=1.8\times10^{-24}$ cm^3	4.1
(b) Altshuler[b] (1953) $\alpha(H^-)=14.6\times10^{-24}$ cm^3	model fails
III. Ionic-covalent resonance $\mu=IeR$ (I=fraction ionic character)	
Pauling[c] (1940)	2.0
IV. *Ab Initio* quantum mechanics $\mu=eR-e\sum_i\int\psi Z_i\Psi d\tau$	
(a) Two electrons	
1. Adamov[d] (1949)	3.5
(b) Four electrons[e]	
1.[f] Hurst, Miller, and Matsen[g] (1957) SO, VB, CI	6.0
2. Hurley[h] (1958) SO, MO, CI	6.3
3. Ormand and Matsen[i] (1958) Elliptical coordinate MO	5.6
4. Platas and Matsen[j] (1958) (a) plus H-atom polarization	5.6
5. Karo and Olson[k] (1959) SCFAO, VB, CI	6.1
6. Karo[l] (1959) SCFAO, MO, CI	6.1
7.[m] Robinson, Stuart, and Matsen[n] (1960) Radially correlated VO, VB, CI	<6.2
8. Ransil[o] (196) SO, MO, CI	5.9
V. Experimental	
Wharton, Gold, and Klemperer[p] (1960)	5.9

[a] W. A. Klemperer and J. L. Margrave, J. Chem. Phys. **20,** 527 (1952).
[b] A. P. Altshuler, J. Chem. Phys. **21,** 2074 (1953).
[c] L. Pauling, *The Nature of the Chemical Bond* (Cornell University Press, Ithaca, New York, 1940).
[d] M. Adamov, Zhur. Fiz. Khim. **23,** 1172 (1949).
[e] SO=Slater orbitals; SCFAO=self-consistent field atomic orbitals; VB=valence bond; MO=molecular orbital; CI=configuration interaction.
[f] Karo and Olsen presented the first 4-electron calculation in the April 1956 MIT Molecular and Solid-State Group Quarterly Report. For results see work cited in footnote 3. The R. P. Hurst, J. Miller, and F. A. Matsen paper was submitted in June, 1956.
[g] R. P. Hurst, J. Miller, and F. A. Matsen, J. Chem. Phys. **26,** 1092 (1957).
[h] A. C. Hurley, J. Chem. Phys. **28,** 532 (1958).
[i] F. T. Ormand and F. A. Matsen, J. Chem. Phys. **29,** 105 (1958).
[j] O. Platas and F. A. Matsen, J. Chem. Phys. **29,** 965 (1958).
[k] See work cited in footnote 2.
[l] See work cited in footnote 3.
[m] This calculation gave the lowest energy of any entry in the table. As was stated in the paper, the calculated dipole moment is probably high since it did not include the hydrogen polarization of number (5) which lowered the dipole moment of number (1) by 0.4 debye.
[n] J. M. Robinson, J. D. Stuart, and F. A. Matsen, J. Chem. Phys. **32,** 988 (1960).
[o] See work cited in footnote 6.
[p] See work cited in footnote 1.

with it to ±0.3 debye. Other methods failed completely. This is the first accurate *ab initio* prediction of a molecular property that has been made[5] and it is, at least, encouraging.

[1] L. L. Wharton, P. Gold, and W. A. Klemperer, J. Chem. Phys. **33,** 1255 (1960).
[2] A. M. Karo and A. R. Olson, J. Chem. Phys. **30,** 1232 (1959).
[3] A. M. Karo, J. Chem. Phys. **30,** 1241 (1959).
[4] The more conventional analysis is

$$\phi-\psi_0=\sum_{n=1} a_n\psi_n.$$

Then

$$E_\phi-W_0\sim\sum a_n^2W_n$$

and

$$\mu_\phi-\mu_{00}\sim\sum_n a_n\mu_{0n},$$

where ϕ is the trial wave function and ψ_n the true wave function. The statement made in the text implies that many of μ_{0n} are zero or small.
[5] For HF, Ransil[6] calculated 1.4 *D* while the experimental value is 1.7 *D*. However, in this case the measurement was made first.
[6] B. Ransil, Revs. Modern Phys. **32,** 239 (1960).

Diamagnetic Susceptibility of Ne, NH_3 and CH_4

K. E. Banyard

Department of Physics, University of Leicester, Leicester, England

(Received November 8, 1960)

In a recent paper[1] the purely diamagnetic contribution χ_r[2] to the molar diamagnetic susceptibility χ was calculated for the gaseous state of the neon-like series of molecules Ne, H_2O, NH_3, CH_4, and NH_4^+ by using some of the wave functions already known. A comparison of the results with the "experimental" values for χ_r enabled a study to be made of the relative accuracy of the wave functions employed. One conclusion which emerged was that for CH_4 the generally accepted experimental χ of -12.2 was thought to be too small and a redetermination of this quantity was suggested.

In a private communication, Barker, Meisenheimer, and Stevenson[3] have kindly provided the writer with a preprint of work to be published elsewhere concerning the measurement of χ for some 30 diamagnetic molecules in the gaseous state. Included in their study was a redetermination of χ for Ne, NH_3, and CH_4. These values are quoted in Table I, column one, along with results from the work cited in footnote 1 which are of particular interest here.

Proceeding as before, it is now seen that for CH_4 the theoretical χ_r, derived from Hartree-Fock wave functions, agrees quite well with the "experimental" value for χ_r based on the new determination for χ. In the case of the Ne and NH_3 we see that the more recent "experimental" values for χ_r are still greater than the theoretical χ_r when derived from analytical central-field wave functions; hence, the previous conclusion that such wave functions result in a radial density which is somewhat too concentrated, is still valid. It is perhaps worthwhile mentioning that the conclusions drawn for H_2O in the work cited in footnote 1 indicate that the radial electron density distribution for NH_3, resulting from the Roothaan treatments of Kaplan[4] and Duncan,[5] is expected to yield a theoretical χ_r which is superior to that quoted here.

For Ne, the Hartree-Fock functions of Worsley[6] have recently come ot our notice and we find that they provide a χ_r of -7.46. This result represents a considerable improvement on the theoretical value quoted in Table I, the remaining discrepancy, when compared with the latest experimental value, is indicative of a slight over-diffuseness of the radial density and prob-

Table I. Comparison of magnetic susceptibilities.

	Experimental				Theoretical
	χ[a]	χ_{hf}[b]	χ_r[c]	χ_r[d]	χ_r
Ne	-6.96 ± 0.14	...	-6.96 ± 0.14	-6.75	-5.8[e]
NH_3	-16.3 ± 0.8	$+4.3$	-20.6 ± 0.8	-23.0	-18.8[e]
CH_4	-17.4 ± 0.8	$+9.3$	-26.7 ± 0.8	$-21.5/-25.3$	$-28.4/-29.0$[f]

[a] Results of Barter, Meisenheimer, and Stevenson.
[b] χ_{hf} is the experimentally-derived paramagnetic contribution to χ.
[c] χ_r is the "experimental" radial contribution to χ derived from footnotes a and b.
[d] The previous "experimental" χ_r quoted in the work cited in footnote 1.
[e] Calculated from analytical central-field wave functions with exchange, see work cited in footnote 1.
[f] Calculated, respectively, from the Hartree-Fock and Hartree-Fock-with-angular-allowance wave functions of I. M. Mills, Mol. Phys. **1,** 99 (1958), see work cited in footnote 1; relevant comments on these wave functions are made by A. F. Saturno and R. G. Parr, J. Chem. Phys. **33,** 22, (1960); K. E. Banyard, J. Chem. Phys. (to be published).

ably arises from the omission in the Hartree-Fock treatment, of correlation effects between electrons with anti-parallel spins.

If the correction for correlation interaction were to have the effect as indicated above for Ne, and recent results[7,8] show that a radial density contraction does seem to be the general trend; then, for the case of CH_4, the inclusion of correlation in the Hartree-Fock treatment with angular allowance might well cause a further improvement in the agreement of the theoretical χ_r with "experiment."

[1] K. E. Banyard, J. Chem. Phys. **33,** 832 (1960).
[2] All values of χ_r, χ_{hf}, and χ are quoted here in units of 10^{-6} emu/mole; χ_r and χ_{hf} are expressed with respect to the center of mass of the molecule as the origin.
[3] C. Barter, R. G. Meisenheimer, and D. P. Stevenson, J. Phys. Chem. **64,** 1312 (1960).
[4] H. Kaplan, J. Chem. Phys. **26,** 1704 (1957).
[5] A. B. F. Duncan, J. Chem. Phys. **27,** 423 (1957).
[6] B. H. Worsley, Can. J. Phys. **36,** 289 (1958).
[7] P. Löwdin and L. Redei, Phys. Rev. **114,** 752 (1959).
[8] B. Dawson, Acta Cryst. **13,** 403 (1960).
Letter K p. 39 Gal. 1X

Erratum: Higher Order Rotation-Vibration Energies of Polyatomic Molecules. IV

[J. Chem. Phys. **29,** 665 (1958)]

GILBERT AMAT

Laboratoire de Chimie Physique, Faculté des Sciences de Paris, Paris, France

AND

HARALD H. NIELSEN

Laboratory of Molecular Structure and Infrared Studies, Department of Physics and Astronomy, The Ohio State University, Columbus, Ohio

(Received November 4, 1960)

A FEW errors in copying from the original manuscript have crept into our paper published two years ago. They are the following:

Equation (3), p. 665, read

$$H^{\dagger} = \cdots \text{ instead of } H^{+}.$$

Table IV, p. 670, in the right side of the 9th formula, read

$$(2)^{\beta'} T^{\text{bcd}} \text{ (replacing } \beta'' \text{ by } \beta').$$

Table V, p. 670, in the right side of the 7th formula delete: $+\frac{1}{2}{}^{\alpha\beta}\Pi$, in the right side of the 10th formula, replace γ by ϵ and ϵ by γ, in the right side of the 11th formula read *ijklmn* (adding *i*) under the first sign $*\Sigma$ and replace the quantity after the second sign $*\Sigma$ by $\epsilon_{ef(k\leq l\leq m)}{}^{j,klm}$.

Table VI, p. 671, in the right side of the 11th formula, read

$$(1+\delta_{am}+\delta_{bm}), \text{ replacing } l \text{ by } b;$$

the formula before the last can be omitted since it can be seen that ${}^{\alpha\beta}\Pi = 0$.

Table VI, continued p. 672, in the left side of the 5th formula, replace *ef* by *e, f*; in the right side of the 8th formula, insert 2 between + and [; add } at the end.

The authors wish to express their gratitude to Dr. S. K. Kurtz who verified the computations involved in this paper and pointed out the errors listed above.

Erratum: Observations of the Thermal Behavior of Radicals in Gamma-Irradiated Ice

[J. Chem. Phys. **32,** 1249 (1960)]

SEYMOUR SIEGEL, L. H. BAUM, SOL SKOLNIK, AND JOHN M. FLOURNOY

Chemical Division, Aerojet-General Corporation, Azusa, California

(Received October 24, 1960)

AS a result of a calculational error the OH radical yields given in this paper are too high by approximately a factor of 3. Therefore, the conclusion drawn from the relatively low yields of H_2O_2 found, namely, that H_2O_2 is not the main product of the OH recombination reaction, may not be a valid one. In fact, if the revised OH radical yields are used, then the H_2O_2 yields discussed are within experimental error of the values predicted on the basis of a simple recombination reaction. However, the conclusion that the recombination reaction $H+OH \rightarrow H_2O$ is the primary reaction, occuring *during* irradiation at 77°K, is not strongly affected by the revision in OH yields.

Erratum: Pressure Dependence of Some Infrared and Vacuum Ultraviolet Bands Occurring in Active Nitrogen

[J. Chem. Phys. **33,** 1112, (1960)]

ROBERT A. YOUNG*

Boeing Airplane Company, Seattle, Washington

(Received November 10, 1960)

THE first paragraph on p. 1116 should be replaced by the following:

Oldenberg and Carlton[20] have related the radiative lifetime τ_A of the $A\ {}^3\Sigma_u{}^+$ state to the lifetime τ_B of the

$B\,^3\Pi_g$ state (now referring to the $v'=0$ level in all cases) in the following manner,

$$\tau_A = 1.6\times10^6\tau_B.$$

Our measurements thus restrict τ_A; $0.24<\tau_A<50$ sec. The lower limit is approximately 10 times that computed by Wilkinson and Mulliken[21] from absorption measurements.

In the paragraph just preceding the Acknowledgements, the inequality $4\times10^{-5}>R(A\,^3\Sigma_u^+)>5.5\times10^{-7}$ should be replaced by $4\times10^{-7}>R(A\,^3\Sigma_u^+)>2\times10^{-9}$. Wherever it occurs, $A\,^3\Sigma_g^+$ should be replaced by $A\,^3\Sigma_u^+$. In footnote 11(a) "frequency" should be replaced by "wavelength."

The radiative lifetime of the $B\,^3\Pi_g$ state, 7×10^{-7} sec, found recently from emissivity measurements of shock heated air[1] is in reasonable agreement with the results presented here.

* Present address: Stanford Research Institute, Menlo Park California.

[1] J. Keck, J. Camm, B. Kivel, and T. Wentink, Jr., Ann. Phys. **7**, 1 (1959).

Notes

The Nuclear Quadrupole and Electron Spin Resonance Spectra of some Chlorine Compounds Including $(Me_3PhN)(FeCl_4)$

C. D. Akon and T. Iredale

Department of Physical Chemistry, University of Sydney, Sydney, Australia

(Received September 26, 1960)

QUADRUPOLE transitions may readily be investigated in chlorine compounds with the aid of continuous wave or super-regenerative oscillators, as the energies of such changes lie within the range of these instruments. We record in this paper quadrupole resonances observed in four organic chlorine compounds, and discuss the absorption found in $(Me_3PhN)^+(FeCl_4)^-$.

The quadrupole transitions have been observed with a self-quenched super-regenerative oscillator of the Dean [1] type. The signal was modulated, using a 50 cps magnetic field, and the resonances were displayed using a narrow band 100 cps amplifier, phase sensitive detector and Varian chart recorder. Frequency measurements were made using a BC 221 wave meter; all our readings are reproducible to ±0.02 Mc. All quadrupole measurements quoted were made at liquid nitrogen temperature 77°K.

First the Cl^{35} resonance in the series α-ω-$(CH_2)_n\,Cl_2$ ($n=1-5$) was investigated. Table I shows the frequencies obtained by the present authors and those of previous workers. The results we have obtained with CH_2Cl_2 and $CH_2Cl\cdot CH_2Cl$ agree well with the previous data. A resonance not previously found was observed in α-ω-$(CH_2)_4Cl_2$. No resonance has yet been recorded for the corresponding mono-substituted paraffin butyl chloride.

TABLE I.

	Resonance frequency Mc	Approx. S/N ratio	Previous results Mc	n
CH_2Cl_2	35.990	100	35.991[a]	1
$Cl(CH_2)_2Cl$	34.361	300	34.361[a]	2
α-ω-$(CH_2)_3Cl_2$	none observed in range 31–40	...	...	3
α-ω-$(CH_2)_4Cl_2$	32.630	100	...	4
α-ω-$(CH_2)_5Cl_2$	none observed in range 31–40	...	...	5
$CH_3CHClCOOH$	do do	...	...	
CH_2ClCH_2COOH	33.65	50	...	

[a] R. Livingston, J. Phys. Chem. **57**, 496 (1953).

However, the Cl^{35} quadrupole frequency in *n*-propyl chloride is 32.968 Mc[2] at 77°K, and this may be taken as the approximate value of the resonance frequency in *n*-butyl chloride. This is seen to be close to the α-ω-$(CH_2)_4Cl_2$ frequency, and is not unexpected since the four paraffinic hydrocarbons will prevent interaction between the end chlorine atoms of the latter. There is a "drop" in the Cl^{35} frequency as n increases from 2 to 4, which is presumably a reflection of the increase in polarity of the bond as n increases. The inductive effect of a longer chain would account for this greater polarity. From another point of view, the "ellipsoidal" form of the electron probability distribution or p character of the bond, is changing to a more "spherical" or s character. But it is extraordinary that the signal to noise ratio (S/N) was so low for the two odd values of n, 3 and 5, that no resonances could be found. No reason can be offered for these negative results at the present time.

The α and β-chloropropionic acids were investigated, and the β-isomer gave a resonance at 77°K, but no response could be obtained from the α isomer. Again no explanation can be given for this negative result. These anomalies may be wrapped up in some crystallization problem which is not readily elucidated.

A very broad apparent absorption was found in $(Me_3PhN)(FeCl_4)$ near 33.3 Mc. On further investigation this was found to be an electron paramagnetic resonance A continuous wave oscillator of the Wang type operating near 30 Mc was used as a source of rf power for the sample placed in the tank coil. The

magnetic field and modulation required to observe the resonance were provided by a Helmholtz coil driven from a Variac transformer. This allowed fields of up to 200-gauss peak to be obtained. The resonance was displayed using a flat amplifier and oscilloscope. Diphenyl picryl hydrazyl whose resonance is known[3] to occur at $g=2.0$ allowed the spectrometer to be calibrated. Attempts to prepare a single crystal of the ($FeCl_4^-$) complex were not successful, but a partially oriented crystal was grown from the melt, and the g value of the paramagnetic resonance was found to be about 2. The resonance was very broad, about 200 gauss, and the linewidth varied with the orientation of the sample to the magnetic field. Using an X-band spectrometer and magnetic field of about 2000 gauss the results at low fields were confirmed. A single line was found with g values of 2.010 ± 0.002, and independent of the orientation of the crystal to the magnetic field. The linewidth was found to lie between 60 and 80 gauss, depending on the crystal orientation. All measurements were made at room temperature. There was no fine or hyperfine structure visible.

Unfortunately the results were not sufficient for us to draw any conclusions from the orbital distribution of the electrons available for bonding in Fe^{III}.

Our thanks are due to Dr. G. S. Bogle of C.S.I.R.O., Sydney, for obtaining the paramagnetic resonance at high field.

One of us (C.D.A.) is indebted to the C.S.I.R.O. for a studentship.

[1] C. Dean (Ph.D. thesis, Harvard University, Cambridge, Massachusetts, 1953).
[2] R. Livingston, J. Chem. Phys. **20**, 1170 (1952).
[3] D. J. E. Ingram, *Spectroscopy at Radio and Microwave Frequencies* (Butterworths Publications, Ltd., 1955).

Degassing of Liquids for Nuclear Spin-Lattice Relaxation Studies*

J. Lees and B. H. Muller†
University of British Columbia, Vancouver, Canada
and
J. D. Noble
University of Wyoming, Laramie, Wyoming

(Received September 30, 1960)

WE wish to report a method for degassing liquids for the purpose of studying their nuclear spin-lattice relaxation time T_1. Previous studies have shown that the T_1 of liquids not degassed is often determined by the dissolved oxygen in the liquid rather than by intrinsic interactions of the pure liquid.[1-3] Reported methods of degassing liquids involve prolonged boiling in vacuo, bubbling of helium, or a freeze-pump-thaw technique.[1-4]

Our method is a simple modification of the gettering technique used by Sandu, Lees, and Bloom[5] to remove oxygen from gases. With the sample kept frozen in the bottom part of a sample tube, a diffuse layer of misch metal is deposited on a spherical surface at the top of the tube by flashing the misch metal in an argon atmosphere at a pressure of a few millimeters. Before and after flashing, the tube is pumped to 10^{-5} or 10^{-6} mm. The tube is sealed off with the sample still frozen. It is not necessary to vaporize the liquid.

Table I. Room temperature nuclear spin-lattice relaxation times of paraffin hydrocarbons. (All times are in seconds.)

Substance	Our values: Untreated sample	Our values: Degassed sample	Other reported values
n-pentane	2 to 9	14.1	4.6[a]
n-hexane	0.77	9.7	2.1[a]
n-heptane	2.3	7.0	2.1[b]

[a] See footnote 6.
[b] See footnote 3.

We have used this technique to prepare samples of *n*-pentane, *n*-hexane, and *n*-heptane, and our results are summarized in Table I. The original samples were pure grade samples from Phillips Petroleum Company. Untreated samples were found to give T_1's of 2 to 9, 0.77, and 2.3 sec, respectively, at room temperature. In the case of pentane, T_1 depended on the freshness of the sample. After treatment, we obtained reproducible times of 14.1, 9.7, and 7.0 sec, respectively. The pentane sample shows no evidence of deterioration after several weeks and it is assumed that the getter will continue to absorb any oxygen which may come off the glass walls.

These values compare with values of 4.6 sec (27°C) for an untreated sample of *n*-pentane and 2.1 sec (28°C) for an untreated sample of *n*-hexane by Benedek and Purcell,[6] and 2.1 sec (28°C) for a "degassed" sample of *n*-heptane by Nolle and Mahendroo.[3]

It is not yet clear whether this technique is applicable to the degassing of water. We have prepared two samples of water this way. The procedure is complicated by the fact that the getter is rapidly attacked by water vapor. We started with a carefully distilled sample of water which gave a T_1 of 3.4 sec at room temperature. Our first treated sample had a T_1 of 4.0 sec which agrees with the value obtained by Chiarotti, Cristiani, and Giulotto[1] when a temperature correction using Simpson and Carr's data was used. In this case, the sample deteriorated after several weeks. Another sample was then prepared which had a T_1 of 3.4 sec before and after treatment. When a sample of this water was deliberately oxygenated, T_1 was reduced to 2.6 sec.

Our results, together with the work of Nolle and Mahendroo,[3] imply that the pressure dependence of T_1 in at least most of the liquids studied by Benedek and Purcell[6] should be interpreted as the pressure dependence of the impurity relaxation rather than the pressure dependence of the intrinsic relaxation of the pure liquids.

The nuclear spin-lattice relaxation time, T_1, of the protons of these samples was measured at 30 Mc by a pulse technique similar to that of Billings and Nolle[7] within an accuracy of about 5%, limited chiefly by temperature control. Studies of the temperature dependence of these samples are in progress and will be reported shortly.

We wish to thank J. F. Harrod for the distilled water sample, and H. S. Sandhu for the use of his vacuum system.

* Supported in part by the National Research Council of Canada and the U. S. National Science Foundation.

† Holder of National Science Foundation Science Faculty Fellowship on leave of absence from the University of Wyoming.

[1] G. Chiarotti, G. Cristiani, and L. Giulotto, Nuovo cimento **1**, 863 (1955).
[2] G. W. Nederbragt and C. A. Reilly, J. Chem. Phys. **24**, 1110 (1956).
[3] A. W. Nolle and P. P. Mahendroo, J. Chem. Phys. **33**, 863 (1960).
[4] J. H. Simpson and H. Y. Carr, Phys. Rev. **111**, 1201 (1958).
[5] H. S. Sandhu, J. Lees, and M. Bloom, Can. J. Chem. **38**, 493 (1960).
[6] G. D. Benedek and E. M. Purcell, J. Chem. Phys. **22**, 2003 (1954).
[7] J. J. Billings and A. W. Nolle, J. Chem. Phys. **29**, 214 (1958).

ν_5 Vibration of Adsorbed Ethylene*

L. H. Little†

Division of Applied Chemistry, National Research Council, Ottawa, Canada

(Received September 12, 1960)

THE infrared-inactive ν_5, C—H stretching vibration of ethylene, has been variously assigned to lines occurring at 3272 cm^{-1} [1] and at 3075 cm^{-1} [2] in the Raman spectrum of liquid ethylene. More recently, a detailed study of the infrared spectra of deuterated ethylenes led Crawford *et al.*,[3] to assign the ν_5 vibration at 3075 cm^{-1}. In the present investigation of the spectrum of ethylene adsorbed at 79°K on porous Vycor glass, evidence is given to support the latter assignment.

Sheppard and Yates[4] have shown that bands which normally occur only in the Raman spectrum, may appear in the infrared spectrum of adsorbed molecules. These vibrations are infrared-forbidden, but appear in the spectrum of the adsorbed material because of perturbation of the molecules by the surface, and loss of molecular symmetry.

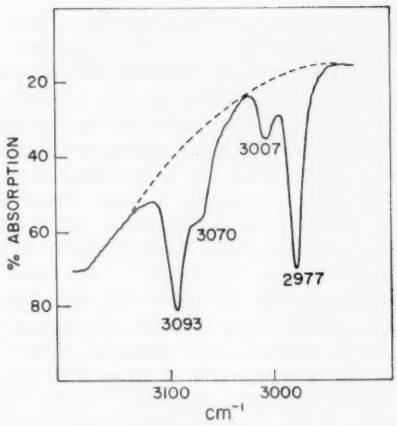

FIG. 1. Infrared spectrum of ethylene adsorbed at 79°K on porous Vycor glass.

The spectrum of ethylene (Fig. 1) adsorbed on porous glass, shows bands at 3093 cm^{-1} and 2977 cm^{-1}, due to infrared-allowed ν_9 and ν_{11}, C—H stretching vibrations, respectively. In addition to these, a band appears at 3007 cm^{-1}, which has been assigned by Sheppard and Yates[4] to the ν_1, totally symmetric, C—H stretching mode. This band appears in the infrared spectrum due to loss of symmetry of the ethylene molecule in the adsorbed state. In the spectrum (Fig. 1), measured with somewhat higher resolution, a fourth band appears at 3070 cm^{-1}.

Herzberg[1] has assigned a weak band at 3075 cm^{-1} in the Raman spectrum of liquid ethylene, to the ν_9 (3105 cm^{-1} in the infrared spectrum of the gas phase) vibration. This band is Raman-forbidden but was said to appear,[1] displaced to lower frequency, because of molecular interaction in the liquid state.

Unless there is more than one type of adsorbed ethylene, the infrared band, appearing at 3070 cm^{-1} in Fig. 1, cannot be assigned to the ν_9 vibration since an intense band occurs at 3093 cm^{-1} due to this vibration. In view of this fact, it is probable that the 3070 cm^{-1} band is due to the ν_5 vibration since no combination of other bands can explain its occurrence.

The relative intensities of the 3070 cm^{-1} and 3093 cm^{-1} bands appear to be independent of surface coverage, suggesting that only one surface species was involved. Both bands were completely removed from the spectrum of the surface by room temperature evacuation of the sample, mass spectrometric analysis of the material so obtained, showed it to be pure ethylene.

The assignment of the ν_5 vibration to 3070 cm^{-1}, is supported by the observation that no band appeared in the spectrum of adsorbed ethylene at 3272 cm^{-1}, the frequency assigned by Herzberg to this vibration. How-

ever, this fact alone would not rule out the assignment of the ν_5 vibration to 3272 cm^{-1} since there is no *a priori* reason why an infrared-forbidden band of surface molecules, should appear with measurable intensity in the spectrum.

* Issued as National Research Council No. 6093.
† National Research Council, Postdoctorate Fellow 1958–1960.
[1] G. Herzberg, *Infrared and Raman Spectra* (D. Van Nostrand Company, Inc., Princeton, New Jersey, 1945), p. 327.
[2] For details see work cited in footnote 1.
[3] B. L. Crawford, J. E. Lancaster and R. G. Inskeep, J. Chem. Phys. **21**, 678 (1953).
[4] N. Sheppard and D. J. C. Yates, Proc. Roy. Soc. (London) **A238**, 69 (1956).

Note on the Sublimation of Ammonium Perchlorate

H. M. Cassel and I. Liebman

Explosives Research Laboratory, Bureau of Mines, Pittsburgh, Pennsylvania

(Received May 6, 1960)

AMMONIUM salts of weaker acids sublime through dissociation, e.g., $NH_4Cl = NH_3 + HCl$. Thus far, however, the mechanism by which ammonium perchlorate (APC) sublimes, has not been definitely established experimentally. Galway and Jacobs,[1] in a recent study of the high-temperature decomposition of APC, express the opinion that APC probably sublimes undissociated, owing to the powerful proton-donating power of perchloric acid, and to the stabilization by hydrogen bonding. An occasional observation by Freeman and Anderson[2] of spheroidal crystallites[3] formed in the sublimation under vacuum of APC, suggested that in this process, precipitation of a liquid phase precedes crystallization.

In an attempt to verify this expectation, a 3/4-in. test tube, 6 in. long, containing about 250 mg pure APC, was heated at the base to 300°C and then evacuated. Temperatures of the glass wall were measured by thermocouples attached at the base and at 1-, 2-, and 3-in. distances. Within a few minutes after closing the outlet to the pump, a deposit of droplets appeared on the glass where the temperature had reached 50°C. On repeating evacuation, these drops coalesced to form larger patches of liquid, which extended to cooler parts of the wall. It was first thought that liquid APC had been formed. However, when pure ammonia was admitted, the liquid drops immediately crystallized. Infrared analysis showed 62% HNO_3 and $12\pm5\%$ $HClO_4$; in addition, the presence of HCl was confirmed by a "wet test." This agrees with a measured *p*H of 3.3 for an aqueous solution of the droplets. The $HClO_4/HNO_3$ ratio as determined, suggests the decomposition reaction:

$$NH_4ClO_4 \approx (HClO_4 + NH_3)/6 + 5(HNO_3 + HCl + H_2O)/6.$$

Accordingly, only one-sixth of the reaction would be simple dissociation. The heat generated upon addition of ammonia is more than 60 kcal and is thus sufficient to evaporate the excess of water and to release a crystalline product, as described.

[1] A. K. Galway and P. W. M. Jacobs, J. Chem. Soc. (London) **1959**, 837.
[2] Information obtained verbally from E. S. Freeman and D. Anderson, The Feltman Research Laboratory, Picatinny Arsenal, Dover, New Jersey.
[3] E. D. Jones, D. S. Burgess, and E. S. Amis, Z. physik. Chem. **4**, 222 (1955).

Ion-Neutral Reactions in the Helium-Hydrogen System

Martin Hertzberg, Donald Rapp, Irene B. Ortenburger, and Donald D. Briglia

Lockheed Missiles and Space Division, Palo Alto, California

(Received August 22, 1960)

WE have measured the appearance potential of the HeH^+ ion, formed by primary ions with average kinetic energy above 10 ev, and have found that it coincides with the appearance potential of the H_2^+ ion. As a result, all three secondary reactions listed below must be considered in the helium-hydrogen system:

$$H_2^+ + H_2 \rightarrow H_3^+ + H \quad (1)$$

$$He^+ + H_2 \rightarrow HeH^+ + H \quad (2)$$

$$H_2^+ + He \rightarrow HeH^+ + H, \quad (3)$$

and it is not permissible to neglect reaction (3) *a priori*, as has been done in obtaining reaction cross sections from the observed secondary to primary current ratios.[1]

Below the appearance potential of the helium ion, only reactions (1) and (3) need be considered, and the ratio of reaction cross sections Q_3/Q_1 was measured to be 0.07 ± 0.03. An analysis of the data in the region above the appearance potential of helium, indicates that reaction (2) proceeds more rapidly than reaction (3) by about a factor of two. These measurements are conclusive proof of the presence of reaction (3) for which evidence has already been obtained in a gaseous discharge study.[2]

If a value of 1.8 ev is assumed[3] for the dissociation energy of the HeH^+ ion into He and H^+, then reaction (2) is 8.3-ev exoenergetic, and reaction (3) is 0.8-ev

endoenergetic. If as has been hypothesized,[4] an endoenergetic ion-neutral reaction would have an activation barrier just equal to its endoenergeticity, measurements of the Q_2/Q_3 ratio at ion energies close to this activation barrier may provide an experimental verification of the binding energy of the HeH^+ ion. The fact that the appearance potential of the HeH^+ ion coincided with that of H_2^+ rather than that of He^+, does not yet prove this hypothesis. The primary H_2^+ ions formed by electron impact will have a distribution of vibrational energies. All H_2^+ ions above the third vibrational level will react exoenergetically via reaction (3). Recent measurements[5] have shown that a substantial number of H_2^+ ions will be formed above the third vibrational level unless the electron energy is controlled more precisely than was possible in this experiment.

In a study of the effect of the rare gases on the radiation induced exchange of hydrogen and deuterium, it was concluded that reactions analogous to (3) could occur for all the rare gas ions.[6] On the other hand, from mass spectrometric investigations, there is evidence that formation via the rare gas ion is dominant for argon and krypton.[7] For the neon-hydrogen system in a gas discharge, formation via the H_2^+ ion has not been considered significant.[8] On the basis of the existing evidence, the following additional conclusions are drawn:

(a) The reaction of the hydrogen molecular ion with a noble gas atom involving proton transfer, is an alternative reaction path for the formation of the rare gas-hydride ion.

(b) Endoenergetic ion-neutral reactions may contribute significantly to the yield of secondary ions when the kinetic energy of the reacting species exceeds the endoenergeticity of the reaction. The attempt to prove this hypothesis in this experiment is complicated by the fact that both exoenergetic and endoenergetic reactions are possible when the primary H_2^+ ions are distributed over a range of vibrationally excited states.

(c) The experimental technique for measuring ion-neutral reactions must provide for proper selection of the reacting ion, either by adequate control of the electron energy, or by mass analysis of the primary ion.

(d) Measurements of the relative rates of such alternate ion-neutral reactions as a function of ion energy, may provide experimental data on the binding energies of molecular ions.

We are grateful to Dr. F. S. Johnson and Dr. W. B. Hanson for their many contributions in guiding the progress of this work, to Professor J. L. Magee and Dr. D. P. Stevenson for valuable discussions, and to Mr. D. McKibbin for designing the ion source used in these experiments.

[1] H. Gutbier, Zeit. Naturforsch. **12a,** 499 (1957).
[2] I. B. Ortenburger, M. Hertzberg, and R. A. Ogg, Jr., J. Chem. Phys. **33,** 579 (1960).
[3] A. A. Evett, J. Chem. Phys. **24,** 150 (1956).
[4] M. Hertzberg, Dissertation, Stanford University (1959).
[5] P. Marmet and L. Kerwin, Can. J. Phys. **38,** 972 (1960).
[6] O. A. Schaeffer and S. O. Thompson, Radiation Research **10,** 671 (1959).
[7] D. P. Stevenson and D. O. Schissler, J. Chem. Phys. **29,** 282 (1958).
[8] M. Pahl and V. Weimer, *Proceedings of the Fourth International Conference on Ionization Phenomena in Gases* (North-Holland Publishing Company, Amsterdam, Holland, 1960), Vol. I, p. 293.

Nuclear Cooling with Metallic Copper

J. J. Fritz, H. J. Maria, and J. G. Aston

Cryogenic Laboratory of the Pennsylvania State University, University Park, Pennsylvania

(Received August 12, 1960)

SEVERAL years ago Kurti *et al.* reported the successful nuclear cooling of metallic copper to temperatures near 10^{-5} degrees K.[1,2] Extension of these experiments to nearly 10^{-6} degrees K was recently reported by Hobden and Kurti.[3] We have partially repeated Spohr's experiments[2] in connection with work on nuclear demagnetization of other materials. This communication reports confirmation of Spohr's results and of some of the features observed by Hobden and Kurti,[3] and describes modifications necessary for a somewhat different experimental arrangement.

The nuclear stage, electronic stage, and heat link used were essentially the same as that used by Kurti *et al.*[1] and described in detail by Spohr.[2] The thermal shield was altered by placing the maganese ammonium sulfate specimen used to cool it above, rather than around, the chrome alum (first stage) specimen, permitting independent observation of the temperatures of both first stage and shield. The entire assembly was mounted directly inside the main bath of liquid helium.

The measuring circuits were substantially the same as those described by Spohr,[2] except that all coils were mounted inside the liquid helium bath. The apparatus was arranged to permit use of an iron magnet powered by steady storage batteries. The copper "ripple shield" used by Spohr[2] was found unnecessary, and was discarded.

The magnet used for these investigations was an iron electromagnet built by the Pacific Electric Motor Company. Using 4-in. pole-pieces with a gap of about 3 in., this magnet produces a field of 21 000 gauss with a power consumption of 45 kw. The helium and nitrogen Dewars had tips of suitable size to fit between the poles. The apparatus was suspended from above, and could be moved vertically so as to place either the first stage or the second stage in the center of the pole-pieces.

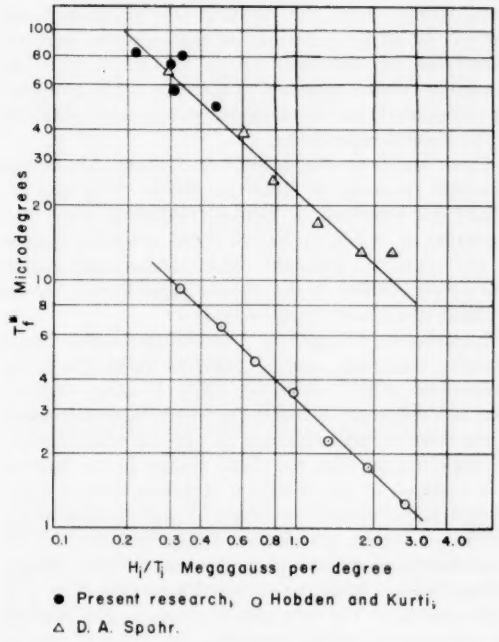

FIG. 1. Cooling of metallic copper.

Shielding of the first stage from the magnetic field during magnetization of the second stage was accomplished by the insertion about the apparatus of two closely fitting pieces of soft iron, forming a hollow block of iron $4\frac{1}{2}\times6\frac{1}{2}$ in. $\times4$ in. (high), each piece supported by a hinged and pinned framework of aluminum alloy. The amount of iron required for this purpose was determined experimentally. The force on the supports at full field was estimated to be about a ton.

The temperature scale used for the first stage was taken from that of Daniels and Kurti,[4] using a small correction to our T^* values based on isentropes and warming curves.

The five experiments reported here starting temperatures (T_i) from 0.023° to 0.037° and magnetic fields (H_i) from 4.9 to 15.0 kgauss, and overlap the lower end of the (H_i/T_i) region covered by Spohr.[1] The results are shown in Fig. 1, along with the six demagnitizations reported by Spohr[1] and the seven reported by Hobden and Kurti.[2]

In Fig. 1 the observed magnetic temperature T_f^* is plotted on log-log scale against H_i/T_i. The straight lines through the data are arbitrary. The spread of about 5% in the observed final temperatures is consistent with susceptibility. Our final temperatures agree with those of Spohr,[2] which were also measured ballistically with about the same apparatus geometry and a (dc) primary field of about 9 gauss, but both sets are about 8 times higher than those of Hobden and Kurti,[3] which were measured with a different apparatus geometry and a much smaller (ac) primary field.

The observed nuclear susceptibility decayed with time in a strict exponential fashion. The decay constant, τ was given by $\tau T_i=0.45$ sec°K, within several percent. Hobden and Kurti[3] observed τT_i of 0.30 with a field of 0.05 gauss and comment that this product doubled when the field was increased to 5 gauss. (Spohr[2] did not succeed in observing exponential deacy.)

We are pleased to report our repetition of the original results of Spohr,[2] and to have observed essentially the same relaxation times as did Hobden and Kurti[3] in their lower (nuclear) temperature range. We see no reason at present to quarrel with their interpretation of τ as the relaxation time for energy transfer between nuclear spin and the electronic system. The eightfold difference in final temperature appears to be related to the measuring fields used and to the difficulty of removing heat of (nuclear) magnetization, but the exact reasons for it are not clear to us.

We wish to express our thanks to Professor J. M. Daniels for invaluable advice in the construction of the apparatus and for assistance during the construction of most of it.

[1] N. Kurti, F. N. H. Robinson, F. E. Simon, and D. A. Spohr, Nature **178**, 450 (1956).
[2] D. A. Spohr, thesis, Oxford University (1958).
[3] M. V. Hobden and N. Kurti, Phil. Mag. [8] **4**, 1092 (1959).
[4] J. M. Daniels and N. Kurti, Proc. Roy. Soc. (London) **A221**, 243 (1954).

The Thermal Diffusion Factor of Helium

F. VAN DER VALK AND A. E. DE VRIES

F.O.M.-Laboratorium voor Massaspectrografie, Amsterdam, Holland

(Received August 29, 1960)

WE measured the thermal diffusion factor of helium in a 9-tube swing separator with a constant lower temperature of 295°K and higher temperatures varying from 370°K to 700°K. The gas used contained 10%[3] He; the tubes of the swing separator were 10 cm long with i.d. of 1 cm; the swinging time was 13.5 sec; the pressure was always near 1 atm. Samples were drawn after two days and analyzed with a mass spectrometer; the resulting values of $\ln Q$ were plotted against $\ln T_{\text{high}}/T_{\text{low}}$. In this plot we obtained within experimental error a straight line with slope 0.555 ± 0.017, giving a constant value of 0.0617 ± 0.0019 for α in this range (Fig. 1).

This obviously is in contradiction with the measurements of Moran and Watson[1] who found a marked

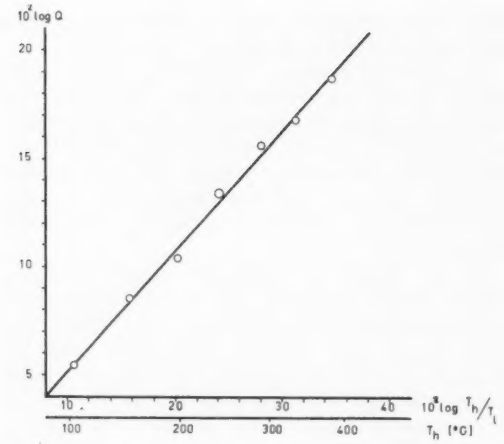

FIG. 1. $\log_{10}$ (separation factor) vs $\log_{10}$ (temperature ratio).

decrease of α towards higher temperatures in this region. However, our value fits excellently with theoretical values for the exp-6-model, using the parameters of Mason and Rice,[2] which indicate a slight decrease of α from 0.0620 at 400°K to 0.0605 at 700°K.

[1] T. I. Moran and W. W. Watson, Phys. Rev. **109,** 1184–90 (1958). Measurements on $^{20}Ne-^{22}Ne$ were in reasonable good agreement with those of Moran and Watson.
[2] E. A. Mason and W. E. Rice, J. Chem. Phys. **22,** 522–35 (1954).

Phase Transition in Ammonium Fluoride*

RICHARD STEVENSON

Eaton Electronics Research Laboratory, McGill University, Montreal, Canada

(Received September 12, 1960)

HIGH-pressure experiments using the piston-displacement method[1] show that a phase transition with an exceptionally large change in volume appears under pressure in ammonium fluoride. A typical $p-V$ isotherm obtained from these experiments is shown in Fig. 1. At room temperature the transition occurs at 3800 atm, with a volume change of approximately 28%. The phase diagram for the substance is given in Fig. 2; the bars represent the range between which the change occurred with pressure increasing and pressure decreasing. At room temperature this "region of indifference" was small, but at liquid nitrogen temperature the transition came about only at the highest pressure available with the apparatus, and recovery started only when the pressure was completely removed. At all temperatures several minutes were required for the transition to go to completion. The change in volume appeared to decrease as the temperature decreased, but no accurate values were obtained at the lower temperatures.

There has been one report[2] of a sharp rise in the dielectric constant of NH_4F at 246°K. This was assumed to represent a phase transition, since the transition at 243°K in NH_4Cl shows a similar change in the dielectric constant. This temperature region was closely studied in the present experiments, but no evidence of a phase change was seen.

At atmospheric pressure ammonium fluoride has a wurtzite structure, and is different from the other ammonium halides which are cubic. Pauling[3] suggests that this difference is due to hydrogen bond formation in the fluoride, with resultant N—H···F coordination. It would appear that the phase change in the fluoride is a collapse of the wurtzite structure into a cubic configuration similar to those found in the other halides. A short calculation (suggested by W. H. Stockmayer) indicates that the size of the volume change is what might be expected for a transition to a cubic structure. The cube root of the molecular volumes for ammonium iodide, bromide, and chloride can be plotted against the sum of the ionic radii for each particular substance. By extrapolating the curve, an estimate of the molecular volume of a hypothetical cubic ammonium fluoride is obtained. This volume is 26% smaller than the actual molecular volume, which

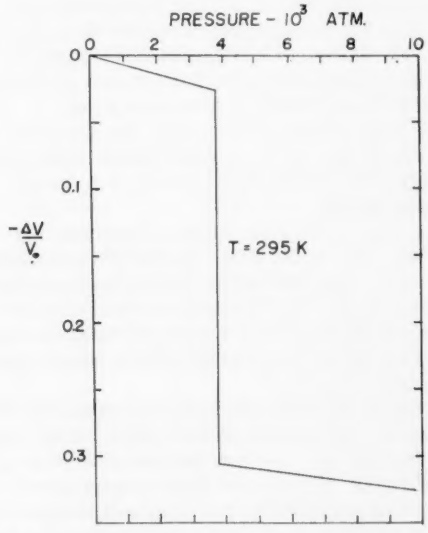

FIG. 1. Pressure-volume isotherm (reduced from the experimental data) at room temperature of NH_4F. The zero pressure phase has a wurtzite structure. Hysterisis associated with the transition is shown in Fig. 2.

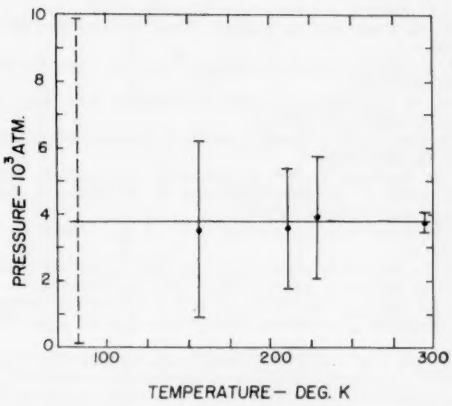

FIG. 2. Phase diagram for NH_4F. The hysterisis of the transition increases enormously as the temperature was lowered.

corresponds very well to the 28% decrease observed in the experiment.

This work was done on apparatus kindly given by Dr. S. C. Collins of the M.I.T. Cryogenic Engineering Laboratory.

* Supported by the Office of Naval Research and in part by the Defence Research Board (Canada).

[1] P. W. Bridgman, Proc. Am. Acad. Arts Sci. **76,** 9 (1945); R. Stevenson, J. Chem. Phys. **27,** 147, 656, 673 (1957).

[2] R. D. Shul'vas-Sorokina and V. D. Evdokimov, J. Exptl. Theoret. Phys. U.S.S.R. **8,** 762 (1938); Acta Physicochim. U.R.S.S. **11,** 291 (1931).

[3] L. Pauling, *The Nature of the Chemical Bond* (Cornell University Press, 1948), p. 300.

Proposal for an Infrared Maser Dependent on Vibrational Excitation*

J. C. POLANYI

Department of Chemistry, University of Toronto, Toronto, Canada

(Received September 15, 1960)

PREVIOUS proposals for the construction of infrared and optical masers (irasers and lasers)[1] envisage population inversion with respect to electronic states. The iraser proposed here would involve inversion between vibrational states.

Einstein transition probabilities for induced emission by vibrational transition are 3–4 orders of magnitude smaller than those for electronic transition, necessitating correspondingly higher concentrations of vibrational species. On the other hand, mean radiational lifetimes for vibrationally excited states are 10^{-1} to 10^{-3} sec, as against 10^{-6} to 10^{-8} sec for electronic, thus facilitating the attainment of the necessary higher concentration of vibrational species. There would be no net gain in using the vibrational medium but for the fact that there is reason to believe that a large number of chemical reactions (association reactions and exchange reactions, in gases) lead to the formation of vibrationally excited products,[2] and that the energy of reaction is converted efficiently into vibration.[3,4] In addition, the vibrational iraser should afford a much wider frequency range, and in pulsed operation, improved possibilities as a coherent amplifier in view of the long mean-life for spontaneous emission.

We shall distinguish between two types of vibrational population inversion: *complete*, with respect to an entire vibrational-rotational band, i.e., "negative vibrational temperature," and *partial*, with respect to a restricted number of vibrational-rotational transitions within a band.

Evidence that chemical reaction can lead directly to *complete* population inversions among freshly formed products of exothermic gaseous reactions, is summarized below. In the reaction $I+Na_2 \rightarrow NaI^\dagger+Na$ (superscript † denotes vibrational excitation in the ground electronic state) 40% of collisions leading to reaction result in formation of $NaI^\dagger$ with vibrational energy ≥ 48.5 kcal/mole.[3] On the assumption that $NaI^\dagger$ is formed at an equal rate in all of the approx. 90 accessible vibrational levels, the writer has calculated that only approx. 20% would be formed with vibrational energy ≥ 48.5 kcal. The experimental results require, therefore, that $NaI^\dagger$ shall be formed at a greater rate in some higher vibrational level(s) than in some adjacent lower one(s). The reaction, $O+O_3 \rightarrow O_2^\dagger+O_2$ appears to form $O_2^\dagger$ more rapidly in $v=13$ than in $v=12$.[5] But $O_2^\dagger$ is infrared inactive. In the analogous reaction $H+O_3 \rightarrow OH^\dagger+O_2$ the rate of $OH^\dagger$ formation, R_V, has been calculated as $R_9 > R_8 > R_7$; $R_4 > R_3 > R_2$.[6]

Partial inversion can occur even though T_V is positive, provided rotational distribution is non-Boltzmann, or $T_R \neq T_V$. For $H+Cl_2 \rightarrow HCl^\dagger+Cl$ under stationary-state conditions, it has been observed that $T_V = 2700°K$, and rotational distribution is non-Boltzmann, but calculable.[4] From the figures it follows that some "high", J' large, P transitions, and low R transitions, have inverted populations.[8] This is more marked for the stationary condition of $OH^\dagger$ produced in the system $H+O_3$; $T_V = 9250°K$ and $T_R \approx 500°K$,[7] from which it follows that approx. 160 out of 648 transitions have inverted populations (calculated by the writer taking $K=1-10$, $J=\frac{1}{2}-21/2$). The 160 inverted transitions comprise the 16 highest P and 2 lowest R transitions for each of the 9 populated vibrational levels.[9]

If the products of the chemical reaction as originally formed, are in an inverted populated distribution, the

experimental conditions which would be expected to favor the maintenance of a *stationary* condition of inversion are as follows: (a) pressure and temperature low to minimize collisional deactivation, with fast flow beyond the reagent mixing point[10] and (b) pulsed reaction, e.g., a pulsed discharge forming bursts of atomic reagent, followed by synchronized pulsed operation as an iraser.

If the method of vibrational excitation, chemical or physical, does not result in an initial population inversion, a complete population inversion under stationary-state conditions might in principle be brought about by (c) specific depopulation of some vibrational levels below the highest populated level by inelastic collisions, that is, by resonant transfer to vibrational or electronic excitation in a collision partner,[11] or (d) specific depopulation by chemical reaction of the vibrators within a limited range of vibrational levels below the highest populated level.[2]

In addition, (e) "partial cooling", should be a more general method,[7] though only offering the possibility of achieving partial inversion where none existed before. For example, if coherent amplification were required, a circulating gas could be heated by thermal pulses[12] at a pressure such that appreciable rotational cooling, but negligible vibrational cooling, occurred before the material entered the iraser cell. The pressure requirement is not stringent since collision efficiencies are substantially less (10^{-1}–$10^{-5}\times$) for vibrational deactivation than for rotational deactivation.

The upper atmosphere could constitute a natural iraser, favored by its long path length. When $OH^{\dagger}$ is present at $T_V \approx 10\ 000°K$,[13] $T_R \approx 227°K$[14]; calculation as before, gives the result that approx. 250 (28 highest P transitions in each of 9 bands) of 648 fundamental transitions will have population inversion. The fundamental OH emission, not yet observed, should therefore give evidence of "self-emission" rather than self-absorption. Enhanced intensity of the sun's continuum at these frequencies would also be expected, i.e., the inverse of the Fraunhofer effect. Similar phenomena may be observed due to the presence of $NaO^{\dagger}$,[15] $NO^{\dagger}$[15] and $NO_2^{\dagger}$[16] in the upper atmosphere.

Note added in proof. P. E. Charters and the writer have recently obtained indications of complete population inversion under stationary-state conditions, between levels $v=2$ and 3 of $HCl^{\dagger}$ formed from $H+Cl_2$ at low pressure; $N_3/N_2 = 1.06_5 \pm .08$ [for a description of the technique see P. E. Charters and J. C. Polanyi, Can. J. Chem. 38, 1742 (1960)].

* This material was presented verbally at a meeting of the Royal Society of Canada on June 8, 1960. The work was performed during the tenure of an Alfred P. Sloan Foundation fellowship, and with support from the National Research Council of Canada.

[1] A. L. Schawlow and C. H. Townes, Phys. Rev. **112**, 1940 (1958); J. H. Saunders, Phys. Rev. Letters **3**, 86 (1959); A. Javan, *ibid.* **3**, 87 (1959).

[2] J. C. Polanyi, J. Chem. Phys. **31**, 1338 (1959).

[3] M. G. Evans and M. Polanyi, Trans. Faraday Soc. **35**, 178 (1939).

[4] J. K. Cashion and J. C. Polanyi, Proc. Roy. Soc. (London) **A258**, 529 (1960).

[5] W. D. McGrath and R. G. W. Norrish, Proc. Roy. Soc. (London) **242A**, 265 (1957).

[6] D. Garvin, H. P. Broida, and H. J. Kostkowski, J. Chem. Phys. **32**, 880 (1960).

[7] The condition $T_R \neq T_V$ is met with, for example, behind shock waves [J. C. McCoubrey and W. D. McGrath, Quart. Revs. (London) **11**, 87 (1957)].

[8] The writer is much indebted to Dr. J. K. Cashion for this calculation.

[9] If T_R were made progressively less than T_V, partial inversion would be evident at first for high P and low R transitions, and then for lower P and lower (or no) R transitions. Inversion with respect to Q transitions would require $T_{V''} \neq T_{V'}$, or $T_{R''} \neq T_{R'}$.

[10] If only 1 or 2 high vibrational levels are populated by the reaction, a stationary condition of population inversion with respect to the level below these high levels would occur even in a static system, owing to the fact that some vibrators relax by way of overtone transitions. [For example, see H. S. Heaps and G. Herzberg, Z. Physik **133**, 48 (1952).] Under these circumstances any process that favors overtone transitions (relaxation at a surface may be an example) will be advantageous.

[11] (a) C. S. Tuesday and M. Boudart, Tech. Note 7. Report OSR-TN-55-67, Princeton University (1955); (b) A. G. Gaydon, Natl. Bur. Standards Circ. No. **523**, 1 (1954).

[12] Pulsed arc image, e.g., see *High Temperature—A Tool For The Future* (Stanford Research Institute, Stanford, California, 1956), p. 15, for references; or pulsed electrical discharge, p. 24.

[13] J. W. Chamberlain and C. A. Smith, J. Geophys. Research **64**, 611 (1959).

[14] J. Connes and H. P. Gush, J. phys. radium (to be published).

[15] Various authors in *The Threshold of Space*, edited by M. Zelikoff (Pergamon Press, New York, 1957).

[16] J. G. Greaves and D. Garvin, J. Chem. Phys. **30**, 348 (1959).

LiOH Hydration Effects in Pressed Alkali Halide Pellets

ROBERT A. BUCHANAN AND WILLIAM A. BOWEN, JR.*

Physics Department, University of California, Los Angeles, California

(Received August 1, 1960)

THE use of pressed alkali halide pellets for sample preparation is a valuable aid to infrared spectroscopists, but several anomalous effects have been reported[1–7] in the literature, which show the need for caution when interpreting spectra obtained in this manner. Yet another effect has been observed during an investigation of LiOH dispersed in various alkali halide pellets, i.e., the very rapid diffusion of water into the already pressed pellet with subsequent formation of the monohydrate of LiOH.

The pellet materials were carefully prepared in a dry box flushed with nitrogen to reduce contamination of the materials due to exposure to atmospheric water and carbon dioxide.

The infrared spectrum of the LiOH pellets shows in

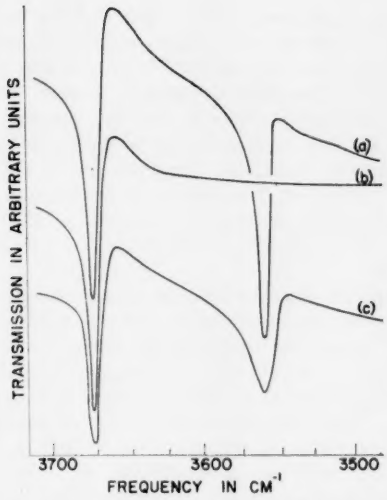

FIG. 1. Infrared spectra of LiOH in KBr pellet: (a) pellet made using normal laboratory procedures; (b) after baking at 300°C in vacuum furnace for 15 min and repressing; (c) after exposure to 90% relative humidity for 1 hr.

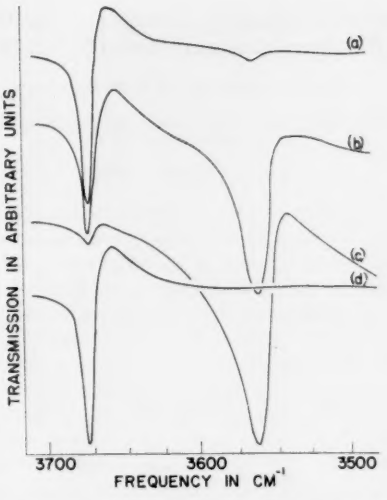

FIG. 2. Infrared spectra of LiOH in RbBr pellet: (a) pellet made using normal laboratory procedures; (b) after exposure to 90% relative humidity for 30 min; (c) after exposure to 90% relative humidity for 1 hr; (d) after baking at 300°C in vacuum furnace for 15 min and repressing.

the LiF region, three absorption bands, two very narrow bands at 3567 cm^{-1} and 3678 cm^{-1}, and a broad band at about 3420 cm^{-1}. Wickersheim[8,9] has identified the 3567 cm^{-1} and 3678 cm^{-1} bands as the $(OH)^-$ ion stretching fundamental of crystalline $LiOH \cdot H_2O$ and LiOH, respectively. The 3420 cm^{-1} band is assigned as primarily the antisymmetric H_2O stretching fundamental. Its presence always comes and goes with the 3567 cm^{-1} (OH^-) fundamental, and hence no further mention will be made of the 3420 cm^{-1} band. Subjecting a pellet to 300°C in a vacuum furnace for 15 min and then repressing, completely removes all traces of the 3567 cm^{-1} band, while increasing the intensity of the 3678 cm^{-1} band. Subsequent exposure of this pellet to a humid atmosphere (90% relative humidity) causes the return of the 3567 cm^{-1} band and a corresponding decrease in the intensity of the 3678 cm^{-1} band. This is illustrated in Fig. 1 for KBr pellets. It appears that heating the pellet drives off the water and converts $LiOH \cdot H_2O$ to LiOH; in addition, the water molecules can diffuse quite easily from the atmosphere back into the pressed pellet to preferentially form $LiOH \cdot H_2O$.

The diffusion of water into pressed pellets of LiOH, has also been observed by first pressing the pellet, noting the intensities of the 3567 cm^{-1} and 3678 cm^{-1} bands, and then exposing the pellet to the humid atmosphere. This treatment also shows an increase in the 3567 cm^{-1} band and a corresponding decrease in the 3678 cm^{-1} band, hence heating is not necessary to obtain the diffusion of water into the pressed pellet.

It has been noticed that exposing LiOH pellets of various alkali halides to the humid atmosphere for fixed periods of time, produces markedly different intensities. Figure 2 shows results obtained for a pellet of RbBr. It is noticed here that almost complete conversion to $LiOH \cdot H_2O$ was accomplished after a 60-min exposure, while in this same period of time only about half of the LiOH was converted to $LiOH \cdot H_2O$ in the KBr pellet (see Fig. 1); hence it is concluded that the diffusion of water into the pressed alkali halide pellets depends in some way upon the alkali halide. No attempt was made to quantitatively determine the diffusion rates for the various alkali halides or the mechanism for this diffusion.

It is concluded from this study that in general, the water molecule is quite mobile in the alkali halide pressed pellet, and if the sample material tends to form hydrates, it may easily do so in the pellet by taking up water molecules from the atmosphere, as well as from the alkali halide itself.

* Present address: U. S. Naval Missile Center, Point Mugu, California.

[1] R. A. Durie and J. Szewczyk, Spectrochim. Acta **8,** 593 (1959).
[2] S. A. Barker, E. J. Bourne, H. Weigel, and D. H. Wiffen, Chem. Ind. (London) **1956,** 318.
[3] V. C. Farmer, Spectrochim. Acta **8,** 374 (1957).
[4] V. M. Meloche and J. E. Kalbus, J. Inorg. & Nuclear Chem. **6,** 104 (1958).
[5] V. C. Farmer, Spectrochim. Acta **8,** 374 (1957).
[6] A. W. Baker, J. Phys. Chem. **61,** 450 (1957).
[7] G. Roberts, Anal. Chem. **29,** 911 (1957).
[8] K. A. Wickersheim, J. Chem. Phys. **31,** 863 (1959).
[9] K. A. Wickersheim, thesis, UCLA, 1958.

experimental conditions which would be expected to favor the maintenance of a *stationary* condition of inversion are as follows: (a) pressure and temperature low to minimize collisional deactivation, with fast flow beyond the reagent mixing point[10] and (b) pulsed reaction, e.g., a pulsed discharge forming bursts of atomic reagent, followed by synchronized pulsed operation as an iraser.

If the method of vibrational excitation, chemical or physical, does not result in an initial population inversion, a complete population inversion under stationary-state conditions might in principle be brought about by (c) specific depopulation of some vibrational levels below the highest populated level by inelastic collisions, that is, by resonant transfer to vibrational or electronic excitation in a collision partner,[11] or (d) specific depopulation by chemical reaction of the vibrators within a limited range of vibrational levels below the highest populated level.[2]

In addition, (e) "partial cooling", should be a more general method,[7] though only offering the possibility of achieving partial inversion where none existed before. For example, if coherent amplification were required, a circulating gas could be heated by thermal pulses[12] at a pressure such that appreciable rotational cooling, but negligible vibrational cooling, occurred before the material entered the iraser cell. The pressure requirement is not stringent since collision efficiencies are substantially less (10^{-1}–$10^{-5}\times$) for vibrational deactivation than for rotational deactivation.

The upper atmosphere could constitute a natural iraser, favored by its long path length. When $OH^{\dagger}$ is present at $T_V \approx 10\ 000°K$,[13] $T_R \approx 227°K$[14]; calculation as before, gives the result that approx. 250 (28 highest P transitions in each of 9 bands) of 648 fundamental transitions will have population inversion. The fundamental OH emission, not yet observed, should therefore give evidence of "self-emission" rather than self-absorption. Enhanced intensity of the sun's continuum at these frequencies would also be expected, i.e., the inverse of the Fraunhofer effect. Similar phenomena may be observed due to the presence of $NaO^{\dagger}$,[15] $NO^{\dagger}$[15] and $NO_2^{\dagger}$[16] in the upper atmosphere.

Note added in proof. P. E. Charters and the writer have recently obtained indications of complete population inversion under stationary-state conditions, between levels $v=2$ and 3 of $HCl^{\dagger}$ formed from $H+Cl_2$ at low pressure; $N_3/N_2 = 1.06_5 \pm .08$ [for a description of the technique see P. E. Charters and J. C. Polanyi, Can. J. Chem. 38, 1742 (1960)].

* This material was presented verbally at a meeting of the Royal Society of Canada on June 8, 1960. The work was performed during the tenure of an Alfred P. Sloan Foundation fellowship, and with support from the National Research Council of Canada.

[1] A. L. Schawlow and C. H. Townes, Phys. Rev. **112,** 1940 (1958); J. H. Saunders, Phys. Rev. Letters **3,** 86 (1959); A. Javan, *ibid.* **3,** 87 (1959).

[2] J. C. Polanyi, J. Chem. Phys. **31,** 1338 (1959).

[3] M. G. Evans and M. Polanyi, Trans. Faraday Soc. **35,** 178 (1939).

[4] J. K. Cashion and J. C. Polanyi, Proc. Roy. Soc. (London) **A258,** 529 (1960).

[5] W. D. McGrath and R. G. W. Norrish, Proc. Roy. Soc. (London) **242A,** 265 (1957).

[6] D. Garvin, H. P. Broida, and H. J. Kostkowski, J. Chem. Phys. **32,** 880 (1960).

[7] The condition $T_R \neq T_V$ is met with, for example, behind shock waves [J. C. McCoubrey and W. D. McGrath, Quart. Revs. (London) **11,** 87 (1957)].

[8] The writer is much indebted to Dr. J. K. Cashion for this calculation.

[9] If T_R were made progressively less than T_V, partial inversion would be evident at first for high P and low R transitions, and then for lower P and lower (or no) R transitions. Inversion with respect to Q transitions would require $T_{V''} \neq T_{V'}$, or $T_{R''} \neq T_{R'}$.

[10] If only 1 or 2 high vibrational levels are populated by the reaction, a stationary condition of population inversion with respect to the level below these high levels would occur even in a static system, owing to the fact that some vibrators relax by way of overtone transitions. [For example, see H. S. Heaps and G. Herzberg, Z. Physik **133,** 48 (1952).] Under these circumstances any process that favors overtone transitions (relaxation at a surface may be an example) will be advantageous.

[11] (a) C. S. Tuesday and M. Boudart, Tech. Note 7. Report OSR-TN-55-67, Princeton University (1955); (b) A. G. Gaydon, Natl. Bur. Standards Circ. No. **523,** 1 (1954).

[12] Pulsed arc image, e.g., see *High Temperature—A Tool For The Future* (Stanford Research Institute, Stanford, California, 1956), p. 15, for references; or pulsed electrical discharge, p. 24.

[13] J. W. Chamberlain and C. A. Smith, J. Geophys. Research **64,** 611 (1959).

[14] J. Connes and H. P. Gush, J. phys. radium (to be published).

[15] Various authors in *The Threshold of Space,* edited by M. Zelikoff (Pergamon Press, New York, 1957).

[16] J. G. Greaves and D. Garvin, J. Chem. Phys. **30,** 348 (1959).

LiOH Hydration Effects in Pressed Alkali Halide Pellets

ROBERT A. BUCHANAN AND WILLIAM A. BOWEN, JR.*

Physics Department, University of California, Los Angeles, California

(Received August 1, 1960)

THE use of pressed alkali halide pellets for sample preparation is a valuable aid to infrared spectroscopists, but several anomalous effects have been reported[1–7] in the literature, which show the need for caution when interpreting spectra obtained in this manner. Yet another effect has been observed during an investigation of LiOH dispersed in various alkali halide pellets, i.e., the very rapid diffusion of water into the already pressed pellet with subsequent formation of the monohydrate of LiOH.

The pellet materials were carefully prepared in a dry box flushed with nitrogen to reduce contamination of the materials due to exposure to atmospheric water and carbon dioxide.

The infrared spectrum of the LiOH pellets shows in

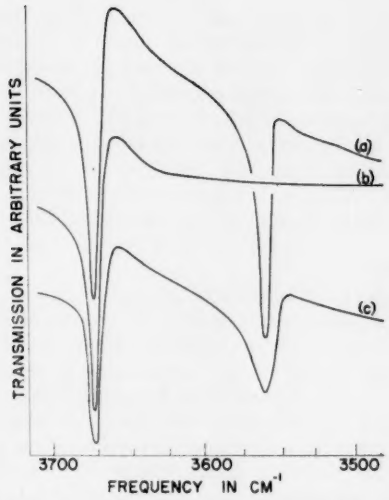

FIG. 1. Infrared spectra of LiOH in KBr pellet: (a) pellet made using normal laboratory procedures; (b) after baking at 300°C in vacuum furnace for 15 min and repressing; (c) after exposure to 90% relative humidity for 1 hr.

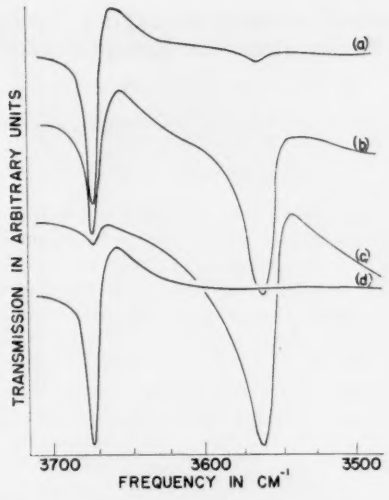

FIG. 2. Infrared spectra of LiOH in RbBr pellet: (a) pellet made using normal laboratory procedures; (b) after exposure to 90% relative humidity for 30 min; (c) after exposure to 90% relative humidity for 1 hr; (d) after baking at 300°C in vacuum furnace for 15 min and repressing.

the LiF region, three absorption bands, two very narrow bands at 3567 cm^{-1} and 3678 cm^{-1}, and a broad band at about 3420 cm^{-1}. Wickersheim[8,9] has identified the 3567 cm^{-1} and 3678 cm^{-1} bands as the $(OH)^-$ ion stretching fundamental of crystalline $LiOH \cdot H_2O$ and LiOH, respectively. The 3420 cm^{-1} band is assigned as primarily the antisymmetric H_2O stretching fundamental. Its presence always comes and goes with the 3567 cm^{-1} (OH^-) fundamental, and hence no further mention will be made of the 3420 cm^{-1} band. Subjecting a pellet to 300°C in a vacuum furnace for 15 min and then repressing, completely removes all traces of the 3567 cm^{-1} band, while increasing the intensity of the 3678 cm^{-1} band. Subsequent exposure of this pellet to a humid atmosphere (90% relative humidity) causes the return of the 3567 cm^{-1} band and a corresponding decrease in the intensity of the 3678 cm^{-1} band. This is illustrated in Fig. 1 for KBr pellets. It appears that heating the pellet drives off the water and converts $LiOH \cdot H_2O$ to LiOH; in addition, the water molecules can diffuse quite easily from the atmosphere back into the pressed pellet to preferentially form $LiOH \cdot H_2O$.

The diffusion of water into pressed pellets of LiOH, has also been observed by first pressing the pellet, noting the intensities of the 3567 cm^{-1} and 3678 cm^{-1} bands, and then exposing the pellet to the humid atmosphere. This treatment also shows an increase in the 3567 cm^{-1} band and a corresponding decrease in the 3678 cm^{-1} band, hence heating is not necessary to obtain the diffusion of water into the pressed pellet.

It has been noticed that exposing LiOH pellets of various alkali halides to the humid atmosphere for fixed periods of time, produces markedly different intensities. Figure 2 shows results obtained for a pellet of RbBr. It is noticed here that almost complete conversion to $LiOH \cdot H_2O$ was accomplished after a 60-min exposure, while in this same period of time only about half of the LiOH was converted to $LiOH \cdot H_2O$ in the KBr pellet (see Fig. 1); hence it is concluded that the diffusion of water into the pressed alkali halide pellets depends in some way upon the alkali halide. No attempt was made to quantitatively determine the diffusion rates for the various alkali halides or the mechanism for this diffusion.

It is concluded from this study that in general, the water molecule is quite mobile in the alkali halide pressed pellet, and if the sample material tends to form hydrates, it may easily do so in the pellet by taking up water molecules from the atmosphere, as well as from the alkali halide itself.

* Present address: U. S. Naval Missile Center, Point Mugu, California.

[1] R. A. Durie and J. Szewczyk, Spectrochim. Acta **8**, 593 (1959).
[2] S. A. Barker, E. J. Bourne, H. Weigel, and D. H. Wiffen, Chem. Ind. (London) **1956**, 318.
[3] V. C. Farmer, Spectrochim. Acta **8**, 374 (1957).
[4] V. M. Meloche and J. E. Kalbus, J. Inorg. & Nuclear Chem. **6**, 104 (1958).
[5] V. C. Farmer, Spectrochim. Acta **8**, 374 (1957).
[6] A. W. Baker, J. Phys. Chem. **61**, 450 (1957).
[7] G. Roberts, Anal. Chem. **29**, 911 (1957).
[8] K. A. Wickersheim, J. Chem. Phys. **31**, 863 (1959).
[9] K. A. Wickersheim, thesis, UCLA, 1958.

Vacuum Ultraviolet Absorption Spectra of Hexafluoroacetone and Hexachloroacetone*

S. R. La Paglia and A. B. F. Duncan

Department of Chemistry, The University of Rochester, Rochester, New York

(Received August 26, 1960)

IT is well known that molecules which contain the carbonyl group absorb in the general region of 2500–3500 A. This absorption is generally accounted for by excitation of an electron from a nonbonding orbital, largely localized on the oxygen atom, to an antibonding orbital which is localized in the CO group.[1,2] In many simply alkyl aldehydes and ketones, absorption[3] also occurs in the general region 1800–2000 A. However, formaldehyde absorbs at somewhat shorter wavelengths (1745 A) and phosgene[4] at still shorter wavelengths (1550 A). It has been suggested[1,2] that in formaldehyde this absorption is the result of excitation

Table I. Ionization potentials and term values for molecules containing the carbonyl group.

Molecule	Term	Ionization potential	Reference
$(CF_3)_2CO$	30 400 cm^{-1}	95 300 cm^{-1}	
Cl_2CO	30 300	95 000	a
H_2CO	30 400	87 710	b
CH_3CHO	28 900	83 900	c, d
Acrolein	29 820	81 500	e
$(CH_3)_2CO$	28 850	80 000	f, g, h
$CH_3COC_2H_5$	28 100	78 740	f, h
Crotonaldehyde	29 000	78 500	e, i
Ketene	30 980	77 500	i
$CH_3COC_3H_7$	26 670	77 370	f, h
Mesityl oxide	31 340	73 010	e, i

[a] See footnote 4.
[b] W. C. Price, J. Chem. Phys. **3,** 256 (1935).
[c] A. D. Walsh, Proc. Roy. Soc. (London) **A185,** 176 (1946).
[d] T. M. Sugden and W. C. Price, Trans. Faraday Soc. **44,** 116 (1948).
[e] A. D. Walsh, Trans. Faraday Soc. **41,** 498 (1945).
[f] See footnote 3.
[g] A. B. F. Duncan and R. S. Holdsworth, Chem. Revs. **41,** 331 (1947).
[h] J. D. Morrison and A. J. C. Nicholson, J. Chem. Phys. **20,** 1021 (1952).
[i] K. Watanabe, J. Chem. Phys. **26,** 542 (1957).
[j] J. P. Teegan, A. D. Walsh, and W. C. Price, J. Chem. Soc. **1951,** 920.

of an electron from the same nonbonding oxygen orbital to a molecular orbital described as $(z_{CH_2}-z_0, a_1)$. Recent theoretical calculations on formaldehyde[5,6] suggest that the form and energy of such a molecular orbital can account for the observed absorption, at least qualitatively, and further suggest that considerable variation in the position of the absorption should occur when H is substituted for by groups of various polarity.

We do not propose to discuss here in detail the shifts relative to formaldehyde which should be expected. A quantitative treatment of this question would require considerable theoretical calculation. Instead, we shall attempt to show empirically that the observed shifts lead to a noteworthy constancy of term value in the first vacuum ultraviolet transition of an extensive series of molecules. The position of the vacuum ultraviolet absorption of the two completely halogenated ketones $(CF_3)_2CO$ and $(CCl_3)_2CO$ is reported for the first time.

The spectra of purified hexafluoroacetone and hexachloroacetone were examined in the region 600–2150 A with a 2-m vacuum spectrograph. At the lowest pressures used, a few microns, hexafluoroacetone absorbs continuously from about 1050 A toward shorter wavelengths. This long-wavelength limit of absorption should approximately represent the ionization potential of the molecule, about 95 000 cm^{-1}. At higher pressures hexafluoroacetone absorbs at longer wavelengths, but at pressures greater than 0.1 mm the long wavelength is constant at about 65 000 cm^{-1}. Hexachloroacetone was also admitted directly into the spectrograph at similar pressures. The beginning of hexachloroacetone absorption was found at about 1500 A and extended toward shorter wavelengths.

In Table I are listed the term values of the next to lowest electronic transition of a variety of carbonyl compounds relative to their minimum ionization potentials; similar relations hold for the higher electronic transitions. It is seen that hexafluoroacetone fits in reasonably well with the terms of such molecules. Although no data exist on the ionization potential of hexachloroacetone, the position of its absorption is in accord with our expectations. The relatively constant term values arise from the close parallel between the spectral shift and the change in minimum ionization potential of the molecule, which in turn depends on the charge distribution in the molecule. This is most clearly seen by comparing the ionization potentials and absorption regions of such molecules as hexafluoroacetone and acetone or phosgene and formaldehyde.

* Part of a dissertation submitted by S. R. La Paglia to the Graduate School of the University of Rochester in partial fulfillment of the requirements for the degree of Doctor of Philosophy. This research was supported in part by the Office of Naval Research.

[1] R. S. Mulliken, J. Chem. Phys. **3,** 564 (1935).
[2] H. L. McMurray, J. Chem. Phys. **9,** 231 (1941).
[3] A. B. F. Duncan, J. Chem. Phys. **8,** 444 (1940).
[4] S. R. La Paglia and A. B. F. Duncan, J. Chem. Phys. **33,** 0000, (1960).
[5] J. M. Foster and S. F. Boys, Revs. Modern Phys. **32,** 303 (1960).
[6] P. L. Goodfriend, F. W. Birss, and A. B. F. Duncan, Revs. Modern Phys. **32,** 307 (1960).